ECSZ Does It

Revisiting the Eastern California Shear Zone

Robert E. Reynolds, editor

California State University Desert Studies Center
2017 Desert Symposium Field Guide and Proceedings
April 2017

This volume is dedicated to

Bennie Troxel

Aug 9, 1920 – Feb 20, 2017

Bennie Wyatt Troxel passed away on Feb 20, 2017; he was 96. He was preceded by his wife of 69 years, Betty Lee Patriquin Troxel, by 3 years. Bennie leaves behind a son and daughter, Wyatt Troxel and Mona Troxel Winter, their spouses, 4 grandchildren, and 9 great-grandchildren.

Bennie was born in Osawatomie, Kansas, on Aug 9, 1920. He served in the U.S. Army Air Corps during WWII flying supplies over The Hump to Burma. After the war, he entered college, eventually earning a BS and MS in geology from UCLA. He completed his course work in 1952 and, at the recommendation of Don Carlisle, was interviewed by Lauren Wright for a position with the California Division of Mines. Lauren hired Bennie, and suggested--as his first project--that Bennie make a geologic map of the north half of the Avawatz Pass 15-minute Quadrangle in southern Death Valley. Bennie liked the idea, and thus began 50+ years of geologic research with Lauren Wright.

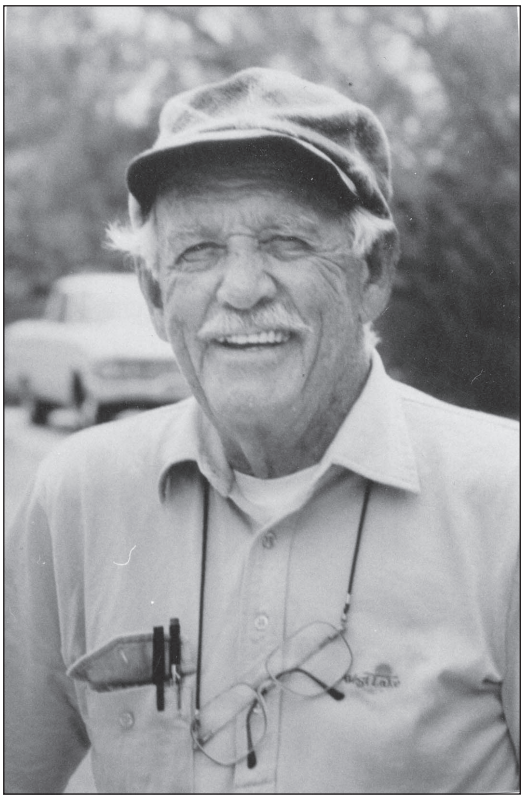

Of the numerous publications by Wright and Troxel, three stand out as modern classics. Because of their mutual interests in Death Valley geology, Levi Noble invited Bennie and Lauren to help map the geology of Noble's Amargosa Chaos in the southern Black Mountains, as well as low-angle faults associated with high-grade metamorphic rocks in the Funeral Mountains. The geology of both areas is extremely complex; Bennie said that all three of them rarely mapped more than 1/10 of a square mile a day. Eventually these maps were published as Geology of the north ½ Confidence Hills Quadrangle, Inyo County, California: The area of the Amargosa Chaos, and Geologic map of the central and northern Funeral Mountains and adjacent areas, Death Valley region, southern California by the California Division of Mines and Geology and USGS, respectively. While mapping the Funeral Mountains, Bennie and Lauren noted that west-dipping normal faults flattened at depth and joined on a common fault plane. They knew that similar fault features existed in the Amargosa Chaos as well as the Alexander Hills, 30 km to the southeast. They published their observations, Shallow-fault interpretation of Basin and Range structure, in 1973. This paper, combined with Ernie Anderson's 1971 paper, Thin skin distension in Tertiary rocks of southeastern Nevada, launched a whole new era of geologic research on crustal extension. To this day, Death Valley is considered one of the best areas to study extensional tectonics on Earth.

Bennie had a quick wit, and was always willing to share a laugh, his knowledge, and a beer with the youngest student or most experienced geologist when they visited Death Valley. When asked recently by his son Wyatt how it was to have slogged through 96 years, Bennie replied "It was nothing, tectonically." When informed of Bennie's death, Rob Negrini, Professor Emeritus of Geology at California State University, Bakersfield, wrote

"It's a sad day when a treasured mentor passes away. He was an inspiration in field. The most observant, sharp mapper I've ever met and, more important, Bennie always made sure there was time to smell the flowers. I'll always remember drinking a beer on the steps of his trailer at the iron mine in the Kingston Range when I was one of his TAs at UC Davis' summer field course. The perch overlooked a set of mountain ranges piled up on top of each other to the horizon culminating with Telescope Peak. Bennie appeared at the doorway after grabbing another beer, opened the pop top, prompting a "phht", and proclaimed "Yep.....another shitty day in Paradise, Rob!"

Here's to an eternity of shitty days in Paradise, Bennie!

—Jim Calzia, Menlo Park, CA, Feb 27, 2017

Front cover: View north of highlands in the Cady Mountains from Sleeping Beauty on the southern margins of the Cady Mountains. Gregor Losson photograph.

Title page: Wash in the Bristol Mountains with Miocene? red conglomerate beds. Jennifer Reynolds photograph.

Back cover: Geologic research in Wilderness Areas such as Broadwell Mesa requires special access and planning. David Miller photograph.

Past volumes may be viewed at: http://nsm.fullerton.edu/dsc/desert-studies-center-additional-information

Table of contents

Active tectonics of the northern Mojave Desert: the 2017 Desert Symposium field trip road log **7**
D.M. Miller, R.E. Reynolds, G.A. Phelps, J. Honke, A.J. Cyr, D.C. Buesch, K.M. Schmidt, G. Losson

The late Cenozoic Eastern California Shear Zone after 25 years of study **45**
D. M. Miller

The Eastern California Shear Zone, Mojave Desert, California **55**
Michael O. Woodburne

Major revisions of the timing, style, magnitude, and cause of Early Miocene extension in the Central Mojave metamorphic core complex and subsequent role of the Eastern California Shear Zone **60**
R. Ernest Anderson, Ph.D.

Characteristics of the Eastern California Shear Zone from Southern Death Valley to the northern Bristol Mountains: a review **71**
Roland H. Brady III

Connecting the Soda–Avawatz and Bristol–Granite Mountains faults with gravity and aeromagnetic data, Mojave Desert, California **83**
Victoria E. Langenheim and David M. Miller

A review of latest Oligocene – earliest Miocene floras of the Mojave Block **93**
Robert E. Reynolds

Analysis of the age and paleomagnetic orientation of the Broadwell Mesa Basalt, Bristol Mountains, CA **97**
G. A. Phelps, J. W. Hillhouse, R. J. Fleck, D. M. Miller, D. C. Buesch, A. Cyr, and K. M. Schmidt

Geochemical variations during development of the 5.46 Ma Broadwell Mesa basaltic volcanic field, California **103**
David C. Buesch

Mineral potential within the Eastern California Shear Zone **118**
Larry M. Vredenburgh

Geology and mineralization of Old Dad Mountain **120**
Larry M. Vredenburgh

Geology and stratigraphy of mineral occurrences in the Bristol and Old Dad Mountains, San Bernardino County, California **124**
Gregg Wilkerson

Daggett—the town history forgot **142**
Daryl Schendel

Mechanisms for post-Bouse (post-5 Ma) deformation in the lower Colorado River region. **145**
K. E. Karlstrom, L. Liu, Q Zhou, L.C.Crossey, J. Thacker, R. Crow, and L. S. Beard

Influence of the Eastern California Shear Zone on deposition of the Mio-Pliocene Bouse Formation: insights from the Cibola area, Arizona **150**
Rebecca J. Dorsey, Brennan O'Connell, Mindy B. Homan, and Scott E. K. Bennett

Hypothesis for post-Bouse distributed deformation of the Lower Colorado River corridor **158**
Jacob O. Thacker, Karl E. Karlstrom, Laura J. Crossey, Ryan Crow, L. Sue Beard, and Rebecca J. Dorsey

Post-9.45 Ma depositional and structural history of the Bear Canyon conglomerate between Indian Pass and Picacho State Recreation Area, southeastern California **165**
Jason W. Ricketts, L. Sue Beard, Ryan Crow, Kevin Coffey, and Gordon B. Haxel

Towards a depositional model for travertines of the Bouse Formation: examples from the southern Blythe Basin **174**
L. C. Crossey, K. E. Karlstrom, R. S. Crow, R.S., C. Ferguson, and R. Dorsey

Geochemical characterization of Bouse carbonates; towards an understanding of Bouse diagenesis **182**
C. Ferguson, L. Crossey, K. Karlstrom, and M. Spilde

Pinto Mountains gold **183**
D. D. Trent

Kokoweef: Still Searching for the Lost River of Gold **188**
Kim Stringfellow

Miocene(?) to Holocene extensional tectonics in the Coyote Mountains, western Salton Trough, southern California **196**
George Morgan and J. R. Morgan

The Mud Hills and Yuha Members of the Deguynos Formation in the northern Coyote Mountains, western Salton Trough, southern California and problems with a right-lateral offset of a hornblende andesite plug by the Painted Gorge Fault **209**
George J. Morgan and JR Morgan

The Ediacaran–Cambrian biotic transition in eastern California and southwestern Nevada and its global context **218**
Michael Strange and Stephen M. Rowland

A survey of lower Cambrian faunas in the southern Great Basin, California and Nevada **226**
Robert G. Eby

Biostratigraphy of nonmarine Miocene gastropods from the Barstow Formation of California **231**
William F. Abersek and Donald L. Lofgren

Environments of the Barstow Formation in the Mud Hills, southeastern California **237**
Katharine M. Loughney

A preliminary restudy of felid footprints housed at the Alf Museum from the Barstow Formation (Miocene) of southern California **241**
Chandler Luebbers, Emily Chu, Andrew A. Farke

The first Pacific Coast record of *Erethizon kleini* (Hystricomorpha, Erethizontidae) **244**
Robert E. Reynolds

Review of the Blancan / Irvingtonian transition in the northern Peninsular Range Province of southern California **251**
Robert E. Reynolds

First report of middle Pleistocene (Irvingtonian) terrestrial megafauna from the Brawley Formation, Superstition Hills, Imperial County, California **257**
Mark A. Roeder and Thomas A. Deméré

The work of W. Morlin Childers: amateur paleontologist and archaeologist **260**
Edgar Bernal Sevilla and Linda Gilbert

The ants (Hymenoptera: Formicidae) of the San Gabriel Mountains of Southern California, USA with an annotated list **266**

James Des Lauriers and Dana Ikeda

Ants of the San Gabriel Mountains in Southern California: keys to the species **280**

James Des Lauriers

Anatomy of Ivanpah Spring, Clark Mountain, San Bernardino County, California **288**

David K. Lynch and Paul M. Adams

Water-resources and land-surface deformation evaluation studies at Fort Irwin National Training Center, Mojave Desert, California **292**

Jill N. Densmore, Justine E. Dishart, David M. Miller, David C. Buesch, Lyndsay B. Ball, Paul A. Bedrosian, Linda R. Woolfenden, Geoffrey Cromwell, Matthew Burgess, Joseph M. Nawikas, David R. O'Leary, Adam R. Kjos, Michelle Sneed, and Justin Brandt

Population dynamics of *Frasera albomarginata* S. Watson "Desert Elkweed" in Mojave National Preserve, San Bernardino County, California **301**

Tom Schweich

Living on the Edge II: Further Investigation of Enhanced Roadside Creosote Growth in the Mojave Desert **306**

David K. Lynch

Flora and fauna of the Holocene Oil Canyon oil-sands from the poorly understood San Joaquin Desert Biozone **310**

Ryan E. O'Dell, Diane M. Erwin, Patricia Holroyd, Brian D. Rankin, and Marwa Ibraheem El-Faramawi

Northern flying squirrel (*Glaucomys sabrinus*) from Kuffel Canyon, San Bernardino Mountains, California **317**

Tom Howe and Peg Eby Howe

Fecundity and reproductive phenology of female Agassiz's desert tortoises (*Gopherus agassizii*) in the Sonoran Desert region of Joshua Tree National Park **319**

Jeffrey E. Lovich, Shellie R. Puffer, Mickey Agha, Joshua R. Ennen, Kathie Meyer-Wilkins, Laura A. Tennant, Amanda L. Smith, and Michael S. Vamstad

Mesocarnivore visitation and interactions with Agassiz's desert tortoises (*Gopherus agassizii*) and their burrows **321**

Shellie R. Puffer, Mickey Agha, Amanda L. Smith, Jeffrey E. Lovich, David Delaney, Joshua R. Ennen, Jessica Briggs, Leo J. Fleckenstein, Laura A. Tennant, Andrew Walde, Terence R. Arundel, Steven J. Price, and Brian D. Todd

From butterflies to bighorns: Multi-dimensional species-species and species-process interactions may inform sustainable solar energy development in desert ecosystems **324**

Steven M. Grodsky, Kara A. Moore-O'Leary, and Rebecca R. Hernandez

Icebows **330**

David K. Lynch and David S. P. Dearborn

Abstracts from proceedings: the 2017 Desert Symposium **333**

Robert E. Reynolds, compiler

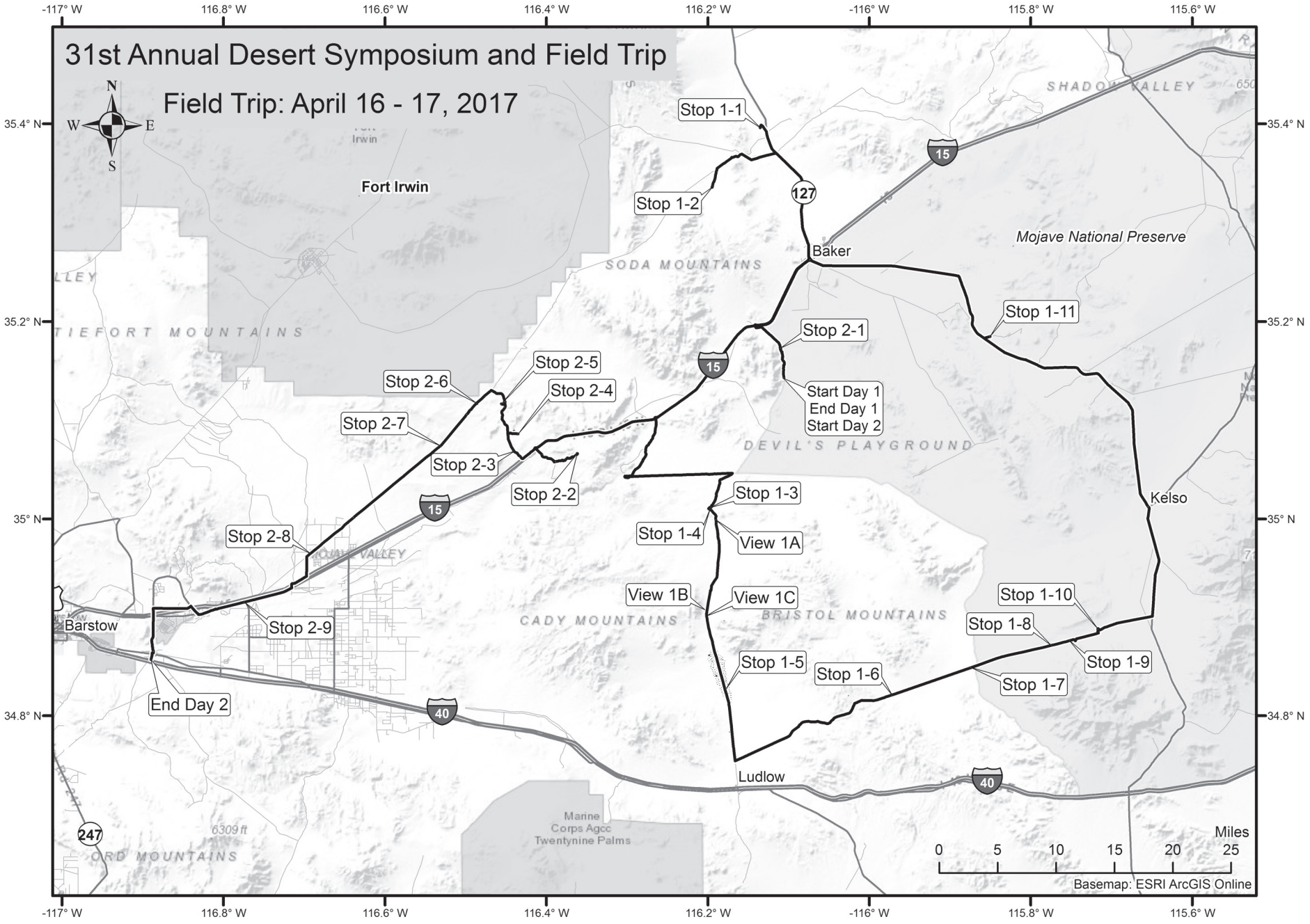
31st Annual Desert Symposium and Field Trip
Field Trip: April 16 - 17, 2017
N
W
E
S
-117° W
116.8° W
116.6° W
116.4° W
116.2° W
-116° W
115.8° W
115.6° W
35.4° N
35.2° N
35° N
34.8° N
Fort Irwin
Irwin
SHADOW VALLEY
Mojave National Preserve
SODA MOUNTAINS
TIEFORT MOUNTAINS
DEVIL'S PLAYGROUND
CADY MOUNTAINS
BRISTOL MOUNTAINS
ORD MOUNTAINS
6309 ft
Baker
Kelso
Barstow
Ludlow
Marine Corps Agcc Twentynine Palms
Stop 1-1
Stop 1-2
Stop 1-3
Stop 1-4
Stop 1-5
Stop 1-6
Stop 1-7
Stop 1-8
Stop 1-9
Stop 1-10
Stop 1-11
Stop 2-1
Stop 2-2
Stop 2-3
Stop 2-4
Stop 2-5
Stop 2-6
Stop 2-7
Stop 2-8
Stop 2-9
Start Day 1
End Day 1
Start Day 2
End Day 2
View 1A
View 1B
View 1C
15
127
40
247
Miles
0 5 10 15 20 25
Basemap: ESRI ArcGIS Online

Active tectonics of the northern Mojave Desert: the 2017 Desert Symposium field trip road log

D.M. Miller[1], R.E. Reynolds[2], G.A. Phelps[1], J. Honke[3], A.J. Cyr[1], D.C. Buesch[1], K.M. Schmidt[1], G. Losson[4]
[1] USGS Menlo Park, CA; [2] Redlands, CA; [3] USGS, Denver, CO; [4] Hermosa Beach, CA

The 2017 Desert Symposium field trip will highlight recent work by the U.S. Geological Survey geologists and geophysicists, who have been mapping young sediment and geomorphology associated with active tectonic features in the least well-known part of the eastern California Shear Zone (ECSZ). This area, stretching from Barstow eastward in a giant arc to end near the Granite Mountains on the south and the Avawatz Mountains on the north (Fig. 1-1), encompasses the two major structural components of the ECSZ—east-striking sinistral faults and northwest-striking dextral faults—as well as reverse-oblique and normal-oblique faults that are associated with topographic highs and sags, respectively. In addition, folds and stepovers (both restraining stepovers that form pop-up structures and releasing stepovers that create narrow basins) have been identified.

The ECSZ is a segment in the 'soft' distributed deformation of the North American plate east of the San Andreas fault (Fig. 1-1), where it takes up approximately 20-25% of plate motion in a broad zone of right-lateral shear (Sauber et al., 1994) The ECSZ (*sensu strictu*) begins in the Joshua Tree area and passes north through the Mojave Desert, past the Owens Valley-to-Death Valley swath and northward, where it is termed the Walker Lane. It has been defined as the locus of active faulting (Dokka and Travis, 1990), but when the full history from about 10 Ma forward is considered, it lies in a broader zone of right shear that passes westward in the Mojave Desert to the San Andreas fault (Mojave strike-slip province of Miller and Yount, 2002) and passes eastward to the Nevada state line or beyond (Miller, this volume).

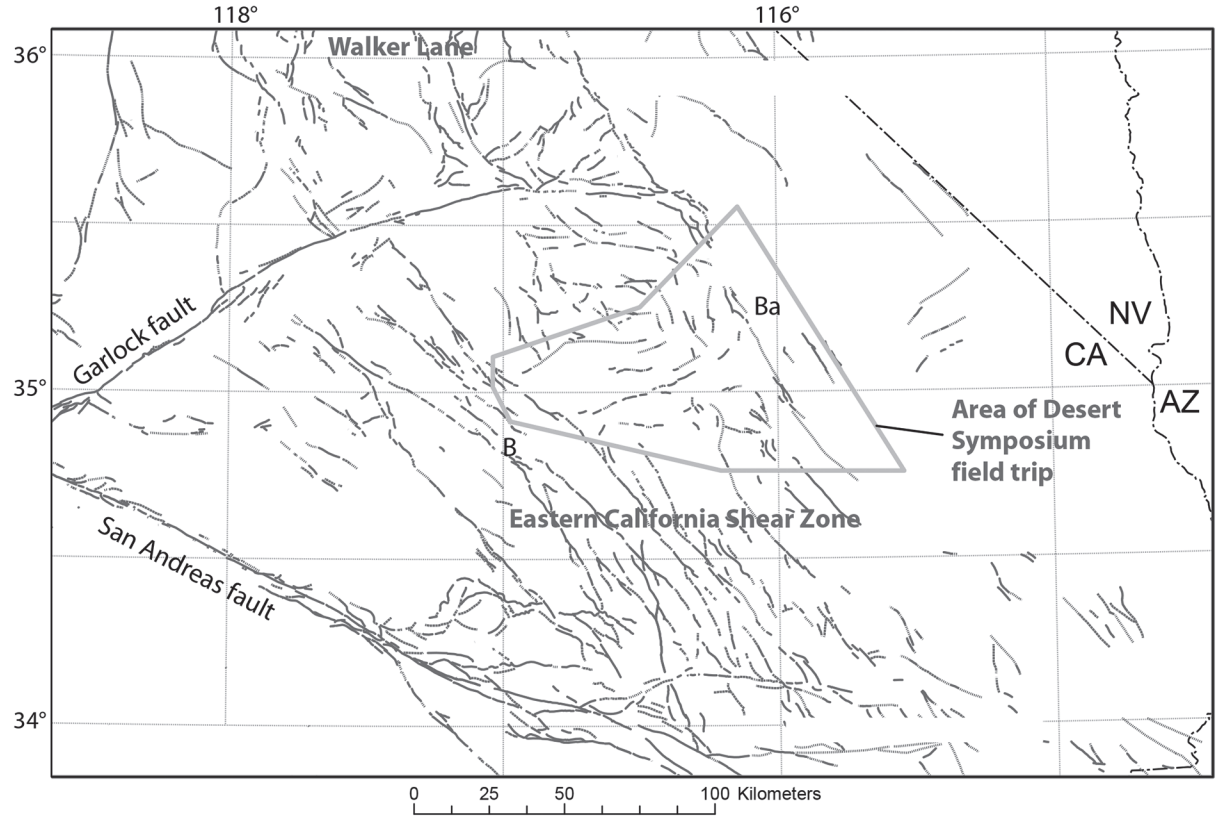

Figure 1-1. Generalized Quaternary fault map showing the ECSZ and the area to be covered by this field trip, after Miller et al. (2007b). B, Barstow, Ba, Baker.

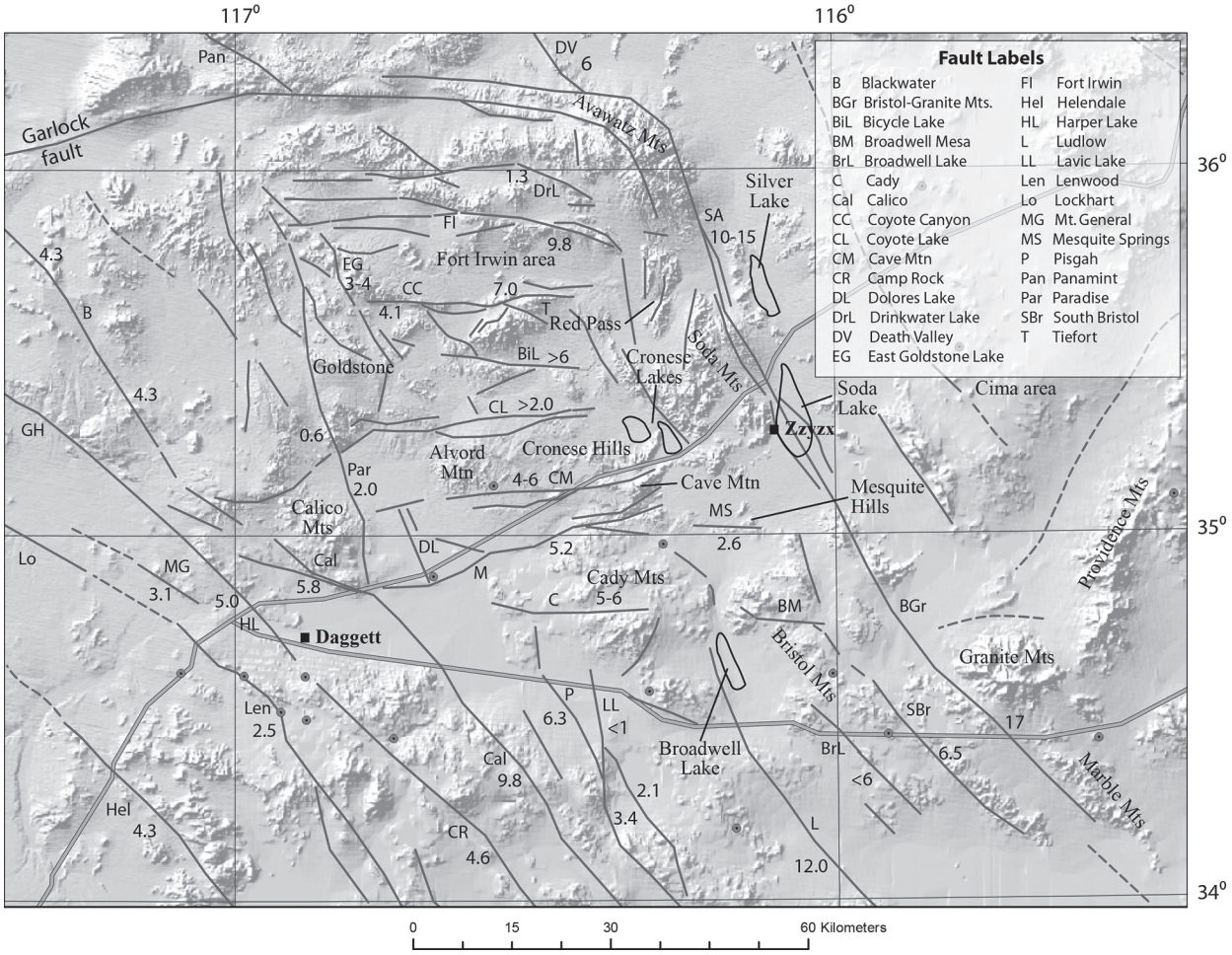

Figure 1-2. Shaded relief map of the field trip area, showing faults and place names. After Miller (this volume).

We will visit several accessible highlights for newly studied faults, signs of young deformation, and packages of syntectonic sediments. These pieces of a complex active tectonic puzzle have yielded some answers to long-standing questions such as:

- How is fault slip transfer in this area accommodated between northwest-striking dextral faults and east-striking sinistral faults?
- How is active deformation on the Ludlow fault transferred northward, presumably to connect to the southern Death Valley fault zone?
- When were faults in this area of the central Mojave Desert initiated?
- Are faults in this area more or less active than faults in the ECSZ to the west?
- What is the role of NNW-striking faults and when did they form?
- How has fault slip changed over time?

Locations and fault names are provided in figure 1-2. Important turns and locations are identified with locations in the projection: UTM, zone 11; datum NAD 83: (**578530 3917335).**

Day 1

Carpooling is mandatory on Day 1. Make carpool arrangements at the symposium on Friday or Saturday. The trip requires 4WD and skill in driving in loose sand and mud. Bring an extra spare tire and full sized shovel, and plan accordingly.

Convene at the Desert Studies Center with a full tank of gas, water, snacks, and protection from sun and wind. Note: part of this day's route is within Mojave National Preserve where special use permits are required for field trips with more than a certain number of vehicles or visitors.

Day 1 will focus on the eastern part of the ECSZ. It will emphasize faults, folds, and geomorphic development of the shear zone, and also touch on earlier history, such as Miocene extensional basins and latest Cretaceous extension. Along the way we will discuss vertebrate paleontology of several sedimentary sequences, linear spring discharge zones that mark youthful faults, and the origin of fissures in playas.

After the first two stops north of Baker, we will travel in a big counterclockwise loop south of I-15. The loop will take us to the outwash from Afton Canyon, south along

Broadwell Valley, across the Bristol Mountains, and north through the Mojave National Preserve via Kelbaker Road. At Zzyzx, convene at the railroad grade of the Tonopah & Tidewater Railroad (T & T), built in 1906 to run north from the Bagdad Chase Mine south of Ludlow, across Broadwell Playa to Mesquite Springs, then north past the salt works of Soda Station (Fulton, 2005) and north across Soda and Silver Lakes through Amargosa Gorge to the lead and silver mines at Tecopa (Myrick, 1963). Leave the Desert Studies Center (DSC) at Zzyzx and proceed north along the edge of Soda Lake.

0.0 (0.0) Drive north on Zzyzx Road from DSC to Zzyzx Overpass, passing several springs with interesting Holocene histories (Day 2, this volume).

0.9 (0.9) Road bears eastward around a lobe of alluvial fan gravel.

1.3 (0.4) Note the presence of (fault controlled?) springs along the playa margin. Soda Lake is underlain by a sedimentary basin, as much as ~1 km deep as estimated by Langenheim et al. (2009) using gravity data. The margins of the basin project toward a strand of the Soda-Avawatz fault to the northwest and a strand of the Bristol Mountains fault to the southeast, suggesting that the basin formed within a releasing step between the two faults. This will be discussed Day 2 at stop 2-1.

1.4 (0.1) SLOW through curves.

1 .6 (0.2) Cross young, light colored fan deposits incised into older, darker fans with pronounced desert pavements. These fans end abruptly at the playa margin. Flow from a spring has leached salts out of the playa and/or added microbial growth that creates a dark stripe into the playa.

1.8 (0.2) SLOW through curves.

2.3 (0.5) Proceed north to I-15.

4.2 (1.9) Road bears left (west).

4.6 (0.4) Road bears right (north).

4.7 (0.1) TURN RIGHT (east) and enter I-15 northbound toward Baker.

5.4 (0.7) Pass through freeway road cuts that expose late Miocene to Pliocene conglomerate forming linear ridges flanked by strands of the Soda–Avawatz fault zone (SAvFZ).

9.8 (4.4) Pass the west Baker off ramp.

10.8 (1.0) Exit at the central Baker off ramp.

11.2 (0.3) Stop at SR 127/Kelbaker Road. TURN LEFT (north) toward Baker.

11.5 (0.3) Cross over I-15 and stop at Baker Boulevard. PROCEED NORTH on SR 127.

ZERO mileage at Baker Blvd.

0.8 (0.8) Cross under powerline at the north end of Baker.

1.9 (1.1) SR 127 bears north, away from the T&T railroad grade. The railroad grade was built rapidly across the smooth, flat playa in 1906 but had to be abandoned when floods of 1916 made the route impassible. A bypass grade was built on higher ground along the east side of SR 127 (Myrick, 1963).

3.3 (1.4) Road bears right (east).

4.4 (1.0) Road bears west.

4.9 (0.5) Note second railroad grade on higher ground along the east side of SR 127.

5.4 (0.5) Road bears left (west).

8.0 (0.2) Note the left turn (west). We will return here to cross Silver Lake unless the playa looks dark, damp, muddy, or wet. Proceed north on SR 127.

At this junction, the second town of Silver Lake was erected on the east side of SR 127 along the new Tonopah and Tidewater (T&T) railroad grade (Myrick, 1963) in 1916 as part of F.M. "Borax" Smith's development of borate mines in Death Valley. It operated between Ludlow and Beatty, Nevada, by way of Silver Lake, Tecopa, and Death Valley Junction. Tracks for the T&T were laid near here in 1906; the line was abandoned in 1939, and steel rails hauled away for scrap. Silver Lake served as a loading station for mines in the hills to the east.

In the spring of 1910, Silver Lake floods for the first time in T&T's history, with water almost up to engine fireboxes. The tracks are raised 6."

In 1916. the Mojave River floods the lake and town again, leaving seven miles of track awash. The T&T railroad cut a trench at the north end of Silver Lake in attempt to drain flooded Silver Lake. That trench was not deep enough to assist with drainage, so the railroad grade was moved east to an elevation of 928 feet, 20 feet above the current playa surface, using materials from the Lila C. Mine. This move involved constructing a new town of Silver Lake on high ground. T&T services were shutdown, causing trains from Crucero to run to Las Vegas, then to Tecopa along the LV & T Route (Myrick, 1992).

9.3 (1.3) Pass the LADWP power line road. (If Silver Lake contains water, use this road to circle west to reach Red Pass Valley). The powerline road runs easterly through the Halloran Hills. The magnitude of detachment faulting during local crustal extension (16 – 10 Ma) is discussed in the Punctuated Chaos Volume (Reynolds and Reynolds, 1996).

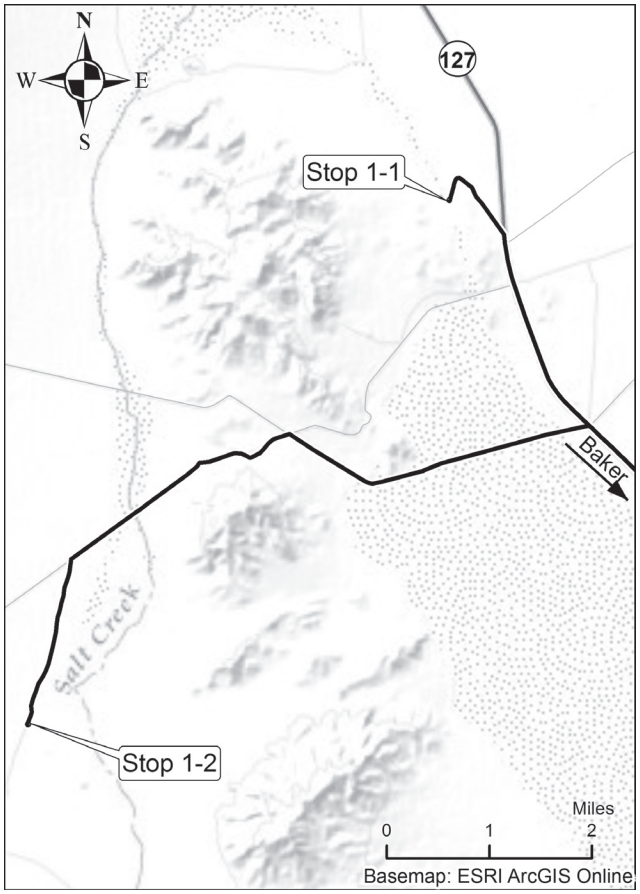

9.5 (0.2) Pass through low hills and enter the Silurian Valley drainage basin.

9.7 (0.2) Pass a road on the west side of SR 127. Ahead, we will pull to the right shoulder and get to this road by a safer route.

10.0 (0.3) STOP on east side of SR 127 across from the "safe" dirt road to west. Leave engine running. **ONE CAR AT A TIME**, check for traffic from both directions and turn left across pavement onto the dirt road. Proceed 0.2 miles to the next paved area.

10.2 (0.2) Regroup. TURN RIGHT and proceed northwest on the dirt road

10.5 (0.3) (**578634 3917600).** The road bends sharply left (southwest) around the toe of the hill. Proceed southwest.

10.7 (0.2) PARK and walk along the east side of the bench.

STOP 1-1: (578530 3917335). Outlet of Lake Mojave and tectonics of the Silurian Valley and Avawatz Mountains.

To the northwest is a view of the massive Avawatz Mountains and their precipitous eastern face. The Soda–Avawatz fault lies along its eastern front, where it transitions, from north to south, from a thrust fault with a probable dextral component to a dextral strike-slip fault with a transpressional dip-slip component (Miller et al., 2007a; Cyr and Miller, this volume; Mendonca, 2007); Fig. 1-3).

The long alluvial fans that grade east from the mountains to the Silurian Valley axis are bowed upward locally in a northwest-aligned zone of deeply incised deposits, with thrusted and folded early to late Pleistocene fan deposits demonstrating that a buried thrust or similar structure affects part of Silurian Valley (Green et al., 2007; Brady, this volume). Contractional deformation may help explain the absence of a deep basin beneath the valley (Langenheim et al., 2009), which has less than 400 m of fill in most of the valley visible from here. The valley apparently formed as a broad downwarp of the basement surface, an origin in accord with the presence of bedrock in the valley axis such as those adjacent to us at this stop. We agree with earlier assessments (Miller et al., 2007a) that Silurian Valley was tectonically created based on this evidence for structural deformation in the Pleistocene. At stop 1-2 we will see the locus of the only deep basin in Silurian Valley; it lies southwest of our current location.

We are near the route of the Salt Lake Trail – Old Spanish Trail that ran from southern Utah past The Springs (Las Vegas) into the Mojave Desert via Resting Spring, Salt Spring (to our north), over Red Pass to Bitter Spring, and south to "Do Not Pass" in the eastern Alvord Mountains. The trail then went southwest to Camp Cady, Daggett, Fish Ponds (Barstow) and through Cajon Pass to San Bernardino and Los Angeles (See Feller, this volume; Walker, 1967; Lyman and Walker, 1997, 1999).

We stand north of Silver Lake, the terminal basin of the Mojave River and the north end of Lake Mojave during the Pleistocene. Spillover from Lake Mojave did not cut completely through the bedrock hills and the deposit we

Figure 1-3. View to the northwest (~315°) of brecciated marble bedrock (upper left) faulted against Quaternary alluvial gravels (middle right) along the Avawatz mountain front. The light-colored fine-grained material is ~8 m of fault gouge composed primarily of finely brecciated marble along with alluvial clasts incorporated toward the right (east).

stand on tells that story. The smooth-surfaced deposit is cut by a steep-walled channel on the west, where the deposit is well exposed. Relict Bt soils of a Pleistocene fan are superimposed by carbonate layers that ring clasts and fill space between clasts. We interpret this as representing the development of soils during the Pleistocene in an un-incised fan, followed by wetland carbonate deposition caused by water leaking through from Lake Mojave. The carbonate formed a resistant upper part of the fan before cutting of the channel by lake spillover. If this scenario is correct, the channel should have been abandoned by 12 to 10 ka when the lake level fell for the last time (Wells et al., 2003); 10.2 ± 0.43 ka luminescence dates on eolian sand banked in the channel (Mahan et al, 2007) support this interpretation. We also tested the luminescence ages in the carbonate within the fan, reasoning that it either would represent the time of wetland accumulation or the time of original fan deposition and soil development. Infra-red stimulated luminescence, the most reliable method, yielded ages of 26.4 ± 1.5 ka at 50 cm depth and 61.1 ± 3.74 ka at 150 cm depth. These ages are most easily interpreted as times of alluvial and illuvial deposition of fine material, rather than wetland aggradation.

Although the terminal lake of the Mojave River lies on our south and overflow occurred here (Wells et al., 2003), the lake overflow apparently did not produce more lakes downstream. The interesting presence of pond turtle in Salt Spring ("Lake" Dumont) sediments north of the Avawatz Mountains and downstream from where we stand suggests a wetland or fluvial connection with Mojave River waters. Bright and Anderson (2007) showed that Mojave River water was not significant at Dumont, and the ostracodes in fine grained sediment are compatible with a spring/wetland system, not a lake. This resolves the conundrum for its age, which predates Lake Mojave, and the lack of a dam to create a lake (Anderson and Wells, 2003). Alternatively, streams from Red Pass (STOP 1-2 ahead) that have been important throughout much of the late Pleistocene, helped to feed this wetland.

Return to vehicles. Drive north to the tip of the ridge.

10.9 (0.2) TURN SHARP RIGHT (southeast).

11.2 (0.3) TURN LEFT toward Hwy 127.

11.4 (0.2) Stop at pavement, look for cross traffic, and TURN RIGHT (south) toward Baker.

12.0 (0.6) Pass the power line at the north end of Silver Lake. If Silver Lake contains water, use this road to circle west into Red Pass Valley.

13.3 (1.3) Slow, TURN RIGHT (west) on the mine road crossing Silver Lake. If the playa looks muddy or wet, do not cross; instead, retrace 1.3 miles north on SR 127 to the powerline road and circle west around playa.

14.7 (1.4) View northwest of a dark butte incised by shorelines of Pleistocene Lake Mojave. The shorelines date between 18 and 11 ka (Wells et al., 2003; Brown et al., 1990; Orr and Warren, 1971).

15.1 (0.4) Pass a gravel pit on the right. The principal source of the gravel was from a wave-built gravel spit. In the walls of the pit, shoreline features can be observed in cross-section. Tufa deposited on cobbles by cyanobacteria is present, as are articulated and disarticulated shells of the mussel, *Anodonta californiensis* (Schneider, 1994; Warren and Schneider, 2000). These shells provided initial dates of Lake Mojave shorelines in a regular progression from 13.7 to 8.4 ka (Orr and Warren, 1971; Brown et al., 1990). These ages have been refined by an experiment to cross-date by multiple methods (Owen et al., 2010). The cross-dating showed that various methods have strengths and weaknesses and each is best interpreted in terms of the specific processes involved, making simple interpretation of an outcrop by a single method potentially misleading. Late Pleistocene fossil fauna from sediments at the north end of Silver Lake have been described (Reynolds, 2004).

15.7 (0.6) Junction. TURN LEFT (southwest) onto the LADWP power line road. The road crosses a ridge of quartzite and winds downhill into Red Pass Valley with pale-colored wetland sediments.

16.9 (1.2) Leave the fans and cross braided streams of the former wetland.

17.4 (0.5) Leave braided streams.

17.9 (0. 4) A BLM wooden sign reads "Cronese Valley" at Tower MCC-VIC, L275-5 (UTM 573703 3912743). TURN LEFT and drive south-southwest past the east side of the fenced artifact enclosure that lies south of the power line road. Cross bladed utility roads and reach a graded mine road flanked by two brown Wilderness Study Area (WSA) stakes that do not exclude entry. Proceed on the graded road south-southwest toward low ridges. The road may occasionally become faint, but it continues straight to reach camp areas on the north tip of the western and eastern ridges.

18.8 (0.9) GO LEFT at the fork.

19.2 (0.3) GO LEFT at the fork.

19.4 (0.2) PARK at the west ridge and walk to outcrop.

STOP 1-2: (573216 3910600). Folds and restraining and releasing stepovers in the Soda-Avawatz fault zone. The low hills in front of us are the result of displacement on NW-striking dip-slip faults between two strands of the NNW-striking Soda-Avawatz Fault Zone (SAvFZ). The SAvFZ extends from the southern Avawatz Mountains in the north (visible from STOP 1-1) across I-15 to Soda Lake playa in the south. The cores of these low hills is composed of upper Miocene to lower Pliocene alluvial and fluvial gravels. Although called the Avawatz Gravels by

Grose (1959), subsequent work has demonstrated that they were derived locally from the igneous and metamorphic bedrock of the Soda Mountains (Gourley, 2000) and are unlike the gravels of the Avawatz Formation.

The hills are surrounded by late Pleistocene to Holocene alluvial fans and stream sediments. These have been mapped and classified based on inset relationships, surface characteristics (pavement, varnish, and depositional microtopography), and the degree of pedogenesis as late Pleistocene (Qia2), latest Pleistocene (Qia1) and Pleistocene-Holocene transition (Qya4) alluvial fans. These are dissected by streams that contain mid-Holocene (Qya3) and younger sediments. New Infrared Stimulated Luminescence (IRSL) geochronology of feldspars places the ages of samples of a Qia2 (35.329744, -116.189507) and a Qya4 (35.331575, -116.189288) deposit at 24.62 ± 1.04 ka and 5.41 ± 0.40 ka, respectively. We consider these to be minimum ages because of complications for luminescence in the Mojave Desert (Roder, et al., 2012) that tends to result in unexpectedly young ages.

At this stop we will see:

1. A view to the southeast from (latitude 35.331397, longitude -116.192134), two Qia2 alluvial fan surfaces that have different surface elevations. Qya4 and younger deposits inset into the Qia2 surfaces do not show similar elevation differences (Fig. 1-4).
2. Imbricated alluvial fan gravels exposed in a stream cut that support a Qia2 surface. The geomorphic surface has been tilted up to the northwest such that the imbrication direction of the gravels points up topographic gradient.
3. Colluvial slopes off of the hills that grade to Qia2 alluvial surfaces and have similar pavement and varnish characteristics (35.328821, -116.185967), whereas younger alluvial fan surfaces are clearly inset into both the hills (35.331077, -116.18827) and Qia2 surfaces (35.331575, -116.189288).
4. One of the faults that have displaced the Mio-Pliocene gravels and tilted them to 110^0/31 south (35.330251, -116.188253).

Figure 1-4. View to the southeast of two Qia2 alluvial fan surfaces. These are developed on alluvial gravels of the same age, but differentially affected by displacement on a minor fault between two strands of the SAvFZ.

Collectively, these features indicate that uplift of the late Cenozoic gravels began prior to Qia2 time and that the most recent displacement on these minor faults of the SAvFZ was between late Qia2 and late Qya4 time.

Not visible to the north in the lowland is a buried basin defined by gravity data (Langenheim and Miller, this volume). It is interpreted as a right step in the Soda-Avawatz fault system (extensional step over), analogous to the pull-apart basin we will discuss at Soda Lake in STOP 2-1. The basin length (~ 9 km) can be used as a proxy for the amount of total offset on the fault system and is consistent with that arrived by correlating magnetic anomalies across the fault. The basin appears to be bisected by a younger strand of the fault if the fault projects across the lowland as inferred by Grose (1959). Return to the powerline road.

20.8 (0.1) TURN RIGHT (northeast) on the powerline road and retrace to Silver Lake Road.

To the northwest, the Iron King Mine (Wright and others, 1953) exposes megabreccia of a large-runout landslide in the Miocene Avawatz Formation. The megabreccia is composed of hydrothermally altered metavolcanic clasts overlain by Paleozoic carbonate clasts (Bishop, 2003). The only possible source for the metavolcanic type megabreccia is in the surrounding hills to the south and east. Because megabreccia masses typically preserve stratigraphy, this provides evidence that this and other nearby Mesozoic metavolcanic basement rock outcrops were once structurally overlain by Paleozoic carbonate, supporting Grose's (1959) hypothesis that a regional-scale allochthon consisting of Paleozoic carbonate once covered the entire Soda Mountains.

In the southwestern Avawatz Mountains, the lower Avawatz Formation contains the only Clarendonian Land Mammal Age Miocene fauna in the Mojave Desert (10.9 Ma; Evernden and others, 1964; Reynolds and Whistler, 1990; Whistler and Reynolds, 1991). This suggests that extensional basins range in age from latest Oligocene and early Miocene from Daggett Ridge near Barstow, through the Cady Mountains and Alvord Mountain, with the youngest fauna in the southern Avawatz Mountains Extensional basins to the east and northeast are much younger, at 14-10 Ma, and may partially overlap with initial ECSZ faulting (Miller, this volume).

23.6 (2.8) TURN RIGHT (southeast) at the powerline Junction with Silver Lake Road and proceed toward SR 127.

24.2 (0.6) Pass a gravel pit.

26.0 (1.8) Stop at pavement of SR 127. Watch for cross traffic. TURN RIGHT (south) toward Baker.

33.2 (2.5) Cross under the powerline at the north edge of Baker. A road west leads to Otto Mountain, a prolific mineralogical species locality.

34.1 (0.9) Stop at Baker Boulevard. Check gas gauge and fill tank if necessary. There are about 140 miles of slow, rough road left along today's route. Cross Main Street and enter I-15 southbound (= west).

34.2 (0.1) Enter I-15 southbound (west).

39.6 (5.4) I-15 cuts through hills composed of gravel, which was deposited during Miocene extension and uplifted by the SAvFZ, part of the ECSZ (Grose, 1957).

45.6 (6.0) The road to the north leads to the Blue Bell Mine, a prolific mineralogical species locality. The ridge on the right is largely composed of granite, but has a prominent red band near its base that appears to be a tuff. Close examination shows that it is altered sheared granite along a low-angle fault.

46.1 (0.5) View of Cave Mountain ahead.

47.1 (1.0) View 2 o'clock of Cat Mountain with cat shaped falling dune.

51.8 (3.7) EXIT the freeway at Basin Road. Continue to Basin Road interchange.

52.0 (0.2) Stop, TURN LEFT (south) and proceed south on BLM route 8712 to the railroad tracks. Pass Ventifact Hill on the left. Lake Manix breached 24.5 ka (Reheis et al, 2012), early during the last glacial maximum, and flooded this area under Lake Mojave (Wells et al., 2003). The area between here and the mouth of Afton Canyon, which was buried by sediment from the river that led from Lake Manix, received huge amounts of sand and gravel excavated from Afton Canyon and the floor of Lake Manix, building a clastic wedge that we will drive up for the next few miles. This wedge rapidly filled proximal Lake Mojave, making a delta and fan. The availability of prodigious amounts of sand from the Mojave River delta caused granitic ventifacts to be carved by the wind (Laity, 2000; Reynolds et al.,2000).

East Cronese Lake lies to the north, and West Cronese Lake is further north through the pass. These "twin lakes" were on an alternate route used by emigrants (Lyman and Walker, 1999) traveling south from Bitter Springs through Cronese lakes to "the caves" and the water in Afton Canyon. Use of the area by Native Americans is well documented (Warren and Schneider, 2000). East Cronese playa is periodically fed by the Mojave River during floods. It has an extensive record of past lakes and human occupations (Schneider, 1989: Warren and Schneider, 2000). A recent paper (Miller and others, 2010) demonstrates late Holocene lakes were present here during the Little Ice Age (~ AD 1650) and Medieval Warm Period (~AD 1290). Proceed south to the sand fields of the Mojave River Sink.

52.7 (0.7) Pass a BLM kiosk at the vehicular open area.

53.9 (1.2) BEAR LEFT onto BLM 8711 at a fork in the road. At the Baxter Iron Mine to the southwest (right fork), Miocene-aged rock avalanches have emplaced iron deposits (hosted by Paleozoic rocks) in a Miocene sedimentary sequence (Lamey, C.A., 1948; Southern Pacific Company, 1964, p. 132.; Leith, 1966; Anderson, 1990; Bishop, 2013).

56.3 (2.4) BEAR RIGHT.

58.2 (1.9) A diversion berm on the right (west) side of the road was built to force the Mojave River flood flows north into East Cronese Basin, protecting the railroad. The Mojave River sporadically followed that route prehistorically, and produced populations of mussels (*Anodonta californiensis*) harvested by the Chemehuevi (Warren and Schneider, 2000).

58.5 (0.3) Cross the Mojave River channel.

58.7 (0.2) Road BLM 8711 bears right (west), parallel to the tracks.

59.3 (0.5) TURN LEFT (south) to the railroad tracks. STOP. Look for trains and cross traffic, then cross the tracks.

59.4 (0.1) Road bears left (east) parallel to tracks.

59.8 (0.4) Pass the derail spur and a right turn to Baxter Wash**.** The Cady Mountains are to the south. The Hector Formation in this part of the northern Cady Mountains ranges in age from 22 Ma to 16 Ma, and vertebrate faunas span the late Arikareean through late Hemingfordian NALMA (Woodburne 1998). Fossil plants recently collectedinclude a sabal palm associated with water reeds. (Reynolds, this volume). These plants were located in sediments beneath the 21.5 Ma basalts (Moseley, 1978; Woodburne and Reynolds, 2010).

64.5 (4.7) Pass a grove of trees on the north side of the tracks.

66.9 (2.4) Look for the "Signal Bridge" over the track. TURN RIGHT (south-southwest) at the first intersection near this structure. We are taking a southerly route along a telegraph/telephone road that was "paved" with Desert Mix—oil and tar spread over gravel classified to a small size (Fig. 1-5). Wooden stubs remain where telegraph poles have been cut down. To the east, a second route parallels the 1906 Tonopah & Tidewater (T &T).

67.9 (1.0) Road bears right (south).

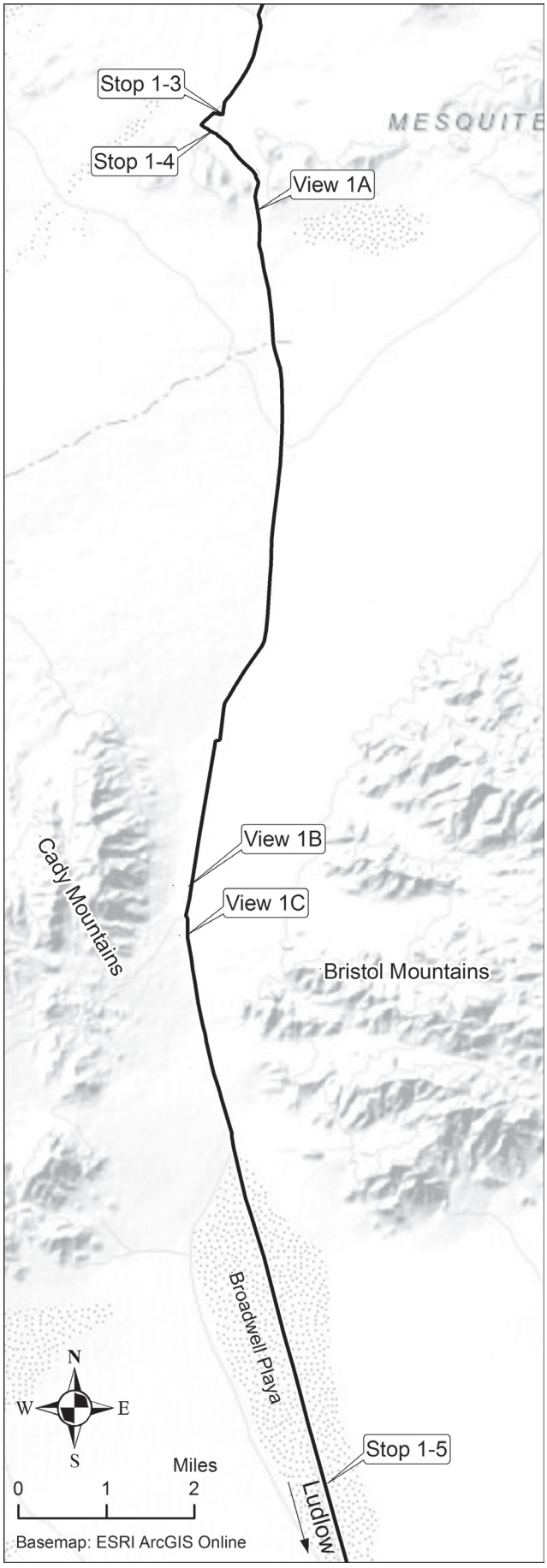

Figure 1-5. Telegraph road between Crucero and Mesquite Spring, stabilized with desert mix asphalt.

68.7 (0.8) Pass a reverse intersection with the telegraph road.

69.0 (0.3) Continue through a second intersection and STAY RIGHT at the next fork in road.

70.0 (1.0) PARK at a complex junction at a mesquite and creosote alignment.

STOP 1-3: **Mesquite Spring fault** (G.A. Phelps). The Mesquite Spring fault is an east-northeast-striking fault zone extending at least the length of the Mesquite Hills (Fig. 1-6). The fault juxtaposes late Pleistocene deposits on the north side of the Mesquite Hills with bedrock of dioritic and granitic intrusive rocks cut by both mafic and felsic dikes. In the eastern and central Mesquite Hills, fault strands tend to strike approximately N75°E, changing strike to primarily due east in the western end of the hills. On the basis of reconnaissance mapping, Miller et al. (2007b) considered that Qya4 latest Pleistocene deposits were warped adjacent to some fault strands, and therefore considered the fault to be active

Fault strands are marked by spring deposits at several locations along the fault, with the largest and most continuous deposits exposed here at the northern edge of the Mesquite Hills and Crucero Road. These deposits can be up to 4 meters high and support various types of vegetation including mesquite trees and grasses.

TURN RIGHT toward the T&T railroad grade.

70.3 (0.3) TURN LEFT (southeast) along the T & T railroad grade that follows white groundwater discharge (GWD) deposits along a fault trace of different orientation. Note the large mesquite and tamarisk trees as well as Native American petroglyphs at Mesquite Spring. The water at Mesquite Spring was reported as "very bad" (Thompson, 1929):

> the water is very highly mineralized. It is very bad, if not unfit, for domestic use, and several persons have become ill after drinking it. It should not be used …for irrigation, and (is)

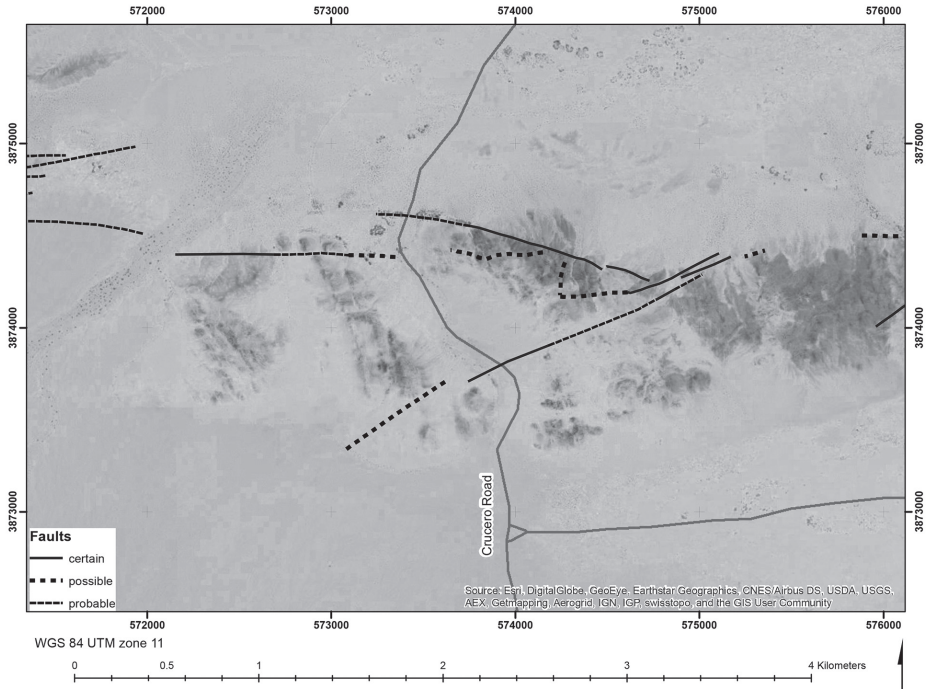

Figure 1-6. Preliminary fault map of the Mesquite Hills showing Mesquite Spring fault strands.

by causing dissolution of rock matrix at the water table, where salts are prevalent.

Proceed southeast. View southwest of Desert Megaphone (Mann, 1998).

80.0 (0.4) BLM Road 7815 joins the T&T railroad berm. Pass a left turn toward an excavation.

80.2 (0.2) The road bears south, away from berm, heading into Broadwell Basin.

80.7 (0.5) Bacon Strip Junction. Pass through the junction with a road to the left running east to join the powerline that runs northeast to the BNSF railroad. This east-trending road leads to the Bacon Strip Ranch and Airport, and continues east to access roads that reach copper (Southern Pacific Company, 1964, p. 109) and tungsten (scheelite; Southern Pacific Company, 1964, p. 153) mines and prospects. Roads to the right (west) lead to cabins.

> unfit for use in boilers because it contains an excessive amount of foaming and scale-forming constituents.

Three roads lead westerly. The road trending northwest curves southwest around hills and a west-northwest road leads to outcrops of Peach Spring Tuff and scattered pieces of agate (Conrotto, 1957). The road running southwest leads to the Southern Pacific pumicite mine (Southern Pacific Company, 1964a), and continues westerly through Hidden Valley to reach Newberry Springs. Continue south-southeast parallel to the T&T railroad grade.

70.6 (0.3) PARK.

STOP 1-4 Mesquite Spring: 572960 3874600. The GWD linear mounds appear to be located on a strike-slip fault. The mounds of carbonate silts on which mesquite grow have been interpreted as GWD deposits based on the poor stratification of carbonate-rich fines appropriate for eolian dust and carbonate precipitation in springs and wetlands (e.g., Pigati et al., 2011). However, flat benches that front the bedrock of the hills just south of these mounds are nearly horizontal, resembling shorelines cut by waves of a big lake. Hooke (1999) interpreted these features as having formed in a huge lake that was continuous from here to northern Death Valley. By this interpretation, the lake must have been deformed, because this south end was uplifted. Deformation of the basin, as well as the near absence of beach deposits, indicates that the lake was ancient. An early Holocene (~8 ka) age of dated organics collected in a black mat from these deposits (M. Reheis, written commun., 2005) make this interpretation unattractive. Alternatively, we suggest that sapping at the margin of a wetland can cause benches such as these

VIEW 1A. View southwest of canyons in the eastern Cady Mountains. Although partly obscured from this view, the east-striking Cady fault (Fig. 1-7) is located at the linear contact between Hidden Valley and the high Cady Mountains to the south. By combining Quaternary surficial deposits map information and crustal structure constraints from buried geophysical signatures, Schmidt and Langenheim (2012) and Schmidt et al. (2012) constrained fault locations and offset rates. Time-averaged sinistral offset rates, estimated from field mapping of displaced Quaternary alluvial fan deposits and from regional age constraints obtained through luminescence and radiocarbon dating techniques, decrease with older deposit age. Late Pleistocene/Holocene deposits yield rates exceeding 1 mm/yr whereas minimum rates for middle to early Pleistocene deposits are as low as 0.02 mm/yr, assuming the time-averaged fault offset ensued immediately following deposit formation. Schmidt and Langenheim (2012) estimated a total sinistral offset of ~6 km along the Cady fault based upon reconstruction of displaced bedrock outcrops and magnetic anomalies. Assuming faulting in the region began ~10 Ma, as recorded by interbedded sediments and volcanics of the Ricardo Group, the average long-term offset rate is ~0.6 mm/yr. Assuming the opening of the Gulf of California to marine incursions by rifting associated with the San Andreas fault system at ~ 6 Ma, the average long-term offset rate is roughly 1 mm/yr.

The Cady fault may represent a significant structural boundary that separates northwest-striking faults to the

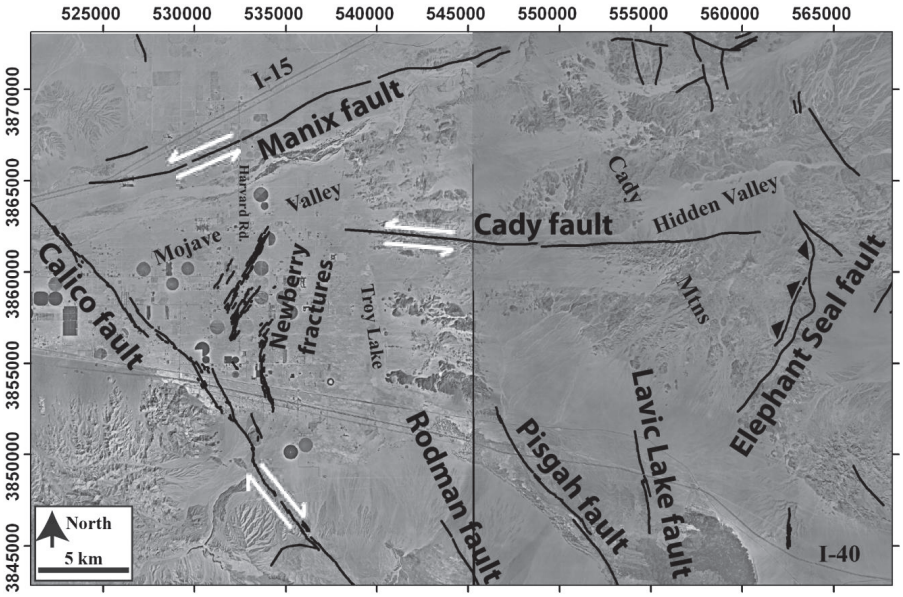

Figure 1-7. Map of the Cady Fault and Quaternary faults surrounding it. View stop 1A lies immediately east of the map.

south, such as the dextral Rodman, Pisgah, and Lavic Lake faults, from east-northeast-striking faults to the north, such as the Manix fault. Quaternary surficial deposits abound in Hidden Valley where they mantle pre-Tertiary granitic basement as well as Miocene volcanic and sedimentary rocks. The Cady fault is flanked to the south by the topographically higher part of the Cady Mountains and cumulative oblique displacement has created the presence of the long east-trending Hidden Valley along the fault. A similar south-side-up relation exists for older Quaternary units, consistent with oblique slip accommodating uplift to the south (Fig. 1-7).

84.5 (3 .8) Turn slightly right (southwest) on Crucero Road toward the T & T grade. We are still travelling on the telegraph road.

85.2 (0.7) The road connects with the T&T railroad berm, crosses the wash, and bears left (south-southwest).

85.6 (0.4) The road turns right (west) and crosses the T&T railroad berm. Proceed south-southwest on the west side of the berm.

85.8 (0.2) A yellow well head is on the right.

86.2 (0.4) View of Miocene(?) red sediments on a steep hill slope to the right (west).

87.1 (0.9) **VIEW 1B: (572750 3863100).** We are at a drainage divide in an alluvial saddle between the Cady and Bristol Mountains. Southward all drainage leads to Broadwell Lake. As we continue south on the road, faults form scarps near hill-fronts on both sides of this valley. The faults on the west form front-facing scarps (face downslope toward the observer) in the steep, bouldery fans (Phelps et al., 2012).

87.2 (0.1) Pass the powerline intersection. The powerline runs northeast to Balch and Sands sidings on the BNSF railroad, and then to Cima. It also runs southwest through a pass in the southern Cady Mountains, on the south side of a major ridge with an incline exploring for gold along a limestone contact (Losson, 2017). Farther southwest, the powerline road passes the Black Butte Mine (Tucker and Sampson, 1931; Rapp et al., 1981; Wright et al., 1953; Southern Pacific Company, 1964, p. 138; Adams, 2015).

Proceed south. Several faults in the eastern Cady Mountains are better viewed from the south, and will be discussed at STOP 1-5.

87.6 (0.4) **VIEW 1C:** One probable fault to the east is represented by a steep, high linear escarpment cut into middle Pleistocene fan deposits. The scarp is straight, and unlikely to have formed by stream side-cutting, because fans here flow west before turning south toward Broadwell Lake. On the west, aligned toes of dark fans are hidden by the T & T grade.

89.0 (1.4) Pass from easterly derived (Bristol Mountains), light colored (granitic) sands to the dark, varnished pavement of fans derived from the Cady Mountains to the west (F8g. 1-8).

Figure 1-8. Light-colored alluvial fans from the Bristol Mountains meet dark, varnished patement on fans from the Cady Mountains.

89.2 (0.2) Pass a gravel pit to the right (west), probably used to collect gravel for T & T rail bed.

89.4 (0.2) Complex intersection at north end of Broadwell Lake playa. Continue south unless playa is wet (Fig. 1-9). **DO NOT ENTER** Broadwell Playa if it appears to be muddy or if it has rained recently (Chevron Gas Station, Ludlow: 760-733-4338). In January 2017, the playa received heavy rain. The elevation at the center of the playa is 1297, and flotsam suggests that the lake filled to 1301 feet, with the shoreline within six feet of the road. Stay right along the west side of the playa on BLM 7815. Do not take BLM 9741. Avoid the road that runs northwesterly to the powerline.]

Figure 1-9. Broadwell Lake, January 2017.

90.5 (1.1) Pass an established road (BLM 7930) that runs west toward the Old Dominion Mine (Southern Pacific Company, 1964, p. 106).

91.3 (0.8) Pass the intersection with bladed road (BLM 9720) that goes west to Preston barite mine (Southern Pacific Company, 1964, p. 136; Dibblee and Bassett, 1966). Look east to the linear fissure of creosote and *Atriplex* shrubs that mark one of several fissures on Broadwell Playa.

92.3 (0.3) Pass an intersection marked by two posts with a bladed road southwest passing through the southeast Cady Mountains to connect with the Hansen Barite Mine (Dibblee, 1967). and the southern powerline.

93.0 (0.7) Pass an intersection with bladed road (BLM 9810) west to prospect trenches.

93.2 (0.2) **STOP 1-5. Broadwell Lake fissures and views of Broadwell Mesa and Cady faults**. VIEW EAST of a lineament of creosote bush (*Larrea tridentata)* and cattle spinach (*Atriplex* sp.) that mark one of several fissures on Broadwell Lake Playa. A 0.7-mile hike northeast across the playa and the T & T grade will reach the east end of the fissure. **NOTE:** Land east of the T&T berm is BLM Wilderness. Walk, but do not drive east of the T&T berm.

Broadwell Lake (G.A. Phelps, K.M. Schmidt, A.J. Cyr, D. C. Buesch, D.M. Miller)

Broadwell Lake is host to numerous giant desiccation stripes, roughly parallel linear features that span the length of the playa at strikes between 030 and 045 degrees (northeast). The features can be traced in imagery for hundreds of meters, and their habit ranges from a faint darkening of playa sediments associated with depressions of a few millimeters, to constructional mounds up to approximately 1 m wide and high (Fig. 1-10). The constructional mounds are vegetated along their apex, with sediments composed of fine sand and silt.

Constructional mounds at Broadwell Lake were excavated by Rasmussen and Associates (1990). The features were found to overlie fissures that extend into the subsurface approximately 3 m. Viewed in cross section, the stripes are wedge-shaped fissures that are wider at the top due to the collapse of the edges subsequent to the fissures formation. No evidence of differential movement was found in the excavations, indicating that the fissures are not faults. Neal et al. (1965) first observed giant vegetation stripes and noted they were associated with playa edges on long, narrow playas, and occurred

Figure 1-10. Oblique view of Broadwell Lake, view to the north. Straight fissures are marked by dark plant growth, and secondary more polygonal patterns can be seen as well. Straight T&T berm passes the length of the playa. Photograph courtesy of Gary Rasmussen.

perpendicular to the margin. Neal et al. (1965) observed that such features on playas in at least two cases were associated with water tables lower than 5 meters, and proposed that the cracks were due to desiccation of the playa sediments at depth.

Messina et al. (2005) observed the formation of a fissure in North Panamint Playa in Death Valley National Park, CA, and suggested that desiccation begins a few meters below the surface, propagates downward and upward until the surface is breached. At that point sediments begin to fill the fissure, which accumulates excess water because it is a local depression. This encourages vegetation, which grows and accumulates sediment as coppice dunes, forming constructional mounds. Neal et al. (1965) suggested that these mounds increase in height, with the plants growing upwards with them, until the roots of the plants are too elevated to receive enough water, after which time the plants die and the constructional features erode back to the level of the playa.

Although these fissures are not faults, they are oriented consistently and in a pattern unusual for playas in the Mojave Desert (based on much mapping by the authors). Fissures more typically are parallel to the playa margin or form polygonal desiccation cracks. Polygonal cracks exist on Broadwell Lake toward the center, and they use these straight northeast-striking fissures as margins (Fig. 1-10). The linear fissures are oriented appropriately to be tensional in the stress framework of the ECSZ, which has maximum stress oriented about N10°E (Schelle and Grunthal, 1996). They probably are related to tectonics of the valley, but a lack of exposed faults in most places provides a sparse framework for interpreting the fissures.

Broadwell playa is narrow and long, oriented nearly northerly, and is flanked by wide piedmonts leading from the Bristol Mountains and Cady Mountains. To the east, the Bristol Mountains have several high peaks on the left (north) that are underlain by Mesozoic granitoids. Southward, the granitoids are overlain by a volcanic-dominated sequence that was mapped by Dibblee (1967) and earlier workers as south-dipping and highly faulted. Virtually the entire range visible from here is composed of these volcanic rocks, which are similar to early Miocene rocks farther south in the Bristol Mountains (Miller, 1994; Harvey, per. comm. To Miller, 2016). Look carefully at the area between the high granitoid peaks and the volcanic rocks farther south for a flat mesa. At this location, the

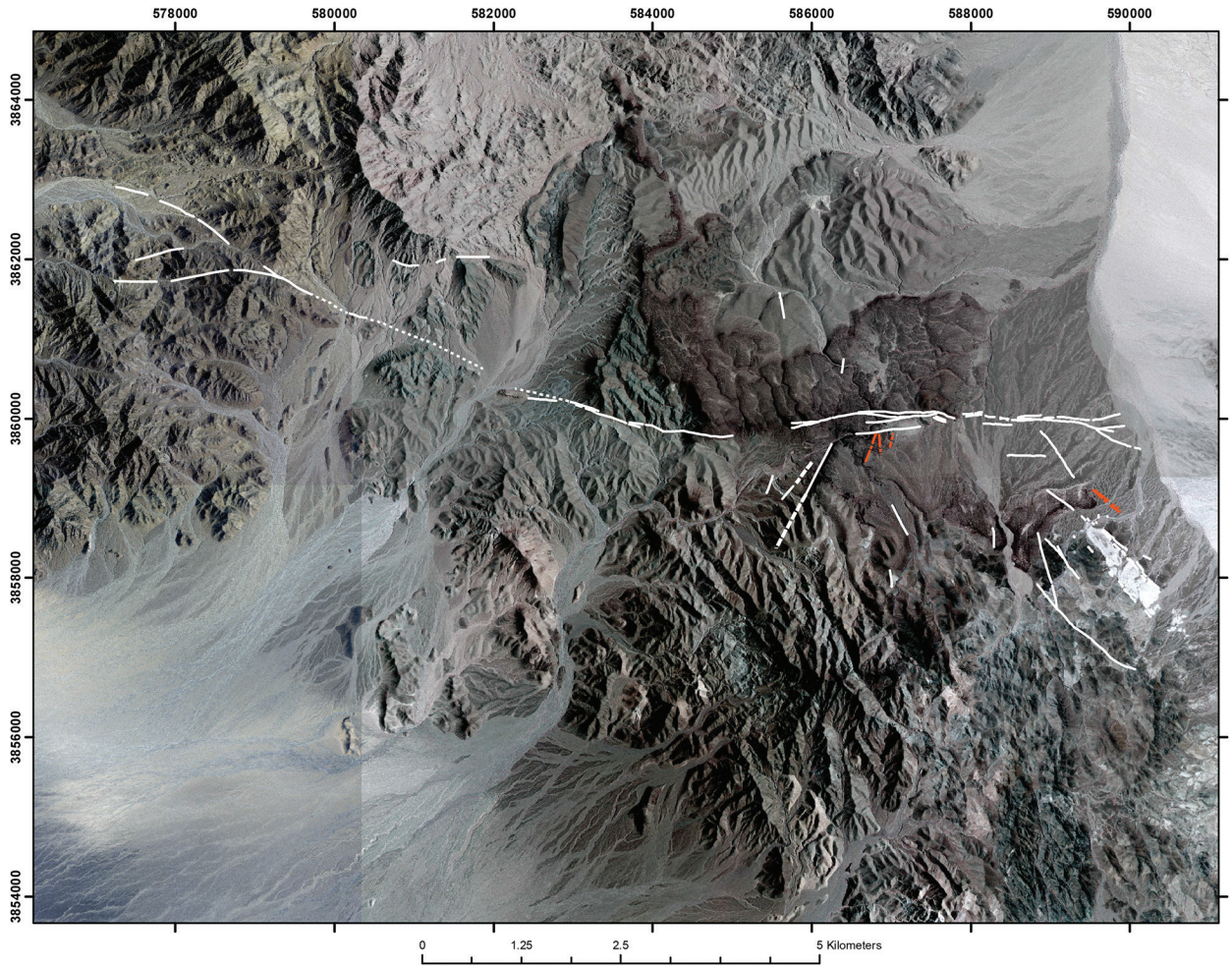

Figure 1-11. Geologic sketch map of the Broadwell Mesa area, northern Bristol Mountains. Preliminary mapping by D.C. Buesch, A.J. Cyr, D.M. Miller, G.A. Phelps and K.M. Schmidt. BMb, Broadwell Mesa basalt; Kg, Cretaceous granite; Jg, Jurassic granite. Heavy white lines are faults.

flat-lying Broadwell Mesa basalt, presumed by Dibblee (1967) to be Quaternary, lies across the dipping Miocene volcanic rocks. Brady (1992) studied this basalt, showing that it is about 5.5 Ma. We have carefully mapped this basalt, now in the center of the Kelso Dunes Wilderness Area, because it was identified by Phelps et al. (2012) as probably cut by an east-striking fault, which, like the Mesquite Spring fault, is anomalous for this part of the ECSZ.

The fault was verified by our detailed mapping (Fig. 1-11). It cuts Pleistocene deposits with soils consistent with 70-100 ka age, forming a narrow zone of graben and horst. At its east end, deposits are consistently faulted up on the south, and the opposite seems to hold farther west at the west margin of Broadwell Mesa. The fault can be followed farther west through the Miocene volcanic rocks and underlying granites, and is last exposed in a position that would have it exit the Bristol Mountains on a WNW orientation, near the subtle divide (view 1B) at the north margin of the Broadwell basin. Geochronology of the basalt (Phelps et al., this volume) and overlying sedimentary deposits is underway, and a number of questions remain outstanding. However, we have determined that: (1) the fault is left-lateral (sinistral) with probably several kilometers of offset of the 5.5 Ma basalt; (2) the basalt flowed into a broad valley that had south- and north-flowing streams that led to a valley axis, and which probably drained eastward; (3) at least one cinder cone eruptive center is essentially on the Broadwell Mesa fault; and (4) the basalt is folded about an east-trending axis. The basalt appears to have flowed into a sag or downwarp based on paleocurrents measured in underlying sediment. Lava ponded near the fault suggests that this was near the axis of the paleovalley. These observations indicate to us that east-trending folds are coincident with sinistral faults, forming valleys along the faults. This pattern also has been observed farther to the northwest in the ECSZ (Miller et al., 2011). Folding occurred over an unknown, but probably significant period of time, perhaps 7 to 4 Ma.

Paleomagnetic directions (Phelps et al., this volume), supplemented by work on chemical trends of magma marked by small changes in rock chemistry in the lava-flow stratigraphy (Buesch, this volume), show that the flows were emplaced rapidly. Phelps et al. (this volume) show that the northern basalt has not rotated a significant amount with respect to the basalt south of the fault, but net rotation of both basalts is poorly constrained. Clockwise vertical-axis rotation is common for fault blocks associated with sinistral faults of the ECSZ (e.g., Schermer et al., 1996) and we continue to evaluate the Broadwell Mesa fault for evidence supporting rotated tectonic blocks.

To the west lies the steep mountain front associated with Cady Peak (Fig. 1-7). Although the Cady fault runs through Hidden Valley west toward the Manix and Calico faults at the southern tip of the Calico Mountains, it does not project straight eastward into Broadwell Valley (Schmidt, this volume). Rather, tectonic strain is accommodated in a complicated manner between the east-striking, left-lateral Broadwell Mesa and Cady faults. At its eastern terminus, the Cady fault intersects or merges with an east-vergent, west-dipping, NNE striking thrust fault, hereafter referred to as the Elephant Seal fault. This abrupt, eastward change in displacement generated rock uplift that has exhumed crystalline basement with high relief, the Cady Mountains, that decreases southward from the Cady fault and the local high of Cady Peak. This may indicate decreased total reverse fault slip on the Elephant Seal fault to the south toward the Lavic Lake Fault. East of the Elephant Seal fault is a broader tectonic accommodation zone containing numerous deformation features that are consistent with shortening associated with a right step in a sinistral fault and also reverse faulting oriented roughly orthogonal to primary sinistral faults. Evidence for a through-going surface trace of an east-striking sinistral fault east of the Cady fault is presently not recognized. The Broadwell Mesa fault is such a candidate, but it lies 20 km to the east and the intervening area is separated by several north-striking, likely oblique dextral, faults. Such complexity of accommodation zone fault structure may indicate that 1) deformation associated with the Cady fault is a spatially and temporally evolving feature that may be lengthening eastward or, more probably that, 2) reverse deformation associated solely with the Elephant Seal fault is stepping eastward. Additionally, the orientations of many of the structures are generally orthogonal, or at a high angle, relative to the expected NNE regional stress field within the ECSZ, and hence represent local complexity of Quaternary tectonic deformation.

Return to vehicles. Proceed south toward second powerline crossing.

93.4 (0.2) Remains of wooden poles run northeast to the east playa margin.

93.7 (0.3) Pass bushes growing in a borrow pit used for road grade material. Nearby, east-west lines of gravel suggest road base material was collected by scraper or Fresno.

94.1 (0.4) Mid-playa road joins our playa margin road. Continue south.

95.0 (0.9) Pass road (BLM 8846) west to Reinerth manganese prospect (Trask, 1950; Leith, 1966; Southern Pacific Company, 1964, p. 106).

95.8 (0.8) Pass road west (BLM 8831) to Andreen manganese prospect (Crook and others, 1943; Leith, 1966; Southern Pacific Company, 1964, p. 106).

95.9 (0.1) Pass road west (BLM 8830).

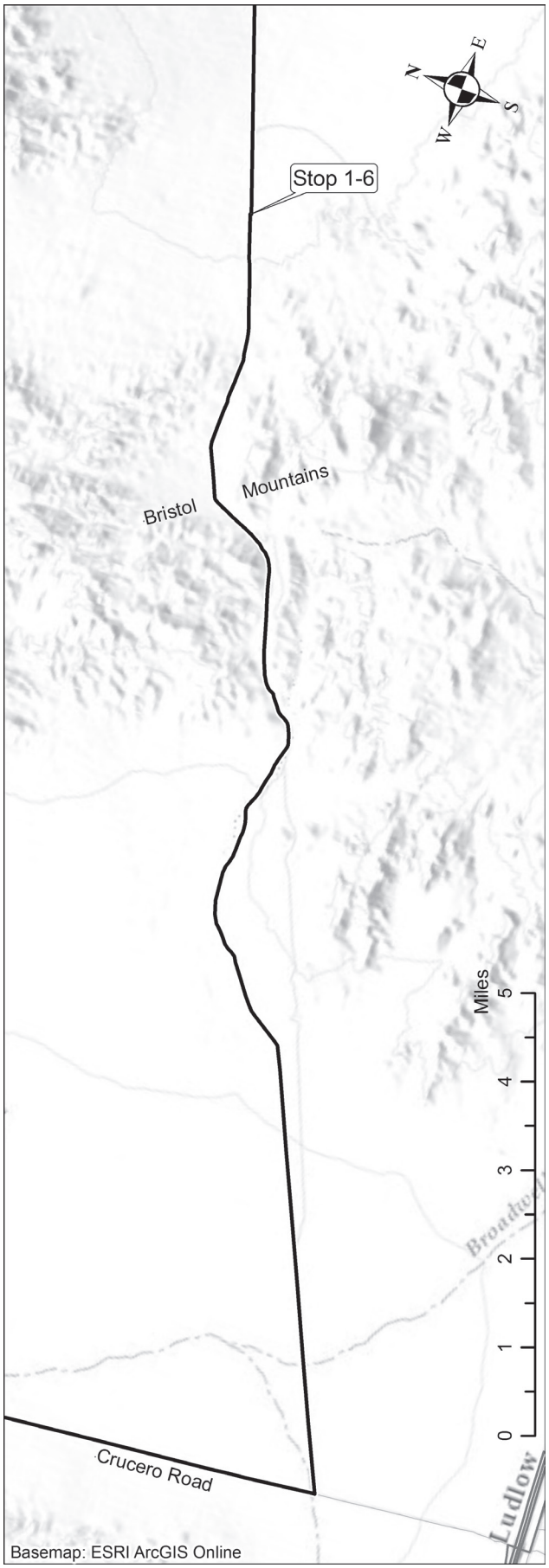

98.0 (2.1) TURN LEFT (northeast) at junction with the powerline road. This utility road (NN015) runs southwest along the south side of the Cady Mountains past the Hansen Barite Mine, Lavic Manganese (Southern Pacific Company, 1964, p. 138; Durrell, 1954; Adams, 2015), the DuPont Strontium deposit (Durrell, 1953), and the mountain crest shaped like a "Sleeping Beauty."

To the northeast, our route along the powerline road passes 30 miles through the Bristol Mountains, along the north side of the Granite Mountains, along the south margin of the Kelso Dunes to Kelbaker Road, and then through Foshay Pass in the Providence Mountains. The road is covered in places with deep dune sand, and there are no towing services at Kelso. 4WD, high clearance vehicles, carpets, boards, and shovels are highly recommended. Remember that deflating your tires can be helpful, but bring a tire pump to reinflate. Proceed northeast on powerline road.

98.1 (0.1) Cross T&T railroad grade (McKenna, 1990).

99.8 (1.7) Leave light-colored sediments being washed north toward Broadwell Playa and cross dark colored gravels from the southern Bristol Mountains.

102.2 (2.4) BEAR LEFT (north) at the fork, and go around the sand hill. Sand on the far side of the hill "is so deep that you could get stuck going downhill" (p. comm. Reynolds to Redmond, 1984).

103.1 (0.9) Pass a hill on the left. View north of Broadwell Mesa.

103.6 (0.5) The road bears right (east-southeast).

104.4 (0.8) The road drops down the terrace into a wash. From here on to the east, the road is firmer.

104.5 (0.1) TURN RIGHT (east).

104.9 (0.4) The road crosses the powerline access road. BEAR LEFT (northeast). Drive through the Bristol Mountains via the road in the wash bottom.

105.4 (0.5) DO NOT TAKE road that bears right (east) uphill. Proceed north-northeast in the wash.

105.7 (0.3) Rejoin the powerline road as it climbs the terrace.

106.4 (0.7) The road crosses a terrace and drops into a wash.

106.8 (0.4) The road bears left (northeast). Avoid canyon and stub roads bearing right (east).

107.6 (0.8) The road bears right (northeast) and leaves the wash. Cross the drainage divide of the Bristol Mountains. Peach Spring Tuff (high mesas to the south) near here shows no vertical-axis rotation, as is typical for many

locations bounded by dextral northwest-striking ECSZ faults (Wells and Hillhouse, 1989).

108.1 (0.5) The road bears right (east), leaves the wash, and ascends onto the eastern high piedmont of the Bristol Mountains.

109.0 (0.9) The road passes a compressor station and the first series of washes.

109.3 (0.3) The road crosses a wash.

109.5 (0.2) Road crosses a second wash.

109.8 (0.3) The road crosses a third wash.

110.2 (0.4) Road crosses a fourth wash.

110.6 (0.4) **STOP 1-6: 594030 3853670. Bristol Mountains tectonics, Late Cretaceous to recent**. We will describe the geology of several features that can be seen from here. Mapping to the south (J. Harvey, unpublished) has traced the South Bristol Fault northwest from the Bristol Lake area to near here. This fault appears to cut middle Pleistocene fan deposits but no younger deposits (Bedford et al., 2012), indicating that it has ceased activity for close to 100,000 yr (Miller et al., 2007) or has had a very low slip rate during its recent history. A valley continues straight to the northwest, along which one or two parallel faults that place Miocene volcanic rocks against Cretaceous granitic rocks are mapped (Dibblee, 1967). In a few places, these faults appear to cut old gravels of uncertain age, and one splay of the faults cuts and displaces the Broadwell Mesa basalt. We consider the South Bristol Fault to continue along this valley at least as far as the intersection with the Broadwell Mesa fault, but details of how the two faults interact are obscured by young stream and alluvial fan deposits, making its extrapolation farther north tentative at best.

New work on gravity-defined basins by G.A. Phelps will be presented that shows a broad basin near our location. A paucity of locally mapped faults makes the interpretation of this basin unclear, but it is tempting to invoke releasing bends in one or more faults as an origin for the basin, analogous to those described by Langenheim and Miller (this volume).

Due north (of us), light-colored rocks form a broad dome in the Bristol Mountains. Mesozoic granitoids in this area are cut by mylonite zones similar to those seen farther northeast in the Teutonia batholith (Miller et al., 1996; Wells et al., 2005), where Cretaceous unroofing was defined by mapping, dating of rocks, and thermochronology. Study of this area by Lee Hess (UNLV) will be presented. Continue east on PL road.

111.3 (0.7) Pass a bladed road south to Strawberry Travertine Onyx Mine (Mitchell, 1998, p. 74). The area to the south is wilderness. Continue east across dark desert pavements.

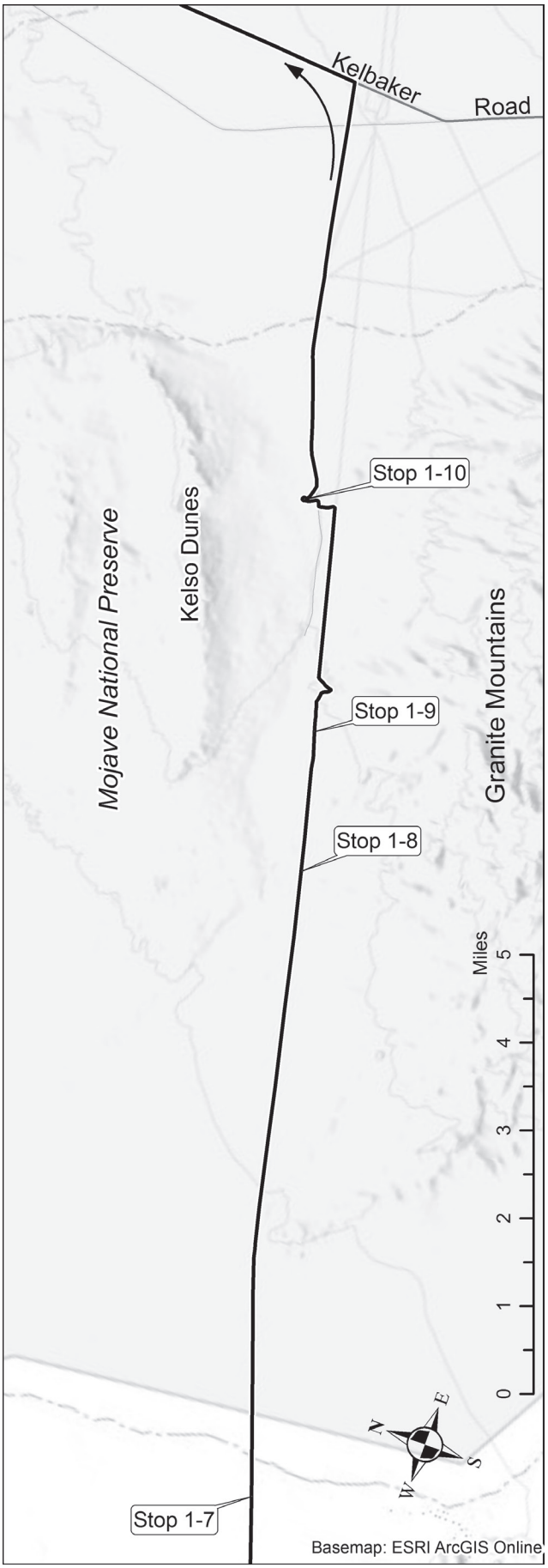

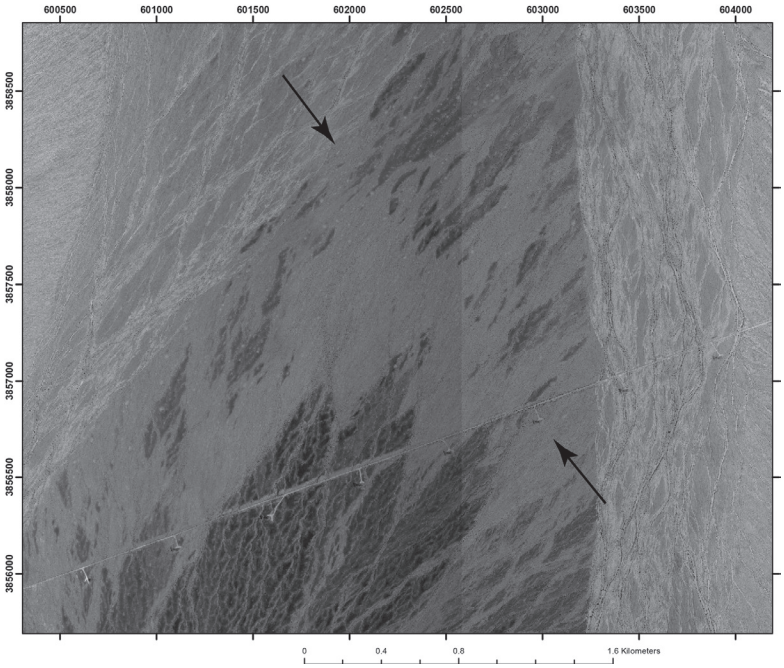

Figure 1-12. National Agriculture Imagery Program (NAIP) image of the area at STOP 1-7 showing linear disruptions of dark, varnished alluvial fan deposits. Linear feature (indicated by black arrows) is the inferred trace of the Bristol-Granite Mountains fault (Bedford et al., 2012).

111.9 (0.6) Cross light-colored arkosic gravels from granitic hills to the north.

114.3 (2.4) Cross reddish-gray gravels and dark red pavemented terraces.

114.5 (0.2) Cross red gravels from the eastern Bristol Mountains.

116.7 (2.2) **STOP 1-7: 602955 3856860 Bristol-Granite Mountains fault**. Here we cross the buried trace of the Bristol-Granite Mountains fault zone (BGMFZ), which is the easternmost fault of the ECSZ as defined by Dokka and Travis (1990). It is marked here by linear truncation of pavement surfaces that are evident on aerial photographs, but any scarps that may be present are very subtle (Figure 1-12). This easternmost fault of the ECSZ has been subject to many interpretations in terms of its role in the shear zone. Langenheim and Miller (this volume) show that it has about 12-17 km (7.5-10.6 mi) of dextral slip, with an apparent northward decrease in offset. The amount of right slip from correlating pairs of aeromagnetic anomalies in the Marble and Old Dad Mountains (15-17 km) -(9.3–10.6 mi) is similar to the result from offset Miocene markers, as modified below, from Lease et al. (2009). This indicates that all of the fault offset is Miocene and younger. Furthermore, gravity and aeromagnetic data indicate that the Bristol-Granite Mountains fault zone is connected to the Soda-Avawatz fault zone, with a curious pattern of alternating stretches of uplift and subsidence that may reflect coupling with faults farther west or east.

Separation across the Bristol-Granite Mountains fault zone: Correlation of the Lost Marble paleovalley (D.C. Buesch and R.O Lease)**.** South of here, across the divide west of the Granite Mountains, a proposed mid Miocene Lost Marble paleovalley in the Old Dad and Marble Mountains provides a separation estimate of 17 km (10.6 mi) for this part of the Bristol-Granite Mountains fault zone.

Lease et al. (2009) described the mid Miocene "Lost Marble paleovalley", which is located in the northern Marble Mountains and northern Old Dad Mountains, California. This paleovalley was offset by the BGMFZ (Fig. 1-13). The youngest rock in the paleovalley is the Peach Spring Tuff (PST, 18.78 Ma from Ferguson et al., 2013). Buesch and Valentine (1986) and Buesch (1991, 1992) described examples of deposition of the PST across pre-existing topography with the tuff filling paleovalleys and onlapping paleo-mountain flanks, including onlap relations in the northern Marble Mountains. Lease et al. (2009) used the thinning and thickening of the PST in the northern Marble and northern Old Dad Mountains to infer locations where the tuff filled a paleovalley. In

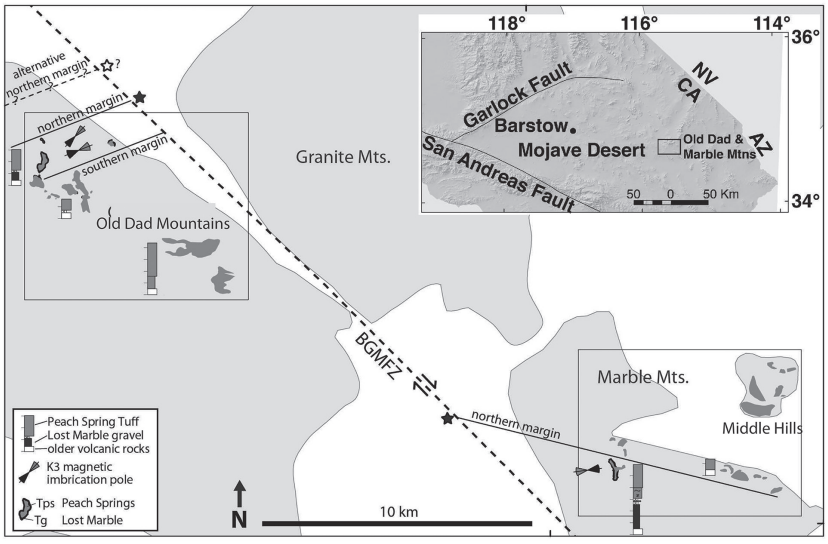

Figure 1-13. Location map of the Old Dad and Marble Mountains, California, with stratigraphic columns, selected anisotropy of magnetic susceptibility data, and projected separated margins of the Lost Marble paleovalley (modified from Lease et al, 2009). Piercing point correlation of the northern margin of the paleovalley (filled star) indicates 17 km of dextral offset along the Bristol-Granite Mountains fault zone (BGMFZ). Boxed areas indicate identical locations of Figures 1-10A and B.

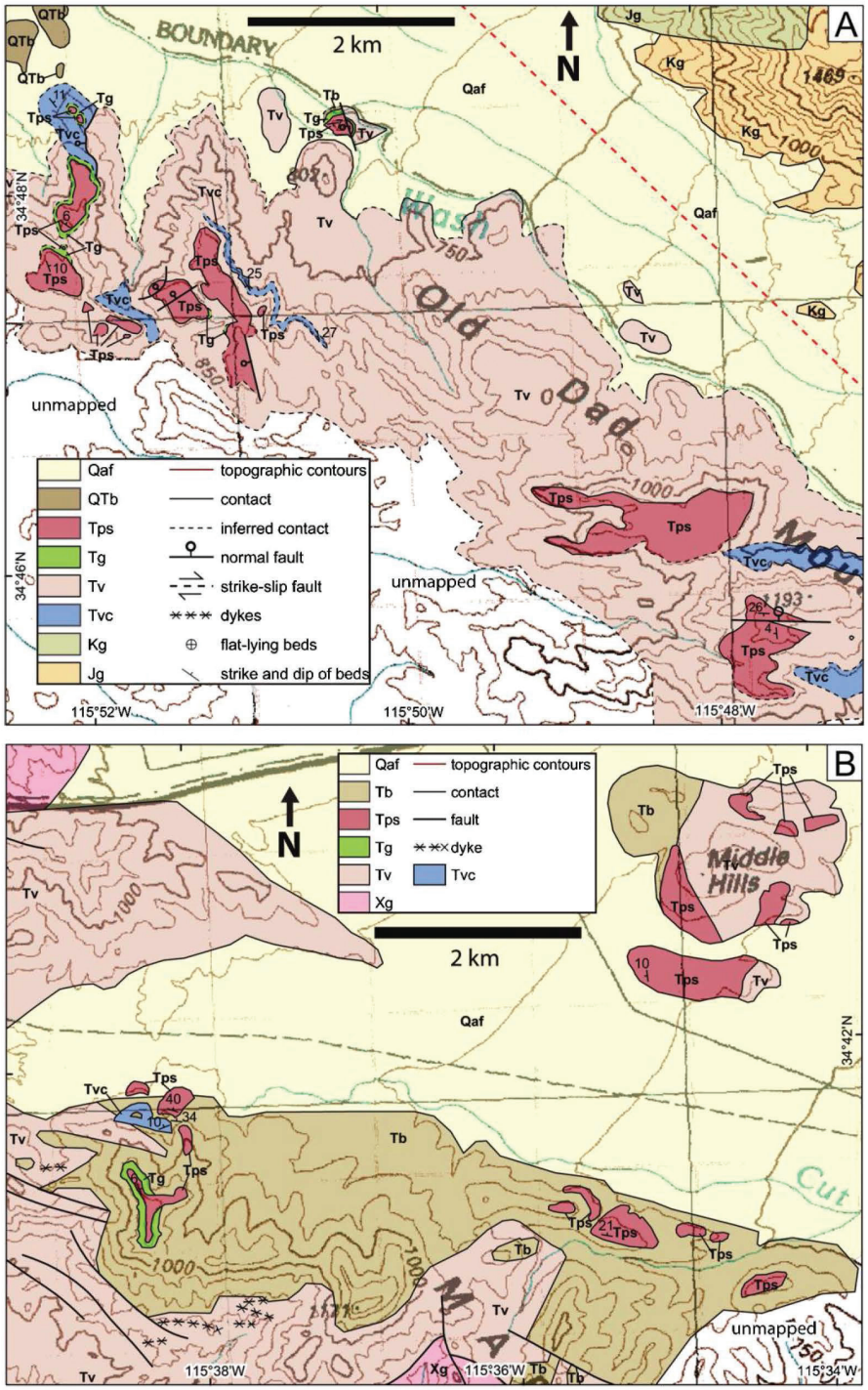

Figure 1-14. Geologic maps of parts of the Old Dad Mountains (A) and northern Marble Mountains (B) from Lease et al (2009). Map symbols: Qaf - Alluvial fan deposits and alluvium (Holocene and Pleistocene); QTb - Basalt (Quaternary and Tertiary); Tps - Peach Springs Tuff (middle Miocene); Tg - Lost Marble gravel (middle Miocene); Tv - Volcanic rocks (early Miocene); Tvc - Volcaniclastic rocks (early Miocene); Tb - Castle basalt (early Miocene); Kg - Granodiorite and porphyritic monzogranite (Cretaceous); Jg - Quartz diorite gneiss, diorite, and granitoid rocks (Jurassic); Xg - Granitoid rocks (Early Proterozoic).

the northern Marble and northern Old Dad Mountains, Lease et al. (2009) described the informally termed "Lost Marble" gravel that locally underlies the PST and is up to 20 m thick, but elsewhere it thins and does not occur beneath the PST. The PST, and locally the Lost Marble gravel, were deposited on various types of basalt to rhyolite lava flows or associated volcaniclastic (tuffaceous) sedimentary rocks (Fig. 1-14). One common feature of paleovalleys, especially when they are filled with hard and erosionally resistant rocks such as lava flows or densely welded and crystallized tuff, is that with time, the topography can become "inverted" where the valley filling deposits ultimately form resistant mesas (Fig. 1-15).

Paleoflow direction indicators (imbrication of clasts) in the Lost Marble gravel and anisotropy of magnetic susceptibility (AMS) in the PST were used to infer local flow directions. In both ellipsoidal sedimentary clasts and AMS fabric, for many rocks, the two longest axes form a plane that is inclined to the base of the deposit, and the shortest axis (which is perpendicular to the other two) is steeply inclined to the base of the deposit. So, the orientation of the short axis of clasts and the steeply inclined AMS axis typically point in the direction of flow.

Definition of the paleovalley was based on the restricted extent of the Lost Marble gravel, and the inferred axial-parallel flow directions in the Lost Marble gravel and the PST (Figure 1-13). The approximated edges of the paleovalley, where the Lost Marble gravel thinned and onlapped against the local volcanic highlands, were projected to the trace of the Bristol-Granite Mountain fault zone (Figure 1-13). An estimation of at least 24 km (15 mi) of right lateral separation of the northern edge of the paleovalley was presented in the original paper (Lease et al., 2009); however, after publication, a scaling error was identified and the revised separation is 17 km (10.6 mi). This value is comparable to the 12-15 km (7.5-9.3 mi) offset determined from geophysical criteria (Langenheim and Miller, this volume).

117.4 (0.7) Leave red gravels and enter light-colored gravels.

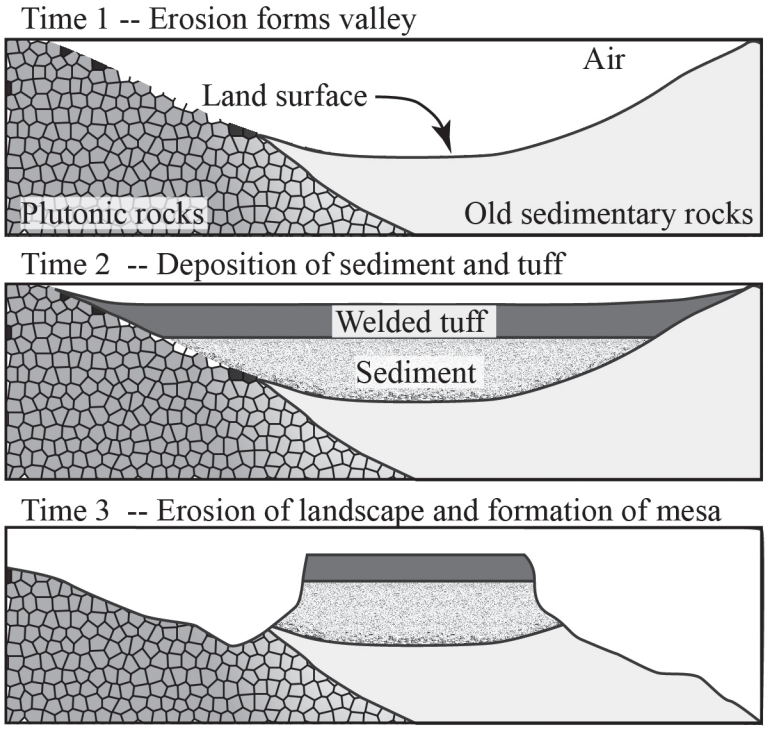

Figure 1-15. Sketch cross sections of paleovalley filling deposits and the formation of inverted topography. Time 1 – Erosion forms valley on different types of rocks. Time 2 – Deposition of sediment and welded tuff into eroded valley. Time 3 – Erosional of welded tuff and underlying sediment exposes and erodes the older rocks to form a new landscape with a mesa.

119.0 (1.6) **606528 3858160.** Pass the north tip of a linear ridge with faulted reddened gravels. This faulted hill was interpreted (Bedford et al., 2012) as caused by a splay of the Bristol-Granite Mountains fault. Proceed east.

119.3 (0.3) Pass a compressor station. Road crosses the second series of washes.

121.6 (2.3) Cross first wash.

121.9 (0.3) Cross second wash.

122.1 (0.2) Cross third wash.

122.3 (0.2) Road crosses fourth wash.

122.4 (0.1) Cross fifth wash.

122.5 (0.1) Pass through sixth wash and park on terrace ahead where vehicles will be visible to oncoming traffic. Walk back to sixth wash to examine stratigraphy.

STOP 1-8: Miocene-Pliocene sediment. Old sedimentary rocks are exposed here. Initial review suggests that coarse-grained, east-dipping (20°) reddish sandstone is the oldest unit. This is overlain by shallow-dipping (10°) coarse, sub-angular, mixed lithology gravels with a deep red matrix. Deposition of relatively unweathered granitic and gneissic breccias followed. The breccia is overlain by coarse conglomerate in a pale red matrix. In turn, this conglomerate is overlain by flat-lying tan arkosic sandstone with pedogenic carbonate.

Return to vehicles, proceed east.

123.7 (1.2) TURN RIGHT (southeast) onto tower stub road and park.

STOP 1-9: 614050 3860020. Granite Mountains tectonics, Late Cretaceous to recent. South of us the imposing Granite Mountains consist mainly of Mesozoic granitoids (Howard et al. 1987). The north margin, near the intersection of the deeply incised piedmont on which we stand and the steep rise of the mountains, is cut by the Bull Canyon fault. This fault consists of finely crushed rock and incipient ductile deformation, and cuts Cretaceous granite. L. Hess and M. Wells (UNLV) will describe their work on this structure and its role in Cretaceous unroofing of the area.

Figure 1-16. East-dipping, coarse Miocene? red sandstones exposed on the north sid eof the Granite Mountains.

The undated extremely coarse sedimentary breccias at our feet, in the deeply incised piedmont that flanks the north margin of the Granite Mountains, may mark Cenozoic unroofing of the Granite Mountains.

To the north, the Bristol-Granite Mountains fault was studied by Brady et al. (1992). Several fault traces cut Miocene sediment and Mesozoic bedrock. One fault trace cuts young Pleistocene deposits (Miller, 2012) that are correlated with deposits dated ~35-25ka.

Retrace to powerline road. Note increasing size of boulders. Continue east, shunting north to the Kelso Dunes park service road.

124.0 (0.3) **CAUTION:** Steep sandy ridge ahead. TURN RIGHT (southeast) to bypass deep sand.

124.1 (0.1) At the top of a boulder ridge, notice north-northwest-trending ridges of boulders to the south-southeast and for two miles to the east. This piedmont has received little study but promises to carry pieces to the puzzle of late Cenozoic tectonics of the Granite Mountains.

125.6 (1.5) Prepare to turn left. The easternmost of the boulder ridges lies ahead. Their eastern face appears to be truncated concordantly along ridge toes following a N60°W bearing. Parallel lineaments occur within the gravel package one-half mile west of the truncated toes. At the north tip of gravel ridges there is a heavily vegetated wash.

125.7 (0.1) TURN LEFT (north) on a narrow road toward Mojave National Preserve Kelso Dunes interpretive center and restrooms.

125.8 (0.1) TURN RIGHT (east-northeast) and proceed along a graded road.

126.9 (1.1) **STOP 1-10 Kelso Dunes**. PARK at visitor information area and discuss formation of Kelso Dunes and their geographic extent. The dunes lie at the east end of a sand stream that starts near Soda Lake, evidently carrying sand deposited after the breaching of Lake Manix. However, composition of the Kelso Dune field varies in different lobes, reflecting admixture of local materials (Lancaster and Tchakerian, 2003; Muhs et al., 2017). PROCEED EAST toward Kelbaker Road.

127.0 (0.1) Pass a dirt road running southeast toward the powerline road. The view ahead (east) shows the southern Providence Mountains (Jurassic granitoids; Miller et al., 1985) and the pink tucked low in the hills on the north side of Foshay Pass mark the location of the Vulcan Mine. North of the pass the crest is dominated by Paleozoic carbonate rocks and Jurassic rhyolite (Hazzard, 1954; Goldfarb et al., 1986; Stone et al., 2017).

128.9 (1.9) Stop at paved Kelbaker Road. Look for cross traffic. TURN LEFT (north) and proceed toward Kelso Depot.

131.8 (2.9) Road bears 10 degrees right (east).

132.7 (0.9) Caution: Road bears 30 degrees left (north). This intersection is with the road to the Vulcan Iron Mine. The mine is located on a contact zone between quartz monzonite and dolomite that contains a magnetite/hematite skarn. During World War II (1942–1949), the Kaiser Steel Corporation produced 2.6 million tons of ore (Wright et al., 1953; Reynolds and Weasma, 2005, p. 10). One and a half miles southeast along this road, is an unusual occurrence of the Bishop Ash (~765,000 years) sandwiched between fan gravels on the west side of the Providence Mountains (Reynolds et al., 2003, p. 20, STOP 3 -5).

135.7 (3.0) SLOW. Road bears right (northeast).

136.2 (0.5) Pass a dirt ramp on the left (west) where Vulcan iron ore was loaded onto rail cars.

136.5 (0.3) Carefully cross railroad tracks near the Kelso Depot, which has been renovated by the National Park Service and serves as an interpretive center. The station was named for a railroad official when it was established on the San Pedro, Los Angeles and Salt Lake Railroad (later, Union Pacific) in 1906 (Gudde, 1969). The small settlement around this important railroad station and yard provided water, gasoline, and food for travelers, who, if traveling by automobile, had reached the "end of the

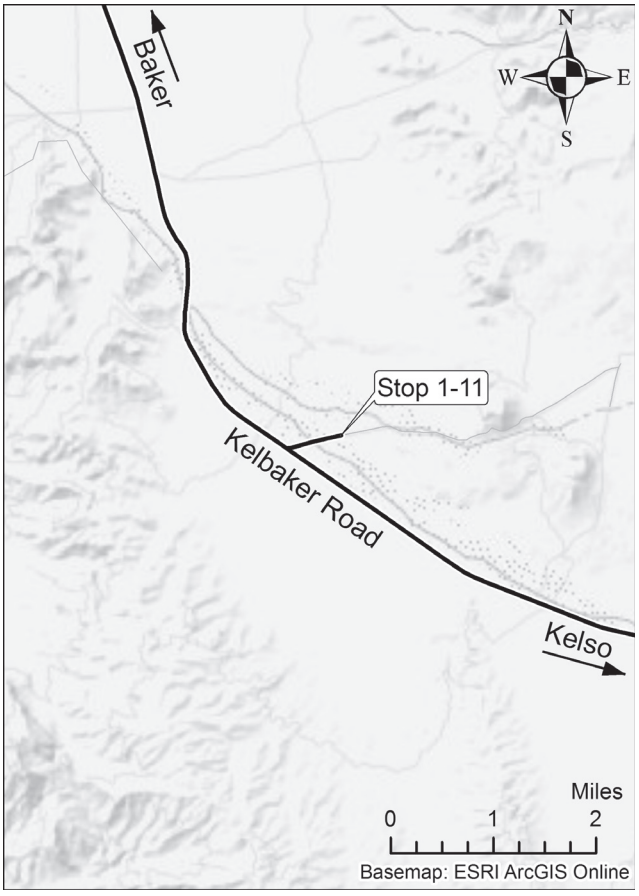

line" in 1917. No reasonably passable road went west along the LA&SLRR. The only exit from Kelso Valley was north, via Cima and Valley Wells, or east to Fenner and then south to National Trails Highway (Thompson, 1921, 1929).

BEAR LEFT (northwest) on Kelbaker Road toward Baker. Pass the right turn (northeast) to Cima.

137.5 (1.0) Kelso Mountains ahead (Vredenburgh, this volume).

139.9 (2.4) View northeast of Cima Dome and Teutonia Peak. (Vredenburgh, this volume; Wilkerson, this volume).

143.5 (3.6) The road bears left (northwest).

144.1 (0.6) The road bears left.

147.0 (2.9) The road bears left.

148.1 (1.1) Road bears right under a transmission corridor.

148.4 (0.3) View to north of Cima volcanic field and cinder cone mining activities to recover light-weight aggregate and road-base material. Differing dips of the basalt flows suggest erosion on this domed granitic pediment through the past several million years.

148.6 (0.2) Left bend in road.

151.0 (2 .4) Pass the left turn to a microwave facility.

151.4 (0.4) Pass left turn (south) to Old Dad Mountain, and canyons exposing Miocene extension-derived basin-filling sediments, landslide deposits, and gravity slide blocks (Barca, 1966; Reynolds, 2001, p. 6). Vredenburgh (this volume) describes the historic mines. Willow Wash Road is on the right. To the north, the Old Government Road from Cedar Canyon meets Willow Wash and continues west past Seventeen Mile Point and the Old Dad Mountain.

155.7 (4.3) TURN RIGHT onto Indian Springs Trail road.

155.9 (0.2) Drop into wash.

156.3 (0.4) **STOP 1-11: Pliocene (?) faults in the Cima Volcanic field.** PARK at the crossroad with vehicles facing Kelbaker Road. Turn to face the basalt flows on the north. The flow on the northeast, which is darkest in color, is about 10,000 years old on the basis of cosmogenic and varnish microlamination dating (Phillips, 2003; Liu, 2003). It is the youngest of the Cima field. Behind it to the north is a long basalt flow, dated at ~0.3 Ma by K-Ar (Dohrenwend et al., 1984). Scarcely visible above and beyond it is an older flow, about 0.5 Ma. That flow, in a position difficult to get to, overlies fault zones of gouge and breccia that formed in the underlying conglomerate (Skirvin and Wells, 1990). Although we concur with Wilshire (1992) that the faults do not cut lava flows (Miller, 2012), Skirvin and Wells interpreted the faults as locally cutting lava flows. Regardless of the exact age of faulting, the northwest strike, vertical dip, and sparse shear indicators show that at least one strike-slip fault is geometrically similar to those of the ECSZ. However, Dokka and Travis (1990) defined the ECSZ as the zone of faults that are active, and by that definition this fault does not belong to the ECSZ. As discussed by Miller (this volume), a broader zone around the ECSZ shows kinematic coordination with the ECSZ and conforms to the age of similar zones of faults southward toward the Gulf of California and northward in the Walker Lane. The faults in the Cima volcanic field provide excellent evidence that the faults of this broader, Miocene to modern, fault system included areas east of the restrictively defined ECSZ. RETRACE to Kelbaker Road.

156.9 (0.6) Stop at Kelbaker Road. Watch for cross traffic. TURN RIGHT (northwest) toward Baker.

158.1 (1.2) SLOW through curves. Note 0.58 Ma basalt to the right that in the past probably ponded against metamorphic rock in hills to left.

160.0 (1.9) Pass the Old Government Road that runs west past Seventeen Mile Point. Seventeen Mile Point was named because it was midway along the 35-mile stretch of the Old Government Road between Marl Spring on the east and Fort Soda (Zzyzx) on the west. The view west after Seventeen Mile Point includes Fort Soda on Soda Lake, and Afton Canyon and Cave Mountain farther west along the Mojave River. View northwest shows Tiefort Mountain (the sharp peak well above most others), and even farther north the prominent Avawatz Mountains.

161.7 (1.7) Slow as Kelbaker Road bears left (west).

172.3 (10.5) STOP at sign after crossing I-15 into Baker. Fill your gas tank and pick up drinks, snacks, and sunscreen for the 90-mile Day 2 trip. Return to DSC at Zzyzx for dinner.

End of Day 1

We have traversed much of the Soda–Avawatz and Bristol–Granite Mountains fault zones, which constitute the eastern boundary of the ECSZ. We have seen parts of the dextral system where faults are identified by their geophysical expression under basins, and places where linear mountain fronts, folds, and localized transpressional popups outline the fault system. West of this fault system, at least two sinistral east-striking faults appear to be interleaved in a zone of dextral faults, and one of these, the Broadwell Mesa fault, is associated with progressive folding during fault activity.

Total offset along the Soda-Avawatz and Bristol-Granite Mountains fault zones is about 15 km, (9.3 mi) but other faults we have seen west of this system have less well-defined offset (and locations in some cases). Faults

east of this system, such as those in the Cima volcanic area, appear to predate the Quaternary but could be kinematically related to the ECSZ faults, suggesting that earlier faulting in the continental deformation zone east of the San Andreas fault deformed a broader zone than the active ECSZ.

DAY 2

Fire Drill Carpooling will be necessary on Day 2. 4WD will be necessary in several places. Plan "jump in" carpool arrangements in advance with friends from Day 1. The Day 2 trip is planned to go west via Cave Mountain, Cronese Hills, and Alvord Mountain. The trip will end east of Barstow near Daggett. High Clearance vehicles or 4WD are recommended.

Today we begin by examining spring discharge deposits near Zzyzx, discussing the history of spring and lake expansions in the past thousand years as well as over the last glacial event. We will also discuss the geophysically determined shape of a pull-apart basin under Soda Lake and its implications for total offset on the Soda-Avawatz fault zone. From there, we travel west by way of several stops in the Afton Road area, north to the powerline road that borders Fort Irwin, and west along that road. The stops will all focus on the primary sinistral faults (Cave Mountain and Manix) of the area as well as minor faults and folds. We will also examine gravels that were deposited by several river systems during the Pliocene and discuss their paleogeographic implications. The trip will end at the historic Alf Blacksmith Shop at Daggett.

Convene at the Desert Studies Center with a full tank of gas, water, snacks, and protection from sun and wind. Pull in behind troop leaders at the T&T railroad berm. Leave the Desert Studies Center at Zzyzx and proceed north along the edge of Soda Lake.

0.9 (0.9) Road bears eastward around the lobe of alluvial fan gravel.

1.3 (0.4) Note the presence of springs along the playa margin.

1.4 (0.1) SLOW through curves.

1.6 (0.2) Cross young, light-colored alluvial fan deposits incised into older, darker varnished fans with desert pavements.

1.8 (0.2) SLOW through curves.

2.3 (0.5) PARK in paved pullout on right side of road, leaving room for traffic to pass. Walk toward edge of playa.

STOP 2-1: 581052 3892590. Spring history along Soda Lake (Jeff Honke). Can we use modern wetlands in the Mojave Desert to clarify Holocene hydrologic variations? The USGS has collected a series of cores surrounding the existing springs near the Desert Research Station here at Zzyzx. To support the sedimentological interpretations of these cores, a series of shallow soil pits were dug around these springs. Both the cores and the soil pits illustrate the potential for recording wet (wetter? cooler?) events in this arid system. In the pits we find black mats of organic material. The aerial extent of wetland vegetation appears to have expanded (up to 100 m beyond current) multiple times during the Holocene, signifying times that were wetter than today. Two distinct units in the uppermost 50 cm of sediment here suggest wetland expansion occurred during the Little Ice Age and the Medieval Warm Period (~1750 AD and ~1250 AD). We will examine these layers and discuss the system morphology, the timing, and the potential paleoclimatic implications. Radiocarbon ages

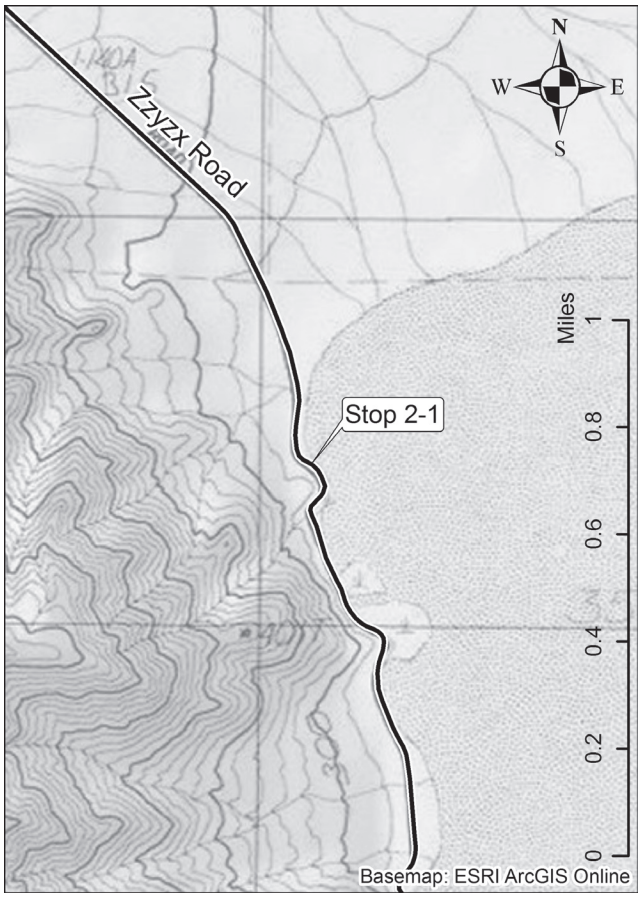

Table 1. Pit depths and ages

Pit-depth	Lab #	Yr BP	±	Calibrated Yr BP	Calibrated Calendar Yr
SL09-9-10	WW10450	300	40	385	1565 AD
SL10-10-12	WW10448	190	110	202	1748 AD
SL14-20-21	A2264	770	25	695	1255 AD
SL24-22-23	A2237	735	35	680	1270 AD
SL34-27-28	WW10449	800	70	733	1217 AD
Calib 7.1.1-Intcal13.14c					

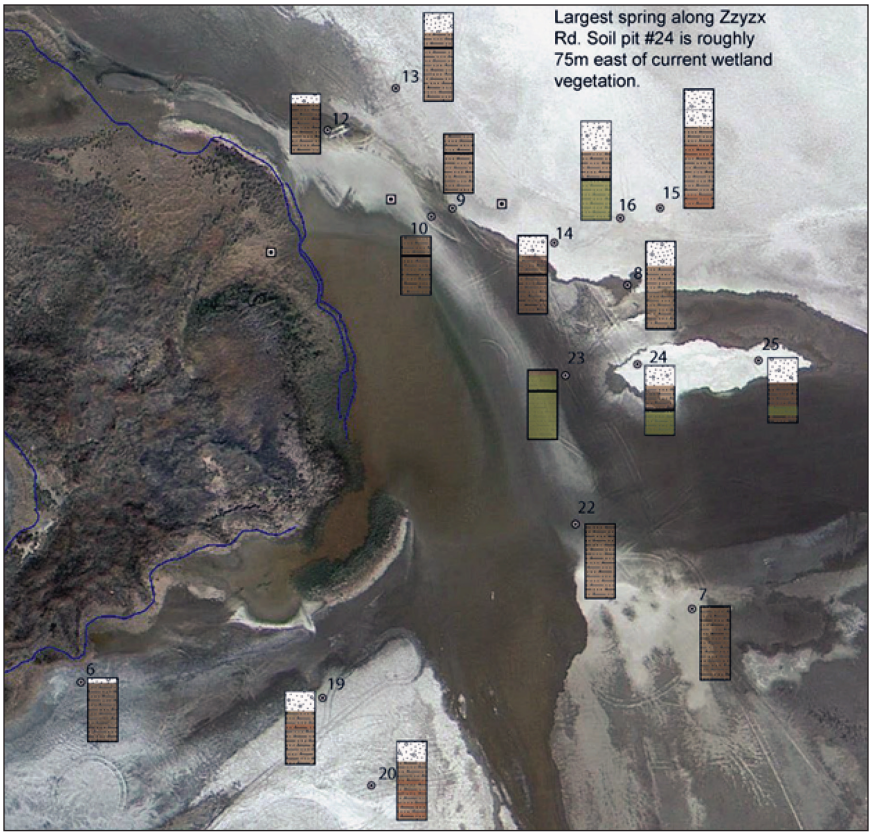

Figure 2-1. Map of a spring complex along the west side of Soda Lake, showing shallow pit samples (circles) with stratigraphic logs. Black bands represent black mats. Blue line encloses modern spring vegetation.

Figure 2-2. Photograph of sample site 9 (Fig. 2-1), view to the south.

obtained follow, and Figures 2-1 and 2-2 illustrate the sites we have studied in this spring complex.

From here we can see the Soda Mountains to the north, where the Soda-Avawatz Fault Zone cuts through in two to four splays mapped first by Grose (1959) and more recently by Cyr (2016). Locally, it is possible that the springs mark a splay of the fault zone where it steps right across Soda Lake in an extensional stepover that created a basin about 12 km (7.5 miles) long and 5 km (3 miles) wide (Langenheim and Miller, 2017).

Lineaments consisting of dunes, springs, and mesquite copses occur on the east side of Soda Lake, probably representing another splay of the fault system (Langenheim and Miller, 2017; Brady, 2017). Brady (1992) mapped several splays of the fault system farther south in the northern tip of the Bristol Mountains, where the faults cut deposits as young as ~30 ka (Bedford et al., 2010; Miller, 2012).

Lake Mojave beach deposits are perched in cemented cliffs in places along the fans west of Zzyzx Road. Tufa cements the jumble of rocks together, indicating that the cemented deposits formed at or just below water level. These beach deposits are about the same elevation as highstand beaches elsewhere around Lake Mojave (Wells et al., 2003), and formed between about 24 and 12 ka. All alluvial fan deposits near the road postdate the lake, which fell to low levels by 10 ka, and the rapid development of varnish on these fans allows them to be subdivided into several Holocene pulses of fan aggradation (Harvey and Wells, 2003; Miller, unpublished mapping).

Return to vehicles. Proceed north to I-15.

4.2 (1.9) Road bears left (west).

4.6 (0.4) Road bears right (north).

4.7 (0.1) Cross over I-15. Turn left (west) and enter I-15 southbound toward Barstow. The light-against-dark color relationship in the ridge on the east side of the piedmont is a contact between the Mio-Pliocene Avawatz gravels (term by Grose, 1959) and the metavolcanic rocks that core the eastern limb of the Soda Mountains. Despite being called the Avawatz gravels, Gourley (2000) used provenance and paleocurrent data to determine that the gravels are

sourced locally from Soda Mountains metavolcanic, metasedimentary, and igneous rocks. At the northern end of this ridge, the gravels are in fault contact with bedrock; this is the western strand of the Soda-Avawatz Fault Zone. About midway down the piedmont, north to south, the fault curves from being oriented ~130° to ~160° and defines the contact between middle and lower members of the Avawatz gravels, which here are in depositional contact with Soda Mountains bedrock. The fault projects under the Holocene alluvium deposited on the piedmont and right beneath the hill we just passed on the north side of I-15 (Fig. 2-3).

Figure 2-3. Road cut with granitic gravels and fault.

10.5 (1.8) Pass Rasor Road exit. Clarence McAuliffe Rasor was Chief Engineer for T&T and later chief of operations for "Borax" Smith's enterprises (Schoffstall, 2010)

11.0 (0.5) View of Cave Mountain, named for the caves in Cave Canyon (later renamed Afton Canyon) near the south base that were cut into Miocene and Pliocene conglomerate by piping and overflow of Lake Manix (Meek, 1989).

12.0 (1.0) View 2 o'clock of Cat Mountain with a cat-shaped dune. Downwind (east) of the Pleistocene Mojave River fluvial plain and Coyote Lake, eolian sand is found covering flat surfaces and covering hill slopes. "Climbing" dunes form on windward slopes when sand is forced up a ridge; "falling" dunes form on the leeward side of ridges, when wind carries sand over the ridge top.

13.5 (1.5) View north of Soda Mountains fault, which cuts diagonally up the west face of the Soda Mountains, crossing over to the north near Red Pass Lake.

15.4 (1.9) Pass Basin Road exit.

17.7 (2.3) Continue past the north side of Cave Mountain, where spectacularly steep fans lie below cliffs of granite and several potential faults and landslides are visible (Jordan, 2017). Large boulders on the fan were in part deposited by debris flows but may also represent landslide runouts. The Cave Mountain fault lies along the north face of the mountain, which is an enormous popup (compressed between two faults and popping up like a greased seed) in the fault system. We will have another view of the south side of this mountain front at STOP 2-2. Oblique air photos taken by Gary Rasmussen reveal linear features in the fans that may be fault splays, but they are difficult to study on the ground because of the coarseness of the fan deposits. The lineaments trend a little north of west, a geometry that would represent transpression, or constraining bends if they are faults related to the Cave Mountain fault.

19.8 (2.4) At the crest of the hill we can see a sand-sheet-draped valley to the south with two prominent dunes near the skyline. Each of these dunes lies on or near the Cave Mountain fault, but the north facing escarpments we see are probably the sides of the dunes, not fault scarps. These longitudinal dunes connect Cave Mountain on the east with low hills farther west. These low western hills are where we will stop next.

23.2 (3.5) The road cut on the left (south) exhibits stratified Miocene(?) gravel and sand cut by several small faults. This unit is named informally the Cave Mountain gravel and we will have another chance to examine it at Stop 2-3. The gray sand makes up much of the deposit in this exposure, with gravel layers standing out in relief because of their coarse grain size and also strong calcite cementation.

23.6 (0.6) Exit at Afton Road.

23.9 (0.3) Stop. TURN LEFT (south), drive over I-15, and continue on the graded dirt of Afton Road.

24.1 (0.2) We are driving on the crest of the Afton Beach Bar, a flat-pebble ridge developed by wave action on the east side of Lake Manix, a position of maximum wave energy from westerly winds. A lagoon once lay east of the beach. (Meek, 1999; Reheis et al., 2012).

24.5 (0.4 At the end of the beach bar, the deposit is faulted against a hill of coarse Cave Mountain gravel (Meek, 1999). This beach was formed ~24.5 ka (Reheis et al., 2013), so the last rupture on this fault (the main strand of the Cave Mountain fault) was latest Pleistocene or Holocene. The fault can be traced west through Lake Manix muds and onward, to the south side of an unnamed small

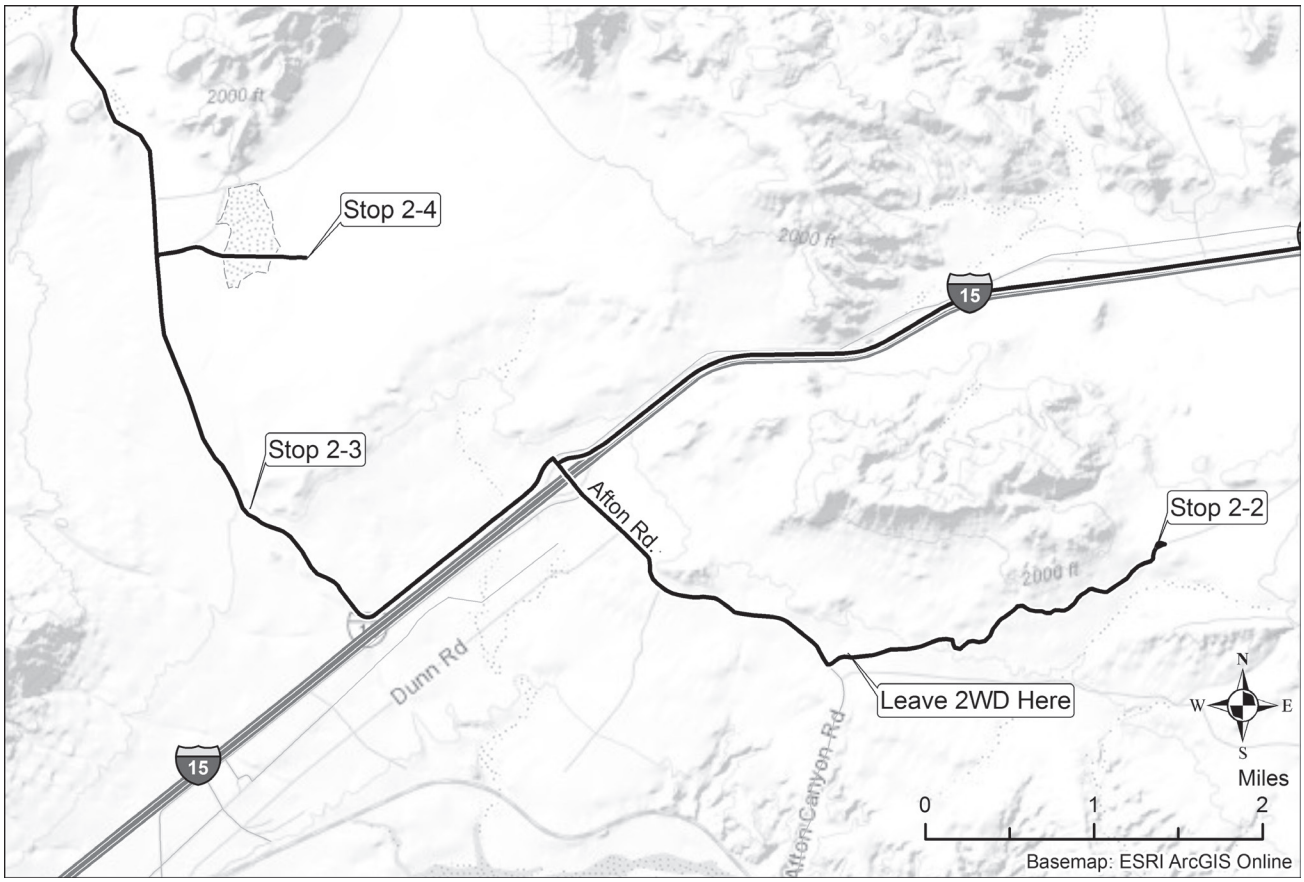

mountain (local name is Dunn Hill) about three miles west of here, on the north side of I-15.

24.7 (0.2) The graded road bears left (east) as it passes a right turn for County Road 20882.

25.1 (0.4) Afton Road bears left (east).

25.5 (0.4) A road runs west north of the power line.

25.6 (0.1) TURN LEFT (east) onto the powerline road, BLM route AC 9624.

25.7 (0.1) PARK low clearance and 2WD vehicles at base of first power tower. Carpooling is VERY necessary through dune sand and rocks for the next several miles.

26.3 (0.6) Switchbacks.

26.7 (0.4) Junction, turn right (southeast) to follow the powerline road.

26.9 (0.2) Stay right at the fork.

27.2 (0.3) The road jogs right.

27.4 (0.2) Stay straight on the right fork up the sandy hill. 4WD recommended.

27.5 (0.1) SLOW at the crest of the hill. Stay in existing tracks as you proceed downward.

27.6 (0.1) TURN SHARP LEFT (west) at the base of the slope, onto main powerline road. Continue west.

27.7 (0.1) Bear right onto a tower service road.

STOP 2-2: Cave Mountain Fault. (**558176 3880533**). At this road cut, examine the gray sandstone interbedded with conglomerate. This is a characteristic exposure of the Cave Mountain gravel, including the calcite-decorated rhizoliths, and a calcareous hardground near the base of the exposure. The gray color may indicate long-term reducing conditions, and is persistent for broad areas of exposure from here to the west and north. However, to the south, toward the Mojave River, the unit changes to alternating red and gray, and eventually to red colors, apparently as a result of the influence of oxidizing environments, as it becomes more gravelly. The Cave Mountain gravel has no reliable age control. It contains sparse pebbles of volcanic rocks, suggesting that it is younger than the regional early Miocene volcanism. It is very similar in terms of color, depositional characteristics, and cementation to the upper part of the "Barstow" Formation of Byers (1960) in Alvord Mountain. However, the Barstow unit has different granitic clasts. If the same in age, it would be middle to upper Miocene (Miller et al., 2011). It is overlain by middle Quaternary alluvial fan deposits and Lake Manix beds (550-25 ka) in various places.

The Cave Mountain granite, present as clasts in the gravel here and forming the mountains east and

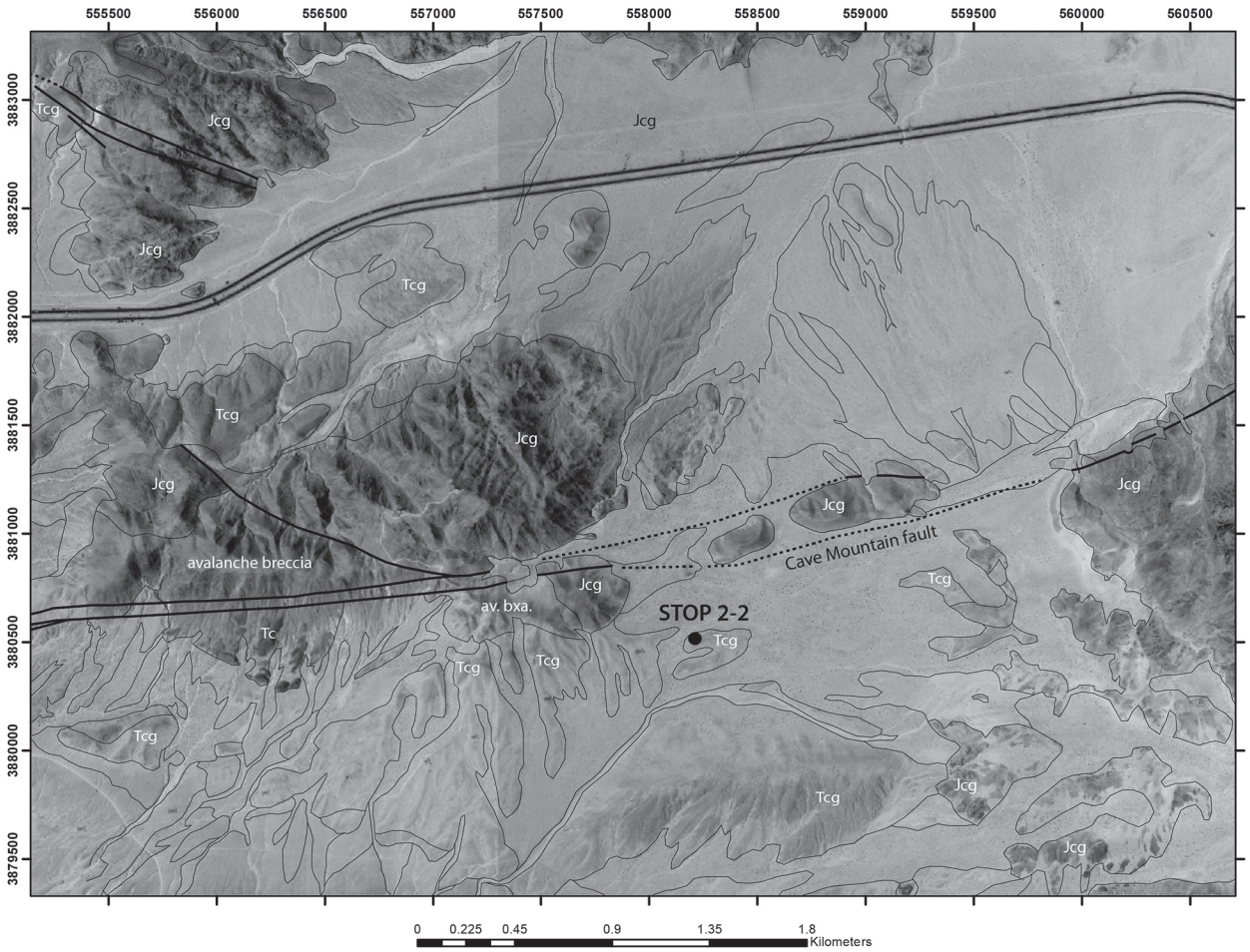

Figure 2-4. Preliminary geologic map of the area west of Cave Mountain. The east-striking Cave Mountain fault shows a few splays in some outcrops. Bedrock of the Cave Mountain granite is overlain westward by thick avalanche breccia deposits of the same rock and other parts of the intrusive suite. These rocks are overlain by the Cave Mountain gravel north of the fault, and by three sedimentary units south of the fault. None of the sedimentary rocks have been dated.

northwest of us, is a distinctive potassium-feldspar-rich, leucocratic (generally less than 5% biotite) granite. It is weakly to strongly foliated, and carries sparse phenocrysts of potassium feldspar. It grades into a porphyritic, more biotite-rich rock that seems to be closely related to dioritic rocks seen in the eastern part of Cave Mountain. All rocks range from weakly foliated to mylonitic, and may have been deformed as part of the East Sierra Thrust system as outlined by Walker et al. (1990) for the Cronese Hills nearby to the west. More on this topic will be presented in the next stops.

Walk to the top of a small hill to the south for a view of features associated with the Cave Mountain fault (Fig. 2-4). These include: (1) the northern steep front of Cave Mountain visible to the east, (2) a long brown shutter ridge(?) of granite to the northeast and below us, (3) eolian sand paths between us and the shutter ridge that farther east become longitudinal dunes directly on the fault, (4) the steep southern, faulted front of granite to the northwest that marks the main trace of the Cave Mountain fault, and (5) linear ridges of the Cave Mountain gravel, such as the one we stand on, that may be controlled both by faults and by resistant bedding in the gently south-dipping unit.

Return to vehicles and retrace west.

28.9 (1.2) TURN LEFT (west) at a spur road.

29.5 (0.6) AFTON ROAD. Collect vehicles from carpooling effort. Drive north along the Lake Manix 25 ka shoreline.

31.2 (1.7) Cross I-15, and TURN LEFT (west) along the paved frontage road on the north side of freeway.

32.5 (1.3) Where the frontage road turns sharply right and pavement ends, it becomes Dunn Road, BLM 8337. Continue north on Dunn Road.

33.0 (0.5) Climb over a gentle rise underlain by the Cave Mountain gravel that has been modified by beach development associated with the highstand (543 m elevation) of Lake Manix.

33.2 (0.2) **STOP 2-3** (**551090 3880795**) **Splay of the Cave Mountain fault.** Descend into the dry wash and park north off the road. Walk upstream to the Cave

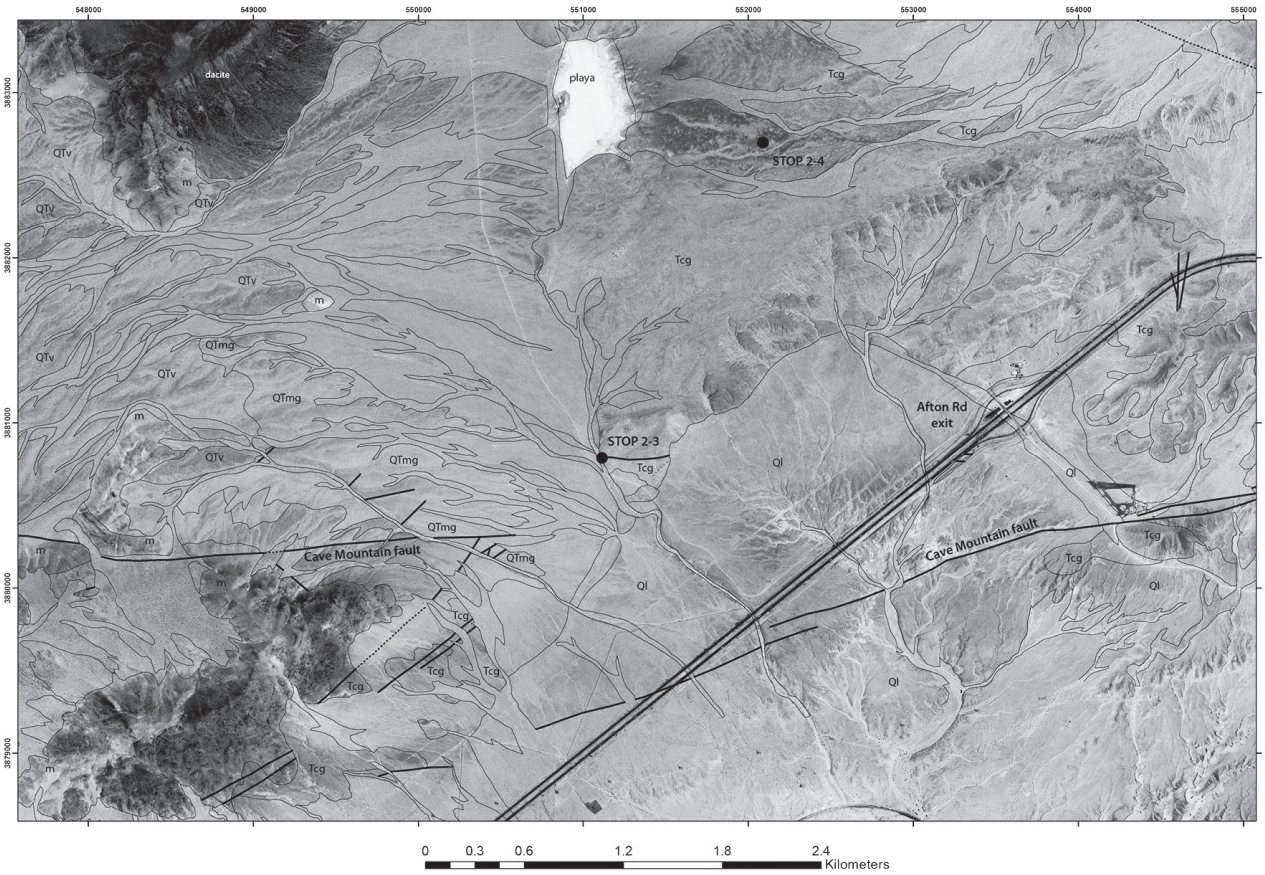

Figure 2-5. Preliminary geologic map of the southern Cronese Hills. The Cave Mountain gravel is widespread east of the line of playas and north of the Cave Mountain fault. South of the fault, it extends from Cave Mountain westward the length of the map. North of the fault and west of playas, volcanic gravel (QTv) derived from the west is locally overlain by coarse alluvial fan gravel that was shed from local hills of metamorphic rocks (QTmg). Fault splays (heavy black lines) bifurcate westward around the informally named, steep-faced Dunn Hill. Blue lines denote shorelines of Lake Manix.

Mountain gravel, which is exposed along the east side. Characteristic deposits in this area consist of gray massive to well-bedded, moderately sorted sand that is arkosic in composition, alternating with conglomerate made up of clasts from the Cave Mountain granite. Both rock types are carbonate cemented to a degree, the conglomerate generally more strongly cemented. A moderate hike up the wash and then east along the north side of this hill provides much better exposures of the gravel unit, especially its interesting sand intervals. The sand intervals are enigmatic, with sedimentary structures indicating fluvial origins but a generally moderately sorted character that commonly is associated with lacustrine deposits. Rhizoliths and hardgrounds, and less common carbonate coats around pebbles, indicate GWD. Interbedded conglomerate is fluvial in origin. This deposit may represent erosion of deeply weathered granitic rock, and deposition in low-energy fluvial plains with shallow groundwater that were episodically covered by sheets of gravel during high-energy stream flow.

At this location, an approximately east-striking high-angle fault cuts the gravel. This is probably a splay of the Cave Mountain fault. Farther west, multiple fault splays are exposed in the same gravel unit, and appear to bifurcate around the un-named pop-up mountain (referred to as Dunn Hill on some maps) to the west of here. Refer to the geologic map for fault locations.

Return to vehicles at Dunn Road, continue north (BLM road 8337).

34.6 (1.4) TURN RIGHT (east) on BLM 8309, toward mine excavation at the edge of the playa. Rocks in alluvial fan deposits here are mainly derived from Jurassic? metavolcanic rocks (Walker et al., 1990) in the Cronese Hills. Mines in this general area exploit iron deposits and decorative rock (Wilkerson, 2015).

34.7 (0.1) BEAR RIGHT (southeast) at junction; then BEAR RIGHT (at second junction).

34.9 (0.2) Cross this unnamed playa.

35.1 (0.2) At the east edge of the playa, proceed east on alluvium.

35.3 (0.2) **STOP 2-4: 551530 3882750 Folded sediment and Cronese fold valley.** Drive and turn carefully on the desert pavement to avoid disturbing the surface. Very subtle hills to the north, south, and east are underlain by the Cave Mountain gravel. This broad, planar surface that slopes gently toward the playa is overlain by Pleistocene deposits and is nearly parallel to bedding in underlying

Figure 2-6. Shallow-dipping Pliocene sediments along the Alvord powerline road.

gravels of possible Miocene age. We suggest that this is a pediment formed on the Miocene (?) gravels; it must have formed during Pliocene to early Quaternary time, and possibly has been tilted down to the west. To the northwest across the playa is a pediment cut into Pliocene gravels that dips gently toward us (east) and again, the dip in late Cenozoic gravel is similar to the slope on the overlying pediment (Fig. 2-6). In general, gravels in the pediments on either side of the playa differ, with unlike provenance, composition, and paleocurrent directions.

The Cave Mountain gravel that forms the subtle hills around us is exposed farther west across the playa in a few places, but always south of the Cave Mountain fault (Fig. 2-7). North of the fault and west of the playa are an older (Pliocene) volcanic gravel and that is overlain by gravel with metamorphic rock clasts. We will see both of these units in STOP 2-5. The volcanic gravel carries clasts of several kinds of volcanic rocks, silicified limestone, and granite and granodiorite similar to rocks in Alvord Mountain. The well-rounded volcanic and silicic rocks are similar to Miocene rocks derived from the Calico Mountains area to the west, and have been traced eastward to the hills south of Alvord Mountain (Miller et al., 2011). These gravels, Pliocene in age, evidently represent east-directed streams in valleys that parallel, and perhaps lie astride, the sinistral Cave Mountain fault. Similar to the evidence for folding along the Broadwell Mesa sinistral fault, the gravels derived from the Calico Mountains suggest that paleogeography was driven by ECSZ faulting and folding. The east-trending paleovalleys may represent a component of north-south shortening associated with the ECSZ. Retrace route across the playa to Dunn road.

36.0 (0.7) Stop at Dunn Road. Look for cross traffic. TURN RIGHT (north) and continue along two more playas in this valley in the Cronese Hills.

36.3 (0.3) Pass a road east to the green rock mine at the north end of a playa.

36.5 (0.2) Road bears left (northwest). Watch for deep windblown sand.

36.7 (0.2) Pass a middle playa.

37.1 (0.4) Road bends right (north-northeast) toward Crucifixion Playa, which was full of water January 2017. This northern playa has creosote bush and crucifixion thorn (Lum et al., 2001) growing on it, highly unusual for clayey and salty playa deposits. All three playas support creosote bushes along their margins, which is characteristic of very young playas that have not added thick clay deposits inhibiting this deep-rooting plant. The playas may be very recent features caused by folding to create a

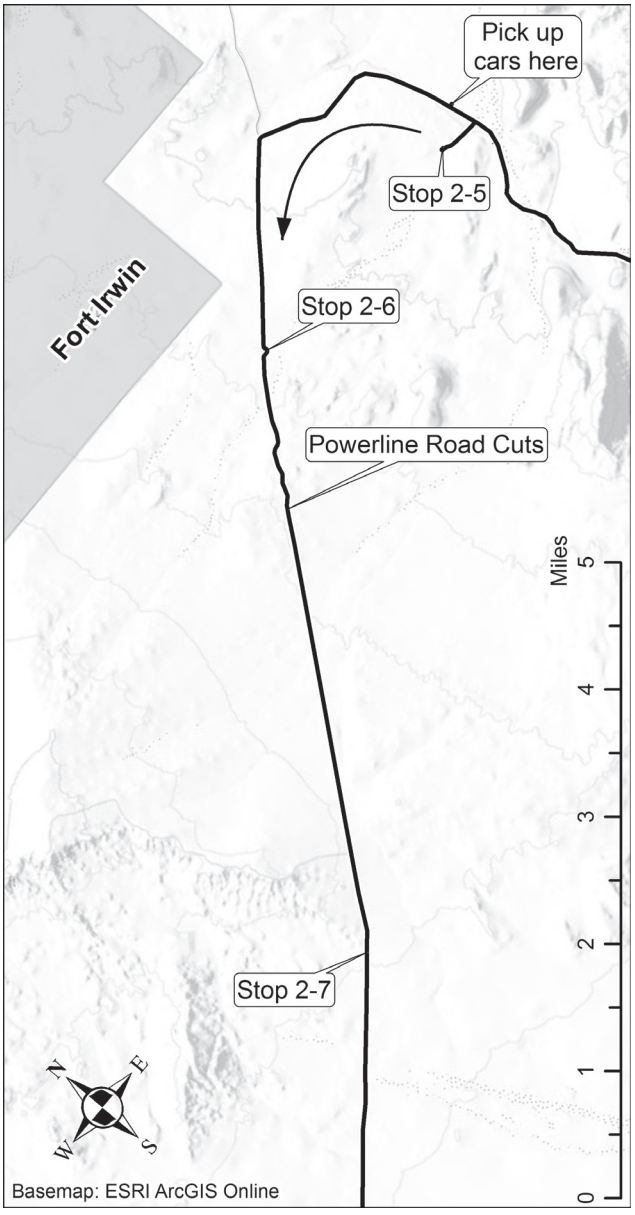

syncline, followed by fans building into the syncline and partitioning it into several small basins.

37.4 (0.3) Pass a right turn at BLM 8329, toward Crucifixion Playa.

37.5 (0.1) Drop into a wash and bear northeast along an east-draining broad alluvial fan system.

38.0 (0.5) On the left (**550010 3885735**) is a small part of a dacite dome of unknown age, probably Miocene. It may be part of a larger dome to the east that lies on metamorphic rocks (Walker et al., 1990).

38.3 (0.3) **550030 3886025** Note major wash on left. We shall return here to take BLM route 8344. Drive ahead and turn right to arrange carpooling.

38.5 (0.2) TURN RIGHT (east) from Dunn Road and park near a linear pile of rocks arranged to look like grave. The inscription reads: Bonnie Keebler Harris grave. The note in the bottle said "December 27, 1872, to whom it may concern: died this day of sickness; too far to travel so will put her here. Bonnie Keebler Harris, born December 1823 in New York, mother of five children. God rest her soul. The bottle and note were replaced with a metal sign, (Mojave River Valley Museum 12-1997). Proceed south on Dunn road to the major wash.

38.8 (0.3) TURN RIGHT (west), up wash on BLM 8344 to Stop 2-5.

STOP 2-5: (**549610 3886120**). **Pliocene sediment derived from sources to the west.** A ridge on the northeast side of the wash is underlain by contrasting facies of Pliocene gravels that dip gently east. The upper sequence contains numerous angular boulders of metamorphic rocks derived from the nearby Cronese Hills. Poor sorting, poorly defined bedding, and very coarse grain size mark this upper unit as alluvial fan deposits. This unit blankets the underlying gravel unit from here southwest to the Cronese Hills but is not observed more than ~1 km to the north. In many places, the transition from lower gravels to this gravel composed of metamorphic rocks contains lenses of carbonate-cemented sand that we interpret as ground water discharge (GWD) deposits. This relation indicates a position for the transition between the gravels was near the valley axis.

The lower gravel is thin-bedded, moderately to poorly sorted, with sparse indicators of stream flow eastward. The unit here is of mixed provenance, containing beds that primarily have volcanic rock clasts and others that mainly contain granitic rock clasts. Northwestward from here, these two provenances are clearly separated as two distinct units that have sources in the Goldstone area (granitic Goldstone gravel) and the Calico Mountains area (volcanic gravel) (Miller et al., 2011). In this location, a thin bed of white ash has yielded a tephrochronological match with the Mesquite tuff (E. Wan, written comm., 2016), about 3.5 Ma, showing that these deposits are Pliocene in age. Note that here, the gentle southeast dip of the gravels is slightly steeper than the stream gradient to the southeast. This stream leads to West Cronese Lake, a playa nearly 330 m lower in elevation. We will show at the next stop that playas were present nearby, to which the two gravel units led and merged. Evidently, after mid-Pliocene time the depocenter was shifted southeast to West Cronese Lake as the trough to our east developed. Near the north end of the trough, ~north-striking faults are mapped (Miller et al., 2014) that may represent structures covered by young materials in the part of the trough we see to our east.

The Pliocene age for mixed volcanic and Goldstone gravels here is important because a broad expanse of gravel and semi-consolidated sandstone from here north into southern Fort Irwin and west to Alvord Mountain has extremely sparse age control. The gravels are much younger than an area in Fort Irwin that contains middle Miocene strata that are overlain by a 12.6 Ma tuff (Swisher, 1992). For both sequences there is great need for more fossil and geochronological data. Return to Dunn Road.

39.1 (0.3) Dunn Road. Stop, look for cross traffic and TURN LEFT (north) on Dunn Road.

39.3 (0.2) Retrieve vehicles parked at Bonnie Keebler Harris grave. Stop, look for cross traffic, and proceed north onDunn Road.

39.9 (0.6) Dunn Road bears west. SLOW as road drops into wash.

40.6 (0.7) Intersection with Alvord Powerline Road BLM 8313. To the northeast of this junction, nearly flat-lying paleosols distinguish Pliocene (?) sediment sections from moderately east-dipping Miocene (?) beds, some of which are rock-avalanche breccias.

Fossiliferous Miocene sediments north of this area, within Fort Irwin, date to 12.6 Ma (Swisher, 1992), and therefore contain the youngest Barstovian LMA fossil locality. If the tephrochronology correlation of CPT V tuff (12.15 ± 0.54) for the Clarendonian fossils low in the Dove Spring Formation (western Mojave Desert) is correct, there is not much time between youngest Barstovian fauna and oldest Clarendonian fauna. A lot happened faunally in that 0.4-million-year transition between the youngest Barstovian and the oldest Clarendonian fauna.

The Barstovian and Clarendonian land mammal ages have significantly different mammal faunas. A simple comparison of large mammal faunal lists from Barstow (Pagnac and Reynolds, 2006, Fig. 11) and the Clarendonian taxa of the Iron Canyon and Ricardo faunas (Whistler et al., Fig 4) and the Avawatz Formation (Reynolds and Whistler, 1991, Table I) shows that of 32 Barstovian genera, 26 (87%) do not occur in Clarendonian faunas, and only 4 (12%) apparently persisted over the transition. Clarendonian faunas in southern California may reflect immigration from outside the region that

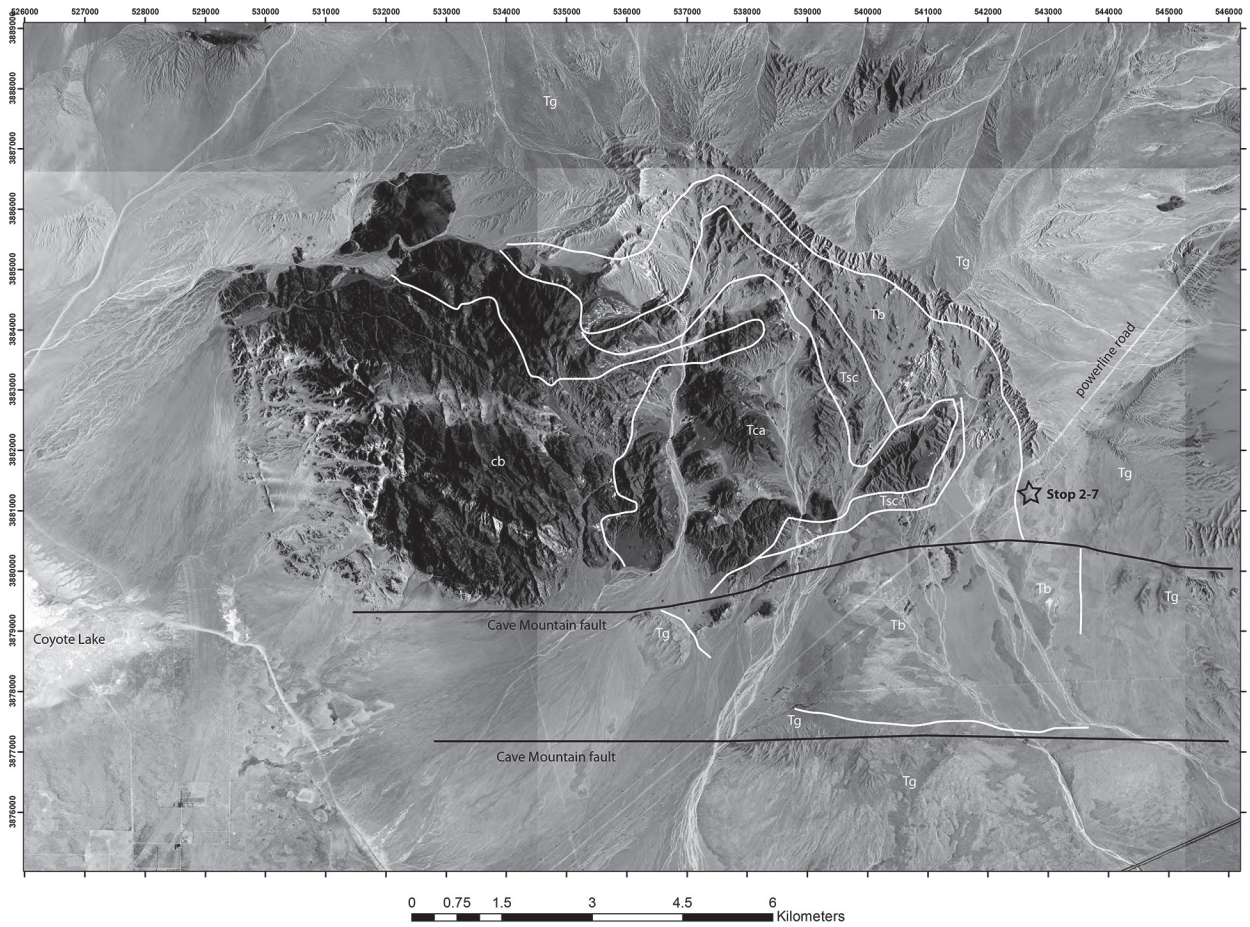

Figure 2-7. Sketch of the overlap gravels associated with Alvord Mountain. Underlying units are broken into Miocene sedimentary rocks (Tb, Barstow Fm.; Tsc, Spanish Canyon Fm.; Tca, Clews Conglomerate and Alvord Mtn. Basalt) and crystalline basement (cb). After Byers (1960) and unpublished mapping by Miller. Black lines are two main strands of the Cave Mountain fault.

followed a marked extinction event of resident Barstovian taxa.

Locally, the Miocene Barstovian age sediments are in strata dipping moderately (15 to 30 degrees). The overlying Pliocene beds at **STOP 2-6** (ahead) are dipping shallowly southeastward. We will not see the unconformity between the two different sediment sequences along this route.

TURN LEFT on powerline road.

42.0 (1.4) **STOP 2-6: (546795 3886150) Miocene and Pliocene sediments at the south edge of Fort Irwin.** PULL LEFT (south) into a round-about power tower service road. The gray, silty playa sediments to the south have not yielded age diagnostic specimens. The playa lies laterally between two sediment sequences, one the Goldstone Gravel, and the other the volcanic gravel. This relation indicates that two distinct stream sources led to the playa. These deposits probably are Pliocene in age, because they lie stratigraphically below the 3.5 Ma deposits of STOP 2-5. Elsewhere, the Goldstone Gravel contains a 3.4 Ma ash (Miller and Yount, 2003). The unconformity between the 12.6 Ma Miocene sediments and the 6-3 (?) Ma gravels and playa sediments is not well exposed near here. Candidates for this unconformity are exposed south of Alvord Mountain (STOPS 1-10 and 1-11, Reynolds and Miller, 2015) and in those localities are notable for a lack of pronounced angularity. Proceed southwest on the powerline road.

43.0 (1.0) Powerline road cuts (**545715 3884925**) consist of Pliocene gravels interfingering with playa sediments; provenance of gravel packages is similar to what we saw at STOP 2-6.

44.2 (1.2) Pass bluffs to the south of gravels bearing volcanic rock clasts. These gravels are not dated here, but appear to underlie, and share lithologic characteristics with, gravels at STOP 2-5 which contain a Pliocene ash.

45.1 (0.9) Cross the divide from the east-flowing drainage basin (to West Cronese Lake) into the west-flowing drainage basin (into Manix Basin). Early on Day 1, we were along the route of the nineteenth century Salt Lake / Old Spanish Trail. After leaving Red Pass and Bitter Spring, the trail passed through this area and continued west-southwest, reaching Camp Cady, then Daggett, and Fish Ponds at Barstow before continuing westerly toward Cajon Pass.

45.9 (0.8) **STOP 2-7: 542743 3881345 Goldstone gravel and overview of Miocene strata of Alvord Mountain (Fig. 2-7).** The arkosic Goldstone Gravel with clasts as large as boulders that were sourced from the Goldstone region of Fort Irwin lies at our feet. The unit is thicker than 100 m here, has east directed paleocurrents and clasts from distant sources that together indicate another east-trending paleovalley that lay astride, in this case, the Coyote Lake fault. The Goldstone gravel can be traced eastward to the playas at and near STOP 2-6 but has not been seen farther east. Nor has it been traced to the Barstovian beds that lie northeast of here. The Goldstone gravel here lies on a thin sandstone unit that in turn overlies the Barstow Formation of Byers (1960). The unconformity at the base of the Goldstone is marked by soils with silica cements (Miller et al., 2011). The unit below the Goldstone Gravel is a granitic-clast conglomerate and sand unit that Byers considered to be separate from the Alvord "Barstow" Formation. It is very similar to the Cave Mountain gravel, although in this area many coarse-grained clasts are locally derived from the Alvord Mountain area. This unit, in turn, grades downward into more tuffaceous sandstone that differs from the overlying granitic-clast conglomerate and sand unit by its interbedded tuffs and pumiceous sandstone. Byers considered the tuffaceous unit to be the upper Barstow Formation. Granite-clast conglomerate and sandstone can be followed east to Cave Mountain, with a change in provenance and perhaps age. The unit has limited age control suggesting that it is older than 6 Ma, and probably older than the ~10 Ma opal in faults cutting it (Miller, 2017).

In the Alvord Mountains area, the "Barstow" Formation (Byers, 1960) does not have all of the marker beds that have been identified elsewhere in the Barstow Formation (Reynolds et al., 2010), and is therefore referred to as "Barstow" Formation.

From this ridge, we have an excellent view west of the "Barstow" Formation, the underlying Spanish Canyon and Clews formations, and crystalline bedrock of Alvord Mountain. The age, sedimentology, and structure of the Spanish Canyon Formation were described by Miller et al. (2011) and Buesch (2014). Continue southwest on the powerline road along the pediment cut into the Barstow Formation.

50.0 (4.1) Caution – dip.

50.1 (0.1) The ridge on the south consists of gravels that overlap the Barstow Formation, similar to those we saw at the last stop but a different stratigraphy (Miller et al., 2011). From the north side of Alvord Mountain, the overlap gravel units wrap east then south along the east side, and then west along the south side, essentially defining a huge domal structure (Fig. 2-7). Was the dome due to "pop up" of Alvord Mountain during the late Pliocene?

50.9 (0.8) Drop into wash.

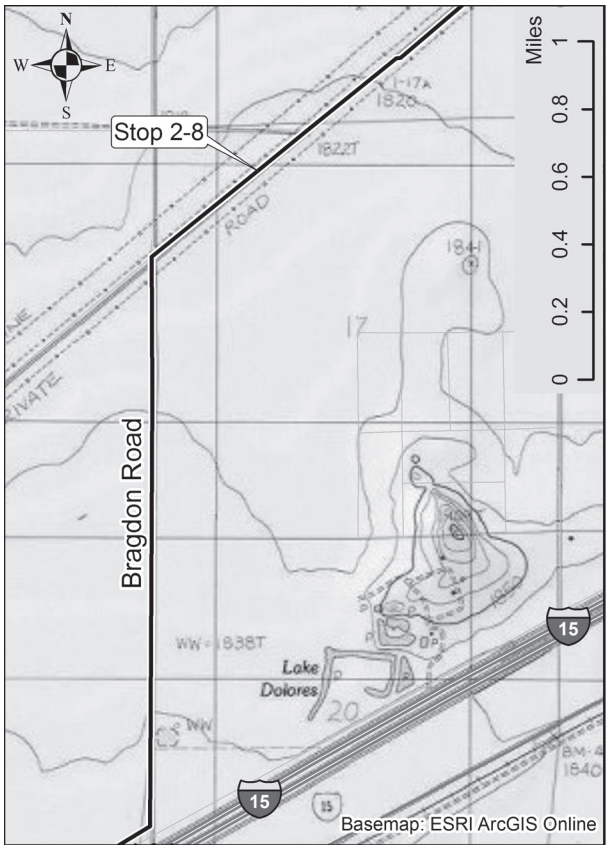

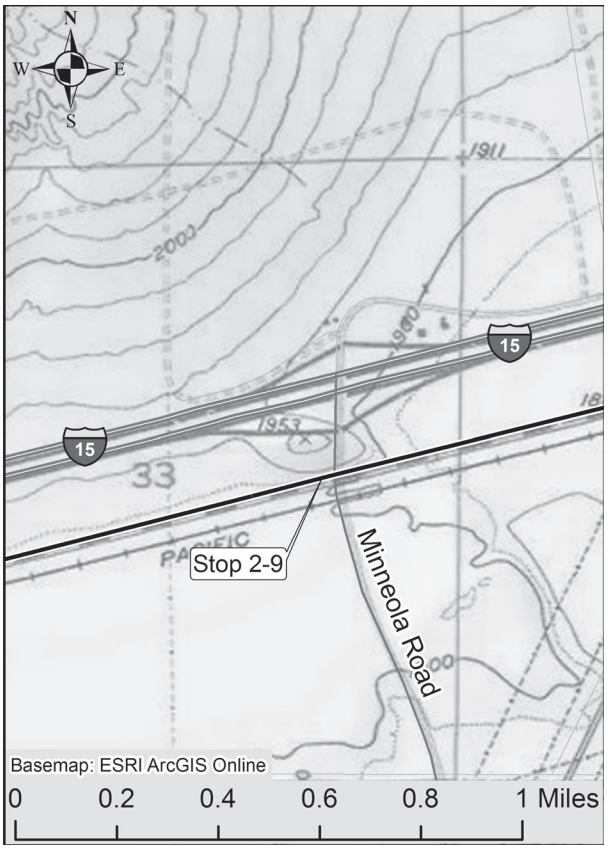

51.2 (0.3) Cross several ridges supported by ~16.2 Ma basalt flows in the central part of the Barstow Formation (Byers, 1960: Miller et al., 2013).

51.9 (0.7) Caution: road washed out ahead.

52.5 (0.6) Avoid dip.

53.4 (0.9) Junction with powerline road from east. Continue past the north end of a ridge underlain by the volcanic gravel unit (Miller et al., 2011).

54.3 (0.9) Drop into Spanish Canyon Wash. Proceed across a broad southwest-sloping alluvial fan that leads to Manix Wash and the Mojave River. Parts of this fan have been scavenged for road base gravel using a Fresno scraper (Lange, 2011).

56.2 (1.9) Cross Alvord Mountain Road that leads north to the Alvord Mine (Vredenburgh, 2011).

57.7 (1.5) Cross a tank road to Fort Irwin.

60.0 (0.3) **532945 3873260** Start onto the east-sloping Mojave River fluvial plain, a transition that is marked in many places by small playas like those we saw in Pliocene deposits at STOP 2-6; note the rolling surface with high ribs that represent inverted stream channels (formed when stream deposits with coarse clasts are eroded, forming resistant ridges that once marked the channels) of the river as we continue onto the plain. Continue southwest on the powerline road.

60.4 (0.4) Pass Harvard Road on left running south to I-15.

61.4 (1.0) Pass Desert View road on left.

61.7 (0.3) Pass a north-south road.

63.0 (1.3) Pass the intersection of Mountain View road and Warbonnett Rd. Miocene basalts of Dolores Hill are to the south.

63.7 (0.7) Pass an intersection with an unnamed east-west road.

63.9 (0.2) **STOP 2-8: Dolores Lake Fault. (528090 3869170**). PULL RIGHT and PARK on a low ridge with a tower maintenance road. The fault here is defined by a ragged scarp about 3–4 m high (Fig. 2-8). It was identified first by Hamilton (1976) as a linear gravity anomaly, and was identified by field mapping by Meek (1994) to the north in Agate Hill. Lidar elevation data has improved our knowledge of the fault by showing that two splays to the south of the I-15 freeway merge to a single strand in this area. The scarp is clearly defined by uplift on the east side, and disconnects of inverted stream channel ridges on either side (Fig. 2-8). Near Agate Hill, the fault bends slightly to the left and becomes more transpressional with clearly defined scarps a few meters high (Dudash, 2006). North of Agate Hill there are as many as three splays of the fault, including one that cuts beach ridges that have been dated about 18 ka in age (Miller and Dudash, unpublished).

Meek (1991) studied a trench excavated along the gas pipeline just north of our location and found no evidence for a fault in that shallow excavation. He suggested that the scarp had been modified by the Mojave River flowing along the feature and scouring it after the last fault rupture. Miller and Dudash agree with that assessment on the basis of our topographic study (Fig. 2-8) that shows the inverted channels of the Mojave River east of the fault to mainly be older than many of those to the west of the fault. Where these channels extend to dated shoreline features in Coyote Lake basin, those lying east of Agate Hill are older than 30 ka, whereas many of those west of Agate Hill are 21-15 ka. One youngest set of channels crosses the fault north of here, in a place where throw on the fault is at a minimum because it transitions from up on the east to up on the west.

The Dolores Lake fault ends southward in a complex junction with the Manix fault, where the area east of the Dolores Lake fault is bowed up to form Harvard Hill. There, Miocene through Pleistocene sediments and volcanic rocks are deformed.

64.2 (0.3) TURN LEFT (south) on Bragdon Road (aka Monastery Road because it leads north to St. Antony Monastery).

65.5 (1.5) Monastery / Bragdon Road ends at Hacienda Road on the north side of I-15. TURN RIGHT (southwest) on Hacienda Road.

75.6 (1.1) Hacienda Road bends left (south) over I-15.

75.8 (0.2) Stop at Yermo Road. Look both ways for cross traffic. TURN RIGHT (southwest) toward Yermo.

79.1 (3.3) PARK west of Minneola Road and walk back to the road cut.

STOP 2-9: Minneola Road Restraining Bend. The road cut along Minneola Road exposes fluvial sediments and gray, silty lacustrine or deltaic fines. The quartzite pebbles in gravelly layers within the deposit mark it as Mojave River sediment. Whether a lake or stream deposit, the sediment (595 m elevation) has been uplifted well above the surrounding fluvial plain (581 m). The uplift is caused by a restraining bend formed at a left bend in the right-lateral Calico fault. The Calico fault, a northwest striking dextral fault, crosses the fluvial plain to our south but turns to a WNW strike at this hill, crossing WNW along the base of the Calico Mountains, where it has a thrust component. At about 1 km northwest of here, the Manix fault strikes west to join the Calico fault, and near that junction, the dextral Paradise fault (locally termed the Tin Can Alley fault; Dudash, 2006) strikes south to a complex 3-fault junction. South from here along the Calico fault, uplift on the southwest side decreases gradually, from

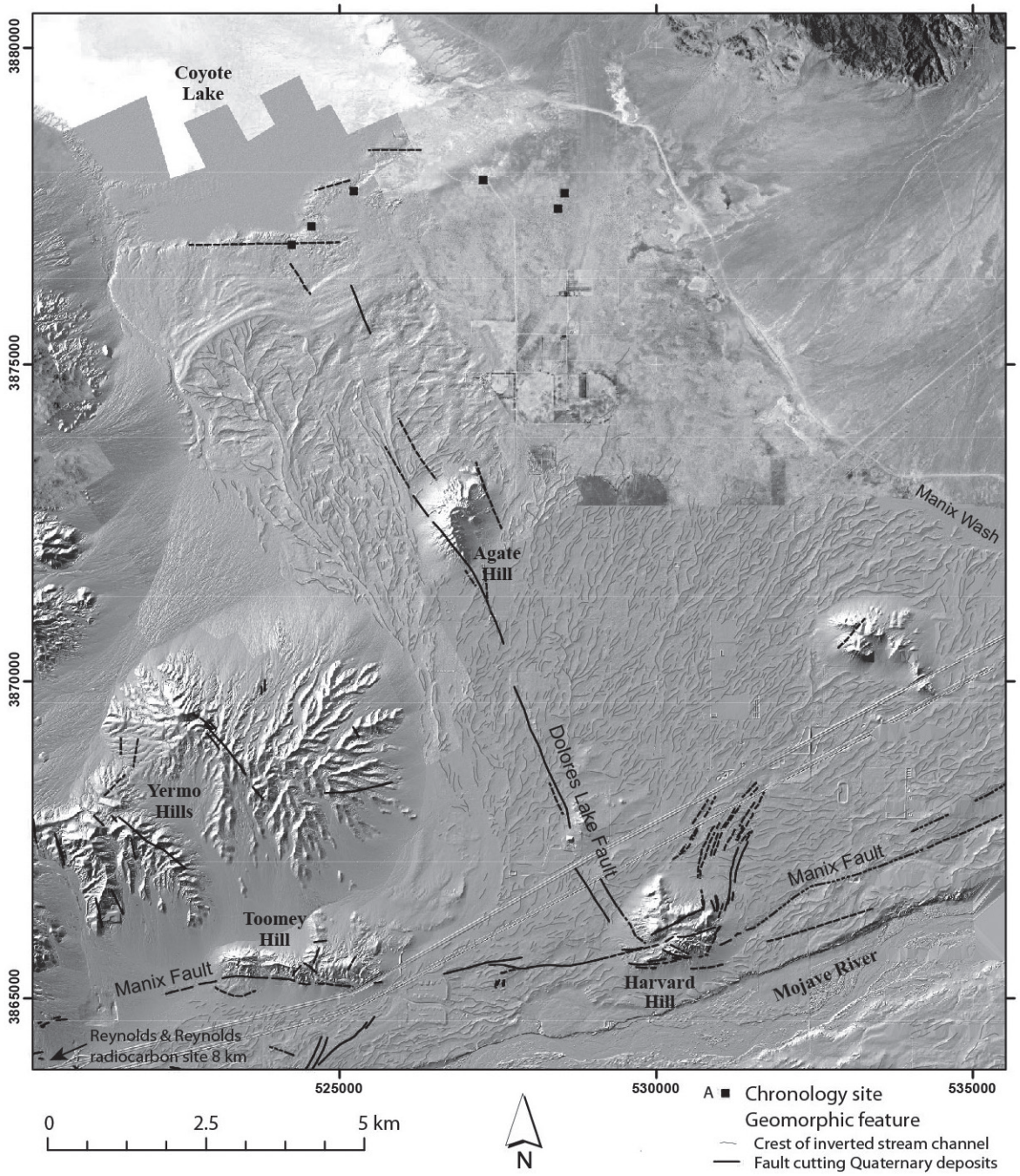

Figure 2-8. Map of the Dolores Lake and other faults, and paleo channels on the Mojave River plain. Based on LiDAR data. Faults in blue, paleochannel crests in gray lines.

about 10 m near the highway to perhaps 5 m near the Mojave River, and generally less than 3 m across the fluvial plain beyond. We will see more evidence for fault control on the Mojave River as we drive upstream.

Return to vehicles and proceed west toward Yermo.

80.3 (1.2) The Calico Lakes resort is southwest of the Agriculture Inspection Station on I-15. Excavation at Calico Lakes recovered a late Pleistocene fauna (fresh water snails, stickleback fish, frogs and toads, lizards and snakes, moles, rabbits, gophers, voles, llama, large camel and horse, Big Horn sheep) dated at ~12 ka (Reynolds and Reynolds, 1985; radiocarbon ages calibrated using Intcal 13). The age and certain elements of the fauna indicate it was a northern extension of Pleistocene "Daggett Pond" and similar datable fine-grained deposits with latest Pleistocene fossils at solar sites on the south side of the Mojave River (Reynolds and Reynolds, 1985, 1991). There is ambiguity in assigning depositional environment to fish, clams, and other fauna recovered because all can live in oxbow lakes, streams, and floodplains of a river system, as well as in a lake. Regardless of the exact environment, it was clearly water-rich and produced thick fine-grained sediment that, although common in much of the fluvial

plain as lenses, is unusual in its thickness and lateral extent here. An earthquake causing uplift on the Calico fault, which would decrease stream gradient to zero or reverse it, is a likely cause for this widespread lake or marsh.

81.3 (1.0) Stop at intersection and TURN LEFT (west) on Yermo Road. The East Yermo entrance to I-15 is to the right.

81.8 (0.5) Pass Second Street. To the south, Second Street crosses the railroad tracks, jogs west and then continues as McCormick Street to cross the Mojave River. There, the north bank of the Mojave River is a series of four benches. These lower by ~2 m increments toward the active drainage. In contrast, the south bank is ~10 m higher in elevation (591 m) than the active drainage (582 m). The south bank bluffs expose many large, well-rounded cobbles of quartzite from Oro Grande that mark the position of the main axial channel at 591 m ~12,000 years ago (Reynolds and Reynolds, 1985). One explanation for benches on the north bank, and not on the south, is that a large pond (Daggett Pond) was formed by the Calico Fault blocking the Mojave River. Eventually, the river breached to the north, and cut benches southward as the channel straightened toward the east-trending axis of the channel.

Another explanation is that the benches were caused by greater uplift on the southwest side of the Calico Fault on the north side of the river compared to the south side. However, along Calico Boulevard, north of Yermo Road, the fluvial plain elevation is ~3.5 m lower than the equivalent surface on the south side of the river.

82.0 (0.2) Pass the Burger Den, the original building for Del Taco. The Del Taco restaurant was opened in Yermo, California on September 16, 1964 by Ed Hackbarth and David Jameson.

82.3 (0.3) Pass Upton's Market.

82.6 (0.3) TURN RIGHT (north) on Calico Road.

83.2 (0.6) Cross I-15 and prepare for a left turn immediately past the west-bound on-ramp.

83.4 (0.2) TURN LEFT (west) on Calico Boulevard.

84.3 (0.9) A landing strip runs north. The colemanite calcining plant of Marion on the Borate & Daggett narrow gauge railroad was located approximately at the north end of the landing strip. Finished product was loaded into rail cars and hauled south to Daggett.

84.4 (0.1) Cross the southwest-trending trace of Mule Canyon Road, which also was the road bed for the Borate & Daggett narrow gauge railroad. The Borate & Daggett ran from the mining town of Borate in the Calico Mountains southwest to the solution ponds east of the Waterloo Mill, then across the Mojave River to loading structures on the Santa Fe Railroad at Daggett (Myrick, 1963).

84.6 (0.2) Pass Happy Trails Road.

85.4 (0.2) Pass the trace of a road from a silver ore mill and Calico Ghost Town southwest past the Waterloo Mill, then across the Mojave River to Daggett.

85.9 (0.5) Stop at Ghost Town Road. Watch for cross traffic. TURN LEFT (south) toward Daggett. The rail bed of the Waterloo Mine railroad is visible 110 m (350 ft) to the west.

86.3 (0.4) Cross under I-15.

86.4 (0.1) Stop at Yermo Road. Proceed south on Yermo–Daggett Road.

86.9 (0.5) The Waterloo Mine railroad bed is visible 300 feet west of the south end of Silver Valley School.

87.8 (0.9) The road bears right (southwest).

87.9 (0.1) View southwest of Waterloo Mill Site foundations at base of Elephant Mountain.

88.3 (0.4) Drop into the Mojave River. Prepare for left turn. Watch for oncoming traffic.

88.7 (0.4) TURN LEFT onto 1st Street.

88.9 (0.2) PARK at the intersection of Mill and 1st streets. Walk to historic Alf Blacksmith Shop and Daggett Historical Society Museum. Return to vehicles, drive south to Santa Fe Road. The Daggett Stone Hotel and Peoples Store are on the left (east).

89.0 (0.1) TURN RIGHT onto Santa Fe Road.

89.1 (0.1) TURN LEFT (south) on Daggett–Yermo Road toward I -40, leading to Barstow, San Bernardino and Los Angeles, or to Bakersfield. If heading to Needles, Flagstaff, or Phoenix, take I-40 east. If going toward Las Vegas, turn right (north) on Daggett–Yermo Road to I-15, then east.

What we have seen

The ECSZ from Baker to Barstow exhibits much steep topography, despite broad tracts of low-relief areas such as the fluvial plain of the Mojave River and some areas flanking the Cronese Hills. The steepest topography is associated with mountain blocks that are caught between two or more flanking faults that cause them to pop up in a restraining stepover. Examples are Cave Mountain and Dunn Hill. Broad, low-relief mountains such as those associated with Alvord Mountain and the Cady Mountains may be caused by doming, with strike-slip faults that traverse them creating local steep topography within the overall dome. Some of the best evidence for uplift can be found where deltaic and lake sediment of

Lake Manix lie above former water levels, and where Mojave River deposits lie above the fluvial plain. Sedimentary sequences from the late Miocene to Pliocene apparently were primarily shed from persistent high ground along an axis of the Calico Mountains northward to the Goldstone area, from which rivers carried distinctive sediment eastward along valleys that mimic locations of sinistral faults.

Deposits in two paleovalleys merged near the area north of the Cronese Hills, meeting at a series of playas. During or preceding this time, gravel and sand were shed over a wide area westward from a Cave Mountain source. We therefore have evidence for modern mountains in the ECSZ having been persistent highs for several million years. Sediment from those highs has spread long distances and accumulated in thin packages, indicating that basins were rare or absent in the region we have traversed. We also have evidence, in the form of domed Pliocene sequences, for these drainage patterns having been disrupted after ~3.5 Ma and before ~500 ka. Clarifying the timing and tectonic drivers of drainage system changes remains a challenge.

Many of the challenges we have encountered on this trip have to do with improving chronologic control on deformed stratigraphic units ranging in age from the late Miocene to the Holocene. We have learned enough about ages of several units to build a framework model for ECSZ tectonism, but much more detail is needed before we will completely understand when important tectonic transitions occurred. In places lacking late Cenozoic units for temporal control, dating fault zone materials where the faults cut Mesozoic or older rocks remains a challenging solution. Another primary challenge is to define the geometry and kinematics of fault linkages, many of which are buried in shallow basins with very young cover that obscures the details. Improved geophysical probing of these critical junctions will be key. Lastly, detailed surface topography provides insights rarely available by any other method. The need for high-resolution topography for the tectonically active Mojave Desert is pressing.

References cited

Adams, Paul M., 2015. Manganese Deposits in the Cady Mountains, San Bernardino County, California. CSU Desert Studies Consortium, p. 206-210.

Anderson, K.C., and Wells, S.G., 2003, Latest Quaternary paleohydrology of Silurian lake and Salt Spring basin, Silurian Valley, California, *in* Enzel, Y., Wells, S.G., and Lancaster, N., eds., Paleoenvironments and paleohydrology of the Mojave and southern Great Basin deserts: Geological Society of America Special Paper 368, p.129-141.

Anderson, Thomas P., 1990, BAXTER IRON/CARBONATE ROCK DEPOSITS SAN BERNARDINO COUNTY CALIFORNIA. Prepared under Authorization of The Surface Mining and Reclamation Act of 1975 at the Direction of The State Mining and Geology Board DMG OPEN-FILE REPORT 90-2, p. 22. Accessed Jan. 2017: http://tinyurl.com/hvjob6b

Barca, R.A., 1966, Geology of the northern part of Old Dad Mountain quadrangle, San Bernardino County, California: California Division of Mines and Geology Map Sheet 7.

Bedford, D. R., Miller, D.M., and Phelps, G.A., 2010, Surficial geologic map of the Amboy 30' by 60' quadrangle, San Bernardino County, California: U.S. Geological Survey Scientific Investigations Map 3109, pamphlet 26 p., scale 1:100,000, available at http://pubs.usgs.gov/sim/3109/

Bishop, K. M., 2013, Rock avalanche setting of the Cave Mountain (Baxter Mine) iron deposits, Afton Canyon, Raising Questions in the Central Mojave. Desert Studies Consortium, California State University, California. p. 107-113.

Brady, R.H. III, 1992, The eastern California shear zone in the northern Bristol Mountains, southeastern California, *in* Richard, S.M., ed., Deformation associated with the Neogene eastern California shear zone, southwestern Arizona and southeastern California: San Bernardino County Museum Special Publication, p. 6-10.

Brady, R.H. III, 2017, Characteristics of the Eastern California Shear Zone from Southern Death Valley to the northern Bristol Mountains: a review, this volume.

Bright and Anderson, 2007, Re-interpretation of Pleistocene Lake Dumont, Salt Spring basin, California, based on ostracode faunal analyses, *in* Miller, D.M., and Valin, Z.C., editors, Geomorphology and tectonics at the intersection of Silurian and Death Valleys, southern California: U.S. Geological Survey Open File Report 2007-1424, p. 51-62, available at http://pubs.usgs.gov/of/2007/ 1424/of2007- 1424.pdf

Buesch, D.C., 1991, Changes in depositional environments resulting from the emplacement of large-volume ignimbrite: *in* Smith, G.A., and Fisher, R.V., eds., Sedimentation in Volcanic Terranes: SEPM Special Publication No. 45, p. 139-153.

Buesch, D.C., 1992, Incorporation and redistribution of locally derived lithic fragments within a pyroclastic flow: Geological Society of America Bulletin, v. 104, p. 1178-1192.

Buesch, D.C., 2014, Interstratified arkosic and volcanic rocks of the Miocene Spanish Canyon Formation, Alvord Mountain area, California—Descriptions and interpretations: *in* Reynolds, R.E., ed, "Not a Drop Left to Drink", California State University Desert Studies Consortium, p. 190-203.

Buesch, D.C., and Valentine, G.A., 1986, Peach Springs Tuff and the volcanic stratigraphy of the southern Cerbat Mtns, Kingman, Arizona: Geological Society of America Cordilleran Section Field Trip Guide and Volume, Field Trip Number 5, p. 7-14.

Byers, F. M., 1960, Geology of the Alvord Mountain Quadrangle, San Bernardino County, California: U.S. Geological Survey Bulletin 1089-A, 71 p.

Conrotto, E. L., 1957, Agate Wonderland in the Cadys: Desert Magazine, November, p. 11-14.

Cyr, A.J., 2016. New surficial geologic mapping reveals change from Pleistocene dextral strike slip to Holocene transpression along the Soda-Avawatz Fault Zone, eastern Mojave Desert, California. Geological Society of

America, Abstracts with Programs, v. 48, n. 4, doi: 10.1130/abs/2016CD-274572.

Dibblee, T.W. Jr., and A. M. Bassett, 1966, Geologic map of the Cady Mountains quadrangle, San Bernardino County, California: U.S. Geological Survey Miscellaneous Investigations Map I-4767, scale 1:62,500.

Dibblee, T.W. Jr., 1967, Geologic map of the Broadwell Lake quadrangle, San Bernardino County, California: U.S. Geological Survey Miscellaneous Investigations Map I-478, scale 1:62,500.

Dibblee, T.W. Jr., 1967, Geologic map of the Ludlow quadrangle, San Bernardino County, California: U.S. Geological Survey Miscellaneous Investigations Map I-477, scale 1:62,500.

Dohrenwend, J.C., McFadden, L.D., Turrin, B.D., and Wells, S.G., 1984, K-Ar dating of the Cima volcanic field, eastern Mojave Desert, California: Late Cenozoic volcanic history and landscape evolution: Geology, v. 12, p. 163-167.

Dokka, R.K., and Travis, C.J., 1990, Late Cenozoic strike-slip faulting in the Mojave Desert, California: Tectonics, v. 9, p. 311-330.

Dudash, S.L., 2006, Preliminary surficial geologic map of a Calico Mountains piedmont and part of Coyote Lake, Mojave Desert, San Bernardino County, California: U.S. Geological Survey Open-File Report 2006–1090, 44 p., scale 1:24,000.

Durrell, C. 1953. Geological investigations of strontium deposits in California: California Division of Mines and Geology Special Report 32: p. 48.

Durrell, C. 1954. Barite Deposits near Barstow, San Bernardino County, California: California Division of Mines and Geology Special Report 39: p. 8.

Evernden, J. F., D. E. Savage, G. H. Curtis and G. T. James. 1964. Potassium argon dates and the Cenozoic mammalian chronology of North America. American Journal of Science, 262: 145-198.

Feller, Walter, 2017, Along the Troubled Trail: Travels with Nicholas Porter (The 1864 Diary of Sarah Jane Rousseau), this volume.

Ferguson, C.A., McIntosh, W.C., and Miller, C.F., 2013, Silver Creek caldera—The tectonically dismembered source of the Peach Spring Tuff: Geology, v. 41, p. 3-6, doi:10.1130/G33551.1.

Fulton, Robert, 2005. Evaporative salt production on Soda Dry Lake. Old Ores: Desert Studies Consortium, California State University, California p. 55-60.

Green, H.L., Redwine, J.L., Miller, D.M., 2007, Reconnaissance studies of soils-geomorphic correlations and late Quaternary deformation of alluvial fan deposits east of the Avawatz Mountains, Mojave Desert, California, *in* Miller, D.M., and Valin, Z.C., editors, Geomorphology and tectonics at the intersection of Silurian and Death Valleys, southern California: U.S. Geological Survey Open File Report 2007-1424, p. 113-140, available at http://pubs.usgs.gov/of/2007/1424/of2007- 1424.pdf

Goldfarb, R.J., Miller, D.M., Simpson, R.W., Hoover, D.B., Moyle, P.R., Olson, J.E., and Gaps, R.S., 1988, Mineral resources of the Providence Mountains Wilderness Study Area, San Bernardino County, California: U.S. Geological Survey Bulletin 1712-D, 70 p.

Gourley, J.R., 2000, Facies analysis of Neogene syntectonic strata in the Soda Mountains, San Bernardino County, California: Implications for constraint on faulting on the Soda-Avawatz Fault Zone: [M.S. Thesis], California State University, Fullerton, 75p.

Grose, L.T., 1959, Structure and petrology of the northeast part of the Soda Mountains, San Bernardino County, California: Geological Society of America, Bulletin, v. 70, p. 1509-1548.

Gudde, E.G., 1975, Gold Camps of California: University of California Press, Berkeley, CA, 467 p.

Hamilton, P., 1976, A geophysical study of the Manix Fault; its tectonic relationship to the western Mohave Desert, San Bernardino County, California: M.S. Thesis, California State University, Los Angeles, California, 101 pp.

Harvey, A.M., and Wells, S.G., 2003, Late Quaternary variations in alluvial fan sedimentologic and geomorphic processes, Soda Lake basin, eastern Mojave Desert, *in* Yehouda Enzel, Stephen G. Wells, and Nicholas Lancaster, eds., Paleoenvironments and Paleohydrology of the Mojave and Southern Great Basin Deserts, GSA Special Paper 368, p. 207-230.

Hazzard, J.C., 1954, Rocks and structures of the northern Providence Mountains, San Bernardino County, Californaia: California Division of Mines Bulletin 170, p. 27-35.

Hooke, R. LeB., 1999, Lake Manly Shorelines in the Eastern Mojave Desert, California: Quaternary Research, v. 52, p. 328-336.

Howard, K.A., Kilburn, J.E., Simpson, R.W., Fitzgibbon, T.T., Detra, D.E., Raines, G.L., and Sabine, Charles, 1987, Mineral Resources of the Bristol/Granite Mountains wilderness study area, San Bernardino county, California: U.S. Geological Survey Bulletin 1712-C, 18 p.

Jordan, F, Jr., 2017, Cave Mountain Faulting and Landsliding, this volume

Laity, Julie. 2000. Ventifacts in the Mojave River Corridor and at "Ventifact Hill." San Benardino County Museum Association; Quarterly 47(2). P. 37-39.

Lamey, C. A., 1948, Cave Canyon Iron-ore Deposits, San Bernardino, California: Calif. Div. Mines, Bull. 129, p. 71-83.

Lancaster, N., and Tchakerian, V.P., 2003. Late Quaternary eolian dynamics, Mojave Desert, California: Geol. Soc. Am. Spec. Pap. 368, 231–249.

Lange, F.W., 2011, Following the tracks of the Fresno: a chronological marker for the historic period, *in* Reynolds, R.E., ed., The incredible shrinking Pliocene: Desert Studies Consortium, California State University, Fullerton, p. 41-46.

Langenheim, V.E., Biehler, S., Negrini, R., Mickus, K., Miller, D.M., and Miller, R.J., 2009, Gravity and magnetic investigations of the Mojave National Preserve and adjacent areas, California and Nevada: U.S. Geological Survey Open-File Report 2009-1117, 28 p., http://pubs.usgs.gov/of/2009/1117.

Langenheim, V.E., and Miller, D.M., 2017, Connecting the Soda-Avawatz and Bristol-Granite Mountains faults with

gravity and aeromagnetic data, Mojave Desert, California, this volume.

Lease, R.O., McQuarrie, N., Oskin, M., and Leier, A., 2009, Quantifying dextral shear on the Bristol-Granite Mountains fault zone: Successful geologic prediction from kinematic compatibility of the Eastern California Shear Zone: Journal of Geology, v. 117, p. 37-53.

Leith, C.K., 1966, Iron and manganese, iron ores of the western United States and British Columbia: U.S. Geological Survey Bulletin 285-E.

Liu, T., 2003, Blind testing of rock varnish microstratigraphy as a chronometric indicator: results on late Quaternary lava flows in the Mojave Desert, California: Geomorphology, v. 53, p. 209–234.

Losson, Gregor, 2017. Established Roads of the Cady Mountains, (Ms on file at BLM Barstow Field Office, Barstow California). pp. 164,

Lum, Maria A., 2003. Crucifixion Thorn. Land of Lost Lakes. Desert Studies Consortium, California State University, California p. 48.

Lyman, Leo and Walker, Cliff, 1997, Water Holes to California. SBCMA 44(2):61-66.

Lyman, Leo and Walker, Cliff, 1999, On the Trail of the 49ers from Bitter Springs to the Cajon Pass. San Bernardino County Museum Quarterly v. 46(3), p. 101-106.

Mahan, S.A., Miller, D.M., Menges, C.M., and Yount, J.C., 2007, Late Quaternary stratigraphy and luminescence geochronology of the northeastern Mojave Desert, with emphasis on the Valjean Valley area, *in* Miller, D.M. and Valin, Z.C., eds., Geomorphology and tectonics at the intersection of Silurian and Death Valleys, southern California: U.S. Geological Survey Open-File Report 2007-1424, p. 63-97.

Mann, Bill, 1998 Guide to 50 Interesting and Mysterious Sites in the Mojave, Vol 1, Shortfuse Publishing, Barstow, CA. p. 44-45.

McKenna, Jeanette A., 1990. Recent Historic and Prehistoric Archaeological investigations in the Broadwell Valley, North of Ludlow, in theMojave Desert, San Bernardino County, California. San Bernardino County Museum Association Quarterly 38(2):50.

Meek, N., 1989, Geomorphic and hydrologic implications of the rapid incision of Afton Canyon, Mojave Desert, California: Geology, v. 17, p. 7-10.

Meek, N., 1991, Report on the Kern River Pipeline Trench in Coyote Basin, California; written comm. from Meek to A. York, 12/15/91, 6 pp.

Meek, N., 1994, The stratigraphy and geomorphology of Coyote Basin, central Mojave Desert, California: San Bernardino County Museum Quarterly, vol. 41, no. 3, p. 5-13.

Meek, N., 1999, New discoveries about the Late Wisconsinan history of the Mojave River system, *in* Reynolds, R. E., and Reynolds, J., eds., Tracks along the Mojave: A field guide from Cajon Pass to the Calico Mountains and Coyote Lake, Volume 46, no. 3, San Bernardino Museum Quarterly, p. 113-117.

Mendonca, J., 2007, Preliminary results on neotectonic and geomorphic evolution of the northeastern Avawatz Mountains, southern Death Valley, California, *in* Miller, D.M., and Valin, Z.C., editors, Geomorphology and tectonics at the intersection of Silurian and Death Valleys, southern California: U.S. Geological Survey Open File Report 2007-1424, p. 141-148, available at http://pubs.usgs.gov/of/2007/1424/of2007- 1424.pdf

Messina, P., Stoffer, P., and Smith, W.C., 2005, Macropolygon morphology, development, and classification on North Panamint and Eureka Playas, Death Valley National Park, California: Earth-Science Reviews, v. 73, no. 1–4, p. 309–322.

Miller, D.M., 1994, Cenozoic deposits in the Lava Hills and southern Bristol Mountains, southeastern California, *in* Sherrod, D.R., and Nielson, J.E., eds., Tertiary Stratigraphy of highly extended terranes, California, Arizona, and Nevada: U.S. Geological Survey Bulletin 2053, p. 99-107.

Miller, D.M., Glick, L.L., Goldfarb, R., Simpson, R.W., Hoover, D.B., Detra, D.E., Dohrenwend, J.C., and Munts, S.R., 1985, Mineral resources and mineral resource potential of the South Providence Mountains Wilderness Study Area, San Bernardino County, California: U.S. Geological Survey Miscellaneous Field Studies Map MF-1780-A, 29 p., scale 1:62,500.

Miller, D.M., Wells, M.L., Dewitt, E., Walker, J.D., and Nakata, J.K., 1996, Late Cretaceous extensional fault system across the northeastern Mojave Desert, *in* Reynolds, R.E., and Reynolds, J., compilers, Punctuated chaos in the northeastern Mojave Desert: San Bernardino County Museum Quarterly, v. 43, no. 1/2, p. 77-84.

Miller, D.M., Menges, C.M., and McMackin, M.R., 2007a, Geomorphology and tectonics at the intersection of Silurian and Death Valleys, southern California: Field trip road log, *in* Miller, D.M. and Valin, Z.C., eds., Geomorphology and tectonics at the intersection of Silurian and Death Valleys, southern California: U.S. Geological Survey Open-File Report 2007-1424, p. 7-49.

Miller, D.M., Dudash, S.L., Green, H.L., Lidke, D.J., Amoroso, L., Phelps, G.A., and Schmidt, K.M., 2007b, A new Quaternary view of northern Mojave Desert tectonics suggests changing fault patterns during the late Pleistocene, *in* Miller, D.M., and Valin, Z.C., editors, Geomorphology and tectonics at the intersection of Silurian and Death Valleys, southern California: U.S. Geological Survey Open File Report 2007-1424, p. 157-171, available at http://pubs.usgs.gov/of/2007/ 1424/of2007- 1424.pdf

Miller, D.M., 2012, Surficial geologic map of the Ivanpah 30' x 60' quadrangle, San Bernardino County, California and Clark County, Nevada: U.S. Geological Survey Scientific Investigations Map 3206, pamphlet 14 p., scale 1:100,000, accessed at https:pubs.usgs.gov/sim/3206.

Miller, D.M., and Yount, J.L., 2002, Late Cenozoic tectonic evolution of the north-central Mojave Desert inferred from fault history and physiographic evolution of the Fort Irwin area, California: Geological Society of America Memoir, 195, p. 173-197.

Miller, D.M., Schmidt, K.M., Mahan, S.A., McGeehin, J.P., Owen, L.A., Barron, J.A., Lehmkuhl, F., Lohrer, R., 2010,

Holocene landscape response to seasonality of storms in the Mojave Desert: Quaternary International, v. 215, p. 45-61.

Miller, D.M., Reheis, M.C., Wan, E., Wahl, D.B., Olson, H., 2011, Pliocene and early Pleistocene paleogeography of the Coyote Lake and Alvord Mountain area, Mojave Desert, California, *in* Reynolds, R.E., ed., The incredible shrinking Pliocene: Desert Studies Consortium, California State University, Fullerton, p. 53-67.

Miller, D.M., 2017 this volume, The late Cenozoic eastern California shear zone after 25 years of study. ECSZ Does It. Desert Symposium proceedings, California State Fullerton, this volume.

Miller, D.M., Hillhouse, J.W., and Reynolds, R.E., 2011, The incredible shrinking Pliocene: Field trip guide, Day 1, in Reynolds, R.E., ed., The incredible shrinking Pliocene: Desert Symposium proceedings, California State Fullerton, p. 6-14.

Miller, D.M., Menges, C.M., and Lidke, D.J., 2014, Generalized surficial geologic map of the Fort Irwin area: Chap. B in Buesch, D.C., ed., Geology and Geophysics Applied to Groundwater Hydrology at Fort Irwin, California, U.S. Geological Survey Open File Report 2013-1024, 11 p., scale 1:100,000, *http://dx.doi.org/10.3133/ofr20131024B*.

Mitchell, J.R., 1998, Gem Trails of Southern California: Gem Guides Book Co., Baldwin Park, CA 91760, p. 176

Moseley, C.G., 1978, Geology of a portion of the northern Cady Mountains, Mojave Desert, California: [M.S. Thesis] University of California Riverside.

Muhs, D.R., Lancaster, N., Skipp, G. L., 2017, A complex origin for the Kelso Dunes, Mojave National Preserve, California, USA: A case study using a simple geochemical method with global applications: Geomorphology, v. 276, p. 222-243.

Myrick, David F. 1963. Railroads of Nevada and Eastern California. Vol. II: The Southern Railroads. Berkeley, Howell North Books. Pp. 455-933.

National Park Service, "Kelso Depot," https://www.nps.gov/moja/learn/historyculture/kelso-depot.htm (visited 1/29/17).

Neal, J.T., 1968, Geology, Mineralogy, and Hydrology of U.S. Playas: Office of Aerospace Research, U.S. Air Force AFCRL-65-266, Environmental Research Paper no. 96, 176 p.

Phelps, G.A., Hillhouse, J.W., Fleck, R.J., Miller, D.M., Buesch, D.C., Cyr, A., and Schmidt, K.M. 2017, Analysis of the Age and Paleomagnetic Orientation of the Broadwell Mesa Basalt, Bristol Mountains, CA this vol

Phillips, F.M., 2003, Cosmogenic ^{36}Cl ages of Quaternary basalt flows in the Mojave Desert, California, USA: Geomorphology, v. 53, p. 199–208.

Pigati, J.S., Miller, D.M., Bright, J.E., Mahan, S.A., Nekola, J.C., and Paces, J.B., 2011, Chronology, sedimentology, and microfauna of groundwater discharge deposits in the central Mojave Desert, Valley Wells, California: Geological Society of America Bulletin, v. 123, p. 2224–2239.

Reheis, M.C., Bright, J., Lund, S.P., Miller, D.M., Skipp, G., and Fleck, R.J., 2012, A half-million year record of paleoclimate from the Lake Manix core, Mojave Desert, California: Palaeogeography, Palaeoclimatology, Palaeoecology, v. 365-366, p. 11-37.

Rasmussen and Associates, 1990, Geologic and Geotechnical feasibility investigation, proposed residuals repository, Broadwell dry lake, north of Ludlow, California: San Bernardino, California, Gary S. Rasmussen and Associates, project no. 2604.3, 89 p.

Reynolds, R.E., 2004. Latest Pleistocene (Rancholabrean) fossil assemblage from the Silver Lake Climbing Dune site, northeastern Mojave Desert, California, California State University Desert Symposium 2004. p. 33-38.

Reynolds, R.E., and Reynolds, J. (eds), 1996. Punctuated chaos in the northeastern Mojave Desert. San Bernardino County Museum Association Quarterly, 43(1,2): 156 p.

Reynolds, R. E., and Reynolds, R. L., 1985, Late Pleistocene faunas from Daggett and Yermo, San Bernardino County, California, *in* Reynolds, R. E., ed., Cajon Pass to Manix Lake: Geological investigations along Interstate 15, San Bernardino County Museum Association Special Publication, p. 175-191.

Reynolds, R. E., and Reynolds, R. L., 1991, Structural implications of late Pleistocene faunas from the Mojave River Valley, California, in Inland southern California: the last 70 million years, ed. M.O. Woodburne, R.E. Reynolds, and D.P. Whistler: Redlands, San Bernardino County Museum Association Quarterly 38, no. 3-4, p. 100-105.

Reynolds, R.E., and Miller, D.M., 2010, Overboard in the Mojave: the field guide: Desert Studies Consortium, California State University Fullerton, p. 7-23.

Reynolds, R.E, 2017, A review of latest Oligocene - earliest Miocene floras of the Mojave Block, this volume.

Reynolds, R.E., Miller, D.M., and Bishop, Kim, 2003. Land of lost lakes, the 2003 Desert Symposium field trip, *in* Land of Lost Lakes, R.E. Reynolds, ed. California State University Desert Studies Consortium: 3-26.

Reynolds, R.E., 2004. Latest Pleistocene (Rancholabrean) fossil assemblage from the Silver Lake Climbing Dune site, northeastern Mojave Desert, California, California State University Desert Symposium 2004. p. 33-38.

Reynolds, R.E., and Whistler, D.P., 1990. Early Clarendonian Faunas of the Eastern Mojave Desert, San Bernardino County, California. Redlands, San Bernardino County Museum Association Special Publication, MDQRC Guidebook.

Reynolds, R.E., and Weasma, Ted, 2005, Old ores: mines and mineral marketing in the east Mojave Desert—a field trip guide: California State University, Desert Studies Consortium: 3-19.

Roder, B. J., Lawson, M. J., Rhodes, E. J., Dolan, J. F., McAuliffe, L. J., McGill, S. F., 2012, Assessing the potential of luminescence dating for fault slip rate studies on the Garlock fault, Mojave Desert, California, USA: Quaternary Geochronology, v. 10, p. 285-290. doi: 10.1016/j.quageo.2012.03.013.

Sauber, J.W., Thatcher, Wayne, Solomon, S.C., and Lisowski, M., 1994, Geodetic slip rate for the eastern California shear zone and recurrence of Mojave desert earthquakes: Nature, v. 367, p. 264-6.

Schelle, H., and Grunthal, G., 1996, Modeling of Neogene crustal block rotation: Case study of southeastern California: Tectonics, v. 15, p. 700-710.

Schendel, Daryl, 2017, Daggett—a town history forgot, this volume.

Schermer, E.R., Luyendyk, B.P., and Cisowski, S., 1996, Late Cenozoic structure and tectonics of the northern Mojave Desert: Tectonics, v. 15, p. 905-932.

Schmidt, K.M., Mahan, S., and Langenheim, V.E., 2012, Constraining Quaternary offset of the Cady fault, eastern California shear zone, southern California, with geologic mapping, luminescence dating, and geophysics: Abstract T33A-2646 presented at 2012 Fall Meeting, AGU, San Francisco, Calif., 3-7 Dec.

Schmidt, K.M. and Langenheim, V.E., 2012, Quaternary offset of the Cady fault, eastern California shear zone, southern California, *in* Searching for the Pliocene: Southern Exposures, Reynolds, R.E. ed., California State University Desert Studies Center 2012 Desert Symposium, p.144-150.

Schneider, J.S., 1994. Fresh water mussels and paleoenvironment at East Cronese Lake, in Kelso Conference Papers 1987–1992. A Collection of Papers and Abstracts from the First Five Kelso Conferences on the Prehistory of the Mojave Desert, G.D. Everson and J.S. Schneider (eds). Museum of Anthropology, California State University, Bakersfield Occasional Papers in Anthropology 4:42-51.

Schoffstall, Patricia A., 2010, Mojave Desert Dictionary. The Mojave River Valley Museum, Barstow, CA 92311, pp. 287.

Skirvin, T.M., and Wells, S.G., 1990, Late Cenozoic structure, geometry, and landscape evolution of the Old Dad Mountain area, California: San Bernardino County Museum Special Publication, p. 73-88

Southern Pacific Company, 1964, Minerals for Industry, Vol. III – Southern California. Accessed Jan., 2017: https://archive.org/details/mineralsforindus95sout

Stone, Paul, Miller, D.M., and Priest, S.S., 2017, Geologic map of the Providence Mountains in the Fountain Peak and parts of the adjacent 7.5-minute quadrangles, San Bernardino County, California: U.S. Geological Survey Science Investigations Map, SIM 3376.

Swisher, C.C. III, 1992, $^{40}Ar/^{39}Ar$ dating and its application to the calibration of the North American Land Mammal Ages: [Ph.D. thesis] University of California Berkeley, 184 p.

Thompson, D.G., 1921, Routes to desert watering places in the Mohave Desert region: U.S. Geological Survey Water Supply Paper 490-B, 183 p.

Thompson, D.G., 1929, The Mojave Desert region, California: U.S. Geological Survey Water Supply Paper 578: 760 p.

Vredenburgh, L.M., 2011, Alvord mine, San Bernardino County, California, *in* Reynolds, R.E., ed., The incredible shrinking Pliocene: Desert Symposium volume, Desert Studies Consortium, California State University Fullerton, p. 47-48.

Vredenburgh, L.M., 2017a, Geology and Mineralization of Old Dad Mountain, this volume.

Vredenburgh, L. M., 2017b, Mineral Potential Within the Eastern California Shear Zone, this volume

Walker, C., 1967, Life and Adventure along the Mojave River Trail. SBCMA, 15(1): pp. 34.

Walker, J.D., Martin, M.W., Bartley, J.M., and Coleman, D.S., 1990, Timing and kinematics of deformation in the Cronese Hills, California, and implications for Mesozoic structure of the southern Cordillera: Geology, v. 18, p. 554–557.

Warren, C.N. and Schneider, J.S., 2000. Archaeology in the Cronese Basin: a history, in Empty Basins, Vanished Lakes, R.E. Reynolds and J. Reynolds (ed). San Bernardino County Museum Association Quarterly 47(2):40-41.

Wells, M.L., Beyene, M.A., Spell, T.L., Kula, J.L., Miller, D.M., and Zanetti, K.A., 2005, The Pinto shear zone; a Laramide synconvergent extensional shear zone in the Mojave Desert region of the southwestern United States: Journal of Structural Geology, v. 27, p. 1697-1720.

Wells, S.G., Brown, W.J., Enzel, Y., Anderson, R.Y., and McFadden, L.D., 2003, Late Quaternary geology and paleohydrology of pluvial Lake Mojave, southern California, *in* Enzel, Y., Wells, S. G., and Lancaster, N., eds., Paleoenvironments and paleohydrology of the Mojave and southern Great Basin Deserts: Special Paper 368: Boulder, Colo., Geological Society of America, p. 79-114.

Wells, R.E., and Hillhouse, J.W., 1989, Paleomagnetism and tectonic rotation of the lower Miocene Peach Spring Tuff: Colorado Plateau, Arizona, to Barstow, California: Geological Society of America Bulletin, v. 101, p. 846–863, doi: 10.1130/0016–7606(1989)101.

Whistler, D.P., and Reynolds, R.E., 1991. Recent revisions to the Clarendonian faunal assemblage from the Avawatz Formation. San Bernardino County Museum Association Quarterly, 38(3, 4):91-92.

Wilkerson, G., 2015, Geology and mining history of the Cronese Mountains, Cave, and northern Cady Mountains, San Bernardino County, California, in Mojave Miocene, R.E. Reynolds, ed.: Desert Symposium proceedings, Desert Studies Consortium California State University Fullerton, p. 211-220.

Wilkerson, 2017, Geology and Stratigraphy of Mineral Occurrences in the Bristol and Old Dad Mountains, San Bernardino County, California, this volume

Wilshire, Howard G., 1992; GIS database by David R. Bedford and Teresa Coleman, 2002, Digital Version of "Open-File Report 92–181: Geologic Map of the Indian Spring Quadrangle, San Bernardino County, California": U.S. Geological Survey Open-File Report 02-272, scale 1:24,000, http://geopubs.wr.usgs.gov/open-file/of02-272/.Woodburne, 19XX; Cady Fauna

Woodburne, M.O. 1998. Arikareean and Hemingfordian faunas of the Cady Mountains, Mojave Desert province, California, pp 197-201 *in* Depositional environments, lithostratrigraphy, and biostratigraphy of the White River and Akrikaree Groups (late Eocene to early Miocene, North America, D.O. Terry Jr., H.E. LaGarry, and R.M. Hunt Jr, (eds.), Geological Society of America Special Paper 325.

Woodburne, M.O., 2017, The Eastern California Shear Zone, Mojave Desert, California, this volume.

Wright, L. A., R. M. Stewart, T. E. Gay and G. C. Hazenbush, 1953, Mines and minerals of San Bernardino County, California, California Journal of Mines and Geology, vol. 49 (1, 2), p. 93.

The late Cenozoic Eastern California Shear Zone after 25 years of study

D. M. Miller
U.S. Geological Survey, 345 Middlefield Rd., Menlo Park CA 94025

Introduction

The Eastern California Shear Zone (ECSZ) was defined by Dokka and Travis (1990) as the part of the Mojave Desert across which active or very young strike-slip faults are known. As such, it ranges from somewhat west of Barstow to Baker, Calif., lying in the central part of the desert. Much study in the 25 years since their influential report has provided a richer and more nuanced view of the ECSZ, and has also provided additional context to the north, south, east, and west. This paper describes the ECSZ, how the shear zone works, some of the advances that have been made in the Mojave Desert, and discusses terminology that should be clarified for future work. I also describe new evidence for ~10 Ma inception of the strike-slip faults overall, and its implications.

The central Mojave Desert lies within a zone of active dextral shear associated with transpressional deformation inboard of the southern San Andreas fault (Fig. 1). This zone presently accommodates 20 to 25% of net shear between the Pacific and North American plates as indicated by geodetic data (8 to 14 mm/yr of dextral shear; Sauber et al., 1994; Miller et al., 2001; Bennett et al., 2003). Schelle and Grunthal (1996) and Hardebeck and Hauksson (1999) described geophysical data demonstrating that brittle behavior of the upper crust extends to about 10 km depth, and that maximum principal stress in the brittle crust is oriented horizontally about 010° to 020°.

The Garlock fault defines the boundary between northern Mojave Desert and Basin-and-Range domains. Some workers (e.g., Frankel et al., 2008) have referred to the strike-slip faults east of the Sierra Nevada as the ECSZ (Fig. 1), whereas others have termed this area the Walker Lane belt. Faulds et al. (2005) used the term Walker Lane for all strike-slip faulting from the Salton trough to northern Nevada.

The active zone of strike-slip faulting (Fig. 2) was termed the ECSZ by Dokka and Travis (1990). Miller and Yount (2002) described a broader region of late Cenozoic faulting that includes all of the western Mojave Desert, where Pleistocene faults are common. East of the strike-slip province in the Mojave Desert is an area sometimes referred to as part of the Basin and Range. This eastern area exhibits strike slip faults ranging from (uncommon) late Quaternary age (Guest et al., 2007) to Pliocene or latest Miocene age (Miller and Wooden, 1993; Mahan et al., 2009).

Quaternary faults within the Mojave Desert have been depicted as occurring over a broad area 150 to 200 km wide, within which dextral faults are spaced fairly evenly, roughly 10 to 20 km apart (Fig. 2). By contrast, strike-slip faults north of the Garlock fault are limited to three principal systems, from west to east – the Owens Valley fault, Panamint fault, and Death Valley fault zone (Fig 2) – which are more widely spaced, about 40 to 60 km apart. Clusters of Holocene faults of the northern Mojave Desert align moderately well with faults to the north of the Garlock fault (Miller et al., 2007).

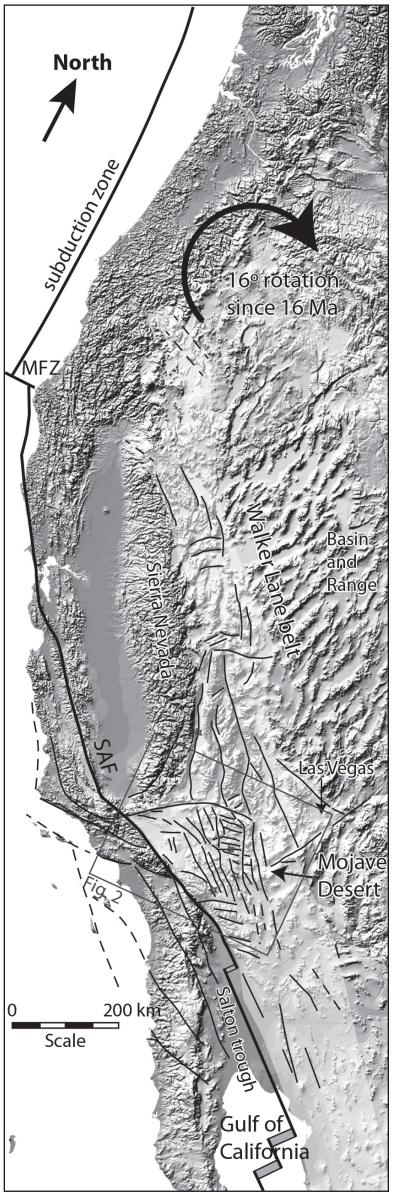

Figure 1. Late Cenozoic strike-slip faults in western North America, and related features such as the Cascadia subduction zone thrust fault. Wide lines represent Pacific-North American plate boundary. MFT, Mendocino Fracture Zone. Blue stars indicate selected historic earthquakes east of the SAF.

Context for strike-slip faulting in the Mojave Desert

The ECSZ in the Mojave Desert is part of a much longer belt of dextral faulting that accommodates plate motion, possibly stretching from Oregon to northwest Mexico. Key to defining the temporal and spatial extents of

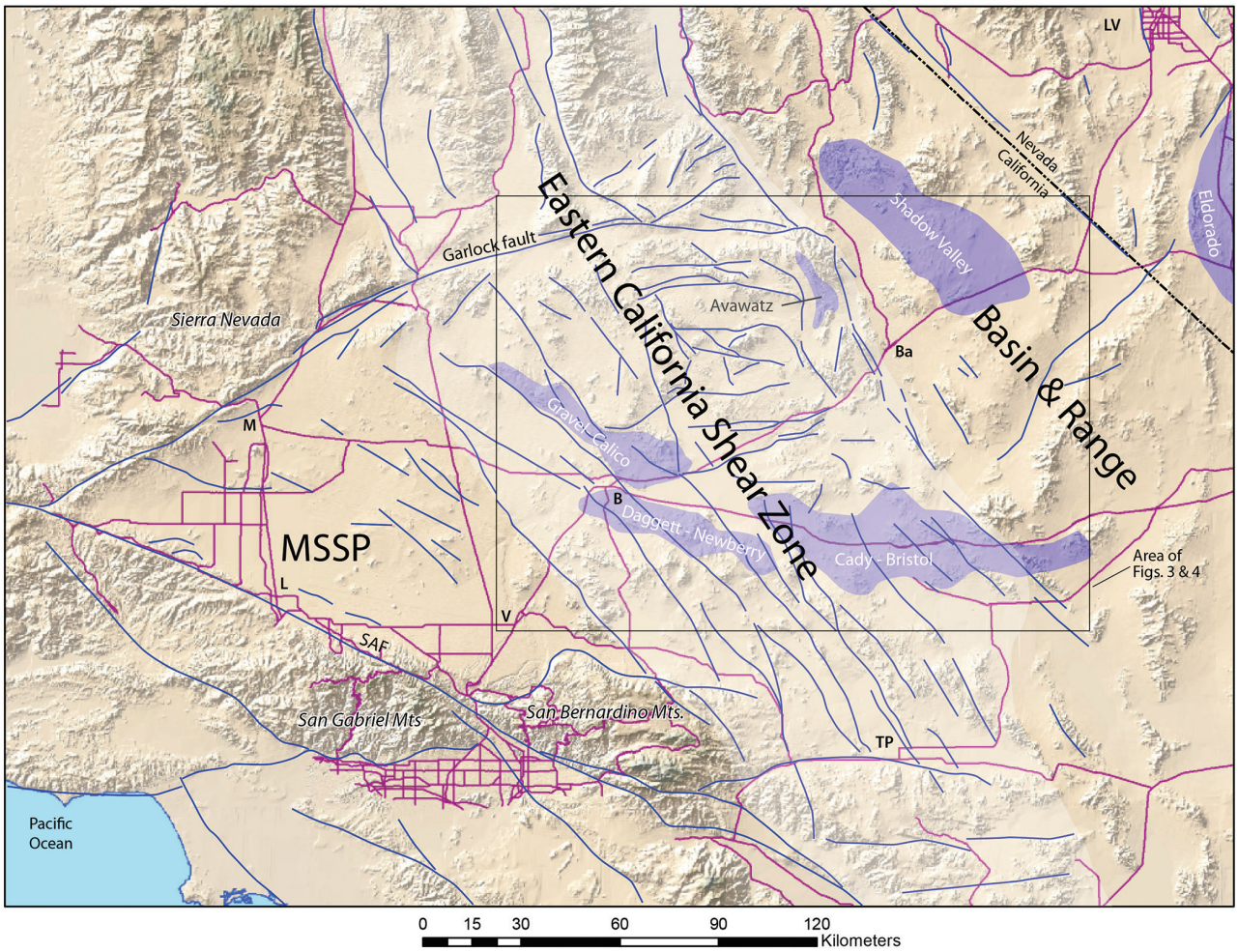

Figure 2. The Mojave Desert part of the Walker Lane belt with ECSZ sector identified. MSSP=Mojave Strike-Slip Province west of the ECSZ. Areas of extensional precursor basins and potentially coeval extensional terranes shown in blue. Faults (blue) generalized from National Quaternary fault database and USGS mapping in the northern Mojave Desert. Major roads indicated by heavy gray lines. Abbreviations for Mojave Desert communities: B, Barstow; Ba, Baker; L, Lancaster; LV, Las Vegas; M, Mojave; TP, Twentynine Palms.

this belt are understanding the mechanisms that drive faulting inboard of the plate boundary and how the plate boundary has changed with time. This topic is beyond the scope of the current paper, but a few key components are discussed below.

South of the U.S.-Mexico border, the Pacific-North America plate boundary developed through three main phases consisting of: (1) transtensional faulting in the area of the future Gulf of California starting 9-10 Ma but possibly as old as 12 Ma, followed by; (2) a shift in the direction of Pacific-North American relative plate motion at ~8 Ma that increased the rate of transtensional faulting and resulted in localization of the plate-boundary in the northern Gulf; and (3) the development of spreading centers at ~6 Ma in the northern Gulf (Bennett and Oskin, 2014; Bennett et al., 2016 and references therein). Thus, if the wide zone of plate-boundary deformation has acted in phase through time, dextral shear in the ECSZ may be expected to have initiated after 12 Ma (possibly ca. 10 Ma), accelerated at 8 Ma, and possibly reorganized and accelerated again at 6 Ma.

The Walker Lane belt (WLB) was described by Stewart (1988) as a belt of NNW-trending mountain ranges that differ from the remainder of the Great Basin (Fig. 1). Although precursor tectonics played a role in development of the belt, Cenozoic dextral faulting (along with sinistral faults in four zones) was a major cause. By this definition, the WLB widens southward from northwest Nevada to the region east of the Sierra Nevada, where it extends east to Las Vegas, and it encompasses the Las Vegas Valley shear zone, which was active ~15-11 Ma (Stewart, 1988). Elsewhere, dextral faulting in the WLB apparently is restricted to inception between 9 and 3 Ma (Faulds et al., 2005; Nagorsen-Rinke et al., 2013). Stewart (1988) noted that the belt includes several highly-extended terranes that are broadly coeval with the WLB; these include Eldorado, the greater Death Valley area, and Yerington complexes. The northern terminus of the WLB has been interpreted to die out near the Oregon border (Faulds et al., 2005) or near Mt. Lassen as complex transpressional transfer westward to the Mendocino Fracture Zone (Sawyer et al., 2013).

Farther north, 16° of clockwise rotation of the Cascades starting ~16 Ma is consistent with dextral shear crossing SW Oregon (Wells and McCaffery, 2013) and ~100 km northward motion of the Sierra Nevada block. Dextral shear in the WLB (42 km; McQuarrie and Wernicke, 2005) may accommodate part of the rotation of the Cascades, although much work is still needed to locate the connecting faults and resolve disparities in timing. West of the SAF, dextral faults parallel to the SAF and east-striking oblique thrust faults are mapped on land, and a deforming zone of submerged crust farther west probably exists. In this area, thinner crust and the possibility for tectonic escape westward may result in kinematics that contrast with those in the Mojave Desert.

Mojave Desert advances and terminology

Pioneering geologists including Hewett, Noble, Troxel, Wright, and Dibblee recognized the presence of numerous northwest-striking strike slip faults in the Mojave Desert. Brady and Dokka proposed that these faults—termed the "Eastern Mojave Shear Zone"—comprise a tectonic boundary between the Mojave and Basin and Range structural domains. Soon thereafter, Dokka and Travis (1990) expanded this concept and changed the name to the "Eastern California Shear Zone". The ECSZ, as noted earlier, is defined as the active set of faults, although the timing was not rigorously defined. Miller and Yount (2002) suggested the term "Mojave strike-slip province" for a broader zone of deformation including the ECSZ and farther west to the Garlock–San Andreas fault intersection because late Pleistocene faults are common west of the ECSZ.

Strike-slip faults east of the ECSZ are poorly dated in most places but widespread (Bedford et al, 2010; Miller, 2012). Limited observations suggest early Quaternary to Pliocene tectonism (Skirvin et al., 1990; Miller and Wooden, 1993). However, farther north the active Stateline fault was proposed to have 30 km of offset and terminate in Ivanpah Valley in an extensional intersection, which started ~5 Ma and was active into Quaternary time (Guest et al, 2007; Mahan et al., 2009). As a result, a view of strike-slip faulting in the Mojave Desert that peers deeper into time than the original ECSZ concept suggests that a much wider zone of dextral faulting needs to be considered.

How old are dextral faults in the Mojave Desert and adjacent regions? The view from the Gulf of California suggests that 12 to 8 Ma transtension may have connected into the Mojave Desert, and that post-8-Ma strike slip faults in the Mojave Desert are likely. Farther north, WLB faults are as old as 9 Ma. If the original definition of WLB is considered, Las Vegas area faults between 15 and 11 Ma should be included. In the Mojave Desert, several constraints indicate that strike-slip faults initiated no earlier than 12-11 Ma: (1) There is no evidence for strike slip control on the basin in which the Barstow Formation (>12.5 Ma) was deposited, nor on older extensional complexes (Glazner et al., 2002). (2) Along the Garlock fault, Loomis and Burbank (1988) argued that a thick sedimentary sequence was related to inception of the fault ~12-10 Ma, although discovery of its offset counterpart in the Summit Range calls that interpretation into question (Frankel et al., 2008). (3) In Fort Irwin, Schermer et al. (1996) demonstrated that fault inception was after deposition of a 10.5 Ma tuff bed. These constraints suggest that dextral faults in the greater Mojave Desert region could be as old as ~12 Ma.

To facilitate discussion of the time-dependent footprint of strike-slip faults in the Mojave Desert region, we propose the following terminology:

The **Eastern California Shear Zone (ECSZ)** is retained for describing the recently active part of the strike-slip system inboard of (east of) the SAF, mostly south of the Garlock fault (i.e., the definition of Dokka and Travis, 1990). We suggest that a useful definition of "recently active" faults is rupture or deformation of widespread deposits that are ~70–100 ka. This definition will include seismically active faults with low recurrence interval.

The **Walker Lane belt (WLB)** is proposed for the full width of the strike slip fault zone in the Mojave Desert including the Stateline fault or even farther east to Las Vegas, and the full extent of dextral shear from Oregon to Mexico (Fig 1).

North of the Garlock fault, the ECSZ as defined above may continue into northern California, but its utility as a subset of the WLB east of the Sierra Nevada is not clear at this time.

Evolution of understanding for strike-slip faults in the Mojave Desert

Our understanding of late Cenozoic fault distribution in the Mojave Desert began with insightful syntheses from geologic mapping studies that first defined patterns of northwest-striking young faults (e.g., Hewett, 1954; Dibblee, 1961). These faults stretch discontinuously from the San Andreas fault to the Garlock fault, but east-striking faults cut parts of the Transverse Ranges and the Fort Irwin area (Hewett, 1954). Garfunkel (1974) presented a kinematic model for dextral shear on most faults of the Mojave Desert, with rigid-block boundary conditions north and south of the Mojave Desert, and predicted that tectonic blocks undergo vertical-axis rotation. The hypothesized 30° counterclockwise rotation of blocks proved wrong, leading to refined kinematic models. Paleomagnetic studies indicated that blocks bounded by northwest-striking faults have undergone little or no rotation, whereas blocks bounded by east-striking sinistral faults have undergone as much as 60° clockwise rotation (e.g., Carter et al., 1987; Luyendyk, 1991; Schermer et. al., 1996).

Dokka and Travis (1990) synthesized knowledge of the geometry, timing, and offset on the known faults of the ECSZ, developing a block model that predicted offsets for all faults, locations of overlapped blocks (transpression),

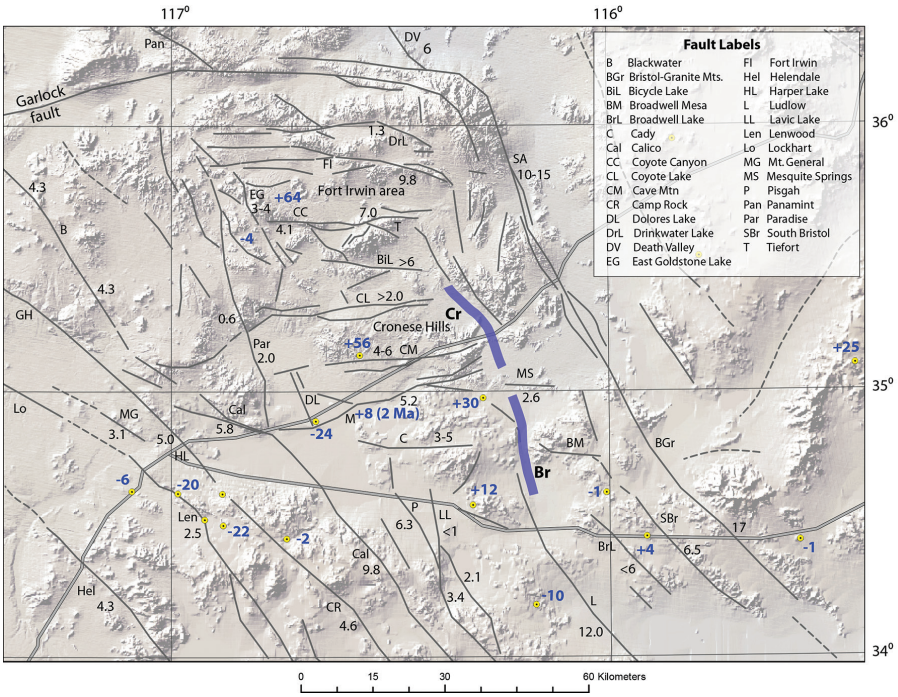

Figure 3. Mojave Desert ECSZ faults showing amount of offset (in km) known along faults (updated in part from Pavlis et al., 1998), and (in bold blue) vertical-axis rotations (Peach Spring Tuff locations shown by yellow dots) updated from Hillhouse et al. (2010). Rotation is + for clockwise, - for counterclockwise. Rotation of +8 is for 2 MY of rotation (Pluhar et al., 1991); others are for early Miocene volcanic rocks. Locations of Cronese (Cr) and Broadwell (Br) lakes troughs are highlighted in blue. Gray lines indicate major roads.

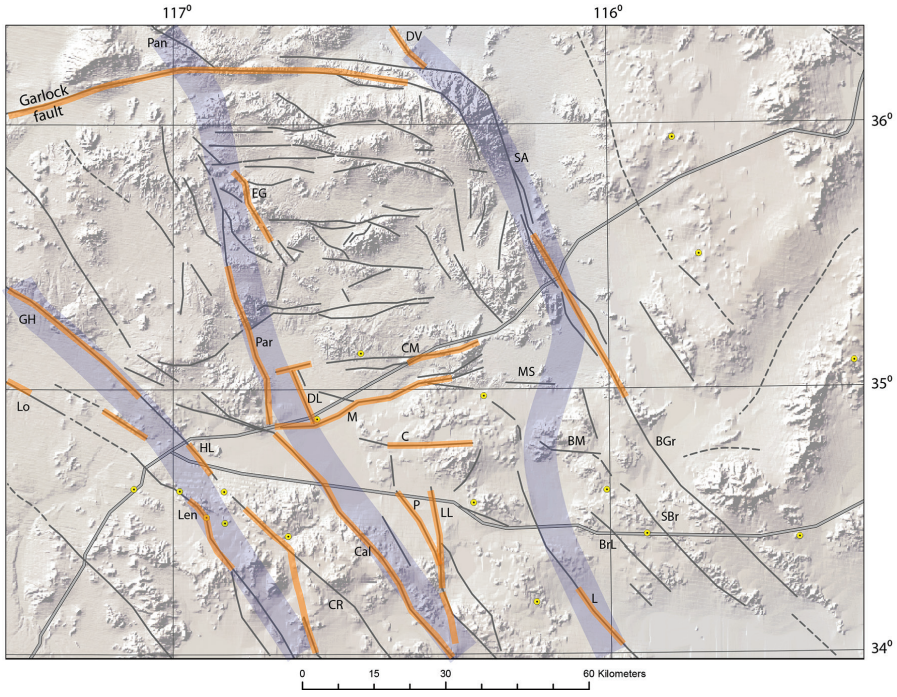

Figure 4. Holocene faults (orange overlay) and possible deep shear zone patterns (blue). Black star show location of Alvord Mountain opal locations in the Cave Mountain fault. Other symbols as in Fig. 3.

and gaps between blocks (transtension). This work made predictions that have been tested, with some confirmed and others refuted. A major advance was analysis of gravity data for the region (Jachens et al., 2002) that showed very few sedimentary basins at block intersections. As a result, the ECSZ is now viewed as transpressional, with contraction from ~010° maximum stress driving not only the strike-slip faulting, but also folds and thrust faults (e.g., Glazner et al, 2002).

Ground ruptures associated with the recent Landers (1992) and Hector Mine (1999) earthquakes in the southern Mojave Desert unexpectedly sliced obliquely NNW across major fault blocks, thus demonstrating that neighboring northwest-striking dextral faults are kinematically linked (e.g., Hauksson et al., 1993). Geologic mapping from the 1930s to 1960s proved inadequate for anticipating the complex rupture patterns of the Landers and Hector Mine earthquakes. Since completion of this early geologic mapping, much has been learned about offset on individual faults, vertical-axis block rotations, ages of key offset rock units along faults, and geodetically determined rates of crustal deformation. However, there have been relatively few advances in the understanding of Quaternary fault networks and associated regional deformation, owing to somewhat limited trenching and paleoseismology studies, limited detailed geologic mapping, and only rare comprehensive studies employing modern concepts of Quaternary pedology and sedimentology, and tectonic geomorphology. The U.S. Geological Survey undertook a series of mapping studies to fill part of this gap in knowledge.

Our regional mapping in the northern Mojave Desert (Miller et al., 2007) focused primarily

on faults that cut Quaternary and Pliocene deposits (Fig. 3). Results verified fault patterns shown on previous maps, and also identified many more faults dissecting blocks that were previously thought to be unbroken. In addition, stratigraphic evidence for the age of latest fault rupture revealed that the spatial distribution of recently active faults in the northern Mojave Desert changed dramatically during the past 200 ka (Miller et al., 2007). Most of the mapped faults were active at the start of this period, then a restricted set was active 30-90 ka, and finally only a few widely spaced zones apparently were active during Holocene time (post-12 ka) (Fig. 3). Our regional mapping spurred more detailed study of several faults from Barstow to Baker, the results of which are partly presented in this volume.

Slip-rate studies focused more attention on the question of which faults are currently the most active, and allowed quantitative comparison of geologic slip rates with geodetic measurements. Oskin et al. (2008) studied a transect of dextral faults through the central ECSZ, and found that the Calico fault (Fig, 3) has the greatest slip rate (~1.6 mm/yr) and that slip rate declines to the east and west. Slip rate for the late Quaternary is approximately half the rate shown by GPS geodesy (10-14 mm/yr; Bennett et al., 2003). Preliminary slip rate data for the late Quaternary are now available for the Cady (0.1 mm/yr; Schmidt and Langenheim, 2015), Manix (0.2–0.6 mm/yr for 3 of 5 strands, Miller unpubl.), and southern Paradise faults (0.04–0.07 mm/yr, Miller unpubl.).

Precursor tectonics

Consideration of faulting as early as 8–12 Ma, or even to 15 Ma near Las Vegas (Stewart, 1988) or 16 Ma in the Cascades (Wells and McCaffery, 2013) requires reevaluation of precursor tectonics and its role in post-10 Ma strike-slip faulting. Extensional terranes occur in many places in the Mojave Desert (Fig. 2), but most of them predate the period of interest. The Barstow Formation and several laterally correlative units that range in age to as young as 14–12 Ma unconformably overlie some of these southerly, early Miocene extensional basin deposits in the central Mojave Desert (Swisher, 1992). These post-extensional deposits preserved in wide, shallow basins have not been recognized as having strike-slip fault controls (Glazner et al., 2002). Farther north, extensional complexes are younger, with ages at Eldorado that are as young as ~14–11 Ma (Anderson, 1971) and at Shadow Valley ~13.5 to ~ 10 Ma (Friedman et al., 1996).

Difficulties in separating precursor basin deposits from syn-WLB orogenic deposits arise because both may be coarse-grained and are rarely well dated, and in many places WLB orogenic sediments are localized in small basins. Unconformities that record inception of WLB faults are generally subtle. Presumably, low-relief relict topography was disrupted by faulting that caused only localized sedimentation, which is generally poorly preserved. Exceptions include long-lived low areas that received sediments for long periods of time in and near the Fort Irwin zone of sinistral faults (Miller et al., 2011). Other examples include the 5.4 Ma basalt flows at Broadwell Mesa, with overlying and underlying sediment that records continuing folding astride a sinistral fault (Miller et al., this volume) and basins within Fort Irwin that contain ~10 Ma tuffs (Schermer et al., 1996; Miller and Yount, 2002) and may record early WLB activity.

Reassessment of fault patterns in space and time based on Quaternary mapping

A provocative result of regional study (Miller et al., 2007) is the discovery of several previously unrecognized ~north-striking faults, many of them in or alongside the Fort Irwin area (Fig. 5). Although this group includes faults striking NNW, due north, and NNE, the great majority of them strike NNW. Most of the faults are best revealed by deformation of Quaternary materials and less so by offsets of bedrock. Similar orientations for the NNW-striking ruptures of the Landers and Hector Mine earthquakes may indicate that new north-striking faults are forming in the Mojave Desert. However, ~north-striking faults are more common than previously

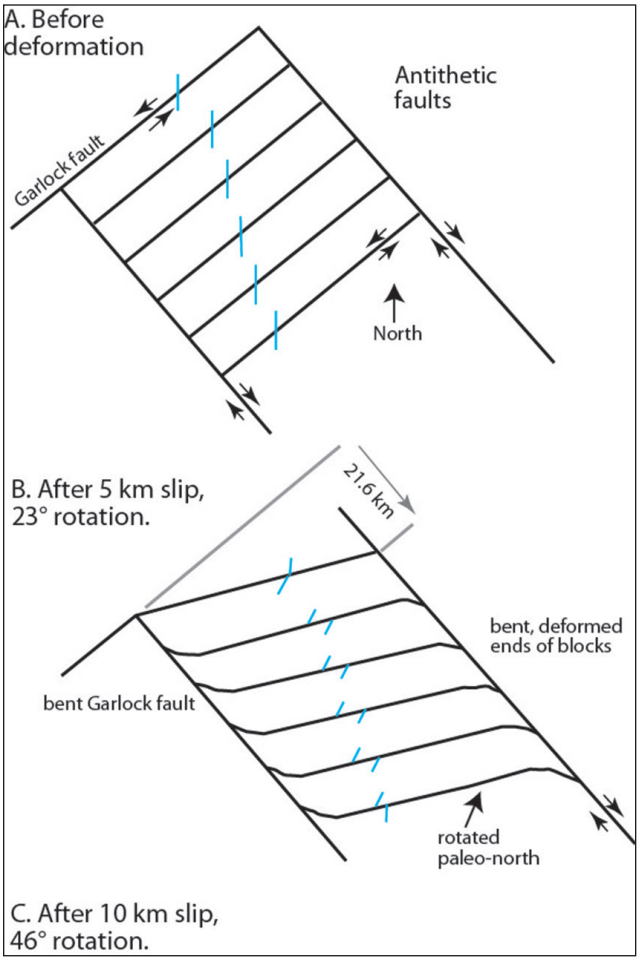

Figure 5. Simple geometric model for sinistral and dextral fault slip associated with vertical-axis block rotations in the Fort Irwin area, modified from Schermer et al. (1996).

recognized, and they form integrated fault zones that probably have been active during much of Quaternary time. Although these faults appear to be relatively newly developed (because bedrock offsets are small compared to many of the block bounding faults previously mapped), Miller et al. (2007) did not establish ages of inception for the faults.

Subsequent detailed study has clarified some of the faults (e.g., Miller et al., this volume). The central Paradise fault northwest of the Paradise Range offsets early Pleistocene deposits more than late Pleistocene deposits, indicating a long Quaternary history with multiple rupture events. Total offset shown in Fig. 3 is based on offset metamorphic rocks in the Paradise Range and aeromagnetic anomalies farther south. North of the Cronese Hills (Fig. 3), shallowly dipping fluvial sand and gravel that contains a ~3.5 Ma ash bed lie near their depocenter, as represented by playa sediment (Miller et al., this volume). However, just 8 km to the east the modern north-trending Cronese trough, over 330 m lower in elevation, is framed by poorly exposed north-striking faults. A similar relation appears to hold in the linear Broadwell Lake trough, with stranded ~5.5 Ma deposits perched high in the Bristol Mountains above Broadwell Lake Valley (Fig. 3). Together, these field relations indicate that many NNW-striking faults have been active during the late Pliocene into the Quaternary, and that they may have formed during Pliocene time.

One striking finding is that many faults with Quaternary expression deform the middle Pleistocene deposits, shown in Figure 4, and fewer deform younger Quaternary deposits (Miller et al., 2007). For this analysis, they evaluated fault history as recorded by multiple ages of deformed deposits, including Pleistocene to Pliocene gravels, and found that most Holocene faults exhibit evidence for multiple ruptures and have been active throughout the late Quaternary time period evaluated. Typical observations that indicate long fault activity are progressively higher scarps in older deposits, multiple slopes on scarps indicating several ruptures, and adjacent highly deformed Pleistocene to Pliocene deposits. It was previously suggested that strike-slip faulting started in eastern areas of the Mojave Desert and migrated westward (Dokka and Travis, 1990; Howard and Miller, 1992). However, the spatial-temporal patterns of faulting determined by our studies suggest that westward younging of faults best applies south of the Mesquite Spring fault and east of the Calico fault. Elsewhere, the pattern is one of reduced area of faults deforming late Pleistocene and early Holocene deposits (Fig. 4). Rather than displaying a simple younging-westward pattern, it indicates a restriction of faults into three relatively widely spaced belts.

The Holocene fault belts include (Fig. 4): (1) the Lockhart and Harper Lake faults in the west, (2) the Paradise and East Goldstone faults farther east, and (3) the Manix and Mesquite Spring faults in the east. Fault belt 1 includes numerous Holocene scarps on stretches of the Lockhart, Lenwood, Harper Lake, Camp Rock, and Mt. General faults. Fault belt 2 includes the Calico fault, which has prominent Holocene scarps and high slip rate (Oskin et al., 2007) but displays no evidence for Holocene rupture northwest of the area where the Manix fault projects west to it (Miller et al., 2007). Rather, the Paradise fault zone north of this intersection has several Holocene scarps, as does the East Goldstone Lake fault. Holocene playas and a few isolated scarps north of Goldstone Lake suggest that Holocene deformation continues north of Goldstone Lake. Fault belt 3 consists of the Manix fault system, which is composed of two to three splays in many places, and the Mesquite Springs fault. The Manix faults are not through-going, but rather step left in scallop-shaped segments. The faults cannot be traced east of Afton Canyon, but farther southeast the Mesquite Spring fault begins and it extends eastward at least 20 km before it is buried by eolian sand. The Manix–Mesquite Spring fault belt exhibits several Holocene scarps as well as large offsets of older Pleistocene deposits and Pliocene deposits (Reheis et al., 2007), and ruptured during the Manix earthquake in 1947 (Richter, 1947). Deformed early Holocene sediment along the Soda–Avawatz fault appears to link with the east-trending part of belt 3.

If the three belts of Holocene faulting are correctly identified, active faults in the northern Mojave Desert have been reduced in number with time. Intervening broad areas may consist of inactive faults or faults with low-slip-rate, large recurrence interval, or more off-fault deformation by folding and tilting than they did in the middle Pleistocene.

The Walker Lane belt in the Mojave Desert: how it works

The WLB in the Mojave Desert (Fig. 2) is geometrically non-uniform in terms of fault spacing and orientation, as it is farther north (e.g., Stewart, 1988). The primary fault geometries are those of dextral NW-striking faults; sinistral faults are subordinate and tend to strike close to easterly. Early work focused on these patterns in active parts of WLB (Carter et al, 1987; Luyendyk et al., 1991), where panels of sinistral faults define east-trending fault blocks framed by dextral faults. Fault block rotation models applied to these panels of sinistral faults use the bookshelf model (Fig. 5), in which a stack of books is tilted to form a set of parallel, inclined books; corresponding simple calculated parameters such as block width, slip on bounding faults, and angular rotation, can be shown to be co-dependent quantities. Because rotation can be measured in some cases by paleomagnetic methods, values for slip can be calculated or, if known, compared with expected values from rotations (e.g., Schermer et al., 1996). Misfits at the southern and northern margins of rotated panels are common, and lead to ambiguities such as south of the Manix and Cady faults (Fig. 3). Here, rotations appear to decline southward from the Manix fault, and

yet faults are parallel. The southern blocks cannot rotate more slowly than the northern ones, or misfits between faults would be common. Did the southern blocks start behaving in parallel with the northern ones only after several m.y. of rotation on the northern ones?

Total offset along faults provides a first-order comparison among faults but is more meaningful when duration of faulting and slip rate changes with time are known. Without a knowledge of these factors, it is difficult to rigorously compare faults using total offset. These difficulties are compounded with the older WLB faults which have poor exposure and fewer datable stratigraphic markers, in general. Some simple relations should hold, such as panels of dextral faults bounded on the north or south by rotating sinistral panels should all have the same offset. Yet they typically do not: Compare the Camp Rock, Calico, and Pisgah faults (Fig. 3), all of which butt southward into the sinistral Pinto Mountain fault. The possibility that the inception of ~north-striking faults is later, and connects across others, complicates geometries and patterns.

What actually drives strain in the WLB? By mapping, we examine the manifestations of the brittle upper ~10 km of crust, which is probably driven by deep-seated shear in zones of uncertain configuration (Behr and Platt, 2014). Studies that examine the coupling between brittle and ductile crust will provide important constraints. Are zones of active faults in the central Mojave Desert a clue? Perhaps they mimic the deeper shear zones (Fig. 4). Inception of the Walker Lane Belt in the Mojave Desert area

Inception of faulting is difficult to determine yet important for linking tectonism to global and regional events, and also for interpreting total offset and slip rates for faults. Model-driven inferences from the perspective of fault development in the Gulf of California indicates inception of dextral faults ~11-6 Ma (Bennett et al, 2016). Similar inferences driven by models of uplift and rotation of the Transverse Ranges suggest younger inception, ~5-2 Ma. North of the Mojave Desert, faults are known to have started between 9 and 3 Ma (Faulds et al., 2005). Henry et al. (2007) and Nagorsen-Rinke et al. (2013) showed Pliocene inception ages in this area. Geologic interpretations of sedimentary basins along the Garlock fault yielded a ~12-10 Ma inception (Loomis and Burbank, 1988), but this interpretation is called into question by discovery of its offset counterpart in the Summit Range (Frankel et al., 2008). Finally, Schermer et al., (1996) showed that a 10.5 Ma tuff bed is offset by Fort Irwin fault as much as older rocks.

South of Alvord Mountain and elsewhere, white to bluish white opal is common in faults strands. Work (Nuriel et al., submitted) with sampled opaline silica from several outcrops along the Cave Mountain fault system (Fig. 3) shows that the opal is deposited by meteoric water. Individual fault outcrops are 2 to 15 meters long, and exhibit highly brecciated and sheared bands of opal material. The opal is most common in poorly dated late Cenozoic conglomerates, but also found in the late Miocene Barstow Formation (Byers, 1960), for which the ages should provide information on the inception faulting.

Opal U-Pb analyses were conducted on the SHRIMP-RG ion microprobe co-operated by U.S. Geological Survey and Stanford University. Calculated ages for opal are based on multiple SHRIMP-RG spot analyses for each opal phase. The U-Pb age was determined by: (1) calculating an equilibrium age based on $^{238}U/^{208}Pb$ vs. $^{206}Pb/^{208}Pb$ on a Tera-Wasserburg concordia, and (2) calculating the $^{206}Pb^*/^{238}U$ age based on weighted average of spot analyses that were corrected for common-lead. The results for three opal samples are: 10.13 ± 0.37 Ma, 11.29 ± 0.77 Ma, and 10.62 ± 0.58 Ma. The ages require that the opal injected a fracture before ~10 Ma, indicating that inception of faulting predates 10 Ma.

It is possible to use rotation rates for sinistral blocks to estimate the age of inception of faulting. The Mojave River Formation (Nagy and Murray,1991; Pluhar et al., 1991) spans 1.5 m.y. from ~0.9 Ma to 2.5 Ma, on the basis of tephra bed correlations. Paleomagnetically determined rotation rates convincingly demonstrate vertical-axis rotation at about 4°/ m.y. If this value is assumed to represent steady state and applied to the total rotation of the northern Cady Mountains (Fig. 3, 30°; Hillhouse et al., 2010) inception of the fault is estimated to be about 7.5 Ma.

We conclude that the inception of sinistral faulting was 10–11 Ma, and any dextral faults coordinated with those blocks must have a similar initiation age.

Discussion

The ECSZ in the Mojave Desert has been a productive concept. I suggest that it be extended in time to include faults no longer active, and to provide compatibility with strike-slip provinces north and south of the Mojave Desert. By including faults that are as old as late Miocene, I suggest that the entire spatial and temporal footprint of strike slip faulting inboard of the SAF can be considered as a regionally extensive zone of related faults that stretches from southern Oregon to the Gulf of California, and I suggest the term "Walker Lane belt" for this diffuse zone of faults.

Fault inception in the ECSZ at about 10–11 Ma, as dated by opal in faults, is compatible with many observations and predictions for fault inception to the north and south, especially if the Las Vegas area is included in the WLB (Stewart, 1988). This inception is 5–6 Ma younger than that predicted by Cascades rotation much farther to the north and ~7 m.y. younger than inceptions ages documented in some parts of the WLB. Dating opal in faults may be a productive approach to improving data for fault inception, particularly in the Mojave Desert where opal is U-rich.

Connecting active slip from southern Death Valley to the transect of faults west of Bristol Lake is problematic.

No through-going faults are mapped, and although young sediment is warped, few faults between Ludlow and Death Valley display Holocene scarps. Does awkward fault geometry preclude rupture, leading to folding and warping, or are faults active but at very low slip rate or recurrence interval? Can a reorganized deep ductile shear zone, below a subhorizontal discontinuity, drive the upper crust faults into new patterns?

Several important questions remain, including:

- Do Eldorado and Shadow Valley extensional terranes interact with early WLB, and if so, how did this interaction work?
- How does transtensional faulting in the Gulf of California area transition to the transpressional faulting of the Mojave Desert, and why?
- What is the timing and kinematic role of NNW-striking faults in the ECSZ?
- Do faults with ~10 Ma inception undergo changes in slip rate or do they have steady rates?
- Where are faults east of the ECSZ and how do they couple to parts of the WLB to the northwest and southeast?

In addition to the traditional approaches that have been applied to identify faults and refine the timing, rates, and kinematics of fault motion in the ECSZ and larger WLB, there are opportunities for applying newer methods, such as more precise geochronology and use of high-resolution topography to evaluate landscape evolution, to address the questions described here. In addition, compiling the detailed mapping that has been completed since Dokka and Travis (1990) defined the ECSZ is a way to explore the details at a more regional scale.

Acknowledgements

I am pleased to acknowledge the sharing of data and ideas by the late David Bedford, as well as by Joe Andrews, Scott Bennett, Roland Brady, David Buesch, Andy Cyr, Stephanie Dudash, Janet Harvey, Vicki Langenheim, Chris Menges, Geoff Phelps, Bob Reynolds, Kevin Schmidt, and Joann Stock. Thank you to careful reviewers Becky Dorsey and Andy Cyr, who improved the manuscript considerably. Work underway with Perach Nuriel, Geological Survey of Israel, has firmly demonstrated the ~10 Ma inception of many ECSZ faults and is changing views of the ECSZ.

References

Anderson, R.E., 1971, Thin skin distension in Tertiary rocks of southeastern Nevada: Geological Society of America Bulletin, v. 82, p. 43-58.

Bedford, D.R., Miller, D.M., and Phelps, G.A., 2010, Surficial geologic map of the Amboy 30' by 60' quadrangle, San Bernardino County, California: U.S. Geological Survey Scientific Investigations Map 3109, pamphlet 26 p., scale 1:100,000, available at http://pubs.usgs.gov/sim/3109/.

Behr, W.M., and Platt, J.P., 2014, Brittle faults are weak, yet the ductile middle crust is strong: Implications for lithospheric mechanics: Geophysical Research Letters, v. 41, p. 8067–8075, doi:10.1002/ 2014GL061349.

Bennett, R.A., Wernicke, B.P., Niemi, N.A., Friedrich, A.M., and Davis, J.L., 2003, Contemporary strain rates in the northern Basin and Range province from GPS data: Tectonics, v. 22, p. 1008, doi: 10.1029/2001TC001355.

Bennett, S.E.K., and Oskin, M.E., 2014, Oblique rifting ruptures continents: Example from the Gulf of California shear zone: Geology, v. 42, p. 215–218, doi: 10.1130/G34904.1.

Bennett, S.E.K., Darin, M.H., Dorsey, R.J., Skinner, L.A., Umhofer, P.J., and Oskin, M.E., 2016, Animated tectonic reconstruction of the Lower Colorado River region: Implications for Late Miocene to present deformation, *in* Going LOCO, Reynolds, R.E. ed.: California State University Desert Studies Center 2016 Desert Symposium, p.73-86.

Carter, J.N., Luyendyk, B.P., and Terres, R.R., 1987, Neogene clockwise rotation of the eastern Transverse Ranges, California, suggested by paleomagnetic vectors: Geological Society of America Bulletin, v. 98, p. 199-206.

Dibblee, T.W., Jr., 1961, Evidence of strike-slip movement on northwest-trending faults in the western Mojave Desert, California: U.S. Geological Survey Professional Paper 424-B, p. B197-199.

Dokka, R.K., and Travis, C.J., 1990, Role of the eastern California shear zone in accommodating Pacific-North American plate motion: Geophysical Research Letters, v. 17, p. 1323-1326.

Faulds, J.E., Henry, C.D., and Hinz, N.H., 2005, Kinematics of the northern Walker Lane: An incipient transform fault along the Pacific–North American plate boundary: Geology, v. 33, p. 505–508, doi: 10.1130/G21274.1.

Frankel, K.L., and 17 others, 2008, Active tectonics of the eastern California shear zone, in Duebendorfer, E.M., and Smith, E.I., eds., Field guide to volcanoes, faults, reefs, dinosaurs, and possible glaciation in selected areas of Arizona, California, and Nevada: Geological Society of America Field Guide 11, p. 43-81

Friedmann, S. J., Davis, G. A., and Fowler, T. K., 1996, Geometry, paleodrainage, and geologic rates from the Miocene Shadow Valley supradetachment basin, eastern Mojave Desert, California, *in* Beratan, K. K., ed., Reconstructing the History of Basin and Range Extension Using Sedimentology and Stratigraphy: Boulder, Colorado, Geological Society of America Special Paper 303, p.85-105.

Garfunkel, Z., 1974, Model for the late Cenozoic tectonic history of the Mojave Desert, California, and its relation to adjacent areas: Geological Society of America Bulletin, v. 85, p. 1931-1944.

Glazner, A.F., Walker, J.D., Bartley, J.M., and Fletcher, J.M., 2002, Cenozoic evolution of the Mojave black of southern California, *in* Glazner, A.F., Walker, J.D., Bartley, J.M., eds., Geologic evolution of the Mojave Desert and southwestern

Basin and Range: Geological Society of America Memoir 195, p. 19-41.

Guest, B, Niemi, N., and Wernicke, B., 2007, Stateline fault system: A new component of the Miocene-Quaternary Eastern California Shear Zone. Geological Society of America Bulletin, v.119, p.1337-1346.

Hardebeck, J.L., and Hauksson, E., 1999, Roles of fluids in faulting inferred from stress field signatures: Science, v. 285, p. 236-239.

Hauksson, E., Jones, L.M., Hutton, K., and Eberhart-Phillips, D., 1993, The 1992 Landers earthquake sequence: Seismological observations: Journal of Geophysical Research, v. 98, p. 19835-19858.

Henry, C.D., Faulds, J. E., dePolo, C.M., 2007, Geometry and timing of strike-slip and normal faults in the northern Walker Lane, northwestern Nevada and northeastern California: Strain partitioning or sequential extensional and strike-slip deformation?: *in* Till, A.B., Roeske, S.M., Sample, J.C., and Foster, D.A., eds., Exhumation Associated with Continental Strike-Slip Fault Systems: Geological Society of America Special Paper 434, p. 59–79, doi: 10.1130/2007.2434(04).

Hewett, D.F., 1954, General geology of the Mojave Desert region, California: *in* Jahns, R.H., ed., Geology of southern California: Californian Division of Mines and Geology, Bulletin 170, v. II, p. 5-20.

Hillhouse, J.W., Miller, D.M., and Turrin, B.D., 2010, Correlation of the Peach Spring Tuff with the geomagnetic polarity time scale and new constraints on tectonic rotations in the Mojave Desert, California, *in* Reynolds, R.E., and Miller, D.M., eds., Overboard in the Mojave: Desert Studies Consortium, California State University Fullerton, p.124-147.

Howard, K.A., and Miller, D.M., 1992, Late Cenozoic faulting at the boundary between the Mojave and Sonoran blocks: Bristol Lake area, California, *in* Richard, S.M., ed., Deformation associated with the Neogene eastern California shear zone, southwestern Arizona and southeastern California: Redlands, CA, San Bernardino County Museum Special Publication 92-1, p. 37-47.

Jachens, R.C., Langenheim, V.E., and Matti, J.C., 2002, Relationship of the 1999 Hector Mine and 1992 Landers fault ruptures to offsets on Neogene faults and distribution of late Cenozoic basins in the eastern California shear zone: Bulletin Seismological Society America, v. 92, p. 1592–1605.

Jachens, R.C., and Langenheim, V.E., 2014, Gravity survey and interpretation of Fort Irwin and vicinity, Mojave Desert, California: in Buesch, D.C., ed., Geology and geophysics applied to groundwater hydrology at Fort Irwin, California: U.S. Geological Survey Open File Report 2013-1024H, 15 p.

Loomis, D., and Burbank, W., 1988, The stratigraphic evolution of the El Paso basin, southern California: Implications for the Miocene development of the Garlock fault and uplift of the Sierra Nevada, Geological Society of America Bulletin, v. 100, p. 12-28.

Luyendyk, B.P., 1991, A model for Neogene rotations, transtension and transpression in southern California: Geological Society of America Bulletin, v. 103, p. 1528-1536.

Mahan, K.H., Guest, B., Wernicke, B., and Niemi, N.A., 2009, Low-temperature thermochronologic constraints on the kinematic history and spatial extent of the Eastern California Shear Zone. Geosphere, v. 5, p. 483-495.

McQuarrie, N., and Wernicke, B.P., 2005, An animated tectonic reconstruction of southwestern North America since 36 Ma: Geosphere, v. 1, p. 147–172, doi:10.1130/GES00016.1.

Miller, D.M., 2012, Surficial geologic map of the Ivanpah 30' x 60' quadrangle, San Bernardino County, California and Clark County, Nevada: U.S. Geological Survey Scientific Investigations Map 3206, pamphlet 14 p., scale 1:100,000, accessed at https:pubs.usgs.gov/sim/3206.

Miller, D.M., and Wooden, J.L., 1993, Geologic map of the New York Mountains area, California and Nevada: U.S. Geological Survey Open File Report 93-198, 10 p., scale 1:50,000.

Miller, D.M., and Yount, J.L., 2002, Late Cenozoic tectonic evolution of the north-central Mojave Desert inferred from fault history and physiographic evolution of the Fort Irwin area, California: Geological Society of America Memoir, 195, p. 173-197.

Miller, D.M., Dudash, S.L., Green, H.L., Lidke, D.J., Amoroso, L., Phelps, G.A., and Schmidt, K.M., 2007, A new Quaternary view of northern Mojave Desert tectonics suggests changing fault patterns during the late Pleistocene, *in* Miller, D.M., and Valin, Z.C., editors, Geomorphology and tectonics at the intersection of Silurian and Death Valleys, southern California: U.S. Geological Survey Open File Report 2007-1424, p. 157-171, available at http://pubs.usgs.gov/of/2007/1424/of2007- 1424.pdf

Miller, D.M., Reheis, M.C., Wan, E., Wahl, D.B., Olson, H., 2011, Pliocene and early Pleistocene paleogeography of the Coyote Lake and Alvord Mountain area, Mojave Desert, California, *in* Reynolds, R.E., ed., The incredible shrinking Pliocene: Desert Studies Consortium, California State University, Fullerton, p. 53-67.

Miller, M.M., Johnson, D.J., Dixon, T.H., and Dokka, R.K., 2001, Refined kinematics of the eastern California shear zone from GPS observations: Journal of Geophysical Research, v. 106, p.2245-2264.

Nagorsen-Rinke, Sarah, Lee, Jeffrey, Calvert, Andrew , 2013, Pliocene sinistral slip across the Adobe Hills, eastern California-western Nevada: Kinematics of fault slip transfer across the Mina Deflection: Geosphere v. 9; p. 37–53; doi:10.1130/GES00825.1.

Nagy, E. A., and Murray, B. C. , 1991, Stratigraphy and intra-basin correlation of the Mojave River Formation, central Mojave desert, California, San Bernardino County Museum Assoc. Quarterly, v. 38, p. 5-30.

Oskin, M., Perg, L., Blumentritt, D., Mukhopadhyay, S., and Iriondo, A., 2007, Slip rate of the Calico fault: Implications for geologic versus geodetic rate discrepancy in the eastern California shear zone: J. Geophysical. Res., 112, B03402, doi:10.1029/2006JB004451.

Oskin, M., Perg, L., Shelef, E., Strane, M., Gurney, E., Singer, B., Zhang, X., 2008, Elevated shear zone loading rate during an earthquake cluster in eastern California: Geology, v. 36, p.507-510.

Pavlis, T. L., L. Serpa, B. Troxel, M. Dean, T. Hartman, and T. Rodosta, 1998, Late Cenozoic deformation in eastern Fort Irwin and its significance for the tectonic history of the Garlock fault system: San Bernardino County Museum Association Quarterly, v. 45, p. 77-83.

Pluhar, C. J., Kirschvink, J. L., and Adams, R. W., 1991, Magnetostratigraphy and clockwise rotation of the Plio-Pleistocene Mojave River formation, central Mojave desert, California, San Bernardino County Museum Assoc. Quarterly, v. 38, p. 31-42.

Reheis, M.C., Miller, D.M., and Redwine, J.L., 2007, Quaternary stratigraphy, drainage-basin development, and geomorphology of the Lake Manix basin, Mojave Desert: U.S. Geological Survey Open-File Report 2007–1281, 31 p.

Richter, C. F., 1947, The Manix (California) earthquake of April 10, 1947: Bulletin of the Seismological Society of America, v. 37(8), p. 171-179.

Sauber, J., Thatcher, W., Solomon, S., and Lisowski, M., 1994, Geodetic slip rate for the eastern California shear zone and the recurrence time of Mojave Desert earthquakes: Nature, v. 367, p. 264-266.

Sawyer, T.L., 2013, The Northern California shear zone—Missing link in the Pacific-North American plate transform margin: Geological Society of America, Cordilleran GSA Section Meeting, 2013 Abstracts with Programs, v. 45, No. 6, p. 59.

Schelle, H., and Grunthal, G., 1996, Modeling of Neogene crustal block rotation: Case study of southeastern California: Tectonics, v. 15, p. 700-710.

Schermer, E.R., Luyendyk, B.P., and Cisowski, S., 1996, Late Cenozoic structure and tectonics of the northern Mojave Desert: Tectonics, v. 15, p. 905-932.

Skirvin, T.M., and Wells, S.G., 1990, Late Cenozoic structure, geometry, and landscape evolution of the Old Dad Mountain area, California: San Bernardino County Museum Special Publication, p. 73-88

Stewart, J.H., 1988, Tectonics of the Walker Lane belt, western Great Basin: Mesozoic and Cenozoic deformation in a zone of shear, *in* Ernst, W.G., ed., Metamorphism and Crustal Evolution of the Western United States, Rubey vol. VII: Englewood Cliffs, New Jersey, Prentice Hall, p. 683–713.

Swisher, C.C. III, 1992, $^{40}Ar/^{39}Ar$ dating and its application to the calibration of the North American Land Mammal Ages: [Ph.D. thesis] University of California Berkeley, 184 p.

Wells, R. E., and Hillhouse, J. W., 1989, Paleomagnetism and tectonic rotation of the lower Miocene Peach Springs Tuff: Colorado Plateau, Arizona, to Barstow, California: Geological Society of America Bulletin, v. 101, p. 846-863.

Wells, R.E., and McCaffrey, Robert, 2013, Steady rotation of the Cascade arc: Geology, v. 41, p. 1027–1030. doi:10.1130/G34514.1

The Eastern California Shear Zone, Mojave Desert, California

Michael O. Woodburne
Department of Geological Sciences, University of California, Riverside 92521

As summarized by Woodburne (2015), the Eastern California Shear Zone (Fig. 1) was active in the Mojave Desert region from about 7 Ma, concomitant and likely associated with oblique extensional opening of the northern Gulf of California. The present report brings additional information to bear on the topic. Whereas overall it appears that Eastern California Shear Zone (ECSZ) tectonism began earlier on the east than the west, generally concordant with the proposal of Dokka and Travis (1990), present evidence suggests a bit of diversity in that regard (Figs. 2, 3).

The Eastern California Shear Zone was originally defined by Dokka and Travis (1990) as the network of faults in the Mojave Desert and adjacent parts of the Death Valley region that comprised a regional zone of diffuse dextral shear. As shown in Fig. 1 the ECSZ is bounded on the north by the Garlock fault, on the west and south by the San Andreas fault, on the south by the Pinto Mtn. fault. The eastern boundary was originally shown as the Mesquite Valley Disturbed Zone and the Granite Mtn. fault, but subsequently (Guest et al., 2007) has been extended eastward to the State Line fault system (SLFZ). Note that the Mesquite Valley Disturbed Zone of Dokka and Travis (1990; MVDZ in Fig. 3), is different than the Mesquite segment of the SLFZ of Guest et al., 2007; SLFZ on Figure 3). Dokka and Travis (1990) considered the ECSZ to be connected to the San Andreas fault system and likely to have accommodated significant (9-14%) of the total shear related to tectonic interaction between the Pacific and North American plates since about 10.6 Ma (see also Dickinson, 1996).

Dokka and Travis (1990) also noted that northwest-striking right-slip faults of the Mojave Desert are (1) discontinuous, with only the Calico–Blackwater fault spanning the entire Mojave Desert (Fig. 3; see also Oskin and Iriondo, 2004), (2) the faults terminate before reaching the Garlock fault, (3) faults south of an irregular line from near Barstow eastward to Ludlow and Soda Lake are continuous, well developed, and with a cumulative slip of >40 km; faults to the north are discontinuous, with <12 km of right slip; and (4) show a northwestward decrease in net slip along most faults.

Dokka and Travis (1990) also proposed that post middle Miocene faulting is partitioned into 6 domains (Fig. 3), which likely deformed and rotated independently of each other; overall deformation was considered to have been on the order of 65 km since the middle Miocene (i.e., the last 11 m.y.). Figure 3 shows the domains, to which has been added the apparent age of early tectonism based on the sedimentary and volcanic data of Fig. 2, and slip magnitudes after Dokka and Travis (1990).

The age and timing of faulting have been difficult to determine. According to Dokka and Travis (1990), the original estimation of the inception of faulting was based on the Calico–Blackwater fault cutting a 13.4 $\pm$ 04 Ma ash of the Barstow Formation, but data developed in individual tectonic sites (Fig. 2) suggests that tectonism, and presumably faulting, began about 5–6 Ma in the older examples, and from about 3 Ma in younger ones. Mahan

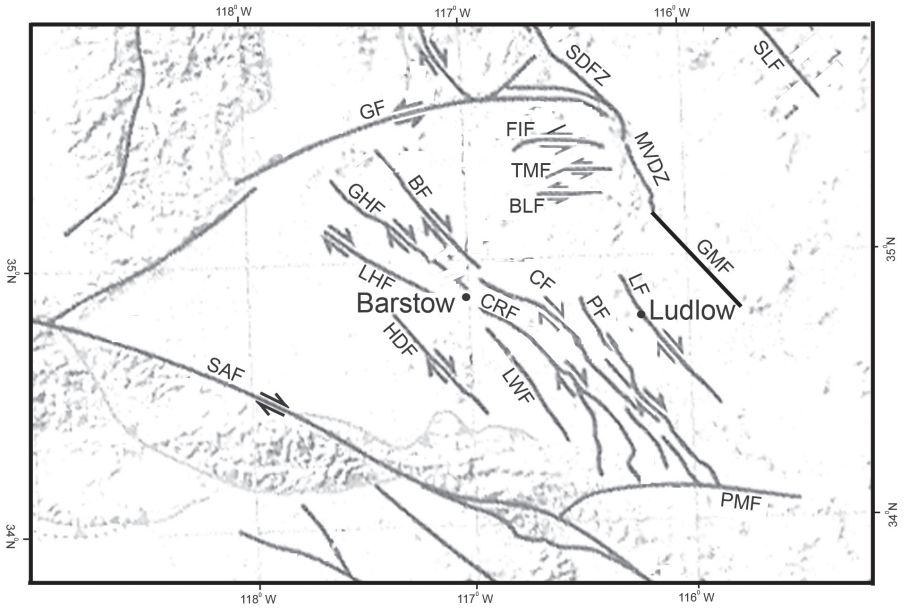

Figure 1. The Eastern California Shear Zone, showing major faults, including the Stateline fault on the east. Modified from Guest et al. (2007; Fig. 1A). Fault names: BF – Blackwater fault; BLF – Bicycle Lake fault; CF – Calico fault; CRF – Camp Rock fault; FIF – Fort Irwin fault; GF – Garlock fault; GHF – Gravel Hills fault; GMF – Granite Mountains fault; HDF – Helendale fault; LF – Ludlow fault; LHF – Lockhard fault; LWF - Lenwood fault; MVDZ – Mesquite Valley Disturbed Zone; PF - Pisgah fault; PMF – Pinto Mountain fault; SAF – San Andreas fault; SDFZ – Southern Death Valley fault zone; SLFZ – Stateline fault zone. Arrows show sense of movement.

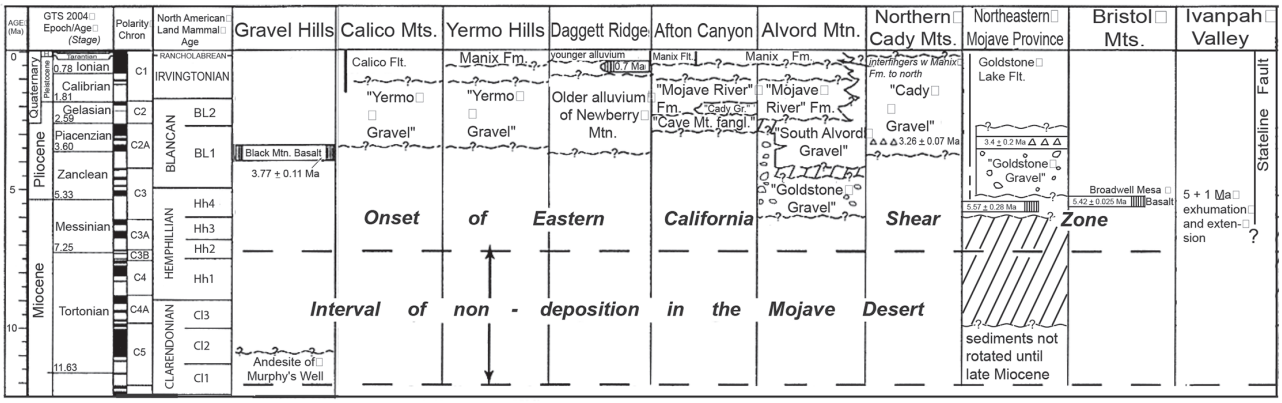

modified from Woodburne (2015, fig. 2)

Figure 2. Late Neogene nonmarine stratigraphy, central Mojave Desert, California. Modified from Woodburne (2015, Fig. 2), with Bristol Mts. and Ivanpah Valley added. Bristol Mts. is after Buesch and Phelps (2016); Ivanpah Valley after Mahan et al. (2009). Sedimentary units discussed in Woodburne (2015).

et al. (2009) suggested that about 30 km of northwest slip on the southern Stateline fault took place during the past 13 Ma, but more likely started after about 6 Ma (Figs. 2, 3).

Whereas Dokka and Travis (1990) focused on a connection between the ECSZ and the San Andreas fault, recent emphasis has been on the tectonic evolution of the Gulf of California. The Gulf of California shear zone was active from about 8 Ma, due to a change in Pacific–North American relative plate motion at that time (Bennett et al., 2013, 2016; Bennett and Oskin, 2014; Darin et al., 2016). Initiation of fault zones in the northern Gulf of California–Salton Trough oblique rift system was followed by widespread marine incursion at ~6.3–6.5 Ma (McDougall, 2008; Dorsey et al., 2011) and reached as far northwestward (McDougall et al., 1999) as San Gorgonio Pass, California (Fig. 4). As noted by Bennett and Oskin (2014), the marine opening is associated with the offset of tuffs dated at just about 6 Ma (6.01 Ma), such offset having been accomplished by elements of the San Andreas fault system in the northern part of the Gulf region. The above lead to the idea that the SAF system was localized (= began its present location) in the Salton Trough region from about 8 Ma, and certainly by 6 Ma, coeval with the initiation of the Gulf of California shear zone in the northern Gulf region (Oskin et al., 2001; Oskin and Stock, 2003a, b; Bennett et al., 2015; Darin et al., 2016). This is taken to support the present working hypothesis that the ECSZ and the adjacent San Andreas fault system were synchronously operational from about 8–6 Ma and likely interrelated.

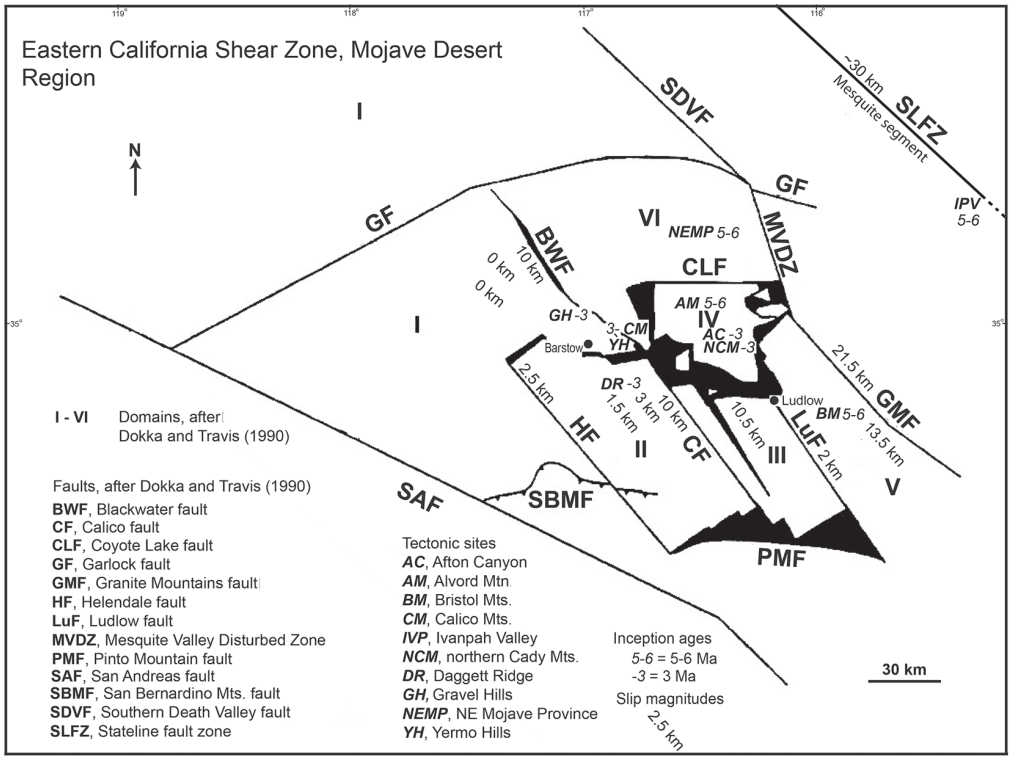

Figure 3, Eastern California Shear Zone, Mojave Desert Region. Tectonic Domains are shown as I-VI, faults labeled, and slip magnitudes after Dokka and Travis (1990, Fig. 5, and Table 1). Tectonic sites and inception ages from this paper. SLFZ follows Mahan et al. (2009). Slip magnitudes for faults follows Dokka and Travis (1990; Table 1). The 13.5 km, slip magnitude in Domain V refers to the Bristol Mts. fault; the 10.5 km magnitude in Domain III to the Pisgah fault, the 3 km and 1.5 km magnitudes in Domain II refer to the Camp Rock and Lenwood faults, respectively, and the 0 km magnitudes in Domain 1 refer to the Gravel Hills (to southwest) and Lockhart faults, respectively. Map location on un-labeled faults follows Dokka and Travis (1990, Fig. 2).

Additional evidence for the northern extension of marine conditions is provided by the Bouse Formation in the Blythe Basin of the Colorado River corridor (Fig. 4). McDougall and Miranda-Martinez (2016) discussed fossiliferous marine units in the base of the Bouse Formation that demonstrate the presence of such conditions at a time between 9 and 5 Ma, with the lower age likely being about ~6.5–6.3 Ma (their figure 3). The above documentation of marine units in the adjacent northern Gulf of California from 6 Ma is compatible with the Blythe data which represent one of the northern-most records of these marine waters at that time, if not somewhat earlier. These data seem to focus the onset of present-day tectonic activity of the local San Andreas fault system starting about 8 Ma, somewhat earlier than the regional marine incursion at ~6.5 Ma.

Evidence for activity within the Eastern California Shear Zone that is concurrent with the San Andreas system is also provided by Mahan et al. (2009), who recorded exhumation of the southern McCullough Range and adjacent northern New York Mts. at 5 ± 1 Ma and contemporaneous extension in the Ivanpah Valley. This information (not noted in Woodburne, 2015) implies activity on the Stateline fault and the location of the eastern limit of post-6 Ma strain in the Eastern California Shear Zone. If the model is accurate, it provides an inference that sharpens the time of inception of the ECSZ, comparable to that suggested by Gan et al. (2003) and Oskin and Stock (2003a), who also supported a kinematic link between the opening of the Gulf of California and the birth of the San Andreas fault system in this region. If the ECSZ faults were active from east to west (Dokka and Travis, 1990:335), and the ca 5 Ma onset of exhumation associated with the Stateline fault system corresponds with the beginning of slip thereon, then more western faults should have younger beginnings. This appears to be borne out with the timing of tectonic activities in the districts shown in figures 2 and 3.

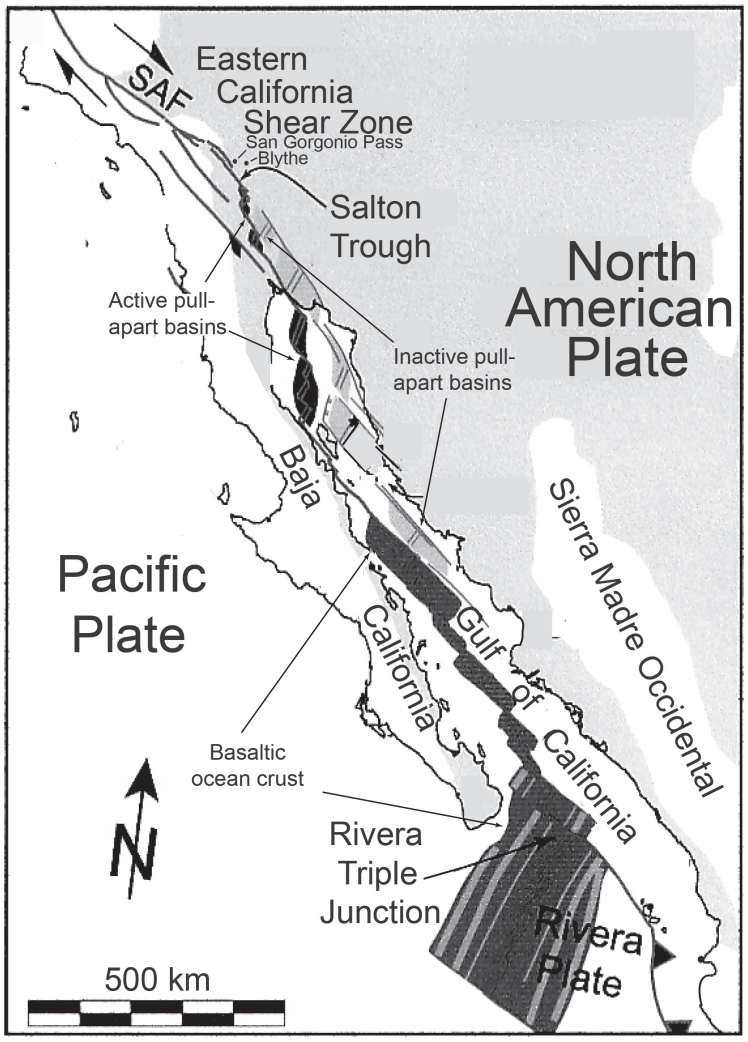

Figure 4. Regional tectonic map of western North America showing the San Andreas fault system boundary between the Pacific and North American plates The active pull-apart basins in the northern Gulf of California are within the area inundated by marine strata from about 6 Ma that reached northward to the San Gorgonio Pass, across the Salton Trough. The active San Andreas fault bounds the Eastern California Shear Zone, and offsets the active pull-apart basins and the basaltic ocean crust, including the Rivera Triple Junction. Adapted from Bennett et al. (2015, Fig. 1A).

The overall picture is compatible with Schermer et al. (1996), who postulated a post ~11–10 Ma slip on ECSZ faults in the northeast Mojave Desert elements of the Northeast Mojave Province (NEMP, Figs. 2, 3). The northeasternmost element of the Mojave Desert ECSZ is found in the Fort Irwin area of the NEMP, north of Alvord Mtn. As noted in Woodburne (2015), a stratigraphic unit known informally as the "Goldstone Gravel" unconformably overlies a basalt dated at 5.57 ± 0.0.28 Ma and contains a tuff in its upper exposures dated at 3.4 ± 0.2 Ma (Schermer et al., 1996) with all units truncated by the Goldstone Lake Fault (Fig. 2). New to the present discussion (Figs. 2, 3), Buesch and Phelps (2016) noted the presence of the Broadwell Mesa Basalt in the Bristol Mts. to the southeast that has been dated at 5.42 ± 0.025 Ma (Fig. 2) with the two basalts being within the age range of the 5 ± 1 Ma exhumation of the Ivanpah Valley as noted above. If Figure 2 is used as an example of Mojave Desert tectonism, it seems to reflect such activity being recorded at about 5–6 Ma in this part of the region, whereas sites to the west of Alvord Mtn. apparently experienced younger episodes, from about 3–4 Ma. The available data appear to generally support the proposal of Dokka and Travis (1990). The units in Afton Canyon (AC; Fig. 3) and northern Cady Mts. (NCM, Fig. 3) suggest a later onset of activity than other places of Domain IV, but Figure 2 was based on presently available data, of which

more are certain to be discovered. Pattern details are still to be developed.

Nuriel et al. (2013) assessed the age of syntectonic opal precipitates in ECSZ fault systems via *in situ* U–Pb SHRIMP (Sensitive High Resolution Ion Microprobe – Reverse Geometry) analysis, and concluded that segments of the sinistral Camp Rock and Cave Mtn. faults were active between 1.5 and 0.2 Ma. Reynolds and Miller (2015, p. 18) cited unpublished work by Nuriel as indicating offset on small sinistral faults that cut the Barstow Formation in the Alvord Mt. area dated at ~9.4–10.2 Ma; such faults being coordinated with the Cave Mtn. fault system (see also Miller et al., 2015). While definitely interesting, no sedimentary context within which to evaluate such activity has yet been described, and hence is not considered further here.

In summary, the following seem to be supported by data currently available: (1) the Eastern California Shear Zone is tectonically integrated with the San Andreas fault, both of which became regionally active at about 6–8 Ma; (2) the eastern domains of the Eastern California Shear Zone (IV–VI) may have begun their activity earlier than more western sites, as proposed by Dokka and Travis (1990), with the exception of domain IV as noted above. As stated by Dokka and Travis (1990; 336) "The cause of this westward shift of activity as well as the implications that this change may have for regional tectonic synthesis and seismic risk assessment are unknown and deserving of greater study." This of course applies to all aspects of the ECSZ.

Acknowledgments

I want to recognize Robert E. and Jennifer F. Reynolds for their significant contribution to fostering an understanding of the historical geology of the Mojave Desert region in southern California over the past 30 years. Bob Reynolds and Rebecca Dorsey provided much appreciated helpful comments to earlier versions of this manuscript, although they do not necessarily agree with the conclusions developed herein.

References.

Bennett, S.E.K., and Oskin, M.E., 2014, Oblique rifting ruptures continents: Example from the Gulf of California shear zone: Geology v.42, p. 215-218, doi: 10.1130/G34904.1.

Bennett, S.E., Oskin, M.E., Iriondo, A., Kunk, M.J., 2016, Slip history of the La Cruz fault: development of a late Miocene transform in response to increased rift obliquity in the northern Gulf of California: Tectonophysics, v. 93, p. 409–435.

Bennett, S.E.K., Oskin, M.E., and Iriondo, A., 2013, Transtensional rifting in the proto-Gulf of California near Bahía Kino, Sonora, México: Geological Society of America Bulletin v. 125, no. 11/12, p.1752-1782. doi: 10.1130/B30676.1.

Bennett, S.E.K., Oskin, M.E., Dorsey, R.J., Iriondo, A., and Kunk, M.J., 2015, Stratigraphy and structural development of the southwestern Isla Tiburón marine basin: Implications for latest Miocene tectonic opening and flooding of the northern Gulf of California: Geosphere, v.11, no. 4, p. 977-1007. doi:10.1130/GES01153.1.

Buesch, D., and Phelps, G., 2016, Architecture, geochemistry, and paleomagnetic directions of the 5.4 Ma Broadwell Mesa basalt volcanic field, Bristol Mountains, California, in Reynolds, R.E., ed., Going Loco: The 2016 Desert Symposium Field Guide and Proceedings, California State University Desert Studies Consortium, p. 253-255.

Darin, M.H., Bennett, S.E.K., Dorsey, R.J., Oskin, M.E., and Iriondo, A., 2016, Late Miocene extension in coastal Sonora, México: Implications for the evolution of dextral shear in the proto-Gulf of California: Tectonophysics, v. 693, p. 378-408.

Dickinson, W.R., 1996, Kinematics of transrotational tectonism in the California Transverse Ranges and its contribution to cumulative slip along the San Andreas transform fault system: Geological Society of America Special Papers, v. 305, p. 1-47.

Dokka, R.K., and Travis, C.J., 1990, Late Cenozoic strike-slip faulting in the Mojave Desert, California: Tectonics, v. 9, no. 2, p. 311-340.

Dorsey, R.J., Housen, B.A., Janecke, S.U., Fanning, C.M., Spears, A.L.F., 2011, Stratigraphic record of basin development within the San Andreas fault system: Late Cenozoic Fish Creek-Vallecito basin, southern California: Geological Society of America Bulletin, v. 123, p. 771–793.

Gan, W., Zhang, P., Shen, Z., Prescott, W.H., and Svarc, J.L., 2003, Initiation of deformation of the Eastern California shear zone: Constraints from Garlock fault geometry and GPS observations: Geophysical Research Letters 30. doi:10.1029/2003GL017090.

Guest, B, Niemi, N., and Wernicke, B., 2007, Stateline fault system: A new component of the Miocene-Quaternary Eastern California Shear Zone: Geological Society of America Bulletin, v.119, p.1337-1346.

Mahan, K.H., Guest, B., Wernicke, B., and Niemi, N.A., 2009, Low-temperature thermochronologic constraints on the kinematic history and spatial extent of the Eastern California Shear Zone: Geosphere, v. 5, no. 6, p. 483-495.

McDougall, K., 2008, Late Neogene marine incursions and the ancestral Gulf of California, in Reheis, M.C., Herschler, R., and Miller, D.M., eds., Late Cenozoic drainage history of the southwestern Great Basin and lower Colorado River region: Geologic and biotic perspectives: Geological Society of America Special Papers 439, p. 355-373. doi: 10.1130/2008.2439(16).

McDougall, K, and Miranda-Martinez, A.Y., 2016, Bouse Formation along the lower Colorado River corridor: tracking the transition from marine estuary to saline lake, in Reynolds, R.E., ed., Going Loco: The 2016 Desert Symposium Field Guide and Proceedings, California State University Desert Studies Consortium, p. 140-144.

McDougall, K., Poore, R.Z., and Matti, J., 1999, Age and paleoenvironment of the Imperial Formation near San Gorgonio Pass, southern California: Journal of Foraminiferal Research, v. 29, no. 1, p. 4-25.

Miller, D.M., Nuriel, P., Oster, J.L., Schmidt, K.M., Reheis, M.C., Cox, B.F., and Maher, K., 2015, Strain partitioning and

timing of strike-slip faulting in the central Mojave Desert, CA, indicated by newly dated latest Miocene, Pliocene, and early Pleistocene deposits, in Reynolds, R.E., ed., Mojave Miocene: The 2015 Desert Symposium Field Guide and Proceedings, California State University Desert Studies Consortium, p. 330-331.

Oskin, M., and Iriondo, A., 2004, Large-magnitude transient strain accumulation on the Blackwater fault, Eastern California shear zone: Geology, v. 32, no. 4, p. 313-316.

Oskin, M., and Stock, J., 2003a, Pacific-North American plate motion and opening of the Upper Delfin basin, northern Gulf of California, Mexico: Geological Society of America Bulletin, v. 115, p.1173-1190.

Oskin, M., and Stock, J., 2003b, Marine incursion synchronous with plate-boundary localization in the Gulf of California: Geology, v. 31, no.1, p.1-6.

Oskin, M., Stock, J., and Martin-Barajas, A., 2001, Rapid localization of Pacific-North American plate motion in the Gulf of California: Geology, v. 29, no.5, p. 459-462.

Nuriel., P., Maher, K., and Miller, D.M., 2013, U-Pb SHRIMP-RG dating of fault-related opals from the Eastern California Shear Zone, in Reynolds, R.E., ed., Raising Questions in the Eastern Mojave Desert: The 2013 Desert Symposium Field Guide and Proceedings, California State University Desert Studies Consortium, p. 287.

Reynolds, R.E., and Miller, D.M., 2015, Mojave Miocene: the field trip, in Reynolds, R.E., ed., Mojave Miocene: The 2015 Desert Symposium Field Guide and Proceedings, California State University Desert Studies Consortium, p. 7-33.

Schermer, E.R., Luyendyk, B.P., and Cisowski, S., 1996, Late Cenozoic tectonics and structure of the northern Mojave Desert: Tectonics, v.15, no.5, p. 905-932.

Woodburne, M.O., 2015, Mojave Desert Neogene tectonics and the onset of the Eastern California Shear Zone, in Reynolds, R.E., ed., Mojave Miocene: The 2015 Desert Symposium Field Guide and Proceedings, California State University Desert Studies Consortium, p. 153-199.

Major revisions of the timing, style, magnitude, and cause of Early Miocene extension in the Central Mojave metamorphic core complex and subsequent role of the Eastern California Shear Zone

R. Ernest Anderson, Ph.D.
USGS geologist emeritus, Kernville, CA

Introduction

Early Miocene strata in the central Mojave metamorphic core complex (CMMCC) were previously interpreted as recording extreme (40-60 km) syndepositional extension above a regional detachment fault system that connected strain from the San Andreas system on the west more than 350 km eastward to the Colorado River extensional corridor (Glazner et al., 2002). Based mainly on field studies, I show that most tilting and folding of the upper-plate strata post-date their deposition, bear little resemblance to structures in extensional allochthons, and account for no more than 4-6 km of extension. Abrupt lateral variations in the structures, textures, mineralogy, and alteration patterns of rocks marking the Waterman Hills detachment fault (WHDF), and local examples of protracted cross-fault flow of fluids, are consistent with small extension. Reported here are critical new data indicating a dilatant emplacement mode for the large (> 400km^2, Walker et al., 1995) early Miocene Waterman Hills pluton (WHP), a mode that allows for a tectonic model of localized extension and uplift as opposed to tectonic exhumation on a regional detachment fault. Also reported are newly discovered field relationships critical to understanding the timing of Neogene sedimentation and deformation, including constraints placed on those processes by the Peach Springs Tuff, exotic-clast conglomerate, and fan-head gravel. All point to uplift that is younger than previously thought and involves faults of the eastern California shear zone (ECSZ).

Province-wide assessments of Neogene extension in the western United States require reliable estimates of strain in widespread, well studied, and well-exposed areas; and knowledge of how extensional strain is interconnected between those areas. Anderson et al. (2013) outlined problems inherent in assuming along-strike connectivity or continuity of strain between areas of known or suspected large extension reaching from central Utah to the CMMCC. Extension, regardless of the validity of magnitude estimates in well-studied areas, lacks along-strike continuity. Metamorphic core complexes of the North American Cordillera are part of that province-wide strain record, as they are considered an expression of extreme extension. Broad gaps exist between the three belts of core complexes and between individual complexes within the belts (Fig. 1), raising the question of whether, or how, extensional strain in the complexes might be connected or how strain might be transferred from one to another. A tectonomagmatic model is applied to the CMMCC consistent with its total structural isolation.

Extension in the CMMCC

The CMMCC is a prime example of geographically isolated uplift (Fig. 1). Whether extensional strain in a restricted core complex (ca. 450 km^2) near the center of a major tectonic block, the Mojave structural block (Glazner et al., 2002), surrounded by few structures indicating similar or coeval extension, could be structurally linked by a detachment fault across distances of hundreds of kilometers was critically evaluated and discounted by Anderson et al. (2013). The amount of extension in the CMMCC was not evaluated. In general, determination of the amount of extension near the center

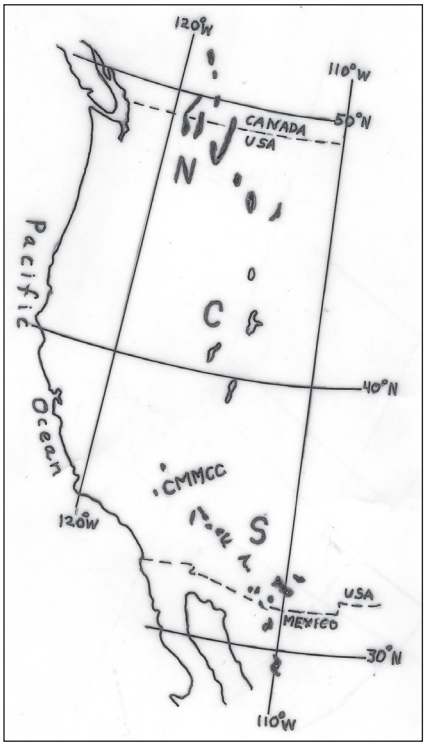

Figure 1— Map showing the distribution of metamorphic core complexes in western North America into north (N), central (C) and south (S) zones (modified from Whitney et al., 2013). CMMCC-Central Mojave Metamorphic Core Complex.

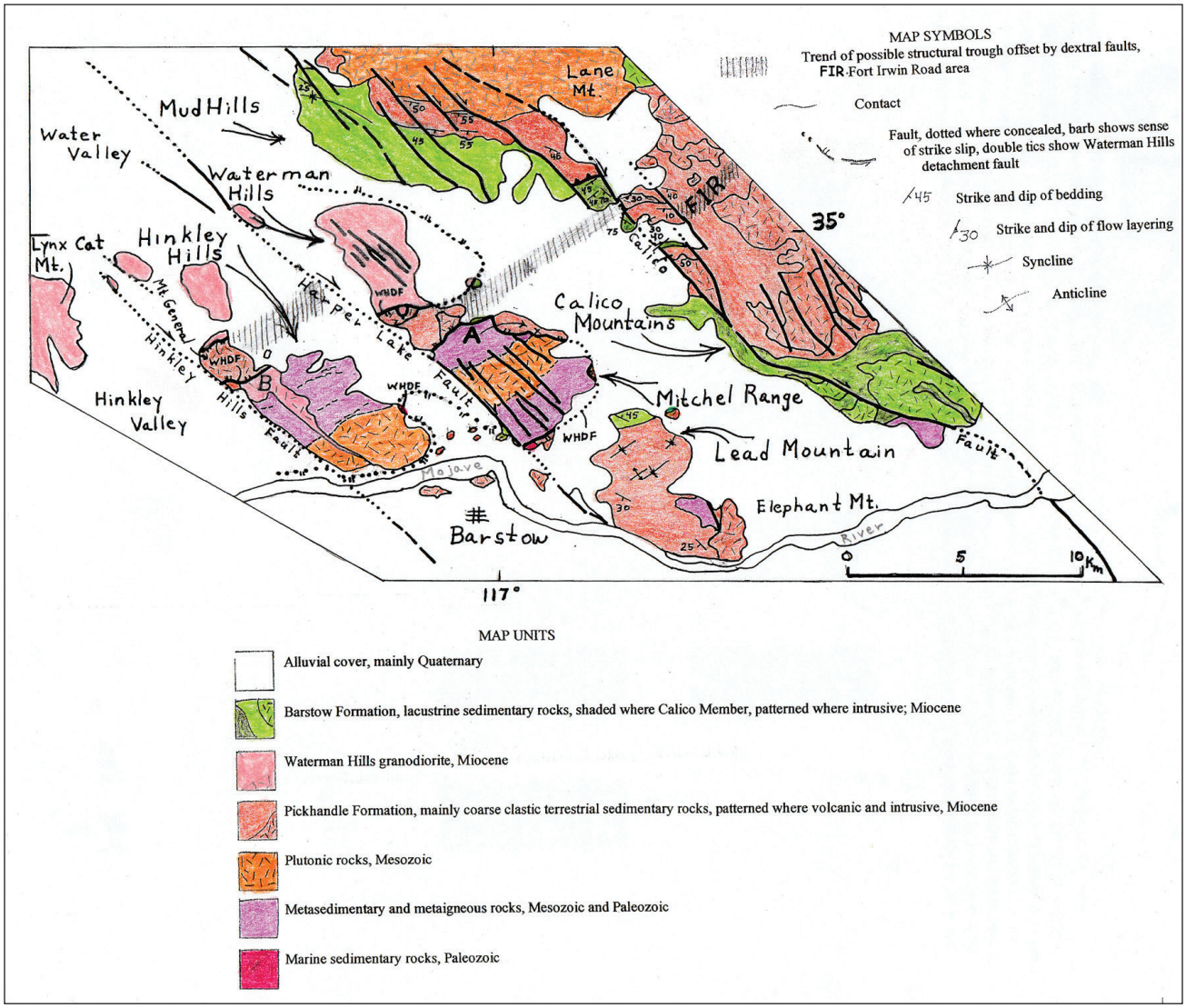

Figure 2— Generalized geologic map of the southeastern CMMCC. Three offset areas of Tertiary rocks exposed in the upper plate of the Waterman Hills detachment fault (WHDF, hachured line) are projected to the northeast (cross ruling) forming northeast trending bands. If right-sense fault offset (McQuarrie and Wernicke, 2005) of the bands is restored, they align into a 20-km-long discontinuous band. Northwest-trending fine dashed lines reflect structural trends internal to the Hinkley Hills and Mitchel Range. The northwest-trending dike system in the Hinkley Hills (B) broadens to the northwest and projects beneath Mount General beyond which it emerges as the Waterman Hills pluton. Map modified from Walker et al. (2002).

of a large structural block, like the Mojave block, lacks the advantage of a nearby static margin, such as the edge of the Colorado Plateau, to which displacements can be referenced. Also, the absence of a clearly defined breakaway fault and/or lateral accommodation structures to which extension can be referenced exacerbates determination of extension magnitude.

Extension in upper-plate rocks

Restoration of right slip on the NW-striking Harper Lake and Calico faults (Martin et al., 1993), places exposures of Pickhandle rocks in the Hinkley Hills, southern Waterman Hills, and the thick (1.5 km) type section of Jackhammer and Pickhandle rocks in the Calico Hills structural blocks in approximate NE alignment along the direction of extension (Fig. 2).

This restored transect of exposed Pickhandle rocks provides an opportunity to estimate the maximum credible amount of extension coeval with deposition of the early Miocene Pickhandle Formation. Study of the spatial and stratigraphic distribution of stratal attitudes shows that the youngest Pickhandle rocks dip as steep as the oldest ones, providing no direct evidence of large syndepositional extension.

For example, in the Hinkley Hills, steep to steeply overturned strata form the west-most exposures high in the stratal assemblage. Also, along the axis of the southwest-plunging Waterman Mine syncline (WMS) in the Waterman Hills (Fig. 3), the average southwesterly dip of beds in the northeast part is 67° (n = 12) and in the southwest part is 66° (n = 12), providing no direct support for syndepositional extensional tilting or growth-fault fanning across the 2 km of continuously exposed strata.

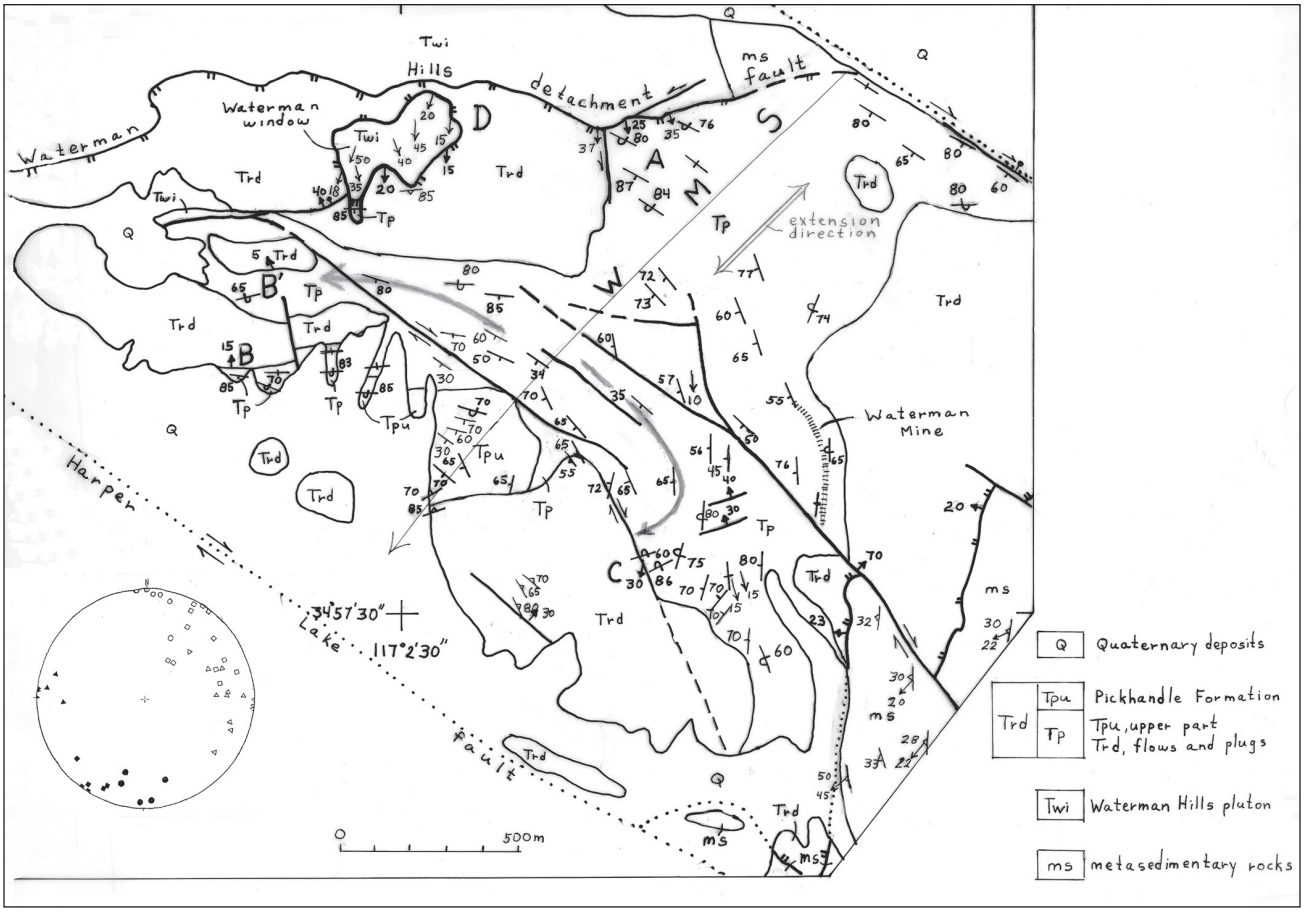

Figure 3— Tectonic map of the steeply southwest-plunging Waterman Mine syncline (WMS) formed in strata of the Pickhandle Formation (Tp; Tpu for upper part) in the southeastern Waterman Hills. The syncline is bounded on the southwest and northeast by right-slip faults and on the north and southeast by the Waterman Hills detachment fault (WHDF, hachured). Tilting of the rocks in the axial region of the WMS has been interpreted as resulting from syndepositional extension (double arrow) (Glazner et al., 1989), but strata along that axis are uniformly steeply tilted, showing that tilting post-dates deposition. The WMS has been interpreted (Anderson and Berger, 2007) as reflecting post-tilting contractional bending strain (large curved arrows in map; circles and triangles representing the separate fold limbs in inset stereographic plot of poles to bedding). Clockwise bending to northerly trends in the southeast limb is consistent with northerly trending foliation in adjacent lower plate metasedimentary rocks in the southeast part of the map. Those northerly trends are part of a coextensive pattern of clockwise bending of initially northeast-trending foliation in the directly adjacent Mitchel Range (Fig. 7). Dips in upper plate strata are steep to overturned throughout most of the northwest limb, possibly reflecting the regional pattern of N-S shortening strain (Bartley et al., 1990). In the SE limb east and southeast of locality C, the strong apparent clockwise bending (>90°) and overturning of strata may reflect bending beyond the end of the dextral fault located to the northwest. Meter-scale reverse faults (not shown in map) at locality B indicate N-S shortening consistent with kinematics of the WHDF in the Waterman window and striae on meter-scale low-angle faults northwest and southwest of the Waterman mine (shown in map by small arrows and values showing plunge of striations). Inset shows lower-hemisphere stereographic plot of poles to bedding (filled symbols reflect overturned beds) in the three separate parts of the syncline: axial region (squares), northwest limb (circles), and southeast limb (triangles); ms, pre-Tertiary metasedimentary rocks.

Along the northeast flank of the Mitchel Range (Fig. 4) and in the southern Calico Mountains, Pickhandle strata mostly strike toward the WHDF, rather than dip toward the fault as expected in an area of strong extension.

Also, Singleton and Gans (2008) found only a subtle unconformity between the Pickhandle and overlying Barstow Formation in the southern Calico Mountains, providing no support for strong syndepositional tilting of the Pickhandle Formation, which is considered to be syntectonic, as opposed to the Barstow Formation, which is considered to be post tectonic. Structures in post-Pickhandle Barstow Formation and younger strata in the Mitchel Range and Calico Mountains show that much of the deformation is post Pickhandle.

Basin formation and filling by approximately 2 km of volcanic and volcanogenic Pickhandle Formation and emplacement of dikes are the main record of Pickhandle-age early Miocene extension (Fig. 5). Generously allowing for 30 % extension associated with these processes, the maximum extension across the exposures is about 3 km. Extension buried beneath basin-fill cover in the basins between the ranges leaves those areas open to speculation, but bedrock structures in directly adjacent areas provide a basis for precluding large components of rifting beneath the basins. The maximum credible extension associated with deposition of early Miocene rocks, although not rigorously constrained, is an order of magnitude less than the 40-60 km inferred in previous studies.

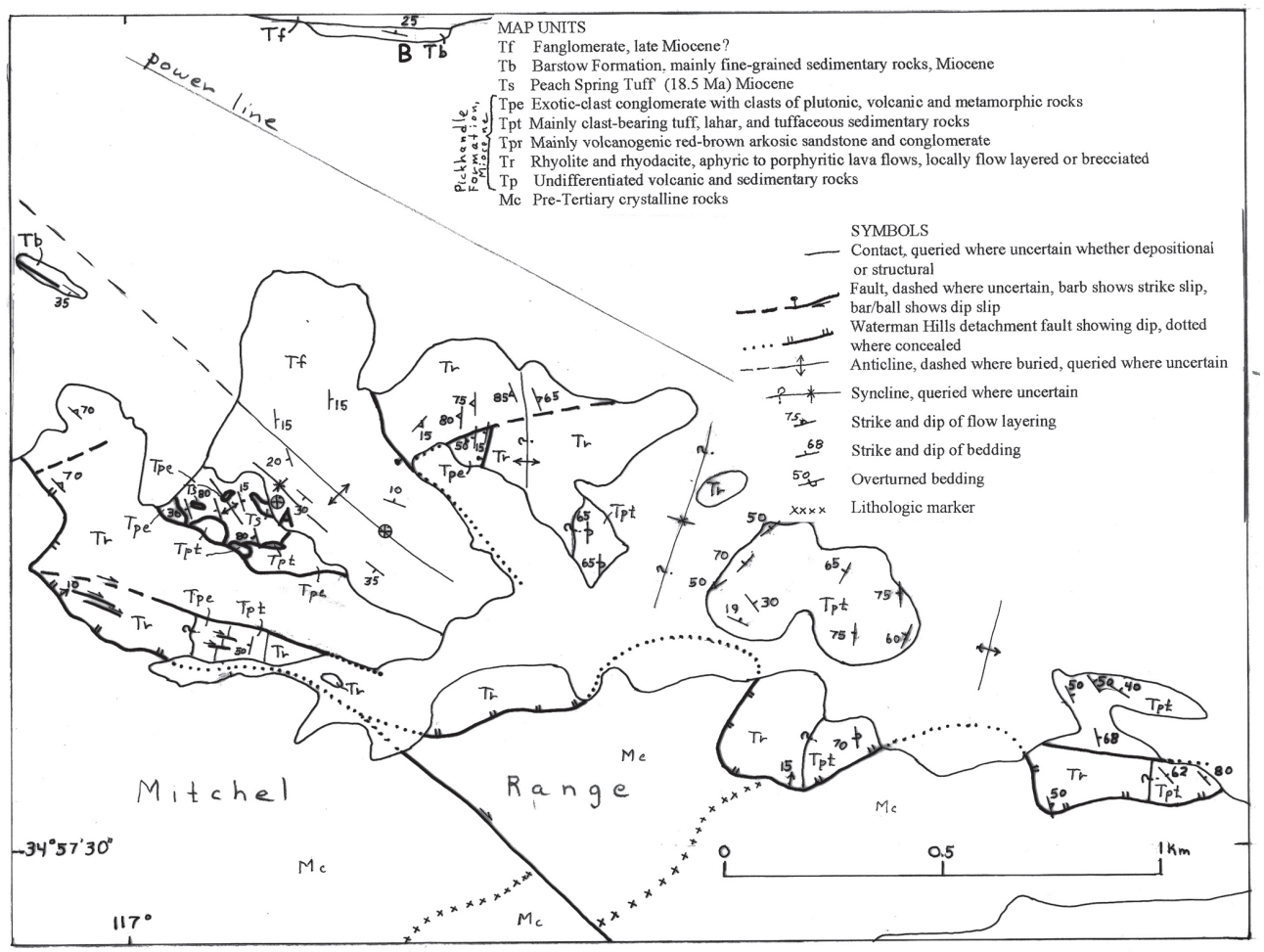

Figure 4— Geologic map of Miocene rocks forming the upper plate of the Waterman Hills detachment fault along the north margin of the Mitchel Range (modified from Fletcher et al., 2002). Stratigraphic tops in overturned beds were determined from fining upward sequences of sand and gravel. If the WHDF records tens of kilometers of NE-directed Miocene extension as suggested in published reports, the expected southwest stratal tilting is sparse. Southwest tilts in the west part are in non-extensional folds. Dip directions in the other parts are variable, and beds closest to the WHDF tend to strike toward, rather than dip toward, the fault. In general, stratal dips provide no direct support for published upper-plate extensional kinematics, and nowhere is there a pattern of growth-fault fanning to support syn-extension deposition. Map shows location of previously unrecognized outcrops of extensionally deformed Peach Spring tuff (Ts) and Barstow Formation (Tb). Gently folded conglomerate and sandstone (Tf), previously mapped as exotic clast conglomerate of the Pickhandle Formation (Fletcher et al., 2002), rests on the 18.8 Ma Peach Spring tuff at locality A and on the Barstow Formation at locality B.

Extension in lower-plate rocks

The challenge of estimating early Miocene lower-plate SW-NE extension differs northwest and southeast of the restored band of exposed Pickhandle rocks. To the northwest, scattered exposures of early Miocene plutonic rocks combine to suggest a mass of batholithic proportions, the Waterman Hills pluton (Fletcher et al., 2002). The southeast part of the pluton consists mainly of previously unrecognized northwest-oriented dikes (Fig. 6 and Google Earth at image width of about 1 km). Extensional dilation associated with dike-on-dike emplacement could equal the full 15 km width of the WHP. To the southeast, where unit contacts and folds in pre-Tertiary rocks trend strongly NE (Fig. 2) and brittle Neogene faults are mainly steep with northwest strikes, large lower-plate extension is limited to the width of Miocene dikes and a stretch factor recorded in widespread mylonitization that I suggest is non-quantifiable because much may be pre-Tertiary. Northwest striking mid-Miocene dikes in the lower plate of the Hinkley Hills directly southeast of Mount General (locality B, Fig. 2) could account for 1-2 km of dilatant extension, but it decreases by a factor of 10 toward the southeast end of the Hinkley Hills. In the other direction, the dike system projects northwestward beneath Mount General and reemerges as the Waterman Hills pluton (Fig. 2) where extension by dike accretion exceeds 90%. Recognition of the strong northwest-increasing dilatant strain gradient for the lower plate places detachment faulting in a local, rather than regional, context. Although the rationale is not detailed herein, the Miocene stretching factor in pre-Tertiary mylonitic rocks that make up the lower plate in the southeast part of the Hinkley Hills and most of the Mitchell Range is conjectured as small.

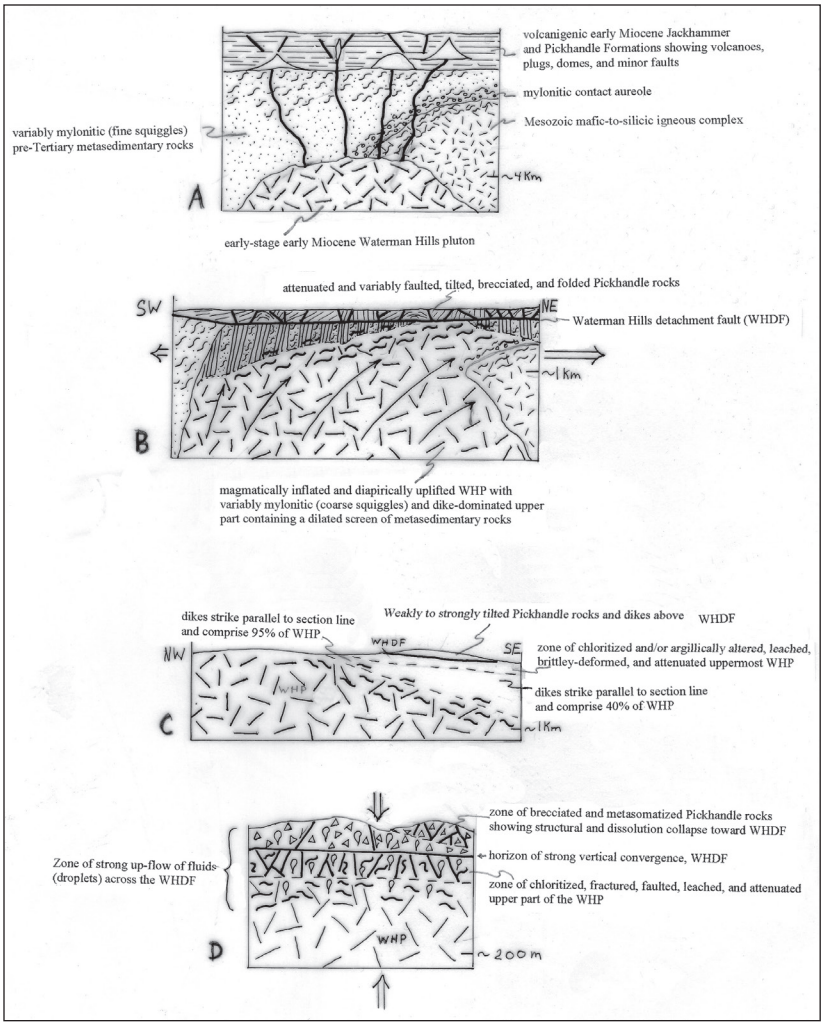

Figure 5—Cross sections illustrating aspects of a tectonomagmatic model of the CMMCC (note contrasts in estimated scaled depth). A. Early-stage link between early Miocene plutonism and volcanism. Also shown are pre-Tertiary mylonitic metasedimentary and metaigneous rocks, especially those linked to the contact aureole of a Mesozoic igneous complex. B. Late-stage relations showing sheeted-dike dilation in upper part of an enlarged and uplifted pluton and overlying volcanogenic carapace shattered in extension (double-shaft arrows) above the dilatant zone. Sketch also illustrates shallow development of mylonite (squiggly lines) during approximately unidirectional northeast-directed spreading. Not illustrated are folds, interpreted herein as mainly pre-Tertiary, of highly varied size beneath the WHDF. C. Dike-parallel sketch emphasizing an increase in dike width and decrease in spacing as the holocrystalline equigranular part of the pluton is approached. D. Sketch emphasizing vertical shortening (double-shaft arrows) resulting from loss of rock volume and gravitational collapse during late-stage magmatic fluid up-flow below and above the WHDF.

The Eastern California Shear Zone in the CMMCC

The ECSZ in the CMMCC is represented by four northwest-striking right-slip faults: from west to east, they are the Lockhart-Lenwood, Hinkley Hills, Harper Lake, and Calico faults (Fig. 2). Cumulative right-sense offset could be > 20 km (McQuarrie and Wernicke, 2005). Off-fault strain in the form of bending and distributed shear could account for an additional > 25% dextral-sense displacement (Shelef and Oskin, 2010). If, as noted above, most tilting of upper-plate rocks in the CMMCC post-dates deposition of the Pickhandle Formation, what part of the total strain in those rocks is associated with the tectonics of the ECSZ? A closely related question, stemming from the observations of Bartley et al. (1990) that widely distributed late Cenozoic N-S shortening in the central Mojave was neither related to extension nor spatially restricted to post-extension transpressional fault bends, is "what part of the shortening strain embodied in folds is associated with the ECSZ"?

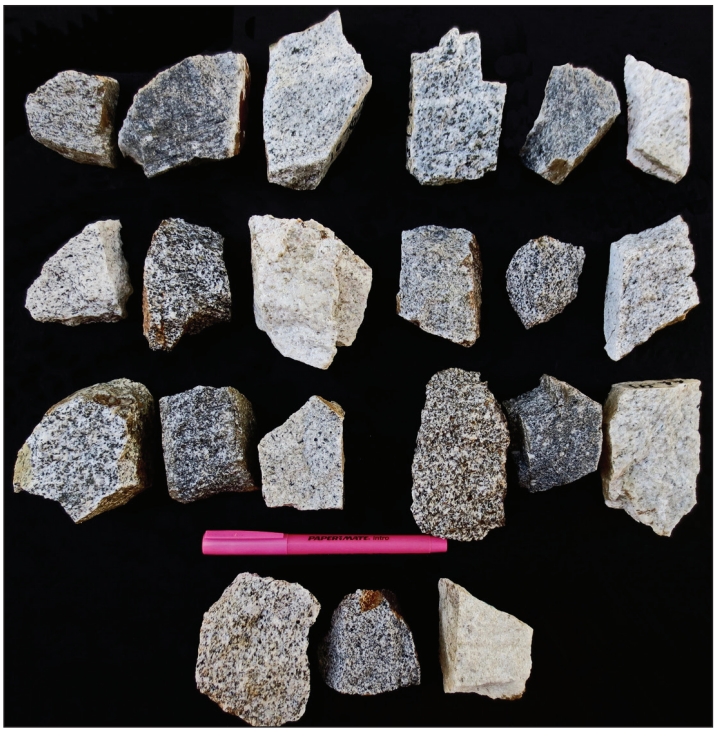

Figure 6—Photo of collection of felsic to mafic rocks of the Waterman Hills pluton. Above pen, each set of three rocks illustrates the medium, dark, and light lithologies of steep northwest striking dikes forming the central part of the pluton. The triplet groups are arranged, book fashion, from southwest in the upper left to northeast in the lower right and cover a 1.3-km-long SW to NE traverse across the central part of the pluton in the Waterman Hills. Together, the mafic and felsic phases comprise less than 20% of the pluton. Below pen, samples represent similar lithologic variation in the massive deeper part of the pluton at the west base of Lynx Cat Mountain where the greatly dominant lithology is medium-colored granite.

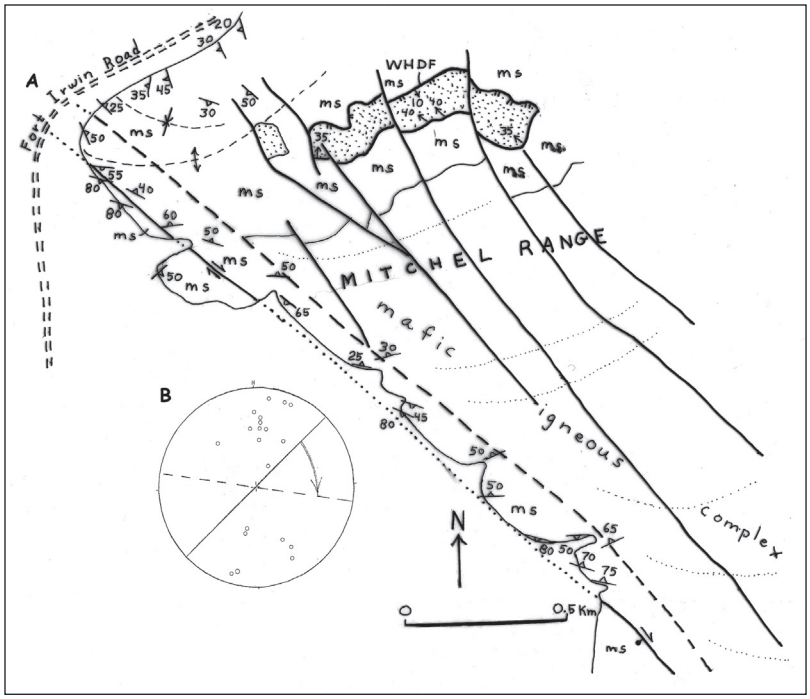

Figure 7—Tectonic map and structure plot. A. Tectonic map of the northwest corner of the Mitchel Range showing a down-dropped northwest-trending horse block of pre-Tertiary mylonitic metasedimentary rocks (ms) between two strands of the Harper Lake fault. Subsidiary faults within the range block are also shown, as are patterns of steep-axis clockwise bending of strike trends of foliation (fine dotted lines) and fold axes (fine dashed lines) in metasedimentary rocks. The strong bending to predominantly NNW strikes in the northwest part continues across the Fort Irwin Road where N-S strikes in metasedimentary rocks parallel strongly clockwise rotated upper plate strata in the WMS (Fig. 2). B. Stereographic lower-hemisphere plot of poles (circles) to diversely dipping foliation in the horse block shown in A. The average strike (dashed line) is about 50° clockwise of the average strike in the center of the adjacent range block (solid line) as shown by the fine dotted lines in A. The rotation is consistent with bending as the dextral Harper Lake fault is approached from the northeast. The diverse dip directions reflect pre-bending folding on northeast-trending axes (Fletcher et al., 1995). The clockwise bending is accompanied by a doubling of plunge of mylonitic lineation (18° to 38°) (not shown). The bending and steepening indicate transpression during range uplift and the strong bending of the lower plate into parallelism with the north-trending southeast limb of the WMS suggests post-extension strain coordination between upper and lower plates.

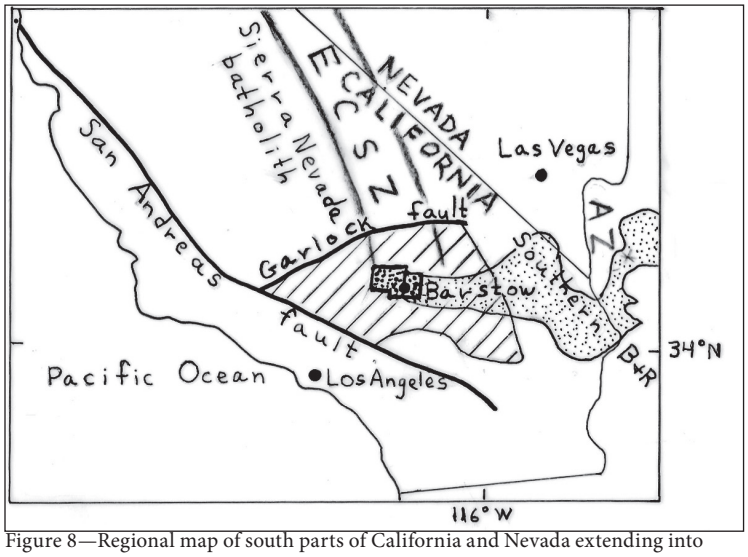

Figure 8—Regional map of south parts of California and Nevada extending into western Arizona (AZ) showing the location of the Mojave structural block (cross ruled) and its bounding faults, the Garlock and San Andreas. Also shown is the eastern California shear zone (ECSZ), the location of Figure 2 (heavy stipple), and the distribution of the Peach Springs Tuff (light stipple).

In the CMMCC, some folding on E-W trends is directly related to the ECSZ. Singleton and Gans (2008) present convincing arguments for interpreting folding of the 19-16.9 Ma Barstow Formation strata in the southern Calico Mountains on approximately E-W trends as related to localized contraction at a restraining bend in the right-lateral Calico fault. Some of the folds are structurally decoupled on a north-directed thrust fault, and the combined folding and faulting account for about 1 km of shortening. A less obvious connection to the ECSZ concerns deformed Barstow Formation strata in the Mud Hills extending eastward into the gap between the eastern Mud Hills and northern Calico Mountains, a gap through which the Calico fault passes (Fig. 2). Barstow strata in that area dip south, are locally folded on E-W axes, and are cut by at least one south-vergent reverse fault. Those structures have broad E-W distribution and do not reflect structural restraint due to bending of the Calico fault. However, Barstow Formation strata directly adjacent to the fault show strong steep-axis bending consistent with right shear, showing that the fault, even where it is optimally oriented for simple right shear, experienced normal sense shortening.

In another example, steep-axis bending of lower plate rocks spatially related to post-extension regional dextral strike slip along an optimally oriented (in terms of plate-margin transform, McQuarrie and Wernicke, 2005) segment of the 135° striking Harper Lake fault at the SW margin of the Mitchel Range. The fault has a conspicuously linear trace, lacking any inflection that could have caused localized folding by structural restraint. Foliation at 20 sites within a 200-m-wide horse block of foliated and lineated pre-Tertiary mylonitized rocks along that fault are shown in Figure 7A. The average strike (dashed line, Fig. 7B) is about 50° clockwise of the prevailing NE-oriented foliation in the adjacent core of the Mitchell range. The bending includes a dip-slip component because the average plunge of mylonitic lineations is about twice (from 18° to 37°) that in a 600-m-wide band directly adjacent the border zone. Barstow Formation strata along the southeast part of the Harper Lake fault dip steeply away from the fault, which locally dips steep beneath the range suggesting dextral transpression. At one locality, dip slip and strike slip striations are well

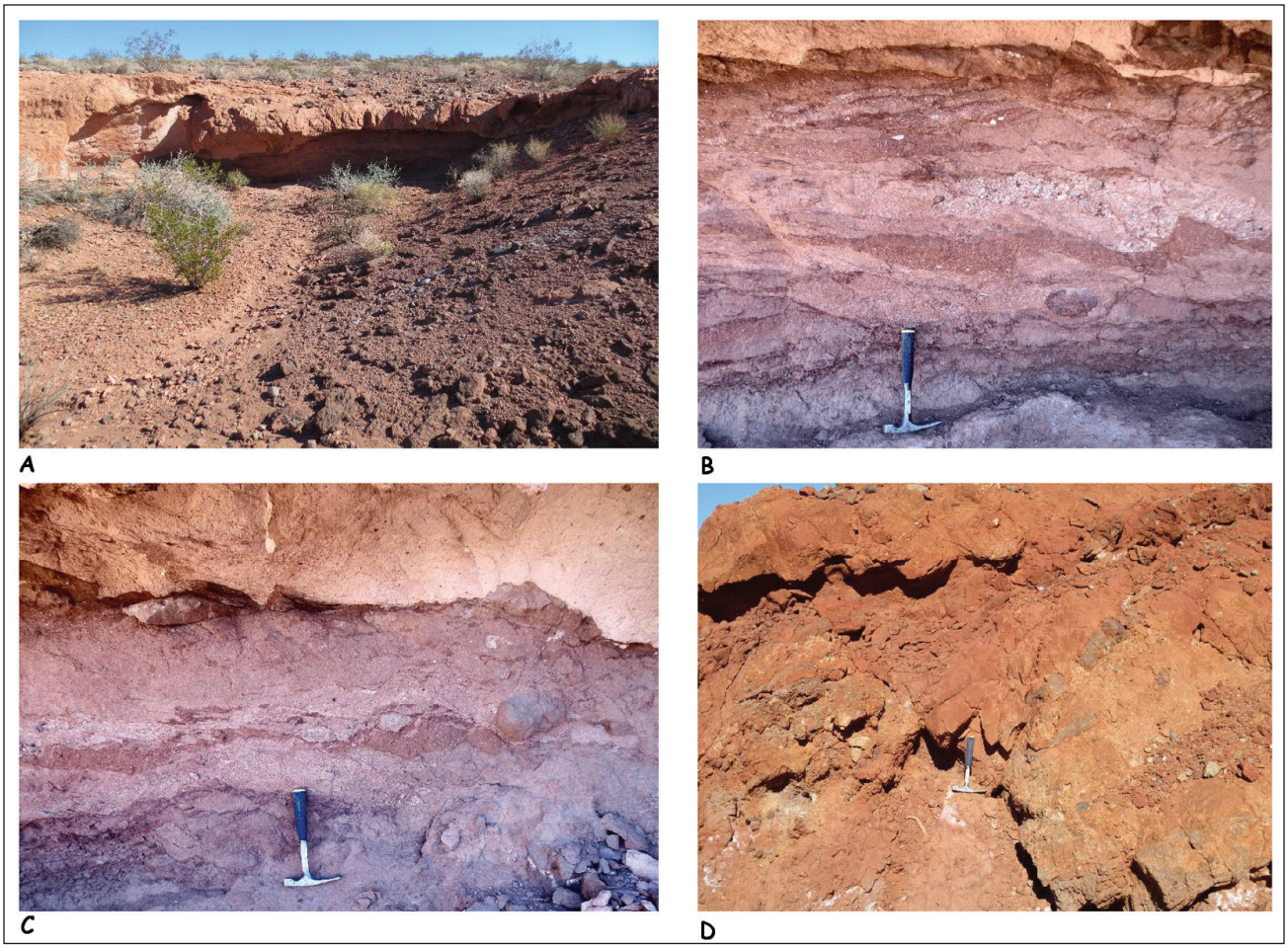

Figure 9—Photos of Peach Springs Tuff on NE flank of the Mitchel Range (Locality A, Fig. 2). A. View of small northerly trending cliff of welded Peach Spring Tuff and underlying volcanogenic conglomerate of the Pickhandle Formation (right foreground). B, C. Photos of faulted base of the tuff in shade in photograph A showing structurally attenuated tuffaceous sedimentary rocks separating the welded Peach Springs from underlying conglomerate. Poorly preserved compaction foliation in the tuff dips about 45° to left (NE) showing that faulting post-dates deposition of the tuff and, consistent with displacements in the tuffaceous sediments, displacement is primarily down in the direction opposite to the regional extension direction. D, View to NW showing wedge-shaped block of Peach Springs Tuff (at hammer) downfaulted into conglomeratic Pickhandle beds.

developed on two separate parallel surfaces showing that young transpressional strain on the Harper Lake fault was capable of being partitioned into reverse-fault uplift and dextral shear. As with the Calico fault in the gap between the Mud Hills and Calico Mountains, evidence for post-Barstow Formation fault-normal shortening at the Harper lake fault is consistent with fault displacement in response to regional N-S shortening as a strain component independent of plate-boundary transform shear.

The large Waterman Mine syncline (WMS) in Pickhandle rocks above the WHDF in the southern Waterman Hills has a steeply SW plunging axis and steep to overturned E-W- and N-S-striking limbs (Fig. 3). Tilting of the strata was likely associated with emplacement, rise, and spreading of the WHP (see below). The fold records post-tilting, post-extension counterclockwise and clockwise bending of strata to form the E-W and N-S limbs respectively as revealed by newly acquired field data showing that the sub-detachment crystalline rocks directly adjacent to the limbs of the WMS are similarly bent around steep axes. The WHDF separating the Pickhandle strata from the crystalline rocks must also be bent. Not only does the WMS differ in architecture from the common and widespread shallow-axis folds in the upper and lower plates of the CMMCC (Fletcher et al., 1995), it is younger and could record a response to N-S shortening rather than NW-SE shortening. These relationships allow for the speculation that the WMS is a product of post tilting N-S shortening during early stages of development of the ECSZ.

In summary, faults of the ECSZ in central Mojave reveal transpressional behavior even where their strike is parallel to the plate-boundary shear direction, a behavior potentially compatible with a regional N-S contractional strain field such as that responsible for the broadly distributed generally E-W folds in Barstow Formation and younger strata. The WMS could reflect the early history of regional contraction. Why a contractional strain field would form locally within the dextral-shear-dominated plate-margin tectonic setting is uncertain.

Importance of the Peach Springs Tuff, exotic-clast conglomerate, and deformed fan-head gravel in defining the age of range uplift in the Central Mojave Desert

The 18.8 Ma Peach Springs Tuff (Ferguson et al., 2013) derived from the Colorado River area (Fig. 8), has a well-documented distribution in the central Mojave Desert (Miller and others, 2010). For the first time, it is identified within the CMMCC. Small exposures (Figs. 4, 9) consisting of tuff with estimated 3% sanidine phenocrysts and sparse small altered biotite and hornblend and accessory sphene and zircon are found on the northeast flank of the Mitchel Range above rocks of the Pickhandle Formation and below conglomerate. The tuff contains a weak foliation that, in thin section, is defined as faint spicules probably representing collapsed shards. The tuff is tilted, faulted, and structurally attenuated (Fig. 9) similar to other upper-plate volcanic rocks in the area. The deformed condition is totally at odds with the post-extension, undeformed condition of equivalent rocks in areas to the east, showing that some extension, and possibly uplift-related attenuation, in the CMMCC is younger than previously thought, consistent with relations noted above.

Newly recognized conglomerate containing cobbles and boulders of densely welded Peach Springs Tuff occur above the Peach Springs Tuff and below and above the overlying Barstow Formation. Some of these conglomerate beds were previously mapped as Pickhandle. The clasts are conspicuously more densely welded than the in-situ tuff forming the exposures on the northeast flank of the Mitchel Range, suggesting the clasts are exotic to the area and that the conglomerates were derived from the east, from the direction of the source caldera. Exotic-clast conglomerates have long been known as common constituents of the middle and upper parts of the Pickhandle Formation, and a northerly source in the Lane Mountain area has been suggested for some (Glazner et al., 2002). Extending the age range of exotic-clast conglomerates from mid Pickhandle to post

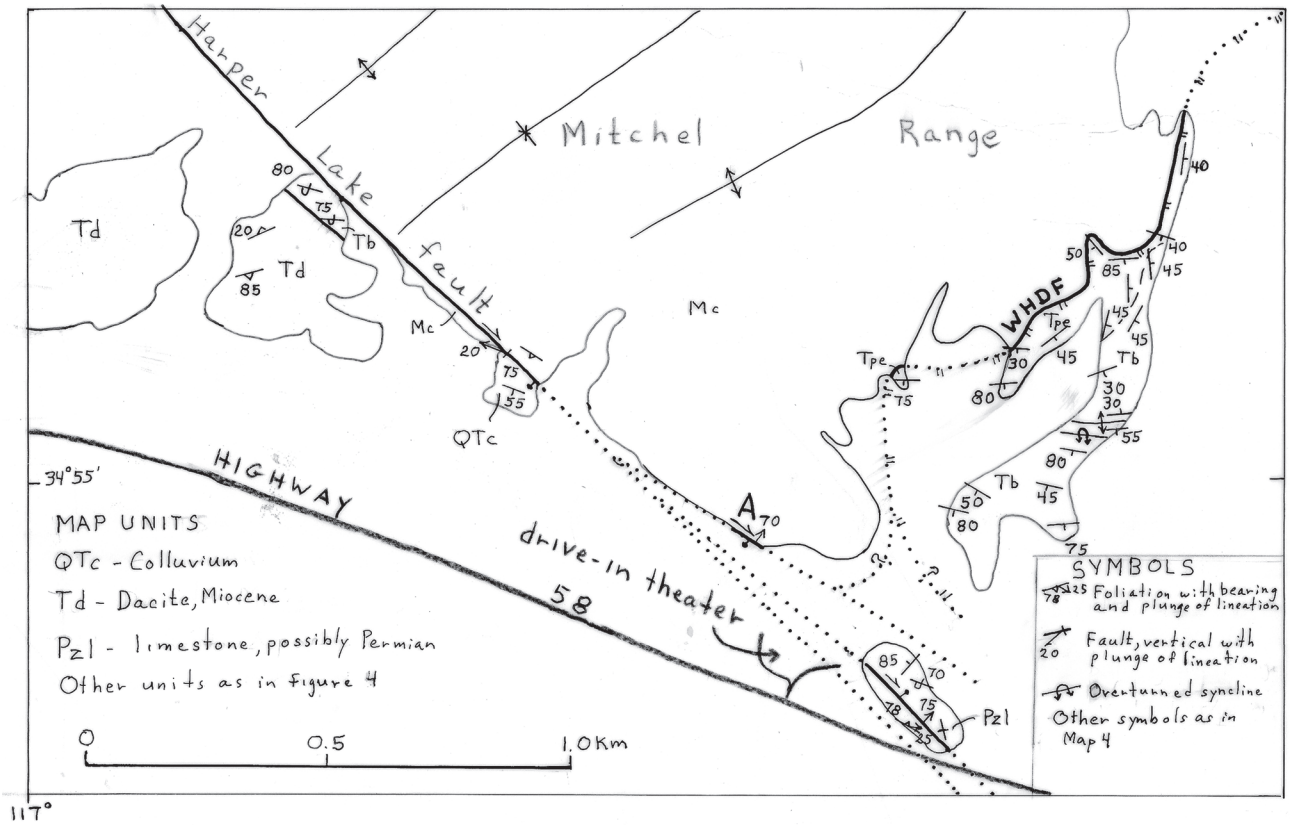

Figure 10—Geologic map of southeast part of the Mitchel Range where the crystalline-rock core is bounded by the intersecting Harper Lake right-slip fault and Waterman Hills detachment fault (WHDF). The upper plate includes previously unmapped thin-bedded, fine-grained clastic sedimentary rocks and minor limestone belonging to the Barstow formation as well as volcanic dacite possibly correlative with "dacite of the Yermo center" mapped in the southern Calico Mountains by Singleton and Gans (2008). These rocks are as strongly deformed as the underlying predominantly polymict plutonoclastic deposits of the Pickhandle Formation (Tpe), showing that deformation here mostly postdates deposition of the Pickhandle, similar to other parts of the Mitchel Range and Waterman Hills as well as the Southern Calico Mountains. Dips are mostly steep to overturned S and SW. East-West contractional folds, including an overturned anticline, in the Barstow Formation strata northeast of the drive-in theater and overturned attitudes along the Harper Lake fault northwest of the theater suggest N-S contraction and dextral transpression rather than extension-style tilting. At site A, dip-slip and strike-slip striations on two separate parallel fault surfaces show that young transpressional strain was capable of being partitioned into reverse-fault uplift and dextral shear. At the SE tip of the range, uncertainty exists as to how, or if, displacement on the Harper Lake fault is coupled to displacement on the WHDF (see queried traces). The possibility exists that the two faults are coupled and that the range block has been uplifted into Miocene strata previously deformed in N-S contraction.

Barstow Formation creates a picture of a stable enduring depocenter in the southern CMMCC, consistent with my claim that extreme early Miocene uplift capable of exhuming mid-crustal mylonite (Fletcher et al., 1995) was either highly localized elsewhere in the CMMCC or did not occur (Anderson et al., in prep).

Barstow Formation strata on the flanks of the Mitchel Range are tilted, and locally overturned, and neither they nor the underlying Pickhandle strata appear to contain clasts of chloritized mylonite that forms the directly adjacent part of the crystalline core of the range block. The first stratigraphic appearance of locally derived clasts of chloritized mylonite is in sharpstone conglomerate along the SW margin of the Mitchel Range directly adjacent to the Harper Lake fault. Those strata represent fan-head deposition and are tilted about 55° away from the range along the dextrally transpressive Harper Lake fault (unit QTc, Fig. 10). Nearby Barstow Formation strata, including rhyodacite flows, are steep to overturned. Together with the greater tilts in the nearby Barstow Formation, the field relations show progressive post-Pickhandle uplift. I speculate that deposition and tilting were late Tertiary and record uplift of the Mitchel Range block during displacement on the transpressive Harper Lake fault of the ECSZ. This speculation is supported by relations at locality A, Figure 10 where dip-slip and strike-slip striations on two separate parallel fault surfaces show young transpressional strain that was partitioned into reverse- and dextral-sense shear.

A tectonic model for the Early Miocene

Unlike core complexes that form at or near the edges of orogenic plateaus, such as those in the lower Colorado extensional corridor, the CMMCC is a relatively small isolated feature that formed near the center of the large Mojave structural block. Whitney et al. (2013) suggested three non-magmatic tectonic models for isolated complexes: block tilt, rolling hinge, and convergent channel flow. Of these, previous investigators favored the rolling hinge model to explain what was perceived as extreme extension during Pickhandle deposition (Bartley and Glazner 1990; Axen and Bartley, 1997). Not only do our studies take exception to extreme extension, Pickhandle rocks do not record of the passage of a rolling hinge. For example, if detachment faulting migrated NE with a trailing rolling hinge in which plutonic and mylonitc lower plate rocks record several kilometers of hinge uplift, a continuous NW-trending welt free of synextensional deposits should span the entire NW-SE extent of the CMMCC. Instead, the Pickhandle strata form a SW-NE band showing no sign of erosional thinning or removal during passage of a rolling hinge. To the extent that they are related to detachment faulting, the flanking mylonites in The Buttes-Hinkley Hills and Waterman Hills-Mitchel Range areas would have to represent two separate rolling hinges or, as I prefer, are simply separate uplifts unrelated to a rolling hinge.

Previous studies of the CMMCC laid the groundwork for adoption of a tectonomagmatic model by noting that plutons are pre-kinematic, synkinematic, and post kinematic and the age span of magmatism encompasses that of extension, (Walker et al., 1995). Rejection of the notion that Pickhandle rocks were tectonically transported into the CMMCC from some unknown source area located to the southwest allows for tectonic modeling of the predominantly volcanic and volcanogenic stratal assemblage of the approximately 24-19 Ma Pickhandle Formation as part of the cogenetic lid of the WHP (Fig. 5D), essentially an early Miocene tectonic model of a syn-volcanic basin directly adjacent to, and partly above, a coeval batholith-size pluton. The present study shows that extension in the basin assemblage was moderate, not extreme, and displacement on the detachment fault was accordingly moderate. In the absence of extreme displacement on a regional detachment fault, what model can best explain uplift and exposure of the pluton and other rocks previously interpreted as coevally mylonitized at mid-crustal depths?

The WHP in the Hinkley Hills-Lynx Cat Mountain area and Waterman Hills is tilted to the southeast on the basis of a northwesterly progression from mainly porphyritic dikes adjacent to upper-plate rocks in the southeast to coarser grained granitoids (emplacement depth estimated at 4-5 km) toward the northwest. Mylonitic fabrics decrease dramatically in the same direction (Fletcher et al., 2002). Also, in its northwest exposures, it consists of massive granitoid bodies lacking in mafic enclaves, pegmatitic or aplitic dikes, or mylonitic fabrics, all of which are common in its shallower southeastern parts. These tilting characteristics, coupled with the mode of pluton emplacement, are critical to defining a tectonomagmatic model for the CMMCC. Growth of the upper part of the pluton by accretion of northwest trending lithologically variable dikes (Fig. 6, and surface exposure as light/dark bands visible in Google Earth at image width of about 1 km) reveals NE-SW dilatant srtain, perhaps across the entire 15-km-wide CMMCC. Mylonitization of only the upper part of the pluton shows that post emplacement stretching forming L-tectonites occurred, not at mid crustal levels as assumed by previous workers, but most likely in the upper 2-3 kilometers where the pluton was emplaced as dikes. If detachment faulting had been responsible for exhuming the pluton, we should expect detachment-parallel plane strain in its upper part, not L-tectonite as exists. Shallow mylonitization was clearly associated with a steep thermal gradient during and following plutonism. Also, tilting to the southeast is not easily incorporated into a detachment fault model. Utilizing elastic failure criteria, tilting in response to large normal displacement should be to the southwest, toward the breakaway fault (King and Ellis, 1990). In the southeastern Waterman Hills, rise of the pluton beneath its cover was 1) only sufficient to expose the dike-dominant upper part, 2) was aided by massive

loss of rock volume by dissolution (Glazner and Bartley, 1991), and 3) was accomplished structurally by collapse on steep faults above and below the WHDF (Fig. 5A, B, D).

If boundary conditions allow for spreading, extension can induce the generation and upward migration of magma as a result of isothermal decompression and dilatancy. Analog modeling by Brun et al. (1994) showed that a localized weak mass, such as a pluton, would rise into a block-tilted overlying layer from which it is separated by a convex-upward fault. Rising magma can induce extension via thermal weakening, forceful injection, and outward spreading as confining pressure lessens. In the CMMCC, mushrooming into an accreting dike swarm may have occurred as confining pressure lessened during magma rise. The result could be defined as an extensional blister (Anderson and Berger, 2007). There may be feedbacks between extension and magmatism: decompression melting can result from extensional thinning and extension can result from magmatic activity that weakens a volume of rock and facilitates extension (Teyssier and Whitney, 2002). As noted by Whitney et al. (2013), partially molten crust in continental areas is likely to facilitate core complex development during extension owing to the dramatic decrease in viscosity and increased buoyancy.

Documentation in the present study of a dike-on-dike emplacement mode for the upper part of the pluton raises the possibility of large-scale synmagmatic dilatant spreading. To form a pluton by dike-on-dike emplacement requires a balance between dilation and magma supply over the period of emplacement. Growth of the pluton is interpreted as the cause of fundamentally fixed-axis tilting and foundering of upper-plate rocks. These relations spawn a tectonomagmatic model of volcanism, volcanogenic sedimentation, extension, shallow mylonitization, and alteration localized above a cogenetic dilatantly emplaced pluton.

A tectonic model for the Eastern California Shear Zone

In the central Mojave Desert, transpressional dextral strike slip of the ECSZ was preceded, and possibly accompanied, by lacustrine and fluvial (conglomeratic) sedimentation and widespread stratal tilting and folding. Although some folds formed at restraining bends in response to the shape of the dextral faults, many did not, and many of those have E-W axes indicating widespread N-S shortening independent of plate-boundary dextral shear (Bartley et al., 1990). Fault-normal shortening is seen at faults that parallel the plate boundary shear direction. A tectonic model of plate-margin shear embedded in a region of N-S shortening best characterizes the ECSZ in the central Mojave Desert area. The model is similar to that defined by major N-S shortening and strike-slip faulting in the Lake Mead area (Anderson et al., 2013). The major difference is the predominance of dextral strike slip in the central Mojave area and sinistral strike slip the Lake Mead area. Prior tectonics also reveal similarities in that they include dilatant accretional emplacement of shallow tilted plutons.

References

Anderson, R.E., Beard, L.S., Mankinen, E.A., and Hillhouse, J.W., 2013. Analysis of Neogene deformation between Beaver, Utah and Barstow, California: Suggestions for altering the extensional paradigm: in Anderson, R.E. ed, Neogene deformation between Central Utah and the Mojave Desert, Geological Society of America Special Paper 499, p. 1-67.

Anderson, R.E., and Berger, Byron, 2007. A blister hypothesis for the central Mojave metamorphic core complex near Barstow, California: Geological Society of America Abstracts with Programs, v. 39, no. 5, p. 227.

Axen, G.J., and Bartley, J.M., 1997. Field tests of rolling hinges: Existence, mechanical types, and implications for extensional tectonics: Journal of Geophysical Research, v. 102, B9, p. 20,515-20,537.

Bartley, J.M., Glazner, A.F., and Schermer, E.R., 1990. North-south contraction of the Mojave block and strike-slip tectonics in southern California: Science, v. 248, p. 1398-1401.

Brun, J.P., Sokoutis, D., and van den Driessche, J., 1994. Analogue modeling of detachment fault systems and core complexes: Geology, v. 22, p. 319-322.

Ferguson, C.A., McIntosh, W.C., and Miller, C.F., 2013. Silver Creek caldera—The tectonically dismembered source of the Peach Spring Tuff: Geology, v. 51, p. 3-6.

Fletcher, J.M., Bartley, J.M., Martin, M.W., Glazner, A.F., and Walker, J.D., 1995. Large-magnitude continental extension: An example from the central Mojave metamorphic core complex: Geological Society of America Bulletin, v. 107, p. 1468-1483.

Fletcher, J.M., Bendixen, J., Fillmore, R., Walker, J.D., Glazner, A.F., and Bartley, J.M., 2002. Geology of the Mitchel Range and Waterman Hills, San Bernardino County, California, in Glazner, A.F., Walker, J.D., and Bartley, J.M., Geologic evolution of the Mojave Desert and southwestern Basin and Range: Geological Society of America Memoir 195, MITWAT on CD-ROM.

Glazner, A.F., Bartley, J.M., and Walker, J.D., 1989. Magnitude and significance of Miocene crustal extension in the central Mojave Desert, California: Geology, v. 17, p. 50-53.

Glazner, A.F., and Bartley, J.M., 1991. Volume loss, fluid flow and state of strain in extensional mylonites from the central Mojave Desert, California: Journal of Structural Geology, v. 13, p. 587-594.

Glazner, A.F., Walker, J.D., Bartley, J.M., and Fletcher, J.M., 2002. Cenozoic evolution of the Mojave block of southern California, in Glazner, A.F., Walker, J.D., and Bartley, J.M., Geologic evolution of the Mojave Desert and southwestern Basin and Range: Geological Society of America Memoir 195, p. 19-41.

King, G.C.P., and Ellis, M.A., 1990. The origin of large local uplift and flank volcanism in extensional regions: Nature, v. 348, p. 689-693.

Martin, M.W., Glazner, A.F., Walker, J.D., and Schermer, E.R., 1993. Evidence for right-lateral transfer faulting accommodating en echelon Miocene extension, Mojave Desert, California: Geology, v. 21, p. 355-358.

McQuarrie, N., and Wernicke, B.P., 2005. An animated tectonic reconstruction of southwestern North America since 36 Ma: Geosphere, v. 1, no. 3, p. 147-172.

Miller, D.M., Leslie, S.R., Hillhouse, J.W., Wooden, J.L., Vasquez, J.A., and Reynolds, R.E., 2010. Reconnaissance geochronology of tuffs in the Miocene Barstow Formation: implications for basin evolution and tectonics in the central Mojave Desert: CSU 2010 Desert Symposium Volume, p. 70-84.

Shelef, E., and Oskin, M., 2010. Deformation processes adjacent to active faults: Examples from eastern California: Journal of Geophysical Research, v. 115, B05308.

Singleton, J.S., and Gans, P.B., 2008. Structural and stratigraphic evolution of the Calico Mountains: Implications for early Miocene extension and Neogene transpression in the central Mojave Desert, California: Geosphere, v. 4, no. 3, p. 459-479.

Teysseir, C., and Whitney, D.L., 2002. Gneiss domes and orogeny: Geology, v. 30, p. 1139-1142.

Walker, J.D., Fletcher, J.M., Fillmore, R.P., Martin, M.W. Taylor, W.J., Glazner, A.F., and Bartley, J.M., 1995. Connection between igneous activity and extension in the central Mojave metamorphic core complex: Journal of Geophysical Research, v. 100, p. 10,474-10, 494.

Walker, J.D., Berry, A.K., Davis, P.J., Andrew, J.E., and Mitsdarfer, J.M., 2002. Geologic map of northern Mojave Desert and southwestern Basin and Range, California: in Glazner, A.F., Walker, J.D., and Bartley, J.M., eds., Geologic evolution of the Mojave Desert and southwestern Basin and Range: Boulder Colorado, Geologic Society of America Memoir 195, scale 1: 250,000.

Whitney, D. L., Teyssier, C., Rey, P and Buck, R.R., 2013. Continental and oceanic core complexes: Geological Society of America Bulletin, v. 125, p. 273-298.

Characteristics of the Eastern California Shear Zone from Southern Death Valley to the northern Bristol Mountains: a review

Roland H. Brady III
Brady and Associates Geological Services, Sacramento California

ABSTRACT—This paper reviews sedimentary continental units and structural relationships that record deposition in rapidly-evolving, syn-tectonic basins along a broad fault zone that extends from southern Death Valley to the Bristol Mountains; these faults are part of the eastern California shear zone. Faulting in this region began in latest Eocene time and continued into the Holocene. In places it is still active. Dextral offset of 20-25 km occurred across this fault zone, mainly on branches east of those presently exposed.

East-directed shortening began in late Miocene and continued into at least the late Pleistocene; it decreases in age and amount of offset southward. This contractile strain may accommodate clockwise rotation of the northeastern Mojave structural block on an axis that lies south of the Bristol Mountains.

Introduction

The most important structural elements of the eastern California shear zone examined here are the Garlock fault zone, and the Death Valley fault zone and its southward extension (Figs. 1 and 2).

Garlock fault zone

The Garlock fault zone is not generally considered to be part of the eastern California shear zone per se. However, since it is a fundamental Quaternary fault system in the region and is kinematically involved with the Death Valley fault zone, it is discussed herein. The Garlock fault zone, the second largest on-shore fault in California, extends 260 km from the San Andreas fault on the west to southern Death Valley on the east, and separates the Mojave structural block to the south from the Basin and Range province to the north.

The Garlock fault zone appears to be a young structure: a growing body of evidence indicates that the inception of slip began between 10 and 7 Ma (Burbank & Whistler, 1987; Loomis & Burbank, 1988). Left-lateral offset of 64 km has been well documented across the fault, and active creep has been measured along its central portion (Smith, 1963; Clark, (1973). Bryant (2000) compiled average slip rates of 11 mm/yr for the western segment of the fault zone, and 1 mm/yr for the eastern segment, with an overall average slip rate of 7 mm/yr. McGill and Sieh (1991) estimated a slip rate of ~3 mm/yr for the eastern Garlock fault in the Avawatz Mountains, with an earthquake recurrence interval of 300-2000 yrs. They also noted that the vertical displacement of

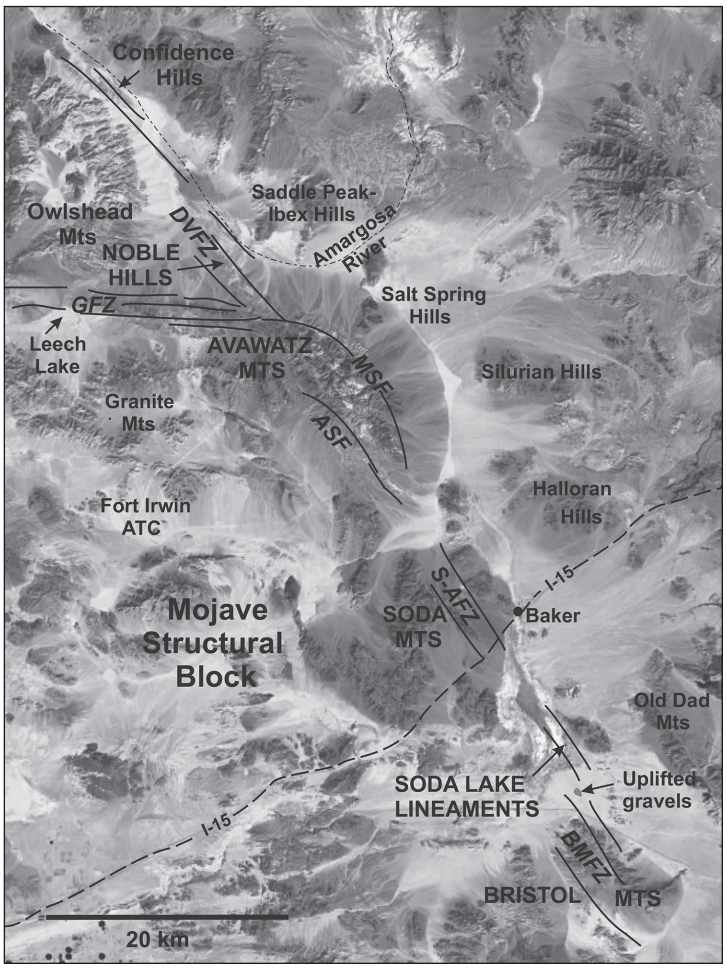

Figure 1. Google Earth location map. Features discussed herein noted in capital letters. DVFZ = Death Valley fault zone, GFZ = Garlock fault zone, MSF = Mule Spring fault, ASF = Arrastre Spring fault, S-AFZ = Soda-Avawatz fault zone, BMFZ = Bristol Mountains fault zone.

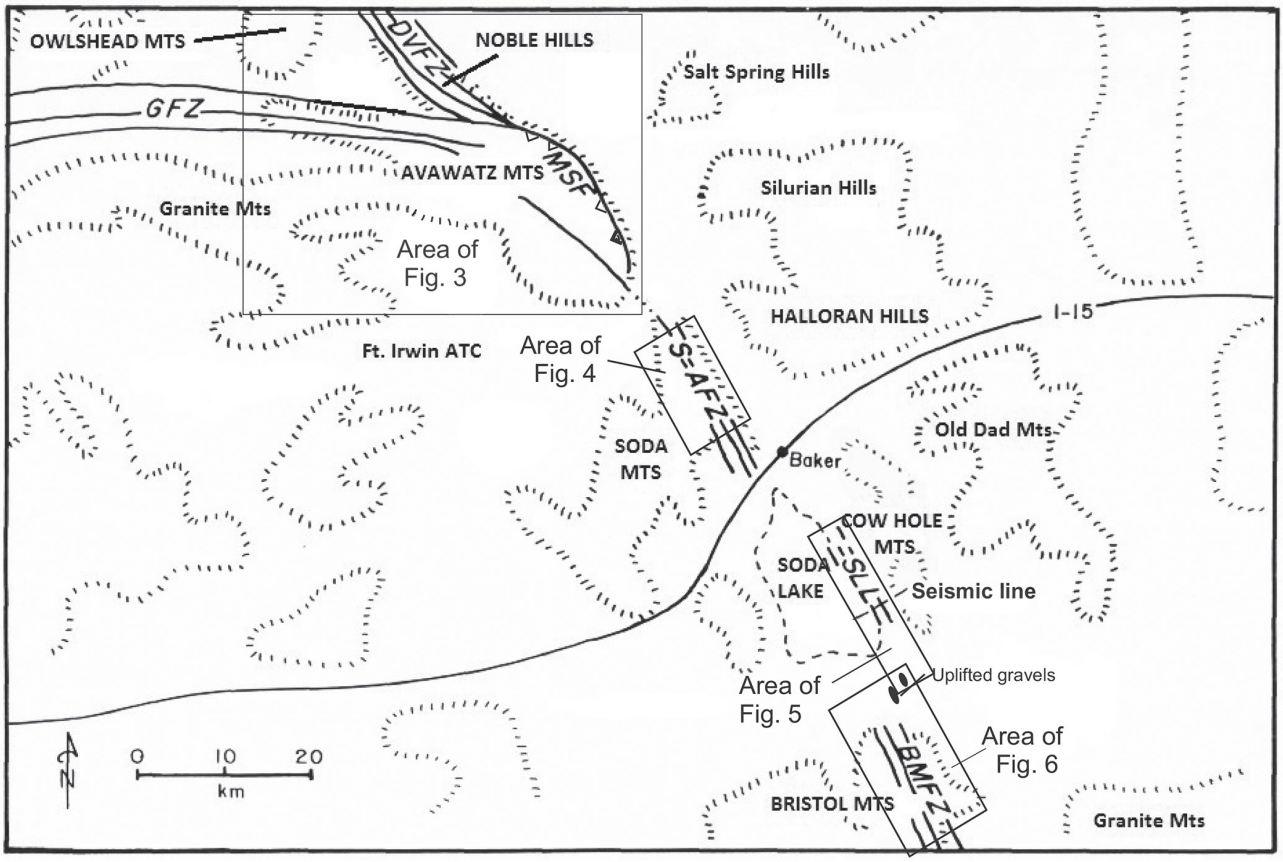

Figure 2. Sketch location map showing areas of other figures. DVFZ = Death Valley fault zone, GFZ = Garlock fault zone, MSF = Mule Spring fault, S-AFZ = Soda-Avawatz fault zone, SLL = Soda Lake lineaments, BMFZ = Bristol Mountains fault zone.

offset Quaternary geomorphic features along the Garlock fault zone on the north side of the Avawatz Mountains is approximately 13% of the total documented left-lateral offset there.

Death Valley fault zone

The Death Valley fault zone is the southern end of a larger fault system at least 210 km long that reaches northward from the Noble Hills to the north end of Death Valley (Fig. 1). Together, this system is generally accepted to have accommodated the pull-apart opening of Death Valley beginning in late Miocene time (Burchfiel and Stewart, 1966). However, its present role in the regional tectonic regime of the eastern California shear zone is unclear.

The Death Valley fault zone, the principal structure examined in this paper, extends through the Confidence Hills to the Noble Hills on the north edge of the Avawatz Mountains (Noble and Wright, 1954) and possibly beyond (Stewart, 1967; Dibblee, 1980; Brady, 1984) (Fig. 1). Where observed, separation across the numerous branches of the Death Valley fault zone is consistently right lateral (Hill and Troxel, 1966) and, although the total has been contested, ranges from 80 km (Stewart, 1967) to less than 8 km (Davis, 1977).

In order to shed light on the age, structural style, and offset history of the eastern California shear zone, this paper examines stratigraphic and structural features in five critical areas from southern Death Valley to the northern Bristol Mountains; from north to south these are: 1) Noble Hills, 2) Avawatz Mountains, 3) Soda Mountains, 4) Soda Lake, and 5) Bristol Mountains (Fig. 2). This examination focuses on understanding the areal extent of dextral and reverse faulting along the southward projection of the Death Valley fault zone through the Soda-Avawatz and Bristol Mountains fault zones.

Noble Hills

The Noble Hills extend 14 km northwestward from the northeastern Avawatz Mountains (Fig. 3) and rise approximately 310 m above the floor of Death Valley. The overall geology of the Noble Hills was originally described by Noble and Wright (1954). Here, the Death Valley fault zone is nearly 5 km across and contains five, sub-parallel branches.

Cenozoic stratigraphy of the Noble Hills

Stratigraphic units in the Noble Hills include hundreds of meters of Tertiary fanglomerate; fluvial conglomerate, sandstone, and claystone; lacustrine clastics, limestone and tuff, and playa gypsum, halite, and dune sand referred to as the Noble Hills assemblage and the Military Canyon formation (Fig. 3). The stratigraphy of these units is detailed in Brady, (1984, 1986) and Brady and Troxel (1999).

Near its base, the oldest sedimentary unit in the Noble Hills assemblage contains a notable purple andesite

agglomerate that yielded at K-Ar date of 11.3 + 0.6 Ma--middle Miocene. Detritus in these beds is composed nearly exclusively of granite and gneiss. This petrology is unlike bedrock in the Avawatz Mountains, which is mainly dark green monzodiorite and metavolcanics of Jurassic age, with lesser bodies of granite, minor roof pendants of Precambrian (Pahrump Group) sedimentary rocks, and Paleozoic marble (Jennings, Burnett, and Troxel, 1962). Paleocurrent data indicates northwest and westward transport. These two factors indicate that the Avawatz Mountains, which lies to the south, was not the sediment source (as discussed in the section Death Valley Fault Zone). However, detritus in the younger strata, and in correlative, tuff-bearing beds in the southern Owlshead Mountains K-Ar dated on biotite at 8.49 + 0.24 and 6.31+ 0.21 Ma (Brady, 1992a) does match bedrock types in the Avawatz Mountains. This sediment was also transported northward, as would be expected.

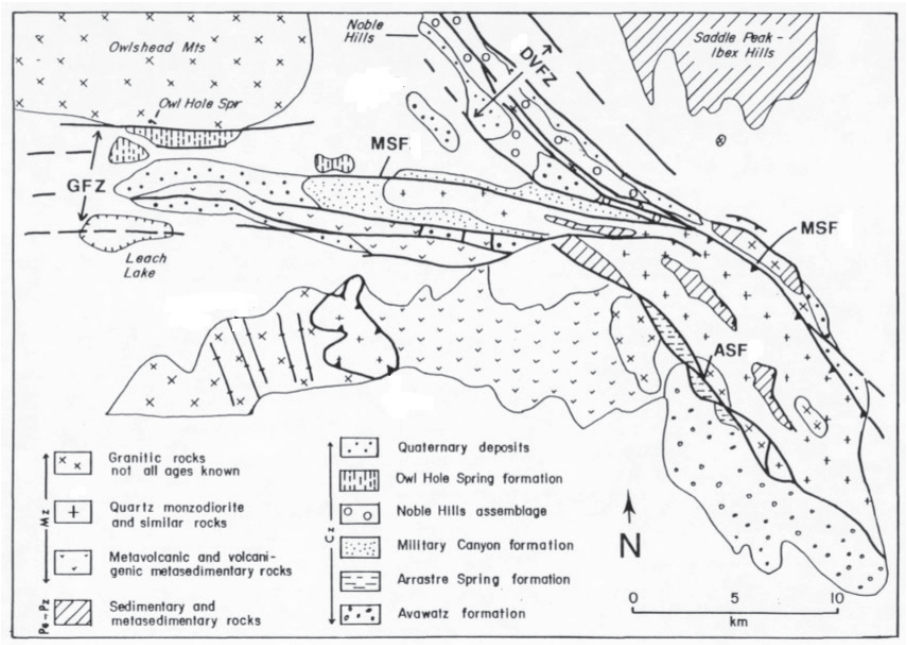

Figure 3. Generalized geologic map of the Avawatz Mountains and Noble Hills. DVFZ = Death Valley fault zone, GFZ = Garlock fault zone, MSF = Mule Spring fault, ASF = Arrastre Spring fault.

A section of monolithologic fanglomerate is well exposed along the eastern edge of the Noble Hills (Fig. 2). The strata dip moderately northeast, and are bounded on both sides by branches of the Death Valley fault zone. The northernmost exposures are conformably overlain by younger alluvial fan deposits. Although the age of the monolithologic fanglomerate is unknown, it is probably Plio-Pleistocene because its characteristics are similar to dated strata of the Owl Hole Spring formation in the southern Owlshead Mountains (Brady, 1992a) (Fig. 3). The fanglomerate is a thickening- and coarsening upward sequence representing a prograding alluvial fan complex. Detritus consists nearly entirely of coarse-grained granite with some vesicular basalt, and a trace of euhedral, smoky quartz crystals. The distinctive petrology of its clasts restricts its source to be the Owlshead Mountains 8-10 km to the northwest. However, the granitic bedrock of the Owlshead Mountains readily breaks down to grus, and nearly all of the detritus in mid and distal alluvial fans presently surrounding the range is finer than a few centimeters in diameter. Coarse conglomerates, such as those in the upper section of the monolithologic fanglomerate, presently extend no farther than 5 km from the bedrock source. This indicates that the monolithologic fanglomerate was originally deposited approximately 5 km closer to the Owlshead Mountains. The implications of this are discussed below.

Death Valley Fault Zone in the Noble Hills

In the Noble Hills, the Death Valley fault zone consists of five, main branches (Fig. 3) and numerous, lesser, sub-parallel faults that form an anastomosing pattern probably representing a complex "flower structure" that merges at depth. Individual branches juxtapose crystalline basement with Miocene and younger strata, and Plio-Pleistocene fanglomerate with younger fan deposits (Fig. 3). This configuration is similar to that in the Confidence Hills 20 km north (Dooley and McClay, 1996), but exposures in the Noble Hills are of a deeper structural level. North of the Noble Hills, fault branches either die out or are buried by ca. 130 alluvial fans (McGill, 1994), that extend eastward from the Owlshead Mountains.

The age of faulting decreases toward the northeast across the Death Valley fault zone. For example, the southwesternmost branch in the Noble Hills which juxtaposes Plio-Pleistocene fanglomerate against Miocene strata, has been folded by movement on younger faults farther northeast in the Noble Hills. The branch along the northeast edge of the Noble Hills is overlain by Quaternary fanglomerate; about 1 km farther northwest this same fanglomerate is faulted. About 3 km northeast of the Noble Hills, en-echelon fault branches uplift Holocene deposits. Butler et al., (1988) showed that the Amargosa River channel is responding to Recent faulting. The estimated dextral displacement of Quaternary sediment is on the order of ~8 km yielding a tentative slip rate of 1-5 mm/yr (Machette & Piety, 2001).

Discussion: Noble Hills

Bedrock in the Avawatz Mountains does not appear to have been the source for sediment in the oldest

stratigraphic units in the Noble Hills. Not only are the main conglomerate clast types--granite and gneiss--not abundant as bedrock, but also, monzodiorite and metavolcanics, the most voluminous types of bedrock in the Avawatz Mountains are absent in the sediment. As well, sediment transport was from east to west, 90 degrees from the Avawatz range, which lies to the south. The most likely provenance is the Halloran Hills located 20-25 km south of the range (Figs. 1 and 2). There, bedrock is mainly composed of granite, gneiss, and minor metasedimentary rocks; pebble counts in Tertiary redbeds are virtually identical to those in the Noble Hills. These relationships would be explained if the Halloran Hills lay east of the Avawatz Mountains during late Miocene time, and shed sediment into the basin. They were then offset 20-25 km south to their present position by dextral shear along the Death Valley fault zone. When the Avawatz Mountains were uplifted, they become the sediment source. This large offset is consistent with the presence of clasts of 18.5-Ma Peach Springs tuff in the Avawatz Formation in the southern part of the range. However, the nearest outcrops of the tuff are some 20 km to the southeast on the east side of the Death Valley fault zone (Glazner, Nielson, Howard, and Miller, 1986).

Although the total slip across the Death Valley fault zone is on the order of 20-25 km, slip across individual branches in the Noble Hills is probably less than 10 km. The greatest offset--on the branch that cuts the Owlshead-derived, monolithologic fanglomerate--is no more than 5 km.

The age of offset appears to decrease eastward. Faults in the western Noble Hills are overlain by Pleistocene fans, but to the east, along the Amargosa River, Holocene lacustrine strata and extensively folded and faulted (Butler et al., 1988). Based on deformation there, Wesnousky (1986) estimated the maximum slip rate to be 3 mm/yr, and the interval between major ruptures to be 1000 years. The slip rate is consistent with values proposed by Brady (1992a).

Avawatz Mountains

Garlock fault zone in the Avawatz Mountains

The Garlock fault zone in the Avawatz Mountains was first noted by Noble and Wright (1954). Hewett (1954) and Troxel et al., (1972) speculated that the fault zone "died out" as a reverse fault on the east flank of the range, but Davis and Burchfiel (1973) contended that it extended some 30-40 km to the east, crossing the Death Valley fault zone. To understand the relationship between the Garlock and Death Valley fault zones Troxel and Butler (1979) mapped the northeastern part of the range. Brady (1986) mapped the entire northern Avawatz Mountains and Brady et al. (1988) described structural and stratigraphic relationships between faulted alluvial fans of the eastern Avawatz Mountains.

In the Avawatz Mountains, The Garlock fault is a vertical, east-striking shear zone approximately 7.5 km across from the southern Owlshead range to the northern Avawatz Mountains (Fig. 1). The zone extends across the entire northern length of the Avawatz Mountains and wraps around to its east side. It contains numerous, anastomosing branches from less than 1 km to over 10 km long that deform bedrock, Tertiary sedimentary units, and Quaternary alluvial fans. McGill (1994) noted that the youngest offsets cut fans in the Avawatz Mountains that are less than 15 ka, and estimated that Holocene slip rates are 1-5mm/yr.

The most fundamental branch of the Garlock fault zone in the Avawatz Mountains is the Mule Spring fault (Fig. 3) because it forms the structural boundary between bedrock, and Tertiary and Quaternary strata to the north, and is the only branch that could accommodate tens of kilometers of slip across it as required by the offset of pre-Tertiary rocks in the Slate Range farther west. In the north-central Avawatz range, the Mule Spring fault strikes east and is vertical; numerous slickenlines indicate slip left-lateral oblique, south side up, as would be expected. However, as the fault wraps around to the northeast, its dip flattens southward, and sense of offset becomes reverse, uplifting the bedrock diorite to its present height of 1876 m. A gravity survey up the front of the range (Brady, 1986) supports the interpretation that the monzodiorite bedrock, although covering more than 50 km^2, is a thin slab 2.2 km thick that overlies less dense rock along a west-dipping fault.

On the basis of apatite fission-track and apatite helium cooling ages from the Avawatz diorite, Chinn (2013) posited that the uplift occurred less than 10 Ma, coinciding with the onset of slip on the Garlock fault zone as suggested by other estimates (Burbank & Whistler, 1987; Loomis & Burbank, 1988). Although Chinn (2013) stated that there is no evidence of vertical motion on the Mule Spring fault since at least late Miocene time, in the east-central part of the range, the fault dips 35 degrees west, and places bedrock monzodiorite over Miocene strata and Pleistocene fanglomerate. At the southernmost end of the range, the Mule Spring fault splays into five branches that dip 45 degrees west, deforming younger Pleistocene fanglomerate (Greene, Redwine, and Miller, 2007).

Detailed field work in the alluvial fans suggest that additional uplift has occurred on blind thrusts beneath the range front (Menges et al. 2005; Mendonca, 2007; Green, Redwine, and Miller, 2007). East-vergent, reverse faults and minor folds deform Pleistocene alluvial fan and debris flow complexes in the range front (Stroud and McGill, 1994). Uplift has also stranded numerous alluvial fans as strath unconformities as much as 10 meters above the active channel (Menges and Miller, 2007). Within these uplifted fans are numerous thrust faults juxtaposing fans of differing grain size against one another (Menges and Miller, 2007). At the southern end of the range,

bedrock is thrust over alluvium. The various contractional structures in the front range of the Avawatz Mountains represent a series of steep, thick-skinned faults that accommodate northeast-directed uplift. The most recent surface deformation on the frontal fold-thrust system is estimated to precede or possibly occur within the latest Pleistocene time. The active front of deformation has not moved far over time, and the structures with younger reverse displacement are those more distal to the Avawatz massif (Menges and Miller, 2007), accommodating the cumulative uplift of the range.

The Arrastre Spring fault in the interior of the range (Fig. 3) is clearly truncated by the Garlock fault and has no evidence of Quaternary activity (Spencer, 1981). Although it was undoubtedly active during the time of initial uplift of the Avawatz Mountains (late Miocene), the Arrastre Springs fault is kinematically isolated and presumably inactive. Although it is parallel to faults on the eastern range front, there is no active slip transfer.

Discussion, Garlock fault

The left-lateral Garlock fault terminates in the Avawatz Mountains along the Mule Spring reverse fault(s), and does not continue farther east as Davis and Burchfiel (1973) proposed.

The Mule Spring fault places the massif of the Avawatz Mountains eastward over the Death Valley fault zone which appears to continue southward beyond the range. This east-directed reverse faulting may, in part, be responsible for the eastward shift of activity along the Death Valley fault zone (Butler et al., 1988).

Uplift on the Mule Spring fault and its subsidiaries can account for the entire height of the range, and would have begun in mid-Miocene time, when monzodiorite- and metavolcanic-derived sediment started infilling the basin to the north. The fault could occupy a pre-existing, low-angle fault such as in the westernmost Avawatz Mountains that cuts Jurassic metavolcanic rocks (Fig. 3).

The transpressional uplift has generated a southwest-to-northeast directed contractional strain across the boundary, indicating a fundamental transition in structural geometries, style, and mechanics of the faulting in this transition, and that at least some slip is transferred between the intersecting faults. This style of faulting could be a response to 30 degrees of clockwise rotation of the northeastern Mojave block (Smith, 1962; Luyendyk, 1991). Regardless, this relationship represents a tectonically significant domain of east-directed, contractile strain within the predominantly dextral eastern California shear zone.

Soda Mountains

The Soda Mountains lie due south of the Avawatz Mountains (Fig. 1). Grose (1959) defined bedrock and Cenozoic units and the main structural framework: the Soda-Avawatz fault zone. Davis (1977) suggested that the Soda-Avawatz fault (zone) (Fig. 4) was the southward continuation of the Arrastre Spring normal fault in the Avawatz Mountains (Fig. 2). Gourley (2000) and Brady mapped the fault zone in detail and examined the stratigraphic and structural relations to resolve the age and style of faulting.

From west to east, the Soda Mountains has three domains (Fig. 3): 1) Mesozoic granitoids with pendants of Paleozoic limestone, Jurassic metavolcanic rock, and quartzites of the distinctive Aztec Sandstone, 2) the Soda-Avawatz fault zone consisting of faulted Tertiary continental strata and bedrock; and 3) Precambrian gneiss, Mississippian-Permian (Bird Spring?) marbles, and Mesozoic granitic rocks.

Cenozoic stratigraphy of the Soda Mountains

Tertiary sedimentary strata of the Soda Mountains correlate with the Miocene Avawatz Formation in the southern Avawatz Mountains to the north (Henshaw, 1939; Grose, 1959) (Fig. 4) where tuff from its lower member yielded a K-Ar date on biotite of 20.9±0.2 Ma (Spencer, 1993).

Three members of the Avawatz Formation are exposed along the Soda-Avawatz fault zone (Gourley, 2000). The lower member is a proximal fan deposit of poorly indurated, boulder-to-cobble conglomerate and minor

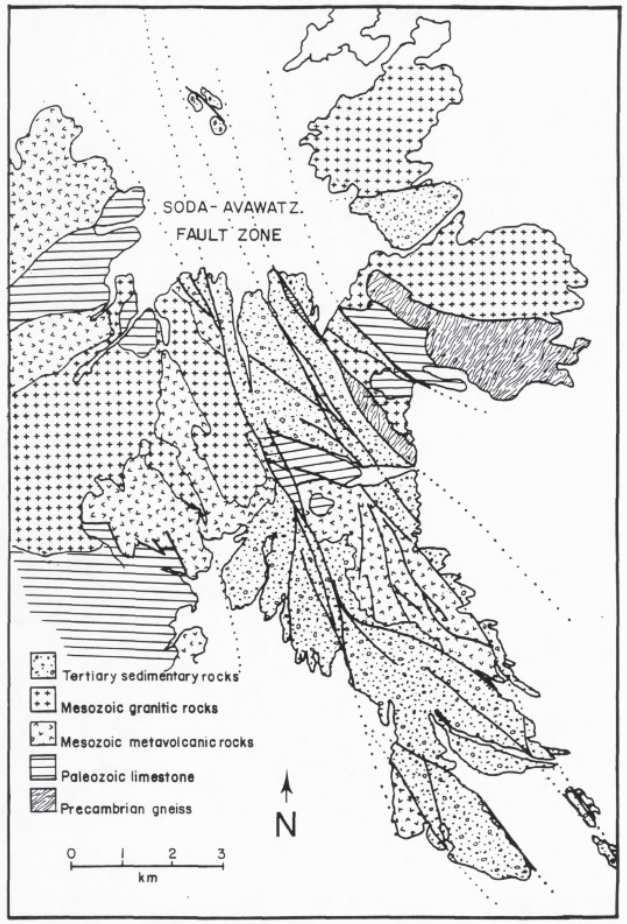

Figure 4. Generalized geologic map of the eastern Soda Mountains along the Soda-Avawatz fault zone.

finer-grained strata. Clast types include metavolcanic, sandstone, granitic rock, gneiss, and breccia from the Bird Springs Formation.

The middle member is well indurated, sandstone, siltstone and minor tuff with interbeds of cobble conglomerate deposited in a mid-fan environment. Clasts are limestone, metavolcanic, granite, intermediate intrusive rock, and quartzite (Aztec Sandstone). On the basis of shard chemistry, one of the tuffs is tentatively correlated to a dated tuff having a K-Ar age of 11.6-11.8 Ma (Brady et al., 1988). In the southwestern part of the area, the middle member conformably overlies the lower member, but elsewhere the contact is faulted.

The upper member is coarse, clast-supported conglomerate having poor bedding and induration. This unit represents deposition in a proximal fan environment, and is difficult to distinguish from the overlying Quaternary alluvial fan deposits.

Point counts of clasts in the Avawatz Formation match bedrock types in the Soda Mountains, with the exception of gneiss in the lower member that is not present in the bedrock here (Gourley, 2000). Paleocurrent directions in the lower and middle members were mainly northward, but in the upper member, stream flow was eastward.

Quaternary fanglomerate lies within the fault zone and is faulted against the Avawatz Formation. Desert pavement with varying degrees of varnish development has formed on its uplifted areas, which are as much as 3-7 m above the modern channels. On the basis of soil development, a deformed surface developed on the unit has been tentatively correlated with the 200,000 year-old Qfo surface of Ritter (1985) in the Silver Lake area.

The Soda-Avawatz fault zone

The Soda-Avawatz fault zone has at least five, near-vertical, through-going branches (Fig. 4). These faults have straight or slightly curved traces, and juxtapose basement rocks with the Avawatz Formation. Domains between the major faults contain numerous smaller shears and folds (Gourley, 2000).

The faults vary from knife-thin to 8 m-wide zones of tectonically powdered rock. Consistently, the faults strike north-northwest, and dip steeply (70-90 degrees) east. Vertical displacement of a few meters both up and down, is common within the zone, but nearly all the fault plane striations rake 10-30° north. Discontinuous, sub-parallel, minor shears are common; these were interpreted to be Mode II Reidel shears, and their geometry is most consistent with dextral faulting. Of 16 sense-of-slip indicators measured, 14 indicate right-lateral and two left-lateral faulting (Gourley, 2000).

Within the fault zone, a shallowly plunging, major anticline and en-echelon syncline in the Tertiary rocks trend about 312°. The anticline's core is composed of metavolcanic rocks, which do not appear to have been folded, indicating that the structure may be related to faulting rather than to regional compression. If so, its geometry is consistent with dextral shear.

Discussion, Soda Mountains

The Miocene Avawatz Formation was deposited in a basin formed by southwest-side-down normal movement that began by 21 Ma and was over by approximately 12 Ma (Spencer, 1990). This is coincident with Cenozoic extension that affected the Mojave region and southern Basin and Range province. The Avawatz Formation overall is an upward-fining, alluvial fan-fluvial-lacustrine complex (retrograding fan). The provenance of its lower member includes bedrock types presently in the Soda Mountains to the west, but paleocurrent directions indicate that sediment was derived from sources to the south and east. Aside from the Soda Mountains, the nearest exposures of similar rocks are in the Cow Hole Mountains on the east side of Soda Lake, some 20 km south (Fig. 1). If this source lay east of the Avawatz Formation depocenter, as it would have if the Halloran Hills were east of the Noble Hills' depocenter, it could have shed sediment into the lower and middle members of the Avawatz Formation (Gourley, 2000). This is consistent with the suggestion in Wadsworth, Ferriz, and Rhodes (1995) that Jurassic metavolcanic rocks of the Soda Mountains Formation were tectonically offset from similar rocks in the Cow Hole Mountains.

Deformation along the Soda-Avawatz fault zone occurred along with deposition of the Avawatz Formation. Accord (1986) conducted a gravity survey in the lowlands just north of the Soda Mountains, and concluded that the depression represented a pull-apart basin associated with dextral slip along the Soda-Avawatz fault zone. Although the main offsets across the faults are right strike-slip, east-directed contractile strain also occurred. Based on seismic refraction data Honeycutt et al., (1986) proposed that the Soda-Avawatz fault zone was an older, strike-slip fault system (as Gross, 1959 contended), later overprinted by east-vergent thrusting.

The maximum displacement across the Soda-Avawatz fault zone is approximately 20 km, but that would have to have occurred on unexposed branches east of those in the Soda Mountains. Deformed fans indicate that movement continued into Quaternary time.

Correlation of the Soda-Avawatz fault zone with the Arrastre Spring fault in the Avawatz Mountains as proposed by Davis (1977) is untenable for two reasons. First, the Arrastre Spring fault is overlain by an undeformed tuff deposited 11-12 my ago (Spencer 1993), whereas deformation along the Soda-Avawatz fault zone has occurred in Quaternary time. Second, unlike the Soda-Avawatz fault zone, which shows primarily strike-slip movement, the Arrastre Spring fault shows mainly dip-slip movement with the west side down (Spencer, 1990).

Structural, stratigraphic, geochronological evidence and gravity geophysical evidence supports the contention

that the Soda-Avawatz fault is a dextral strike-slip system similar in structural style, age, and displacement to the Death Valley fault zone. East-directed shortening occurred as a late phase.

Soda Lake

Soda Lake Lineaments

Soda Lake playa is situated approximately 5 km south of the town of Baker and occupies the basin between the Soda Mountains and the Old Dad Mountains (Fig. 1). Active sand dunes cover the southern end of the playa, separating it from the Bristol Mountains 4 km farther south. Steven Wells and his students (pers. comm., 1987) pointed out two pronounced lineaments on black-and-white air photos that cross the east-central part of Soda Lake (playa) (Fig. 5). On satellite imagery, there are six pronounced and three less obvious lineaments became evident along the eastern margin of the playa (Brady et al. 1988). The lineaments trend north-northwest in a zone several meters wide, each ranging from 0.5 to nearly 3 km long. Herein, the zone is referred to as the Soda Lake lineaments.

The Soda Lake lineaments are formed by sub-parallel rows of fresh-water phreatophyte plants, mainly mesquite. The land surface is smooth and nearly flat, and is punctuated by coppice dunes that have formed around the mesquite, accentuating the relief of the lineaments.

Mesquite bushes are salt-intolerant. Here, their growth is conspicuous because they are in a highly soda-saline area of the playa and are surrounded by salt-tolerant and salt-loving plants such as pickleweed and salt grass. Most likely the regional groundwater gradient from the Old Dad and Cow Hole Mountains slopes west toward Soda Lake. Water from wells in the alluvial fans just east of Soda Lake is of potable quality, whereas the water beneath Soda Lake is too saline for use (R. Foster, pers. comm., 1987; manager, Zzyzx Research Station). The botanical lineaments appear to have formed above narrow, planar, vertical groundwater barriers of high permeability that are intercepting the groundwater on the east side of the lake, and causing it to flow upward to the surface through the overlying salt- and soda-bearing playa deposits along north-northwest striking, high-angle faults-that are the southward projection of the Soda- Avawatz fault zone.

Gravity, magnetic and seismic studies were undertaken across the lineaments and into Soda Lake in collaboration with R. Negrini and students from California State University, Bakersfield. Taken together, the seismic and gravity data indicate that the subsurface consists of a body of mixed but high velocities (Layer 2) that lie 7 -15 m beneath an upper layer (Layer 1) of uniformly low velocity. Below the lineaments, the interface between these layers is irregular, or varying depth beneath the ground surface. Conversely, west of the lineaments, out in the lakebed, the subsurface is considerably more uniform geophysically, and the Layer l/Layer 2 interface is smoother. Whereas

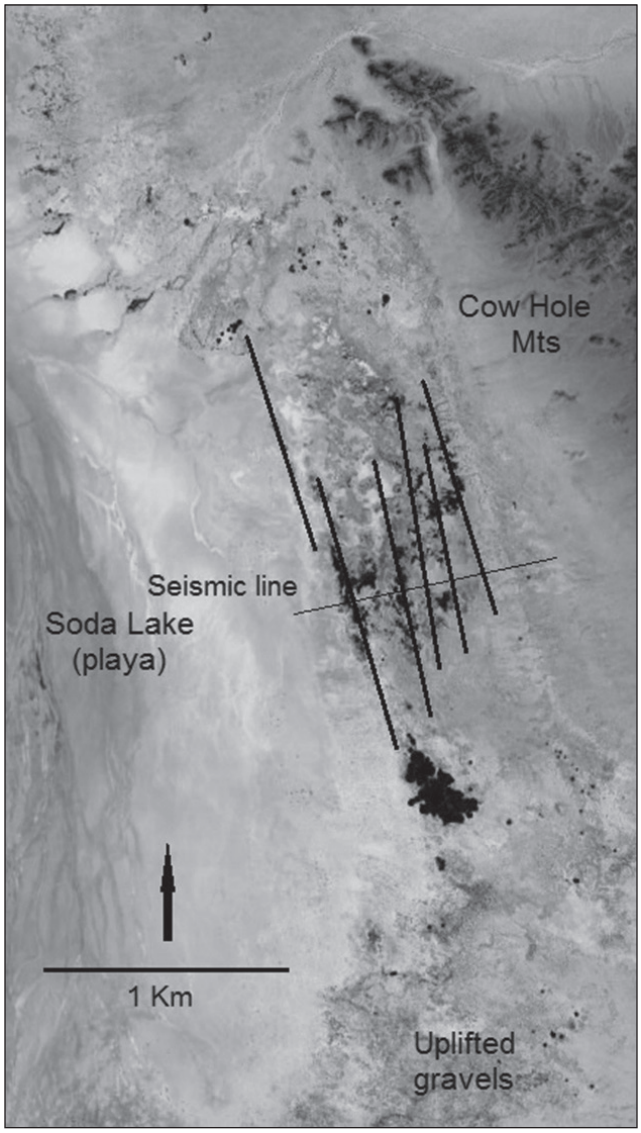

Figure 5. Google Earth image of the Soda Lake lineaments showing position of seismic line, and uplifted gravels.

between the lineaments, the boundaries between individual velocity "blocks" within Layer 2 do not align precisely with the individual lineaments, the overall boundary of mixed velocities in Layer 2, and the irregular interface between Layers 1 and 2 correlates well with the zone of lineaments overall.

The geophysical data are consistent with the interpretation that the Soda Lake lineaments are northwest-striking, high-angle faults. Because fresh groundwater is at or near the surface along the lineaments, the zone of high permeability, likely corresponding to the faults, also reaches the surface. This indicates that the faults have probably moved during Quaternary time.

Uplifted gravels

Several isolated bodies of mainly granitic-derived gravel, each several tens of m^2, protrude through the dune sand at the southeastern end of Soda Lake (S. Wells, pers. comm., 1987) (Figs. 5, 6). The bodies are approximately 7

km southeast of and directly aligned with the Soda Lake lineaments. The two most likely genetic interpretations are: (1) they are remnants of high-standing, relict Pleistocene gravel bars from ancient Soda Lake or (2) they are older gravel deposits that have been uplifted (or folded) along sub-parallel faults.

The gravels are probably not gravel bars because: (1) their position is not coincident with other known shoreline features, (2) the clasts are moderately sorted and sub-angular to sub-rounded granite rather than being well-rounded and well-sorted as are clasts in other Pleistocene bars of Soda Lake (Wells et al., 1984), and (3) the conglomerates lack the southward, back -dipping imbrication characteristic of other beach bars of Soda Lake.

Most likely, the gravels are uplifted, distal portions of older Quaternary or late-Tertiary alluvial fans emanating from the Bristol Mountains. Their presence indicates that the faults causing the Soda Lake lineaments may continue beyond the southeastern margin of Soda Lake and, because the outcrops are topographically higher than the surrounding dunes, the conglomerate may have been uplifted during Quaternary (Holocene?) time. Unfortunately, sand dunes obscure any intervening surface expressions of the gravels or faults.

Discussion, Soda Lake

The geometry and hypothesized origin of the lineaments on the east side of Soda Lake, and the (deformed?) fan gravels at its south end are consistent with the presence of northwest-striking, high-angle, Holocene(?) faults here. Although the relationships here do not constrain the amount or sense of slip, these features align with the southward projection of the Soda-Avawatz fault zone.

Northern Bristol Mountains

The northern Bristol Mountains (Fig. 1) are the southernmost area examined herein. The mountains lie at the south edge of Soda Lake. Formerly accessible only with great difficulty by four-wheel drive along dry washes, they now lie within the Wilderness area of the Mojave National Preserve, so are closed to vehicles.

Since reconnaissance work of Basset and Kupfer (1964), the only mapping of the area is that of Brady (1992b) and Francke-Loriz (1993). The northern Bristol Mountains are composed mainly of Mesozoic granitic rock and minor amounts of Precambrian (?) gneiss on the western margin. Large slabs of C-S mylonite lie along the east side of the range, but unfortunately were not seen in place. The range is flanked on the west by thick deposits of conglomerate and is partly buried by Quaternary and Holocene sand dunes on the north.

Cenozoic stratigraphy of the Bristol Mountains

The northern Bristol Mountains contain five (described) sequences of faulted and folded Cenozoic sedimentary strata that were deposited in syntectonic basins along the northwest-striking Bristol Mountains fault zone. On Figure 6, these are noted as the Plio-Pleistocene fanglomerate; and the Coppermine Wash, Boulder Wash, Balch Wash, and Tortoise Wash sequences named for the informal declivities in which they lie (Brady, 1992b). The most elevated of these strata, the Balch Wash sequence, lies nearly 350 m above the floor of Soda Lake.

The sedimentary sequences range from 23 to 130 m thick, and consist of locally-derived (granitic and metavolcanic) conglomerate, arkosic sandstone, sandy siltstone, limestone, basalt and tuff, deposited in proximal to distal alluvial fans and lake margins. Basalt in a basal conglomerate of the section of the Balch Wash sequence (Fig. 6) yielded a K-Ar age of 27 ± 0.6 Ma on feldspar. A rhyolite tuff closely overlying the basalt yielded a concordant K-Ar age of 26.0 ± 0.6 Ma and 26.7 ± 0.6 Ma on biotite and hornblende, respectively. An older fanglomerate near Balch Wash consists of cobble conglomerate, thinning and fining upward to sandstone and sandy siltstone, and represents a retrograding alluvial fan. Clasts are mainly granitic with Tertiary volcanics, and minor quartzite and marble—bedrock types not presently exposed in the Bristol Mountains. Its age is unknown, but presumed to be Plio-Pleistocene. The fanglomerate is in low-angle fault contact with the Balch Wash sequence.

Eroded patches of relict Quaternary alluvial fan deposits unconformably overlie the Tertiary sequences and bedrock. In places these gravels are faulted into the Tertiary rocks. The clasts are composed nearly entirely of green and pink granite clasts presumably derived from local bedrock. Recent erosion has channeled to depths of 9 m, causing the upper surface of the gravels to be abandoned as a surface of deposition. The upper surface has low bar-and- swale micro-topography, relief is due to single clasts. Desert varnish is dark and thick, and the undersides of clasts are reddened to 2.5YR 5/6 (Munsell). Underlying soil has a strong cambic B horizon and a well-developed petrocalcic horizon. Stephen Wells (pers. comm., 1990) examined the surface and suggested that it was strikingly similar to the Late Pleistocene "Qf1" of Ritter (1985) in the Silver Lake area east of the Soda Mountains. This fan surface is truncated in several places on both the east and west sides forming east-facing scarps 1-1.5 m high.

Bristol Mountains fault zone

The northern Bristol Mountains fault zone possesses a marked northwest-trending topographic grain produced by sub-parallel, vertical faults, some of which extend the length of the range (Brady, 1993c). Lesser-developed faults strike north and are from one to two kilometers long. Some faults solely juxtapose bedrock, but others bound basins filled with Tertiary and Quaternary continental strata. Quaternary fan deposits and surfaces are clearly offset by northwest or north-striking faults. All of the major faults in the range are marked by intense

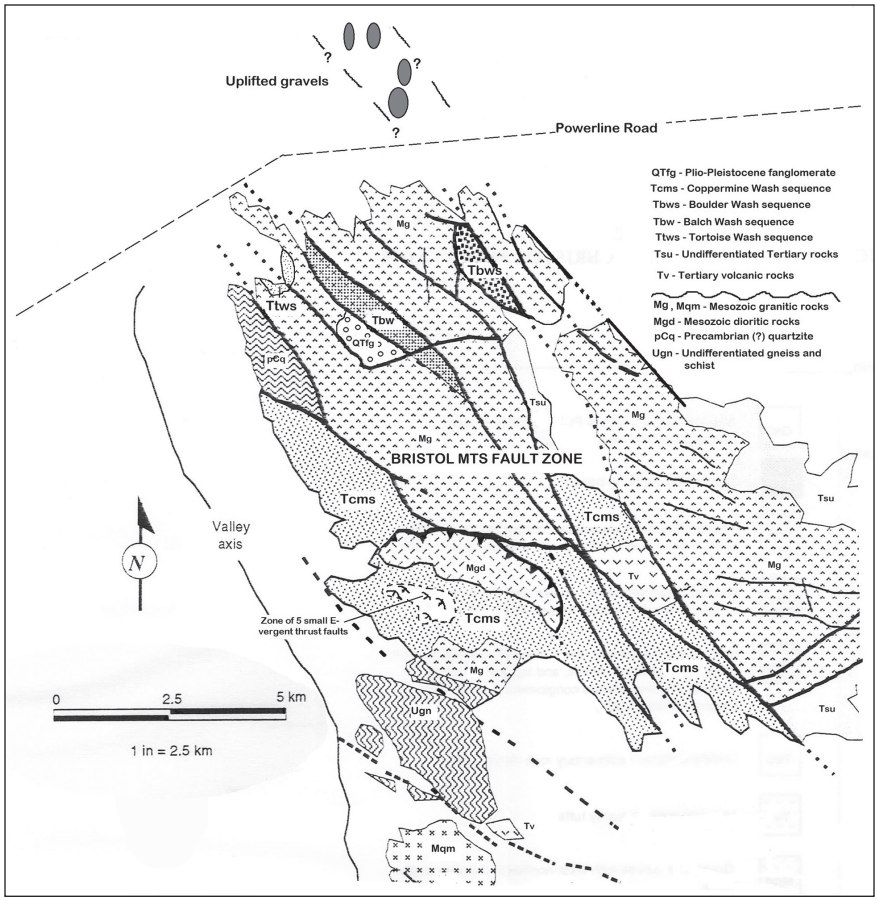

Figure 6. Generalized geologic map of the northern Bristol Mountains and uplifted gravels south of Soda Lake. Locations of Cenozoic sedimentary strata indicated.

brecciation; in some places the rock has been sheared to sand and gouge, but in others the fault breccia includes fragments up to 8 m in diameter.

The most prominent faults are those that bound the Balch Wash and Boulder Wash sequences (Fig. 6). On the east is a zone of sub-parallel, north-northwest striking, vertical faults that place the sedimentary strata against granitic rock. Within 50 m of the fault zone, beds are complexly cut by minor high- and low-angle faults and are broadly to tightly folded. In several places, fault-bounded slabs of granitic bedrock are tectonically intersheaved with Tertiary strata and with the overlying fanglomerate. The fault zone varies from several discreet, well-defined faults, to a diffuse mass of sheared and altered rock nearly 45 m across in which the granitic protolith is all but indistinguishable. There are numerous, sub-parallel, minor faults whose separation appears to be limited to a few tens of meters. Near-horizontal slickenline orientations in gouge indicate that the dominant shear sense is right lateral.

A fault between the Balch Wash and Boulder Wash sections juxtaposes pink granitic rock on the east, against highly chloritic-altered green, granitic rock on the west. Although the aerial limits of the chlorite alteration were not exposed, for a distance of 8 km neither rock type crops out on the opposite side of the fault. It is unlikely that the chloritic alteration developed after the faulting because it is confined to the west side of the fault, and the protolith is the same kind of granitoid as exists across the fault.

Reverse faults

In the south-western part of the range, a prominent reverse fault places granitic rocks, eastward over the Miocene(?) Coppermine Wash sequence (Fig. 6). The amount of slip is unconstrained, but the nearest exposure of rocks similar to those of the hanging wall is 6 km to the southwest.

Five other, small, reverse faults cut fan deposits in the western flank of the Bristol Mountains, and are described in detail in Francke-Loriz (1993) (Fig. 6). The faults dip north (280/20N, 269/35N, 277/77N), northwest (060/30N), and southeast (060/30E). They all have well-developed surfaces marked by clay and siliceous gouge. Some have associated gash fractures and steeply-raking slickenlines. All faults offset Pleistocene(?) fanglomerate having Stage II petrocalcic horizons and 5 cm-thick cambic B horizons. Where visible, offsets are less than a meter, but two are unconstrained. None show surface expression.

Discussion, Northern Bristol Mountains

The five sedimentary sequences that lie between these faults were most likely deposited in pull-apart basins as evolving alluvial fans. The Eocene sequence and the older fanglomerate both include sediment not exposed in the Bristol Mountains, and which could have been shed from sources then to the east. If so, the source area would now lie southeast of the Bristol Mountains, and displacement would have occurred along faults east of the range.

Major faults in the northern Bristol Mountains strike north-northwest, and align with the southern projection of the Soda-Avawatz fault zone and the Soda Lake lineaments, although the latter appear somewhat further east. This could indicate that the fault zone is particularly broad, or that a right step (releasing step) occurs between the segments. The brittle style of deformation indicates that faulting occurred at a high strain rate and at fairly shallow levels. Although the S-C mylonite on the eastern slopes of the range was not seen in place so could not be measured, its presence indicates ductile faulting occurred on a now uplifted surface.

The Bristol Mountains fault zone is most likely strike-slip because: 1) the fault traces are straight, 2) fault planes

are consistently near vertical, 3) the rake of slickenlines is near horizontal, and 4) the geometry of the pull-apart basins is consistent with dextral shear.

The offset across the Bristol Mountains fault zone is likely greater than 8 km because basement rocks are juxtaposed over that distance on a single branch. The close connection between bedrock types and sediment provenance in the Bristol Mountains indicates that dextral offset along any one strand does not exceed the 15-km length of the range; though cumulative offset east of the range may be greater.

Since the age of volcanic rocks in the Balch Wash sequence is latest Eocene, and since these sequences are most likely correlative, at least in part, faulting along the Bristol Mountain fault zone must have begun by that time. The upward-decreasing deformation in the sedimentary strata indicates that faulting was most intense between deposition of the lower unit (approximately 26 Ma) and deposition of the older (Pleistocene?) fanglomerate, although faulting continued at least into the Pleistocene. East-directed reverse faulting involved Miocene(?) sedimentary strata and Pleistocene fans.

Conclusions

The Death Valley fault zone and its southward continuation, and adjacent Mule Spring thrust and associated faults represents the approximate eastern boundary of the eastern California shear zone in this area (Dokka and Travis, 1990; Miller and Yount, 2002).

Similarities in geometry, age of inception, structural style, relationship to sedimentary basins, and age of most recent offset indicate that a broad zone of right-lateral faults extends from southern Death Valley to the northern Bristol Mountains. Right steps along these faults formed pull-apart basins that filled with fluvial and lacustrine rocks beginning in latest Eocene time. The offset across this zone is 20-25 km based on sediment provenance and paleocurrent directions. However, large offset occurred east of the presently exposed fault traces. Deposition and faulting within reached a maximum during Miocene and Pliocene, but has been decreased since then.

East-directed reverse faulting all along this zone occurred synchronously with dextral shear, and continued into the late Cenozoic. The greatest uplift and eastward displacement occurred in the Avawatz Mountains. Lesser faulting occurred in the Soda Mountains and in the southwestern Bristol Mountains. If this southward decrease in east-directed fault displacement is a response to clockwise rotation of the northern Mojave terrane, it indicates that either rotation is occurring on several, individual tectonic blocks, or that the rotational axis for the entire rotation lies south of the Bristol Mountains.

Acknowledgement

This paper is dedicated to my mentor and friend Bennie Wyatt Troxel who passed away Feb. 20, 2017. I owe so much to you. Without your expertise, insights, and kindness throughout my formative years, I would not be the geologist or person I now am. Thank you Bennie, and farewell.

References

Acord, J., 1986, A gravity study of the Soda-Avawatz fault zone, San Bernardino County, California {M.S. thesis]: Bakersfield, California State University, 78 p.

Basset, A.M. and Kupfer, D.H., 1964, A geologic reconnaissance in the southeastern Mojave Desert, California: California Division of Mines and Geology, Special Report 83.

Brady, R. H. III, 1984, Neogene stratigraphy of the Avawatz Mountains between the Garlock and Death Valley fault zones, southern Death Valley, California: Implications as to late Cenozoic tectonism: Sedimentary Geology v. 38, no. 1-4, p. 127-157.

Brady, R.H. III, 1986, Cenozoic geology of the northern Avawatz Mountains in relation to the intersection of the Garlock and Death Valley fault zones, San Bernardino County, California [Ph.D. thesis]: Davis, California, University of California, 292 p.

Brady, R. H. III, 1992a, Neogene sedimentary rocks in the southern Owlshead Mountains: Constraints on displacement of the eastern Garlock fault zone *in* Sherrod, D.R., and Nielsen, J.E., eds. Tertiary Stratigraphy of Highly Extended Terranes: US Geological Survey Bulletin 2053, p. 13-18.

Brady, R.H. III, 1992b, Cenozoic stratigraphy and structure of the northern Bristol Mountains, California *in* Sherrod, D.R., and Nielsen, J.E., eds. Tertiary Stratigraphy of Highly Extended Terranes: US Geological Survey Bulletin 2053, p. 25-28.

Brady, R. H. III, 1992c, The eastern California shear zone in the northern Bristol Mountains, southeastern California. *in* Reynolds, R. E., ed. Deformation associated with the Neogene eastern California shear zone, southwestern Arizona and southeastern California: Redlands, California, San Bernardino County Museum, p. 6.

Brady, R.H. III, and Troxel, B.W., 1999, The Miocene Military Canyon Formation: Depocenter evolution and constraints on lateral faulting, southern Death Valley, California *in* Wright, L.A. and Troxel, B.W., Cenozoic basins of the Death Valley region: Geological Society of America Special Paper 333, p. 277-288.

Brady, R. H., III, Clayton, J., Troxel, B. W., Verosub, K. L., Cregan, A., and Abrams, M., 1988, Thematic mapper and field investigations at the intersection of the Death Valley and Garlock fault zones California: Remote Sensing and Environment, v. 28, p. 207-217.

Bryant, W., compiler, 2000, Fault number 69a, Garlock fault zone, Western Garlock section, in Quaternary fault and fold database of the United States: U.S. Geological Survey website, http://earthquakes.usgs.gov/regional/qfaults

Burbank, D., Whistler, D., 1987, Temporally constrained tectonic rotations derived from magnetostratigraphic data: Implications for the initiation of the Garlock fault, California: Geology, v. 15, p. 1172-1175.

Burchfiel, B.C. and Stewart, J.H., 1966, "Pull-apart" origin of the central segment of Death Valley, California: Geological Society of America Bulletin, v. 77, p. 439-442.

Butler, P.R., B.W. Troxel and Verosub, K.L., 1988, Late Cenozoic history and styles of deformation along the southern Death Valley fault zone, California: Geological Society of America Bulletin, v. 100, p. 402-410.

Chin, L.D., 2013, Blind contractional faulting responsible for exhumation of the eastern Garlock fault, Avawatz Mountains, California: [abs] Geological Society of America Abstracts with Programs, v. 45, no. 7, p. 596.

Clark, M.M., 1973, Map showing recently active breaks along the Garlock and associated faults, California: U.S. Geological Survey Miscellaneous Geological Investigations Map 1-741.

Davis, G.A., 1977, Limitations on displacement and southward extent of the Death Valley fault zone, California: California Division of Mines and Geology Special Report 129, p. 12-33.

Davis, G.A. and Burchfiel, B.C., 1973, Garlock fault, an intracontinental transform structure, southern California: Geological Society of America Bulletin, v. 84, p. 1407-1422.

Dooley, T., and McClay, K., 1996, Strike-slip deformation in the Confidence Hills, southern Death Valley fault zone, eastern California, USA: Journal of the Geological Society of London, v. 153, p. 375-387.

Francke-Loriz, C., 1993, Application of satellite image analysis to Quaternary geology and engineering fault studies: Northern Bristol Mountains, San Bernardino County, California [M.S. thesis]: Fresno, California State University, 113 p.

Glazner, A. F., Nielson, J. E., Howard, K. A., and Miller, D. M., 1986, Correlation of the Peach Springs Tuff, a large-volume Miocene ignimbrite sheet in California and Arizona: Geology, vol. 14, p. 840-843.

Gourley, J. R., 2000, Facies analysis of Neogene syntectonic strata I the Soda Mountains, San Bernardino County, California: Implications for constraint of faulting on the Soda-Avawatz fault zone [M.S. thesis]: Fresno, California State University, 65 p.

Green, H.L., Redwine, J. L., and Miller, D.M., 2007, Reconnaissance studies of soils-geomorphic correlations and late Quaternary deformation of alluvial fan deposits east of the Avawatz Mountains, Mojave Desert, California in Miller, D.M., and Valin, Z.C., eds., 2007, Geomorphology and tectonics at the intersection of Silurian and Death Valleys, southern California—2005 Guidebook, Pacific Cell Friends of the Pleistocene: U.S. Geological Survey Open-File Report 2007–1424, p. 113-140.

Grose, L.T., 1959, Structure and petrology of the northeast part of the Soda Mountains, San Bernardino County, California: Geological Society of America Bulletin, v. 70, p. 1509-1548.

Henshaw, P.C., 1939, A Tertiary mammalian fauna from the Avawatz Mountains, San Bernardino County, California: Carnegie Institution of Washington Publication 514, p. 1-30.

Hewett, D.F., 1954, General geology of the Mojave Desert region, California, *in* Jahns, R.H., ed., Geology of Southern California: California Division of Mines and Geology Bulletin 170, c. 2, p. 5-20.

Hill, M.L., and Troxel, B.W., 1966, Tectonics of Death Valley region, California: Geological Society of America, Bulletin, v. 77, p. 435-438.

Honeycutt, T.K., Malinconico L.L., and Marzolf, J.E., 1986, Geophysical study of the Soda-Avawatz fault zone in the Soda Mountains: Evidence for east vergent thrusting: Geological Society of America Abstracts with Programs, Cordilleran Section, v. 18, n. 2, p. 118.

Jennings, C. W., 1994, Fault activity map of California and adjacent areas with location and ages of recent volcanic eruptions: California Geologic Data Map Series, Map No. 6. California Division of Mines and Geology, 1: 250,000 scale.

Jennings, C.W., Burnett, J.L, and Troxel, B.W., 1962, Geologic map of California, Trona sheet: California Division of Mines and Geology, 1:250,000 scale.

Loomis, D., and Burbank, W., 1988, The stratigraphic evolution of the El Paso basin, southern California: Implications for the Miocene development of the Garlock fault and uplift of the Sierra Nevada, Geological Society of America Bulletin, v. 100, no. 1, p. 12-28.

Luyendyk, B.P., 1991, A model for Neogene crustal rotations, transtension, and transpression in southern California: Geological Society of America Bulletin, v. 103, p. 1528–1536.

Machette, M., Piety, L., compilers, 2001, Fault number 143b, Southern Death Valley fault zone, Nobel Hills section, in Quaternary fault and fold database of the United States: U.S. Geological Survey website, http://earthquakes.usgs.gov/hazards/qfaults, accessed 2/12/2017.

McGill, S.F., 1994, Holocene slip rate of the easternmost Garlock, fault, Avawatz Mountains, California, *in* Reynolds, J., ed., Abstracts from proceedings—The 1994 Desert research symposium: Quarterly of San Bernardino County Museum Association, v. 41, no. 3, p. 24.

McGill, S., and Sieh, K., 1991, Surficial offsets on the central and eastern Garlock fault associated with prehistoric earthquakes. Journal of Geophysical Research, v. 96, p. 21597-21621.

Mendonca, J., 2007, Preliminary results on neotectonic and geomorphic evolution of the northeastern Avawatz Mountains, southern Death Valley, California *in* Miller, D.M., and Valin, Z.C., eds., Geomorphology and tectonics at the intersection of Silurian and Death Valleys, southern California, 2005 Guidebook, Pacific Cell Friends of the Pleistocene: U.S. Geological Survey Open-File Report 2007–1424, p. 141-148.

Menges, C.M. and Miller, D. M., 2007 Geomorphology and tectonics at the intersection of Silurian and Death Valleys: Field trip road log *in* Miller, D.M., and Valin, Z.C., eds., Geomorphology and tectonics at the intersection of Silurian and Death Valleys, southern California, 2005 Guidebook, Pacific Cell Friends of the Pleistocene: U.S. Geological Survey Open-File Report 2007–1424, p. 24-37.

Menges, C., Pavlis, T., McMackin, M., Serpa. L., and Bennett, R., 2005, Geomorphic and structural evidence for significant neotectonic contractional strain within southern Death Valley and bordering areas, eastern California. Geological Society of America Abstracts with Programs, v. 37, no. 7, p. 69.

Miller, D. M., and J. C. Yount (2002), Late Cenezoic tectonic evolution of the north-central Mojave Desert inferred from fault history and physiographic evolution of the Fort Irwin area, California, in Geologic evolution of the Mojave Desert and Southwestern Basin and Range, edited by A. F. Glazner, J. D. Walker, and J. M. Bartley, J. M.,: Geological Society of America Memoir 195, Geological Society of America, Boulder, CO., pp. 173.

Noble, L.F., and Wright, L.A., 1954, Geology of the central and southern Death Valley region, California, *in* Jahns, R.H., ed., Geology of Southern California: California Division of Mines and Geology Bulletin 170, c. 2, p. 143-160.

Ritter, J.B., 1985, Late Quaternary piedmont stratigraphy of the Salt Spring Hills area, eastern Mojave Desert, California, *in* Hale, R.G., ed., Quaternary lakes of the eastern Mojave Desert, California, Field Trip Guide: Pacific Cell, Friends of the Pleistocene, p. 101-112.

Spencer, J.E., 1990, Late Cenozoic extensional and compressional tectonism in the southern and western Avawatz Mountains, southern California *in* Wernicke, B.F., ed. Basin and Range extensional tectonism near the latitude of Las Vegas, Nevada: Geological Society of America Memoir, no. 176, p. 317-335.

Spencer, J. E., 1993, Stratigraphy of the Avawatz Formation, southern Death Valley region, southeastern California *in* Sherrod, D. R., and Nielson, J.E., eds. Tertiary Stratigraphy of highly extended terranes, California, Arizona, and Nevada: US Geological Survey Bulletin 2053, p. 19-20.

Smith, G.I., 1962, Large lateral displacement on the Garlock fault, California, as measured from an offset dike swarm: American Association of Petroleum Geologists Bulletin, v. 46, p. 85-104.

Stewart, J.H., 1967, Possible large right-lateral displacement along fault and shear zones in Death Valley-Las Vegas area, California and Nevada: Geological Society of America Bulletin, v. 78, p. 131-142.

Stroud, J., and McGill, S., 1994b, Late Quaternary activity on a thrust fault in the northeastern Avawatz Mountains, Mojave Desert, California: San Bernardino County Museum Association Quarterly, v. 41, no. 3, p. 30-31.

Troxel, B.W., Wright, L.A., and Jahns, R.H., 1972, Evidence for differential displacement along the Garlock fault zone, California: Geological Society of America Abstracts with Programs, Cordilleran Section, v. 4, n. 3, p. 250.

Troxel, B.W., and Butler, P.R., 1979, Tertiary and Quaternary fault history of the intersection of the Garlock and Death Valley fault zones, southern Death Valley, California: Report submitted to U.S. Geological Survey, Menlo Park, California, 29 p.

Wadsworth, W.B., Ferriz, H., and Rhodes, D., 1995, Structural and stratigraphic development of the Middle Jurassic magmatic arc in the Cowhole Mountains, eastern Mojave Desert, California *in* Miller, D., and Busby, C., eds,, Jurassic magmatism and tectonics of the North American Cordillera: Geological Society of America, Special Paper 299, p. 327-349.

Wells, S.G., McFadden, L.D., Dohrenwend, J.C., Bullard, T.F., Feilberg, B.F., Ford, R.L. Grimm, J.P., Miller, J .R., Orbock S.M., and Pickle, J.D., 1984, Late Quaternary geomorphic history of Soda Mountains piedmont and Silver Lake playa area: Geological Society of America Annual Meeting Guidebook, n. 14, p. 69-87.

Wesnousky, S.G., 1986, Earthquakes, Quaternary faults and seismic hazard in California: Journal of Geophysical Research, v. 91, p. 12587-12631.

Connecting the Soda–Avawatz and Bristol–Granite Mountains faults with gravity and aeromagnetic data, Mojave Desert, California

Victoria E. Langenheim[1] and David M. Miller[2]
U.S. Geological Survey, Menlo Park, CA, [1]zulanger@usgs.gov; [2]dmiller@usgs.gov

ABSTRACT—The Soda–Avawatz and Bristol–Granite Mountains faults are considered by some to form the northeastern margin of the eastern California shear zone yet their connectivity and extents are obscured by surficial deposits and the estimates of total right-lateral offset from geologic data range from 0 to as much as 24 km. We use gravity and recently released detailed aeromagnetic data to map strands of these faults, examine structure within the fault zones and provide estimates of right-lateral offset. Gradients in gravity and aeromagnetic data define physical property contrasts that coincide with mapped strands of the faults and allow for extension of these faults, where concealed, to indicate continuity between the Soda–Avawatz and Bristol–Granite Mountains faults. Gravity data reveal local tectonic basins west of Silver Lake, beneath Soda Lake, and southwest of the Marble Mountains that are approximately 9–15 km long, 3–5 km wide, and 1–1.5 km deep. The basins are located where the local fault traces strike more northerly than the overall fault zone strike, suggesting that these basins are transtensional (pull-apart). If the lengths of these basins can be used as a proxy for right-lateral offset, the Soda–Avawatz and Bristol–Granite Mountains faults may have up to 9–15 km of post-early Miocene offset, consistent with our offset estimates from correlative magnetic anomalies across the fault zone.

Introduction

The Eastern California Shear Zone (ECSZ) is an important zone of active faulting that accommodates distributed right-lateral shear (Dokka and Travis, 1990; Sauber et al., 1994) and kinematically links motion on the San Andreas fault with transtensional deformation on the southern Death Valley fault zone and other fault zones north of the Garlock fault (Fig. 1). The ECSZ strikes approximately north-south across the Mojave Desert and eastern Transverse Ranges, yet details of how Miocene to Quaternary dextral shear is and has been partitioned onto various faults are incompletely understood in many cases. Geodetic data reveal that as much as 25% of the ~ 50 mm/yr slip budget across the North American–Pacific plate boundary occurs within the shear zone (Sauber et al., 1994), yet these data cannot always resolve slip on closely-spaced faults with low slip rates. Paleoseismological constraints on recent fault slip rates are available in some cases (e.g., Rockwell et al., 2000), and estimates based on offset of Quaternary markers have also been made in places (e.g., Miller and Yount, 2002). Total offset along faults since their late Miocene initiation is a necessary metric for defining long-term behavior of the ECSZ. Here we use pre-mid-Cenozoic features to estimate

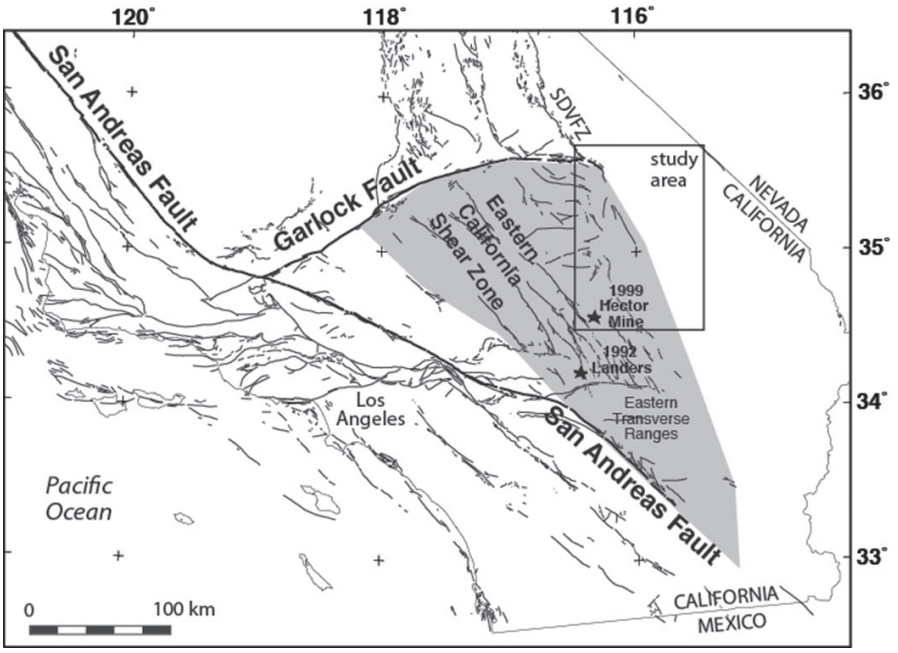

Figure 1. Index map showing study area within the Eastern California Shear Zone (shaded region). Stars, epicenters of recent M7+ earthquakes in the Mojave Desert. SDVFZ, Southern Death Valley fault zone.

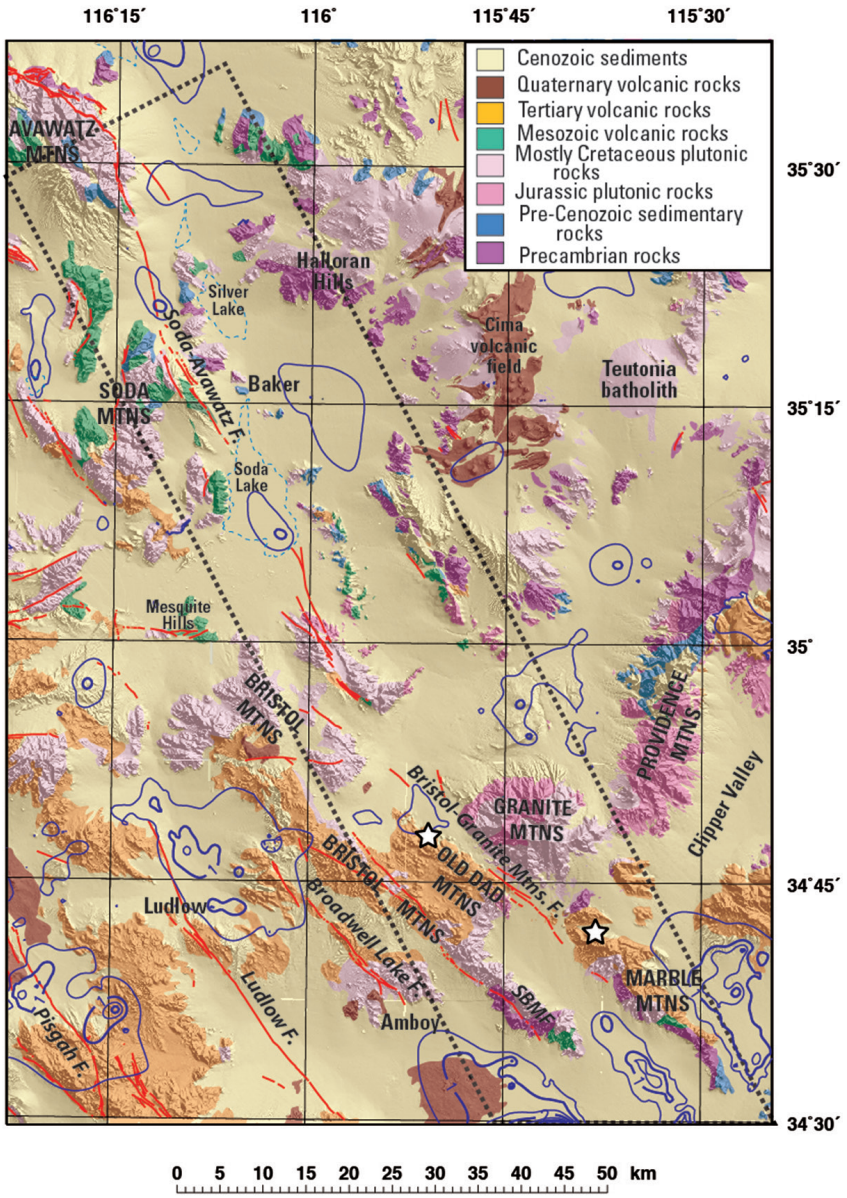

Figure 2. Simplified geologic map from Miller et al. (2007a) and Jennings et al. (1977). Red lines, faults from Miller et al. (2007b, 2014). Dashed blue lines, playas. Stars mark the location of the early Miocene(?) Lost Marble paleovalley gravels (Lease et al., 2009). Dark blue lines, 0.5 km contours of basin thickness from Langenheim et al. (2009) and Jachens and Langenheim (2014). Black box shows extent of maps in Figure 5. SBMF, South Bristol Mountains fault.

total (or cumulative) fault offset for two major structures along the northeastern margin of the ECSZ.

Geologic estimates of offset for individual faults in the ECSZ can range widely, especially where surficial deposits or complex structure obscure offset markers or connections between faults. For parts of the ECSZ where detailed geologic mapping of offset features either does not exist or is obscured by young surficial deposits, offset estimates are based on kinematic model predictions, such as those of Dokka and Travis (1990), Richard (1993), Glazner et al. (2002), McQuarrie and Wernicke (2005), and Bennett et al. (2016). Some of these models predict gaps and overlaps between fault blocks in addition to offset estimates. For the region surrounding the M7+ Landers and Hector Mines earthquakes (Fig. 1), Jachens et al. (2002) used detailed aeromagnetic data to examine cumulative offsets in basement rocks and gravity data to test whether model predictions of gaps between fault blocks result in deep basins filled with low-density Cenozoic deposits. This analysis showed that geophysical data can augment offset estimates based on geologic mapping, particularly those areas covered by young deposits. However, the analysis did not include the eastern part of the ECSZ due to an absence of detailed aeromagnetic data there at that time.

The northeastern margin of the ECSZ is considered by some (e.g., Brady, 1992; Glazner et al., 2002) to be the Soda–Avawatz and Bristol–Granite Mountains faults. Whether these faults are a continuation of the southern Death Valley fault zone south of the Garlock fault has been the subject of debate (Davis, 1977, Glazner et al., 2002). It also remains unclear how or if the Soda–Avawatz and Bristol–Granite Mountains faults connect and how much offset they have accommodated. We take advantage of recently released detailed aeromagnetic data and previously published basement depth estimates based on gravity data to address these questions.

Previous work

The Soda–Avawatz fault was first described by Grose (1959) as a N25°W-striking fault zone that juxtaposes distinctly different packages of pre-Cenozoic rocks in the northeast Soda Mountains west of the town of Baker, CA (Fig. 2). Farther north, the fault changes to a more northerly strike as it continues along the eastern margin of the Avawatz Mountains. Grose (1959) found evidence of right-lateral motion, such as near-horizontal slickenlines, apparent reversal of throw, and *en echelon* arrangement of folds and secondary faults along the fault zone. He could not, however, document the amount of offset because he could not match correlative geologic features across the fault, but speculated that the offset probably exceeds 5 km. Brady (1984) proposed a minimum of 20 km of right-lateral offset based on correlation of clasts in the Tertiary deposits in the

Avawatz Mountains to bedrock sources in the Halloran Hills and Gourley (2000) inferred a minimum of 20 km based on clast compositions and paleocurrent directions in the Tertiary Avawatz Formation.

The Granite–Bristol Mountains fault was first described by Gamble (1959a ,b) in a pair of unpublished reports for the Southern Pacific Company. As summarized by Howard et al. (1987), the fault juxtaposes Cretaceous granodiorite in the Granite Mountains against Tertiary volcanic rocks exposed in the Old Dad Mountains (Fig. 2) and dips steeply northeast. A change in magnetic patterns (northeast-striking magnetic stripes southwest of the fault versus small, irregularly shaped anomalies northeast of the fault in Fig. 3) and a prominent linear northwest-trending gravity gradient (Fig. 4) also mark the Granite–Bristol Mountains fault in this area (Howard et al., 1987). Offset estimates along this stretch of the fault range from 0–10 km based on the alignment of Tertiary rhyolite flows and metavolcanic rocks (Howard and Miller, 1992) to >24 km based on alignment of gravels beneath the Miocene Peach Spring tuff (see white stars in Figs. 2, 3, and 4 for correlative locations of this "Lost Marble paleovalley" of Lease et al., 2009). This estimate has been revised to 17 km by David Buesch (in Miller [2017]).

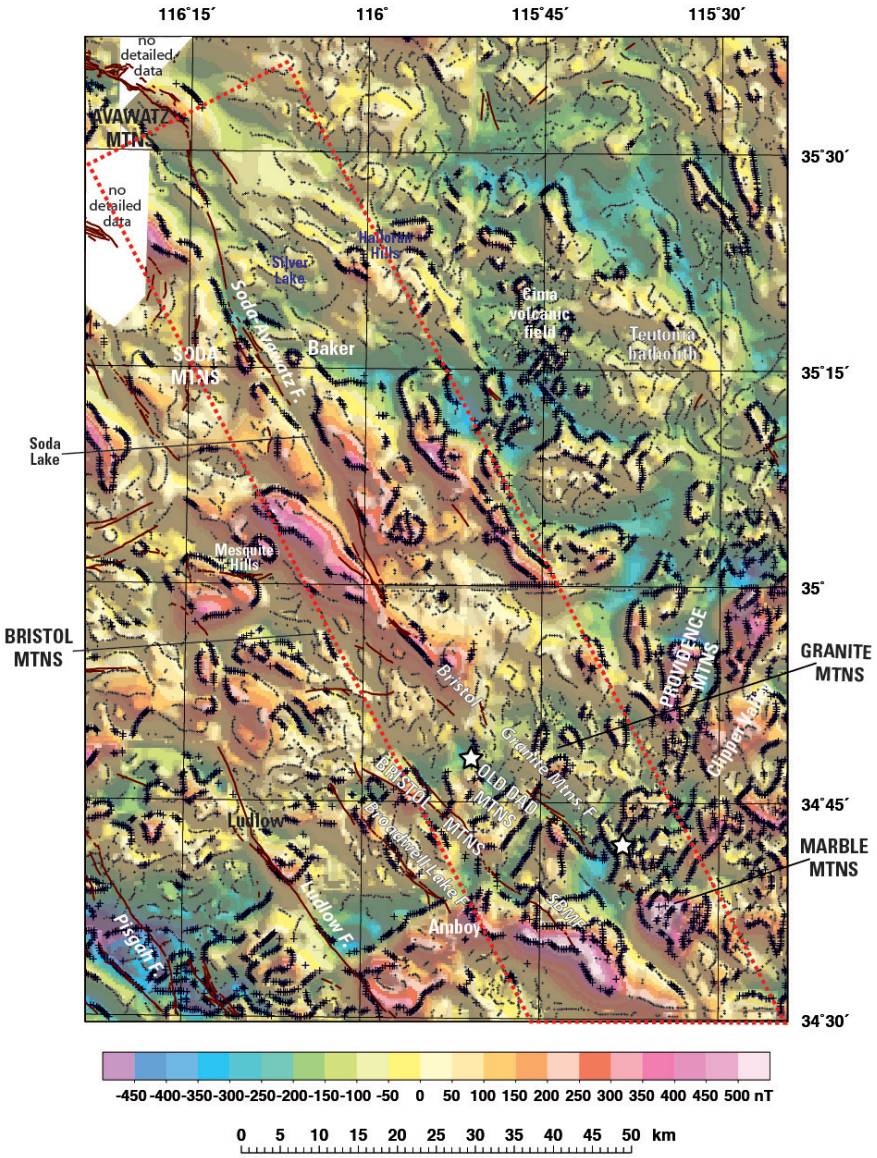

Figure 3. Aeromagnetic map. Red dashed line, extent of maps in Fig. 5. Plus signs, locations of maximum horizontal gradients, with smaller symbols denoting gradient values below the mean value and larger symbols denoting gradient values above the mean value. See Figure 2 caption for explanation of lines and symbols.

The Granite–Bristol Mountains fault has also been mapped in the northern Bristol Mountains by Laird (1959), Davis (1973), Brady (1992), Bedford (2010) and Miller (2012). The northern Bristol Mountains are characterized by a strong northwest-trending grain that results from multiple, subparallel, vertical right-lateral faults whose amount of slip has not been determined with certainty because of an absence of piercing points. Offset of the contact between chloritically altered granitic and unaltered granitic rocks suggests at least 6 km of right slip on one of the longer, more prominent faults within the zone (Brady, 1992), with a postulated maximum of 15 km across the fault zone (Brady, 1993).

Palinspastic reconstructions predict offsets along these two fault zones that range from 4 to 45 km. The lower estimate is from Glazner et al. (2002) who assumed that offset on the southern Death Valley fault (ranging from 8 km by Davis [1977] to 20 km by Brady [1984]) continues southward onto the Soda–Avawatz fault and then is divided equally between the Bristol–Granite Mountains, the southern Bristol Mountains, and the Ludlow faults, with an average offset of ~ 4 km on each fault. Richard (1993) estimated no more than 16 km of right slip based on relationships and reconstructions in southeastern California. Larger estimates of fault offset include 21.5, 24, and 27 km by Dokka and Travis (1990), Bennett et al. (2016), and McQuarrie and Wernicke (2005), respectively, based on their regional reconstructions for

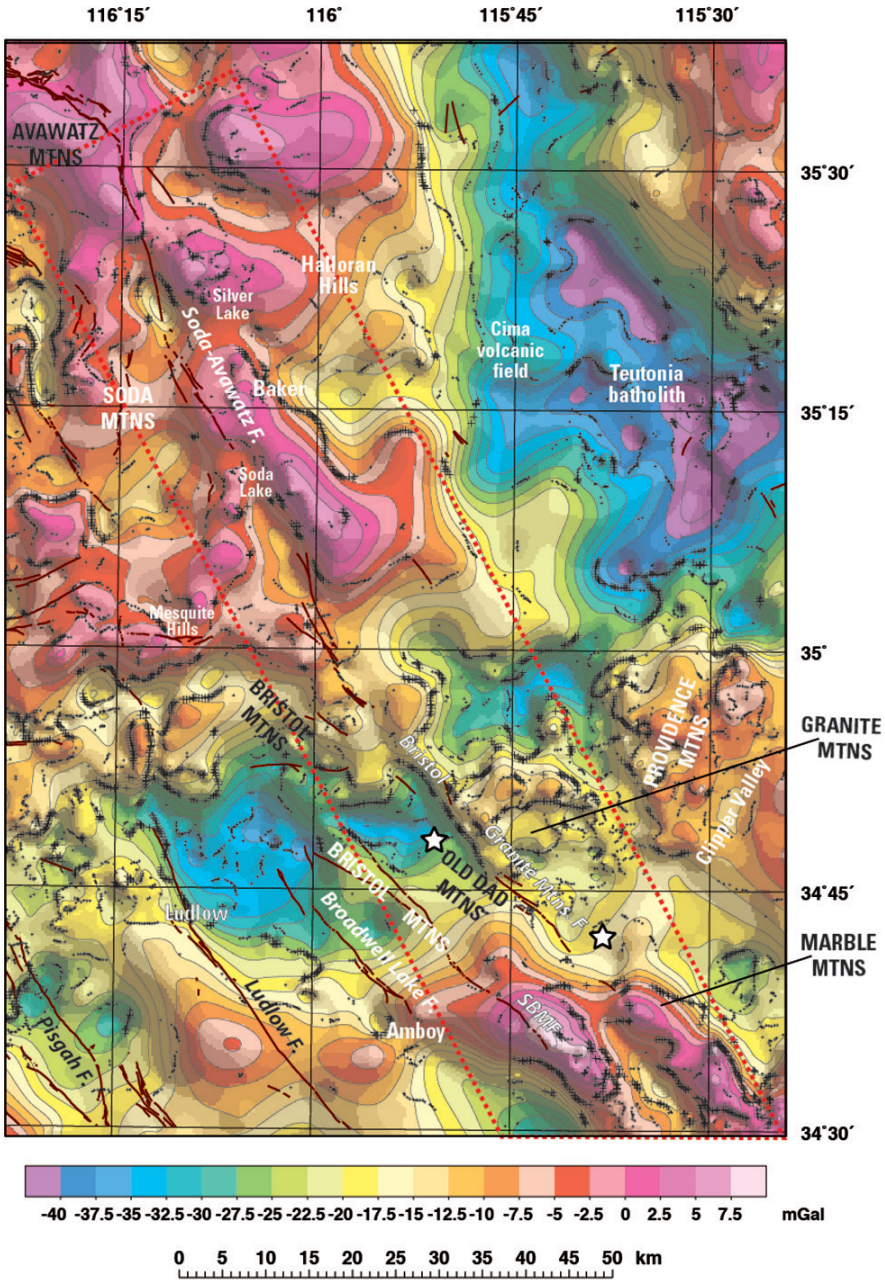

Figure 4. Isostatic gravity map. Red dashed line, extent of maps in Fig. 5. Plus signs, locations of maximum horizontal gradients, with smaller symbols denoting gradient values below the mean value and larger symbols denoting gradient values above the mean value. See Figure 2 caption for explanation of lines and symbols.

the Bristol–Granite Mountains fault, and 45 km on the Soda–Avawatz fault, called the South Death Valley fault by McQuarrie and Wernicke (2005). Dokka and Travis (1990) continue slip north from the Bristol–Granite Mountains fault onto the "Mesquite Valley disturbed zone", which they describe as a sinuous belt of basins between Ludlow and Soda Lake that formed as a result of distributed normal and strike-slip faults that include the Soda–Avawatz fault.

Geophysical data and methods

We use previously published gravity and aeromagnetic data in this analysis. Aeromagnetic data are from multiple surveys that are a subset of those compiled in Langenheim et al. (2009) and Langenheim and Jachens (2014). These surveys were flown along flight lines spaced ≤1.6 km apart. All but the northwest part of the study area (white areas in Fig. 3) was flown at a spacing of 800 m and all of the study area was flown at a nominal height of 305 m above terrain, except for the northwest corner, which was flown at a height of 50 m. As discussed in more detail in the open-file reports, the survey data were processed to reflect crustal magnetization and merged to form a seamless dataset (Fig. 3). Sedimentary deposits are generally weakly magnetic and thus the magnetic data allow us to map basement features beneath Cenozoic basin deposits.

The gravity data, consisting of 3,406 measurements unevenly distributed throughout the study area, are from compilations by Langenheim et al. (2009) and Jachens and Langenheim (2014) for the Mojave National Preserve and Fort Irwin Training Center. See these reports for details of data sources and processing of these data that resulted in isostatic residual gravity anomalies (Fig. 4), which reflect density variations in the upper to middle crust. One of the most significant upper-crustal density contrasts in the Mojave Desert is that between low-density Cenozoic deposits and denser basement rocks (which are defined to be pre-Cenozoic in age; Jachens et al., 2012). Inversions using gravity, geologic map, and well data (Langenheim et al., 2009; Jachens and Langenheim, 2014) provide estimates of Cenozoic basin thickness throughout the study area (blue contours in Fig. 2).

For both the gravity and magnetic data, we use the maximum horizontal gradient method (Cordell and Grauch, 1985; Blakely and Simpson, 1986) to locate edges of density and magnetization sources (+s in Figs. 3 and

4). Before calculating the gradient maxima, we filter the magnetic data to remove the dipole effect of the Earth's magnetic field, transform the magnetic field into an equivalent gravity field, and enhance anomalies produced by shallow sources (Fig. 5c; depth < 2 km; see Langenheim and Jachens [2014] for more information). Gradient maxima occur directly over vertical or near-vertical contacts that separate rocks of contrasting densities or magnetizations so this technique is ideal for locating strike-slip faults where they juxtapose rocks of contrasting physical properties.

Magnetic anomalies can also be used to constrain the amount of cumulative strike-slip offset (horizontal separation) on strike-slip faults because these anomalies are generally sourced by physical property variations within the crystalline basement rocks. Estimates of offset based on magnetic data benefit from the even data spacing throughout the study area and often yield sharply defined anomalies. This approach offers a means of evaluating and refining offset estimates based on geologic data and helps to identify additional offset features where magnetically transparent Cenozoic sedimentary deposits conceal bedrock evidence for fault offset. Magnetic and gravity anomalies used to infer offset carry ambiguity where the anomalies cannot be tied directly to geologic features observed at the surface. In some cases, anomalies sourced at depth may be inaccurately correlated. By using multiple sets of displaced anomalies, we have more confidence in our correlations.

The specific technique we use to identify offset magnetic anomalies is that used by Jachens et al. (2002) west and south of our study area and analogous to that used to identify offsets of exposed geologic features. We search along the trace of a candidate fault for elongate magnetic anomalies that are sub-perpendicular to the fault and whose magnetic sources appear to be truncated at the fault trace (piercing point). We then search the opposite fault block for similar anomalies that are truncated against the opposite side of the fault and estimate the magnitude of offset by measuring the along-fault separation between corresponding distinctive features of the anomaly. Given the flight-line spacing of aeromagnetic data in our study area, the resolution of magnetic features from the gridded data is approximately 0.4 km. We suggest these data can help identify linear magnetic features in map-view with an uncertainty of 0.6 km, as previously proposed by Jachens et al. (2002) using similar resolution aeromagnetic data.

Results and discussion

We first describe the geophysical expression of the Soda–Avawatz and Bristol–Granite Mountains faults, followed by a discussion of offset geophysical features and basins developed within the fault zones.

Geophysical expression of the Soda–Avawatz and Bristol–Granite Mountains fault zones

Both the Soda–Avawatz and Bristol–Granite Mountains fault zones are marked by prominent gravity and magnetic gradients (Fig. 3–5). The northernmost segment of the Soda–Avawatz fault that bounds the eastern Avawatz Mountains coincides with a gravity gradient and the eastern edges of narrow west-northwest-trending magnetic anomalies. As the mapped trace continues to the south towards mapped traces in the bedrock of the Soda Mountains, it cuts across a gravity low (L1 in Fig. 5b) and magnetic trough that strike 20° more westerly than the surficial Quaternary fault trace. In this reach, the fault is inferred from the positions of three small hills that may represent pop-ups (Grose, 1959), but other geometries are possible. The edges of these lows are parallel to the mapped bedrock traces in the Soda Mountains, which are well characterized by nearly coincident magnetic gradients (Fig. 5c). The gravity expression of the bedrock trace is a relatively subtle gradient with denser rocks on the east side of the mapped trace (G1 in Fig. 5b). This area, however, has few gravity measurements to fully characterize the gradient.

The mapped traces of the Soda–Avawatz fault do not continue southeast of the Soda Mountains (Fig. 2). However, Brady et al. (1989) and Brady (1992) have suggested that the Soda–Avawatz fault connects to lineaments mapped along the eastern edge of Soda Lake and continues further south as the Bristol–Granite Mountains fault, referring to gravity data that were unpublished at the time. The gravity data (subsequently published by Langenheim et al. [2009]) do indicate a low beneath the southern part of Soda Lake (L2 in Fig. 5b) that is bound on the northeast by a prominent gradient that is aligned with the bedrock trace in the Soda Mountains. These data also indicate a subtler, sub-parallel gradient located 4–5 km to the southwest that is roughly aligned with the northern trace of the Bristol–Granite Mountains trace. Aeromagnetic data show a 2 to 5-km-wide, nearly 30-km-long, fairly linear low between the Soda Mountains trace south to the northern Bristol Mountains trace (between f' and d in Fig. 5c), supporting a structural connection between the Soda–Avawatz and Bristol–Granite Mountain faults.

The Bristol–Granite Mountains fault is fairly well expressed in the potential-field data. In the northern Bristol Mountains, the northern fault trace forms the eastern margin of a magnetic high (d in Fig. 5c). Farther south, the trace marks the western edge of a magnetic body (d' in Fig. 5c), which we use to locate the fault 7–8 km southeast of bedrock outcrops. Given the steepness of the anomaly, Hendricks (2007) estimated the depth to the top of the magnetic body is 1–2 km; he speculated that the source is extensive iron mineralization (commonly in skarns in this part of the Mojave Desert) or intrusion of Tertiary igneous rocks along the fault zone. We note that the magnetic high broadens to the southeast (near

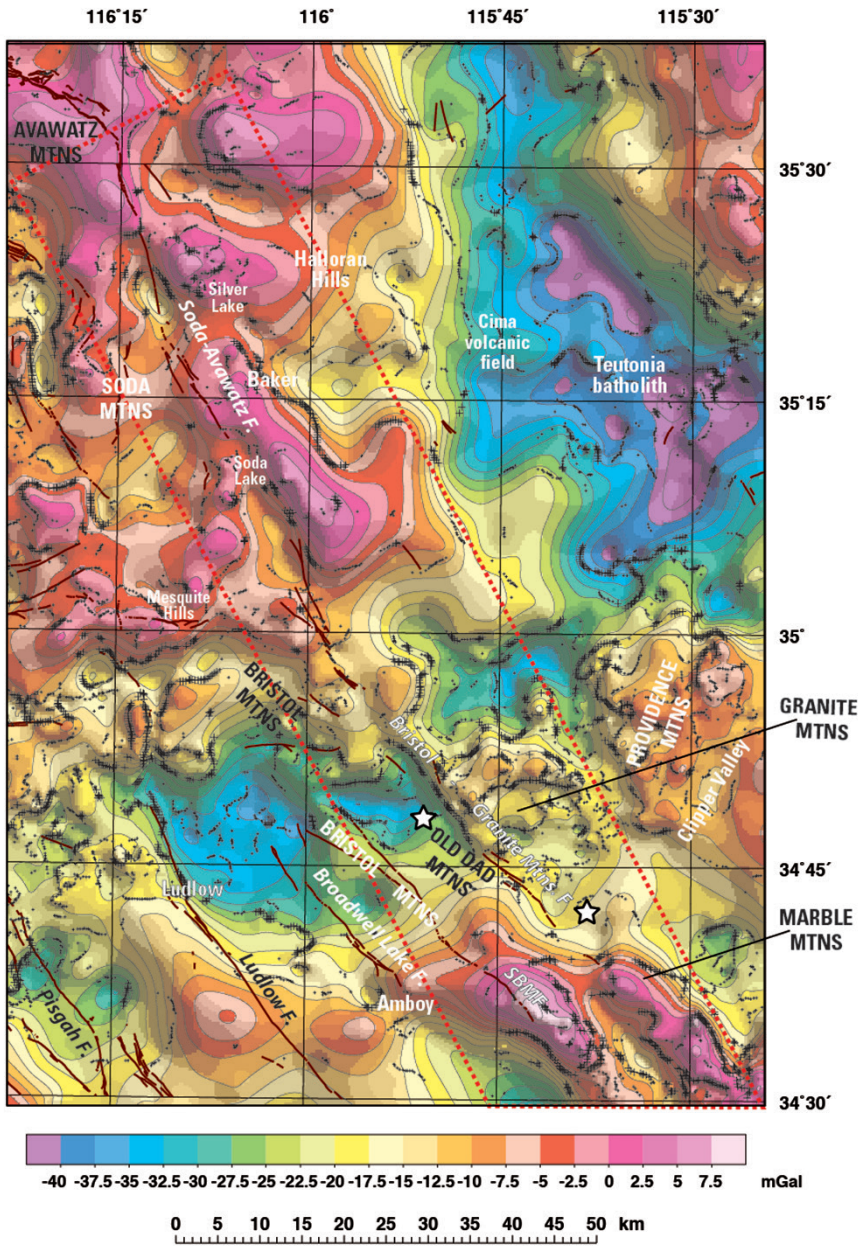

Figure 5. A) Simplified geologic strip map that shows basins (blue contour lines from fig. 2), and gravity (dotted brown lines) and magnetic (dashed black lines) gradients. B) Gravity map that shows correlation of northwest edge of gravity highs (G2-G2') and gravity lows (L3-L3') across the southern part of the Bristol–Granite Mountains fault and additional features discussed in text. Same color contour intervals as shown in Fig. 4. Thick, dashed dark blue lines, highlighted gravity gradients from A). C) Aeromagnetic map filtered to enhance shallow sources with pairs of correlated magnetic anomalies labeled a-h and a' to h'. Thick, dashed white lines, highlighted magnetic gradients from A).

d' in Fig. 5c) and is accompanied by somewhat higher gravity values (H1 in Fig. 5b), suggesting that the body is not restricted to the fault zone and is instead truncated by the fault in this area. For this stretch of the fault, the gravity data show a weak gradient, with denser rocks to the northeast of the fault, which becomes pronounced southeast of magnetic high d'.

The pronounced gravity gradient along the southwestern margin of the Granite Mountains, as discussed in Howard et al. (1987), results from the fault juxtaposing lower-density Tertiary volcanic rocks against denser granodiorite. In this 20-km-long stretch, the fault also separates a northeast-trending magnetic grain southwest of the fault from a weaker, less organized magnetic anomaly pattern to the northeast. At the southern end of the gravity gradient, it reverses facing direction, now with denser rocks to the southwest against less dense rocks to the northeast for a distance of ~25 km. Farther south, along the southwest margin of the Marble Mountains, the gravity gradient along the mapped fault trace reverses facing direction again and forms the northeast margin of a basin that is estimated by Langenheim et al. (2009) to be 1.5 km deep (Fig. 2). This stretch of the projected fault is marked by a narrow magnetic low. The low could be caused by alteration, but no evidence of mineralization to support this hypothesis has been found (Howard et al., 1987). We posit that the low is primarily caused by deepening of the basement surface, as indicated by the gravity low and data in various reports prepared for Cadiz Land Company (e.g., Black, 1997).

Estimates of cumulative offset on the Soda–Avawatz and Bristol–Granite Mountains faults

Analysis of the gravity and magnetic anomalies along and adjacent to mapped traces of the Soda–Avawatz and Bristol–Granite Mountains faults provides support for kinematically connecting the two faults as a significant fault zone in the ECSZ. We correlate eight magnetic features across the Soda–Avawatz and Bristol–Granite Mountains faults that indicate right-lateral offsets ranging from 8 to 17 km (Fig. 5c; Fig. 6). If our pairs of correlated anomalies are correct, this suggests that offset may decrease from 16–17 km in the southern part of the study area, to about 12 km near Soda Lake, and 8–11 km between the Soda and Avawatz Mountains.

Fault offsets determined by gravity data are less certain because of the uneven distribution of gravity measurements and the uncertainty in basement gravity

field due to basin deposits. One possible correlation is the northeast edge of a dense body corresponding with Jurassic plutonic complexes south of the Granite Mountains that appears to be offset about 15 km (G2-G2' in Fig. 5b), consistent with the offset estimated using the magnetic data. The gravity lows to the northwest of G2 and G2' also appear to be offset by ~ 15 km (L3 and L3'), although this correlation is complicated by ambiguities in the basement gravity field.

Another proxy for displacement is the length of pull-apart or transtensional basins formed at releasing steps or bends in strike-slip fault systems. We suggest that gravity lows within the fault zone west of Silver Lake, beneath Soda Lake, and southwest of the Marble Mountains formed as pull-apart basins in right steps or releasing bends in this right-lateral fault system. The basin southwest of the Marble Mountains is linear, about 15–16 km long, 2–3 km wide, and ~1.5 km deep. The northeast margin of the basin is parallel to and aligned with the southward projection of the Bristol–Granite Mountains fault mapped east of the Old Dad Mountains, whereas the southwest basin margin is roughly aligned with a concealed northwest-striking fault southeast of the study area (Howard, 2002). This fault may have Quaternary offset if it is part of the slickensided surface found in deposits of probable Quaternary age at a depth of 78 m in a drillhole about 20 km southeast of the study area beneath Cadiz Lake (Bassett et al., 1959; Howard, 2002). Both basin margins are marked by linear gravity and magnetic gradients, suggesting fault control. A plausible mechanism for forming this basin is a right step between two strands of the Bristol–Granite Mountains fault zone.

The gravity data indicate a basin beneath Soda Lake, but the exact dimensions of the basin are not as well constrained by gravity measurements, especially on its western margin. The north-northwest-trending basin is about 12 km long, ~ 1 km deep, and as much as 5 km wide. A pull-apart origin was suggested for the basin based on previously unpublished gravity data (Brady, 1992). The northeast margin coincides with gravity and magnetic gradients that are aligned with the southern projection of the Soda–Avawatz fault mapped in the Soda Mountains. The southwest basin margin is roughly aligned with the northward projection of the eastern, more westerly-trending strand of the Bristol–Granite Mountains fault. Thus the basin lies within a right step between the projections of the Soda–Avawatz and Bristol Mountains faults. The southwest margin of the basin is especially well expressed by a linear magnetic gradient that appears to step east beneath the gravity low and thus may represent a fault strand that forms a more direct connection between the Soda–Avawatz and Bristol–Granite Mountains faults.

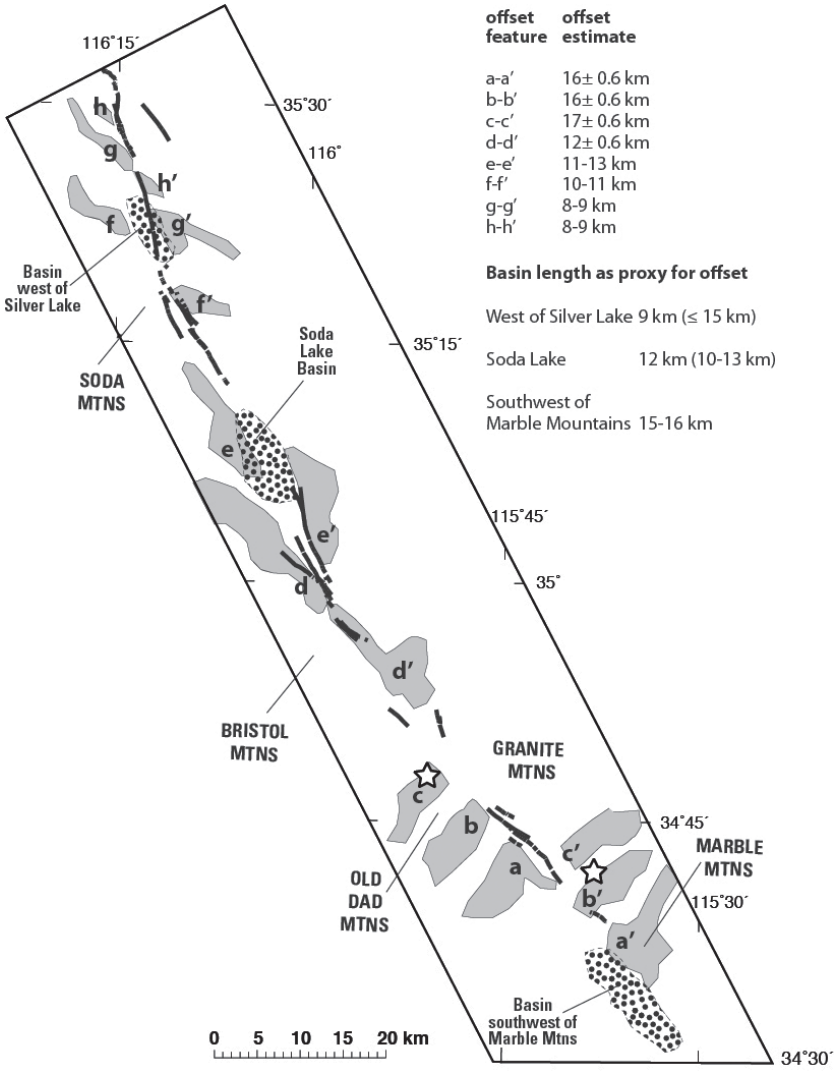

Figure 6. Map of offset features (gray polygons) and pull-apart basins (stippled pattern) along the Soda-Avawatz and Bristol-Granite Mountains fault zones (heavy black lines), with offset estimate summary.

The northwest-trending basin west of Silver Lake is about 9 km long, 3–4 km wide and 1.5 km deep. Brady et al. (1989) suggested that the gravity low reflected a basin formed by strike-slip faults. Both northeast and southwest margins are well expressed by gravity and magnetic gradients and are parallel to the fault traces mapped in the Soda Mountains. Again, this basin as defined by gravity lies within a right step between two strands of the fault, whereas the inferred location of the Quaternary strand bisects the basin. Sandbox models of strike-slip basins show that faulting in extensional stepovers evolve such that younger fault strands commonly evolve and connect together to bisect the strike-slip basin formed by older,

possibly unconnected fault strands (Dooley and McClay, 1997).

Fault offset inferred from the length of the tectonically-controlled basins within the Soda–Avawatz and Bristol–Granite Mountains faults ranges from ~9 km to ~15 km, consistent with offsets estimated by the correlation of magnetic anomalies. Additionally, the estimates from the analysis of the geophysical data are within those proposed from geologic mapping, at least for the southern part of the fault system. There, the revised offset estimate of the Lost Marble gravels (17 km; David Buesch, road log day 1, this volume) is more consistent with the 15–17 km from offset estimates derived from our geophysical analysis. Our geophysical estimates are less consistent with the 24 km estimate originally presented by Lease et al. (2009). This suggests that all of the 15–17 km of cumulative fault offset on the Soda–Avawatz and Bristol–Granite Mountains faults occurred after deposition of the early Miocene(?) Lost Marble gravels, which are overlain by the Peach Springs tuff dated at 18.78 Ma by Ferguson and others (2013).

The offsets inferred from the geophysical analysis for the northern part of the system are similar to those of Davis (1977), but significantly lower than those inferred by Brady (1984) and Gourley (2000). The discrepancy may result from an underestimation of the length of the basin west of Silver Lake, as the location of the southeast basin margin is not as well constrained by gravity measurements. However, the basin is no more than 15 km long, given the presence of basement outcrops to the southeast. The discrepancy also could result from overestimation of offset by clast compositions and paleocurrent indicators, given possible complications from mid-Miocene extension/transtension that influenced the deposition of the lower Avawatz Formation (Spencer, 1990). More work is needed to reconcile these different estimates of offset before evaluating the impact of apparent diminishing northward cumulative offset on this fault system and the implications for various palinspastic models for deformation in this part of the ECSZ.

The geophysical results point to an interesting pattern of alternating stretches of uplift (basement outcrop) and subsidence (basins) along the Soda–Avawatz and Bristol–Granite Mountains fault zone. The uplift and subsidence likely results from transpression and transtension, respectively, within the fault zone. These segments average 15–20 km in length; they may indicate coupling with faults farther west (or east) or otherwise provide hints about how the eastern margin of the ECSZ interacts within the broader shear zone.

Acknowledgments

We thank reviewers Scott Bennett and Geoffrey Phelps for their reviews and the National Cooperative Geologic Mapping Program of the U.S. Geological Survey for support.

References

Bassett, A.M., Kupfer, D.H., and Barstow, F.C., 1959, Core logs from Bristol, Cadiz, and Danby dry lakes, San Bernardino County, California: U.S. Geological Survey Bulletin 1045-D, p. 97-138.

Bedford, D. R., Miller, D.M., and Phelps, G.A., 2010, Surficial geologic map of the Amboy 30' by 60' quadrangle, San Bernardino County, California: U.S. Geological Survey Scientific Investigations Map 3109, pamphlet 26 p., scale 1:100,000, available at http://pubs.usgs.gov/sim/3109/.

Bennett, S.E.K., Darin, M.H., Dorsey, R.J., Skinner, L.A., Umhoefer, P.J., and Oskin, M.E., 2016, Animated Tectonic Reconstruction of the Lower Colorado River Region: Implications for Late Miocene to Present Deformation, in Reynolds, R.E. ed., Going LOCO--Investigations along the lower Colorado River: Proceedings for the 2016 Desert Symposium, p. 73-86, http://nsm.fullerton.edu/dsc/images/DSCdocs/DS_2016_Going_LOCO.pdf.

Black, W.E., 1997, Seismic reflection survey, Cadiz Valley, Cadiz, California: Report prepared for the Cadiz Land Company, San Bernardino, Calif., 23 p.

Blakely, R.J., and Simpson, R.W., 1986, Approximating edges of source bodies from magnetic or gravity anomalies: Geophysics, v. 51, p. 1494-1498.

Brady, R.H., III, 1984, Neogene stratigraphy of the Avawatz Mountains between the Garlock and Death Valley fault zones, southern Death Valley, California: Implications as to late Cenozoic tectonism: Sedimentary Geology, v. 38, p. 127-157.

Brady, R.H., III, 1992, The Eastern California Shear zone in the northern Bristol Mountains, southeastern California in Richard, S.M., ed., Deformation associated with the Neogene Eastern California Shear Zone, southwestern Arizona and southeastern California: San Bernardino County Museum Special Publication 92-1, p. 6-10.

Brady, R.H., III, 1993, Cenozoic stratigraphy and structure of the northern Bristol Mountains, California in Sherrod, D.R. and Nielson, J.E., eds., Tertiary stratigraphy of highly extended terranes: U.S. Geological Survey Bulletin 2053, p. 25-28.

Brady, R.H., III, Clayton, J., Verosub, K.L., Cregan, A., Troxel, B.W., and Abrams, M., 1989, Kinematics at the intersection of the Garlock and Death Valley fault zones, California: Integration of TM data and field studies: NASA Grant NAS5-28754 Final Report, 1982 p. http://ntrs.nasa.gov/archive/nasa/casi.ntrs.nasa.gov/ 19890012892.pdf

Cordell, L., and Grauch, V.J.S., 1985, Mapping basement magnetization zones from aeromagnetic data in the San Juan Basin, New Mexico in Hinze, W.J., ed., The Utility of Regional Gravity and Magnetic Anomaly Maps: Society of Exploration Geophysicists, Tulsa OK, p. 181-192.

Davis, G.A., 1973, Geologic studies of the hypothesized Death Valley fault zone, in Southern California Edison Company, Information concerning site characteristics, Vidal Nuclear Generating Station, vol. 5, Appendix 2.5-E, Attachment A, p. E-A-1 to E-A-17.

Davis, G.A., 1977, Limitations on displacement and southeastward extent of the Death Valley fault zone,

California: California Division of Mines and Geology Special Publication 129, p. 29-33.

Dokka, R.K., and Travis, C.J., 1990, Late Cenozoic strike-slip faulting in the Mojave Desert, California: Tectonics, v. 9, p. 311-330.

Dooley, Tim, and McClay, Ken, 1997, Analog modeling of pull-apart basins: American Association of Petroleum Geologists Bulletin, v. 81, p. 1804-1826.

Ferguson, C.A., McIntosh, W.C., and Miller, C.F., 2013, Silver Creek caldera—The tectonically dismembered source of the Peach Spring Tuff: Geology, v. 41, p. 3-6, doi:10.1130/G33551.1.

Gamble, J., 1959a, Geology and mineral resources of Township 8 North, Ranges 11 and 12 East, San Bernardino County, California: San Francisco, Calif., Southern Pacific Company, unpub. report and 1:24,000-scale map, 22 p.

Gamble, J., 1959b, Geology and mineral resources of Township 9 North, Ranges 11 and 12 East, San Bernardino County, California: San Francisco, Calif., Southern Pacific Company, unpub. report and 1:24,000-scale map, 18 p.

Glazner, A.F., Walker, J.D., Bartley, J.M., and Fletcher, J.M., 2002, Cenozoic evolution of the Mojave block of southern California, in Glazner, A.F., Walker, J.D., and Bartley, J.M., eds., Geologic Evolution of the Mojave Desert and Southwestern Basin and Range: Geological Society of America Memoir 195, p. 19-41.

Gourley, J.R., 2000, Facies analysis of Neogene syntectonic strata in the Soda Mountains, San Bernardino County, California: Implications for constraint on faulting on the Soda-Avawatz fault: California State University, Fresno, M.S. thesis, 66 p.

Grose, L.T., 1959, Structure and petrology of the northeast part of the Soda Mountains, San Bernardino County, California: Geological Society of America Bulletin, v. 70, p. 1509-1548.

Hendricks 2007 California in Theodore, Ted, ed., Geology and mineral resources of the East Mojave National Scenic Area, San Bernardino County, California: U.S. Geological Survey Bulletin 2160, [available at http://pubs.usgs.gov/bul/b2160/, last accessed February 2, 2009].

Howard, K.A., 2002, Geologic map of the Sheep Hole Mountains 30 by 60 quadrangle, San Bernardino and Riverside counties, California: U.S. Geological Survey Miscellaneous Field Studies Map MF-2344, http:// pubs.usgs.gov/mf/2344.

Howard, K. A., and Miller, D. M. 1992, Late Cenozoic faulting at the boundary between the Mojave and Sonoran blocks: Bristol Lake area, California in Richard, S.M., ed., Deformation associated with the Neogene Eastern California Shear Zone, southwestern Arizona and southeastern California. Redlands, CA, San Bernardino County Museum Special Publication 92-1, p. 37–47.

Howard, K.A., Kilburn, J.E., Simpson, R.W., Fitzgibbon, T.T., Detra, D.E., Raines, G.L., and Sabine, Charles, 1987, Mineral Resources of the Bristol/Granite Mountains wilderness study area, San Bernardino county, California: U.S. Geological Survey Bulletin 1712-C, 18 p.

Jachens, R.C., and Langenheim, V.E., 2014, Gravity survey and interpretation of Fort Irwin and vicinity, Mojave Desert, chapter H of Buesch, D.C., ed., Geology and geophysics applied to groundwater hydrology at Fort Irwin, California: U.S. Geological Survey Open-File Report 2013-1024, 11 p., http://dx.doi.org/ 10.3133/ofr20131024H.

Jachens, R.C., Langenheim, V.E., and Matti, J.C., 2002, Relationship of the 1999 Hector Mine and 1992 Landers fault ruptures to offsets on Neogene faults and distribution of Late Cenozoic basins in the Eastern California Shear Zone: Bulletin of the Seismological Society of America, v. 92, p. 1592-1605.

Jennings, C.W., Strand, R.G., and Rogers, T.H., 1977, Geologic map of California: California Division of Mines and Geology, scale 1:750,000.

Laird, R.T., 1959, Geology and mineral resources of Township 10 North, Ranges 9 and 10 East, San Bernardino Meridian, San Bernardino County, California: San Francisco, Calif., Southern Pacific Company, unpub. report, scale 1:24,000, 28 p.

Langenheim, V.E., Biehler, S., Negrini, R., Mickus, K., Miller, D.M., and Miller, R.J., 2009, Gravity and magnetic investigations of the Mojave National Preserve and adjacent areas, California and Nevada: U.S. Geological Survey Open-File Report 2009-1117, 28 p., http://pubs.usgs.gov/of/2009/1117.

Langenheim, V.E., and Jachens, R.C., 2014, Aeromagnetic data, processing, and maps of Fort Irwin and vicinity, California, chap. I of Buesch, D.C., ed., Geology and geophysics applied to groundwater hydrology at Fort Irwin, California: U.S. Geological Survey Open-File Report 2013–1024, 18 p. http://dx.doi.org/10.3133/ofr20131024I.

Lease, R.O., McQuarrie, N., Oskin, M., and Leier, A., 2009, Quantifying dextral shear on the Bristol-Granite Mountains fault zone: Successful geologic prediction from kinematic compatibility of the Eastern California Shear Zone: Journal of Geology, v. 117, p. 37-53.

McQuarrie, N., and Wernicke, B. P. 2005. An animated tectonic reconstruction of southwestern North America since 36 Ma. Geosphere, v. 1, p. 147–172.

Miller, D.M., 2012, Surficial geologic map of the Ivanpah 30' x 60' quadrangle, San Bernardino County, California and Clark County, Nevada: U.S. Geological Survey Scientific Investigations Map 3206, pamphlet 14 p., scale 1:100,000, accessed at https:pubs.usgs.gov/sim/3206

Miller, D.M., and others, 2017, Active Tectonics of the Northern Mojave Desert: The 2017 Desert Symposium Field Trip Road Log *in* Reynolds, R.E., ed., 2017 Desert Symposium Field Guide and Proceedings, California State University Desert Studies Center, Zzyzx, CA, this volume.

Miller, D.M., and Yount, J.C., 2002, Late Cenozoic tectonic evolution of the north-central Mojave Desert inferred from fault history and physiographic evolution of the Fort Irwin area, California, *in* Glazner, A.F., Walker, J.D., and Bartley, J.M., eds., Geologic Evolution of the Mojave Desert and Southwestern Basin and Range: Geological Society of America Memoir 195, p. 173-197.

Miller, D.M., Miller, R.J., Nielsen, J.E., Wilshire, H.G., Howard, K.A., and Stone, Paul, 2007a, Geologic map of the East Mojave National Scenic Area, California *in* Theodore, Ted, ed., Geology and mineral resources of the East Mojave National Scenic Area, San Bernardino County, California:

U.S. Geological Survey Bulletin 2160, [available at http://pubs.usgs.gov/bul/b2160/, last accessed February 2, 2009].

Miller, D.M., Dudash, S.L., Green, H.L., Lidke, D.J., Amoroso, L., Phelps, G.A., and Schmidt, K.M., 2007b, A new Quaternary view of northern Mojave Desert tectonics suggests changing fault patterns during the late Pleistocene, *in* Miller, D.M., and Valin, Z.C., editors, Geomorphology and tectonics at the intersection of Silurian and Death Valleys, southern California: U.S. Geological Survey Open File Report 2007-1424, p. 157-171, available at http://pubs.usgs.gov/of/2007/ 1424/of2007- 1424.pdf

Miller, D.M., Menges, C.M., and Lidke, D.J., 2014, Generalized surficial geologic map of the Fort Irwin area, San Bernardino County, California, chap. B *of* Buesch, D.C., ed., Geology and Geophysics applied to groundwater hydrology at Fort Irwin, California: U.S. Geological Survey Open-File Report 2013–1024, 11 p., scale 1:100,000. *http://dx.doi.org/10.3133/ofr20131024B*

Richard, S.M., 1993, Palinspastic reconstruction of southeastern California and southwestern Arizona: Tectonics, v. 12, p. 830-854.

Rockwell, T.K., Lindvall, S., Herzberg, M., Murbach, D., Dawson, T., and Berger, G., 2000, Paleoseismology of the Johnson Valley, Kickapoo, and Homestead Valley faultsL clustering of earthquakes in the eastern California shear zone: Bulletin of the Seismological Society of America, v. 90, p. 1200-1236.

Sauber, J.W., Thatcher, Wayne, Solomon, S.C., and Lisowski, M., 1994, Geodetic slip rate for the eastern California shear zone and recurrence of Mojave desert earthquakes: Nature, v. 367, p. 264-6.

Spencer, J.E., 1990, Late Cenozoic extensional and compressional tectonism in the southern and western Avawatz Mountains, southeastern California *in* Wernicke, B.P., ed., Basin and Range extensional tectonics near the latitude of Las Vegas, Nevada: Geological Society of America Memoir 176, p. 317-333.

A review of latest Oligocene – earliest Miocene floras of the Mojave Block

Robert E. Reynolds
CSU Desert Studies Research Associate, Redlands, CA. 92373, bob.reynolds220@gmail.com

ABSTRACT— Fossil floras in the Bristol and Cady Mountains, Wild Horse Mesa, and in the Barstow formation range in age from 24 Ma to 17 Ma. These floras, when viewed in combination with associated invertebrate and vertebrate fossils, allow inferences about habitat for the Mojave Desert sequence of mammalian faunas that span the Arikareean / Hemingfordian NALMA transition from latest Oligocene to earliest Miocene time. Taxa of many of these floras suggest streams and wetlands, wooded slopes, and distant uplands with piñon and juniper.

Introduction

The Mojave Block lies between the left lateral Garlock fault on the north, the right-lateral San Andreas fault on the southwest, and is poorly defined to the east. During the mid Oligocene, the block was a pediment that had been stripped of Paleozoic and Mesozoic sediments, leaving a relatively smooth surface cut into Cretaceous granitic rocks that were undergoing erosion. The signature appearance of this surface is one of low relief, stained with red-orange leisengang rings, covered with granitic grus, lag cobbles of quartzite, with a scatter of occasional large spheroidal bounders. This pre-Miocene erosional surface (Oberlander, 1972; Reynolds, 1992; Reynolds, 1995j) was disrupted by crustal extension during Late Oligocene through early Miocene time. Extensional faulting helped create the present day topography and developed initial drainage routes through the dismembered terrain. Sedimentary basins resulting from extensional listric-normal faulting contain fossil faunas and floras: the southern Bristol Mountains flora, Cady Mountain flora, Wild Horse Mesa flora (18.5 Ma; McCurry, 1995; Reynolds and others, 1995), floras from the Barstow Formation in the Calico Mountains (Jenkins, 1986; Reynolds, 2013), and the dated sequence of floras from the Barstow Formation in the Mud Hills (17 – 14 Ma; Alf, 1970; Reynolds and Schweich, 2013, 2015).

Southern Bristol Mountains flora

The southern Bristol Mountains fossils occur below an ash bed that produced a U-Pb zircon age of 23.8 ± 0.4 Ma (1 Sigma) (Harvey and others, 2010; Reynolds and others, 2015), making these latest Oligocene plants the oldest flora from the Mojave Block. The plant fossils are identified as palm root, the grass *Tomlinsonia* sp., the fern *Acrostichium* sp., and structures with 3 to 5 pore-like openings reminiscent of vascular bundles like that of pre-palm or pre-yucca (*Protoyucca* sp.). Fresh water gastropod (*Lymnaea sp.*) and fern suggest a subtropical climate for plants and animals that lived along a riparian streamside.

Cady Mountains flora

The Cady Mountains flora, found in the western portion of the Hector Formation in the northern Cady Mountains, is preserved in siliceous limestone near the base of the earliest Miocene section described by Moseley (1978). This lacustrine-paludal bed is located in the basal sandstone and conglomerate of Unit Ts1 (Moseley, 1978). Ts1 underlies several undated basalt and ignimbrite flows that are overlain by basalts flow Tb2 dated at 21.5 Ma (Moseley, 1978), suggesting that the Cady Mountains Flora dates to 22 Ma, in latest Arikareean time. The Cady Mountains plant taxa include *Sabalites* sp. (Fig 1), the sable palm and *Tomlinsonia* sp. (siliceous grass) (Figs 2a, b, c). These taxa grow at the edges of brackish marshes and roots are preserved in subsurface strata (Fig. 3).

Wild House Mesa flora

The Wild Horse Mesa Flora was recovered from tuffaceous shale of the Winkler Formation deposited in shallow lakes located above the PST (18.8 Ma, Ferguson and others, 2013) and below the WHM tuff of 17.7 Ma (McCurry, 1995; Reynolds 1995). *Sequoidendron langsdorfi* was reported from the Wild Horse Mesa sediments (Hazzard, 1954), and pine-like needles suggest the presence of

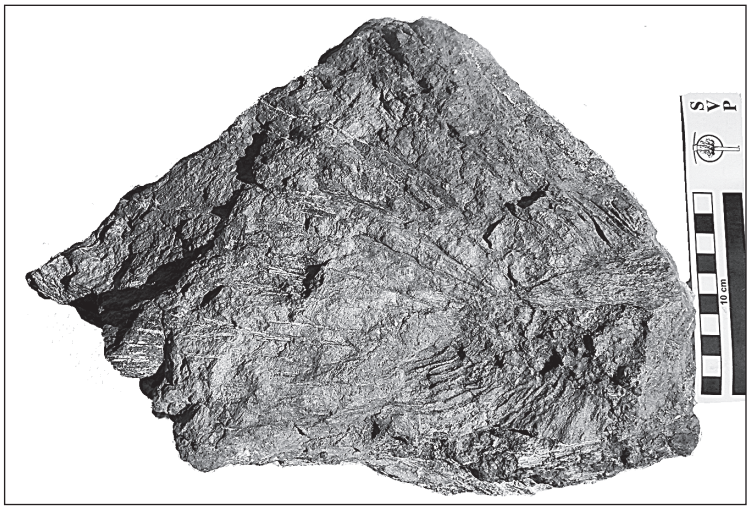

Figure 1: Cady Mountains flora, *Sabalites* sp., Sabal Palm

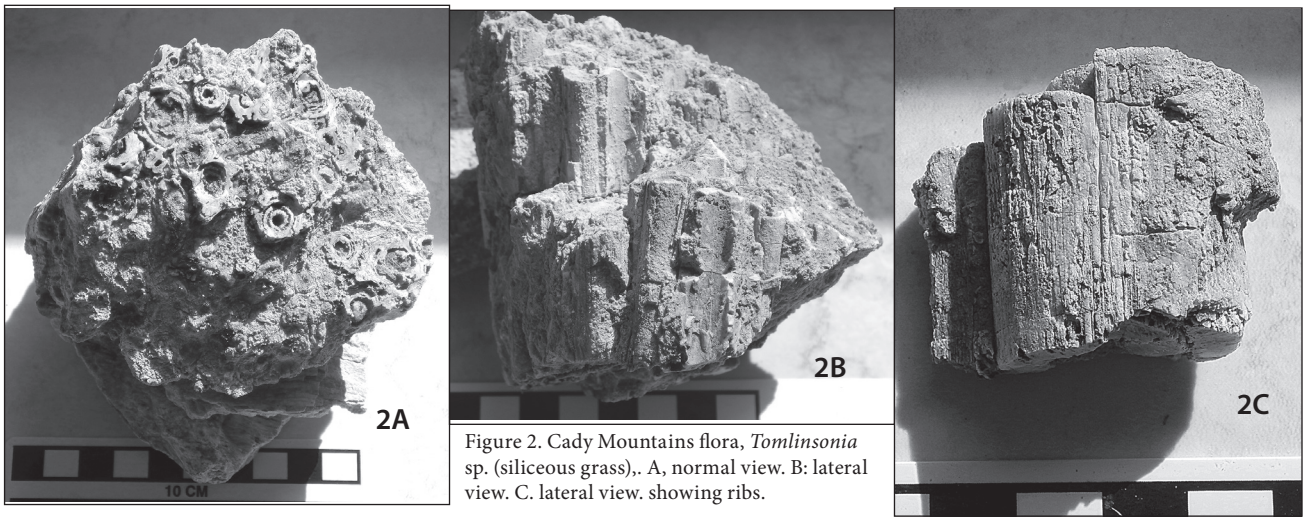

Figure 2. Cady Mountains flora, *Tomlinsonia* sp. (siliceous grass),. A, normal view. B: lateral view. C. lateral view. showing ribs.

Figure 3: Rhizoliths in freshwater limestone (Gregor Losson photo).

Pinaceae in addition to Taxodiacea growing around this five-mile-wide, well-drained highland depocenter.

Barstow formation floras

The Barstow Formation spans time from 19 – 12.5 Ma and extends from Black Canyon east-southeast through the Calico, Alvord, and southern Cady Mountains to the vicinity of Ludlow, California (Reynolds, and others, 2010.

Barstow Formation, Calico Mountains. Palm and palm root weathers from sediments dating between 17 and 15.5 Ma. One silicified palm base was recovered from a gravel pit near Minneola Road. This was probably washed east from the vicinity of other palm occurrences at Little Borate Canyon, then south along the Yermo Land Fill road.

Barstow Formation, Lenwood flora (n. d.).

A palm base was collected near the intersection of the SR-58 cutoff to Mojave and West Main Street in eastern Yermo.

Barstow Formation, Little Borate Canyon, Calico Mountains.

During the recovery of silicified insects from calcareous stomatolites in lacustrine silts, mosses and moss spores, charophyte (green algae) spore cases, leaves and seeds were collected, but descriptions apparently remain unpublished (Palmer, 1957; Jenkins, 1986).

Barstow Formation, Mud Hills, Rainbow Loop Flora (16.3 Ma).

The Rainbow Loop Flora (RLF) is located at the top of the Brown Platy Limestones (BPL) sequence and below the Strontium–Borate (Sr-B) horizon (Reynolds and others, 2010), the former dated magnetostratigraphically between 16.4–16.2 Ma at a locality half a mile west. This flora (Alf, 1970; Reynolds and Schweich, 2013, 2015) has 27 plant taxa representing several habitats (Table 1).

Table 1: Rainbow Loop Taxa by Community

Community	Genus	Common name
Aquatic	*Carex*?	sedge
	Typha?	cat tail
Riparian	*Acer*?	maple
	Salix?	willow
	Aracaceae	palm
Woodland	*Quercus*	oak
	Fraxinus	ash
	Juglans sp	walnut
	Rhamnaceae (*Ceanothus*? or *Rhamnus*?)	buck thorn
	Rosaceae, c.f., *Prunus*	rose family
	Rubiaceae	madder
	Rosaceae, c.f., *Cercocarpus*	mountain mahogany
	Cupressaceae, c.f., *Juniperus*	juniper
Upland	*Purshia*	bitterbrush
	Cupressaceae, c.f., *Juniperus*	juniper
Distant Upland	*Pinaceae*	pine

Table 2: Chronostratigraphic relationship of floras.

Locality	Date	Riparian	Combined Woodland
South Bristol Mountains	23.8 Ma	palm, *Tomlinsonia* sp. (grass)	
Cady Mountains Flora	22 Ma	palmetto, *Tomlinsonia* sp. (grass)	
Wild Horse Mesa	18.5 Ma	*Sequoidendron* sp.	pine
Barstow Formation, Calico Mountains	17 – 15.5 Ma	palm, green algae, mosses	
Rainbow Loop Flora	16.3 Ma	cattail, maple, willow, palm	oak, ash, Juniper, pine
Solomon Skyline	14.8 Ma		walnut, spruce
Slug Bed Pollen	14.8 Ma	sedges, cattails, horsetails, palm, willow cottonwood	walnut
Hell Gate Flora	14.2 Ma		walnut

Discussion

The central Mojave Miocene floras from 24 Ma to 14 Ma have lacustrine, stream bank, and riparian components (Table 2). They include water reeds and aquatic plants, shore-line reeds, grasses, riparian trees, palms and palmettos, and logs of woodland species that were washed into flowing or still water. Walnut trees grew in many areas. These fossiliferous deposits reflect drainages that developed from east to west as extensional tectonism waned. The combined woodland species suggest that forested highlands with oak, juniper, sequoia and pine survived extension and associated erosion.

In support of habitat data provided by floras, beavers (*Anchitheriomys*? sp.) are present in the Lower and Upper Cady Mountains Local Faunas (17.3 Ma, Miller, 1980, Woodburne, 1998). Other beaver genera (*Monosaulax* sp., Lindsay, 1972) are present at 14.8 Ma in the Barstow Formation of the Mud Hills. Although these large rodents can travel short distances over dry land, they move from one stream or pond to another along a riparian corridor. The floras in the wetlands and lakes of the Barstow Formation were apparently stable year round, since the stickleback fish that they supported mandate a drainage connection at 16 Ma from the central Mojave to the Pacific Ocean (Bell and Reynolds, 2010).

Acknowledgements

This work was conducted under the authorization of Jim Shearer, archaeologist, Bureau of Land Management, Barstow Field Office (BLM Permit No. CA-10-00-007P). Thanks to Don Lofgren and Andrew Farke for accepting specimens of the plants into the Raymond Alf Museum of Paleontology in Claremont, CA. Tom Schweich was a great help with fossil plant identification. Assistance with field work by Tom and Peggy Howe, Mark Roeder, Quintin Lake, Gregor Losson, and the Larson family, is acknowledged. Gregor Losson assisted with fieldwork and photography.

References cited

Alf, R.M. 1970. A preliminary report on a Miocene Flora from the Barstow Formation, Barstow, California. Southern California Academy of Science, 69(3-4): 183-189.

Bell, Michael A., and Robert E. Reynolds, 2010. Miocene and Late Pleistocene stickleback spines from the Mojave Desert, California; Desert Symposium Volume, California State University, Desert Studies Consortium. p. 162-168.

Ferguson, C.A., McIntosh, W.C., and Miller, C.F., 2013, Silver Creek caldera—The tectonically dismembered source of the Peach Spring Tuff: Geology, v. 41, p. 3-6, doi:10.1130/G33551.1.

Fisk, Lanny H., and David F. Maloney, 2015. Palynology of the "Slug Bed" in the middle Miocene Barstow Formation in the Mud Hills, Mojave Desert, southern California. Desert Symposium Volume, California State University, Desert Studies Consortium. p. 130-135

Harvey and others, 2010. Expanding the late Oligocene/early Miocene tectonic, magmatic and sedimentary history in the South Bristol Mountains, Desert Symposium Volume, California State University, Desert Studies Consortium, p. 283.

Hazzard, J. C., 1954. Rocks and structure of the northern Providence Mountains, San Bernardino County, California, in Jahns, R. H., ed., Geology of Southern California. California Division of Mines Bulletin, 170 (IV):27-36.

Jenkins, John E., 1986. Miocene invertebrates from the Calico Mountains, San Bernardino County, California. San Bernardino County Museum Association quarterly, Vol. 33(4), pp. 42.

Lindsay, E.H. 1972. Small mammal fossils from the Barstow Formation, California. University of California Publications in Geological Sciences 93:104p.

McCurry, Michael, D. R. Lux, and Kevin L. Mickus, 1995. Neogene Structural Evolution of the Woods Mountains Volcanic Center, East Mojave National Scenic Area. San Bernardino County Museum Association quarterly, Vol. 42(3), p. 75-80.

Miller, S.T., 1980. Geology and mammalian biostratigraphy of a part of the northern Cady Mountains, Mojave Desert, California: U. S. Geol. Surv. Open File Report 80-878, 122 p.

Moseley, C.G. 1978. Geology of a portion of the northern Cady Mountains, Mojave Desert, California. University of California, Riverside, Department of Earth Sciences (Master's thesis).

Oberlander, T. M., 1972. Morphogenesis of granitic boulder slopes in the Mojave Desert, California. Journal of Geology, 80:1-19.

Palmer, A. R. 1957. Miocene arthropods from the Mojave Desert. U. S. Geological Survey Professional Paper 294-G, p. 237-280.

Reynolds, R.E., 1992. The Tertiary Pioneertown sequence, *in* Old routes to the Colorado, J. Reynolds, ed. Redlands, San Bernardino County Museum Association Special Publication 92-2:31-33.

Reynolds, R. E., 2013. Non-vertebrate fossils in the Miocene Barstow Formation, central Mojave Desert, California. 2013 Desert Symposium Volume, California State University, Desert Studies Consortium. p. 99-102.

Reynolds, Robert E., Janet Harvey, Axel K. Schmitt, and Tomas Spinks, 2015. Fossil plants, gastropods and camel tracks from Early Miocene sediments in the southern Bristol Mountains, Mojave Desert, California. Desert Symposium Volume, California State University, Desert Studies Consortium. p. 200-205.

Reynolds, R.E., Hunt, R., and Albright, B., 1995. Rhinoceros in Lanfair Valley *in* Ancient surfaces of the East Mojave Desert, Reynolds, R.E. (compiler) and J. Reynolds (ed). San Bernardino County Museum Association Quarterly, 42(3): p. 107- 110.

Reynolds, R. E., D. M. Miller, M. O. Woodburne, and L. B. Albright, 2010. Extending the boundaries of the Barstow Formation in the central Mojave Desert; Desert Symposium Volume, California State University, Desert Studies Consortium. p.148-161.

Reynolds, R. E., and T. A. Schweich, 2013. The Rainbow Loop Flora from the Mud Hills, Mojave Desert, California. Desert Symposium Volume, California State University, Desert Studies Consortium. p. 39-48.

Reynolds, Robert E., and Thomas A. Schweich, 2015. Additions to the floras of the Barstow Formation in the Mud Mills, Mojave Desert, California. Desert Symposium Volume, California State University, Desert Studies Consortium. p. 119-129.

Woodburne, M.O. 1998. Arikareean and Hemingfordian faunas of the Cady Mountains, Mojave Desert province, California, pp 197-201 *in* . Depositional environments, lithostratrigraphy, and biostratigraphy of the White River and Akrikaree Groups (late Eocene to early Miocene, North America, D.O. Terry Jr., H.E. LaGarry, and R.M. Hunt Jr, (eds.),. Geological Society of America Special Paper 325.

Analysis of the age and paleomagnetic orientation of the Broadwell Mesa Basalt, Bristol Mountains, CA

G. A. Phelps, J. W. Hillhouse, R. J. Fleck, D. M. Miller, D. C. Buesch, A. Cyr, and K. M. Schmidt
U.S. Geological Survey. Middlefield Road, Menlo Park, California

ABSTRACT—To add to the regional paleomagnetic data documenting block rotation in eastern California, we determined the age and paleomagnetic rotation of the Broadwell Mesa basalt, a basalt in the Bristol Mountains, CA as part of an effort to constrain the timing and rotation of blocks adjacent to the fault. The east-striking sinistral Broadwell Mesa fault cuts and separates the basalt into two outcrops. An 40Ar/39Ar date from the northern outcrop yields an age of 5.46 ± 0.04 Ma. Two sites consisting of 40 paleomagnetic cores from the basalt indicate the basalt is reversely magnetized and that there has been no significant rotation (< 11°) between the two basalt outcrops.

Introduction

The Broadwell Mesa basalt is a series of at least 10 flows emanating from at least one cinder cone vent atop Broadwell Mesa, located in the Mojave Desert of southern California (fig. 1). The basalt forms a plateau along the western crest of the Bristol Mountains. It has two major outcrops, one with an area of approximately 4.6 km^2 exposed mostly north of the fault, and the other an area of approximately 1.4 km^2 exposed to the southeast of the northern outcrop, south of the fault. The northern outcrop is composed of a series of flows primarily north of, and truncated by, the east-striking, sinistral Broadwell Mesa fault, and the other a series of flows exposed approximately one kilometer south of the fault and east of the easternmost edge of the northern outcrop (consistent with sinistral slip). The flows have no intervening sedimentary horizons between them, they have similar stratigraphic position and structural orientation, and they have physical and chemical similarities, indicating that the north and south outcrops form part of the same unit (Buesch and Phelps, 2016).

The Broadwell Mesa basalt was first mapped by Gardner (1940), who considered the basalt to be Pleistocene and structurally undisturbed. He described the unit as variable in thickness, and postulated a maximum thickness of 400 feet (122 m) (Gardner, 1940). The basalt was later mapped by Kupfer and Bassett (1962), who refined the mapped boundaries of the unit

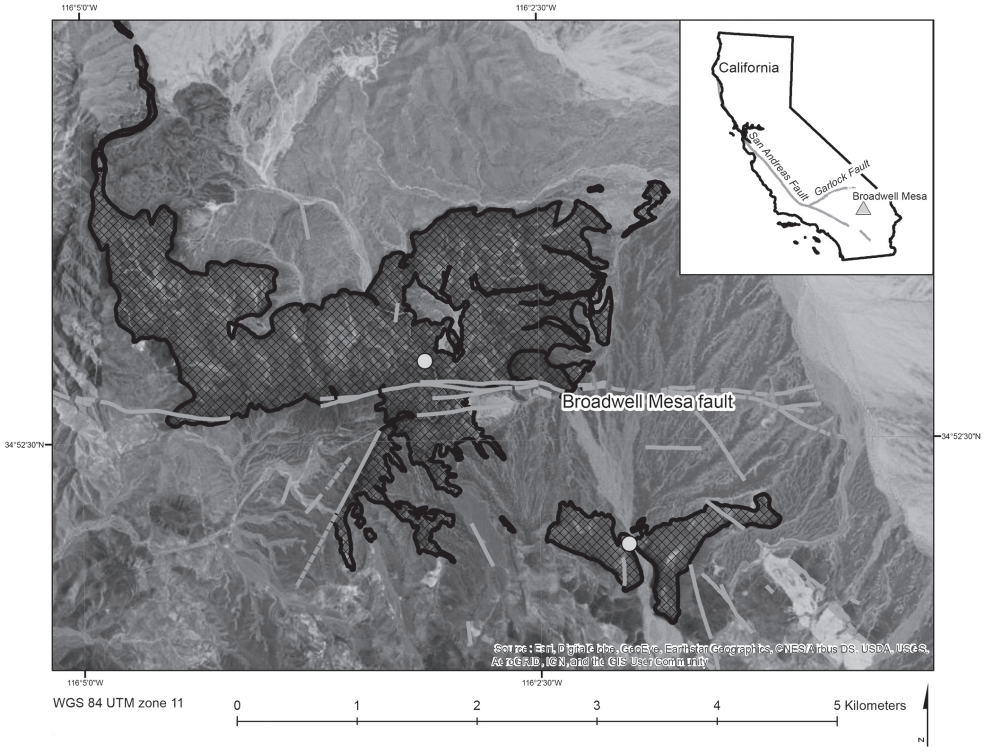

Figure 1. Broadwell Mesa basalt (black hachure) and Broadwell Mesa fault (red lines, dashed where approximately located). Sample locations for the outcrops north and south of the fault are shown as green dots. Based on unpublished mapping by the authors that revises Phelps et al. (2012).

TABLE 1. PALEOMAGNETIC DATA FOR BROADWELL MESA BASALT

Sample	Location*		Remanent Magnetization				Magnetic	Hand Sample
	Easting	Northing	Declination	Inclination	Angular Std. Dev.	Magnetization	Susceptibility	
	(meters)	(meters)	(degrees)	(degrees)	(degrees)	(A/m)	(10^{-3} SI)	
~~3J856-1~~	586637	3860258	158.8	-33.7	0.6	2.15	75.0	M13BM-1350-1A
3J857-1	586637	3860258	161.0	-34.0	0.7	2.20	78.3	M13BM-1350-1A
3J858-1	586637	3860258	160.9	-33.6	0.4	1.95	74.0	M13BM-1350-1A
3J859-1	586637	3860258	161.8	-39.5	0.6	3.12	90.9	M13BM-1350-1B
3J860-1	586637	3860258	180.4	-41.5	0.4	3.16	89.8	M13BM-1350-1B
3J861-1	586637	3860258	169.0	-39.3	0.3	2.84	78.9	M13BM-1350-1B
3J862-1	586637	3860258	174.4	-37.0	9.0	3.49	53.0	M13BM-1350-2A
3J863-1	586637	3860258	169.4	-32.8	0.7	6.46	69.5	M13BM-1350-2A
3J864-1	586637	3860258	170.4	-35.3	0.4	6.39	59.6	M13BM-1350-2A
3J865-1	586637	3860258	170.6	-26.6	0.5	1.01	135.3	M13BM-1350-2B
3J866-1	586637	3860258	170.2	-28.5	0.5	1.00	131.6	M13BM-1350-2B
3J867-1	586637	3860258	186.6	-33.9	19.5	8.43	127.3	M13BM-1350-2B
3J868-1	586637	3860258	184.1	-41.1	0.9	1.54	56.3	M13BM-1350-3A
3J869-1	586637	3860258	183.5	-45.3	0.8	1.30	51.9	M13BM-1350-3A
3J870-1	586637	3860258	189.6	-52.9	0.9	1.17	50.8	M13BM-1350-3A
3J871-1	586637	3860258	158.6	-32.8	1.0	1.34	43.0	M13BM-1350-3B
3J872-1	586637	3860258	157.3	-29.6	0.7	1.33	42.9	M13BM-1350-3B
3J873-1	586637	3860258	159.0	-28.0	0.8	1.34	42.2	M13BM-1350-3B
3J874-1	586637	3860258	136.7	-23.0	0.5	1.21	256.5	M13BM-1350-4A
3J875-1	586637	3860258	134.6	-25.9	5.3	8.86	185.1	M13BM-1350-4A
3J876-1	586637	3860258	168.9	-37.2	0.9	9.03	27.3	M13BM-1350-4B
3J877-1	586637	3860258	167.6	-36.9	1.1	8.63	26.0	M13BM-1350-4B
3J878-1	586637	3860258	177.1	-29.8	1.0	9.02	26.3	M13BM-1350-4B
3J879-1	586637	3860258	170.8	-42.1	0.8	1.46	34.3	M13BM-1350-5A
3J880-1	586637	3860258	174.1	-42.0	0.6	1.77	42.1	M13BM-1350-5A
3J881-1	586637	3860258	167.0	-44.6	0.6	1.37	33.7	M13BM-1350-5A
3J882-1	586637	3860258	167.0	-39.0	1.0	1.08	46.7	M13BM-1350-5B
3J883-1	586637	3860258	168.7	-36.7	0.9	5.93	46.0	M13BM-1350-5B
3J884-1	586637	3860258	179.1	-27.7	8.5	5.63	39.6	M13BM-1350-5B
Bootstrap Spherical Median:		168.5	-36.7	68th quantile: 1.6	95th quantile: 3.7			
3J885-1	586637	3860258	170.2	-26.6	1.4	1.18	63.2	M13BM-1077B
3J886-1	588337	3858724	171.3	-27.7	0.3	1.33	59.1	M13BM-1077B
3J887-1	588337	3858724	173.8	-29.1	0.6	1.23	50.4	M13BM-1077B
3J888-1	588337	3858724	145.1	-43.9	1.2	1.16	68.9	M13BM-1077C
3J889-1	588337	3858724	155.4	-43.0	0.3	3.24	93.9	M13BM-1077C
3J890-1	588337	3858724	159.8	-40.5	1.1	1.73	78.2	M13BM-1077D
3J891-1	588337	3858724	161.3	-41.4	0.8	1.16	58.1	M13BM-1077D
3J892-1	588337	3858724	159.1	-40.7	0.6	3.11	84.4	M13BM-1077D
3J893-1	588337	3858724	147.7	-40.6	0.5	1.15	49.1	M13BM-1077A
3J894-1	588337	3858724	150.9	-45.8	1.0	1.23	55.3	M13BM-1077A
3J895-1	588337	3858724	150.6	-49.2	1.0	1.23	52.3	M13BM-1077A

*UTM zone 11 NAD83

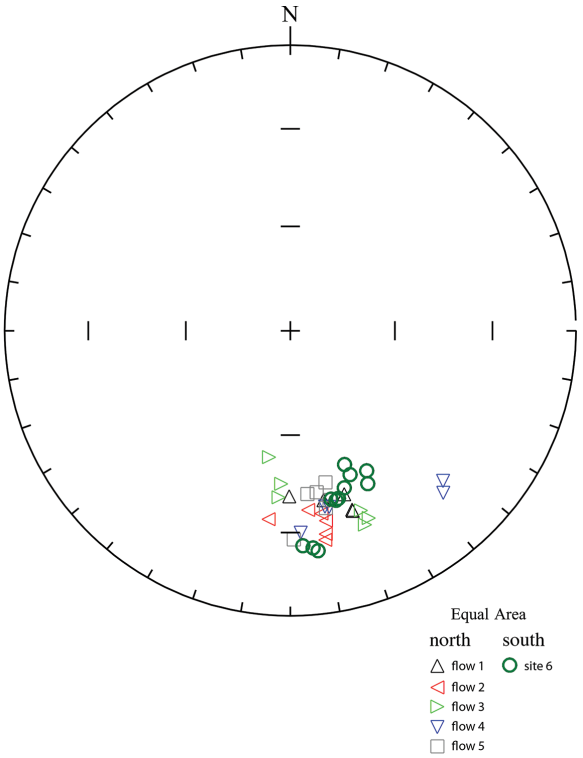

Figure 2. Paleomagnetic directions of five flows from the northern outcrop (uncorrected for tilt) and one from the southern outcrop of the Broadwell Mesa basalt. Flows are numbered lowest to highest in the northern outcrop; site 6 is from the southern outcrop. Plots were generated using the open-source software Paleomag-Tools v. 4.2 (Hounslow, 2011).

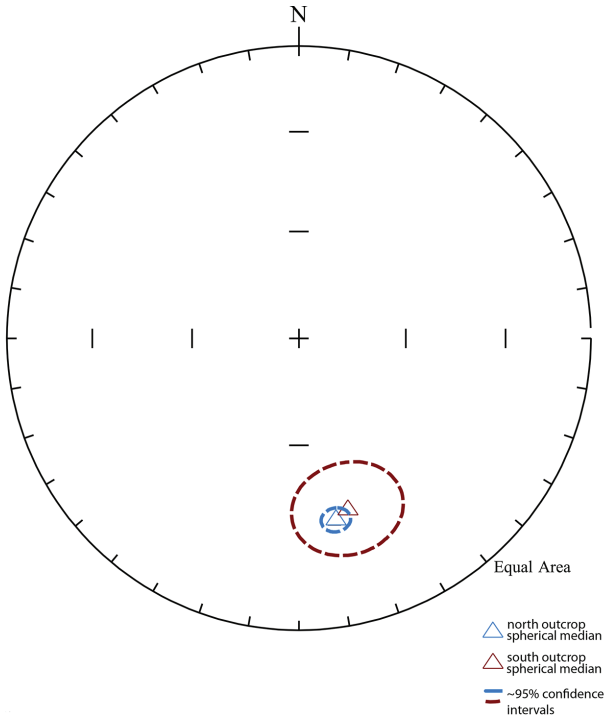

Figure 3. Spherical median paleomagnetic directions for the northern and southern outcrops, and their approximate 95% confidence intervals. Plots were generated using the open-source software Paleomag-Tools v. 4.2 (Hounslow, 2011).

and identified the basalt as Quaternary. Dibblee (1967) adopted this age (1967) and did not significantly change the mapped boundaries of the outcrops, but did map a fault cutting the very southwestern-most edge of the northern basalt outcrop that we now consider the western extension of the Broadwell Mesa fault. Although Phelps et al. (2012) used areal photography to map the Broadwell Mesa basalt at the 1:100,000 scale, the boundaries remained essentially unchanged except for the addition of the Broadwell Mesa fault, a previously unrecognized east-striking fault that cuts the basalt and adjacent Late Pleistocene alluvial deposits to the east (fig. 1). Brady (1992) reported a K-Ar age date of 5.28 +/- 0.13 Ma for the Broadwell Mesa basalt, and noted it was underlain by tilted volcanic and sedimentary rocks similar to the Balch Wash sequence exposed in the northeastern-most Bristol Mountains. Buesch and Phelps (2016) published a preliminary description and analysis of the age and paleomagnetic data, which are revised in this paper.

Late Pleistocene alluvial fan deposits capped by mature desert pavements lie in the intervening area between the northern and southern Broadwell Mesa basalt outcrops (fig. 1). The southern basalt outcrop is tilted 7° to the northeast, and aeromagnetic data (Soda Lake Survey in Langenheim, 2014) show a continuous magnetic low beneath the alluvial fan deposits from the southern to the northern outcrop, suggesting Broadwell Mesa basalt is present in the subsurface between the two outcrops. This is further evidence that the basalt outcrops are part of the same unit.

In the following sections we investigate the age and direction of remanent magnetization of the northern and southern outcrops of the Broadwell Mesa basalt in an effort to constrain timing and relative rotation adjacent to the Broadwell Mesa fault.

Methods

$^{40}Ar/^{39}Ar$ Chronology

The Broadwell Mesa basalt was collected for isotopic $^{40}Ar/^{39}Ar$ age dating from the northern basalt outcrop (fig 1). The sample was taken from the highest of 6 flows (Buesch and Phelps, 2016; Buesch, 2017, this volume) exposed along the wall of a canyon that cuts through the basalt unit. This flow had little to no alteration of olivine and groundmass, the least altered of the exposed flows.

The sample was crushed to a grain size of 180-250 micrometer grain size and all phenocrysts were removed by magnetic separation. Two splits were taken from the bulk groundmass separate and analyzed independently using the $^{40}Ar/^{39}Ar$ incremental-heating technique (e.g., McDougall and Harrison, 1999) at the USGS in Menlo Park, CA. Analytical results of both samples exhibited significant amounts of nuclear recoil of Ar, yielding no

TABLE 2. TILT-CORRECTED REMNANT MAGNETIZATION DIRECTION

Sample name	Tilt-corrected remnant magnetization		Hand sample name
	Declination (degrees)	Inclination (degrees)	
3J885-1	173.0	-23.4	M13BM-1077B
3J886-1	174.2	-24.4	M13BM-1077B
3J887-1	176.7	-25.5	M13BM-1077B
3J888-1	151.5	-43.3	M13BM-1077C
3J889-1	161.3	-41.2	M13BM-1077C
3J890-1	165.0	-38.3	M13BM-1077D
3J891-1	166.6	-39.0	M13BM-1077D
3J892-1	164.4	-38.5	M13BM-1077D
3J893-1	153.3	-39.7	M13BM-1077A
3J894-1	157.5	-44.5	M13BM-1077A
3J895-1	158.1	-47.9	M13BM-1077A
Bootstrap Spherical Median: 164.1 -38.8 68^{th} quantile: 2.7 95^{th} quantile: 14.2			

valid age plateau, and ages were calculated as "recoil model ages", a technique described in (Fleck et al., 2014). These model ages are defined as the integrated age of contiguous temperature increments and fractions of increments in a centered fraction of the age spectrum. Results of age studies reported in Fleck et al. (2014) and in Hagstrum et al. (2016) document the general validity of this approach for samples that do not yield well-defined plateau ages.

Paleomagnetic sample collection and measurement

A total of 14 oriented samples were collected from the northern and southern outcrops (Buesch and Phelps, 2016; Fig. 1); the northern site is also the site of the whole-rock $^{40}Ar/^{39}Ar$ sample. Two oriented hand samples were collected from each of five consecutive flows north of the Broadwell Mesa fault (in this paper flows are labeled 1 to 5 from bottom to top), and one outcrop (labeled 6) close to each other from a single flow south of Broadwell Mesa fault. Hand samples were oriented in the field using a Brunton compass, drilled, and re-oriented on an orientation stage in the lab to obtain oriented core samples. When size allowed, we collected three oriented cores from each hand sample, for a total of six oriented cores per flow. In two instances, hand samples were only large enough to recover two oriented cores, resulting in two flows (flow 4 and the southern flow) with only five oriented samples. Remanent magnetism and susceptibility were then measured using superconducting magnetometer. The specimens were not given any demagnetization treatment. NRM was reported for each oriented core sample, resulting in at least 5 measurements (typically 6) per flow (Table 1). The directions measured from the cores yielded no indication of significant magnetic deflection across five flows in the northern outcrop, and we assume that the southern outcrop behaves similarly.

We did not apply a tilt correction to the flows of the northern outcrop because they are sub-horizontal, but did apply a tilt correction to the flow of the southern outcrop using in-house tilt-corredction software. To obtain the tilt correction we measured multiple vertical joint fractures from the middle of the flow as well as the orientation of several nearly vertically elongated vesicles near the base of the flow. Assuming the joint fractures occur perpendicular to the lower and upper surfaces of the flow, and the flow was deposited horizontally, Schmidt Equatorial Equal-Area stereonet analysis of the joint fractures yields an estimated dip of 7° NE and a strike of 323°. Typically, vesicles in the basalt are spherical to slightly ellipsoidal; however locally, larger elongate vesicles formed, and as a result of buoyancy they rose vertically into the flow. At this southern outcrop, the vertically oriented vesicles (some of which were deformed by the flowing lava) indicate a northerly dip of between 0 and 10°, consistent with the quantitative results obtained from analyzing the joint fractures. The paleomagnetic directions for the southern outcrop were then corrected for the estimated strike and dip of 323° and 7°. The resulting paleomagnetic directions for the southern outcrops are listed in Table 2 and shown in Fig. 2.

Two primary sources of uncertainty are possible with this sampling method. The first is uncertainty at the outcrop, because taking an oriented hand sample with a Brunton compass, coring and then reorienting the hand sample, is a less precise way of obtaining oriented sample than drilling and orienting the sample in the field. The latter was precluded because the basalt lies within a wilderness area. The Brunton compass can also be affected by magnetic deflections caused by proximity to the basalts and adjacent strongly magnetized areas due to lightning strikes. Generally this sampling method is considered accurate to 5°-10°.

Statistics used uor inferring paleomagnetic direction

The most commonly applied method of estimating the center of a population from paleomagnetic data is to assume a spherical Gaussian distribution and measure the sample mean. The use of such an approach relies on the assumption that the data are unimodal, isotropic, and rotationally symmetric. In this case confidence intervals are estimated using standard formulas (e.g. Lowrie, 1997). However, if the assumptions are violated then the statistical estimates may be incorrect, and the confidence intervals unreliable. Sampling methods that are prone to occasional bias in the recorded sample orientation, such as those used to sample the Broadwell Mesa basalt, could produce skewed distributions that would violate these

assumptions. In the case of our study, because the total number of measurements (sample size) is rather small, one or two paleomagnetic direction outliers, resulting from potential bias in the determination of sample orientation in one or both of the field and lab, could unduly influence the estimate of the mean.

A less restrictive approach is to assume only that the distribution of paleomagnetic direction is unimodal. In this case the spherical median of the paleomagnetic directions can be used to estimate the central tendency of their distribution. The spherical median was chosen as a measure of central tendency to robustly determine the best estimate of the remanent paleomagnetic direction for both outcrops. Use of the spherical median helps mitigate uncertainty introduced by possible bias. Confidence intervals around the spherical median were determined by bootstrapping techniques (Tauxe et. al., 1991; Chernick, 2008).

The spherical median is more difficult to calculate than the spherical mean, as it requires an optimization approach to solve the spherical median equation. We follow the method of Fisher et al. (1987) for defining and calculating the spherical median, which they define as the result that minimizes the following equation:

$$, \quad \sum_{i=1}^{n} \cos^{-1}(\tilde{x}x_i + \tilde{y}y_i + \tilde{z}z_i) \qquad (1)$$

where ~ indicates the direction cosines of the vectors x, y, and z, and x, y, and z (without the ~) are the Cartesian coordinates of the paleomagnetic vector.

Minimizing this equation minimizes the sum of the arc lengths from the spherical median to each sample vector. The Nelder-Mead optimization algorithm was used to solve for the spherical median (R Core Team, 2015).

We used bootstrap resampling to calculate the median statistic (Tauxe et. al., 1991; Chernick, 2008). In bootstrap resampling, a sample of the same size as the original is drawn from the data using sampling with replacement. In any given bootstrap resample, some values are chosen twice (or more) while others are not chosen at all. Statistics based on bootstrap resamples generally provide good estimates of a given population statistic, assuming the original sample is an adequate representation of the population (Chernick, 2008).

We assume that the paleomagnetic directions measured from northern and southern outcrops (fig. 2; tables 1 and 2) represent samples from two separate statistical populations, and we then compare the spherical median of these populations (north and south). We generated 1000 bootstrap resamples for each of the northern and southern outcrops and calculated the spherical median for each bootstrap resample. The spherical median of the original sample for each group (northern and southern) was chosen as the median value for the outcrop. The bootstrap resamples were used to estimate the standard error of the spherical median. The 68th and 95th confidence intervals for both the northern and southern medians were chosen according to the percentile approach (choosing the value within which 68% and 95% of the data fall, respectively). The median values for each outcrop and their confidence intervals are shown in fig 3.

Bootstrapped confidence intervals for the mean direction of a paleomagnetic sample can be unreliable for sample sizes less than about 20 (Tauxe et. al., 1991), so the confidence intervals for the southern basalt outcrop may underestimate the true confidence intervals. Chernick (2008) suggested that confidence intervals become unreliable for sample sizes less than 10. To our knowledge the behavior of the bootstrapped median confidence intervals for small (< 20) samples of paleomagnetic data have not been investigated. The wide confidence interval for the spherical median of the southern basalt may result from a small sample size. We show the confidence interval as calculated for the southern basalt outcrop, with the caveat that further investigation (e.g. Tauxe et al., 1991) is warranted.

We used the bootstrap resamples to find the distribution of the angular difference between the median of the northern and southern outcrops (10^6 differences) in order to calculate the amount and uncertainty of vertical axis rotation. The median value and confidence intervals were derived in the same manner as previously specified. Note that a property of differencing medians is that the median of sample A minus the median of sample B in general does not equal the median of all samples in A minus all samples in B:

$$median(A) - median(B) \neq median(A - B) \qquad (2)$$

We choose the right-hand side of equation (2) to estimate the vertical axis rotation between the northern and southern outcrops because it directly measures the desired statistic.

Results

Age of the Broadwell Mesa basalt

The two splits of a groundmass separate of the basalt yielded ages of 5.468±0.059 and 5.450±0.045 Ma, respectively, providing a weighted mean age of 5.46±0.04 Ma relative to an age of 28.20 Ma for the Fish Canyon sanidine standard (note that the Fish Canyon sanidine standard has changed slightly since Buesch and Phelps, 2016). Both analyses showed significant effects from nuclear recoil of Ar isotopes and both have been reduced as "recoil model ages" (Fleck et al., 2014). The ages place eruption of the Broadwell Mesa basalts in the uppermost part of the Gilbert Reversed Polarity Chron (Ogg, 2012). Note that an age of 5.42±0.035 Ma for the Broadwell Mesa basalt was reported by Buesch and Phelps (2016). This value was relative to a previously assessed age of 28.02 Ma for the Fish Canyon sanidine.

Paleomagnetic Direction and Amount of Rotation

Our results show that the Broadwell Mesa basalt is reversely magnetized (fig. 2), consistent with its age within the Gilbert Reversed Polarity Chron and its expression as a local low in aeromagnetic data.

The spherical medians of the northern and (tilt corrected) southern outcrops are (168.5°, -36.7°)±1.6 and (164.1°, -38.8°)±2.7, respectively. The confidence intervals of the two directions show that the remanent magnetic directions of the northern and southern flows are within about 2 standard deviations of each other, and therefore cannot be distinguished using the available data (fig 3).

The amount of rotation was determined by the median difference between all combinations of the bootstrap samples of the northern and southern basalt flows. The median amount of rotation (positive numbers indicate clockwise rotation) relative to the southern outcrop, 4.7° ± [3.6°, 6.5°] (the 68th quantile) and ± [-3.5, 11.0] (for the 95th quantile, the negative value indicates counterclockwise rotation). Note that these directions differ from Buesch and Phelps (2016) due to a re-assessment of the tilt correction. Thus at the 95% confidence level our measurements include the possibility of zero rotation, indicating that the measured rotation between the northern and southern outcrops is not significant. From this we conclude that motion along the Broadwell Mesa fault has not rotated the adjacent blocks relative to one another since 5.46 million years ago.

Any use of trade, firm, or product names is for descriptive purposes only and does not imply endorsement by the U. S. Government.

References

Brady III, R.H., 1992, The Eastern California Shear zone in the northern Bristol Mountains, southeastern California: *in* Richard, S.M., ed., Deformation associated with the Neogene Eastern California Shear Zone, southwestern Arizona and southeastern California: Redlands, CA., San Bernardino County Museum Special Publication, p. 6-10.

Buesch, D., and Phelps, G., 2016, Architecture, geochemistry, and paleomagnetic directions of the 5.42 Ma Broadwell Mesa basalt volcanic field, Bristol Mountains, California: *in* R. E. Reynolds, *ed*. Going Loco – Investigations along the Lower Colorado River, 2016 Desert Symposium Field Guide and Proceedings April 2016.

Buesch, D., 2017, Geochemical variations during development of the 5.4 Ma Broadwell Mesa basalt volcanic field, California: (this volume)

Chernick, M.R., 2008, Bootstrap Methods: A Guide for Practitioners and Researchers (2nd ed): Wiley-Interscience, Hoboken, N.J., 400 pp.

Dibblee, T.W., Jr., 1967, Geologic map of the Broadwell Lake quadrangle, San Bernardino County, California: U.S. Geological Survey Miscallaneous Geologic Investigations Map I–478, scale 1:62,500.

Fisher, N.I., Lewis, T., and Embleton, B.J.J., 1987, Statistical Analysis of Spherical Data: Cambridge University Press, Great Britain, 329 pp.

Fleck, R.J., Hagstrum, J.T., Calvert, A.T., and Evarts, R.C., 2014, $^{40}Ar/^{39}Ar$ geochronology, paleomagnetism, and evolution of the Boring volcanic field, Oregon and Washington, USA: Geosphere, v. 10, no. 6, p. 1283-1314, doi:10.1130/GES00985.1.

Gardner, D.L., 1940, Geology of the Newberry and Ord Mountains, San Bernardino County, California, California Journal of Mines and Geology, v. 36, no. 3, p. 257–292.

Hagstrum, J.T., Fleck, R.J., Evarts, R.C., and Calvert, A.T., 2016, Paleomagnetism and $^{40}Ar/^{39}Ar$ geochronology of the Plio-Pleistocene Boring Volcanic Field: Implications for the geomagnetic polarity time scale and paleosecular variation: Physics of the Earth and Planetary Interiors, v.262, p.101-115, http://dx.doi.org/10.1016/j.pepi.2016.07.008.

Hounslow, M.W., 2011. Palaeomag-Tools v. 4.2, program for analysis of 2-D and 3-D directional data. Available from: http://www.lancaster.ac.uk/people/hounslow/resources/software/pmagtool.htm

Kupfer, D.H., and Bassett, A.M., 1962, Geologic reconnaissance map of part of the southeastern Mojave Desert, California: U.S. Geological Survey Miscellaneous Field Investigations MF–205, scale 1:125,000.

Langenheim, V.E., and Jachens, R.C., 2014, Aeromagnetic data, processing, and maps of Fort Irwin and vicinity, California, chap. I of Buesch, D.C., ed., Geology and geophysics applied to groundwater hydrology at Fort Irwin, California: U.S. Geological Survey Open-File Report 2013–1024, 18 p. http://dx.doi.org/10.3133/ofr20131024I.

Lowrie, W., 1997, Fundamentals of Geophysics: Cambridge University Press, Cambridge, U.K., 354 pp.

McDougall, I., and Harrison, T.M., 1999, Geochronology and Thermochronology by the $^{40}Ar/^{39}Ar$ Method, 2nd edition, Oxford University Press, New York, USA, 269 p.

Ogg, J.G., 2012, Geomagnetic polarity time scale, in Gradstein, F.M., et al., eds., The Geologic Time Scale 2012: Oxford, Elsevier, p. 85–113.

Phelps, G.A., Bedford, D.R., Lidke, D.J., Miller, D.M., and Schmidt, K.M., 2012, Preliminary surficial geologic map of the Newberry Springs 30' x 60' quadrangle, California: U.S. Geological Survey Open-File Report 2011–1044, pamphlet 68 p., 1 sheet, scale 1:100,000. (Available at http://pubs.usgs.gov/of/2011/1044/.)

R Core Team, 2015, R: A language and environment for statistical computing: R Foundation for Statistical Computing, Vienna, Austria, https://www.R-project.org/.

Tauxe, L., Kylstra, N., and Constable, C., 1991, Bootstrap Statistics for Paleomagnetic Data: Journal of Geophysical Research, v. 96, no. B7, p. 11,723-11,740.

Geochemical variations during development of the 5.46 Ma Broadwell Mesa basaltic volcanic field, California

David C. Buesch
USGS Menlo Park Office, dbuesch@usgs.gov

ABSTRACT—The 5.46±0.04 Ma Broadwell Mesa basalt and associated basaltic volcanic field in the western Bristol Mountains, California, formed a ~6 km2 volcanic flow field with architecture including numerous lava flows, a ~1.1 km2 lava lake, and a ~0.17 km2 cinder cone. The local number of lava flows varies from one along the margins of the field to as many as 18 that are stacked vertically, onlapped by younger flows, or are laterally adjacent to each other. Geochemical plots of 40 hand samples indicate that all lava flows are basalt and that the field is slightly compositionally zoned. Typically, there is a progressive change in composition in sequentially overlying lava flows, although in some flow sequences, the overlying flow has an "across trend" step in composition, and a few have an "against trend" step in composition. The progressive compositional change indicates that the magmatic composition evolved during the history of the field, and the "across trend" and minor "against trend" steps probably represent periods of crystal fractionation or reinjection of magma during hiatuses in eruptions. The lack of clastic sedimentary rocks or even aeolianite interstratified with the lava flows probably indicates that the Broadwell Mesa volcanic field was short-lived.

Introduction

The 6 km^2 Broadwell Mesa volcanic field, located in the western Bristol Mountains, California (Figure 1), consists of basalt exposed in broad areas covered by one to as many as 18 locally exposed lava flows, a lava lake, and a cinder cone. The Broadwell Mesa basalt has a K-Ar age of 5.28±0.13 Ma (Brady, 1992); however more recently, a whole-rock 5.46±0.04 Ma age by the Ar^{40}/Ar^{39} technique has been obtained on one of the youngest basalt flows in the central part of the field (Phelps and

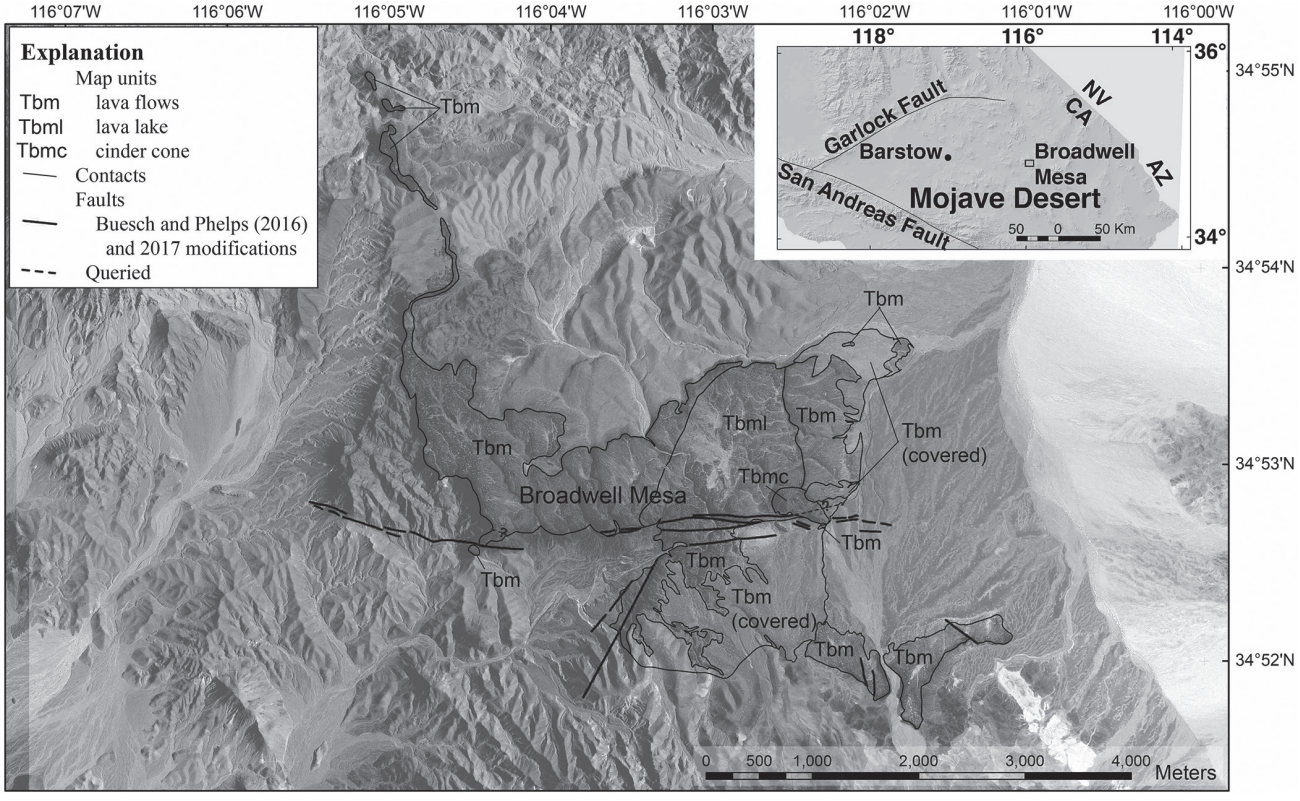

Figure 1. Location of, and volcano morphologic areas in, the Broadwell Mesa volcanic field.

Table 1. Sample identification and locations.

Location	UTMe	UTMn	Area	Sample[1]	Position	Description
1077	588337	3858724	SEsf	BM-1077A	core	Same lava flow; Pmag samples
1077	588337	3858724	SEsf	BM-1077B	core	Same lava flow; Pmag samples
1077	588337	3858724	SEsf	BM-1077C	core	Same lava flow; Pmag samples
1077	588337	3858724	SEsf	BM-1077D	core	Same lava flow; Pmag samples
1350	586637	3860258	MCnf	BM-1350-1B	core	Same series; Pmag samples
1350	586637	3860258	MCnf	BM-1350-2A	core	Same series; Pmag samples
1350	586637	3860258	MCnf	BM-1350-3A	core	Same series; Pmag samples
1350	586637	3860258	MCnf	BM-1350-4B	core	Same series; Pmag samples
1350	586637	3860258	MCnf	BM-1350-5A	core	Same series; Pmag samples
1162	586589	3860282	MCnf	BM1162-LF3	core	
1163	586585	3860346	MCnf	BM1163-LF4a	core	
1165	586583	3860360	MCnf	BM1165-LF3A	core	Same 1165 section
1165	586583	3860360	MCnf	BM1165-LF3B	near top	Same 1165 section
1165	586583	3860360	MCnf	BM1165-LF4	core	Same 1165 section
1171	588337	3858758	SEsf	BM1171a	block	Talus block from flow 2232-LFJ?
1177	588280	3858344	SEsf	BM1177	core	Only 1 flow
1186	587853	3860040	SEifz	BM1186a	block, near top	Possibly in fault slice
1220	587490	3860171	CCnf	BM1220	core	LF in cindercone crater
1221	587025	3860057	LLifz	BM1221	block	Mantling hillslope near fault
2134	586363	3859759	MCifz	BM2134-F1	core	Same section as 2175-F4
2140	586645	3860249	MCnf	BM2140-F3a	core	LF3a in 1350 5-flow series
2151	586794	3860007	MCifz	BM2151-LF3a	core	Same 2151-2157 section
2153	586805	3859980	MCifz	BM2153-LF4a	core	Same 2151-2157 section
2157	586810	3859947	MCifz	BM2157-LF7a	lower core	Same 2151-2157 section
2161	586714	3859866	MCifz	BM2161-LF1	upper core	Same 2166 section
2161	586714	3859866	MCifz	BM2161-LF6	core	Same 2166 section
2175	586388	3859745	MCifz	BM2175-LF4	upper core	Same section as 2134-F1
2180	586871	3860415	LLnf	BM2180	upper core	Only 1 flow
2182	586412	3860640	LLnf	BM2182a	upper core	Only 1 flow
2231	588314	3858736	SEsf	BM2231-LFM	core	Same 2231-2235 section
2232	588320	3858739	SEsf	BM2232-LFJ	upper core	Same 2231-2235 section
2233	588335	3858753	SEsf	BM2233-LFL	core	Same 2231-2235 section
2234	588327	3858731	SEsf	BM2234-LFF	core	Flow with 1077 4-pmag samples
2235	588330	3858734	SEsf	BM2235-LFK	upper core	Same 2231-2235 section
2246	584470	3859768	SWsf	BM2246a	lower core	Only 1 flow; samples ~1 m apart
2246	584470	3859768	SWsf	BM2246b	lower core	Only 1 flow; samples ~1 m apart
2254	584607	3859898	SWsf	BM2254	core	Only 1 flow
2257	584706	3859946	SWnf	BM2257-LF1	lower core	Only 2 flows
2258	584600	3860110	SWnf	BM2258-LF3	upper core	Same 2259-2258 section
2259	584595	3860103	SWnf	BM2259-LF1a	core	Same 2259-2258 section

[1] Samples were typically in "A" and "B" (or "a" and "b" pairs). Sample BM2140-LF3a is a separate flow between LF3 and LF4.

others, this volume). The Broadwell Mesa basalt was emplaced unconformably (locally with angularity) on folded and faulted Miocene volcanic and sedimentary rocks (Dibblee, 1967; Brady, 1992, 1993; Phelps and others, 2012; Buesch and Phelps, 2016). Understanding the eruption history and development of the volcanic field is based on the physical stratigraphy and geochemical variations described in this paper. In a broader sense, the stratigraphy and architecture of the field is being studied to provide insights into the (1) geography of the area during the time the field developed, (2) magma petrogenesis of the field, and (3) history of the east-striking Broadwell Mesa fault in the eastern part of the Eastern California Shear Zone (Dokka and Travis, 1990),

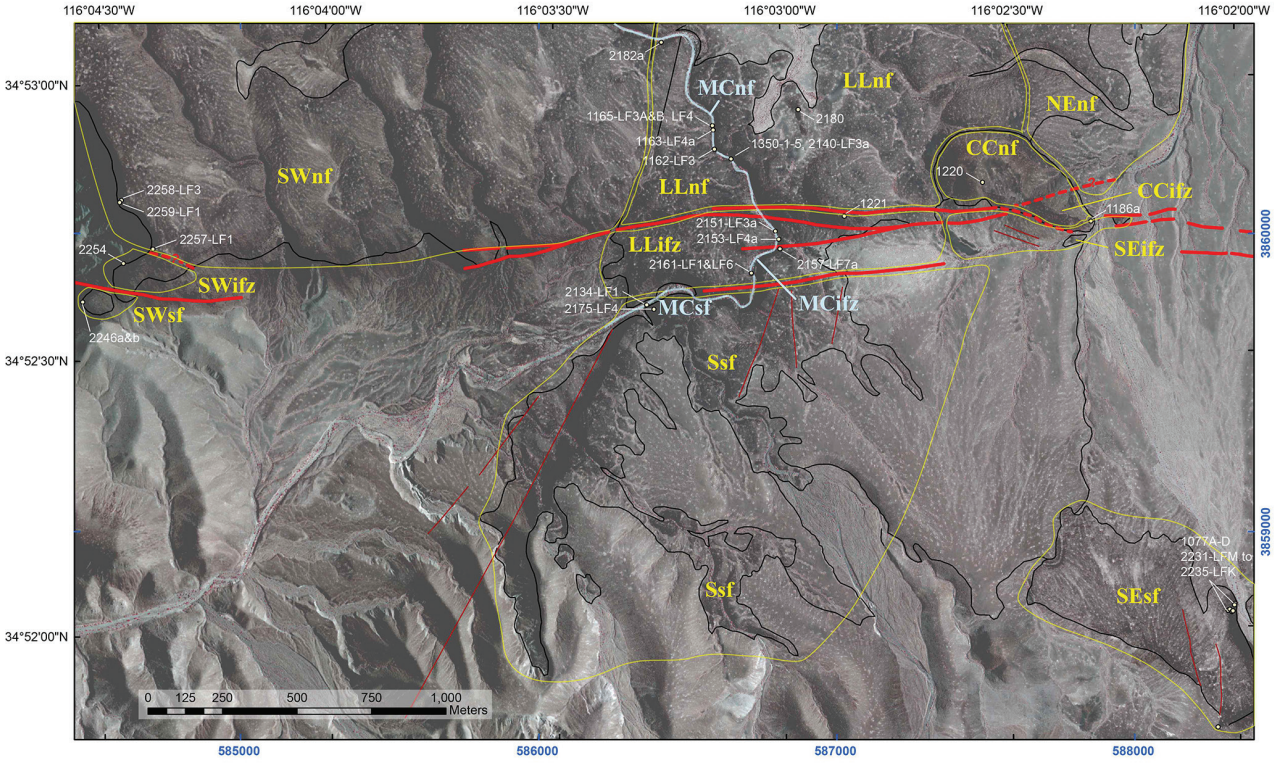

Figure 2. Map of geographic areas and sample locations. Faults and contacts are from Figure 1, but small faults not aligned with the Broadwell Mesa faults have thinner lines. List of symbols: Yellow lines – boundaries of areas; Cyan line – trace of exposures in the Main Canyon area; CC – cinder cone; LL – lava lake; MC – main canyon; NE – northeast; NW – northwest; S – south; SE – southeast; SW - southwest; nf – north of fault; ifz – in fault zone; sf – south of fault.

which is more broadly defined as the Mojave strike-slip province (Miller and Yount, 2002).

Physical stratigraphy of the field

As a field-based and conceptual framework for working in the Broadwell Mesa volcanic field, a descriptive hierarchical system of lava flow features and morphology has been applied to scales from an individual flow to the full field. The hierarchy is helpful for providing qualitative estimates of time and duration from the development of lava flow features to the complete history of the entire volcanic field.

1. Flow buds and lobes—Buds and lobes are protrusions of lava along the edges of a flow (buds are smaller than lobes), and are small compared to their associated flow.
2. Simple flow—A simple flow has well developed upper and lower cooling features (such as vesiculated zones or typically fine-grained layers) that parallel the upper and lower surfaces of the flow, and these features differ from a possibly slightly coarser-grained and differently vesiculated texture in the core.
3. Compound flow—A compound flow has well developed upper and lower cooling features (such as fine-grained layers and vesiculated zones) compared to a typically coarser-grained and differently vesiculated core; however, there are one or more partially developed selvages of vesiculated or finer-grained rock compared to adjacent rocks. These selvages are interpreted as being formed during pulses of lava that (A) overwhelms and engulfs a partially cooled outer surface, or (B) congealed along slightly cooled surfaces on the margins of lava tube walls. It is possible that along the trace length of a flow, or across the width of a flow, it can transform from a simple flow to a compound flow because the features that are used to identify each flow type were developed locally.
4. Flow unit—A flow unit (or sequence) consists of several stacked, onlapped, or laterally adjacent flows, where the boundaries between different lobes and flows have poorly to moderately developed upper, lower, or lateral cooling structures.
5. Eruptive episode—An episode consists of lava flows or sequences during an effectively continuous eruption, and is followed by a hiatus in the eruption that could have lasted months, years, or decades. Episodes might be indicated by the occurrence of clastic or aeolianite sediments deposited between lava flows.
6. Eruptive cycle—An eruptive cycle can consist of one or more episodes, but the cycle represents the duration of activity of the volcano or volcanic field.

Locations of samples

Some samples were collected from exposures of specific lava flows or features, such as tumuli, and these samples

are identified with the field location number (i.e., BM1165). However, many samples are from lava flows from local exposures or measured sections, and these samples have additional identifiers. For samples from a measured section, lava flows are identified as "Local Flow" and the stratigraphic position (number) within the section (for example, LF1 is the lowest exposed lava flow, and LF6 is the 6th flow in the vertical sequence). In sections where a flow was traced into the section from one location to another, the lowest local flow could inherit the previous identifier (such as LF3). This "LF nomenclature" is only for uniquely identifying the relative positioning of local flows, and is not an indicator of the stratigraphic position within the full volcanic field. All rock samples were located with a handheld GPS (units differed based on collector) and coordinates are listed in Table 1.

Within the field there are three main morphological areas—the cinder cone, the lava lake, and the outflow area (that is, outside the lava lake)—and the field can be divided into 14 geographic areas. In addition to the morphologic areas, the areas are divided into (1) areas north, within, and south of the Broadwell Mesa fault zone, and (2) geographic areas (northwest, southeast, etc.), or along the main canyon that transects the field (Figure 2).

Stratigraphy and features of lava flows

All lava flows are porphyritic olivine basalt; however, the amount, size, and minerals as phenocrysts (crystals 1-5 mm long) and mini-phenocrysts (crystals 0.25-1 mm) can vary from flow to flow, and these crystals are in a seriate groundmass that consists of microlites (crystals less than 0.25 mm) and parts of the groundmass that are aphanitic when using a 10x hand lens. Vitreous green olivine formed phenocrysts and mini-phenocrysts (3-7 percent and 0-7 percent, respectively). Translucent to slightly white plagioclase formed phenocrysts and mini-phenocrysts in some flows (1-3 percent and 7-20 percent, respectively), but others have neither. Locally, vitreous black grains of pyroxene form mini-phenocrysts. Olivine, plagioclase, and pyroxene form the microlite assemblage of the main constituents in the groundmass and typically comprise 8 to 40 percent of the rock. Variations in the amount, size, and phenocryst and mini-phenocryst phases occur in different flows. For example, in measured section 1350 where samples were collected for paleomagnetic properties and geochronology, the abundance and size of olivine phenocrysts increase up section, olivine mini-phenocrysts decrease up section, plagioclase phenocrysts decrease up section, and plagioclase mini-phenocrysts decrease slightly up section (with no plagioclase mini-phenocrysts in local flow 3). Some flows are texturally zoned with fewer and smaller phenocrysts and mini-phenocrysts near the top and bottom of a flow compared to the core (Figure 3). This textural zoning results either from cooling of the lava flow, or arrival of slightly different compositions of magma during the emplacement. The arrival of lava at a specific location can probably span a period of time; for example, the outer part of a lava flow cools and congeals while the core continues to flow in the center. If the supply of lava to the core continues, the flow might "inflate" (that is, get thicker), or if the flow of lava through the core wanes and the lava flows away, a lava tube forms.

All lava flows, regardless of thickness and length, typically have fine-grained margins with small vesicles (both resulting from rapid cooling), and these margins differ from coarser-grained cores that can have fewer or more (but possibly larger) vesicles. Typically, vesicles in lava flows occur in three size ranges. All flows have mini- to micro-vesicles (less than 2 mm), most flows have small

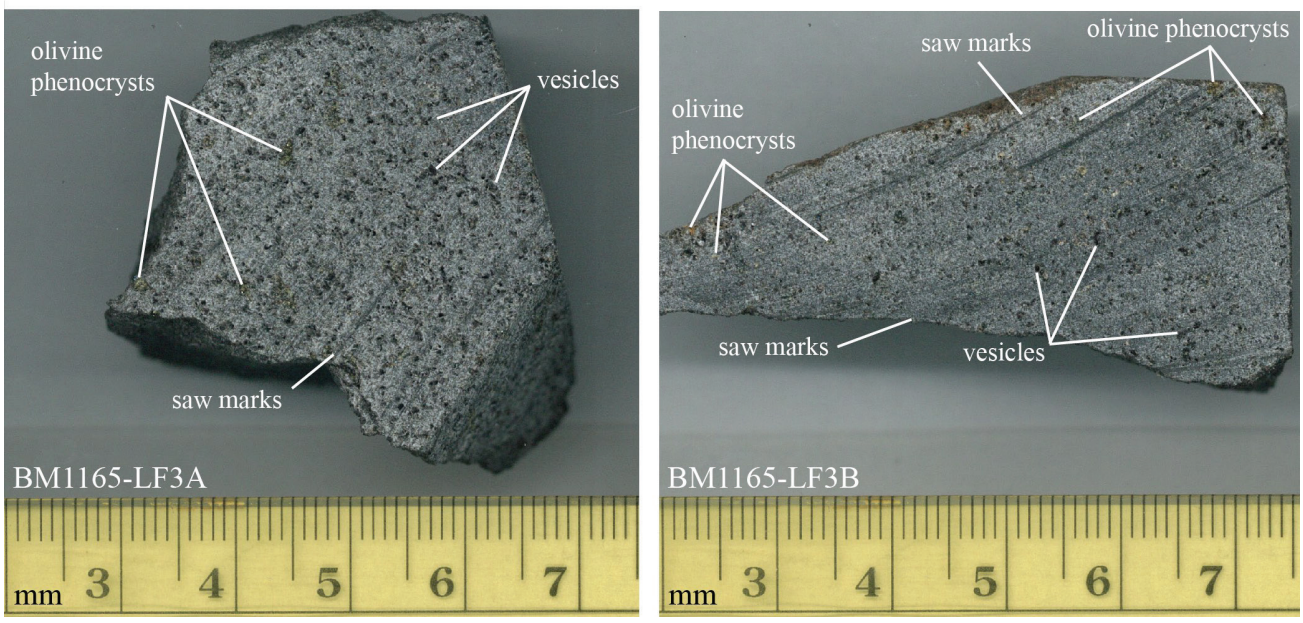

Figure 3. Scanned images of cut faces on basalt samples BM1165-LF3A (core), and BM1165-LF3B (near top). Olivine phenocrysts are medium dark green. Vesicles are dark gray to black

vesicles (2-10 mm), and some flows have large vesicles (10-30 mm). Many lava flows have planar to curviplanar flow tops and edges that are indicative of fluid flows. Some lava flows have "ropy" structures and very fine-grained surfaces that are typical of pahoehoe lava flows, although these features are easily eroded after the surface has been exposed. A few lava flows have small amounts of clinker (reddish brown, typically slightly scoriaceous, basaltic clasts) along the top or at the base. Only one lava flow has a moderately well developed lava tube.

Stratigraphy and features in lava flows outside the lava lake

In the main part of the field (that is, not in the lava lake), the simple and compound lava flows are mostly tabular, 0.3-5 m thick, and traceable for 10-1000 m. One lava flow along the northwestern edge of the field is at least 4.5 km long. Locally there are areas with complicated multiple onlapping lobes and flows. In most areas of the field, the base of the basalt section is not exposed. Along the margins of the field, typically there is only one, 0.5-2 m thick, lava flow that represents the lateral onlapping onto pre-basalt deposits. Missing from the stratigraphic sequence of lava flows are any clastic or aeolianite depsoits, even along the margins of the field where incursions of sediment would have been possible.

Several details of the lava flows are notable. (1) Some flows are broadly arched, as indicated by the onlapping relations of younger flows. (2) Some flows have tumuli, a domed part of the upper surface of a lava flow that can be several meters across and several meters high, and typically, the crests of the tumuli have one or more fractures or crevasses. Locally, lava flows that moved across crevasses in the tops of subjacent lava flows resulted in the filling of the crevasses to form what initially appears to be a pseudo-dike that transects the lower lava flow. (3) There is one well-formed, approximately 1.5 m tall, lava tube that occurs in local flow LFC in the southeastern area (area SEsf, see Figure 6). (4) In many lava flows, there are near-vertical, typically 2-6 cm diameter, pipes of coarsely vesiculated lava (with 10-25 percent, 2-15 mm vesicles), and some flows have nearly horizontal, 1-2 cm thick, vesicle "sills" that intersect pipes to form trellis-like structures. (5) Typically, vesicles are less than 3 mm in diameter and spherical to ellipsoidal; however, many lava flows have large-diameter (10-15 mm) and vertically elongate vesicles. These elongated vesicles, some of which formed near the cooling basal contact, buoyantly rose through the lava and were bent in the direction of flow.

Stratigraphy and features of the lava lake

The lava lake north of the Broadwell Mesa fault has an area of ~1.1 km^2 and is locally bounded by marginal levees. Along the eastern margin of the lake the lava flows are thicker in the lake area and thinner where they spilled over the edge of the lake and flowed away. In the area of the lava lake, the simple and compound lava flows are mostly tabular, 1-15 m thick, and traceable for 10-400 m along the main canyon, and in other parts of the lava lake one flow along the eastern side might be traceable for as much as 800 m (based on aerial photographic interpretations). Locally, there are smaller and thinner complicated multiple and onlapping lobes and flows. In the main canyon area of the lava lake at location 1350 (north of the fault zone), the measured section of 6 lava flows is 26 m thick (base of section not exposed). In addition to having many thick lava flows, many of these flows contain (1) near-vertical vesiculated pipes, (2) vesicle "sills" of coarsely vesiculated lava, and (3) locally these pipes and sills combine to form trellis-like structures.

In and south of the Broadwell Mesa fault zone, the lava lake is difficult to identify and more work is needed. Lava flows exposed along the Main Canyon area in and south of the fault have numerous thick and laterally continuous flows that are similar to the flows in the lava lake north of the fault, and these flows might be in the southern part of lava lake. At locations 2134 and 2175 (a single lava flow sequence south of the fault), a section of 5 lava flows is ~24 m thick (base of section not exposed).

As is true for most areas in the field, the base of the basalt section in the lava lake is not exposed, so the complete thickness of the section remains undetermined. One area where the base of the lava lake section is exposed is where the uppermost flows of the lake onlap the northeastern sector of the cinder cone.

Stratigraphy and features of the cinder cone

The cinder cone is the only clearly identifiable vent area. The cinder cone is elongate parallel to the Broadwell Mesa fault (it is 460 m long, 360 m wide, and ~30 m high), and in detail consists of two adjacent cones. Most of the cinder cone material consists of scoria lapilli that vary from black or dark gray to red, and locally there are beds of yellow to brownish yellow sideromelane clasts. Fusiform or spindle-shaped bombs occur locally, and a few cored bombs up to 1.7 m in diameter were formed as fragments of agglutinate with fragment-centered radiating cooling fractures. Locally, along the outer slopes and within the crater area there are thin basalt flows. Sample BM1220 is from a thin lava flow in the northern crater.

Stratigraphic positions of important samples

The locations, local lava flow identifiers, and the stratigraphic positions of samples in the lava flows are listed in Table 1 and displayed in Figure 2. Below are listed a few samples for which the stratigraphic relations within a section or the position of the sample in a flow are particularly important to understanding the physical and geochemical stratigraphic data.

1165-LF3A, LF3B, LF4 – At this location are three locally exposed lava flows with LF3 overlain by LF4. Sample LF3A is from the core, and LF3B is from near the top of the flow (Figure 3).

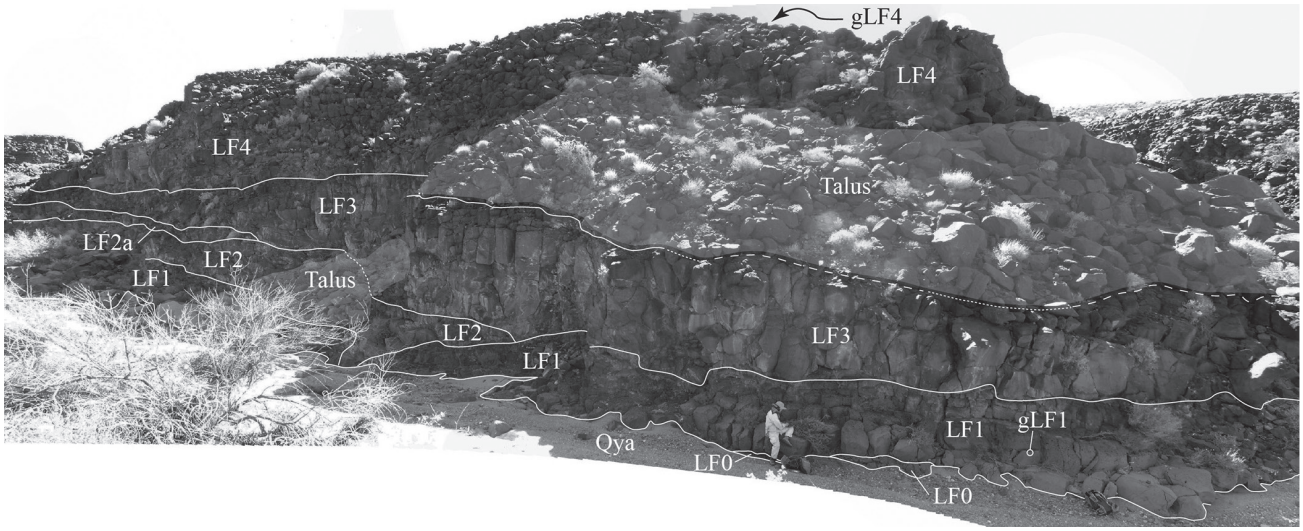

Figure 4. Panorama photograph of local lava flows LF0 to LF4 in the southwestern part the Main Canyon located south of the Broadwell Mesa fault (area MCsf). From the base of LF1 to top of LF4 is 24 m. gLF1 and gLF4 are locations of wavelength dispersive X-ray fluorescence (wdXRF) samples and sample sites are 2134-LF1 and 2175-LF4.

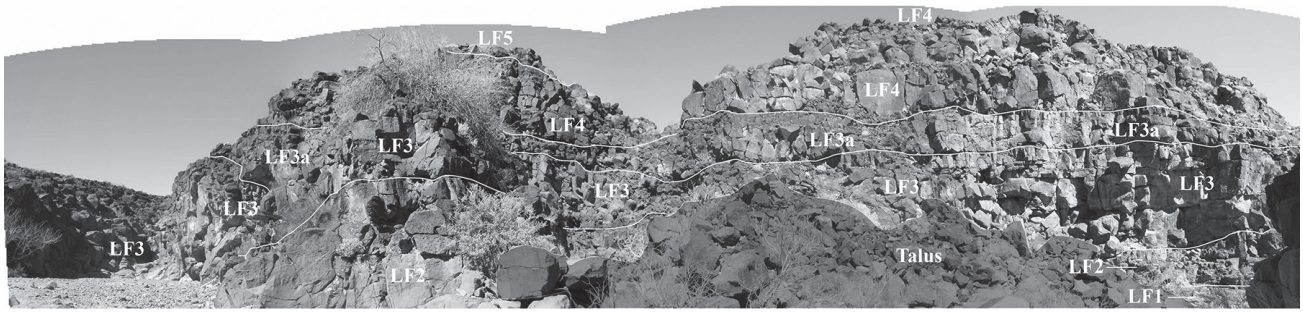

Figure 5. Panorama photograph of local lava flows LF1 to LF5 in the Main Canyon located north of the Broadwell Mesa fault at sample site 1350-1 to 1350-5 (area MCnf). From the near the top of LF1 to top of LF4 is 26 m. From the top of the water fall on the left (labeled LF3) to LF3 at right side of image is ~60 m.

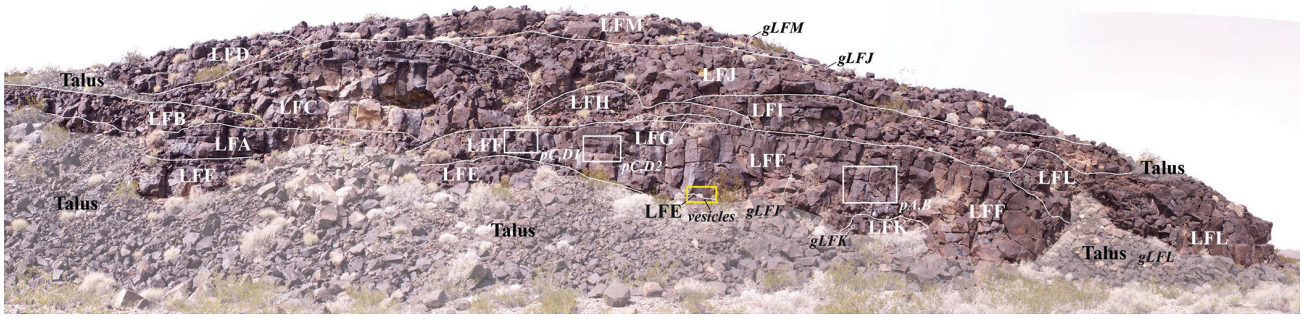

Figure 6. Panorama photograph of local lava flows LFA to LFM at GPS sites 2231 to 2235 in the southeastern part of the field (area SEsf). From the near the top of LFK to top of LFM is 17 m. gLFK, gLFF gLFL, gLFJ, and gLFM are wdXRF sample sites. Paleomagnetism samples 1077A&B were from the area labeled pA,B in LFF. Samples 1077C&D were from either area labeled pC,D1 or area pC,D2, and both areas are in LFF. Flow deformed vesicles at base of LFF in yellow box labeled "vesicles". Local flow LFC has a lava tube that is approximately 1.5 m tall.

1220 – Sample 1220 is from a small lava flow located in the cinder cone crater.

2134-LF1 to 2175-LF4 – At these locations are five locally exposed lava flows (Figure 4).

1350-1 to -3, 2140-LF3a, 1350-4 to 5 – At this location are six locally exposed lava flows with samples for geochemical, paleomagnetic, and geochronologic data (Figure 5).

2235-LFK to 2231-LFM and 1077A-D – At these locations are 13 local lava flows with samples for geochemical and paleomagnetic data (Figure 6). Samples LFK to LFM are precisely located (each has a GPS location). The four samples (1077A-D) were collected for paleomagnetic analysis prior to delineation of the detailed lava flow sequence, and the lava flow was identified as LFF. Samples 1077A-D have a single GPS location, and detailed locations were documented with sketch maps and photographs. Samples 1077A and B were collected within a 2x3 m area in one part of the flow, and 1077C and D were collected within a 1.5x2 m area in another part of the flow. The two possible

Table 2. Selected geochemistry of samples.
[Major elements in wt %; Trace elements in ppm; Al/Ti ratio from ppm]

Field No.	SiO2	TiO2	Al2O3	MgO	Na2O	K2O	Ba	Co	Cr	Nb	Ni	Zr	Al/Ti
2013 samples													
1077A	49.4	2.94	14.8	6.31	3.49	1.29	331	40.1	260	42	112	271	5.05
1077B	49.3	2.85	14.8	7.00	3.41	1.24	407	40.1	250	41	121	263	5.20
1077C	49.7	2.96	14.6	6.76	3.45	1.27	359	40.9	230	43	108	274	4.95
1077D	49.7	2.81	14.7	7.16	3.38	1.22	296	41.5	260	41	116	263	5.21
1350-1B	50.2	2.74	14.8	6.39	3.44	1.07	297	39.0	220	33	100	235	5.40
1350-2A	49.9	2.52	14.8	7.54	3.35	0.97	236	44.6	280	30	128	213	5.85
1350-3A	50.4	2.47	15.0	7.08	3.45	0.91	211	43.3	260	28	117	207	6.09
1350-4B	50.5	2.21	14.3	8.26	3.24	0.83	241	49.5	250	20	173	168	6.49
1350-5A	50.4	2.24	14.8	7.76	3.29	0.79	224	48.4	230	21	159	171	6.62
2014-2015 samples													
1162-LF3	50.3	2.53	15.1	6.80	3.36	0.92	240	40.7	259	25	113	191	5.96
1163-LF4a	51.0	2.31	14.6	7.56	3.32	0.80	232	44.3	228	19	156	166	6.32
1165-LF3A	50.7	2.37	14.7	7.56	3.31	0.84	238	44.5	242	18	153	156	6.21
1165-LF3B	50.7	2.47	14.6	6.89	3.37	0.88	252	41.4	216	19	124	169	5.90
1165-LF4	51.1	2.26	14.8	7.30	3.38	0.80	237	42.4	241	18	141	160	6.55
1171a	50.3	2.47	15.0	7.02	3.37	0.84	478	41.2	244	22	118	177	6.09
1177	50.1	2.48	15.1	7.18	3.24	0.73	229	43.6	238	21	125	176	6.10
1186a	49.5	2.85	15.5	4.87	3.58	1.18	269	32.7	146	31	51	204	5.44
1220	51.1	2.86	15.4	5.56	3.62	1.14	393	33.8	162	33	65	225	5.38
1221	50.5	2.39	14.8	6.88	3.38	0.86	271	42.2	229	19	123	163	6.18
2134-F1	49.0	2.90	14.7	7.38	3.29	1.23	329	40.2	289	37	134	250	5.07
2140-LF3a	50.2	2.46	14.8	7.38	3.33	0.88	220	40.6	248	23	122	179	6.03
2151-LF3a	51.0	3.07	15.1	4.89	3.59	1.22	281	34.1	155	32	63	246	4.92
2153-LF4a	50.4	2.54	14.8	7.19	3.30	0.84	230	42.0	266	23	125	179	5.84
2157-LF7a	51.2	2.46	14.7	6.57	3.46	0.83	273	39.5	208	20	108	177	5.98
2161-LF1	50.3	2.68	15.2	6.50	3.39	1.03	251	38.1	236	27	94	205	5.65
2161-LF6	50.2	2.49	14.9	7.43	3.33	0.79	256	42.3	267	23	127	180	5.96
2175-LF4	50.2	2.64	15.1	6.79	3.38	0.95	247	39.5	260	26	104	200	5.73
2180	50.9	2.36	15.5	6.62	3.40	0.80	253	40.6	240	19	116	163	6.58
2182a	50.0	2.67	15.2	6.85	3.36	1.01	249	38.7	244	27	100	207	5.70
2231-LFM	50.2	2.40	14.7	7.75	3.31	0.77	213	43.7	277	20	144	168	6.12
2232-LFJ	50.4	2.50	15.0	6.91	3.34	0.86	220	40.3	238	23	109	190	6.00
2233-LFL	49.3	2.90	14.9	7.44	3.37	1.18	290	39.1	276	35	115	241	5.14
2234-LFF	49.2	2.87	14.7	7.54	3.37	1.22	334	38.7	275	35	118	237	5.14
2235-LFK	50.0	2.92	14.8	6.64	3.40	1.30	334	37.2	261	36	117	243	5.05
2246a	49.7	2.92	15.0	6.67	3.43	1.19	295	36.4	246	34	104	232	5.14
2246b	49.6	2.99	14.9	6.79	3.41	1.19	292	37.6	246	34	103	234	4.98
2254	50.0	2.72	14.8	7.15	3.31	0.96	250	39.6	260	27	108	202	5.42
2257-LF1	49.8	2.76	14.9	7.23	3.35	1.09	294	38.7	271	32	111	223	5.40
2258-LF3	49.1	2.62	15.1	7.17	3.30	0.96	249	39.1	266	28	114	199	5.75
2259-LF1a	48.8	2.91	14.6	7.68	3.37	1.23	310	39.6	279	36	128	241	5.02

detailed positions for C and D are based on the perspective of the original photographs and sketches.

2257 to 2259 – Samples 2259-LF1 and 2258-LF3 are part of a 9 m thick sequence of 3 lava flows. 2257-LF1 is the lower of 2 flows located ~200 m from the 2259-2258 section. It is possible that 2257-LF1 correlates to LF2 in the section 2259-2258.

Geochemistry

Forty samples were collected from lava flows in most areas of the volcanic field to evaluate local, vertical, and lateral geochemical variations. Geochemical analyses are from two submissions to the USGS contract laboratory: (1) 9 samples from field locations 1077 and 1350 that were collected in 2013, and (2) 31 samples from the rest of the field that were collected in 2014 and 2015. Eleven major element oxides were analyzed with wavelength dispersive X-ray Fluorescence (wdXRF) and 55 trace elements were analyzed with ICPAES-MS. Although there is a full set of data for these samples, only the major oxides, trace elements, or element ratios described in this paper are listed in Table 2. Major element oxides were summed and normalized for use in TAS and Harker diagrams. Major elements measured with ICPAES-MS were not normalized because the analyses in the run containing 1077 and 1350 did not contain Si. Trace elements measured with ICPAES-MS were plotted as reported, or were used as ratios.

All values from the 2013 and 2014-2015 analyses were within the quality assurance and quality control (QA-QC) acceptable limits for each run. The 2013 and 2014-2015 runs included analyses of different reference materials. For the 2014-2015 analyses, the reference materials were two basalts and one andesite, so they were very close to the compositions in Broadwell Mesa samples. The differences between the reference materials analyzed during the run compared to the published values (the "Compared to Defined") are

Table 3. Comparison of reference materials during analytical runs to certified values. [Bold type are values within the range of the Broadwell Mesa samples (min, max, average) and used to calculate the "Compared %" and "Error of Average. Underlined values highlighted by the laboratory and recommended using "Compare to Mean".]

	wdXRF	wdXRF	wdXRF	wdXRF	wdXRF	wdXRF	ICPAES	ICPAES	ICPAES	ICPAES	ICPAES	ICPAES	ICPAES
2014-2015 samples	SiO_2	TiO_2	$Al2O_3$	MgO	Na_2O	K_2O	Ba	Co	Cr	Nb	Ni	Zr	
Min	48.80	2.26	14.60	4.87	3.24	0.73	213	32.7	146	18	51	156	
Max	51.20	3.07	15.50	7.75	3.62	1.30	478	44.5	289	37	156	250	
Average	50.15	2.64	14.94	6.91	3.38	0.98	274	39.8	242	27	114	199	
Compared %[1]	0.52	1.81	-0.72	1.11	0.00	-0.57	-1.02	0.27	2.10	-10.53	-11.22	-12.77	
Error of the Average[2]	0.26	0.05	-0.11	0.08	0.00	-0.01	-2.81	0.11	5.09	-2.79	-12.79	-25.46	
Reference Material													
BCR-2	54.5	2.34	13.6	3.61	3.16	1.82	670	37.1	20	11	15	164	
Compared to Defined	100.74	103.54	100.74	100.56	**100.00**	101.68	98.10	**100.27**	111.11	100.00	100.00	**87.23**	
Defined Value	54.1	2.26	13.5	3.59	**3.16**	1.79	683	**37**	18	11	15	**188**	
Mean	54.20	2.28	13.47	3.59	3.15	1.80	669.73	38.10	18.39	11.45	16.08	174.50	
AMH-1	60.7	0.87	17.5	3.24	4.16	1.22	319	18.6	42	7	37	130	
Compared to Defined	100.60	102.87	99.83	102.66	98.86	**99.43**	**98.98**	99.57	102.71	84.13	114.34	89.04	
Defined Value	60.337	0.8457	17.53	3.156	4.208	**1.227**	**322.3**	18.68	40.89	8.32	32.36	146	
BHVO-1	50.2	2.85	13.7	7.31	2.24	0.52	135	43.3	287	17	114	148	
Compared to Defined	**100.52**	105.17	**99.28**	**101.11**	99.12	**100.00**	97.12	96.22		**89.47**		82.68	
Compared to Mean		**101.81**							**102.10**		**88.78**	90.02	
Defined Value	**49.94**	2.71	**13.8**	**7.23**	2.26	**0.52**	139	45	--	**19**	--	179	
Mean	49.83	**2.80**	13.66	7.26	2.24	0.53	127.73	45.07	**281.09**	17.91	**128.41**	164.41	

[1] "Compared %" equals the ("Compared to Defined"-100).
[2] The "Error of the Average" equals the "Average" x "Compared % / 100.

Table 3 (cont.). Comparison of reference materials during analytical runs to certified values. [Bold type are values within the range of the Broadwell Mesa samples (min, max, average) and used to calculate the "Compared %" and "Error of Average. Italics values are outside the range of the Broadwell Mesa samples.]

	wdXRF	wdXRF	wdXRF	wdXRF	wdXRF	wdXRF	ICPAES	ICPAES	ICPAES	ICPAES	ICPAES	ICPAES
2013 samples	SiO_2	TiO_2	$Al2O_3$	MgO	Na_2O	K_2O	Ba	Co	Cr	Nb	Ni	Zr
Min	49.30	2.21	14.30	6.31	3.24	0.79	211	39.0	220	20	100	168
Max	50.50	2.96	15.00	8.26	3.49	1.29	407	49.5	280	43	173	274
Average	49.94	2.64	14.73	7.14	3.39	1.07	289	43.0	249	33	126	229
Compared %	1.05	1.52	0.67	-3.40	0.00	1.09	-7.23	0.00	-8.33	7.41	3.28	4.15
Error of the Average	0.52	0.04	0.10	-0.24	0.00	0.01	-20.91	0.00	-20.74	2.46	4.13	9.51
Reference Material												
DGPM-1	*79.6*	*0.56*	9.46	*0.58*	0.1	*2.77*	*1180*	*1.3*	*110*	11	*23*	*427*
Recovery[3]	*0.9975*	*1.0000*	0.9895	*1.0357*	1.1111	*1.0109*	*0.9277*	*0.9559*	*0.9167*	1.1224	*1.5333*	*1.0415*
Compared to Defined	*99.75*	*100.00*	98.95	*103.57*	111.11	***101.09***	***92.77***	*95.59*	***91.67***	112.24	*153.33*	***104.15***
Defined Value	*79.8*	*0.56*	9.56	*0.56*	0.09	***2.74***	***1272***	*1.36*	***120***	9.8	*15*	***410***
GSP-2	*67.3*	*0.67*	15	*0.94*	2.78	*5.47*	*1260*	*7.3*	*20*	29	*29*	*561*
Recovery	*1.0105*	*1.0152*	1.0067	*0.9792*	1.0000	*1.0167*	*0.9403*	*1.0000*	*1.0000*	1.0741	*1.7059*	*1.0200*
Compared to Defined	***101.05***	***101.52***	**100.67**	*97.92*	**100.00**	*101.67*	*94.03*	***100.00***	*100.00*	**107.41**	*170.59*	*102.00*
Defined Value	***66.6***	***0.66***	**14.9**	*0.96*	**2.78**	*5.38*	*1340*	***7.3***	*20*	**27**	*17*	*550*
GSP-QC	*68.4*	*0.67*	14.6	*1*	2.58	*5.2*	*1280*	*7.2*	*20*	28	*20*	*570*
GSP-QC	*68.4*	*0.66*	14.6	*0.99*	2.59	*5.2*	*1260*	*6.4*	*20*	28	*25*	*596*
Recovery	*1.0163*	*0.9925*	1.0139	*0.9660*	1.0299	*1.0058*	*0.9621*	*1.0675*	*0.9050*	1.2174	*1.8000*	*1.1255*
Compared to Defined	*101.63*	*99.25*	101.39	***96.60***	102.99	*100.58*	*96.21*	*106.75*	*90.50*	121.74	*180.00*	*112.55*
Defined Value	*67.3*	*0.67*	14.4	***1.03***	2.51	*5.17*	*1320*	*6.37*	*22.1*	23	*12.5*	*518*
Lab internal (Ni ppm)												
STD-SY-4											*15*	
Recovery											*1.1538*	
Compared to Defined											*115.38*	
Defined Value											*13*	
STD-RTS-3A											*63*	
Recovery											*1.0328*	
Compared to Defined											***103.28***	
Defined Value											***61***	

[3] "Recovery" is reported by the laboratory as equals the measured value divided by the Defined value.

typically 0-2 percent, but some trace elements showed a difference of 10-13 percent (selected data in Table 3). For the 2013 analyses, the reference materials were two dacites and one rhyolite, so only three of the selected major or trace elements were within the range of the Broadwell Mesa basalt compositions. The differences between the reference materials analyzed during the run compared to the published values (the "Compared to Defined") are typically 0-3 percent, but some trace elements showed a difference of 3-8 percent (selected data in Table 3). There are two important relations of these "Compared to Defined" data. (1) The compared data for each element were used to calculate the "Compared %" (which equals the "Compared to Defined"-100). The Compared % was used to determine how much error might be attributed to the average value, or the "Error of the Average" (which equals the "Average" x Compared % / 100). The Compared % indicates that for some elements there are only minor differences (less than a factor of 2) between the 2013 and 2014-2015 data, but for other elements the differences can be as much as a factor of 7. (2) This "calibrated but outside the range of basalt" indicates that the 2013 data are of good quality, but for some comparisons between 2013 and 2014-2015 data, detailed differences should not be pushed too far. Having issued this caution, the data for the 1350-1B to 1350-5A samples are typically well within the range of nearby samples from 2014-2015, and the 1077A-D samples are close, but slightly different than the nearby samples from 2014-2015.

Samples analyzed for geochemistry were chosen because they were representative of the lava flow and consisted of pristine minerals and groundmass. Olivine, plagioclase, and pyroxene were typically vitreous, although some olivine in some lava flows had surfaces or parting planes that had been converted to iddingsite. Typically, samples had less than (to much less than) 1 percent, fine-grained, secondary minerals that coated the walls of vesicles.

TAS and Harker diagrams

On a total alkalis (Na_2O+K_2O wt%) versus silica diagram (TAS), all 40 samples plot well within the upper part of the basalt region (Le Maitre, 1989). Typically, samples with lower SiO_2 have higher total alkalis, and there is a gradational change to samples with higher SiO_2 having lower total alkalis (Figure 7). Two samples outside this general trend include 1220 and 2151-LF3 (a lava flow from the cinder cone crater, and a lava flow low in the sequence in the fault zone, respectively). There is a slight gap in the data in the ranges from 49.9-50.1 wt % SiO_2 and 4.4-4.5 wt % total alkalis; however, this gap does not necessarily indicate there are two distinct compositional populations because for many of the local lava flow sequences there were lava flows that were not sampled. One noteworthy caveat about TAS diagrams is that although the samples used are not obviously altered, Si, Na, and K are all susceptible to an increase or decrease as a result of alteration or secondary mineralization.

Harker diagrams are plots of major element wt % versus SiO_2 wt %, and these diagrams for the Broadwell Mesa basalt have similar trends as the TAS diagram. For example, TiO_2 wt % versus SiO_2 wt % (Figure 8) has similar gradational trends for samples from lower SiO_2 and higher TiO_2 to samples with higher SiO_2 and lower

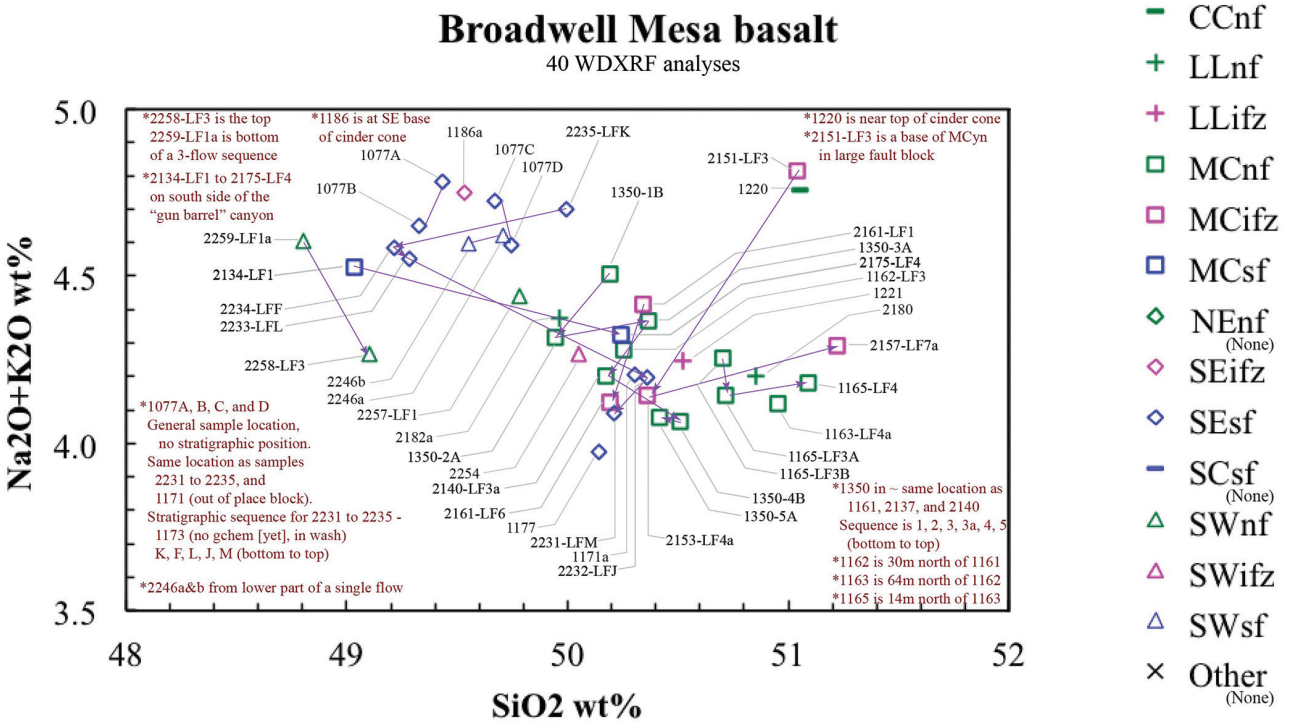

Figure 7. Total alkali (Na_2O+K_2O wt%) versus silica diagram for basalts at Broadwell Mesa. All data within the basalt field from Le Maitre (1989).

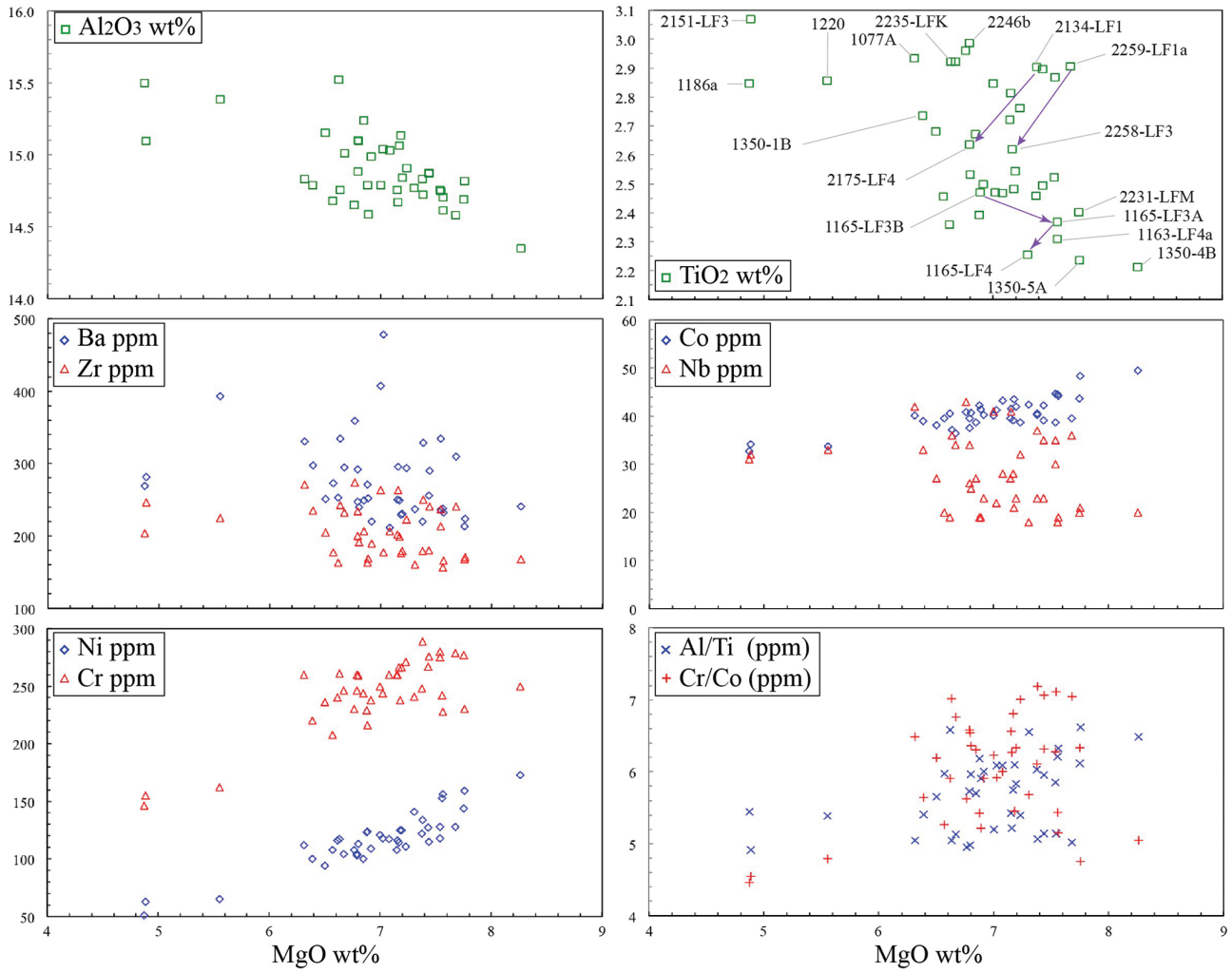

Figure 8. Harker diagram of TiO_2 versus SiO_2.

TiO_2. As with the TAS diagram, there is a similar subtle gap about 49.9 wt % SiO2, but this might result from simply not sampling lava flows with these compositions.

Two general trends in the data are evident with data plotted by geographic area and lower to higher stratigraphic position (or in the "sequence of arrival" of lava at a location such as in the samples at 1165) (Figure 7 and 8). (1) More data south of the fault have lower SiO_2 and more data north of the fault have higher SiO2. One possible influence on this distribution is that many locations south of the fault are from sections deposited on the pre-basalt substrate whereas many locations north of the fault are where the base of the section is not exposed and these samples might represent the last erupted lava. (2) The typical stratigraphic trend is from lower SiO_2 and higher TiO_2 to higher SiO_2 and lower TiO_2; for example, 2234-LFF to 2232-LFJ. Locally, some data in a sequence have values that are "across" or "against" this general trend. Two examples where values are across the trend are 2151-LF3 to 2153-LF4, and 2161-LF1 to 2161-LF6. The sample series 1165-LF3B to 1165-LF3A to 1165-LF4 crosses the trend line twice, and the series 1350-1B to 1350-2A to 1350-3A to 2140-LF3a crosses the trend three times.

For context, the "Error of the Average" for TiO_2 in the 1165-LF3B to 1165-LF3A samples is 0.05 ppm, and the difference between LF3B and LF3A is 0.10 ppm (Tables 3 and 2). Two examples where values are against the trend are 2235-LFK to 2234-LFF, and 1350-4 to 1350-5.

Element and element ratio plots

Bi-plot graphs of major element (wt %), trace elements (ppm), or element ratios show relations in data that vary from well correlated to poorly correlated. Figure 9 includes selected major and trace elements, or element ratios versus MgO wt%. MgO wt % was chosen as the X-axis because this is commonly done for rocks that are influenced by crystallization of olivine and pyroxene. The major and trace elements in Figure 9 are depicted because they tend to be stable in basaltic rocks and are immobile during alteration or weathering. Ni, Cr, Co (ppm) and Al_2O_3 wt % are all well correlated to MgO wt %, TiO_2 wt % is moderately correlated to MgO wt %, and Ba, Nb, and Zr (ppm) are poorly correlated to MgO wt %. The element ratios of Al/Ti and Cr/Co (both from the ppm data) are moderately correlated to MgO wt %.

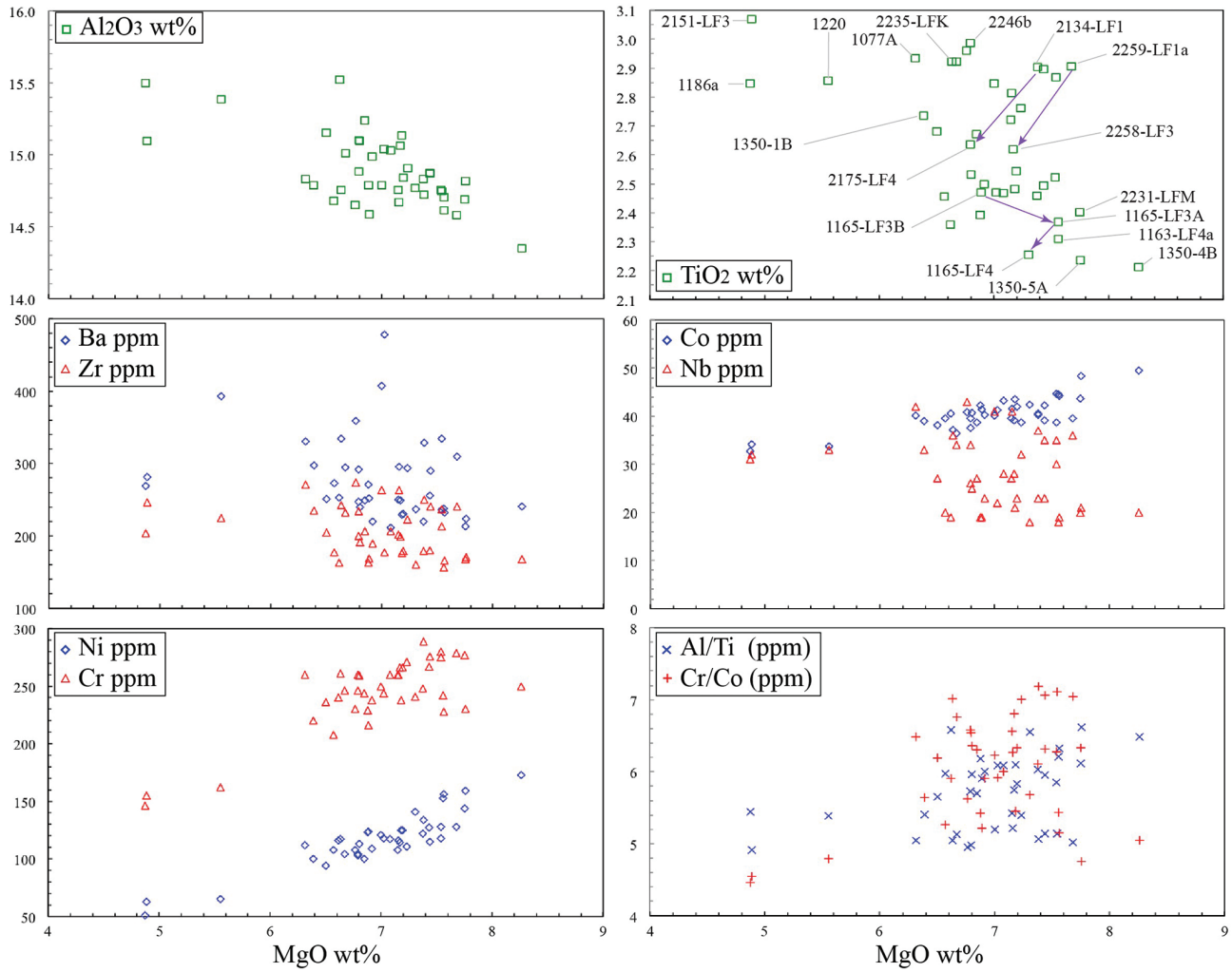

Figure 9. Selected major element oxide compositions, trace element abundances, and element ratios versus MgO wt %.

To aid in the correlation to the TiO_2 Harker diagram (Figure 8), selected samples in Figure 9 are labeled that show some of the (1) beginnings and endings of stratigraphic sequences, (2) three local sequences, and (3) "outliers" from the general trend. The two longer sequences that define the overall "along" the trend of increasing MgO wt % (details not shown) include 1350-1 to 1350-5 and 2235-LFK to 2231-LFM. The local sequences that have across trends include 2134-LF1 to 2175-LF4 and 2259-LF1a to 2258-LF3. The local 1165 sequence has an along the trend increase in MgO wt % from the upper shell (LF3B) to the core (LF3A) and an across trend from LF3A to the core in LF4. Samples 1350-4 to 1350-5 have a slight against the trend decrease in MgO wt %.

Use of element ratio bi-plot graphs are helpful to use if element data have not been normalized. Not normalizing the element (or oxide) data can result for several reasons, including not having a full set of data because some of it was not collected. For example, ICPAES-MS data on Si was not collected for the 9 samples from 2013. Also, for a different part of the Broadwell Mesa basalt study, a portable X-ray Fluorescence (pXRF) was used to collect data in the field but it does not measure the full range of elements as the xdXRF; therefore, comparing pXRF and wdXRF data without the use of ratios might be challenging. Figure 10 is representative of element ratio bi-plot graphs for the Broadwell Mesa basalt, and many of the trends observed in this graph also occur in other graphs such as the TAS and Harker diagrams. There is a general trend of increasing Al/Ti and decreasing Zr/Cr with increasing stratigraphic position. There is a slight "gap" at about 5.1 ppm Al/Ti, and several of the local sections have sequences that span this gap. There are local examples of sequences that are across the trend (2153-LF4a to 2157-LF7a, 1165-LF3A to 1165-LF4, and 1350-2A to 1350-3A to 2140-LF3a), and a few examples are against the trend (1350-4B to 1350-5A and 2234-LFF to 2233-LFL).

Another way to display the vertical and lateral geochemical variability is to plot one elemental component (such as Al/Ti) by area and stratigraphic position (Figure 11). Lava flows with the lowest Al/Ti ratios (<5.0) are stratigraphically lowest (some

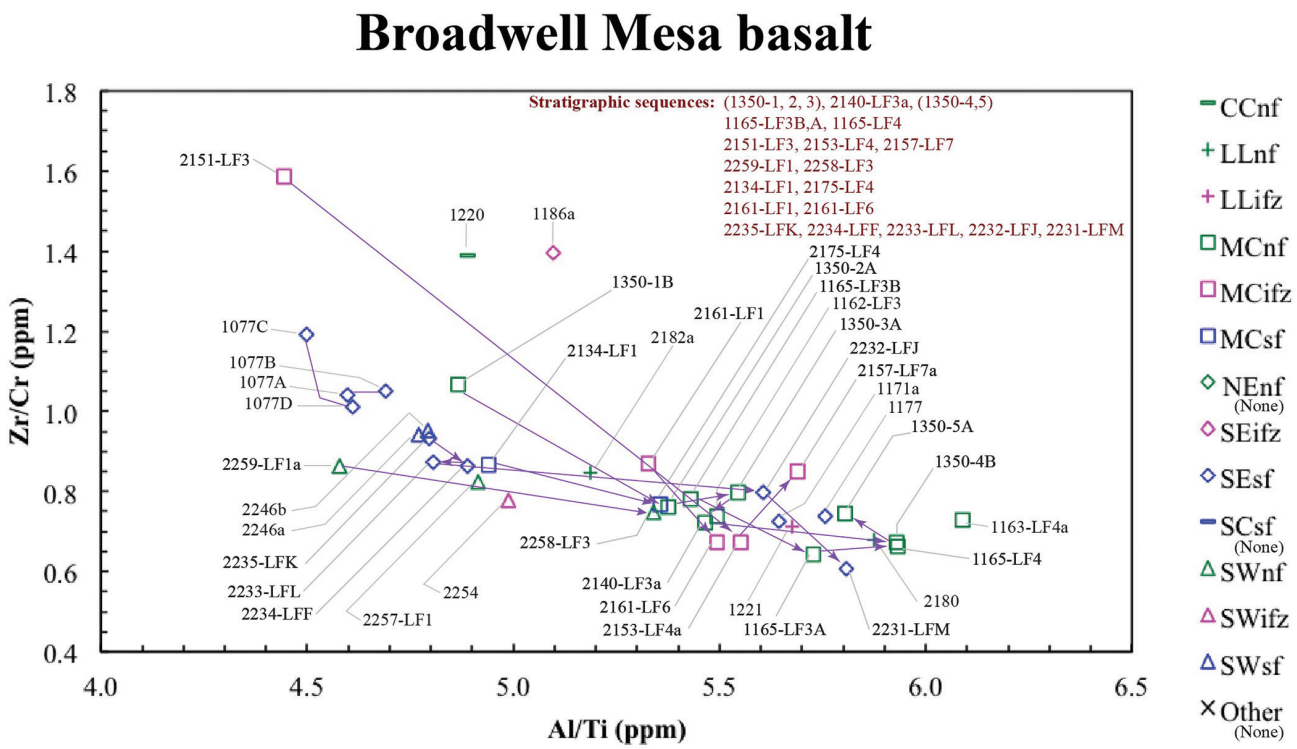

Figure 10. Zr/Cr versus Al/Ti plot.

representing the first lava deposited in that area), and these flows occur across the field. Several flows in this category are from the southwestern and southeastern exposures, and some are from the central part of the field in the Main Canyon area, including in the vent crater of the 25-m high cinder cone (1220). Lava flows with the intermediate Al/Ti ratios (5.0-5.6) occur in several parts of the field, and are within the section or locally form the top of the section. In several sequences, including the 2235-LFK to 2231-FLM sequence, a few lava flows were not sampled, but might be of these intermediate compositions. Lava flows with the highest Al/Ti ratios (>5.6) are stratigraphically highest (representing the last lava deposited in that area), and these flows occur in the lava lake, main canyon north of the fault, and southeast areas.

Samples from a small lava flow in the vent crater of the cinder cone (1220) and a lava flow from the main canyon area within the Broadwell Mesa fault zone (2151-LF3) typically plot near each other on all geochemical plots, but outside the typical distribution of the data. These two samples have some of the highest SiO_2, Na_2O+K_2O, TiO_2, MgO, Al_2O_3, and Zr/Cr values, and lowest Ni, Cr, Co, and Al/Ti values. On several of the element plots, lava flow 1186a (which is from near the base of the cinder cone in the southeastern part of the fault area) also has similar values. These similarities suggest that the eruptions that formed these three lava flows might have occurred within a short period of time. There is no spatial context for lava flow 1186a, but lava flow 2151-LF3 is at the base of a five-flow sequence and the cinder cone is overlain by lava flows from the lava lake, so both of these flows were probably erupted relatively early in the history of the field.

Geochemical evolution of the field

The progressive changes in composition for sequentially overlying lava flows (for example, increase in SiO_2, MgO, and Al/Ti), and for some flow sequences with "across trend" and "against trend" steps in composition, occur in many parts of the field (Figure 7, 9, 11). These trends are displayed differently depending on which type of graph is used. Typically, these compositional trends are from sequences of lava flows; however, in one lava flow (1165-LF3) there are differences between samples from the core to near the top of the same lava flow. Additionally, several elements including Ni, Cr, and Co (ppm) and Al_2O_3 wt % are well correlated (to strongly compatible) with MgO wt %, and TiO_2 wt % is moderately correlated to MgO wt %. Magma composition modeling of the Broadwell Mesa basalt data has not been conducted.

Trends in Broadwell Mesa basalt major and trace element data are similar to those identified by Farmer and others (1995) for 31 samples of basalt flows from the nearby Cima volcanic field 36 km northeast of the Broadwell Mesa volcanic field. Farmer and others (1995) analyzed major and trace elements, and numerous isotopes. The well-correlated (strongly compatible) trends of Ni and other elements with MgO wt % are attributed to clinopyroxene ± olivine fractionation. Farmer and others (1995) used isotopic analyses to argue that the basalts in the Cima area resulted from partial melting of the asthenosphere, and was not contaminated by interaction

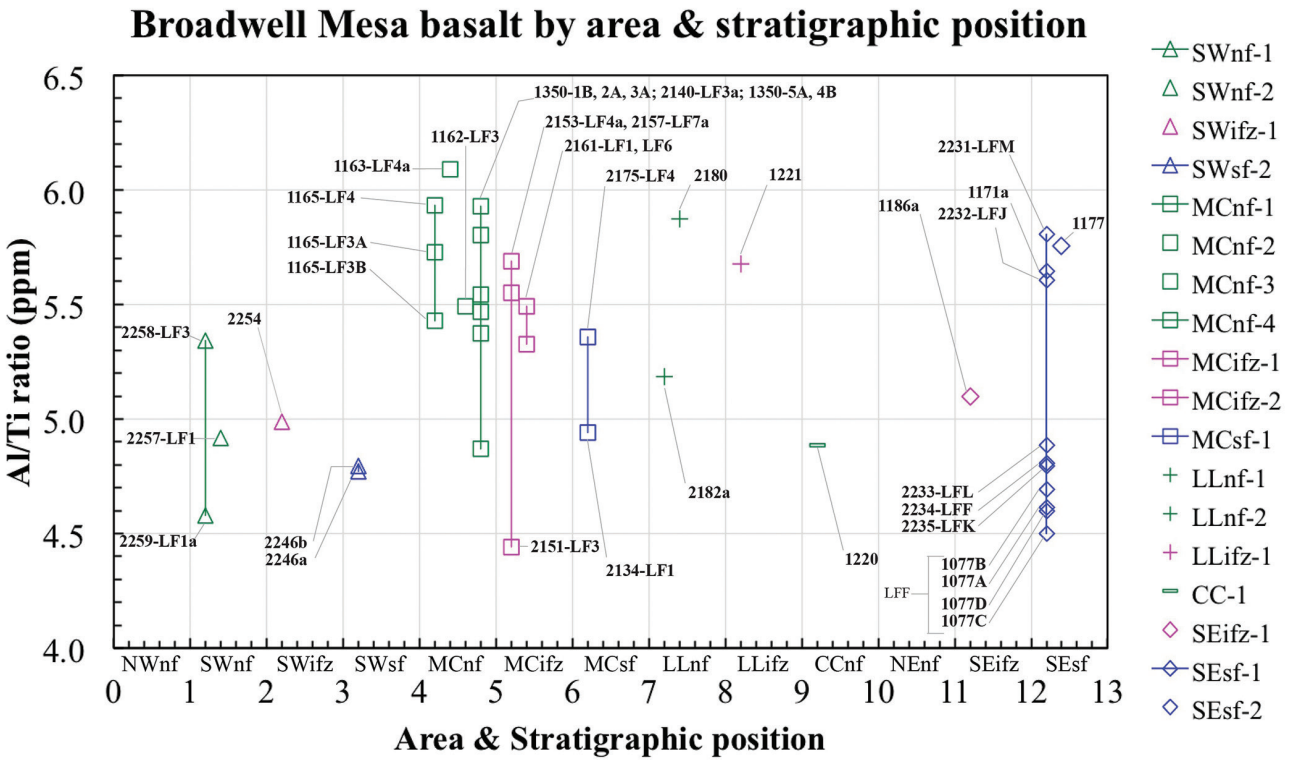

Figure 11. Plot of the Al/Ti ratio versus the area and stratigraphic position of the samples. Areas are arranged from west to east, and within each area samples or stratigraphic sequences are arranged from north to south. In the list of symbols, the hyphenated numbers are the numbers of stratigraphic sequences (with connecting lines) or individual samples (no line) in each area.

with crustal materials. Although the modeling results by Farmer and others (1995) have not been applied to the Broadwell Mesa volcanic field directly, they are at least consistent with the geochemical zonation of the Broadwell Mesa data.

The typical trend (or evolution) of the geochemistry is from lower to higher SiO_2, MgO, Ni, Cr, and Al/Ti and higher to lower Na_2O+K_2O, TiO_2, Al_2O_3, and Zr/Cr. The fact that these trends occur from the small scale within a single lava flow up through several flows to the full section (both vertically and laterally), indicates the eruptions incrementally tapped a continuously changing magmatic system that was probably undergoing various amounts of partial melting of the source rocks, resupply of magma, and fractional crystallization.

Conclusion

The Broadwell Mesa volcanic field is not a very large field (~6 km^2), but within the basaltic compositions of lava flows, the field is compositionally zoned. The eruptive history and development of the volcanic field are based on physical stratigraphy and geochemical variations within and between the lava flows. Small-scale features of the lava flows (especially variations in the amounts and sizes of phenocrysts and vesicles in the upper and lower rapidly cooled parts of the flow compared to the internal core, and deformation of vesicles resulting from flow of the core relative to the chilled outer margins) provide context to physical and geochemical processes of lava flow emplacement. For example, local flow 1165-LF3 has changes in textures and geochemistry from the upper chilled margin to the core that indicate zonation by continuous (but successive) emplacement of lava that changed composition during the eruption. The similarity in, or small progressive geochemical changes between, stratigraphically adjacent lava flows might indicate that the flows are part of a flow unit. In flow sequences where there are moderate to large steps in geochemistry (which is not just apparent because of a lack of sampling), these steps probably represent periods of time (hiatuses) in the eruptions where the bulk composition of the magma changed as a result of increased partial melting or crystal fractionation.

Most lava flows are simple and some are compound, and several might be parts of one or more lava flow units. The geochemistry of these simple lava flows to lava flow units does change within a stratigraphic section, so it supports the general correlation of flow and flow units, but detailed flow unit correlations across the field cannot yet be done with the available data. One set of possibly related flow units might be those associated with lava flows 2151-LF3, 1220, and 1186a because they all tend to have slightly different compositions compared to the rest of the field. These stratigraphic differences in geochemistry might be consistent with eruption during two or more eruptive episodes; however, the lack of clastic sedimentary rocks or even aeolianite interstratified with the lava flows probably indicates that the Broadwell Mesa volcanic field is a single eruptive episode with a (relatively) short eruptive cycle.

Acknowledgements

I want to acknowledge the helpful discussions and interactions with my colleagues on the Broadwell Mesa team including David Miller, Geoff Phelps, Kevin Schmidt, and Andy Cyr. Their knowledge on the mapping of the Miocene rocks and Quaternary deposits and faulting, and observations of the basalt flows, has been an invaluable framework for examining this basaltic field. Reviews by Robert Fleck and Drew Downs (both USGS) were very helpful and greatly appreciated. The interpretations of the physical and geochemical stratigraphy described herein are all mine.

References

Brady, R.H. III, 1992, The Eastern California Shear zone in the northern Bristol Mountains, southeastern California: in Richard, S. M., ed., Deformation associated with the Neogene Eastern California Shear Zone, southwestern Arizona and southeastern California: Redlands, CA., San Bernardino County Museum Special Publication, p. 6-10.

Brady, R.H. III, 1993, Cenozoic stratigraphy and structure of the northern Bristol Mountains, Calif.: *in* Sherrod, D.R. and Nielson, J.E., (eds.), Tertiary stratigraphy of highly extended terranes, California, Arizona, and Nevada, U.S. Geological Survey Bulletin 2053, p. 25–28.

Buesch, D.C., and Phelps, G.A., 2016, Architecture, geochemistry, and paleomagnetic directions of the 5.42 Ma Broadwell Mesa basalt volcanic field, Bristol Mountains, California: in Reynolds, R.E., ed, "Going LOCO: Investigations along the Lower Colorado River", California State University Desert Studies Consortium, p. 253-255. (Available at http://nsm.fullerton.edu/dsc/images/DSCdocs/DS_2016_Going_LOCO.pdf)

Dibblee, T.W., Jr., 1967, Geologic map of the Broadwell Lake quadrangle, San Bernardino County, California: U.S. Geological Survey Miscellaneous Geologic Investigations Map I–478, scale 1:62,500.

Dokka, R.K., and Travis, C.J., 1990, Role of the eastern California shear zone in accommodating Pacific-North American plate motion: Geophysical Research Letters, v. 17, p. 1323–1326.

Farmer, G.L, Glazner, A.F., Whilshire, H.G., Wooden, J.L., Pickthorn, W.J, and Katz, M., 1995, Origin of late Cenozoic basalts at the Cima volcanic field, Mojave Desert, California: Journal of Geophysical Research, v. 100, no. B5, p. 8399-8415.

Le Maitre, R.W. (ed), 1989, *A Classification of Igneous Rocks and Glossary of Terms*, Blackwell Scientific, Boston, Mass., 93p.

Miller, D.M., and Yount, J.L., 2002, Late Cenozoic tectonic evolution of the north-central Mojave Desert inferred from fault history and physiographic evolution of the Fort Irwin area, California, in Glazner, A.F., and Walker, J.D., eds., Geologic evolution of the Mojave Desert and southwestern Basin and Range: Geological Society of America Memoir 195, p. 173-197.

Phelps, G.A., Bedford, D.R., Lidke, D.J., Miller, D.M., and Schmidt, K.M., 2012, Preliminary surficial geologic map of the Newberry Springs 30' x 60' quadrangle, California: U.S. Geological Survey Open-File Report 2011–1044, pamphlet 68 p., 1 sheet, scale 1:100,000. (Available at http://pubs.usgs.gov/of/2011/1044/.)

Phelps, G.A., Hillhouse, J.W., Fleck, R.J., Miller, D.M., Buesch, D.C., Cyr, A., and Schmidt, K.M , this volume, Analysis of the Age and Paleomagnetic Orientation of the Broadwell Mesa Basalt, Bristol Mountains, CA.

Mineral potential within the Eastern California Shear Zone

Larry M. Vredenburgh
U. S. Bureau of Land Management, 3801 Pegasus Dr., Bakersfield, CA 93308, lvredenb@blm.gov

The California Desert Conservation Area: modelling mineral potential

A desert study program had been initiated by the Bureau of Land Management (BLM) as early as 1968, but completion of the study acquired upmost urgency when President Richard Nixon signed an executive order on February 8, 1972 requiring a program of off-road vehicle management of all federal lands (Los Angeles Times, 2 Mar 1975, p. 31). Further, each agency was given 6 months to develop and issue regulations, "to provide for administrative designation of the specific areas and trails on public lands on which the use of off-road vehicles may be permitted, and areas in which the use of off-road vehicles may not be permitted, and set a date by which such designation of all public lands shall be completed." On November 1, 1973, the BLM published the "Record for the Interim Critical Management Program (ICMP) for Recreation Vehicle Use on the California Desert," fulfilling the requirement of the executive order.

Shortly after the completion of the ICMP the BLM published notices seeking public input for an updated ICMP (Los Angeles Times, 15 Aug 1974, p. 74). During this time (1973 -1974) BLM began hiring subject matter experts to evaluate the resources for the existing environment of the California Desert. This new effort envisioned evaluating 27 areas and preparing Resource Use Plans (Los Angeles Times 8 July 1976, p 51). The BLM estimated the planning effort would be completed in 1982 (Los Angeles Times 2 Mar 1975, p. 33).

On October 21, 1976 Congress passed the Federal Land Policy and Management Act (FLPMA). This legislation was the Bureau of Land Management's "organic act" which established the agency's purpose and direction, it also established the 25 million acre California Desert Conservation Area (CDCA). In FLPMA Congress directed the agency to complete a land use plan for the CDCA by September 30, 1980. Congress actually funded this mandate, and perhaps even more surprisingly the plan was completed on time.

BLM hired subject matter experts to assemble and lead teams to assess the resources of the CDCA. The plan elements included, cultural resources, Native American coordination, wildlife, vegetation, wilderness, wild horse and burro management, livestock grazing, recreation, mineral resources, energy production and utility corridors, and land-tenure adjustment.

Jean Juilland, was hired by BLM in 1973 to evaluate Geology, Energy and Mineral (GEM) resources. He was born in Romania in 1928. He earned a diploma in Mining Technology at the Haileybury School of Mines in Canada, and completed his BSc, and MSc, at Michigan Technical University, with post-graduate studies at Stanford University. He mined and did mineral exploration in Peru, and was a mine geologist and then production planner for the underground gold mine McIntyre Porcupine Mines in Schumacher, Ontario, Canada. Also, Jean worked for Texas Instruments in Colorado. He then did exploration for Geophoto, a wholly-owned subsidiary of Texas Instruments. He was their senior geologist and assistant manager in Brisbane, Australia. He later became the company's projects manager for mineral exploration throughout Australia. He consulted for Placer Amex, Inc.

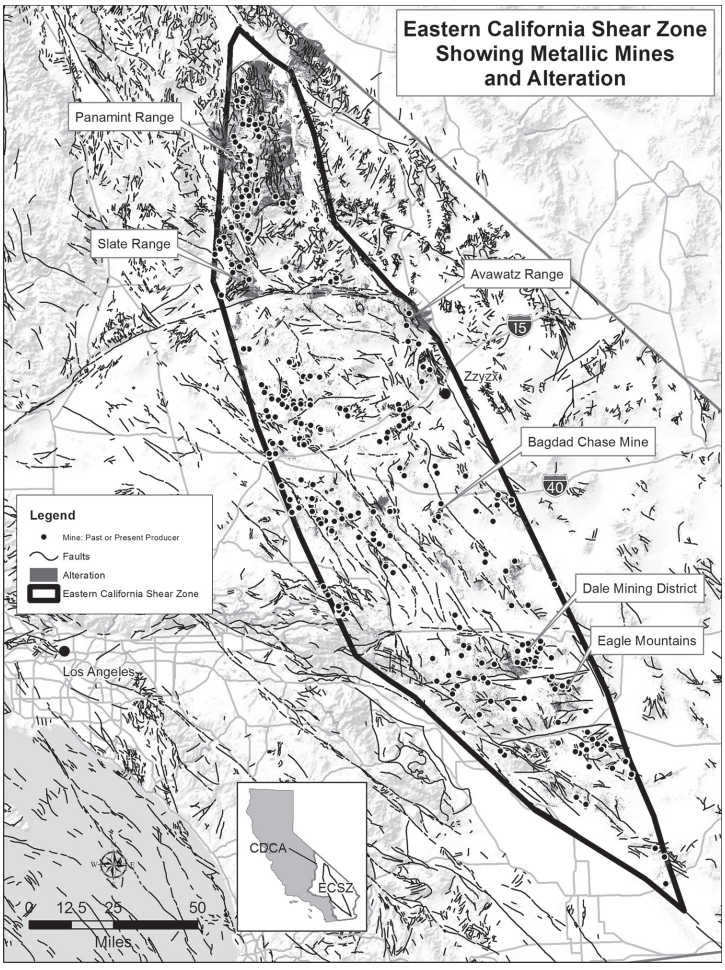

in California while doing his doctoral research on the Lights Creek Stock.

Evaluation of the mineral resources of the CDCA was a huge task. Jean approached it with some of the latest techniques – airborne geophysics, enhanced imagery, and a landscape scale drainage sediment geochemical survey.

Stream Sediment samples were collected from 1240 sites. Two samples were collected from each site; one sample was sieved, the other was sieved and panned, resulting in a heavy mineral concentrate. These samples were analyzed using semiquantitative, direct-current arc-emission spectrography.

A "Landsat Enhancement Project" was delivered August 1979 by General Electric, Space Division. Products included a lineament map, tonal anomaly map (inferred areas of hydrothermal alteration), and a regional statistical analysis of metallic mineral potential. Data used in the statistical analysis included a weighted score for lineaments, favorable lithology, and known mineral occurrences. A 10km grid cell was used.

Another contract assembled a computerized list of mineral occurrences. The U. S. Geological Survey's Mineral Resources Data System (MRDS) hadn't been invented yet! This data was one of the layers used in the GE statistical analysis.

Besides these high-level studies, there was an aggressive field component as well. One assignment I had was to investigate a prominent, inferred area of hydrothermal alteration as defined from Landsat imagery high in the Avawatz Range.

The minerals staff divided the CDCA into 75 separate areas and, using all the available data, wrote reports summarizing the GEM Resources in that area. However, not all of the area reports were completed before the completion of the Desert Plan.

This was all accomplished long before the personal computer, and due to technical difficulties, GIS technology, was not used. Most of the information was reduced to mylar overlays for evaluation and interpretation.

Mineral potential within the Eastern California Shear Zone

Today, to assemble this data requires less than an hour. The US Geological Survey has created an interactive map service with all of these data sets as well as many others https://mrdata.usgs.gov/general/map.html

Each data set has a link which will lead you to the raw data. And, if you aren't GIS savvy, they have kmz files available to use with Google Earth.

And if that isn't enough data, there's more! Zoom into your area of interest and when you click on the map, a table pops up that displays the following data sets: geology, airborne geophysical surveys, estimates of undiscovered mineral resources, mine locations (MRDS), National Geochemical Database (this includes the BLM geochemical survey), global assessment of undiscovered copper resources, mine features from USGS topo maps, and a list of all references in the National Geologic Map database. All this data can easily be downloaded.

To experiment with some of these data sets I added areas of inferred hydrothermal alteration (Mars, 2013), USGS MRDS mine location, and faults. I didn't run a geostatistical query on this data, and of course many other data sets could have been added. Just eye-balling the overlap of these themes, the following mines / areas stand out: Panamint Range, Slate Range. Avawatz Range, Dale Mining District, Eagle Mountains. Of course, the test would be to thoroughly study an area with alteration with no mines.

Acknowledgements

I would like to thank Sue Marcus, a former co-worker on the Desert Plan Staff, for sending me a copy of Jean Juilland's obituary, "Jean Juilland SME An Appreciation by Sue Marcus."

Bibliography

Environmental Analysis Record for the Interim Critical Management Program for Recreation Vehicle Use on the California Desert. November 1, 1973, US Department of the Interior Bureau of Land Management, California Desert Staff. 572 p. https://archive.org/details/interimcriticalm00unit

Executive Order 11644--Use of off-road vehicles on the public lands https://www.archives.gov/federal-register/codification/executive-order/11644.html

Mars, John C., 2013, Hydrothermal Alteration Maps of the Central and Southern Basin and Range Province of the United States Compiled From Advanced Spaceborne Thermal Emission and Reflection Radiometer (ASTER) Data, US Geological Survey Open-File Report 2013-1139 https://pubs.usgs.gov/of/2013/1139/

Jean Juilland 1928-2016, Obituary http://www.legacy.com/obituaries/mercurynews/obituary.aspx?pid=181603589

Philip Fradkin, 825,000 Desert Acres May Be Closed to Off-Road Vehicle Use, Los Angeles Times 19 Sep 1973, p. 7.

Prelat, A.E., Kowalik, W.S., Lyon, R.J.P., 1979, Mineral exploration evaluation of part of the California Desert Conservation Area, based on integration of Landsat data with geological and airborne geophysical data: unpublished SLM contract no. YA -512-CT8-234.

The California Desert Conservation Area Plan, US Department of the Interior, Bureau of Land Management, Desert District, Riverside, California, 1980. https://archive.org/details/californiadesert5115unit

Vredenburgh, Larry M., 1988, Geology and Mineral Resources of the Avawatz Mountains Resource Area, San Bernardino County, California in Geology of the Death Valley Region South Coast Geological Society, Guidebook 16 pp. 305-344

Geology and mineralization of Old Dad Mountain

Larry M. Vredenburgh
U. S. Bureau of Land Management, 3801 Pegasus Dr., Bakersfield, CA 93308, lvredenb@blm.gov

Geology

No single rock type dominates Old Dad Mountain and its surrounding area. Rock types include Early Proterozoic gneiss and granitoid rocks (Xg), Jurassic Aztec Sandstone (Ja), Mesozoic volcanic and sedimentary rocks (Mzv), Late Proterozoic and Cambrian siliciclastic rocks (PZs), and Tertiary volcanic rocks (Tv1). Old Dad Mountain is underlain by a resistant knob of limestone which is part of the Devonian to Permian limestone (PDl).

Hewett (1956) reported the presence of granite, schist, and quartzite intruded by syenite dikes in the Proterozoic rocks in this general area (Theodore, 2007, p. 111).

The oldest structure is a Lower (?) Jurassic unconformity overlain by Aztec Sandstone. The northwest-trending Powerline Canyon shear zone is exposed just south of Jackass Canyon. The Playground thrust fault truncates these older structures. Extensional tectonics during Miocene time resulted in the Old Dad normal fault. The steep slopes that formed on both sides of the Old Dad Mountain fault block by erosion or downfaulting became the source of numerous landslides of brecciated rock, as well as glide blocks, during Neogene time (Dunne, 1977).

Hewett (1956, p. 113) surmised gold mineralization at mines in the north of Old Dad Mountain may be related to the intrusion of the Sands granite. At the Paymaster Mine, a massive quartz vein occurs in pre-Cambrian gneiss. Gold bearing quartz veins at the Brannigan and Oro Fino Mines occur in quartzite, shale, and dolomite of the Upper Precambrian to Lower Cambrian Wood Canyon formation, Stirling quartzite and Johnnie formation (Hewitt, 1956, p. 38).

Mining history and economic geology

During the 1850s, an Indian foot trail that evolved into the Mojave Road first crossed the middle of Old Dad Mountain, then went around it (Casebier, 1975, p. 54, 86, 90). During 1853 and 1854, Lieutenant Amiel Weeks Whipple conducted a survey along the 35th parallel from Fort Smith, Arkansas, to Los Angeles, California. He crossed the range, with the aid of Mohave Indian guides,

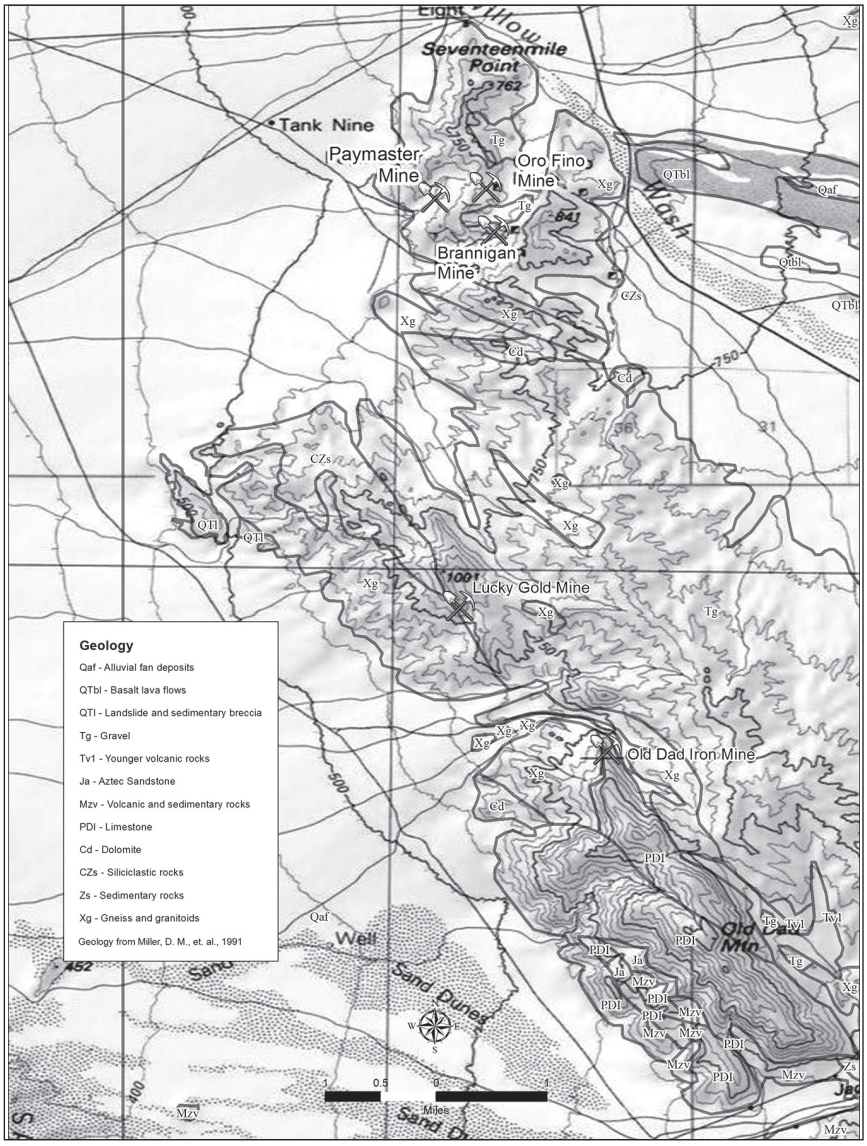

Preliminary geologic map of the East Mojave National Scenic Area, California, U.S. Geological Survey, 1991

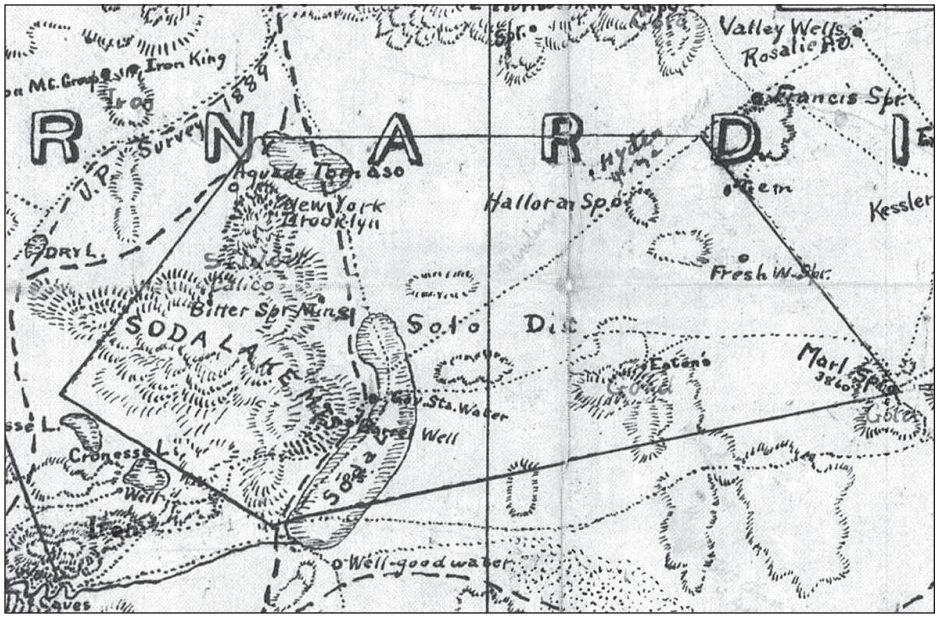

A portion of Crowell's Miner's Map. 1903 Edition Showing the Solo Mining District

at Jackass Canyon and Rocky Ridge (35.111n, 115.794w). This canyon, now traversed by powerlines that originate at Hoover Dam, is in the middle of the range. The difficult route over Rocky Ridge wasn't used after the fall of 1859 in favor of an easier route around the north end of Old Dad Mountain at Seventeen Mile Point (Casebier, 1988, p. 294-295).

The Solo Mining District was established February 18, 1889 (May Queen Mine, Mineral Survey 2814, Notes) during a time of mining activity in the Soda Mountains. As created, the district extended eastward to encompass Old Dad Mountain.

In April 1902, Bob Yancey, "an old and well known desert prospector," is credited with discovery of rich gold ore near Seventeen-Mile Point. An article in the San Bernardino Evening Transcript screamed "A stampede of miners, Bob Yantzey's [actually spelled Yancey] Discovery is filling up the desert with men – the ledges are large and extensive." Within a month of this report, former mayor of Los Angeles Fred Eaton had "secured 21 mining claims here."

Nearly a year later, in January 1903, a Nevada cattleman named Greeley purchased a claim from Nathaniel Mount and several other business men of Barnwell. Of course, this purchase aroused new interest. In April 1903, an article stated "Mr. E. E. Palmer, Mr. Geo. Rose, Mr. J. J. Brady and Mrs. U. J. Stewart" had staked several claims at Seventeen-Mile Point.

Fred Eaton had acquired the claims under a $30,000 bond, spent $7,000 on building trails and sinking a shallow shaft, but he was caught in the financial panic of 1907 and abandoned the bond.

In March 1909 the "Eaton group" of four claims was sold by Henry Ward and A. L. Buys to a group of men from Los Angeles doing business under the name Precious Metals Development Company. These men included John L. Witney, former manager of the McCracken mine located in Arizona; Dick Ferris, a well-known actor; and Harmon D. Ryus, former manager of the White automobile dealership in Los Angeles. A couple of months later they were reported to have purchased the Ward mine for $18,000.

Soon they began surveying the site for a mill, and the route for a pipeline to Indian Spring, located 5 miles away to the northeast. Also, they began work on a 700 foot long cross-cut adit, and sinking two shafts.

A four-stamp mill finally was installed in August 1910. About this same time the mine started being referred to as the Witney. The cross-cut had been completed as well as 140 and 85-foot deep shafts. All together some 2,000 feet of drifts and other underground had been driven.

The mill seemed to have been successful in recovering gold from free milling ore. On January 19, 1912, the Barstow Printer reported, "J. T. Keough, manager of the Precious Metals Development Co., at Seventeen mile Point, came in Monday with a gold brick weighing 32 ounces, the result of a 72-hours run with their two stamp Nisson mill." Apparently this reference to a 2-stamp mill was in error, since later in the year it is again referred to as a 4-stamp mill.

This mine, known as the Eaton, Witney, or Whitney – and later as the Paymaster—was not the only mine in the vicinity. Other mines mentioned during this 10-year period include the following; unfortunately their locations are unknown.

- The Palmyra group of four claims owned by William Yeoman and Bob Yancey, "from which many years ago, beautiful free gold specimens were obtained and exhibited" (*Mining World*, April 11, 1908).
- The Paymaster, Red Boy and California groups owned by J. V. Robison and Henry Ward (*Mining World*, April 11, 1908)
- Bell Mine, owned by Julius Myers, "Has free gold rock. . . it is jewelry gold" (Barstow *Printer*, Jan. 12, 1912).
- The Stillwell brothers have sent forward a carload of twenty-four tons from Seventeen-Mile Point of an estimated value of 60 percent lead and about half an ounce of silver to each unit of lead (Los Angeles *Mining Review*, June 5, 1909, p. 19)

- The Big Bonanza group of four claims has about 350 ft. of tunnel development. The vein is quartzite, about 32 ft. in width and gives assay values across its entire width of $18 in gold to the ton (*Mining World*, Apr. 11, 1908)

In 1912 the Big Bonanza mine attracted the attention of the San Francisco *Call, (*April 14, 1912). The newspaper reported,

> J[oel] V[aughn] Robison, formerly superintendent of the Yankee Girl; mine in the Bullfrog district of southern Nevada, came into Randsburg from the Big Bonanza group, a property, which he owns and is operating at Seventeen Mile Point in the northern part of San Bernardino county. He brought several samples of ore, which attracted general attention. These samples, to use the favorite expression among mining men, are, literally "shot full of gold," and will assay at a conservative estimate between $700 and $800. They are selected, however, and do not represent an average of the ledge which Robison says will yield about $8 through the, entire width of 40 feet.
>
> The property is situated in the Silver lake country, 17 miles, east of the Tonopah and Tidewater railroad. Robison says that he has completed 600 feet of development work on the Big Bonanza claim. This consists of a 225 foot crosscut to the ledge which was reached at a depth of 275 feet and drifts in both directions. The ledge is between well defined walls and the ore is easily mined. Robison has a deal on to turn the property over to eastern people who propose to work it on a more extensive scale.

Due to increased mining activity in the area, in 1931, W. B. Tucker, with the California Division of Mines, prepared a special report on the Halloran Springs Mining District. Two important discoveries were catalysts for activity in this district. Just south of Seventeen Mile Point, on March 11, 1930, M. A. Sisley and John Herrod discovered high grade gold quartz on the Brannigan Claims, and on November 19, 1930 A. A. Brown and Ralph Brown discovered high-grade gold quartz at what became known as the Telegraph mine, located at Halloran Springs.

Following the discovery of gold at the Brannigan mine, between 1938 and 1940 the mine yielded 51 tons of ore which contained 59 ounces of gold and 20 ounces of silver, which was milled nearby (Hewett, 1956, p. 122).

The Oro Fino Mine was active in 1902, between 1937 and 1941, and in 1948. US Bureau of Mines records (Hewett, 1956, p. 122) show 528 tons which yielded 400 ounces of gold and 20,594 ounces of silver. Prior to 1943,

Ore car at the Brannigan Mine, 1976. Photo by the author.

(Tucker and Sampson, 1943, p. 457) report the mine yielded 4,000 tons which averaged $50 per ton.

According to Wright *et al*, (1953, p. 78) the Paymaster yielded between $50,000 and $100,000 between 1900 and 1953.

Acknowledgements

I would like to thank Chris Ervin, Archivist for the Mojave Desert Heritage and Cultural Association, for assistance researching the Mojave Trail.

References

Barca, R.A., 1966, *Geology of the northern part of the Old Dad Mountain quadrangle, San Bernardino County, California:* California Division of Mines and Geology, Map 7, scale 1:62,500

Casebier, D. G., 1975, *The Mojave Road* (Tales of the Mojave Road Publishing Co.: Norco, CA).

Casebier, D.G., 1988, *Guide to the East Mojave Heritage Trail, Ivanpah to Rocky Ridge* (Tales of the Mojave Road Publishing Co.: Norco, CA), p. 294-295

Crowell, R. A., 1903, *Miners Map of Death Valley and the Proposed Salt Lake R. R's*

Dunne, G.C., 1977, *Geology and structural evolution of Old Dad Mountain, Mojave Desert, California*: Geological Society of America Bulletin, v. 88, p. 737-748.

Hensher, Alan, 1988, *Silver Lake*, *in* Casebier, D.G., 1988, *Guide to the East Mojave Heritage Trail, Ivanpah to Rocky Ridge* (Tales of the Mojave Road Publishing Co.: Norco, CA), pp. 161 -166.

Hewett, D.F., 1956, *Geology and mineral resources of the Ivanpah quadrangle, California and Nevada*: U.S. Geological Survey Professional Paper 275, p. 120 – 122.

May Queen Mine Mineral Survey 2824, Notes Vol. 22-20.

Miller, David M., Miller, Robert J., Nielson, Jane E., Wilshire, Howard G., Howard, Keith A., and Stone, Paul, 1991, *Preliminary geologic map of the East Mojave National Scenic Area, California*, U.S. Geological Survey Open File Report 91-435

Theodore, Ted G., editor, 2007, Geology and Mineral Resources of the East Mojave National Scenic Area, San Bernardino County, California, U.S. Geological Survey Bulletin 2160

Tucker, W. B., 1931, *Halloran Springs Mining District, California Division of Mines Report 27*, p. 321 - 333.

Tucker, W. B., 1943, *Los Angeles Field Division, Mineral Resources of San Bernardino County*: California Division of Mines Vol. 39, No. 4.

Vredenburgh, L. M., Shumway, G.L., Hartill, R. D., 1981, *Desert Fever, an overview of mining in the California Deser*t (Living West Press: Canoga Park, CA).

Vredenburgh, Larry M., 1994. *Fort Irwin and Vicinity: History of Mining Development, in* Robert E. Reynolds, *Off Limits in the Mojave Desert*, San Bernardino County Museum Association Special Publication 94, p. 81 - 90.

Wilshire, Howard G., 2002, *Digital Version of Open-File Report 92–181: Geologic Map of the Indian Spring Quadrangle, San Bernardino County, California*, U.S. Geological Survey Open-File Report OF 02-272.

Wright, L. A., Stewart, R. M., Gay, T. E., Hazenbush, G. C., 1953, *Mines and Mineral Deposits of San Bernardino County, California*, California Journal of Mines and Geology, Vol. 49, pp. 72, 76, 78, 98; Table pp. 47, 52, 53, 68, 72, 75, 82

In 1906, drivers raced from Los Angeles to the San Gabriel Mountains, http://www.sbsun.com/events/20150112/in-1906-drivers-raced-from-los-angeles-to-the-san-gabriel-mountains San Bernardino Sun. Accessed Feb. 10, 2017.

Barstow *Printer*: Aug. 12, Dec. 23, 1910, Feb. 3, Apr. 28, 1911, Jan. 12, 19, Apr. 5, Nov. 1, 1912; Los Angeles *Herald*: Nov. 2, 1909; Los Angeles *Mining Review*: May 24, 1902; Apr. 27, May 15, 22, Jun. 5, 26, 1909; May 13, 1911, p. 21; Los Angeles *Times*: Jan. 30, 1903; Apr. 27, Mar. 25, 28, Nov. 2, 1909; *Mining and Scientific Press*: Aug. 20, 1910; *Mining World*: May 8, 1909; Apr., 1908, Mar. 4, 1911; *Pacific Coast Miner:* Apr., 1903; Redlands *Citrograph*: May 3, 1902; San Bernardino County *Sun*: Aug. 7, 1910; Oct. 10, 1911; San Bernardino *Evening Transcript:* Apr. 30, 1902; Salt Lake *Mining Review*: Apr. 30, 1909; San Francisco *Call*: Apr. 14, 1912

Geology and stratigraphy of mineral occurrences in the Bristol and Old Dad Mountains, San Bernardino County, California

Gregg Wilkerson
yosoygeologo@gmail.com

In the Bristol and Old Dad Mountains there are 91 mineral occurrences (MRSD database of the U.S. Geological Survey, 2011). A study area that includes these mines is illustrated in Figure 1 and a generalized geologic map of this study area is given in Figure 2. A geologic mosaic of the Bristol and Old Dad Mountains and a stratigraphic compilation for this mosaic are at:

Geologic Mosaic: https://www.academia.edu/31563585/Geologic_Mosaic_of_the_Bristol_and_Old_Dad_Mountains_San_Bernardino_County_California

This map is compiled from Jennings and others (1962), Hewett (1956), Keith (2002), Redford (2003), Dibblee, 2008a, 2008b and 2008c, Bedford and others (2006) and Kumpfer and Basset (1962). This mosaic is designed for plotting on Arch E (36" x 43") size paper.

Stratigraphic Compilation: https://www.academia.edu/s/fcc88741e3/stratigraphic-compilation-for-the-bristol-and-old-dad-mountainsxlsx?source=link

An ArcGIS map package for the mosaic can be downloaded from http://vredenburgh.org/gw/pdf/DS2017

A map showing the locations of the 91 mine locations that is designed for plotting on Arch E (36" x 43") size paper is found at: https://www.academia.edu/s/f1902781ba/mines-and-mineral-occurances-of-the-bristol-and-old-dad-mountains-san-bernardino-county-california?source=link

Of the 91 mine in the study area, 36 are classified by USGS as occurrences, 30 as prospects, 14 as past producers, 3 as producers, and 5 deposits of unknown status.

Table 1 is a list of mineral occurrences with mineral commodities, surface host rocks, and grade ranges (if reported).

Table 2 is an alphabetic listing of the 91 mines and mineral occurrences in the Bristol and Old Dad Mountains with commodity, development status, references, PLSS-TRS, and latitude/longitude information.

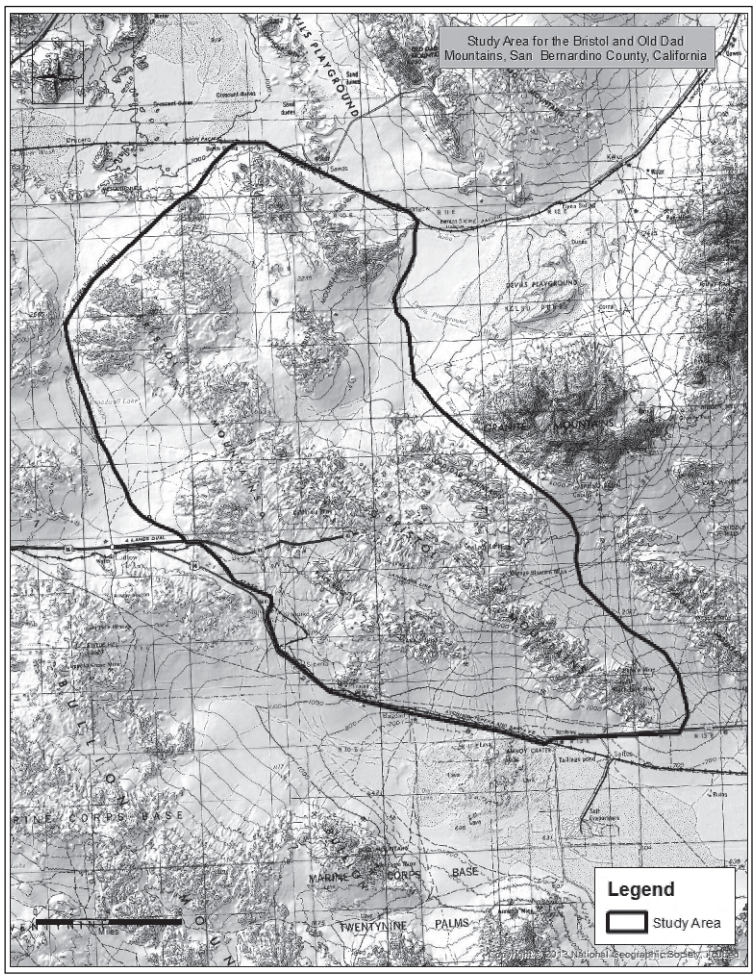

Reports for the named mines and mineral occurrences in Table 1 can be downloaded from : https://www.academia.edu/s/f1902781ba/mines-and-mineral-occurances-of-the-bristol-and-old-dad-mountains-san-bernardino-county-california?source=link

Reports for the mines and mineral occurrences identified by name in Table 1 are found on Academia.edu at the URL's listed in Table 3.

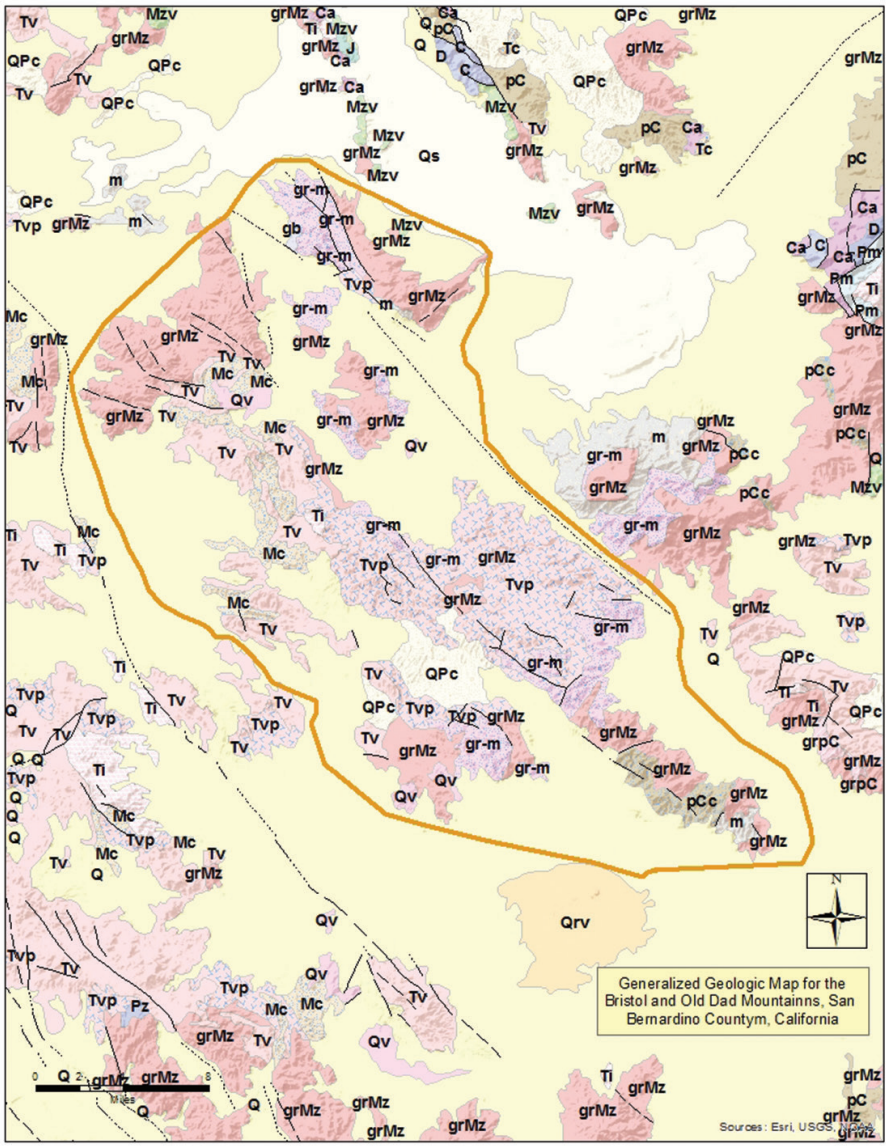

Legend

- Q Quaternary; alluvium, lake, playa, and terrace deposits
- Qs Quaternary; marine and nonmarine sand deposits
- Qls Quaternary; nonmarine, landslides
- Qg Quaternary; nonmarine, glacial till and moraines
- Qrv Quaternary-Recent; volcanic flow rocks
- Qrvp Quaternary-Recent; volcanic pyroclastic and mudflow deposits
- Qv Quaternary; volcanic flow rocks
- Qv? Quaternary; volcanic flow rocks (uncertain correlation)
- Qvp Quaternary; pyroclastic and volcanic mudflow deposits
- Qvp? Quaternary; pyroclastic deposits (uncertain correlation)
- Tv Tertiary; volcanic flow rocks
- Tvp Tertiary; pyroclastic and volcanic mudflow deposits
- Ti Tertiary; shallow intrusive rocks
- grCz Tertiary; granitic plutonic rocks
- grCz? Tertiary; granitic plutonic rocks (uncertain correlation)
- P Pliocene; marine sandstone, shale, siltstone, conglomerate
- QPc Pleistocene - Pliocene; nonmarine sandstone, shale, gravel
- M Miocene; marine sandstone, shale, siltstone, conglomerate
- M? Miocene; marine sedimentary rocks (uncertain correlation)
- Mc Miocene; nonmarine sandstone, shale, conglomerate
- Tc Tertiary; nonmarine sandstone, shale, conglomerate
- O Oligocene; marine sandstone, shale, siltstone, conglomerate
- Oc? Oligocene; nonmarine sedimentary rocks (uncertain correlation)
- Oc Oligocene; nonmarine sandstone, shale, conglomerate
- E Eocene; marine sandstone, shale, siltstone, conglomerate
- Ec Eocene; nonmarine shale, sandstone, conglomerate
- Ep Paleocene; marine sandstone, shale, siltstone, conglomerate
- E-Ep Eocene - Paleocene; marine sedimentary rocks
- TK Tertiary-Cretaceous; marine sedimentary and metasediment rocks
- gr undated granitic rocks
- grMz Mesozoic; granite, quartz monzonite
- grMz? Mesozoic; granite, quartz monzonite (uncertain correlation)
- gb Mesozoic; gabbro and dioritic rocks
- um Mesozoic; ultramafic rocks
- gr-m Mesozoic-Precambrian; granitic and metamorphic rocks
- ls Mesozoic-Paleozoic; limestone, dolomite and marble
- sch Mesozoic-Paleozoic; schist
- m pre-Cenozoic; metasedimentary and metavolcanic rock
- Mzv Mesozoic; volcanic and metavolcanic rocks
- mv pre-Cenozoic; metavolcanic rocks
- K Cretaceous; marine sedimentary rocks
- K? Cretaceous; marine sedimentary rocks (uncertain correlation)
- Ku-Ep Paleocene - upper Cretaceous; marine sedimentary rocks
- Ku? Upper Cretaceous; marine sedimentary and metasediment rocks (uncertain correlation)
- Ku Upper Cretaceous; marine sedimentary and metasediment rocks
- Kl Lower Cretaceous; marine sedimentary and metasediment rocks
- Kl? Lower Cretaceous; marine sedimentary rocks (uncertain correlation)
- KJf Cretaceous - Jurassic: Franciscan Complex - shale, chert, limestone
- KJfm Cretaceous - Jurassic: Franciscan Complex melange
- M+KJfs Miocene marine sedimentary rocks & Cretaceous - Jurassic: Franciscan Complex schist
- KJfs Cretaceous - Jurassic: Franciscan Complex schist, blueschist
- J Jurassic; marine sedimentary and metasediment rocks
- J? Jurassic; marine sedimnetary rocks (uncertain correlation)
- Tr Triassic; marine sedimentary and metasediment rocks
- grPz Paleozoic and Permo-Triassic; granitic rocks
- Pz Paleozoic; metasedimentary rocks
- Pzv Paleozoic; metavolcanic rocks
- Pm Permian; marine sedimentary and metasediment rocks
- C Carboniferous; marine sedimentary and metasediment rocks
- D Devonian; Marine sedimentary and metasediment rocks
- SO Silurian-ordovician; marine sedimentary and metasediment rocks
- Ca Cambrian; marine sedimentary and metasediment rocks
- pC pre-Cambrian; marine sedimentary and metasediment rocks
- pCc Precambrian; igneous and metamorphic rocks
- grpC Pre-Cambrian; granite, syenite, anorthosite
- grpC? Pre-Cambrian; granite, syenite, anorthosite (uncertain correlation)
- Water

Table 1

Commodity	No. of" deposits	Significant deposits	Surface host rock (see Geologic Mosaic)	Grade range (if reported)
Barite-Barium	5	Kit Fox	"pl" = Pre-Tertiary light colored plutonic rocks; "gr" = Mesozoic granite; "Qa" Quaternary deposits (as placers); "Ta"= Oligocene-Miocene andesite	
Bentonite	1	Siberia Clay Prospect	"Qoa" = Older alluvium lakebed deposit	
"Calcium, Gypsum-Anhydrite"	1	Bristol Dry Lake (formerly National Chloride Co. of America; Hollar Chemical Co.; and Saline Products Co.)	"Qoa" = Older alluvium lakebed deposit	Lime (CaO)= 28.1%
				Sulphur trioxide (SO8)= 34.9%
				Water driven off at 60° C.= 00.8%
				Water driven off at 300° C.= 05.2%
				Chlorine (Cl) = 01.4%
				Iron oxide (Fe2 03) = 01.0%
"Chromium, Molybdenum"	1	Unnamed Chromium Occurrence	"ml"= Crystalline limestone; "pl"= light colored plutonic rocks; Pre-Tertiary	
Clay	1	Siberia Clay Prospect	Lakebed deposit in "Qoa" = Older alluvium; Quaternary	
Copper	19	"NW Windy Point, Gold Coin, Orange Blossom, Hercules"	"pm"= Undifferentiated plutonic and metamorphic rocks: Pre-Tertiary; "m"= Undifferentiated metamorphic rocks: Pre-Tertiary; "Qa"= Alluvium; "QTh" = High Gravels: "QTt"= Tuff: Quaternary	
Dolomite-Magnesite	3	"E. Amboy Dolomite, Allison Garnet"	"ml"= Crystalline limestone: Pre-Tertiary	
Garnet	1	Allison Garnet	"ml"= Crystalline limestone: Pre-Tertiary	
Gold	15	"Billy Boy, Rainbow Lode, Sunrise, Hercules, Orange Blossom"	"m"= Undifferentiated metamorphic rocks; "ml"= Crystalline limestone; "pm"= Undifferentiated plutonic and metamorphic rocks; "pl"= light colored plutonic rocks: Pre-Tertiary; "Qoa"= Older Alluvium: Quaernary.	1.7 oz/ton (Orange Blossom)0.9 oz/Ton (Rainbow)
Iron	7	"Black Jack, Iron Hat"	"pm"= Undifferentiated plutonic and metamorphic rocks; "ml"= Crystalline limestone: Pre-Tertiary	"59-60% Fe, 0.12% Ti, 0.030-0.316% S, and 0.017-0.019% P, 4.9 % silica"
Lead	1	Golden Eagle	"pm"= Undifferentiated plutonic: Pre-Tertiary	
Limestone	3	Snowcap	"ml"= Crystalline limestone; "pm"= Undifferentiated plutonic and metamorphic rocks: Pre-Tertiary	
Manganese	2	"Reinerth Prospect, Incas Manganese Mine"	""QTvg"= gravels and pyroclastic rocks, tuffaceous sandstone and tuff: Tertiary or Quaternary ; "gr"= granite: Mesozoic"	Gold=0.02 oz/ton

continues

Table 1 (continued)

				Silver=5.2 oz/ton
				Manganese =23.9 percent
Onyx	1	"Reinerth Prospect, Ribbon Rock"	""QTvg"= gravels and pyroclastic rocks, tuffaceous sandstone and tuff; "QTuv"= Undifferentiated volcanic rocks: Tertiary or Quaternary "	
Perlite	22	"Unnamed Prospect, Glassy Rock Perlite"	"Tb"= basalt: Oligocene-Miocene	
			"Tif"= intrusive felsite: Miocene	
			"Tpf"= perlite: Miocene	
Pumice	3	Dish Hill Volcanic Cinders	"Qb"= basalt: Quaternary	
Sand and Gravel	2	Unnamed Locations	"Qoa" = Older alluvium; Quaternary; "QTuv"= Undifferentiated volcanic rocks: Tertiary or Quaternary	
Uranium	1	Hope Mine	"pl"= light colored plutonic rocks; Pre-Tertiary	
Zinc	1	Unnamed Occurrence	"hd"= hornblende diorite: "gr"=granite; Mesozoic	

Table 2.

Site name	Commodity	Status	References	PLSS-TRS	Latitude	Longitude
Allison Garnet	Garnet	Occurrence	"{Deposit:: CALIF. JOUR. MINES AND GEOL., V. 49, 1953, TABULATED LIST,} {Deposit:: P. 174.}"	6N 13E Sec. 30 SBM	34.58062000040	-115.66303000000
Amboy Iron Deposits	Iron	Occurrence	"{Deposit:: WRIGHT, L.A., ET AL 1953: MINES AND MINERAL RESOURCES SAN BERNARDINO; CA. JOUR. MINES AND GEOLOGY, VOL. 49, NOS. 1 & 2, P. 87-90}{Reserve-Resource:: WRIGHT, L.A. ET AL, 1953, P. 90}"	6N 12E Sec. 07 SBM	34.61862999960	-115.76278000000

continues

Table 2 (continued)

Amboy Iron Deposits	Iron	Prospect	"{Deposit:: CALIF. JOUR. MINES AND GEOL., V. 49, 1953, P. 87-88.}{Deposit:: SOUTHERN PACIFIC CO., 1964, MINERALS FOR INDUSTRY,}{Deposit:: VOL. III - SOUTHERN CALIFORNIA: P. 131.}{Deposit:: THE LOCATEIONS GIVEN IN THE ABOVE REFERENCES DO NOT AGREE.}"	6N 12E Sec. 17 SBM	34.61391999980	-115.74974000000
Billie Boy	Gold	Past Producer	"SOUTHERN PACIFIC COMPANY, 1964, MINERALS FOR INDUSTRY, SOUTHERN CALIFORNIA, V. 3, P. 11"	6N 10E Sec. 05 SBM	34.64445999990	-115.96973000000
Billie Boy Claim	Gold	Prospect	"{Deposit:: SOUTHERN PACIFIC CO., 1964, MINERALS FOR INDUSTRY,} {Deposit:: VOL. III - SOUTHERN CALIFORNIA: P. 116.}"	6N 10E Sec. 05 SBM	34.64442000030	-115.96974000000
Black Jack	Iron	Past Producer	"{Deposit:: MINERALS FOR INDUSTRY-SOUTHERN CALIFORNIA, 1964: SOUTHERN PACIFIC CO., VOL. III, P. 131}{Deposit:: WRIGHT, L.A. ET AL, 1953: MINES AND MINERAL RESOURCES SAN BERNARDINO; CA. JOUR. MINES AND GEOLOGY, VOL. 49, NOS. 1 & 2, P. 91-93.}"	6N 13E Sec. 30 SBM	34.58363000010	-115.65972000000
Black Jack Deposit	Iron	Prospect	"{Deposit:: CALIF. JOUR. MINES AND GEOL., V. 49, 1953, P. 91-93.}{Deposit:: SOUTHERN PACIFIC CO., 1964, MINERAL FOR INDUSTRY,}{Deposit:: VOL. III - SOUTHERN CALIFORNIA: P. 131.}"	6N 13E Sec. 30 SBM	34.58442000030	-115.66193000000

continues

Table 2 (continued)

Bonner	Copper	Prospect	"{Deposit:: SOUTHERN PACIFIC CO., 1964, MINERALS FOR INDUSTRY,} {Deposit:: VOL. III - SOUTHERN CALIFORNIA: P. 106.}"	9N 8E Sec. 10 SBM	34.89220999990	-116.13365000000
Bristol Dry Lake Pit	"Calcium, Gypsum-Anhydrite"	Producer	"{Deposit:: HESS, F.L., 1910, A RECONNAISSANCE OF THE GYPSUM DEPOSITS OF}{Deposit:: CALIFORNIA: USGS BULL. 413, P. 25-27.}{Deposit:: CLOUDMAN, H.C. AND OTHERS, 1919: REPORT 15 OF THE STATE}{Deposit:: -897.}{Deposit:: HERN PACIFIC CO, SAN STONE, R.W. AND O"	6N 12E Sec. 27 SBM	34.57502000020	-115.72054000000
Chalmers	"Dolomite, Magnesite"	Prospect	"{Deposit:: CALIF. JOUR. MINES AND GEOL., V. 49, 1953, TABULATED LIST,} {Deposit:: P. 152.} {Deposit:: SOUTHERN PACIFIC CO., 1964, MINERALS FOR INDUSTRY, VOL. III-}{Deposit:: SOUTHERN CALIFORNIA, P. 162-163.}"	6N 13E Sec. 29 SBM	34.58442000040	-115.64913000000
Dish Hill Volcanic Cinders	Pumice	Past Producer	"CALIF. JOUR. MINES AND GEOL., V. 49, 1953, P. 187."	6N 10E Sec. 16 SBM	34.61002000020	-115.94474000000
E. Amboy Dolomite	"Dolomite, Magnesite"	Occurrence		6N 13E Sec. 31 SBM	34.56671999970	-115.65833000000
Elsie Prospect	Gold	Prospect		6N 10E Sec. 05 SBM	34.64391999970	-115.96254000000
Glassy Rock Perlite	Perlite	Past Producer	"{Deposit:: CALIF. JOUR. MINES AND GEOL., V. 49, 1953, P. 187-188.}{Deposit:: SOUTHERN PACIFIC CO., 1964, MINERALS FOR INDUSTRY}{Deposit:: VOL. II - SOUTHERN CALIFORNIA: P. 179.}"	8N 10E Sec. 33 SBM	34.73752000020	-115.95144000000

continues

Table 2 (continued)

Gold Coin	"Copper, Au, Ag"	Past Producer	"{Deposit:: WRIGHT, L. A., ETAL, 1953 , MINES AND MINERAL DEPOSITS, SAN BERNARDINO COUNTY; CALIF. JOUR. MINES AND GEOLOGY, VOL. 49 , NO. 1 & 2 ; DIV. OF MINES, P. 17 (AP.}{Production:: WRIGHT, L. A., 1953 , P. 17 (AP.) (SEE REF.)}"	7N 11E Sec. 24 SBM	34.68696000010	-115.78584000000
Golden Eagle	Lead	Occurrence	"CALIF. DIV. MINES BULLETIN 144, 1948, P. 306."	6N 12E Sec. 22 SBM	34.60281999990	-115.72304000000
Hercules	"Copper, Gold"	Past Producer	"{Deposit:: TUCKER, W. B. AND SAMPSON, R. J., 1931 , LOS ANGELES FIELD DIVISION; 27TH REPT. STATE MINERALOGIST; CALIF. MIN. BUR., P. 273} {Deposit:: WRIGHT, L. A., ETAL, 1953 , MINES AND MINERAL DEPOSITS, SAN BERNARDINO COUNTY; CALIF. JOUR. MINES AND GEOL"	7N 11E Sec. 17 SBM	34.69835000040	-115.85834000000
Hercules	"Gold, Copper"	Past Producer	"{Deposit:: CALIF. JOUR. MINES AND GEOL., V. 49, 1953, TABULATED LIST,} {Deposit:: NO. 32, P. 12.}{Deposit:: SOUTHERN PACIFIC CO., 1964, MINERALS FOR INDUSTRY,}{Deposit:: VOL. III - SOUTHERN CALIFORNIA: P. 118.}"	7N 11E Sec. 08 SBM	34.71172000000	-115.85274000000
Home	"Copper, Gold"	Occurrence	"WRIGHT, L. A., ETAL, 1953 , MINES AND MINERAL DEPOSITS, SAN BERNARDINO COUNTY; CALIF. JOUR. MINES AND GEOLOGY, VOL. 49 , NO. 1 & 2 ; DIV. OF MINES, P. 12 (AP."	7N 11E Sec. 07 SBM	34.71223999990	-115.87612000000

continues

Table 2 (continued)

Home	Copper	Prospect	"{Deposit:: CALIF. DIV. MINES REPORT, V. 27, 1931, P. 273.} {Deposit:: CALIF. JOUR. MINES AND GEOL., V. 49, 1953, TABULATED LIST,} {Deposit:: P. 12.}{Deposit:: SOUTHERN PACIFIC CO., 1964, MINERALS FOR INDUSTRY,}{Deposit:: VOL. III - SOUTHERN CALIFORNIA: P."	7N 11E Sec. 07 SBM	34.71172000040	-115.87524000000
Hope Mine	Uranium	Occurrence	"{Deposit:: MINOBRAS, 1978, URANIUM DEPOSITS OF ARIZONA-CALIFORNIA-}{Deposit:: NEVADA: P. 91.}"	6N 13E Sec. 18 SBM	34.60611999960	-115.66643000000
Iron Hat	Iron	Producer	{Deposit:: CALIF JOUR MINES & GEOL V.49 NOS 1&2 JAN-APRIL 1953 PP95-6}{Deposit:: BULL. 129 P99;USGS QUAD CADIZ CAL.1956 & CJMG V 49 NO 1 PL 1}	6N 11E Sec. 19 SBM	34.59945999990	-115.88334000000
Jack Frost	"Limestone, General"	Occurrence	"{Deposit:: SOUTHERN PACIFIC CO., 1964, MINERALS FOR INDUSTRY, VOL. III-}{Deposit:: SOUTHERN CALIFORNIA, P. 175.}"	6N 12E Sec. 26 SBM	34.58442000010	-115.69303000000
Kit Fox	Barium-Barite	Prospect	"{Deposit:: CALIF. DIV. MINES AND GEOL. OPEN-FILE REPORT 88-3, 1988,} {Deposit:: NO. 2, APPENDIX A AND PLATE 2.}"	9N 10E Sec. 34 SBM	34.82941999980	-115.91804000000
Lady Lou	Copper	Occurrence	"{Deposit:: AUBURY, L. E., 1908 , COPPER RESOURCES OF CALIFORNIA BULL. 50 ; CALIF. MIN. BUR., P. 340} {Deposit:: WRIGHT, L. A., ETAL, 1953 , MINES AND MINERAL DEPOSITS, SAN BERNARDINO COUNTY; CALIF. JOUR. MINES AND GEOLOGY, VOL. 49 , NO. 1 & 2 ; DIV. OF MI"	7N 11E Sec. 11 SBM	34.70696000040	-115.81001000000

continues

Table 2 (continued)

Lady Lou	"Copper, Gold"	Occurrence	"{Deposit:: CALIF. JOUR. MINES AND GEOL., V. 49, 1953, TABULATED LIST,} {Deposit:: NO. 40, P. 14.}{Deposit:: SOUTHERN PACIFIC CO., 1964, MINERALS FOR INDUSTRY,}{Deposit:: VOL. III - SOUTHERN CALIFORNIA: P. 105.}"	7N 11E Sec. 11 SBM	34.71172000020	-115.80644000000
Nw Windy Point	Copper	Producer		6N 12E Sec. 13 SBM	34.61031999980	-115.68303000000
Orange Blossom	"Copper, Gold"	Prospect	"{Deposit:: CALIF. JOUR. MINES AND GEOL., V. 49, 1953, TABULATED LIST,} {Deposit:: NO. 46, P. 17.}{Deposit:: SOUTHERN PACIFIC CO., 1964, MINERALS FOR INDUSTRY,}{Deposit:: VOL. III - SOUTHERN CALIFORNIA: P. 105.}"	7N 11E Sec. 24 SBM	34.68672000030	-115.78614000000
Propane Tank Prospect	"Gold, Coper"	Prospect		7N 12E Sec. 30 SBM	34.66892000010	-115.77754000000
Pumping Station Prospect	"Gold, Silver, Copper"	Prospect		7N 11E Sec. 26 SBM	34.66642000010	-115.80444000000
Rainbow Lode	Gold	Prospect	"{Deposit:: SOUTHERN PACIFIC CO., 1964, MINERALS FOR INDUSTRY,} {Deposit:: VOL. III - SOUTHERN CALIFORNIA: P. 118.}"	7N 11E Sec. 25 SBM	34.66672000010	-115.78554000000
Rainbow Lode	Gold	Past Producer	"SOUTHERN PACIFIC COMPANY, 1964, MINERALS FOR INDUSTRY, SOUTHERN CALIFORNIA, V. 3, P. 11"	7N 11E Sec. 25 SBM	34.66835000030	-115.78028000000
Reinerth Prospect	Manganese	Past Producer	"CALIF. DIV. MINES BULLETIN 152, 1950, P. 206."	8N 9E Sec. 10 SBM	34.79781999970	-116.02025000000
Ribbon Rock	Semiprecious Gemstone	Prospect	"{Deposit:: CALIF. JOUR. MINES AND GEOL., V. 49, 1953, TABULATED LIST,} {Deposit:: P. 141.} {Deposit:: SOUTHERN PACIFIC CO., 1964, MINERALS FOR INDUSTRY,} {Deposit:: VOL. III - SOUTHERN CALIFORNIA: P. 189.}"	8N 10E Sec. 08 SBM	34.79691999970	-115.96664000000

continues

Table 2 (continued)

Santischi Perlite	Perlite	Prospect	"{Deposit:: CALIF. DIV. MINES AND GEOL., V. 49, 1953, TABULATED LIST,} {Deposit:: P. 163.} {Deposit:: SOUTHERN PACIFIC CO., 1964, MINERALS FOR INDUSTRY,} {Deposit:: VOL. III - SOUTHERN CALIFORNIA: P. 179.}"	7N 11E Sec. 09 SBM	34.71251999990	-115.83894000000
Siberia Clay Prospect	Bentonite	Occurrence	"RAPP, J.S., AND VREDENBURGH, L.M., 1992, INDUSTRIAL MINERAL RESOURCE POTENTIAL OF TERTIARY PLAYA DEPOSITS OF THE FORT IRWIN AREA, SAN BERNARDINO COUNTY, CALIFORNIA: SOCIETY FOR MINING, METALLURGY, AND EXPLORATION, INC. PREPRINT NUMBER 92-44, 9 P"	7N 9E Sec. 09 SBM	34.71669000010	-116.05085000000
Siberia Deposit	Clay	Prospect	"{Deposit:: CALIF. JOUR. MINES AND GEOL., V. 39, 1943, P. 512.} {Deposit:: CALIF. JOUR. MINES AND GEOL., V. 49, 1953, TABULATED LIST,} {Deposit:: P. 139.} {Deposit:: SOUTHERN PACIFIC CO., 1964, MINERALS FOR INDUSTRY,} {Deposit:: VOL. III - SOUTHERN CALIFORNIA"	7N 9E Sec. 04 SBM	34.72722000010	-116.04975000000
Silver Creator Placer	Barium-Barite	Prospect		6N 12E Sec. 30 SBM	34.57502000040	-115.76754000000
Snowcap	"Limestone, General, Dolomite"	Prospect	"{Deposit:: CALIF. JOUR. MINES AND GEOL., V. 49, 1953, TABULATED LIST,} {Deposit:: NO. 459, P. 156.}{Deposit:: SOUTHERN PACIFIC CO., 1964, MINERALS FOR INDUSTRY,}{Deposit:: VOL. III - SOUTHERN CALIFORNIA: P. 171.}"	6N 13E Sec. 30 SBM	34.58082000030	-115.66583000000

continues

Table 2 (continued)

Sunrise	Gold	Past Producer	"SOUTHERN PACIFIC COMPANY, 1964, MINERALS FOR INDUSTRY, SOUTHERN CALIFORNIA, V. 3, P. 11"	7N 12E Sec. 18 SBM	34.70029999970	-115.76862000000
Sunrise	"Gold, Copper"	Prospect	"{Deposit:: SOUTHERN PACIFIC CO., 1964, MINERALS FOR INDUSTRY, VOL. III}{Deposit:: - SOUTHERN CALIFORNIA: P. 118.}"	7N 12E Sec. 18 SBM	34.70031999960	-115.76864000000
Unnamed	Gold	Past Producer	"SOUTHERN PACIFIC COMPANY, 1964, MINERALS FOR INDUSTRY, SOUTHERN CALIFORNIA, V. 3, P. 12"	10N 9E Sec. 23 SBM	34.94000999980	-116.00446000100
Unnamed Barite Prospect	Barium-Barite	Prospect	"{Deposit:: SOUTHERN PACIFIC CO., 1964, MINERALS FOR INDUSTRY,} {Deposit:: VOL. III - SOUTHERN CALIFORNIA: P. 160.}"	11N 10E Sec. 33 SBM	34.99361000020	-115.92473999900
Unnamed Dolomite Occurrence	"Dolomite, Magnesite"	Occurrence	"{Deposit:: SOUTHERN PACIFIC CO., 1964, MINERALS FOR INDUSTRY, VOL. III-}{Deposit:: SOUTHERN CALIFORNIA, P. 171.}"	6N 12E Sec. 25 SBM	34.58111999970	-115.67893000000
Unnamed Iron Occurrence	Iron	Occurrence	"{Deposit:: SOUTHERN PACIFIC CO., 1964, MINERALS FOR INDUSTRY,} {Deposit:: VOL. III - SOUTHERN CALIFORNIA: P. 134.}"	10N 10E Sec. 06 SBM	34.98330999980	-115.96945000000
Unnamed Limestone Occurrence	"Limestone, General"	Occurrence	"{Deposit:: SOUTHERN PACIFIC CO., 1964, MINERALS FOR INDUSTRY, VOL. III-}{Deposit:: SOUTHERN CALIFORNIA, P. 177.}"	7N 12E Sec. 05 SBM	34.72641999980	-115.74004000000
Unnamed Location	Perlite	Unknown	LETTER 1/21/57 MIN DEPT BRANCH W/ OPEN FILE REPT ON MOJAVE D	10N 10E Sec. 14 SBM	34.95781000020	-115.90304000000
Unnamed Location	Zinc	Unknown	LETTER 1/21/57 MIN DEPT BRANCH W OPEN FILE REPT ON MOJAVE DE	10N 8E Sec. 24 SBM	34.94531000010	-116.09085000000

continues

Table 2 (continued)

Unnamed Location	Pumice	Unknown	LETTER 1/21/57 MIN DEPT BRANCH W OPEN FILE REPT ON MOJAVE DE	9N 8E Sec. 17 SBM	34.87310999990	-116.16305000000
Unnamed Location	"Sand and Gravel, Construction"	Unknown	LETTER 1/21/57 MIN IND DEPT BRANCHW/ OPEN FILE ON MOJAVE	8N 10E Sec. 20 SBM	34.76831999960	-115.96194000000
Unnamed Location	"Sand and Gravel, Construction"	Unknown	LETTER OF 1/21/57 MIN DEPT BRANCH W/OPEN FILE REPT ON MOJAVE	7N 9E Sec. 12 SBM	34.71192000000	-115.99944000000
Unnamed Location	Perlite	Occurrence	LETTER OF 1/21/57 MIN DEPT BRANCH W/OPEN FILE REPT ON MOJAVE	8N 10E Sec. 25 SBM	34.75561999990	-115.89113999900
Unnamed Mine	Gold	Past Producer		6N 13E Sec. 32 SBM	34.56811999960	-115.65113000000
Unnamed Mineral Occurrence	"Chromium, Molybdenum"	Occurrence		8N 10E Sec. 24 SBM	34.76891999960	-115.89894000000
Unnamed Occurrence	Iron	Occurrence	"MINERALS FOR INDUSTRY-SOUTHERN CALIFORNIA, 1964: SOUTHERN PACIFIC CO., VOL. III, P. 13"	10N 10E Sec. 06 SBM	34.98362000010	-115.97085000000
Unnamed Occurrence	"Copper, Ag, Au"	Occurrence	"{Deposit:: SOUTHERN PACIFIC CO., 1964, MINERALS FOR INDUSTRY,} {Deposit:: VOL. III - SOUTHERN CALIFORNIA: P. 111.}"	10N 8E Sec. 13 SBM	34.95560999980	-116.09665000000
Unnamed Perlite Occurrence	Perlite	Occurrence	"{Deposit:: SOUTHERN PACIFIC CO., 1964, MINERALS FOR INDUSTRY,} {Deposit:: VOL. III - SOUTHERN CALIFORNIA: P. 180.}"	8N 10E Sec. 17 SBM	34.78312000010	-115.96164000000
Unnamed Perlite Occurrence	Perlite	Occurrence	"{Deposit:: SOUTHERN PACIFIC CO., 1964, MINERALS FOR INDUSTRY, VOL. III-}{Deposit:: SOUTHERN CALIFORNIA, P. 180.}"	8N 10E Sec. 26 SBM	34.75442000030	-115.90974000000
Unnamed Perlite Occurrence	Perlite	Occurrence	"{Deposit:: SOUTHERN PACIFIC CO., 1964, MINERALS FOR INDUSTRY, VOL. III-}{Deposit:: SOUTHERN CALIFORNIA, P. 180.}"	8N 10E Sec. 35 SBM	34.74031999950	-115.91024000000

continues

Table 2 (continued)

Unnamed Perlite Occurrence	Perlite	Occurrence	"{Deposit:: SOUTHERN PACIFIC CO., 1964, MINERALS FOR INDUSTRY, VOL. III-}{Deposit:: SOUTHERN CALIFORNIA, P. 180.}"	8N 10E Sec. 34 SBM	34.74001999960	-115.92724000000
Unnamed Perlite Occurrence	Perlite	Occurrence	"{Deposit:: SOUTHERN PACIFIC CO., 1964, MINERALS FOR INDUSTRY,} {Deposit:: VOL. III - SOUTHERN CALIFORNIA: P. 180.}"	7N 11E Sec. 01 SBM	34.72581999960	-115.78774000000
Unnamed Perlite Occurrence	Perlite	Occurrence	"{Deposit:: SOUTHERN PACIFIC CO., 1964, MINERALS FOR INDUSTRY, VOL. III-}{Deposit:: SOUTHERN CALIFORNIA, P. 180.}"	8N 9E Sec. 25 SBM	34.75442000040	-115.98274000000
Unnamed Perlite Occurrence	Perlite	Occurrence	"{Deposit:: SOUTHERN PACIFIC CO., 1964, MINERALS FOR INDUSTRY,} {Deposit:: VOL. III - SOUTHERN CALIFORNIA: P. 180.}"	8N 10E Sec. 27 SBM	34.75861999960	-115.92644000100
Unnamed Perlite Occurrence	Perlite	Occurrence	"{Deposit:: SOUTHERN PACIFIC CO., 1964, MINERALS FOR INDUSTRY,} {Deposit:: VOL. III - SOUTHERN CALIFORNIA: P. 180.}"	8N 11E Sec. 32 SBM	34.74171999970	-115.85914000000
Unnamed Perlite Occurrence	Perlite	Occurrence	"{Deposit:: SOUTHERN PACIFIC CO., 1964, MINERALS FOR INDUSTRY, VOL. III-}{Deposit:: SOUTHERN CALIFORNIA, P. 180.}"	8N 11E Sec. 36 SBM	34.74061999970	-115.78864000000
Unnamed Perlite Occurrence	Perlite	Occurrence	"{Deposit:: SOUTHERN PACIFIC CO., 1964, MINERALS FOR INDUSTRY, VOL. III-}{Deposit:: SOUTHERN CALIFORNIA, P. 180.}"	8N 9E Sec. 11 SBM	34.79172000040	-116.00505000000
Unnamed Perlite Occurrence	Perlite	Occurrence	"{Deposit:: SOUTHERN PACIFIC CO., 1964, MINERALS FOR INDUSTRY,} {Deposit:: VOL. III - SOUTHERN CALIFORNIA: P. 180.}"	9N 8E Sec. 13 SBM	34.86751000000	-116.09725000000

continues

Table 2 (continued)

Unnamed Perlite Occurrence	Perlite	Occurrence	"{Deposit:: SOUTHERN PACIFIC CO., 1964, MINERALS FOR INDUSTRY,} {Deposit:: VOL. III - SOUTHERN CALIFORNIA: MAP III.}"	7N 9E Sec. 02 SBM	34.72722000000	-116.01554000000
Unnamed Perlite Occurrence	Perlite	Occurrence	"{Deposit:: SOUTHERN PACIFIC CO., 1964, MINERALS FOR INDUSTRY, VOL. III-}{Deposit:: SOUTHERN CALIFORNIA, P. 180.}"	7N 11E Sec. 05 SBM	34.72781999960	-115.85804000000
Unnamed Perlite Occurrence	Perlite	Occurrence	"{Deposit:: SOUTHERN PACIFIC CO., 1964, MINERALS FOR INDUSTRY, VOL. III-}{Deposit:: SOUTHERN CALIFORNIA, P. 180.}"	8N 11E Sec. 30 SBM	34.75532000050	-115.87504000000
Unnamed Perlite Occurrence	Perlite	Occurrence	"{Deposit:: SOUTHERN PACIFIC CO., 1964, MINERALS FOR INDUSTRY,} {Deposit:: VOL. III - SOUTHERN CALIFORNIA: P. 180.}"	8N 11E Sec. 31 SBM	34.74141999960	-115.87444000000
Unnamed Perlite Occurrence	Perlite	Occurrence	"{Deposit:: SOUTHERN PACIFIC CO., 1964, MINERALS FOR INDUSTRY, VOL. III-}{Deposit:: SOUTHERN CALIFORNIA, P. 180.}"	8N 11E Sec. 18 SBM	34.78442000000	-115.87584000000
Unnamed Perlite Occurrence	Perlite	Occurrence	"{Deposit:: SOUTHERN PACIFIC CO., 1964, MINERALS FOR INDUSTRY, VOL. III-}{Deposit:: SOUTHERN CALIFORNIA, P. 180.}"	8N 10E Sec. 36 SBM	34.74032000020	-115.89224000000
Unnamed Perlite Occurrences	Perlite	Occurrence	"{Deposit:: SOUTHERN PACIFIC CO., 1964, MINERALS FOR INDUSTRY, VOL. III-}{Deposit:: SOUTHERN CALIFORNIA, P. 180.}"	7N 10E Sec. 02 SBM	34.72531999970	-115.91024000000
Unnamed Prospect	Barium-Barite	Prospect		9N 8E Sec. 22 SBM	34.86251000030	-116.12525000000
Unnamed Prospect	Tungsten	Prospect	"{Deposit:: SOUTHERN PACIFIC CO., 1964, MINERALS FOR INDUSTRY, VOL. III-}{Deposit:: SOUTHERN CALIFORNIA, P. 152.}"	7N 12E Sec. 05 SBM	34.72221999990	-115.74414000000

continues

Table 2 (continued)

Unnamed Prospect	Barium-Barite	Prospect		9N 8E Sec. 17 SBM	34.87311000040	-116.16414999900
Unnamed Prospect	"Copper, Au"	Prospect	"{Deposit:: U.S. GEOLOGICAL SURVEY MISC. GEOL. INVESTIGATIONS MAP I-478,}{Deposit:: 1967, TEXT, P. 3.}"	10N 9E Sec. 02 SBM	34.98331000030	-116.00945000000
Unnamed Prospect	"Gold, Copper"	Prospect	"{Deposit:: SOUTHERN PACIFIC CO.,M 1964, MINERALS FOR INDUSTRY,}{Deposit:: VOL. III - SOUTHERN CALIFORNIA: P. 124.}{Deposit:: CALIF. DIV. MINES AND GEOL. OPEN-FILE REPORT 88-3, 1988,}{Deposit:: NO. 1, APPENDIX A, P. 39, AND PLATE 2.}"	10N 9E Sec. 23 SBM	34.94061000020	-116.00445000000
Unnamed Prospect	Gold	Prospect		6N 13E Sec. 31 SBM	34.57112000020	-115.67193000000
Unnamed Prospect	Copper	Prospect	"{Deposit:: SOUTHERN PACIFIC CO., 1964, MINERALS FOR INDUSTRY,}{Deposit:: VOL. III - SOUTHERN CALIFORNIA: P. 105.}"	7N 11E Sec. 23 SBM	34.67892000000	-115.80024000000
Unnamed Prospect	"Copper, Gold"	Prospect	"{Deposit:: U.S. GEOLOGICAL SURVEY MISC. GEOL. INVESTIGATIONS MAP I-478,}{Deposit:: 1967, TEXT, P. 3.}"	9N 8E Sec. 15 SBM	34.87500999990	-116.13255000000
Unnamed Prospect	Gold	Prospect		6N 13E Sec. 32 SBM	34.57251999990	-115.65052999900
Unnamed Prospect	Copper	Prospect	"{Deposit:: SOUTHERN PACIFIC CO., 1964, MINERALS FOR INDUSTRY,}{Deposit:: VOL. III - SOUTHERN CALIFORNIA: P. 105.}"	7N 11E Sec. 23 SBM	34.68192000040	-115.80554000000
Unnamed Prospect	Perlite	Past Producer	"{Deposit:: U.S. GEOLOGICAL SURVEY MISC. GEOL. IVESTIGATIONS MAP I-478,}{Deposit:: 1967, TEXT, P. 3.}"	9N 8E Sec. 24 SBM	34.86000999990	-116.09665000000

continues

Table 2 (continued)

Unnamed Prospect	"Silver, Gold, Manganese"	Prospect	"{Deposit:: SOUTHERN PACIFIC CO., 1964, MINERALS FOR INDUSTRY,} {Deposit:: VOL. III - SOUTHERN CALIFORNIA: P. 144.}"	9N 8E Sec. 09 SBM	34.88940999990	-116.14115000000
Unnamed Prospect	Copper	Prospect	"{Deposit:: U.S. GEOLOGICAL SURVEY MISC. GEOL. INVESTIGATIONS MAP I-478,}{Deposit:: 1967, TEXT, P. 3.}"	10N 9E Sec. 02 SBM	34.98310999960	-116.00945000000
Unnamed Volcanic Cinder Occurrence	Pumice	Occurrence	"{Deposit:: SOUTHERN PACIFIC CO., 1964, MINERALS FOR INDUSTRY,} {Deposit:: VOL. III - SOUTHERN CALIFORNIA: P. 182.}"	6N 10E Sec. 11 SBM	34.62471999960	-115.90894000000
Windy Point Shaft	Copper	Prospect		6N 13E Sec. 18 SBM	34.61471999990	-115.66613000000
Winifred Group	"Copper, Gold"	Past Producer	"{Deposit:: WRIGHT, L. A., ETAL, 1953 , MINES AND MINERAL DEPOSITS, SAN BERNARDINO COUNTY; CALIF. JOUR. MINES AND GEOLOGY, VOL. 49 , NO. 1 & 2 ; DIV. OF MINES, P. 22 (AP.}{Production:: WRIGHT, L. A., 1953 , P. 22 (AP)}"	7N 11E Sec. 29 SBM	34.66696000030	-115.86584000000
Winifred Group	"Copper, Gold"	Past Producer	"{Deposit:: CALIF. JOUR. MINES AND GEOL., V. 49, 1953, TABULATED LIST,} {Deposit:: NO. 58, P. 22.}"	7N 11E Sec. 29 SBM	34.66811999980	-115.85914000000

Table 3

MINE NAME	URL
Allison Garnet	https://www.academia.edu/s/23d6c340be/allison-garnet-occurrence-bristol-mountains-san-bernardino-county-california?source=link
Amboy Iron Deposits	https://www.academia.edu/s/eefd9e6cb8/amboy-iron-mines-bristol-mountains-san-bernardino-county-california?source=link
Billy Boy Gold Mine	https://www.academia.edu/s/7875163d6a/billy-boy-gold-mine-bristol-mountains-san-bernardino-county-california?source=link
Black Jack Iron	https://www.academia.edu/s/64d11ad965/black-jack-iron-mine-bristol-mountains-san-bernardino-county-california?source=link
Bristol Dry Lake Gypsum-Anhydrite	https://www.academia.edu/s/8a8e97f96e/bristol-dry-lake-calcium-gypsum-anhydrite-halite-deposit-bristol-mountains-san-bernardino-county-california?source=link
Dish Hill Volcanic Cinders	https://www.academia.edu/s/2f99bbb103/dish-hill-volcanic-cinders?source=link
Glassy Rock Perlite	https://www.academia.edu/s/6cfd0cc92b/glassy-rock-perlite-mine-bristol-mountains-san-bernardino-county-california?source=link
Golden Eagle Lead	https://www.academia.edu/s/c876adbb68/golden-eagle-lead-mine-bristol-mountains-san-bernardino-county-california?source=link
Hercules Cu-Au	https://www.academia.edu/s/28cbf65ae9/hercules-au-cu-mine-bristol-mountains-san-bernardino-county-california?source=link
Hope Uranium	https://www.academia.edu/s/20a0ffc767/hope-uranium-prospect-bristol-mountains-san-bernardino-county-california?source=link
Inca Manganese	https://www.academia.edu/s/575c645bb2/incas-magnesium-mine-bristol-mountains-san-bernardino-county-california?source=link
Kit Fox Barite Prospect	https://www.academia.edu/s/0dc5756fb7/kit-fox-barite-mine-bristol-mountains-san-bernardino-county-california?source=link
NW Windy Point Copper	https://www.academia.edu/s/d36fce920a/nw-windy-point-copper-mine-bristol-mountains-san-bernardino-county-california?source=link
Orange Blossom and Gold Con Mines	https://www.academia.edu/s/955a6dfd37/orange-blossom-and-gold-coin-cu-au-ag-mine?source=link
Rainbow Lode Gold	https://www.academia.edu/s/b4d3662503/rainbow-lode-mine-bristol-mountains-san-bernardino-county-california?source=link
Reinerth Prospect	https://www.academia.edu/s/5d4688dcd4/reinerth-prospect-bristol-mountains-san-bernardino-county-california?source=link
Ribbon Rock Onyx	https://www.academia.edu/s/f688dc1541/ribbon-rock-onyx-mine-bristol-mountains-san-bernardino-county-california?source=link
Siberian Clay Prospect	https://www.academia.edu/s/d47af20e54/siberia-clay-prospects-bristol-mountains-san-bernardino-county-california?source=link
Snowcap Limestone	https://www.academia.edu/s/b3e033a4ca/snowcap-limestone-occurrence-bristol-mountains-san-bernardino-county-california?source=lin
Sunrise Au-Cu	https://www.academia.edu/s/d4dae27744/sunrise-gold-mine-bristol-mountains-san-bernardino-county-california?source=link
Unnamed Chromium Occurrence	https://www.academia.edu/s/9b93f74edb/unnamed-chromium-occurrence-bristol-mountains-san-bernardino-county-california?source=link
Unnamed Perlite Mine	https://www.academia.edu/s/fc48f6d3e0/unnamed-perlite-mine-bristol-mountains-san-bernardino-county-california?source=link
Unnamed Sand and Gravel Deposit 01	https://www.academia.edu/s/d3a1317af2/unnamed-sand-and-gravel-deposit-no-1-bristol-mountains-san-bernardino-county-california?source=link
Unnamed Sand and Gravel Deposit 02	https://www.academia.edu/s/ad9f17157a/unnamed-sand-and-gravel-deposit-no-2-bristol-mountains-san-bernardino-county-california?source=link
Unnamed Zinc	https://www.academia.edu/s/c5a16a8d49/unnamed-zinc-prospect-bristol-mountains-san-bernardino-county-california?source=link
Geology and Mineral Occurrences of the Bristol and Old Dad Mountains	https://www.academia.edu/s/8ca8ef641c/geology-and-mineral-occurrences-of-the-bristol-and-old-dad-mountains-san-bernardino-county-california-text?source=link

References and bibiliography

Bedford, David R., David M. Miller, and Geoff A. Phelps, 2006, Preliminary Surficial Geologic Map of the Amboy 30 x 60 Minute Quadrangle, California, U.S. Geological Survey, Open File Report 2006-1165, Sheet 1 of 1.

Dibblee, Thomas W. Jr., 1967, Geologic Map of the Broadwell Lake Quadrangle, San Bernardino County, California, U.S. Geological Survey, Miscellaneous Geological Investigations, Map I-478.

Dibblee, Thomas W., Jr., 2008a, Geologic Map of the Alvord Mountain and Cave Mountain 15 Minute Quadrangles, San Bernardino County, California, Dibblee Foundation Map #DF-395.

Dibblee, Thomas W., Jr., 2008b, Geologic Map of the Broadwell Lake 15 Minute Quadrangle, San Bernardino County, California, Dibblee Foundation Map #DF-395.

Dibblee, Thomas W., Jr., 2008c, Geologic Map of the Deadman Lake and Lead Mountain 15 Minute Quadrangles, San Bernardino County, California, Dibblee Foundation Map #DF-388..

Dibblee, Thomas W., Jr., 2008d, Geologic Map of the Ludlow and Bagdad 15 Minute Quadrangles, San Bernardino County, California, Dibblee Foundation Map #DF-396.

Fox, L.K. and Miller, D.M., 1990, Jurassic granitoids and related rocks of the southern Bristol Mountains, southern Providence Mountains, and Colton Hills, Mojave Desert, California: Geological Society of America, Memoir 174, scale 1:312,500.

Hewett, D. F., 1956, Geologic Map and Sections of the Ivanpah Quadrangle, California-Nevada, in Geology and Mineral Resources of the Ivanpah Quadrangle California-Nevada, U.S. Geological Survey, Professional Paper 275, Plate 1.

Howard, Keith A., 2002, Geologic Map of the Sheep Hole Mountains 30' x 60' Quadrangle, San Bernardino and Riverside Counties, California, Miscellaneous Field Studies MF-2344, Sheet 1 of 2.

Jennings, Charles W., John L. Burnett and Bennie W. Troxel, 1962, Trona Sheet, Geologic Map of California, Olaf P. Jenkins Edition, California Division of Mines and Geology.

Kumpfer, Donald H. and Allen M. Basset, 1956,U.S. Geological Survey, Preliminary geologic map of part of the southeastern Mojave Desert, California: U.S. Geological Survey, Open-File Report OF-56-74, scale 1:120,000.

Kumpfer, Donald H. and Allen M. Basset, 1962, Reconnaissance Map of Part of the Mojave Desert, California, in "A Geologic Reconnaissance of the Southeastern Mojave Desert", California Division of Mines and Geology Special Report 83 and U.S. Geological Survey Mineral Investigations Field Studies Map MF-205 scale 1:125K.

Penhoel, L ., 1951, Lillian and Magnetite Mine, Bristol Mountains, California, Private report, 1951. Cited by Wright and others, 195, p. 87.

Rapp, J.S., and L.M. Vredenburgh, 1992, Industrial Mineral Resource Potential of Tertiary Playa Deposits of the Fort Erwin Area, San Bernardino County, California, Society for Mining and Metallurgy and Exploration Inc., Preprint No. 92-44, 9p.

Redford, David R., 2003, Surficial and Bedrock Geological Database of the Kelso 7.5 Minute Quadrangle, San Bernardino, California, U.S. Geological Survey, Open File Report OF 03-501.

Redford, David R., David M. Miller and Geoff A Phelps, 2006, Preliminary Surficial Geologic Map an Database of the Amboy 30x60 Minute Quadrangle, California, U.S. Geological Survey, Open File Report 2006-1165.

Southern Pacific Company, 1964, Minerals for Industry, Volume III – Southern California, California Division of Mines and Geology, Special Report 95, 242 pages plus maps. The data in this report is based on geologic maps Southern Pacific produced pre-1964 covering two townships each. These maps create a mosaic of township geologic maps throughout much of the Mojave Desert.

Tucker, W.B. and R.J.S. Sampson, 1943, Mineral Resources of San Bernardino County, California Journal of Mines and Geology, v. 39, n. 2, p. 247-549, pl. 7.

Wright, Lauren A., Richard M. Stewart, Thomas E. Gay, Jr., and George C. Hazenbush, 1953, Mines and Mineral Deposits of San Bernardino County, California, California Journal of Mines and Geology, v. 49, 192 pages plus maps.

Daggett—the town history forgot

Daryl Schendel
President, Daggett Historical Society, PO Box 105, Daggett CA 92327, Drs8r14@aol.com

Many travelers consider the little town of Daggett as nothing more than a bunch of rundown buildings and shacks doomed to time and negligence. No fast food, no gas, just a corridor from the I-40 to I-15 or a slow stretch along Route 66. If you blink, you will miss it, but wonder why was this town here. This town has more history than you can shake a stick at, and it is the intention of the Daggett Historical Society to bring it back to life. Our society, reincarnated after 16 years and going full steam, has 100 members and is growing. The Daggett history comes from those that either grew up or still live in town. History flows in by means of pictures, letters or oral history recordings. Every day, another piece of the puzzle falls into place and what is assumed is examined for authenticity.

During the 1880s Daggett was indeed the hub of transportation and supply for the area and tied in directly with Calico and surrounding mining areas. Following is a short list of persons and places that are each a tale in themselves. When all brought together, they bring the true story of Daggett to life.

One of the major players in Daggett was Seymour Alf and his famous 20 Mule Team Wagons. Five of the wagons are known for sure to have been built in his blacksmith shop. Should you go to the visitors center at the Borax mine in Boron, the wagons out front were built in Daggett by Seymour. Seymour not only hauled borax ore 11 miles from the mining town of Borate to Daggett, but had wagons and mules capable of moving buildings, many

Daggett, view to the west circa 1918

Daggett, 1918

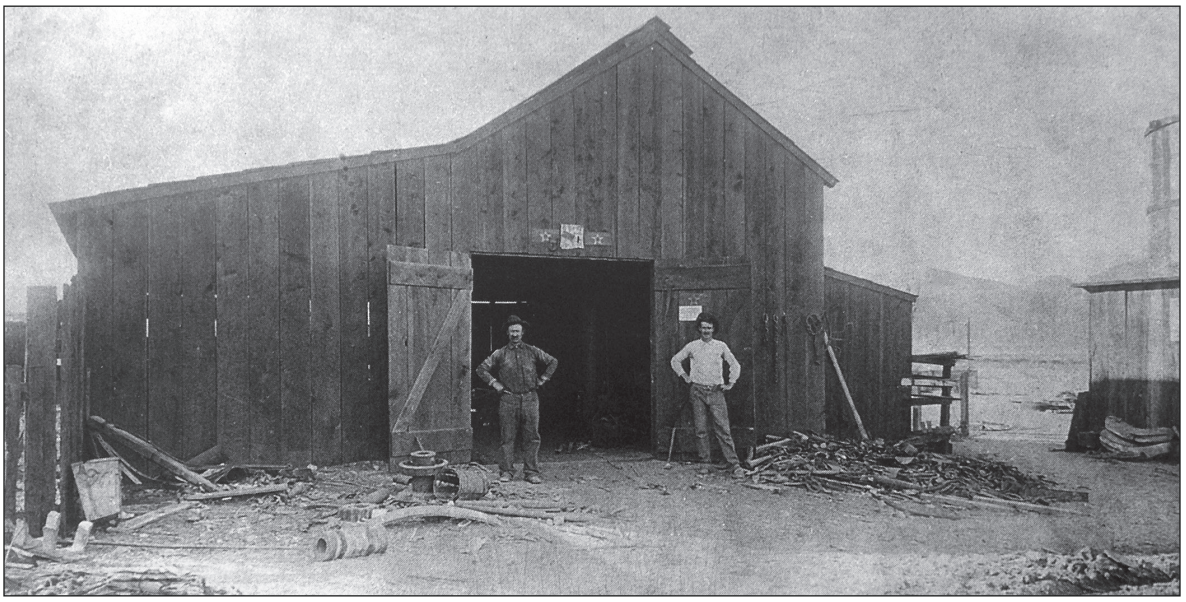

Alf's Blacksmith Shop

Table 1. Notable names in Daggett history

NAME OR LOCATION	IMPORTANCE	DATE
Mormon, Mojave and Spanish Trails	Led to Daggett	
Mojave River/Fish Ponds	Watering hole west of Daggett on Mojave Trail	1880s
Southern Pacific Railroad	Finished to Daggett	1882
Union Pacific Railroad	Took over the Los Angeles and Salt Lake Railroad running through Daggett	1921
Atlantic Pacific–Santa Fe Railroad	Arrived in Daggett	1884
Lt. Governor John Daggett	Town site of Calico Junction changed to Daggett in his honor	1883
Stone Hotel	Originally called Railroad Hotel, name changed to Stone Hotel in 1888. Active 1884–1930+	1884
Seymour Alf/Alf's Blacksmith Shop	After fire this is rebuilt and still standing	1890
Fouts Brothers Garage	Originally built as a repair roundhouse in Marion. Moved once more before its current location in 1912.	1880s
Daggett Ditch/Farming	Historic irrigation project on the Mojave River that ran 4 miles upstream to the Van Dyke Ranch	1901
Mulcahy Brothers	Early Calico miners and owners of many mining claims, including the Maggie Mine. The brothers continued mining long after the silver bust by 1907. Last Mulcahy mines were still worked in the 1980s.	1884
Death Valley Scotty	Scotty was a frequent guest at the Stone Hotel. His colorful life included working as a swamper for the 20 mule team, and a stint at railroading, but he was best known as owner of Scotty's Castle in Death Valley.	1885
Borate/20 Mule Team	Borax mines 3 miles from Calico/Alf's teams hauled	
Jonas Osborne/Osborne wagons	Respected Pioneer and mine owner. Built and patented a steam tractor and wagons to haul salt from Danby.	1893
Francis Marion Smith	The Borax King, Pacific Borax Company	
Waterloo Mill	Serviced entire Silver Valley, 60 stamps strong	
Old Dinah	Huge steam tractor used for Borax. Lasted only a year because of constant maintenance and major problems with sand and steep grades.	1894
Falconer	Saloon keeper, real estate investor, and owner of the Stone Hotel 1892–1917	1888
Marcus Pluth	Miner/mining operator who sold one of his cement claims in Victorville for a million dollars	1907
Homer/Frank Ryerson	Pioneer Meat Market; butcher & fresh meat supplier. The building is now the Desert Market	1893
Theodore and Dix Van Dyke	Well known father & son ranchers, they also served as judges in their later years	1900
Casper Sanger	Started the Oro Grande (Waterloo) mining company, major Calico Silver producer, shipped from Daggett	1884
Daggett Cemetery/250 guests since 1800s	First burials had unmarked graves. First marked grave is a 5-year-old child buried in 1888.	1860

from the Calico area. Seymour also was a road builder and his Fresnos sit at the blacksmith displaying their wear and tear. Many local roads serve as documentation of his grading skills and are still in service today.

The tools and equipment that built these wagons sit, eager to go to work, in his shop that stands tall and intact and dates back to the 1880s. To walk inside you would swear Seymour closed up the night before, after a hard day's work. In August, 2013, Lawrence (Larry) Alf passed away and the legacy of Alf's Blacksmith Shop was in jeopardy of being lost forever, or passed around for profit and gain. From 1951 to his death in 2013 Larry let no one enter, disturb, or visit this shrine to his grandfather, Seymour, not even family. For this we thank him and

now understand his thinking. As so often happens, those in charge of the estate knew very little of the history, but dollar signs prevailed and somehow fate allowed this historic site to stay intact, escaping auction.

The Daggett Historical Society is a proud owner of a wonderful museum that has been in limbo for over 16 years and I am proud to say it will soon be open to the public again. On the same note the Historical Society is now the proud owner of the famous Stone Hotel and we are actively pursuing grants and funding to secure and protect this structure. We are working hard to put Daggett back on the historical map and any contributions, whether artifacts, stories, or monetarily will be met with open arms. If nothing else, become a member of our Society and join our efforts.

Mechanisms for post-Bouse (post-5 Ma) deformation in the lower Colorado River region.

K. E. Karlstrom[1], L. Liu[2], Q Zhou[2], L.C.Crossey[1], J. Thacker[1], R. Crow[3], and L. S. Beard[3]
[1]Department of Earth and Planetary Sciences, University of New Mexico, Albuquerque, N.M. 87131; [2]Department of Geology, University of Illinois, Champaign, Ill., [3]U.S. Geological Survey, Flagstaff, Ariz,

Introduction

The Bouse Formation records the first arrival of the Colorado River to sea at the proto-Gulf of California between 5.3 and 4.8 Ma. The river was propagating downstream by basin spillover (Blackwelder, 1934; House et al. 2008) and groundwater sapping (Crossey et al., 2015) at about the same time that the Gulf of California was opening northwards (Bennett et al., 2016). Debates and continued research focus on **where** (Yuma basin or Blythe basin), **when** (5.3 or 4.8 Ma), and **how** the river met the sea. New research on the nature of any syn- and post-5 Ma deformation of the Bouse Formation in the lower Colorado River corridor is important for resolving current debates. Numerous papers use present elevations of Bouse and Bullhead outcrops to indicate near-original depositional elevations; these data then define lake geometries, lake highstands, basin paleodepths (Spencer et al., 2008; 2013; Miller et al., 2014; Pearthree and House, 2014) and geometry of Bullhead fill terrace treads (Howard et al., 2015). An alternative hypothesis is that Bouse outcrops have been significantly deformed and their original depositional elevations reflect some combination of lake levels, faulting, epeirogenic uplift, and tilting. Debates about the marine (Buising, 1990; McDougall et al., 2014, Dorsey et al., 2016; O'Connell et al., 2017) versus non-marine (Spencer and Patchett, 1997; House et al., 2008; Pearthree and House, 2014; Bright et al., 2016) depositional setting for the Bouse Formation of the Blythe basin corresponds to the deformation versus no-deformation models because Bouse elevations in Yuma are well below sea level and marine fossils and sedimentary facies within the Bouse are found at elevations of about 120 m asl in the Blythe basins (McDougal and Martinez, 2014). Complexities of incomplete preservation of Bouse and Bullhead Formations, and uncertainty about whether Pliocene sea level was 56 m below modern sea level to 39 m above it (Miller et al., 2005; Raymo et al., 2009) are important considerations for endmember marine+deformation and non-marine+no-deformation hypotheses.

This paper pursues the marine+deformation hypothesis which states that the Bouse Formation of the Yuma and lower Blythe basins was deposited near sea level in a mixed marine/estuarine depositional setting and syn- and post-5 Ma deformation have changed original Bouse depositional elevations by 100s of meters. Testing of this hypothesis is important for understanding the birth of the Colorado River system and how the 4–5 Ma Colorado River was "graded" to sea level (Howard et al., 2013; Crow et al., 2014; 2016). As shown in Figure 1, the "buzz saw" model (Karlstrom et al., 2007; 2008) applies the concept that differential incision along a "graded" continental-scale river is an indication of differential uplift, where sections that of the river that are incising faster are being uplifted relative to more slowly incising segments. The concept has caveats involving deciphering local (fault-related) versus regional (epeirogenic) differential incision (e.g. internal debate continues on whether high incision in the footwall of the Toroweap fault is the result of localized fault-related

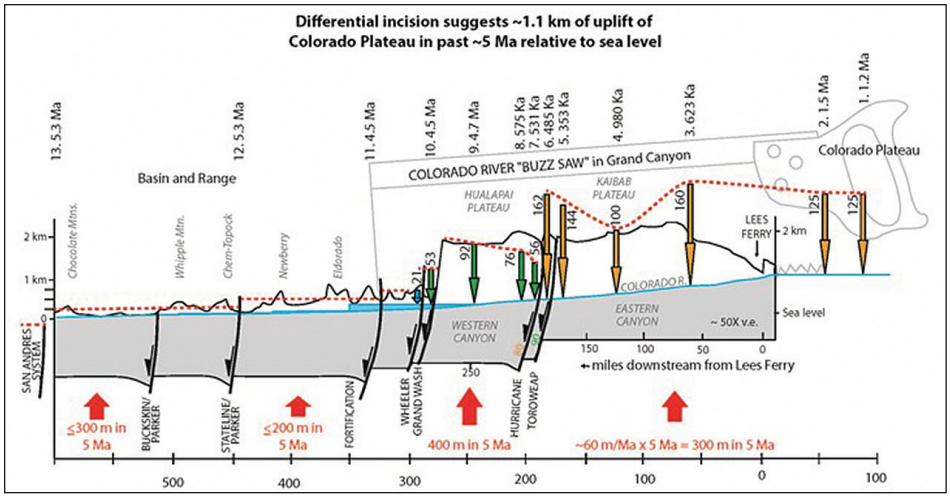

Figure 1. Buzz saw model using differential incision amounts over 5 Ma to estimate uplift of the Colorado Plateau. Numbers at top show time period of each incision constraint; different colored incision arrows and red dashed line represent variably uplifted blocks.

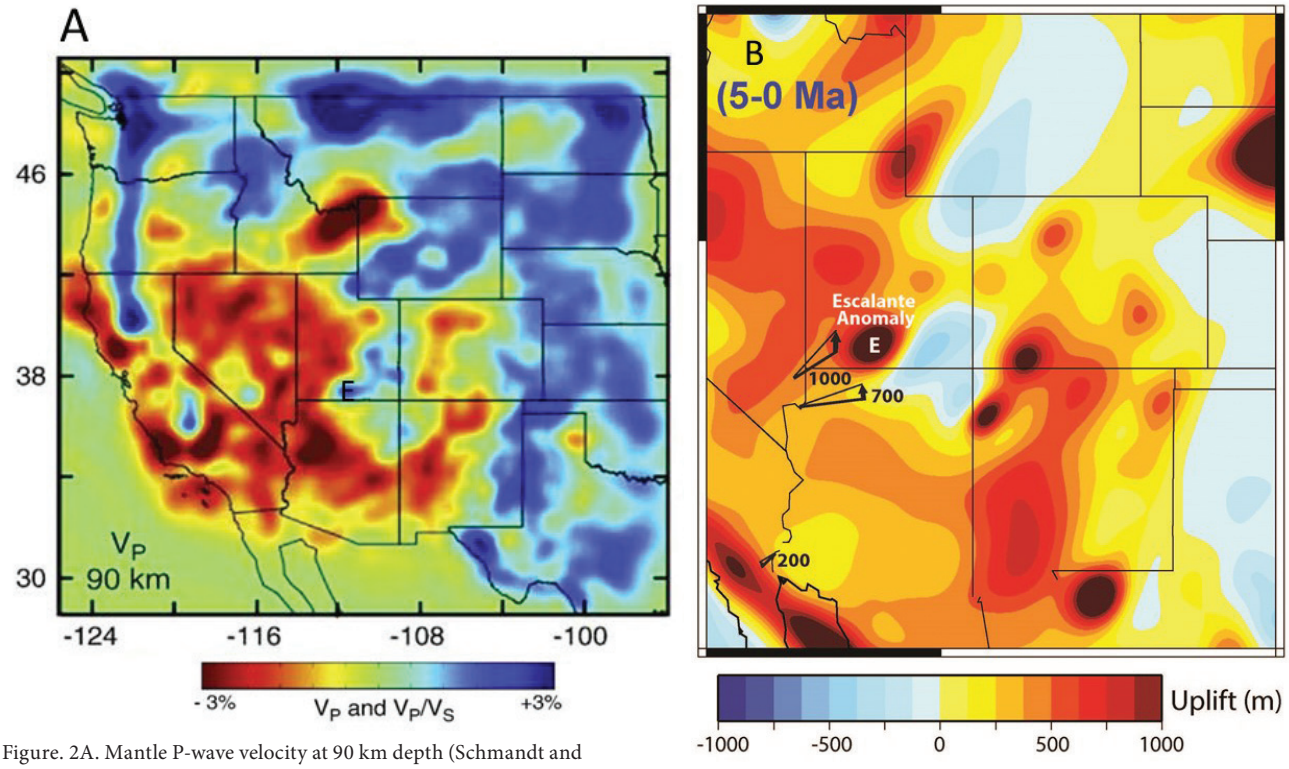

Figure. 2A. Mantle P-wave velocity at 90 km depth (Schmandt and Humphreys, 2010). 2B. Changes of dynamic topography (0-5 Ma) due to mantle flow in the last 5 Ma via a "backward flow model" where the sign of gravity is reversed. Numbers are magnitude in meters of geologically inferred differential uplift. Delamination has been postulated under the Escalante anomaly (E) as a driver of Plateau uplift (Levander et al. 2012). Tomographic model in the lower Colorado River region is near the edge of USAarray coverage and hence resolution is not as good as within the array interior.

uplift or regional block uplift), assumption of semi-steady incision for comparisons of reaches, and understanding of transient knickpoints and other geomorphic adjustments to river profiles (Darling and Whipple, 2015).

Mechanisms

Three mechanisms may have interacted to significantly modify (by 100s of m) Bouse and Bullhead outcrops relative to their original depositional elevations.

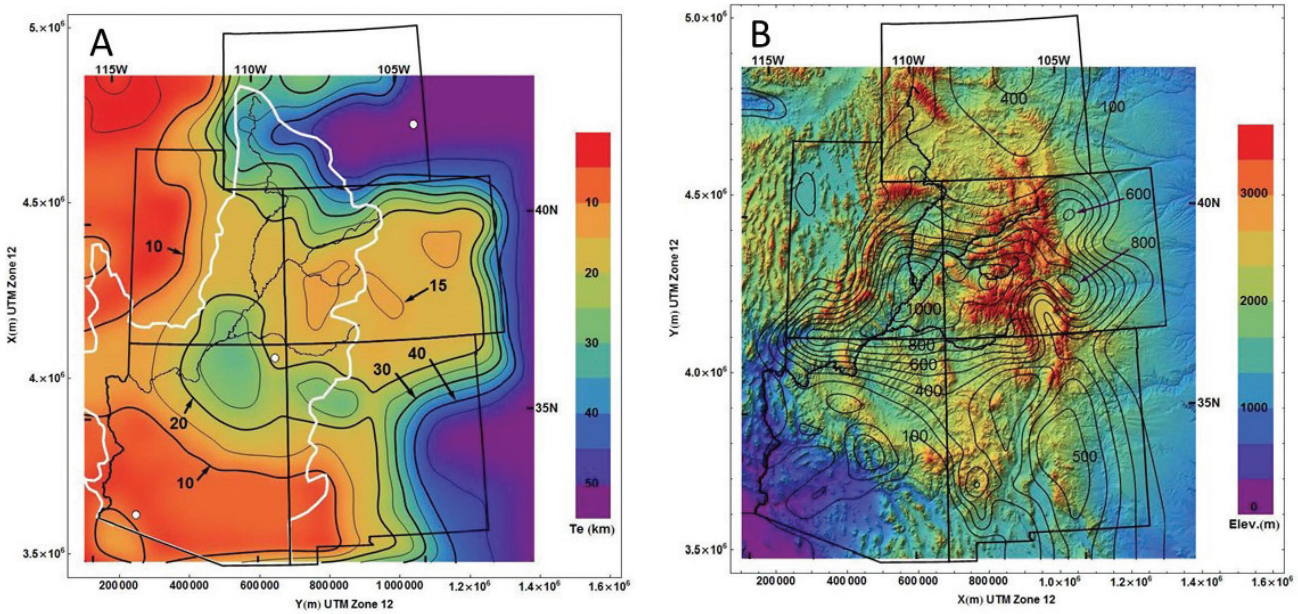

Figure 3A. Effective elastic thickness of the lithosphere (*Te*) in km (after Lowry et al., 2000); *Te* varies from <10 km in the Basin and Range to 50 km in the continental craton. White dot in SW Arizona has a isostatic response radius of about 50 km. Figure 3B. Contours of flexural isostatic uplift for the spatially variable effective elastic thickness shown in A; contour interval is 100 m (from Lazear et al., 2013).

I) Thacker et al. (this volume) propose a testable kinematic model similar to that of Bennett et al. (2016) where diffuse dextral shear related to the San Andreas plate margin and Eastern California shear zone is expressed in the lower Colorado River corridor as: NW-striking dextral strike slip fault systems (e.g. Algodones and Stateline systems), normal-slip reactivation of Miocene N-S faults (e.g. forming grabens parallel to the river that downdropped Bouse outcrops), and contractional reactivation of E-W Miocene structures with reverse faults and anticlinal upwarping (e.g Chocolate Mountains; Beard et al., 2016). Additional work to map and quantify slip on syn- and post-5 Ma structures is needed and underway (Bennett et al., 2016; Dorsey et al., 2016; Crow et al., 2016; Thacker et al., this volume; Ricketts et al., this volume).

II) Mantle velocity variations beneath western U.S (Fig. 1A; Schmandt and Humphreys, 2010) show large perturbations of seismic wave speed in the upper mantle of 6 % in VP that take place across sharp (< 100 km wide) interfaces (Karlstrom et al., 2012). Various types of geodynamic modeling efforts are underway that convert velocity to temperature, density, and viscosity. These models are faithful to global mantle flow fields and plate kinematics, including subduction of the Farallon slab (Liu, 2015). Figure 2 shows a model taken from a full western U.S. plate-scale model that uses the modern mantle flow field and runs it backwards in time ("backwards advection") for 5 Ma. We then estimate the surface responses to evolving mantle densities, such that some regions of the western U.S. are found to subside and others to uplift in the past 5 Ma. The model shows potential uplift of the Colorado Plateau above the Escalante anomaly (E) relative to the lower Colorado River corridor of about 700 m (dark red to orange), in general agreement with the buzz saw model of Figure 1. In the southern Colorado River region, it shows that mantle flow could drive uplift of the Gulf of California relative to the Blythe basin, opposite of geologic data that show Bouse Formation may have been uplifted about 150 m in the Blythe basin relative to the Yuma basin. However, the model ignores isostatic subsidence due to crustal thinning in the Gulf of Califoria which may dominate over mantle flow forces. These models are preliminary, but make an argument that mantle flow and broad epeirogenic uplift may explain significant differential surface upift/ subsidence such that it is unlikely that Bouse outcrops across the region have remained at their same depostional elevations for the past 5 Ma.

III) A third mechanism of uplift that may have contributed to change in elevation of Bouse outcrops involves isostatic rebound that accompanies differential erosion. Figure 3 illustrates this concept. Rebound modeling for differential erosion of the Colorado Plateau-Rocky Mountain region over the past 10 Ma was done by Lazear et al. (2013) based on variable elastic thickness calculations from Lowry et al. (2000). This work showed that differential rebound has shorter wavelength and higher amplitude with decreasing elastic plate thickness. The lower Colorado River corridor has 5-10 km elastic thickness such that relatively short wavelength uplift due to differential rebound is possible. The Lazear et al., (2013) models dealt with erosion of Paleozoic and Mesozoic strata from the Colorado Plateau-Rocky Mountain region and suggested minimal rebound due to this erosion in the lower Colorado River corridor.

However, a next set of isostatic models needs to consider erosion of bedrock in the jagged ranges east and west of the Colorado River (e.g. The Needles) and deposition into river-parallel basins. Assuming erosion rates of 100 m/Ma, about 500 m of bedrock in the last 5 Ma may have been eroded and redistributed in pediment fans and in lower Colorado River basins. This may help explain differential uplift/subsidence at the 100-m-scale perpendicular to the Colorado River (over length scales of 50 km) that may have modified Bouse outcrop elevations. Cross sections drawn perpendicular to the river show that Bouse outcrops are more steeply dipping than younger pediment fan surfaces. At the 10 to 100-m scale, Bouse outcrops drape across topography and this has led to the inference that the full 100s-m-scale elevation changes between the lowest parts of each basin near the Colorado river and the basin flanks can be explained due to rapid filling of a deep lake basins and deposition of Bouse carbonates as a "bathtub-like" coating as lake levels rose (Pearthree and House, 2014). An alternative hypothesis that needs examining is that some component of the 100 –m-scale variations in outcrop elevation transverse to the river may be due to variable isostatic rebound due to enhanced erosion in the ranges and deposition in the basins.

Conclusions

The relative importance of potential differential uplift mechanisms described above is unknown and requires focused fieldwork and modeling. The active neotectonic setting of this region includes: I) the San Andreas plate margin/ Eastern California shear zone (since 12 Ma), II) the dramatic variation in mantle seismic velocities that seem to require mantle flow forces and buoyancy variations with 100s- to 1000-m-scale differential surface responses, and III) differential erosion that can result in differential rebound at the 100 m vertical scale and 1 km horizontal scale. Given the neotectonic setting, it is likely that I-III all interacted and that the least likely hypothesis is that the elevations of Bouse outcrops have remained the same over the past 5 million years.

References cited

Bennett, S.E., Darin, M.H., Dorsey, R.J., Skinner, L.A., Umhoeffer, P.J., and Oskin, M.E., Animated tectonic reconstruction of the Lower Colorado River region: Implications for late Miocene to Present deformation: 2016 Desert Symposium volume, p. 73-86.

Blackwelder, E., 1934, Origin of the Colorado River: Geological Society of America Bulletin, v. 45, p. 551–566, doi:10.1130/GSAB-45-551.

Bright, J., Cohen, A.S., Dettman, D.L., Pearthree, P.A., Dorsey, R.J., and Homan, M.B., 2016, Did a catastrophic lake spillover integrate the late Miocene early Pliocene Colorado River and the Gulf of California?: Microfaunal and stable isotope evidence from Blythe basin, California-Arizona, USA. Palaios, v. 31, p. 81-91.

Buising, A. V., 1990, The Bouse Formation and bracketing units, southeastern California and western Arizona: Implications for the evolution of the proto-Gulf of California and the lower Colorado River: Journal of Geophysical Research, v. 95, p. 20111-20132.

Crossey, L.C., Karlstrom, K.E., Dorsey, R., Pearce, J., Wan, E., Beard, L.S., Asmerom, Y., Polyak, V., Crow, R.S, Cohen, A., Bright, J., Huth, 2015, The importance of groundwater in propagating downward integration of the 6-5 Ma Colorado River System: Geochemistry of springs, travertines and lacustrine carbonates of the Grand Canyon region over the past 12 million years: Geosphere, v. 11, no. 3, p. xx-, doi:10.1130/GES01073.1.

Crow, R., Karlstrom, K. E., Darling, A., Crossey, L. J., Polyak, V., Granger, D., Asmerom, Y., and Schmandt, B., 2014, Steady incision of Grand Canyon at the million-year timeframe; a case for mantle-driven differential uplift: Earth and Planetary Science Letters, v. 397, p. 159-173. doi:10.1016/j.epsl.2014.04.020.

Crow et al., 2016. Integrating lower Colorado River alluvial deposits and Grand Canyon incision constraints to reconstruct paleo Colorado River profiles and determine Colorado Plateau uplift: 2016 Desert Symposium volume.

Dorsey, R.J., O'Connell, B., Homan, M., and Howard, K., 2016, Upper Limestone of the Southern Bouse Formation: Evidence for Unsteady Origins of the Colorado River: Short Paper for 2016 Desert Symposium Volume.

House, P.K., Pearthree, P.A., and Perkins, M.E., 2008, Stratigraphic evidence for the role of lake spillover in the inception of the lower Colorado River in southern Nevada and western Arizona, in Reheis, M.C., Hershler, R., and Miller, D.M., eds., Late Cenozoic Drainage History of the Southwestern Great Basin and Lower Colorado River Region: Geologic and Biotic Perspectives: Geological Society of America Special Paper 439, p. 335–353.

Howard K.A., House, P.K., Dorsey, R.J., Pearthree, P.A., 2015, River-evolution and tectonic implications of a major Pliocene aggradation on the lower Colorado River: The Bullhead Alluvium: Geosphere, v. 11; no. 1; p. 1–30; doi:10.1130/GES01059.1.

Karlstrom, K.E., Crow, R., McIntosh, W., Peters, L., Pederson, J., Raucci, J., Crossey, L.J., Umhoefer, P., and Dunbar, N., 2007, 40Ar/39Ar and field studies of Quaternary basalts in Grand Canyon and model for carving Grand Canyon: Quantifying the interaction of river incision and normal faulting across the western edge of the Colorado Plateau: Geological Society of America Bulletin, v. 119, p. 1283–1312, doi:10.1130/0016-7606(2007)119[1283:AAFSOQ]2.0.CO;2.

Karlstrom, K.E., Crow, R, Crossey, L.J., Coblentz, D., and van Wijk, J., 2008, Model for tectonically driven incision of the less than 6 Ma Grand Canyon: Geology, v. 36, no. 11, p. 835–838, 36, doi:10.1130/G25032A.1, with Data Repository 2008218.

Karlstrom, K.E., Coblentz, D., Dueker, K., Ouimet, W., Kirby, E., Van Wijk, J., Schmandt, B., Kelley, S., Lazear, G., Crossey, L.J., Crow, R., Aslan, A, Darling*, A., Aster, R., MacCarthy*, J., Hansen, S.M., Stachnik, J., Stockli, D.F., Hoffman, M., McKeon, R., Feldman, J. Heizler, M., Donahue, M.S., and the CREST working group, 2011, Surface response to mantle convection beneath the Colorado Rocky Mountains and Colorado Plateau: Lithosphere, v. 4 p. 3-22.

Lazear, G., Karlstrom, K., Aslan, A., and Kelley, S., 2013, Denudation and flexural isostatic response of the Colorado Plateau and southern Rocky Mountains region since 10 Ma: Geosphere, v. 9, no. 4, p. 792-814. doi:10.1130/ges00836.1.

Levander, A., Schmandt, B., Miller, M. S., Liu, K., Karlstrom, K. E., Crow, R. S., Lee, C. T. A., and Humphreys, E. D., 2011, Continuing Colorado Plateau uplift by delamination; style convective lithospheric downwelling: Nature, v. 472, no. 7344, p. 461-465. doi:10.1038/nature10001.

Liu, L., 2015, The ups and downs of North America: Evaluating the role of mantle dynamic topography since the Mesozoic: Reviews of Geophysics, v. 53, no. 3, p. 1022-1049. doi:10.1002/2015rg000489.

Lowry, A.R., Ribe, N.M., and Smith, R.B., 2000, Dynamic elevation of the Cordillera, western United States: Journal of Geophysical Research, v. 105, p. 23371– 23390, doi:10.1029/2000JB900182.

McDougall, K., and Miranda Martinez, A.Y., 2014, Evidence for a marine incursion along the lower Colorado River corridor: Geosphere, v. 10, p. 828-841.

Miller, D.M., Reynolds, R.E., Bright, J.E., Starratt, S.W., 2014, Bouse Formation in the Bristol basin near Amboy, California, USA: Geosphere, v. 10, p. 462-475, doi:10.1130/GES00934.1.

Miller, K.G., Kominz, M. a, Browning, J. V, Wright, J.D., Mountain, G.S., Katz, M.E., Sugarman, P.J., Cramer, B.S., Christie-Blick, N., and Pekar, S.F., 2005, The Phanerozoic record of global sea-level change.: Science (New York, N.Y.), v. 310, no. 5752, p. 1293–1298, doi:10.1126/science.1116412.

O'Connell, Dorsey, R.J., and Humphreys, E.D., 2016, Tidal rhythmites in the southern Bouse Formation as evidence for post-Miocene uplift of the lower Colorado River corridor: Geology, v. 45, p. 99-102, DOI: 10.1130/G38608.1.

Pearthree, P.A., and House, P.K., 2014, Paleogeomorphology and evolution of the early Colorado River inferred from relationships in Mohave and Cottonwood valleys, Arizona, California, and Nevada: Geosphere, v. 10, p. 1139-1160, doi:10.1130/GES00988.1.

Raymo, M.E., Hearty, P., De Conto, R., O'Leary, M., Dowsett, H.J., Robinson, M.H., and Mitrovica, J.X., 2009, PLIOMAX: Pliocene maximum sea level project: PAGES News, v. 17, no. 2, p. 58–59, doi:10.1029/2004PA001071.

Schmandt, B. and Humphreys, E., 2010, Complex subduction and small-scale convection revealed by body-wave tomography of the western United States upper mantle: Earth and Planetary Science Letters, 297, v. 3, p. 435-445.

Spencer, J.E., and Patchett, P.J., 1997, Sr isotope evidence for a lacustrine origin for the upper Miocene to Pliocene Bouse Formation, lower Colorado River trough, and implications for timing of Colorado Plateau uplift: Geological Society of America Bulletin, v. 109, p. 767-778.

Spencer, J.E., Pearthree, P.A., and House, P.K., 2008, An evaluation of the evolution of the latest Miocene to earliest Pliocene Bouse lake system in the lower Colorado River valley, southwestern USA, in Reheis, M.C., Hershler, R., and Miller, D.M., eds., Late Cenozoic Drainage History of the Southwestern Great Basin and Lower Colorado River Region: Geologic and Biotic Perspectives: Geological Society of America Special Paper 439, p. 373–388, doi:10.1130/2008.2439(17).

Spencer, J.E., Patchett, P.J., Pearthree, P.A., and House, P.K., Sarna- Wojcicki, A.M., Wan, E., Roskowski, J.A., and Faulds, J.E., 2013, Review and analysis of the age and origin of the Pliocene Bouse Formation, lower Colorado River Valley, southwestern USA. Geosphere, v. 9, no. 3, p. 444-459.

Influence of the Eastern California Shear Zone on deposition of the Mio-Pliocene Bouse Formation: insights from the Cibola area, Arizona

Rebecca J. Dorsey[1], Brennan O'Connell[1], Mindy B. Homan[1,2], and Scott E. K. Bennett[3]
[1]*Department of Earth Sciences, University of Oregon, Eugene, Oreg. rdorsey@uoregon.edu*
[2]*Current Address: Devon Energy Corp, Oklahoma City, Okl.*
[3]*U.S. Geological Survey. Middlefield Road, Menlo Park, California, sekbennett@usgs.gov*

Introduction

The Eastern California Shear Zone (ECSZ) is a wide zone of late Cenozoic strike-slip faults and related diffuse deformation that currently accommodates ~20–25% of relative Pacific–North America plate motion in the lower Colorado River region (Fig. 1A; Dokka and Travis, 1990; Miller et al., 2001; Guest et al., 2007; Mahan et al., 2009). The ECSZ is kinematically linked southward to dextral faults in the northern Gulf of California (Bennett et al., 2016a), and it may have initiated ca. 8 Ma when major strike-slip faults developed in the northern Gulf and Salton Trough region (Bennett et al., 2016b; Darin et al., 2016; Woodburne, 2017). Thus deformation related to the ECSZ occurred in the lower Colorado River region during deposition of the Bouse Formation, which is commonly bracketed between 6.0 and 4.8 Ma (House et al., 2008; Sarna-Wojcicki et al., 2011; Spencer et al., 2013) and may be as old as 6–7 Ma in the south (McDougall and Miranda Martínez, 2014, 2016). Post-4.5 Ma broad

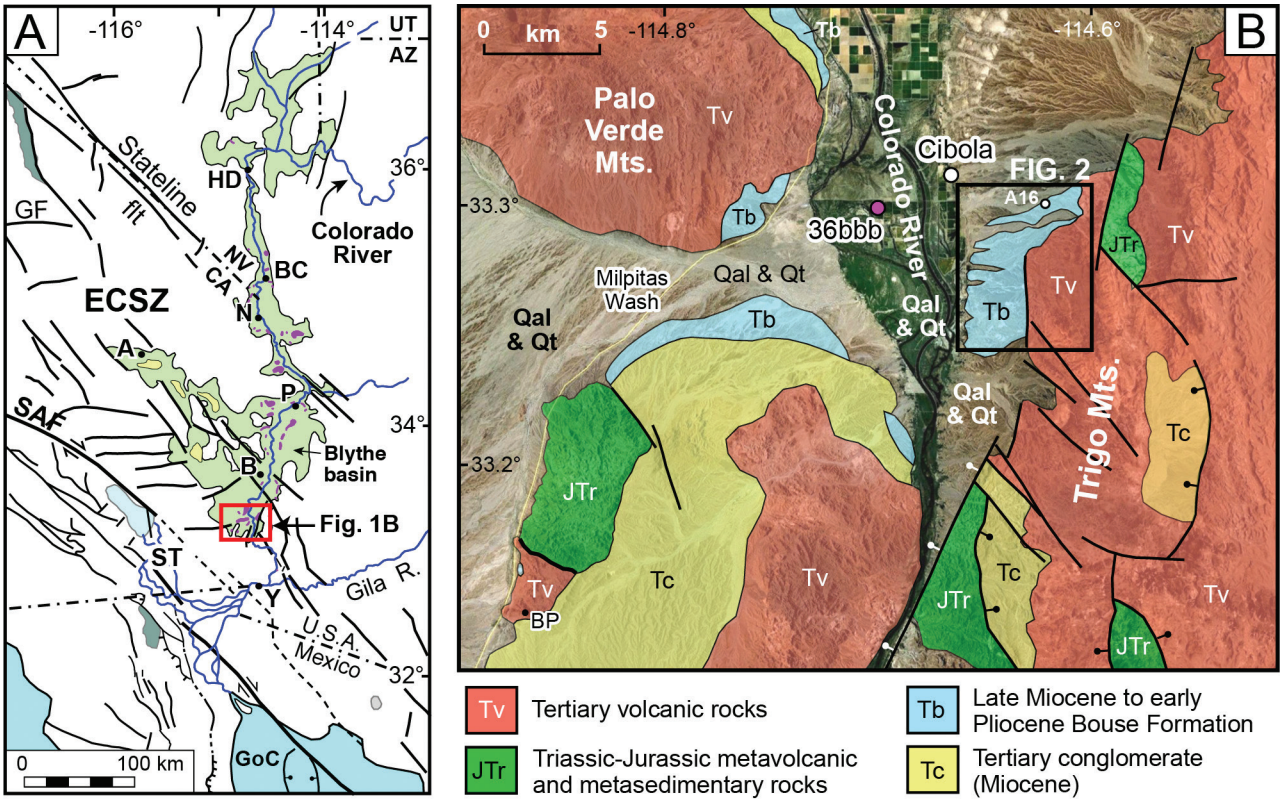

Figure 1. (A) Map of the lower Colorado River region highlighting faults, surface exposures of the Bouse Formation (purple), modern dry lakes (yellow), and inferred distribution of Bouse paleo- lakes (pale green; Spencer et al., 2008). Abbreviations: A, Amboy; B, Blythe; BC, Bullhead City; ECSZ, eastern California shear zone; GF, Garlock fault; GoC, Gulf of California; HD, Hoover Dam; N, Needles; P, Parker; SAF, San Andreas fault; ST, Salton Trough; Y, Yuma. (B) Simplified geologic map of the southern Blythe basin and surrounding ranges (compiled from Sherrod and Tosdal, 1991). BP = Buzzards Peak; 36bbb is a water well with Bouse Formation recorded to 92 m depth (Metzger et al., 1973). "Qal and Qt" is Quaternary alluvium and terrace deposits (undifferentiated).

Figure 2. Satellite image of the Cibola area showing location of measured sections and stratigraphic panels. Trace of normal fault from Homan (2014), Gootee et al. (2016), and this study. Location labels starting with "A" are sections from Homan (2014), labels starting with "B" are sections measured by B. O'Connell (unpubl. data). Location shown in Fig. 1B.

sagging is recognized along the lower Colorado River (Howard et al., 2015), but the possibility that faults of the ECSZ influenced local to regional subsidence patterns during deposition of the Bouse Formation has received little attention to date (e.g., Homan, 2014; O'Connell et al., 2016).

The Bouse Formation is a widespread sequence of late Miocene to early Pliocene deposits exposed discontinuously along the lower Colorado River corridor (Fig. 1A). In the southern Blythe basin it consists of three regionally correlative members: (1) Basal Carbonate, consisting of supratidal and intertidal mud-flat marls,

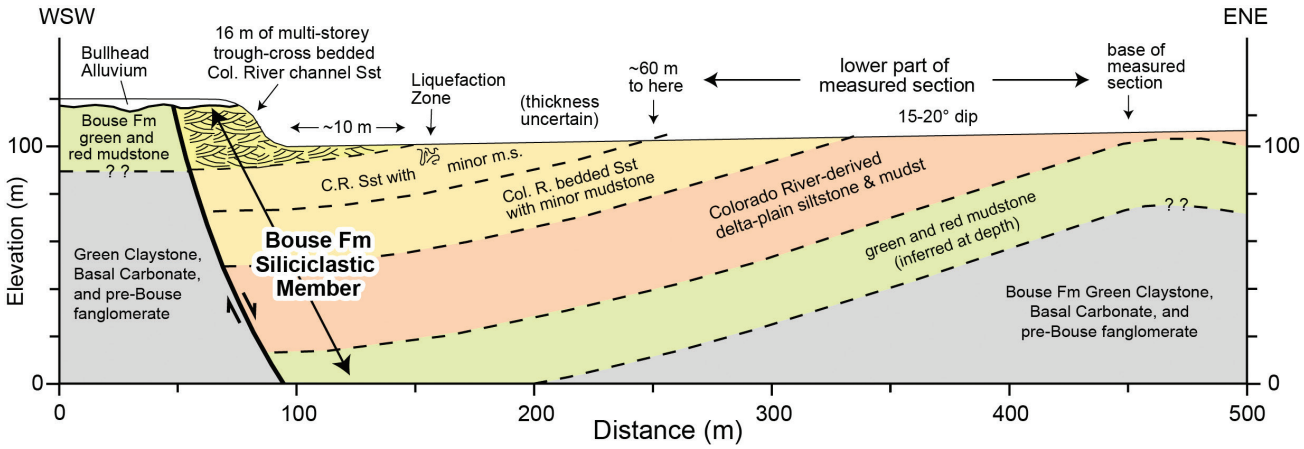

Figure 3. Geologic cross section across NE-dipping normal fault and thick hanging-wall section of Bouse Formation Colorado-River delta and channel deposits (Siliciclastic Member) in lower Hart Mine Wash. Line of section shown in Fig. 2.

intertidal and shallow subtidal bioclastic grainstone and conglomerate, and subtidal marl; (2) Siliciclastic member, consisting of Colorado River-derived green claystone, red mudstone and siltstone, and cross-bedded river channel sandstone; and (3) Upper Bioclastic member fossiliferous sandy calcarenite, coarse pebbly grainstone, and calcareous-matrix conglomerate (Homan, 2014; Dorsey et al., 2016; O'Connell et al., 2016, 2017). The southern Bouse Formation has been interpreted as recording deposition in either a lake (Spencer and Patchett, 1997; Spencer et al., 2008, 2013; Bright et al., 2016) or shallow marine setting (Buising, 1990; McDougall, 2008; McDougall and Miranda Martínez, 2014; O'Connell et al., 2017).

In this paper we summarize key results from five field seasons of detailed stratigraphic analysis south of Cibola, Ariz. (. 1). The data reveal systematic stratal thinning and thickening, pinch-outs, and wedging patterns in the Bouse Formation that we conclude were produced by syn-depositional tilting in response to growth of normal faults near the eastern margin of the basin. Similar stratal patterns in other nearby areas suggest widespread structural controls on deposition of the Bouse Formation. A palinspastic reconstruction of the lower Colorado River region at 5 Ma, modified from Bennett et al. (2016), provides insight to regional fault geometries in the ECSZ that may have controlled syn-depositional tilting and subsidence in Bouse depocenters shortly prior to and during initiation of the Colorado River.

Results

The Bouse Formation is well exposed in modern washes southeast of Cibola, Ariz. (Fig. 1B). Figure 2 shows the map distribution of Bouse Formation carbonate units, location of measured sections, and transects used to construct two stratigraphic panels. In the southern and central part of the map area, the Bouse Formation is truncated on the east by a steeply (60–70°) west-dipping normal fault (Homan, 2014; Gootee et al., 2016; this study). In western Hart Mine Wash a well exposed *northeast*-dipping normal fault cuts ~80–100 m of SW-dipping Colorado River siltstone, mudstone and sandstone in the hanging wall (Figs. 2, 3). This fault is located along-strike northwest of the west-dipping normal fault (Fig. 2), but it is not known if the two fault exposures are the same fault or two separate faults. In either case, the along-strike change in fault strike, dip, and sense of offset suggests a component of strike-slip motion on the fault in this area. This fault and hanging-wall deposits are unconformably capped by Bullhead Alluvium, and the section contains an interval of convolute bedding and large-scale liquefaction features that are typical of earthquake-induced seismites (Fig. 3).

Figure 4 shows two detailed stratigraphic panels that were constructed by correlating measured sections using laterally continuous stratigraphic contacts. Stratal architecture in the panels is restored to its original geometry by hanging units from reliable stratigraphic datums that we infer to represent paleo-horizontal surfaces based on the overall fine grain size and low energy of the deposits (e.g., Homan, 2014; O'Connell et al., 2017). In the Marl Wash panel, the base of the upper fanglomerate (Tfg2 in Fig. 4B) likely was deposited with a gentle west dip at the margin of a fan delta that prograded into the standing body of water recorded by the Bouse Upper Bioclastic member. Since we do not know *a-priori* the primary dip on the base of Tfg2, we also assign this datum a horizontal original dip, a choice that does not noticeably affect the resulting stratal architecture or structural interpretations.

The Hart Mine Wash panel (Fig. 4A) reveals a thin carbonate platform in the east represented by Bouse basal bioclastic limestone, and a gently west-tilted monocline defined by systematic westward thickening and wedging of the Basal Carbonate and green claystone of the Siliciclastic member. Units are inferred to thicken westward into the subsurface using the same angle of thickening that we document with surface exposures of lower bioclastic limestone and green claystone. The queried fault at depth is suggested as a possible control on the observed stratal thickening and wedging patterns.

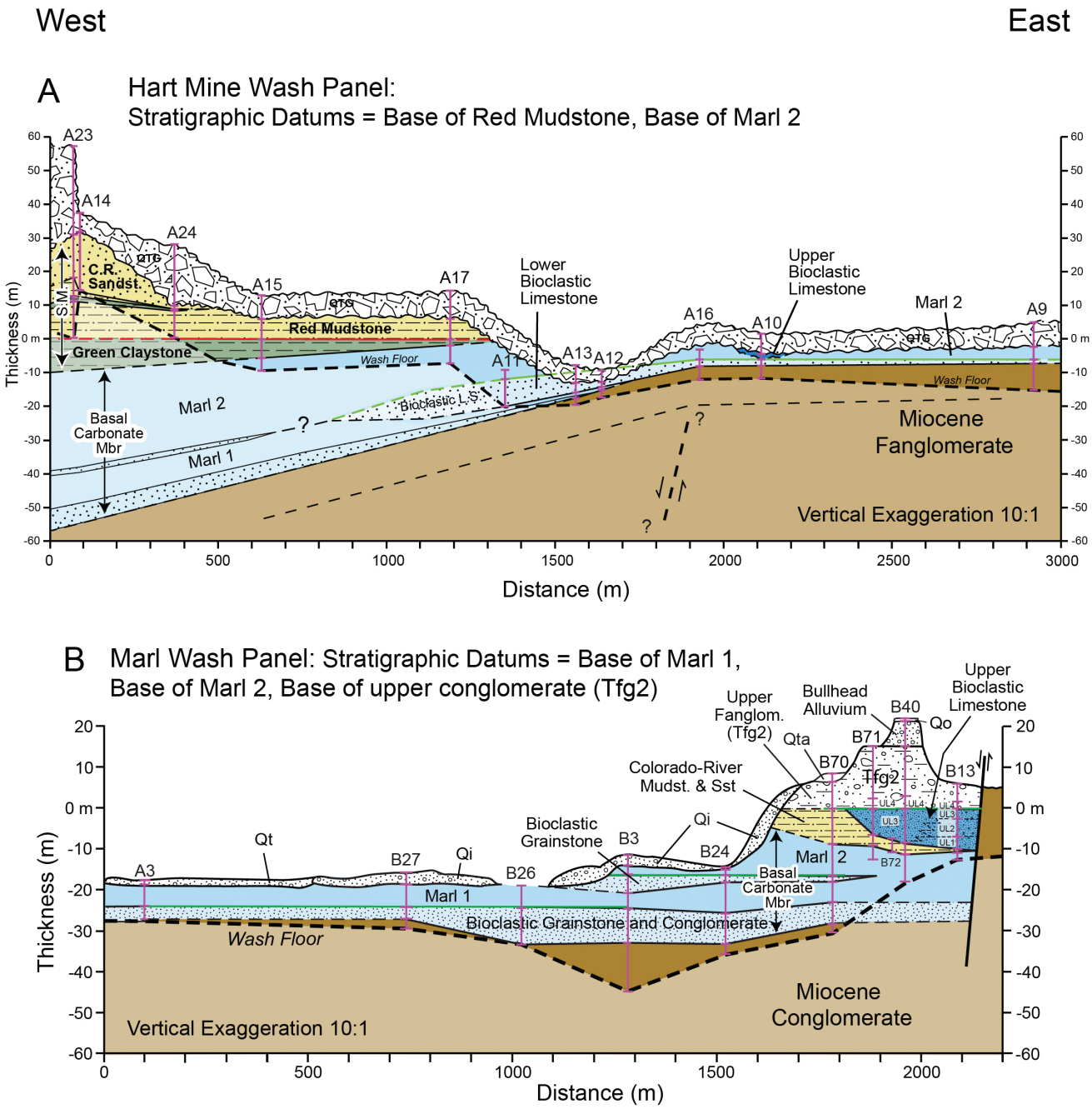

Figure 4. Restored stratigraphic panels for the Bouse Formation south of Cibola, AZ. (A) Hart Mine Wash displays a thin platform of carbonate in the east and westward thickening of Basal Carbonate and green claystone west of section A16, defining an overall monocline geometry. S.M. is siliciclastic member. (B) Marl Wash panel shows relatively uniform thickness of the Basal Carbonate member, westward thickening of the Siliciclastic member, and eastward thickening of the Bouse Upper Bioclastic member. Qta, Qi, Qt, and Qo are Quaternary gravel units of Gootee et al. (2016). UL1-UL4 are facies of the Upper Bioclastic member (O'Connell et al., 2016). Colored horizontal lines are stratigraphic datums. Darker colors represent units exposed above the wash floor, and lighter shades are units inferred below wash floor. Wash floor appears deformed because sections are restored to pre-deformation coordinates. Location of panels in Fig. 2.

Westward thickening in this panel may be a result of tilt on the northeast-dipping fault normal fault in lower Hart Mine Wash (Fig. 3), or growth folding above the propagating tip of a blind west-dipping normal fault, or both.

The Marl Wash panel displays relatively uniform thickness of Basal Carbonate in the western and central parts (Fig. 4B). The eastern part of this panel reveals westward thickening of the Bouse Siliciclastic member away from the normal fault, and eastward thickening of Upper Bioclastic member toward the fault. Importantly, the upper fanglomerate (Tfg2) conformably overlies the Upper Bioclastic member near the fault, and it rests unconformably on Colorado River mudstone and sandstone west of there in section B70. This indicates that accommodation space was produced close to the fault *during deposition of Upper Bioclastic Limestone and Tfg2,* while accommodation was being destroyed by uplift

and erosion to the west at B70, yielding a structural relationship produced by tilting toward the fault. The eastern part of the panel thus defines a "double wedge" geometry consisting of a westward-thickening stratal wedge (Siliciclastic member) overlain by an eastward-thickening wedge (Upper Bioclastic member), which records syn-depositional tilting first away from and then toward the normal fault.

Based on data presented above, we propose a two-stage model (Fig. 5) for the evolution of normal faults that controlled deposition of the Bouse Formation in the Cibola area. This is a composite conceptual model that combines observations of: (1) westward thickening wedge geometries in Basal Carbonate and green claystone in Hart Mine Wash (Fig. 4A) and Siliciclastic member in Marl Wash (Fig. 4B); and (2) eastward thickening of Upper Bioclastic Limestone in a stratal wedge that dips toward the normal fault in Marl Wash (Fig. 4B). In Stage 1, syn-depositional westward tilting and stratal thickening occurs by growth of a monocline above the tip of a west-dipping, propagating blind normal fault at depth (Fig. 5A). In Stage 2, the normal fault propagates up to and breaches the surface, creating new accommodation space by eastward tilting toward the fault in a new fault-related monocline (Fig. 5B). This model was developed to explain similar double-wedge geometries in syn-rift deposits in the Gulf of Suez (Gawthorpe et al., 1997), and is widely applied to fault-related stratal architecture in other extensional rift-basin systems (e.g., Hardy and McClay, 1999; Jackson et al. 2006).

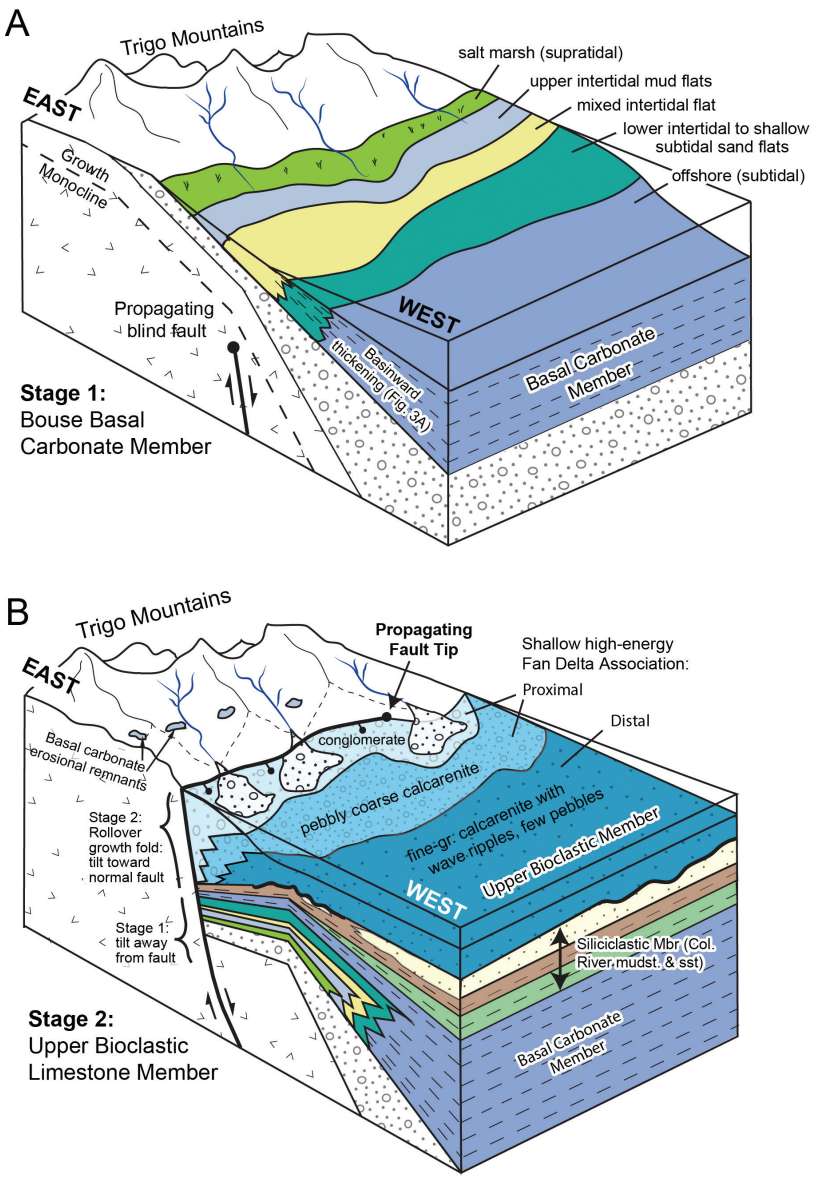

Figure 5. Proposed two-stage model for structural control on deposition of the Bouse Formation south of Cibola. (A) Stage 1: propagating blind normal fault causes westward tilting and stratal thickening toward basin depocenter. (B) Stage 2: fault breaches the surface and creates new accommodation space by eastward tilting toward the normal fault in a fault-related growth monocline (e.g., Gawthorpe et al., 1997)

Discussion and Conclusions

Data presented above show that syn-depositional fault-related tilting exerted an important control on production of accommodation space and resulting thickness variations in the Bouse Formation south of Cibola. This conclusion is highlighted by observations near the NE-dipping fault in lower Hart Mine Wash (Fig. 3): (1) the 80–100 m thick section of Colorado-River deltaic and channel sandstones in the hanging wall is by far the thickest exposed section of Siliciclastic member south of Blythe; (2) the fault and hanging-wall section are erosionally capped by ~4.5-Ma Bullhead Alluvium, and thus fault slip and tilting are pre-Bullhead (syn-Bouse); and (3) the hanging-wall section contains locally abundant convolute beds (seismites) and a large-scale liquefaction zone that likely record earthquakes on nearby faults, possibly the fault that cuts the section. Other patterns of stratal thickening and wedging south of Cibola (Figs. 4, 5) provide additional evidence for syn-depositional tilting due to slip on normal faults in this area.

The Hart Mine Wash panel reveals intra-formational westward thickening of about 50 m over a ~2 km distance, indicating an internal dip of ~1.4° (Fig. 4A). This angle predicts westward thickening of ~170 meters over 7 km from the hinge of the monocline at section A16 to well 36bbb in the Colorado River Valley (Fig. 1B). The maximum depth of Bouse Formation siliciclastic muds and sands in this well is 92 m (26 m below sea level) where it is a minimum of 52 meters thick (basal limestone was not encountered; Metzger et al., 1973), consistent with

the prediction. This comparison suggests that syn-Bouse westward tilting can explain the increase in thickness from Hart Mine Wash to the subsurface beneath the Colorado River floodplain, though the NE-dipping normal fault in lower Hart Mine Wash complicates this pattern and may suggest additional structural controls on stratigraphic thickness variations in this area.

Similar stratal wedge geometries in other parts of the southern Blythe basin are consistent with syn-depositional basinward tilting and subsidence. In the southeast Palo Verde Mountains (Fig. 1B) Bouse Formation deposits dip 5-7° to the east and thicken to the east via stratal wedging, not onlap (Homan, 2014). Faults in several locations cut the Bouse Siliciclastic member and are unconformably overlain by un-faulted Upper Bioclastic member, and in western Milpitas wash (Fig. 1B) the Upper Bioclastic member unconformably caps the Basal Carbonate member (Homan, 2014). Structural controls on syn-Bouse subsidence are further indicated by the regional map pattern which shows modern dry lakes bounded by active faults of the ECSZ, with Bouse Formation present in the subsurface beneath the dry lakes (Fig. 1A; Howard and Miller, 1992; Jachens and Howard, 1992).

We therefore propose that the distribution of basinal depocenters that contain the Bouse Formation (Fig. 1A) is at least in part controlled by the distribution and kinematics of linked dextral and oblique normal faults that were active in this region during late Miocene to early Pliocene time. We present a palinspastic reconstruction of the ECSZ and lower Colorado River region at 5 Ma (Fig. 6; modified from Bennett et al., 2016a) illustrating the interaction of active faults that may have controlled formation of Bouse-age depocenters. NW-striking dextral faults are connected through a series of broad releasing stepovers to dextral faults that link southeast to a major late Miocene to early Pliocene dextral shear zone in coastal Sonora, Mexico (Bennett et al., 2016b; Darin et al., 2016). We infer that this fault network was active during deposition of the Bouse Formation and exerted a direct control on formation of basinal depocenters via fault-related tilting similar to processes documented in this study south of Cibola. Abundant NW-striking faults east and southeast of here in the Trigo Mountains (Fig. 1B) probably are kinematically linked and related to syn-Bouse faults documented in this study.

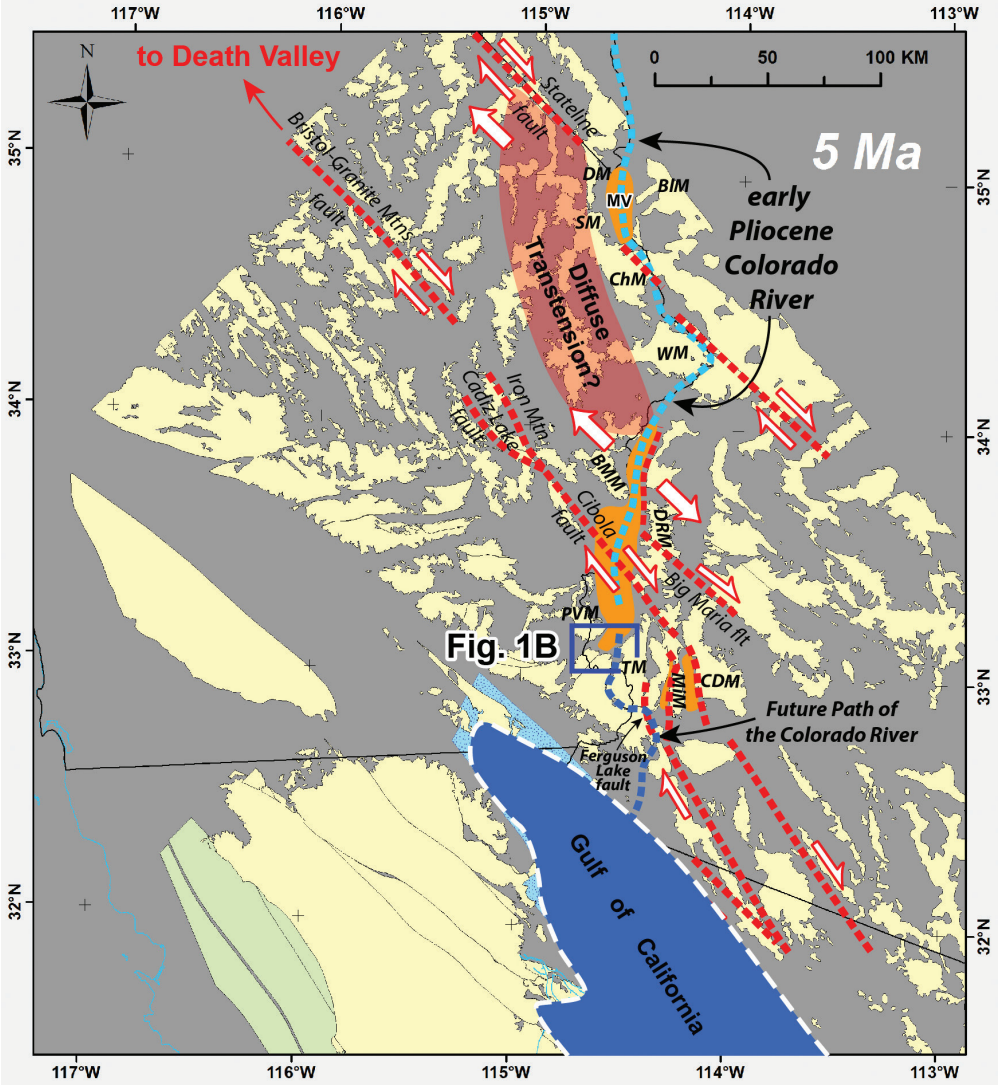

Figure 6. Palinspastic reconstruction of the ECSZ and lower Colorado River region at 5 Ma during deposition of the Bouse Formation, modified from Bennett et al. (2016a). Orange areas indicate basins that are predicted to open and subside due to extension or transtension (MV = Mohave Valley). Political boundaries are fixed in present-day coordinates for reference. Animation is available at: https://youtu.be/htzdDLW3-aQ. Mountain Ranges (yellow): BMM - Big Maria Mtns; BlM - Black Mtns; CDM - Castle Dome Mtns; ChM - Chemehuevi Mtns; DM - Dead Mtns; DRM - Dome Rock Mtns; MiM - Middle Mtns; PVM - Palo Verde Mtns; SM - Sacramento Mtns; TM - Trigo Mtns; WM - Whipple Mtns.

We further suggest that syn-Bouse diffuse transtension and subsidence throughout much of the lower Colorado River corridor may have formed deep basins in releasing stepovers (Fig. 6). For

example, a ~3-km deep sedimentary basin is present beneath the Mohave Valley (Saltus and Jachens, 1995), though the age of subsurface sediments is not well known. Active fault-controlled subsidence in the ECSZ may have also contributed to setting and modifying the path of the early Colorado River during its initiation ca. 5 Ma. The predictions of this model need to be tested in future studies of stratal architecture, detailed geologic and structural mapping, and gravity surveys of subsurface basins.

Acknowledgments

This study was supported by funding from the Sedimentary Geology and Paleobiology Program of the National Science Foundation (EAR-1546006). Vicki Langenheim and Kris McDougall provided constructive reviews of this paper. Laurie Crossey, Karl Karlstrom, Keith Howard, and Brian Gootee are thanked for insightful discussions. Any use of trade, firm, or product names is for descriptive purposes only and does not imply endorsement by the U.S. Government.

References Cited

Bennett, S.E.K., Darin, M.H., Dorsey, R.J., Skinner, L.A., Umhoefer, P.J., and Oskin, M.E. (2016a) Animated tectonic reconstruction of the Lower Colorado River region: implications for Late Miocene to Present deformation. *In:* Reynolds, R.E. (Ed.) 2016 Desert Symposium Field Guide and Proceedings, California State University Desert Studies Center, Zzyzx, Calif., p. 73-86.

Bennett, S.E., Oskin, M.E., Iriondo, A., Kunk, M.J., 2016b, Slip history of the La Cruz fault: development of a late Miocene transform in response to increased rift obliquity in the northern Gulf of California. Tectonophysics. v. 93, p. 409–435.

Bright, J., Cohen, A.S., Dettman, D.L., Pearthree, P.A., Dorsey, R.J. and Homan, M.B., 2016, Did a catastrophic lake spillover integrate the late Miocene early Pliocene Colorado River and the Gulf of California?: Microfaunal and stable isotope evidence from Blythe basin, California-Arizona, USA. Palaios, v. 31, p. 81-91.

Buising, A.V., 1990, The Bouse Formation and bracketing units, southeastern California and western Arizona: Implications for the evolution of the proto–Gulf of California and the lower Colorado River. Journal of Geophysical Research, v. 95, p. 20,111–20,132.

Darin, M.H., Bennett, S.E.K., Dorsey, R.J., Oskin, M.E., and Iriondo, A., 2016, Late Miocene extension in coastal Sonora, México: Implications for the evolution of dextral shear in the proto-Gulf of California. Tectonophysics, v. 693, p. 378-408.

Dokka, R.K., and Travis, C.J., 1990, Late Cenozoic strike-slip faulting in the Mojave Desert, California. Tectonics, v. 9, p. 311-340.

Dorsey, R.J., O'Connell, B., Homan, M., and Howard, K.A., 2016, Upper limestone of the southern Bouse Formation: Evidence for unsteady origins of the Colorado River. *In:* Reynolds, R.E. (Ed.) 2016 Desert Symposium Proceedings, California State University Desert Studies Center, Zzyzx, Calif., p. 145-153.

Gawthorpe, R. L., Sharp, I., Underhill, J. R., and Gupta, S., 1997, Linked sequence stratigraphic and structural evolution of propagating normal faults. Geology, v. 25, p. 795-798.

Gootee, B.F., Pearthree, P.A., House, P.K., Youberg, A., Spencer, J.E., and O'Connell, B., 2016, Geologic map of the Cibola 7 ½' Quadrangle and the northwestern part of Cibola SE 7 ½' Quadrangle, La Paz County, Arizona, and Imperial County, California. Arizona Geological Survey Digital Map DGM-117, scale 1:24,000, with text.

Guest, B, Niemi, N., and Wernicke, B., 2007, Stateline fault system: A new component of the Miocene-Quaternary Eastern California Shear Zone. Geological Society of America Bulletin, v.119, p.1337-1346.

Hardy, S., and McClay, K., 1999, Kinematic modelling of extensional fault-propagation folding. Journal of Structural Geology, v. 21, p. 695-702.

Homan, M.B., 2014, Sedimentology and stratigraphy of the Miocene-Pliocene Bouse Formation near Cibola, Arizona and Milpitas Wash, California: Implications for the early evolution of the Colorado River [M.S. thesis]. Eugene, University of Oregon, 116 p.

House, P.K., Pearthree, P.A., and Perkins, M.E., 2008, Stratigraphic evidence for the role of lake spillover in the inception of the lower Colorado River in southern Nevada and western Arizona, *in* Reheis, M.C., Hershler, R., and Miller, D.M., eds., Late Cenozoic Drainage History of the Southwestern Great Basin and Lower Colorado River Region: Geologic and Biotic Perspectives. Geological Society of America Special Paper 439, p. 335-353.

Howard, K.A., and Miller, D.M., 1992, Late Cenozoic faulting at the boundary between the Mojave and Sonoran blocks: Bristol Lake area, California. *In*: Richard, S.M. (ed.) Deformation associated with the Neogene Eastern California Shear Zone, southwestern Arizona and southeastern California. Redlands, CA, San Bernardino County Museum Special Publication 92-1 p. 37-47.

Howard, K.A., House, P.K., Dorsey, R.J., and Pearthree, P.A., 2015, River-evolution and tectonic implications of a major Pliocene aggradation on the lower Colorado River, the Bullhead Alluvium. Geosphere, v. 11, p. 1–30; doi:10.1130/GES01059.1.

Jachens, R.C., and Howard, K.A., 1992, Bristol Lake basin: A deep sedimentary basin along the Bristol-Danby Trough, Mojave Desert. *In:* Reynolds, R.E. (ed.) Old Routes to the Colorado. Redlands, CA, San Bernardino County Museum Special Publication 92-2, p. 57-59.

Jackson, C.A.L., Gawthorpe, R.L., and Sharp, I.R., 2006, Style and sequence of deformation during extensional fault-propagation folding: examples from the Hammam Faraun and El-Qaa fault blocks, Suez Rift, Egypt. Journal of Structural Geology, v. 28, p. 519–535.

Mahan, K.H., Guest, B., Wernicke, B., and Niemi, N.A., 2009, Low-temperature thermochronologic constraints on the kinematic history and spatial extent of the Eastern California Shear Zone. Geosphere, v. 5, p. 483-495.

McDougall, K., 2008, Late Neogene marine incursions and the ancestral Gulf of California, In: Reheis, M.C., Hershler, R., and Miller, D.M. (eds.) Late Cenozoic drainage history of the southwestern Great Basin and lower Colorado River region:

Geologic and biotic perspectives. Geological Society of America Special Paper 439, p. 355-373.

McDougall, K., and Miranda Martinez, A.Y., 2014, Evidence for a marine incursion along the lower Colorado River corridor. Geosphere, v. 10, p. 1-28.

McDougall, K., and Miranda Martinez, A.Y., 2016, Bouse Formation along the lower Colorado River corridor: tracking the transition from marine estuary to saline lake. In: Reynolds, R.E. (Ed.) 2016 Desert Symposium Field Guide and Proceedings, California State University Desert Studies Center, Zzyzx, Calif., p. 140-144.

Metzger, D.G., Loeltz, O.J., and Irelan, B., 1973, Geohydrology of the Parker-Blythe-Cibola area, Arizona and California: U.S. Geological Survey Professional Paper 486-G, 130 p.

Miller, M.M., Johnson, D.J., Dixon, T.H., and Dokka, R.K., 2001, Refined kinematics of the eastern California shear zone from GPS observations, 1993–1994. Journal of Geophysical Research, v. 106, p. 2245–2263,

O'Connell, B., Dorsey, R.J., Homan, M., Gootee, B.F., and House, P.K., 2016, Structural controls on stratigraphic architecture of the southern Bouse Formation near Cibola, Arizona. In: Reynolds, R.E. (Ed.) 2016 Desert Symposium Field Guide and Proceedings, California State University Desert Studies Center, Zzyzx, Calif., p. 171-175.

O'Connell, B., Dorsey, R.J., and Humphreys, E.D., 2017, Tidal rhythmites in the southern Bouse Formation as evidence for post-Miocene uplift of the lower Colorado River corridor. Geology, v. 45, p. 99–102.

Saltus, R.W. and Jachens, R.C., 1995, Gravity and basin-depth maps of the Basin and Range Province, Western United States: U.S. Geological Survey Geophysical Investigations Map 1012, 4 sheets, scale 1:2,500,000.

Sarna-Wojcicki, A.M., Deino, A.L., Fleck, R.J., McLaughlin, R.J., Wagner, D., Wan, E., Wahl, D., Hillhouse, J.W., and Perkins, M., 2011, Age, composition, and areal distribution of the Pliocene Lawlor Tuff, and three younger Pliocene tuffs, California and Nevada. Geosphere, v. 7; p. 599- 628.

Sherrod, D.R., and Tosdal, R.M., 1991, Geologic setting and Tertiary structural evolution of southwestern Arizona and southeastern California. Journal of Geophysical Research, v. 96, p. 12,407-12,423.

Spencer, J.E., and Patchett, P.J., 1997, Sr isotope evidence for a lacustrine origin for the upper Miocene to Pliocene Bouse Formation, lower Colorado River trough, and implications for timing of Colorado Plateau uplift. Geological Society of America Bulletin, v. 109, p. 767-778.

Spencer, J.E., Pearthree, P.A., and House, P.K., 2008, An evaluation of the evolution of the latest Miocene to earliest Pliocene Bouse lake system in the lower Colorado River valley, southwestern USA, In: Reheis, M.C., Hershler, R., and Miller, D.M., eds., Late Cenozoic drainage history of the southwestern Great Basin and lower Colorado River region: geologic and biotic perspectives. Geological Society of America Special Paper 439, p. 375–390.

Spencer, J.E., Patchett, P.J., Pearthree, P.A., and House, P.K., Sarna-Wojcicki, A.M., Wan, E., Roskowski, J.A., and Faulds, J.E., 2013, Review and analysis of the age and origin of the Pliocene Bouse Formation, lower Colorado River Valley, southwestern USA. Geosphere, v. 9, p. 444–459.

Woodburne, M.O., 2017, The Eastern California Shear Zone, Mojave Desert, California. *In:* Reynolds, R.E. (Ed.) 2017 Desert Symposium Field Guide and Proceedings, California State University Desert Studies Center, Zzyzx, Calif., this volume.

Hypothesis for post-Bouse distributed deformation of the Lower Colorado River corridor

Jacob O. Thacker[1], Karl E. Karlstrom[1], Laura J. Crossey[1], Ryan Crow[2], L. Sue Beard[2], and Rebecca J. Dorsey[3]
[1]*Department of Earth and Planetary Sciences, University of New Mexico, Albuquerque, NM, 87131, USA*
[2]*U.S. Geological Survey, 2255 N. Gemini Drive, Flagstaff, AZ 86001, USA*
[3]*Department of Earth Sciences, University of Oregon, Eugene, OR, 97403, USA*

Introduction and background

Deposits of the >6-4.8 Ma Bouse Formation and ~4.5-3.8 Ma post-Bouse Bullhead Alluvium are present both in the subsurface and as erosional remnants within successive basins along much of the Lower Colorado River (LoCR). These deposits record the first arrival and integration of the Colorado River to the proto-Gulf of California (Bouse Formation) and aggradation of the Colorado River as a continent-scale river system (Bullhead Alluvium). Within basins, Bouse deposits occur at a range of elevations, and have been interpreted to represent the filling of lakes, leaving behind Bouse carbonates as a bathtub-like coating draped on paleotopography as lakes filled (Pearthree and House, 2014). Draping across topography at vertical scales of tens of meters is clearly evident by outcrops within the Yuma Proving Grounds. First-order observations show that the highest Bouse deposits are hundreds of meters higher on the flanks of basins than at their center (Pearthree et al., 2016). Additionally, a longitudinal (N to S) ~200 m change in elevation of Bouse deposits is evident across the Topock Divide (Fig. 1). Here, deposits north of the divide are at a maximum elevation of ~560 m elevation, while deposits to the south are at ~360 m elevations (Pearthree and House, 2014). Similarly, the highest Bouse deposits across the Chocolate Mountains divide are 300-400 m higher to the north (Metzger, 1968) and in wells to the south, near Yuma, Arizona (Olmstead et al., 1973). These elevation differences have been suggested to record the eventual spilling of the lake water southward to successively lower basins whereby topographic divides (Fig.1) blocked first-arriving river water into large inland lakes before eventually integrating and continuing their course downstream to the proto-Gulf of California (Spencer et al., 2012; Pearthree and House, 2014). $^{87}Sr/^{86}Sr$ values have been cited as evidence for a generally non-marine origin for the Bouse Formation (Spencer and Patchett, 1997). In this model, lakes are envisioned as 300-500 m deep, with present outcrop elevations reflecting original depositional elevation.

An alternative hypothesis is that tectonic activity associated with the evolving San Andreas plate boundary and Eastern California shear zone (ECSZ) may have influenced the observed elevations of Bouse and Bullhead strata after they were deposited. The rarity of mapped scarps and discrete structures within the study area suggests that deformation may be diffuse. In particular, deformation within the LoCR corridor at and between the Topock and Chocolate Mountain divides (e.g. Beard et al., 2016) may be manifested through diffuse transtensional strain whereby dominant structures consist of NW-SE –oriented distributed dextral systems, N-S-oriented normal faults, and E-W-oriented contractional structures (antiformal structures and reverse faults) (Fig. 1). In order to test these competing hypotheses, we have begun a compilation of faults and have targeted key locations for structural analysis and mapping.

Our preliminary assessment through the integration of diverse datasets suggests the viability of this second hypothesis of diffuse Pliocene-Recent tectonism throughout the LoCR corridor. Datasets include geologic data from past and active mapping (e.g. Faulds et al., 2004; Gootee et al., 2016; House et al., 2004; Howard et al., 2013), detailed observations of fault and stratigraphic relationships in the southern Blythe basin (Homan, 2014), depth-to-bedrock data (Richard et al., 2007), structural analysis (this study), high-precision GPS surveying of Bouse and post-Bouse deposits (in progress USGS effort), geospatial analysis of Colorado River deposits (Crow et al., 2016; in progress USGS effort), subsurface data (Metzger et al., 1973) fault and subsurface compilations (in progress USGS effort; this study), geodetic estimates (Kreemer et al., 2010), and historical seismicity in the study area (Yang et al., 2012). This paper is a progress report of this current evidence for Pliocene-Recent deformation in the LoCR corridor.

Evidence in the Chocolate Mountains and Blythe Basin

Evidence for elevation change of Bouse outcrops across the Chocolate Mountain divide (Fig. 1) includes paleontological (McDougall and Martinez, 2014) and stratigraphic (O'Connell et al., 2017) observations that suggest the Bouse Formation in the southern Blythe basin is marine. "Non-marine" Sr isotopic values (Spencer and Patchett, 1997) may be attributable to mixing in an estuary setting, somewhat analogous to modern San

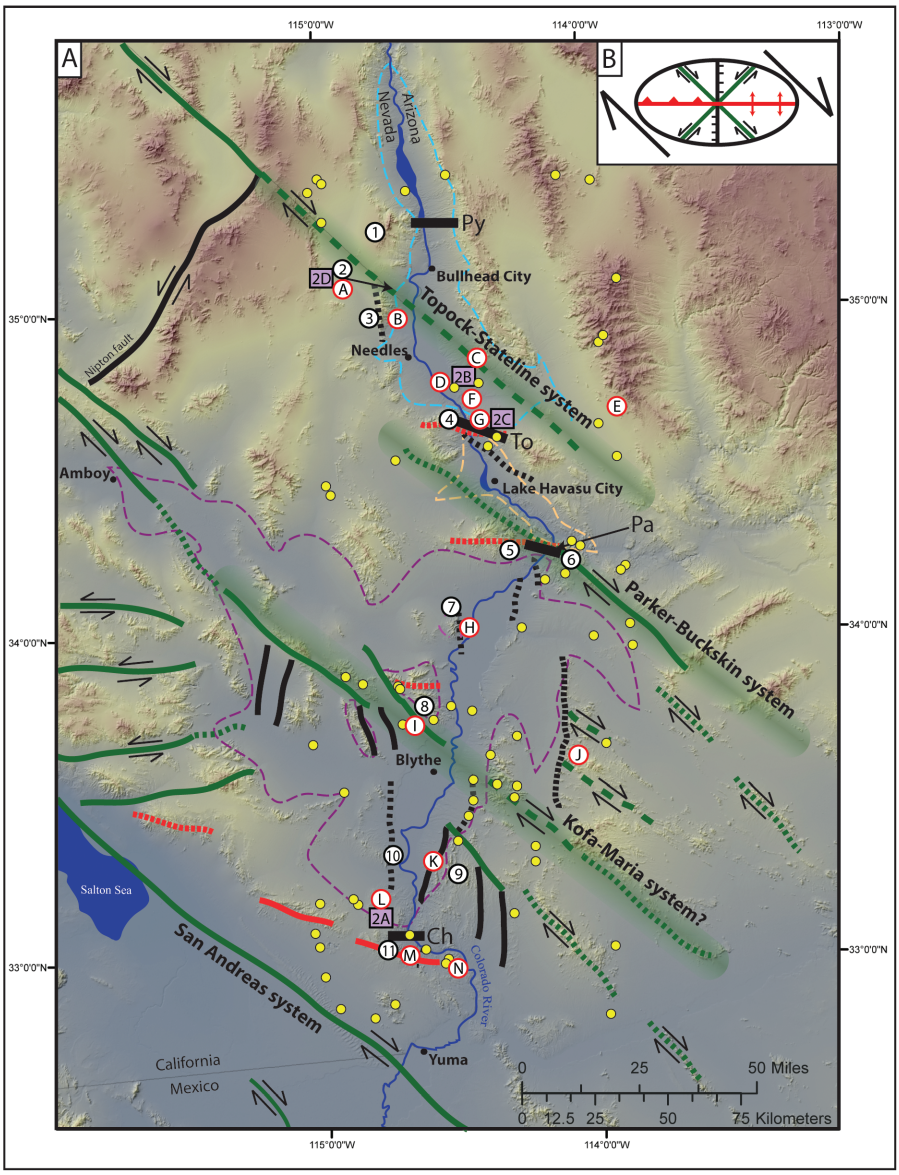

Figure 1: A) Digital elevation model of the Lower Colorado River corridor and surrounding region showing present evidence and our hypothetical tectonic framework (structures). References for present evidence listed unless from this study. Note that solid lines represent mapped structures or structural systems, while dashed represent inferred and dotted represent hypothetical. Basin outlines are approximate. Earthquakes shown were queried only along the LoCR corridor (e.g., Salton Sea seismicity omitted). Earthquake magnitudes not distinguished by size; all are less than magnitude 4. B) Schematic right-lateral shear couple with expected structures shown. Color-coded to structures in A.

Francisco Bay (Crossey et al., 2015). Interpreted marine facies of the Bouse Formation reach elevations of 120 m in the Blythe basin (McDougal and Martinez, 2014), and Beard et al. (2016) suggested that about ~300 m of <5 Ma tectonic uplift across the Chocolate Mountains divide would be needed to create a barrier between the Yuma basin and the Blythe basin to cut off the proposed Bouse marine inlet. Support for syn- and post-Bouse deformation in the southern Blythe basin include: (1) deformation of the Bouse in the southern Trigo Peaks of Arizona (Buising, 1990; Gootee et al., 2016); (2) a recently discovered syn-Bouse normal fault in lower Hart Mine Wash that has demonstrably 80-100 m of throw (Dorsey et al., this volume); (3) possible tilting of Bouse outcrops due to growth of the Chocolate Mountain anticlinorium (Beard et al., 2016); (4) stratal wedging and pinch-out patterns in the Bouse Formation that indicate syn-depositional fault-controlled tilting (O'Connell et al., 2017; Dorsey, et al., this volume); and (5) localities where faults that cut the Bouse Formation are unconformably overlapped by un-faulted younger Bouse deposits or Bullhead Alluvium (Homan, 2014).

Work on the Chocolate Mountains anticlinorium (Ricketts et al., 2011; Beard et al., 2016; Ricketts et al., this volume) suggests the region just south of the Chocolate Mountains divide records mid- to late-Miocene deformation related to the evolution of the San Andreas plate boundary system. Within this region, deformation is expressed through NW-oriented dextral faults and the EW-trending Copper Basin reverse fault. These structures cut the Bear Canyon conglomerate to the east of the Chocolate Mountains in and

around Bear Canyon (Point L, Fig. 1; Ricketts et al., 2011; Girty et al., 2012; Ricketts et al., this volume). A 9.45 Ma basalt that is interbedded with the youngest Bear Canyon conglomerate deposits suggests post-9.45 Ma deformation (Ricketts et al., 2011; Girty et al., 2012; Ricketts et al., this volume). Quaternary deposits here, however, have not been shown to be deformed, suggesting no active tectonism.

Within the Blythe basin, we suggest N-S faults sub-parallel to the river, as displayed on figures in Sherrod and Tosdal (1991), have normal slip. The Blythe basin shows subsidence of the Bouse Formation and Bullhead gravels in the subsurface (Metzger et al., 1973; Pearthree et al., 2016) that is possibly explained by river-parallel grabens. Evidence for small-displacement N-S normal faults includes syn-Bouse structures within the Blythe basin (Buising, 1990; Dorsey et al., this volume). At the Big Fault (Point K, Fig. 1), Bouse Formation strata are displaced with a throw of ~20 m (Gootee et al., 2016) along a N-S-striking, west-dipping normal fault. Across the basin (near Buzzard Peak; Point L, Fig. 1), two small N-S-striking east-dipping normal faults cut Bouse marl with a collective throw of ~ 1 m (Fig. 2A). Though small, the east-directed down-dropping of these structures is compatible with tectonic subsidence in the southern Blythe basin. Dextral slip on NW-striking faults that obliquely cross the Colorado River are also hypothesized in this area.

Dispersed NW-SE dextral strike slip faults have also been inferred in the Plomosa Mountains near Quartzite, AZ (Miller and McKee, 1971) (Fig. 1). To the south, interesting NW-SE topographic trends in the Kofa and Dome Rock mountains are along-strike with dextral faults in the Big Maria Mountains. Other work in the area (Richard and Dokka, 1992; Miller et al., 2014) shows fault systems (the Packard Well fault) to the southwest of the Big Marias in line with this topographic trend. A post-Bouse structure known as the Blythe graben (Schell and Wilson, 1981) is also found along this system, and displaces Quaternary alluvial fan deposits. Subsurface data show the deepest Bouse deposits in this vicinity (Metzger et al., 1973), but work on the distribution of subsurface Bouse deposits (in progress) is required to more clearly define the role of faulting.

Evidence within the vicinity of Topock Divide

The Needles area also shows evidence for syn- and post-Bouse deformation (Points B-G, Fig. 1). The Needles graben (Point C, Fig. 1) is a NW-SE trending structure along-strike with the Stateline fault system. Here, early- to mid-Pleistocene surfaces are offset by ~ 4-5 m (Pearthree et al., 1983). Approximately 10 km to the SW, a considerably smaller graben is observed within post-Bouse river sediments (Fig. 2B). These sediments, mapped as the deposits of the Santa Fe Railroad (Howard et al., 2013), dip 15° SW. Interestingly, these structures also correspond roughly with a ~1000 m geophysically estimated depth-to-bedrock (substantially deeper than the surrounding area) (Richard et al., 2007), thicker and deeper subsurface Bouse deposits (Point D, Fig. 1; Metzger et al., 1973), the continuation of geophysically defined faults (Beard et al., 2011), and a change in topographic trend from ~N-S to NW-SE (Point E, Fig. 1). Three-dimensional geospatial analysis of Colorado River deposits (Crow et al., 2016; in progress USGS effort) show variations in the highest Bullhead outcrops in this vicinity (Fig. 3) that could partly be explained by cumulative displacement on such faults. A 100 m "jump" in the highest definitive Bullhead Alluvium outcrops is coincidental with the Needles Graben. Although this is suggestive of tectonic control, it can also be explained by incomplete preservation. The highest Bouse outcrops are at similar elevations north and south of the inferred Stateline-Topock fault system (515-530 m and 500-540 m, respectively). Therefore, the ~200 m elevation difference across Topock Divide would require another structure. Within Topock Divide itself (Topock Gorge), perched side-stream gravels suggest young incision (Point G, Fig. 1; Fig. 2C), and the age and sharpness of the bedrock gorge are in need of explanation.

South of the Topock Divide, the Buckskin-Rawhide metamorphic core complex is cut by post-detachment E-W extensional and NW-striking strike-slip faults that have an estimated 7-9 km of total post-12 Ma dextral offset (Singleton, 2015; Singleton et al., 2016). A youthful, Plio-Quaternary age for dextral faulting in this area is inferred from: (1) a small pull-apart basin that controls modern topography at a releasing step-over on the Mineral Wash fault; (2) constriction of the Bill Williams River where it is crossed by the Swansea fault; (3) right-lateral deflection of modern drainages; (4) a large beheaded Quaternary alluvial fan; and (5) other evidence of recent stream captures that suggest an unstable disequilibrium landscape adjusting to fault-controlled base-level change. New work is needed to assess the age and structural significance of these critical relationships. Along-strike projection of this system may be en echelon with the Stateline fault system, and, therefore, be an influential structural system in our hypothetical tectonic framework.

Additional new observations are compatible with the distributed deformation hypothesis. At Point B in Fig. 1, 23° southeast dip in basal marl of the Bouse Formation has been interpreted as a primary "drape" with no post-depositional tilting (Pearthree and House, 2014). However, detailed inspection shows that interbedded marly claystone and clayey marl overlying the basal marl also dip ~20-23° SE, much steeper than primary dip expected for these facies, suggesting significant post-depositional tilting. At Manchester Beach, N-S mafic dikes (42-62°W dip) crosscut ~15 Ma Newberry Granite. Two locations show right-separations of ~3 and ~5 m where washes cut through the dikes at the point of separation and trend ~140° in the down-wash direction (Point A, Fig. 1; Fig. 2D). This trend is similar to the strike of the Stateline

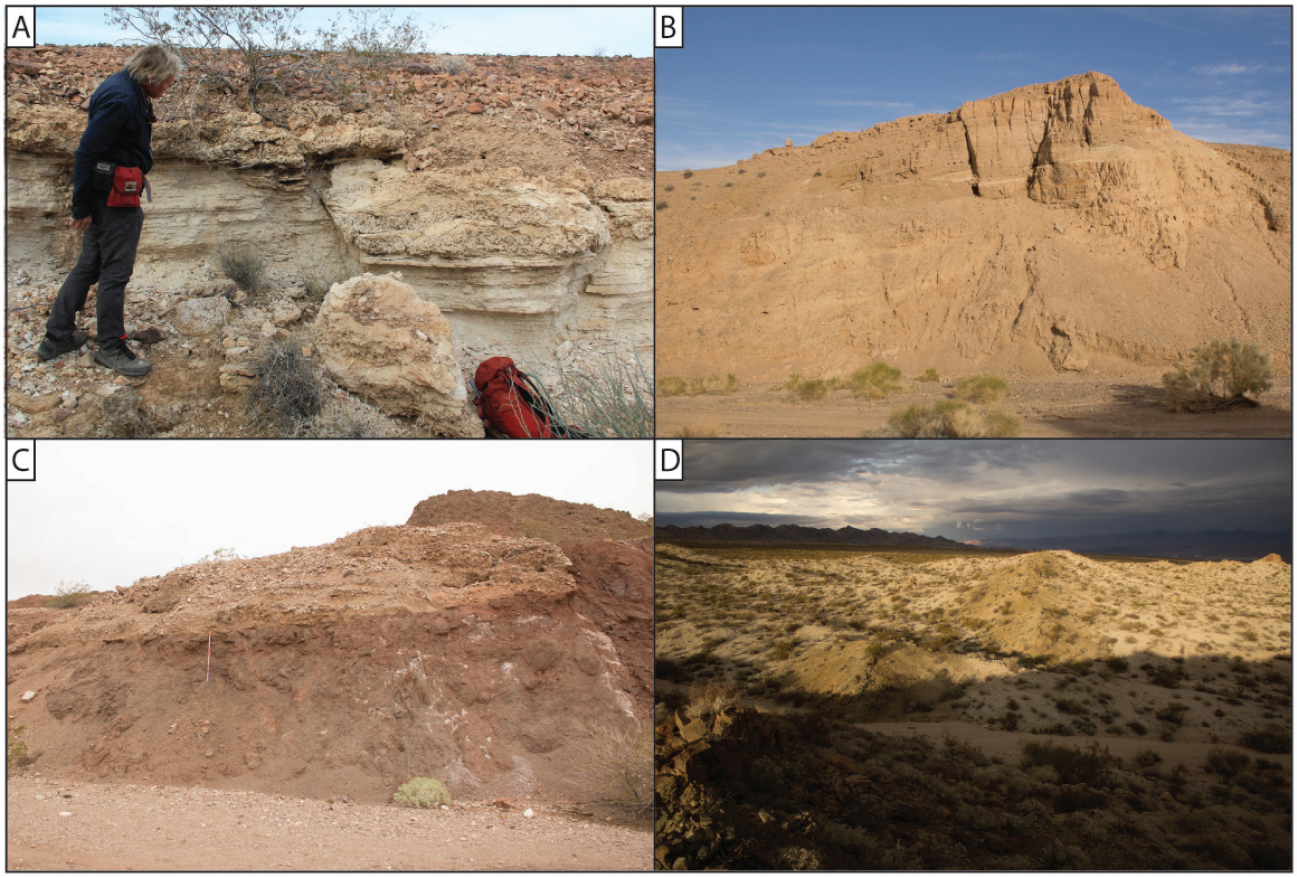

Figure 2: Evidence for Pliocene-Recent deformation in the LoCR, locations shown on Figure 1. A) Small faults near Buzzard Peak showing ~ 1 m total throw. Faults strike ~N-S and dip ~60E. View is to north. Photo: Laura Crossey. B) Small graben in ~15° SW tilted beds of post-Bouse river sediments, suggesting Pliocene or younger deformation. Bush ~1 m tall; view to north. C) Down-cutting of presently active wash (foreground) ~3 m through older wash material (at top) and basement rock in Topock Divide. Tape extended to one meter. D) Right-separated dike at Manchester Beach; separation ~5 m. Wash trends ~310, similar to and along-strike with the Stateline fault system. Dikes intrude ~15 Ma Newberry Granite, suggesting middle Miocene or younger deformation and continuation of the Stateline fault system to the LoCR. View to north.

fault system (Fig. 1; Guest et al., 2007; Mahan et al., 2009). However, slickenlines and discrete structures have not been found, precluding determination of these features as truly strike-slip. Interestingly, further south, a large (~10 m) left separation was also identified. This orientation is permissible within a dextral system (Fig. 1B). Because of a lack of structures offsetting the Bouse Formation in this area (due to limited preservation), the timing of these right-separated dikes can only be constrained to younger than <15 Ma.

Evidence from geodesy and historical seismicity

Geodetic measurements (Kreemer et al, 2010), Earthquake focal mechanisms (Yang et al., 2012), and a preliminary summary of historic seismic activity (Fig. 1) within the LoCR region show diffuse low magnitude seismicity. Evidence may suggest active deformation of the Chocolate Mountain anticlinorium. Focal mechanisms within this area are dominantly NW-striking dextral strike-slip faults, though a single focal mechanism east of the Chocolate Mountains (Point N, Fig. 1) is suggestive of E-W striking reverse faulting, and may be related to movement along the Copper Basin reverse fault (Ricketts et al., 2011; this volume).

A query of historic seismicity (earthquake.usgs.gov) within the study area was conducted for the period of 1800 to present. These results are shown on Figure 1, and exclude quarry blasts and earthquakes reported with negative depths. North of the Trigo Mountains, a N-S linear trend is observed, as well as possible NW-SE linear trends near the Buckskin-Rawhide metamorphic core complex that are compatible with distributed dextral motion as suggested by Singleton (2015) and Singleton et al. (2016). To the southwest of the Big Maria Mountains, a string of seismicity is observed that correlates with the Blythe graben (Point I, Fig. 1) and Packard Well fault. The remainder of seismic activity is sparse, but appears distributed throughout the region. This is consistent with Kreemer et al.'s (2010) estimates of 1.4 mm/yr diffuse extension in the northern LoCR.

Evidence from river profile constructions

Distributed tectonic activity associated with the ECSZ may also have influenced the elevations of Bouse and Bullhead strata across the Topock divide near Needles,

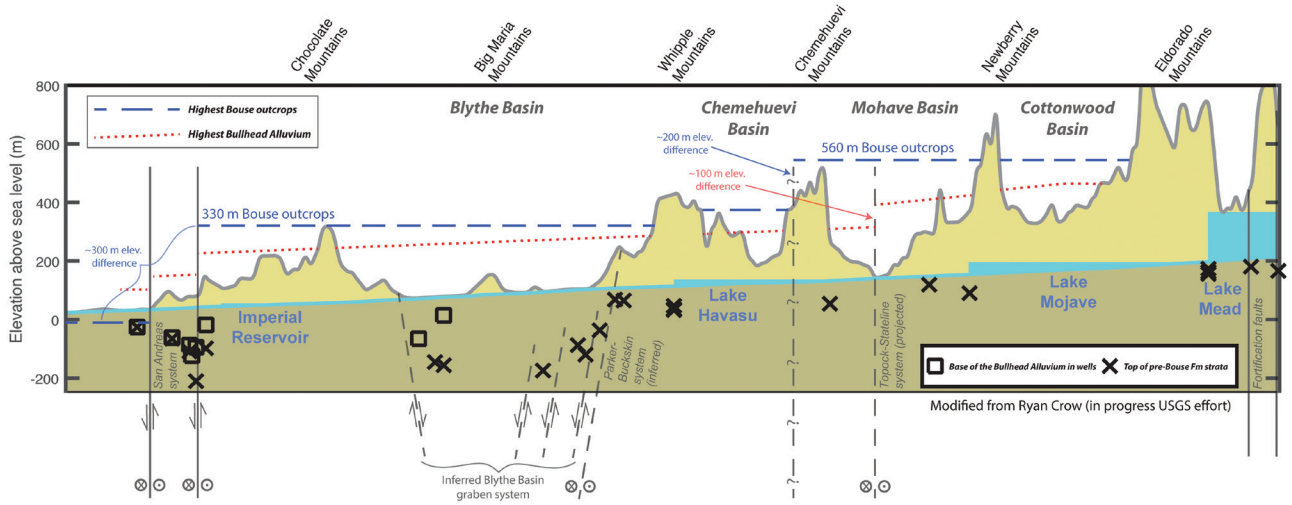

Figure 3: Lower Colorado River profile showing highest Bouse outcrops (blue dashed lines) and the Bullhead alluvium (red dotted lines). Inferred (dashed) and known (solid) faults and fault systems are shown. Elevations are from continued mapping and high-precision GPS measurements. Modified from Ryan Crow (in progress USGS effort).

as best evidenced by river profile constructions (Fig. 3). Subtle deformation may be related to southeastern continuations of the Stateline fault system (Guest et al., 2007; Mahan et al., 2009). Geospatial analysis of Colorado River outcrops along the LoCR show marked differences in elevations of Bouse deposits in the Mohave-Cottonwood (~550-560 m), Chemehuevi (~360 m), and the Blythe (~330 m) basins (Pearthree and House, 2014). Bouse deposits are also interpreted in the subsurface of all basins, while Bullhead deposits are interpreted in the subsurface of the southern Blythe Basin (Fig. 3). Some component of this elevation change could be related to distributed N-side-up throw and localized tectonic subsidence.

A hypothetical tectonic framework for the LoCR

Figure 1 shows a testable hypothesis for distributed syn- and post-Bouse deformation associated with the ECSZ whereby the LoCR's tectonic history has been influenced by Pacific/North American plate boundary motion. Deformation has taken place since the mid- to late Miocene (e.g. Atwater, 1989; Ricketts et al., 2011; Bennett et al., 2016), and may be ongoing. Regionally, structures that are observed and inferred in the study area fit into a right-lateral shear couple, bounded by the San Andreas fault to the south and the Stateline fault system to the north (Fig. 1B). In particular, distributed deformation may be through transtension, in that reactivated N-S normal faults and NW-SE dextral shear systems are likely prevalent. This transtensional hypothesis builds on the work of Bennett et al. (2016). In this regard, tectonic basin subsidence could have occurred through a mixture of distributed deformation within a far-field dextral stress regime (shear couple), as well as soft-linkages between en echelon dextral systems (such as in the Needles area). From north to south, potential systems in need of investigation include the Stateline-Topock system, the Parker-Buckskin system, the possible Kofa-Maria system, and the San Andreas system (Fig. 1). Basin-bounding E-W ranges would likely experience N-S directed compression within a right-lateral shear couple, and the N-S LoCR corridor itself may be the result of N-S grabens formed during extensional reactivation of older Miocene faults.

Conclusions

We have presented a hypothetical tectonic framework model that could account for some of the differences in elevations of Bouse and post-Bouse strata along the LoCR corridor. This hypothesis invites integration of diverse datasets, and acquisition of new structural data to test whether Pliocene to Recent deformation in the study area could be the result of distributed transtension. Further work is required, such as a comprehensive compilation of faults and new subsurface data on the distribution and depths of the Bouse Formation in the subsurface. But, even the subtle Pliocene-Recent tectonism presently identified within the LoCR corridor suggests modification of the fill-and-spill model, and seems to argue that some component of the observed elevation differences of Bouse outcrops could be the result of tectonic activity.

Acknowledgments

Support for this research is through the National Science Foundation grant EAR-1545986. We wish to thank Phil Pearthree and Kyle House for providing us with valuable outcrop locations, and to acknowledge the Yuma Proving Grounds for granting us access. We also wish to thank Brandon Schmandt for his input on geodetic estimates, and Jason Ricketts and John Singleton for their thorough reviews of the manuscript.

References

Atwater, T., 1989, Plate tectonic history of the northeast Pacific and western North America, *in* Winterer, E.L., Hussong, D.M., Decker, R.W., eds., The Eastern Pacific Ocean and

Hawaii: Boulder, Colorado, Geological Society of America, The Geology of North America, v. N.

Beard, L.S., Haxel, G.B., Dorsey, R.J., McDougal, K.A., Jacobson, C.E., 2016, Late Neogene deformation of the Chocolate Mountains Anticlinorium: implications for deposition of the Bouse Formation and early evolution of the Lower Colorado River, *in* Going Loco: Investigations along the Lower Colorado River, 16th, California State University Dessert Studies Consortium, p. 87-90.

Beard, L.S., Kennedy, J., Truini, M., Felger, T., 2011, Geologic map of Detrital, Hualapai, and Sacramento valleys and surrounding areas, northwest Arizona: U.S. Geological Survey Open-File Report Map 2011-1225, scale 1:250,000.

Bennett, S.E.K., Darin, M.H., Dorsey, R.J., Skinner, L.A., Umhoefer, P.J., Oskin, M.E., 2016, Animated tectonic reconstruction of the Lower Colorado River region: implications for Late Miocene to Present deformation, *in* Going Loco: Investigations along the Lower Colorado River, 16th, California State University Dessert Studies Consortium, p. 73-86.

Buising, A. V, 1990, The Bouse Formation and bracketing units, southeastern California and western Arizona: Implications for the evolution of the proto-Gulf of California and the lower Colorado River: Journal of Geophysical Research-Solid Earth and Planets, v. 95, no. B12, p. 20111–20132.

Crossey, L.C., Karlstrom, K.E., Dorsey, R., Pearce, J., Wan, E., Beard, L.S., Asmeron, Y., Polyak, V., Crow, R.S., Cohen, A., Bright, J., Pecha, M.E., 2015, Importance of groundwater in propagating downward integration of the 6-5 Ma Colorado River system: Geochemistry of springs, travertines, and lacustrine carbonates of the Grand Canyon region over the past 12 Ma: Geosphere, v. 11, n. 3, p. 660-682.

Crow, R.S., Karlstrom, K.E., Howard, K.A., Beard, L.S., House, P.K., Sharp, W., Polyak, W., Peters, L., Asmerom, Y., McIntosh, W., Block, D., Crossey, L.C, 2016, Integrating lower Colorado River alluvial deposits and Grand Canyon incision constraints to reconstruct paleo Colorado River profiles and determine Colorado Plateau uplift, *in* Going Loco: Investigations along the Lower Colorado River, 16th, California State University Desert Studies Consortium, p. 87-90.

Dorsey, R.J., O'Connell, B., Homan, M.B., Bennett, E.K., this volume, Influence of the Eastern California shear zone on deposition of the Mio-Pliocene Bouse Formation: Insights from the Cibola area, Arizona.

Faulds, J.E., House, P.K., Pearthree, P.A., Bell, J.W., and Ramelli, A.R., 2004, Preliminary geologic map of the Davis Dam quadrangle and eastern part of the Bridge Canyon quadrangle, Clark County, Nevada and Mohave County, Arizona. Nevada Bureau of Mines and Geology Open- le report 03-5, scale 1:24,000.

Girty, G.H., Muela, K.K., Olson, H., Sutton, L., Biggs, M., Sainsbury, J., Ricketts, J.W., Errthum, R., Colby, T.A., Carrasco, T., Gordon, E., and Pelbath, T., 2012, Toward a unified model for the geologic and tectonic history of the region between Indian Pass and Picacho State Recreation Area, southeastern California, *in* Wirths, T.A. (ed.), Picacho and the Cargo Muchachos: San Diego Association of Geologists, San Diego, Ca, p. 53-86.

Gootee, B.F., Pearthree, P.A., House, P.K., Youberg, A., Spencer, J.E., O'Connell, B., 2016, Geologic map of the Cibola 7½' Quadrangle and the northwestern part of Cibola SE 7½' Quadrangle, La Paz County Arizona, and Imperial County, California: Arizona Geological Survey Digital Map DGM-117, scale 1:24,000, with text.

Guest, B., Niemi, N., Wernicke, B., 2007, Stateline fault system: A new component of the Miocene-Quaternary Eastern California shear zone: GSA Bulletin, v. 119, n. 11/12, p. 1337-1346.

Homan, M.B., 2014, Sedimentology and stratigraphy of the Miocene-Pliocene Bouse Formation near Cibola, Arizona and Milpitas Wash, California: Implications for the early evolution of the Colorado River [M.S. thesis]: Eugene, University of Oregon, 116 p.

House, P.K., Howard, K.A., Bell, J.W., and Pearthree, P.A., 2004, Preliminary geologic map of the Arizona and Nevada parts of the Mt. Manchester Quadrangle. Nevada Bureau of Mines and Geology Open-File Report 04-04, 1:24,000.

Howard, K.A., John, B.E., Nielson, J.E., Miller, J.M.G., Wooden, J.L., 2013, Geologic map of the Topock 7.5' Quadrangle, Arizona and Califronia: U.S. Geological Survey Scientific Investigation Map 3236, scale 1:24,000.

Kreemer, C., Blewitt, G., Hammond, W.C., 2010, Evidence for an active shear zone in southern Nevada linking the Wasatch fault to the Eastern California shear zone: Geology, v. 38, n. 5, p. 475-478.

Mahan, K.H., Guest, B., Wernicke, B., Niemi, N.A., 2009, Low-temperature thermochronologic constraints on the kinematic history and spatial extent of the Eastern California shear zone: Geosphere, v. 5, n.6, p. 483-495.

McDougall, K., Martinez, A.Y., 2014, Evidence for a marine incursion along the lower Colorado River corridor: Geosphere, v. 10, p. 828-841.

Metzger, D.G., 1968, The Bouse Formation (Pliocene) of the Parker-Blythe-Cibola area, Arizona and California: U.S.G.S Professional Paper 600-D, p. D126-D136.

Metzger, D.G., Loeltz, O.J., Irelna, B., 1973, Geohydrology of the Parker-Blythe-Cibola Area, Arizona and California: U.S.G.S Professional Paper 486-G, p. 130.

Miller, D.M., Reynolds, R.E., Bright, J.E., Starratt, S.W., 2014, Bouse Formation in the Bristol basin near Amboy, California, USA: Geosphere, v. 10, n. 3, p. 462-475.

Miller, F.K., McKee, E.H., 1971, Thrust and strike-slip faulting in the Plomosa Mountains, southwestern Arizona: GSA Bulletin, v. 82, n. 3, p. 717-722.

O'Connell, B., Dorsey, R.J., Humphreys, E.D., 2017, Tidal rhythmites in the southern Bouse Formation as evidence for post-Miocene uplift of the lower Colorado River corridor: Geology, v. 45, n. 2, p. 99-102.

Olmsted, F.H., Loeltz, O.J., and Irelan, B., 1973, Geohydrology of the Yuma Area, Arizona and California: U.S. Geological Survey Professional Paper 486-H, p. 1–227.

Pearthree, P.A., House, P.K., 2014, Paleogeography and evolution of the early Colorado River inferred from relationships in the Mohave and Cottonwood valleys,

Arizona, California, and Nevada: Geosphere, v. 10, n. 6, p. 1-22.

Pearthree, P.A., House, P.K., Gootee, B.F., Crow, R.S., Youberg, A., Bright, J., Howard, K.A., 2016, A perspective on lake filling, spilling, river incision and aggradation, and deformation during the early Pliocene in the Blythe Basin, Arizona and California: GSA Abstracts with Program, v. 48, n. 7.

Pearthree, P.A., Menges, C.M., Mayer, L., 1983, Distribution, recurrence, and possible tectonic implications of late Quaternary faulting in Arizona: Arizona Geological Survey Open-File Report 83-20, 44 p.

Richard, S.M., Dokka, R.K., 1992, Geology of the Packard Well fault zone, southeastern California, *in* Richard, S.M., ed. Deformation associated with the Neogene Eastern California Shear Zone, southwestern Arizona and southeastern California: Redlands, CA, San Bernardino County Museum Special Publication, p. 71-74.

Richard, S.M., Shipman, T.C., Greene, L., Harris, R.C., 2007, Estimated depth to bedrock in Arizona: AZGS Digital Geologic Map DGM-52, 1:1,000,000 scale, 9 p.

Ricketts, J.W., Girty, G.H., Sainsbury, J.S., Muela, K.K., Sutton, L.A., Biggs, M.A., Voyles, E.M., 2011, Episodic growth of the Chocolate Mountains anticlinorium recorded by the Neogene Bear Canyon conglomerate, southeastern California, U.S.A.: Journal of Sedimentary Research, v. 81, p. 859-873.

Ricketts, J.W., Beard, L.S., Crow, R., Coffey, K., and Haxel, G.B., this volume, Post-9.45 Ma depositional and structural history of the Bear Canyon conglomerate between Indian Pass and Picacho State Recreation Area, southeastern California.

Schell, B.A, Wilson, K.L., 1981, Regional neotectonic analysis of the Sonoran Desert: U.S. Geological Survey Open-File Report 82-57, 61 p.

Sherrod, D.R., Tosdal, R.M., 1991, Geologic setting and Tertiary structural evolution of Southwestern Arizona and Southeastern California: JGR, v. 96, p. 12407-12423.

Singleton, J.S., 2015, The transition from large-magnitude extension to distributed dextral faulting in the Buckskin-Rawhide metamorphic core complex, west-central Arizona: Tectonics, v. 34, pg. 1685-1708.

Singleton, J.S., Seymour, N.M., Reynolds, S.J., 2016, Distributed Neogene dextral faulting across Arizona's metamorphic core complexes: Superposition of the Pacific-North America plate boundary on the southern Basin and Range: GSA Abstracts with Programs v. 48, n. 4.

Spencer, J.E., and Patchett, P.J., 1997, Sr isotope evidence for a lacustrine origin for the upper Miocene to Pliocene Bouse Formation, LCR trough, and implications for timing of Colorado Plateau uplift: GSA Bulletin, v. 109, p. 767–778.

Spencer, J.E., Patchett, P.J., Pearthree, P.A., House, P.K., Sarna-Wojcicki, A.M., Wan, E., Roskowski, J.A., Faults, J.E., 2013, Review and analysis of the age and origin of the Pliocene Bouse Formation, lower Colorado River Valley, southwestern USA: Geosphere, v. 9, n. 3, p. 444-459.

Yang, W., Hauksson, E., Shearer, P.M., 2012, Computing a large refined catalog of focal mechanisms for southern California (1981-2010): Temporal stability of the style of faulting: Bulletin of the Seismological Society of America, v. 102, p. 1179-1194.

Post-9.45 Ma depositional and structural history of the Bear Canyon conglomerate between Indian Pass and Picacho State Recreation Area, southeastern California

Jason W. Ricketts[1], L. Sue Beard[2], Ryan Crow[2], Kevin Coffey[3], and Gordon B. Haxel[2]
[1]*Department of Geological Sciences, The University of Texas at El Paso, 500 W. University Ave, El Paso, TX 79902*
[2]*Geology, Minerals, Energy, and Geophysics Science Center, U.S. Geological Survey, 2255 N. Gemini Drive, Flagstaff, AZ 86001*
3Department of Earth, Planetary, and Space Sciences, University of California, Los Angeles, Los Angeles, CA. 90095-1567

Introduction

Constraining the timing and extent of Neogene north-south-oriented contraction and related dextral shear in southeastern California has implications for opening of the proto-Gulf of California, integration of the Colorado River, and uplift along the lower Colorado River corridor. The area lying between Indian Pass and Picacho State Recreation Area (PSRA) preserves a remarkable record of Oligocene and younger deformation documenting the transition from a Paleogene convergent margin to a Neogene transform setting dominated by dextral strike-slip faults. In eastern California, deformation related to the younger transform setting is expressed through development of the Eastern California Shear Zone, a 100-km-wide zone of dextral shear that initiated about 12-10 Ma (Dokka and Travis, 1990a, 1990b). Within the Indian Pass-PSRA region, the Bear Canyon conglomerate (BCC) forms an extensive alluvial sequence that unconformably overlies a package of ca. 23-Ma volcanic and epiclastic rocks, the Jurassic Winterhaven Formation, a probably Jurassic orthogneiss unit, and the Upper Cretaceous to Paleogene Orocopia Schist. The BCC is itself internally faulted and folded about the Chocolate Mountains anticlinorium (Ricketts et al., 2011), a series of elongate domes cored by the Orocopia Schist that extend from central Arizona to the San Andreas fault (Fig. 1) (e.g. Dillon, 1975; Haxel, 1977; Dillon et al., 1990; Jacobson et al., 2002; Haxel et al., 2002). In and around Bear Canyon, the BCC can be subdivided into three separate unconformity-bounded sequences, designated from oldest to youngest, SI, SII, and SIII (Fig. 2).

The purpose of this paper is to summarize what is currently known about the depositional and structural history of the BCC, with a focus on the more recent post-9.45-Ma history. Preliminary studies of the BCC described main outcrop localities and provided evidence that western exposures of this unit have been translated northwest during slip along the San Andreas fault system (Haxel and Dillon, 1973; Dillon, 1975; Peterson, 1975; Dillon and Ehlig, 1993). Although detailed studies of the BCC have previously been undertaken in the region between Indian Pass and PSRA (e.g. Hughes, 1993; Girty et al., 2006, 2012; Ricketts et al., 2011), a comprehensive understanding of the depositional conditions and subsequent deformation remains lacking. Therefore, this paper is also an opportunity to present some tentative conclusions based on new observations, and provide avenues for future research.

Geologic setting

The structurally lowest unit exposed in the region is the dominantly quartzofeldspathic Orocopia Schist, which reached amphibolite-grade peak metamorphic conditions (Jacobson et al., 2002). This unit forms the core of the Chocolate Mountains anticlinorium (Figs. 1, 2). The Orocopia Schist is separated from the overlying

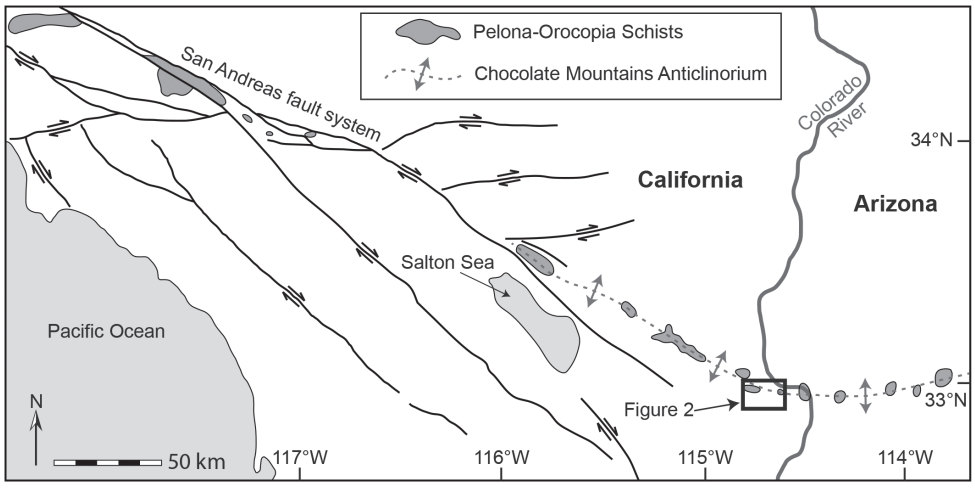

Figure 1. Simplified regional tectonic setting, highlighting major faults related to the San Andreas fault system and the trace of the Chocolate Mountains antoclinorium. Figure is modified from Yin (2002).

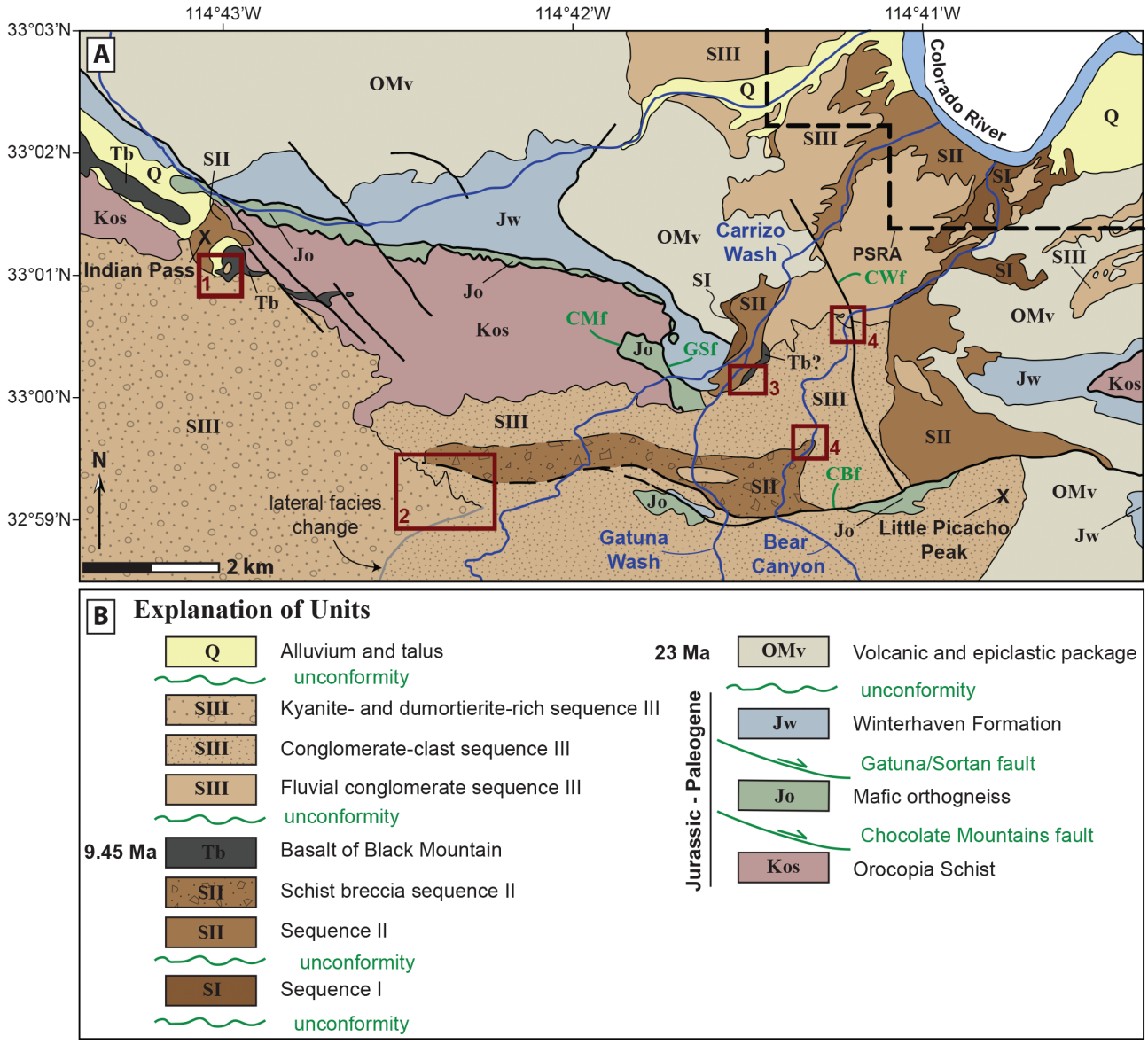

Figure 2. Simplified geologic map of the region between Indian Pass and Picacho State Recreation Area, southeastern California highlighting exposures of the Bear Canyon conglomerate. Red boxes with numbers refer to the locations of Bear Canyon conglomerate depositional relationships depicted in Figure 3. CBf – Copper Basin fault; CMf – Chocolate Mountains fault; CWf – Carrizo Wash fault; GSf – Gatuna/Sortan fault; PSRA – Picacho State Recreation Area. Figure is modified from Ricketts et al. (2011).

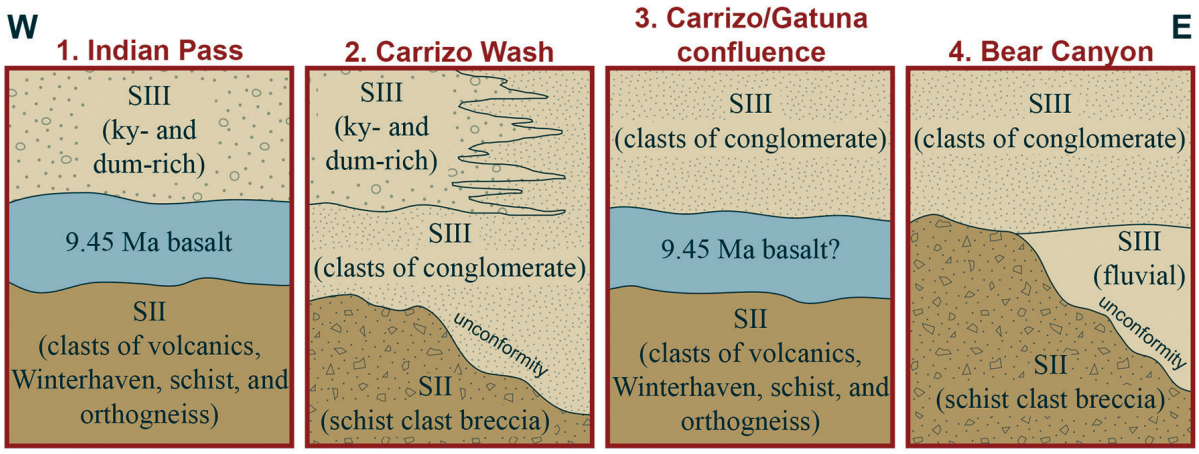

Figure 3. Schematic diagrams illustrating depositional relationships at different locations from Indian Pass to PSRA. Locations are shown in Figure 1. dum – dumortierite; ky – kyanite.

mafic orthogneiss unit by the Chocolate Mountains fault. This structure probably originated as a thrust that was responsible for initial burial of the Orocopia Schist, but was later reactivated as an extensional detachment fault at approximately 52-50 Ma (Dillon et al., 1990; Simpson, 1990; Jacobson et al., 2002; Yin, 2002). The mafic orthogneiss unit contains Al-rich plagioclase and hornblende having compositions that suggest middle- to upper-amphibolite peak metamorphic conditions (Oyarzabal et al., 1997). The mafic orthogneiss and Orocopia Schist lie within the footwall of the Gatuna/Sortan detachment fault and are juxtaposed against the Winterhaven Formation in the hanging wall. The Winterhaven includes metasedimentary and metavolcanic rocks that reached chlorite-grade greenschist metamorphic conditions. $^{40}Ar/^{39}Ar$ thermochronologic data suggest that the Gatuna/Sortan fault exhumed the package of metamorphic rocks to near-surface levels from ca. 28-24 Ma (Jacobson et al., 2002, 2007).

A 1.2-km-thick unit of volcanic and epiclastic rocks rest unconformably on the metamorphic basement. These rocks consist of basaltic to andesitic lava flows, trachyte, lahars, epiclastic breccia, and pyroclastic accumulations (Crowe, 1978; Girty et al., 2006; Biggs, 2008; Sainsbury, 2010). U-Pb zircon geochronology from the oldest and youngest rocks of the volcanic package yield eruption ages of 23.4 ± 0.4 Ma (Needy et al., 2007) and 23.5 ± 1 Ma (Biggs, 2008), respectively, indicating very rapid and near-synchronous deposition of the entire volcanic and epiclastic package.

The BCC was deposited on the ca. 23-Ma volcanic rocks, and the two are separated by an angular unconformity. The BCC crops out extensively in the region between Indian Pass and PSRA (Fig. 2). Thick exposures are preserved along the length of Bear Canyon, where the BCC was deposited within a depression in the axis of the Chocolate Mountains anticlinorium (Ricketts et al. 2011). To the east and west, the BCC thins against topographic highs that are composed of Orocopia Schist, mafic orthogneiss, and Winterhaven Formation, which form structural highs along the anticlinorium. Exposures of the BCC extend to the southwest, where they drape against the southern limb of the Chocolate Mountains anticlinorium. Although detailed mapping of these deposits has yet to be completed, the BCC also extends south to at least the Cargo Muchacho Mountains, and west beyond Indian Pass.

Depositional patterns of the Bear Canyon Conglomerate

In Bear Canyon and Carrizo Wash, the BCC was deposited as at least three separate sequences, each separated by an angular unconformity. Detailed mapping and sedimentological work, moreover, show that each sequence is itself composed of multiple lithologic types deposited in a range of depositional conditions, and contains clasts derived from multiple provenance locations (Ricketts, 2010; Ricketts et al., 2011). Many of these sedimentary rocks reflect very local drainages during the Miocene when drainage patterns were controlled by the Chocolate Mountains anticlinorium and rock units that core this feature, although there is also evidence for north-flowing drainages that introduced exotic clasts, as described below. Figure 3 provides a tentative correlation of units from Indian Pass to Bear Canyon, as described below.

Sequence I

Sequence I mostly crops out within Bear Canyon along the northeastern edge of the field area, although a separate small outcrop is preserved to the west near Carrizo Wash (Fig. 2). Sequence I is composed of clast- and matrix-supported, medium- to thick-bedded, poorly- to well-sorted conglomerate (Ricketts et al., 2011). Clasts in sequence I range in size from granules to boulders, and are entirely derived from the underlying ca. 23-Ma volcanic and epiclastic package. Further, clast counts in sequence I show an unroofing sequence and suggest that these sediments were derived from the dissection of the underlying ca. 23-Ma volcanic rocks (Girty et al. 2006). Along the northern end of Bear Canyon, sequence I is separated from sequence II by a ~6° angular unconformity. Farther south in Bear Canyon, it is capped by flat-lying gravels of sequence III (Fig. 4A).

Sequence II

Sequence II crops out in Carrizo Wash and to the east of Bear Canyon, and is truncated to the south by the Copper Basin fault (Fig. 2). It directly overlies multiple units, including sequence I, the ca. 23-Ma volcanic package, and the Winterhaven Formation. It is similar to sequence I in that it is made up of clast- and matrix-supported, medium- to thick-bedded, poorly to well-sorted conglomerate. Clast assemblages in both sequences contain subequal proportions of the various types of volcanic rock, but those in sequence II also contain abundant clasts of the underlying metamorphic basement. The presence of clasts of basement rocks indicates that by the time sequence II was deposited, the ca. 23-Ma volcanic rocks had been eroded through in some locations (Ricketts et al., 2011). Clast counts and paleoflow indicators all suggest that most, if not all of sequence II exposed between Indian Pass and PSRA was derived from local sources and funneled into the growing depression in the Chocolate Mountains anticlinorium (Ricketts et al., 2011). In Bear Canyon, sequence II is separated from sequence III by a ~15° angular unconformity.

To the south near the Copper Basin fault, the upper part of sequence II is made up of a distinctive sedimentary breccia that contains more than 90% angular clasts of Orocopia Schist. These deposits commonly show coarse-tail reverse grading, a wide range in clast size, and very thick beds which indicate deposition primarily by debris flows. These beds can be traced to the west of Carrizo

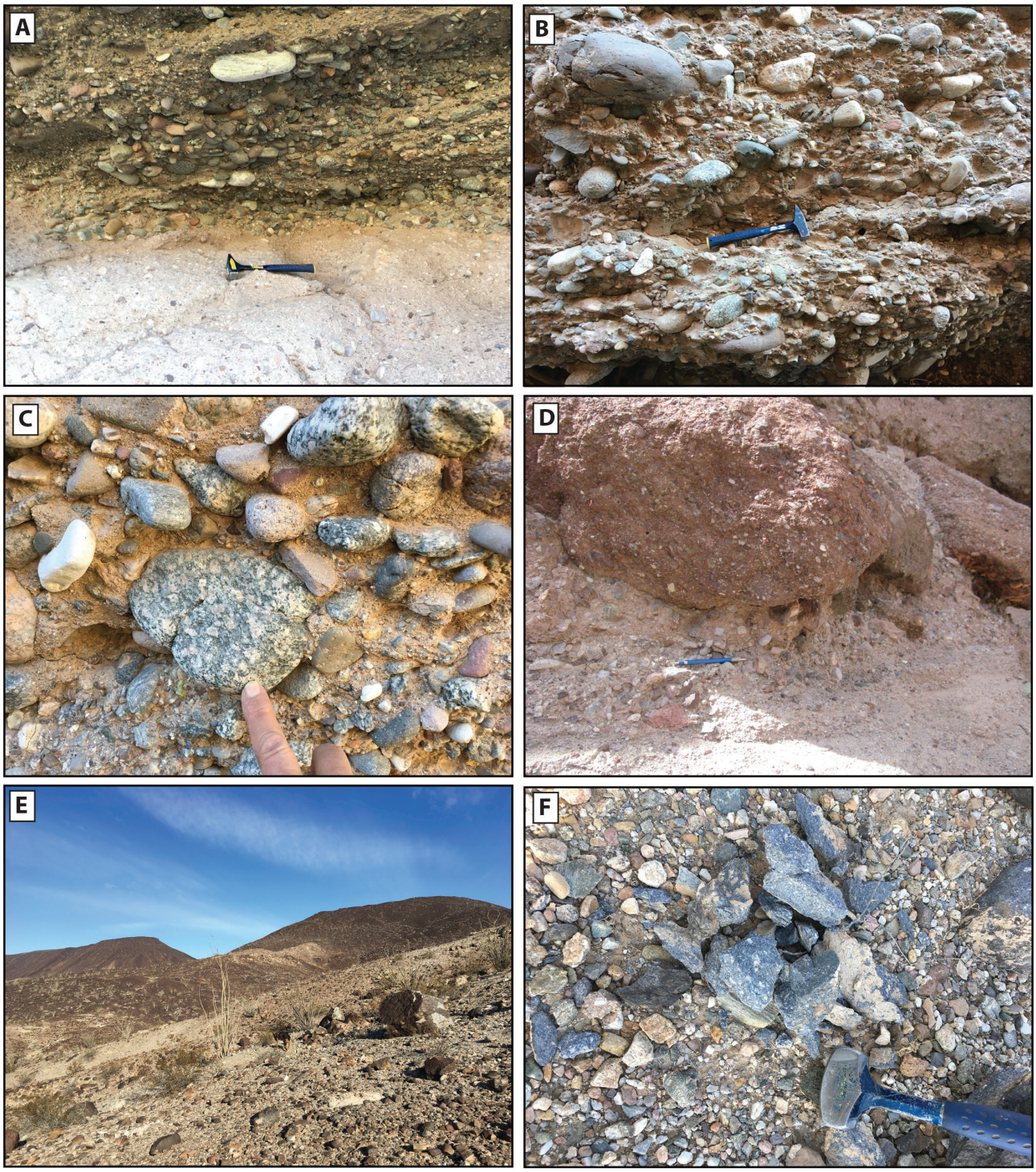

Figure 4. A. Depositional contact between sequence I and sequence III in Bear Canyon. Sequence I only contains clasts of 23-Ma volcanic rock, whereas sequence III contains a wide variety of clasts, including abundant mesocratic orthogneiss. Photo by L.S. Beard. **B.** View looking west of the oldest facies of sequence III in Bear Canyon. Note the well-rounded nature of the clasts and the imbrication suggestive of northward transport. Photo by L.S. Beard. **C.** Close-up of mesocratic orthogneiss clast in the oldest facies of sequence III in Bear Canyon. Note the abundance of these clasts in the photo compared to other rock types. These clasts are tentatively suggested to have been derived from the Cargo Muchacho Mountains to the south based on textural similarities. Photo by L.S. Beard. **D.** Younger facies of sequence III in Bear Canyon containing abundant pebble- to boulder-sized clasts of older, dark reddish-brown conglomerate. Photo by G.H. Girty. **E.** View of sequence III deposits south of Indian Pass with boulder-sized clasts of mesocratic orthogneiss. In the background, these deposits can be seen deposited on top of the basalt of Black Mountain. Photo by L.S. Beard. **F.** Clast of bluish gray dumortierite in sequence III south of Indian Pass. Photo by L.S. Beard.

Wash, where they parallel the southern edge of the Gavilan hills (Figs. 2, 3).

Sequence III

Sequence III caps older BCC deposits in Bear Canyon and Carrizo Wash (Fig. 2). In Gatuna Wash, sequences II and III are separated by an undated basalt flow. In this region sequence III is composed of two main lithologic units that can be easily identified in the field. The underlying unit is composed of clast-supported conglomerate that accumulated in a series of 1-2 m deep asymmetric alluvial channels. Well-developed imbrication consistently suggests these channels were north-flowing (Fig. 4B) (Ricketts et al., 2011). Clasts are typically well-sorted and rounded, and a significant proportion of them are derived from an orthogneiss source. Although these orthogneiss clasts have not yet been studied in detail, in hand sample they differ from the mafic orthogneiss that crops out to the east and west by having higher abundances of 1-2 cm K-feldspar phenocrysts and lesser amounts of biotite and muscovite (Fig. 4C). They range from weakly to strongly foliated. These clasts appear similar to exposures of mesocratic quartz monzonite that crop out along the eastern side of the Cargo Muchacho Mountains to the south, which contain large K-feldspar phenocrysts that are embedded within a finer-grained matrix of biotite and hornblende. These mafic minerals typically project into the larger K-feldspar phenocrysts, making the grain edges appear fuzzy (Dillon and Ehlig, 1993). This particular texture is also observed in the clasts of orthogneiss in Bear Canyon (Fig. 4C). These observations suggest a more far-traveled and distal source, which is unlike any other BCC deposit in the local area. The fluvial, orthogneiss-bearing conglomerate of sequence III interfingers with, and transitions into, the youngest lithologic unit exposed in and around Bear Canyon. These deposits are made up of clast- and matrix-supported beds that are typically poorly sorted. Although these deposits contain clasts from the underlying metamorphic basement, they also contain a significant volcanic-clast population, which gives these beds a distinctive pinkish hue. In addition, these youngest deposits contain clasts of dark reddish-brown, well-indurated older conglomerate (Fig. 4D). These conglomerate clasts range in size from ~ 5 cm to at least 3-4 m in diameter. The relative abundance of these conglomerate clasts increases to the southeast, and the maximum clast size increases in the same direction. Although additional research is necessary to confirm, a probable source for these clasts is Little Picacho Peak (Fig. 2), which is composed of well-indurated conglomerate having a dark reddish-brown color.

Sequence III extends to the southwest along the southern flank of the Gavilan Hills, where clasts of conglomerate continue to decrease in size and abundance until they are not observed. Immediately west of Carrizo Wash, these deposits interfinger with, and are overlain by, conglomerate that contains abundant clasts of mesocratic orthogneiss (Figs. 2, 3). These clasts range in size from pebbles to boulders, and make up a majority of the clast population. These deposits differ, however, from the fluvial, orthogneiss-bearing conglomerate at the base of sequence III because they are not as well-rounded, and they do not form the same sequence of nested channels with well-developed imbrication. This unit of sequence III west of Carrizo Wash can be traced to Indian Pass, where they directly overly the basalt of Black Mountain, with a reported $^{40}Ar/^{39}Ar$ age of 9.45 ± 0.27 Ma (Muela, 2011). At Indian Pass, mesocratic orthogneiss clasts are still present, although they are commonly boulder-sized (Fig. 4E). In addition, sequence III deposits at this location also contain distinctive kyanite- and dumortierite-rich clasts (Fig. 4F) that have not been observed in and around Bear Canyon, but have been found as far east as Carrizo Wash. These are tentatively suggested to have been derived from outcrops in the Cargo Muchacho Mountains, where kyanite is abundant in veins at some localities (e.g. Dillon and Ehlig, 1993).

Neogene structural evolution

Depositional patterns are best understood within the context of the local structural development of the area, which greatly affected the timing, extent, and style of BCC deposition. Extension concentrated along the Gatuna/Sortan faults at 28-24 Ma (Jacobson et al., 2002, 2007) resulted in exhumation of the Orocopia Schist to near-surface levels and the initial formation of the Chocolate Mountains anticlinorium as an extensional megamullion structure. The hingeline of this large-scale fold produced a series of culminations, such as within the Gavilan Hills, and depressions, such as in the region of Bear Canyon. Paleocurrent and provenance studies of the BCC within and surrounding Bear Canyon suggest that sequences II and III were locally derived and funneled into the north-south-trending depression in the anticlinorium (Ricketts et al., 2011). Extensional deformation persisted into the Miocene because the package of ca. 23-Ma volcanic and epiclastic rocks is strongly deformed by normal faults that are related to, and sole into, the Gatuna/Sortan master detachment (Sainsbury, 2010). Although the BCC preserves minor normal faults with relatively small offset, it was not strongly deformed by this extensional event. Rather, as described below it preserves ample evidence for north-south-oriented contraction which persisted until younger than 9.45 Ma (Ricketts et al., 2011).

Evidence for post-9.45-Ma deformation

All three sequences of the BCC have been variably faulted and folded about the Chocolate Mountains anticlinorium. The 9.45-Ma basalt of Black Mountain currently provides the most concrete evidence for the timing of deposition and deformation of the BCC. At Indian Pass, the basalt directly overlies sequence II and underlies sequence III of the BCC (Fig. 2). At this location the basalt dips ~10° south along the southern limb of

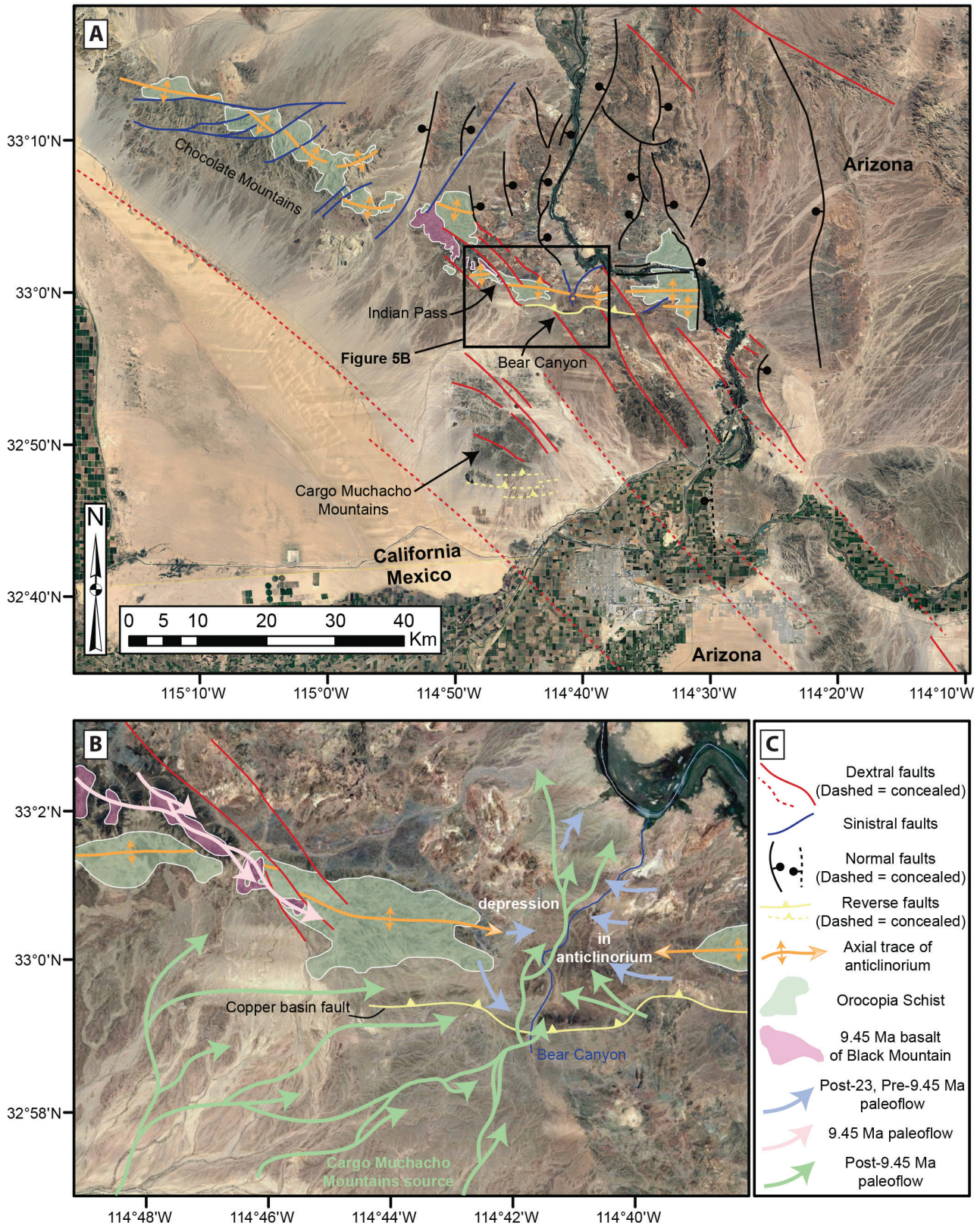

Figure 5. A. Regional tectonic setting of the study area highlighting systems of dextral, sinistral, and reverse faults that overprint earlier-formed normal faults. Outcrops of Orocopia Schist and the basalt of Black Mountain are highlighted, and the trace of the Chocolate Mountains anticlinorium through the study area is shown. Figure is modified from Beard et al. (2016). **B.** Summary of paleoflow indicators and their known timing constraints. The depression in the Chocolate Mountains anticlinorium is located between structural highs exposing Orocopia Schist to the east and west. See text for details of suggested paleoflow patterns. **C.** Explanation of map units. Base photos are from Google Earth.

the Chocolate Mountains anticlinorium (Ricketts et al., 2011). As described previously, sequence III overlying the basalt of Black Mountain contains abundant cobble- to boulder-sized mesocratic orthogneiss and kyanite- and dumortierite-bearing clasts. 5 km to the east this unit transitions laterally into, and overlies, sequence III of the BCC that contains abundant clasts of preexisting conglomerate (Figs. 2, 3). In Carrizo Wash, an enigmatic outcrop of basalt is exposed along the eastern edge of the wash (Fig. 2). Ricketts et al. (2011) originally mapped this as part of the underlying ca. 23-Ma volcanic package. 23-Ma basalt flows, however, are commonly altered by hydrothermal metasomatism and preserve abundant amygdules filled with quartz or calcite (Girty et al., 2012). The basalt in Carrizo Wash does not share these characteristics, suggesting it may be a younger flow. In addition, detailed mapping shows that this flow overlies sequence II, and directly underlies sequence III, similar to relationships at Indian Pass (Fig. 2). If this basalt flow is equivalent to the basalt of Black Mountain, this would further suggest that all of sequence III of the BCC is younger than 9.45 Ma. Dating of this basalt flow, which is currently underway, would further test this hypothesis.

Between Bear Canyon and Gatuna Wash, bedding orientations within sequence III define a broad, east-west-trending anticline that is similar in orientation to the Chocolate Mountains anticlinorium. Strike-slip faults cutting all three sequences of the BCC are evidenced by well-defined fault surfaces with subhorizontal slickenlines. In addition, the axial traces of folds in sequence III between Gatuna Wash and Little Picacho Peak are offset, and display left- and right-lateral separation. The most prominent of these strike slip faults is informally referred to as the Carrizo Wash fault (Fig. 2) (Ricketts et al., 2011). Although detailed mapping of the three sequences has yet to be completed to the south, the Bear Canyon and Carrizo Wash faults appear to be truncated against the east-west-trending Copper Basin fault (Ricketts et al., 2011; Girty et al., 2012). This fault dips steeply south and places mafic orthogneiss in the hanging wall against sequences II and III deposits in the footwall, suggesting reverse movement (Sutton, 2010). In the immediate footwall of the Copper Basin fault, bedding orientations within sequences II and III define a fault-parallel syncline that extends east from Little Picacho Peak and west to at least Carrizo Wash and possibly farther (Ricketts et al., 2011). The above structural observations, coupled with the preliminary correlation of BCC units from Bear Canyon to Indian Pass, suggest that fold growth, strike-slip faulting, and reverse movement along the Copper Basin fault all post-date the eruption of the basalt of Black Mountain at 9.45 Ma.

How young is the most recent deformation?

Beard et al. (2016) suggested that the post-BCC shortening strain as documented by Ricketts et al. (2011) was a result of left-stepping dextral faults (Fig. 5A). They suggested a broad northwest belt of distributed dextral shear developed during the late Miocene time as part of the Gulf of California shear zone (Bennett and Oskin, 2014; Bennett et al., 2016). In their model, the western part of the shear zone stepped left along the southwest side of the Chocolate Mountains anticlinorium, imposing a shortening strain that enhanced the anticlinorium and formed the Copper Basin reverse fault (Fig. 5A). The eastern part of the shear zone east of the Chocolate Mountains linked northward to segments of the Eastern California shear zone.

The age and relative timing of this post 9.45 Ma deformation sequence is poorly constrained. However, the linkage between the Gulf of California and Eastern California shear zones through southeastern California and southwestern Arizona was most likely active in late Miocene to Pliocene (Fig. 3 in Bennett et al., 2016) and, by inference, produced the transpressional steps into the Chocolate Mountains. Additional post-5 Ma faulting and gentle fold-related tilting are suggested by faults that are known to cut and post-date the Bouse Formation (e.g. Gootee et al., 2016) and by gentle tilting and warping of the Bouse (see discussion in Beard et al., 20160.

These structural patterns, coupled with provenance studies of the BCC as described previously, shed light on paleoflow directions through time in the region between Indian Pass and PSRA (Fig. 5B). Sequences I and II were locally-derived, and funneled into the growing depression in the Chocolate Mountains anticlinorium between 23 and 9.45 Ma. At 9.45 Ma, the basalt of Black Mountain flowed southeast along a paleodrainage that cut obliquely across the east-west-trending Chocolate Mountains anticlinorium. Based on clast composition and imbrication of clasts, sequence III was derived from the south, with a likely source in the Cargo Muchacho Mountains. These fluvial streams likely took advantage of the low-lying depression in the anticlinorium, and flowed north parallel to Bear Canyon after 9.45 Ma (Fig. 5B).

Future research and conclusions

Future research in this area will likely be aimed at further constraining the timing and style of Neogene deformation preserved in the BCC. To do this, detailed sedimentological studies need to be undertaken to correlate different sequences and tie them to known time stratigraphic markers such as the basalt of Black Mountain. Initial work in the region between Little Picacho Peak and Carrizo Wash will need to be extended to the south of the Copper Basin fault, and to the west towards Indian Pass. This will also help to refine the post-9.45-Ma paleodrainages depicted in Figure 5B. Second, detailed kinematic studies of faults cutting different sequences of the BCC need to be undertaken in order to understand the style, extent, and possible timing of deformation preserved in these rocks. Although the majority of faults that cut the BCC are relatively small offset, they can nonetheless provide important

information regarding the state of strain, which can then be compared to more regional trends. Lastly, although there is ample evidence for post-9.45-Ma deformation in the BCC, it is more difficult to constrain exactly when deformation ceased in this region. In an attempt to provide additional temporal constraints, efforts will focus on finding ash layers in the youngest sequence III layers in an attempt to date when they were deposited. If found, these ash layers could provide the most robust evidence for constraining the timing of youngest deformation in this region. Although the undated basalt in Carrizo Wash, between sequences II and III, is likely associated with the 9.45-Ma Black Mountain eruption, in-progress $^{40}Ar/^{39}Ar$ dating of this flow may require revisions to the ages of the BCC subunits.

In conclusion, the Neogene BCC between Indian Pass and PSRA preserves a remarkable record of Oligocene and younger deformation. Detailed sedimentological and structural studies suggest that the BCC is composed of three sequences that are each separated by an angular unconformity. New observations now allow for a tentative correlation of these units from Indian Pass to Bear Canyon. Sequence III directly overlies the 9.45-Ma basalt of Black Mountain at Indian Pass and is also folded about the Chocolate Mountains anticlinorium. A series of strike-slip faults cutting sequence III of the BCC are truncated by the east-west-trending Copper Basin reverse fault. These structures are all consistent with a tectonic environment dominated by north-south shortening. Post-9.45-Ma deformation in the region between Indian Pass and PSRA is consistent with development of the Eastern California Shear Zone and therefore records early evolution of the San Andreas transform fault system in southeastern California.

Acknowledgments

The research reported here builds off of the data and interpretations from Ricketts et al. (2011), which was supported by NSF EAR-091163 awarded to G.H. Girty at San Diego State University. Geochemical data for clasts within the Bear Canyon conglomerate are available from the Journal of Sedimentary Research Data Archive: http://www.sepm.org/pages.aspx?pageid=269. Robert Powell and Jacob Thacker reviewed this manuscript and provided helpful comments.

References

Beard, L.S., Haxel, G.B., Dorsey, R.J., McDougall, K.A., and Jacobson, C.E., 2016, Late Neogene deformation of the Chocolate Mountains anticlinorium: Implications for deposition of the Bouse Formation and early evolution of the Lower Colorado River, *in* Reynolds, R.E., ed., Going LOCO: investigations along the Lower Colorado River: Desert Symposium Field Guide and Proceedings, p. 176-184.

Bennett, S.E.K., and Oskin, M.E., 2014, Oblique rifting ruptures continents: Examples from the Gulf of California shear zone: Geology, v. 42, p. 215-218, doi: 10.1130/G34904.1.

Bennett, S.E.K., Darin, M.H., Dorsey, R.J., Skinner, L.A., Umhoefer, P.J., and Oskin, M.E., 2016, Animated tectonic reconstruction of the Lower Colorado River Region: Implications for late Miocene to Present deformation, *in* Reynolds, R.E., ed., Going LOCO: Desert Symposium Field Guide and Proceedings, p. 73-86.

Biggs, M.A., 2008, Miocene volcanic rocks and conglomerates, SE California: evidence for Neogene reactivation of the Chocolate Mountains anticlinorium [M.S. thesis]: San Diego, San Diego State University, 30 p.

Crowe, B.M., 1978, Cenozoic volcanic geology and probable age of inception of basin-range faulting in the southeasternmost Chocolate Mountains, California: Geological Society of America Bulletin, v. 89, p. 251-264.

Dillon, J.T., 1975, Geology of the Chocolate and Cargo Muchacho Mountains, southeasternmost California [Ph.D. thesis]: Santa Barbara, University of California, 405 p.

Dillon, J.T., and Ehlig, P.L., 1993, Displacement on the southern San Andreas fault, *in* Powell, R.E., Weldon, R.J., II, and Matti, J.C., eds., The San Andreas fault system: Displacement, palinspastic reconstruction, and geologic evolution: Geological Society of America Memoir 178, p. 199-216.

Dillon, J.T., Haxel, G.B., and Tosdal, R.M., 1990, Structural evidence for northeastward movement on the Chocolate Mountains thrust, southeasternmost California: Journal of Geophysical Research, v. 95, p. 19953-19971.

Dokka, R.K., and Travis, C.J., 1990a, Late Cenozoic strike-slip faulting in the Mojave Desert, California: Tectonics, v. 9, p. 311-340.

Dokka, R.K., and Travis, C.J., 1990b, Role of the Eastern California shear zone in accommodating Pacific-North American plate motion: Geophysical Research Letters, v. 17, p. 1323-1326.

Girty, G.H., Stephenson, D., Canfield, A., Marsh, J., Middleton, T., Rayburn, J., Sisk, M., Verdugo, D., Moniz, R., Gunter, J., Nielsen, J., Gasca, C., Rowland-Smith, A., Smith, M., Lovering, K., Campbell, K., Castenada, F., Gray, R., and Campbell, C., 2006, Geology of the Picacho State Recreation Area, SE California: implications for the timing of formation of the Chocolate Mountains anticlinorium, *in* Girty, G.H., and Cooper, J., eds., Using stratigraphy, Sedimentology, and Geochemistry to Unravel the Geologic History of the Southwestern Cordillera: A volume in honor of Patrick L. Abbott: Pacific Section, SEPM, Book 101, p. 77-96.

Girty, G.H., Muela, K.K., Olson, H., Sutton, L., Biggs, M., Sainsbury, J., Ricketts, J.W., Errthum, R., Colby, T.A., Carrasco, T., Gordon, E., and Pelbath, T., 2012, Toward a unified model for the geologic and tectonic history of the region between Indian Pass and Picacho State Recreation Area, southeastern California, *in* Wirths, T.A. (ed.), Picacho and the Cargo Muchachos: San Diego Association of Geologists, San Diego, Ca, p. 53-86.

Gootee, B.F., Pearthree, P.A., House, P.K., Youberg, A., Spencer, J.E., and O'Connell, B., 2016, Geologic map and report of the Cibola area, La Paz County, Arizona, and Imperial County, California: Arizona Geological Survey Digital Geologic Map 112 (DGM-112), scale 1:24,000, 21 p.

Haxel, G.B., 1977, The Orocopia Schist and the Chocolate Mountains thrust, Picacho-Peter Kane Mountain area,

southeasternmost California [Ph.D. thesis]: Santa Barbara, University of California, 277 p.

Haxel, G., and Dillon, J., 1973, The San Andreas fault system in southeasternmost California. Stanford Univ. Publications Geol. Sci, v. 13, p. 322–33.

Haxel, G.B., Jacobson, C.E., Richard, S.M., Tosdal, R.M., and Grubensky, M.J., 2002, The Orocopia Schist in southwestern Arizona: Early Tertiary oceanic rocks trapped or transported far inland, *in* Barth, A. ed., Contributions to Crustal Evolution of the Southwestern United States: Geological Society of America, Special Paper 365, p. 99-128.

Hughes, K.M., 1993, The conglomerate of Bear Canyon (Miocene), Chocolate Mountains, southeastern Calif., *in* Sherrod, D.R., and Nielsen, J.E., eds., Tertiary Stratigraphy of Highly Extended Terranes, California, Arizona, and Nevada: U.S. Geological Survey, Bulletin 2053, p. 213-216.

Jacobson, C.E., Grove, M., Stamp, M.M., Vucic, A., Oyarzabal, F.R., Haxel, G.B., Tosdal, R.M., and Sherrod, D.R., 2002, Exhumation history of the Orocopia Schist and related rocks in the Gavilan Hills area of southeasternmost California, *in* Barth, A., ed., Contributions to Crustal Evolution of the Southwestern United States: Geological Society of America, Special Paper 365, p. 129-154.

Jacobson, C.E., Grove, M., Vucic, A., Pedrik, J.N., and Ebert, K.A., 2007, Exhumation of the Orocopia Schist and associated rocks of southeastern California: relative roles of erosion, synsubduction, tectonic denudation, and middle Cenozoic extension, *in* Cloos, M., Carlson, W.D., Gilbert, M.C., Liou, J.G., and Sorensen, S.S., eds., Convergent Margin Terranes and Associated Regions – a tribute to W.G. Ernst: Geological Society of America, Special Paper 410, p. 1-37.

Muela, K.K., 2011, Timing and style of Miocene deformation, Indian Pass and Picacho State Recreation Area, SE California, U.S.A. [M.S. thesis]: San Diego, San Diego State University, 44 pg.

Needy, S.K., Wooden, J.L., Barth, A.P., and Jacobson, C.E., 2007, Geochronology of igneous rocks in the Chocolate Mountains region as a means to interpret the tectonic evolution of southeastern California: Geological Society of America, Abstracts with Programs, v. 39, p. 407.

Oyarzabal, F.R., Jacobson, C.E., and Haxel, G.B., 1997, Extensional reactivation of the Chocolate Mountains subduction thrust in the Gavilan Hills of southeastern California: Tectonics, v. 16, p. 650-661.

Peterson, M.S., 1975, Geology of the Coachella Fanglomerate, *in* Crowell, J. C., ed., San Andreas Fault in Southern California: Special Report 118, California Division of Mines and Geology, Sacramento, p. 119–126.

Ricketts, J.W., 2010, Miocene growth of a depression in the axis of the Chocolate Mountains anticlinorium recorded by the Bear Canyon conglomerate, SE California [M.S. thesis]: San Diego, San Diego State University, 50 p.

Ricketts, J.W., Girty, G.H., Sainsbury, J.S., Muela, K.K., Sutton, L.A., Biggs, M.A., and Voyles, E.M., 2011, Episodic growth of the Chocolate Mountains anticlinorium recorded by the Neogene Bear Canyon conglomerate, southeastern California, U.S.A.: Journal of Sedimentary Research, v. 81, p. 859-873, doi: 10.2110/jsr.2011.66.

Sainsbury, J.S., 2010, Timing of extension, N-S shortening, and conjugate strike-slip faulting in the evolution of the Chocolate Mountains anticlinorium: evidence from the Gavilan Hills, SE California [M.S. thesis]: San Diego, San Diego State University, 42 p.

Simpson, C., 1990, Microstructural evidence for northeastward movement on the Chocolate Mountains fault zone, southeastern California: Journal of Geophysical Research, v. 95, p. 529-537.

Sutton, L.A., 2010, The Copper Basin fault, a newly recognized reverse fault in the lower Colorado River region, SE California: implications for Miocene-Pliocene N-S shortening within the Eastern California Shear Zone [M.S. thesis]: San Diego, San Diego State University, 42 p.

Yin, A., 2002, Passive-roof thrust model for the emplacement of the Pelona-Orocopia Schist in southern California, United States: Geology, v. 30, p. 183-186.

Towards a depositional model for travertines of the Bouse Formation: examples from the southern Blythe Basin

L. C. Crossey[1], K. E. Karlstrom[1], R. S. Crow[2], R.S., C. Ferguson[1], and R. Dorsey[3]
[1] *University of New Mexico,* [2] *USGS Flagstaff,* [3] *University of Oregon*

The Bouse Formation provides a sedimentary record of the first arrival of the Colorado River, water and sediment, as it was integrated from the Colorado Plateau to the proto-Gulf of California approximately 4.8-5.3 Ma (House et al., 2008; Spencer et al., 2013). This unit is generally thin (1-100s m) but widespread within basins in the lower Colorado River corridor from Lake Mead to Yuma (Fig. 1). The lower (informal) member of the Bouse Formation is predominantly carbonate; the middle part (the "interbedded unit" of Metzger et al., 1973) consists mainly of siliciclastic deposits, including Colorado River-derived clays, silt, and sand; and the upper member is sandy to gravel-rich bioclastic limestone and locally derived conglomerate that was recently recognized in in the upper member of the southern Blythe basin. This paper focuses on basal carbonates of the Blythe basin. Two depositional models for the Bouse in this basin are considered: (1) deposition in a freshwater lake (e.g., Spencer et al., 2008; 2013); and (2) a marine estuary, as proposed for the southern part of the corridor (e.g., Miller et al., 2014; McDougall and Miranda-Martinez, 2014; Crossey et al., 2015; Homan, 2014; O'Connell et al., 2016; 2017).

This paper focuses on the travertine (aka tufa) facies of the Bouse with a goal of understanding the different origins of Bouse carbonates and follows interpretations of Crossey et al. (2016). Dorsey et al. (2016) describe three carbonate facies in the southernmost part of the corridor: (1) lower bioclastic limestone and "tufa" that are interpreted to represent high-energy shallow water (including tidal) environments; (2) a marl succession that is interpreted to record precipitated carbonate settling below wave base in a large body of water; and (3) an upper unit of fossil-rich calcarenite and conglomerate (Gootee et al., 2016) that overlies the other carbonate facies, mudstone, and cross-bedded Colorado River sandstone,

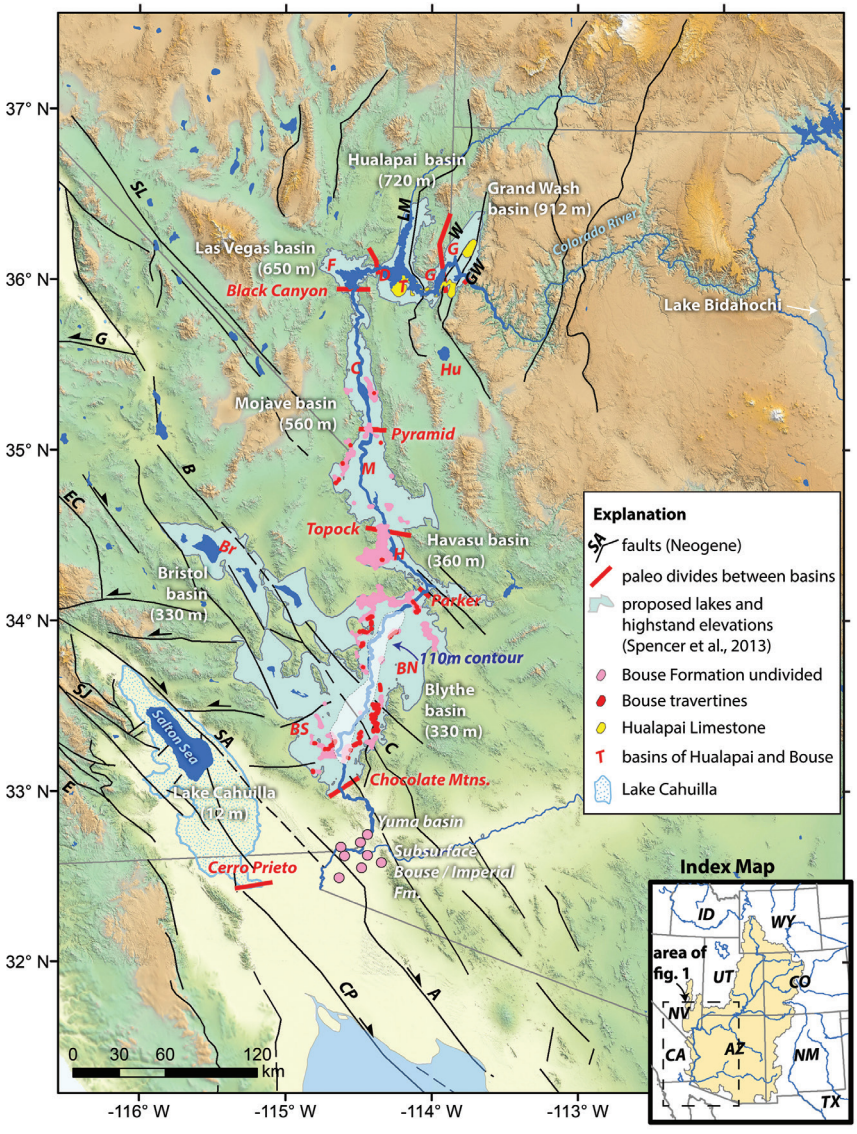

Figure 1. Distribution of the Bouse Formation; Red= Bouse travertine; Pink= Bouse Fm. undivided. This paper focuses on travertines from the Blythe basin: general locations indicated with black stars. The blue arrow indicates the location of the 110m elevation contour, which corresponds to the highest elevation of interpreted marine facies in the Blythe basin. Modified from Crossey et al. (2016).

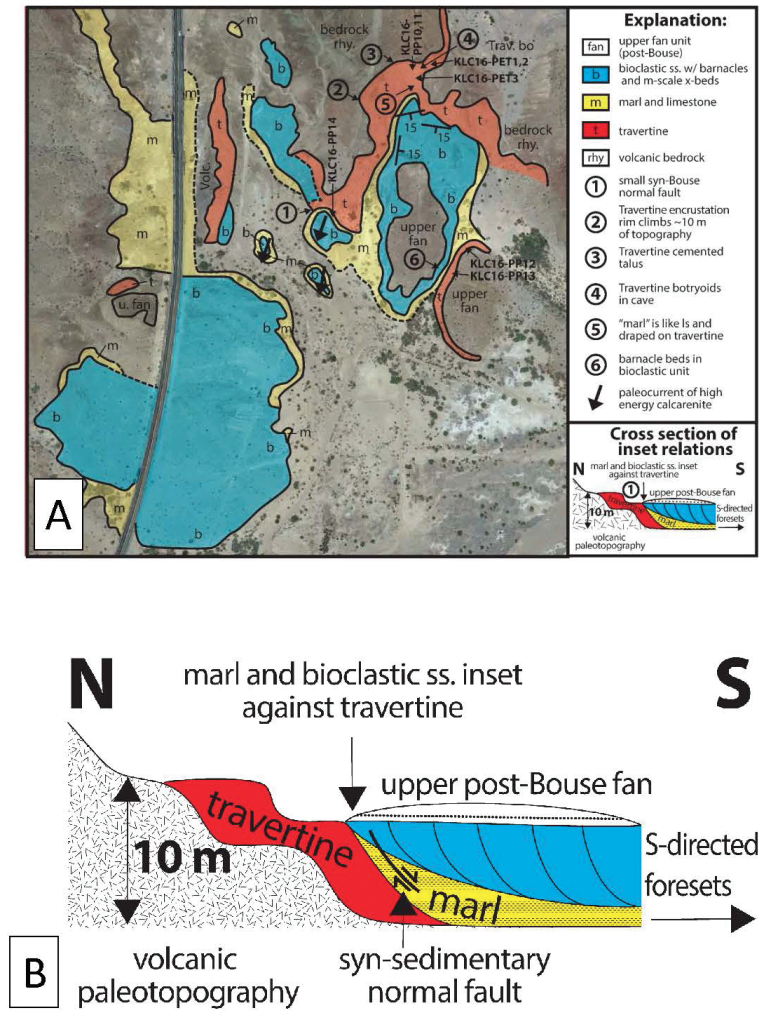

Figure 2. (A) Geologic map of the Bouse Formation at Petroglyph Park; Red= Bouse travertine; Blue=bioclastic sst., Yellow-marl & ls. (B) Schematic cross-section from north to south across the map area illustrating marl onlapping travertine, and high-energy facies inset into both.

and is locally interbedded with mudstone. Here we argue that the travertine deposits constitute a widespread and definable facies as well.

We emphasize that the travertine facies of the Bouse records the first arrival of carbonate- oversaturated waters (the "carbonate factory") that deposited basal Bouse carbonates and hence the need to develop a depositional model for this facies and how it relates to the overlying bioclastic limestone, marl, and calcarenite facies of the Bouse Formation. The term travertine is used here as the more inclusive term and refers to *chemically-precipitated continental limestone that forms as groundwater discharge deposits at spring outlets, and in lakes and streams, via precipitation of calcite from waters that are supersaturated with respect to calcium carbonate* (Ford and Pedley, 1996; Pentecost, 2005). The term "tufa" is sometimes used interchangeably as a mapping term for porous carbonates that occur in spring mounds and "tufa towers" around lakes. However, we prefer the term "travertine" and use it inclusively with no implied interpretation about temperature of the depositing waters, as this is generally unknown for inactive/fossil systems. The term travertine, in our usage, encompasses a very wide range of freshwater carbonate textures (Fig. 2; see also Crossey et al., 2016).

As also summarized by Crossey et al. (2016), fresh-water carbonates form according to a well-recognized suite of chemical reactions (Pentecost, 2005; Crossey et al., 2006, 2009). For waters to become supersaturated with respect to CO_2, an "external" CO_2 source (e.g. soil gas and/or magmatically derived volatiles) is needed to make waters aggressive enough to dissolve calcite in regional aquifers. The dissolution reaction is: $extCO_{2(g)} + H_2O + CaCO_{3(limestone)} \rightarrow Ca^{+}_{2\,(aq)} + 2HCO^{-}_{3\,(aq)}$. The precipitation phase of travertine involves degassing of CO_2 due to pressure drop (as artesian waters move upward) and/or turbulence (e.g. due to groundwater discharge or wave action) via the reaction: $Ca^{+}_{2\,(aq)} + 2HCO^{-}_{3\,(aq)} \rightarrow CO_{2(g)}\uparrow + H_2O + CaCO_{3(travertine)}$. When groundwater carries calcium, for example, mixing with an alkaline lake can result in localized supersaturation. Biological influences can also facilitate travertine precipitation of calcite by changing saturation state of waters or by algal trapping of fine grained carbonate. Formation of Bouse travertines is interpreted here as ultimately due to spillover of alkaline waters derived from Lake Hualapai (Crossey et al., 2015), but groundwater mixing and amplification of the degree of carbonate supersaturation by biologic processes as represented by the tube cast facies of the travertine results in the remarkable localized precipitation.

Bouse travertines are most voluminous in the Blythe basin, but they have been found in all Bouse basins (Fig. 1). Interestingly, they occur throughout the Blythe basin on east, center, and west sides of the basins, near the mapped highest elevations of Bouse outcrops (~ 330 m asl), and near the modern Colorado River (~ 100 m asl). Extensive mapping by various workers (Pearthree and House, 2014 and references therein) shows that travertine occurs in conjunction with paleo shoreline deposits and is found in numerous locations draped against (encrusted on in our interpretation) bedrock of a variety of lithologies (Fig. 2A). The transect from lowest to highest elevations imply time transgressive deposition, possibly with components of post-depositional tilting. Encrustations on underlying paleotopography indicate a rough landscape at outcrop scale exceeding 10s of m of relief. Large 'reef' complexes (Fig. 3 & 4; sensu Benson, 1994) and apparent shoreline deposits rimming paleotopography need special

emphasis in more refined depositional models. Field relationships with other Bouse carbonate facies consistently indicate that travertine accumulations (encrustations) are first, or early; travertine generally pre-dates and is occasionally coeval (interbedded) with marl and calcarenite. Where preserved, marl carbonates (deposited from a water column) are typically inset (Fig. 2B). Travertine-coated cobbles and boulders, and clasts of travertine are also found in the lag gravels and fanglomerates below the basal Bouse marl and bioclastic carbonate (Fig. 3, 4). Thus, we infer that Bouse travertines are likely time transgressive (timescale unknown) but were deposited mainly before other Bouse carbonates were deposited at a given locality.

Our depositional model for Bouse travertine relies on a close analog documented in tufa mounds and shoreline tufas of Pyramid Lake and Lake Lahontan (Benson, 1994; 2004), tufa mounds in Mono Lake (Dunn, 1953; Scholl and Taft, 1964), stromatolites in groundwater springs (Wolaver et al., 2013), and shoreline deposits around both marine and lake basins. Remarkably similar travertine morphology is illustrated in figures 3 and 4. Marine examples include Shark Bay and the Coorong delta (Australia).

Using these analogs, the distribution of travertine outcrops suggests two likely controls on deposition: subaqueous groundwater inputs along faults and lake-margin seepage that interact with shoreline wave action. Fault control (or modulation) of deposition of travertine seems likely to provide a source of excess CO_2, and possibly calcium, and locating springs along fault conduits. Additional mapping of Bouse travertine mounds similar to those observed in the Palo Verde and Trigo Mountains may help define source springs. However, preserved travertine deposits are quite extensive in some areas and encrust complex topography, and few direct fault- travertine associations are yet documented with the exception of several rare carbonate veins. A lake-shore origin similar to Pyramid Lake, Nevada for the travertine is thus our preferred interpretation for the occurrences seen to date as this might provide turbulence needed for degassing, form the concentric geometry of travertine outcrops around paleotopography (aka shorelines), and explain the general association of travertine with basin highstands in terms of a basin transgression. If so, the presence of similar mound complexes at low elevations and encrustations across paleotopography might be ascribed to lacustrine transgression in which travertine is older than other carbonate facies at any location.

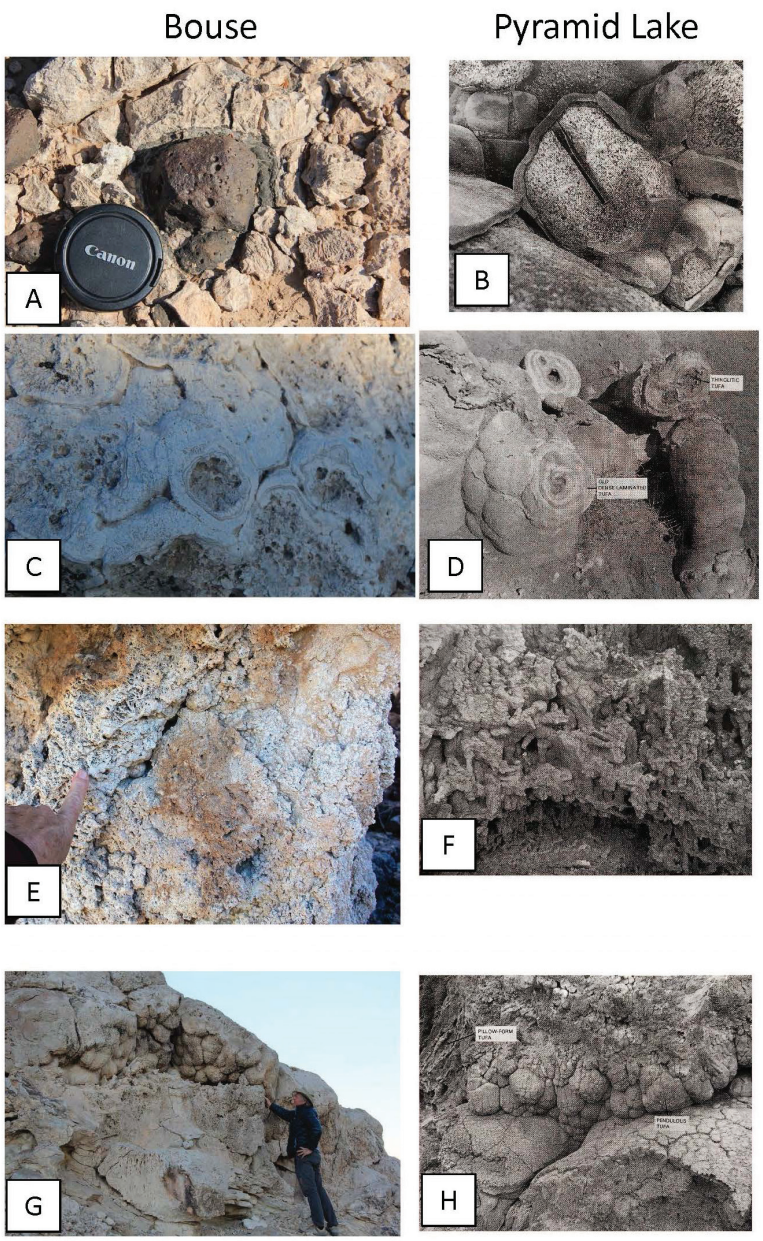

Figure 3. Comparison of Bouse travertine (left photo for each pair) and Pyramid Lake (right, from Benson, 1994) (A, B). Dense carbonate rinds on clasts. (C, D) Concentrically laminated travertine tubes and botryoids (Bouse ~4-10 cm diameter; Pyramid lake up to 50 cm). (E, F) small-diameter tubular 'tufa' (mm- to cm-scale). (G, H) 'Pendulous or mammillary forms 20-50 cm diameter.

Geochemical tests for origin of the travertine are underway and include multi-tracer analysis of travertine versus other Bouse carbonate facies. If spring inputs were important sources, the travertine may show higher $^{87}Sr/^{86}Sr$ when groundwater flowpaths were through Precambrian granites relative to low $^{87}Sr/^{86}Sr$ young volcanic bedrock. The presence of silica diagenesis, local manganese mineralization, and geothermal-associated trace elements like B, Br, Li may help establish any geothermal inputs. A lakeshore origin may show

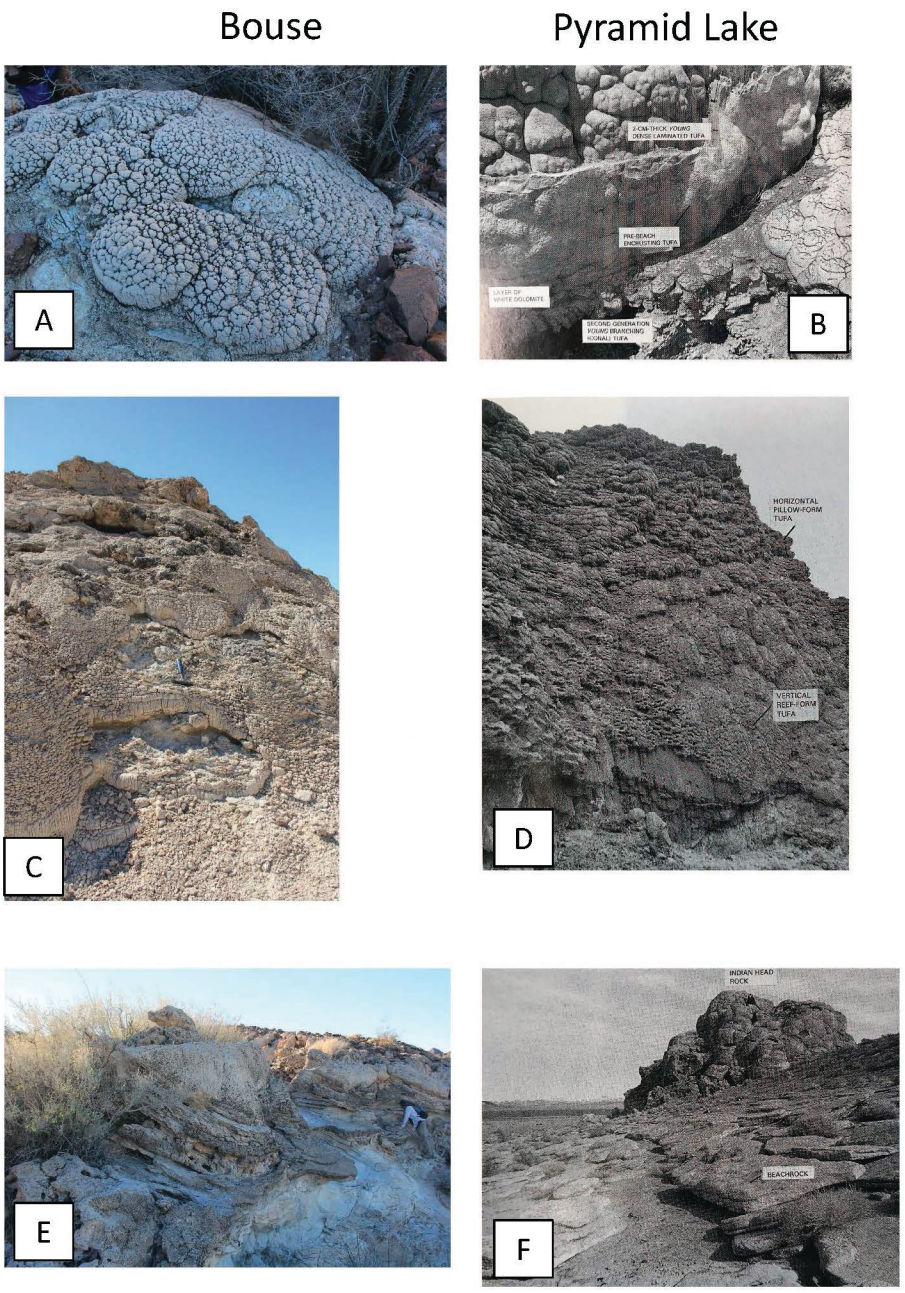

Figure 4. Comparison of Bouse travertine (left photo for each pair) and Pyramid Lake (right, from Benson, 1994) (A, B). Mature branching conal or cauliflower-shaped morphology. (C, D) Reef-form tufa morphology (described by Benson, 1994). Both locations show encrustation of travertine on near-vertical bedrock exposures. (E, F) Onlapping, inset relationships of dipping marl (left, Palo Verde Mountains) and beachrock (right, Pyramid Lake) onto encrusting travertines.

significant degassing and fractionation of stable isotopes. Another important aspect of travertine is that they may be datable using U-Pb dating to help establish the timeframe for Bouse deposition. For example, in the current spill-and-fill model for downward integration of the Colorado River system (Spencer et al., 2013; Pearthree and House, 2014), travertine deposits record rising lake levels in each basin. With progressive filling and spilling of basins, travertine deposits in northern basins travertines would generally be older than southern basins. Depending on how rapidly these postulated lakes filled, it might also be possible to distinguish the ages of the lowest and highest travertine deposits in each basin, and make inferences about gradual versus sudden filling of the basin.

Geochemical work to date shows wide variation in C and O stable isotopes of Blythe basin travertine, with some studies (Crossey et al., 2015) showing fairly well behaved linear mixing trend between river-like endmembers in ($d^{18}O$,$d^{13}C$) of (-8,-5) to marine-like endmembers of (0,0) and other studies (Bright et al., 2016) showing reproducible chemostratigraphy in several location and a more scattered C-O plot. A linear isotopic mixing trend observed in travertine is very similar to values from the overlying marls, but both are dramatically different from similar mixing arrays seen in our Pyramid Lake analog whose endmembers are displaced by + 5 in $d^{13}C$. Geochemical studies are ongoing, but at present, evidence for both carbonate and silica diagenesis of carbonates raises caution about interpreting measured values as primary; this alteration may also affect attempts at U-Pb dating (Crow et al., 2014). We envision that subaqueous encrustations of carbonate may have been diagenetically altered during rising and falling water levels and therefore microscampling is needed to reveal any least/unaltered carbonate geochemistries. Sample analysis methods (microdrilling versus dissolution) may help explain the different isotopic results found by different studies (linear versus more scattered) if biogenic influences produced heavier $d^{13}C$ in the fossil-bearing marls.

Nevertheless, preliminary impressions are as follows. (1) Deposition of the first Bouse carbonate involved precipitation of carbonate encrustations on local paleotopography via degassing of carbonic waters, groundwater-supplied calcium, and biological

influences; this could have happened in a mixed or stratified estuarine or lacustrine environment based on the C-O mixing trend (if this trend is borne out by further analyses and can be shown to be primary). (2) Bouse marls represent carbonate that rained out of the (rising but fairly quiescent) water column as chemical precipitates and fine grained carbonate, likely in a mixed marine- estuary environment in the Blythe basin, based on the paleontology and stabel isotopic C-O mixing trend. (3) In the southern Blythe basin, the presence of onlapping bioclastic carbonates with abundant tidal sedimentary facies and tidal rhythmites in the basin axis (O'Connell et al., 2017) suggests the possibility that the basin first filled with lake waters (1 and 2), then the lake drained or lowered substantially, and later a regional marine transgression produced widespread tidal deposits. Lake and marine transgressions separated by a short-lived lowstand might explain the diagenetic alteration documented or suspected in some samples.

Acknowledgements

This paper received funding from the Sedimentary Geology and Paleobiology Program of NSF (grants EAR-1545986 to Crossey and Karlstrom; EAR-1546006 to Dorsey) from the Sedimentary Geology and Paleobiology Program. The paper benefitted from numerous discussions with LoCO Bouse colleagues from the USGS-Flagstaff and AZGS. The manuscript benefitted from a thorough and constructive review by Phil Pearthree of the Arizona Geologic Survey.

References Cited

Benson, L., 1994, Carbonate deposition, Pyramid Lake Subbasin, Nevada: 1. Sequence of formation and elevational distribution of carbonate deposits (Tufas): Palaeogeography, Palaeoclimatology, Palaeoecology, 109, pp. 55-87.
Benson, L., 2004, The Tufas of Pyramid Lake, Nevada: U.S. Geological Survey Circular 1267, 14 p.

Bright, J., Cohen, A.S., Dettman, D.L., Pearthree, P.A., Dorsey, R.J., and Homan, M.B., 2016, Did a catastrophic lake spillover integrate the late Miocene early Pliocene Colorado River and the Gulf of California?: Microfaunal and stable isotope evidence from Blythe basin, California-Arizona, USA. Palaios, v. 31, p. 81-91.

Bright, J., Cohen, A.S., Dettman, D.L., Pearthree, P.A., Dorsey, R.J., and Homan, M.B., 2016, Did a catastrophic lake spillover integrate the late Miocene early Pliocene Colorado River and the Gulf of California?: Microfaunal and stable isotope evidence from Blythe basin, California-Arizona, USA. Palaios, v. 31, p. 81-91.

Crossey, L.J., Fischer, T.P., Patchett, P.J., Karlstrom, K.E., Hilton, D.R., Newell, D.L., Huntoon, P., Reynolds, A.C., and de Leeuw, G.A.M., 2006, Dissected hydrologic system at the Grand Canyon: Interaction between deeply derived fl uids and plateau aquifer waters in modern springs and travertine: Geology, v. 4, p. 25–28, doi:10.1130/G22057.1.

Crossey, L.J., Karlstrom, K.E., Springer, A.E., Newell, D., Hilton, D.R., and Fischer, T., 2009, Degassing of mantle- derived CO2 and He from springs in the southern Colorado Plateau region—Neotectonic connections and implications for groundwater systems: Geological Society of America Bulletin, v. 121, p. 1034–1053, doi:10.1130/B26394.1.

Crossey, L.J., Karlstrom, K.E., Dorsey, R., Pearce*, J., Wan, E., Beard, L.S., Asmerom, Y., Polyak, V., Crow, R.S, Cohen, A., Bright*, J., Huth, 2015, The importance of groundwater in propagating downward integration of the 6-5 Ma Colorado River System: Geochemistry of springs, travertines and lacustrine carbonates of the Grand Canyon region over the past 12 million years: Geosphere, v. 11; no. 3; p. 660–682; doi:10.1130/GES01073.1.

Crossey, L.C., Karlstrom, K.E., Crow, R.S., House, P.K., Pearthree, P. 2016, Travertines of the Bouse Formation. In: Reynolds, R.E. (Ed.) 2016 Desert Symposium Proceedings, California State University Desert Studies Center, Zzyzx, CA, p. 166-170.

Crow, R., Karlstrom, K., Crossey, L., Polyak, V., Asmerom, Y., and House, K., 2014, Deciphering the evolution and origin of the lower Colorado River and uplift of the Colorado Plateau: Preliminary U-Pb carbonate dating results and future directions: Abstract EP41A-3498 presented at 2014 Fall Meeting, AGU.

Dorsey, R.J., O'Connell, B., Homan, M., and Howard, K.A., 2016, Upper limestone of the southern Bouse Formation: Evidence for unsteady origins of the Colorado River. In: Reynolds, R.E. (Ed.) 2016 Desert Symposium Proceedings, California State University Desert Studies Center, Zzyzx, CA, p. 145-153.

Dunn, J.R., 1953, The origin of the deposits of tufa in Mona Lake: Journal of Sedimentary Petrology: v. 23, p. 18-23.

Ford, T.D., and Pedley, H.M., 1996, A review of tufa and travertine deposits of the world: Earth-Science Reviews, v. 41, p. 117–175, doi:10.1016/S0012-8252(96)00030-X.

Gootee, B.F., Pearthree, P.A., House, P.K., Youberg, A., O'Connell, B., and Bright, J., 2016, A sequence stratigraphic interpretation of the upper bioclastic unit capping the Bouse Formation in the Cibola area, Arizona and California. In: Reynolds, R.E. (Ed.) 2016 Desert Symposium Field Guide and Proceedings, California State University Desert Studies Center, Zzyzx, CA, p. 154-159.

Homan, M.B., 2014, Sedimentology and stratigraphy of the Miocene-Pliocene Bouse Formation near Cibola, Arizona and Milpitas Wash, California: Implications for the early evolution of the Colorado River: MS Thesis, University of Oregon.

House, P.K., Pearthree, P.A., and Perkins, M.E., 2008, Stratigraphic evidence for the role of lake spillover in the inception of the lower Colorado River in southern Nevada and western Arizona, in Reheis, M.C., Hershler, R., and Miller, D.M., eds., Late Cenozoic Drainage History of the Southwestern Great Basin and Lower Colorado River Region: Geologic and Biotic Perspectives: Geological Society of America Special Paper 439, p. 335–353.

McDougall, K., and Miranda Martínez, A.Y., 2014, Evidence for a marine incursion along the lower Colorado River corridor: Geosphere, v. 10, p. 842-869, doi:10.1130/GES00975.1.

Metzger, D.G., Loeltz, O.J., and Irelna, B., 1973, Geohydrology of the Parker-Blythe-Cibola Area, Arizona and California: U.S. Geological Survey Professional Paper 486-G, p. 1–130.

Miller, D.M., Reynolds, R.E., Bright, J.E., Starratt, S.W., 2014, Bouse Formation in the Bristol basin near Amboy, California, USA: Geosphere, v. 10, p. 462-475, doi:10.1130/GES00934.1.

O'Connell, B., Dorsey, R.J., Homan, M., Gootee, B.F., and House, P.K., 2016, Structural controls on stratigraphic architecture of the southern Bouse Formation near Cibola, Arizona. In: Reynolds, R.E. (Ed.) 2016 Desert Symposium Field Guide and Proceedings, California State University Desert Studies Center, Zzyzx, CA, p. 171-175.

O'Connell, B., Dorsey, R.J., and Humphreys, E.D., 2017, Tidal rhythmites in the southern Bouse Formation as evidence for post-Miocene uplift of the lower Colorado River corridor: Geology, v. 45, p. 99–102.

Pearthree, P.A., and House, P.K., 2014, Paleogeomorphology and evolution of the early Colorado River inferred from relationships in Mohave and Cottonwood valleys, Arizona, California, and Nevada: Geosphere, v. 10, p. 1139-1160, doi:10.1130/GES00988.1.

Pentecost, A., 2005, Travertine: Berlin, Springer Verlag, 445 p.

Scholl, D.W. and Taft, W.H., 1964, Algae, contributions to the formation of calcareous tufa, Mono Lake, California: Journal of Sedimentary Petrology: v. 34, p. 309-319.

Spencer, J.E., Pearthree, P.A., and House, P.K., 2008, An evaluation of the evolution of the latest Miocene to earliest Pliocene Bouse lake system in the lower Colorado River valley, southwestern USA, in Reheis, M.C., Hershler, R., and Miller, D.M., eds., Late Cenozoic Drainage History of the Southwestern Great Basin and Lower Colorado River Region: Geologic and Biotic Perspectives: Geological Society of America Special Paper 439, p. 373–388, doi:10.1130/2008.2439(17).

Spencer, J.E., Patchett, P.J., Pearthree, P.A., House, P.K., Sarna-Wojcicki, A.M., Wan, E., Roskowski, J.A., Faulds, J.E., 2013, Review and analysis of the age and origin of the Pliocene Bouse Formation, lower Colorado River Valley, southwestern USA: Geosphere, v. 9, p. 444-459, doi:10.1130/GES00896.1.

Wolaver, B.D., Crossey, L.J., Karlstrom, K.E., Banner, J.L., Cardenas, M.B., Ojeda, C.G., Sharp, J.M., 2013, Identifying origins of and pathways for spring waters in a semiarid basin using He, Sr, and C isotopes: Cuatrociénegas Basin, Mexico: Geosphere 9 (1), 113-125.

Geochemical characterization of Bouse carbonates; towards an understanding of Bouse diagenesis

C. Ferguson[1], L. Crossey[1], K. Karlstrom[1], and M. Spilde[2]
[1]Department of Earth and Planetary Sciences, [2]Institute of Meteoritics, ferguson33@unm.edu

Debates about the marine versus non-marine origin of the Bouse Formation consider a range of datasets including sedimentary structures, paleontology, and geochemistry. Geochemical arguments involve strontium (Sr) isotopes as well as carbon (C) and oxygen (O) stable isotopes which are compared to modern values for marine and non-marine settings. Such comparisons rely on whether or not the carbonates retain their primary composition. This paper examines the Bouse carbonates using stable isotope, Sr and SEM/microprobe data with now recognized distinctions between different types of carbonate facies including marl, travertine, calcarenite and carbonate-cemented bioclastic units. The major goals are to decipher any diagenetic alteration that may have changed the primary compositions of the carbonates, and also understand the scale and nature of those changes.

Preliminary work has concentrated on the carbonates of the Blythe basin where marine fossils are found (McDougal et al., 2016). Stratigraphic studies interpret marine tidal facies and rhythmites (O'Connell et al., 2016), where Sr values are distinctly non-marine (Spencer et al., 2011) but where mixing models of radiogenic inputs to marine setting may allow models for intermittent marine environments (Crossey et al., 2015). Textural evidence from cut slabs shows mottled carbonate textures indicating complex compositions. Stable isotope work on visibly distinct micro-drilled subsamples is underway to compare any carbonate variation and determine diagenetic versus primary portions. At present, we hypothesize that there has been a major carbonate diagenesis that has altered portions of the carbonate such that primary values are not assured.

Microprobe data reveals large percentages (up to ~ 30%) of amorphous silica intergrown with carbonate in wormy textures. This silica replaces forams and other fossils and is interpreted to represent an important silica diagenetic event. This same event could explain formation of petrified wood in Bouse and Bullhead gravel outcrops (Spinks, 2016). Next steps are to compile semi-quantitative SEM data on the variations in Bouse carbonate and silica composition at the microscale. Our present working hypothesis is that Bouse carbonates have undergone both silica and carbonate diagenetic events that have modified primary compositions such that interpreting and understanding the original environment relies on finding un-/ least-altered portions of the samples and then applying suitable microscale analyses.

Acknowledgements

This paper received funding from NSF grants EAR 1545986 from the Sedimentary Geology and Paleobiology Program.

References

Crossey, L.J., Karlstrom, K.E., Dorsey, R., Pearce, J., Wan, E., Beard, L.S., Asmerom, Y., Polyak, V., Crow, R.S, Cohen, A., Bright, J., Huth, 2015, The importance of groundwater in propagating downward integration of the 6-5 Ma Colorado River System: Geochemistry of springs, travertines and lacustrine carbonates of the Grand Canyon region over the past 12 million years: Geosphere, v. 11; no. 3; p. 660–682; doi:10.1130/GES01073.1.

Crossey, L.C., Karlstromm, K.E., Crow, R.S., House, P.K., Pearthree, P., 2016, Travertines of the Bouse Formation. In: Reynolds, R.E. (Ed.) 2016 Desert Symposium Field Guide and Proceedings, California State University Desert Studies Center, Zzyzx, CA, p. 166-170.

McDougall, K. and Miranda-Martinez, A.Y., 2016, Bouse formation along the lower Colorado River corridor: tracking the transition from marine estuary to saline lake. In: Reynolds, R.E. (Ed.) 2016 Desert Symposium Field Guide and Proceedings, California State University Desert Studies Center, Zzyzx, CA, p. 140-144.

O'Connell, B., Dorsey, R.J., Homan, M., Gootee, B.F., and House, P.K., 2016, Structural controls on stratigraphic architecture of the southern Bouse Formation near Cibola, Arizona. In: Reynolds, R.E. (Ed.) 2016 Desert Symposium Field Guide and Proceedings, California State University Desert Studies Center, Zzyzx, CA, p. 171-175.

Pearthree, P.A., and House, P.K., 2014, Paleogeomorphology and evolution of the early Colorado River inferred from relationships in Mohave and Cottonwood valleys, Arizona, California, and Nevada: Geosphere, v. 10, p. 1139-1160, doi:10.1130/GES00988.1.

Pentecost, A., 2005, Travertine: Berlin, Springer Verlag, 445 p.

Spencer, J.E., Patchett, P.J., Roskowski, J.A., Pearthree, P.A., Faulds, J.E., and House, P.K., 2011, A Brief review of Sr isotopic evidence for the setting and evolution of the Miocene Pliocene Hualapai-Bouse lake system In: Beard, L.S., Karlstrom, K.E., Young, R.A., and Billingsley, G.H., eds., CREvolution 2—Origin and evolution of the Colorado River system, workshop abstracts: U.S. Geological Survey Open-File Report 2011-1210, p. 250-259.

Spinks, 2016, Pliocene fossil woods from the Colorado River delta: What do we know?. In: Reynolds, R.E. (Ed.) 2016 Desert Symposium Field Guide and Proceedings, California State University Desert Studies Center, Zzyzx, CA, p. 189-192.

Pinto Mountains gold

D. D. Trent
Geologist, rockdoctrent@gmail.com

ABSTRACT—The Dale Mining District was the most productive gold mining district in the eastern Transverse Ranges. The major mines were in an area of about four square miles. Among those mines the Supply Group and the Carlyle were two of the most significant. From 1915 to 1942 the Supply Group (the Supply, Jean, and Nightingale mines) produced about 67,000 oz. of gold, the largest production from the entire Dale Mining District. The Carlyle Mine, about one mile northeast of the Supply Mine, from 1936 to 1939 produced $124,000 from 13,256 tons of gold-silver-lead-copper ore; production figures from 1938 to 1942 are unknown but the gross value of concentrates was reported to be $2,411.33 per ton. This paper will focus on the history, geology and development of these two significant mining operations.

Introduction

The Dale Mining District was the major mining district in the Pinto Mountains in San Bernardino County, and the most productive gold mining district in the eastern Transverse Ranges. For example, in 1899 the Dale District was reported to be producing over $6,000 a month (Ekman, et al, 1968, p. 141). In addition to gold, lesser amounts of lead, silver, and copper were by-products. The principal mines, in an area of about four square miles, consisted of the Supply Group, Carlyle, Ivanhoe, O.K., Brooklyn, Bon Ton, and Virginia Dale (Cloudman et al, 1919, p. 801; Ruff et al, 1992, p. 227-228). The Supply Group consisted of the Supply, Jean, and Nightingale mines. The Nightingale, also known the as the Lorman, as indicated on U.S. Geological Survey topographic maps, but it is also reported elsewhere as the Lohrman or Luhrman. The following will discuss the Supply Group and the Carlyle, two of the most significant mines in the district.

Supply Mine Group (Supply, Jean and Nightingale–Lorman)

Location: Secs. 21, 22, 27, 28, T. 1 S., R. 12 E., S.B.M; 34° 3' 41" N, 115° 43' 14" W, in the Pinto Mountains about 20 miles east of Twentynine Palms in the Dale Mining District,

Years of operation: 1900(?)–1915; 1930–1942.

Production: Pre 1915, 50,000 oz. gold. 1930–1942, 17,000 oz. gold (Ruff et al, 1982, p. 239). Collectively, the Supply Group yielded about $1.5 million in gold ore, the largest production from the entire Dale Mining District. This value may include production from the Gold Crown Mine. Of the total production, about one-half was produced by the large-scale operation of the Supply Mine when it was owned by the Seal of Gold Mining Company and later by Charles Schwab's United Greenwater Copper Company, all of which was prior to 1915 when water seepage ended mining at the Supply Mine.

History The Supply Mine was located in 1894 by Frank Sabathe. About ten years later his partner, Jack Killian, established the Seal of Gold Mining Company and began serious work on the property. By 1904, a cyanide mill was operating with water piped 3.5 miles from a well on

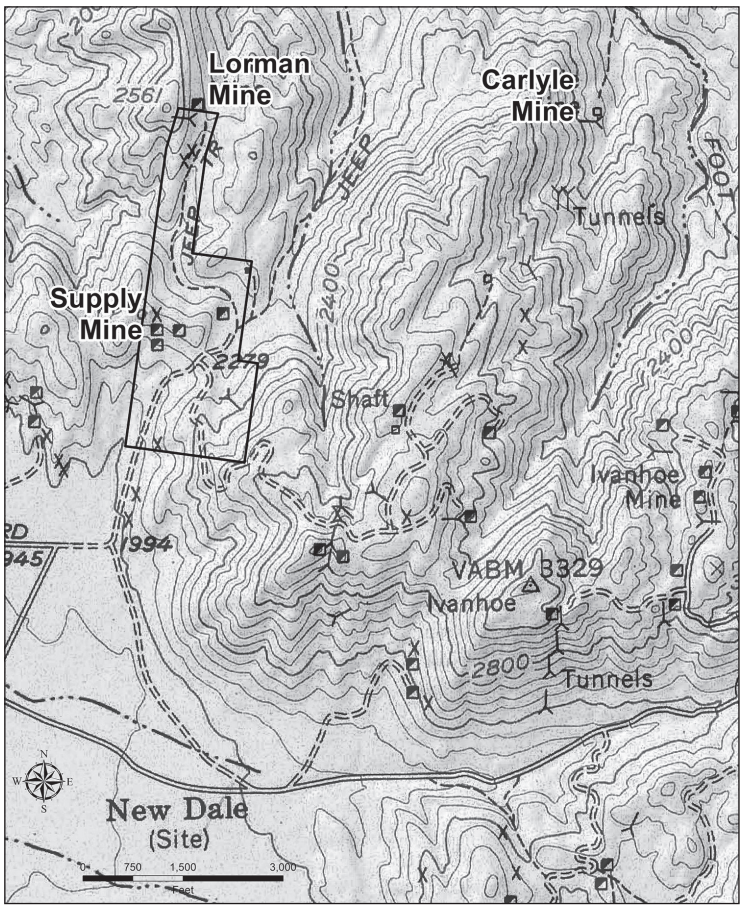

Fig. 1. Topographic map showing the locations of the Supply Group, Carlyle, other nearby mines and prospects in the Dale Mining District.

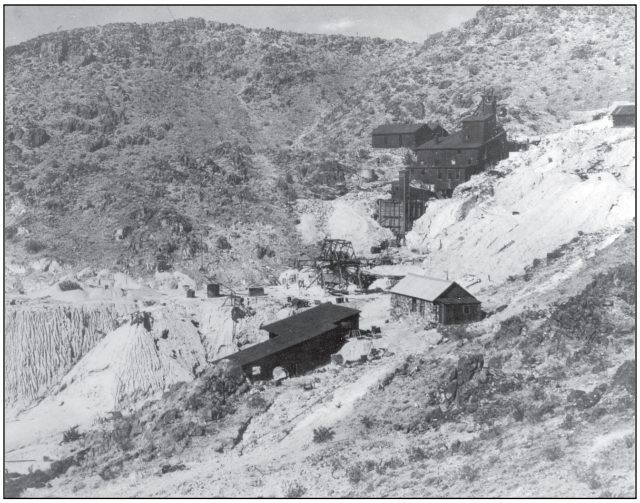

Fig. 2. Supply Mine, 1941. (NPS photo).

Dale Dry Lake (Mining and Scientific Press, 1904, p. 355). The mine was leased to a Mr. Tartarian for about two years, but the property reverted back to the Seal of Gold Company (Harrington, 1943, p. 14). From 1911 to 1915, the mine became a large-scale operation when leased to Charles Schwab's United Greenwater Copper Company. During these years the property employed some 80 men and supported the nearby mining town of New Dale. Seeley G. Mudd and Frank Wiseman acquired and worked the mine in the early 1920s and in 1927 leased the mine to the Arrowhead Development Company of Tonopah, Nevada. By 1929 the mine was idle (Mining and Scientific Weekly, 1927, p. 581; Smith, 2006, p. 69-70).

A second period of large-scale mining began during the Great Depression years of the 1930s. In 1932 the locally owned Gold Crown Mining Company began cleaning up stockpiles and old waste rock dumps from which 87 ounces of gold were recovered worth about $1,500. Beginning in 1933 the company stabilized the underground workings, which had suffered from many years of abandonment, rebuilt surface structures, constructed a new bunkhouse, and installed a telephone system (Greene, 1983, p. 70; Jones, 1946, p. 2-3). Restoring the Supply's mill was considered but instead the company decided to construct a new state-of-the art mill at the Gold Crown property south of New Dale in Riverside County. Newly mined ore and old tailings from the Supply were trucked to the new mill for processing. The company eventually relocated its mill to the Nightingale (Lorman) operation, one mile north of the Supply (Greene, 1983, p. 71), (34° 3' 39"N, 115° 43' 14" W). Operations ended in 1942 by Order L-208 of the U.S. War Production Board, which shut down most nonessential mining for the duration of World War II, and the mine and mill were dismantled in December. Small-scale mining continued for several years following World War II. Observations at the mine site suggest limited activity on the property in the 1970s (Green, L. W., 1983, p. 71-72; Wright et al, 1953, p. 82).

Fig. 3. Site of the Supply Mine, 2006. (D.D. Trent photo).

Geology Tucker and Sampson (1940, p. 63) report several steeply dipping north striking quartz veins with widths of 4 to 12 ft in andesite porphyry. The major focus was the Supply–Nightingale vein. My surface observations in 2006 revealed the veins to be about one to two ft wide and Howard (2002) reports the country rock as Jurassic age porphyritic quartz monzonite bleached white by albite alteration. The rocks are tentatively correlated to similar rocks (Jagiello, 1991) in the Bullion Mountains.
Development The Supply vein was worked by an inclined shaft that reached a depth of 1,250 ft. Development included numerous levels and over 5,000 ft of underground workings. The Jean vein, parallel to and about 1,000 ft east of the Supply vein, was developed by a 200–ft inclined shaft with less extensive workings than in the Supply. When taken over by the Gold Crown Company in 1930 the mining activity moved about 3,600 ft north of the Supply to develop the Nightingale (Lorman) Mine. The Nightingale appears to have worked the same gold-quartz vein as that at the Supply, hence the name Supply–Nightingale vein. The Nightingale, with a 60-ft steel headframe, sunk a two-compartment shaft on the vein to a depth of 675 ft. Several levels at 75-ft intervals were driven with the underground workings

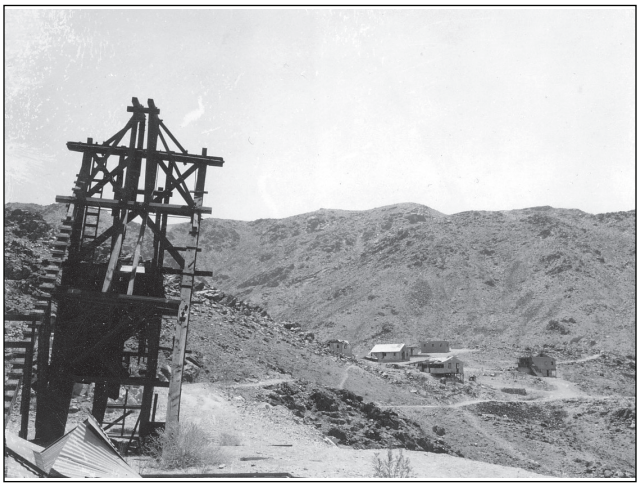

Fig. 4. Head frame of the Jean Mine, with the bunkhouse and other buildings of the mine's camp in the distance, 1959. (NPS photo).

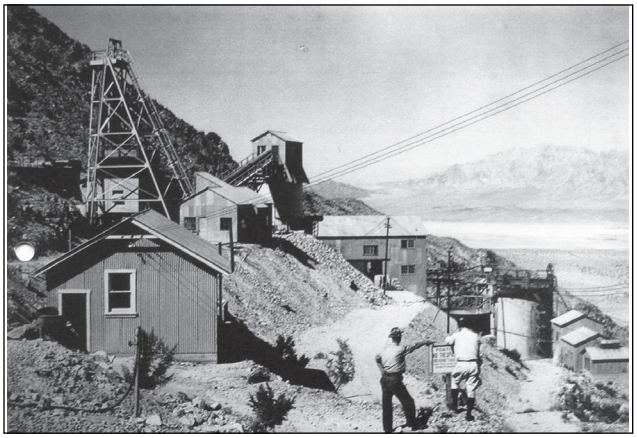

Fig. 5. Nightingale (Lorman) Mine and the Gold Crown Corporation mill, 1941. Dale Dry Lake in the distance. (NPS photo).

Fig. 6. Site of the Nightingale (Lorman) Mine and mill, 2006. (D.D. Trent photo).

totaling about 6,000 ft. By the late 1930s all the operations had shifted to the Nightingale Shaft and mill (Tucker and Sampson, 1940. p. 82). Prior to 1938, ore from the Supply property was treated by dry crushing and cyanidation in the mill at the Gold Crown mine in Riverside County. At the new Nightingale mill the ore was wet-ground to minus 100-mesh in a cyanide solution. The Nightingale mill incorporated the latest 1930s state-of-the-art equipment as illustrated by the mill flow sheet.

Recovery was reported at 95 percent with a loss in the tailings of 80 cents to $1.00. Ore grade is reported to have averaged $12 per ton. The mill also processed contract ore from nearby mines. Power for the mill machinery was provided by a 300 hp, 4-cylinder Fairbanks-Morse diesel engine, direct connected to a 170 K.V.A. generator. A 75-hp electric motor drove a 300-cu ft Ingersoll-Rand air compressor for drilling underground. Water for the mill operations was pumped two miles from a 265-ft deep well. (Tucker and Sampson, 1940, p. 62-63).

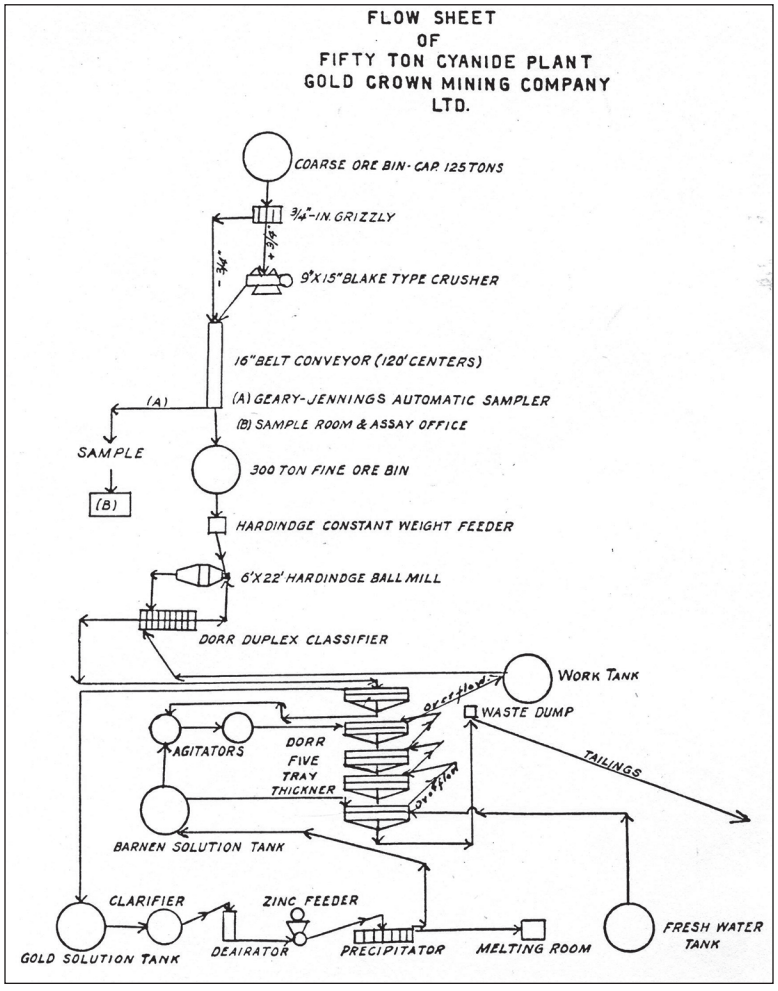

Fig. 7. Flow sheet of the Gold Crown mill circuit at the Nightingale (Lorman) mine, Tucker and Sampson, 1940, p. 64).

Carlyle Mine

Location: Sec. 11, 14, 1S, 12E, SBM (projected); 34° 4' 37" N, 115° 42' 7" W, on the northeast slope of the Pinto Mountains in the Dale Mining District, about 23 mi southeast of Twentynine Palms (Wright et al, 1953, p. 73) and about a mile northeast of the Supply Mine.

Years of operation: Mining began in the early 1900s but little is known of its early operations; June 1936–March 1938; April 1939–October 1942 (Wright et al, 1953, p.73; Tucker and Sampson, 1940, p. 61).

Production: From 1936–1939 the operation produced $124,000 from13,256 tons of gold-lead-silver-copper ore. Production figures from 1938–1942 unknown but the gross value of concentrates was reported to be $2,411.33 per ton (Tucker and Sampson, 1940, p. 62; Wright et al, 1953, p.74).

History As with the Supply Group, the Carlyle Mine had two periods of major production: the 1910s and the 1930s. Little is known of the earlier operation (Smith, 2006,

Fig. 8. Carlyle mill, ca.1937. Note aerial tram cables for transporting ore to the mill. ca. 1937 (NPS photo).

Fig. 9. Site of the Carlyle mill, 2006. (D.D. Trent photo).

p. 72) other than a brief statement by Cloudman et al (1919, p. 803):

Opened up quite extensively and has changed hands within the last few months, and development work is carried on steadily and continuously . . . and that the erection of reduction works is now contemplated.

In the 1920s to early 1930s, a small reduction mill was constructed to recover values of gold, silver, and lead by use of a jig, floatation cells and a concentrating table, and an aerial tram was constructed to carry ore from the mine to the mill. Several small operators worked the property from 1931 to 1932 (Smith, 20006, p. 73). Large-scale mining at the Carlyle began in 1935 when the Carlyle Mining Company of Beverly Hills (later to become the Carlyle Mining Corporation) purchased the property. The company increased the underground workings, built a large blacksmith shop, added a compressor and pipeline to supply compressed air for pneumatic drilling, and constructed a second aerial tramway, 2,680 ft long, to carry ore from the upper mine to the mill (Wright, 1953, p. 74; Smith 2002, p. 74 and 118). These aerial trams were the only aerial trams used in any Southern California mines. A local Twentynine Palms company, Camco Mining, leased the property from 1939 to 1941 but little is known of Camco's activities. Mining activity ceased in 1942 for the duration of World War II by order of the War Production Board, and there is no evidence of any post war mining activity at the Carlyle property (Smith, 1983, p. 76).

Geology: Tucker and Sampson (1940, p. 61) report the ore body was a quartz vein in a fault zone with a diorite footwall and a granodiorite hanging wall. However, Howard (2002) reports the country rock as Jurassic age porphyritic quartz monzonite bleached white by albite alteration. The rocks are tentatively correlated to similar rocks (Jagiello, 1991) in the Bullion Mountains. Gold mineralization was finely disseminated and associated with lead minerals, galena, anglesite, cerrusite, and with silver minerals, pyrargyrite, polybasite, and stephanite (Tucker and Sampson, 1940, p. 61).

Development: In 1939 the underground workings consisted of a lower 1,500 ft tunnel in quartz diorite, from which no ore was recovered, and the main working tunnel about 330 ft above the lower tunnel that extended south 1,200 ft on the vein. Five ore shoots were developed on this level. Among the workings were drifts, crosscuts, two raises driven to surface and one ore shoot stoped to

Fig. 10. Carlyle mill, ca. 1937. (NPS photo).

Fig. 11. Carlyle mill and lower mine workings, waste rock dump, aerial tram cables, and aerial tram tower on the skyline, ca. 1937. (NPS photo).

Figure 12. Winch at the Carlyle mine.

the surface. Levels were driven at 30 ft and 80 ft and the ore shoot developed on these levels was 60 ft long and 6 ft wide, with high-grade silver ore on the footwall and gold ore on the hanging wall. Gold was reported to average $12 per ton. Twelve men were employed in the mine and mill in 1940 (Tucker and Sampson, 1940, p. 61-62). Ore from the upper workings was trammed in one-ton cars to an ore bin (70 ton capacity) from which it was carried to the mill by the 2,680 ft aerial tram equipped with two buckets, each with a capacity of 1500 lbs.

Floatation concentrate from cleaner cells was reported to carry $800 to $1000 per ton. Heads carried from $10 to $20 per ton in gold, with $3 to $6 per ton silver. Tailings from the mill flow were sent to a Dorr thickener and from there to a tailings dump.

Power for the mill was provided by a 225-hp, 3-cylinder, Fairbanks-Morse diesel direct connected to a 150 K.V.A. generator. Water was supplied from a 135-ft deep well on the southern edge of Dale Dry Lake by a pumping plant. A three-stage plunger booster pump lifted the water 900 ft through a pipeline for two miles to supply water to the mill -- a state-of-the-art flotation plant with a capacity of 60 tons per day. Treated ore recovered 80 to 90% of the gold, and 75% of the silver. The concentrates also included small amounts of copper, lead, iron, arsenic, antimony, and bismuth (Tucker and Sampson, 1940, p. 61-62; Greene, 1983, p. 118).

Acknowledgements

I am indebted to Wayne Steinmetz and Ted Reeves for invaluable assistance and companionship in the field, to Larry Vredenburg for suggestions that greatly improved the text and provided the map, and to Melanie Spoo, Curator of Collections at Joshua Tree National Park, for her help in acquiring vintage photographs.

References

Cloudman, H.C., Huguenin, Emile, and Merrill, F.J.H., 1919, Mines and mineral resources of San Bernardino County. Report of the State Mineralogist **15**, p.1-125.

Ekman, A., Parker, I.H., Storms, W.H., 1968, Old mines and ghost towns of California. Fort Davis, Texas.

Greene, Linda W., 1983, Historic resource study: a history of land use in Joshua Tree National Monument. Denver Service Center, National Park Service manuscript.

Harrington, John, 1943, Flight from New Dale. Westways **35**, no. 3.

Howard, Keith A., 2002, Geologic Map of the Sheep Hole 30' x 60'Quadrangle, San Bernardino and Riverside Counties, California. U.S. Geological Survey Misc. Field Studies Map MF-2344, two sheets.

Jagiello, Keith, Christie, J.M., and Blom, R.M., 1992, Horizontal separation of major late Cenozoic strike-slip faults in the Twenty-nine Palms region, Mojave Desert, California, *in* Richard, S.M., ed., Deformation associated with the Neogene eastern California shear zone, southeastern California and southwestern Arizona: Redlands, Calif., San Bernardino County Museum Special Publication 92–1, p. 48–53.

Jones, H.W., 1946, Pinto Basin gold. Desert Spotlight 1, no. 7, p. 2-3.

Mining and Scientific Press, November 26, 1904).

Ruff, Robert W., Mark E. Unruh and Paul A. Bogseth, 1982, Mineral resources of the eastern Transverse Ranges of southern California, *in* Fife, D.L., and Minch, John A., editors, Geology and mineral resources of the California Transverse Ranges: Santa Ana. South Coast Geological Society, p. 222-249.

Smith, J.L.K., 2006, A land of plenty: Depression mining and landscape capital in the Mojave Desert, California. Ph.D. dissertation, University of Nevada, Reno.

Tucker, W.B., and Sampson, R.J., 1940, California Journal of Mines and Geology, **36**, no. 1.

Wright, Lauren, Stewart, R.M., Gay, T.E., and Hazenbush, G.C., 1953, Mines and mineral deposits of San Bernardino County; California Journal of Mines and Geology **49**, nos. 1 & 2, p. 49-192.

Kokoweef: Still Searching for the Lost River of Gold

Kim Stringfellow
The Mojave Project, mail@kimstringfellow.com

> Either Uncle Earl Dorr discovered the richest gold deposit in the United States…or he was the most imaginative liar in the state of California.[1]
>
> *—Ray Dorr, nephew of Earl Dorr, Argosy magazine, September 1967*

This dispatch concerns the fabrication and distortion of legends over time. Specifically, it delves into a fascinating saga revolving around a conjectured Mojave Desert gold strike of epic proportions still actively sought to this day by an eclectic and persistent group of quixotic speculators: Earl P. Dorr's Lost River of Gold.

In 1933, scattered newspaper articles appeared across Southern California extolling the grandeur and beauty of some recently discovered massive limestone caves within the Mojave's Providence Mountains near the old Bonanza King Mine. Known today as Mitchell Caverns, these geological wonders were named after Jesse E. "Jack" Mitchell who had initially explored the caves in 1929 and would later market them into a popular recreational destination accessible from the National Trails Highway better known as Route 66.

Writer Philip Johnston's detailed observations of these particular subterranean treasures were published in the August 1933 issue of *Touring Topics,* a precursor to *Westways* that is still in print today. Johnston's article, "Crystal Caverns of the Mojave," along with its accompanying photographs celebrated the beauty and geological mystery of the caves and speculated what future speleological discoveries in the Mojave Desert awaited.

In response, several regional newspapers including the *San Bernardino Sun* dated August 5, 1933, ruminated further: "Miners and prospectors have suspected for years that these caverns may be connected by a great underground river that rises somewhere in the center of Nevada, fed by the winter snows of Nevada's numerous mountain ranges, and passing southward through the Mojave desert and then on to the Colorado River." The column goes on to state how "this great river has not been discovered. In fact, *it may exist only in the imagination of desert dwellers whom [sic] thoughts of water are recurring constantly. But the legend prevails.*"

Mythic accounts of buried treasure and lost mines had been circulating amongst desert prospectors for years. Author John D. Mitchell (no relation to the Caverns recreational promoter) published several collections

SECTION TWO
INLAND EMPIRE

The San Bernardino Daily Sun

WEDNESDAY MORNING, OCTOBER 17, 1934

Giant Mojave Desert Caverns Readily Accessible to Travel

This is a view of one of the gigantic caverns on the Mojave desert. The cave shown here is one of a vast system of caverns believed to extend for 300 miles from the southern tip of Nevada through southeastern California to Mexico. This is the belief expressed by A. W. Plummer, Hollywood photographer and desert explorer who has exhibited pictures he has taken of some of the caves.

COUNTY TAKES STEPS TO BAR ILLEGAL VOTES

3,000 Falsely Registered Are Warned They Face Arrest if Their Ballots Are Cast

Agencies in San Bernardino county interested in preserving the sanctity of the ballot and insuring an honest election on Nov. 6 were moving swiftly last night to prevent the 3,000 illegally registered voters in San Bernardino county from participating in the coming election.

Announcement that there are at least 3,000 illegal registrations in this county was made several days ago by County Clerk Harry L. Allison. It was followed by an announcement in Los Angeles county that 100,000 illegal registrations had been discovered and an immediate survey of the situation was ordered in the other counties of southern California.

CANVASS OPENS TODAY

District Attorney Stanley Mussell, Sheriff Ernest Shay, and the foreman of the grand jury, Truman H. Wiggins, last night indicated that any attempt to vote on these illegal registrations would be a short road to the penitentiary. In addition, Merriam-Hatfield headquarters, through Arthur J. Brown, chairman, and the Democratic Merriam-for-Governor club, through Dr. L. W. Ayers, its president, declared a canvass of the city of San Bernardino would begin this morning to determine what the probability is of wholesale illegal voting. County Clerk Allison had expressed the opinion that many of these illegal

IDENTIFICATION

Natural Scenic Wonders Mecca For Scientists, Tourists; Part of Huge System

HATFIELD WILL

Figure 1. A.W. Plummer's photograph of the Mitchell Caverns appears in an October 17, 1934 variation of the *Herald Express* article in the *San Bernardino Sun* proposing that the cavern is part of a vast subterranean system interconnecting the American Southwest. Image courtesy Anna Garcia.

of these yarns starting with "Lost Mines of the Great Southwest" in 1933. Beginning 1940, *Desert Magazine* began reprinting Mitchell's "lost mine" stories every few months well in into the 1950s.

"Death Valley Gold," published in March 1940, told the tale of two "Pahute" brothers that had discovered a limestone cave at the edge of a dry lake somewhere in Death Valley leading into a "dome-shaped cavern with a dark pool of water at the bottom."[2] Here, water bubbled up from some unknown depth along with "great amounts of heavy black sand piled on the terraces around the lake" that upon close inspection "sparkled with small nuggets and flakes of gold." Strangely, the water body seemed to be affected tidal movements.[3] After gathering the gold laden sand to pack out, one of the brothers decided to take a quick swim in the pool when suddenly the water along with the man were sucked into the chasm. The man's body was never to be recovered. Notably, the illustration's caption accompanying the story reads: "Neither Mr. Mitchell nor *Desert Magazine* would attempt to defend the authenticity of this tale."

In August 1951, Mitchell's "Cave of the Golden Sands" appeared in *Desert Magazine's* August issue. This first person account, told to the author by an older gent at a Nevada mining camp *at the turn of the century*, shared a similar storyline but with a mysterious lone prospector as the main protagonist who claimed that he collected four pounds of gold nuggets from a "black sand deposit near Clark Mountain northeast of Nippeno (Nipton)."[4] This cave was said to be located just above the western edge of a dry lake—most likely Ivanpah from the description. While exploring the cave the prospector discovered a long tunnel leading to an amphitheater-like grotto "full of churning water" that appeared to ebb and flow as if controlled by tidal surges. The water would erupt miraculously "twice every 24 hours" and then drain furiously via a whirlpool only to reveal a black sand beach gleaming with gold.

By fall of 1934, an equally fantastic account of long-forgotten Hollywood photographer and desert explorer A.W. Plummer was published front-page in the September 28 *Los Angeles Evening Herald Express*, proclaiming, "330-Mile California Cave System Rediscovered." The unsubstantiated story posits his theory that a "system of giant underground caves, through which flows a mighty subterranean river" extends for some 300 miles from southern Nevada to the Mexican border.

The problem with Plummer's assumption is that geologists had already discounted the possibility that an underground river of this magnitude could exist within the eastern Mojave. The article goes on to state that Plummer was exhibiting his photographs of 14 cavern openings "strung out over 300 miles in a jagged and twisting line" that he had been documenting over the last three years. Plummer noted that he was not the original discoverer of the caves—Native Americans and Spanish explorers had long known about their existence—but that he was the first to postulate that these were part of an immensely linked cavern system spreading across the American Southwest. Plummer had concluded this through personal observation including the presence of "fresh winds" emanating from within the depths of the various cave openings he had explored.

In December 1935, *Westways* had published a follow-up to Johnston's 1933 *Touring Topics* article, retracing much of his previous report, with the exception that he mentions the surprising discovery of a certain prospector named E.P. Dorr along with his affidavit outlining in detail his "three days" odyssey through passages of a great cavern."[5] Dorr's treasure was not within the Providence Mountains but in Kokoweef Peak, located about 35 miles north as the crow flies in the Ivanpah Mountain Range. This was the first public acknowledgement of Dorr's 1934 affidavit and it appears that he had contacted Johnston is his effort to make his story public.

From its inception, Dorr's story was riddled with discrepancies. Variations of the account made attempts to unravel an accurate story and factual chain of events extremely complicated. But legend has it that Earl Dorr first learned of Kokoweef's vast hidden treasure from three Indian brothers—Oliver, Buck and George Peysert—said to have been previous hired hands at his father's Colorado Springs' ranch during the 1890s [6]. At least this is the story outlined at kokoweef.com.

Allegedly inspired by tribal lore, the Peysert brothers had set off from the Dorr Ranch sometime between 1903-05 in search of Kokoweef's untold riches said to be centered around this 6,037-foot peak situated three miles south of the Mountain Pass in California and about 19 miles west of the Nevada state line on Interstate-15.

Within six short weeks of their arrival the Peysert brothers had gained access into a subterranean cave system via Kokoweef's Crystal Cave—one of three solution cavities inside the peak that developed along fault contacts. Kokoweef Peak is composed of Mississippian and Pennsylvanian limestone, which can slowly be dissolved in acidic rainwater, snow melt and percolating groundwater. The waters that dissolved the limestone followed fissures along faults of late Mesozoic age. Although the limestone formations are between 340-300 million years old, the actual dissolution to form caverns started much later, probably in the Ice Age, only a million years in age [7].

After purportedly exploring several miles of serpentine labyrinth interspersed with deep vertical karst and vast limestone ledges, to the brother's amazement an enormous underground river materialized. More astonishing was how the black sand beach was rich in placer gold. After liberating as much of the gold-laden sand as they could carry on their backs, the three began their ascent out of the cavern—but not before tragedy struck when brother George plunged into the river to his death [8].

Distraught but determined, the two brothers made their way back to civilization, traded in their extremely

Figure 2. The Kokoweef beacon at Mountain Pass on I-15 that continues to lure tourists and treasure seekers to the famed mine. Photo: Kim Stringfellow.

profitable discovery to the U.S. Mint, then allegedly deposited more than $57,000 between banks in Needles and Las Vegas. The legend further suggests that the brothers never revisited Kokoweef again as tribal custom forbade them from entering the cave after their sibling's unfortunate demise.[9] This tragic incident would not deter Earl Dorr, a "cowboy turned prospector" now in his late 30s, who supposedly set off during the late 1920s to undergo his own odyssey to locate Kokoweef's golden bonanza.

Kokoweef Peak lies in a verdant Joshua tree woodland accessible by car from the Bailey Road exit off Interstate 15. Heading east on Baily, drivers will pass the blue and white beacon signaling the way to Kokoweef, Inc. about three miles down a series of dirt roads. It is here where this larger-than-life legend continues to play out, captivating treasure hunters, hungry investors and curious thrill seekers for well over 80 years.

As mentioned earlier, extensive cave systems do exist throughout the Mojave Desert. Mitchell Caverns (currently closed) features a trio of immense limestone caves with spectacular travertine "draperies," stalactites, stalagmites, helictites and other wondrous subterranean mineral formations. Kokoweef Peak has three considerable, nearly vertical caverns named Kokoweef, Crystal and Kin Sabe—a misspelling of *Quien sabe,* Spanish for "who knows?"

And, true, a rich diversity of mineral wealth is centered in the region. Standard Mines Company shipped thousands of tons of copper ore rich in gold and silver from here at the turn of the century, and telltale signs of early Spanish mines can be discerned on ledges and rock outcrops throughout the area. The Molycorp mine looms north of the I-25 and when in production extracted rare earth elements used in cell phones, TVs, fuel cells, and photovoltaics.

Fantastic as it seems, Dorr also claimed success in locating the Peysert brother's subterranean mother lode—at least this is the story that most treasure magazines proffering the legend seem to suggest. The holy grail of the Dorr legend is an affidavit notarized in Pasadena on November 16, 1934, published in the *California Mining Journal*'s November 1940 issue *six years after it was notarized*. In this document, Dorr and an unnamed accompanying civil engineer began their explorations of "certain caverns" during May of 1927, spending *four days* in the cave system and traveling "a distance between eight and nine miles." Nowhere in this affidavit does it mention Kokoweef Peak or Crystal Cave as the actual location, nor is there any mention of the Peysert Brothers.

To confuse matters more there are at least two affidavit versions floating around— Kokoweef.com claims that their copy of the hand-typed document notarized on December 10, 1934, is the *original*—even though the notarized date on the first affidavit *is a month earlier.* Still, the two documents share much of the same information with the exception that the second "original" version names a "Mr. Morton" as the civil engineer and states how Dorr had first been made aware of the caverns through the Peysert Brothers. Suspiciously, these crucial details were added after the November 16 version. Future published references of Dorr's story in treasure magazines would print either affidavit interchangeably.

The imaginative details of Dorr's find are truly out of this world. Below are verbatim excerpts from the November 1934 affidavit version:

> This is to certify that there is located in San Bernardino County, California, about two hundred and fifty miles from Los Angeles, a certain caverns…From the mouth of the cave we descended about 2000 feet. There, we found a canyon, which, on our altimeter, measured about 3000 to 3500 feet deep. We found the caverns to be divided into many chambers, filled and embellished with the usual stalactites and stalagmites, besides many grotesque and fantastic wonders that make the caverns one of the marvels of the world.
>
> On the floor of the canyon there is a flowing river which by careful examination and measurement (by triangulation) we estimated to be about 300 feet wide and with considerable depth. The river rises and falls the tides of the sea—at high tide, being approximately 300 feet wide, and at low tide, approximately 10 feet wide and four feet deep.
>
> When the tide is out there is exposed on both sides of the river from 100 to 150 feet of black beach sand which is very rich in gold value. The sands are from 4 to 11 feet deep…We explored the ledge sands for a distance of more than eight miles, finding little variation in the depth and width of the sands.

The second affidavit dated December 10, 1934, embellishes the story further:

> One [stalactite], the largest seen, is 27 feet in diameter and hangs 1,510 feet down into a 3000 foot canyon. This great stalactite is perpetually washed by water flowing over it and falling into the dark canyon depths. The huge glistening white crystal *is 500 feet longer than the Eifel Tower*, and challenged us with amazement and wonder.

Dorr goes on to state within the December affidavit that his last conversation with Oliver and Buck Peysert was at his home in Pasadena on November 10, 1934—six days after the first affidavit was notarized. Finally, both affidavits declare that the 2.5 pounds of sand collected along the ledges were assayed at $2,145.47 per yard or $20.67 per ounce by John Herman in Los Angeles—although no record of this document seems to exist [10]. With gold hovering at $1,355.00 per ounce as of August 2016, the stated assay would translate into billions of dollars today.

The fabrications of Dorr's story that arose soon after the publication of his affidavit in the 1940 *California Mining Journal* are legendary and, not surprisingly, fraught with inconsistencies. For instance, one version of the yarn suggests that Mr. Morton became dreadfully ill while inside Crystal Cave and had to be lugged back to the surface single-handedly by Dorr where he was met by two prospector acquaintances that just happened to be camping outside the cave's entrance. The men supposedly helped Dorr bring Morton out and down the mountainside and while doing so, ended up eyeing the gold-laden sand thereby exposing Dorr's windfall [11].

The story shatters into a multitude of versions at this point. Some accounts propose that Dorr set a blast charge sealing the passage before or even just after coming up to the surface and encountering the two men. Others have Dorr returning at some later point to do so in his effort to conceal from claim jumpers. Another version suggests that Dorr blew the entrance while the two prospectors were *inside,* entombing them and thus sealing their fate. Of course, their remains were not discovered during subsequent explorations of Crystal Cave and if they hadn't been victims of Dorr's wrath then these two characters (who, if available, would be able to back his story) were never heard of again. Rather conveniently, too, "Mr. Morton" failed to physically materialize to corroborate Dorr's affidavit.

It is true that a Southern California Grotto (the Pasadena based chapter of the National Speleological Society) exploratory team of 34 cavers led by renowned spelunker Dr. William Halliday, found DORR smoked with a carbide lamp onto the ceiling in two locations during their November 1948 caving exploration. The group additionally noted DORR at a deeper location above a pile of flowstone rubble with the ghosted black line suggesting that a blast charge could have been set here previously [12].

Although not stated in either affidavit, later published accounts would state that while exploring the cavern for some length Dorr and Morton observed a fissure allowing daylight to stream in, signaling the possibility of another portal entrance. This partially suggests why Dorr purportedly blasted the Crystal Cave entrance shut, gambling that he would later, and perhaps effortlessly, locate a secondary access point after the dust settled down. The problem was he could not find this elusive entrance. To make matters worse, another miner, Pete Ressler (rumored to have run with the Butch Cassidy gang), held most of the claims in and around Kokoweef Peak so Dorr was not able to stake a claim at this original Crystal Cave entry point.

The publication of Dorr's story in Johnston's *Westways* article in 1935, along with his affidavit, convinced Herman Wallace and some other willing Los Angeles investors to bankroll his project—a feat during the lean Depression years. That same year the syndicate formed Crystal Cave Mining Corporation. By 1939, they had bought out Ressler's 14 Kokoweef area claims for $5,000 and began tunneling an *adit* from Kin Sabe in an effort to connect with Crystal Cave—but this endeavor was unsuccessful.

Undeterred, the outfit attempted another linkup from Kokoweef Cave, but in the process discovered something else—high-grade zinc ore. When refined, zinc can be used

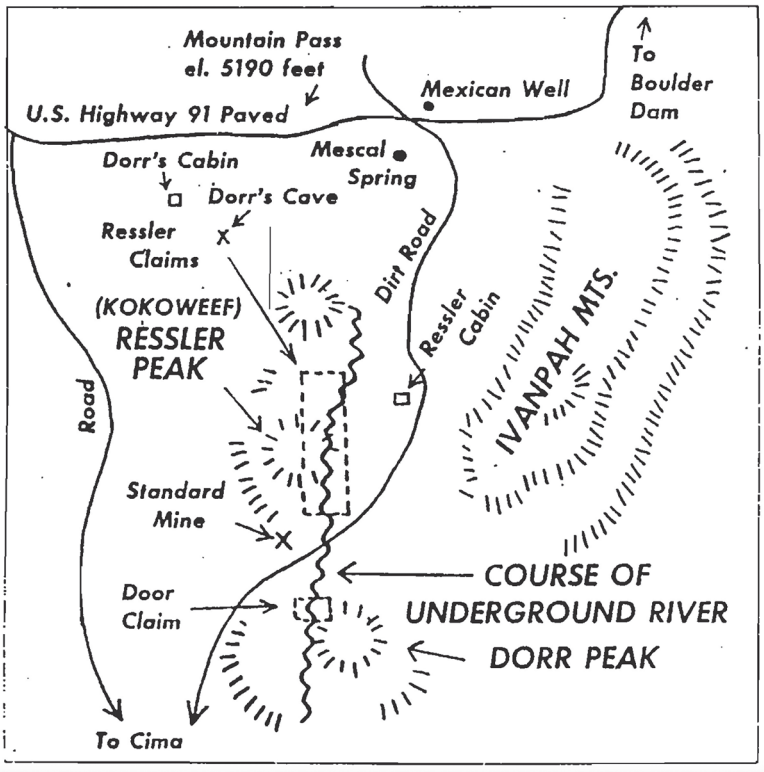

Figure 3. Ray Dorr's 1967 Argosy Magazine map showing the location of Dorr's cave and cabin in the Mescal Range, about 5 miles north of Kokoweef Peak.

for brass manufacturing, galvanization processes, tire production and other industrial uses deemed crucial for the burgeoning war effort. This discovery—along with the Federal Government's 1933 Executive Order 6102 that banned private ownership of gold coin, bullion and other monetary forms along with the 1942 ban on the extraction of non-strategic metals such as gold during wartime—brought the entire operation to a standstill. If the zinc strike had not been discovered as certain world events aligned, the Crystal Cave Mining Corporation may have continued in their search for Earl's River of Gold.

Sometime in the mid- to late 1930s, Dorr began independently tunneling a possible connection to the illusive portal at one of his area claims in the Mescal Range near the old U.S. Highway 91 (now Interstate 15)—located about five miles north of Kokoweef and Dorr peaks. Here, not far from the shack that Dorr built, is a canyon leading to a steep hillside cave where he apparently dug a 100-foot shaft *seemingly* to nowhere, which was later abandoned after Dorr moved on to find paying work [13]. When Dorr died in 1957 during a mining accident, it was said that he only had a few hundred dollars to his name.

There is no doubt Earl P. Dorr explored Kokoweef's Crystal Cave and several others nearby in the years before 1934. To what extent we will never know. What he discovered during his explorations remains conjecture. The subterfuge he chose to promote was likely embellished with local lore, fueled by his contemporaries' front-page accounts of fantastic discoveries, driving him to dream up a more imaginative speleological wonder in his effort to lure investors to grubstake him in his search for the Mojave's fictionalized Lost River of Gold.

Dorr's fabrication continues to tempt others to follow in his footsteps in the never-ending saga to unlock the mysteries of Kokoweef. But these endeavors often end in folly. For instance, in 1959 two illegal treasure hunters set a blast deep within Crystal Cavern, only to asphyxiate to death from toxic dynamite fumes.

In 1963, a near shootout erupted at Kokoweef between drill workers hired by Emmet J. Culligan, of water softening fame, and Charles O. Thompson, a former Corona high school track star residing in Llano, California, who had at the time leased a mining option with a group of investors from Crystal Cave Mining Corporation. Culligan's men were conducting exploratory drilling in the area spurned, not surprisingly, by his own interest in underground rivers. Thompson later filed a court injunction against the retired water-softening mogul and his partners, charging that Culligan's activities were infringing upon his legitimate mining operation, thus igniting a lengthy court battle.

Meanwhile, Culligan was busy drilling 12 miles south of Kokoweef at Cima with a traditional water-drilling rig, but upsized to an oil drill rig that he had purchased and brought over from Long Beach, California. The team did manage to punch a "blow hole" where fresh air miraculously flowed, suggesting that it was connected to other cavern network openings. Culligan, who was less interested in locating gold and more so in finding water, looked into obtaining industrial strength dye he called "red smoke" that he planned to drop inside the opening and then fly around the area to map where the smoke escaped from other geological orifices—except that the U.S. Army failed to provide him with the chemical for private use. In the end, Culligan spent upwards of $75,000 of his own money to fund the project, and Thompson got into hot water himself for failing to pay back taxes on mining claims.

This well-publicized court case, along with intrigue driven by the plethora of treasure hunting magazines peddling the ever-popular Dorr legend, continued to stoke renewed interest in locating the Mojave's Lost River of Gold.

> "Be ensured the enthusiasm remains." — Kokoweefinc.net

By 1972, a new group of "gold-blind" Kokoweef enthusiasts, organized under the auspices of Concave Mining Company, had leased the now patented Kokoweef claim and were soon hard at work in their effort to locate a cavern passage into Dorr's alleged River of Gold. To offset exploratory expenses, they began conducting public tours for $2.50 per person and hawked ornamental mineral specimens brought out of the cave by the truckload.

In 1974, after investors revolted over embezzlement allegations, a new company formed, Legendary Kokoweef Caverns, Inc., which issued new unregistered stock and interest-bearing notes. Under their direction, a horizontal 750-foot tunnel under Crystal Cave along with a 150-foot inclined raise sited upward were completed, allowing them to vigorously clean out debris from the bottom of the cave network. However, embroiled nearly ten years with concerns over financial and legal liabilities, they, too, had abandoned their lease.

By the mid-1980s, a North Las Vegas military surplus storeowner named Larry Hahn had taken the helm as head of Explorations Inc. of Nevada, which reorganized in 2006 as Kokoweef, Inc. with Hahn appointing himself as president/treasurer along with a 51-percent stockowner share in the corporation. The current operation, still headed by Hahn, is funded through stockholder monies from 300 to 500, to as many as 1,000 investors, who on average have each purchased a minimum of $600 dollars in Kokoweef, Inc. stock. At least 11 individual investors have sunken $100,000 each into the enterprise [14]. Day-to-day operations are run by a small group of amateur investor volunteers living either full- or part-time on site, including several retired gaming employees, a former sheriff, and a near doppelganger for Hunter S. Thompson who just happens to have graduated from the same high school as I did in Kent, Washington, five years before me.

Ralph Lewis, working today as a union electrician, caught the Kokoweef bug in 1979 just after his honorable

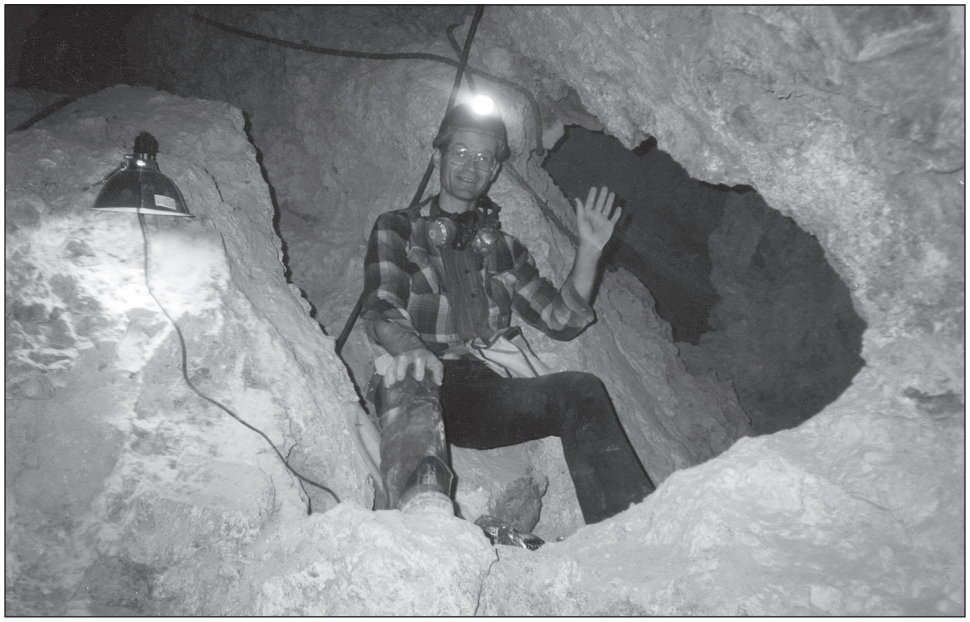

Figure 4. Ralph Lewis photographed at the purported blocked entrance at the bottom of Crystal Cave. About 5 feet above Lewis' head (out of the image frame) is the infamous carbide smoked DORR letters. Photo: Robert "Bob" Lauten.

discharge from the army. He had been tipped about the Dorr legend by his brother who had read about Kokoweef in the 1967 *Argosy Magazine* article authored by Ray Dorr, one of Earl's nephews. Lewis had planned to spend only two weeks visiting the site, but ended up staying on for two years as a volunteer worker. He lived on and off at the camp, which he somewhat affectionately nicknamed "Squalorville," until 2001, including an eight-year full-time stint at the Kokoweef mill site. Over time Lewis gained extensive knowledge of the peak's cavern system through "drilling, blasting, mucking and mapping," and has conducted tours into the Crystal Cave for dozens of interested parties, including several documentary film crews.

Lewis stated over the past 45 years at least 20 distinct tunnels, shafts and raises of varying lengths totaling well over a mile have been completed inside the private holdings at Kokoweef Peak. The tunnels feature colorful names such as Hillary's Hole and the Psychic Decline. Lewis became close friends with Willard Dorr Jr., another of Earl's nephews. He was later the recipient of Willard's estate along with numerous photos and documents relating to Earl Dorr after Willard Jr. died in 2000.

Lewis—a former Kokoweef true believer—is now a self-described "truth seeker" who is highly certain that Dorr never accessed his River of Gold from within Kokoweef Peak. However, he still holds out on the possibility that Dorr or others found ingress to the purported cavern system at a different location. Having spent years conducting research on the subject, including assisting with 21 costly on-site electronic geophysical surveys funded somewhat ironically with the inheritance from Willard Jr. plus a substantial chunk of his own personal savings, he is compelled to share a fact-based backstory for the treasure-obsessed public. Detailed, if somewhat cryptic essays of his theories including a riddle-filled poem are published at kokoweef.com. Lewis' outlook is partially driven by his own determined quest for the truth reinforced by a family tragedy—his father fell victim to a mining investment scam that forced him to lose all of his life savings when the deal did not pan out as planned.

Lewis' sleuthing led him to a Denver cemetery in his search for the mysterious "Peysert" Indian Brothers. He did locate *Peyser* headstones here, but learned that these particular ancestors were likely of European descent and definitely not Native American. One Peyser was said to be a mining broker and the other a wealthy jeweler. He has theorized that "Kokoweef" is a misspelling of *Coco-weep*, which he believes translates into "wet cave"—the name of a forgotten canyon first described in an 1870 Clark Mining District map. Finally, when it comes to the DORR letters found in the depths of Crystal Cave, Lewis flatly states that it doesn't necessarily mean that Dorr inscribed this himself. From his exhaustive research and physical examinations he is convinced that Dorr's purported dynamited blocked passageway found deep in the mountain is simply a hoax.

But more convincingly, Lewis woke up to Dorr's deception after locating and reviewing an obscure April 1942 Department of the Interior National Park Service (NPS) report. The report was from an investigation of various caves within the Clark Mountains and Mescal Range "as far as Kokoweef Peak"—conducted to discern if these particular caverns were of "sufficient importance to warrant their further consideration for park or monument purposes." The investigation had been initiated when a Mr. John Q. Little along with his partner, "a prospector named Dorr," had filed an application for a special use permit for developing certain area caverns for the public. T.R. Goodwin, the acting superintendent for Death Valley National Monument, dispatched a NPS investigative crew that included Mr. Alberts, a naturalist; Mr. Grunigen, an engineer; and Mr. Oakes, a park ranger. Dorr acted as field guide.

The NPS staff reported in internal correspondence, dated May 1, 1942, that "no cavern of scientific, education, or recreational value was located in the area." More pointedly, the report—titled *Special Report: Investigation*

Figure 5. A photograph from the original 1942 NPS investigation report debunking Dorr's alleged Crystal Cave entry point. Dorr, who acted as field guide, is pictured in the center of the group. Image courtesy Ralph Lewis.

of Cave Sites and Claims in Vicinity of Mescal Range, Calif.—stated on page 6:

> Either Mr. Dorr actually found one of the chimeras of the Mojave Desert—the fabulous underground river along the banks of which occurred black sands, rich with gold nuggets—or he has heard the tale so long that he has come to believe it in all sincerity.

On page 9 it follows with:

> They [the NPS field crew] found no evidence of any artificial closing of the chimney either by lasting [sic] rock, or erection of a barrier. This is interesting in the light of Dorr's story, and local legend having it that this chimney [Kokoweef's Crystal Cave] was the former means of entrance into the underground river with rich black sands.

Mr. Lewis has been known to tell people, "If I'd done my homework first and had read the 1942 government report in 1979, I probably would not have stayed at Kokoweef for more than two weeks."

These days Lewis feels that Kokoweef, Inc. investors would be better off capitalizing on a "billion dollar" mineral sulfide deposit revealed by the electronic surveys or perhaps just plain old tourism. He continues to pursue his independent research in the quest for truth regarding the Kokoweef legend.

+++

The only hard data to come out of Kokoweef Peak is one that has nothing to do with mineral wealth. Beginning in 1972, paleontologist/geologist Bob Reynolds—the former Curator of Earth Sciences at the San Bernardino County Museum—at the request of the cave's owners, led a research team into Kokoweef Cave to excavate and remove more than five and a half tons of loose sediment containing more than 200,000 fossil and skeletal remains from the Latest Pleistocene period. The excavations took place from 11 to 45 feet below the cave's trestle. All material had to be packed out manually without mechanical hoists, which Reynolds still remembers as "backbreaking work." The retrieved fossiliferous sediments deposited less than 11 thousand years ago bore bone fragments of coyote, large and small camels, deer, pronghorn, horse, marmots, voles, bats, shrews, and birds including condors. This collection is considered the most extensive late Pleistocene cave fauna from the East Mojave.

Coincidentally, Reynolds is himself less than six degrees separated from the Kokoweef legend. His great-aunt Lois Turner lived in a boarding house in Pasadena that Dorr frequented during the early 1930s. She recounted years later how Dorr would make calls from the house pay telephone to promote his River of Gold story and referred to him as a "shady character" [15]. Reynolds heard a similar description when interviewing Riley Bembry of Riley's Camp who was a butcher in Cima in the 1930s. At town gatherings and dances, Bembry noted

that "Dorr was a loner, hanging around the fringes of the crowd…"

When asked if such a monumental underground river could remain hidden in this region, Reynolds said:

> Don't look at the cave, don't look at the peak, look at the geology and topography. Kokoweef Peak reaches 6,000 feet and the original entrance to the cave is at 5,800 feet. Although the limestone of the peak is easily dissolved to form cavities and caverns, geologic maps suggests that it is sitting on insoluble granite at the elevation of Piute Valley (5,000 feet) at the base of the peak. Looking east into Ivanpah Valley, the slopes consist of gneiss, a rock as insoluble as granite, that is exposed to a low elevation of 2,900 feet. Looking west down Piute Valley toward Cima Road and Valley Wells in Shadow Valley, granite is exposed at 3,800 feet. *So, there are generally insoluble rocks for about 2,000 feet below the base of the limestone and almost a half mile below the original cave entrance.* Both Ivanpah and Shadow valleys have spring and ponds, and lakes that are dry unless filled by thunder showers. If there were a "lost river" below those valleys, spring and rainwater would disappear into it along faults [16].

In the end, Earl P. Dorr seems to have hoodwinked himself—believing in his own elaborate fabrication simply because he had invested so much time and energy into inventing the story. After all, even Ray Dorr commented that his uncle had a "vivid imagination." Was Dorr a clever liar that ended up believing his own ruse? That he continued searching for another entrance into the Mojave's mythic River of Gold well into the 1940s—even after his Crystal Cave Mining Corporation partners gave up on the endeavor and the 1942 NPS report confirmed that it was improbable—suggests that there was something Dorr was after or even possibly *hiding.* Whatever it was, though, Dorr ended up taking that secret to his grave.

Acknowledgments

I would like to thank Anna Garcia, principal water resources hydrogeologist at the Mojave Water Agency, for sharing her extensive research archive on Kokoweef. Very special thanks go out to Ralph Lewis and Bob Reynolds for sharing insights and personal stories related to this fascinating legend.

Notes:

[1] The 1967 *Argosy* magazine article written by Ray Dorr identified Uncle Dorr's middle initial incorrectly as *M*, when it was actually *P.*

[2] Considering the date of publication, one could argue that Mitchell revised the Dorr legend for his own purposes but it more or less suggests how during the early part of the 20th century numerous versions of the Mojave's Lost River of Gold myth were circulated widely throughout the transient prospecting community.

[3] Not so farfetched since Devils Hole is affected by semidiurnal tidal movements.

[4] Technically the cave described in the story would need to be *northwest* of Nipton to be positioned geographically on the western shore of Ivanpah Dry Lake.

[5] The two known notarized affidavits state that it took Dorr and his engineer four days to explore the cave system.

[6] The range of articles on the subject sometime state that the Peysert Brothers were either of Chemehuevi or Paiute descent, or simply referred to as "Indian."

[7] Evans, James R., 1971. Geology and mineral deposits of the Mescal Range quadrangle, San Bernardino County, California. California Division of Mines and Geology map sheet 17, scale 1:62,500; Reynolds, R.E., R.L. Reynolds, C.J. Bell, N.J. Czaplewski, H.T. Goodwin, J.I. Mead, and B. Roth, 1991. The Kokoweef Cave faunal assemblage. San Bernardino County Museum Association Special Publication, SP91-1:97-103.

[8] In Bob Ausmus' "The Legend of the Kokoweef," *Guide to the East Mojave Heritage Trail (Ivanpah to Rocky Ridge) No.14* by Dennis Casebier and the Friends of the Mojave Road, October 1988, Ausmus states that the legend begins with "Paiute" brothers first locating the river, who "returned with lumber for constructing a sluice box, and within six weeks produced $57,000 worth of gold from their placer mining operation" 239.

[9] The author consulted with Chemehuevi elder and Native scholar Matthew Leivas Sr. on whether there are any tribal histories relating to the Mojave's "lost river of gold." Leivas said that he was not aware of any "tribal lore" vaguely supporting the legend.

[10] The December 10, 1934, affidavit on Kokoweef.com states an amount of $2,144.47 per yard not $2,145.47.

[11] See Ausmus "The Legend of Kokoweef."

[12] For further reading see: Halliday, William R. *Adventure Is Underground*. New York. Harper & Brothers, Publishers, 1959.

[13] The major fault under these peaks run east/west and there appears to be a branch of the fault under Kokoweef that angles upwards to this location. If one believes in Dorr's story, then it is possible that a linkup could be found at this location. Source: Dorr, Ray. *Argosy* magazine.

[14] Email correspondence with Bob Reynolds on July 26, 2016 with the author.

[15] Email correspondence with Bob Reynolds on July 25, 2016 with the author. For more information see: Reynolds, R.E. et al. "The Kokoweef Cave Faunal Assemblage." SBCMA Spec. Publ. MDQRC 91, May 1991.

[16] Ibid.

Miocene(?) to Holocene extensional tectonics in the Coyote Mountains, western Salton Trough, southern California

George Morgan and J. R. Morgan
georgemorgan@cox.net

ABSTRACT—Three extensional tectonic episodes, dating from Miocene(?) to late Pleistocene, are recorded in the local stratigraphy of the Coyote Mountains, southern California. Each episode has its own particular set of normal faults, grabens and distinctive package of syn- and post-extensional sediments. The first episode is correlated with Basin and Range extension that took place in Sonora, Mexico. The second episode is correlated with the opening of the Gulf of California. The third episode is correlated with the West Salton Detachment Fault after the Coyote Mountains had started to move northward from Sonora under the influence of the San Andreas fault system.

Introduction

The Coyote Mountains (CMs) are a small, fish hook-shaped mountain range located in southern California (see Figure 1). The mountain range is north of Interstate 8, northeast of Ocotillo, Imperial County, California and 20 kilometers north of the international border with Mexico. The western part of the CMs is situated in San Diego County and the eastern part lies in Imperial County. The CMs are located on the western edge of the Salton Trough with the Peninsular Ranges Batholith further to the west (see Figure 1). The CMs are bounded on the southwest

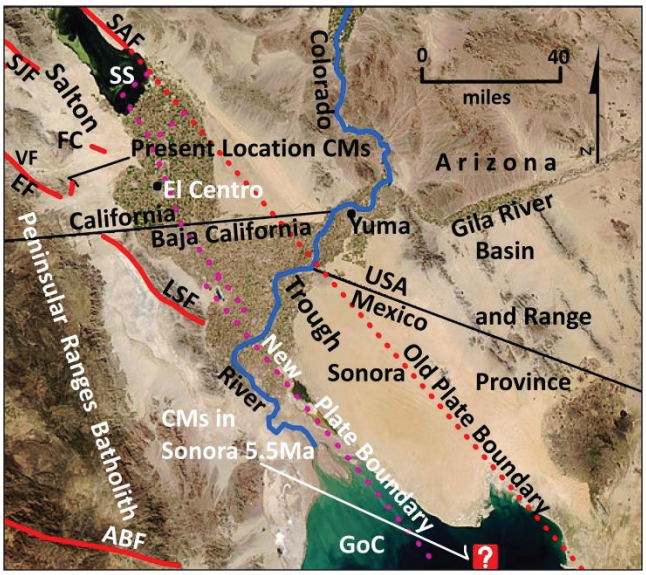

Figure 1. Location Map of the Salton Trough and the Coyote Mountains in California and Sonora, Mexico. **ABF**—Agua Blanca Fault, **EF**—Elsinore Fault, **FC**—Fish Creek Mountains, **GoF**—Gulf of California, **LSF**—Laguna Salada Fault, **SAF**—San Andreas Fault, **SJF**—San Jacinto Fault, **SS**—Salton Sea, **VF**—Vallicetos-Split Mountain-Fish Creek Basin. Red square with query is the paleogeographic location of the Coyote Mountains at 5.5 Ma by Winker and Kidwell (1996) in Sonora, Mexico. We agree the paleogeographic location for the CMs was somewhere in Sonora, Mexico. NASA photograph.

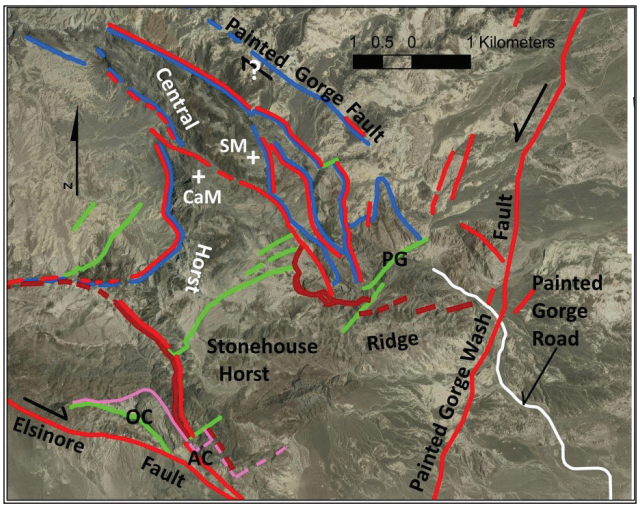

Figure 2. Map of the fish hook area of the CMs and some of the faults in the CMs. **OC**—Ocotillo Canyon. **AC**—Alverson/Fossil Canyon. **PG**—Painted Gorge. **CaM** – Carrizo Mountain. **SM** – Switchback Mountain The active right-lateral Elsinore Fault forms the southwestern side of the CMs and the active left-lateral Painted Gorge Wash Fault forms a boundary on the east-southeastern side of the CMs. Pink lines-first extensional episode normal faults. Brown lines-second extensional episode normal faults. Blue lines-third extensional episode normal faults. Red lines—1 Ma strike-slip faults (Steely et al., 2009). Green faults-other faults. The normal faults of the three episodes outline the half grabens, grabens and horsts associated with the three extensions. White line—Painted Gorge Road. Red faults that are close and parallel to older normal faults represent reactivation of the older normal fault as 1 Ma right-lateral faults. The horst for the first extensional episode is the topographic high, metamorphic core of Stonehouse Ridge. The normal faults of the second and third episodes are found on the east and west sides of the topographic high, metamorphic, fish hock shaped, core of the CMs. We refer to this area as the Central Horst. Christensen (1957) named the Painted Gorge Fault and mapped it as a normal fault. Some workers believe the Painted Gorge Fault to be a right-lateral fault. A recent fault scarp on the Pained Gorge Fault the shows very little strike-slip movement and more dip-slip movement with the east side up (Morgan and Morgan, this volume). Older offsets across the Painted Gorge Fault appear to be dip-slip with the east side up. We believe the Painted Gorge Fault is a normal fault that is a part of the third extensional episode found in the CMs (this paper). We are having trouble mapping the Painted Gorge Fault continuously to and crossing the Painted Gorge drainage (Morgan and Morgan this volume).

by the active right-lateral Elsinore Fault (Dibblee, 1954) and on the east-southeast by the active left-lateral Painted Gorge Wash Fault (Morgan and Morgan, 2005) (see Figure 2).

The CMs consist of an uplifted crystalline basement core overlaid by Cenozoic sediments accumulated before and during the ongoing opening of the Gulf of California. The sedimentary column represents, first, a Miocene age non-marine depositional environment, then a Miocene through Pliocene marine depositional environment, and finally a Pliocene to Pleistocene non-marine depositional environment. A tectonic reconstruction by Winker and Kidwell (1996) place the CMs in Sonora, Mexico before 5.5 Ma. We believe the CMs, as discussed in this paper, were affected by Basin and Range extensional tectonic regime found in Sonora. With continuing episodes of extensional tectonics and the opening of the Gulf of California by the San Andreas Fault System, the CMs moved northwest from Sonora to their present location.

In 2001 we started mapping the CMs at a 1:2000 scale and have found the mapping to be challenging. Some of those who have worked in the CMs describe them as complicated. They are right. Mapping by the authors continues and we may revise the concepts presented here.

Basement

The basement of the present-day CMs consists of an uplifted crystalline core of marbles, schists, cherts, banded cherts, quartzites and amphibolites. These units represent Paleozoic(?) (Dibblee, 1954; Miller and Dockum, 1983) age miogeosynclinal to flysch sediments we believe were deposited in a passive continental margin in Sonora, Mexico. Blaettler (1991) studied the petrology of the amphibolites and concluded they originated as basalts. Morgan and Morgan (2015) reported relic pillow structures in some of the outcrops Blaettler previously studied. The amphibolites may represent relic basalts flows in a marine environment.

Starting before and/or during the Jurassic, the passive continental margin in Sonora became an active margin and the marine sediments were intruded, deformed, and regionally metamorphosed. Some of the igneous rocks associated with the active margin in the CMs are: diorite, gabbro, dikes of various compositions, foliated tonalite and a gneiss. All of these rocks are Jurassic (about 162 Ma based on U/Pb dating by Morgan and Morgan, 2015). Cretaceous igneous rocks have not been found and in the CMs. The Jurassic(?) deformation has destroyed all the original sedimentary relationships. During the deformation the metamorphic and igneous rocks of the CMs were uplifted and the metamorphics were left with steeply dipping foliation and tight folds.

Cenozoic sedimentation and extensional tectonics

From the Cretaceous to Oligocene, rock units are either absent or have yet to be identified in the CMs. During the Eocene, rivers flowed from eastern Sonora, across the crystalline basement terrane that contained the CMs and the Peninsular Ranges Batholith, to the Pacific Ocean (Link and Abbott, 1991). The only indication of these Eocene rivers in the CMs are the distinct, well indurated, silicified meta-volcanic cobbles associated with the Eocene rivers, which are sporadically found as reworked clasts in the lower fanglomerates of the Split Mountain Group below the Alverson Formation (Ruisaard, 1979 renamed the Alverson Volcanics of Dibblee, 1954).

Following the erosional episode represented by the Eocene rivers and beginning in the Oligocene, Basin and Range extension took place in Sonora (Nourse et al., 1994; McDowell, et al., 1997). In the CMs, the Basin and Range extension (the first extensional episode of three) is represented by normal faulting and deposition of syn-extensional Miocene age sediments of a lower part of the non-marine Split Mountain Group (Winker and Kidwell, 1996) deposited in an extensional half graben in the southern CMs (see Figure 2 and 4). Deposited in and outside of this graben are post-extensional sediments and the volcanics of the Alverson Formation that are an upper part of the Split Mountain Group (see Figure 3 and 15). Field evidence indicates that the volcanics completely buried the CMs (Morgan and Morgan, 2015). Deposited in and outside of this half graben are marine and non-marine sediments of the Miocene Viejo Formation (Morgan and Morgan, 2016), a lower part of the Imperial Group (Winker and Kidwell, 1996).

The Viejo Formation contains nine plus marine transgressional-regressional (T-R) sequences that interfinger with five plus non-marine fanglomerates deposited in the slowly subsiding CMs (Morgan and Morgan, 2015). In the CMs we define a transgression

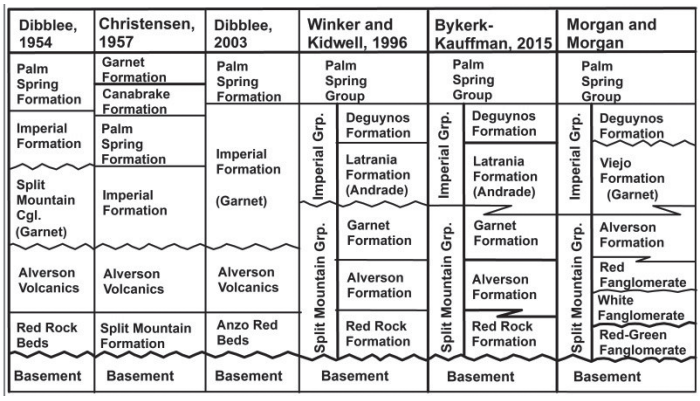

Figure 3. Edited columnar sections from Dibblee (1954, 2003), Christensen (1957), Winker and Kidwell (1996) and Bykerk-Kauffman (2015) for units they used in the CMs that are discussed in this paper. Our working columnar section, "Morgan and Morgan" is only for the CMs. Only the relative age of units is shown. **(Garnet)**—designates units of other authors that contain Christensen's Garnet Formation. **Cgt**—conglomerate. **Grp**—Group.

as a rise in sea level and a regression as a fall in sea level: regional uplift or subsidence is not controlling the transgressions or the regressions found in the CMs. The transgression and the regression together form a sequence of marine sediments. The marine sedimentary sequence in the CMs starts with a locally derived, high energy, basal conglomerate deposited on an unconformity, then deposition of a sandstone, followed by deposition of a low energy mudstone topped by another unconformity. The easily eroded mudstone is often missing from the sequence. Angular unconformities, between many of the T-R sequences, attest to the tectonic activity taking place during the deposition of the Viejo Formation. In the CMs, when the sea level is low, non-marine, locally derived, fanglomerates were sometimes deposited between the T-R sequences. There is field evidence that the youngest marine member of the Viejo Formation covered the CMs completely (Morgan and Morgan, 2015) Marine members that are low in the Viejo Formation interfinger with basalt flows that are in the upper part of the Alverson Formation (younger than 16.9 Ma U/Pb, detrital zircons age dating, Morgan and Morgan, 2015). The interfingering of Imperial Group sediments (Viejo) with the volcanics of the Alverson Formation was first reported by Woodring (1931). The Viejo Formation may represent an early arrival of the Gulf of California, at least in the CMs. Dorsey (2012) reports the Gulf of California arriving in the Vallecito–Split Mountain–Fish Creek Basin, to the north of the CMs (see Figure 1), about 6.2 Ma.

During the deposition of the Miocene Imperial Group sediments (Winker and Kidwell, 1996) in the CMs, the tectonic regime changed from Basin and Range extension to right-lateral transtension associated with the San Andreas Fault system and the opening of the Gulf of California (Hamilton, 1961; Umhoefer, 2011). During this interval, a second extensional episode is preserved as curved normal faults and half grabens on the east and west sides of the CMs. Field evidence indicates the second extensional episode can be associated with the opening of the Gulf (this paper). With this change to lateral movement, the CMs started to move toward the northwest starting about 5.5 Ma (Winker and Kidwell, 1996). As the CMs moved northwest, they came under the depositional influence of the Colorado River. In the CMs, the Pliocene marine Deguyños Formation, an upper part of the Imperial Group (Winker and Kidwell, 1996), and the non-marine Pliocene to Pleistocene Palm Spring Group (Winker and Kidwell, 1996), recorded these changes in tectonics and sedimentation. Internally the Deguyños Formation deposited around the CMs contains angular unconformities that are related to T-R sequences controlled by sea level changes (Morgan and Morgan, 2015). Both the Deguyños Formation and the sediments of the Palm Spring Group are widespread in the Salton Trough and may have completely covered the CMs (Winker and Kidwell,1996).

As the CMs moved north, a third extensional episode occurred that we believe is associated with the West Salton Detachment (Axen and Fletcher, 1998). This third extension episode produced normal faults, horsts, grabens, and a half graben on the east and west sides of the CMs. In the western Salton Trough, movement on the West Salton Detachment ended about 1Ma with the onset of right-lateral faulting (Steely et al., 2009). Dating the end of the third episode in the CMs is speculative as radiometric age dates are lacking, but the third extensional episode we have mapped in the CMs ends with right-lateral faulting about the same time as Steely et al. (2009) proposed.

In the last 1 Ma the CMs have under gone a rapid, episodic and disproportional topographic uplift and erosion leaving the CMs with unstable slopes and five plus terraces on the mountain flanks. On the east side of the CMs, the terraces merge eastward to a common base level (Morgan and Morgan, 2015). Morgan and Morgan (2015) recognized that at least one marine member of the Viejo Formation underwent soft sediment deformation during the recent uplift. The rapid, episodic and disproportionate uplift of the CMs took place along strike-slip and older extensional-normal faults. Some of the extensional normal faults may have been reactivated as 1 Ma strike-slip faults.

The CMs are now located near the western edge of the Salton Trough; are dominated by active right and left-lateral faulting, and are being differentially uplifted.

Stratigraphic nomenclature by other workers in the Coyote Mountains

Others have studied and are studying the CMs and have different explanations for the complex geology. Winker and Kidwell (1996) reorganized the columnar section for the Vallecito-Split Mountain-Fish Creek Basin (VSFCB) northwest of the CMs (see Figure 1). For the most part they used the nomenclature work out in the VSFCB to describe the geology they mapped in the CMs (see Figure 3). Winker and Kidwell (1996) recognized only one transgression for the Imperial Group in the VSPFCB and the CMs. The Andrade Member of the Latrania Formation (see Figure 3) represents their transgression in the CMs. Winker and Kidwell do not recognize that the Andrade Member of the Latrania Formation in the CMs interfingers with the volcanic flows of the Alverson Formation. Morgan and Morgan (2016) replaced, only in the CMs stratigraphy, the Latrania Formation with the Viejo Formation containing nine plus T-R marine sequences that interfinger with five plus non-marine fanglomerates (see Figure 3).

The Garnet Formation is another Cenozoic unit that Winker and Kidwell redefined. The Garnet Formation has had a storied history. The placement of the Garnet Formation in a columnar section depends strongly on who was mapping and when they mapped. The Garnet was initially given status as a formation by Christensen (1957) for the gravels (fanglomerates) found in what appears to be a channel in the topographic, metamorphic core of

the southern CMs. He believed the unit to be Quaternary in age and above the Canebrake Formation (see Figure 3). Christensen never designated a type section for the Garnet.

Dibblee (1954) mapped the Garnet as Split Mountain Conglomerate. In later mapping, Dibblee (2003) combined his Split Mountain Conglomerate (Garnet) and other fanglomerates stratigraphically above the Alverson with the Imperial Formation. We agree with Dibblee's later interpretation. Morton (1977) following Christensen's interpretation and showed the Garnet as Quaternary gravels on his map. Winker and Kidwell (1996) expanded the Garnet Formation to include all gravels (fanglomerates) in the CMs stratigraphically above the Alverson Formation and below(?) the Latrania Formation, Imperial Group. Winker and Kidwell then placed their Garnet Formation in the Split Mountain Group above the Alverson and below the Latrania. Winker and Kidwell describe their Garnet as having marine "toes" (?). The only marine Cenozoic sediments in the CMs are in the Imperial Group. We believe that Winker and Kidwell's marine "toes" are their Garnet interfingering with Imperial Group marine sediments. Morgan and Morgan (2012) mapped Christensen's Garnet on the crest on the CMs between two transgressional-regressional marine sequences of the Imperial Group.

Ann Bykerk-Kauffman and her students in their mapping of the CMs used Winker and Kidwell's Latrania Formation (Andrade Member) and Garnet Formation for the past 20 years. They consider the different T-R sequences of the Viejo to be lithofacies of the Andrade Member (personal communication). Caldwell and Bykerk-Kauffman (2015) use another concept to explain the different levels of the Latrania Formation (Andrade), our Viejo T-R sequences, found in the CMs. They state: "The Latrania Formation appears to have been simultaneously deposited at varying depths–wherever the topography was gentle enough to retain sand." Ann and her students do not reconized the Andrade Member of the Latrania Formation interfingering with the basalt flows of the Alverson Formation.

Ann Bykerk-Fauffman divided Christensen's Garnet into an upper Quaternary gravel and lower gravel (Garnet?) in the central crest of the CMs (personal communication). Bykerk-Kauffman and her students map all the fanglomerates in the CMs as the Garnet Formation (lower gravel?) defined by Winker and Kidwell (1996). Brenneman and Bykerk-Kauffman (2012) discovered that there is Imperial Group marine sediments (Latrania?) below her lower gravel, as defined by her, at the crest of the CMs. Ann Bykerk-Kauffman (2015) shows in her columnar section an upper part of the Garnet of Winker and Kidwell (1996) interfingering with the marine Latrania Formation that is above the Garnet. Does Bykerk-Kauffman's Garnet or part of Winker and Kidwell's Garnet interfinger with the Imperial Group?

We have replaced, only in the CMs stratigraphic column, the Latrania Formation with the Viejo Formation in an attempt to clear up the formational ambiguities that exist in the nomenclature for the CMs. The Viejo Formation with its nine plus marine T-R sequences, some of which interfinger with the volcanics of the Alverson Formation, we believe, is a better fit for the geology we have mapped in the CMs. Our mapping indicates that the Garnet as Christensen described and the other similar fanglomerates above the Alverson Formation are not one fanglomerate unit but are several different fanglomerate units. In the CMs these different non-marine fanglomerates interfinger with the nine plus marine T-R sequences of the Viejo Formation (Morgan and Morgan, 2016). Because Christensen's Garnet Formation interfingers with marine T-R sequences of the Viejo Formation, we have demoted the use of the Garnet name to member status in the Viejo Formation. We use the members of the Viejo Formation to help us define and constrain the three extensional tectonics episodes we have mapped in the CMs.

Winker and Kidwell (1996) define the wide spread, in the Salton Trough, marine mudstones and silts of the Deguyños Formation as being the first sediments in the CMs to be influence by the arrival of Colorado River. In the CMs this definition of the Deguyños holds. The Deguynos formation is found, for the most part, in the topographic low areas around the basement core of the CMs. Internally within the Deguynos Formation, around the CMs, there is evidence of T-R sequences that are controlled by sea level changes.

Extensional tectonics

Dennis Kerr (1982) was the first to recognize in the Fish Creek and Coyote Mountains the presence of continental-sediments deposited in an extensional setting and situated stratigraphically below the Miocene aged volcanics of the Alverson Formation. Similar continental-sediments are found beneath Miocene volcanics south of the international border in the Sierra Cucapa and the Sierra da Mayors Mountains, Baja California. North of the border and in the vicinity of the CMs, continental sediments under Miocene volcanics are located in the Volcanic Hills (Fourt, 1979). In the Davies Valley area we have found continental-sediments under Miocene Volcanics. In our ongoing mapping of the Coyote Mountains (CMs) we not only recognize the extensional-continental sediments below the Miocene volcanics that Kerr (1982) did, we recognize two additional extensional episodes. Each of these episodes, including Kerr's, has its own set of normal faults, half grabens, grabens, horst, and distinct package of syn-extensional sediments. The first extensional episode described outcrops on the southern side of the CMs. The igneous and metamorphic basement core rocks of Stonehouse Ridge (See Figure 2) are mapped as the horst block for this first episode. The second and third extensional episodes outcrop on the east and west

side of the igneous and metamorphic, block shaped, core that is north of Stonehouse Ridge. This is the hook in the geographic layout of the CMs and we refer to this area as the Central Horst (see Figure 2). Stonehouse Ridge Horst and the Central Horst form the topographic high areas of the CMs.

First Extensional Episode

Winker and Kidwell (1996) place the CMs geographically in Sonora, Mexico before 5.5 Ma and it is Sonora where the first and oldest extensional tectonic episode occurred. During the Oligocene the Basin and Range extension started in Sonora (Nourse et al., 1994). In the southern CMs the first extensional episode resulted in an east-west aligned half graben containing syn- and post-extensional sediments and volcanics (see Figures 2 and 4). Stonehouse Ridge is the horst block for the first extension. The direction of extension of this episode is to the south-southeast. An east-northeast normal-fault forms the northern boundary of a part of this graben (see Figures 2 and 4). This normal fault and other normal faults of this first episode are thought to be rooted to the main Basin and Range Detachment which is presumed to be at depth under the CMs. A southern part of the graben has been removed by younger faulting. Two zones of accommodation cuts the graben into thirds. The original orientation of this basin was probably more north-northwest which is the orientation of extensional grabens as presently found in Sonora (McDowell, et al., 1997). The change in the elongation direction of the graben as presently found in the CMs implies a clock-wise rotation of about 90° after the first extensional episode ended.

The Red-Green and White Fanglomerates of the non-marine, Miocene Split Mountain Group are believed to be the syn-extensional sedimentation of this first extensional episode. These two fanglomerates units are below the U/Pb 17.1 Ma dated (Morgan et al., 2012) volcanics of the Alverson Formation. In the CMs we have mapped three fanglomerates and the Alverson Formation as part of Winker and Kidwell's (1996) Split Mountain Group. The Red-Green and White Fanglomerates are a lower part of the Split Mountain Group (See Figures 3 and 15). The Red-Green and White Fanglomerates are not only found in the half graben but are found north of the half graben forming buttress unconformities with the basement rocks of the Stonehouse Ridge Horst (see Figures 6 and 7). The Red-Green and White Fanglomerates are only associated with this half graben. The age of the Red-Green and White Fanglomerates may be Oligocene, but these fanglomerates are not at the bottom of the stratigraphic section in Ocotillo Canyon and without a radiometric age date we consider the two fanglomerates to be lower Miocene.

Stratigraphically above the Red-Green and White Fanglomerates units are the post-extensional Red Fanglomerate unit and volcanics of the Alverson Formation, an upper part of the Miocene Split Mountain Group. The Red Fanglomerate and volcanics of the Alverson Formation bury some of the normal faults, half grabens and zones of accommodation of the first extensional episode. These first episode post-extensional units were deposited on the horst and graben but appear not to be disturbed by the first extension. An upper part of Red Fanglomerate interfingers with basalts of a lower part of the Alverson Formation as seen in the geographic divide between Ocotillo Canyon and Alverson Canyon (Morgan and Morgan, 2015). The Viejo Formation

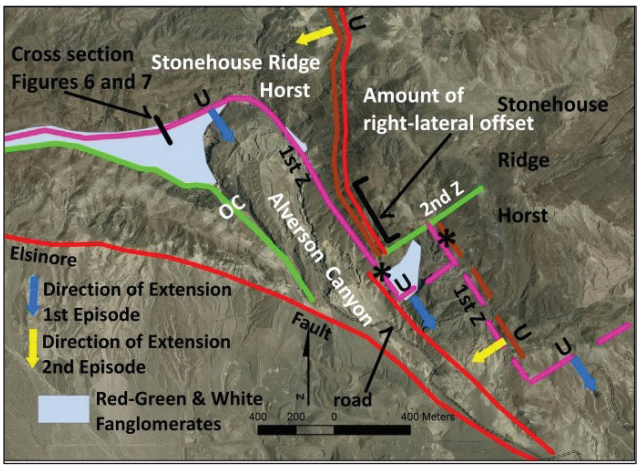

Figure 4. Map of Ocotillo Canyon (**OC**), Alverson Canyon (Fossil Canyon), the first extensional episode (Basin and Range extension that took place in Sonora) and a southern part of the western, second extensional episode. Pink lines—three normal faults of the first episode strike east-northeast and two zones of accommodation (**1st Z**) striking north-northwest. The "**U**" are on the up sides of the normal faults. The extension of first episode was to the south-southeast. The southern two normal faults and grabens of the first episode are buried by the Red Fanglomerate and volcanics of the Alverson Formation. These two normal faults and grabens are inferred to be there by the presence of the Red-Green and White Fanglomerates on the southern sides of buttress unconformities formed on the Stonehouse Horst. This is the same geological relationship that is present on the northern side of Ocotillo Canyon where a normal fault of first episode is observed (Figures 6 and 7). The brown lines are two normal faults that are a part of the western, second extensional episode in the CMs. Extension during the western second episode is to the southwest. The east-northeast green fault is a western, second episode zone of accommodation between the two normal faults and the two half grabens of the second episode. North of the second zone of accommodation, the northern normal faults of the second episode cut and offset the first episode's half graben and a western part of the Stonehouse Ridge Horst. After extension ended in the CMs, this northern normal fault of the second episode was reactivated as a 1 Ma right-lateral fault (red line), and further separated the northern, first episode normal fault and half graben from the southern pair of first episode normal faults and half grabens by an estimated 400 m. South of the second zone of accommodation, the southern, south-southeast, second episode, normal fault offsets marker beds in the post-extensional sediments (Viejo Formation) of the first episode vertically from the same units on Stonehouse Ridge Horst by an estimated 220 m (between the two asterisks of this figure). South of the second zone of accommodation and after the end of extensional faulting in the CMs, a 1 Ma right-lateral fault (red line), that appears to be an extension of the northern, second episode, right-lateral, reactivated fault, cuts the sediments in the second southern graben. The east-west to south-southeast green fault just east of the Elsinore Fault truncated and removed a southern part of the first episode half graben. The Elsinore Fault also cuts the half grabens and truncated many of the faults of the first and second episodes.

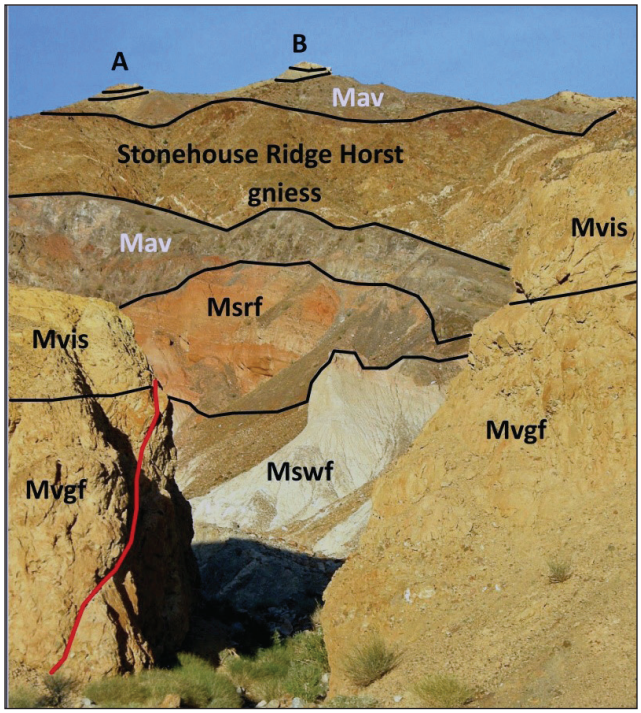

Figure 5. Looking east from Alverson Canyon, across at a southern part of the graben of the western second extensional episode and at the contact between marine Imperial T-R Member (**Mvis**) and the non-marine Green Fanglomerate (**Mvgf**) Member of the Viejo Formation (see Figure 4, western askerisk). This contact is repeated at the buttes A and B, (see Figure 4, eastern asterisk) on the skyline with an estimated 220m of vertical throw. **Mswf**—White Fanglomerate, Split Mountain Group. **Msrf**—Red Fanglomerate, Split Mountain Group. **Mav**—undifferentiated basalt flows of the Alverson Formation, Split Mountain Group. **Mvgf**—non-marine Green Fanglomerate Member of the Viejo Formation, Imperial Group. **Mvis**—marine Imperial T-R Member of the Viejo Formation, Imperial Group. The red line is a 1 Ma fault that is south of the second zone of accommodation and is associated with the south-southeast 1Ma right-lateral fault of the western second episode (see Figures 2 and 4). Note on the skyline the basalt flow of the Alverson Formation rests directly on Stonehouse Ridge Horst without intervening Red-Green (Msrg), White (Mswf) or Red (Msrf) Fanglomerates.

(Morgan and Morgan, 2016), a lower part of Winker and Kidwell's (1996) Imperial Group was also deposited undisturbed on the horst and graben of the first extension. Lower units of the Viejo interfinger with upper volcanic flows of the Alverson Formation (Woodring, 1932; Morgan and Morgan, 2015). The upper units of the Split Mountain Group and the Viejo Formation date the end of the first extensional episode.

Later the east-west half graben and a part the Stonehouse Ridge Horst of the first extensional episode were cut by north-south trending normal faults, west side down, of the western second extensional episode (see Figures 2 and 4). The syn-extensional sediments of this western second episode include the Red Fanglomerate, the volcanics of the Alverson Formation, Spilt Mountain Group and the marine and non-marine sediments of the Viejo Formation, Imperial Group. The southern part of the second episode south-southeast normal fault offsets marker beds of the syn-extensional sediments of the Viejo

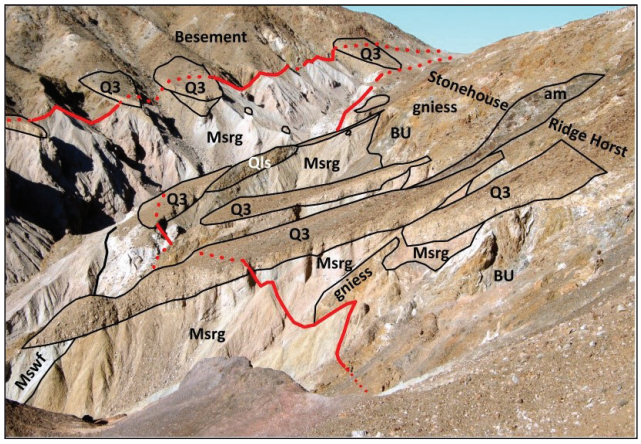

Figure 6. Looking west at the simplified geology of the northern part of Ocotillo Canyon. The normal fault that forms the northern boundary of the first episode's half graben is in the foreground. The southern fault that truncated and removed a southern part of the half graben is in the background. Both faults strike to the west and narrow the graben. **am**—amphibolite. **BU**—buttress unconformity. **Q3**—Terrace 3. **Qls**—landslide. **Msrg**—Red-Green Fanglomerate, Split mountain Group. **Mswf**—White Fanglomerate, Split Mountain Group. Note that the Red-Green fanglomerates form buttress unconformities with the basement rocks of the Stonehouse Ridge Horst, north of the normal fault. The geology of this view is also a part of the western, second episode, northern half graben.

Formation on the half graben from the same marker beds on the Stonehouse Ridge Horst vertically by an estimated 220m (see Figure 4 asterisks and Figure 5). After all the extensions in the CMs ended (about 1 Ma, Steely et al., 2009), we believe the western, second episode, north-south normal fault was reactivated as a 1 Ma right-lateral fault and offset the east-west basin and the Stonehouse Ridge Horst by an estimated 400m (see Figure 4). A 1 Ma lengthening of this reactivated right-lateral north-south normal fault continued south and cut the syn- and post-extensional sediments of the first and second episode.

The recent, rapid, episodic and disproportional topographic uplift of the CMs took place, after 1Ma, and is taking place along the right-lateral faults and the older normal faults. We believe the original normal fault of the first extensional episode, at the cross section (see Figures 4, 6 and 7), now appears as a reverse fault as a result of the recent uplift of the CMs.

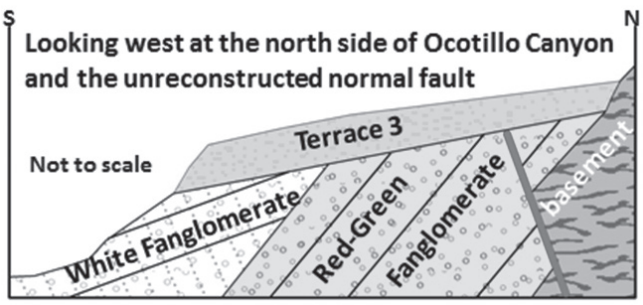

Figure 7. Simplified geological cross section of Figure 5, the northern part of the half graben of the first extensional episode. The normal fault is not reconstructed and its dip is the result of the recent uplift of the CMs.

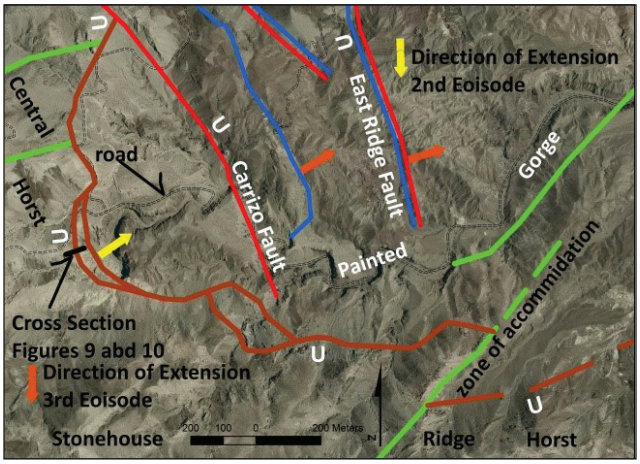

Figure 8. Simplified map of the east side of the Central Horst and the north side of Stonehouse Ridge Horst and the eastern second extensional episode. The brown line marks the normal curved fault and outlines a half graben of the eastern second extensional episode. In the field the fault is made evident by volcanics of the Alverson Formation in the graben faulted against basement rocks of the Central and Stonehouse Ridge Horsts. The eastern second episode extension was to the east-northeast on the east side of the Central Horst. Blue lines are normal faults that belong to the eastern third extensional episode. Extension during the third episode on the east side of the Central Horst was to the east-northeast. Red lines are 1 Ma right-lateral faults; if they are close and parallel to an older normal fault; the older normal fault has been reactivated as a 1 Ma right-lateral faults. Christensen's (1957) Carrizo Fault truncates the northern part of the curved normal fault of the eastern second episode but does not cut the southern, east-west straight part of the curved fault. Note a green east-northeast fault offsetting right-laterally the straight section of the curved normal fault just north of Stonehouse Ridge. This may be a zone of accommodation. "U"—up thrown side of the normal faults. The black line is the cross section in Painted Gorge Amphitheater (see Figures 9 and 10).

There are minor thrust faults found in the southern CMs and we believe they are related to strike-slip movement on second episode north-south reactivated 1 Ma right-lateral fault and its right-lateral extension to the south. The thrust faults are widely dispersed in and confined to the first extensional episode's half grabens. Because of the complex geology within the half grabens the faults can only be followed for, at most, a few tens of meters. The thrust faults cut the syn-extensional sediments of both the first episode and the western, second episode. We have not been able to estimate the amount of throw on the thrust faults but it appears not to significantly disrupt the columnar section. These thrust faults were first recognized by Ann Bykerk-Kauffman and her students (personal communication). The thrusting direction is to the north-northwest and dips on the thrust faults are generally to the south. We have observed that the dips on thrust faults in the northern part of the grabens are steeper than the dips on thrust faults in the southern parts of the grabens. The thrusting appears to have taken place early in the uplift of the CMs. This is the only place where thrust faults have been recognized in the CMs.

Second extensional episode, east side of the Coyote Mountains

A second younger extensional episode is preserved on the east and west sides of the Central Horst in the CMs (Figure 2, 8 and 11). On the eastern side of the Central Horst (Figure 8) the second episode is represented by syn-extensional sediments and volcanics of the Alverson Formation associated with a curved (map view) normal fault and a half graben found north of Stonehouse Ridge and centered around the western part of Painted Gorge drainage. The curved normal fault is defined by the volcanics of the Alverson on the graben faulted against the crystalline basement of the Central and Stonehouse Ridge Horsts. Extension for the eastern second episode is to the east-northeast. Deposited on basement rocks, the volcanics of the Alverson Formation and marine sediments of the Viejo Formation are the syn-extensional sediments that help to define the eastern, second episode, half graben. The Red Fanglomerate does not crop out within the half graben, but is presumed to be below the Alverson. On the Central Horst, the Red Fanglomerate, volcanics of the Alverson and the Viejo marine sediments form buttress unconformities with the basement rocks. The Red-Green and White fanglomerates are not found under the Red Fanglomerate on the Central Horst and is presumed to be absent under the Red Fanglomerate in the eastern, second episode, half graben.

Morton (1966) was the first to map the eastern, second episode, curved normal fault as curved and we agree with his interpretation. Dibblee (1954, 2003) shows the curved fault as a straight fault on the north side of Stonehouse Ridge. Christensen (1957) mapped this fault as two faults. The curved northern branch truncates the straight east-west branch. Bykerk-Kauffman mapped the northern part of the curved normal fault as the Gorge End Fault and mapped straight east-west part of the curved normal fault is another fault. Bykerk-Kauffman's northern Gorge End Fault is truncated by the EW straight fault (personal communication). Bykerk-Kayffman also has the north end of her Gorge End Fault truncated by younger faulting. We believe the curved normal fault of the eastern second episode may be rooted in the already existing Basin and Range Detachment at depth under the CMs.

Horst and grabens of the third and youngest extensional episode forms and truncates the northern edge of the eastern second extensional episode (see Figure 2 and 8). We believe after the end of the third extensional episode in the CMs, many of the normal faults associated with the third episode were reactivated as 1 Ma right-lateral strike-slip faults. These reactivated faults cut the basement, basalts of the Alverson and presumably units of the Viejo in the half graben of the eastern second episode. The 1 Ma right-lateral strike-slip Carrizo Fault (Christensen, 1957) truncates the northern end of the curved normal fault of the eastern second episode, but does not cut the southern, east-west straight part of the curved fault (see Figures 2 and 8). None of the reactivated

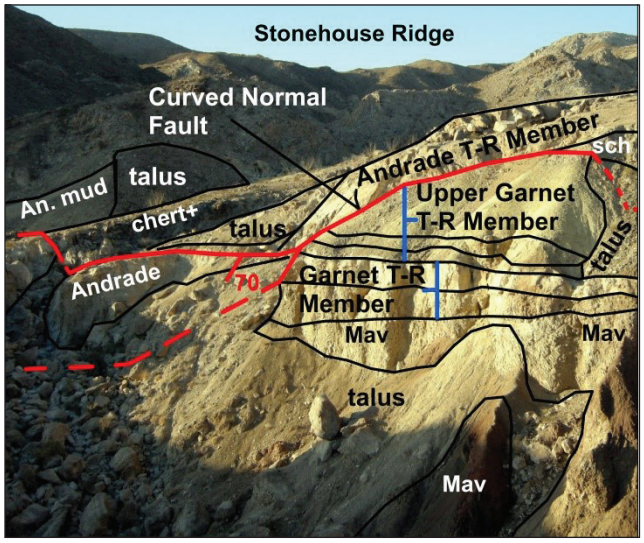

Figure 9. Looking SW at the simplified geology in the Painted Gorge Amphitheater with Stonehouse Ridge in the background (see Figure 8). Three transgressional-regressional members of the Viejo Formation are represented in the amphitheater area. From the oldest to youngest: the **Garnet T-R Member**, the **Upper Garnet T-R Member** and the **Andrade T-R Member**. All T-R units are marine and members of the Viejo Formation. **An. Mud**—Andrade mudstone. **Mav**—basaltic flows of the Alverson Formation. **sch**—schist basement.

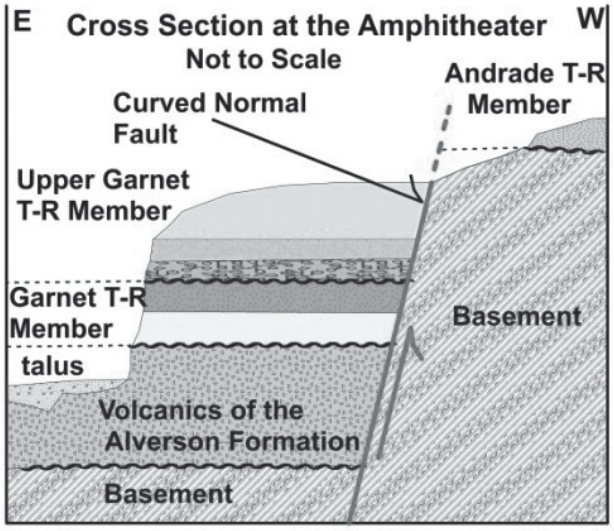

Figure 10. Simplified geological cross section at the Painted Gorge Amphitheater showing the Viejo marine T-R sequences and the curved normal fault of the second extensional episode. All T-R members are marine.

right-lateral faults we have so far mapped cross the graben and cut the straight east-west portion of the eastern, second episode, curved fault. An east-northeast fault does cut the straight east-west branch of the curved fault with a right-lateral offset (see Figures 2 and 8). This offset may be an old zone of accommodation. Other east-northeast faults in this area of the CMs are presumed to be or are left-lateral. This is an area of the CMs that we are still mapping.

The syn-extensional sediments in the half graben of the eastern second episode include the Red Fanglomerate, volcanics of the Alverson Formation and marine transgressional-regressional (T-R) sediments of the Viejo Formation. There are several volcanic plugs found on the graben. It appears sedimentary units of the Deguyños Formation are not involved with the eastern second episode. There is only one marker bed that is common to the half graben of the eastern second episode and the Central Horst. The marker bed is the marine Garnet T-R Member of the Viejo Formation and indicates an estimated vertical throw of approximately 160 meters between the half graben and the Central Horst. The Garnet T-R Member is only found on the half graben near the cross section in Figure 6. We refer to this area as the Pained Gorge Amphitheater.

In the Amphitheater the marine Andrade T-R Member of the Viejo is stratigraphically above the Upper Garnet T-R Member, which is above the Garnet T-R Member (see Figures 9 and 10) of the Viejo Formation. Winker and Kidwell (1996) used the term Andrade for their only unit of the Latrania Formation in the CMs. Winker and Kidwell block out a particular recognizable part of the their Andrade as a limestone. We believe a better description of their limestone would be calcarenite. We have used this very recognizable calcarenite and the name Andrade to define a particular T-R sequence of the Viejo Formation. Andrade was just too good a name to throw away. The curved fault cuts the Andrade T-R Member with an estimated throw of 3m, west side up. The marine Andrade T-R member is easily found in several places on the half graben and Central Horst. If the estimated 3 m is the result of recent (1 Ma) uplift of the CMs, then the eastern second extensional episode ended before the deposition of the Andrade T-R Member. If the 3m offset is the result of slip on the curved fault during the eastern second extensional episode then the end of the second episode is after the deposition of the Andrade T-R Member.

Second extensional episode, west side of the Coyote Mountains

On the west side of the Central Horst, are two half grabens associated with two normal faults of the western, second extensional episode (see Figures 2, 4 and 11). The more southern and smaller half graben and its south-southeast normal fault were discussed in conjunction with the first extensional episode. Both half grabens on the west side are truncated by the Elsinore Fault. The larger and more northern half graben of western second episode is associated with a normal fault that is also curved. The syn-extensional sediments of the western second episode are found on the northern half graben and on the Central Horst. In places the fault zone of the curved normal fault between the half graben and the Central Horst is three plus meters wide. The curved normal fault is east of Alverson Canyon and somewhat parallels the southern part of the Canyon. Following the curved normal fault to the north, the fault cuts an east-west branch of the

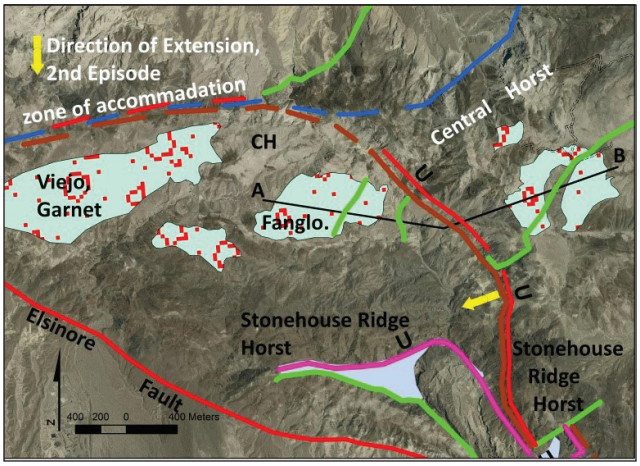

Figure 11. Simplified geological map of the west side of the Central Horst and the western second extensional episode. Pink lines—normal faults first extensional episode. Brown lines—normal faults second extensional episode. The brown curved normal fault outlies a half graben of the western second episode that is truncated by the right lateral Elsinore Fault. Blue lines—normal faults of the third extensional episode. Green lines—other faults. Red lines—1 Ma right-lateral faults. Red faults near and parallel to normal faults indicate reactivation of the normal fault as a 1 Ma right-lateral fault. Unit highlighted is the Garnet Fanglomerate Member of the Viejo Formation, Imperial Group. A to B, a cross section highlighting the vertical offset of the Garnet Fanglomerate (see Figure 12). "**U**"- up thrown side of the normal fault. **Fang**—Fanglomerate. **CH**—Central Horst rocks found in the half graben. Note that a western part of the first episode half graben and a western part of the Stonehouse Ridge Horst are now a southern part on the western, second extensional,northern half graben.

Alverson Canyon before it starts to turn west. The western, second episode, curved normal fault continues to turn west and joins a zone of accommodation that it shares with the western, third extensional episode, normal fault. The western, second episode, curved normal fault at depth under the CMs may also be rooted in the already existing Basin and Range Detachment Fault.

The syn-extensional sediments associated with the western second episode are the Red Fanglomerate and volcanics of the Alverson Formation, an upper part of the Split Mountain Group and the marine and non-marine members of the Viejo Formation, a lower part of the Imperial Group. We believe that marine sediments of the Deguyños Formation, an upper part of the Imperial Group, are not involved with the second extensional episode. A volcanic plug and cone with basalt flows of the Alverson are found on the western, second episode, northern half graben. Volcanics flows of the Alverson are found on the basement rocks of the Central Horst. We have not found a marker bed in the volcanics we can trace between the half graben and the horst. Under the volcanics on the western, second episode, half graben are found White and Red Fanglomerates of the Split Mountain Group. The White Fanglomerate on the western second episode graben is associated with a western part of first extensional episode half graben that is now a southern part the western, second episode, half graben (see Figure 11). The White Fanglomerate is not found under the volcanics on the Central Horst.

Unconformably deposited on the Garnet Fanglomerate Member of the Viejo Formation on the Central Horst are units of the marine Garnet T-R Member of the Viejo Formation. This is the same Garnet T-R Member of the Viejo Formation that is associated with the eastern, second episode, curved normal fault and half graben. West the western normal fault of second episode, the Garnet Fanglomerate is also unconformably overlain by the Garnet T-R (see Figure 12). The vertical throw across the western, second episode, northern curved normal fault is estimated to be 210 meters. This value is close to the estimated 220 meters of an estimated vertical throw across the western, second episode, south-southeast normal fault that is south of the second zone of accommodation (see Figures 4 and 5) .

McDowel et al. (1997) observes that the extensional tectonics of the Basin and Range in Sonora may have continued and been "coeval with initial evolution" of the right-lateral transtension tectonics that produced the Gulf of California. The Red Fanglomerate and the most of the volcanics of the Alverson Formation predate the arrival of marine sediments in the CMs but are involved with the second episode. With the deposition of the syn-extensional, marine sediments of the Viejo Formation during the second episode, one can assume that the Gulf of California arrived in the CMs. The influence of the Colorado River did not arrive in the CMs until the deposition of the Deguynos Formation (Winker and Kidwell, 1996). The CMs had to have started north out of Sonora (opening of the Gulf) before the arrival of the Deguynos, during the deposition of the Viejo Formation. The second extensional episode fits the time frame that McDowell, et al. has for the continuing of the Basin and Range extension to the opening of the Gulf of California.

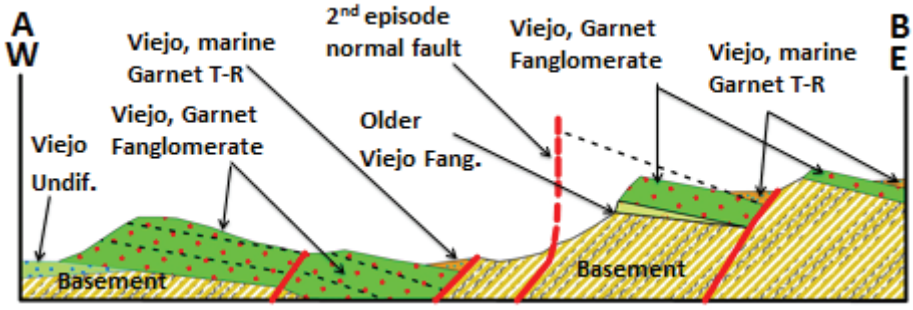

Figure 12. Cross Section A to B (see Figure 11). Simplified geology not to scale. Red lines—faults. Dotted lines—bedding plains. **Undiff**—undifferentiated. **Fang**—Fanglomerate. The vertical throw between the Garnet T-R west of the western, second episode, normal fault and the Garnet T-R east of the normal fault is estimated to be 210 meters.

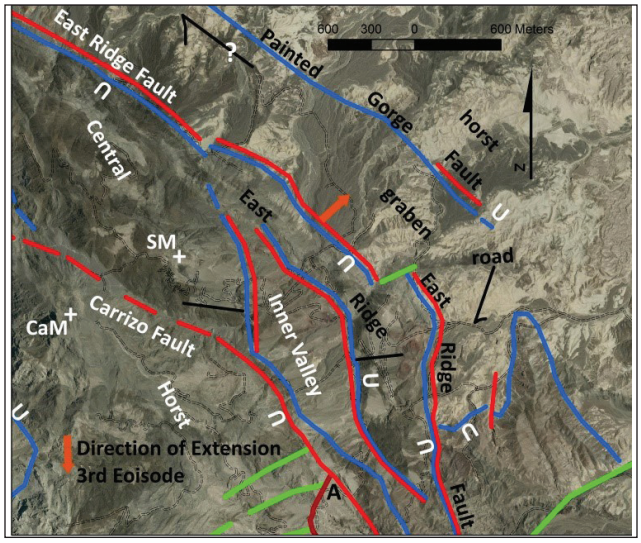

Figure 13. Simplified geological map of the east side of the Central Horst and the horst and grabens of the western third extensional episode. Brown lines—second episode faults. Blue lines—third episode faults. Red lines—1 Ma active strike-slip right-lateral faults. Green lines—other faults. Red lines near and parallel to older faults indicate the older fault has been reactivated as a 1 Ma right-lateral fault. Red line under the word Fault in Painted Gorge Fault is a recent fault scarp, east side up with little right-lateral offset. The east-northeast green line separating the two branches of the East Ridge Fault may be an old zone of accommodation of the reactivated normal fault. **CaM**—Carrizo Mountain. **SM**—Switchback Mountain. "**U**"—are on the up-thrown side of the normal faults. The black lines on Switchback Mountain and East Ridge represent the south side of a fanglomerate channel that is offset by an estimated 250 meters, right-laterally across Inner Valley. Inner Valley is a graben and East Ridge is a horst. Near "A" in the figure, the Carrizo Fault offsets a landslide by an estimated 140 meter right-laterally.

After the end of extension tectonics in the CMs, the CMs underwent a recent, rapid, differential topographic uplift. This uplift probably took place and may be presently taking place on the east and west side of the CMs along reactivated strike-slip faults and very probably along the curved normal faults of the second episode. On the east side there are two duplex structures on the eastern, second episode, curved normal fault that may be a response to the uplift of the CMs or to strike-slip movement trying to straighten out the curved normal fault (see Figure 8). On the west side of the CMs uplift along the western, second episode, curved normal, reactivated as a 1 Ma right-lateral, fault could explain its wide fault zone. Contacts between basement units, across the western second episode curved normal fault, show apparent right lateral offset (Morgan and Morgan, 2015).

The Deguyños Formation(?) mudstone is found on the east side of the southern part of reactivated, west side, northern, second episode, western curved normal fault. Some of the mudstone along the fault may be Viejo Formation. At one time the CMs were buried by the Deguyños Formation and the Palm Spring Group. Strike-slip faulting during the rapid, episodic and disproportionate uplift of the CMs would involve the Deguyños. We have not found Deguyños deposited on the western graben of the second episode or the Central Horst.

Third extensional episode

The third and youngest extensional episode is associated with West Salton Detachment that was active from late Miocene to the Pleistocene (Axon and Fletcher, 1998) and is represented by a series of horst and graben structures found on the east and west sides of the Central Horst (see Figures 2, 8, 13 and 14). Large parts of the Central Horst that is between the east and west parts of the third episode have not been mapped. Large parts of the western half graben have also not been mapped. The marine sediments of the Deguyños Formations (an upper part Imperial Group) and the non-marine sediments of the Palm Spring Group (Winker and Kidwell, 1996) are syn-extensional sediments involved with this extension. An upper marine member of the Viejo Formation (a lower part of the Imperial Group) may also be syn-extensional sediments of the third episode. The volcanics of the Alverson Formation and the Viejo Formation of are the syn-extensional sediments of the second extensional episode. A horst and several grabens of third episode truncate and form the northern edge of the eastern second episode confirming that the second episode is older than the third episode.

Steely et al., (2008) has the West Salton Detachment in the western Salton Trough, cut by right-lateral faults thus, for the most part, ending movement on the West Salton Detachment about 1 Ma. Right-lateral faulting in the CMs appears to end the third extensional episode about the same time. The main West Salton Detachment is probably at depth below the CMs and may be the reactivated original Basin and Range Detachment surface. In the CMs not only does the onset of right lateral faulting end the movement on the normal faults of this last extension episode, but there is evidence that the traces of some of the normal faults of the three episodes may have been reactivated as 1 Ma right-lateral faults.

East Side of the Third Extensional Episode

On the east side of the Central Horst are a sequence of north-south to north-northwest aligned horst and grabens stepping off to the east (see Figure 14). Starting from the Central Horst there is the Carrizo Fault, a graben (Inner Valley), an unnamed fault, a horst (East Ridge), East Ridge Fault, another graben, Painted Gorge Fault and on the northeast side of Painted Gorge Fault another horst. The East Ridge Fault is the northeast boundary of the igneous and metamorphic core of the CMs (Morgan and Morgan, this volume). To the north, East Ridge joins the Central Horst and becomes one ridge with the loss of Inner Valley. The extension of the eastern third episode was to the northeast.

The syn-extensional sediments found on the east side of the Central Horst are of the Alverson Formation(?), marine Viejo Formation(?) marine Deguynos Formations

and non-marine sediments of the Palm Spring Group. We have not found units that allow us to estimate the amount of throw on the normal faults that control the horst and grabens.

After the end of the third extensional episode, some of the traces of the eastern, third episode, normal faults were reactivated as 1 Ma right-lateral faults. The East Ridge Fault is an example of a third episode normal fault that has been activated as a 1 Ma right-lateral fault.

Starting on the west side of the Central Horst, Christensen's (1957) Carrizo Fault, a right-lateral fault, offsets a western curved normal fault of the third episode. The south-southeast Carrizo Fault then cuts the Central Horst separating Switch Back Mountain from Carrizo Mountain. As the Carrizo Fault leaves the Central Horst it turns more southerly and reactivates an east side, third episode, normal fault. The Carrizo Fault continues to the south-southeast and truncated the curved normal fault of the eastern second episode (Figures 2, 8 and 14). Near the northern truncation of the eastern, second extensional episode, curved fault, the Carrizo Fault offsets a landslide that formed on the Central Horst right-laterally by minimum of 140 meter (see "A" Figure 13).

An early Pleistocene(?) fanglomerate channel starting from near Switchback Mountain, presumably crossed Inner Valley, a graben, and can be found crossing East Ridge, a horst. The southern edge of the channel shows an estimated 250 meters of right-lateral offset across the 1 Ma faults that form the Inner Valley Graben (see Figure 13). We have not found the fanglomerate channel east of East Ridge.

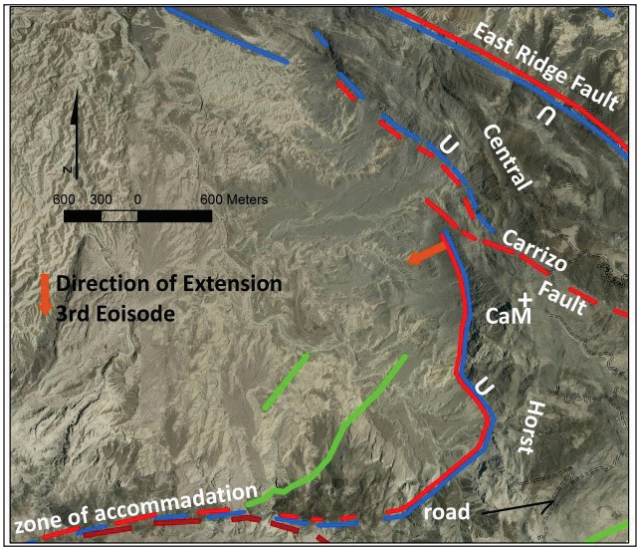

Figure 14. West side of the Central Horst, the curved normal fault and a half graben of the western third extensional episode. **CaM**—Carrizo Mountain. "**U**"—are on the up-thrown side of the normal faults. Brown lines—second episode fault. Blue lines—third episode faults. Red lines—1 Ma right-lateral faults. Green lines—other faults. Red lines near and parallel to older faults indicate the older fault may have been reactivated as a 1 Ma right-lateral fault. Note Carrizo Fault offsetting the western, third episode, curved normal fault right-laterally. Extension of the western third episode was in a southwest direction. The graben is made up of syn-extensional sediments belonging to the Deguyños Formation, Imperial Group (marine mudstones and silts) and of the Palm Spring Group (non-marine sediments). If units of Deguyños Formation and the Palm Spring Group were deposited on the Central Horst, they have been removed. Vertical throw on the third episode curved normal fault on the western side of the Central Horst is estimated to be a minimum of +900 m at Carrizo Mountain based on the height of the eroded(?) exposed scarp. The western, third episode, curved fault has probably been reactivated as a 1 Ma right-lateral fault. Some of this throw may be the result of the recent uplift of the CMs along the reactivated western, third episode, curved normal fault.

The Third Extensional Episode on the West side of the Central Horst

Western Third Extensional Episode

On the west side of the CMs the third extensional episode is represented by a curved normal fault and a half graben. Large areas of the Central Horst and the half graben of the western third extensional episode have yet to be mapped. Extension was to the south-southwest. The northern part of the curved normal fault above the Carrizo Fault, forms the western side of the fish hook/Central Horst of the CMs (Figures 2 and 14). The curved fault continues south and curves to the west on the north side of the zone of accommodation it shares with the curved normal fault of the western second episode. The curved normal fault of the third extensional episode may be rooted in a detachment surface that is the reactivated Basin and Range Detachment. The southern part of the western, third episode, curved fault, we believe has been reactivated as a 1 Ma right-lateral fault.

The western third extensional episode half graben contains marine sediments of the Deguynos Formation and non-marine sediments of the Palm Spring Group. A marine member of the upper part of the Viejo Formation may also be present. Alverson Formation and older units have not been found in the half graben. Marine Viejo Formation units have been deposited on the west side of the Central Horst forming buttress unconformities. No Deguyños or Palm Spring units have been found deposited on the Central Horst. It is assumed that at one time the CMs were buried by sediments of the Deguyños and Palm Spring.

The beginning of right-lateral faulting ended the extensional tectonics in the CMs. The right-lateral Elsinore Fault terminating the western edge of the western, third episode, half graben would be an example of this change in tectonics. Part of the recent, rapid, episodic and disproportional topographic uplift of the CMs have taken place and may be taken along the reactivated western curved normal fault of the third episode. The two faults (green) that cut the sediments in the western, third episode, half graben may be part of a duplex structure trying to straighten out the curved normal fault (see Figure 14).

Conclusions

The first extensional episode appears to be related to the Basin and Range extension when the CMs were in Sonora, Mexico. The second extensional episode may have taken place in the CMs before and during the opening of the Gulf of California and before the onset of the West Salton Detachment. This would validate McDowell et al, (1997) premise that the extensional tectonics in Sonora continued through to the opening of the Gulf of California. The third extensional episode we believe is associated with the West Salton Detachment. The West Salton Detachment is wide spread in the western Salton Trough (Axen and Fletcher, 1998). The normal faults of the three extensional episodes may be rooted to the same detachment surface at depth below the CMs, the Base and Range Detachment. There seems to have been continuous extensional tectonics (see Figure 15) taking place from possibly before the Miocene in the CMs that ended with the onset of right-lateral faulting about 1 Ma (Steely et al., 2009). A question to be asked: are the first two extensional tectonic episodes we have in the CMs more wide spread in the western Salton Trough?

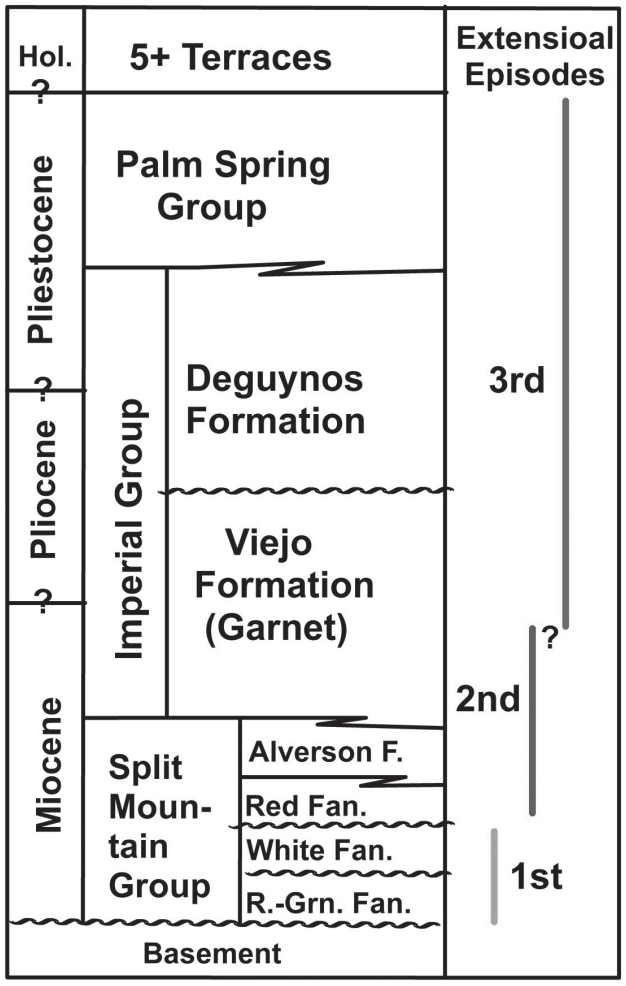

Figure 15. The three extensional episodes found in the CMs are shown in relation to the group and formational units they affect and their relational ship to each other. The "?" marks between the Cenozoic time units are questing the age boundaries in the sedimentary units. The "?" mark between the second and third episodes is questing the timing of the end of the second and the start of the third episode. **F**—Formation. "**Rd-Grn Fan**"—Red-Green. Fanglomerate. **Fan**—Fanglomerate.

Thanks to: John Prall for help in writing and editing this paper, Bill Elliott, Mike Hart, Ann Bykerk-Kauffman, Eric Frost, Stephen Schellenberg, Monte Marshall, Gordon Gastil, Gary Axen, Larry Busch, Charles Winker, Jerry Treiman, Jim Senn and the BLM for a mapping permit.

References

Axen, G. J., and Fletcher, J. M., 1998, Late Miocene-Pliocene extensional faulting, northern Gulf of California, Mexico, and Salton Trough, California: International Geological Review, V. 40, p. 217-244.

Blaettler, Karen Griffith, 1991, A petrographic study of an amphibolite outcrop in the Coyote Mountains, Imperial County, California, San Diego State University, Under Graduate Research Report, V. 53.

Caldwell, G. and Bykerk-Kauffman, A., 2015, Evaluation Of Late Neogene Sediments On The Northern Flank Of The Central Coyote Mountains: Paleotopographic Setting And Sediment Sources Of The Late Miocene Latrania Formation During Initial Stages Of A Marine Incursion: Pacific Section of the American Association of Petroleum Geologist, 2015 Conference Technical Program.

Brenneman, M. J. and Bykerk-Kauffman, A., 2012, Complex paleotopography and faulting near the Elsinore Fault, Coyote Mountains, southern California, abstract #T23D-2417, American Geophysical Union Fall Meeting.

Christensen, A. D., 1957, Part of the geology of the Coyote Mountains area, Imperial County, California: Unpublished M.S. thesis, University of California at Los Angeles, 188p.

Dibblee, T. W., 1954, Geology of the Imperial Valley region, California, in Jahns, R. H., ed., Geology of southern California: California Division Mines Bulletin, v. 170, p. 21-28.

Dibblee, T. W., 2003, Geology of the Coyote Mountains, Imperial and San Diego Counties, California, In, M.L. Murbach and M.W. Hart (eds.), Geology of the Elsinore Fault Zone, San Diego Region: San Diego Association of Geologist, San Diego, South Coast Geological Society, Santa Ann, California, p.117-123.

Dorsey, R.J. (2012), Earliest delivery of sediment from the Colorado River to the Salton Trough at 5.3 Ma: Evidence from Split Mountain Gorge. In: Reynolds, R.E. (ed.) Searching for the Pliocene: Southern Exposures. *Proceedings of the 2012 Desert Symposium*, p. 88-93.

Fourt, R., 1979, Post-batholithic Geology of the Volcanic Hills and Vicinity, San Diego County, California, San Diego State University, Master Thesis.

Hamilton, W.B., 1961, Origin of the Gulf of California: GSA Bull., 72, p1307-1318

Kerr, D., (1982), Early Neogene continental sedimentation, western Salton Trough, California, M. S. Thesis, San Diego State University, 138 p.

Link, M. H., and Abbott, P. L., 1991, Eocene sedimentary history, San Diego, California: overview and Field trip stops,

in Abbott, P. L., and May, J. A., eds., 1991, Eocene geological history San Diego Region, Pacific section SEPM, Vol. 68, p.1-26.

McDowell, F.W., Roldán-Quintana, J., and Amaya-Martínez, R., 1997, Interrelationship of sedimentary and volcanic deposits associated with Tertiary extension in Sonora, Mexico: Geological Society of America Bulletin, v. 109, p. 1349–1360, doi: 10.1130/0016-7606(1997)109<1349: IOSAVD>2.3.CO

Miller, R, H., and Dockum, M. S., 1983, Ordovician conodonts from metamorphosed carbonates of the Salton Trough, California: Geology, v. 11, p. 410-412.

Morgan, G. J., and Morgan, J. R., 2005, The Painted Gorge Wash Fault: recent left-lateral faulting, east side Coyote Mountains, Imperial County, California: Bloom, D. M., ed. Geology and history of southeastern San Diego County, California, San Diego Association of Geologists, p.189-204.

Morgan, G. J. and Morgan, J. R., 2012, Garnet Wash Formation and the Imperial Group: a new look at old problems, Coyote Mountains, western Salton Trough, Imperial County, southern California, USA. GSA, Abstract and Programs, Vol. 44, No. 3, p. 11.

Morgan, J. R., Morgan, G. J. and Pecha, M., 2012, U/Pb dating of tuffs from the Alverson Volcanics in the Fossil Canyon and Painted Gorge areas of the Coyote Mountains, western Salton Trough, California, GSA, Abstract and Programs, Vol. 44, No. 3, p. 22.

Morgan, G. J., and Morgan, J. R., 2015, Overview of the Geology of the southern Coyote Mountains, Salton Trough, Imperial County, southern California. In Wagner, R., ed., Geology of the Coyote Mountains, southern California: San Diego Association of Geologists, p.77-87.

Morgan, G. J. and Morgan, J.R., 2016, Viejo Formation: a new formation for the Imperial Group sediments in the southern Coyote Mountains, Salton Trough, southern California, GSA Cordilleran Section, Abstract Paper No. 28-10.

Morton, P. K., 1977, Geology and mineral resources of Imperial County, California: California Division of Mining and Geology, County Report No.7.

Nourse, J. A., Anderson. T. A., and Silver, L. T., 1994, Tertiary metamorphic core complexes in Sonora, northwest Mexico: Tectonics, v.13, p. 1161-1182

Ruisaard, C. I., 1979, Stratigraphy of the Miocene Alverson Formation, Imperial County, California: Masters of Science Thesis, San Diego State University, 125p.

Steely, A. N., Janecke, S. U., Dorsey, R. J., and Axen, G. J., 2009, Early Pleistocene initiation of the San Felipe fault zone, SW Salton Trough, during reorganization of the San Andreas fault system: Geological Society of America Bulletin, v. 121, P. 663-687, doi. 10.1130/B26239.1.

Umhoefer, P. J., 2011, Why did the Southern Gulf of California rupture so rapidly?—Oblique divergence across hot, weak lithosphere along a tectonically active margin: GSA Today, V. 21, Issue 11, pp. 4-10.

Winker, C. D., and Kidwell, S. M., 1996, Stratigraphy of a marine rift basin: Neogene of the western Salton Trough, California, in Abbott, P. L., and Cooper, J. D., eds., Field Conference Guidebook and Volume for the Annual Convention: San Diego, California, American Association of Petroleum Geologists, Pacific Section, p. 295-336.

Woodring, W. P., 1931, Distribution and age of the Tertiary Deposits of the Colorado Desert: Carnegie Institution of Washington Publication 148, p. 1-25

The Mud Hills and Yuha Members of the Deguynos Formation in the northern Coyote Mountains, western Salton Trough, southern California and problems with a right-lateral offset of a hornblende andesite plug by the Painted Gorge Fault

George J. Morgan and JR Morgan
georgemorgan@cox.net

ABSTRACT—Mud Hills and Yuha Members of Deguyños Formation are found in the northern Coyote Mountains, south of the Carrizo Wash, in southern California. The intrusive Alverson Formation volcanic plug/s of hornblende andesite on the east side of the Coyote Mountains may not be offset by the Painted Gorge Fault, as many believe. The Painted Gorge Fault, located northeast of the metamorphic core of the Coyote Mountains is not the "prominent" face the northeast side of the mountains.

Introduction

The Coyote Mountains (CMs) are a small fish hook shaped mountain range located in southern California (see Figure 1). The mountain range is north of Interstate 8, northeast of the small town of Ocotillo, Imperial County, California and 20 kilometers north of the international border with Mexico. The western part of the CMs is situated in San Diego County and the eastern part lies in Imperial County. The CMs are located on the western edge of the Salton Trough with the Peninsular Ranges Batholith further to the west (see Figure 1). The CMs are bounded on the southwest by the active right-lateral Elsinore Fault (Dibblee, 1954) and on the east-southeast by the active left-lateral Painted Gorge Wash Fault (Morgan and Morgan, 2005) (see Figure 2).

The CMs consists of an uplifted crystalline basement core overlaid by Cenozoic sediments accumulated before and during the ongoing opening of the Gulf of California. The sedimentary column represents, first a Miocene age non-marine depositional environment, than a Miocene through Pliocene age marine depositional environment and finally a Pliocene to Pleistocene age non-marine depositional environment. A tectonic reconstruction by Winker and Kidwell (1996) place the CMs in Sonora, Mexico before 5.5 Ma. We believe the CMs, (Morgan and Morgan this volume) were affected by Basin and Range extensional tectonic regime found in Sonora. With continuing episodes of extensional tectonics and the opening of the Gulf of California by the San Andreas Fault System, the CMs moved northwest from Sonora to their present location.

In 2001 we started mapping the CMs at a 1:2000 scale and have found the mapping to be challenging. Some

Figure 1. Location Map of the Salton Trough and the Coyote Mountains in California and Sonora, Mexico. **ABF** - Agua Blanca Fault, **EF** - Elsinore Fault, **FC** - Fish Creek Mountains, **GoF**-Gulf of California, **LSF** - Laguna Salada Fault, **SAF** - San Andreas Fault, **SJF** - San Jacinto Fault, **SS** - Salton Sea, **VF** - Vallicetos-Split Mountain-Fish Creek Basin. Red square with query is the paleogeographic location of the Coyote Mountains 5.5 Ma by Winker and Kidwell (1996) in Sonora, Mexico. We agree the paleogeographic location for the CMs was somewhere in Sonora, Mexico. NASA photograph

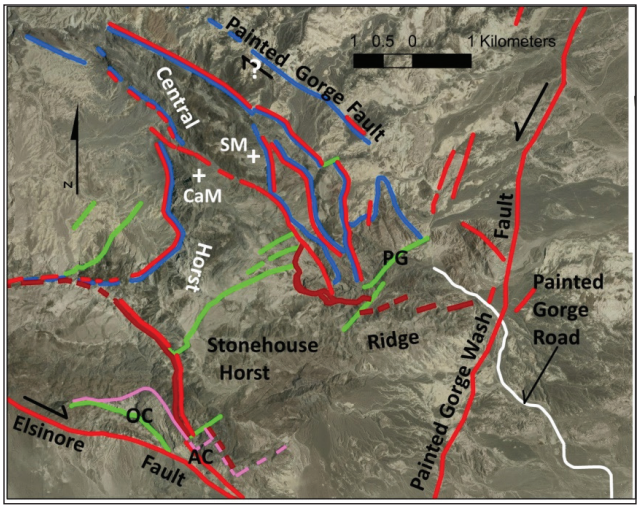

Figure 2. Map of the fish hook of the CMs and some of the faults in the CMs. **OC** - Ocotillo Canyon. **AC** - Alverson/Fossil Canyon. **PG** - Painted Gorge. **CaM** – Carrizo Mountain. **SM** – Switchback Mountain. Pink lines - first extensional episode normal faults. Brown lines - second extensional episode normal faults. Blue line - third extensional episode normal faults. Red lines - younger than 1 Ma strike-slip faults. Green faults- other faults. The normal faults of the three episodes outline the half grabens, grabens and horsts associated with the extensions (Morgan and Morgan this volume). White line - Painted Gorge Road. Red faults that are close and parallel to older normal faults represent reactivation of the older normal fault as 1 Ma right-lateral faults. The horst for the first extensional episode is the topographic high, metamorphic core of Stonehouse Ridge. The normal faults of the second and third episodes are found on the east and west sides of the topographic high, metamorphic, fish hook, core of the CMs. We refer to this area as the Central Horst (Morgan and Morgan this volume). Christensen (1957) named the Painted Gorge Fault and mapped it as a normal fault. Some workers believe the Painted Gorge Fault to be a right-lateral fault. A recent fault scarp on the Pained Gorge Fault the shows very little strike-slip movement and more dip-slip movement with the east side up (this paper). Older offsets across the Painted Gorge Fault appear to be dip-slip with the east side up. We believe the Painted Gorge Fault is a normal fault that is a part of the third extensional episode found in the CMs (Morgan and Morgan this volume).

of those who have worked in the CMs describe them as complicated. They are right. Mapping by the authors continues and we may revise the concepts presented here.

Basement

The basement of the present day CMs consists of an uplifted crystalline core of marbles, schists, cherts, banded cherts, quartzites and amphibolites. These units represent Paleozoic(?) (Dibblee, 1954; Miller and Dockum, 1983) age miogeosynclinal to flysch sediments we believe were deposited in a passive continental margin in Sonora, Mexico. Blaettler (1991) studied the petrology of the amphibolites and concluded they originated as basalts. Morgan and Morgan (2015) reported relic pillow structures in some of the outcrops Blaettler previously studied. A conclusion can be made that the amphibolites represent relic basalts flows in a marine environment.

Starting before and/or during the Jurassic, the passive continental margin in Sonora became an active margin and the marine sediments were intruded, deformed, and regionally metamorphosed. Some of the igneous rocks associated with the active margin in the CMs are: diorite, gabbro, dikes of various compositions, foliated tonalite and a gneiss. All of these rocks are Jurassic (about 162 Ma based on U/Pb dating by Morgan and Morgan, 2015). Cretaceous igneous rocks have not been found and in the CMs. The Jurassic(?) deformation has completely destroyed all the original sedimentary relationships. During the deformation the metamorphic and igneous rocks of the CMs were uplifted and the metamorphics were left with steeply dipping foliation and tight folds.

Cenozoic sedimentation and extensional tectonics

From the Cretaceous to Oligocene, rock units are either absent or have yet to be identified in the CMs. During the Eocene, rivers flowed from eastern Sonora, across the crystalline basement terrane that contained the CMs and the Peninsular Ranges Batholith, to the Pacific Ocean (Link and Abbott, 1991). The only indication of these Eocene rivers in the CMs are the occurrence of distinct, well indurated, silicified meta-volcanic cobbles, associated with the Eocene rivers, which are sporadically found as reworked clasts in the lower fanglomerates of the Split Mountain Group below the Alverson Formation (Ruisaard, 1979 renamed the Alverson Volcanics of Dibblee, 1954).

Following the erosional episode represented by the Eocene rivers and beginning in the Oligocene, Basin and Range extension took place in Sonora (Nourse et al., 1994; McDowell, et al., 1997). In the CMs, the Basin and Range extension (the first extensional episode of three) is represented by normal faulting and deposition of syn-extensional Miocene age sediments of a lower part of non-marine the Split Mountain Group (Winker and Kidwell, 1996) deposited in an extensional half graben (this paper). The half graben is located in the southern CMs (see Figure 2). Deposited in and outside of this graben are post-extensional sediments and the volcanics of the Alverson Formation (Morgan and Morgan this volume) that are an upper part of the Split Mountain Group. Field evidence indicates that the volcanics completely buried the CMs (Morgan and Morgan, 2015). Deposited in and outside of this half graben are marine and non-marine sediments of the Miocene Viejo Formation (Morgan and Morgan, 2016), a lower part of the Imperial Group (Winker and Kidwell, 1996).

The Viejo Formation contains nine plus marine transgressional-regressional (T-R) sequences that interfinger with five plus non-marine fanglomerates deposited in the slowly subsiding CMs (Morgan and Morgan, 2015). In the CMs we define a transgression as rise in sea level and a regression is a fall in sea level. Regional uplift or subsidence is not controlling the transgressions or the regressions found in the CMs. The transgression and the regression together form a sequence of marine sediments. The marine sedimentary sequence in the CMs start with a locally derived, high energy,

basal conglomerate deposited on an unconformity, then, deposition of a sandstone followed by deposition of a low energy mudstone topped by another unconformity. The easily eroded mudstone is often missing from the sequence. Angular unconformities, between many of the T-R sequences, attest to the tectonic activity taking place during the deposition of the Viejo Formation. In the CMs, when the sea level is low, non-marine, locally derived, fanglomerates were sometimes deposited between the T-R sequences. There is field evidence that the youngest marine member of the Viejo Formation covered the CMs completely (Morgan and Morgan, 2015) Marine members that are low in the Viejo Formation interfinger with basalt flows that are in the upper part of the Alverson Formation (younger than 16.9 Ma U/Pb, detrital zircons age dating, Morgan and Morgan, 2015). The interfingering of Imperial Group sediments (Viejo) with the volcanics of the Alverson Formation was first reported by Woodring (1931). The Viejo Formation may represent an early arrival of the Gulf of California, at least in the CMs. Dorsey (2012) reports the Gulf of California arriving in the Vallecito-Split Mountain-Fish Creek Basin, to the north of the CMs (see Figure 1), about 6.2 Ma.

During the deposition of the Miocene Imperial Group sediments (Winker and Kidwell, 1996) in the CMs, the tectonic regime changed from Basin and Range extension to right-lateral transtension associated with the San Andreas Fault system and the opening of the Gulf of California (Hamilton, 1961; Umhoefer, 2011). During this interval, a second extensional episode is preserved as curved normal faults and half grabens on the east and west sides of the CMs. Field evidence indicates the second extensional episode can be associated with the opening of the Gulf (Morgan and Morgan this volume). With this change to lateral movement, the CMs started to move toward the northwest starting about 5.5 Ma (Winker and Kidwell, 1996). As the CMs moved northwest, they came under the depositional influence of the Colorado River. In the CMs, the Pliocene marine Deguyños Formation, an upper part of the Imperial Group (Winker and Kidwell, 1996), and the non-marine Pliocene to Pleistocene Palm Spring Group (Winker and Kidwell, 1996), recorded these changes in tectonics and sedimentation. Internally the Deguyños Formation deposited around the CMs contains angular unconformities that are related to T-R sequences controlled by sea level changes (Morgan and Morgan, 2015). Both the Deguyños Formation and the sediments of the Palm Spring Group are wide spread in the Salton Trough and may have completely covered the CMs (Winker and Kidwell,1996).

As the CMs moved north, a third extensional episode occurred that we believe is associated with the West Salton Detachment (Axen and Fletcher, 1998). This third extension episode produced normal faults, horsts, grabens and a half graben on the east and west sides of the CMs (Morgan and Morgan this volume). In the western Salton Trough, movement on the West Salton Detachment ended about 1Ma with the onset of right-lateral faulting (Steely et al., 2009). Dating the end of the third episode in the CMs is speculative as radiometric age dates are lacking, but the third extensional episode we have mapped in the CMs ends with right-lateral faulting about the same time as Steely et al. (2009) proposed.

In the last 1 Ma the CMs have under gone a rapid, episodic and disproportional topographic uplift and erosion leaving the CMs with unstable slopes and five plus terraces on the mountain flanks. On the east side of the CMs, the terraces merge eastward to a common base level (Morgan and Morgan, 2015). Morgan and Morgan (2015) recognized that at least one marine member of the Viejo Formation underwent soft sediment deformation during the recent uplift. The rapid, episodic and disproportional topographic uplift of the CMs took place along strike-slip and older extensional-normal faults. Some of the extensional normal faults may have been reactivated as 1 Ma strike-slip faults.

The CMs are now located near the western edge of the Salton Trough; are dominated by active right and left-lateral faulting, and are being disproportionally uplifted.

Yuha and Mud Hills

In our continuing mapping of the Coyote Mountains(CMs) we have found Mud Hill and Yuha

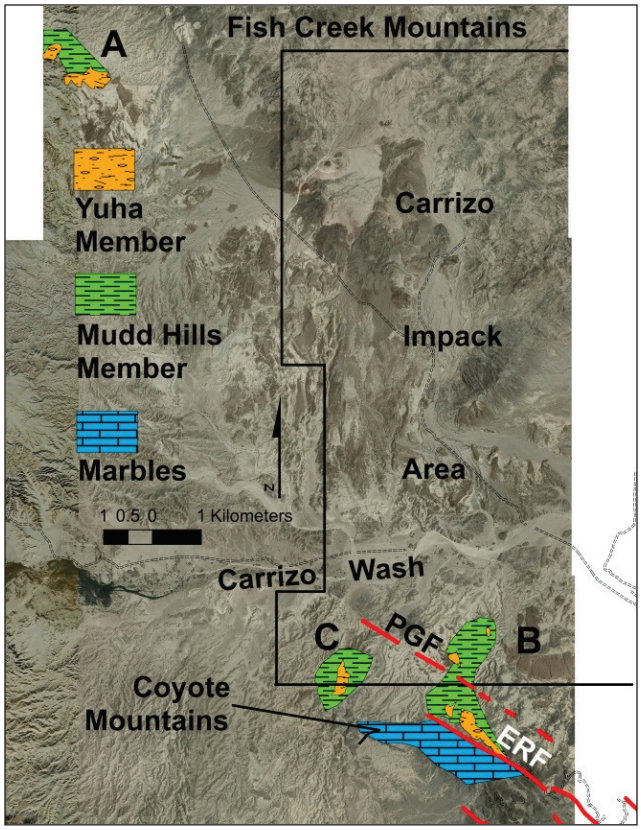

Figure 3. Map of the locations of the Mud Hills and Yuha Members of the Deguyños in the Fish Creek Drainage and in the northern CMs. "A" location of Figure 4. "B" the location of Figures 5 and 6. "C" the location of Figure 7. PGF - extension of the Painted Gorge Fault. ERF - East Ridge Fault.

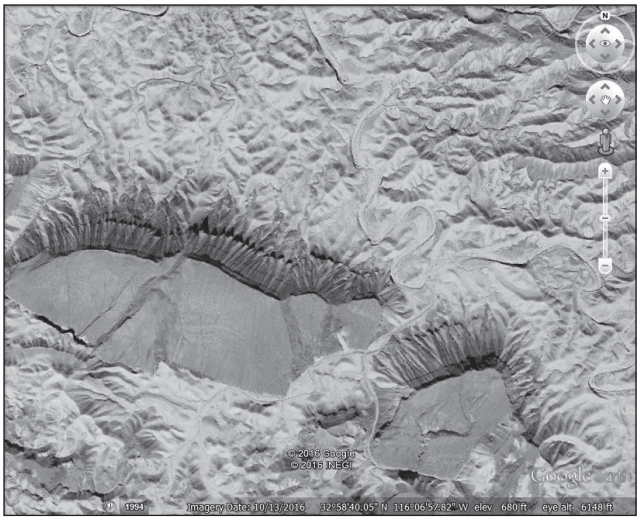

Figure 4. "A" in Figure 3, Winker and Kidwell's (1996) type area for the Mud Hills and Yuha Members of the Deguynos Formation. Note the shadow on the Elephant Knees, which is the base of the Yuha Member, below the thick, tan coquina bed forming the resistant bed that forms the top of the cuestas.

Figure 5. Northern part of "B" in Figure 3. Thick coquina beds in the Yuha have almost been completely removed. Note shadow on the Elephant Knees under the coquina beds.

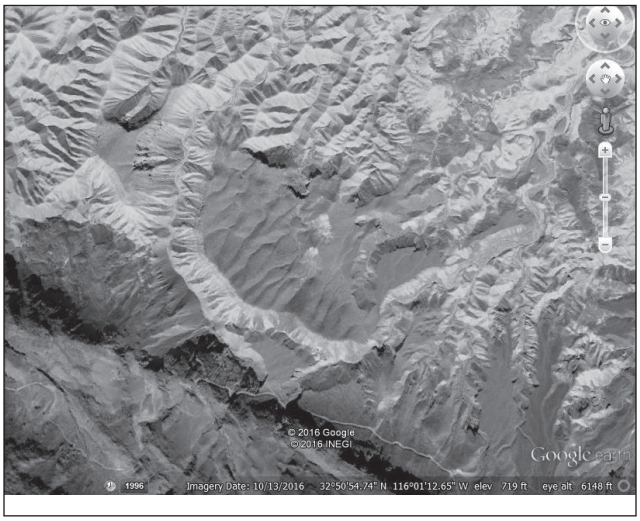

Figure 6. Southern part of area "B" in Figure 3. The thick coquina beds of the Yuha Member are evident. The Elephant Knees are not as prominent but is represented by the gray unit below the tan coquina bed. The East Ridge Fault separates the Mud Hills and Yuha Members from the marbles of the Coyote Mountains.

Figure 7. This is the area "C" in Figure 3. The Elephant Knees are not as well developed as in Figures 4, 5 and 6.

Members of the Deguynos Formation (Winker and Kidwell, 1996) in the northern part of the CMs south of Carrizo Wash(see Figure 3). Winker and Kidwell (1996) extend the Mud Hills and Yuha Members in to the Carrizo Impact Area where they have these units become the Lavender Canyon Member(?). The Mud Hills and Yuha units we mapped are south of the Carrizo Wash and look very much like the units Winker and Kidwell mapped along the south side of Fish Creek drainage (see Figures 4, 5, 6 and7). These units even have recognizable Elephant Knees. In one area south of the Impact Area, the Mud Hills and Yuha units are faulted against the northeast edge of the CMs (see Figure 3 and 6) along the East Ridge Fault (Morgan and Morgan this paper). The Mud Hill and Yuha Members form a stratigraphic horizon that crosses the basin from Fish Creek drainage to the CMs. These units will help with unraveling of the complex stratigraphy that is found in and around the CMs and aid with the correlation of sedimentary units between the CMs and Vallecito Basin-Split Mountain-Fish Creek Basin.

Painted Gorge Fault and Hornblende Andesite Plugs

With our detailed mapping (1:2000 scale) we have a somewhat different geological interpretation then Bykerk-Kauffman, et al. (2016), Ruisaard (1979), Morton (1977), Christensen (1957) and Dibblee (1954, 2003), for the two hornblende andesite plugs that flank the Painted Gorge drainage on the eastern side of the Coyote Mountains and other geological problems. We have not completed

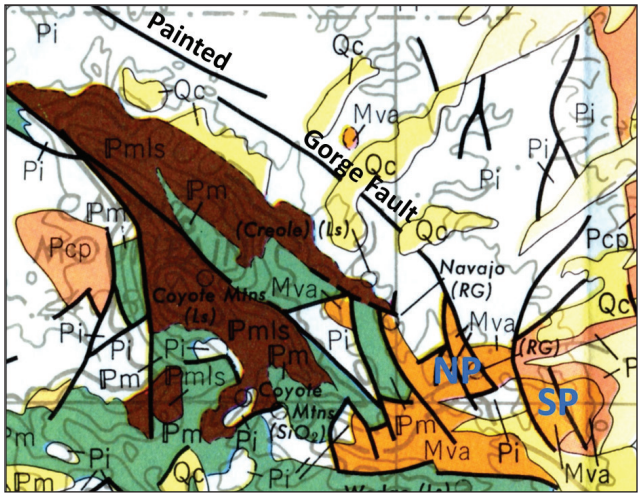

Figure 8. A part of Morton's (1977) map for the CMs showing the Painted Gorge Fault and the two hornblende andesite plugs. "**NP**' - northern plug. '**SP**" - southern plug. Dibblee (1954, 2003), Christensen(1957), and Ruisaard (1979) did not recognize a fault on the northeast side of the metamorphic core of the CMs. All show the Painted Gorge fault turning south and forming the eastern side of the northern plug. We are having difficulty mapping the Painted Gorge making the turn to the east side of the northern plug. The Pained Gorge Fault before it makes the turn is a dip-slip fault with the east side up. The Painted Gorge Fault on the east side of the northern plug is dip-slip fault, west side up.

our mapping of this area, but we have several working hypothesis.

> From Bykerk-Kauffman et al. abstract: "The northeastern flank of the range is dominated by the Painted Gorge fault (PGF)."

Christensen (1957) named the Painted Gorge Fault because it crossed the Painted Gorge drainage. We believe the Pained Gorge Fault is not the "dominate" northeast edge of the Coyote Mountains. The next north-northwest fault to the west of the Painted Gorge Fault is the East Ridge Fault (see Figures 9 and 10). This fault has east block Deguynos (an upper part of the Imperial Group) mudstones and silts in contact with west block basement

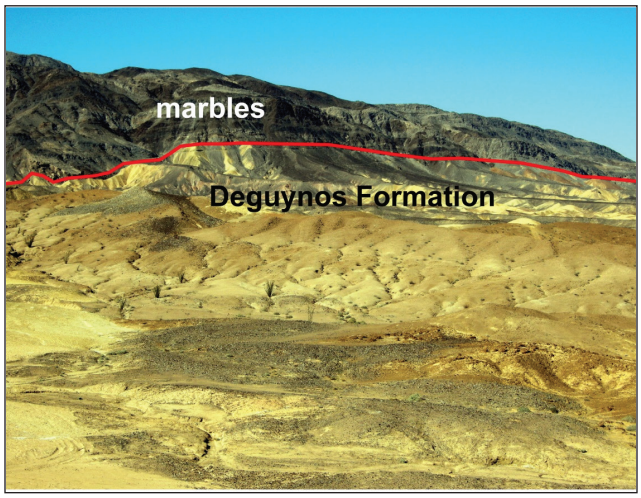

Figure 10. Looking west to northwest at the northeast side of the CM. Red line - East Ridge Fault

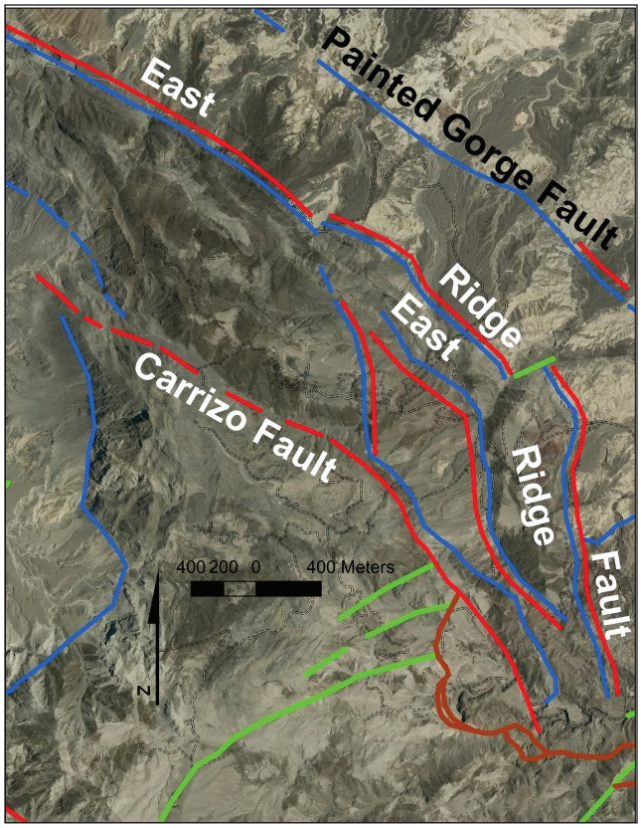

Figure 9. East Ridge Fault is the blue line on the east to northeast side of the igneous and metamorphic core of the CM. East Ridge is a horst made primarily of metamorphic rocks. There is a graben between East Ridge Fault and the Painted Gorge Fault. Blue lines - third extensional episode faults, brown lines - second extensional episode faults, green lines - other faults and red lines - 1 Ma right-lateral fault (Morgan and Morgan this volume). Red lines near and parallel to blue faults indicate that the blue fault was reactivated as a 1 Ma right lateral fault after extensional tectonics ended about 1 Ma in the western Salton Trough (Steely, et. al., 2009).

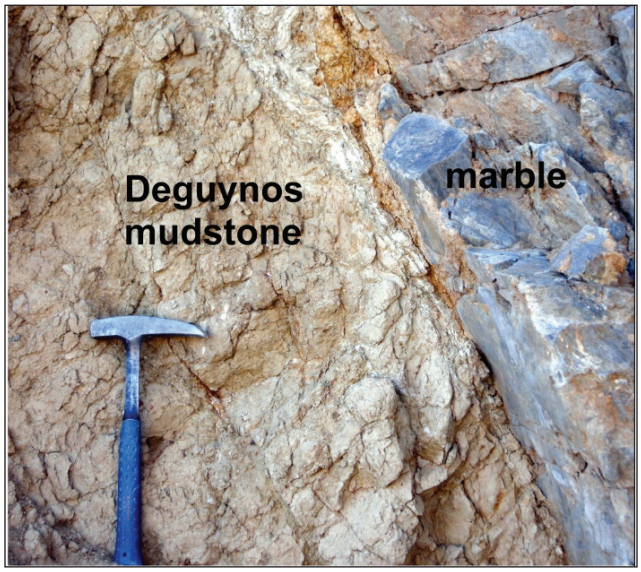

Figure 11. Looking south at East Ridge Fault. Photo was taken just north on the green left-lateral fault that offsets the East Ridge Fault in Figure 9. Dip of the fault is 70° to the west. Mudstones and silts of the Deguyños are sheared and not deposited against the fault.

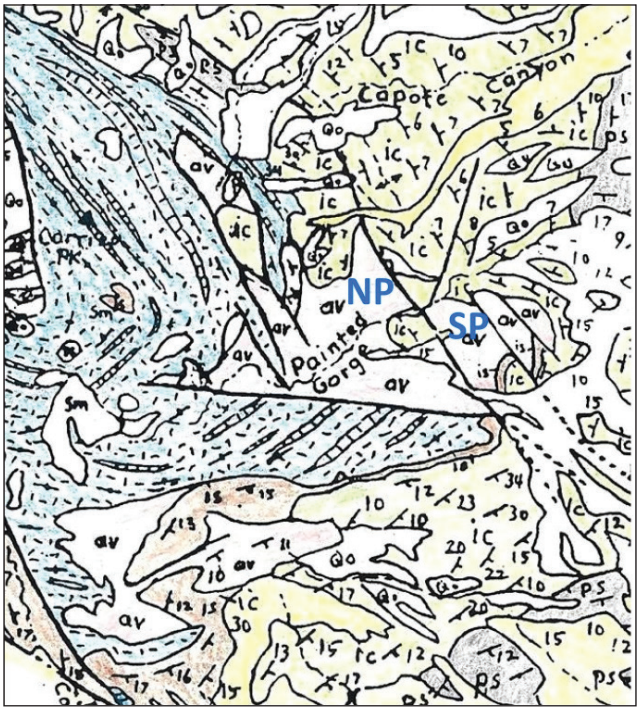

Figure 12. Part of Dibblee's (1954) map: the area of the two hornblende andesite plugs. "**NP**" - northern plug. "**SP**" - southern plug. Note several north-northwest faults, including the Painted Gorge Fault(between the two plus), cross the Pained Gorge drainage. Some of the faults continue south of the southern plug.

rocks along a steep, west dipping, east-side down fault surface (Figure 11) that is not a buttress unconformity, as some believe. The East Ridge Fault was a normal fault that belonged to the third of three extensional episodes found in the Coyote Mountains (Morgan and Morgan, this volume). In the last 1Ma the East Ridge Fault has been reactivated as right-lateral fault. The fault has been involved with the recent, rapid, episodic and disproportional topographic uplift of the CM. As the East Ridge Fault approaches the Painted Gorge drainage the Deguyños Formation is replaced with volcanics of the Alverson Formation on the east side of the fault. We believe that this fault is the northeast edge of the core of the CM and can be followed to the northwest along the edge of the CM. This fault places Mud Hill and Yuha Members of the Deguynos Formation against the northeast side of the CM south of the Carrizo Impact Area (this paper).

> We reinterpret it (PGF) as a right lateral strike-slip fault with ~1 km of displacement, as evidenced by an offset hornblende andesite body.

In order for this to be true there has to be an active north-northwest fault on the western side of the southern plug. Dibblee, 1954 Figure 12 and Dibblee, 2003 Figure 13, Christensen (1957) Figure 14, Ruisaard (1979) Figure 16 and Bykerk-Kauffman, personal communication, all show an extension of the north-northwest Painted Gorge fault on the west side of the southern plug. Morton (1977)

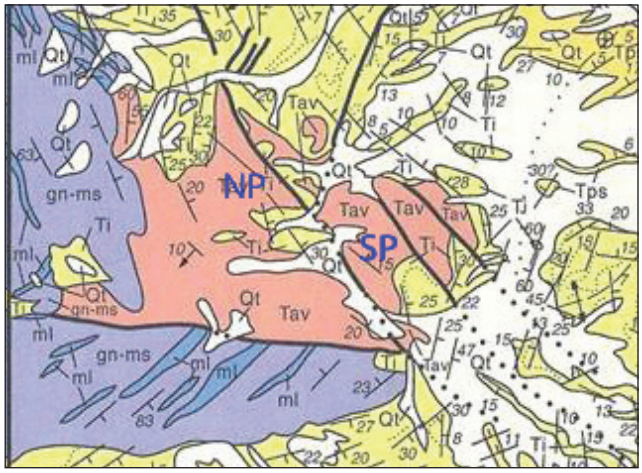

Figure 13. A part of Dibblee's 2003 map. "**NP**" - northern plug. "**SP**" - southern plug. Note many of the faults to the west of the northern plug have been removed. The Painted Gorge Fault and other north-northwest faults still cross the Painted Gorge drainage and continue south of the southern plug.

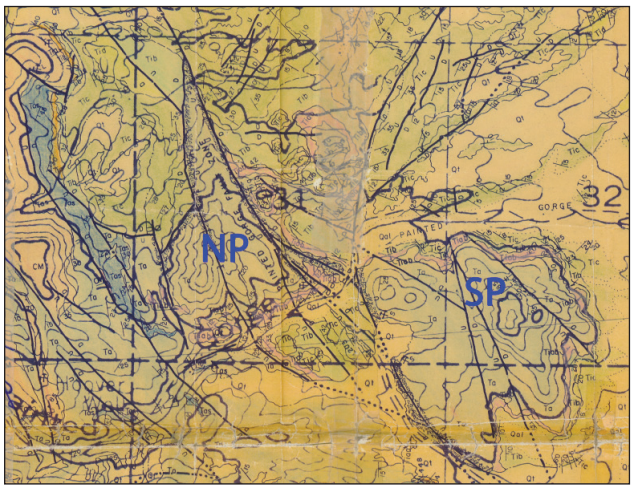

Figure 14. Christensen's Map of the area around the Painted Gorge Fault and the two plugs. "**NP**" - northern plug. "**SP**" - southern plug. Note the breccia along the north-northwest Painted Gorge fault that cross the Painted Gorge drainage and continue on the west side of the southern plug. Christensen considers the breccia in the plus to be fault related. Note also the other north-northeast faults that cross the Pained Gorge drainage and continue south of the southern plug.

Figure 15 with a slightly different interpretation also shows a fault on the west side of the southern plug.

Christensen mapped breccia along the faults he mapped in and on the sides of the plugs. He believes the breccia he mapped is a product of faulting. This may be one of the reasons he extends his Painted Gorge fault to the south along the west side of the southern plug. There is brecciation along parts of the western side of the southern plug. Our mapping has lead us to believe that most of the breccia found in the plugs is the result of at least three episodes of intrusion, a younger hornblende andesite plug intruding and brecciating a cold older hornblende andesite plug. This relationship can be found in both hornblende andesite plugs. Another scenario for producing a breccia along the edge of the plugs can occur when an active

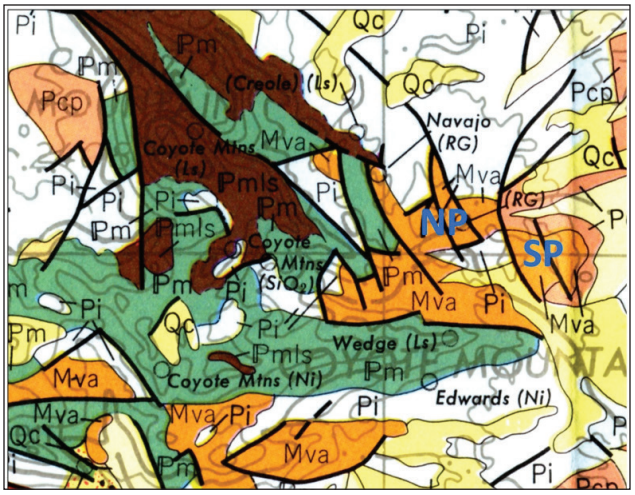

Figure 15. Morton's (1977) Map. "**NP**" - northern plug. "**SP**" - southern plug. The fault on the west side of the south plug is connected to an east-northeast fault. The east-northeast faults tend to left-lateral strike-slip faults. Note that Morton's Painted Gorge Fault does not cross the Painted Gorge drainage and the faults in the southern plug do not continue south of the southern plug.

Figure 16. Ruisaard (1979) broke out the hornblende andesite plugs as a separate volcanic unit of the Anderson Formation. "**NP**" - northern plug. "**SP**" - southern plug. Note that Ruisaard has many of his north-northwest faults cross the Painted Gorge drainage.

intrusion with an outer chilled zone, brecciates that chill zone through continued emplacement.

South of Painted Gorge drainage and west of the southern plug we have not found an active or inactive north-northwest fault cutting Terrace 3, cutting the Deguynos mudstone under Terrace 3, cutting the exposures of basalt on both sides of the road, cutting the southern plug or offsetting the very active, oblique, left-lateral, east-northeast Painted Gorge Wash Fault (Morgan and Morgan, 2005) (see Figure 17). The Painted Gorge Wash Fault does cut all but the youngest Qal in several washes. Our mapping leads us to believe that the Pained Gorge Fault and other north-northwest faults, for the most part, do not cross the Painted Gorge drainage west of the southern plug (zone of adjustment?). Morton (1966) mapped the north-northwest faults not crossing the Painted Gorge drainage. We believe that the two exposures of hornblende andesite represent a bifurcated plug with slight, questionable left-lateral offset or are two independent plugs. We have map an east-northeast fault, presumably left-lateral, in the Painted Gorge drainage south of the northern plug but the fault does not cut Terrace 3 when followed to the west. We have mapped other east-northeast faults in the area west of the southern plug; none are displaced by a north-northwest fault.

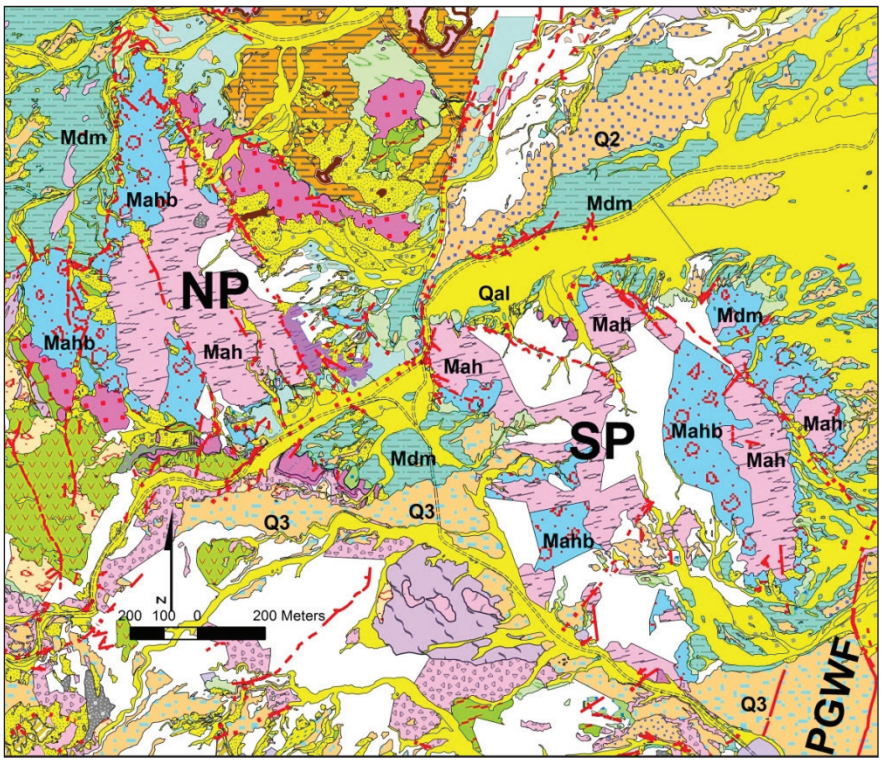

Figure 17. A draft map of part of our 1:2000 scale map showing the area around the two(?) andesite plugs. "**NP** "- northern plug. "**SP**" - southern plug. **Qal** - alluvium. **Q2** - Terrace 2. **Q3** - Terrace 3. **Mdm** - Deguynos mudstone. **Mah** - Alverson intrusive hornblende andesite plugs. **Mahb** - Alverson brecciated hornblende andesite plug material. **PGWF** - Painted Gorge Wash Fault. There are no north-northwest faults west of the northern plug that cross the Pained Gorge drainage. There is a north-northwest fault on the east side of the north plug, but there is no north-northwest fault on the west side of the southern plug. We have not found any north-northwest fault on the west side of the southern plug cutting the Terrace 3 or the Deguyños mudstone under the Terrace 3. We have not found a north-northwest fault cutting the basalt plug or the basalt flow that is west of the southern plug. There are several east-northeast faults on the west side of the southern plug but they do not show any offset cause by a north-northeast fault. The internal geology of the two plugs does not appear to match.

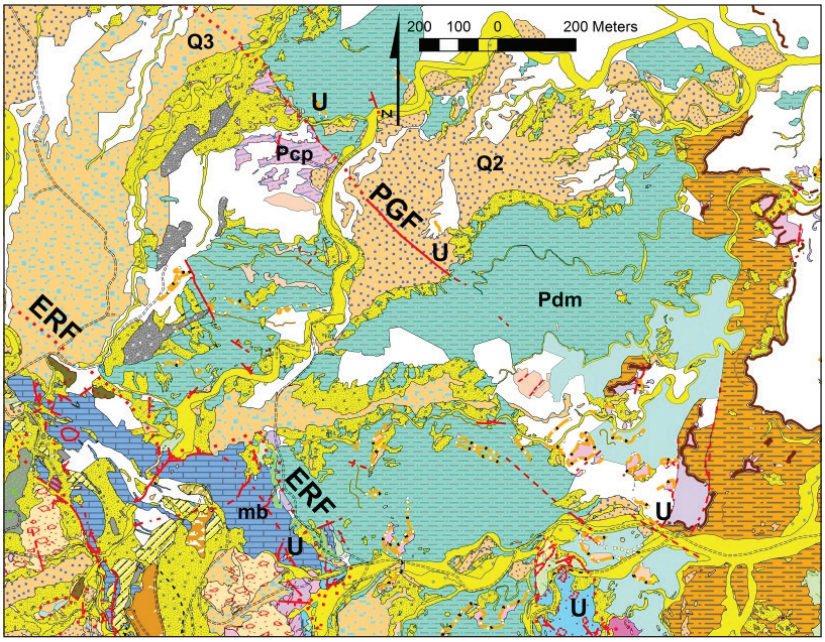

Figure 18. Area at the southern end of the Painted Gorge fault. **PGF** - Painted Gorge Fault. **ERF** - East Ridge Fault. **U** - up side of the fault. **Q2** - Terrace 2. **Q3** - Terrace 3. **Mb** - marbles. **Pdm** - Deguynos Formation. **Pcp** - Palm Spring Group mudstones.

"Fault scarps on alluvial deposits reveal that the PGF is active".

Our mapping shows Christensen's Painted Gorge Fault cutting our Terrace 2, but it does not cut the Qal, Qoa or Terrace 1. The scarp is about 0.6m high, east side up. The Painted Gorge Fault also appears not to cut other Terraces (another Terrace 2 and a Terrace 3) to the north (see Figure 18). Further to the north and in the south part of the Carrizo Impact Area, the PGF separated two outcrops of the Mud Hills and Yuha Members of the Deguynos Formation (Figure 3). The Painted Gorge Fault scarp on Terrace 2 shows very little right-lateral offset, not the kilometer of recent offset that Bykerk-Kauffman et al.(2016) propose to be offsetting the two exposures of the hornblende andesite plugs.

We are even having trouble mapping the Painted Gorge Fault southeast of Terrace 2, cutting marker beds and forming a link with the fault, that is west side up, found on the east side of the northern hornblende andesite plug (see Figure 18). We believe that the fault on the east side of the northern plug is related to the recent uplift of the CM and may not be a part of the Painted Gorge Fault. This is area we have not finished mapping. We believe, as Christensen did, that the PGF fault is prominently a dip-slip normal fault with the east side up. The older stratigraphy along the fault also shows east side up on the Painted Gorge Fault. The Painted Gorge's recent scarp that cuts Terrace 2 may be under the influence of the left-lateral faults to the southeast.

The Painted Gorge Fault, the East Ridge Fault and other normal faults made horst and graben structures that are found on the east side of the CMs. These normal faults appear related to the West Salton Detachment (Morgan and Morgan, this volume). There is evidence that the traces of some of these normal faults have been reactivated as strike-slip faults (Morgan and Morgan, this volume).

Thanks to: John Prall, Bill Elliott, Mike Hart, Ann Bykerk-Kauffman, Eric Frost, Stephen Schellenberg, Monte Marshall, Gordon Gastil, Gary Axen, Larry Busch, Charles Winker, Jerry Treiman, Jim Senn and the BLM for a mapping permit.

References

Axen, G. J., and Fletcher, J. M., 1998, Late Miocene-Pliocene extensional faulting, northern Gulf of California, Mexico, and Salton Trough, California: International Geological Review, V. 40, p. 217-244.

Blaettler, Karen Griffith, 1991, A petrographic study of an amphibolite outcrop in the Coyote Mountains, Imperial County, California, San Diego State University, Under Graduate Research Report, V. 53.

Bykerk-Kauffnam, A., Janecke, S. U., Ewing, C. S., Brenneman, M. J., Caldwell, G. R. and Gentry, A. C., 2016, A complex fault network in an active zone of distributed right-lateral shear, Coyote Mountains, southern California, GSA Annual Meeting, abstract.

Dibblee, T. W., 1954, Geology of the Imperial Valley region, California, in Jahns, R. H., ed., Geology of southern California: California Division Mines Bulletin, v. 170, p. 21-28.

Dibblee, T. W., 2003, Geology of the Coyote Mountains, Imperial and San Diego Counties, California, In, M.L. Murbach and M.W. Hart (eds.), Geology of the Elsinore Fault Zone, San Diego Region: San Diego Association of Geologist, San Diego, South Coast Geological Society, Santa Ann,

California, p.117-123.

Dorsey, R.J. (2012), Earliest delivery of sediment from the Colorado River to the Salton Trough at 5.3 Ma: Evidence from Split Mountain Gorge. In: Reynolds, R.E. (ed.) Searching for the Pliocene: Southern Exposures. *Proceedings of the 2012 Desert Symposium*, p. 88-93.

Christensen, A. D., 1957, Part of the geology of the Coyote Mountains area, Imperial County, California: Unpublished M.S. thesis, University of California at Los Angeles, 188 p.

Hamilton, W.B., 1961, Origin of the Gulf of California: GSA Bull., 72, p1307-1318.

Link, M. H., and Abbott, P. L., 1991, Eocene sedimentary history, San Diego, California: overview and Field trip stops, in Abbott, P. L., and May, J. A., eds., 1991, Eocene geological history San Diego Region, Pacific section SEPM, Vol. 68, p.1-26.

Miller, R, H., and Dockum, M. S., 1983, Ordovician conodonts from Metamorphosed carbonates of the Salton Trough, California: Geology, v. 11, p. 410-412.

Morgan, G. J., and Morgan, J. R., 2005, The Painted Gorge Wash Fault: recent left-lateral faulting, east side Coyote Mountains, Imperial County, California: Bloom, D. M., ed. Geology and history of southeastern San Diego County, California, San Diego Association of Geologists, p.189-204.

Morgan, J. R., Morgan, G. J. and Pecha, M., 2012, U/Pb dating of tuffs from the Alverson Volcanics in the Fossil Canyon and Painted Gorge areas of the Coyote Mountains, western Salton Trough, California, GSA Cordilleran Section, Abstract and Programs, Vol. 44, No. 3, p. 22.

Morgan, G. J. and Morgan, J. R., 2015, Overview of the Geology of the southern Coyote Mountains, Salton Trough, Imperial County, southern California. In Wagner, R., ed, Geology of the Coyote Mountains, southern California: San Diego Association of Geologists, p.77-87.

Morgan, G. J. and Morgan, J.R., 2016, Viejo Formation: a new formation for the Imperial Group sediments in the southern Coyote Mountains, Salton Trough, southern California, GSA Cordilleran Section, Abstract Paper No. 28-10.

Morton, P. K., 1977, Geology and mineral resources of Imperial County, California: California Division of Mining and Geology, County Report No.7.

Ruisaard, C. I., 1979, Stratigraphy of the Miocene Alverson Formation, Imperial County, California: Masters of Science Thesis, San Diego State University, 125p.

Steely, A. N., Janecke, S. U., Dorsey, R. J., and Axen, G. J., 2009, Early Pleistocene initiation of the San Felipe fault zone, SW Salton Trough, during reorganization of the San Andreas fault system: Geological Society of America Bulletin, v. 121, P. 663-687, doi. 10.1130/B26239.1.

Umhoefer, P. J., 2011, Why did the Southern Gulf of California rupture so rapidly?—Oblique divergence across hot, weak lithosphere along a tectonically active margin: GSA Today, V. 21, Issue 11, pp. 4-10.

Winker, C. D., and Kidwell, S. M., 1996, Stratigraphy of a marine rift basin: Neogene of the western Salton Trough, California, in Abbott, P. L., and Cooper, J. D., eds., Field Conference Guidebook and Volume for the Annual Convention: San Diego, California, American Association of Petroleum Geologists, Pacific Section, p. 295336.

Woodring, W. P., 1931, Distribution and age of the Tertiary Deposits of the Colorado Desert: Carnegie Institution of Washington Publication 148, p. 1-25.

The Ediacaran–Cambrian biotic transition in eastern California and southwestern Nevada and its global context

Michael Strange[1] and Stephen M. Rowland[1]
[1]*Department of Geoscience, University of Nevada Las Vegas*

Introduction

In his 1989 book *Wonderful Life*, Stephen Jay Gould presented the now iconic Burgess Shale fauna as the epitome of what evolution was able to accomplish in diversifying animal life during the Cambrian Explosion. While it would be difficult to exaggerate the role the Burgess Shale fauna has played in our understanding of the diversification of multicellular animals, it is important to remember that the Burgess Shale postdates the beginning of the Cambrian Period—the nominal ignition of the Cambrian Explosion—by more than thirty million years. An understanding of the dynamics of the Cambrian Explosion and the events leading up to it requires us to look even deeper into the past, into the murky paleontological mists of the Proterozoic Eon.

The Eastern California/southwestern Nevada region is one of the most important regions in the world for research on the fossiliferous strata that straddle the Neoproterozoic-Cambrian boundary, and recent discoveries and analyses of these fossils have shed new light on events and processes that were occurring during this seminal episode in Earth history. Here we provide a review of the current status of research on the paleontology of the Neoproterozoic-Cambrian boundary in eastern California and southwestern Nevada, along with the global context in which these fossils occur.

Regional stratigraphy

Figure 1 summarizes the regional Ediacaran-Cambrian stratigraphy across eastern California and southwestern Nevada. During the Nineteenth and most of the Twentieth centuries, the base of the Cambrian System was defined by the first occurrence of trilobites, once thought to be the earliest fossilized animals. However, in the early Twentieth Century, German geologists working in Namibia discovered some pre-trilobite, non-mineralized, frond-like fossils (Xiao, 2008). In the 1940s, similar fossils were found in the Ediacara Hills of South Australia (Glaessner, 1961). Pre-trilobite fossils, including some conical ones with phosphatic or calcium carbonate shells, were later found in many other places in the world. This led to an intense debate within the community of Cambrian paleontologists about how to define the base of the Cambrian Period. Because the base of the Cambrian also defines the base of the Phanerozoic Eon—literally "the eon of visible animals"—many researchers favored redefining the base of the Cambrian downward, to include at least some of these newly discovered, pre-trilobite fossils. This debate culminated in 1992 with the international adoption of a new definition of the base of the Cambrian Period. This expanded Cambrian System does not, however, extend low enough to include most of the pre-trilobite, animal-appearing fossils. Notably the famous molds and casts of soft-bodied organisms of Namibia, South Australia, and elsewhere—so-called Ediacara-type fossils—remain true pre-Cambrian fossils. These are diagnostic fossils of the Ediacaran (ee-dee-AK-a-run) Period, which was formally established by the International Union of Geological Sciences in 2004 (Knoll et al., 2006). Small tubular and conical fossils—some of which have biomineralized skeletons while others do not—also occur in the Ediacaran Period.

In deciding how to define the Ediacaran-Cambrian boundary, biostratigraphers wrestled with the problem of a lack of suitable body fossils. They ultimately chose a morphologically distinctive type of burrow named *Treptichnus pedum* as their index fossil. By international agreement, an assemblage of trace fossils including *T. pedum* occurs in the Cambrian but not in the Ediacaran. The boundary is formally defined as the base of the *T. pedum* Assemblage Zone in an exposure in Newfoundland, Canada (Geyer and Landing, 2016). This is the only biostratigraphic boundary in the geologic time scale that is defined by a trace fossil.

In the strata of the Death Valley region and southern Mojave Desert, the lowest occurrence of *T. pedum*—and therefore the Ediacaran-Cambrian boundary—is in the Lower Member of the Wood Canyon Formation; farther northwest, in the White-Inyo Mountains of Inyo County, California and in adjacent Esmeralda County, Nevada, the boundary occurs in the Esmeralda (middle) Member of the Deep Spring Formation (Fig. 1)(Corsetti and Hagadorn, 2000, 2003; Hagadorn and Waggoner, 2000; Hagadorn et al., 2000; Rowland and Rodriquez, 2014; Smith et al., 2016a).

The redefinition of the base of the Cambrian System/Period resulted in an increase in the thickness of Cambrian strata and an older date for its beginning (now determined to be 541.0 Ma; Gradstein et al., 2012). Ever since the Cambrian Period was originally defined in the 1830s, it had been divided into three epochs: Early,

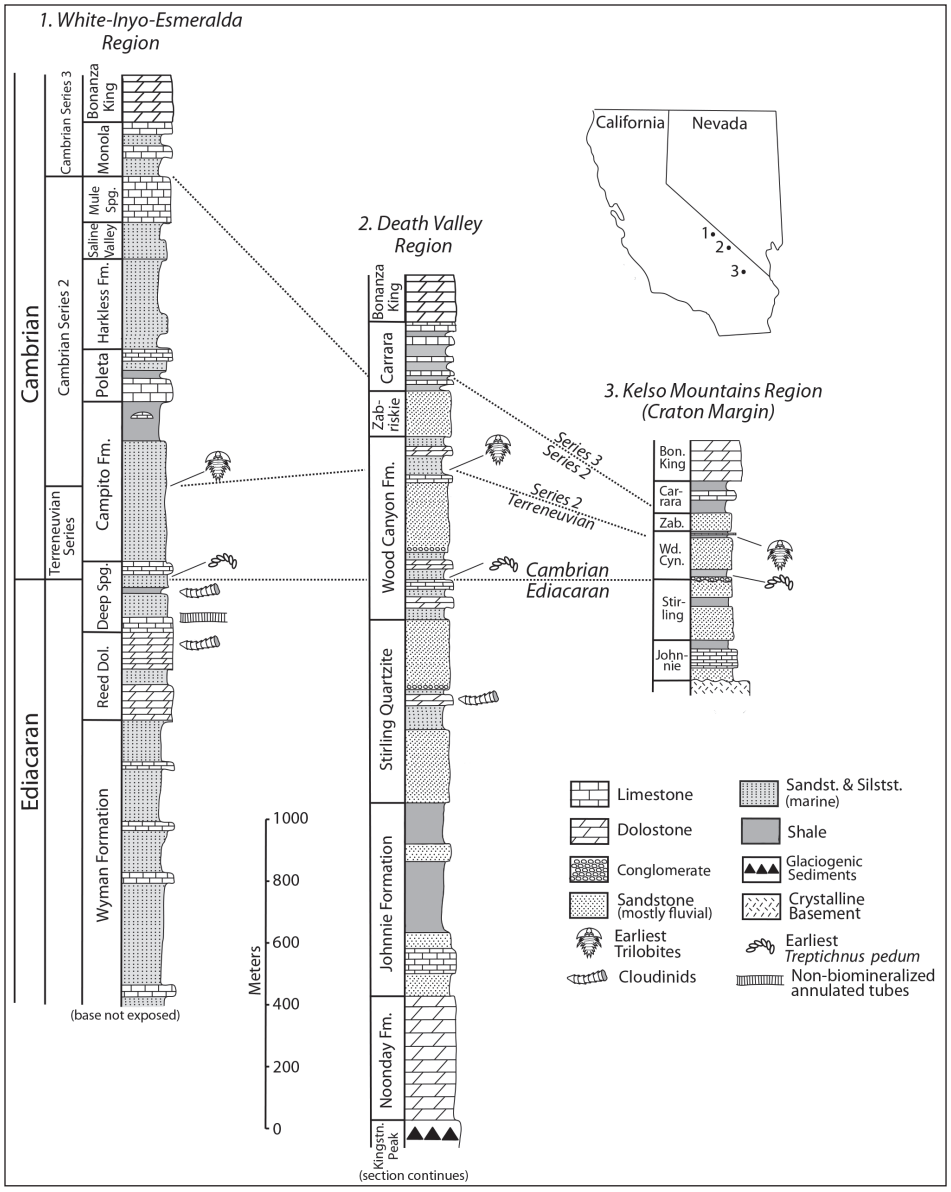

Figure 1. Generalized stratigraphic columns of Ediacaran and Cambrian strata in eastern California. Adapted from Hagadorn et al. (2000) and Corsetti and Hagadorn (2003).

Middle, and Late (Berry, 1968). Lowering the boundary to a position well below the first occurrence of trilobites added a considerable thickness of strata to the Cambrian System. In the Death Valley region, for example, approximately 400 meters of formerly pre-Cambrian strata were suddenly added to the Cambrian System. Cambrian stratigraphers were discomfited by this increased thickness in the Lower Cambrian Series, and an international commission ultimately decided to abandon the traditional tripartite subdivision of the Cambrian in favor of a quadripartite scheme (Gradstein et al., 2012). This new stratigraphic framework is reflected in Figure 1. The Terreneuvian Series is the newly-added pre-trilobite interval. *Terre Neuve* is the French name for Newfoundland, where the type section of this series is located. Series 2 is the stratigraphic interval formerly known as the Lower Cambrian, and Series 3 is the interval formerly known as the Middle Cambrian. These two series/epochs will eventually be given geographic locality-based names, after type sections (global stratotype sections and points—GSSPs) are chosen. The stratigraphic interval formerly known as the Upper Cambrian (not shown in Figure 1), is now the Furongian Series, named after its stratotype section in China. The age of the Terreneuvian/Series 2 boundary is 521 Ma, and the age of the Series 2/Series 3 boundary is 509 Ma (Gradstein et al., 2012). Thus the approximately 700 meters of the Wood Canyon Formation, Zabriskie Quartzite, and basal Carrara in the Death Valley column of Figure 1, between the earliest occurrence of *T. pedum* and the extinction of olenellid trilobites (marking the end of Series 2) represents 32 million years.

As illustrated in Figure 1, the Ediacaran and Cambrian strata of eastern California thicken dramatically toward the northwest. The sedimentary facies also change. In the Kelso Mountains and Death Valley regions, thick intervals of fluvial sandstone and conglomerate are dominant lithologies, while carbonate intervals are relatively thin. In stark contrast, roughly one hundred kilometers to the northwest, fluvial facies are absent and carbonate intervals are thick. (The proximity of these contrasting facies may be exaggerated somewhat due to Cenozoic tectonism.) The strata in these two adjacent regions are so different that—below the Cambrian-Series-3 Bonanza King Formation—none of the Ediacaran and Cambrian stratigraphic intervals in the Death Valley region are known by the same formation names in the White-Inyo-Esmeralda region. The rocks in the Death Valley region were deposited in proximal continental-shelf and fluvial braid-plain environments; braided-stream sandstones and conglomerates alternate with peritidal shallow-marine deposits. Northwestward into the White-Inyo-Esmeralda region, these facies transition into distal, shallow-shelf,

storm-dominated, exclusively marine settings with shelf-margin reefs (Christie-Blick et al., 1989; Mount and Rowland, 1981; Rowland et al., 2008).

A wormworld rauna in the garden of Ediacara

Within the past several years, to better understand the confluence of evolutionary events and environmental factors that enabled metazoan diversification to explode in the Cambrian, researchers have been aggressively focusing on the Ediacaran fossil record. This effort includes detailed studies of the famous, Ediacara-type fossils first reported from Namibia and South Australia (e.g., Narbonne, 2005; Vickers-Rich and Komarower, 2007; Xiao, 2007; Fedonkin et al., 2008; Tarhan et al., 2017). But it also includes the study of a less well-known, terminal Ediacaran, miniature vermiform fauna—nicknamed the "wormworld" biota by Schiffbauer et al. (2016a)—which includes the earliest biomineralizing taxa (see also Schiffbauer, 2016).

Both types of Ediacaran fossils have been reported from eastern California and southwestern Nevada (Hagadorn and Waggoner, 2000; Hagadorn et al., 2000; Smith et al., 2016b), but it is the "wormworld" fauna that has attracted the most recent attention. "Wormworld" taxa have actually been known to occur in this region for half a century; Taylor (1966) described some poorly preserved, calcareous, tubular fossils from the uppermost Reed Dolomite. He named them *Wyattia reedensis*, in honor of U.C. Berkeley paleontology professor J. Wyatt Durham. In the early 1980s a fauna of tubular fossils was described from the Dunfee (lower) Member of the Deep Spring Formation at Mt. Dunfee, in Esmeralda County, Nevada (Mount et al., 1983; Signor et al., 1983). Several new skeletal taxa were described in this lower Deep Spring fauna, however Grant (1990) later synonymized them, together with *Wyattia*, concluding that they all were closely related to, or con-generic with, *Cloudina* (although *Wyattia* is an earlier named taxon and therefore has priority over *Cloudina*). *Cloudina*, as originally described by Germs (1972), consists of a series of nested, conical, calcite tubes, flared at their openings, often forming a curved or sinuous shell morphology. In recent years, morphologically similar, non-mineralized, or weakly mineralized, fossils named *Conotubus* have been placed with *Cloudina* in the family Cloudinidae. Cloudinids are restricted to the Ediacaran Period.

Figure 2 illustrates non-biomineralized cloudinids from the Esmeralda (middle) Member of the Deep Spring Formation at Mt. Dunfee. These fossils were first reported by Oliver (1990), but remained unstudied until recently. They were rediscovered, along with an additional fossiliferous horizon in the Dunfee (lower) Member of the Deep Spring Formation, and reported by Smith et al. (2016a). These two horizons contain disparate assemblages of the "wormworld" fauna. The stratigraphically lower of the two horizons contains abundant casts and molds of a tubular fossil that Smith et al. (2016) identified as *Gaojiashania*, a genus previously known only from the Gaojiashan Lagerstätte of South China. They tentatively assigned other specimens to *Wutubus*, another tubular genus previously known only from South China. Along with the tubular organisms, the newly studied Deep Spring horizons contain several ichnotaxa of trace fossils. The upper fossil-bearing horizon in the Esmeralda Member has also yielded a tiny, non-biomineralized alga of unknown division-level affinity, *Elainabella deepspringensis* (Rowland and Rodriguez 2014)(Fig. 3). Smith et al. (2016a) reported the occurrence of relatively abundant, poorly preserved *Cloudina* specimens throughout the Dunfee (lower) Member of the Deep Spring Formation, and as far down in section as the Reed Dolomite, the stratigraphic level where Taylor (1966) had recovered his *Wyattia* specimens.

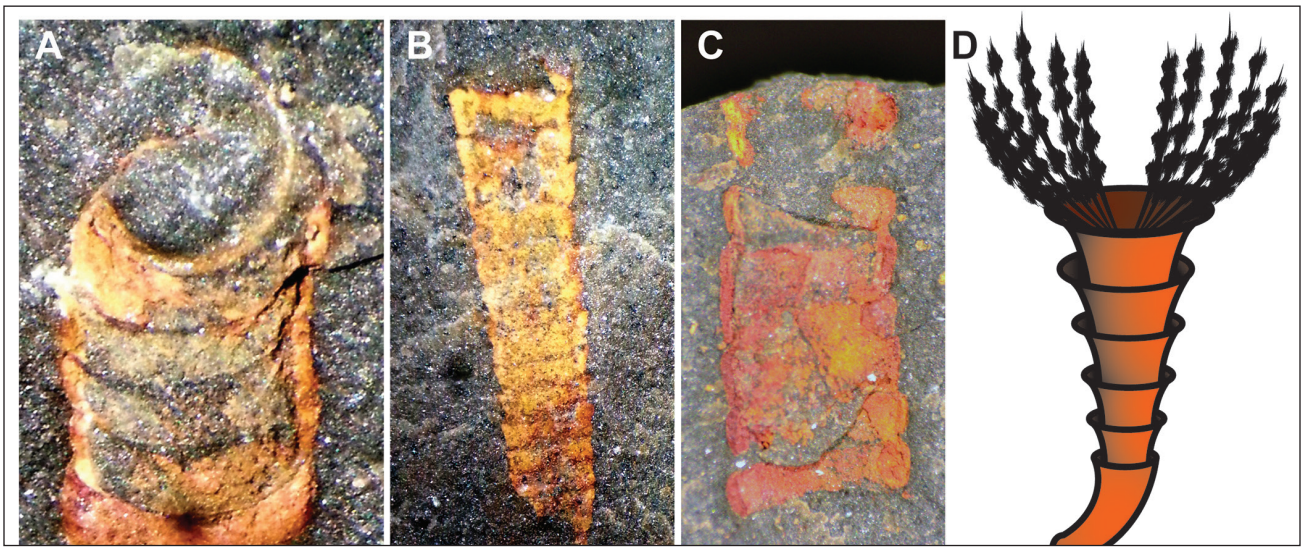

Figure 2. (A, B, C) Tubular vermiform fossils (Cloudinids and Cloudinid-like forms) from the Esmeralda (middle) Member of the Deep Spring Formation, Mount Dunfee, Nevada. (D) hypothesized reconstruction of recalcitrant tube wall and unpreserved, fan-shaped feeding structures of *Conotubus*.

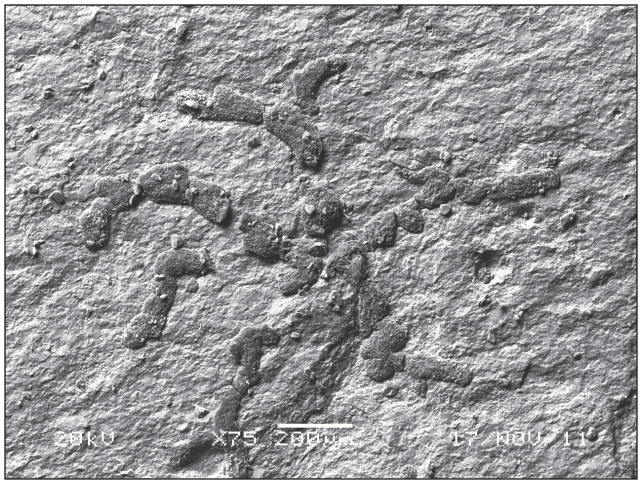

Figure 3. SEM image of *Elainabella deepspringensis*, a tiny, non-biomineralized alga from the Esmeralda (middle) Member of the Deep Spring Formation at Mt. Dunfee. The fossil is approximately 1 mm wide. From Rowland and Rodriguez (2014)

Biostratigraphically, the "wormworld" fauna of the Deep Spring Formation displays an enigmatic pattern of biomineralization. Biomineralized *Cloudina* appears lower in the section than the non-biomineralized cloudinid *Conotubus*. This is contrary to the anticipated pattern in which non-biomineralizing forms would logically be expected to evolve first; biomineralization would be expected to come later, culminating with the dawn of the Cambrian and the explosively evolving menagerie of biomineralizing taxa. In the Denying Formation of South China, in fact, biomineralization follows the anticipated script: the soft-tissue cloudinid *Conotubus*, together with a diverse assemblage of other annulated vermiforms, disappears from the record well before the first appearance of biomineralized *Cloudina* (Cai et al., 2010). This enigmatic disparity between the relative positions of biomineralized and non-biomineralized cloudinids in South China and southwestern North America may be resolved with future discoveries. However, the occurrence of soft-tissue, non-biomineralized vermiforms in the Deep Spring Formation stratigraphically above *Cloudina* indicates that these non-mineralizing members of the "wormworld" fauna survived well after the development of biomineralization in *Cloudina* and any selective pressures which may have caused it, such as an increased level of predation (Hua et al. 2003). The emerging picture suggests that the evolution of biomineralization in the Ediacaran Period is not a simple story of the gradual, progressive acquisition of this ability by vermiform animals. Whatever abiotic and ecological factors contributed to the evolution of biomineralized skeletons, their influence evidently fluctuated through time.

Diverse assemblages of metazoan trace and body fossils, as well as many other putative metazoans and classic Ediacarans, have been found in the Wood Canyon Formation. Hagadorn and Waggoner (2000) reported finding fourteen taxa in a variety of lithologies in the Wood Canyon and adjacent strata. These assemblages contain some taxa that are members of the "wormworld" fauna. *Cloudina*, for example, occurs in the middle carbonate units of the Sterling Quartzite (Hagadorn et al., 2000). However, definitive taxonomic assignments of many of these fossils are impossible; the style of preservation often does not preserve the detail needed to identify important morphological features.

Biotic change recorded in the rrace fossil record

A major challenge in studying the Ediacaran-Cambrian transition globally is the dearth of stratigraphic sections containing multiple sedimentary facies. Trace fossils are best preserved in siliciclastic-dominated facies (sandstone-siltstone-shale), while carbonate-dominated facies record secular isotopic changes (especially those of carbon isotopes) in seawater that are not recorded in siliciclastic rocks. In Ediacaran and Cambrian research—more than in any other interval of geologic time—the combination of trace fossils in siliciclastic rocks and chemostratigraphic signals in carbonate rocks is critical for inter-regional and inter-continental correlation, and also for teasing the details of biotic change out of the stratigraphic record. A major reason the eastern California and southwestern Nevada stratigraphic sections have played such an important role in the history

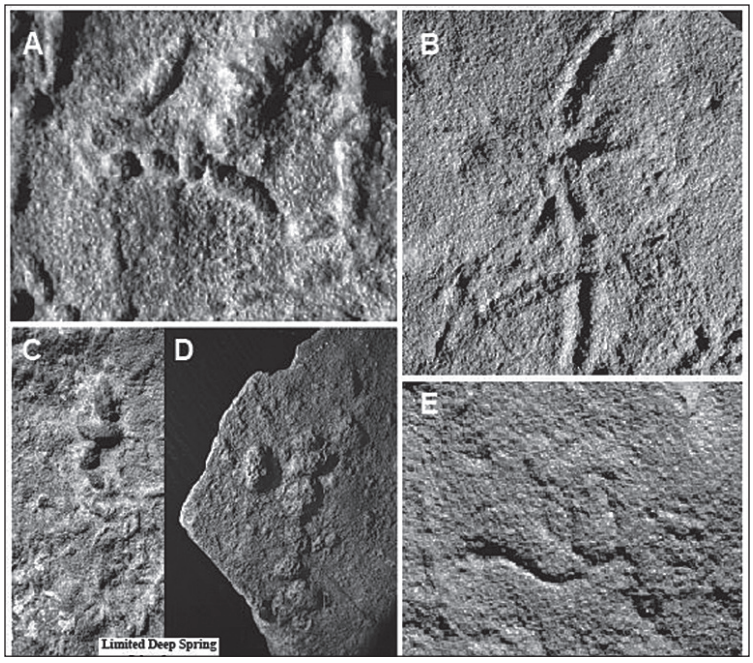

Figure 4. Trace fossils typical of the Lower Assemblage in the Death Valley region, consisting of simple, shallow burrows. (A) *Treptichnus pedum* from the Wood Canyon Formation. (C-D) *Treptichnus pedum* from the Deep Spring Formation. (B, E) Simple, shallow traces from the Wood Canyon Formation in the Montgomery Mountains, Nye County, Nevada.

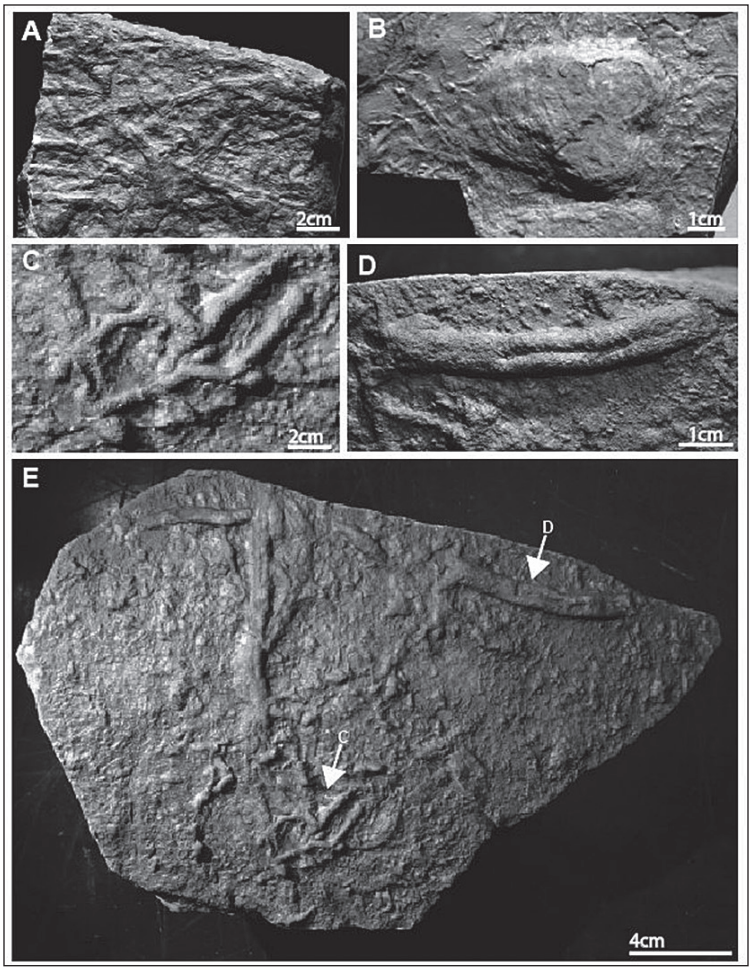

Figure 5 (left). Trace fossils typical of the Middle Assemblage in the Death Valley region, consisting of complex, mostly shallow burrows. (A) Large undifferentiated burrows. (B) *Rusophycus*, a trilobite burrow. (C) Small undifferentiated burrows from slab in "5E." (D) Bilobed *Helminthoidichnites* burrow from slab in "5E." (E) slab showing diversity of burrows typical of the Middle Assemblage with arrows indicating where magnified images were taken for images "5D" and "5E."

of research on the Ediacaran-Cambrian transition is that these are mixed-facies sections, with both siliciclastic and carbonate intervals. This allows the record of carbon isotopic excursions to be integrated with the trace fossil record (Corsetti and Hagadorn, 2000, 2003; Smith et al., 2016a). Here we briefly review the dynamic pattern of biotic change recorded in the trace fossil record across the Ediacaran-Cambrian boundary in this region.

The Wood Canyon Formation contains abundant sandstone, siltstone, and shale, which provide ideal substrates for infaunal (living *within* the sediment) habitats and the preservation of the organisms' behaviors as trace fossils. Therefore, in sections such as those in the Death Valley region (Fig. 1), the story of the Cambrian explosion is told through the diversification and increasing complexity of trace fossils (Figs. 4-8). The trace fossil record thus serves as a proxy for bilaterian benthic activity (Jensen et al., 2005).

Generally speaking, the trace fossils become morphologically more complex, and they record increasing behavioral complexity, upward through the section. The quality of preservation and ambiguity of many of the trace fossils often makes taxonomic assignments difficult. For this reason, we will focus more on the general trends across the boundary and less on specific ichnotaxa. As illustrated in Figures 4-8, the trace fossil record across the Ediacaran-Cambrian transition in the Death Valley regional strata changes episodically; it can be divided into three ichnofaunal assemblages: lower, middle, and upper. In the White-Inyo-Esmeralda region the different sedimentary facies of the Deep Spring Formation, compared to the Wood Canyon Formation, presents a different manifestation of the incipient Cambrian explosion than that of the Wood Canyon Formation. Trace fossils are relatively rare in the Deep Spring Formation, while in the Mt. Dunfee section, at least, tubular fossils seem quite common and widespread. So the dominant themes of the Ediacaran-Cambrian transition there is one of the advent of biomineralization, increased diversification of the epifaunal (living *on* the sediment surface) community, and the expansion of the Ediacaran food web (Smith et al. 2016a, Schiffbauer et al. 2016). The Mount Dunfee section provides the best opportunity for assemblage comparisons of "wormworld" faunas throughout the world. Past studies in the Wood Canyon Formation, along with recent discoveries yet to be explored in detail (Smith et al., 2016b), suggest that a similar suite of tubular taxa exist there as well.

When discussing the preservation of the behavior of early animals as recorded in their trace fossils, it is important to consider evolving sedimentary systems during the latest Neoproterozoic. The earliest burrowing animals lived in a pre-substrate-revolution world, meaning that they lived in and on non-bioturbated sediments with extensive microbial mats. During this time, finely laminated sediments could be deposited with little or no sediment mixing between layers, allowing for the preservation of shallow burrowing behaviors. The generalized view of trace fossil evolution during the early stages of the Cambrian explosion is one of increasing size, diversity, and depth of burrow penetration (Fig. 8). Trace fossils in the Lower Assemblage follow this generalized view perfectly, with small, shallow burrowers being the first to appear below the Ediacaran-Cambrian boundary (Figs. 4, 7, 8). Deeper burrowing by larger animals follows in progressively younger strata (Figs. 5, 6, 7, 8). Biostratigraphically, simple traversing burrows with an occasional loop appear in the Lower Member of the Wood Canyon (Fig. 4B,E); these burrows have traditionally been referred to the ichnogenera *Planolites*, *Helminthoidichnites*, and *Palaeophycus* (Fig. 8). Within the lower member, Hagadorn and Waggoner (2000)

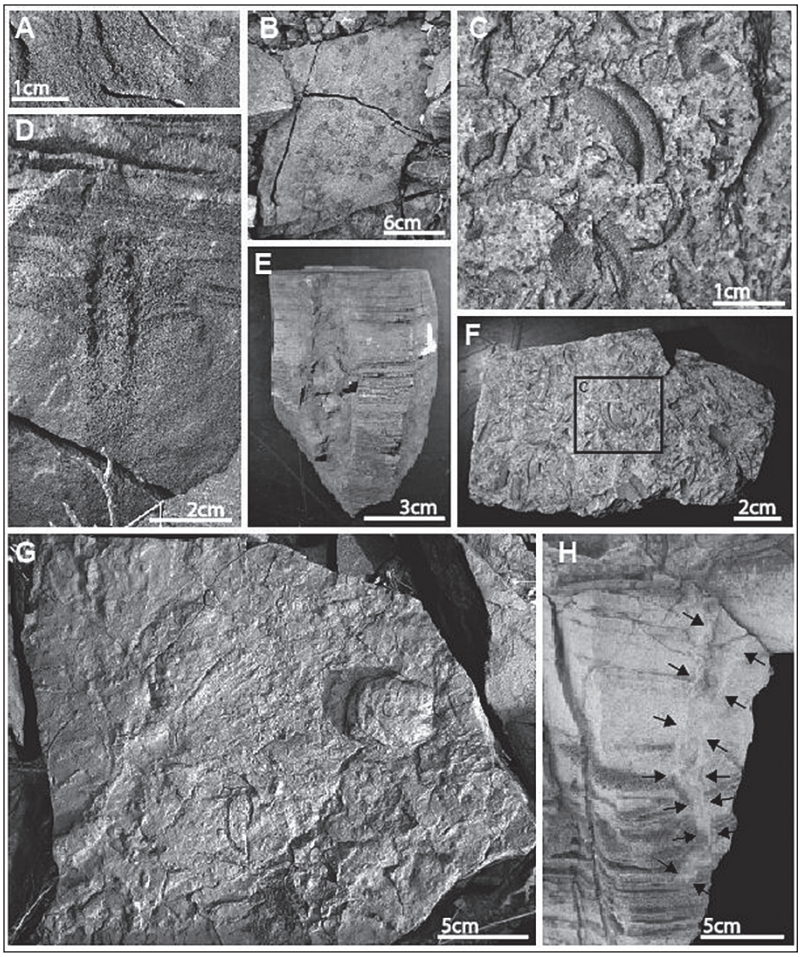

Figure 6. Traces and body fossils typical of the Upper Assemblage of the Death Valley region comprised of large, complex, and deep burrows. (A) *Harlaniella*. (B) dense cluster of *Skolithos*-like vertical burrows. (C) Magnified image of trilobite cephalon in "F." (D-E,H) large, complex, vertical burrows. (F) slab containing abundant trilobite hash. (G) large slab containing highly diverse traces *Rusophycus, Treptichnus pedum,* and *Skolithos.*

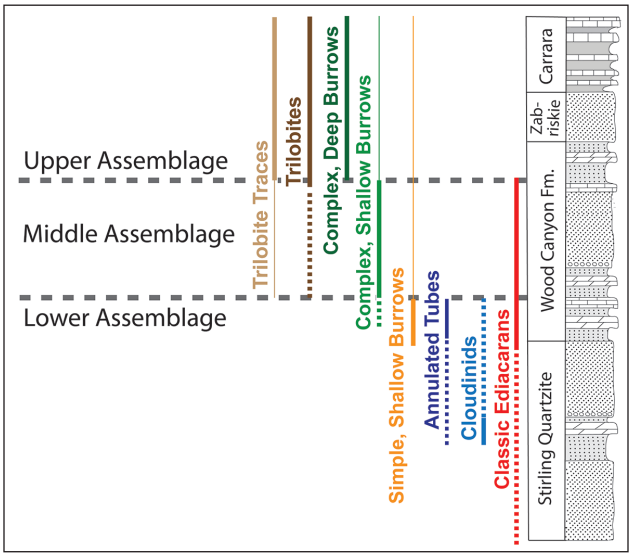

Figure 7. Biostratigraphic ranges of various generalized groups within the Death Valley region. Representative trace fossils in each assemblagae are illustrated in Figs. 4, 5, and 6. Schematic reconstructions of each assemblage are shown in Fig. 8. Note the trend toward deeper and more complex trace fossils through time.

and Waggoner and Hagadorn (2002) identified several other fossils including multiple tubular taxa preserved as casts and molds—*Archaeichnium*, *Cloudina*, *Corumbella*, and *Onuphionella*—and three members of the older Ediacara-type biota—*Ernietta, Swartpuntia,* and *Tirasiana* (Fig. 8). Collectively, these organisms comprise the "Lower Assemblage" of Ediacaran fossils and trace fossils in the Wood Canyon Formation, occurring within the biostratigraphic interval that extends from the first appearance of Ediacaran organisms up to the first occurrence of *Treptichnus pedum*.

The global distribution of Ediacaran body fossils, such as those represented in the lower panel of Figure 8, has led to a wide variety of interpretations concerning their origin and extinction (Narbonne, 2005; Vickers-Rich and Komarower, 2007; Xiao, 2007; Fedonkin et al., 2008; Laflamme et al., 2013), specifically in connection to the later radiation of animal life in the Cambrian. A sparse assemblage of Ediacaran organisms has been found throughout the Death Valley Region. Most of these come from the Wood Canyon Formation and include *Swartpuntia*, *Eldonia*, and *Tirisiania* (Hagadorn et al., 2000; Hagadorn and Waggoner, 2000; Waggoner and Hagadorn, 2002). Unconfirmed reports of the holdfast-fossil *Aspidella* (represented as a *Charnia*-like organism in the lower panel of Fig. 8) may extend the geographic range of Ediacara-type organisms into the Deep Spring Formation. The Ediacara-type taxa seem to have gone extinct globally prior to the beginning of the Cambrian (Xiao, 2008; Laflamme et al., 2013), and this pattern holds true in the Death Valley region. The Lower Assemblage contains the highest mixture of classic Ediacara-type organisms and members of the "wormworld" fauna.

The "Middle Assemblage" (Figs. 7, 8) consists of organisms found between the first occurrence of *Treptichnus pedum* and the first occurrence of trilobite body fossils. This assemblage represents the beginning of minor bioturbation and an increased complexity of trace fossils. Because the trilobite trace fossil *Rusophycus* first appears well below the first trilobite body fossils, future biostratigraphic studies should be able to constrain the beginning of deep burrowing behaviors at the end of the Middle Assemblage instead of at the appearance of trilobites. The most prominent ichnotaxa within the Middle Assemblage include the large trilobite resting trace *Rusophycus* (Fig. 5B), the enigmatic, bilobed trace fossil *Helminthoidichnites* (Fig. 5A, D, E), and abundant

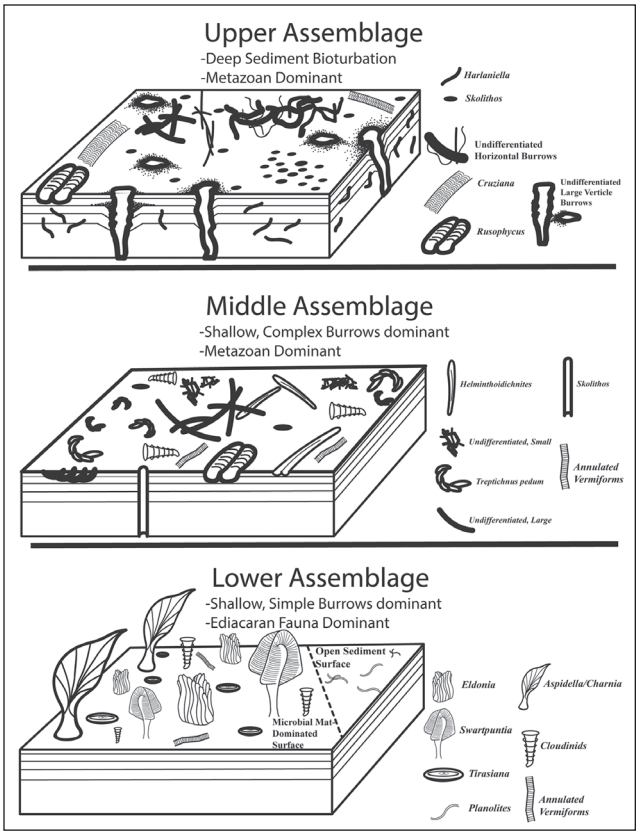

Figure 8. Reconstructions of three fossil assemblages in the Death Valley region. In the middle and upper assemblages, emphasis has been placed on trace fossil diversity. See Fig. 7 for graphical representation of assemblages.

Treptichnus pedum (Fig. 5E). However, a high diversity of complex burrow systems can be found with a variety of shapes and sizes (Figs. 5, 8). Importantly, the majority of trace makers in this assemblage created traces which penetrated only shallowly into the sediment. The exception is the occasional vertical burrow *Skolithos*.

Trace fossils of the "Upper Assemblage" were made by larger animals with the ability to burrow deeply into the sediment (Fig. 8). Massive amounts of bioturbation begin with the introduction of this assemblage, with burrows that pass though many layers of sediment (Fig. 6D, E, H). While many of these large burrows are difficult to differentiate, many are similar to the simple, vertical Skolithos burrows in the Middle Assemblage, however in the Upper Assemblage they occur in dense clusters (Figure 6B).

Conclusions

The beautifully exposed, mixed-carbonate-and-siliciclastic, Ediacaran-and-Cambrian strata of eastern California and southwestern Nevada preserve the story of the biotic transition from the Proterozoic to the Phanerozoic eons as well as it is preserved anywhere in the world, from the monotonous tranquility of the early Ediacaran seafloor to the riot of autotrophs, heterotrophs, and mixotrophs interacting in complex marine ecosystems in the Cambrian.

The story of the Cambrian Explosion is recorded in great detail in these rocks, resplendent as they are with diverse assemblages of trace and body fossils, and with the recorded signals of global environmental events. As researchers become more skilled at deciphering these signals—at reading the story written in code in the strata—our understanding of this episode in Earth history and the history of life will continue to sharpen.

Acknowledgments

Thanks to Bob Reynolds for encouraging us to contribute this paper. Discussions with James Hagadorn, Jim Schiffbauer, and Emmy Smith contributed significantly to this review; their insights are gratefully acknowledged. This research has been supported in part by a grant from the Geological Society of America to M.S.

References

Berry, W.B.N., 1968, *Growth of a Prehistoric Time Scale*. San Francisco: W.H. Freeman, 158 p.

Cai, Y., Hua, H., Xiao, S., Schiffbauer, J., and Li, P., 2010, Biostratinomy of the late Ediacaran pyritized Gaojiashan Lagerstätte from southern Shaanxi, South China: Importance of event deposits. PALAIOS, v. 25, p. 487-506.

Christie-Blick, N., Levy, M., Mount, J. F., Signor, P. W. and Link, P. K., 1989, Paleontology of the Lower Cambrian Waucoban Series in Eastern California and Western Nevada. *In* Late Proterozoic and Cambrian Tectonics, Sedimentation, and Record of Metazoan Radiation in the Western United States: Pocatello, Idaho, to Reno, Nevada 20-29 July, 1989. American Geophysical Union, Washington, D. C.. doi: 10.1029/FT331p0047.

Corsetti, F.A., and Hagadorn, J.W., 2000, Precambrian-Cambrian transition: Death Valley, United States. Geology, v. 28, p. 299-302.

Corsetti, F.A., and Hagadorn, J.W., 2003, The Precambrian-Cambrian transition in the Southern Great Basin, USA. The Sedimentary Record, v. 1, no. 1, p. 4-7.

Fedonkin, M.A., Gehling, J.G., Grey, K., Narbonne, G.M., and Vickers-Rich, 2008, *The Rise of Animals: Evolution and diversification of the Kingdom Animalia*. Baltimore: Johns Hopkins University Press, 343 p.

Germs, G.J.B., 1972, New shelly fossils from Nama Group, South West Africa. American Journal of Science, v. 272, p. 752-761.

Geyer, G., and Landing, E., 2016, The Precambrian-Phanerozoic and Ediacaran-Cambrian boundaries: a historical approach to a dilemma. *In* Brasier, A.T., McIlroy, D., and McLoughlin, N., (eds.), *Earth System Evolution and Early Life: a Celebration of the Work of Martin Brasier*. Geological Society, London, Spec. Publ. 448, http://doi.org/10.1144/SP448.10.

Glaessner, M.F., 1961. Pre-Cambrian animals. Scientific American, v. 204, no. 3, p. 72-78.

Gradstein, F.M., Ogg., J.G., Schmitz, M.D., and Ogg, G.M., 2012, *The Geologic Time Scale 2012*. Amsterdam: Elsevier, 1144 p.

Grant, S.W.F., 1990, Shell structure and distribution of *Cloudina*, a potential index fossil for the terminal Proterozoic. American Journal of Science, v. 290-A, p. 261-294.

Grazhdankin, D., 2004. Patterns of distribution in the Ediacaran biotas: facies versus biogeography and evolution. Paleobiology, v. 30, no. 2, p.203-221.

Hagadorn, J.W., and Waggoner, B.M., 2000, Ediacaran fossils from the southwestern Great Basin, United States. Journal of Paleontology, v. 74, p. 349-359.

Hagadorn, J.W., Fedo, C.M., and Waggoner,B.M., 2000, Early Cambrian Ediacaran-type fossils from California: Journal of Paleontology, v. 74, p. 731-740.

Hua, H., Pratt, B., and Zhang, L., 2003, Borings in *Cloudina* Shells: Complex predator-prey dynamics in the terminal Neoproterozoic: PALAIOS, v. 18, p. 454-459.

Jensen, S., Droser, M.L., and Gehling, J.G., 2005, Trace fossil preservation and the early

evolution of animals. Palaeogeography, Paleoclimatology, Palaeolecology, v. 220, p. 19-29.

Knoll, A.H., Walter, M.R., Narbonne, G.M., Christie-Blick, N., 2006, The Ediacaran Period: a new addition to the geologic time scale. Lethaia, v. 39, p. 13-30.

Laflamme, M., Darroch, S., Tweedt, S., Peterson, K., and Erwin, D., 2013, The end of the Ediacara biota: Extinction, biotic replacement, or Cheshire Cat?. Gondwana Research, v. 23, p. 558-573.

Mens, K. 2003, Early Cambrian tubular fossils of the genus *Onuphionella* from Estonia. Proc. Estonian Acad. Sci. Geol, 52, 2, 89-97.

Mount, J.F., and Rowland, S.M., 1981, Grand Cycle A (Lower Cambrian) of the Southern Great Basin: A product of differential rates of relative sea-level change. In Taylor, M.E., ed., *Short Papers for the Second International Symposium on the Cambrian System*, U.S. Geol. Survey Open File Report 81-743, p. 143-146.

Mount, J.F., Gewirtzman, D.A., and Signor, P.W., 1983, Precambrian-Cambrian transition problem in western North America: Part I, Tommotian fauna in the southwestern Great Basin and its implications for the base of the Cambrian System. Geology, v. 11, p. 225-226.

Narbonne, G.M., 2005, The Ediacara biota: Neoproterozoic origin of animals and their ecosystem. Annual Review of Earth and Planetary Sciences, v. 33, p. 421-442.

Narbonne, G.M., and Saylor, B.Z., 1997. The youngest Ediacaran fossils from southern Africa. Journal of Paleontology, v. 71, p. 953-967

Nelson, C., 1978, Late Precambrian–Early Cambrian stratigraphic and faunal succession of eastern California and the Precambrian–Cambrian boundary: Geological Magazine, v. 115, p. 121, doi: 10.1017/s0016756800041169.

Oliver, L., 1990, Stromatolites o the Lower Cambrian Deep Spring Formation: Mount Dunfee, Esmeralda County, Nevada. M.S. thesis, University of Nevada Las Vegas, 150 p.

Rowland, S.M., and Rodriguez, M.G., 2014, A multicellular alga with exceptional preservation from the Ediacaran of Nevada. Journal of Paleontology, v. 88, p. 263-268.

Rowland, S.M., Oliver, L.K., and Hicks, M., 2008, Ediacaran and early Cambrian reefs of Esmeralda County, Nevada: Non-congruent communities within congruent ecosystems across the Neoproterozoic/Paleozoic boundary. *In* Duebendorfer, E.M., and Smith, E.I., eds., Geol. Soc. Amer. Field Guide 11, p. 83-100, doi: 10.1130/2008.fld0911(04).

Schiffbauer, J.D., 2016, The age of tubes: A window into the biological transition at the Precambrian-Cambrian boundary. Geology, v. 44, p. 975-976.

Schiffbauer, J.D., Huntley, J.W., O'Neil, G.R., Darroch, S.A.E., Laflamme, M., and Cai, Y., 2016, The Latest Ediacaran Wormworld Fauna: Setting the ecological stage for the Cambrian Explosion: GSA Today, v. 26, no. 11, p. 4-11.

Signor, P.W., III, McMenamin, M.A.S., Gewirtzman, D.A., and Mount, J.F., 1983, Two new pre-trilobite faunas from western North America. Nature, v. 303, p. 415-418.

Smith, E.F., Nelson, L.L., Strange, M.A., Eyster, A.E., Rowland, S.M., Schrag, D.P. and Macdonald, F.A., 2016a, The end of the Ediacaran: Two new exceptionally preserved body fossil assemblages from Mount Dunfee, Nevada, USA. Geology, v. 44, p. 911-914.

Smith, E.F., Nelson, L.L., Tweedt, S.M., and O'Connell, N., 2016b, A link between latest Ediacaran biotic assemblages globally: New fossil finds from the Lower Member of the Wood Canyon Formation in Death Valley. Geol. Soc. Amer. Ann. Mtg., Abstract No. 184-7.

Tarhan, L.G., Droser, M.L., Gehling, J.G., and Dzaugis, M.P., 2017, Microbial mat sandwiches and other anactualistic sedimentary features of the Ediacara Member (Rawnsley Quartzite, South Australia): Implications for interpretation of the Ediacaran sedimentary record. PALAIOS, v. 32, p. 181-194.

Taylor, M.E., 1966, Precambrian mollusc-like fossils from Inyo County, California. Science, v. 153, p. 198-201.

Vickers-Rich, P., and Komarower, P., eds., 2007, *The Rise and Fall of the Ediacaran Biota*. Bath: The Geological Society, 464 p.

Waggoner, B., and Hagadorn, J. W., 2002, New fossils from terminal Neoproterozoic strata of

Southern Nye County, Nevada. *In* Corsetti, F.A., ed., *Proterozoic–Cambrian of the Great Basin and Beyond*, pp. 87–96, SEPM Volume and Guidebook 93.

Xiao, S., 2008, Rise and demise of ghostly animals. Science, v. 319, p. 1618-1619.

A survey of lower Cambrian faunas in the southern Great Basin, California and Nevada

Robert G. Eby
3619 Underwood Street, Houston, TX 77025 bobeby@gmail.com

ABSTRACT—Fossiliferous lower Cambrian sedimentary rocks are exposed in many mountain ranges of the southern Great Basin from central Nevada southward to the central Mojave Desert and from California's White and Inyo Mountains eastward into western Utah. The fossil faunas in these rocks include, in addition to the relatively common olenelline trilobites, two other orders of trilobites, articulate and inarticulate brachiopods, hyolithids, archaeocyathids, echinoderms, small conical fossils of uncertain affinities, and remains of soft-bodied panarthropods. These fossils are in an easterly thinning wedge of sedimentary rocks formed as the Late Proterozoic to Cambrian seas prograded eastward from the continental margin onto the craton. The thickest sections, in the White and Inyo Mountains, continue upward from Proterozoic through Cambrian and higher sedimentary rocks while the thinnest sections, in the eastern areas, contain only uppermost lower Cambrian and higher sedimentary rocks.

Introduction

Charles Doolittle Walcott (1891) first suggested subdividing the Cambrian System into Lower, Middle and Upper Series. Walcott (1912) further suggested the name Waucoban be used for the lower Cambrian after fossiliferous sections near Waucoba Springs in the northern Inyo Mountains of California. Historically, the Cambrian has been subdivided on the basis of its trilobite faunas, with the lower Cambrian of most of North America defined by the range of trilobites of the suborder Olenellina. While the lower-middle Cambrian boundary was rather well defined at the extinction level of the olenellines, the base of the lower Cambrian has long been poorly defined. This is because no trilobites and few other fossils had been found below the lowest occurrence of the olenellines.

The arrangement of the continents today is very different than during the Cambrian because of the continual rearrangement of the earth's surface by plate tectonics. While most of North America, including Greenland, belonged to a single paleo-continent referred to as Laurentia, pieces of other continents have since been added and parts have been taken away. Northern Scotland was part of Laurentia that was lost when the Atlantic Ocean opened and coastal New England, the Canadian maritime provinces and eastern Newfoundland belonged to the paleo-continent Avalonia. The fossil faunas of these paleo continents seem to have been very different from one another, usually not even sharing the same families. Because of these differences, precise correlations between the continents can be quite difficult.

While the lower Cambrian had been defined by the range of the Olenellina, the sedimentary rocks below the Cambrian, the Precambrian, had historically been seen to largely lack fossils. However, with time and more study, various fossil types were recognized to consistently occur below the oldest olenellines. These older fossil types were not seen to range through the Precambrian, rather their lowest occurrences were often not far below the lowest trilobites. The progression of the recognition of the lower boundary of the Cambrian has been described with references by Palmer (1998). Presently, the International Union of Geological Sciences, through its Subcommission on Cambrian Stratigraphy, has refined and renamed the subunits of the Cambrian so that they may be recognized internationally (Gradstein, *et al*., 2012). This subdivision is shown in figure 1 where some of the series and stages have been given provisional numerical names until formal names are adopted.

Whereas the Cambrian had previously been subdivided into the three Lower, Middle and Upper Series, it is now subdivided into four series. Furthermore, another entire system, the Ediacaran, has been identified below the Cambrian. The Ediacaran is based on a fossil fauna of rare small shelly fossils of unknown affinities and enigmatic

<table>
<tr><td colspan="6">Ordovician System</td></tr>
<tr><td rowspan="11">Cambrian System</td><td>485</td><td rowspan="3">Furongian Series</td><td>Stage 10</td><td rowspan="3">"Upper" Cambrian</td><td rowspan="5"></td></tr>
<tr><td>Jiangshanian</td></tr>
<tr><td>497</td><td>Paibian</td></tr>
<tr><td rowspan="3"></td><td rowspan="3">Series 3</td><td>Guzhangian</td><td rowspan="3">"Middle" Cambrian</td></tr>
<tr><td>Drumian</td></tr>
<tr><td>509</td><td>Stage 5</td><td>Delmaran</td></tr>
<tr><td rowspan="2"></td><td rowspan="2">Series 2</td><td>Stage 4</td><td rowspan="4">"Lower" Cambrian</td><td>Dyeran</td></tr>
<tr><td>521</td><td>Stage 3</td><td>Montezuman</td></tr>
<tr><td rowspan="2"></td><td rowspan="2">Terreneuvian</td><td>Stage 2</td><td rowspan="2">Begadean</td></tr>
<tr><td>541</td><td>Fortunian</td></tr>
<tr><td colspan="6">Ediacaran System</td></tr>
</table>

Figure 1. International Cambrian zonation showing currently recognized ages of boundaries and approximate correlations to Laurentian zonation.

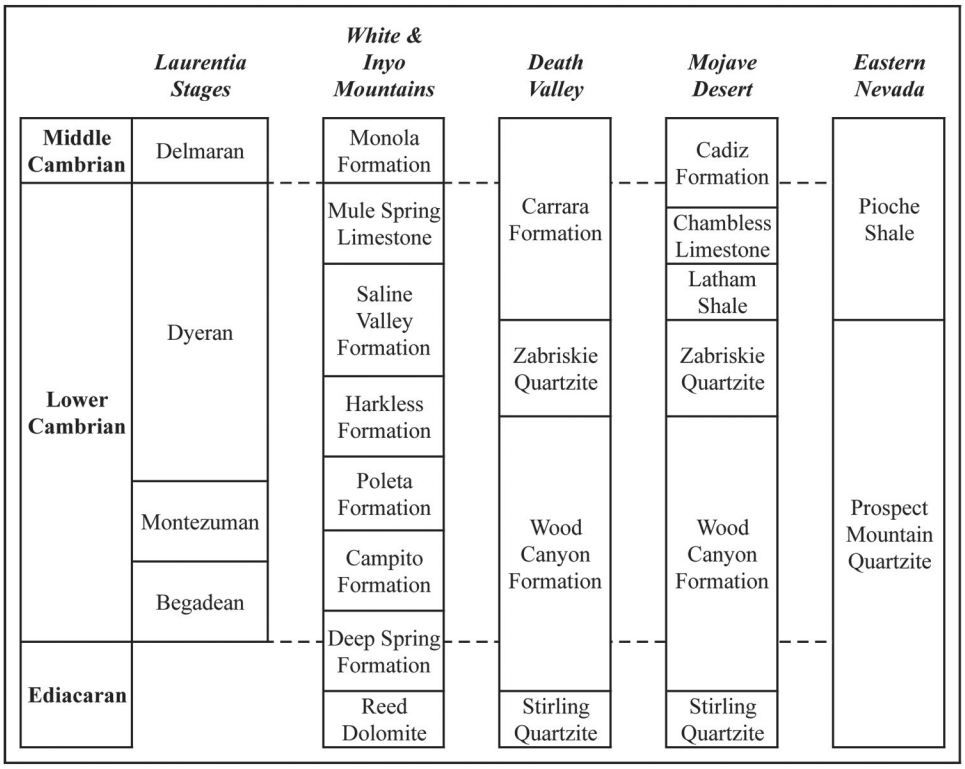

Figure 2. Correlations of the various stratigraphic units in the four areas of the Southern Great Basin areas with lower Cambrian exposures. The Laurentian lower Cambrian stages are also shown. Note that the columns here are not to scale as the upper units are somewhat thinner than the lower ones and the stratigraphic columns represented on the left are much thicker than those on the right.

impressions of soft-bodied animals in sedimentary rocks. The lowest Cambrian stage, the Fortunian of the Terreneuvian Series, is based on the earliest occurrences of trace fossils left by animals that burrowed into the sediments, the earliest being *Treptichnus pedum*. Older animals are thought to have lived on or slightly above the seafloor and did not burrow into it. The next Cambrian stage, Stage 2 of the Terreneuvian, is defined by the first occurrence of small shelly fossils, many attributable to primitive mollusks, and the heavily calcified sponge group Archaeocyatha. The Terreneuvian Series in Laurentia has been named the Begadean (Palmer, 1998) to simplify intra-continental correlation. The oldest trilobites, of the Olenellina, first appear in the following Cambrian Stage, Stage 3 of Series 2. This corresponds to the lower half of Walcott's Waucoban and has been named the Montezuman (Palmer, 1998) within Laurentia. Within Laurentia, this stage includes the range of the Olenellina but is below the range of the family Olenellidae and its genus *Olenellus*. The next higher stage, Stage 4 of Series 2, corresponds to the upper half of Walcott's Waucoban and has been named the Dyeran (Palmer, 1998, Webster, 2011a) in Laurentia. Within Laurentia, this stage is defined by the range of the Olenellida family and its *Olenellus* genus. It is overlain by the Middle Cambrian Stage 5 of Series 3, named the Delmaran in Laurentia.

Stratigraphy

The Lower Cambrian rocks in the region discussed here are exposed over an area of roughly 15,000 square miles. Stratigraphically, they range in thickness from no more than 250 meters in the southeast to well over 1,500 meters to the northwest representing an onshore to offshore distance of more than 250 miles (Stewart, 1970). Because of these great ranges, it is not surprising that coeval stratigraphic sections have greatly differing lithologies, both in detail and through the entire section. Therefore, rock units in nearby areas have been given differing formational names that have successfully been applied over many decades of research. The greatest differences in contemporaneous stratigraphic sections are seen to represent differences across depositional dip, from onshore to offshore. At the same time, stratigraphic differences along depositional strike, that is parallel to shore, are seen to be much less. In general, four areas have been taken as representing these varying distances along depositional dip and the formation names from these areas have been successfully applied along depositional strike. These four areas are: 1) the White and Inyo Mountains of California and the neighboring Esmeralda County, Nevada; 2) the area around Death Valley National Park and the Spring Mountains of Nevada; 3) the central Mojave Desert area of California and 4) the area farther north in eastern Nevada. Diagrammatic lower Cambrian stratigraphic columns for these four areas and their correlations are shown in figure 2.

Paleontology

The principal information here is shown in figures 3A and 3B. There, 12 localities in the southern Great Basin with relatively well-described lower Cambrian faunas are listed. These localities are indicated on figure 4. In figure 3A the olenelline trilobites found in these areas are listed with Xs indicating occurrences described in the available literature. Likewise, figure 3B lists the non- olenelline trilobites and the other invertebrate taxa described in the literature. Over the last few decades, the systematic relationships of the Olenellinae has been significantly

		White & Inyo Mountains, CA	Split Mountain, NV	Last Chance Range, CA	Grapevine Mountains, CA	Funeral Mountains, CA	Groom Range, NV	Eagle Mountain, CA	Resting Springs Range, CA	Nopah Range, CA	Desert Range, NV	Pioche District, NV	Marble Mountains
Olenellin Trilobites	*Arcuolenellus arcuatus*				X	X							
	Arcuolenellus megafrontalis											X	
	Bolbolenellus euryparia							X		X			
	Bolbolenellus brevispinus		X									X	
	Bristolia bristolensis		X	X		X	X	X	X	X		X	X
	Bristolia anteros		X	X	X	X	X			X	X		X
	Bristolia brachyomma									X	X		
	Bristolia fragilis		X		X	X	X	X		X	X	X	
	Bristolia harringtoni		X									X	
	Bristolia insolens		X									X	
	Bristolia mohavensis												X
	Daguinaspis sp.	X											
	Eopeachella angustispina											X	
	Fallotaspis spp.	X											
	Holmia rowei	X											
	Holmiella sp.	X											
	Laudonia prima	X											
	Lochmanolenellus gracile	X		X	X	X							
	Mesonascis cylindricus				X								
	Mesonascis fremonti					X	X	X	X	X		X	X
	Nephrolenellus multinodus				X	X	X	X	X		X	X	
	Nephrolenellus geniculatus						X					X	
	Nevadia weeksi	X											
	Nevadella addyensis	X		X	X	X							
	Nevadella baculentis	X											
	Olenellus chiefensis						X					X	
	Olenellus clarki	X			X	X	X	X	X	X	X	X	X
	Olenellus fowleri						X					X	
	Olenellus gilberti	X	X		X	X	X	X	X	X	X	X	X
	Olenellus granulatus	X											
	Olenellus howelli				X					X			
	Olenellus nevadensis	X			X	X	X		X		X	X	X
	Olenellus puertoblancoensis				X		X			X		X	X
	Olenellus terminatus						X					X	
	Olenellus sp.			X									
	Paranephrolenellus spp.											X	
	Peachella brevispina							X		X		X	
	Peachella iddingsi			X	X	X	X		X	X	X		X
	Peachella sp.	X											
	Wanneria sp.	X		X									

		White & Inyo Mountains, CA	Split Mountain, NV	Last Chance Range, CA	Grapevine Mountains, CA	Funeral Mountains, CA	Groom Range, NV	Eagle Mountain, CA	Resting Springs Range, CA	Nopah Range, CA	Desert Range, NV	Pioche District, NV	Marble Mountains
Non-Olenellin Trilobites	*Antagmus sp.*	X										X	
	Bonnia spp.	X		X									
	Crassifimbra spp.									X		X	
	Goldfieldia pacifica	X											
	Ogygopsis batis	X											
	Olenoides sp.	X											
	Oncocephalus sp.	X											X
	Oryctocephalites palmeri											X	
	Periomma sp.									X			
	Stephensaspis ativus	X											
	Syspacephalus sp.	X											
	Zacanthopsis contractus	X											
	Zacanthopsis eperephes	X											
	Zacanthopsis levis		X									X	
	Zacanthopsis palmeri											X	
	Zacanthopsis sp.						X						
Brachiopods	*Acrotreta sp.*	X										X	
	Acrothele sp.	X										X	
	Billingsella highlandensis	X											
	Dictyonina pannula											X	X
	Eothele spurri												X
	Hadrotreta primaaea												X
	Kutorgina spp.	X										X	
	Lingulella sp.	X											
	Mikwitzia occidens	X											X
	Micromitra spp.	X											
	Nisusia spp.	X											X
	Obolella spp.	X											
	Paterina prospectensis												X
	Pompekium argentium	X											
	Spinulothele dubia	X											
	Swantonia weeksi	X											X
	Wimanella highlandensis												
Echinoderms	*Gogia sp.*	X											X
	Helicoplacus spp.	X		X	X	X							
	Polyplacus kilmeri	X											
	Stromatocystites	X											
	Waucobella nelsoni	X											
	Edrioasteroidea gen. sp.	X											
Archaeocyathida		X		X	X	X	*	*	*	*	*	*	X
Hyolithes spp.		X	*	*	*	*	*	*	*	*	*	*	X
Girvanellid oncolites		X	*	*	*	*	*	*	*	*	*	*	X

Figures 3A and 3B. Tables of the occurrences of species of lower Cambrian faunas in 12 areas of the Southern Great basin. Figure 3A lists only the olenellin Trilobites and Figure 3B lists the non-olenellin trilobites and other invertebrate fossils from available literature. For each location, all lower Cambrian taxa described in the literature from there are listed regardless of their stratigraphic occurrences.

revised, with many species formerly assigned to *Olenellus* reassigned to several new genera, such as *Bolbolenellus* and *Nephrolenellus* (Palmer and Repina, 1993, Palmer, 1998 and Lieberman, 1998, 1999). The fossils listed for each location represent all the lower Cambrian species and genera described from that location, grouping together taxa from differing stratigraphic horizons. Two of the specimens listed, at the bottom of figure 3B, are shown with asterisks for most localities. That is because hyolith fossils are somewhat common in most fossiliferous sections but are not commented on because they seem to not be stratigraphically significant. The other group, girvanellid oncolites, are actually ellipsoidal to sub-spherical sedimentary features formed by cyanobacteria, such as *Girvanella*. They seem to form by overgrowths on core particles and are rolled around by water currents to become rounded. During the Cambrian, they appear to have been formed under intertidal or very shallow subtidal conditions and are rather common in shallow water limestones.

While there are more than 40 mountain ranges and other areas of significant lower Cambrian outcrops in the southern Great Basin, most have not had detailed paleontological sampling. Many of these areas have had preliminary sampling by field geologists to identify rock ages but not many more than the 12 listed here have been seriously studied paleontologically. Three of these areas have been very well studied and therefore have

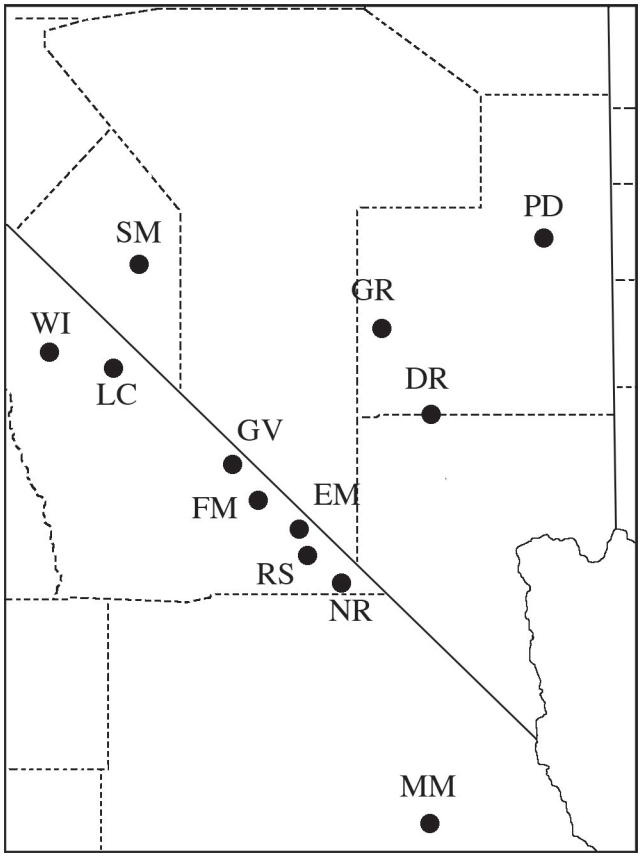

Figure 4. Map of the southern Great Basin of California and Nevada showing the general locations of the fossil localities discussed here. WI: White and Inyo Mountains; SM: Split Mountain; LC: Last Chance Range; GV: Grapevine Mountains; FM: Funeral Mountains; GR: Groom Range; EM: Eagle Mountain; RS: Resting Springs Range; NR: Nopah Range; DR: Desert range; PD: Pioche District; MM: Marble Mountains.

longer lists of described fossils. The area of the White and Inyo Mountains of California and the adjacent area in western Esmeralda County, Nevada, have been known for their Cambrian rocks since the mid 19th century. It was here that Walcott established his type section for the Waucoban stage. In addition, the University of California has long had its summer geology field camp here and generations of students have mapped the area. The district around the old mining town of Pioche, Nevada also has excellent lower Cambrian exposures that became well known because some of the uppermost lower Cambrian rocks were frequently mineralized with silver ore. Later study also found that some horizons contained silicified fossils that could be extracted by dissolving the limestone in weak acid. The third area is in the Marble Mountains of the central Mojave Desert. Although the fossiliferous interval there is relatively thin and represents only the uppermost lower Cambrian, this area seems to be so well studied because of its easy access by amateur paleontologists.

White and Inyo Mountains, California (also neighboring western Esmeralda County, Nevada) data comes from many sources, all summarized in Signor and Mount (1985). Split Mountain, Nevada data comes from Webster (2011b). Palmer and Halley (1979) provide data for the Last Chance Range, California, Grapevine Mountains, California, Funeral Mountains, California, Groom Range, Nevada, Eagle Mountain, California, Resting Springs Range, California, Nopah Range, California, and the Desert Range, Nevada. Hunt and Maybe (1966) also provided some data for the Last Chance Range, Grapevine Mountains and the Funeral Mountains, all of California. Webster *et al.* (2011) also provided data for the Groom Range, Nevada. Data for the Pioche District, Nevada come from Webster (2011c) and Palmer in Merriam (1964). Mount (1980) provided the data for the Marble Mountains, California.

References

Gradstein, F. M., Ogg, J. G., Schmitz, M. D. and Ogg, G. M., eds., 2012, The Geologic Time Scale 2012, Volume 1, Elsevier, Oxford, 1176 pp.

Hunt, C. B. and D. R. Mabey, 1966, Stratigraphy and Structure, Death Valley, California, U. S. Geol. Surv. Profess. Paper 494-A, Washington, D. C., 168 pp.

Lieberman, B. S., 1998, Cladistic analysis of the Early Cambrian olenelloid trilobites, Journal of Paleontology, 72, p. 59-78.

Lieberman, B. S., 1999, Systematic Revision of the Olenelloidea (Trilobita, Cambrian), Peabody Museum of Natural History, Yale University, Bulletin 45, 160 pp.

Merriam, C. W., 1964, Cambrian Rocks of the Pioche Mining District, Nevada, U. S. Geol. Surv. Profess. Paper 469, Washington, D. C., 63 pp.

Mount, J. D., 1980, Characteristics of Early Cambrian faunas from eastern San Bernardino County, California, So. Calif. Paleo. Soc. Spec. pub. no. 2, p. 19-23.

Palmer, A. R., 1998, Terminal Early Cambrian extinction of the Olenellina: Documentation from the Pioche Formation, Nevada: Journal of Paleontology, v. 72, p. 59-78.

Palmer, A. R. and R. B. Halley, 1979, Physical Stratigraphy and Trilobite Biostratigraphy of the Carrara Formation (Lower and Middle Cambrian) in the Southern Great Basin, U. S. Geol. Surv. Profess. Paper 1047, Washington, D. C., 171 pp.

Palmer, A. R. and L. N. Repina, 1993, Through a Glass Darkly: taxonomy, phylogeny and biostratigraphy of the Olenellina, Lawrence KS: Univ. Kans. Paleontol. Contrib., New Series 3, 35 pp.

Signor, P. W. and J. F. Mount, 1985, Lower Cambrian stratigraphic paleontology of the White–Inyo Mountains of eastern California and Esmeralda County, Nevada, p. 6-15, in Hall, C. A. and D. M. Young, eds. Natural History of the White-Inyo Range, Eastern California and Western Nevada and High Altitude Physiology, White Mtn. Res. Sta. Symp. Vol.1, 241 pp.

Stewart, J. H., 1970, Upper Precambrian and Lower Cambrian Strata in the Southern Great Basin, California and Nevada, U. S. Geol. Profess. Paper 620, Washington D. C., 212 pp.

Walcott, C. D., 1891, Correlation Papers – Cambrian, Bull. U. S. Geol. Surv. 81.

Walcott, C. D., 1912, Group terms for the Lower and Upper Cambrian series of formations, Cambrian geology and Paleontology, Smiths.Misc. Colln. 57, no. 10, p. 305-307.

Webster, M., 2011a, Trilobite biostratigraphy and sequence stratigraphy of the upper Dyeran (traditional Laurentian "Lower Cambrian") in the southern Great Basin, U. S. A., p. 121-154, in Hollingsworth, J. S., F. A. Sundberg and J. R. Foster, eds., Cambrian Stratigraphy and Paleontology of Northern Arizona and Southern Nevada: Museum of Northern Arizona Bulletin 67, Flagstaff, Arizona.

Webster, M. 2011b. Upper Dyeran litho- and biostratigraphy of the Split Mountain area, Nevada. p. 236-246, in Hollingsworth, J. S., F. A. Sundberg and J. R. Foster, eds., Cambrian Stratigraphy and Paleontology of Northern Arizona and Southern Nevada: Museum of Northern Arizona Bulletin 67, Flagstaff, Arizona.

Webster, M. 2011c. Litho- and biostratigraphy of the Dyeran-Delamaran boundary interval in the Pioche-Caliente region, Nevada. p. 203-215 *in* J. S. Hollingsworth, J. S., F. A. Sundberg, and J. R. Foster, eds., *Cambrian Stratigraphy and Paleontology of Northern Arizona and Southern Nevada*. Museum of Northern Arizona Bulletin **67**, Flagstaff, Arizona.

Webster, M., L. B. McCollum, and F. A. Sundberg. 2011. Upper Dyeran and Lower Delamaran litho- and biostratigraphy of the northern Groom Range, Nevada. p. 226-236, *in* J. S. Hollingsworth, J. S., F. A. Sundberg, and J. R. Foster, eds., *Cambrian Stratigraphy and Paleontology of Northern Arizona and Southern Nevada*. Museum of Northern Arizona Bulletin **67**, Flagstaff, Arizona.

Biostratigraphy of nonmarine Miocene gastropods from the Barstow Formation of California

William F. Abersek [1] and Donald L. Lofgren [2]
[1] *The Webb Schools, Claremont, California 91711*
[2] *Raymond M. Alf Museum of Paleontology, Claremont, California 91711*

Introduction

The Barstow Formation comprises a concave belt of alluvial and lacustrine sediment, extending for 83 km between the Gravel Hills on the west and the Cronese Basin on the east in the Mojave Desert of California (Woodburne et al., 1990). The formation is best known for its fossil rich outcrops located within the Mud Hills, approximately 10 miles north of Barstow, California (Figure 1). Besides an abundance of vertebrate fossils, the Barstow Formation has yielded a considerable number of Miocene gastropods (Taylor, 1954; Plyley et al., 2013; Abersek et al., 2016).

The earliest work on gastropods from the Barstow Formation was by Dwight Taylor who attended Webb School of California, a secondary school in Claremont, California, in the late 1940s. He worked closely with Raymond Alf, a paleontologist/science teacher who eventually founded the museum that bears his name on the Webb campus. Shortly after completing his undergraduate degree, Taylor (1954) published his study of Barstow Formation gastropods, describing eight species from seven localities, four of which were new.

Beginning in the early 1990s, crews from the Raymond M. Alf Museum of Paleontology (RAM) have made significant collections of gastropods from the Barstow Formation. These collections were briefly described by Plyley et al. (2013) and compared to gastropods from the Temblor Formation of central California. Soon thereafter, description of gastropods from the Lake Bed locality (locality 3 of Taylor, 1954) and the geologic setting and paleoecology of the site, were provided by Abersek et al. (2016). However, the remainder of the RAM gastropod collection from the Barstow Formation has not been described. Also, in contrast to detailed biostratigraphic studies of the mammalian fauna of the Barstow Formation (Woodburne et al., 1990; Pagnac, 2009), a biostratigraphic analysis of gastropods from the formation has yet to appear.

Here, we document the lithostratigraphic position of RAM gastropods from the Lake Bed site (Abersek et al., 2016) and hundreds of other specimens from six RAM additional localities in the Barstow Formation. Based on these data, we provide the first biostratigraphic analysis of gastropods from the Barstow Formation. Detailed description of the entire RAM Barstow Formation mollusk collection will appear soon (Lofgren et al., in preparation).

Materials and methods

Gastropods in the RAM collections are from seven localities in the Barstow Formation: the Lake Bed (RAM V200025), Slug Bed (RAM V200515, RAM V94183), Chert Ridge Quarry (RAM V201202), Snail Farm (RAM V201201), *Helminthoglypta alfi* Type Locality (RAM V200114), Quarry 5 (RAM I99015), and the Bird Bone Bed (RAM V98004). The RAM collection has representatives of all eight of the gastropod species described by Taylor (1954) and one unnamed new taxon. Significant efforts to identify the RAM gastropod collection began with Plyley et al. (2013). A description of all nine species was presented by Abersek et al. (2016) based on specimens from the Lake Bed locality. Specimens from the other six localities were identified using the figures and descriptions provided in Abersek et al. (2016).
Measurements of the stratigraphic sections discussed in the text or shown in Figure 2 were compiled thusly: V98004 and Easter Quarry sections, November 2010, by D. L. Lofgren and P. Liskanich; Lake Bed section, November 2015, by D. L. Lofgren, W. F. Abersek, and M. Fassler; Chert Ridge Quarry (and Snail Ridge), Slug Bed, *Hemicyon* Tuff, and Unnamed Faulted sections,

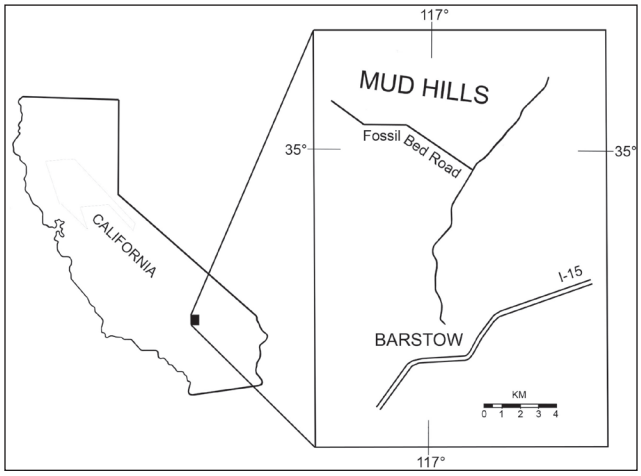

Figure 1. Location of the Barstow Formation within the Mud Hills, Mojave Desert, California (adapted from Steinen 1966).

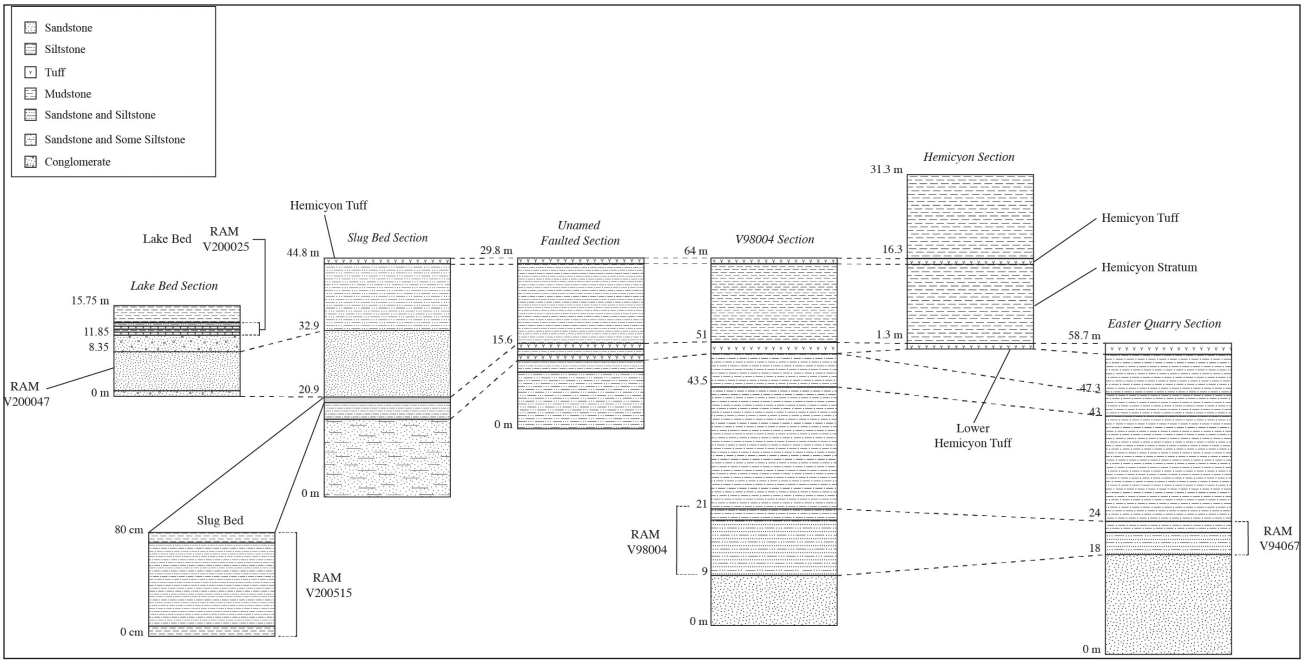

Figure 2. Correlation of stratigraphic sections from the upper member of the Barstow Formation showing lateral relationships between major gastropod-bearing sites and the *Hemicyon* Tuff along Fullers Earth Canyon and outcrops to the east (SE 1/4 section 15 and SW 1/4 Section 14, township 11 north, range 2 west); Easter Quarry Section about 1.8 km east of Lake Bed Section, strata thicknesses in meters, except for Slug Bed locality (V200515) detail which is in centimeters.

October 2016, by W. F. Abersek and D. L. Lofgren. Figure 2 includes standard rock textures provided by the United States Geological Survey. A standard Jacob's staff was used to measure all stratigraphic sections in meters. General geographic locations for RAM gastropod localities are given in Figure 2 or in text; GPS coordinates available to qualified investigators by request.

RAM Barstow Formation gastropod localities

Abersek et al. (2016) and Taylor (1954) identified eight mollusk species from the Barstow Formation, two of which are conically spiraled (*Lymnaea mohaveana* and *Lymnaea megasoma*) and five of which are discoidally spiraled (*Helminthoglypta alfi*, *Menetus micromphalus*, *Planorbula mojavensis*, *Pristiloma chersinellum*, and *Vallonia cyclophorella*). The other species is the 'slug' *Craterarion pachyostracon*. Abersek et al. (2016) also identified an unnamed discoidal gastropod and described it as "species indeterminate," although it bears some similarity to *Helminthoglypta alfi*.

Of the seven Barstow localities where RAM crews recovered gastropods, the Lake Bed locality (RAM locality V200025) has the most diverse number of species (Figure 3) and its most common is the aquatic species *Lymnaea mohaveana* (Abersek et al., 2016). The Lake Bed is also the type locality of *Lymnaea mohaveana*, *Craterarion pachyostracon*, and *Menetus micromphalus* (Taylor, 1954), and the only locality where "species indeterminate" has been found (Abersek et al., 2016). *Craterarion pachyostracon* is extremely common at the Slug Bed (RAM localities V200515 and V94183) (Figure 3), but this site was as yet undiscovered when Taylor (1954) completed his study of Barstow Formation gastropods.

The seven RAM localities that yield gastropods are described below. The Lake Bed, the Slug Bed, and the Bird Bone Bed (RAM locality V98004) are shown in their stratigraphic positions in relation to one another and to the *Hemicyon* Tuff (Figure 2). The four others are discussed in relation to their stratigraphic position compared to the Skyline or Oreodont tuffs. All RAM sites are in the upper member of the Barstow Formation except for Quarry 5, which is in the middle member.

Lake Bed, RAM Locality V200025 (locality 3 of Taylor, 1954). The Lake Bed is composed of 40-50 cm of brown mudstone with thin beds of siltstone located between two 4 cm thick tuffaceous marls (Abersek et al., 2016). Fossil mammals and gastropods are both abundant in the Lake Bed and all of the nine known gastropod taxa from the Barstow Formation are present at the site (Figure 3) (Abersek et al., 2016). A 15.75 m thick section encompasses the Lake Bed which is in an arroyo referred to as Bird Canyon (see map in Lindsay, 1972: fig. 1). Based on approximate stratigraphic position, the Lake Bed locality is certainly stratigraphically below the *Hemicyon* Tuff (equals *Hemicyon* Tuff of Woodburne et al., 1990, which overlies the *Hemicyon* stratum containing abundant mammals). But the top of the Lake Bed section is faulted just above the locality, so the available outcrop does not preserve the relative stratigraphic positions of the Lake Bed and *Hemicyon* Tuff (Figure 2). Lindsay (1972) estimated that the Lake Bed was about 10 m below the *Hemicyon* Tuff and this seems to be reasonable based on

extrapolated lithostratigraphic correlations from the Slug Bed section (Figure 2). The base of the Lake Bed section is also faulted so that highly disturbed remnants of Slug Bed sediment occur on the fault scarp in Bird Canyon.

Slug Bed, RAM Locality V200515 and V94183. The Slug Bed is composed of about 80 cm of siltstone and mudstone (Figure 2) in which specimens of the slug *Craterarion pachyostracon* abound. A few specimens of *C. pachyostracon* were also recovered from the Lake Bed (Figure 3), but this rare taxon has not been reported elsewhere in North America. Unlike most other gastropod bearing sites in the Barstow Formation, specimens of species other than *C. pachyostracon* at the Slug Bed are very fragile and are destroyed as they erode. Thus, only one adult specimen of *Lymnaea mohaveana* has been recovered, except for a possible crushed specimen of *Helminthoglypta alfi* (Figure 3).

Many small elements of mammals occur in the Slug Bed, the most common of which are isolated teeth or jaw fragments of a beaver identified by Lindsay (1972) as *Monosaulux pansus*. The 44.8 m Slug Bed section indicates that the *Hemicyon* Tuff is about 23 m above the Slug Bed (Figure 2). Also, extrapolating strata from the V98004 section and Unnamed Faulted section between the V98004 and Slug Bed sections, the Slug Bed appears to be approximately laterally equivalent to the Lower *Hemicyon* Tuff (Figure 2). The throw of the fault between the Slug Bed section and the Unnamed Faulted section is about 29 m, but stratigraphic units can be easily traced across this fault because of excellent exposures. Similarly, there is another fault between the Unnamed Faulted section and the V98004 section, but the Lower *Hemicyon* Tuff and *Hemicyon* Tuff are laterally traceable across the fault (Figure 2).

RAM Locality V98004, Bird Bone Bed. The V98004 section is 64 m thick and encompasses the Lower *Hemicyon* Tuff, *Hemicyon* Tuff, and RAM locality V98004, which is composed of 12 m of mostly siltstone (Figure 2) that has yielded a rich mammalian fauna (Lofgren et al, 2014). The V98004 stratigraphic interval yielded the holotype of *Megahippus mckennai* (Tedford and Alf, 1962) and an M2 of the proboscidean *Gomphotherium*, the oldest known record of this taxon from the Barstow Formation (Lofgren et al., 2010; Lofgren et al., 2012). The site is also notable for its large concentration of small vertebrate bones in a 10 cm thick siltstone lens (one meter in width), of which over 50% are avian elements (Lofgren et al., 2014). Three specimens of *Helminthoglypta alfi* were also recovered from this siltstone lens (Figure 3).

The two tuffs and other strata from the V98004 section can be traced to the east across a couple of minor faults to the *Hemicyon* Stratum and Easter Quarry sections, which contain the Frick Quarry sites of the same names. Specimens from Easter Quarry and the *Hemicyon* Stratum (often called *Hemicyon* Quarry) are housed at the American Museum of Natural History in New York. The fossil rich *Hemicyon* Stratum occurs high in the 15 m interval of strata between the Lower *Hemicyon* Tuff and *Hemicyon* Tuff, but this same interval in the V98004 section is not significantly fossiliferous. Also, 6 m of the Easter Quarry section are laterally equivalent to strata that comprise RAM locality V98004 (Figure 2) and the two

	Lake Bed V200025	Slug Bed V200515	Chert Ridge Quarry V201202	Snail Farm V201201	*H. alfi* Type Locality V200114	Quarry 5 I99015	Bird Bone Bed V98004
Lymnaea mohaveana	321	1					
Lymnaea megasoma	15		4				
Craterarion pachyostracon	5	Approx. 5000					
Helminthoglypta alfi	3	1			144		3
Menetus micromphalus	3		1		2		
Planorbula mojavensis	14		122	72	1	1	
Pristiloma chersinellum	41						
Vallonia cyclophorella	2				1		
Species Indeterminate	3						

Figure 3. Number of specimens per gastropod taxon recovered from the seven RAM localities. Stratigraphic position of sites shown in Figure 2 or discussed in text.

intervals have a similar concentration of well preserved, black-gray fossils. The 6 m interval in the Easter Quarry section is known as RAM locality V94067 (Lofgren et al., 2014) and the Frick Easter Quarry is located in the upper part of this 6 m interval.

Chert Ridge Quarry, RAM Locality V201202 (SE ¼, Section 9, Township 11 north, Range 2 west). Chert Ridge Quarry is another Frick quarry, but actually is three quarries spaced about 200 meters laterally that were centered on excavation of a bone rich tuffaceous siltstone. The middle quarry produces 95% of the gastropod specimens found by RAM crews. Measuring up from the Skyline Tuff (50 cm thick and well exposed in this area), RAM locality V201202 is about 39 m above the Skyline Tuff. The *Hemicyon* Tuff is mapped in this vicinity (Woodburne et al., 1990), but a number of tuffs were found above the Skyline Tuff and we could not distinguish which was the *Hemicyon* Tuff. Chert Ridge Quarry (V201202) yielded more than one hundred gastropods, over 90% of which were *Planorbula mojavensis* (Figure 3). Four specimens of *Lymnaea megasoma* and a single specimen of *Menetus micromphalus* were also recovered.

Snail Farm, RAM Locality V201201 (SE ¼, Section 9, Township 11 north, Range 2 west). This site is about 200 m east of Chert Ridge Quarry (V201202) and is in a tuffaceous siltstone that is approximately stratigraphically equivalent to the one represented by V201202. Seventy two specimens of *Planorbula mojavensis* were collected from the Snail Farm (V201201), but no other species were found.

Helminthoglypta alfi Type Locality, RAM Locality V200114 (locality 1 of Taylor, 1954) (NW ¼, Section 24, Township 11 north, Range 2 west). This site is within Rainbow Basin and is stratigraphically equivalent to the type locality of *Dyseohyus fricki*, a species of peccary described by Stock (1937) and Woodburne (1969). Raymond Alf and his student Bill Webb found the skull and jaw fragments of this peccary in 1936 and donated them to Stock at the California Institute of Technology (Lofgren and Anand, 2010). The type locality of *H. alfi* is about 105 m above the Skyline Tuff. The *Hemicyon* Tuff does not extend into Rainbow Basin (Woodburne et al., 1990), so determining the stratigraphic position of V200114 relative to the *Hemicyon* Tuff is not possible. Taylor (1954) only recovered *H. alfi* from this site, but RAM crews have collected two specimens of *Menetus micromphalus*, and one each of *Planorbula mojavensis* and *Vallonia cyclophorella* (Figure 3). However, the site is indeed dominated by *H. alfi* as 144 specimens are present in the RAM collections.

Quarry 5, RAM Locality I99015 and V94026 (NE ¼, Section 23, Township 11 north, Range 2 west). Quarry 5 represents a channel lag deposit about 10 m above the Oreodont Tuff, based on mapping by Woodburne et al. (1990). This channel fill contains a high concentration of bone (elements often water worn) and was discovered and excavated by Ray Alf and Webb students for over two decades (Lofgren and Anand, 2010). Only *Planorbula mojavensis* is known from the site; this record is based on a single specimen, the only gastropod in the RAM collections from the middle member of the Barstow Formation.

Gastropod biostratigraphy and discussion

The stratigraphic ranges of the nine gastropod species from seven RAM localities are shown in Figure 4. All of the species occur in the upper member of the Barstow Formation in outcrops stratigraphically between the Skyline Tuff and the *Hemicyon* Tuff (Figure 2 and 4). These taxa comprise an upper member interval characterized by the co-occurrence of *Lymnaea mohaveana*, *Lymnaea megasoma*, *Helminthoglypta alfi*, *Menetus micromphalus*, *Planorbula mojavensis*, *Pristiloma chersinellum*, *Vallonia cyclophorella*, and *Craterarion pachyostracon*. Although little is currently known about the gastropod assemblages of the middle or Owl Conglomerate members of the Barstow Formation, and upper member gastropod zone could be loosely defined as those taxa that occur between the Skyline Tuff and *Hemicyon* Tuff (Figure 4). Thus, it would be equivalent to the lower half (interval between the Dated Tuff and *Hemicyon* Tuff) of the *Megahippus mckennai*/*Merycodus necatu*s Interval Zone of Pagnac (2009: fig. 3) of the Ba 2 biochron, a biostratigraphic zonation based on mammalian megafauna (Tedford et al., 2004). The geochronology of this gastropod "zone" would span a little less than 1.0 Ma, as although the Skyline Tuff has not been dated, the Dated Tuff in Rainbow Basin (only 18 m above Skyline Tuff) is about 14.8 Ma and the *Hemicyon* Tuff is about 14.0 Ma (Woodburne et al., 1990).

The only gastropod recovered from the middle member in the RAM collections is a specimen of *Planorbula mojavensis* from Quarry 5, a site about 10 m above the Oreodont Tuff (Figure 4). Thus, definition of a gastropod zone for the middle member is not possible and it is not known if taxa from the "upper member zone" occur lower in the section, except for *P. mojavensis*. The Oreodont Tuff has been dated at 15.9 Ma (Woodburne et al., 1990) and all that can be determined thus far is that the geochronologic range of *P. mojavensis* spans about 2 Ma (15.9 Ma to 14.0 Ma) based on its occurrence in both the upper and middle members of the Barstow Formation.

The middle member is similar to the upper member in that both are highly fossiliferous at certain outcrops and have yielded a very large number of fossil vertebrates, mainly mammals. However, even after extensive prospecting of outcrops of the middle member in the Rainbow Basin and Coon Canyon areas for more than two decades by RAM crews, only the single specimen of *Planorbula mojavensis* was found. The reason for this is not clear, but may be related to depositional setting.

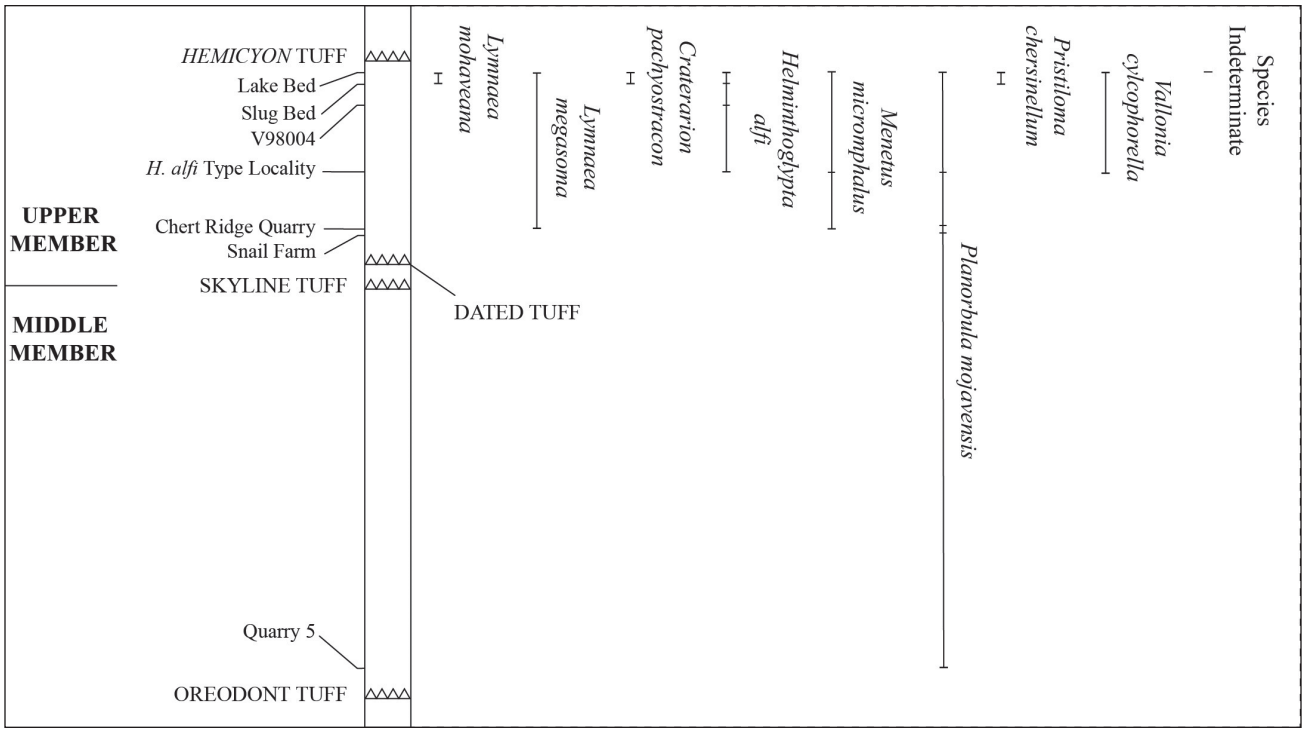

Figure 4. Stratigraphic ranges of gastropods based on taxa recovered from seven RAM localities that occur in either the middle or upper members of the Barstow Formation Isotopic dates of the *Hemicyon* Tuff and Oreodont Tuff are about 14.0 Ma and 15.8 Ma respectively (Woodburne et al., 1990). Only a single specimen of Planorbula mojavensis is known from the middle member.

The upper member is composed mostly of lacustrine sediments, with minor coarse grained clastic beds (Woodburne at al., 1990) and all the RAM sites in the upper member appear to represent lacustrine deposits. The middle member between the Oreodont and Skyline tuffs in the Rainbow Loop area is composed mainly of alluvial and conglomeratic sandstone (Woodburne et al., 1990), and between Rainbow Basin and Coon Canyon some of the vertebrate bearing units are clearly channel fill deposits containing abundant bone (Quarry 5, for example). Thus, the difference in the number of gastropods recovered from the two members may be related to their differences in depositional setting.

Mammalian faunal differences are significant between the middle and upper members of the Barstow Formation (Pagnac, 2009: fig. 3). One explanation is that about 15 million years ago, shrubs and deciduous hardwoods were replaced by tougher foliage as the result of climatic warming and a decrease in precipitation, so mammals with teeth adapted to soft vegetation disappeared from the Barstow region (Pagnac and Reynolds, 2006). It would be interesting to test this hypothesis by contrasting gastropods from the middle and upper members to see if these gastropod assemblages differ significantly. Climatic differences that apparently affected the Barstow Formation mammalian assemblage about 15 Ma may have had little effect or a major effect on invertebrate assemblages. This can't be addressed based on the RAM collections, as the RAM biostratigraphic record of gastropods is almost entirely limited to the upper member of the formation. We recommend that this study be extended to the collections of other institutions that have a significant number of well documented Barstow Formation gastropods to address this issue.

This is the third paper in a series concerning gastropod paleontology of the Barstow Formation based on RAM collections (Plyley et al., 2013; Abersek et al., 2016). In the future, RAM field crews will be concentrating on recovery of gastropods and other invertebrates from the middle member of the Barstow Formation.

Acknowledgments

We thank students and faculty of The Webb Schools who assisted in collecting the RAM gastropod sample from the Barstow Formation. We also thank J. Shearer and the Barstow Field Office of the California Bureau of Land Management for permits, M. Woodburne for reviewing the manuscript, and the Mary Stuart Rogers Foundation and Augustyn Family Fund for financial support.

References

Abersek, W. F., Fassler, M. L., and D. L. Lofgren. 2016. Nonmarine Gastropods from the Lake Bed Locality, Upper Member, Barstow Formation, California. Pp. 276-283, in R. E. Reynolds (ed.), Going Loco, investigations along the Colorado River. The 2016 Desert Symposium Field Guide and Proceedings, California State University Desert Studies Consortium.

Lindsay, E. H., 1972. Small mammal fossils from the Barstow Formation, California. University of California Publications in Geological Sciences 93:1-104.

Lofgren, D. L., and R. S. Anand. 2010. 75 years of fieldwork in the Barstow Formation by the Raymond Alf Museum of Paleontology. Pp. 169-176, in Reynolds, R. E. and D. M.

Miller (eds.), Overboard in the Mojave, 20 million years of lakes and wetlands and abstracts of proceedings of the 2010 Desert Symposium, California State University Desert Studies Consortium.

Lofgren, D. L., Hess, A., Silver, D., and P. Liskanich, 2012. Review of proboscideans from the Middle Miocene Barstow Formation of California. Pp. 125-134, in: R.E. Reynolds (ed.). Search for the Pliocene: the southern exposures. The 2012 Desert Symposium Field Guide and Proceedings, California State University Desert Studies Consortium.

Lofgren, D. L., Kwon, C. Todd, J., Marquez, S., Holliday A., Stoddard, R. and P. Kloess. 2014. Preliminary analysis of an important vertebrate bearing horizon with abundant avian material from the upper member of the Barstow Formation of California. Pp. 155-164, in R. E. Reynolds (ed.), Not a drop left to drink. The 2014 Desert Symposium Field Guide and Proceedings, California State University Desert Studies Consortium.

Lofgren, D. L., Pagnac, D., Liskanich, P., Hess, A., and D. Silver. 2010. Proboscideans from the Middle Miocene Barstow Formation of California. Journal of Vertebrate Paleontology, Programs and Abstracts 2010:146.

Pagnac, D. C., 2009. Revised large mammal biostratigraphy and biochronology of the Barstow Formation (Middle Miocene), California. Paleobios 29:48-59.

Pagnac, D. C. and R. E. Reynolds. 2006. The Fossil Mammals of the Barstow Formation. Pp. 65-70, in R. E. Reynolds (ed.), Making Tracks Across the Southwest. The 2006 Desert Symposium Field Guide and Abstracts from Proceedings, California State University Desert Studies Consortium.

Plyley, A. S., Lofgren, D. L., and A. A. Farke, 2013. Nonmarine gastropods from the Temblor and Barstow formations of California. Pp. 68-72, in R. E. Reynolds (ed.), Raising Questions in the Central Mojave Desert. The 2013 Desert Symposium Field Guide and Proceedings, California State University Desert Studies Consortium.

Steinen, R. P., 1966. Stratigraphy of the middle and upper Miocene, Barstow Formation, California. (m.s. thesis): University of California-Riverside, 150 pp.

Stock, C. A., 1937. A peccary skull from the Barstow Miocene, California. National Academy of Sciences Proceedings 23:398-404.

Taylor, D. W., 1954. Nonmarine mollusks from the Barstow Formation of Southern California. United States Geological Survey Professional Paper 254–C: 57-80.

Tedford, R. H., and R. M. Alf. 1962. A new *Megahippus* from the Barstow Formation, San Bernardino County, California. Bulletin of the Southern California Academy of Sciences 61:113-122.

Tedford, R. H., Albright III, L. B., Barnosky, A. D., Ferrusquia-Villafranca, I., Hunt Jr., R. M., Storer, J. S., Swisher II, C. C., Voorhies, M. R., Webb S. D., and D. P. Whistler. 2004. Mammalian biochronology of the Arikareean through Hemphillian interval (late Oligocene through early Pliocene epochs). Pp. 169-231, in M. O Woodburne (ed.), Late Cretaceous and Cenozoic mammals of North America. Columbia University Press, New York.

Woodburne, M. O., 1969. Systematics, biogeography, and evolution of *Cynorca* and *Dyseohyus* (Tayassuidae). Bulletin of the American Museum of Natural History 141:271-356.

Woodburne, M. O., Tedford, R. H. and C. C. Swisher III. 1990. Lithostratigraphy, biostratigraphy, and geochronology of the Barstow Formation, Mojave Desert, southern California. Geological Society of America Bulletin 102:459-477.

Environments of the Barstow Formation in the Mud Hills, southeastern California

Katharine M. Loughney[1,2]
[1] *Museum of Paleontology, University of Michigan, 1109 Geddes Ave., Ann Arbor, MI 48109*
[2] *Department of Earth & Environmental Sciences, University of Michigan, 1100 North University Ave., Ann Arbor, MI 48109*

ABSTRACT—Environmental and geochemical proxies such as phytoliths and biomarkers permit the reconstruction of past environmental conditions. In the middle Miocene Barstow Formation, such proxies reveal that environments changed over time from alluvial fan and playa lakes to extensive floodplains and wetlands. Vegetation was dominated by trees and shrubs during most of this time, and habitats varied between woodlands and forested grasslands. Open habitat grasses became more prevalent near the top of the depositional sequence where forested grasslands covered the landscape. Habitats became more favorable for mammals and sites of fossil preservation increased along with this environmental transition.

Introduction

The Barstow Formation (19.3 – 13.3 Ma) in the Mojave Desert of southern California (Fig. 1) was deposited during the height of Neogene tectonic and volcanic activity in western North America. The Middle Miocene Climatic Optimum (MMCO; ~17–14 Ma), an interval of global warming, also occurred during the deposition of the Barstow Formation. The Barstow Formation has higher mammal diversity than any other middle Miocene formation from the Great Basin (Badgley et al., 2015), indicating that environments of deposition were attractive habitats for mammals or were conducive to fossil preservation.

In this paper, I summarize the results of my ongoing research on environmental change through the deposition of the Barstow Formation. This work is part of recent efforts by numerous workers to examine Miocene faunal change (Pagnac, 2009; Woodburne and Reynolds, 2010; Badgley et al., 2015) and to reconstruct paleoenvironments in the Mojave region (Reynolds et al., 2010; Smiley et al., 2015; Loughney and Smith, 2015; Smiley et al., in review; Loughney and Badgley, in review). Through these efforts, we are better able to understand how the fauna and environments of the Mojave relate to other North American Miocene settings.

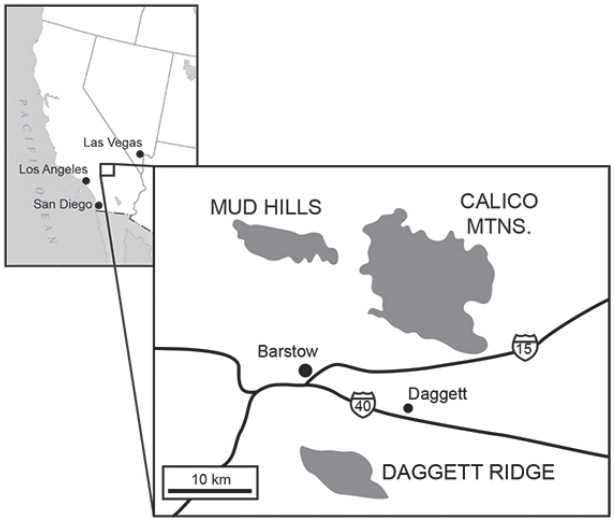

Figure 1. Map showing location of outcrops of the Barstow Formation near Barstow, California.

Tectonics and climate are the main drivers of sedimentation in interior basins (Shanley and McCabe, 1994) and serve as major controls on local environments and the plants and animals that are able to inhabit the area. As tectonic activity in the central Mojave region declined, depositional environments changed. Facies analysis and environmental proxies permit the reconstruction of vegetation and broad environmental conditions through the deposition of the Barstow Formation (Loughney and Badgley, in review). Environmental change is reflected in the stratigraphy of the Barstow Formation in the Mud Hills, which fines upward from coarse sandstone and conglomerate low in the section to mudstone near the top of the sequence (Fig. 2). Paleoenvironmental indicators sampled directly from sediment also provide important insight into how depositional environments changed through these tectonic and climatic transitions. These environments varied in their potential as habitat for plants and animals and as settings that preserve fossils.

Geological background

The Basin and Range physiographic province was created during widespread Neogene extension between ~35 – 14 Ma (McQuarrie and Wernicke, 2005; Dickinson, 2002). During this time, the highly dissected terrain of the Basin and Range physiographic province formed through detachment-style faulting, resulting in many geographically restricted basins. The Mojave tectonic block in southeastern California contains numerous

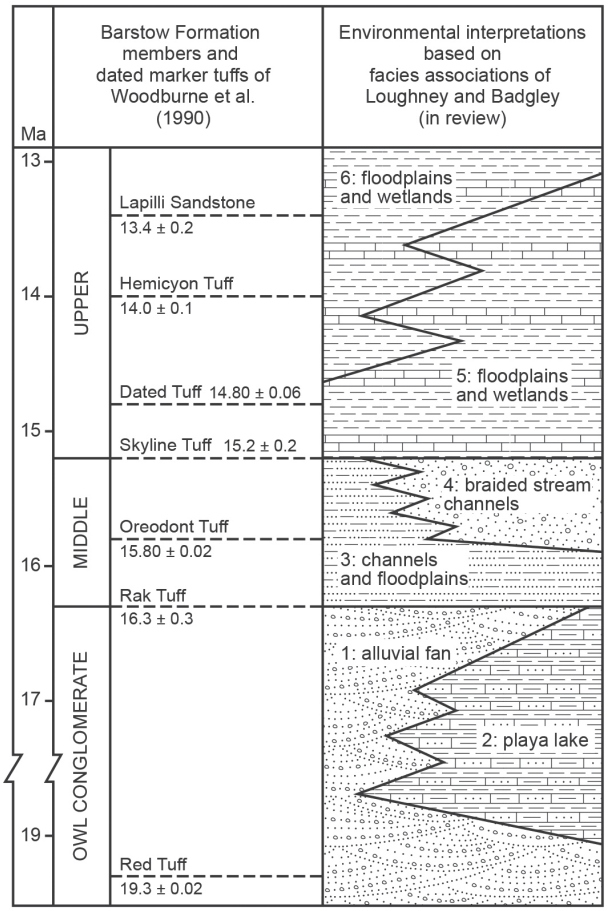

Figure 2. Stratigraphy and geochronology of the Barstow Formation, with lithological members, ages of dated tuff units, lithostratigraphy, and correlation to facies associations of Loughney and Badgley (in review).

depositional basins that formed during regional extension in the early Miocene (~23 – 18 Ma; Glazner et al. 2002), which were then filled with sediment through the middle to late Miocene. The Barstow Formation in the central Mojave Desert (Fig. 1) was deposited in one such basin during the middle Miocene.

The Barstow Formation is divided into three members on the basis of broad differences in lithology (Fig. 2; Woodburne et al., 1990). The Owl Conglomerate Member is characterized by conglomerate and sandstone, the Middle Member is characterized by sandstone and mudstone, and the Upper Member is characterized by mudstone and marl. Within these members, the facies can be grouped into facies associations that represent the dominant alluvial processes and environments at the time of deposition (Loughney and Badgley, in review).

Fossil localities (vertebrate, plant, and trace fossils) are present throughout the Barstow Formation in the Mud Hills, with the majority of localities occurring in the Upper Member. Of 149 representative localities examined, 80% are in the upper part of the formation (Table 1). The lateral and vertical distribution of facies associations, the evidence for vegetation, and the increasing number of fossil localities indicate that environments became more hospitable to plants and animals over time.

Environmental reconstruction

Three different sources of information provide a basis for inferring changes in paleoenvironments in the Barstow Formation: facies analysis, stable isotopes of carbon and hydrogen from biomarkers, and phytoliths. Sediment samples for biomarker and phytolith analyses were collected throughout the formation from each major facies association (Fig. 3).

Compound-specific biomarkers are plant-derived biomolecule residues that provide evidence of paleovegetation. Aquatic and terrestrial plants produce carbon chains of varying lengths in varying abundance (Freeman and Pancost, 2014). The average carbon chain length (ACL) of a sample is indicative of the types of plants contributing to the sample, such that grasses produce many odd-numbered chains of 31-35 carbon atoms, and trees and other woody plants produce odd-numbered chains of 25-35 carbon atoms (Freeman and Pancost, 2014).

Isotopic ratios of carbon and hydrogen can be measured from biomarkers and are used to interpret plant functional types and the environmental conditions under which plants grew. Fractionation differences between C_3 and C_4 photosynthetic pathways result in broad differences in $\delta^{13}C$ values for different functional types. In modern ecosystems, isotopic values from C_3 plants (trees, shrubs, some grasses) range from -35‰ to -22‰, and values of C_4 grasses range from -19‰ to -9‰ (Koch, 1998). Hydrogen isotopes are used to reconstruct relative moisture availability, with more negative values indicating wetter conditions and more positive values indicating drier conditions.

Phytoliths are microscopic silica bodies that are precipitated in the cells of plants. These bodies can be taxonomically diagnostic and are used to reconstruct vegetation and habitat composition (Piperno, 2006). Phytoliths derived from trees and woody plants are grouped as forest indicators (FI) and grass silica short cells (GSSCs) are produced by open- and closed-habitat grasses. The ratio between FI and GSSC phytoliths is used to reconstruct the amount of woody cover on the landscape and whether habitats are open- or closed- canopied (Strömberg, 2002).

Barstow paleoenvironments

Values of carbon and hydrogen isotopes from biomarkers sampled in the Mud Hills varied through the Barstow Formation. Mean carbon isotope values range from -29.8‰ to -25.5‰ (Fig. 4), indicating that environments were dominated by C_3 vegetation—likely a combination of trees, shrubs, and grasses—over the depositional history of the formation. Average ACL values indicate that biomarkers were derived mainly from trees or shrubs, with minor input of longer chain lengths from grasses.

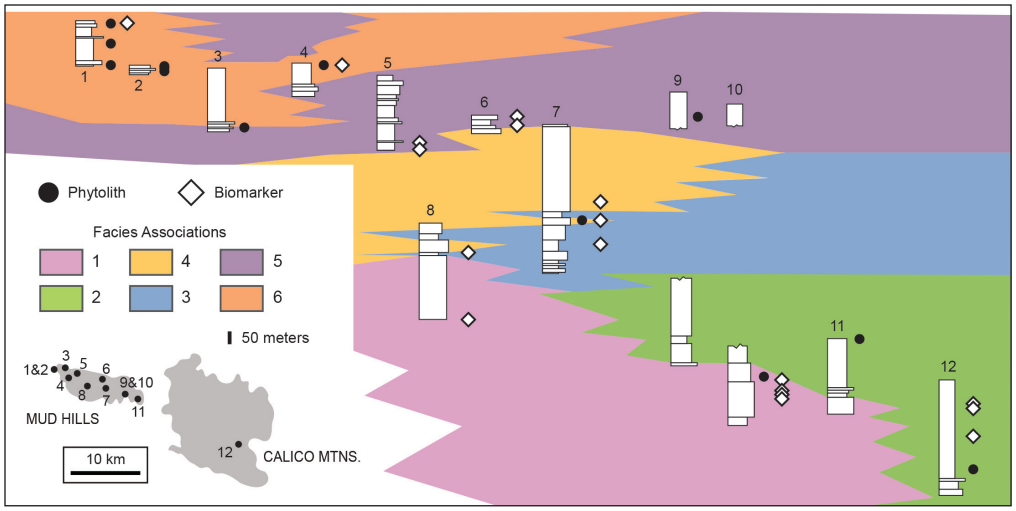

Figure 3. Stratigraphic sections measured in the Mud Hills and Calico Mountains showing the distribution of major facies associations and locations of phytolith and biomarker samples. Modified from Loughney and Badgley (in review).

Hydrogen values range from -203‰ to -167‰ (Fig. 4), reflecting local differences in moisture availability across the Barstow landscape and among facies associations.

Facies association 1 is roughly equivalent to the Owl Conglomerate Member in the Mud Hills; it is characterized by thick conglomerate and coarse sandstone representing the deposits of alluvial fans (Fig. 2). Facies association 1 grades laterally into facies association 2 in the eastern Mud Hills (Fig. 3). Facies association 2 includes thick sequences of alternating thin-bedded claystone, sandstone, and marl deposited in a large playa lake (Reynolds et al., 2010) that was contemporaneous with the alluvial fan deposits of facies association 1 (Loughney and Badgley, in review). Biomarkers from facies association 1 indicate that these environments were dominated by C_3 vegetation. Rare phytoliths from the Owl Conglomerate Member show that grasses were present at this time (Loughney and Smith, 2015). Charophyte fossils preserved in facies association 2 in the Mud Hills show that the lake margins were vegetated, but no phytoliths are preserved in this facies association.

The Middle Member of the Barstow Formation encompasses the deposits of facies associations 3 and 4, which are characterized by sandstone units bounded by mudstone (Fig. 2). Facies association 3 represents the deposits of channels and proximal floodplains. The stacked sandstone bodies of facies association 4 represent channel deposits of braided streams with limited floodplain deposits (Loughney and Badgley, in review). Biomarker results show a drying trend through the deposition of the Middle Member, coinciding with the peak of the MMCO, stratigraphically above the Oreodont Tuff, dated at 15.8 Ma (Woodburne et al., 1990). Phytoliths are sparse in the Middle Member but indicate that habitats were forested, and that open-habitat grasses were present (Table 1; Loughney and Smith, 2015).

Facies associations 5 and 6 comprise the Upper Member and are mudstone-dominated, with marl and sandstone representing important components (Fig. 2). These facies associations represent well-developed floodplains with localized wetlands and ponds. These floodplains were extensively vegetated, as indicated by abundant root casts and phytoliths. Phytoliths indicate that vegetation was a mixture of forest and grasslands, with palm trees forming important components of grasslands. Palm savannas are close analogs to the types of habitats that formed late in the depositional history of the Barstow Formation in the Mud Hills (Loughney and Smith, 2015).

Environments of deposition in the Mud Hills changed substantially over the deposition of the Barstow Formation. These environments transitioned from seasonally dry playas and alluvial fans to locally wet floodplains through time. This transition coincides with the MMCO, although it remains unclear what effect climate played in Neogene environmental and vegetation changes in the Mojave region. The ability of later-forming, well-vegetated Barstow environments to support mammals contributed to the number of fossil localities in the Upper Member. These environments represent depositional settings that preserve abundant vertebrate remains (Table 1; Koster, 1987; Loughney and Badgley, in review).

Questions remain about the environments that existed in the Barstow Formation. Future areas of research include expanding paleoenvironmental reconstructions to other Barstow outcrops,

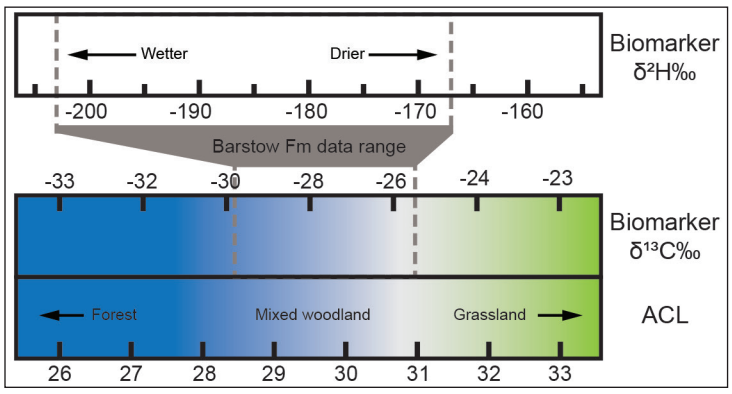

Figure 4. Results from ^{2}H, ^{13}C, and ACL analyses with approximate correlations of $\delta^{13}C$ and ACL values to habitat type.

examining the lateral variability of habitats, and reconstructing paleoecological associations between mammals and environments in the past. Through these efforts we can better constrain the timing and extent of vegetation and environmental transitions, especially in response to the MMCO. This project and ongoing work will help to put the Barstow Formation in context with other fossiliferous geological formations of the Mojave region.

References

Badgley, C., Smiley, T.M., and Loughney, K.M., 2015, Miocene mammal diversity of the Mojave region in the context of Great Basin mammal history, *in* Reynolds, R.E., ed., The Mojave Miocene: 15 Million Years of History, California State University Desert Studies Consortium, Zzyzx, p. 34-43.

Dickinson, W.R., 2002, The Basin and Range Province as a composite extensional domain: International Geology Review, v. 44, p. 1-38.

Freeman, K.H., and Pancost, R.D., 2014, Biomarkers for terrestrial plants and climate, *in* Turekian, H.D., and Holland, K.K., eds., Treatise on Geochemistry, p. 395-416.

Glazner, A.F., Walker, J.D., Bartley, J.M., and Fletcher, J.M., 2002, Cenozoic evolution of the Mojave block of southern California: Geological Society of America Memoirs No. 195, p. 19-41.

Koch, P.L., 1998, Isotopic reconstruction of past continental environments: Annual Review of Earth and Planetary Sciences, v. 26, p. 573-613.

Koster, 1987, Vertebrate taphonomy applied to the analysis of ancient fluvial systems, *in* Ethridge, F.G., Flores, R.M., and Harvey, M.D. (eds.), Recent Developments in Fluvial Sedimentology, Society of Economic Paleontologists and Mineralogists Special Publication No. 39, p. 159–168.

Loughney, K.M., and Smith, S.Y., 2015, Phytoliths from the Barstow Formation through the middle Miocene Climatic Optimum: Preliminary results, *in* Reynolds, R.E., ed., The Mojave Miocene: 15 Million Years of History, California State University Desert Studies Consortium, Zzyzx, p. 51-58.

Loughney, K.M., and Badgley, C., in review, Facies, environments, and fossil preservation in the Barstow Formation, Mojave Desert, California: PALAIOS.

McQuarrie, N., and Wernicke, B.P., 2005, An animated tectonic reconstruction of southwestern North America since 36 Ma: Geosphere, v. 1, p. 147-172.

Pagnac, D., 2009, Revised large mammal biostratigraphy and biochronology of the Barstow Formation (middle Miocene), California: PaleoBios, v. 29, p. 48-59.

Piperno, D.R., 2006, Phytoliths: A Comprehensive Guide for Archaeologists and Paleoecologists: Lanham, Maryland, AltaMira Press, 238 p.

Reynolds, R.E., Miller, D.M., Woodburne, M.O., and Albright, L.B., 2010, Extending the boundaries of the Barstow Formation in the central Mojave Desert, *in*, Reynolds, R.E., ed., Overboard in the Mojave: 20 Million Years of Lakes and Wetlands, California State University Desert Studies Consortium, Zzyzx, p. 148-161.

Shanley, K.W., and McCabe, P.J., 1994, Perspectives on the sequence stratigraphy of continental strata: AAPG Bulletin, v. 78, p. 544-568.

Smiley, T.M., Hyland, E.G., and Cotton, J.M., 2015, Approaches for reconstructing paleoenvironments in the Cajon Valley and Crowder formations, southern California, *in*, Reynolds, R.E., ed., The Mojave Miocene: 15 Million Years of History, California State University Desert Studies Consortium, Zzyzx, p. 251-258.

Smiley, T.M., Hyland, E.G., Cotton, J.M., and Reynolds, R.E., in review, Evidence of early C4 grasses, habitat drying, and faunal response during the Miocene Climatic Optimum in the Mojave Region: Palaeogeography, Palaeoclimatology, Palaeoecology.

Strömberg, C.A.E., 2002, The origin and spread of grass-dominated ecosystems in the late Tertiary of North America: Preliminary results concerning the evolution of hypsodonty: Palaeogeography, Palaeoclimatology, Palaeoecology, v. 1-2, p. 59-75.

Woodburne, M.O., Tedford, R.H., and Swisher, C.C., III, 1990, Lithostratigraphy, biostratigraphy, and geochronology of the Barstow Formation, Mojave Desert, southern California: Geological Society of America Bulletin, v. 102, p. 459-477.

Woodburne, M.O., and Reynolds, R.E., 2010, The mammalian litho- and biochronology of the Mojave Desert Province, *in*, Reynolds, R.E., ed., Overboard in the Mojave: 20 Million Years of Lakes and Wetlands, California State University Desert Studies Consortium, Zzyzx, p. 124-147.

A preliminary restudy of felid footprints housed at the Alf Museum from the Barstow Formation (Miocene) of southern California

Chandler Luebbers[1], Emily Chu[1], Andrew A. Farke[2]
[1]*The Webb Schools, 1175 West Baseline Road, Claremont CA 91711*
[2]*Raymond M. Alf Museum of Paleontology, 1175 West Baseline Road, Claremont CA 91711*

ABSTRACT—The Barstow Formation of San Bernardino County, California, preserves a rich Miocene (Barstovian NALMA) vertebrate ichnoassemblage. Many previously described and figured specimens are housed at the Raymond M. Alf Museum of Paleontology (Claremont, California), but most have not been studied using modern ichnological techniques. Here, we reexamine a sample of 19 individual tracks presumably made by Felidae. All were collected as individual prints, although some may be from disassociated trackways. Precise locality data are uncertain in some cases, hindering reassociations. Tracks were measured and digitized using photogrammetry, allowing a clearer differentiation of features on each individual print. The tracks range in length from 56 mm to 78 mm, and were originally assigned to two ichnospecies (*Felipeda bottjeri* and *Felipeda scrivneri*) based on differences in shape (e.g., relative elongation and the angle between digits). Differences between tracks are subtle, and even though measurements show some footprints are more elongated than others, we conclude that they potentially represent differences between manual and pedal tracks or else reflect taphonomic effects. Thus, we suggest that there is only one felid ichnotaxon (*F. bottjeri*) in the Alf Museum sample from the Barstow Formation.

Introduction

The Barstow Formation of southern California dates to the Miocene (Hemingfordian–Barstovian NALMA, ~19.3–13.4 Ma), and it hosts abundant vertebrate trace and body fossils (Pagnac 2009; Woodburne et al. 1990). Felids are a rare component of the faunal assemblage, represented by body fossils of *Pseudaelurus intrepidus* and *Nimravides* sp., and trace fossils assigned to *Felipeda scrivneri* and *Felipeda bottjeri* (Lofgren et al. 2006; Pagnac 2009). Both *Pseudaelurus intrepidus* and *Nimravides* sp. are roughly similar in size to the modern-day cougar (Lofgren et al. 2006).

The cat tracks described in this paper (Figures 1, 2) were collected by Ray Alf and students from The Webb School of California as individual prints in the 1950s and 1960s, and are housed at the Raymond M. Alf Museum of Paleontology (RAM) in Claremont, California (Lofgren et al. 2006). Some may be from weathered out trackways, but locality data are unclear in many cases, making associations difficult to determine. Based on a recent review of records, some tracks that had previously been assigned to a general Barstow track locality (RAM V94281) were able to be more precisely assigned and associated (to RAM V201103; see Table 1). Where precise data are known, all tracks are from the Middle Member of the Barstow Formation, below Skyline Tuff (sensu Woodburne et al. 1990).

Sarjeant et al. (2002) described the Alf Museum felid tracks and assigned them to two ichnospecies, *Felipeda bottjeri* and *Felipeda scrivneri*. Tracks assigned to *F. bottjeri* were identified as more elongate and narrower than those of *F. scrivneri,* among other differences. Reynolds and Milner (2012) later reviewed these same occurrences and others from California and Utah, but evaluated the tracks in a taxonomy-free approach (i.e., they were only referred to as Felidae, without any reference to ichnotaxon). Here, we present a preliminary redescription and reevaluation of the 19 felid tracks from the Barstow Formation in the Alf Museum collection. Our hope is that this will spur additional research into the variation, taphonomy, and ichnotaxonomy of tracks from the Barstow Formation.

Material and methods

All fossils are housed at the Raymond M. Alf Museum of Paleontology. We used digital calipers to measure each print to the nearest mm (Table 1). In order to create digital models, we took approximately 25 photos of each print from different angles using an iPhone 6 and reconstructed photogrammetric models using Agisoft PhotoScan Professional 1.1.6.2038. Terminology follows that of Sarjeant et al. (2002) and Reynolds and Milner (2012).

Description

All specimens are natural casts (relief) of tracks (Table 1, Figures 1, 2). Nine out of the 19 tracks from the RAM collection are complete. All are isolated prints and lack obvious claw marks. Each of the complete tracks has a

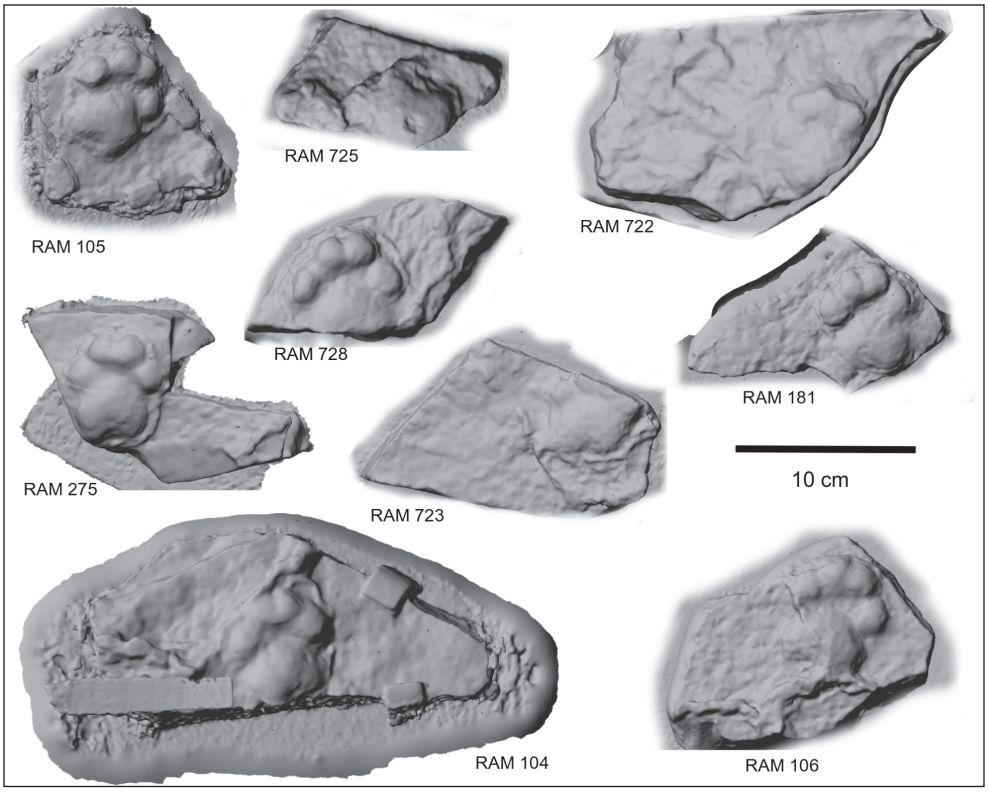

Figure 1. Digital surface models of track fossils from the Barstow Formation assigned to Felidae.

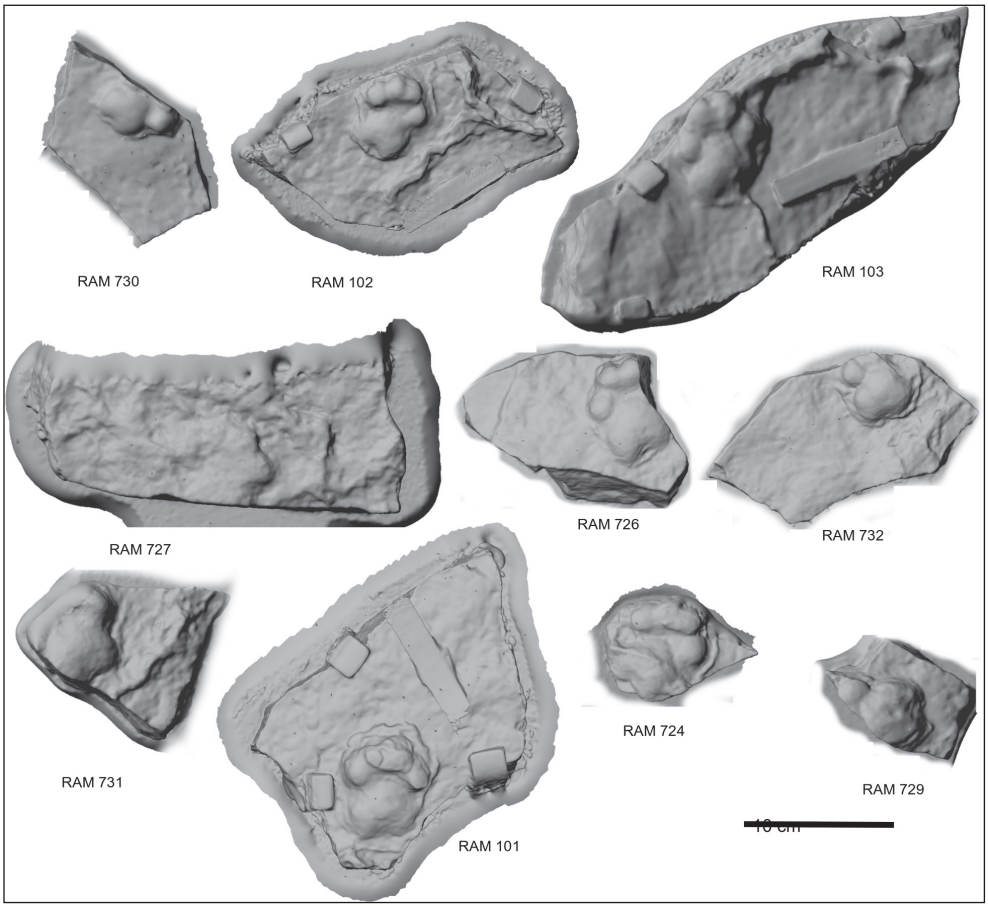

Figure 2. Digital surface models of track fossils from the Barstow Formation assigned to Felidae.

similar, generally circular shape and a cleft on the heel of the metapodial pad (bilobed). Every print has four digits, and all of the digits are oval in overall shape, with a width to length ratio of approximately 1:1.14. The metapodial pad of each track is roughly ovoid and bilobed where preserved, with a width to length ratio of approximately 1.1:1, and the digits span wider than the central pad for all tracks. The two middle digits of each track are more anteriorly placed than the two outside digits, and the toes form an arch along the top of the central pad. The length:width ratio varies slightly between prints (Table 1).

Some tracks, such as RAM 724 and RAM 106, have a protruding thin ridge superimposed over the track (Figures 1, 2). Based on their irregular positions, we hypothesize that the ridges are most likely sediment deformation. Two tracks, RAM 725 and RAM 729, have small indentations on the central pad, which are also most likely caused by sediment deformation. RAM 727, RAM 722, and RAM 723 do not have distinct impressions and have shallow indentations for most features of the track. However, digits and metapodial pads can still be faintly seen. RAM 727 is missing part of the lower central pad, RAM 722 is missing part of the metapodial pad, and RAM 723 only partially preserves its four digits.

Discussion

A single Barstow Formation specimen in the Alf Museum collection (RAM 105) was previously assigned to *Felipeda scrivneri*, RAM 105 (Sarjeant et al. 2002); the holotype of this ichnotaxon is from younger sediments in Death Valley. Relative to specimens of *F. bottjeri*, tracks of *F. scrivneri* are described as less elongate and with a greater overall angulation of digits, in addition to a more prominent separation between the digital pads and the metapodial pads. Based on our examination of the RAM specimens, we hypothesize that variation in digital/metapodial pad separation is at least in part a function of substrate consistency and/or other taphonomic factors. Furthermore, relative elongation of the overall track is variable, and also likely due to being either a manus/pes track or individual variation. For instance, the length/width ratio of the track varies between 1.15 and 1.25 in *F. bottjeri* identified by Sarjeant et al. (2002), contrasting with 1.12 in the *F. scrivneri* referred specimen (Table 1). However, we suggest that the latter is within the potential realm of variation for the former, particularly when considering differences between manus and pes. We also attempted to measure interdigital angles, but due to the variation in preservation as well as the relatively round shape of the digital pads, it was difficult to take consistent measurements. Considering the overall evidence, we suggest that only a single felid ichnotaxon (*Felipeda bottjeri*) is represented by the Alf Museum sample from the Barstow Formation.

Based on our preliminary observations, we suggest that a more comprehensive evaluation of felid tracks from the Barstow Formation would be fruitful, including fossils from other collections as well as description of *in situ* trackways. In particular, more thorough documentation of variation is necessary, as is a more detailed comparison with other known felid tracks.

Acknowledgements

We thank D. Lofgren for providing helpful guidance and R. Reynolds for input on a previously published abstract regarding this research. The Barstow Field Office of the US Bureau of Land Management has provided continuous assistance for studies by the Alf Museum within the Barstow Formation, under permit CA-15-06P.

Bibliography

Lofgren, D.L., J.A. Greening, C.F. Johnson, S.J. Lewis, and M.A.Torres. 2006. Footprints on the sands of time: fossil tracks at the Raymond Alf Museum of Paleontology and management of tracks on public lands. In America's Antiquities: 100 Years of Managing Fossils on Federal Lands, S.G. Lucas, J.A. Spielman, P.M. Hester, J.P. Kenworthy, and V.L. Santucci, eds. New Mexico Museum of Natural History and Science Bulletin 34. p. 109-118.

Pagnac, D. 2009. Revised large mammal biostratigraphy and biochronology of the Barstow Formation (Middle Miocene), California. PaleoBios 29:48-59.

Reynolds, R.E. and A.R.C. Milner. 2012. Early Neogene cat tracks from California and Utah, in Reynolds, R.E. (ed.), Searching for the Pliocene: Southern Exposures.Fullerton, California: California State University Desert Studies Consortium. p. 153-159.

Sarjeant, W.A.S., R.E. Reynolds, and M.M. Kissell-Jones. 2002. Fossil creodont and carnivore footprints from California, Nevada, and Wyoming, in Reynolds, R.E. (ed.), Between the Basins: Exploring the Western Mojave and Southern Basin and Range Province. Fullerton, California: California State University Desert Studies Consortium. p. 37–50.

Woodburne, M. O., Tedford, R. H., and Swisher, C. C. 1990. Lithostratigraphy, biostratigraphy, and geochronology of the Barstow Formation, Mojave Desert, southern California. Geological Society of America Bulletin. 102:459-477.

The first Pacific Coast record of *Erethizon kleini* (Hystricomorpha, Erethizontidae)

Robert E. Reynolds
CSU Desert Symposium Research Associate, Redlands CA 92374, bob.reynolds220@gmail.com

ABSTRACT—A new specimen of small *Erethizon sp.* from the Unnamed Sandstone in the California Oaks area of Murrieta, Riverside County, CA is described. Its stratigraphic position below the Bishop Ash (760,000 ky) suggests an age of about one million years, or the middle Irvingtonian North American Land Mammal Age (NALMA). This specimen, from Peninsular Range Province of southern California, fills gaps in the time line for the *Erethizon* sp. lineage, and helps distinguish Blancan through Irvingtonian species west of the Rocky Mountains. Its small size and certain morphologic characteristics suggest that this specimen represents *Erethizon kleini*.

Background

Fossil porcupines in North and South America have been assigned to two genera over the last forty five years: *Erethizon* sp. and *Coendou* sp. Since Frazier's (1981) revision, all fossil or recent porcupines north of the Yucatan peninsula are assigned to Erethizon sp. The earliest North American record of *Erethizon* (*E. stirtoni*) is from the late Blancan Wolf Ranch locality in southeastern Arizona (Harrison, 1978; Frazier, 1981). *E. stirtoni* (White, 1968; Frazier, 1981; White and others, 2006) was identified from the middle Blancan into mid Irvingtonian Vallecito Creek local fauna at Anza Borrego State Park. Other occurrences of *Erethizon* species are from southern California. The *E. cascoensis* occurrences in the San Timoteo Formation span the period between medial Blancan, at 2.5 Ma through early Irvingtonian, 1.3 Ma (White, 1970; Albright, 1999). The California Oaks (Cal Oaks) *Erethizon* dates from less than 0.85 Ma (Reynolds and Reynolds, 1990a, 1990b) and greater than the overlying Bishop Ash (760,000k).

The block of sediment that contained the specimen was collected in the 1980s. Recent preparation has produced a partially complete, closely associated, and sometimes articulated skeleton of a sub-adult porcupine (*Erethizon* sp.; Table 1.) Mandibles with dentition, upper dentition, and cranial fragments are present.

Table 1. Inventory list of *Erethizon* from California Oaks locality

A2239-2060-A	Left and right upper incisors
A2239-2060-B	L dP4/
A2239-2060-C	L P4/
A2239-2060-D	L M1/; (worn, with striations)
A2239-2060-E1	L M2/ M3/ Slight wear, with strong roots. Reverse side is -2060-E2
A2239-2060-E2	Manus with cuboid, 3 metacarpals w. loose epiphyses & sesmoids present, 3 first phalanges, 1 second phalange
A2239-2060-F	R dP4 very worn, roots dissolving
A2239-2060-G	R P4 Unworn, unrooted
A2239-2060-H	R M1/
A2239-2060-I	R M2/
A2239-2060-J	R M3/
A2239-2060-K	L mandible /I, p/4, m/1, m/2,
A2239-2060-L	L dp/4
A2239-2060-M	L m/3 rooted, slightly worn
A2239-2060-N	R mandible and associated ramus, w. /I, Rt p/4, m/1, m/2, m/3,
A2239-2060-O	R dp/4
A2239-2061	unused designation
A2239-2062	Metatarsals and phalanges
A2239-2063	Distal tibia
A2239-2064	Femur fragments
A2239-2065	Right astragulus
A2239-2066	Metapodials
A2239-2067	Phalanges A=1st, B=2nd, C=terminal
A2239-2068	Proximal fragments of terminal phalanges
A2239-2069	Caudal vertebra

Systematic paleontology

Order Rodentia
Suborder Hystricomorpha Brandt, 1855
Family Erethizontidae Thomas 1897
Erethizon Cuvier, 1822
Erethizon sp. Frazier, 1981,
Erethizon kleini Frazier, 1981, p. 43.

Holotype—UF 21473, left mandible with incisor and p4-m3. Condyle and angular process broken.

Type Locality—Inglis IA, Citrus County, Florida. A sinkhole–cave fill on the north side of the Cross-Florida barge Canal approximately 3 miles east of U. S. Highway 98 south of Inglis, Florida.

Age—Early Irvingtonian

Distribution—Principle sample from west- and east-central Florida.

Diagnosis—Notably smaller than any other species of *Erethizon*; otherwise closely resembling *E. dorsatum* morphologically.

Referred Specimen—SBCM Locality number: SBCM 5.6.155, FN: Q-4-26-1. California Oaks Development on Antelope Road (C. A. R.) in Murrieta, Riverside County, California. Located north of the junction of California Oaks Road and Jackson Avenue.

Description

The specimen is a partially articulated skeleton with complete dentition (Appendix, Table 2). Cranium and post cranial vertebrae and limb elements are crushed and some missing. Based on worn fourth premolars, and erupting or slightly worn molars the Cal Oaks specimen is a subadult. Vertebral discs are not fused, and epiphyses of limbs, metapodials and phalanges are unfused. Front and hind carpals, tarsals and phalanges are present and provide opportunity for study and comparison

Discussion

The relationship between *Erethizon* sp. and *Coendou* sp. has previously been discussed by White (1970) and a revision by Frazier (1981) followed. The latter presented measurements of at least 200 specimens from 65 localities in North America. Frazier (1981, Fig. 4, p. 10) indicates that Blancan through Recent porcupine species from across North America as far south as southern Mexico are referable to *Erethizon* sp., while those along the Yucatan Peninsula are of the genus *Coendou* sp.

The Cal Oaks *Erethizon* sp. (A2239-2060) was compared with measurements of comparable elements from the four species described by Frazier (1981: *E. bathygnathum*, *E. cascoensis*, *E. kleini*, and *E. dorsatum*). The specimen was also compared to three Recent sub-adult comparative specimens of *Erethizon* (Table 2).

Table 2. Measurements of *Erethizon* specimen from California Oaks locality

Upper Dentition		mm	mm		A2239-
Left	Right	L	W		
I/		4.3	4.2		2060A
dP4/		5.1	5.1	Very worn, roots dissolving	2060-B
P4/		5.8	5.4	Unworn, unrooted	2060-C
M1/		5.4	5.4	Unworn, unrooted	2060-D
M2/		5.7	5.8	Slight wear, strong roots	2060-E
M3/		5.2	5.3	Slight wear, ??? strong roots	2060-E
	I/	4 .8	4 .4		2060A
	dP4/	5.1	5.1	Very worn, roots dissolving	2060-F
	P4/	5.8	5.4	Unworn, unrooted	2060-G
	M1/	5.7	6.0	Unworn, unrooted	2060-H
	M2/	5.4	5.4	Slight wear, strong roots	2060-I
	M3/	5.2	5.2	Worn, strong roots	2060-J
Lower Dentition		**mm**	**mm**		**A2239-**
Left	**Right**	**L**	**W**		
/I		3.9	3.5	Lt mandible w. p/4, m/1, m/2; anterior most worn	2060-K
dp/4		5.7	M4.1	Very worn, roots dissolved	2060-L
p/4		5.9	4.9	In wear	2060-K
m/1		5.8	5.2	Moderate wear	2060-K
m/2		6.0	5.4	Slight wear	2060-K
m/3		5.8	4.9	Isolated m/3 slightly worn	2060-M
	/I	3.9	3 .6	Rt mandible w. Rt p/4, m/1, m/2, m/3,	2060-N
	dp/4	5.5	4.5	Worn	2060-O
	p/4	un	un	Unworn frag.	2060-N
	m/1	5.5	5.4	Moderate wear	2060-N
	m/2	5.9	5.6	Slight wear	2060-N
	m/3	5.5	5.1	Isolated m/3 slightly worn	2060-N
		xxx	23.3	Alveolar length of lower tooth row	
		14.8	13.4	Length lower diastema	
		17.9	18.2	Depth mandible at p4/	
		9.9	13.6	Depth mandible at m2/	
		22.4	20.9	Length symphysis	

Diagnosis

Frazier (1981, Figure 2, p. 6) gives suggestions for positions of measurement that distinguish *Coendou* from *Erethizon*. In the case of the Cal Oaks specimen the small size would suggest *Coendou*. However, distinctive characteristics of *Erethizon* sp. are present, as discussed by White (1968) and amplified by Frazier (1981). These diagnostic characteristics are:

- P4 of most *Erethizon* specimens is usually larger than M1. The Cal Oaks P4 is slightly longer than the M1 (7% Table 1) but equal in width. Cal Oaks tooth width dimensions of P4 and M1 are equivalent to subadults of *E. kleini*, and at the large end of adult *Coendou* (Frazier, 1981, Fig. B-9). The relative size of the subadult Cal Oaks specimen and the size of P4 and M1 support diagnosis of Erethizontidae.
- The Cal Oaks P4 has an internal reentrant (hypoflexus, Fig. 1), which is a variable characteristic in fossil *Coendou* and *Erethizon*. Frazier (1981, p. 21) notes that abrasion scratches on cheek teeth of *Erethizon* are less than 30° relative to the long axis of the dental row. Those at angles greater than 35° indicate *Coendou*. The

Table 3: Measurements of comparative subadult *Erethizon dorsatu*m dentition (A500-1028, Nelsen-1, SM360)

Lt maxilla	**dP4**	**P4**	**M1**	**M2**	**M3**
Length	5.7	6.4-6.6 **A6.5**	5.8-6.3- **A6.1**	6.3-6.4-6.1 **A6.3**	6.1-6.2 **A6.2**
Width	6.3	6.2-6.9 **A6.6**	6.2-6.3- **A6.3**	6.3-7.4-6.3 **A6.7**	6.1-6.3 **A6.2**
Rt maxilla	**dP4**		**M1**	**M2**	**M3**
Length	5.9	6.4-6.6 **A6.5**	5.9-6.4-6.1 **A6.1**	6.3-5.7-6.1 **A6.0**	6.5-6.2 **A6.4**
Width	6.2	6.6-6.9 **A6.8**	6.0-5.9-6.2 **A6.0**	6.7-7.3 **A6.8**	5.7-6.2 **A6.0**
Lt mandible	**dP4**	**P4**	**M1**	**M2**	**M3**
Length	7.0 –u--6.6= **A6.8**	**7.6**	6.2 –u-6.1-**A6.2**	6.3-u-6.1 **A6.2**	u-u-6.7 **A6.7**
Width	5.6-u-6.9= **A6.3**	**6.1**	6.3-u-5.8 **A6.1**	6.1-u-5.8 **A6.0**	u-u-5.7 **5.7**
Rt mandible	**dP4**	**P4**	**M1**	**M2**	**M3**
Length	**7.0**	**7.4**	6.2-5.9 **A6.1**	6.2-5.9 **A6.1**	6.4
Width	**5.96.2**		6.4-5.6 **A6.0**	6.4-6.1 **A6.3**	5.8

A = Average measurement. All measurements in millimeters

Cal Oaks specimen has faint scratches on one molar that are less than 30° to the long axis of the tooth row, supporting an assignment to *Erethizon.*

- The upper incisor length / width (Table 1) ratio corresponds with the lowest points of adult *E. dorsatum*, is well below any subadults of fossil *E. dorsatum,* and is higher than *Coendou* sp. The ratio of lower incisor length to width is below those of subadult *E. kleini* and at the very high end of adult *Coendou*.
- Anteriorally convergent mandibular tooth rows are a characteristic of *Erethizon*, and noticeable in the Cal Oaks *Erethizon* (Fig. 3). In *Coendou* sp., the tooth rows are subparallel.
- The angular process of the mandible from Cal Oaks is inflected medially, as in *Erethizon*, and the interior surface is convex.
- The alveolar length of the lower tooth row (Table 2) corresponds to subadults of *E. dorsatum* and adults of *E. kleini*, and is at the very high end of adult *Coendou* sp.
- Diastema length (Table 1) corresponds to that in subadults of *E. dorsatum* from the east coast of North America, to subadults of *E. kleini,* and to the highest range of adult *Coendou* measurements.
- The depth of mandible at two positions (Table 2) corresponds with subadults of *E. dorsatum* and the upper range of *Coendou*.
- The length of the symphysis (Table 2) compared to the length of the lower diastema is well below the subadult range of *Erethizon* sp. and at the low- central range of *Coendou*.
- The astragulus of *Erethizon* sp. is less derived than that of the arboreal *Coendou* sp. (Frazier, 1981, Fig. 18, p. 38; Fig A). The Cal Oaks specimen is close to the size and morphology of that figured for *E. kleini* (Frazier, 1981, Fig. 18C).

Summary

Tooth size and morphology, mandibular dimensions, and abrasion scratches support referral of the Cal Oaks specimen to *Erethizon*. Comparison of dental size and ratios indicates that the subadult Cal Oaks porcupine is much smaller than most subadults of the genus *Erethizon* sp. Measurements show that the subadult Cal Oaks specimen is as large as the largest of adult *Coendou* sp. The scope of this study did not include direct comparisons with *E. kleini* specimens.

The Cal Oaks specimen is referred to *Erethizon* sp. cf. *E. kleini* small, based on:

- Anteriorally convergent lower tooth row,
- convex mandibular angle,
- Tooth abrasions less than 30 degrees relative to long axis of tooth row.
- Incisor dimensions.
- Premolar and first molar (upper and lower) measurements
- Dimensions and morphology of astragulus
- Frazier (1981) in his diagnosis states: *E. kleini,* an early Irvingtonian *Erethizon,* is "…notably smaller than any other species of *Erethizon;* otherwise closely resembling *E. dorsatum* morphologically."

Although the Cal Oaks specimen falls within the lowest size range of *Erethizon* sp., and is comparable to *E. kleini* in size, it should be noted that the referral is questionable since *E. kleini* is known only from Gulf Coast fossil faunas in Florida of early and middle Irvingtonian LMA. Additionally, the Cal Oaks specimen lower incisor dimensions are less those of *E. kleini*, a character that, on the other side of the continent, might be a result of adaptation to local flora and habitat. The lack of small fossil porcupines from Blancan through Irvingtonian deposits between the Peninsular Range of southern California and Florida is a notable absence from the fossil record.

The presence of a small erethizontid in the northern Peninsular Range of California suggests the possibility of an early Irvingtonian dispersal of small porcupines along the Pacific coast comparable to that which took *E. kleini* around the Gulf Coast to Florida.

The scope of this study did not encompass physical comparisons to other small size members of *Erethizon* sp. Following such studies, the Cal Oaks specimen may

Figure 1. Anterior view of upper incisor pair in matrix (2239-2060-A).

Figure 2. Anterior view of lower incisors in left and right mandibles (2239-2060-K, -N).

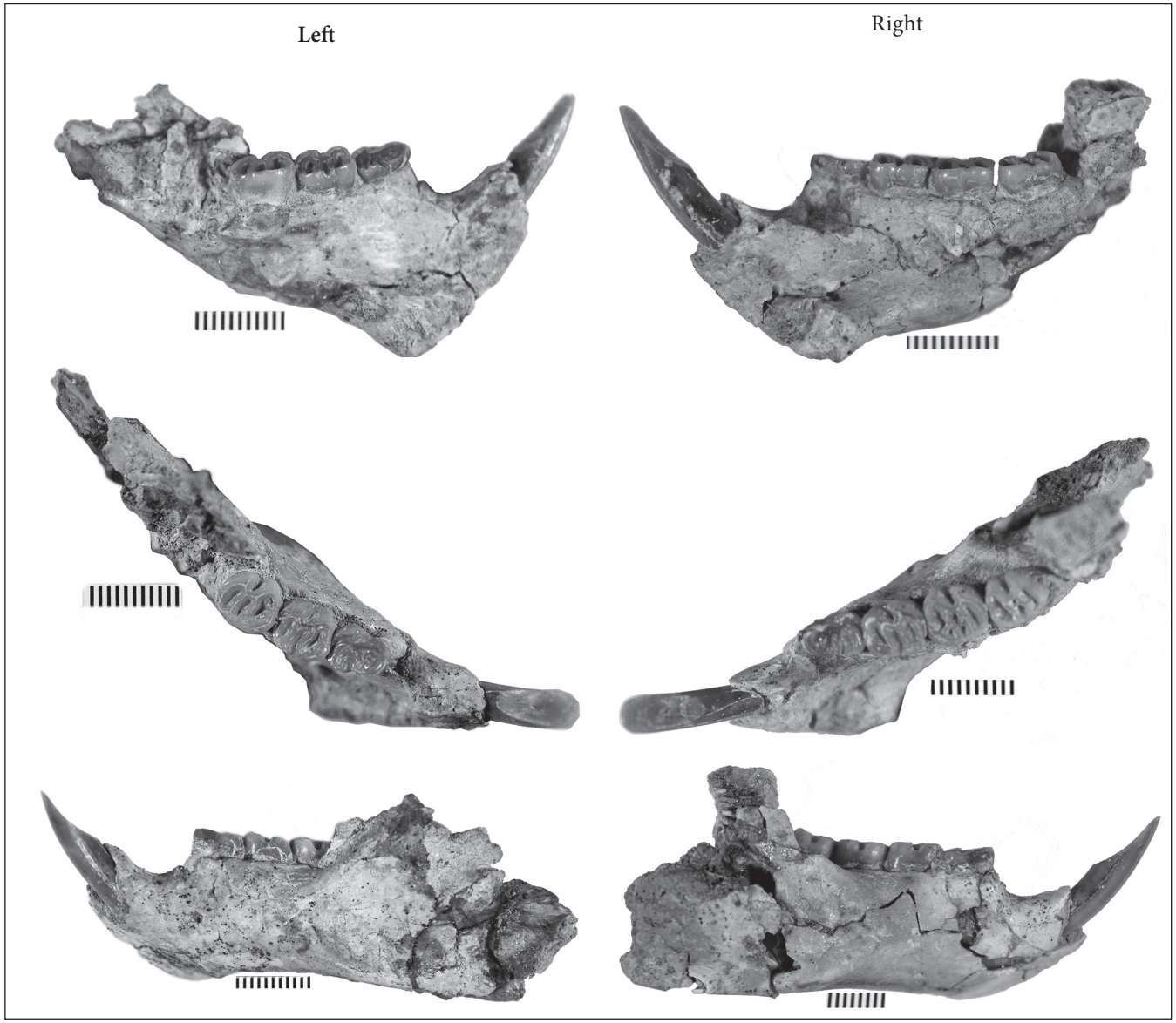

Figure 3. Interior, occlusal and exterior views of lower left mandible (2239-2060-K) and lower right mandible (2239-2060-N). Occlusal views show anterior convergence of tooth row toward mid-line at symphysis.

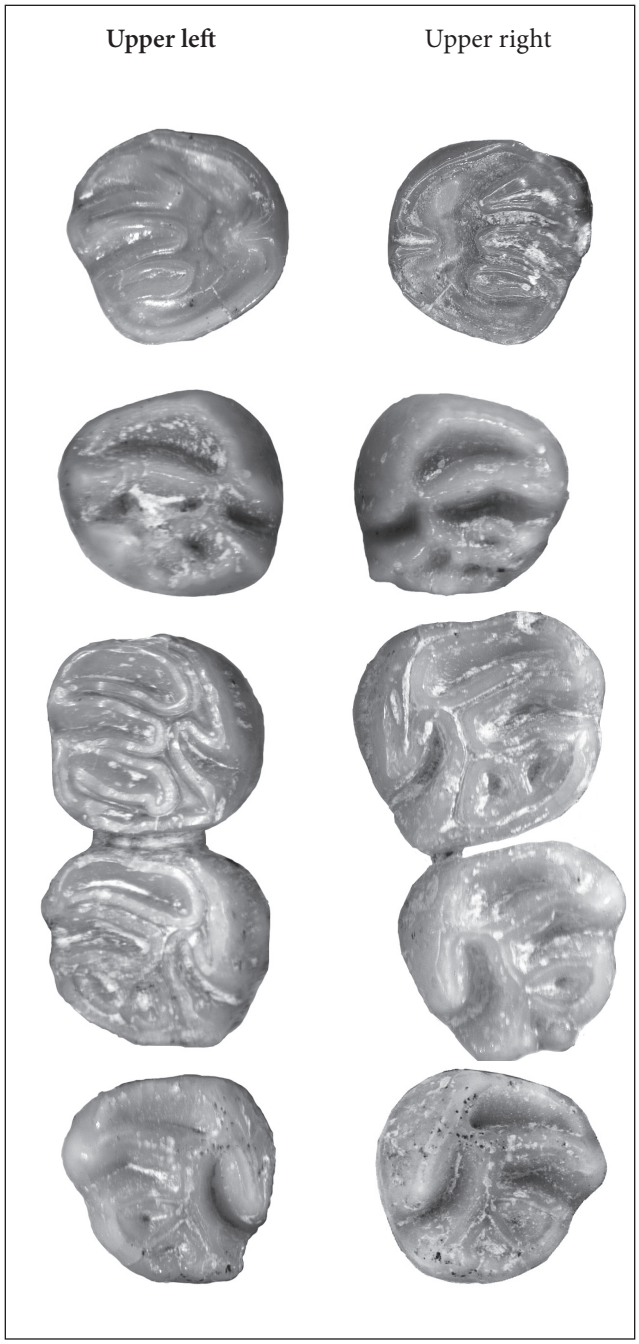

Figure 4. Composite view of upper left and right cheek teeth (dP4 and P4 – M3). Not to scale.

Figure 5. Composite view of lower left and right cheek teeth (dp4 and p4 – m3) Not to scale.

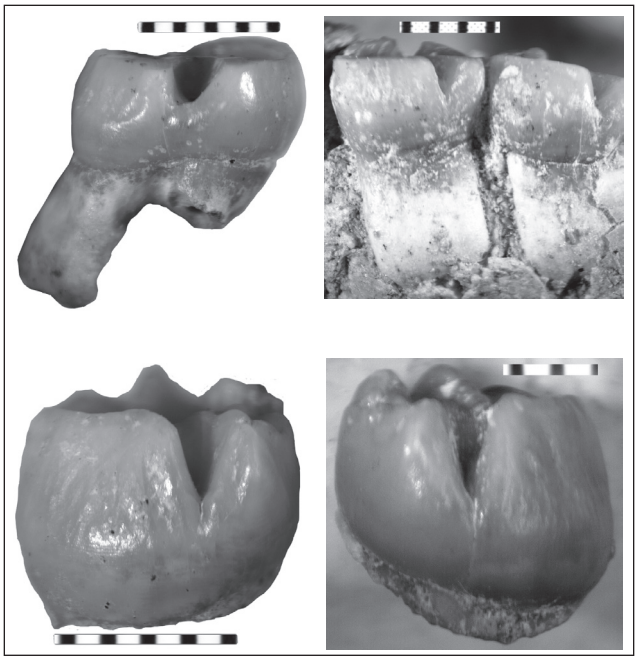

Figure 6: Crown height of selected cheek teeth (-2060-L dp4; -2060-C P4; -2060 E M2; -2060-J M3).

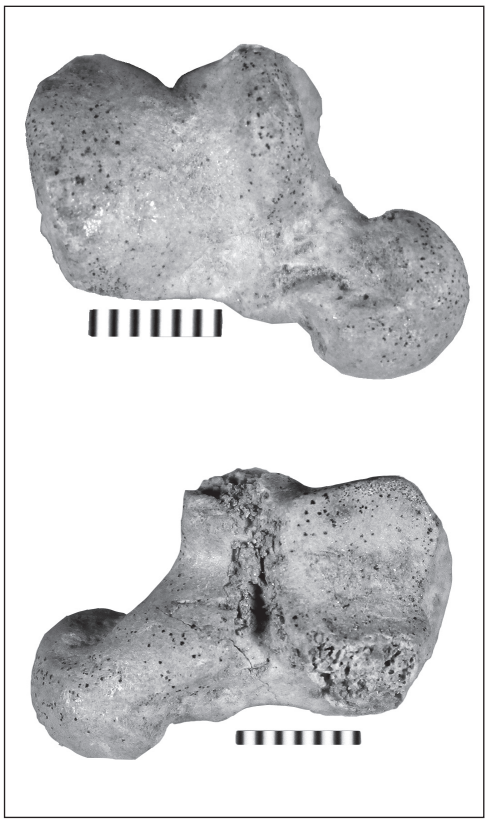

Figure 7: Right astragulus, dorsal and ventral views (2239-2065).

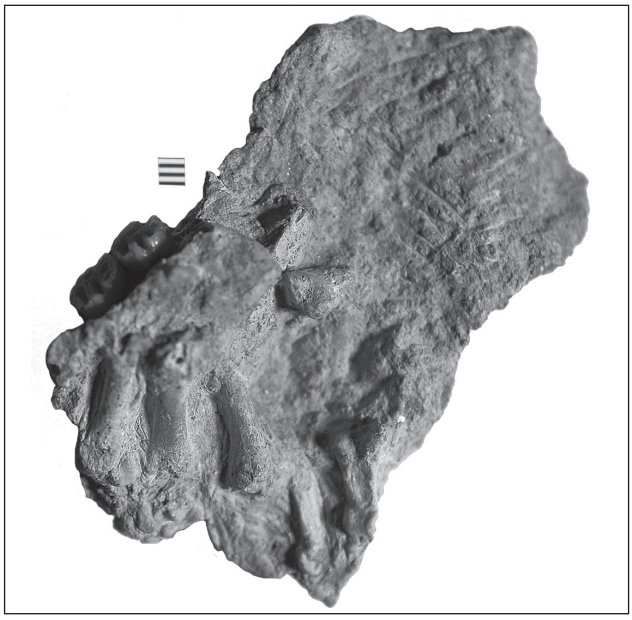

Figure 8: Articulated manus (-2060-E2) with cuboid, metacarpals, loose epiphyses, sesmoids, 3 first phalanges, 1 second phalange.

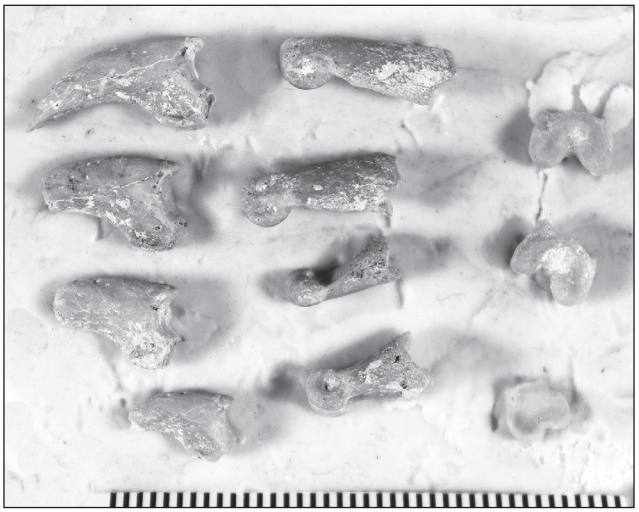

Figure 9: Isolated first, second and terminal phalanges (A2239-2067-A, -B, -C).

warrant description as a new species, small in size, that lived contemporaneously with and occupied slightly different habitats than *E. cascoensis*, *E. dorsatum* or *E. kleini*.

Acknowledgments

I thank Barry Albright for review of the paper. Thanks also go to Ian Gilbert, Curator of Earth Sciences, SBCM, and Will Abersek, Alf Museum, for photographing specimens. Quintin Lake discovered and recovered the specimen and did preliminary preparation. Richard L. Reynolds did intermediate preparation and preliminary identification. I thank SBCM Director Melissa Russo and Ian Gilbert for access to the SBCM paleontological collections as well as research time and space. Thanks, as usual, to J. Reynolds for support at SBCM and review of this report.

References

Albright, L.B., III, 1999b, Biostratigraphy and Vertebrate Paleontology of the San Timoteo Badlands, Southern California: University of California Publications in Geological Sciences, vol. 144, pp. 1121.

Frazier, Michael K., 1981. A revision of the fossil Erethizontidae of North America. Bull. Florida State Mus., Biol. Sci. 27(1): 1-76.

Harrison, J.A., 1978, Mammals of the Wolf Ranch Local Fauna, Pliocene of the San Pedro Valley, Arizona: University of Kansas Museum of Natural History Occasional Papers, v. 73, pp. 1–18.

Reynolds, R.E., and Reynolds, R.L., 1990a. A new, late Blancan faunal assemblage from Murrieta, Riverside County, California. Redlands, San Bernardino County Museum Association Quarterly, 37(2).

Reynolds, R.E., and Reynolds, R.L., 1990b. Irvingtonian? faunas from the Pauba Formation, Temecula, Riverside County, California. Redlands, San Bernardino County Museum Association Quarterly, 37(2).

Reynolds, R.E., and Reynolds, R.L., 1991. The Pleistocene Beneath our Feet: Near-surface Pleistocene Fossils in Inland Southern California Basins, *in* Inland southern California: the last 70 million years, M.O. Woodburne, R.E. Reynolds , and D.P. Whistler, ed. Redlands, San Bernardino County Museum Association Quarterly 38(3,4):41-43.

White, J. A.,1968. A new porcupine from the middle Pleistocene of the Anza-Borrego Desert of California. With notes on mastication in *Coendou* and *Erethizon*. Contrib. Sci. Los Angeles Co. Mus. Nat. Hist. 136: 1-15

White, J. A., 1970. Late Cenozoic porcupines (Mammalia, Erethizontidae) of North America. Amer. Mus. Novit. 2421:1-15.

White, J.A., H. Wagner, and G.T. Jefferson, 2006, The Small Fossil Mammals: Rodents, Rabbits and Their Relatives. Pp. 235–251. *In* Jefferson and Lindsay, 2006, *Eds.* Fossil Treasures of the Anza-Borrego Desert, p. 394.

Review of the Blancan / Irvingtonian transition in the northern Peninsular Range Province of southern California

Robert E. Reynolds
CSU Desert Studies Research Associate, Redlands CA 92373, bob.reynolds220@gmail.com

ABSTRACT— The San Timoteo Formation has produced the El Casco Substation fossil assemblage that was recovered down section and a half mile east of the previously described El Casco Fauna locality. The San Timoteo Formation provides critical data about the climatic, botanic, and zoologic transitions through three North American Land Mammal Ages (NALMA)—Hemphillian, Blancan and early Irvingtonian. The five million year span of deposition (6.2–0.5 Ma) encompasses a period of time that contains mammalian radiations from South America and Asia into North American.

The fossil assemblage from the El Casco Substation includes an associated fauna and flora. Each has been studied separately, so are referred to as Substation Fauna and Substation Flora. The Substation Fauna consists of 65 taxa while the Substation Flora contains 12 plant taxa. Twenty-six mammalian taxa are geographical and temporal range extensions. This exceptional assemblage from a single sedimentary interval has only 13 taxa in common with those reported previously from all five members of the entire San Timoteo Formation. The Substation Fauna contains eight genera of riparian and aquatic mollusks, stickleback fish, three salamanders, a frog, giant tortoise, pond turtle, lizards, and snakes. Ducks and rails imply aquatic habitats. Small mammals include shrew and mole, temporal extensions for heteromyids and cricetids, and the earliest record of the microtine *Allophaiomys* sp. entering the southwestern United States. Large herbivores include deer, camelids, horse, giant sloths *Paramylodon* sp. and *Nothrotheriops* sp. and partial skeletons of the sabertoothed cats *Homotherium* sp. and *Smilodon gracilis*.

The taxa of the Substation Fauna indicate a late Blancan NALMA. The taxa from the stratigraphically higher El Casco locality suggest an Irvingtonian NALMA except for the *Plesippus*, a holdover species. Therefore, in the Peninsular Range Province of southern California, the Blancan to Irvingtonian transition lies between 1.7 and 1.4 Ma, the respective ages of the Substation Fauna and the El Casco Fauna..

Setting

El Casco (elevation 2,080') is in San Timoteo Canyon, south of and between Beaumont and Redlands, in western San Gorgonio Pass, Riverside County, California. The pass, summit elevation 2,600', developed along the San Andreas fault zone and forms a natural break between the San Bernardino Mountains to the north (elevation 11,272') and the San Jacinto Mountains to the south (elevation 10,215' elevation). The pass separates the east-central portion of the Transverse Range geological province from the north end of the Peninsular Range geological province.

History of investigations

The San Timoteo Formation has produced a very significant assemblage of terrestrial vertebrates and plants spanning the last 5.7

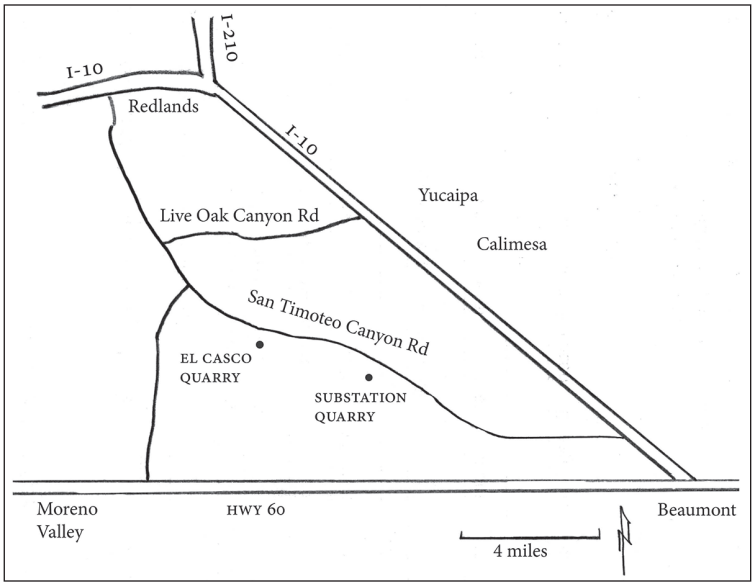

Figure 1. Vicinity map.

Table 1. Pliocene and Pleistocene North American Land Mammal Ages and Faunas			
Period	NALMA	Age Ranges	Fossil Faunas
Holocene		0.01 Ma–present	
Pleistocene	Rancholabrean	0.2 Ma–0.01 Ma	
	Irvingtonian	1.35Ma–0.2 Ma	0.9 Ma Shutt Ranch
	Irvingtonian		1.4 Ma El Casco
	Blancan/Irvingtonian transition	1.72 Ma–1.35 Ma	
	Late Blancan	2.5 Ma–1.72 Ma	1.7 Ma El Casco Substation
Pliocene	Middle Blancan	4.1 Ma–2.58 Ma	
	Early Blancan	4.9 Ma–4.1 ma	
Simplified from Bell and others, 2004, Finney, 2011			

million years. Fossils in the formation have been the subject of investigations for nearly a century (Frick, 1921; 1933; Reynolds and Reeder, 1991; Matti and Morton, 1975). A total of 36 plant taxa have been recorded from the formation that helps decipher past topography and rainfall patterns (Axelrod, 1966, 1976). The most recent comprehensive studies of the formation (Albright, 1999) recorded 42 animal taxa such as camels, deer, horses, sloths, elephants, tapirs, dogs, bears, rabbits, and rodents from over 14 localities.

The El Casco Substation was constructed by Southern California Edison on a 40-acre parcel. Just 240,000 cubic yards of fossiliferous sediments were disturbed. Salvage by trained monitors from LSA, an environmental consulting firm, between September 2009 and January 2011, and screen washing of sediments, recovered 15,900 specimens: 2,800 plants, 1,000 invertebrates and 12,000 vertebrates.

The Substation site is located in a portion of the San Timoteo Formation that lies stratigraphically above a Blancan NALMA locality (311, Albright, 1999) with abundant vertebrate taxa and 1150 feet below an overlying locality with Irvingtonian NALMA fauna (350, the El Casco Fauna, Albright, 1999). Thus, the Substation Fauna is stratigraphically positioned to provide information on the transition from the older Blancan to the younger Irvingtonian NALMA.

Stratigraphy

West-trending San Timoteo Canyon (Fig. 1) bisects the Upper Unit (Unit 4; Albright, 1999) of the San Timoteo Formation Unit 4. This canyon contains the boundary between the Pliocene Epoch and the Pleistocene Epoch, around 2.58 Ma (Finney, 2011) as well as the faunal transition from the Blancan (Bl) North American Land Mammal Age (NALMA) to the Irvingtonian (Ir) NALMA (Table 1). The stratigraphic units become younger to the northeast. Sediments at Shutt Ranch, Calimesa, contain the youngest fauna in the San Timoteo Formation, dating to approximately 0.9 million years (Ma) (Reynolds and Reeder, 1991; Albright, 1999). Sediments overlying Unit 4 have been referred to as the sedimentary deposits of Live Oak Canyon (Matti and others, 2015).

The San Timoteo Formation on the substation parcel was mapped as containing landslide topography (Qls; Morton, 2004), but fresh exposures show only minor stratigraphic offsets. Canyon bottoms contain terraced surfaces of late Pleistocene to Holocene fluvial fill (Qf). San Timoteo Creek and tributaries contain active channel fill (Qw).

The El Casco locality (Fig. 1) is 2.5 miles west of the SCE El Casco Substation locality in the upper San Timoteo Formation (Albright, 1999; Morton, 2004). The stratigraphic position of these two localities can be compared by using measurements from the top of a thick, cliff-forming arkosic sandstone marker bed that occurs down-section from both localities. The El Casco locality is approximately 160 meters upsection from the arkosic sandstone, while the Substation locality is approximately 100 meters upsection.

The arkosic sandstone corresponds with Albright's magnetostratigraphic sample No. 317 at 2.0 Ma (C2r.1r). The El Casco locality produced magnetostratigraphic sample No. 350, corresponding to 1.4 Ma (upper C1r.2r). The Substation location is projected as approximately 1.7 Ma. The magnetostratigraphic samples taken from the bottom to the top of the Substation excavation produced a reversed magnetic signature (Hillhouse, 2010; p. c. to Reynolds), reinforcing the possibility of representing lower C1r.2r at a date less than 1.77 Ma, the Olduvai normal magnetozone (Table 2).

Table 2. Stratigraphic and magnetostratigraphic relationships					
Ma	Chron	Albright 1999 Locality	Locality Name	NALMA *Bell et al. 2004	NALMA This paper
	C1 n	400			
0.8	C1r.1r		Shutt Ranch L. F.		
0.9	C1r.1r	360	mammoth		
	C1r.1n	359		**Irvingtonian***	
1.4	C1r.2r	350	**El Casco L. F.**	**Blancan**	**Irvingtonian**
	C1r.2r				**faunal turnover**
1.7	C1r.2r		**Substation L. F.**		**Blancan**
	C2n				
2.0	C2r.1r	317	arkosic sandstone marker		
2.5	C2r21r				

Faunal significance

The total number of taxa — 77 plants, invertebrates and vertebrates — is larger than any other single late Blancan NALMA locality in California. The Arroyo Seco and Vallecito Creek faunas from Anza-Borrego Desert State Park contain a higher taxon count, but the count represents the combined taxa from many sites (Jefferson, 2008). The stratigraphic position of the mammalian taxa at the Substation site will help interpret timing of the Blancan/Irvingtonian transition (Bell and others, 2004) west of the Rocky Mountains on the North American continent, which may be different than that described previously (Bell and others, 2004) .

Substation faunal list

INVERTEBRATES
INSECTS
Bembrix sp. ..... sand wasp
Psychomyiidae ..... caddisfly larva

MOLLUSKS
Deroceras sp. ..... slug test
Amnicola sp. ..... conispiral gastropod
Physa sp. ..... conispiral gastropod
Succinea sp ..... conispiral gastropod
Pupilla sp. ..... conispiral gastropod
Vertigo sp. ..... conispiral gastropod
Vallonia sp. ..... planispiral gastropod
Helisoma sp. ..... planispiral gastropod

LOWER VERTEBRATES:
FISH
Gasterosteus sp. ..... stickleback

AMPHIBIANS
Ambystoma sp ..... salamander
Batrachoseps sp. ..... salamander
Ensatina sp ..... salamander
Hyla sp. ..... tree frog
Pelobatidae or Bufonidae ..... frog or toad

TORTOISE/TURTLE
Actinemys sp. ..... pond turtle
Hesperotestudo sp. ..... giant tortoise

SERPENTES
Colubridae ..... snake
Crotalidae ..... pit viper

LACERTILIA
Elgaria sp. ..... alligator lizard
Annielidae ..... legless lizard
Iguanidae ..... iguanid lizard
Sceloporus sp ..... spiny lizard
Phrynosoma sp. ..... horned lizard
Plestiodon sp. ..... skink

BIRDS
Aphelocoma californica ..... scrub jay
Passeriformes ..... perching birds
Fringillidae ..... finches
Porzana carolina ..... sora rail
Oxyura jamaicensis ..... ruddy duck

SMALL MAMMALS:
INSECTIVORA
cf. *Notiosorex* sp. ..... shrew
Sorex sp. ..... long-tailed shrew
Scapanus sp. ..... mole

LAGOMORPHA
Sylvilagus sp ..... cottontail

SCIURIDAE
Xerospermophilus sp., cf. *mohavensis* ancestral Mojave ground squirrel

HETEROMYIDAE
Perognathus sp A ..... pocket mouse
Perognathus sp B ..... small pocket mouse
Perognathus sp. C ..... pocket mouse
Dipodomys sp A ..... kangaroo rat
Dipodomys sp B ..... kangaroo rat
Dipodomys sp C ..... kangaroo rat
Dipodomys sp D ..... kangaroo rat
Prodipodomys sp ..... ancestral kangaroo rat

GEOMYIDAE
Thomomys sp.cf. *T. bottae* ..... Botta's pocket gopher

CRICETIDAE
Peromyscus sp. ..... pocket mouse
Peromyscus (sm) sp. cf. *P. hagarmanensis* ..... pocket mouse
Neotoma sp. ..... wood rat
Neotoma sp (large) ..... wood rat
Neotoma prefuscipes ..... wood rat
Neotoma (Paraneotoma) fossilis ..... extinct wood rat
Onychomys sp. cf. *O. pedroensis* ..... grasshopper mouse
Baiomys sp. (small) ..... pygmy mouse
Reithrodontomys rexroadensis ..... harvest mouse

MICROTINAE
Allophaiomys sp ..... ancestral vole
Ondatra? ..... muskrat

LARGE MAMMALS
XENARTHRA
Nothrotheriops sp. ..... Shasta ground sloth
Paramylodon harlani ..... Harlan's ground sloth

PERISSODACTYLA
Equus bautistensis ..... horse

ARTIODACTYLA
Odocoileus sp ..... deer
Odocoileus sp (large) ..... large deer
Paleolama sp. ..... llama
Gigantocamelus sp? ..... giant camel

CARNIVORA
Mephitis mephitis? ..... skunk
Smilodon gracilis ..... saber cat
Homotherium serum ..... scimitar cat
Pantera onca? ..... Jaguar

Small mammal biochronology

Prodipodomys sp. is a Blancan indicator that did not survive into the Irvingtonian (Albright, 1999; Bell and others, 2004). The Substation Fauna heteromyids and cricetids share more than ten taxa in common with four older localities(to 2.5 Ma) in the San Timoteo Formation, and only three in common with the overlying 1.4 Ma El Casco Fauna (Albright, 1999) (Table 2). This suggests that the Substation Fauna (1.7 Ma) may represent a Late Blancan fauna, the Blancan thought to end across the continent at about 1.72 Ma (Bell and others, 2004). However, in an attempt to exclude "*Plesippus*" from the Irvingtonian, those authors suggest that the Irvingtonian in southern California may start later than the 1.4 Ma El Casco locality, due to the presence of "*Plesippus*" at that site.

Large mammal biochronology

Paramylodon sp. and *Nothrotheriops* sp. appear around 2 Ma in the Vallecito–Fish Creek Badlands of Imperial County, CA (McDonald, 2004). The earliest western US date for *Odocoileus* sp. is 2.2 Ma at Anza Borrego (Murray, 2006). The camelids *Paleolama* sp and *Gigantocamelus* sp. are present from 2.2—0.9 Ma at Anza-Borrego (Webb and others, 2006). *Homotherium* sp. appears in the late Blancan (Bell and others, 2004) and *Smilodon gracilis* is known from late Blancan to middle Irvingtonian (2.2–1.0 Ma) deposits from Imperial County (Shaw and Cox, 2006). The Substation large mammals (Table B) reinforce a late Blancan age.

Table 3 suggests that a faunal turnover from Blancan to Irvingtonian NALMA time occurred between deposition of the Substation locality (1.7 Ma) and the El Casco Locality (1.4 Ma). Of the selected taxa in Table 3, ten of the Substation taxa are present down section, while only four are known from upsection.

Substation flora

The associated Substation flora is distinct from other southern California floras of similar age as it contains plants from aquatic and foothill communities, along with riparian and upland slope communities.

Aquatic community
- *Equisetum* sp. (horse tail)
- *Sparganium* sp. (bur-reed)
- *Typha* sp. (common cattail)

Riparian community
- Betulaceae (birch)
- *Platanus* sp. (sycamore)
- *Populus* sp. (cottonwood, aspen, or poplar)
- *Salix* sp. (willow)

Foothill slopes
- *Magnolia* sp. (magnolia)
- *Quercus* sp. (oak)
- *Rhododendron* sp. (rhododendron)
- *Robinia*? (locust)

Upland slopes
- *Pinus* sp. (pine)

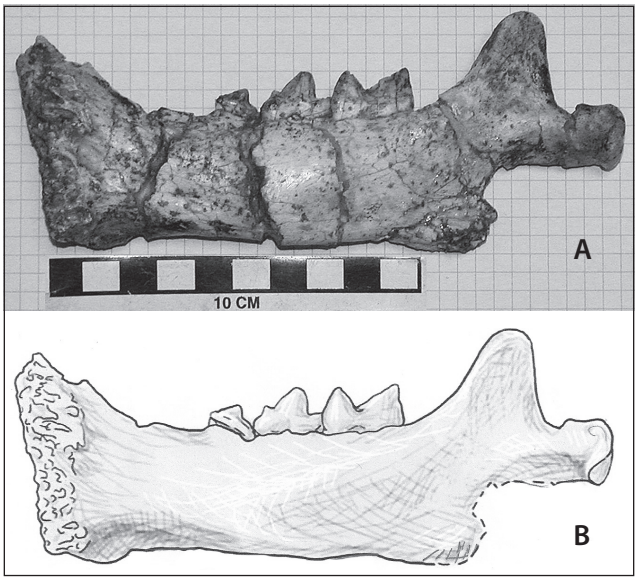

Figure 2. (a) Smilodon graciilis right mandible. b: *Smilodon gracilis*, right mandible. Illustration by Katura Reynolds

The transition from the Blancan into the Irvingtonian NALMA is diachronous and poorly constrained. Albright (1999) originally described the El Casco Local Fauna of 1.4 Ma as early Irvingtonian. However, Bell and others (2004) chose to include the El Casco fauna in the late Blancan, in part to exclude the "*Plesippus*" of El Casco (Albright, 1999) from the Irvingtonian, leaving the Bl/Ir transition date in California between 1.4–1.3 Ma (Bell and others, 2004).

This report places the El Casco Substation Fauna in the late Blancan NALMA, an assignment supported by age ranges of the heteromyidae, cricetinae and microtinae from the Substation that appear earlier and lower in the San Timoteo sedimentary section than the El Casco fauna (Albright, 1999). In particular, *Prodipodomys* sp., *Neotoma (Paraneotoma) fossilis,* and *Onychomys* sp. cf. *O. pedroensis* do not elsewhere range into the Irvingtonian NALMA (Lindsay, 2008). Table B suggests that a faunal turnover occurs between deposition of the Substation locality (1.7 Ma) and the El Casco Locality (1.4 Ma). To paraphrase Bell and others (2004), this faunal turnover between 1.7 and 1.4 Ma might be the beginning of the "Irvingtonian as it is traditionally recognized in California" were it not for their decision to include the El Casco fauna and its "*Plesippus*" in the Blancan. This report suggests that the Substation Fauna is late Blancan NALMA and the fauna from the El Casco locality is Irvingtonian, but contains one Blancan holdover, *Plesippus* sp.

Summary

The excavation for the SCE El Casco Substation produced 15,909 specimens from the San Timoteo Formation, including 2,816 plant specimens, 1,013 invertebrate specimens, and 12,080 vertebrate specimens. These fossils have been identified and curated into the Western Science

TABLE 3: Stratigraphic ranges of selected taxa from the San Timoteo Formation

Location	L	195	304	311	Substation	El Casco 350	Mammoth
Chron (from Albright, 1999a)		C2r.2r	C2An.2n	C2An.1n	C1r.2r	C1r.2r	C1r.1r
Perognathus sp A	S	—	—	S	ELCS		
Perognathus sp B				S	ELCS		
Perognathus sp C		S	—	—	ELCS		
Dipodomys sp A		S	—	—	ELCS		
Dipodomys sp B			S	—	ELCS		
Dipodomys sp C				S	ELCS		
Dipodomys sp D					ELCS	S	—
Prodipodomys sp	S	—	S	S	ELCS		
Thomomys sp. cf. *T. bottae*					ELCS	S	—
Peromyscus hagarmanensis	S	S	S	S	ELCS		
Neotoma prefuscipes					ELCS	S	—
Neotoma (P.) fossilis					ELCS		
Onychomys pedroensis					ELCS		
Baiomys sp	S	—	—	—	ELCS		
Reithrodontomys rexroadensis		S	—	—	ELCS		
Allophaiomys sp					ELCS		
Ondatra?					ELCS	S	
"Plesippus" francescana						S	
Equus bautistensis					ELCS	S	
Paleolama sp.					ELCS		
Smilodon gracilis					ELCS		
Homotherium serum					ELCS		
Pantera onca?					ELCS		
Mammuthus sp.							M
A = Anza-Borrego (Jefferson & Lindsay 2006); ELCS = El Casco Substation; L = Lower in section; S = San Timoteo Fm. (Albright 1999)							

Center, Hemet, as 1,922 groups of specimens. Together, this assemblage of specimens constitute the basis for the description of the El Casco Substation Flora of 12 plant taxa and the El Casco Substation Fauna with 65 animal species, for a combined total of 77 taxa.

The Blancan Substation Fauna provides new data for describing the transition of mammals from the Blancan (2.5 MA) to Irvingtonian (1.4 MA) Land Mammal Ages at a time between 1.65 MA and earlier than 1.4 Ma. The age range of 1.77 MA to 1.65+ MA is assigned to the El Casco Substation Fauna. The El Casco Fauna of 1.4 MA (Albright, 1999) contains Irvingtonian taxa, except for the genus Plesippus sp. The significant faunal turnover between the Substation and El Casco that indicates the Blancan/Irvingtonian transition would be at approximately 1.5 MA.

Acknowledgments

I thank M. O. Woodburne for his review of this manuscript. The author acknowledges important support provided by Southern California Edison during fossil recovery, preparation, identification and curation. Help with specimen identification came from George Jefferson and Jeannie Johnstone at Anza Borrego Desert State Park (large herbivores and felids); Chris Shaw and Shelly Cox at George C. Page, La Brea Discoveries (large felids and herbivores). Douglas Morton (USGS emeritus) and Jonathan Matti (USGS) visited the site and offered opinions on stratigraphic relationships. We thank Darla Abigt Radford for assistance with curation into the collections of the Western Science Center.

References cited

Albright, L.B., III. 1999. Biostratigraphy and vertebrate paleontology of the San Timoteo Badlands, Southern California. University of California Publications in Geological Sciences 144: 1121.

Bell, C.J., E.L. Lundelius, Jr., A.D. Barnosky, R.W. Graham, E.H. Lindsay, D.R. Ruez, Jr., H.A. Semken, Jr., S.D. Webb, and R.J. Zakrzewski. 2004. The Blancan, Irvingtonian, and Rancholabrean Mammal Ages; pp. 232-314 in M. O. Woodburne, (ed.), Cenozoic Mammals of North America, Geochronology and Biostratigraphy. University of California Press, Berkeley, California.

Jefferson, G.T. 2008. A catalog of Blancan and Irvingtonian vertebrates and floras From Arizona, Southern California, Nevada, Utah and North Western Mexico. Manuscript, Stout Research Center, Anza-Borrego Desert State Park 107 p.

Jefferson, G.T., and L. Lindsay (eds) 2006. The Fossil Treasures of the Anza-Borrego Desert. Sunbelt Publications, San Diego, California 394 p.

Lindsay, E.H. 2008. Cricetidae. p. 456–479, in C. M. Janis, G. F. Gunnell and M. D. Uhen (eds.), Evolution of Tertiary Mammals of North America, 2: 795.

Matti, J.C., and D.M. Morton. 1993. Paleogeographic evolution of the San Andreas fault in Southern California: a reconstruction based on a new cross-cut fault correlation,

pp. 107–159 in R. E. Powell, R. J. Weldon, and J. C. Matti, J.C. (eds.), The San Andreas Fault System: Displacement, Palinspastic Reconstruction, and Geologic Evolution. Geological Society of America Memoir 178 p.

Matti, J.C., D. M. Morton, and V.E. Langenheim, 2015. Geologic and Geophysical Maps of the El Casco 7.5′ Quadrangle, Riverside County, Southern California, with Accompanying Geologic-Map Database. USGS Open-File Report 2010–1274. Accessed March, 2017. https://pubs.er.usgs.gov/publication/ofr20101274

McDonald, H.G. 2006. The ground sloths: invaders from South America. p. 161-174 in , G. T. Jefferson, and L. Lindsay (eds). The Fossil Treasures of the Anza-Borrego Desert. Sunbelt Publications, San Diego, California. p. 329-338.

McDonald, H.G., and V.L. Naples. 2008. Xenarthra. p. 147–160 in: C. M. Janis, G. F. Gunnell and M. D. Uhen (eds.), Evolution of Tertiary Mammals of North America 2: 795.

Morton, D.M. 2004. Geologic map of the Santa Ana 30′ × 60′ quadrangle, Southern California,1:100,000. U. S. Geological Survey Open File Report (OFR) 99-172, V.2-2004.

Murray, L.K. 2006. The smaller artiodactyls: peccaries, oxen, deer, and pronghorns, pp. 273-287 in G. T Jefferson,., and L. Lindsay, (eds.), The Fossil Treasures of the Anza-Borrego Desert. Sunbelt Publications, San Diego, California.

Shaw, Christopher A., and Shelly M. Cox, 2006, The large Carnivorans: Wolves, Bears and Big Cats, . pp. 177–191 in G. T. Jefferson, and L. Lindsay (eds.), The Fossil Treasures of the Anza-Borrego Desert. Sunbelt Publications, San Diego, California.

Webb, S.D. 1998. Cervidae and Bovidae, pp. 508–519 in C. M. Janis, K. M. Scott and L. L. Jacobs (eds.), Evolution of Tertiary Mammals of North America, 1: 691.

Webb, S.D., K. Randall, and G.T. Jefferson. 2006. Extinct camels and llamas of Anza-Borrego, pp. 293–310in G. T Jefferson and L. Lindsay (eds). The Fossil Treasures of the Anza-Borrego Desert. Sunbelt Publications, San Diego, California.

First report of middle Pleistocene (Irvingtonian) terrestrial megafauna from the Brawley Formation, Superstition Hills, Imperial County, California

Mark A. Roeder[1] and Thomas A. Deméré[1]
Department of Paleontology, San Diego Natural History Museum, P.O. Box 121990, San Diego, CA 92112; maroeder1731@aol.com, tdemere@sdnhm.org

Introduction

Since 2012, paleontological reconnaissance fieldwork conducted in the Superstition Hills in western Imperial County has resulted in new fossil discoveries at several sites in deformed strata mapped as the Brawley Formation. Recovered fossils include locally abundant shells of freshwater gastropods and bivalves, monotypic assemblages of brackish water bivalves, sparse skeletal remains of freshwater and marine bony fishes, and isolated teeth of small terrestrial reptiles and mammals (Roeder and Remeika, 2014). During the 2016 field season isolated bones of a tortoise and large-bodied land mammals were discovered in the southern part of the Superstition Hills. These discoveries increase the number and diversity of vertebrate fossils known from the Brawley Formation. What follows is a preliminary description of the new terrestrial reptile and mammal fossils and a preliminary interpretation of the significance and implications of these fossils in understanding the paleobiology and paleoecology of Pleistocene deposits of the western Salton Trough.

Geologic Setting

The Superstition Hills is an area of low, eroded badlands in the western Salton Trough that has been uplifted and folded along the WNW striking Superstition Hills Fault and related NE striking sympathetic faults (e.g., Elmore Ranch Fault) (Kirby et al., 2007). These faults lie within the southern portion of the San Jacinto Fault Zone and are active, having ruptured as recently as 1987 (Hudnut et al., 1989).

The middle Pleistocene Brawley Formation (Dibblee, 1954) is well exposed throughout the Superstition Hills in a series of faulted anticlines and synclines (Dibblee, 1984, 2008). Over 600 meters of strata consisting primarily of light gray claystones and thin sandstones with occasional intervals of pebbly sandstones were mapped by Dibblee (2008) in the area. Dibblee (1984) suggested that deposition of the Brawley Formation occurred under generally the same conditions as those of the Borrego Formation (i.e., a large, below sea level brackish water lake). However, more recent work suggests a more complex depositional history for the Brawley Formation.

Besides the Superstition Hills, the Brawley Formation also crops out as badlands to the north in the San Felipe Hills and west of Salton City, to the south at Superstition Mountain, and in the Durmid Hills east of the Salton Sea. In other areas of the Salton Trough, the Brawley Formation is widely present in the subsurface. Magnetostratigraphic work by Kirby et al. (2007) in the San Felipe Hills dates the Brawley Formation at about 1.1 to 0.5 Ma (*mega annum*). These authors note that the Brawley Formation and the coeval Ocotillo Formation (Dibblee, 1954) typically (but not everywhere) lie unconformably on lacustrine strata of the Borrego Formation. Kirby et al. (2007) also provide detailed discussions of the Brawley Formation and Ocotillo Formation, describing the lithologic and depositional complexity of both rock units. For the Brawley Formation, Kirby et al. (2007) note that this rock unit contains not only fluvial, lacustrine, and deltaic deposits associated with the ancient Colorado River delta, but also contains locally derived basin sediments associated with aeolian, playa lake, and alluvial fan settings. In addition, work by these and other researchers have shown that the Brawley Formation in the San Felipe Hills and Durmid Hills also contains evidence of several marine incursions (Kirby et al., 2007; Roeder and Remeika, 2014; Roeder and LaFollette, 2015).

Paleontology

Fossils reported from the Brawley Formation include well-preserved shells of freshwater (lacustrine) and brackish water (lagoonal) mollusks, ostracods, and diatoms recovered from exposures in the San Felipe Hills (Kirby et al., 2007), rare remains of freshwater vertebrates and small-bodied terrestrial vertebrates (Table 1) collected as a result of screenwashing of *Rangia* shell beds exposed in the northern Superstition Hills (Roeder and Remeika, 2014), and rare tests of brackish water, benthic foraminifers from strata exposed in the San Felipe Hills (Kirby et al., 2007). The latter records indicate that

the "Brawley Lake" basin possibly had periodic connections to the ancestral Gulf of California during the middle Pleistocene.

Recent paleontological reconnaissance fieldwork has resulted in the discovery, at one site (SDNHM Locality 7289), of isolated, fragmentary, permineralized bones of large-bodied land mammals weathering out on the surface (Table 1). The recovered fossils include post-cranial elements assigned to tortoise, horse, and camel as described below.

Table 1. List of fossil vertebrates from the Brawley Formation, Superstition Hills, Imperial County, CA.

Taxon	Common Name	Element	Depositional environment
Osteichthyes			
Gila sp.	Chub	Pharyngeal teeth	Fluvial, deltaic, lacustrine
Cynoscion parvipinnus	Short-finned corvina	otoliths	Lagoon, estuarine, shallow marine
Reptilia			
Gopherus sp.	Desert tortoise	carapace fragment	Upper delta plain
Crotalus sp.	Rattlesnake	fang	Upper delta plain
Mammalia			
Microtus sp.	Vole	teeth	Upper delta plain
Perognathus sp.	Pocket mouse	teeth	Upper delta plain
Dipodomys sp.	Kangaroo rat	teeth	Upper delta plain
Equus sp.	Horse	rib, tibia, phalanx	Upper delta plain
Camelidae indet.	Camel	scapula fragment	Upper delta plain

Figure 1. Pleistocene mammal fossils from SDNHM Locality 7289, Brawley Formation, Superstition Hills. A-C. *Equus* sp. (SDNHM 146796), proximal phalanx. A. palmar view. B. anterior view. C. dorsal view. D. Camelidae (SDNHM 146800), right scapula, distal end. Scale bars equal 2 cm.

Reptilia
Testudinidae
cf. *Gopherus* sp.

Referred specimens: SDNHM 146795 carapace margin fragment

The carapace fragment measures 31.6 mm by 14.2 mm by 4.6 mm and is sharply broken. It preserves grooves for epidermal scutes and was found on the ground surface as float. The thickness and surface texture of this fragment is consistent with carapace elements of the common desert tortoise, *Gopherus*.

Perissodactyla
Equidae
cf. *Equus* sp.

Figs. 1A, B, C

Referred specimens: SDNHM 146796, proximal phalanx; SDNHM 146797, capitulum of anterior rib; SDNHM 146798 partial right tibia, proximal end; SDNHM 146799 partial rib.

The nearly complete proximal phalanx measures 83.8 mm in length, with a distal trochlear width of 42.8 mm and a dorsoventral thickness of 26.3 mm. The fossil was found on the ground surface as float. The overall size of the phalanx is consistent with proximal phalanges of medium-sized horses. Other skeletal elements tentatively assigned to *Equus* sp. include the capitulum of an anterior rib, the sharply broken shaft of a rib, and a badly weathered proximal fragment of a right tibia. The rib shaft was found partially *in situ* in a cross-bedded sandstone, while the other elements were found as float.

Artiodactyla
Camelidae

Fig. 1D

Referred specimens: SDNHM 1467800, partial right scapula, distal end.

A distal end of a large camelid scapula preserves the anterodorsal portion of the glenoid cavity, the dorsal portion of large coracoid process, and the distal terminus of the scapular spine. The bone is strongly permineralized and sharply broken and was found as float.

Discussion

In the Superstition Hills, the recovery of horse and camel remains, of freshwater invertebrates (*Anodonta* sp.) and freshwater bony fish (*Gila* sp.), and of brackish water invertebrates (*Rangia* sp.) and marine bony fish (*Cynoscion*

parvipinnus) is evidence for a diversity of depositional environments, including upper delta plain , delta plain distributary channel, and delta front lagoon, respectively. These various facies of the Brawley Formation fit within a broader depositional system that was dominated by the Pleistocene Colorado River delta. However, as noted by Kirby et al. (2007), other facies of the Brawley Formation suggest a more complex depositional history in which locally-derived sediments were transported into the western and northern portions of the Brawley Formation depositional basin by ephemeral streams associated with fluvial and alluvial fan facies of the Ocotillo Formation. During the interval of time represented by the Brawley Formation, the interplay of these various depositional environments largely repeated geologic events first established during the Pliocene. These events include episodic filling of the Salton Trough by northward flowing flood waters of the ancestral Colorado River to form large lacustrine bodies of water that subsequently desiccated when flow from the Colorado River was diverted to the south side of the delta and back into the head of the proto-Gulf of California (Dorsey, 2006). It was in a setting like this that the ecologically diverse invertebrate and vertebrate assemblages of the Brawley Formation lived.

Taphonomically, the isolated and fragmentary nature of the megafaunal remains described above suggests a process of breakup of skeletons on the Pleistocene delta floodplain followed by reworking during flood conditions and eventual transport and deposition of isolated skeletal elements in distributary channels. Cassiliano (1999) reported a similar taphonomic process for vertebrate fossils found in the Arroyo Diablo Formation as exposed in the Vallecito Creek-Fish Creek area of Anza Borrego Desert State Park. These taphonomic conditions of the Brawley Formation appear to stand in contrast to those evident for the coeval Ocotillo Formation, from which more complete skeletons of a diversity of Pleistocene land mammals have been recovered (Jefferson and Lindsay, 2006).

Conclusions

Although fragmentary and few in number, the terrestrial vertebrate fossils reported here serve as an indication of the paleontological potential of the Brawley Formation strata exposed in the Superstition Hills. Applying the Potential Fossil Yield Classification (PFYC) criteria used by the Bureau of Land Management (BLM, 2007) and the U.S. Forest Service, we suggest that the Brawley Formation should be assigned a PFYC 4 ranking. With increased oversight by BLM managers and with additional paleontological walkover surveys, it is hoped that the rich paleontological history of this rock unit will be more fully revealed.

Acknowledgements

Field work was conducted under BLM Paleontological Permit CA-16-09P and fieldwork authorization number CA-670-017-048EA01 for the BLM El Centro Field Office. This manuscript benefited from review comments by George T. Jefferson.

References

Bureau of Land Management (BLM). 2007. Potential Fossil Yield Classification (PFYC) System for Paleontological Resources on Public Lands. Instruction Memorandum No. 2008-009, released October 15, 2007.

Cassiliano, M.L. 1997. Taphonomy of mammalian fossils across the Blancan-Irvingtonian boundary: Palm Spring Formation, Anza Borrego Desert of southern California. Palaeogeography, Palaeoclimatology, Palaeoecology 129:81–108.

Dibblee, T.W. Jr. 1954. Geology of the Imperial Valley region, California. In, R.H. Jahns (ed.), Geology of southern California. California Division of Mines, Bulletin 170, chapter 2:21-28.

Dibblee, T.W., Jr. 1984. Stratigraphy and tectonics of the San Felipe Hills, Borrego badlands, Superstition Hills, and vicinity. In, C.A. Rigsby (ed.), The Imperial Basin-Tectonics, Sedimentation, and Thermal Aspects. Pacific Section S.E.P.M. guidebook: 31-44.

Dorsey, R. 2006. Stratigraphy, tectonics, and basin evolution in the Anza-Borrego Desert region. In, G.T. Jefferson and L. Lindsay (eds.), Fossil Treasures of the Anza-Borrego Desert. Sunbelt Publications, San Diego, California, p. 89-104.

Hudnut, K.W., L. Seeber, and T. Rockwell. 1989. Slip on the Elmore Ranch Fault during the past 330 years and its relation to slip on the Superstition Hills Fault. Bulletin of the Seismological Society of America 79:330-341.

Jefferson, G.T. and L. Lindsay. 2006. Fossil Treasures of the Anza Borrego Desert. Sunbelt Publications, San Diego, California. 394 p.

Kirby, S.M., S.U. Janecke, R.J. Dorsey, B.A. Housen, V.E. Langenheim, K.A. McDougall, and A.N. Steely. 2007. Pleistocene Brawley and Ocotillo formations: evidence for initial strike-slip deformation along the San Felipe and San Jacinto fault zones, southern California. Journal of Geology 115:43-62.

Roeder, M.A. and P. Remeika. 2014. A preliminary report on new records of fossils from the Brawley Formation (middle to late Pleistocene), northern Superstition Hills, Imperial County, California. In, R.E. Reynolds (ed.) Not a Drop Left to Drink. 2014 Desert Symposium, California State University Desert Studies Center, p. 123.

Roeder, M.A. and P.I. LaFollette. 2015. New fossil records from the middle Pleistocene Brawley Formation of Imperial and San Diego counties, southern California. Southern California Academy of Sciences, Abstracts with Programs, p. 109.

The work of W. Morlin Childers: amateur paleontologist and archaeologist

Edgar Bernal Sevilla [1] and Linda Gilbert [2]
[1] *Imperial Valley Desert Museum, Ocotillo, CA 92259,*
[2] *Colorado Desert District Stout Research Center, Borrego Springs CA 92004*

As any American southwestern enthusiast will tell you, there are few things more captivating than a desert landscape. The great deserts of the American southwest have fascinated western visitors since the first Spaniards came in search of gold and glory. Today, rather than conquistadors and missionaries, the southwest is full of archaeologists, naturalists, geologists, hikers, off-roaders, and campers who all share a love for what many consider a desolate region. This passion for the desert captured the heart of a young El Centro, California resident named Willie Morlin Childers, though he usually forsook the Willie and went by Morlin Childers.

Morlin Childers' commitment led him to embrace most of the activities of the modern desert lover; and whereas he is most well-known for his archaeology, his dedication to the desert included the search for fossils, study of the geology of the Colorado Desert, and a deep interest in desert lore. He was a prolific archaeologist and paleontologist of the Imperial Valley and surrounding areas; he even has a species of ancient valley sea urchin named after him (Grant and Hertlein, 1956). While exploring the Imperial Valley desert in 1971, Childers made a find that would change his archaeological career and forever immortalize him in the mythology of the Imperial Valley: the skeleton of what came to be known as the Yuha Man.

Paleontology

Morlin Childers' family moved to El Centro when he was nine. He called himself "a real product of the desert" (Smith, 1981:1), As a youth and young man, Morlin spent as much time in the desert as he could. In the early 1940s he began to collect fossil marine invertebrates – shells of pectens, gastropods, oysters and corals from the sands and clays of the Imperial Group, found in local shell beds in Alverson Canyon, the Coyote Mountains and the Yuha Buttes.

G Dallas Hanna and the California Academy of Science

But to find the fossils was not enough, Childers wanted to know what genera and species they represented, so in 1955 he sent samples and photographs to G Dallas Hanna of the California Academy of Science (CAS) in San Francisco (Grant and Hertlein, 1956). Hanna was the author of Paleontology of Coyote Mountain, Imperial County, California (Hanna, 1926) and was a well-known expert on the Imperial Group and "Latrania Sands" (Hanna, 1926).

Their correspondence continued into the 1960s, with Childers sending specimens and photographs (Childers, personal correspondence with G Dallas Hanna, April 17, 1962) and Hanna enlisting Curator of Invertebrate Paleontology at the CAS, Leo Hertlein to identify them. In a letter to Childers, Hanna said "Dr. Hertlein has worked on your echinoids as thoroughly as he can" (Hanna personal correspondence with W.M. Childers, May 29, 1962). One of the samples turned out to be a new species of sea urchin (Figure 1) and Hertlein and his colleague U.S. Grant IV named it for Morlin Childers – Schizaster morlini (Grant and Hertlein, 1956).

Figure 1 Example of *Schizaster morlini* ABDSP[IVCM] 4001/I183, 31x39 mm., from 3D image prepared by JGilbert and GVogeli, Anza-Borrego Desert Paleontology Society

In 1962, Hanna wrote to Dr. Ted Downs, Curator of Vertebrate Paleontology for the Los Angeles County Museum (LACM), to introduce Childers (Hanna, 1962). Downs had a State Park collecting permit and had been working in the Anza-Borrego area since 1954. They met, and Childers became a go-to resource for Downs – arranging for flights over the desert, a collecting trip to Laguna Salada in Baja California, Mexico, a helicopter to help remove sacks of matrix for sieving, trips to the Yuha Desert, Imperial County, California – and he joined them on field surveys, meeting many of the geologists and paleontologists working with Downs, including George J. Miller (Downs, 1962-1964). Professor Richard Merriam (University of Southern California, USC, head of geology) became a longtime collaborator on Childers' projects and adventures. Merriam brought along a "fresh assistant professor of geology", Dr. Jim Bischoff, who observed about Childers, "…he clearly loved the desert, as did I. He was full of curiosity about the natural world." (Bischoff, personal communication to authors, 2017).

Childers' desert adventures were told in the stories he wrote for Desert Magazine in the 1960s (Childers, 1964; 1966; 1967). His adventures, such as *A Whale of a Trip to*

Baja (Huffman, 1964), *Explorer Rediscovers Lost Lake in Mexico*, (Ryan, 1963) and *Three Cheat Death in Colorado River Triumph* (Ryan, 1964) appeared in the Los Angeles Times and other newspapers. Bischoff said of Childers, "From time to time Morlin would call me on the phone and invite me to accompany him on some expedition or another to see some feature he had discovered. I always enjoyed doing so." (Bischoff, personal communication to authors, 2017).

A discussion with Hanna, about a sandstone formation that Childers photographed (Figure 2) turned into an article published in CAS magazine Pacific Discovery, that included photographs taken by Hanna of similar formations in Santa Cruz, California (Childers, 1964).

In his 1968 paper *Three Late Cenozoic Molluscan Faunules from Baja California with a Note on Diatomite from West of San Felipe*, Dr. Hertlein thanked Morlin Childers for providing a collection of 26 species of echinoids, mollusks and gastropods from previously unvisited localities in Baja California, Mexico (Hertlein, 1968). He observed, "A number of species in the present assemblage are characteristic of the Imperial fauna and one may infer that the strata containing them were deposited approximately contemporaneously with those of the Imperial formation in southeastern California." (Hertlein, 1968:402). He also thanked San Diego State University (SDSU) geology Professor Edwin Allison for providing the stratigraphic relationship of the Childers fossil beds. The diatomite "Note" is also a thank you to Childers for a sample of diatomite containing 32 identified species, although he added "This however is just a small sampling of the flora." (Hertlein, 1968:405). All these collections were placed in the CAS fossil repository.

Childers' contacts with CAS were broken in the early 1970s with the death of Hanna (1970) and Hertlein (1972). But 1971 was an eventful year. It marked the transition from his earlier interest in invertebrate fossils with his new passion - Early Man.

SDSU Masters student Thomas E. Stump was intrigued by the similarity of the Imperial corals, mollusks and gastropods to the fauna of the Caribbean and was told about Childers' invertebrate collection by Allison. In 1972 as Stump was writing his thesis *The Stratigraphy and Paleontology of the Imperial Formation in the Western Colorado Desert*, (Stump, 1972). The Childers' collection became part of his research. Stump met with Childers' wife, Lucille, and selected a portion of the collection to take with him. He identified the specimens, including 10 new species. But, he never met Morlin Childers (Stump personal communication to authors, 2017).

Stump's 1972 thesis documented in detail the relationship between over 120 invertebrate fossils found in the Imperial Group and the living species found in the Caribbean – something that had been recorded but not systematically described by William Healey Dall, Curator of the Department of Mollusks, United States National Museum in his *Scientific Results of the Explorations of the U.S. Fish Commission Steamer Albatross between 1887 and 1888* from the coast of Chesapeake Bay through the Strait of Magellan and up the coast of California, (Dall,1889). In 1974, Stump returned the Childers invertebrates. Subsequently, those specimens were donated to the Imperial Valley College Museum (Spencer, T., Imperial Valley College correspondence with W.M. Childers, May 16, 1974).

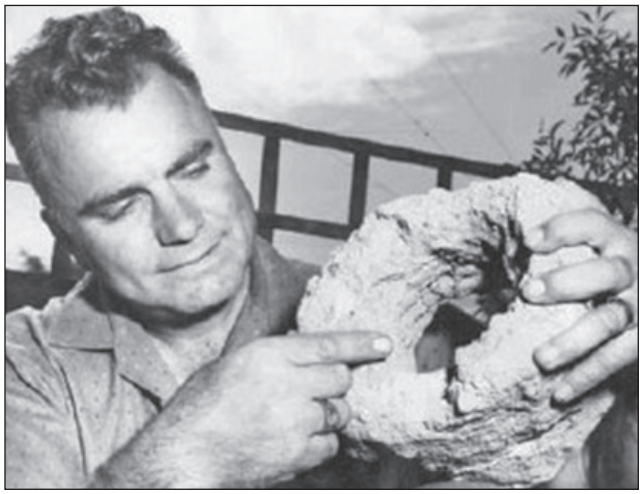

Figure 2. Morlin Childers with a "sandstone chimney" 1964 from the IVDM Morlin Childers collection..

Calico Archaeological Conference 1970

The Calico Conference was a turning point in Childers' career. Many luminaries of the field attended the conference to debate the Pleistocene dates emerging from the site. Childers was not invited, but he managed to gain entry with a press pass. He attempted to show a few archaeologists some of the tools he had collected but they refused to look at them (Minshall, 1978). In a last ditch attempt, Childers approached archaeology superstar Dr. Louis Leakey himself. Not only did Leakey agree to see them, but he agreed that they were indisputably manmade and likely very ancient. Dr. Leakey's proclamation undoubtedly had a great impact on Childers and he would spend the rest of his career advocating for early (Pleistocene) man in the Americas.

The first skeleton—Truckhaven Man

Childers, while roaming the desert in 1971 with geologists Dick Merriam and Jim Bischoff (Bischoff, personal communications with authors 2017), found a pile of stones near the unincorporated community of Truckhaven, California, on the northwest bank of the Salton Sea (Childers, Tom, personal communication to author Sevilla April 11 2016). To the untrained eye, a pile of stones is a pile of stones, but Childers saw from caliche buildup around the stones, what appeared to be a random pile of rocks a camper might have left behind, was actually placed in antiquity. Following further analysis, he deduced that the pile was most likely a burial cairn. Childers leased the

Figure 3: Navy helicopter from the IVDM Morlin Childers collection.

land from the owner and contacted Dr. Erlinda Burton, a Professor of archaeology at the local Imperial Valley College (Childers et al., 1973).

Dr. Burton assigned her archaeology students to excavate the burial site. Childers arranged for a U.S. Navy helicopter to fly the skeleton out on May 15, 1971 (Childers, personal correspondence with Captain J. Evans Jr. of the U.S. Navy, May 20,1971)

The excavators used shellac to hold the matrix together. Unfortunately the shellac contaminated the bone such that direct radiocarbon dating on bone collagen could not be performed. Instead, Childers arranged, at the suggestion of his friend Julian D. Hayden, to have the bones dated based on the carbon content of bone apatite (Hayden, personal correspondence with W.M. Childers, July 22, 1971). The date that came back was 4,990 ± 250 BP (years before present). Due to the unreliability of bone apatite dating and the unremarkable result, Childers moved on to his next discovery, which occupied his remaining years.

The second skeleton—Yuha Man

Childers knew where there was another cairn. Time for excavation was of the essence since the site was in danger from off-road vehicles and pothunters, who had destroyed 15 similar cairns throughout the Yuha Desert before 1972 (Childers,Tom personal communication to Sevilla 2017). Before beginning work, Childers obtained an Antiquities Act Permit – 72-CA-001 and the excavation was undertaken as a salvage with the participation of the Bureau of Land Management (BLM) following the protocols of the time and observed by other leading archaeologists and geologists. (Figure 4). Despite rain at the dig site, Childers, his associates, and Imperial Valley College (IVC) students from one of his classes were able to remove the skeleton from its location and safely transport it to IVC. In the fall 1972, the BLM was the first to publish the Yuha Man discovery, noting "the careful trenching and sifting of extremely small portions of a find in a charted order often preserve fossils and artifacts of an antiquities site…" (Evans, 1972:5).

"Great care was taken to secure sites and samples of caliche complying with the restrictions stated by Williams and Polach" (Childers, 1974:9). Dr. Jim Bischoff sent caliche samples from the matrix surrounding the skeleton to be radiocarbon dated by Geochron Labs (Geochron Lab Report, 1972), which resulted in a date of 21,500 +2,000 -1,000 BP (Childers,1974). Cairn caliche was sent to University of California, Los Angeles where it was dated using radiocarbon analysis to 22,125 ± 400 BP (Childers et al., 1973). "Preliminary tests on samples of the bones showed such a low protein content that radiocarbon dating was not attempted – the whole skeleton would have to have been destroyed." (Childers, 1983:122).

Once the findings were published in Nature (Bischoff et al., 1976), there was immediate resistance to their interpretation of the age of burial. Childers' date was double the accepted time of man's entry into North America, putting Childers squarely at odds with the "Clovis First" model of the peopling of the Americas, in which nomadic big game hunters followed their prey over the Bering Land Bridge no earlier than about 13,000 BP. Ervin Taylor criticized the use of caliche for dating in Childers' work before the end of 1972 (Taylor, 1972).

Research and controversy

Childers used the next few years to bolster his arguments, although he also experienced some setbacks. To validate the amino acid racemization dates, early in 1976 Childers buried a thermometer at the location where the Yuha Man was found. Amino acid racemization dating, a technique pioneered by Dr. Jeffrey Bada, UCSD, in which amino acid racemization (the process by which left-handed amino acids turn right-handed at the death of an organism) ratios are examined in order to get the date of an organism's death. Whereas temperature affects the rate at which amino acids racemize, knowing the average temperature to which a specimen was exposed is crucial

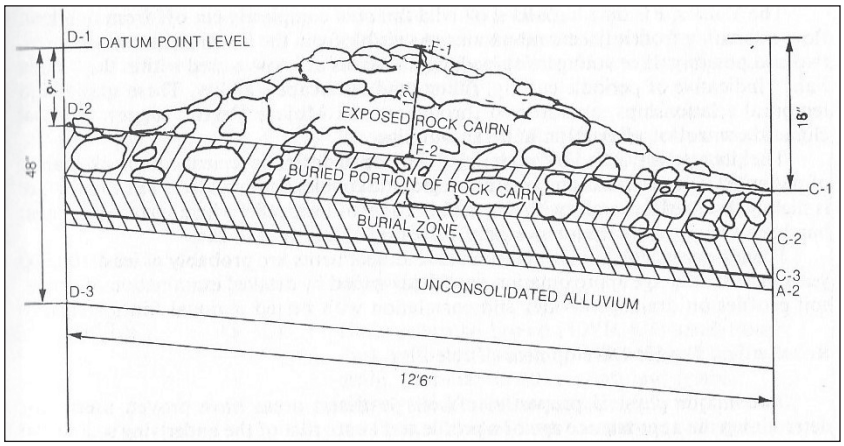

Figure 4. Yuha Burial Diagram from *The Interrelationships of Geology, Geography and Archaeology in the Yuha Desert,* p123, IVDM Morlin Childers Collection

to this technique. Two months later, he returned to find a campfire in the exact spot of his instruments, ruining his experiment. In his Preliminary Report on Yuha Man, Childers (1973) posited that temperatures taken from a Brawley weather station would be consistent with those of the Yuha Desert.

The use of caliche dating was criticized in a series of articles by L. A. Payen, C. H. Rector, and R. E. Taylor (University of California Riverside, UCR), E. Ritter (BLM, Riverside), and J. E. Ericson (Los Angeles County Museum of Art). They first remarked, "Evidence is presented demonstrating that the C-14 dates of around 22,000 years BP should be viewed with extreme caution, especially because of the inherent problem in soil carbonate dating." (Payen, et.al., 1978:448).

They criticized the fact that ^{14}C dating was not conducted directly on the bones. They added that Thorium-230 dating (which was done at a USC laboratory) was in its infancy and so should not be considered reliable (Payen, et al., 1978:449).

"In addition, the presence of late-appearing cultural material at the locality conflicts with the purported antiquity of the site." (Payen et al., 1978:448). They pointed out that cultural material found near the burial, though not necessarily associated with it, was of Holocene age, so it was younger than the age Childers and his associates espoused. They added that the cultural material should definitely be taken into account when ascertaining the date of the burial, although it is not an explicit indicator of age (Payen et.al., 1978: 451).

Bischoff, Childers, and R. J. Schlemon (1978) responded that there were flaws in the Payen et al. (1978) analysis of the soil and stratigraphy, particularly that one of the washes in their diagram was actually just a veneer and was not deep enough to be an actual wash. The site had been excavated in 1971, Shlemon returned in 1978 to conduct additional fieldwork, while Payen's group revisited the site several years after the excavation.

Bischoff, et al. (1978) pointed out that Payen et al. (1978) denouncing of caliche dating was irrelevant because multiple samples of caliche used for the dating all returned similar dates. And they stated that the Payen et al. assertion that direct carbon dating was not conducted was also an unnecessary statement due to the fact that Bischoff had originally mis-stated how much collagen was found in the bones, (Bischoff, 1976) pointing out that to get the correct amount of collagen levels for a sample would result in the destruction of the entire skeleton to obtain the ^{14}C date (Bischoff, et al.,1978).

Payen et al. (1979) responded, stating that Childers' earlier stratigraphic assumptions were likely due to the skeleton sinking a few inches, pointing to the reported discrepancies in the depth of the burial, which they called "a confused situation." They also reiterated the unreliability of dating caliche, pointing out that caliche growth had been observed in WWII graves in Algiers, Algeria, showing that caliche growth is variable and is by no means an indicator of antiquity.

The theft

In August of 1980, the Imperial Valley College Barker Museum was burglarized. Nothing was stolen except for photographs, negatives, and other materials about the Yuha Man. Two months later, the Smithsonian Institution informed the Imperial Valley College that it was going to appropriate the Yuha remains. On November 17, 1980, when the locked storage room that the skeleton was stored in was opened to prepare the skeleton for shipping to the Smithsonian, the Yuha Man was discovered to have been stolen. An FBI investigation was conducted to find the bones but nothing came of it (Ellensburg Daily Record, 1980). There are several versions of the story of this disappearance and it remains a "cold case".

But if the skeleton thief's goal was to keep the skeleton from being re-dated, luck was not on their side. Some bone fragments of Yuha Man's hand, foot, and rib were found overlooked by the thief, along with fragments possessed by Bischoff and Pauline Stedt of the UCR Department of Anthropology, and thus, with the advancement of technology, by 1984, these fragments were sufficient for Carbon-14 dating using tandem accelerator mass spectrometry. The fragments were dated at the University of Arizona Tucson laboratory and none were found to be older than 4,000 years, placing the Yuha Man firmly in the Holocene and out of the Pleistocene era that Childers previous had proposed and fought for. (Stafford et al., 1984: 446-47).

Dr. Tom Stafford, the lead researcher behind the new dating effort, sent Childers his results a few months before publishing Childers got in one last jab at the Riverside researchers, telling Stafford in a letter that "It is refreshing to have the age of the Yuha Bones investigated utilizing a purely scientific approach, without apparent prejudice or speculation." (Childers personal correspondence to Tom Stafford, December 5, 1983.).

Childers continued work on the archaeology of the Yuha Desert. "What has really been a preliminary reconnaissance of the Yuha Desert – even though it has involved many years of work and the collection of thousands of artifacts – has revealed that the archaeology of the area presents problems every bit as complex as those of geology." (Childers, 1984).

Age Assignments Re-evaluated

The following year, *Major Revisions in the Pleistocene Age Assignments for North American Human Skeletons by C-14 Accelerator Mass Spectrometry: None Older Than 11,000 C-14 Years B.P.* was published by Taylor et al. (1985). Before this article was written, Childers had extensive support for his dates. Many other skeletons throughout North America, particularly California, had been dated in excess of 20,000 years. In the years between the mass spectrometry Carbon-14/13 dating of Yuha Man and the

Figure 5. Tom Lee and Morlin Childers in the Yuha Desert from *The Interrelationships of Geology, Geography and Archaeology in the Yuha Desert,* p119, from the IVDM Morlin Childers collection

Taylor et al., 1985 paper, nearly all of these skeletons were re-dated using this new method and none of them were older than 11,000 years (Taylor et al, 1985).

His contributions

Two years later, Childers passed away. Despite ultimately being wrong about the age of Yuha Man, Childers' contributions to science and desert studies are numerous. His paleontological collection led to the discovery of at least one new invertebrate species. The fossil specimens he collected are housed in the major repositories in California – California Academy of Science, Los Angeles County Museum, San Diego Natural History Museum and Colorado Desert District Stout Research Center. His work with the Yuha Man comprised the lead article in the 1972 edition of the BLM's *Our Public Lands*. It helped foster scientific interest in the deserts of California, thus leading to increased political pressure to protect the deserts from vandals and reckless recreation. He published over a dozen papers and magazine articles on archaeology, geology, and desert lore. He involved leading archaeologists and geologists such as: George F. Carter, Reiner Protsch, George M. Stanley, James Bischoff, Richard Merriam, Malcolm Rogers, Kenneth L. White, Emma Lou Davis, Carl L. Hubbs, Julian Hayden, Bob Begole, Margaret Weide, Paul Ezell, Thomas Lee, Rose Tyson, Don Crabtree, Louis Payen, Ervin Taylor, Carol Rector, Eric Ritter, JE Erickson, Roy Schlemon, Jay Von Werlhof, Michael Barker, Erlinda Burton, and surely more – not all of whom agreed with him. The Childers Archaeological Collection, recently acquired by the Imperial Valley Desert Museum, and the Childers Invertebrate Collection, recently acquired by the Stout Research Center, are both now available for the first time since Childers' passing. As the collections are studied by a new generation of researchers, perhaps Morlin Childers still has more contributions to make.

> "That's the way stuff gets found. No one at Berkeley or UCLA would have ever found that Yuha burial. The fact that a person doesn't have a fancy degree doesn't mean he can't develop a very observant eye." Emma Lou Davis on Morlin Childers (Smith, 1981):35.

Acknowledgments

Thank you to Dr. Lyndon Murray and George T. Jefferson for their rigorous editing and insightful discussions of the issues.

References

Bischoff, J. L., R. Merriam, W.M. Childers, R. Protsch. 1976. Antiquity of Man Indicated by Radiometric Dates on the Yuha Burial Site. Nature. 261: 128-129. (13 May 1976)

Bischoff, J. L., W. M. Childers, and R. J. Schlemon. 1978. Comments on the Pleistocene Age Assignment and Associations of a Human Burial from the Yuha Desert, California: A Rebuttal. American Antiquity 43(4) (October 01, 1978): 747-49.

Bischoff, J. L., W. M. Childers, R. Protsch, and R. J. Schlemon. 1979. Reply to Payen Et Al., II. American Antiquity 44(3) (July 01, 1979): 599.

Childers, W. M. 1964. Sandstone Chimneys of the Imperial Formation. Pacific Discovery. 17 (Jan-Feb):29-31

Childers, W. M. 1966. Ghosts of Port Isabel. Desert Magazine, 29 (11) (November, 1966):25-26

Childers, M. 1967. Mystery of Santa Maria. Desert Magazine, 30 (6) (June, 1967):5-7

Childers, W. M., E. Burton, and M. A. Barker. 1973. A Preliminary Report on a Burial Excavated in the Yuha Desert of Imperial County, California. Report. Riverside: Bureau of Land Management, California Desert District Office

Childers, W. M. 1974. A Preliminary Report on a Yuha Burial. Anthropological Journal of Canada,12, (1):2-9

Childers, W. M. 1977. Ridgeback Tools of the Colorado Desert. American Antiquity. 42 (2) (April):242-248

Childers, W. M., H. L. Minshall. 1980. Evidence of Early Man Exposed in Yuha Pinto Wash. American Antiquity. 45 (2) (April):297-398

Childers, W. M. 1983. The Interrelationships of Geology, Geography and Archaeology in the Yuha Desert. Anthropological Journal of Canada, 21:101-127

Dall, W. H. 1889. Preliminary Report on the Collection of Mollusca and Brachiopoda Obtained in 1887-88. Proceedings of the United States National Museum.12:219-362

Davis, E. L., K. H. Brown, J. Nichols. 1972. Evaluation of Early Human Activities in the California Desert. Great Basin Foundation for the Bureau of Land Management.

Downs, T. D. 1962-1964. Field Notes. 1962:10-12: 1963:14-22: 1964:48-50

Ellensburg Daily Record, 1980. From School Closet, Skeleton's Theft Investigated., November 22, 1980.

Evans, T. 1972. Our Public Lands: Yuha Man Pushes Back Frontier of Knowledge, the official publication of the Bureau of Land Management.

Geochron Lab Report 1972: Sample #GX2342, Shellac Contaminated Bone. Cambridge, MA

Grant, U. S., IV and L. G. Hertlein. 1956. Schizaster Morlini, A New Species of Echinoid from the Pliocene of Imperial Valley California. Southern California Academy of Sciences 55(2)

Hanna, G D. 1926. Paleontology of the Coyote Mountains, Imperial County, California. Proceedings of the California Academy of Sciences, 4th Series 14:427-503

Hertlein, L. G. 1968. Three Late Cenozoic Molluscan Faunules from Baja California with Note on Diatomite from West of San Felipe. Proceedings of the California Academy of Sciences, 4th Series 20 (19): 401-405

Huffman, I. 1964.A Whale of a Trip to Baja, Desert Magazine 27 (12):7-8

Minshall, H.L. 1978. The Broken Stones: 83-96. Copley Books.

Payen, L. A., C H. Rector, E. Ritter, R. E. Taylor, and J. E. Ericson. 1978. Comments on the Pleistocene Age Assignment and Associations of a Human Burial from the Yuha Desert, California. American Antiquity 43 (3) (July 01, 1978): 448-53

Payen, L. A., C. H. Rector, E. W. Ritter, and R. E. Taylor. 1979. Reply to Bischoff, Childers, and Shlemon. American Antiquity 44 (3) (July 01, 1979): 596-99.

Ryan, J. 1963. Explorer Rediscovers Lost Lake in Mexico. Los Angeles Times, June 23:190

Ryan, J. 1963. Three Men Plan to Ride Gulf Wave Up Colorado River Aboard Cruisers. Los Angeles Times, August 11:281

Ryan, J. 1964. Three Cheat Death in Colorado River Triumph. Los Angeles Times. January 2:19

Smith, G. 1981. Discovery in the Desert. Westways Magazine. (January):32-35

Stafford, T. W., A. J. T. Jull, T. H. Zabel, D. J. Donahue, R. C. Duhamel, K. Brendel, C. V. Haynes, J. L. Bischoff, L. A. Payen, and R. E. Taylor. 1984. Holocene Age of the Yuha Burial: Direct Radiocarbon Determinations by Accelerator Mass Spectrometry." Nature 308, (5958): 446-47.

Stump, T. E. 1972. Stratigraphy and Paleontology of the Imperial Formation in the Western Colorado Desert. Master of Science Thesis. San Diego State University 132pp.

Taylor, R. E. 1972. U.C.R Carbon Dating Facility. Press Statement by Ervin Taylor regarding the Caliche Date of the Yuha Burial. News release, San Diego, San Diego Union Tribune.

Taylor, R. E., L. A. Payen, C. A. Prior, P. J. Slota, R. Gillespie, J. A. J. Gowlett, R. E. M. Hedges, A. J. T. Jull, T. H. Zabel, D. J. Donahue, and R. Berger. 1985. Major Revisions in the Pleistocene Age Assignments for North American Human Skeletons by C-14 Accelerator Mass Spectrometry: None Older Than 11,000 C-14 Years B.P. American Antiquity 50 (1).

White, K., G. F. Carter, W. M. Childers. 1979. Geomorphology and Time. Anthropological Journal of Canada. 17 (3):16-23

The ants (Hymenoptera: Formicidae) of the San Gabriel Mountains of Southern California, USA with an annotated list

James Des Lauriers[1] and Dana Ikeda[2]
1Department of Biology, Chaffey College, Alta Loma, CA 91737, JIMDESL39@gmail.com
[2]Department of Biological Science, Northern Arizona University, Flagstaff, AZ 86001, USA, Dana.Ikeda@nau.edu

ABSTRACT—We conducted a long term ant sampling program over a period of 16 years along elevational and vegetation gradients in the San Gabriel Mountains of Southern California. Four major findings emerged. 1) We present the first annotated species list, including natural history notes and locations for each species, for this region. 2) We detected 96 species of ants in the San Gabriel Mountains which represents 36% of the 270 species known to occur in California. 3). Five of the species detected were found at elevations higher than previously observed. 4) Despite the high human impact in the area, only two of those species are introduced from outside California. 5) Contrary to previous studies, we found no evidence that species diversity declines with increasing elevation. This study represents a first step in examining the plant community associations of the ant assemblage, the contribution of low elevation ant communities to the montane fauna and the impact of heavy recreational use and urban encroachment on ant species diversity.

Ants constitute an ecologically dominant, taxonomically diverse group of terrestrial arthropods. They contribute to many decomposition and ecosystem processes including predation, soil disturbance and hemipteran tending, particularly in the soil litter horizon. The composition of the various ant functional groups (Andersen 2010, Parr et al. 2005) modulates many ecological interactions (Burger et al. 2003). Ant soil excavation and foraging behaviors move nutrients and seeds and their predation on other arthropods alters the population dynamics of many species. An understanding of ant diversity and plant community associations will permit the detection of developing ecological impacts of a changing climate and intense recreational use.

The San Gabriel Mountains are nearly surrounded by a highly urbanized region including the Los Angeles

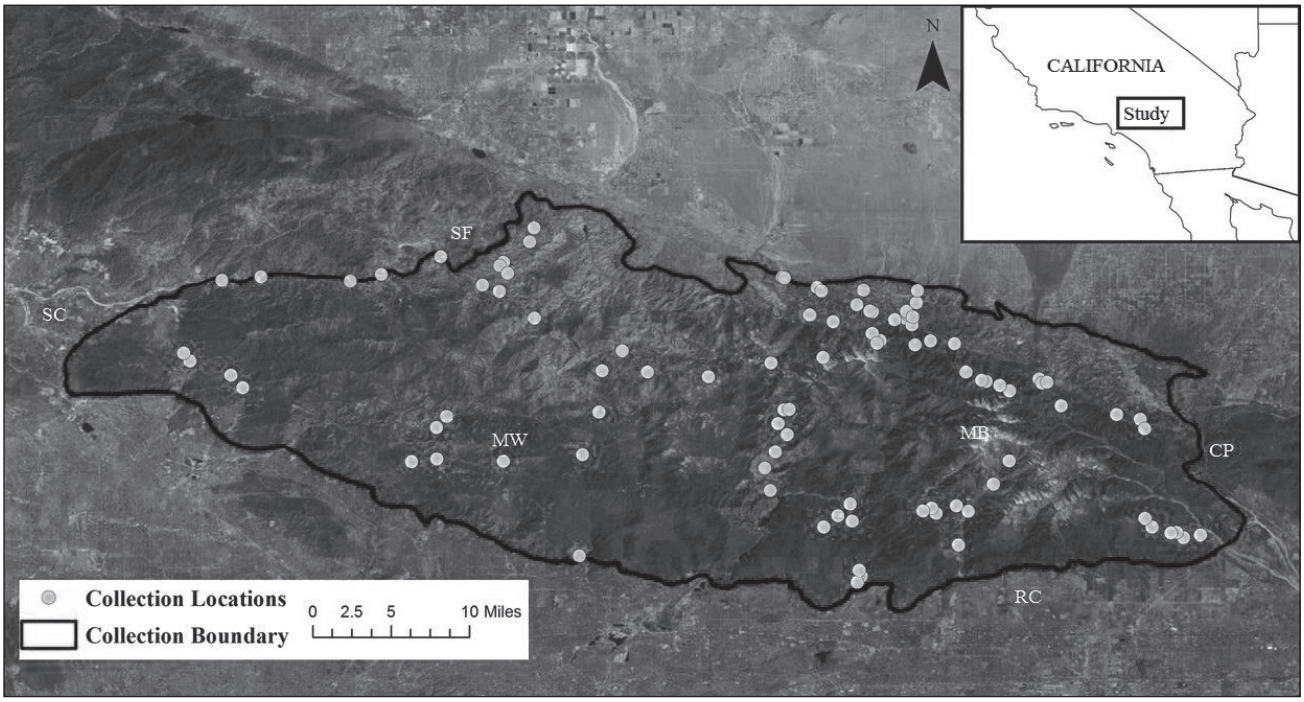

Figure 1. The San Gabriel Mountains study area. The collecting locations are indicated by the yellow points and the red line indicates the perimeter of the study area. Landmarks: CP – Cajon Pass; MB – Mount Baldy at N34.2766°, W117.4713°; MW – Mount Wilson; RC – Rancho Cucamonga; SC – Santa Clarita; SF – San Fernando Pass.

Basin on the south and the Antelope Valley on the north. The mountains get intense recreational use throughout the year and at the same time the mountains provide a significant part of the domestic water supply to the adjacent communities. The need to protect both the recreational and natural resources has been recognized by the inclusion, in 2015, of part of the range in the National Parks system. Monitoring the health of the resource is a clear necessity.

This complex, fire-dominated mosaic of plant communities is an attractive place to study the rich ant fauna. Ward (2005) reviewed the ants of California mostly at the generic level. Ant surveys of Southern California include two in San Diego County (Hunt 1973, Suarez et al. 1998), one in a desert-facing canyon near Palm Springs (Wheeler and Wheeler 1973) and another of Santa Cruz Island (Wetterer et al. 2000) but we have been unable to find any study of the local region. This study represents the first attempt to thoroughly survey the ants of the San Gabriel Mountains with particular attention paid to the elevational and plant community associations of the species.

Materials and Methods

The east-west trending San Gabriel Mountains separate the Los Angeles basin's Mediterranean climate on the south from the Mojave Desert on the north. At 10,064 ft., Mt San Antonio is the high point of the range. The range lies between San Fernando Pass on the west and Cajon Pass on the east, a distance of about 60 mi. The range is about 20 mi wide and includes an area of about 980 mi^2. On the south side, the elevation of the base of the range is at about 2000 ft. and rises abruptly from the valley floor. The plant communities there are dominated by scrub and chaparral communities of various species composition with oak and mixed conifer communities extending to the high ridges. Precipitation on these highest slopes ranges from 30-40 inches. On the north side, at elevations around 4000 ft. junipers mark the base, then Pinyon/Juniper woodlands give way to Conifer/Oak forests with White Fir forests on the highest ridges. These north-facing communities receive 15-20 in. of precipitation, much of it in the form of winter snow. Geologically, the range, along with the others of the Transverse Ranges, is produced by the movement of the Pacific Plate against the North American Plate along the San Andreas Rift Zone. Schoenherr (1992) and Millar (2012) offer overviews of the natural history and the climatic and vegetation history of the region.

Ants were systematically collected across the length and breadth of the San Gabriel Mountains throughout the year between 1999 and 2015. Ants were collected by hand, pitfall traps, Burlese funnel sampling, various bait traps on the ground or hanging in vegetation and by night-lighting. Traps were generally left in place for a year or more and refreshed five or more times per year, generally monthly to allow sampling across seasons. A trap array consisted of four 3.6 in. dia. disposable plastic beverage cups containing radiator fluid. Abensperg-Traun and Steven (1995) as well as Borgelt and New (2005) discuss the statistical advantage of using traps as large as these. A stiff plastic roof supported by 4 long nails embedded in the ground was placed about one inch above the cup to keep rain and litter from falling into the cup while not restraining the ground movement of arthropods. Traps were haphazardly placed on the north sides of bushes or overhanging boulders under the dripline thus protecting the trap from intense summer heat. Hand collecting included opportunistic wandering and surface scanning; turning stones, fallen logs, rotten stumps and litter; breaking twigs; chopping in standing and fallen dead wood; lifting dead bark, digging into active nests and sieving litter.

For the purposes of this study the limits of the mountain range are defined visually on the south side by the abrupt increase in the general slope of the land. On the north side, the range is defined by the lowest local elevation of Pinyon/Juniper woodland or Desert Chaparral (Fig. 1). Heavily modified habitats were avoided which explains the highly dissected margin of the study area.

We used the United States Department of Agriculture Forest Service's CALVEG layers (Cleland et al. 2004) to classify collection sites based on the dominant vegetation type present according to the Regional Dominance Type 1 field description. Collection sites were classified by vegetation type using the ArcMap software (ESRI 2009). A tabulation of sampling effort and the associated vegetation types with their areas are presented in Table 1.

Ants were identified by reference to Wheeler and Wheeler (1973, 1986), Snelling (1973, 1976, 1982), Snelling et al. (2014) and unpublished keys by Snelling and George (1979). The website AntWeb.org has auto-montage images of all of California's ant species (Ward 2016). Identifications of most species in the annotated list (marked at the end of the name by *) were checked by Andrew Suarez (then at UC, Berkeley) or Philip Ward (UC, Davis). Matthew Prebus (UC, Davis) checked the identification of some newly described *Temnothorax*

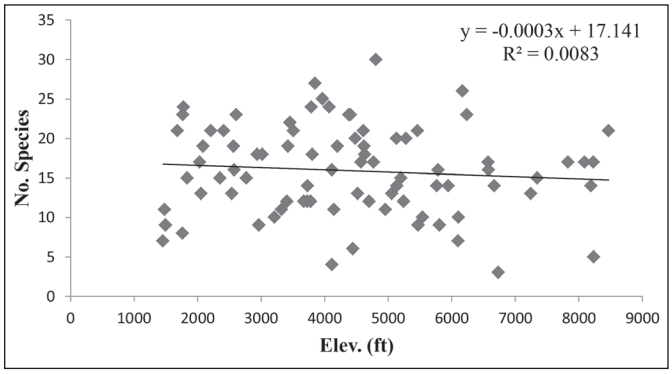

Figure 2. The number of ant species collected at 92 locations in the San Gabriel Mountains plotted against elevation. There is no correlation between elevation and species density.

Table 1. Sampling effort in relation to relative cover of vegetation types.

VEGETATION TYPE	Area (mi^2)	% of Area	% Samp. Effort	Trap Nights	No. Sites
Lower montane mixed chaparral	277.98	29.8	32.4	91613	14
Ceanothus Mixed chaparral	81.30	8.7	2.3	6590	5
Scrub oak	62.45	6.7	5.2	14763	6
Bigcone Douglas Fir	60.38	6.5	2.5	7154	4
Canyon live oak	56.79	6.1	4.7	13227	7
Semi Desert chaparral	37.68	4.0	10.2	28769	14
Mixed conifer fir	35.85	3.8	1.4	3948	1
Soft scrub mixed chaparral	25.55	2.7	1.2	3360	2
Upper montane mixed chaparral	23.76	2.6	2.7	7542	3
Birchleaf Mountain Mahogany	21.87	2.4	0.9	2505	1
Mixed conifer pine	21.67	2.3	1.1	3132	1
Mixed chaparral transition	19.09	2.1	2.6	7405	4
Singleleaf pinyon pine	18.25	2.0	2.2	6166	2
Jeffrey Pine	17.75	1.9	2.9	7777	3
Sumac shrub	17.49	1.9	1.2	3246	2
Chamise	17.17	1.8	4.2	11958	4
Eastside pine	15.63	1.7	6.7	18790	7
Barren	14.71	1.6	1.1	3132	1
California Sagebrush	12.31	1.3	1.2	3360	2
Desert mixed shrub	11.48	1.2	2.3	6488	3
Urban developed general	7.94	0.9	2.9	8102	4
Interior mixed hardwood	7.48	0.8	0.8	2105	1
Coast live oak	7.02	0.8	1.7	4736	2
California Juniper	5.57	0.6	1.0	2688	1
Douglas fir Ponderosa Pine	4.62	0.5	0.7	1916	2
Great Basin Desert Mixed Scrub	2.70	0.3	1.1	3072	1
Riparian mixed hardwood	2.65	0.3	2.2	6155	1
Scalebroom	0.72	0.1	0.4	1065	1
Ponderosa pine	0.68	0.1	0.6	1675	1
50 Unsampled Vegetation Types	43.95	4.7	0.0	0	0
TOTAL	932.49	100.0	100.1	282439	100
Total Study Area = 935.33 mi^2		Study Area minus waterways = 932.49 mi^2			

and Gordon Snelling checked the identifications of *Neivamyrmex*. The natural history notes were gleaned from the literature and from our own observations while Functional Group designations, food and nest records come from the sources cited above as well as Andersen (1997, 2010), Mackay and Mackay (2002), and Wheeler and Wheeler (1973). The entire dataset including the exact locations of all collecting sites are available upon request from either author. Specimens of every species we encountered in the field have been deposited in the Bohart Museum at the University of California, Davis.

Results

This survey sampled ants using pitfall traps at 100 locations scattered throughout the range and included 282,439 trap nights. These sampling locations were chosen opportunistically with wintertime access and vegetative diversity in mind. An additional 112 locations were casually sampled by hand collecting and other records were gleaned from the literature. Pitfall traps accounted for 96% of all species records, hand collecting accounted for 4% and the other methods yielded less than 1% of the records.

The survey produced 11,370 species records including 284,697 individual specimens in 30 genera containing 96 species, two of which are introduced from outside the region. The California ant fauna contains 45 genera including about 245 native species and 25 introduced species (Ward 2016) and thus, the San Gabriel Mountains contain approximately 40% of the native ant diversity and 8% of the introduced species. The collection includes five subfamilies; Myrmicinae (45 spp.), Formicinae (35 spp.), Dolichoderinae (7 spp.), Dorylinae (5 spp.), Ponerinae (2 spp.) and Pseudomyrmecinae (1 sp.). Four genera, *Camponotus* (11 spp.), *Temnothorax* (11 spp.), *Myrmecocystus* (10 spp.) and *Pheidole* (9 spp.), contributed 42% of the species and 30% of the individual records. And finally, the four commonest species were *Formica moki* (1006 records), *Crematogaster mormonum* (921), *Camponotus semitestaceus* (814) and *Pheidole hyatti* (790).

The 29 sampled vegetation types included 95.3% of the total area of the mountain range. There were 50 un-sampled vegetation types that, in the aggregate, covered the remaining 4.7% of the area. The sampling effort was in rough proportion to the relative cover of sampled vegetation types and is portrayed in Table 1.

We estimated total ant species richness in the San Gabriel Mountains using the Chao2 estimator (Gotelli and Colwell, 2001), $S_{est} = S_{obs} + (Q_1)^2 / 2Q_2$ where S_{est} is the estimated number of species in the community, S_{obs} equals the observed number of species, Q_1 is the number of species represented by a single individual, and Q_2 is the number of species represented by two individuals. In this expression the rarest species in the sample are used to estimate the number of un-sampled rare species that occur in the sampled area.

Our sampling revealed 97 species, including five species represented by a single record, $Q_1 = 5$ and five other species represented by only two records, $Q_2 = 5$. Thus, $S_{est} = 96 + 25/10 = 98.5$ estimated total species. We found that our collection sampled all but about three species. Thus our observed species richness approximates

the estimated richness. However, since samples are ordinarily underestimated and biased against rare species (Dornelas et. al. 2012, Gotelli and Colwell 2001, Mao and Colwell 2005, Tista and Fiedler 2011) it is likely that a number of additional species remain to be discovered.

We also examined the hypothesis that ant species richness is mediated by elevation (either temperature or moisture). From the complete sample we eliminated sites that had fewer than 1,000 trap nights and more than 10,000 trap nights. That was done to eliminate extreme outliers. The remaining 92 locations accumulated 6315 species records from 231,736 trap nights. The average number of species at a site was 17 (range 3-37). When species number is plotted against elevation, we found that species density, that is, the number of species recorded at sampled elevations, showed no correlation between species number and elevation, (Fig. 2).

Species Accounts

Identifications of most species in the annotated list (marked at the end of the name by *) were checked by Andrew Suarez (then at UC, Berkeley) or Philip Ward (UC, Davis). The locations listed in each note are arranged in a more or less counter-clockwise sequence around the mountain range and most were selected with ease of access in mind. They are representative of the various sites where the species was collected. Distances associated with road names are reported in road miles. Vegetation types are listed in each note from low to high elevation.

Formicinae

Acanthomyops – See *Lasius* in this list

Brachymyrmex depilis Emery 1893
Generalist Cryptic species. Tends hemipterans. Distributed widely across the continent in a wide variety of habitats. Pinyon/Oak scrub, *Ceanothus* Chaparral, Pine/Oak Forest between 2350-7300 ft. Jun-Nov. Alates, Aug-Nov. Nest subterranean, under stones. 16 records. San Gabriel Cyn Rd, 0.5 mi e Coldbrook Cpgd; Mt Baldy Rd at 2875 ft.; Big Rock Canyon; Hwy N3, 1 mi n Mill Creek Summit; Sand Canyon Rd, 1.1 mi w Bear Divide Rd.

Camponotus anthrax Wheeler, W. M. 1911*
Subordinate Camponotini. Honeydew feeder. Ceanothus Chaparral, Pine/Oak Forest between 3400-6700 ft. Every month. Alates, Nov. Nest in soil under stones. 28 records. Mt Baldy Rd, Hogback; Hwy 138, 2 mi w Hwy I15; 2 mi w Wrightwood, Mt Emma Rd x Hwy N3.

Camponotus clarithorax Creighton 1950*
Subordinate Camponotini. Honeydew feeder. Oak/Chamise Chaparral, Riparian Woodland, Pine/Oak Forest between 2300-3900 ft. Feb-Oct. Nest in oak cavities. 10 records. Mt Baldy Rd, Hogback; W Fork Cucamonga Cyn; Day Cyn, Etiwanda.

Camponotus dumetorum Wheeler, W. M. 1910
Subordinate Camponotini. Honeydew feeder. Listed by Mallis (1941) as commonly occurring in the chaparral below 2000 ft. Our records are from Chamise Chaparral, Canyon Oak woods between 2400-4700 ft. Jan-Nov. Alates, June. 45 records. Along Hwy N2 between Mill Creek Summit and Hwy N3; Aliso Cyn Rd, 6 mi se Soledad Cyn Rd. We have no record of this species east of Mt Wilson.

Camponotus essigi Smith, M. R. 1923*
Subordinate Camponotini. Honeydew feeder. Manzanita/Chamise chaparral, Pine/Oak Woodland between 1780-6600 ft. Mar-Oct. Nest in decaying wood. 18 records. Ball Flat, 7 mi w Wrightwood; Hwy N2, 1 mi n Mill Creek Summit; Hwy N3, 1 mi s Mt Emma Rd.

Camponotus hyatti Emery 1893*
Subordinate Camponotini. Honeydew feeder. Non-native grassland, chaparral, Pinyon/Juniper Woodland, Pine/Oak Woodland, coniferous forest between 1780-7500 ft. Every month. Alates, October. Nest in beetle or termite galleries in standing dead wood. 167 records. Mt Baldy Rd at 2875 ft.; Glendora Ridge Rd; Ball Flat, 7 mi w Wrightwood; Big Rock Cyn Rd; Mescal Cyn Rd, 2.0 mi n Hwy N4; Soledad Cyn Rd 9.2 mi e Hwy 14.

Camponotus laevigatus (Smith, F. 1858)*
ubordinate Camponotini. Honeydew feeder. Oak chaparral, Pine/Oak Woodland, Incense Cedar/*Pseudotsuga* between 4600-5700 ft. May-Aug. Nest in conifer logs. 4 records. Mt Baldy Rd, 1 mi n Mt Baldy Village; San Sevaine Rd, Lytle Creek; East Blue Ridge Rd, 1.3 mi sw Wrightwood; Mescal Cyn Rd, 2.0 mi n Hwy N4.

Camponotus quercicola Smith, M. R. 1954*
Subordinate Camponotini. Feeds on honeydew, nocturnal predator, scavenger. Oak/conifer woods, White Fir/Jeffrey Pine forests between 2700-8500 ft. Jan-Oct. Alates, May-Aug. Nest in dead wood galleries in living oaks. 101 records. Cucamonga Cyn; San Sevaine Rd, Lytle Creek; Mescal Cyn Rd, 2.0 mi n Hwy N4; Hwy N2, 0.9 mi w Snow Crest; Largo Vista Rd x Hwy N4. Gadau et al. (1999) in an extended description of natural history indicate that it is strongly arboreal but we commonly collect them in pitfall traps placed on the ground. See the description of *C. vicinus*. *C. quercicola* might be confused with the black form of *C. vicinus*. *C. quercicola* has a sharp petiolar node when viewed in profile and it has no erect hairs on the dorsum of the pronotum.

Camponotus sansabeanus (Buckley 1866)*
Subordinate Camponotini. Omnivorous scavenger. *Ceanothus* Chaparral, Joshua/Juniper Woodland, Pinyon/Juniper Woodland between 3600-4900 ft. Jan-Nov. Nest in soil, some under stones. 17 records. Mescal Cyn Rd, 2.8 mi n Hwy N4; Hwy N4, 0.9 mi e Valyermo PO; 2 more

records from Snelling and George (Unpublished records), 2 mi s Pearblossom; 4 mi se Pearblossom.

Camponotus semitestaceus Snelling 1970*
Subordinate Camponotini. Honeydew feeder. Hemipteran tender. Chaparral, Pinyon/Sage Scrub, Pine/Oak Woodland, White Fir/Jeffrey Pine Forest 1450-8700 ft. Every month.

The records for this low elevation species above about 6,000 ft. are likely erroneous due to misidentifications of *C. vicinus* which does extend to the high ridges. This problem was pointed out by one reviewer. Alates, Mar-Jun and Oct. Nest under stones. 814 records. San Gabriel River Canyon; Mt Baldy Rd at 2875 ft.; Ontario Peak; 1 mi e Wrightwood, Hwy N3; Little Tujunga Cyn 0.7 mi w Wildlife Waystation; Hwy N3 1 mi s Mt Emma Rd.

Camponotus vicinus Mayr 1870*
Subordinate Camponotini. Honeydew on roots, Hemipteran tender, carrion. Tend scales on roots, scavenge insects, carrion. Chaparral, Oak/conifer woods, White Fir/Jeffrey Pine forest between 2080-8500 ft. Every month. Alates, Jun-Sept. Nest under objects on ground. 382 records. Little Tujunga Cyn Rd at Dillon Divide; Mt Baldy, Manker Flats; San Sevaine Rd, Lytle Creek; 2 mi e Wrightwood. In addition to the typical form of this species – black head and gaster with red thorax– there is an all-black form in the San Gabriels. Mescal Cyn Rd, 2.0 mi n Hwy N4 is a reliable collecting site. It superficially resembles *C. quercicola* and might be confused with that species at first glance. The black form can be distinguished from *C. quercicola* in having a rounded node on the petiolar crest when viewed in profile and also in having several erect hairs on the dorsum of the pronotum.

Camponotus yogi Wheeler, W. M. 1915*
Subordinate Camponotini. Tend hemiptera. Chaparral, Riparian woodland, Oak/Pine Woodland between 1500-6600 ft. Every month. Alates, May-Oct. Nest in dead wood galleries or under stones. 124 records. Mackay and Mackay (2002) report that *Temnothorax andrei* is occasionally found in the nests of this species in New Mexico. San Gabriel Canyon; Glendora Ridge Rd; San Sevaine Rd, Lytle Creek; 2 mi w Wrightwood; Mescal Cyn Rd, 2.8 mi n Hwy N4; Largo Vista Rd, 1 mi n Hwy N4; Sand Cyn Rd, 1.1 mi w Bear Divide Rd.

Formica francoeuri (=*pilicornis*) Bolton 1995*
Opportunist. Feeding opportunist. Seen carrying aphids. Chaparral, riparian boulder wash, *Cercocarpus*/Pinyon Woodland, Pine/Oak, Pine/*Ceanothus* Woodland between 1470-7350 ft. Every month. Alates, Apr-Sept. Nest in soil under stones. 204 records. In some locations this species is so abundant that it seems to exclude nearly every other ant species—the largest sample contained more than 4000 individuals. *Temnothorax anaphalantus* was consistently collected at the same site where these huge samples were obtained. San Gabriel River Canyon; San Antonio Canyon; Lone Pine Canyon, 5 mi e Wrightwood; Prairie Fork Canyon at 7,000 ft.; Mescal Cyn Rd, 0.2 mi n Hwy N4; Hwy N4, 0.8 mi w Elk Camp; Soledad Cyn Rd, 4.2 mi e Hwy 14.

Formica argentea W. M. Wheeler 1912*
Opportunist. Scavenger. Nearctic and occurs throughout western Europe and in Japan. Mallis (1941) reported this species from Kelly's Camp in Icehouse Canyon. He referred to it as *F. fusca*. Mt. Baldy at 8500 ft. in White Fir forest. Yellow Pine/White Fir Forest between 6570-8500 ft. Apr-Oct. Nest in rotten wood or in soil under objects. 47 records. East Blue Ridge, Guffy Cpgd, 1.6 mi s Wrightwood, East Blue Ridge Rd, 1.3 mi sw Wrightwood; Lupine Cpgd, Rd 3N39.

Formica gnava Buckley 1866*
Opportunist. Seen tending aphids, gather floral nectar. Oak Chaparral, Pinyon/Juniper Woodland between 2030-5160 ft. May-Sept. Mackay and Mackay (2002) found them nesting under large, flat rocks producing no mound. Six records. Mescal Canyon, 2 mi n Hwy N4; Mt Emma Rd, 2.5 mi n Hwy N3; Aliso Cyn Rd, 6 mi se Soledad Cyn Rd.

Formica moki Wheeler, W. M. 1906*
Opportunist. Hemipteran tender. Chaparral, Riparian woodland, Pinyon/Juniper Woodland, Pine/Oak Woodland, Jeffrey Pine Forest between 1450-8250 ft. Every month. Alates, May-Oct. Nest in soil under stones. 1006 records. San Gabriel River Canyon; East Etiwanda Canyon; Angeles Crest Hwy, 7 mi w Wrightwood; Mt Emma Rd x Hwy N3. This is the most frequently encountered species in this study.

Formica subpolita Mayr 1886*
Opportunist. Honeydew feeder. Scrub Oak chaparral, Pine/Oak Woodland, Coniferous Forest between 3730-8500 ft. Mar-Nov. Alates, August. Nest in soil and under stones. 49 records. San Sevaine Rd, Lytle Creek; Hwy N2, 4 mi w Wrightwood; Hwy N2, 3.1 mi w Cloudburst Summit.

Formica xerophila Smith 1939
Opportunist. Hemipteran tender. Nest in soil and under stones or wood. In March and June, 2015 Mark Ikeda collected workers at Spruce Canyon, 3 miles south of Mt. Baldy Village at 2875 ft. in Chamise chaparral.

Lasius alienus (Foerster 1850)*
Cold Climate Specialist. Occurs from Japan, through North America to Germany. Feed on live and dead insects, honeydew. *Ceanothus* chaparral, Scrub Oak Chaparral, White Fir/Oak Forest between 2875-8500 ft. Every month. Alates, every month. Nest in soil or rotting wood. 91 records. 1 mi n Mt Baldy Village; Hwy N2, 6 mi w Wrightwood; Hwy N2 at Islip Saddle; East Blue Ridge Rd, 1.3 mi s Wrightwood.

Lasius (Acanthomyops) californicus Wheeler, W. M. 1917*
Cold Climate Specialist. Cryptic species, tend root coccids and aphids. A temporary social parasite on other *Lasius.* Chaparral, Pinyon/Juniper Woodland, Pine/Oak

Woodland, Coniferous Forest between 1680-8500 ft. Every month. Alates, May-Nov. Nest in soil under rocks. 52 records. Manker Flats on Mt Baldy; San Sevaine Rd, Lytle Creek; Largo Vista Rd,1 mi n Hwy N4; Hwy N2, 6 mi w Wrightwood; Mt Emma Rd, 2.5 mi n Hwy N3.

Lasius nr *flavus**

Cold Climate Specialist. Probably feeds on live and dead insects, honeydew. Two records of single queens. 4570-5160 ft. August. Nest in soil. Recently burned Scrub Oak and in Ceanothus, pinyon woodland. San Sevaine Rd; Mescal Cyn, 2.0 mi n Hwy N4.

Myrmecocystus colei Snelling 1976

Hot Climate Specialist. Scavenger, predator, honeydew feeder. Pinyon/sage woodland, Chaparral between 2000-4800 ft. Feb-Sept. Nest is compact, clayey soil. Four records. This species is an endemic to this region. Snelling (1976) reports these locations; Eaton Canyon and Cajon Canyon. Our records include Soledad Cyn Rd 10.7 mi e Hwy 14; Largo Vista Rd 1 mi n Hwy N4.

Myrmecocystus creightoni Snelling 1971*

Hot Climate Specialist. Scavenge insects, honeydew feeder. Riversidean Scrub wash, Chaparral, Pinyon/Juniper Woodland between 1570-6200 ft. Dec-Jul. Nest in exposed soil. 10 records. Like the previous species, it is a southern California endemic. Mescal Cyn Rd, 2.8 mi n Hwy N4; Ball Flat, 7 mi w Wrightwood; Hwy N4, 2.5 mi w Largo Vista Rd; 2-6 mi sse Pearblossom along Ft. Tejon Rd; Mt Emma Rd, 0.5 mi n Hwy N3.

Myrmecocystus flaviceps Wheeler, W. M. 1912*

Hot Climate Specialist. Scavenger, predator, honeydew gatherer. Buckwheat flats, *Ceanothus* Chaparral, Pinyon/Juniper Woodland between 1800-4800 ft. Mar-Sept. Nest in exposed soil. 6 records. Cobal Cyn, Claremont; Big Rock Cyn Rd; Largo Vista Rd, 1 mi n Hwy N4; Aliso Cyn Rd 5.0 mi se Soledad Cyn Rd.

Myrmecocystus kathjuli Snelling 1976

Hot Climate Specialist. Scavenger, predator, honeydew feeder, flower nectar. Pinyon/Juniper Woodland at 4400 ft. August. Nest in deep sand in desert washes. One record from 8 mi se Pearblossom by Roy Snelling. His description places the site in Big Rock Canyon.

Myrmecocystus kennedyi Snelling 1969*

Hot Climate Specialist. Nectar, honeydew gatherer, Scavenger of dead arthropods found in the heat of the day. Oak/Juniper scrub, Great Basin Sage. 3550-4900 ft. Jan-Oct. Nest in well-drained, exposed sandy soils. Nine records. This desert species evidently just creeps into the northern margins of the range. Swarthout Cyn Rd, 0.5 mi se Lone Pine Cyn Rd; Mescal Cyn Rd, 2.8 mi n Hwy N4; Hwy N4, 2.1 mi w Largo Vista Rd; Mt Emma Rd, 2.5 mi n Hwy N3.

Myrmecocystus mexicanus Wesmael 1838

Hot Climate Specialist. Feed on honeydew, flower nectar, dead insects and carrion. Joshua/Juniper, Joshua/Oak Woodland 3600-4000 ft. September. Nest in coarse soil on high ground. Snelling (1976) reports 2 records. 2 mi sse Pearblossom along Ft. Tejon Rd; Cajon Canyon along Hwy 138.

Myrmecocystus mimicus Wheeler, W. M. 1908*

Hot Climate Specialist. Feed on honeydew, flower nectar, live and dead insects including termites, tend aphids. Chaparral, Pinyon/Juniper Woodland between 1800-6000 ft. Feb-Nov. Nest in clayey soil, often with the entrance hidden in a grass clump. 18 records. Cobal Canyon, Claremont; Mt Baldy Rd at 2875 ft.; Rd 3N31, 3 mi e Wrightwood; Largo Vista Rd, 1 mi n Hwy N4; Mt Emma Rd, 2.5 mi n Hwy N3.

Myrmecocystus semirufus Emery 1893*

Hot Climate Specialist. Scavenger, predator, nectar feeder. Records from Snelling (1976), "disturbed chaparral 2 mi s Pearblossom. Various dates". Nest exposed, coarse soil, often on a slope. They tolerate extremely high summer soil temperatures; anecdotally as high as 57°C. We have 11 records. Apr-Sept. 3500-3850 ft. Hwy N4, 0.7 mi e Valyermo PO.

Myrmecocystus testaceus Emery 1893*

Hot Climate Specialist. Feeds on honeydew, plant secretions, live and dead insects. Chaparral, Pinyon/Juniper Woodland, Conifer/Oak Woodland between 1200-7850 ft. Every month. Alates, Oct-Mar. Nest in exposed soil. 301 records. Eaton Cyn, La Cañada; Cobal Cyn, Claremont; Glendora Mtn Rd, 5 mi w Mt Baldy Village; Ball Flat, 7 mi w Wrightwood; Hwy N2, 0.5 mi e Dawson Saddle; Mt Emma Rd, 0.5 mi n Hwy N3.

Myrmecocystus wheeleri Snelling 1971*

Hot Climate Specialist. Food includes dead insects, probably honeydew. White Sage Scrub, chaparral, Juniper Woodland between 1750-5100 ft. May-Nov. Nest in exposed soil. 26 records. Day Canyon, Etiwanda; Swarthout Rd, 0.5 mi s Lone Pine Cyn Rd; Mescal Cyn Rd, 2.8 mi n Hwy N4; Little Rock Dam; 6 mi se Pearblossom along Ft. Tejon Rd; Big Rock Cyn Rd; Soledad Cyn Rd, 9.2 mi e Hwy 14.

Nylanderia magnella Kallal and LaPolla 2012*

Formerly *N.* cf *terricola*. The current status of the nomenclature remains unsettled (PS Ward in. litt.). Opportunist. Generalist feeder, omnivorous scavenger. *Ceanothus* Chaparral, Buckwheat/Yerba Santa Scrub between 1650-5100 ft. Every month. Alates, Feb-Nov. Nest in soil under wood or stone. 66 records. San Gabriel Canyon, 0.5 mi e Cold Brook Campground; Mt Baldy Rd at 2875 ft.; San Sevaine Rd; Big Rock Canyon Rd; Hwy N4, 0.9 mi e Valyermo PO; Soledad Cyn Rd, 1.9 mi e Hwy 14.

Polyergus vinosus Trager 2013

Social Parasite. An obligate slave-making (duloticous) species. It parasitizes *Formica moki* exclusively (Trager 2013). Chaparral, Alder Woodland, Canyon Oak/Sugar Pine between 2600-5700 ft. Jun-Nov. Nest in soil often

under stones. Alates, Jun-Aug. 47 records. Raiding columns may be observed in the late afternoon during the summer. Mt Baldy Rd at 2875 ft.; Glendora Mtn Rd, 3.9 mi w Mt Baldy Village; San Sevaine Rd, Lytle Canyon; Hwy N2, 0.6 mi w Chilao; Mescal Cyn Rd, 2.0 mi n Hwy N4; Mt Emma Rd, 1.5 mi n Hwy N3.

Prenolepis imparis (Say 1836)*
Cold Climate Specialist. Feeds on honeydew, fluid from decaying fruit, omnivore. Chaparral, Pinyon/Juniper Woodland, Oak/Maple woods, White Fir/Jeffrey Pine Forest between 1450-8500 ft. Every month. Alates, every month. Nest in soil under stones. 763 records. In some winter samples it is the only species collected. San Gabriel River Canyon; Mt Baldy Rd at 2875 ft.; Lone Pine Cyn Rd, 2 mi e Wrightwood; Largo Vista Rd, 1 mi n Hwy N4; Mt Emma Rd x Hwy N3. We have found it slowly foraging next to snow banks on sunny midwinter days.

Myrmicinae

Aphaenogaster occidentalis (Emery 1895)*
Opportunist. Generalist forager. Root hemipterans found in nests. Scrub Oak, Pine/Oak Woodland, Coniferous Forest between 3700-7850 ft. Jan-Nov. Alates, Jul-Oct. Nests under stones. 47 records. San Sevaine Rd, Lytle Creek Canyon; East Blue Ridge Rd; Prairie Fork Cyn at 6700 ft.; Hwy N4, 1 mi e Elk Camp; Hwy N2, 5 mi w Wrightwood; Mescal Cyn Rd, 1.0 mi n Hwy N4.

Cardiocondyla mauritanica Forel 1890*
Opportunist. Opportunist scavenger and predator. We have two records - one from San Dimas Canyon in a riparian woodland, the other from San Antonio Canyon in Chamise chaparral, May-Aug. Alates, August. Elev. 1490-2875 ft. It is a widely introduced tramp species that was probably introduced into California in imported nursery stock. Nests are typically tiny and cryptic, placed in disturbed soil in sunny places.

Crematogaster californica Wheeler, W. M. 1919*
Generalist Myrmicine. Tend aphids and coccids. Chaparral, Riparian Woodland between 1450-5500 ft. Every month. Alates, Sept-Nov. Nest in soil under stones. 190 records. Mt Baldy Rd at 2875 ft.; Glendora Mtn Rd, 5.1 mi w Mt Baldy Village; Day Canyon, Etiwanda; Hwy N4, 0.9 mi e Valyermo.

Crematogaster coarctata Mayr 1870*
Generalist Myrmicine. Tend coccids under soil. *Ceanothus* Chaparral, *Arctostaphylos* Chaparral, Oak/Chamise Chaparral, Yellow Pine Forest between 1450-6600 ft. Every month. Alates, Jul-Sept. 95 records. Nest in soil under stone or bush. Charlton Flat, Mt Baldy Rd at 2875 ft.; Ball Flat, 7 mi w Wrightwood; Little Tujunga Cyn, 0.7 mi w Wildlife Waystation.

Crematogaster depilis Wheeler, W. M. 1919*
Generalist Myrmicine. Plant nectar, honeydew, carrion. Hemipteran tending generalist. *Ceanothus* Chaparral, Joshua/Juniper Woodland, Pine/Oak Woodland between 2870-6000 ft. Oct-May. Nest, soil in and among roots. 7 records. Mt Baldy Rd at 2875 ft.; Hwy N4, 0.7 mi e Valyermo; 2 mi s Pearblossom; 1.5 mi e Wrightwood.

Crematogaster hespera Buren 1968
Generalist Myrmicine. Probably hemipteran tending generalist. G. and R. Snelling (in litt.) found this species at Blue Ridge; Hwy N2 and at Manker Flat at Mt Baldy in Conifer/Oak forests at 6100-7450 ft. April. Buren (1968) reports it from Big Dalton Cyn, Glendora. In New Mexico the species frequently associates with cottonwoods (Mackay & Mackay, 2002). Nest in dead wood cavities. We have no record of our own.

Crematogaster marioni Buren 1968*
Generalist Myrmicine. Oak/Ceanothus, Oak/juniper between 3900-6250 ft. It probably is arboreal preferring to nest in oaks or manzanita (Buren 1968). Jun-Oct. Eight records. 0.6 mi e Mt. Wilson Rd; Largo Vista Rd, 1 mi n Hwy N4; Mt Emma Rd, 2.5 mi n Hwy N3. One of Buren's (1968) paratypes is from "Pasadena".

Crematogaster mormonum Wheeler, W. M. 1919*
Generalist Myrmicine. Hemipteran tending, scavenger, predator. All communities from chaparral through Coniferous Forest between 1500-8250 ft. Every month. Alates, Jun-Dec. Nest in wood or under stones. 921 records. Mt Baldy Rd at 2875 ft.; Lone Pine Cyn Rd; Largo Vista Rd, 1 mi n Hwy N4; Ball Flats, 7 mi w Wrightwood; East Blue Ridge Rd. This species is among the most frequently encountered species in the range.

Crematogaster mutans Buren 1968*
Generalist Myrmicine. Tend scale insects. Chaparral, Manzanita/juniper woodland. 2800-4900 ft. May-Aug. Six records. Mt Baldy Rd; Mescal Cyn, 2.8 mi n Hwy N4.

Buren (1968) suggested that, based on queen morphology (body size much smaller than is typical for the genus), this species might be a temporary parasite of either *C. californica* or *C. mormonum*. At the two locations in this study, *C. mormonum* is the common sympatric congener. We have found no subsequent mention of the suggestion.

Leptothorax – See *Temnothorax* in this list

Manica bradleyi (Wheeler, W. M. 1909)*
Cold Climate Specialist. Montane specialist. Feed on insects and seeds, perhaps other ants (Wheeler and Wheeler 1986). White Fir/Yellow Pine Forest at 8200-8500 ft. May-Oct. Alates, October. Nest under objects or in exposed soil. 21 records. Guffy Cpg, East Blue Ridge Rd. individual workers can be found slowly foraging in exposed places in the evening.

Messor – See *Veromessor* in this list

Monomorium ergatogyna Wheeler, W. M. 1904*
Opportunist. Generalist omnivore. Chaparral, Pine/Oak Woodland, Coniferous Forest between 1680-8500 ft. Every month. Alates, Jul-Oct. Nest in soil or handy cavity. 129 records. Mt Baldy Rd at 2875 ft.; East Blue Ridge Rd, 1.6

mi sw Wrightwood; 1 mi e Elk Camp; Ball Flat, 7 mi w Wrightwood; Largo Vista Rd, 1 mi n Hwy N4; Aliso Cyn Rd, 5.0 mi se Soledad Cyn Rd.

Myrmica punctinops Francoeur 2007*
Cold Climate Specialist. Generalist predator, scavenger. Pine/Oak forest, Yellow Pine/White Fir Forest, between 5200-8500 ft. May-Oct. Alates, August. Probably nest under stones. 37 records. Mt Wilson near observatory; East Blue Ridge Rd; Hwy N2, 0.6 mi e Chilao.

Myrmica rugiventris (Smith, M. R. 1943)*
Cold Climate Specialist. Generalist predator, scavenger. Feed on arthropods, some plant matter. Manzanita Chaparral, Pine/Oak Forest between 4600-6200 ft. Every month. Alates, July. Probably nest under stones. 23 Records. San Gabriel Cyn Rd, 0.1 mi e Crystal Lake Rd; Mt Baldy Rd, Manker Flat; Largo Vista Rd, 1 mi n Hwy N4; Ball Flat, 7 mi w Wrightwood; Hwy N2, 1 mi n Mill Creek Summit.

Pheidole nr *barbata**
Generalist Myrmicine. Seed harvester, scavenger. *Ceanothus* chaparral, Scrub Oak between 2850-3500 ft. May-Jun. Nest probably in sandy places. 7 records. Mt Baldy Rd at 2875 ft.; Aliso Cyn Rd, 5.0 mi se Soledad Cyn Rd. The specimens in this sample closely resemble *P. barbata* but PS Ward distinguishes the specimens that he has seen.

Pheidole californica Mayr 1870*
Generalist Myrmicine. Seed harvester. *Ceanothus* Chaparral between 1750-2900 ft. Apr-Aug. 4 records. Nest in exposed soil or under stones, oak galls. Nest in exposed soil or under stones, oak galls. Chaffey College Preserve, Alta Loma (not within the boundary of the study area); Mt Baldy Rd at 2875 ft.

Pheidole cerebrosior Wheeler, W. M. 1915*
Generalist Myrmicine. Seed harvester, scavenger. *Ceanothus* Chaparral, Pine/Oak Woodland between 1750-7250 ft. Jan-Nov. Nest under stones. 41 records. Mt Baldy Rd at 2875 ft.; 0.3 mi n Vincent Gap, Hwy N2; Mt Emma Rd x Hwy N3; Aliso Cyn Rd, 5.0 mi se Soledad Cyn Rd. In the Mojave Desert we have collected individuals of this species alive in the tumulus piles of *Pogonomyrmex rugosus*.

Pheidole clydei Gregg 1950
Generalist Myrmicine. Scavenger on dead arthropods. Roy Snelling (Los Angeles Co. Museum, label dated 30 Sept. 1965) had one record from Big Rock Creek at an elevation of 4500 ft. Nest in cracks in boulders and cliffs. Nocturnal forager. We collected near the reported site for a year without encountering this species.

Pheidole desertorum Wheeler, W. M. 1906*
Generalist Myrmicine. Omnivore. Aggressive predator and scavenger, rarely gather seeds. Joshua/Juniper and Pinyon/Oak Woodland between 3600-5500 ft. Sept-Feb. Nest under stones. 6 records. Hwy N4, 2.5 mi w Largo Vista Rd; 2 mi s Pearblossom.

Pheidole gilvescens Creighton & Gregg 1955*
Generalist Myrmicine. Seed harvester, scavenger. Pinyon/Oak, Oak/Juniper Woodland between 4050-4900 ft. Jan-Oct. Nests in dry, exposed sites. 6 records. Big Rock Canyon Rd; Mt Emma Rd, 2.5 mi n Hwy N3.

Pheidole hyatti Emery 1895*
Generalist Myrmicine. Omnivore and seed harvester. Non-native grasslands, Chaparral, Conifer/Oak Woodlands, Yellow Pine/White Fir Forest between 1450-8500 ft. Every month. Nest in soil under plants. Alates, May-Oct. 790 records. San Dimas Cyn, LaVerne; Johnson Pasture, Claremont; Mt Baldy Rd at 2875 ft.; Lone Pine Cyn, 1.5 mi e Wrightwood; Ball Flats 7 mi w Wrightwood; East Blue Ridge Rd; Hwy N2 at Islip Saddle; Aliso Cyn Rd, 5.0 mi se Soledad Cyn Rd.

Pheidole rugulosa Gregg 1959*
Generalist Myrmicine. Omnivore and seed harvester. A single record from the literature, 2 mi s Pearblossom in Joshua/Juniper Woodland at 3600 ft. We have 5 records from Mt Baldy Rd at 2875 ft. in *Ceanothus* Chaparral. May-Oct. Nest in exposed soil or under stones. The chaparral records are notable for a typical desert species, (PS Ward pers. com.).

Pheidole sciophila Wheeler, W. M. 1908*
Generalist Myrmicine. Omnivore, seed harvester. *Ceanothus* chaparral, Pinyon/Sage woodland, Jeffrey Pine forests between 1750-6250 ft. May-Sept. Nest obscure, often close to stem of a shrub. 16 records. Mt Baldy Rd at 2875 ft.; Largo Vista Rd, 1 mi s Hwy N4; Aliso Cyn Rd, 5.0 mi se Soledad Cyn Rd.

Pogonomyrmex californicus (Buckley 1867)
Hot Climate Specialist. Food includes seeds, vegetation, dead insects. Disturbed places, non-native grasslands, Chaparral, Scrub Oak Woodlands between 1450-5200 ft. Mar-Oct. Nest in exposed sandy soil. 35 records. Mt Baldy Rd at 2875 ft.; San Sevaine Rd, Lytle Creek; Soledad Cyn Rd, 4.2 mi e Hwy 14. This species is a typical occupant of sandy sites in the valleys. It is typically replaced upslope at about 2000 ft. by *P. subnitidus.* Four records above 4500 ft. were on south-facing exposures that had been burned in the previous few years. It has a ferocious sting. Beware!

Pogonomyrmex montanus MacKay 1980
Hot Climate Specialist. Food includes seeds, vegetation, dead insects. Yellow Pine/White Fir Forest edges between 6550-8500 ft. May-Oct. Alates, October. Nest in exposed sandy soil. 23 records. East Blue Ridge Rd.

P. subnitidus is limited to lower elevations than is *P. montanus*. The highest record that we have for *P. subnitidus* is 6000 ft. Mackay (1980) reports *P. montanus* at elevations above 4900 ft. in the San Bernardino Mountains. We have never found them together at a single location.

Pogonomyrmex rugosus Emery 1895
Hot Climate Specialist. Feeds on seeds, plant bits, dead insects. Chaparral and Pinyon/Juniper Woodland. One record of this common desert species at Mt Emma Rd 1.5 mi n Hwy N3, chaparral at 4200 ft. July. Nest in exposed soil. The tumulus pile contains large amounts plant material cast out of the nest. We have never encountered the species on the coastal side of the range.

Pogonomyrmex subnitidus Emery 1895*
Hot Climate Specialist. Feeds on seeds, insects and pollen. Gleans mammalian scat containing seeds – coyote scat particularly. Chaparral, Scrub Oak between 2050-6000 ft. Nest in exposed soil. Mark Ikeda (pers. comm.) showed that the nest entrance is moved from sun to shade from spring to summer thus extending the foraging day. Jan-Nov. Alates, Apr-Sept. 424 records. San Gabriel Canyon; Mt Baldy Rd at 2875 ft.; Hwy N4, Mescal Cyn Rd, .02 mi n Hwy N4; 1 mi e Largo Vista Rd; Hwy N3, 1 mi s Mt Emma Rd.

Pyramica – See *Strumigenys* in this list

Solenopsis CA-01
Cryptic Species. Predator. A single record from the San Gabriel River Canyon at an elevation of 2100 ft. from 17 Feb 1963 by RR Snelling. Chamise/Black Sage Chaparral. We had a trap array at that location for eighteen months during 2005-06 and didn't encounter the species. It is a minute, cryptic species to be on the lookout for.

Solenopsis molesta (Say 1836)*
Cryptic Species. Predator. Feeds on brood and refuse in the nests of larger ants near whose nests they reside. Grassland, chaparral, Conifer/Oak Woodland, Yellow Pine/White Fir Forest between 1450-8250 ft. Every month. Alates, Jun- Oct. Nest under stones or in nests of larger ants. 249 records. Subterranean pitfall traps yield large numbers of them. San Gabriel Canyon; Johnson Pasture, Claremont; Manker Flats, Mt Baldy; Lone Pine Cyn, 1.5 mi e Wrightwood; East Blue Ridge, 1.5 mi s Wrightwood; Largo Vista Rd, 1 mi n Hwy N4; Mt Emma Rd, 2.5 mi n Hwy N3.

Solenopsis xyloni McCook 1880*
Tropical Climate Specialist. Feeds on seeds, omnivore, raids other ants. Riparian Woodland, chaparral, Pinyon/Oak Woodland, Yellow Pine/White Fir Forest between 1450-8500 ft. Every month. Alates, Apr-Aug. Nest under stones or litter, exposed soil. 623 records. San Dimas Cyn, La Verne; Mt Baldy Rd at 2875 ft.; Day Cyn, Etiwanda; Ball Flat, 7 mi w Wrightwood; Largo Vista Rd, 1 mi n Hwy N4; Mt Emma Rd, 1.5 mi n Hwy N3.

Stenamma californicum Snelling 1973*
Cold Climate Specialist. Preys on litter microarthropods. *Ceanothus* chaparral, Bay/Oak Riparian Woodland, Yellow Pine/White Fir Forest between 1470-5130 ft and a single additional record at 8200 ft. Jan-Nov. Alates, Jan-Aug. Nest in litter, soil or rotten wood. 29 records. Mt Baldy Rd at 2875 ft.; San Sevaine Rd, Lytle Creek; East Blue Ridge Rd, 1.5 mi s Wrightwood; Hwy N2, 2.2 mi s Hwy N3; Little Tujunga Cyn Rd at Dillon Divide.

Stenamma diecki Emery 1895*
Cold Climate Specialist. Preys on litter microarthropods. Chaparral, Riparian Woodland, Pine/Oak Woodland between 1450-7850 ft. Every month. Nest in litter, soil or rotten wood. Alates, Jan-Jun. 119 records. San Dimas Cyn, LaVerne; Mt Baldy Rd at 2875 ft.; Glendora Mtn Rd, 5.1 mi w Mt Baldy Village; San Sevaine Rd, Lytle Creek; Largo Vista Rd at Hwy N4; Hwy N2, 2.2 mi s Hwy N3. Branstetter (2012) puts this undescribed taxon in *S.* mgb 101 in California, distinguishing it from *S. diecki* elsewhere. *S. diecki* does not occur in California.

Stenamma smithi Cole 1966*
Cold Climate Specialist. Probably preys on litter microarthropods. Jeffrey Pine mixed with Little Sage between 5200-6300 ft. Mar-Nov. Alates, March. Seven records. Hwy N2, 3.1 mi w Cloudburst Summit; Sulfur Springs Rd, 2 mi n Chilao. Snelling (1973) makes no mention of the natural history of the species. Allred (1982) describes them nesting in sagebrush and juniper duff in Utah.

Strumigenys (=Pyramica) californica (Brown 1950)*
Cryptic Species. Predator. Feeds on collembola in the litter. Three records of dealate queens in *Ceanothus* and Chamise Chaparral, Elderberry/Sycamore gully between 1680-2875 ft. Oct-Dec after the early rains of the season. San Dimas Cyn; Mt. Baldy Road at 2875 ft.

Temnothorax anaphalantus (= CA-06) Snelling, et al 2014*
Cold Climate Specialist. Probably a generalist scavenger. Oak/Chamise Chaparral, Scrub Oak/*Prunus*, willow riparian margin between 1450-6000 ft. Feb-Nov. Alates, Jun-Sept. One nest record from dead wood in Montane Chaparral (Snelling et al, 2014). Alates, Jun-Sept. We have 48 records. San Gabriel Cyn Rd; Glendora Mtn Rd, 0.4 mi e Horse Cyn; Mt Baldy Rd at 2875 ft.; Mescal Cyn Rd, 0.2 mi n HwyN4. At several locations we have found it in what seems to be a close spatial association with dense *Formica francoeuri* populations that can exclude nearly all other ground dwelling ant species.

Temnothorax andrei (Emery 1895)*
Cold Climate Specialist. A generalist forager. Chaparral, Oak Scrub, Pine/Oak Woodland, Coniferous Forest between 1450-8500 ft. Every month. Alates, Jun-Dec. Nest under stones. Their nests may occasionally be found in the nests of *Camponotus yogi* (Mackay and Mackay 2002). 291 records. San Gabriel Canyon; Mt Baldy Rd at 2875 ft.; Largo Vista Rd, 1 mi s Hwy N4; Hwy N2, 6 mi w Wrightwood; East Blue Ridge Rd, 1.5 mi s Wrightwood; Soledad Cyn Rd, 4.2 mi e Hwy 14.

Temnothorax caguatan (= CA-03) Snelling, et al 2014*
Cold Climate Specialist. Probably a generalist scavenger. *Ceanothus* Chaparral, Pinyon/Scrub Oak Woodland, Canyon Oak association, Yellow Pine Forest between 2600-8300 ft. Feb-Nov. Alates, Sept-Nov. Nests strictly

arboreal (Snelling et al. 2014). 28 records. San Gabriel Cyn Rd near Crystal Lake; Glendora Mtn Rd, 2.5 sw San Gabriel River; East Blue Ridge Rd, 2 mi sw Wrightwood; Mt Wilson Observatory; Mt Baldy Rd at 2875 ft.; Ball Flat, 7 mi w Wrightwood; East Blue Ridge Rd, 1.3 mi sw Wrightwood; Hwy N4 x Largo Vista Rd. This species resembles *T. rugatulus*. They can be distinguished. In *T. caguatan* the petiolar node is broadly triangular and the posterior face is nearly straight when viewed in profile whereas in *T. rugatulus* the posterior face of the petiolar node is convexly curved.

Temnothorax gallae (Smith, M. R. 1949)*
Cold Climate Specialist. Probably a generalist forager. *Ceanothus* Chaparral, Pinyon/Oak Woodland, White Fir forests between 2800-8500 ft. May-Sept. Nests in gall cavities in Canyon Live Oak (Mackay and Mackay 2002) and probably other plant cavities. Six records. Mt Baldy Rd at 2875 ft.; East Blue Ridge, 1.6 mi sw Wrightwood; Hwy N2, 0.5 mi e Dawson Summit; Hwy N3, 1 mi s Mt Emma Rd.

Temnothorax neomexicanus (Wheeler, W. M. 1903)*
Cold Climate Specialist. A generalist forager. Chaparral, pine/chaparral, Pinyon/Juniper Woodland between 1650-6200 ft. Feb-Dec. Nest in soil under stone. 54 records. Mt Baldy Rd at 2875 ft.; Ball Flat, 7 mi w Wrightwood; Largo Vista Rd, 1 mi n Hwy N4; Mt Emma Rd, 0.5 mi n Hwy N3.

Temnothorax nevadensis (Wheeler, W. M. 1903)*
Cold Climate Specialist. A generalist scavenging forager. Chaparral, Oak/Juniper Woodland, Pine/Chaparral Woodland, Yellow Pine/White Fir Forest between 1750-8500 ft. Mar-Dec. Alates, September. Nest in soil under stones. 89 records. Mt Baldy Rd at 2875 ft.; Ball Flat, 7 mi w Wrightwood; East Blue Ridge Rd, 1.5 mi s Wrightwood; Hwy N4, 1 mi e Largo Vista Rd; Mt Emma Rd, 2.5 mi n Hwy N3.

Temnothorax nitens (Wheeler, W. M. 1903)*
Cold Climate Specialist. Scavenger, prey on soil microarthropods, tend aphids. Chaparral, Pinyon/Juniper Woodland, Pine/Oak Woodland, White Fir Forest between 2200-8500 ft. Feb-Oct. Alates, September. Nest under stones or arboreal. 28 records. Glendora Mtn Rd, 3.9 mi w Mt Baldy Village; San Sevaine Rd, Lytle Creek; Hwy N2 at Vincent Gap; Hwy N2, 0.5 mi e Dawson Saddle; Lone Pine Cyn Rd, 5 mi e Wrightwood; Largo Vista Rd, 1 mi n Hwy N4.

Temnothorax paiute (= CA-08) Snelling, et al 2014*
Probably a Cold Climate Specialist. Nothing is known about the biology of this recently described species (Snelling et al. 2014). Records from Lone Pine, CA and the Nevada Nuclear Test Site are more than 50 years old. Feb-Nov. We have four records from the Clark Mtns north of Ivanpah in Pinyon/Juniper Woodland at about 5400 ft. and four records, May-Dec., from Hwy N4, 0.7 mi and 0.9 mi e Valyermo Post Office at an elevation of around 3800 ft. in mixed Juniper/Cottonwood Woodland. The specimens from Valyermo are darker than the type material (Matt Prebus, 2014 in litt.). This species is quite an exciting find.

Temnothorax rugatulus (Emery 1895)*
Cold Climate Specialist. A generalist scavenging forager. Chaparral, Pine/oak Forest, Yellow Pine/White Fir Forest between 1750-8500 ft. Mar-Dec. Alates, Mar-Aug. Nest under stones or rotten wood, occasionally arboreal (Wheeler and Wheeler 1986). 81 records. San Gabriel Cyn Rd, 0.1 mi w Crystal Lake Rd; EastBlue Ridge, 1.6 mi sw Wrightwood; Hwy N4 x Largo Vista Rd; Hwy N2 0.5 mi e Dawson Saddle. To distinguish this species from *T. caguatan* see the note for that species.

Temnothorax wardi (=CA-02) Snelling, et al 2014*
Cold Climate Specialist. Probably a generalist scavenger. Chaparral, Pinyon/Oak Scrub between 2500-5700 ft. Mar-Oct. No nest records. 23 records. Glendora Mtn Rd, 3.4 mi w Mt Baldy Village; San Sevaine Rd, Lytle Creek at 4567 ft. (the type locality for the species); Mescal Cyn Rd, 2.0 mi n Hwy N4; Big Rock Cyn Rd; Soledad Cyn Rd, 10.7 mi e Hwy 14. Specimens have been collected in pitfall traps or by hand on nest middens of *Forelius* species.

Temnothorax whitfordi (Mackay 2000)*
Cold Climate Specialist. Feeding ecology not known. Pinyon/Juniper Woodland 4800 ft. along Largo Vista Rd 1 mi n Hwy N4. January. A single record. Ron Alten found one nest containing dozens of workers 8 ft above ground in buprestid beetle galleries in Juniper. Mackay and Mackay (2002) reports that they are uncommonly aggressive in defense of the nest and that they deliver a painful sting. Alten concurs.

Veromessor andrei (Mayr 1886)
Hot Climate Specialist. Feed on grass, grass blades, flower parts and seeds. Joshua/Juniper woodland, Buckwheat-rich communities, Chaparral, Oak Woodland between 1800-6200 ft. Every month. Alates, July. Nest in compact, exposed soils. 45 records. Johnson's Pasture, Claremont; Mt Baldy Rd, Hogback; 5 mi se Palmdale; Mt Emma Rd x Hwy N3; Soledad Cyn Rd, 10.7 mi e Hwy 14.

Veromessor pergandei (Mayr 1886)*
Hot Climate Specialist. Flower parts, insects, seed harvester. Riversidean Fan Scrub, Juniper/Yucca Woodland between 1550-4650 ft. May-Jul. Alates, May. Nest in exposed soil. 5 records. Day Canyon, Etiwanda; Acton; Hwy N3, 1 mi w Mill Creek Summit. This species has been much studied in the context of optimal foraging strategies. They are polymorphic, don't sting and are reliably active even during dry seasons and so lend themselves to manipulative field studies.

Dolichoderinae

Dorymyrmex bicolor (Wheeler, W. M. 1906)*
Dominant Dolichoderinae. Warm Temperate hemipteran tending opportunist. All habitats between chaparral and Yellow Pine Forest from 1450-6750 ft. Every month.

Alates, May-Oct. Nest on exposed soil. 205 records. San Gabriel River; Mt Baldy Rd at 2875 ft.; San Sevaine Rd, Lytle Creek; Mtn High Ski Area, 2 mi w Wrightwood; Largo Vista Rd, 1 mi n Hwy N4; Mt Emma Rd x Hwy N3; Aliso Cyn Rd, 6.0 mi se Soledad Cyn Rd.

Dorymyrmex insanus (Buckley 1866)*
Opportunist. Hemipteran tending opportunist. Chaparral, Scrub Oak, Pine/Oak woodland, Coniferous Forest between 1450-8250 ft. Every month. Alates, Feb-Oct. Nest on exposed soil. 647 records. Nests can be found in almost any warm, disturbed bit of soil all around the range.

Forelius mccooki (McCook 1880)*
Dominant Dolichoderinae. Hemipteran tending scavenger. *Ceanothus* Chaparral at 1700-6200 ft. Every month. Nest in soil or under stones. 33 records. Mt Baldy Rd at 2875 ft.; Ball Flat, 7 mi w Wrightwood; Hwy N4, 2.5 mi w Largo Vista Rd; Mt Emma Rd, 1.5 mi n Hwy N3. This and the next species are very closely related and might hybridize (PS Ward, pers. com., 2010).

Forelius pruinosus (Roger 1863).
Dominant Dolichoderinae. Hemipteran tending scavenger. Chaparral, Pine/Oak Woodlands, Yellow Pine/White Fir Forest between 1450-8500 ft. Every month. Alates, Jun-Aug. Nest in soil or under stones. 264 records. Cobal Cyn, Claremont; Mt Baldy Rd at 2875 ft.; Glendora Mtn Rd, 3.4 mi w Mt Baldy Village; Rd 3N31, 3 mi e Wrightwood; Hwy N4, 2.1 mi w Largo Vista Rd; Mt Emma Rd x Hwy N3; Aliso Cyn Rd, 6.0 mi se Soledad Cyn Rd.

Linepithema humile (Mayr 1868)*
Dominant Dolichoderinae Hemipteran tending opportunist. The species evidently came from Argentina and has also been distributed widely by commerce in Asia and South America. The species is widely distributed in Mediterranean climates around the world. Outside their native range in South America they form "supercolonies", that is, any individual is welcome in any nest and so they form populations of billions of individuals. The population in our area extends from northern Baja California to southern Oregon. Wild (2004, 2007) provided a thorough taxonomic treatment of this genus.

In California this enormous supercolony is accompanied by four smaller satellite supercolonies that maintain strongly contested borders where neighboring supercolonies abut one another (Thomas et al. 2006). The species typically requires mild coastal habitats or irrigated places in the inland valleys. Nest in moist soil and under objects. 37 records from noncultivated sites between 1450-4500 ft. Every month. Alates, May-Sept. Chaffey College Preserve in Alta Loma, 10 records from the North Etiwanda Habitat Preserve at Day Canyon (Andrea Cabrera, pers. comm. 2012) and another 12 from San Dimas Canyon. Yerba Santa/buckwheat, Chamise chaparral. Every month. San Gabriel Cyn Rd, 2.0 mi s Crystal Lake; Hwy N4, 0.7 mi e Valyermo PO; Aliso Cyn Rd, 5.0 mi se Soledad Cyn Rd. None of these listed locations are irrigated nor are they close to irrigated places. This suggests that some populations are adapting to the summer aridity of the range—not welcome news.

Liometopum occidentale Emery 1895*
Dominant Dolichoderinae. Hemipteran tending opportunist. Gathers live and dead insects. Any habitat where there are oaks between 1650-8300 ft. Nest in oak cavities and oak litter. Every month. Alates, Mar-June. 269 records. San Gabriel Cyn Rd, 2.0 mi s Crystal Lake; Johnson Pasture, Claremont; Glendora Mtn Rd, 3.4 mi w Mt Baldy Village; Largo Vista Rd at Hwy N4; Hwy N4, 6 mi w Wrightwood; Mt Emma Rd x Hwy N3.

Tapinoma sessile (Say 1836)*
Opportunist. Hemipteran tending opportunist. All habitat types between 1450-8500 ft. Every month. Alates, Mar-Nov. Nest in soil or any handy cavity. 841 records. San Dimas Reservoir, La Verne; Day Cyn, Etiwanda; Lone Pine Cyn, 1 mi e Wrightwood; East Blue Ridge Rd; Hwy N2, 6 mi w Wrightwood; Hwy N2, 1 mi n Mill Creek Summit; Mt Emma Rd, 1.5 mi n Hwy N3.

Ponerinae

Hypoponera CA-01*
Cryptic Specialist Predator. Hypogaean generalist predator, probably on collembola and other small soil arthropods. *Ceanothus* Chaparral, Pinyon/Juniper Woodland between 1750-4850 ft. May-Oct. Alates, Jun. Nest underground. Six records. San Gabriel Cyn Rd, 2 mi s Crystal Lake; Mt Baldy Rd at 2875 ft.; Largo Vista Rd, 1 mi n Hwy N4; Aliso Cyn Rd, 5.0 mi se Soledad Cyn Rd.

Hypoponera opacior (Forel 1893)*
Cryptic Specialist Predator. Hypogaean generalist predator, probably on collembola and other small soil arthropods.*Ceanothus* Chaparral, Scrub Oak, California Bay riparian woodland between 2050-4150 ft.; Jun-Aug. Nest underground. Alates, Aug. Three records. San Gabriel Cyn Rd, 2 mi s Crystal Lake; Glendora Mtn Rd, 0.5 mi sw San Gabriel River; Mt Baldy Rd, 2875 ft.

Pseudomyrmecinae

Pseudomyrmex apache Creighton 1953
Tropical Climate Specialist. Feed on honeydew, scavenge, prey on arthropods. Chaparral, Juniper Woodland, Oak Woodland between 1750-5850 ft. Every month. Alates, Jul-Aug. Nest in dead wood galleries of *Arctostaphylos* and *Ceanothus* and other woody plants. 35 records. Upper Tujunga Rd; Johnson Pasture, Claremont; Mt Baldy Rd at 2875 ft.; Mt Baldy Rd at Hogback; Glendora Mtn Rd, 3.4 mi w Mt Baldy Village; Lone Pine Cyn Rd, 2 mi e Wrightwood; Little Tujunga Cyn Rd, 3.6 mi w Dillon Divide; Mt Emma Rd, 2.5 mi n Hwy N3.

Dorylinae

Neivamyrmex californicus (Mayr 1870)*
Tropical Climate Specialist. This species' range is limited to the California Floristic Region which confuses the Functional Group designation. Prey on various ants, especially *Pheidole*, and other insects. Oak-rich chaparral, Pine/Oak Woodland, Yellow Pine Forest between 2200-8250 ft. May-Jan. Bivouac in soil, nests of other ants and litter cavities. 59 records. Mt Baldy Rd at 2875 ft.; San Sevaine Rd, Lytle Creek; Guffy Cpg, 1.9 mi sw Wrightwood; Hwy N2, 6 mi w Wrightwood; Big Rock Cyn Rd; Mt Emma Rd, 1.5 mi n Hwy N3. The morphological and biological distinctions between this species, *N. nigrescens* and *N. opacithorax* are discussed by Ward (1999). The relationships are complex and subtle.

Neivamyrmex minor (Cresson 1872)
Tropical Climate Specialist. Predator on various ants, especially *Pheidole*, and other insects. One record from 2.5 mi sse Valyermo in Pinyon/Juniper Woodland at 4800 ft., (Los Angeles Co. Museum). Various summer dates. Nest in soil and litter cavities. We have no records. This species is known only from males, mostly collected at lights during the summer. Snelling and Snelling (2007, p. 481) suggest that *N leonardi* will turn out to be the worker of this species. Serendipitously, we had two collecting locations within about ½ mile of the cited record in similar habitat that ran for more than a year and collected no *N. leonardi*.

Neivamyrmex nigrescens (Cresson 1872)*
Tropical Climate Specialist. Predator on various ants, especially *Pheidole*, and other insects. Chaparral between 1450-4900 ft. with a single record at 8230 ft. This upper limit is much higher than the 4660 ft reported by Ward (1999). Apr-Nov. Bivouac in soil and litter cavities. Schnierla (1958) reports that in southeastern Arizona the colonies of this species reach 150,000-200,000 individuals. Dejean et al. (2013) report on the various responses of prey species to its raids.150 records. Mt Baldy Rd at 2875 ft.; Glendora Mtn Rd, 5.1 mi w Mt Baldy Village; San Sevaine Rd, Lytle Creek; East Blue Ridge Rd, 1.6 mi s Wrightwood; Hwy N4, 2.1 mi w Largo Vista Rd; Mt Emma Rd, 1.5 mi n Hwy N3.

See note in the *N. californicus* entry. There is a form of this species that Ward (1999, p. 86) refers to as the "shiny form" in which the typical sculpturing on the head and pronotum is replaced by an untextured, shiny surface. There is a zone of introgression between the typical and shiny forms on the north side of the San Gabriel Mountains. We have two records of this shiny form from Mt Emma Rd, 2.5 mi n Hwy N3 and 0.9 mi e Valyermo PO on Hwy 4.

Neivamyrmex opacithorax (Emery 1894)*
Tropical Climate Specialist. Predator on ant brood and other insects. Buckwheat flats, Chaparral between 2000-4650 ft. Apr-Oct. Nest in soil and litter cavities. 35 records. Mt Baldy Rd at 2875 ft.; Glendora Mtn Rd, 3.9 mi w Mt Baldy Village; Soledad Cyn Rd, 4.2 mi e Hwy 14; Hwy N3, 1 mi s Mt Emma Rd. See taxonomic note in the *N. californicus* entry.

Discussion

Four major findings emerged from our survey of the ants of the San Gabriel Mountains in southern California. First, particular comment is warranted concerning the upper elevation records for five of the species. We have a number of records for *Neivamyrmex californicus, N. nigrescens, Forelius pruinosus, Dorymyrmex insanus* and *Solenopsis xyloni.* Each of them has been recorded repeatedly at several locations on different collection dates thousands of feet above the expected elevation range of the species. For instance, Wheeler and Wheeler (1973) did not find any such high elevation records in Deep Canyon near Palm Springs. Our records are mostly from sunny exposures on East Blue Ridge (above 8,000 ft.) and Prairie Fork Canyon (at 7,000 ft.). We are convinced that the records are valid but, except for the sunny, warm exposures in a warming climate, we have no explanation for the causes of these dramatic upward extensions of their ranges. One reviewer remains skeptical.

Second, these mountains are immediately adjacent to an enormous human population and the Angeles National Forest gets extremely heavy recreational use. In addition, there are several residential communities and developed inholdings within the perimeter of the study area. We are surprised that only *Linepithema humile* and *Cardiocondyla maruritanica*, the only two of the 25 non-native species in California, have managed to insert themselves into the native ant community. We think it likely that collecting within these residential communities and in their disturbed margins will reveal more species of non-native ants. The impact of invasive ants on native communities is frequently severe and deserves attention (Holway et al. 2002; Wittman 2014).

Third, the moisture and temperature gradients that are generally related to elevation invite the suggestion that ant species diversity also varies along an elevational gradient. Machac et al. (2011) showed that such a gradient does exist in some temperate mountain ranges, that species density declines with increasing elevation and that it is mediated by temperature. Arnan et al (2015) suggest that ant communities' resilience to climatic temperature change is related to mean annual temperature and temperature seasonality. In the present study our analysis of the species density across the elevation gradient on both north-facing and south-facing exposures (Fig. 2) shows no correlation between species number and elevation. These results suggest that different ant assemblages may respond differently to novel thermal trends. The fact that we pooled north-facing and south-facing locations into one analysis may have obscured local patterns, in fact, that is likely to be the case.

Lastly, the several canyons that drain northward into the desert deserve more careful study as they might provide access into the mountains by a number of desert species that were not detected by this survey and those species may form interesting associations with the more montane ant fauna. As a tantalizing example, we recorded workers of four desert species in the range far from expected habitats. *Formica xerophila, Pheidole* nr *barbata, P. rugulosa* and *Crematogaster depilis* were collected in San Antonio Canyon in *Ceanothus* chaparral at an elevation of 2875 ft. on the south side of the range. The presence of workers is evidence of established nests in an unexpected vegetation type. Their presence invites more focused collecting as that might reveal something of the nature of the biogeographic barriers that filter the ant faunas of the Mojave Desert and the Los Angeles Basin.

The Transverse Ranges of southern California have long been recognized as a biogeographic barrier between the Mojave Desert on the north and the Los Angeles Basin on the south (Gottscho 2016 and references therein). There also appear to be both a geological and a biological rift between the western Transverse Ranges (Sierra Pelona and those westward) and the eastern Transverse Ranges (San Gabriel, San Bernardino and San Jacinto Ranges). The San Fernando Pass demarcates one major break and Cajon Pass creates another. Chatzimanolis and Caterino (2007) demonstrated distinct genetic breaks in populations of insects, birds and reptiles across both of these physical features. The results of the present study will provide a basis for comparison with the ant faunas of the adjacent mountain ranges – the Sierra Pelona across the San Fernando Pass to the west and the San Bernardino Mountains across Cajon Pass on the east.

Conclusions

There are many aspects of the ecology of ants in this mountain range that have not been addressed here. Species associations within particular vegetation types, elevation gradients, north-south facing habitat exposure and functional group associations can all be extracted from our data set. We anticipate that those topics will be the subject of subsequent studies.

Acknowledgements

Mark Ikeda's continuing conversations about the ant literature have materially improved our understanding of the subject. He also provided specimens for the voucher collection and a critical reading of the manuscript. The willingness of Philip Ward and Andrew Suarez to check the identifications of many specimens made the study possible. Matt Prebus checked the identification of a number of newly described *Temnothorax*. Gordon Snelling checked the identification of *Neivamyrmex,* read a draft of the manuscript and contributed a number of army ant records. Two anonymous reviewers of an earlier draft of this paper provided very substantial suggestions that greatly improved the paper.

Chris Chandler, GIS Specialist, San Bernardino National Forest, provided the mapping files that made the vegetation analysis possible. John C. Donoghue II did a vegetation analysis of an early draft of this study. A permit for access to restricted areas was provided by the Lytle Creek office of the San Bernardino National Forest in 2004 and Marty Dumpis of the Angeles National Forest provided an access permit after the Grand Prix fire of 2003. We appreciate all of their generous help.

Literature Cited

Abensperg-Tran, M., and D. Steven. 1995. The effects of pitfall trap diameter on ant species richness (Hymenoptera: Formicidae) and species composition of the catch in a semi-arid eucalypt woodland. Australian J. Ecology, 20: 282-287.

Allred, D. M. 1982. Ants of Utah. Great Basin Nat., 42(4):415-511.

Andersen, A. N. 1997. Functional groups and patterns of organization in North American ant communities: a comparison with Australia. J. Biogeog., 24:433-460.

—. 2010. Functional groups in ant community ecology. p 142-143. in Lach, L, CL Parr, KL Abbot. 2010. Ant Ecology. Oxford Univ Press, London, xvii + 402 pp.

Arnan, X., N. Bluthgen, R. Molowny-Horas, and J. Retana. 2015. Thermal characterization of European and communities along thermal gradients and its implications for community resilience to temperature variability. Front. Ecol. Evol. 3: 138 doi:10.3389/fero.2015.00138.

Borgelt, A., and T. R. New. 2005. Pitfall trapping for ants in mesic Australia: the influence of trap diameter. J. Insect Conservation, 9:219-221.

Branstetter, M. G. 2012. Origin and diversification of the cryptic ant genus *Stenamma* Westwood (Hymenoptera: Formicidae), inferred from multilocus molecular data, biogeography and natural history. Syst. Emtomol. 37(3):478-496.

Buren, W. F. 1968. A review of the species of *Crematogaster*, sensu stricto, *in* North America (Hymenoptera, Formicidae) Part II. Descriptions of new species. J. Georgia Entomol. Soc., 3:91-121.

Burger, J. C., R. A. Redak, E. B. Allen, J.T. Rottenberry, and M. E. Allen. 2003. Restoring arthropod communities in Coastal Sage Scrub. Conservation Biology. 17(2):460-467.

Chatzimanolis, S., and M. S. Caterino. 2007. Toward a better understanding of the "transverse range break": lineage diversification in southern California. Evolution 61(9):2127-2141.

Cleland, D. T., J. A. Freeouf, G. J. Norwacki, C. Carpenter, J. E. Keys, and W. H. McNab. 2004. Subregions of the conterminous United States. Washington, DC: U.S. Department of Agriculture, Forest Service.

Dejean, A., B. Corbara, O. Roux, and J. Orivel. 2013. The antipredator behaviors of Neotropical ants towards army ant raids (Hymenoptera: Formicidae).Myrmecol. News, 19:17-24.

Dornelas, M., A. E. Magurran, S. T. Buckland, A. Chao, R. L. Chazdon, R. K. Colwell, T. Curtis, K. J. Gaston, N. J. Gotelli, M. A. Kosnik, M. BcGill, J. L. McCune, H. Morlon, P. J. Mumby, L. Øvreås, A. Studeny, and M. Vellend. 2012. Quantifying temporal change in biodiversity: challenges and

opportunities. Proceedings of the Royal Society, B. doi: 10.1098/rspb.2012.1931.

ESRI. 2009. ArcMap 9.3. Environmental Systems Research Institute, Redlands, California.

Gadau, J., S. G. Brady, and P. S. Ward. 1999. Systematics, distribution and ecology of an endemic California *Camponotus quercicola* (Hymenoptera: Formicidae). Ann. Entomol. Soc. Am., 92(4):514-522.

Gotelli, J. J., and R. K. Colwell. 2001. Quantifying biodiversity: procedures and pitfalls in the measurement and comparison of species richness. Ecology Letters, 4:379-391.

Gottscho, A. D. 2016. Zoogeography of the San Andreas Fault system: Great Pacific Fracture Zones correspond with spatially concordant phylogeographic boundaries in western North America. Biol. Res. (2016) 91:235-254.

Holway, D. A., L. Lach, A. V. Suarez, N. D. Tsutsui, and T. J. Case. 2002. The causes and consequences of ant invasions. Ann. Rev. Ecol. Syst. 2002. 33:181-233.

Hunt, J. H. 1973. Comparative ecology of ant communities in Mediterranean regions of California and Chile. Unpubl. Ph.D. dissertation, Univ. Calif., Berkeley. 131 p.

Machac, A., M. Janda, R. R. Dunn, and N. J. Sanders. 2011. Elevational gradients in phylogenetic structure of ant communities reveal the interplay of biotic and abiotic constraints on diversity. Ecography, 34:364-371.

Mackay, W. 1980. A new harvester ant from the mountains of Southern California (Hymenoptera: Formicidae). Southwestern Nat., 25(2):150-156.

— and E. Mackay. 2002. The Ants of New Mexico (Hymenoptera: Formicidae). The Edwin Mellen Press, Lewiston, NY, USA, 398 pp.

Mallis, A. 1941. A list of the ants of California with notes on their habits and distribution. Bull. So. Calif. Acad. Sci., XL(1):61-100.

Mao, C. X., and R. K. Colwell. 2005. Estimation of species richness: mixture modes, the role of rare species and inferential challenges. Ecology 86(5):1143-1153.

Millar, C. 2012. Geologic, climatic, and vegetation history of California. In: Baldwin, et al. 2012. The Jepson Manual: Vascular Plants of California. 2nd ed. Univ. Calif. Press, xvii + 1400 pp.

Parr, C. L., B. J. Sinclair., A. N. Andersen, K. J. Gaston, and S. L. Chown. 2005. Constraint and competition in assemblages: a cross-continental and modeling approach for ants. Am. Nat. 165(4):481-494.

Schnierla, T. C. 1958. The biology and behavior of certain Nearctic army ants: last part of functional season, southeastern Arizona. Insectes Sociaux, 5:215-255.

Schoenherr, A. 1992. A Natural History of California. Univ. Calif. Press, Berkeley. California Natural History Guides: 56, Univ. Calif. Press, Berkeley, xi + 772 pp.

Snelling, G. C., and R. R. Snelling. 2007. New synonymy, new species, new keys to *Neivamyrmex* army ants of the United States, pp. 459-550. In: Snelling, R. R., B. L. Fisher, and P. S. Ward (eds). Advances in Ant Systematics (Hymenoptera: Formicidae): Homage to E. O. Wilson – 50 Years of Contributions. Memoirs of the Amer. Entomol. Institute, 80.

Snelling, R. R. 1973. Studies on California ants. 7. The genus *Stenamma* (Hymenoptera: Formicidae). Contributions in Science (Los Angeles), 245: 1-38.

—. 1976. A revision of the honey ants, genus *Myrmecocystus* (Hymenoptera: Formicidae). Nat. Hist. Mus. Los Angeles Co. Sci. Bull., 24, 163 pp.

—. 1982. A revision of the honey ants, Genus *Myrmecocystus* , first supplement (Hymenoptera: Formicidae). Bull. So. Cal. Acad. Sci., 81(2): 69-86.

—, M. L. Borowiec, and M. M. Prebus. 2014. Studies on California ants: a review of the genus *Temnothorax* (Hymenoptera, Formicidae). ZooKeys, 372:27-89.

— and C. D. George. 1979. The taxonomy, distribution and ecology of California desert ants. Report to Calif. Desert Play Program, Bureau of Land Mgmt, USDA. 335 + 89 pp. BLM contract No. CA-060-CT8-000007.

Suarez, A. V., D. T. Bolger, and T. J. Case. 1998. Effects of fragmentation and invasion on native ant communities in coastal Southern California. Ecology, 79(6):2041-2056.

Tista, M., and K. Fiedler. 2011. How to evaluate and reduce sampling effort for ants. J. Insect Conservation. 15:547-559.

Thomas, M. L., C. M. Payne-Makrisa, A. V. Suarez, N.D. Tsutsui and D. A. Holway. 2006. When supercolonies collide: territorial aggression in an invasive and unicolonial social insect. Molecular Ecology 15:4303-4315.

Trager, J. C. 2013. Global revision of the dulotic ant genus *Polyergus* (Hymenoptera, Formicidae, Formicinae, Formicini). Zootaxa, 3722 (4): 501-548 (2013).

Ward, P. S. 1999. Deceptive similarity in army ants of the genus *Neivamyrmex* (Hymenoptera: Formicidae): taxonomy, distribution and biology of *N. californicus* (Mayr) and *N. nigrescens* (Cresson). J. Hym. Res., 8(1):74-97.

—. 2005. A Synoptic review of the ants of California (Hymenoptera: Formicidae). Zootaxa, 936: 1-68 (2005).

—. 2016. AntWeb: Ants of California. Available from: https://www.antweb.org/page.do?name=california. Accessed 3 May 2016.

Wetterer, J. K., P. S. Ward, A. L. Wetterer, J. T. Longino, J. C. Trager, and S. E. Miller. 2000. Ants (Hymenoptera: Formicidae) of Santa Cruz Island, California. Bull. So. Cal. Acad. Sci., 99(1):25-31.

Wheeler, G. C., and J. N. Wheeler. 1973. Ants of Deep Canyon: Colorado Desert, California. Philip Boyd Deep Canyon Desert Research Center, Univ. Calif, Riverside, xiii + 162 pp.

—, and —. 1986. The Ants of Nevada. Nat. Hist. Mus. Los Angeles Co., vii + 138 pp.

Wild, A. L. 2004. Taxonomy and distribution of the Argentine Ant, *Linepithema humile.* Ann. of the Entomol. Soc. Amer. 97: 1204-1215.

—. 2007. Taxonomic revision of the ant genus *Linepithema* (Hymenoptera: Formicidae). Univ. Calif. Publ. Entomol. 126:1-151.

Wittman, S. E. 2014. Impacts of ants on native ant communities (Hynemoptera: Formicidae). Myrmecol. News. 19:111-123.

Ants of the San Gabriel Mountains in Southern California: keys to the species

James Des Lauriers
Dept. Biology, Chaffey College, Alta Loma, CA 91737, JIMDESL39@gmail.com

The east-west trending San Gabriel Mountains separate the Los Angeles basin's Mediterranean climate on the south from the Mojave Desert on the north. At 10,064 ft., Mt San Antonio is the high point of the range. The range lies between San Fernando Pass on the west and Cajon Pass on the east, a distance of about 60 miles. The range is about 20 miles wide and includes an area of about 980 mi^2. On the south side, the base of the range is at about 2000 ft. and rises abruptly from the valley floor. The plant communities there are dominated by scrub and chaparral communities of various composition with oak and mixed conifer communities extending to the high ridges. Precipitation on these highest slopes ranges from 30-40 inches. On the north side, at elevations around 4000 ft., junipers mark the base, then Pinyon/Juniper woodland gives way to Conifer/Oak forests with White Fir forests on the highest ridges. These communities receive 15-20 inches of precipitation, much of it in the form of winter snow. Geologically, the range, along with the others of the Transverse Ranges, is produced by the movement of the Pacific Plate against the North American Plate along the San Andreas Rift Zone. Schoenherr (1992) and Millar (2012) offer overviews of the natural history and the climatic and vegetation history of the region.

This complex, fire-dominated mosaic of plant communities is an attractive place to study the rich ant fauna. Ant surveys of Southern California include one in San Diego County (Suarez et al., 1998) and another of Santa Cruz Island (Wetterer et al., 2000) but I have been unable to find any study of the local region. Ward (2005) reviewed the ants of California mostly at the generic level. Ward's paper includes keys to the genera of California ants.

With this literature in hand I set out to survey the ants of the range beginning in 1999. Since then I have recorded 97 species collected throughout the range. Des Lauriers and Ikeda (under review) describe the results of this survey and provide an annotated list, natural history notes for each species and some biogeographical inferences. The identification of these species has been quite a challenge given the sparse literature and the dynamic state of the taxonomy. To help my own efforts and those of my collaborators I have produced a set of sixteen keys. A key was made for each genus that contains species that can't be confidently distinguished by visual inspection of the automontage images found at AntWeb.org.

This anthology of keys to the workers includes the genera *Camponotus, Crematogaster, Forelius, Formica, Hypoponera, Lasius, Myrmecocystus, Myrmica, Neivamyrmex, Nylanderia, Pheidole, Pogonomyrmex, Pseudomyrmex, Solenopsis, Stenamma* and *Temnothorax*. User-friendly keys to the genera can be found in Fisher and Cover (2007) and Ward (2005). You should use one of these keys to identify your specimen to genus. Then consulting the appropriate key in this anthology will get you to species. **If there is no key to the genus you are interested in** among the keys in this anthology, it is because the genus contains only one or two species recorded within the range and it can be identified by visual comparison with the images of California species at AntWeb.org. https://www.antweb.org/adm1.do?name=California. Those species appear in the alphabetical list of species that follows.

Aphaenogaster occidentalis, Brachymyrmex depilis, Cardiocondyla mauritanica, Dorymyrmex bicolor and *D. insanus, Linepithema humile, Liometopum occidentale, Manica bradleyi, Monomorium ergatogyna, Myrmica punctinops* and *M. rugiventris, Polyergus vinosus, Prenolepis imparis, Strumigenys californica, Tapinoma sessile, Veromessor andrei* and *V. pergandei*.

Unless otherwise indicated these keys are to workers and include those species found in the San Gabriel Mountains and immediate environs.

I identified ants by reference to Wheeler and Wheeler (1986), Snelling (1973, 1976, 1982), Snelling and George (1979), Snelling et al., (2014) and AntWeb.org. The website has automontage images of all of California's ant species and is kept up to date. Identifications of most species were checked by Andrew Suarez (then at UC, Berkeley) or Philip Ward (UC, Davis). Matthew Prebus (UC, Davis) checked the identification of some newly described *Temnothorax* and Gordon Snelling checked the identifications of *Neivamyrmex*.

These keys are a work in progress and I would appreciate it if you direct my attention to errors or suggested improvements. Additional species will surely be detected within the range. I would greatly appreciate having those records pointed out to me so that they can be added to the growing faunal list. I'd particularly like to thank Mark Ikeda for his help in working through some of the difficult couplets and for these many years of collaboration. Students at Chaffey College helped by using earlier versions of these keys and by pointing out errors and ambiguities.

Keys follow in alphabetical order

CAMPONOTUS

There are twenty two species in California eleven of which are recorded in the San Gabriel Mountains. In constructing the key extensive use was made of the following sources; Ward (2005) and Wheeler & Wheeler (1986). The key is supported by the images of California ants found at AntWeb.org. Two words of caution are warranted. In the San Gabriels *C. vicinus* includes a black form as well as the typical bicolored form and C. *semitestaceus* does not display the lobule at the base of the scape that typifies the species elsewhere. Small individuals are frequently unkeyable.

1 Head, in profile, evenly arched from clypeal apex to vertex. ..2
Head, in profile, obliquely truncate below antennal insertions. (subg. *Myrmaphaenus*). ..... *yogi*

2(1) Clypeus without median notch, thickened; major workers > 8 mm long. 3
Lower margin of median lobe of clypeus with narrow notch in middle, thin, weakly convex and semicircularly depressed; major worker < 8 mm long. (subg. *Myrmentoma*). 4

3(2) Clypeus carinate to feebly so, if latter then scape flattened at base. (subg. *Tanaemyrmex)*..... 8
Clypeus more or less ecarinate; scapes never flattened at the base. (subg. *Camponotus*). 7

4(2) Mesosomal profile distinctly depressed at metanotal suture. . ... *hyatti*
Mesosomal profile not depressed at metanotal suture. 5

5(4) In profile view, crest of petiolar node narrowly sharp. 6
In profile view, crest of petiolar node rounded..... *anthrax*

6(5) In front view, malar area with conspicuous short erect or suberect hairs; propodeal profile angular..... *clarithorax*
In front view, malar area without erect or suberect hairs except a few at base of mandible; integument subpolished to shiny. …..... *essigi*

7(3) Dorsal surface of head and mesosoma with numerous erect hairs; when viewed in profile, node of petiole rounded; body surface with bluish metallic sheen. ..... . *laevigatus*
Dorsal surface of head and mesosoma with no or few erect hairs; when viewed in profile, node of petiole sharp; body surface shiny black. ..... . *quercicola*

8(3) Base of scape flattened, at least slightly broader at base than immediately beyond. 10
Scape narrowest at base, weakly flattened. 9

9(8) Integument hairy, pubescence on tergites 3 and 4 longer than distance between hairs. ..... *vicinus*
Integument less hairy; length of pubescence on tergites 3 and 4 about equal to distance between hairs. ..... *maritimus** (* This species has not been collected in the San Gabriels but its known range toward the west is close.)

10(8) Margins of head of major, in frontal view, distinctly convergent toward mandibular bases; scape with small lateral lobule at base; apex of scape of major exceeding vertex corner by at least its apical breadth 11
Head of major quadrate, margins strongly convergent immediately above mandibular base; scape base broad, flattened, not lobulate; apex of scape of major exceeding vertex corner, if at all, by less than its apical breadth ..... *sansabeanus*

11(10) Lobule at flattened base of scape conspicuous in all sizes of workers. . ..... *dumetorum*
Lobule at flattened base of scape absent or only a suggestion of it in the largest workers (this condition seems to be limited to this region). …..... . *semitestaceus*

CREMATOGASTER

There are ten species of *Crematogaster* in California seven of which have been recorded in the San Gabriel Mountains. *C. larreae* and *C. opuntiae* are desert species that might be found at lower elevations on the north side of the range. This key to the workers is modified from Wheeler and Wheeler (1986) and from the AntWiki site http://www.antwiki.org/wiki/Key_to_western_US_Crematogaster. The characters are often ambiguous and individuals with worn hairs add to the uncertainty. The photos at AntWeb.org are very helpful.

1. Anteroventral tooth of petiole strikingly large; head subquadrate; postpetiole trapezoidal in dorsal view, wider in front, with straight; petiole much broader than in all the other species. ..... *mutans*
Without this combination of characters. 2

2. Pronotum sides densely, conspicuously punctate; thorax without erect hairs or with a single erect hair on each pronotal shoulder. (Hairs may be worn. Check several specimens.) . . 3
Pronotum sides with some other type of sculpture or else 2 or more hairs on each pronotal shoulder. 6

3. Thorax and gastral tergites without erect hairs, **may be worn**. Check several specimens. 4
An erect hair on each pronotal shoulder, **may be worn.** Check several specimens. 5

4. Head and thorax reddish. ..... … *depilis*
Head and thorax black or dark brown. … ..... *larreae*

5. Pubescence appressed on scape and head, hairs on 1st gastral tergite about one hair length apart ..... *opuntiae*
Pubescence suberect on scape (look along the distal 1/3) and head, hairs on 1st gastral tergite closer than one hair length apart. 9

6. Lower mesopleuron with distinct striae (very fine lines). . 7
Lower mesopleuron without striae, or a mere hint of one or two. …..... . *hespera*

7. Scape not, or scarcely, surpassing occipital corner in large specimens; mesonotal declivity smoothly curved or inconspicuous; thorax weakly punctuate; occiput shiny. ..... . *marioni**
Scape surpassing occipital corner by 1 or 2 diameters; mesonotal declivity **abrupt and angular. . .....** . 8

8. Head entirely striatopunctate; dull. ..... *coarctata*

Head above eyes smooth and shining or with only weak striae. ..... . *mormonum*

9. In dorsal view, postpetiole subquadrate and anterolateral corners of petiole broadly rounded. ..... . *mutans*
In dorsal view, postpetiole narrower in front than in back and anterolateral corners of petiole more acute..... *californica*
* Chaparral, arboreal, on manzanita, oak, riparian on oak.

FORELIUS

1. A few standing hairs along the anterior margin of the scape (viewed from above against a dark field) .....*mccooki*
No standing hairs along the anterior margin of the scape. ..... *pruinosus*

FORMICA

Formica is a large, complex Holarctic ant genus. Most of the species are northern or are associated with wooded areas. There are 43 species in California. I have modified the key of Wheeler and Wheeler (1986) so that this key includes only the six species so far known to occur in the San Gabriel Mountains. The key is strongly supported by the images in Wheeler & Wheeler (1986). This key is derived directly from Francoeur (1973). All of the species in this key are in the *fusca* species group. On three occasions while collecting along East Blue Ridge near Guffy Camp I have seen an ant that is in the *rufa* or *sanguinea* Group. It might be *F. aserva* but I've never been quick enough to collect it under the thorny *Ceanothus* thickets. Keep a sharp eye out for a surprise.

1. Eyes with short, erect hairs arising from between the facets; all body surfaces covered with short, erect hairs..... *Francoeuri* 2

2. Strongly polymorphic; thorax opaque or subopaque; dorsal gastric hairs long; surface strongly shining..... . *subpolita*
Feebly polymorphic or monomorphic; other characters otherwise. 3

3. Concolorous black, blackish. .....*.argentea*
Bicolored: head and thorax red, often infuscated with patches of reddish brown, especially on dorsum; gaster black or blackish brown. 4

4. Epinotum high, its angle distinct. ..... *gnava*
Epinotum long and low, its angle reduced to an even convexity. 5

5. Scale of petiole low and, in profile, thick and broadly rounded at summit, both faces convex but anterior moreso. . *xerophila*
Scale of petiole high and, in profile, thin and angulate at summit. ..... *moki*

HYPOPONERA

Perhaps all four of the species of *Hypoponera* that occur in California also occur in the San Gabriel Mountains or the immediate environs. I have records from the range for *H.* CA-01 and *H. opacior* and for *H. punctatissima* from nearby Ontario. The keys that I've seen all seem to trace their ancestry to Creighton (1950). I've made a key that works for the Southern California material that I have at hand.

1. Mesopleuron smooth and shiny, lacking punctures ..... *punctatissima*
Mesopleuron partly to entirely granulate or punctate. 2

2. Head and dorsal pronotum nearly bare of pubescence, a few appressed hairs may be present. CA-01
Head and dorsal pronotum densely clothed with appressed to decumbent pubescence. 3

3. Petiole in lateral view narrower dorsally than ventrally, the anterior and posterior faces not parallel; Head and body punctate over a smooth and shiny background. *opacior*
Petiole in lateral view not narrowed dorsally, the anterior and posterior faces parallel; head and body punctate-granulate, the background surface not particularly shiny. ..... *opaciceps*

LASIUS

Of the seventeen species of *Lasius* in California I have collected only three in the San Gabriel Mountains. For high quality images of all of these species see AntWeb.org. I think it likely that more of the subterranean species will be discovered in the range. Hand collecting and digging along the shallow roots of shrubs may be rewarded.

1. Color dark and eyes fully developed. ..... *alienus*
Color pale to tan and eyes much reduced. 2

2. Eye with fewer than about 20 facets; propodeum sparsely hairy. ..... nr *flavus*
Eye with more than about 20 facets; propodeum abundantly hairy. ..... *californicus*

MYRMECOCYSTUS

There are 22 species of *Myrmecocystus* in California. Of those, ten occur in the San Gabriel. Snelling (1976, 1982) revised the genus and produced keys to all three castes. Here I have modified the worker key so that it contains only the 10 species that have so far been recorded in the range. The images at AntWeb.org are very helpful.

Key to the Subgenera: Workers

1. Integument either: (a) bicolorous, head and thorax ferruginous, gaster black; (b) unicolorous, ferruginous or orange; (c) unicolorous blackish or dark brown; mandibles six or seven toothed; eye small, maximum diameter less than to slightly exceeding length of first flagellomere; ocelli present, sometimes obscure in small individuals; diurnal, matinal or crepuscular. 2
Integument light yellow or brownish yellow; mandibles eight to ten toothed; eye large, maximum diameter much exceeding length of first flagellomere; ocelli absent or much reduced; nocturnal..... *Myrmecocystus*

2. Small (HL not exceeding 1.26 mm), uniformly blackish or dark brown, usually with anterior one-third of head paler; erect hairs very reduced on head and; pubescence sparse on head. ..... *Eremnocystus*
-- Larger (HL exceeding 0.83 mm), either bicolorous or ferruginous; usually abundantly hairy, erect hairs numerous on head and thorax, appressed pubescence usually dense on third tergum; diurnal. ..... *Endiodioctes*

Key to the species of Subg. *Myrmecocystus*: Workers

1. Large, highly polymorphic species, head length 1.0-2.0 mm or more, usually in excess of 1.3 mm; metanotal suture usually impressed and propodeum as long as high or longer, juncture of dorsal and posterior faces broadly rounded. ..... . *mexicanus*

Smaller, moderately polymorphic species, head length 0.8-1.4 mm; metanotal suture not impressed; propodeum higher than long, juncture of dorsal and posterior faces abruptly rounded, often subangulate. ..... *testaceus*

Key to the species of Subg. Eremnocystus: Workers

1. Antennal scape and dorsum of propodeum without fully erect hairs. ..... *creightoni*

Antennal scape, usually, and dorsum of propodeum, always, with some fully erect hairs. ..... *colei*

Key to the species of Subg. *Endiodioctes*: Workers

1. Abundantly hairy species: 20+ erect hairs on malar area in frontal view; scape, femora and tibiae with numerous suberect to erect hairs on all surfaces; first three (usually four) terga with dense pubescence; head width of major usually in excess of 1.7 mm. . ..... *semirufus*

Less hairy species: fewer than 20 erect hairs on malar area in frontal view, usually fewer than 6; scape and femora often sparsely hairy ; third tergum often sparsely pubescent: head width of major less than 1.7 mm. 2

2. Malar area, in frontal view, with six or more erect hairs evenly distributed between eye and base of mandible. 3

Malar area, in frontal view, with not more than four erect hairs, these confined to lower half, near base of mandible. . 4

3. Tergum IV conspicuously pubescent in specimens with pronotal width in excess of 1.0 mm; erect hairs present on at least half of distance between inner eye margin and antennal socket; punctures of frontal lobes and frons of variable size and irregularly distributed. ..... *semirufus*

Tergum IV with pubescence, when present, very widely scattered: erect hairs present only adjacent to eye margin, not extending more than 0.25 of distance between eye and antennal socket; punctures of frontal lobes and frons uniformly minute, evenly distributed. ..... *flaviceps*

4. Longest occipital hairs clearly longer than minimum eye diameter in majors. 5

Longest occipital hairs no more than 0.6 X minimum eye diameter usually about 0.5. 6

5. Hairs on dorsal face of hind femur appressed to subappressed; frontal lobes and frons finely, closely and uniformly punctate; mandible septemdentate: abdomen usually wholly orange-ferruginous. ..... *wheeleri*

Hairs on dorsal face of hind femur suberect, conspicuous; frontal lobes finely and very irregularly punctate with large impunctate areas; mandible octodentate; abdomen usually black, often with basal two or three terga extensively yellowish. ..... *kathjuli*

6. Tergum III with little or no pubescence. 7

Tergum III with dense pubescence. ..... *flaviceps*

7. Pubescence very sparse on face; head often subpolished and shiny; side of head of large worker often converging; head, thorax and legs brownish. . ..... *mimicus*

Pubescence abundant on face; head usually distinctly tessellate, not notably shiny; side of head straight in frontal view; head, thorax and legs ferruginous (top of head may be slightly brownish). ..... *kennedyi*

MYRMICA

There are eight species of *Myrmica* in California with two of them in the San Gabriel Mountains. The key is supported by the images of California ants found at AntWeb.org.

1. Lower mesopleuron conspicuously rugose; epinotal spine much longer than the width of its apparent base... *punctinops*

Lower mesopleuron faintly or not rugose; Epinotal spine about as long as the width of its apparent base. .... *rugiventris*

NEIVAMYRMEX

The ants in the genus *Neivamyrmex* were revised by Snelling and Snelling (2007) and Snelling & George (1979) surveyed the army ants of the California deserts. There are nine species in California. I have modified their keys so that this key includes only the four species so far known to occur in the San Gabriel Mountains. The key is supported by the images of California ants found at AntWeb.org. and those in the original papers which are available online.

The taxonomy of this genus appears to be in a state of uncertainty. Most are very poorly known within our area. Males are commonly attracted to lights. Workers are, as a rule, collected in pitfall traps or at night when the foraging or emigration columns may be encountered. Bivouaced colonies are rarely located. Some species, such as *N. leonardi,* are probably wholly subterranean.

There are two pairs of species that are of particular interest. *N. minor* is known only from males and has been collected south of Pearblossom. *N. leonardi* is known only from workers. These two species may actually be a single species. Two other species that occur in the immediate region, *N. mojave* (only males known) and *N. nyensis* (only workers known) are also likely to be a single species (Snelling & Snelling, 2007).

WORKERS

1. Node of petiole, from above, elongate, clearly longer than broad; largest workers more than 5 mm long. …… 2

Node of petiole, from above, stout, about as broad as long; largest workers 3-4 mm long; HW not exceeding 1.0 mm. ..... *leonardi*

2(l). Head more or less shiny, not densely sculptured and opaque; at least side of pronotum usually distinctly shiny. 3

Head and mesosoma opaque, densely and often coarsely sculptured). ..... *nigrescens* (part)

3(2). Basal margin of mandible evenly curved into masticatory margin, without a tooth or corner at their junction. 4

Basal margin of mandible straight, forming distinct tooth or angle with masticatory margin. 5

4(3). Dorsal surface of propodeum distinctly depressed below level of mesonotum; metafemur long, 6.4 x as long as deep. ..... *nigrescens* (shiny form)

Dorsal surface of propodeum not distinctly depressed; metafemur shorter, 5.2 x as long as deep. ..... *californicus*
5(3). Mesosoma largely or entirely conspicuously roughened and opaque or semiopaque; head relatively broad. .... . *opacithorax*
Mesosoma smooth and shiny, with only occasional indications of sculpturing on mesosoma**;** head relatively narrow; a small species. ..... *nyensis*

MALES
1. Mandible sickle-shaped. ..... *minor*
Mandible not sickle-shaped. 2

2(1). From above, dorsal surface of head forming distinct ridges over antennal sockets; mesosomal dorsum subopaque to opaque. …..... *nigrescens* (typical form)
From above, dorsal surface of head rounded, not forming distinct ridges over antennal sockets; Mesosomal dorsum moderately shiny. ..... *opacithorax*

NYLANDERIA
The California species of ants in the genus *Nylanderia* were revised by Kallal and LaPolla (2012). There are 5 species in California one of which is an undescribed species represented by a single record. I have made the key so that it includes only the three described species so far known to occur in, **or near** the San Gabriel Mountains. The key is supported by the images of California ants found at AntWeb.org and those in the original paper which is available online at AntWeb.org.

1. Vertex of the head in frontal view concave; a desert species. ..... *hystrix*
Vertex of head in frontal view convex; diverse habitats.... 2

2. Eye length ¼ head length or more; domestic habitats; color dark brown. ..... *vividula*
Eye length less than ¼ head length; undisturbed natural habitats; color light brown. ..... *magnella*

Vividula and *magnella* workers are often exceedingly difficult to separate on morphological grounds. However the males are easily separable. In frontal view the head length exceeds the head width (measured just above the eyes) in *N. vividula*. In *N magnella* those dimensions are about equal. Also consult the original paper, p. 41 for genital structure differences.

PHEIDOLE
The California species of ants in the genus *Pheidole* appear not to have been specifically studied in a single publication. There are 27 species in California. Snelling and George (1979) surveyed the desert ants of California and have keys for each of the castes. I have modified their key so that it includes the 8 species so far known to occur in the San Gabriel Mountains. Take note of the fact that images of both major and minor workers are presented for each species.

The key to the species groups is adapted from Wilson (2003). The workers of *Pheidole* are dimorphic with the majors having exceedingly enlarged heads as well as more robust bodies. Minor workers far outnumber majors and the keys nearly always require that you have specimens of both forms. Thus, collecting methods must be able to confidently associate majors and minors as members of one species. Sampling directly from nests is the only sure way of having that confidence.

Key to the Species Groups
1. Along with the bidentate or toothless hypostoma of the major, the major and minor have a roughly quadrate or short-rectangular head shape; i.e., in full-face view, the lateral margins of the head are straight to weakly curved, and the head capsule is as wide or almost as wide as it is long. Minor: eyes large compared to head size, the ratio of Eye Length to Head Length is 0.14 to 0.40. ..... *pilifera* group
Either the major and minor have moderately to strongly curving sides of head; or the ratio of Eye Length to Head Length in the minor is 0. 15 or less; or both of these traits are present. ..... *fallax* group

Key to the Pilifera Group (modified from Snelling and George 1979.)

Minor Workers
1. Head sharply narrowed behind eyes to form a short neck at occipital margin; Head Length about 1.3-1.4 times Head Width. ..... *desertorum*
Head weakly to moderately narrowed behind eyes, not forming neck at occipital margin; Head Length about 1.2 times Head Width. ..... *hyatti*

Major Workers
1. Apex of antennal scape surpassing occipital margin; mesial pair of gular teeth slender, spiniform. . *desertorum*
Apex of antennal scape not attaining occipital margin; when gular teeth present, mesial pair usually triangular..... *hyatti*

Key to the Fallax Group (modified from Snelling and George 1979.)

Minor Workers
1. Dorsum of head and thorax (usually) largely smooth and shiny; punctulate, when present, obscure and limited in extent; mesonotum, in profile, often evenly curved or straight; scape exceeding occipital margin, if at all, by one-fifth its length or less. 2
Head and thorax closely and sharply punctulate with shiny areas along middle of head and promesonotum; mesonotum angulate in profile; scape surpassing occipital margin by about one-fourth its length. ..... *sciophila*

2. Propodeum conspicuously punctulate, with short, but distinct, spines or teeth; occipital margin usually distinctly concave; postpetiole, in profile more or less distinctly nodose. 3
Propodeum weakly punctulate or smooth and shiny, without spines or teeth, at most angulate at juncture of basal and posterior faces; occipital margin flat or weakly concave; postpetiole not nodose in profile. ..... . nr *barbata* (There are two taxa here. One is typical *P. barbata* while the other is determined by P. Ward in 2005 to be nr *barbata*. To my eye those specimens resemble a pale *P. rugulosa*.)

3. EL at least 1.5 x OMD, interocular distance no more than 3.0 x Eye Length, usually much less. 4
EL no more than 1.1 x OMD, interocular distance about 3.5 x Eye Length. ..... *rugulosa*

4. Promesonotal hairs slender, flexuous, longest about equal to EL, clearly greater than MOD. ..... *gilvescens*

Promesonotal hairs stout, stiff, longest about equal to MOD. 5

5. Occipital lobes and promesonotal dorsum smooth and shiny; tibial hairs few and decumbent to erect. 6
Occipital lobes and promesonotal dorsum dull due to microsculpture and punctulae; tibial hairs abundant and erect. ..... *cerebrosior*

6. Entire mesopleura **coarsely punctate**. ..... *rugulosa*
Mesopleura faintly, partially punctate. ..... *californica*

Major Workers

1. Mesial pair of gular teeth absent; tops of occipital lobes' sculpture rugulose or distinctly transversely striate. 2
Gular teeth various; tops of occipital lobes smooth and shiny, or variously sculptured, but not striate. 3

2. Tops of occipital lobes distinctly transversely striate; mesial pair of gular teeth absent. ..... . *rugulosa*
Tops of occipital lobes more or less coarsely rugulose. ..... *californica*

3. Gular teeth absent; longest genal hairs at least 0.35 mm; OMD equal to, or less than EL. ..... nr *barbata*
At least one pair of gular teeth; longest gular hairs no more than 0.25 mm, usually less than 0.20; OMD usually greater than EL. 4

4. Dorsum of head mostly smooth and shiny with scattered coarse, piligerous punctures; promesonotal dorsum similar or with coarse transverse rugulae with moderately punctulate interspaces; mesial pair of gular teeth absent. 5
Dorsum of head and promesonotum densely granulopunctate; mesial pair of gular teeth present, spiniform. ..... *sciophila*

5. Propodeal spines acute and well developed; standing hairs on frons sparse or absent. ..... *cerebrosior*
Propodeal spines little more than angular denticles; standing hairs on frons numerous. ..... *gilvescens*

GLOSSARY

EL = Eye Length ..... **MOD** = Minimum Ocular Diameter
OMD = Oculomandibular Distance

POGONOMYRMEX

The California desert species of ants in the genus *Pogonomyrmex* were described by Johnson & Overson (2009) and by Snelling & George (1979). Trager (1998) has keys to the entire genus. There are 18 species in California. I have modified their keys so that this key includes only the four species so far known to occur in the San Gabriel Mountains. The key is supported by the images of California ants found at AntWeb.org. and those in the original papers which are available online. These ants are armed with a **ferocious sting. Beware!**

1. Venter of petiole (where ventral process would be) with 1 or more distinct setae. ..... *rugosus*
Venter of petiole without setae. … 2

2. Propodeal spines present. 3
Propodeal spines absent. ..... *californicus*

3. Cephalic interrugal spaces with beaded sculpture. *montanus*
Cephalic interrugal spaces not beaded. ..... *subnitidus*

PSEUDOMYRMEX

Pseudomyrmex apache is the only member of the genus so far collected in the San Gabriel Mountains or the immediate environs. I have collected *P. pallidus* at Whitewater wash west of Palm Springs and so I made keys modified from Ward (1985) that work for the California material that I have at hand.

WORKERS

1. Eyes short (REL = 0.39-0.44). Scape length subequal to EL (SI = 0.9- 1.0). ..... . *apache*
Eyes longer (REL = 0.45-0.54). Scape length shorter than EL (SI = 0.68-0.86). . ..... *pallidus*

QUEENS

1. Larger (HW = 0.85-1.03), HL = 1.28-1.46). Eyes relatively short (REL2 = 0.52-0.58). ..... *apache*
Smaller (HW = 0.66-0.92, HL = 0.82-1.15). Eyes longer (REL2 = 0.59-0.71). .. .. *pallidus*

MALES

1. Head broader (CI > 0.80) and not densely punctate. Eyes shorter, EL about half head width (REL2 = 0.50-0.57) .. *apache*
Head elongate (CI < 0.80) and upper half densely punctate. Eyes relatively longer, EL about three-forths head width head width (REL2 = 0.71-0.83). ..... . *pallidus*

GLOSSARY

CI = HW/HL	**HW** = Head width	**SI2** = SL/EL
EL = Eye length	**REL** = EL/HL	**SL** = Scape length
HL = Head length	**REL2** = EL/HW	

SOLENOPSIS

There are eleven species of *Solenopsis* in California three of which have been collected in the San Gabriel Mountains. There are an additional three that may be found around the periphery of the range. I have made this key so that it includes the six species that occur in, or near, the San Gabriel Mountains. The key derived from Mackay (2002) and Pacheco and Mackay (2013).

S. amplychila and *S. aurea* are desert species that might be encountered on the lower north slopes. *S. invicta* is the imported and invasive fire ant. I have records of it from as nearby as Rancho Cucamonga, Fontana and Ontario so this species might be encountered along the suburban interface with undisturbed habitats.

Solenopsis CA-01 is known from a single location only - Hwy 39, in San Gabriel Canyon at an elevation of 2100 ft. It was collected by Roy Snelling in 1963. I collected at that location for 18 months without recording the species.

1. Eye containing fewer than 15 facets. ..... (Thief Ants) 2
Eye containing more than 20 facets. ..... (Fire Ants) 3

2. Eye contains only 1 or 2 facets poorly defined; head elongate, head length about 1.4X the head width. ...CA-01
Eye contains several well defined facets; head less elongate, head length about 1.3X the head width. ...*molesta*

3. Gaster color dark brown-black. 4

Gaster color yellow-red. 5

4. Clypeus with median tooth; mandibles with 4 teeth; petiolar process reduced to absent. ..... *invicta*
Clypeus without a median tooth; mandibles with 3 teeth, in some there is a fourth small, isolated proximal tooth; petiolar process distinct. ..... *xyloni*

5. Major workers. 6
Minor workers. 7

6. In majors, two clypeal teeth distinct. ..... *aurea*
In majors, clypeal teeth reduced. ..... *amblychila*

7. In minor workers pronotal standing hairs number 6-8. ..... *amblychila*
In minor workers pronotal standing hairs number about 10. ..... *aurea*

STENAMMA

The California species of ants in the genus *Stenamma* were revised by Snelling et al (1973). There are twenty species in California. I have modified his key so that it includes only the three species so far known to occur in the San Gabriel Mountains. S. *heathi* is also included although it has not been collected in the range. It has been collected both north and south of the range. The key is supported by the images of California ants found at AntWeb.org. and those in the original paper which is available online.

1. Median lobe of clypeus prolonged beyond clypheal margin, in frontal view apex truncate; eyes relatively large, OMD 1.0-1.8 x EL. ..... *smithi*
Median lobe of clypeus short, not exceeding clypeal margin, in frontal view apex appearing notched; eyes relatively small. 2

2. First tergite half or more densely and closely punctulate, with scattered coarse piligerous punctures and with fine striae over basal half, forming reticulae anteriorly; head and thorax evenly rugoso-reticulate. ..... *heathi*
First tergite usually smooth and shiny; if sculptured, sculpture limited to basal third or less, consisting of fine punctulae and/or fine divergent basal striae; head and thorax usually not regularly rugoso-reticulate. 3

3. First sternite conspicuously sculptured, at least at sides, usually much of segment densely punctulate or basal third with conspicuous striae, either coarse or fine; first tergite usually conspicuously sculptured. ..... *californicum*
First sternite wholly smooth and shiny, without punctulation or striae; first tergite largely smooth and shiny, but with usual short, separated divergent striae at base. ..... *diecki**

GLOSSARY

EL – Greatest diameter eye length.
OMD – Oculo-mandibular distance.

* *S. diecki* is part of a difficult species complex. *S. diecki* does not occur in Southern California mainland. The local, undescribed taxon is given the code name *Stenamma* mgb101, (in Litt., PS Ward, 2017).

TEMNOTHORAX

The California species of ants in the genus *Temnothorax* was recently revised by Snelling, et al (2014). There are twenty-two species in California. I have modified their key so that it includes only the eleven species so far known to occur in the San Gabriel Mountains. *T. pseudandrei* is also included with the hope that it will be discovered on the cottonwoods along the north side of the range. The key is supported by the images of California ants found at AntWeb.org. and those in the original paper.

1. Antenna 11-segmented. 2
Antenna 12-segmented. 4

2(1). Propodeal spines longer than 0.5 x distance between their bases, PSI 19-30; pronotal dorsumcoarsely areolate-rugose or at least irregularly rugose. 3
Propodeal spines dentiform, always much less than 0.5 x distance between their bases, PSI 6-10; pronotal dorsum dull and reticulate, without coarse areolae or rugae. ..... *whitfordi*

3(2). Petiole node profile subacute dorsally, with dorsal face rounding evenly into posterior face of node; petiole 0.97-1.04 times longer than high in profile when length is measured on a plane parallel to the venter of the petiole, from the anterior flange of the peduncle to the posterior margin of the petiole and the height is measured from the top of the node to the ventral margin of the petiole in a plane orthogonal to the length measurement; metafemur slender, 4.0-4.7 times longer than wide in dorsal view; ground-nesting, occasionally arboreal. ..... *rugatulus*
Petiole node broadly rectangular, with an oblique angle between the dorsal and posterior faces of node; petiole 1.04-1.18 times longer than high in profile; metafemur stout, 3.5-4.2 times longer than wide in dorsal view; exclusively arboreal nesting species ..... *caguatan*

4(1). First gastral tergum moderately to slightly shiny, most of disc distinctly finely sculptured. 10
First gastral tergum smooth and shiny, appearing polished, devoid of sculpture other than scattered minute piligerous punctures. 5

5(4). Petiole node triangular to subtriangular in profile. 6
Petiole node rounded to rectangular in profile. (The trait is subtle. Run both lugs of the couplet.) 7

6(5). Propodeal spines as long as, or longer than, distance between their bases, PSI 20-26; arboreal species nesting in galls and dead twigs. ..... *gallae*
Propodeal spines distinctly shorter than the distance between their bases, PSI 10-16; arboreal or ground nesting species. ..... *nitens*

7(5). Propodeal spines as long as, or slightly shorter than the distance between their bases, PSI 15-24; light to dark brown ground nesting species. ..... *nevadensis*
Propodeal spines distinctly shorter than the distance between their bases, PSI 4-17; either arboreal or ground nesting; color variable. 8

8(7). Postpetiole wide, PPW 1.47-1.98 x PTW. 9
Postpetiole narrow, PPW 1.23-1.43 x PTW. 11

9(8). Postpetiole narrow relative to petiole, PPW 1.47-1.76 x PTW; mesosomal dorsum reticulate and variously rugose in part, but not coarsely areolate with microreticulate interspaces. ..... *neomexicanus*

Postpetiole wide relative to petiole, PPW 1.79-1.98 x PTW; pronotal disc and dorsal face of propodeum coarsely areolate with microreticulate interspaces. ..... *wardi*

10(4). Mesosomal dorsum with metanotal groove impressed, pronotum distinctly higher than base of propodeum. .. *paiute*

Metanotal groove not impressed, mesosoma forms a smooth convex profile. ..... a*naphalantus*

11(8). Cephalic venter with scattered fine setae; frons, in profile, with short setae present along entire length, from base of clypeus to posterior margin. ..... *andrei*

Cephalic venter without setae; frons, in profile, with few or no setae, but with 2 on lower vertex and 4 across posterior margin. ..... *pseudandrei*
(Look for *T. pseudandrei* on cottonwoods on the north side of the range; arboreal.)

Glossary

CI - Cephalic Index: (HW/HL) x (100).
FI - Femoral Length Index: (HFL/HW) x (100).
HFL - Hind Femoral Length: Maximum length of hind femur in dorsal view, excluding trochanter.
OI - Ocular Index: (EL/HL) x (100).
PPW - Postpetiole Width: Maximum width of postpetiole in dorsal view.
PSI - Propodeal Spine Index: (PSL/HL) x (100).
PI - Petiole index: (PPW/PTW) x (100)
PSL - Propodeal Spine Length: the tip of the measured spine, its base, and the center of the propodeal concavity between the spines must all be in focus. Using a dual-axis micrometer, the spine length is measured from the tip of the spine to a virtual point at its base where the spine axis meets orthogonally with a line leading to the median point of the concavity.
PTW - Petiole Width: Maximum width of petiole in dorsal view.
SI - Scape Index: (SL/HL) x (100).

References

Creighton, WS. 1950. *The Ants of North America*. Bull. Mus. Comp. Zool. Vol 104: 585 pp. Des Lauriers, J and D Ikeda. Under review. So. Calif. Acad. Sci. Bull.

Fisher, BL and SP Cover. 2007. The Ants of North America: a Guide to the Genera. Univ. Calif. Press, Berkeley. 194 pp.

Francoeur, A 1973. Revision Taxonomique des Especes Neartiques du Group Fusca, Genre *Formica* (Hymenoptera: Formicidae. Mem. Soc. Entomol. Quebec. 3: 1-316.

Johnson, RA and RP Overson. 2009. A New North American Species of *Pogonomyrmex* (Hymenoptera: Formicidae) from the Mohave Desert of Eastern California and Western Nevada. J. Hym. Res. 18(2): 305-314.

Kallal, RJ and JS LaPolla. 2012. Monograph of *Nylanderia* of the World. Part II. *Nylanderia* in the Nearctic. ZooTaxa 3508: 1-64.

Mackay, W. 2002. The Ants of New Mexico. The Edwin Mellen Press, UK. 399 pp.

Millar, C. 2012. Geologic, Climatic, and Vegetation History of California. in: Baldwin, et. al. 2012. The Jepson Manual: Vascular Plants of California. 2nd ed. Univ. Calif. Press. Pp 49-67.

Pacheco, J. and W. Mackay. 2013. The Systematics and Biology of the New World Thief Ants of the Genus Solenopsis (Hymenoptera: Formicidae). The Mellen Press, UK. 500 pp.

Schoenherr, A. 1992. A Natural History of California. Univ. Calif. Press, Berkeley. California Natural History Guides: 56, Univ. Calif. Press, Berkeley 772 pp.

Snelling, RR. 1973. Studies on California Ants. 7. The Genus Stenamma (Hymenoptera: Formicidae). Contributions in Science (Los Angeles), 245: 1-38.

___. 1976. A Revision of the Honey Ants, Genus Myrmecocystus (Hymenoptera: Formicidae). Nat. Hist. Mus. Los Angeles Co. Sci. Bull., 24. 163 pp.

___. 1982. A Revision of the Honey Ants, Genus Myrmecocystus, First Supplement (Hymenoptera: Formicidae). Bull. So. Cal. Acad. Sci., 81(2): 69-86.

___, ML Borowiec, and MM Prebus. 2014. Studies on California Ants: a Review of the Genus Temnothorax (Hymenoptera, Formicidae). ZooKeys, 372: 27-89.

___, and CD George. 1979. The Taxonomy, Distribution and Ecology of California Desert Ants (Hymenoptera: Formicidae). Report to Calif. Desert Plan Program. Bureau of Land Management, USDA 335 + 89 pp.

___, GC and RR Snelling. 2007. New Synonymy, new Species, new keys to Neivamyrmex Army Ants of the United States, pp. 459-550. In Snelling, R. R., B. L. Fisher, and P. S. Ward (eds.). Advances in Ant Systematics (Hymenoptera: Formicidae): Homage to E. O. Wilson – 50 years of Contributions. Memoirs of the American Entomological Institute, 80.

Suarez, AV, DT Bolger and TJ Case. 1998. Effects of Fragmentation and Invasion on Native Ant Communities in Coastal Southern California. Ecology, 79 (6): 2041-2056.

Trager, SW. 1998. The World of the Harvester Ants. Texas A&M Univ. Press. 213 pp.

Ward, PS. 1985. The Nearctic Species of the Genus Pseudomyrmex (Hymenoptera: Formicidae). Quaestiones Entomologicae 21: 209-246.

___.2005. A Synoptic Review of the Ants of California (Hymenoptera: Formicidae). Zootaxa, 936: 1-68 (2005).

Wetterer, JK, PS Ward, AL Wetterer, JT Longino, JC Trager and SE Miller. 2000. Ants (Hymenoptera: Formicidae) of Santa Cruz Island, California. Bull. So. Cal. Acad. Sci., 99(1): 25-31.

Wheeler, GC and JN Wheeler. 1986. The Ants of Nevada. Nat. Hist. Mus. Los Angeles Co. 138 pp. Wilson, EO. 2003. Pheidole in the New World: A Dominant, Hyperdiverse Ant Genus. Harvard Univ. Press. 794 pp.

Anatomy of Ivanpah Spring, Clark Mountain, San Bernardino County, California

David K. Lynch and Paul M. Adams
Thule Scientific

ABSTRACT—Ivanpah Spring is located in Precambrian gneissic granite in the eastern foothills of Clark Mountain within the Mojave National Preserve. The country rock has been modified immediately upstream and downstream of the dike, the down stream portions being heavily altered by hydrolysis of country rock to a yellowish-brown dusty coating of quartz, caliche and clay. Spring hydrology appears to be associated with or controlled by a pegmatite dike of K-feldspar and quartz.

1. Introduction

Ivanpah Spring[1] is one of many seeps in the Clark Mountain area. The spring is 15 kilometers (km) SW of the intersection of I-15 and the California-Nevada border (Primm), and 8 km north of Mountain Pass, CA (Figure 1). It is about two km northeast of the Clark Mountain Fault System[2] and a km southwest of the Ivanpah Fault[3] in a former gold and silver mining area with many diggings and ruins[4]. The Ivanpah ghost town at Willow Spring is 0.7 km northwest of Ivanpah Spring. *Ivanpah* means "good water" in southern Piute[5].

The spring lies in a Precambrian metamorphic complex of foliated gneissic granite with occasional pink K-feldspar pegmatite dikes[3]. In this paper we describe the spring's geology and topographic setting, present a geologic section sketch and discuss a number of aspects of water movement in the spring's vicinity.

2. Methods

The site was visited several times during the winter of 2016-2017, both before and after heavy rains in the area. The elevation profile along the lowest part of the ravine (thalweg) was measured, the surface geology mapped and rock samples were taken from outcrops above and below the spring for laboratory analysis. Samples were cut and polished to expose the mineralogy. Field tools were a Garmin 60csx GPS receiver, laser range finder and surveying equipment. In the laboratory we used a tile saw and polishing tools, a scanning electron microscope (SEM) and an energy-dispersive X-ray spectrograph (EDS) for elemental composition and for general mineral identification.

3. The spring and its immediate surroundings

Figure 2 shows a surveyed geological sketch map that summarizes our main findings. We present it here to identify different rock units in the figures that follow.

The spring, a low flow rate (~1 liter/minute) seep, emerges from near the base of a rock wall (Figure 3) and flows down a linear ravine (heading of 56° E of N) for about 60 meters before sinking below ground into alluvial soil. Both upstream and downstream, the ravine wall contains competent outcrops. Float has been carried from the mountains above by the ephemeral stream that appears to be responsible for cutting the ravine. The rock

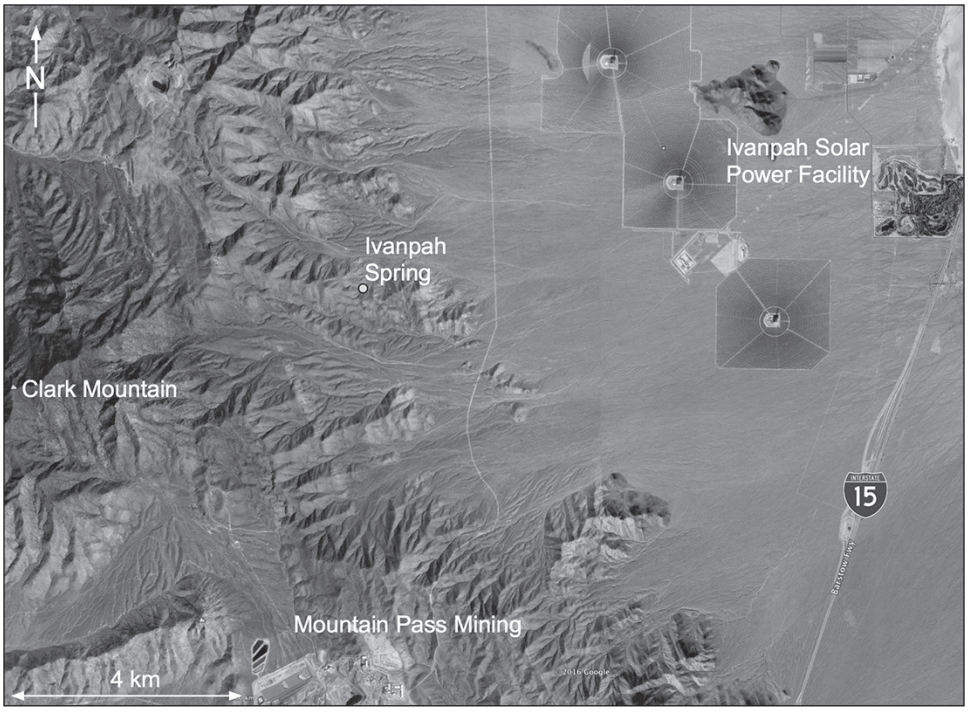

Figure 1. Location of Ivanpah Spring (adapted from Google Earth imagery). The NNW trending Clark Mountain Fault system is evident SW of Ivanpah Spring.

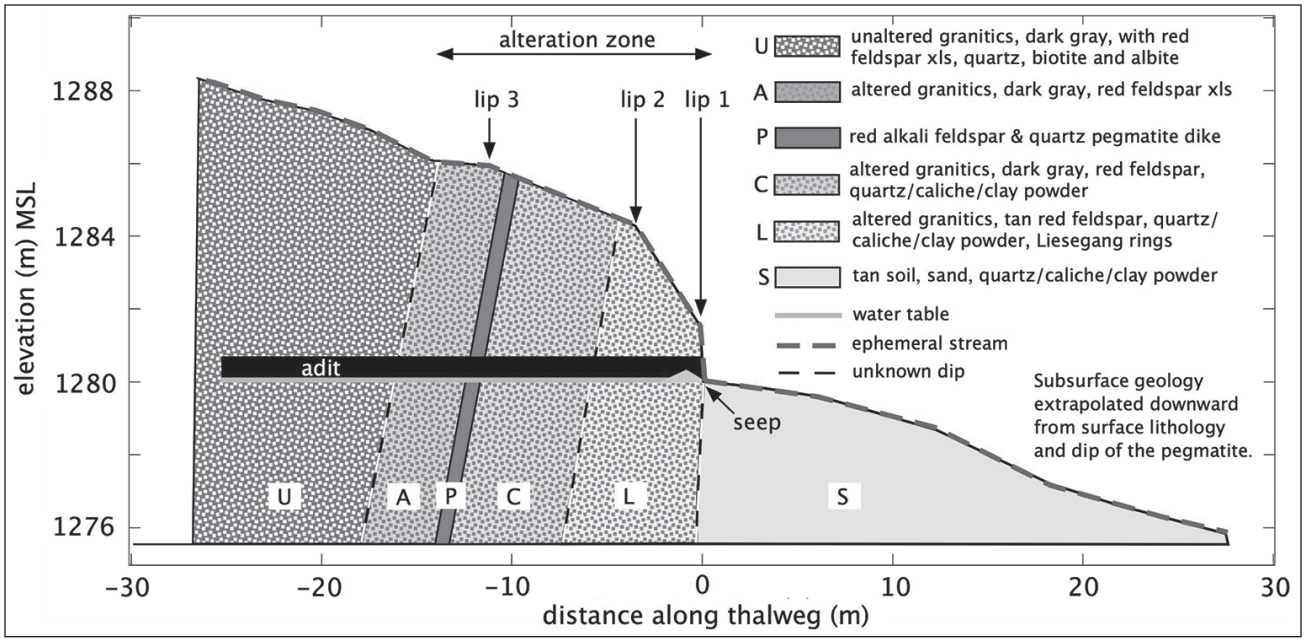

Figure 2. Surveyed elevation profile of the thalweg with rock units and water levels. Ivanpah Spring is indicated as the "seep". As judged by eye based on color, texture, gross mineralogy and the presence of yellow-orange powder, there were six different rock units (U, A, P, C, L and S). None of the subsurface dips are known, so the U-A, C-L and L-S contact dips are indicated with dashed lines. The A-P and P-C contact dips are also similarly uncertain because the shape of the subsurface pegmatite could not be determined.

in the spring's vicinity upstream and down stream and including the alteration zone is heavily jointed gneissic granite.

The spring has two branches, one emerging from soil adjacent to a well dug by miners (south arm) and the other (north arm) surfacing at the base of a vertical wall (~2 m high) of altered granite containing abundant Liesegang Rings[6,7] (Figure 4). The mouth of the spring lies within what appears to be a hydrologic alteration zone (Figure 2). It extends about 14 m along the ravine, which contains an obvious red pegmatite dike transecting the ravine (Figure 5). The surface exposure of the dike is about 11 m (horizontally) upstream of the seep.

The dike is hard and compact, and is composed of K-feldspar and quartz (leucogranite, also called alaskite). Its surface exposure is about half a meter wide. With a dip and strike of 79°S and N30W, the dike is nearly perpendicular to the direction of stream flow.

The colors of the exposed rocks along the thalweg are markedly different above and below the dike (Figure 6). Outcrops lining the ravine downstream of the dike and extending about eighty meters show significant coatings of yellow-orange powder composed of clay, quartz, caliche (effervesces in HCl) and possibly minor amounts of Fe_XO_Y. Rocks above the dike do not have this coating. Some of the downstream deposits were seen above the elevation level of the present day spring.

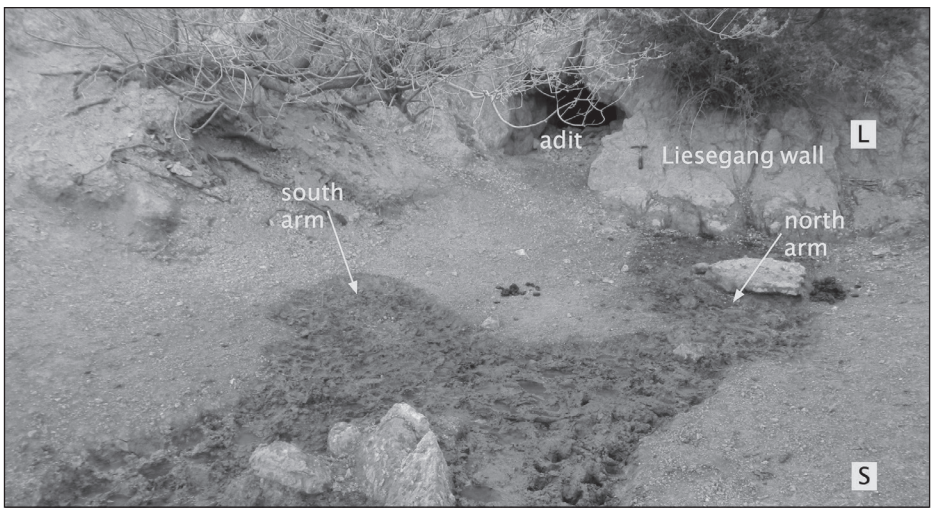

Figure 3. Mouth of Ivanpah Spring. Two seep arms merge to form the spring. One emerges from the base of the Liesegang wall, the other surfaces through tan-yellow soil that is sometimes covered in cow dung, as seen here as dark mud. The surface topography just below the adit changes as the ephemeral spring cascades down over its mouth and deposits sediment, sometimes making the two arms appear to merge. Note rock hammer on Liesegang wall for scale. Labeled rock units are from Figure 2.

The adit is 26 m long and extends horizontally into the rock with a bearing from the entrance of about 230°. Although there is water on the adit floor, water does not flow out because a small mound of local rock rubble has been piled against the entrance. An open well sits atop the southern shoulder of the ravine approximately 13 m east of the

Figure 4. Small area of the Liesegang wall showing concentric ring structure. The parent rock is gneissic granite and it has been chemically altered by hydrolysis. Labeled rock unit is from Figure 2

seep. The well water's surface elevation is the same as the water in the adit and the seep to within the measurement uncertainty (±10 cm). Well water depth is unknown. At no location above the seep was any water seen coming out of the rock, nor was there any standing water or wet soil upstream of the dike except immediately following a rain.

Thalweg soils differed markedly above and below the dike. The upstream soil is sandy, well drained and the grains do not adhere to each other. It is composed of quartz and feldspar, small amounts of biotite and a number of components that probably originated upstream, perhaps from a significant distance. The downstream soil is soft, crumbly and somewhat cohesive, though easily reduced to powder between the fingers. It is composed of the same material that coats the downstream granite: powdery quartz, caliche and clay. The downstream sample was taken as close as possible to the thalweg, but owing the presence of manure, it was necessary to scrape it from the surface about a meter to one side of the spring flow. The overall impression is that the differences in soils are the result of hydrolysis by the spring. The downstream soil is most likely a groundwater discharge deposit, the evaporation of water from the seep leading to deposition of metal cations, carbonates, etc.

4. Discussion

As exposed on the surface, the pegmatite dike is the hardest and least fractured unit, and together with an altered unit A it forms a lip (Lip 3, Figure 2) with a sharp drop in the thalweg. With an obvious dike immediately upstream of the Liesegang wall and seep, the spring would seem to be a *joint or fracture* spring[8]. Furthermore, the sharp topographic change of the thalweg in the alteration zone seem unlikely to be coincidental to the spring's emergence. In view of the dike's apparent water impermeability, its location suggests that it is acting as an aquatard to ground water. Yet water is getting though the dike to form the seep, so there are probably cracks in the dike below the surface through which water can pass to the mouth of the spring. It also seems likely that groundwater encountered the dike and was forced upward to discharge on the surface. Such a mechanism could explain the yellowish deposits downstream of the dike.

The spring was undoubtedly present before any mining activity in the area. Topography and Liesegang rings tell us that. The reason why the adit was dug is not known but it could have been to increase the flow rate of the spring and to supply miners with water. The adit and drainage mechanism is similar to excavations known as qanats that have been used for thousands of years in desert regions to passively extract water from sloping terrain[9]. Regardless of the reason, the adit may have locally modified the geometry of underground water movement and the seep itself.

The yellow powder (quartz, caliche and clay) is seen on downstream outcrops that are above the elevation of the current

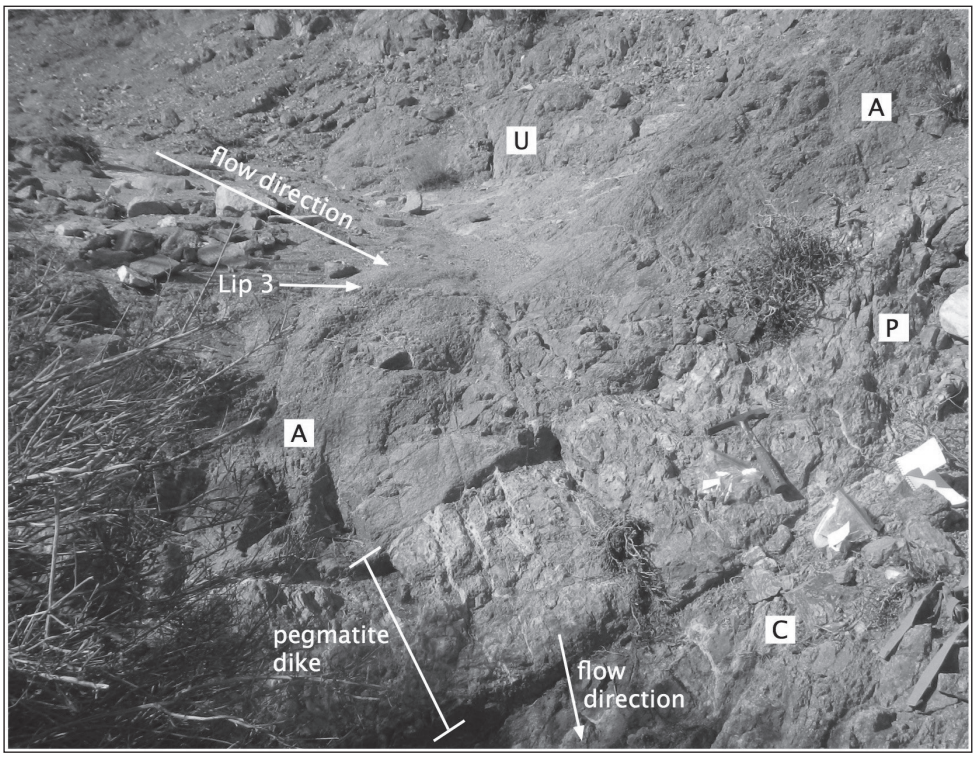

Figure 5. View of altered region. Note rock hammer (right) for scale. The red K-feldspar pegmatite dike P has been intruded into the gneissic granite country rock U, A and C. Rocks A and C appear to be altered by hydrolysis and C seems to have been more heavily or differently altered. Labeled rock units are from Figure 2.

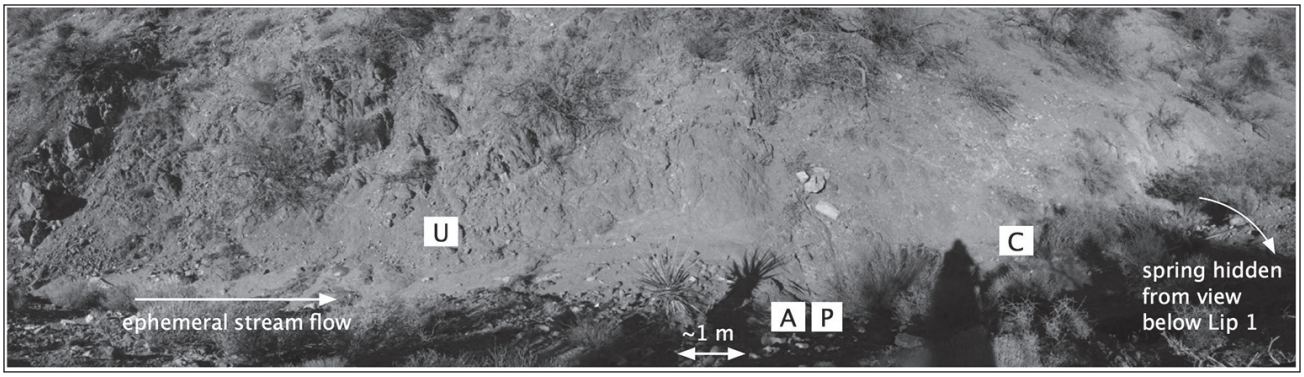

.Figure 6. Panoramic view of the ravine and alteration zone. Labeled rock units are from Figure 2. The pegmatite P is slightly right of center and is exposed for several meters on either side of the ravine. To the left (upstream), the unaltered country rock U is more or less uniformly brown at this scale, but to the right of the pegmatite (downstream) the surface rock is heavily coated with yellow-orange powder C. Both components persist for about eighty meters downstream before gradually disappearing as the original unaltered country rock becomes evident, the same as the unaltered rock about five meters upstream of the dike. Photograph taken upstream of the spring, here hidden from view below Lip 1 (Figure 2). The enhanced vegetation at far right marks the spring's emergence.

seep. This may suggest that the water table and/or seep were once at a higher elevation. This could be explained by down cutting by the ephemeral stream that lowered the ravine's elevation, leaving exposed the outcrops with yellow powder on either side that we see today. Alternatively, the current location of the nick point at the Liesegang wall could be the result of headward erosion by the ephemeral stream that is slowly moving upstream, especially if the stream flow rate was much higher during the last glacial period.

Although the dip of the pegmatite at the surface has been measured (~79° S), its subsurface geometry is not known. Therefore the dips of the U-A, C-L and L-S contact are uncertain. It may be possible to retrieve the dips by measuring where the contacts intersect the adit. Being 26 meters long, the adit would appear to extend through the entire alteration zone.

Acknowledgements

The authors would like to thank owner Gerald L. Sauer for permission to visit and investigate the spring, and Joe Peralta for field support. We are also grateful to Krishangi Groover for a thorough review of the paper and Bob Reynolds for many useful comments.

References

1. 35.540310°, -115.529617°, 1280m MSL

2. Jessey, David R., Don W. Tarman, Miho Waki, and Suzanne M. Baltzer, A Field Investigation of the Clark Mountain Fault Complex, San Bernardino County, California, in The Changing Face of the Eastern Mojave Desert, proceedings of the 2001 Desert Symposium, R. Reynolds (ed.), California State University Fullerton (2001)

3. Hewett, D.E., 1956, Geology and mineral resources of the Ivanpah Quadrangle, California and Nevada: U.S. Geological Survey Professional Paper 275, 172 p.

4. Digonnet, Michel, Hiking the Mojave Desert: Natural and Cultural Heritage of Mojave National Preserve, Wilderness Press, 462 pp. (2013)

5. Gudde, Erwin Gustav, 1000 California Place Names: Their Origin and Meaning, University of California Press (1969)

6. Liesegang, R. E.,"Ueber einige Eigenschaften von Gallerten", Naturwissenschaftliche Wochenschrift, Vol. 11, Nr. 30, 353-362 (1896)

7. Decelles, P.G. and Gutschick, R.C., Mississippian wood-grained chert and its significance in the western interior United States. Journal of Sedimentary Petrology, **53**: 1175-1191 (1983)

8. Davis, Stanley N. and Roger J. M. Dewiest, Hydrogeology, New York, John Wiley & Sons, 463 pp. (1966)

9. Schreiber, Katharina and Josué Lancho Rojas, Irrigation and society in the Peruvian desert : the puquios of Nasca, Lexington Books, 172 pp. (2003)

Water-resources and land-surface deformation evaluation studies at Fort Irwin National Training Center, Mojave Desert, California

Jill N. Densmore[1], Justine E. Dishart[2], David M. Miller[3], David C. Buesch[3], Lyndsay B. Ball[4], Paul A. Bedrosian[4], Linda R. Woolfenden[1], Geoffrey Cromwell[5], Matthew Burgess[5], Joseph M. Nawikas[6], David R. O'Leary[5], Adam R. Kjos[5], Michelle Sneed[1], and Justin Brandt[1]

[1]*California Water Science Center, U.S. Geological Survey, 6000 J Street Placer Hall, Sacramento, CA 95819*

[2]*Directorate of Public Works, Environmental Division, U.S. Army, ATTN: IMNT-PWE, PO Box 105085, Bldg 602, Fifth Street, Fort Irwin, CA 92310*

[3]*Geology, Minerals, Energy, & Geophysics Science Center, U. S. Geological Survey, 345 Middlefield Road, Menlo Park, CA 94025*

[4]*Crustal Geophysics and Geochemistry Science Center, U.S. Geological Survey, Denver Federal Center, Bldg 20, MS 964,Denver, CO 80225*

[5]*California Water Science Center, U.S. Geological Survey, 4165 Spruance Road, Suite 200, San Diego, CA 92101*

[6]*California Water Science Center, U.S. Geological Survey, 10775 Pioneer Trail, Suite 102, Truckee, CA 96161*

ABSTRACT—This report is intended to provide an overview of recent water-resources and land-surface deformation studies at the NTC.

Introduction

The U.S. Army Fort Irwin National Training Center (NTC), in the Mojave Desert, obtains all of its potable water supply from three groundwater basins (Irwin, Langford, and Bicycle) within the NTC boundaries (fig. 1; California Department of Water Resources, 2003). Because of increasing water demands at the NTC, the U.S. Geological Survey (USGS), in cooperation with the U.S. Army, completed several studies to evaluate water resources in the developed and undeveloped groundwater basins underlying the NTC. In all of the developed basins, groundwater withdrawals exceed natural recharge, resulting in water-level declines. However, artificial recharge of treated wastewater has had some success in offsetting water-level declines in Irwin Basin. Additionally, localized water-quality changes have occurred in some parts of Irwin Basin as a result of human activities (i.e., wastewater disposal practices, landscape irrigation, and/or leaking pipes). As part of the multi-faceted NTC-wide studies, traditional data-collection methods were used and include lithological and geophysical logging at newly drilled boreholes, hydrologic data collection (i.e. water-level, water-quality, aquifer tests, wellbore flow). Because these data cover a small portion of the 1,177 square-mile (mi^2) NTC, regional mapping, including geologic, gravity, aeromagnetic, and InSAR, also were done. In addition, ground and airborne electromagnetic surveys were completed and analyzed to provide more detailed subsurface information on a regional, base-wide scale. The traditional and regional ground and airborne data are being analyzed and will be used to help develop preliminary hydrogeologic framework and groundwater-flow models in all basins. This report is intended to provide an overview of recent water-resources and land-surface deformation studies at the NTC.

Physiographic and geologic setting

The NTC is in the Mojave Desert region of southern California, about 35 miles (mi) north-northeast of Barstow (fig. 1). The NTC lies in a heavily faulted and geologically complex area within the Eastern California Shear Zone and is bounded by the Garlock Fault to the north (fig. 2). Typical of many parts of the Mojave Desert, the geology and landscape of the Fort Irwin area consists of rugged mountains separated by broad valleys.

A wide variety of rock types and faults lie within the NTC boundary (Miller and others, 2014). Pre-Tertiary (Mesozoic and older) plutonic rocks, including minor amounts of metamorphic and sedimentary rocks, form many of the mountains with local accumulations of Tertiary (Miocene to Pliocene) volcanic and sedimentary rocks (fig. 2). Between these mountains lie broad valleys that contain basin-fill deposits, i.e., Quaternary and Tertiary deposits (Miller and others, 2014). The western part of the NTC lies along the eastern and southern edges of the Tertiary (Miocene) Eagle Crags Volcanic Complex that included thick accumulations of lava flows, pyroclastic rocks (fallout tephra deposits and ignimbrite), and volcaniclastic and tuffaceous sandstone and conglomerate (Sabin, 1994). Toward the eastern part of the NTC, the basin-fill deposits become progressively finer grained. Basin-fill deposits in the eastern part of the NTC consist of fine- to coarse-grained alluvium and partly consolidated deposits including thick sections of clays and lacustrine deposits observed in borehole lithological and geophysical logs (Miller and others, 2014; Kjos and others, 2014).

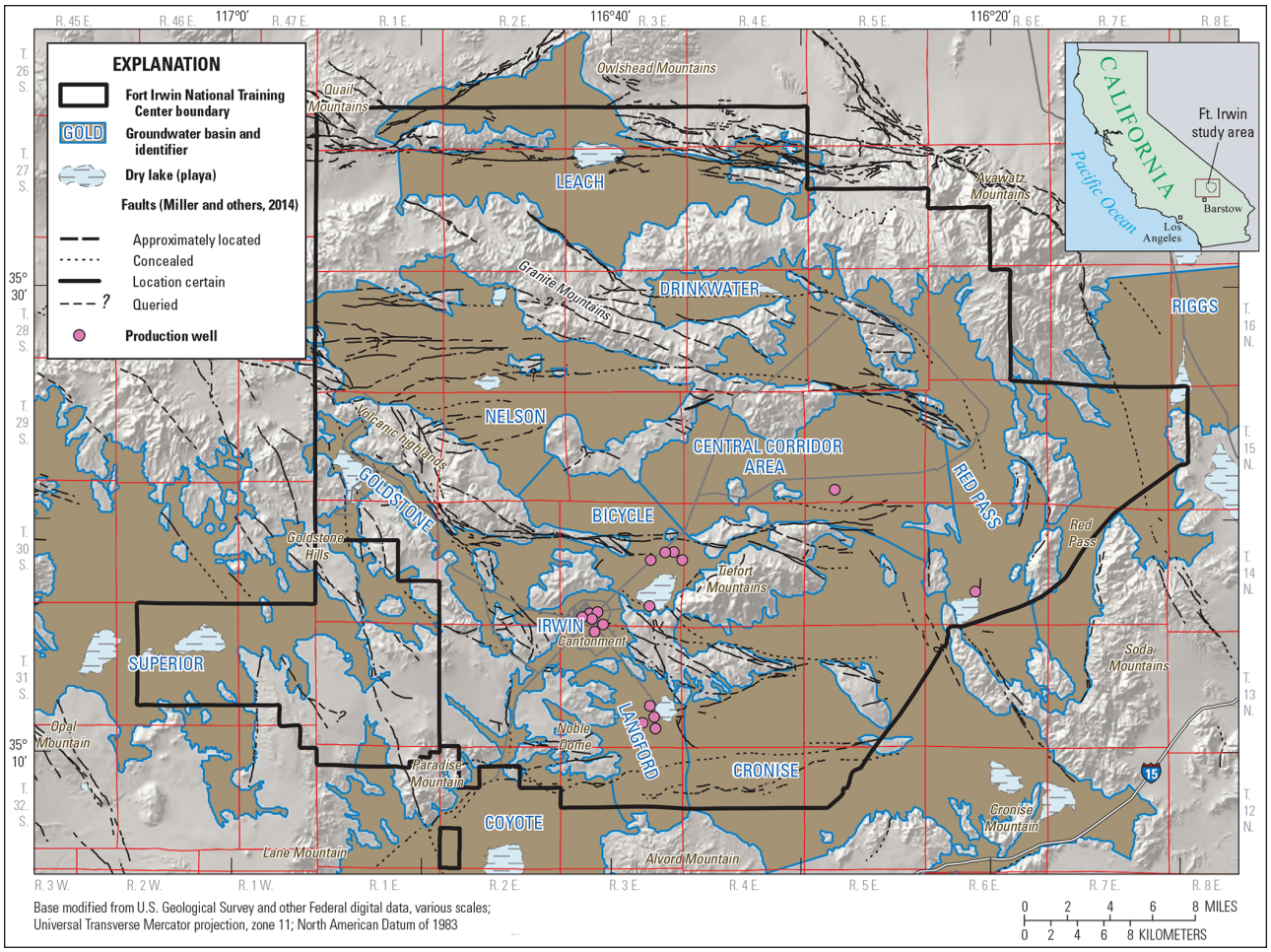

Figure 1. Map showing groundwater basins and production wells, Fort Irwin National Training Center, California (From Kjos and others, 2014; basins modified from California Department of Water Resources, 2003).

Numerous faults cross the NTC (fig. 2). Quaternary faults in the NTC area belong to the Eastern California Shear Zone and include sinistral, east-west striking faults that characterize the central part of the NTC, and the contrasting dextral northwest-southeast striking faults that border the east and west margins. Oblique and thrust faults also are present at the base of some of the local mountains. About half of the faults are active and exhibit Holocene rupture. For more details on the geology, see Miller and others (2014).

Hydrologic setting

The hydrogeology of the NTC is typical of many basins in the Mojave Desert. Basins are underlain by the pre-Tertiary basement complex of plutonic and metamorphic rocks. Volcanic rocks, predominantly in western basins, have highly variable permeability; some volcanic rocks are welded whereas others are highly fractured and may yield water, where fractured. The basin fill consists of semi-consolidated to unconsolidated Tertiary and Quaternary deposits derived from the surrounding mountains. The Quaternary deposits are generally more permeable than the Tertiary deposits and typically have higher water yield where saturated. The numerous faults crossing the NTC control the lateral extent and movement of groundwater.

Limited natural recharge occurs from precipitation runoff and infiltration along ephemeral washes and near the bases of the surrounding mountains, primarily during winter rains or short summer thunderstorms (Densmore and Londquist, 1997). Local precipitation data are limited. Historical records from the Goldstone ECHO 2, California, weather station (043498) in Goldstone Basin from December 01, 1973, to July 31, 2006, indicate an average annual precipitation of 5.80 in. (Western Region Climate Center, 2009); although this average can vary greatly from year to year. Surface runoff from storms occurs primarily in the higher topographic area of the volcanic highlands including the Nelson and Goldstone Basins in the west and in the local internal mountain ranges in the central and northern parts of the base, such as the Tiefort, the Granite, and the Avawatz Mountains (fig. 1). Runoff from the storms then infiltrates at the base of the mountain fronts and along the washes. Groundwater flows from these recharge areas toward the low areas in flow-through basins and playas within terminal basins. The depth to groundwater and direction of groundwater flow are also affected by the

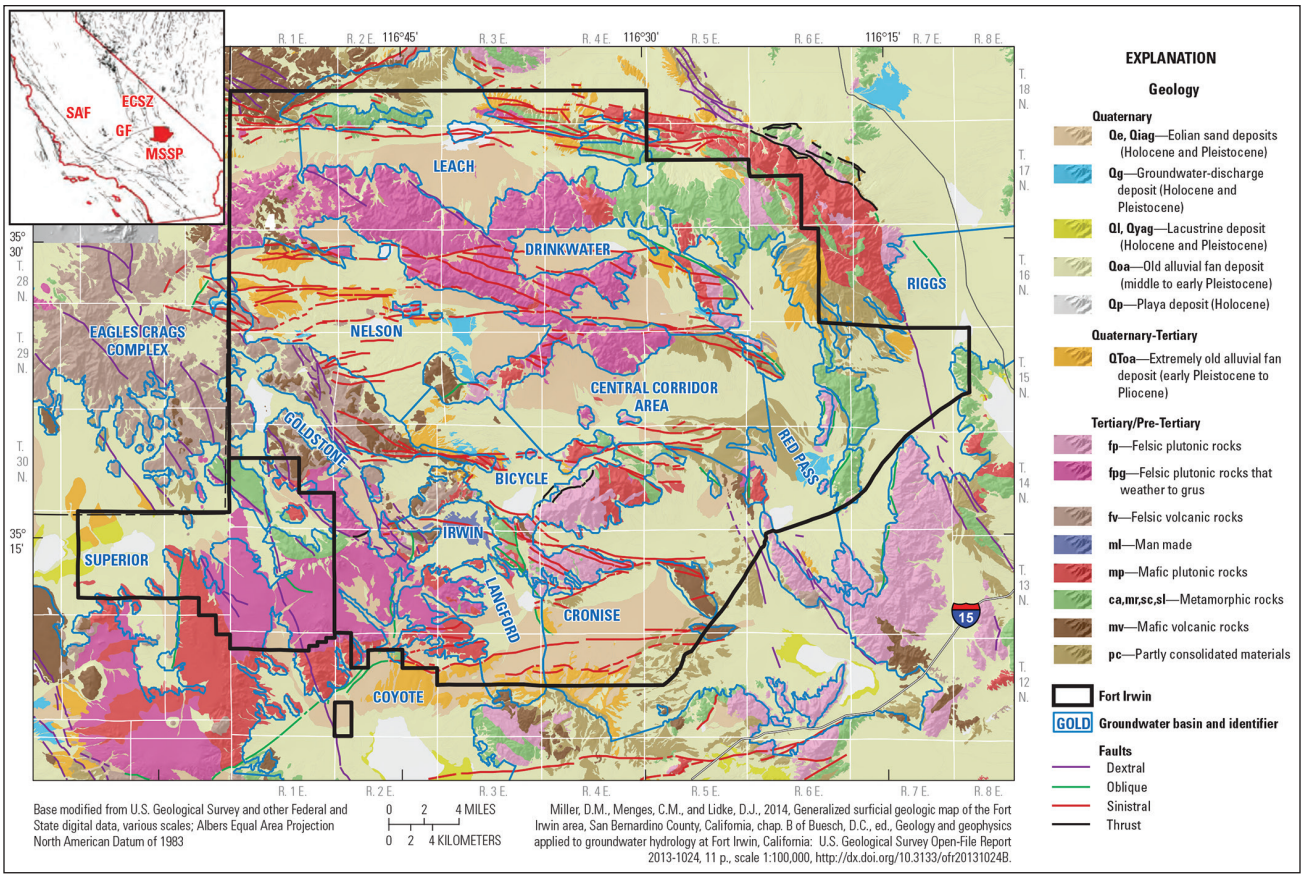

Figure 2. Map showing generalized surficial geology and faults at Fort Irwin National Training Center, California (ECSZ, Eastern California Shear Zone; GF, Garlock Fault; MSSP, Mojave Strike-Slip Province; SAF, San Andreas Fault).

distribution of faults, locations and amount of recharge and discharge, and aquifer hydraulic properties. In some basins, groundwater discharges by subsurface flow through saddles and along faulted or fractured zones in the bedrock.

Groundwater basins at Fort Irwin

The groundwater basins, as defined by the California Department of Water Resources (2003), which underlie the NTC are: the Langford Valley, Bicycle Valley, Coyote Lake Valley, Goldstone Valley, Superior Valley, Red Pass Valley, Avawatz Valley (locally called Drinkwater), Leach Valley, Cronise Valley, and Riggs Valley Basins. For simplicity in this study, these basins are referred to as Langford, Bicycle, Coyote, Goldstone, Superior, Red Pass, Drinkwater, Leach, Cronise, and Riggs Basins (figs. 1 and 2). Additionally, Langford Basin is subdivided into two subbasins by California Department of Water Resources (2003), and referred to as Irwin and Langford Basins. On the basis of groundwater divides, Bicycle Basin is subdivided into Bicycle and Nelson subbasins, referred to as Bicycle and Nelson Basins in this report; likewise, Red Pass Basin is subdivided into Central Corridor area and Red Pass subbasins, referred to as Central Corridor area and Red Pass Basin in this report. The basins have been grouped into developed and undeveloped basins for the following discussion.

Developed Basins

Three basins (Irwin, Langford, and Bicycle Basins) have been developed for groundwater production and have considerable historic hydrologic data including lithological, geophysical, water-level, and water-quality data. Although Coyote Basin has also been developed with pumping wells, Coyote Basin is not included in this discussion because it lies mostly outside of the NTC boundary. The NTC infrastructure (i.e., housing, offices, food and shopping) is in Irwin Basin; the airfield is in Bicycle Basin. Subsurface flow and infrequent surface drainage out of Irwin Basin is to the southeast through an unnamed wash into Langford Basin. From 1941 to 1995, most of the groundwater pumpage at the NTC was from Irwin Basin. Groundwater pumping began in Bicycle and Langford Basin in 1967 and 1992, respectively. Groundwater pumped from the Bicycle and Langford Basins is transported through pipelines to Irwin Basin, where it is blended with water pumped from Irwin Basin. Since the mid-1990s, pumpage from Irwin Basin has decreased and has been replaced by pumpage from Langford and Bicycle Basins. Groundwater-flow models were constructed for these developed basins to aid NTC personnel in managing their limited water supply (Densmore and Londquist, 1997; Densmore, 2003; Voronin and others, 2013; Voronin and others, 2014;

Densmore and others, 2010; and Densmore and others, written commun., 2017a).

Groundwater levels. Prior to groundwater development, the groundwater-surface altitudes[1] beneath Irwin, Langford, and Bicycle Basins were about 2,305, 2,114, and 2,225 feet (ft), respectively. Groundwater pumping, since as early as 1941, has resulted in water-level declines in Irwin, Langford, and Bicycle Basins. Water levels near the center part of Irwin Basin declined more than 30 ft during 1953-67, then recovered about 16 ft during 1967-82, and again declined about 15 ft during 1982-92 (Densmore, 2003). Since 1992, the disposal of treated wastewater and reduction of pumpage in Irwin Basin have resulted in water-level recovery of about 40 ft. Water-level declines ranged from as much as 40 ft over 19 years (from 1992-2011) in Langford Basin to as much as 100 ft over 43 years (from 1967-2010) in Bicycle Basin (Voronin and others, 2014; Densmore and others, written commun., 2017a).

Water Quality, Source, and Age. Water-quality changes have occurred in some parts of the basins as a result of pumping in these basins. In Irwin Basin, elevated nitrate and dissolved solids concentrations are present in some wells as a result of wastewater-disposal practices (Densmore and Londquist, 1997). Naturally occuring poor-quality water also occurs in the southern part of Langford Basin and along the northwest side of Bicycle Lake playa in Bicycle Basin (Voronin and others, 2014; Densmore and others, written commun., 2017a). Stable isotopes of groundwater samples from these basins are isotopically lighter than local precipitation, indicating that present-day meteoric waters are not the source of recharge in these basins (Densmore and Londquist, 1997; Voronin and others, 2014; Densmore and others, written commun., 2017a). Age dating of water samples from these basins indicates that most of the groundwater recharged prior to 1952 and is more than 14,000, 12,000, and 15,000 years old in Irwin, Langford, and Bicycle Basins, respectively (Densmore and Londquist, 1997; Voronin and others, 2014; Densmore and others, written commun., 2017a). However, water from some wells in areas affected by wastewater-treatment disposal and irrigation-return flows in Irwin Basin contained measureable tritium indicating that groundwater recharge occurred after 1952 (Densmore and Londquist, 1997).

Undeveloped Basins

The undeveloped basins include Nelson, Goldstone, Superior, the Central Corridor area, Red Pass, Cronise, Drinkwater, Leach, and Riggs Basins. The undeveloped basins have little to no lithologic or historical hydrologic data. Beginning in 2010, geophysical and hydrogeologic data were collected to characterize the size and shape of these basins, the geohydrologic properties of the basin-fill materials, and water quality of the groundwater. The goal was to assess groundwater availability in the undeveloped basins.

Basin Characterization. Recent (2010-16) investigations of the undeveloped basins involved the collection of geophysical data to characterize the size and shape of the basins, drilling to characterize the geohydrology, construction of monitoring wells to provide a means to collect groundwater-quality samples, and to conduct hydrologic testing of aquifer properties. For more details, see Buesch (2014); Miller and others (2014); Bloss and Bedrosian (2015); Bedrosian and others (2014); Burgess and Bedrosian (2014); Jachens and Langenheim (2014); Langenheim and Jachens (2014); Kjos and others (2014); Nawikas and others (written commun., 2017); Densmore and others (2016); Miller and others, 2016; Bedrosian and others, 2016; Buesch and O'Leary, 2016; O'Leary and others (2016); Ball and others (2016). These data provide input for preliminary hydrostratigraphic and groundwater-flow models to evaluate groundwater availability in the undeveloped basins (Cromwell and others, 2016; Woolfenden and others, 2016).

Geophysical Surveys. Geophysical surveys were completed to estimate the size and shape of groundwater basins, characterize the subsurface stratigraphy, provide estimates of depth to water, and identify areas of saline or poor-quality water. Because one survey method does not supply all the necessary information, multiple geophysical survey techniques were used to enhance and support the interpretation of results from other methods. The geophysical techniques included gravity, aeromagnetic, ground transient-electromagnetic (TEM), and airborne electromagnetic (AEM) surveys.

Gravity surveys were completed over parts of the NTC during 2010-11. Data were collected in Nelson and Goldstone Basins, in the southern part of Superior Basin, Central Corridor area, Red Pass, Drinkwater, Leach, Cronise, and Riggs Basins. The gravity data were modeled together with available regional gravity data to produce a depth to bedrock map of the entire NTC (Jachens and Langenheim, 2014). Additional gravity data were collected during 2015-16 to refine an area in Goldstone Basin.

Aeromagnetic surveys were effective in defining faults because of the presence of magnetic and non-magnetic Pre-Tertiary (Mesozoic) plutons underlying the study area. Pre-existing aeromagnetic data were available for most of the NTC, with the exception of the northern basins. New aeromagnetic data were collected in Leach Basin during 2010-11 and in Nelson, Goldstone, Superior, and Red Pass Basins and Central Corridor area during 2015. The major faults that cross through and offset pluton boundaries, as well as buried volcanic flows, are readily mapped using existing and new aeromagnetic surveys. These data, in conjunction with the gravity and AEM data, were used to help define the structure and geometry of the groundwater basins (Langenheim and Jachens, 2014).

1 In this report, altitudes are referenced to the North American Vertical Datum (NAVD 88)

Ground TEM surveys were completed to map the contact between relatively high-yield alluvial deposits and low-yield Tertiary sediments, as well as changes in water salinity with depth. The TEM geophysical method measures the electrical resistivity of the subsurface at depths from 10s to 100s of meters at a given location, typically referred to as a sounding. Initially, TEM soundings were completed near existing wells with downhole geophysical logs to determine if measurable electrical resistivity contrasts occurred at the water table and at known stratigraphic contacts. Because a TEM sounding is non-invasive and can be conducted in a few hours, this technique is much less expensive than drilling wells, and TEM soundings could then be used to guide the location of future wells. Data collected at wells were used to ground-truth the TEM and the airborne geophysical data (Burgess and Bedrosian, 2014). During 2010-11, 79 soundings were conducted in all basins in areas determined by the gravity and aeromagnetic surveys to have the highest probability for water production.

Airborne electromagnetic (AEM) surveys, ground truthed with TEM surveys, were used to map contacts of different stratigraphic units, thicknesses of aquifers, and changes in water salinity with depth over large areas. AEM surveys were also useful for providing geologic data and estimates of water quality in areas where ground-based geophysical techniques are difficult or restricted, such as Leach Basin, that has been a bombing range for more than 50 years. AEM data were collected in Leach Basin during 2010-11, and in Nelson, Goldstone, Superior, Central Corridor area, and Red Pass Basins during 2015, to evaluate aquifers in these basins as potential water supplies. These data were used in conjunction with the gravity and aeromagnetic data to help define the structure of the groundwater basins and provide subsurface resistivity maps. These data also aid in refining hydrostratigraphic frameworks and, ultimately, model layers in the groundwater-flow models (Bedrosian and others, 2014; Ball and others, 2016). Preliminary results of the AEM surveys highlight the strong geophysical contrasts across faults and between crystalline basement, volcanic flows and domes, and basin-fill deposits that are likely to substantially influence groundwater flow in this geologically-complex and tectonically active region.

Exploration Drilling. Exploration drilling and collection of hydrologic, lithologic, and stratigraphic data from boreholes provides data needed to better assess the water resources of the basin (Kjos and others, 2014). Seventeen multiple-well monitoring sites and 7 test wells were constructed between 2009-12 (Kjos and others, 2014) in all undeveloped basins, except Drinkwater and Leach Basins, where previously described data indicated the highest potential for water-resource development. The multiple-well monitoring sites contain one to three 2-inch polyvinyl chloride (PVC) piezometers that allow for water-level measurements and depth-dependent water-quality sampling. The test wells were constructed of 6- to 8-inch PVC and perforated within coarse-grained water-bearing deposits.

Hydrologic Testing. Hydrologic testing was conducted to provide data to assess the hydraulic properties of the NTC aquifer system. Aquifer and slug tests were conducted using the test wells and monitoring wells, respectively, upon completion of drilling to provide information on aquifer properties at each well (Nawikas and others, written commun., 2017). These tests were analyzed to estimate aquifer transmissivity and well yields, and showed that these undeveloped groundwater basins are highly variable both within and between basins. Additionally, wellbore flow (or velocity) logs were collected in selected test wells under pumped and unpumped conditions to determine contributions of flow from aquifer zones penetrated by the wells. Water-quality samples were also collected at discrete depths to determine differences in water quality with depth to supplement the wellbore flow analysis. Wellbore flow was simulated for each well by using an integrated flow-analysis tool, AnalyzeHOLE, to evaluate aquifer properties and heterogeneity (Halford and Kuniansky, 2002). Simulated hydraulic conductivity values derived from the calibrated simulations ranged from <0.01 to 60 ft/day (O'Leary and others, 2016). Flow profiles collected from the selected test wells under pumped conditions showed increasing groundwater flowing from shallower to deeper screens within the wells, and indicate higher yields from deeper aquifers in the wells tested. Overall, wellbore flow simulation results show good correlation with the interpretations of geologic, hydrogeologic, geophysical, and airborne electromagnetic survey data (O'Leary and others, 2016).

Groundwater levels and surface-water altitudes. Water levels were measured sporadically between 2011 and 2016 from the newly drilled sites. Water levels measured in 2012 ranged from as shallow as 55 ft below land surface in Cronise Basin to as deep as 525 ft below land surface in Central Corridor area (Kjos and others, 2014). Although the data set is limited, water levels in the undeveloped basins have not varied much year to year, as expected, because there is 1) limited natural recharge, similar to the developed basins, and 2) little to no pumping, unlike the developed basins. For comparison of water levels amoung basins, water-level measurements were converted to water-surface altitude using a common datum (fig. 3). Higher water-surface altitudes are located primarily in the higher topographic areas of the volcanic highland in the north and western basins at the NTC; lower water-surface altitudes are located primarily in the central, southern, and eastern basins. Large differences in water-surface altitude between adjacent basins or over short distances suggests that there is limited hydraulic connection between or within some of the basins. The water-level data provide historical benchmarks and current observations for trend analysis and also aid as a constraint during development of groundwater-flow models that will be

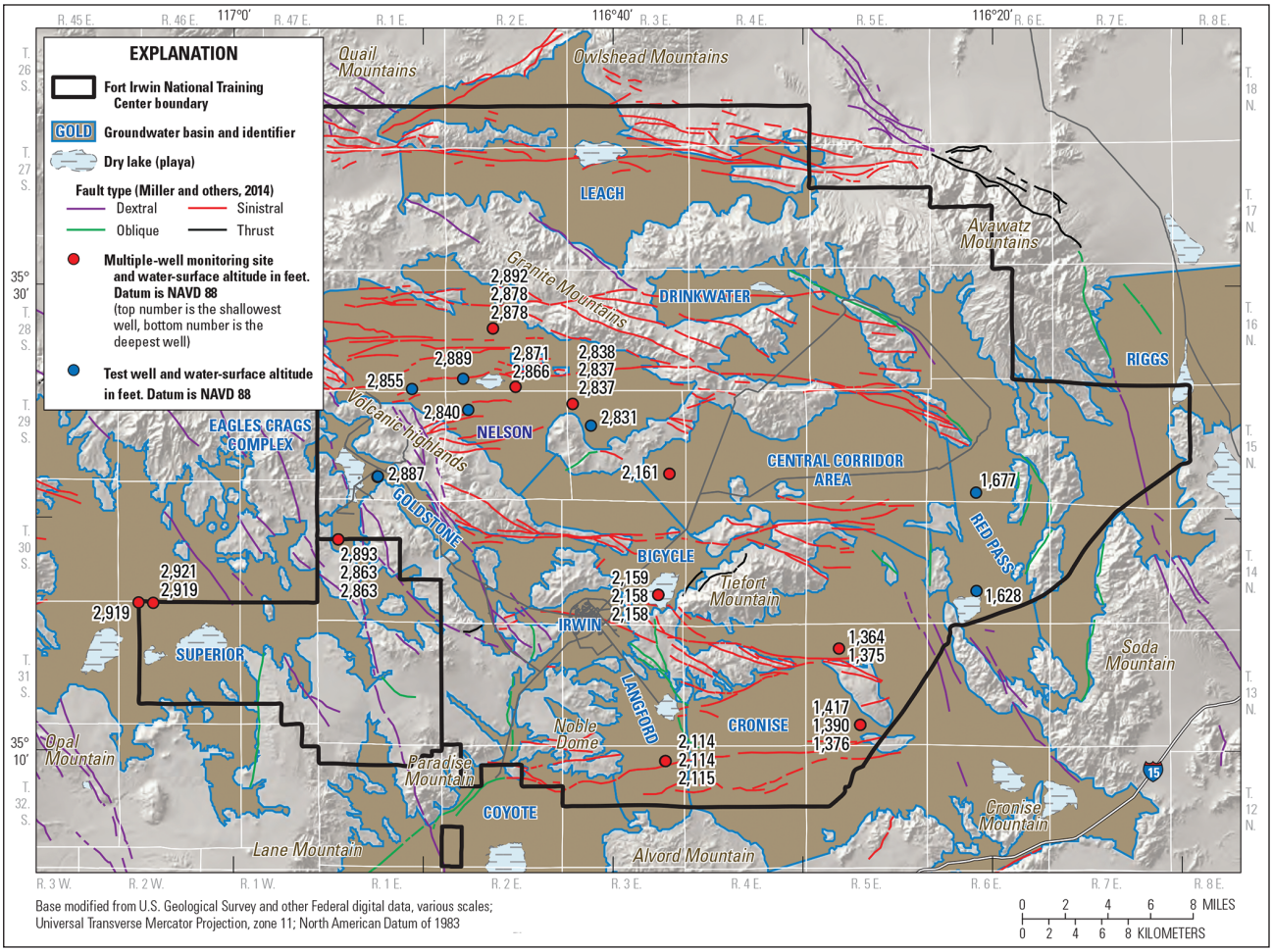

Figure 3. Map showing groundwater basins, wells drilled in 2011-12, and groundwater-surface altitudes during 2011-12, Fort Irwin National Training Center, California (water-level data from Kjos and others, 2014; basins modified from California Department of Water Resources, 2003).

used by NTC water personnel in managing their limited water-supply resources.

Water Quality, Source, and Age. Water-quality data were collected sporadically between 2011 and 2012 from newly drilled wells to determine the groundwater quality within the basins and to help delineate potential locations of poor-quality groundwater (Kjos and others, 2014). Samples were analyzed for major ions, selected trace elements, stable isotopes of oxygen and hydrogen, and the radioactive isotopes of tritium and carbon-14.

Groundwater from wells in Nelson and Superior Basins, in Central Corridor area, and on the south western edge of Goldstone Basin is characterized as a sodium-bicarbonate type water; groundwater from wells in Goldstone and Cronise Basins is characterized as a sodium-chloride type water (Nawikas and others, written commun., 2017). Specific conductance in most basins ranged from about 367 to 1,590 µS/cm (fig. 4; from data presented in Kjos and others, 2014). Poor-quality water (>1,600 µS/cm; the secondary maximum contaminant level; U.S. Environmental Protection Agency, 2013) was present in Goldstone and Cronise Basins. Arsenic and fluoride concentrations were variable, depending on type of geologic deposits. Arsenic ranged from less than 3 to 179 µg/L and fluoride ranged from less than 1 to 15 mg/L (Kjos and others, 2014). The U.S. Environmental Protection Agency maximum contaminant levels for arsenic and fluoride are 50 µg/L and 4 mg/L, respectively (U.S. Environmental Protection Agency, 2013).

Land-surface deformation

Land-surface deformation is a worldwide occurrence driven by a number of processes including tectonics, volcanism, subsidence due to groundwater withdrawals, as is the case in the Central Valley of California (e.g., Galloway and others, 1999), or land-surface expansion, as is the case of clay sediments of a playa swelling from re-saturation after playa inundation. Land-surface failures, in the form of fissures and sink-like depressions, formed between 2005 and 2014 on the Bicycle Lake playa in Bicycle Basin. These types of land-surface failures often are indicative of differential (spatially variable) land subsidence (Galloway and others, 1999). The Bicycle Lake playa is used as an aircraft runway for transporting troops and supplies. Because of the immediate hazards to users of the runway, monitoring and evaluation of land-surface deformation were undertaken that included

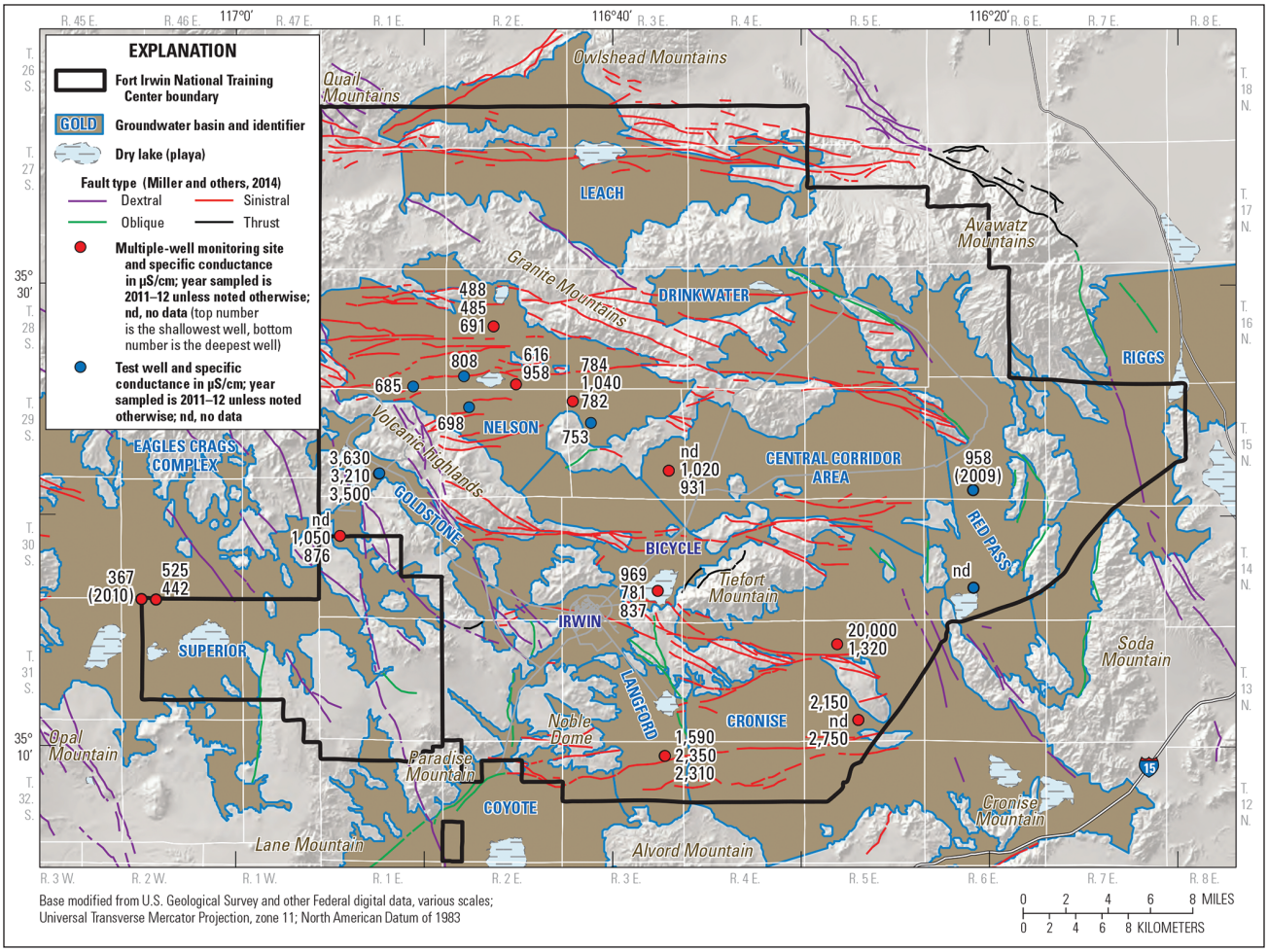

Figure 4. Map showing groundwater basins, wells drilled in 2011-12, and specific conductance during 2011-12, Fort Irwin National Training Center, California (conductivity data from Kjos and others, 2014; basins modified from California Department of Water Resources, 2003).

Interferometric Synthetic Aperture Radar (InSAR), leveling, tape extensometer, Light Detection and Ranging (lidar), and geophysical (Electromagnetic Resistivity Tomography [ERT] and Electromagnetic Induction [EMI]) surveys (Densmore and others, 2010; Densmore and others, written commun., 2017b). InSAR interferograms show spatially variable subsidence magnitudes with a maximum of about 420 millimeters (16.5 inches) between 1992 and 2015. Subsidence rates calculated from InSAR interferograms are variable. The rates of subsidence were lower between 2009 and 2015 than during the previous decade (Densmore and others, written commun., 2017b). Results of leveling data show differential subsidence occurred along a survey transect across the playa and into the area of maximum subsidence. Repeated tape-extensometer measurements across the main runway fissure from April 2009 to January 2016 suggest widening of the fissure was variable over time. A baseline terrestrial lidar survey of the main runway fissure was conducted in January 2009 to enable tracking the evolution of this feature. Subsurface imaging of the main runway fissure with a series of ERT surveys in 2008 suggests that the fissure may extend more than 15 ft into the subsurface (Densmore and others, written commun., 2017b). To assess correlation between water-level changes and land-surface deformation in Bicycle Basin, water-level changes related to groundwater pumpage were also evaluated.

During December 2015, while USGS repeated EMI surveys to monitor land-surface deformation in Bicycle Basin, Fort Irwin requested that land-surface deformation be examined in Red Pass Basin where sink-like depressions were reported on Red Pass Lake playa. A baseline EMI survey was conducted in 2015 on Red Pass Lake playa and on the nearby gravel runway. During this survey several large sink-like depressions and 2 fissures were documented on the playa. InSAR images, created from 1992-2015 overflights for the Bicycle Basin subsidence monitoring, were examined to look for any recent subsidence in Red Pass Basin; however, no recent subsidence was detected. Because there is very little pumpage in Red Pass Basin, water levels in Red Pass Basin are stable, unlike Bicycle Basin. Red Pass Basin lies within dextral faults of the Eastern California Shear Zone that bound the NTC to the east. As part of the land-surface deformation study, preliminary numerical experiments of desiccation and tectonic processes are being conducted to evaluate the driving mechanisms for macro-polygon

formation (Densmore and others, written commun., 2017b).

Summary

A multifaceted, interdisciplinary study is being undertaken at the NTC to explore the groundwater resources and land-surface deformation in a series of developed and undeveloped basins in the Mojave Desert. These desert basins are located in a generally data-poor and geologically complex region. Geologic mapping and geophysical surveys have provided surficial and subsurface information about the groundwater basins within the area. Groundwater levels and water quality vary between basins and suggest limited hydrologic connectivity between basins; however, further study is needed to thoroughly assess basin interconnectivity. Geologic and groundwater-flow models are currently being developed to test hypotheses about the hydrogeologic setting and to build the foundation for quantitative analyses of groundwater availability at the NTC. Preliminary numerical experiments are being conducted to evaluate desiccation and tectonic as driving mechanisms for macro-polygon formation and land-surface deformation at the NTC.

Acknowledgments

The authors acknowledge Chris Woodruff, Kevin Ellett, Jim Howle, Andy Morita, Diane Rewis, Mike Carpenter, Mike Solt, Vicki Langenheim, Bob Jachens, Tony Brown, Charlie Brush, Carl Carlson, and Peter Martin for their assistance on various parts of these studies. The authors also acknowledge the helpful personnel at Range Control for keeping us safe on base.

References cited

Ball, L.B., Bedrosian, P.A., Woolfenden, L., Buesch, D.C., Miller, D.M., and Densmore, J.N., 2016, From Resistivity to Model Framework: Developing 3D Hydrostratigraphy from Airborne Electromagnetic Data in the Nelson Basin, Northern Mojave Desert, in Geological Society of America Abstracts with Programs. v. 48, no. 7; doi: 10.1130/abs/2016AM-285558; https://gsa.confex.com/gsa/2016AM/webprogram/Paper285558.html

Bedrosian, P.A., Ball, L.B., Miller, D.M., Menges, C.M., Buesch, D.C., and Densmore, J.N., 2016, Why So Blue? The Distribution, Origin, and Deformation of Electrically Conductive Stratigraphic Units within the Northeast Mojave Strike-Slip Province, in Geological Society of America Abstracts with Programs. v. 48, no. 7; doi: 10.1130/abs/2016AM-285496; https://gsa.confex.com/gsa/2016AM/webprogram/Paper285496.html

Bedrosian, P.A., Ball, L.B., and Bloss, B.R., 2014, Airborne electromagnetic data and processing within Leach Lake Basin, Fort Irwin, California, chap. G of Buesch, D.C., ed., Geology and geophysics applied to groundwater hydrology at Fort Irwin, California: U.S. Geological Survey Open File Report 2013–1024, 20 p., http://dx.doi.org/10.3133/ofr20131024G.

Bloss, B.R., and Bedrosian, P.A, 2015, Laboratory electrical resistivity analysis of geologic samples from Fort Irwin, California, chap. E of Buesch, D.C., ed., Geology and geophysics applied to groundwater hydrology at Fort Irwin, California: U.S. Geological Survey Open-file Report 2013-1024, 104 p., http://dx.doi.org/10.3133/ofr20131024E.

Buesch, D.C., and O'Leary, D.R., 2016, Using Borehole Data to Establish Lithostratigraphic Geophysical Units (LGUS) for Hydrogeologic Modeling, Fort Irwin, California, in Geological Society of America Abstracts with Programs. v. 48, no. 7; doi: 10.1130/abs/2016AM-283757; https://gsa.confex.com/gsa/2016AM/webprogram/Paper283757.html

Buesch, D.C., 2014, Introduction to the geologic and geophysical studies of Fort Irwin, California, chap. A of Buesch, D.C., ed., Geology and geophysics applied to groundwater hydrology at Fort Irwin, California: U.S. Geological Survey Open-File Report 2013–1024, 8 p., http://dx.doi.org/10.3133/ofr2013102A.

Burgess, M.K., and Bedrosian, P.A., 2014, Time-domain electromagnetic surveys at Fort Irwin, San Bernardino County, California, 2010–12, chap. F of Buesch, D.C., ed., Geology and geophysics applied to groundwater hydrology at Fort Irwin, California: U.S. Geological Survey Open-File Report 2013–1024, 64 p., http://dx.doi.org/10.3133/ofr20131024F.

California Department of Water Resources, 2003, Bulletin 118—Statewide groundwater basin map. version 3 (October 2003): California Department of Water Resources database, accessed November 3, 2011, at http://water.ca.gov/groundwater/bulletin118/gwbasins.cfm; Fort Irwin region: http://water.ca.gov/groundwater/bulletin118/southlahontan.cfm

Cromwell, G., Ball, L.B., Bedrosian, P.A., Miller, D.M., Buesch, D.C., Densmore, J.N., and Woolfenden, L., 2016, Integrated Hydrogeologic Framework Model for two Groundwater Basins at Fort Irwin National Training Center in the Mojave Desert, California, in Geological Society of America Abstracts with Programs. v. 48, no. 7; doi: 10.1130/abs/2016AM-282902; https://gsa.confex.com/gsa/2016AM/webprogram/Paper282902.html

Densmore, J.N. 2003, Simulation of ground-water flow in the Irwin Basin Aquifer System, Fort Irwin National Training Center, California: U.S. Geological Survey Water-Resources Investigations Report 2002-4264, 69 p., at https://pubs.er.usgs.gov/publication/wri024264

Densmore, J.N., Ellett, K.M., Sneed, M., Brandt, J., Howle, J.F., Morita, A., Borela, R., and Bobet, A., undated, Evaluation of Land Subsidence and Ground Failure Hazards at Bicycle Basin, Fort Irwin National Training Center, California, 1992-2015: U.S. Geological Survey [written communication, 2017b].

Densmore, J.N., Ellett, K., Howle, J., Carpenter, M., and Sneed, M., 2010, Monitoring land-surface deformation on Bicycle Lake playa, Fort Irwin, California, USA: in Land Subsidence, Associated Hazards and the Role of

Natural Resources Development---Proceedings of the 8th International Symposium on Land Subsidence, October 17-22, 2010, Queretaro, Mexico: International Association of Hydrological Sciences Publication 339.

Densmore, J.N., and Londquist, C.J. 1997, Ground-water hydrology and water quality of the Irwin Basin at Fort Irwin National Training Center, California: U.S. Geological Survey Water-Resources Investigations Report 97-4092, 159 p., at https://pubs.er.usgs.gov/publication/wri974092

Densmore, J.N., Miller, D.M., Buesch, D.C., Ball, L.B., Bedrosian, P.A., Cromwell, G., and Woolfenden, L., 2016, Overview on Integrating Remote Sensing with Traditional Methods in Hydrologic, Geologic, and Water-Exploration Studies at Fort Irwin National Training Center in the Mojave Desert, California, in Geological Society of America Abstracts with Programs. v. 48, no. 7; doi: 10.1130/abs/2016AM-285096; https://gsa.confex.com/gsa/2016AM/webprogram/Paper285096.html

Densmore, J.N., Woolfenden, L.R., Rewis, D.L., Martin, P.M., Sneed, M., Ellett, K.M., Solt, M., and Miller, D.M., undated, Geohydrology, Geochemistry, and Numerical Simulation of Groundwater Flow and Land Subsidence in the Bicycle Basin, Fort Irwin National Training Center, California: U.S. Geological Survey [written communication, 2017a].

Galloway, D.L., Jones, D.R., and Ingebritsen, S.E., 1999, Land subsidence in the United States: U.S. Geological Survey Circular 1182, 175 p., at https://pubs.usgs.gov/circ/circ1182/

Halford, K. J., and Kuniansky, E. L., 2002, Documentation of Spreadsheets for the Analysis of Aquifer-Test and Slug-Test Data: U.S. Geological Survey Open-File Report 02-197, 54 p., at https://pubs.usgs.gov/of/2002/ofr02197/

Jachens, R.C., and Langenheim, V.E., 2014, Gravity survey and interpretation of Fort Irwin and vicinity, Mojave Desert, California, chap. H of Buesch, D.C., ed., Geology and geophysics applied to groundwater hydrology at Fort Irwin, California: U.S. Geological Survey Open-File Report 2013–1024, 11 p., http://dx.doi.org/10.3133/ofr20131024H.

Kjos, A.R., Densmore, J.N., Nawikas, J.M., and Brown, A.A., 2014, Construction, water-level, and water-quality data for multiple-well monitoring sites and test wells, Fort Irwin National Training Center, San Bernardino County, California, 2009–12: U.S. Geological Survey Data Series 788, 139 p., https://dx.doi.org/10.3133/ds788.

Langenheim, V.E., and Jachens, R.C., 2014, Aeromagnetic data, processing, and maps of Fort Irwin and vicinity, California, chap. I of Buesch, D.C., ed., Geology and geophysics applied to groundwater hydrology at Fort Irwin, California: U.S. Geological Survey Open-File Report 2013–1024, 18 p., http://dx.doi.org/10.3133/ofr20131024I.

Miller, D.M., Buesch, D.C., Ball, L.B., Bedrosian, P.A., Densmore, J.N., and Langenheim, V.E., 2016, Formation and Destruction of Sedimentary Basins along Sinistral Faults, Fort Irwin, CA, Applied to Groundwater Availability, in Geological Society of America Abstracts with Programs. v. 48, no. 7; doi: 10.1130/abs/2016AM-280476; https://gsa.confex.com/gsa/2016AM/webprogram/Paper280476.html

Miller, D.M., Menges, C.M., and Lidke, D.J., 2014, Generalized surficial geologic map of the Fort Irwin area, San Bernardino County, California, chap. B of Buesch, D.C., ed., Geology and geophysics applied to groundwater hydrology at Fort Irwin, California: U.S. Geological Survey Open-File Report 2013–1024, 11 p., scale 1:100,000, http://dx.doi.org/10.3133/ofr20131024B.

Nawikas, J.M., Densmore, J.N., Brown, A., O'Leary, D., Buesch, D.C., and Izbicki, J.A., undated, Summary of Hydrologic Testing, Fort Irwin National Training Center, San Bernardino, CA: U.S. Geological Survey [written communication, 2017].

O'Leary, D.R., Buesch, D.C., Miller, D.M., Densmore, J.N., and Nawikas, J.M., 2016, Wellbore Flow Simulations for Test Wells, Fort Irwin National Training Center, California, in Geological Society of America Abstracts with Programs. v. 48, no. 7; doi: 10.1130/abs/2016AM-283279; https://gsa.confex.com/gsa/2016AM/webprogram/Paper283279.html

Sabin, A.E., 1994, Geology of the Eagle Crags volcanic field, northern Mojave Desert, China Lake Naval Air Weapons Station, California, [Ph.D. Thesis]: Golden, Colorado School of Mines, 209 p., https://dspace.library.colostate.edu/handle/11124/170512

U.S. Environmental Protection Agency, 2013, Drinking water contaminants: U.S. Environmental Protection Agency, accessed May 3, 2013, at http://www.epa.gov/safewater/contaminants/index.html.

Voronin, Lois M.; Densmore, Jill N.; Martin, Peter; Brush, Charles F.; Carlson, Carl S.; Miller, David M., 2013. Geohydrology, geochemistry, and groundwater simulation (1992–2011) and analysis of potential water-supply management options, 2010–60, of the Langford Basin, California: U.S. Geological Survey Scientific Investigations Report 2013-5101, 86 p., at https://pubs.er.usgs.gov/publication/sir20135101

Voronin, L.M., Densmore, J.N., and Martin, Peter, 2014, Analysis of potential water-supply management options, 2010–60, and documentation of revisions to the model of the Irwin Basin Aquifer System, Fort Irwin National Training Center, California: U.S. Geological Survey Scientific Investigations Report 2014–5081, 34 p., at http://dx.doi.org/10.3133/sir20145081.

Western Region Climate Center, 2009, Goldstone ECHO 2—California (043498) Period of Record Monthly Climate Summary. December 01, 1973, to July 31, 2006: Western Region Climate Center database, accessed February 6, 2017, at http://www.wrcc.dri.edu/cgi-bin/cliMAIN.pl?ca3498.

Woolfenden, L., Ball, L.B., Bedrosian, P.A., Cromwell, G., O'Leary, D.R., Miller, D.M., Buesch, D.C., and Densmore, J.N., 2016, Simulating Groundwater-Flow Systems in Basins having Sparse Data at Ft. Irwin National Training Center in the Mojave Desert, California, in Geological Society of America Abstracts with Programs. v. 48, no. 7; doi: 10.1130/abs/2016AM-285439; https://gsa.confex.com/gsa/2016AM/webprogram/Paper285439.html

Population dynamics of *Frasera albomarginata* S. Watson "Desert Elkweed" in Mojave National Preserve, San Bernardino County, California

Tom Schweich
420 Arapahoe Street, Golden, CO 80403

ABSTRACT—*Frasera albomarginata* S. Watson [Syn: *Swertia albomarginata* (S. Watson) Kuntze] commonly called "Desert Elkweed" is a semelparous perennial herb that is found on limestones or other carbonate-based thin soils among pinyons and junipers of the American southwest. In the eastern Mojave the species is found on Clark Mountain, the New York and Providence Mountains, and the Mid Hills between them. Sixteen years of observational data from the Mid Hills of Mojave National Preserve show that the population size of *F. albomarginata* S. Watson is highly variable and dependent on precipitation to maintain its population and to reproduce. The future of a *F. albomarginata* seedling is quite uncertain, and many die without normal to above-normal rainfall . A local population must maintain a soil seed bank to sustain its presence over several "bad" years.

Introduction

Desert Elkweed, *Frasera albomarginata* S. Watson, is a pretty little plant found occasionally in Pinyon-Juniper woodlands of southwestern USA deserts. It grows low to the ground with a rosette of green leaves (Figure 1). The leaves have a small white edge, or margin, around the green leaf; hence the name albo- (white) -marginata (-margined).

F. albomarginata flowers only once in its life history and then dies, and is therefore called semelparous, if you like Latin, or monocarpic, if you prefer Greek. Sometimes *F. albomarginata* is described as a biennial. This may be an accurate description for plants growing near the center of its range. However, in the eastern Mojave, it rarely flowers in its second year. Though Desert Elkweed grows for more than one year, it does not form woody tissue, which makes it a perennial herb, or forb.

When *F. albomarginata* flowers, it sends up a stem which is 8 to 24 inches (2-6 dm) tall and has very thin leaves arranged around the stem in a whorl. The flowers are about 1 inch (2.5 cm) in diameter, with greenish-white petals that have purple dots (Figure 2). Nectar, to attract pollinating insects, is secreted in pits which are located well out on the petals.

The genus name of *Frasera* was first applied to this distinctly North American genus by Walter (1788) in his *Flora Caroliniana*, and is named for J. Fraser, a Scottish collector of North America plants, 1750–1811. For much of its subsequent history, *Frasera* was often included in *Swertia* (cf., Card, 1931, and Post, 1956), which explains why the taxon is sometimes called *Swertia albomarginata* (S. Watson) Kuntze. However, recent molecular work, including that of Chassot, et al. (2001) has shown that *Swertia* in the broad sense is highly paraphyletic and that

Figure 1. Typical rosette of *Frasera albomarginata* leaves (stake is ¼" in diameter).

Figure 2. Flowers of *Frasera albomarginata* (scale approximate).

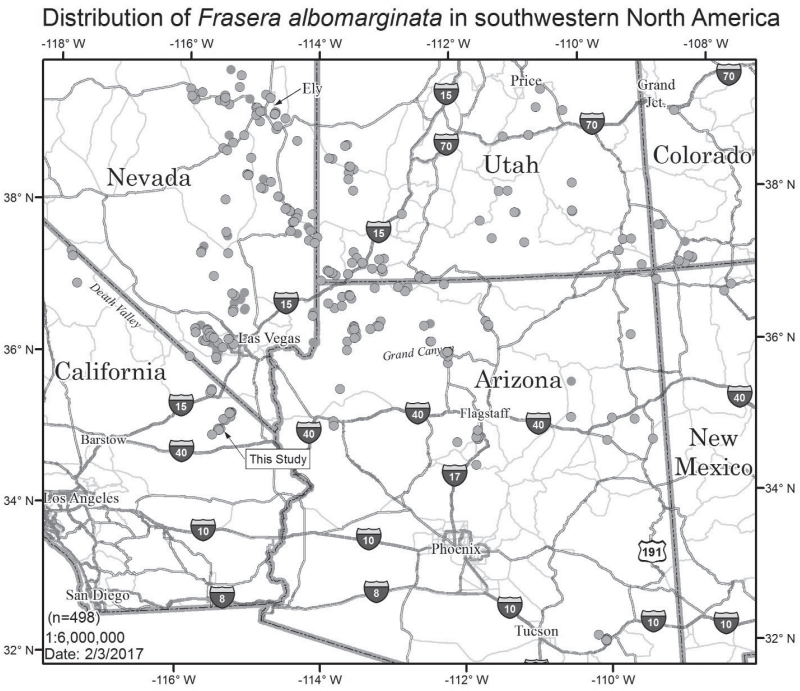

Figure 3. Collection sites of *Frasera albomarginata* in southwestern North America, based on herbaria specimens.

Frasera should stand on its own as a North American genus of Gentianaceae.

The type (first described specimen) of *F. albomarginata* was collected near Saint George, in southwestern Utah in 1870 by Dr. Edward Palmer. The label on the specimen says, "S. E. Utah." However, there is good evidence that this is a transcription error. Sereno Watson (1871) wrote the first description, incorporating Palmer's collections into his botanical volume of the report on King's geological exploration of the fortieth parallel.

The geographic distribution of *F. albomarginata* is shown in Figure 3. The data points are 498 vouchers, 54 of which were collected by the author, at 44 herbaria. The westernmost occurrence is on top of the Last Chance Range, Death Valley National Park. There is a disjunct population at the former mining town of Johnson, Cochise County, Arizona, and the easternmost populations are found mostly in the Four Corners area of Colorado and New Mexico. The densest populations are found in a belt from Saint George, Utah, through Beaver Dam State Park, Nevada, to the vicinity of Ely and Eureka, Nevada. There are also numerous collections in the Spring Mountains near Las Vegas, Nevada. In the eastern Mojave, *F. albomarginata* is found on the limestones of Clark Mountain, the New York and Providence Mountains, and the Mid Hills between them. This study was conducted on outcrops of the informally-named lacustrine limestone of the Winkler Formation of Pinto Mountain (35.1756°, -115.3865°, WGS 1984, elev. 1672 m.) and Wild Horse Mesa (35.0472°,-115.4581°, WGS 1984, elev. 1558 m.).

Field Work

Two 25 m^2 plots were established on April 30, 1996 in Mojave National Preserve: one on the north face of Wild Horse Mesa (Figure 4), and the other on the south face of Pinto Mountain.

Individuals of *Frasera albomarginata* were marked with a numbered stake. Initially observations were made two or three times per year. However, it soon became evident that such frequent visits were damaging the meager soil. Visits were scaled back to once a year, in late Spring when the species is likely to be flowering. The plots were not burned by the Hackberry Complex Fire, June 23-27, 2005, although some of the surrounding vegetation was singed

Data collected included: Date, plant number, linear dimensions in three dimensions, number of basal leaves, and life stage. Life stages were defined as: Seedling (1st-year rosette), Dormant, Rosette (2+ year), Bud, Flower, Fruit, and Death. The stages of Bud, Flower, and Fruit were taken to represent successful reproduction because the plots were visited only once a year. Data were aggregated across the two plots. While the populations followed similar patterns, there were generally more plants at Wild Horse Mesa than Pinto Mountain.

Data were collected through May 28, 2012, providing 17 annual observations over 16 years of continuous data collection for the two plots.

Figure 4. Typical *Frasera albomarginata* habitat at Wild Horse Mesa, San Bernardino County, California

The total data set includes data from 322 individual plants. However, it was not possible to determine the age of the 100 plants growing in the plots when the plots were established. Therefore, data for those plants was excluded when calculating the life table. Similarly, there were 27 live plants, which were not attempting to reproduce when the plots were removed, and the data for those plants was also excluded. This results in full life-cycle data for 195 plants through the 16-year period.

Weather data (Summary of the Day) was obtained for Mitchell Caverns from March 11, 1958 to April 30, 2011, at which time Providence Mountains State Park was closed for repairs. Mitchell Caverns is 15 km. southwest of, and 240 m. lower than the north face of Wild Horse Mesa and 28 km. southwest of, and 350 m. lower than the Pinto Mountain plot.

Other sources of weather data in the eastern Mojave are quite limited. The Mid Hills RAWS station has operated intermittently since September 23, 1991, but provides only temperature data, not precipitation. Other stations in the eastern Mojave include Amboy, Baker, and Needles, California, but these are much removed in distance and elevation from locations where *F. albomarginata* is found.

Precipitation and temperature data were aggregated monthly. The data was then normalized by month, e.g., all the data points for the Augusts in the data set were normalized to the average for all Augusts. The other months were normalized in the same manner. The normalized data was then smoothed with a 24-month weighted average. The 24-month smoothing period was selected subjectively by comparison to population size data. It is circular to compare explanatory data smoothed to a good fit with the data it is purported to explain. For this reason no statistical analysis was attempted. Subjectively, though, the smoothed data visually suggests that accumulated precipitation over time, even year to year, better explains population and reproduction than shorter-term values.

Results

Unsurprisingly, population size and reproduction are highly variable and at a gross level appear to be explained by rainfall. Within those tentative conclusions, there are other subtle unexplained points, such as whether the population increase in 2004 is better explained by monthly rainfall than by 24-month smoothed rainfall.

The greatest number of plants and the most plants in flower were found in 2006, the year after a very wet summer. There were 126 plants, 113 at Wild Horse Mesa

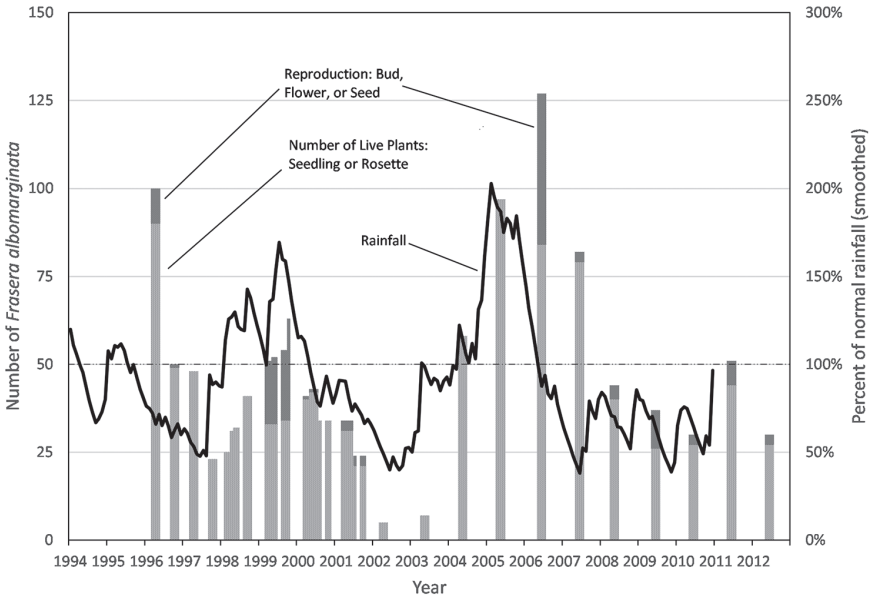

Figure 5. Number of live and reproducing *F. albomarginata* compared to 24-month weighted average of normalized rainfall at Mitchell Caverns, California. Plant population data points = 322

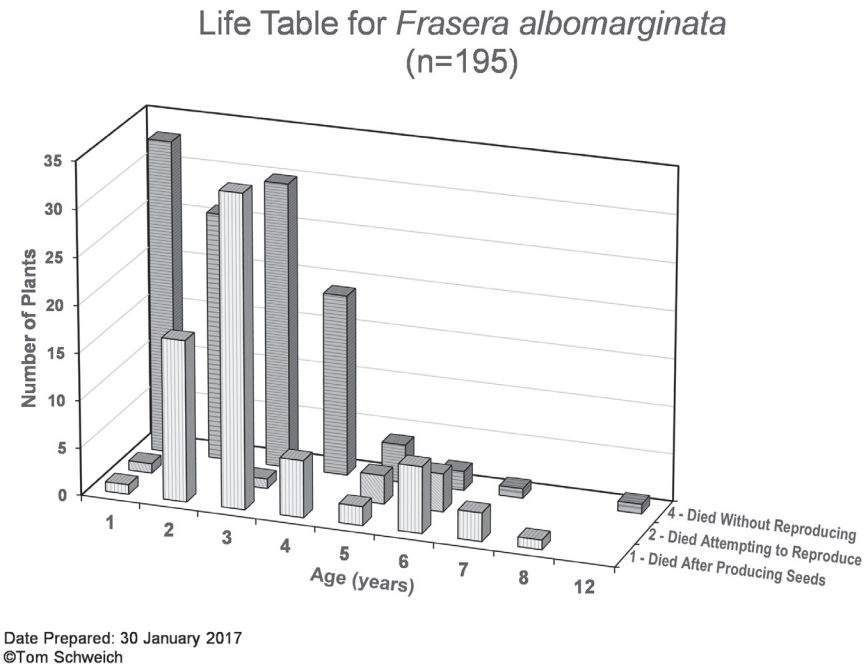

Figure 6. Life table for 195 *Frasera albomarginata* monitored over the 16 year period at Pinto Mountain and Wild Horse Mesa in the eastern Mojave Desert.

and 13 at Pinto Mountain. The least number of plants was found in 2002 after the drought years of 2001-2002. There were five live plants, four at Wild Horse Mesa, and one at Pinto Mountain. The mean number of live plants over the 16 year period was 58.4 (± 36.3, 1sd).

Figure 5 compares the number of live and reproducing *F. albomarginata* to the 24-month normalized rainfall data from Mitchell Caverns. (The population bars have also been artificially widened so that they are more visible.) It is clear that the population increases typically occur after periods of above normal rainfall, and that significant reproduction occurs only following periods of extraordinary rainfall. The year 2000 is an exception in that there was near-normal rainfall, but there was neither a population increase nor substantial reproduction. A speculative explanation would suggest that plants with reproductive capacity bloomed the previous year, and that few plants growing in 2000 were capable of transitioning to reproduction.

The rapid increase in population from five plants in 2002 to 145 plants in 2006 without any intervening seed production shows that *F. albomarginata* is dependent on a soil seed bank to sustain itself through dry years.

A similar comparison of population size versus monthly temperature did not show a pattern similar to that of rainfall.

Figure 6 shows a life table for 195 plants that completed a full life cycle during the period of this study. Of these 195 plants:

- 116 (59.5%) died without ever attempting to reproduce.
- 34 (17.4%) died in the first year of life.
- 9 (4.6%) dried up and died while attempting to reproduce.
- 70 (35.9%) successfully reproduced (set seed).

Over 16 years of observations the most successful reproduction event, i.e., flowering and setting of seed, was in 2006 when 43 plants (32,5%) of 132 plants found were observed to be flowering or setting seed. Smaller amounts of seed were produced in three years: 1999 (19 plants), 2009 (11 plants), and 1996 (10 plants).

The most common age at reproduction is year three. This is more likely the result of germination and rainfall intervals than an inherent character of the species.

In summary, life for *Frasera albomarginata* in Mojave National Preserve is quite uncertain. Death without reproduction is the most common life outcome. In dry years, plants simply die, or even die as they are attempting to flower.

Additional Observations

Various attempts to germinate seed were all met with failure. Several very fresh seeds may have germinated once, but the seedlings quickly perished, presumably from damping-off. Mature seed never germinated in my experiments, regardless of treatment. In a third attempt, three inches of soil from a 2 foot by 2 foot plot were transported to my garden, spread out in a 3 inch deep plot, and watched for several years without observing a *F. albomarginata* seedling.

There is one anecdote about transition to flowering from rosette state, and this only from an accidental experiment. Four rosettes were dug up for a transplant experiment. They were wrapped in a damp paper towel, and placed in an ice chest. Three days later, when removed from the ice chest, all four plants were growing flower stalks. This suggests that transition to flowering is both very rapid and opportunistic.

Observations of open flowers show that they are visited by many different bees and flies.

In general, *F. albomarginata* is found in more dense populations near the center of its range. Particularly outstanding are populations found in Beaver Dam State Park and Silver King Pass, Lincoln County, Nevada. Predation was rarely seen in the eastern Mojave and, then, the entire flower stalk was eaten, perhaps by deer or cattle. Although, anecdotally, the plants were more likely to perish from being stepped-on, rather than being eaten. Insect predation also seems to be limited to the center of the species' range. There is a small worm that eats the pith of the flowering stalk, which has been seen primarily at Beaver Dam State Park. An entry/exit hole was often seen at the top on an internode.

Frasera albomarginata is one of several semelparous arid-land *Frasera* found in the American Southwest. It is also not the only *Frasera* with white-margined leaves. Other common *Frasera* with white margined leaves are *F. paniculata* and *F. puberulenta*.

Frasera puberulenta Davidson, is very similar to *F. albomarginata* and was at one time considered a variety of *F. albomarginata*. It is found along the eastern Sierra Nevada and at a few locations in the western Great Basin.

Frasera paniculata Torr. (Syn: *F. utahensis* M. E. Jones) is another common species of desert *Frasera* and is sometimes confused with *F. albomarginata*. It is found in the sandier habitats of northern Arizona and southern Utah. Reports of *F. paniculata* occurring in Nevada, such as those found in GBIF and EOL, are mistaken in my opinion.

The desert species of *Frasera*, including *F. albomarginata*, *F. paniculata*, and *F. puberulenta* of the eastern Sierra Nevada, are thought to have evolved from *Frasera speciosa* Griesb. (Kartesz, 1988). *Frasera speciosa* is sometimes called Monument Plant because of its shape and size. Another common name is Elkweed, from which I extrapolate a common name of Desert Elkweed for *F. albomarginata*.

Conclusions

Frasera albomarginata is an attractive, delicate-appearing forb that appears to be restricted to carbonate-based soils in the eastern Mojave Desert. Freezing winters with snow is the primary source of precipitation, and long, hot, dry summers, with unpredictable cloudbursts, present unique

challenges for a plant whose family—Gentianaceae —is normally associated with more moist climates. Being semelparous, *F. albomarginata* must establish a seed bank in the soil that can maintain viability over several "bad" years. The presence of *F. albomarginata* adds to the beauty of the desert experience, and its ecology should be instructive in how organisms cope with a difficult and unpredictable desert environment.

Acknowledgements

The National Park Service graciously renewed my research permit year after year. I am grateful to the referee for their constructive input.

Literature Cited

Card, Hamilton H., 1931. A Revision of the Genus *Frasera*. Annals of the Missouri Botanical Garden, Vol. 18, No. 2 (Apr., 1931), pp. 245-282.

Chassot, P., S. Nemomissa, Y.-M. Yuan, and P. Küpfer. 2001. High paraphyly of *Swertia* L. (Gentianaceae) in the Gentianella-lineage as revealed by nuclear and chloroplast DNA sequence variation. Plant Systematics and Evolution. 229(1-2):1-21.

Kartesz, John Thomas. 1988. A flora of Nevada. Ph.D. dissertation, University of Nevada, Reno, 1988.

Post, Douglas M. 1956. Studies in the Gentianaceae: *Frasera* and *Swertia* of North America. Ph.D. dissertation. University of California, Berkeley. 1956.

Walter, Thomas. 1788. Flora Caroliniana. London: 1788.

Watson, Sereno. 1871. Volume 5, Botany. pp. in King, Clarence. Report of the Geological Exploration of the Fortieth Parallel. Professional Papers of the Engineer Department, U. S. Army. 18. Washington: Government Printing Office, 1871.

Living on the Edge II: Further Investigation of Enhanced Roadside Creosote Growth in the Mojave Desert

David K. Lynch
Thule Scientific, david@alumni.caltech.edu

ABSTRACT—Enhanced creosote growth on ridges lining two-lane paved roads on fans in the Mojave Desert is investigated using new field measurements and approximate calculations. Clear evidence is presented for ponding of water uphill of the uphill ridge, further enhancing growth. We argue that a temporary reservoir of water may exist following a rainstorm beneath one or both ridges. Such reservoirs would promote ruderal creosote growth, as would capillary action, which is able to raise water from the ditch into the ridge. Based on the geometry of creosote root growth in the context of ridge geometry, we suggest that some root growth would be parallel to the ridges to seek ditch water.

1. Introduction

Creosote growth in the Mojave Desert is known to be enhanced on elevated ridges constructed during road building alongside two lane paved roads[1-3] (Figure 1). The first order explanation is that runoff from the paved road collects in the ditches next to the ridges, thereby providing extra water for nearby plants. Furthermore, the uncompacted ridge soil is looser than the undisturbed desert soil and this allows easier penetration of water and a better medium for root growth[4], even though the ridges are usually higher than the level of the road and certainly higher than water in the ditch. In this paper we will extend previous analyses[4] of ruderal (disturbed) creosote growth based on field observations, known soil properties and the mechanics of water diffusion in porous media. We will also speculate on root geometry in the vicinity of desert roads.

2. Field observations

In the winter of 2016 and 2017, a number of surveys were made in Death Valley National Park, Panamint Valley and the Lake Los Angeles region of the Mojave Desert in order to investigate creosote growth adjacent to two-lane paved roads. Over 1200 miles of two-lane, paved roads were observed with attention paid to roadside growth, followed by examination on Google Earth. One such visit was timed to be a day after a rainstorm and we were able to find many roadside ditches with standing water. Standing water in roadside ditches a day or two after a rain tells us that the soil is poorly drained (Figure 2). Poorly drained soil is almost always composed of small particles like silt and clay. Such soils have small pore spaces and thus water diffusion by capillary action is expected to be significant. Capillary action can move water horizontally and raise water above the level of standing water in a ditch and into the ridges. In contrast, well-drained soil is composed of large particles (sand, gravel) where capillary action is weak. In this case water percolation tends to be dominated by gravity and diffuses more-or less downward.

Field observations show that on a fan, enhanced creosote growth tends to be strongest on the uphill ridge (Figure 3). The uphill ridge is bounded by two water sources: the uphill ditch water and water that collects immediately uphill of it (Figure 4). Also evident in the field and on satellite imagery are many discrete areas of light colored soil just uphill of and immediately adjacent to the uphill ridge. These are dried up ponded sediments composed of clay, and are almost completely absent downhill of the downhill ridge. Thus we have clear

Figure 1. Enhanced Creosote growth on the elevated ridges on either side of Trona Wildrose Road in Panamint Valley. Note the more widely spaced and smaller creosote bushes in the undisturbed soil well away from the road.

Figure 2. Standing water in a ditch near Lake Los Angeles following rain. Creosote is growing vigorously on the elevated ridge constructed when the road was built.

evidence of water collecting right next to and on either side of the uphill ridge. We interpret this to mean that the more vigorous growth on the uphill ridge compared to the downhill ridge is a direct result of two water sources rather than just one (downhill ditch).

For water to collect uphill of the uphill ridge, it must have flowed over the surface, either as sheet flow or in drainages. This again suggests that the desert surface is composed of poorly drained soil. Measurements of the hydraulic conductivity of Mojave Desert soils correspond to soils that are primarily silt or clay[5], consistent with what has been previously discussed.

3. Transient water diffusion in the vadose zone

Diffusion of water through unsaturated soil is described by Richards Equation[6,7], a partial differential equation with no general analytic solutions. Solutions are obtained numerically using codes such as HYDRUS 1D[8]. A key parameter in the equation is the hydraulic conductivity (denoted K in Richard's equation) that has units of speed (m/s), though this is not the speed at which water diffuses, only being proportional to it. K is a 2nd rank tensor[9,10], the nine components of which are virtually never known, though scalar values have been measured[11]. It also varies spatially, especially vertically in different soil horizons, and can range over ten orders of magnitude depending on soil type and specifics of the measurements. The solution of Richards equation relies on applying boundary conditions and for a road, they are difficult to define numerically. For these reasons, modeling moisture flow in soils is difficult, and especially so near roads whose soils have been disturbed by road building. We will therefore perform a simple approximate numerical analysis to bound the various solutions as a guide to future investigations.

During and after a rainstorm on a fan, water can collect at three locations along the road: the downhill ditch, the uphill ditch, and uphill of the uphill ridge (Figure 4). Diffusion of this water into the soil depends on soil particle sizes. In sand and gravel, gravity is the dominant force and water tends to diffuse downward with little horizontal movement. For smaller particles sizes like silt and clay, capillary action is dominant and water diffuses in all directions and upward into the ridge. Thus we must always keep in mind that diffusion speed and direction are correlated with particle size, resulting in anisotropic diffusion.

Since the flow is transient, let's ask how long it would take for water to diffuse from the three regions and into two locations: under a ridge and under the road. This question is motivated by the suggestion that there may be enduring water reservoirs under and near the road after a rain.

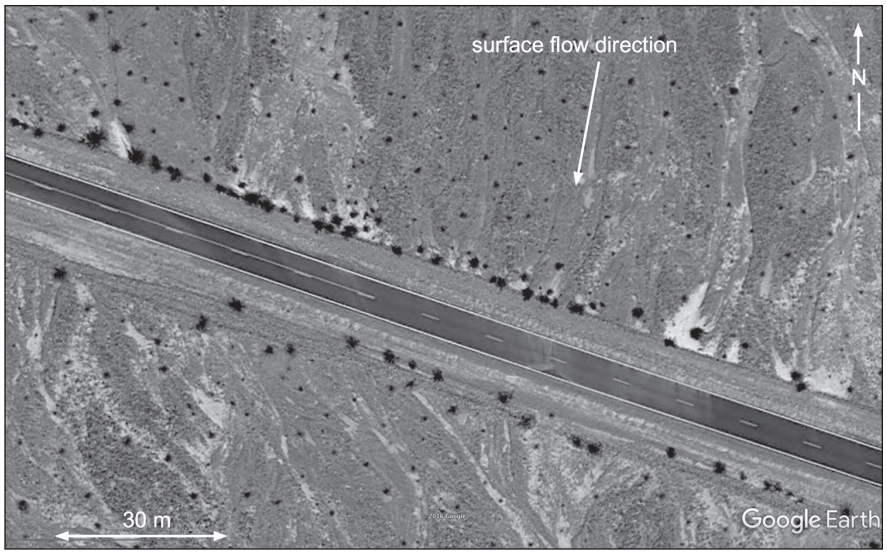

Figure 3. Google Earth image of a section of Scotty's Castle road. Enhanced creosote growth is obvious on either side of the road but it is more vigorous on the uphill ridge than on the downhill ridge. Also obvious immediately uphill of the uphill ridge are areas of light soil that are dried out ponded sediments, primarily clay. These occur because the uphill ridge acts as a barrier to surface flow on the fan. Note the absence of the dried up ponded sediments on the downhill side of the road. Stronger uphill growth and ponded sediments both occur most strongly when the flow direction is perpendicular to the road.

Let us assume that the typical desert rainstorm lasts two days. We demonstrate here that it matters very little if the time we choose varies by a factor of two (e.g., one day or four days). The horizontal distance from a ditch to a ridge is about 1 m, and the distance from a ditch to a location directly beneath the road is about 10 m. Thus the minimum speeds at which water can diffuse to reach the ridge and the road center in two days are 0.5 days and 5 days, respectively (i.e., 1m/2 days and 10m/2 days). Based on published infiltration and percolation rates[12,13], the speed to reach the ridge corresponds to silt or

clay. The much higher speed to reach the road center corresponds to sand. But diffusion in sand is dominated by gravity and with little or no capillary action to spread the water sideways; the water would be expected to move downward, not laterally under the road.

Infiltration and exfiltration take place at different rates (hysteresis)[14-16], the former being 2-3 times faster than the latter. Infiltration is driven by the hydraulic head (standing water depth) and exfiltration is controlled by diffusion to the surface followed by evaporation. While it may take two days for water to infiltrate, it will take four to six days for it to exfiltrate, i.e., dry out and leave the subsoil dry again, or in its pre-rain state. Thus if there is a reservoir under a ridge, it will endure for several more days (~4) than it would in the undisturbed desert field away from the road, giving the creosote a few more days of moisture after each rain. If there are six rains per season, the ruderal plants have an extra ~24 days of available moisture during which to grow.

The observations of Figures 1-3 are typical of most roadside creosote distributions, but there are exceptions too. Many factors influence creosote growth that can dominate the processes outline above. Occasionally one may find places where no enhancement is found or enhancement that is slightly stronger below the downhill ridge. Sometimes small creosote bushes are found growing in the ditch between the road and the ridge, though they are invariably smaller than those growing on the adjacent ridge. Other enhancements are found away from the road in water courses and obvious drainages, unsurprising because water collects there. In general, however, most two lane roads through the desert where creosote grows show roadside enhancement.

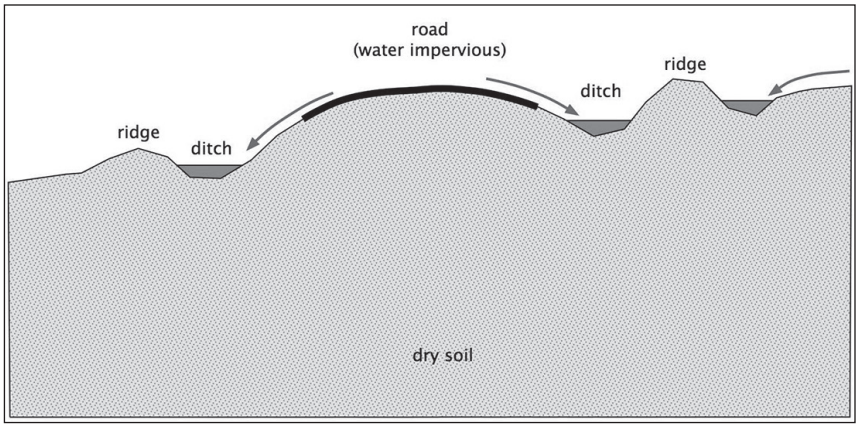

Figure 4. Section diagram of a paved desert road on a fan. Water can collect in three places: in the two ditches from runoff from the impervious pavement, and from surface flow down the fan where it ponds up adjacent to and immediately uphill of the uphill ridge.

4. Geometry of creosote growth on a ridge

Creosote roots in undisturbed soil tend to be shallow, typically about one meter in depth, though some have deeper-reaching tap roots[17]. One meter is also approximately the height of the roadside ridges, and thus there may be a coincidental match between root depth and ridge height that optimizes root growth.

In undisturbed soil, creosote roots grow radially outward from the plant's base, extending about four-to-five meters in all directions for mature plants (Figure 5). Such radial growth is not possible on roadside ridges whose width is only about one meter. With ditch water lying parallel to and immediately adjacent to the ridges, creosote roots would be expected to grow towards the water. To do so they would have to grow inside the ridge and parallel to the ditch, forming a roughly linear bundle of roots.

5. Summary and conclusions

Field observations show that after a rainstorm in the Mojave Desert, many roadside ditches have standing water for a few days after the rain. This is due to poorly drained soil composed of small particle, silt or clay. On a desert fan, water collects on either side of the uphill ditch and this promotes more vigorous ruderal creosote growth than on the downhill ridge, though both ridges show enhanced growth compared to the undisturbed desert surface. Order-of-magnitude (or better) analyses suggest that there may be a water reservoir under the uphill ridge, and probably a lesser reservoir under the downhill ditch, both being the result of capillary action and lateral (sideways) diffusion of water. These simple calculations suggest that water can reach under the ridges but not under the road. It should be noted that ditch soils may be different than the soils in the undisturbed desert floor.

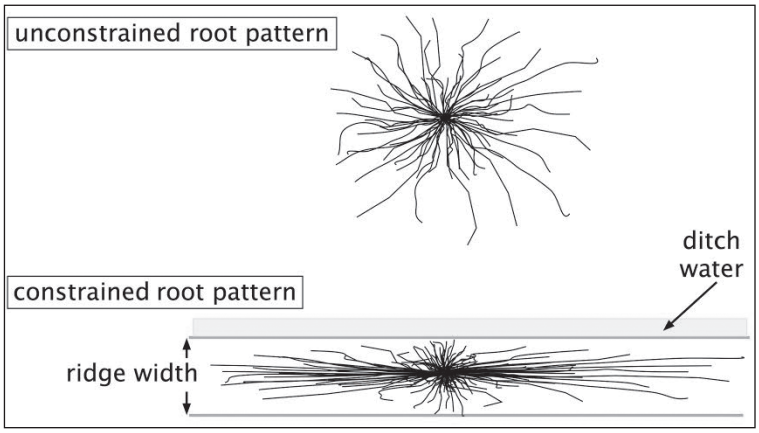

Figure 5. Map view diagram of creosote roots. In the open desert, creosote roots can grow freely in all directions. But when constrained to grow in the roadside ridges, they may grow parallel to and within the ridge. Such growth also would bring the roots in closer contact with water along the ditch, and directly above any subsurface water reservoir.

There is an apparent coincidence between mature creosote root depth and ridge heights, both being about one meter. This coincidence may enhance creosote growth compared to the undisturbed desert surface that adds to the enhancement of roadside vigor. Some creosote roots on ridges bounding desert roads may be partially constrained to grow within the ride and parallel to the ditches, as opposed to growing uniformly radially. Such constrained growth would lead to roughly linear root packages that grow inside and along the ridge, and toward the ditch water.

The results presented above do not consider evaporation of ditch water or evapotranspiration by the creosote, both of which influence water balance in the upper vadose zone. Some recent computations[18] suggest that in most cases evaporation and evapotranspiration do not significantly change the results presented here.

The observations and calculations reported here are largely qualitative and in some cases speculative. All of the results can be investigated by direct measurement and by numerical modeling. We urge the community of desert scientists to pursue the topics discussed here.

Acknowledgements.

I would like to acknowledge David C. Buesch (USGS), David M. Miller (USGS), Darren R. Sandquist (CSUF) for useful comments on this topic during the 2016 Desert Symposium. I also thank Julian A. Scott (USFS), Peter A. Livingston (CPSU) and Tony VanCuran (UC Davis) for reviewing and making valuable comments on the results presented here.

References

1. Johnson, Hyrum B., Frank C Vasek and Terry Yonkers, "Productivity, diversity and stability relationships in Mojave Desert roadside vegetation.", Bulletin of the Torry Botanical Club, 102 (3) 106-115 (1975)

2. Clark, David D, "An analysis of construction effects on vegetation and soils of the Colorado Desert : final report", California State University, Fullerton. Dept. of Biology; Systems Control, Inc; United States. Bureau of Land Management (1979)

3. Lightfoot, David C. and Walter G. Whitford, "Productivity of Creosotebush Foliage and Associated Canopy Arthropods Along a Desert Roadside", The American Midland Naturalist, 125(2) 310-322 (1991)

4. Lynch, David K., Living on the edge: enhanced roadside growth of creosote bush (Larrea tridentata), In Going Loco, proceedings of the 2016 Desert Symposium, R. Reynolds (ed.), Desert Studies Center, California State University Fullerton, 236

5. Young, M.H., E.V. McDonald, T.G. Caldwell, S.G. Benner, and D.G. Meadows. 2004. Hydraulic properties of a desert soil chronosequence in the Mojave Desert, USA. Vadose Zone J. 3:956-963.

6. Richards, L.A., 1931. Capillary conduction of liquids in porous mediums. Physics 1, 318–333.

7. Pachepsky, Yakov, Dennis Timlin, Walter Rawls, Generalized Richards' equation to simulate water transport in unsaturated soils, Journal of Hydrology 272 (2003) 3–13

8. https://www.ars.usda.gov/pacific-west-area/riverside-ca/us-salinity-laboratory/docs/hydrus-1d-model/

9. Duque, Carlos, Peter Engesgaard and Majken C. Looms, Full Tensor Representation of anisotropy in hydraulic conductivity: effects of simulating discharge of groundwater to lakes, XIX International Conference on Water Resources CMWR 2012 University of Illinois at Urbana-Champaign June 17-22, 2012

10. Cisler, J., On the tensor concept of unsaturated anisotropic hydraulic conductivity, Water Resources Research, 8, #2, 525–528 (1972)

11. http://www.structx.com/Soil_Properties_007.html

12. http://qcode.us/codes/sacramentocounty/view.php?topic=14-14_10-14_10_110

13 https://www.ag.ndsu.edu/publications/home-farm/individual-home-sewage-treatment-systems

14. http://www.nrcresearchpress.com/doi/pdf/10.4141/cjss62-033

15. http://ntl.bts.gov/lib/38000/38500/38567/OTCREOS7.1-11-F.pdf

16. https://nicholas.duke.edu/people/faculty/katul/93WR00094.pdf

17. Gibbens R. P. and J. M. Lenz, Root Systems of some Chihuahuan Desert Plants, Journal of Arid Environments, 49, Number 2, October 2001 , 221-263

18. Livingston, Peter A., Personal communication (2017). "The infiltration rate of a silty to clayey soil is around 0.05 inches per hour (1.2 inches per day). If the ditches have 4 inches of standing water and the storm has moved off, then the evaporation rate is probably around 0.2 inches per depending on temperature, humidity, and wind. At 1.4 inches per day the ditch would be dry in about 2.86 days. During this time 2.38 inches of water will have infiltrated into the soil. A "dry" silty clay loam soil still has about 2.6 inches of water per foot of soil This water is not available to the plant as the soil water pressure is greater than a plant can withdraw. The available water holding capacity of a silty clay loam soil is 1.8 inches of water per foot of depth, so over time the 2.38 inches of water will drain down, by gravity, to a depth of 1.32 ft. In Beatty Nevada in May, 2005[19], the bare soil evaporation was an average of .047 inches per day and the average evapotranspiration of creosote bushes in the area was 0.075 inches per day. This is for an individual plant. Assuming the plants cover 80% of the vegetated strip, then the weighted average rate of water use from the strip is 0.069 inches per day. The 1.8 inches of available water stored in the soil would actively sustain the plants for 26 days. After 26 days the plants would go into a semi dormant state."

19. Garcia, C. Amanda, Michael J. Johnson, Brian J. Andraski, Keith J. Halford, and C. Justin Mayers, Portable Chamber Measurements of Evapotranspiration at the Amargosa Desert Research Site near Beatty, Nye County, Nevada, 2003–06, USGS Scientific Investigations Report 2008-5135 (2008)

Flora and fauna of the Holocene Oil Canyon oil-sands from the poorly understood San Joaquin Desert Biozone

Ryan E. O'Dell[1], Diane M. Erwin[2], Patricia Holroyd[2], Brian D. Rankin[2], and Marwa Ibraheem El-Faramawi[2]
[1]*Department of the Interior, Bureau of Land Management, Central Coast Field Office, Marina CA, 93933, rodell@blm.gov;*
[2]*University of California-Berkeley, Museum of Paleontology, 1101 Valley Life Sciences Building, Berkeley, CA, 94720*

ABSTRACT—A thick partially-exposed outcropping of oil-sands is located in Oil Canyon ~12 km north of Coalinga, California on AERA Energy Corporation property. AERA geologists and personnel over the years have referred to the surface seep as part of the "Temblor Tar Cap." Here we report for the first time on the fossil vertebrates, insects, and plants discovered thus far at the Oil Canyon tar seep. Vertebrate remains include a partial skeleton of a relatively large bird with remnants of the wings, the articulated limb bones of a smaller bird, isolated feathers, partial skeletons of pocket mice, and a bobcat jaw. The insects include abundant carbonized three-dimensional and compressed remains of dragonflies, grasshoppers, beetles and lepidopterans (butterflies and or moths). To date, the only identifiable plant macrofossils are leaf impressions of Tucker's oak, *Quercus john-tuckeri*, leaf fragments of *Typha* (cattail), and combined carbonized compression - casts of the inflated inflorescence stems of buckwheat, possibly *Eriogonum nudum* var. *indictum*, which grows in the area today. The fossil data together with new radiocarbon age estimates and geologic context indicate the Holocene landscape and climate in the vicinity of the Oil Canyon seep at the western edge of the San Joaquin Valley between 11,320 (minimally) and 10,150 YBP was relatively wetter and cooler than today. Our preliminary findings suggest the presence of a small pond within a localized perennial wetland. Cattail grew at the margin but current evidence suggests it was not abundant. Herbaceous and shrubby groundcover would have included buckwheats growing on the surrounding slopes, with trees of *Q. john-tuckeri* growing at much lower elevation than today, closer to the depositional basin and in close proximity to the Oil Canyon drainage.

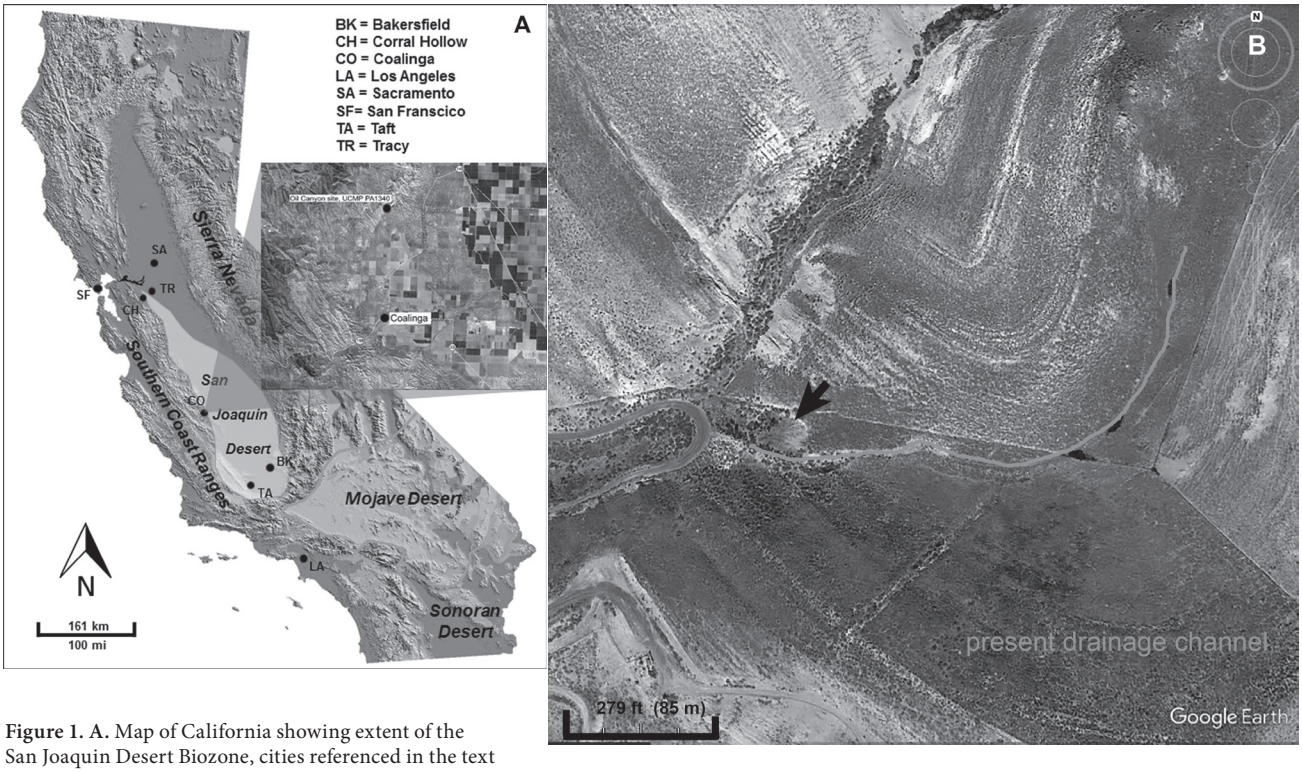

Figure 1. A. Map of California showing extent of the San Joaquin Desert Biozone, cities referenced in the text and location of the Oil Canyon site near Coalinga (outset). **B.** Google Earth satellite view of the Oil Canyon deposit (arrow) and course of the present-day drainage channel.

Introduction

The San Joaquin Desert occupying the San Joaquin Valley is the most imperiled and poorly recognized desert in California (Germano et al. 2011) (Fig. 1A). Average annual temperature from the northern limit of the desert at Corral Hollow near the city of Tracy to the southern limit between the cities of Taft and Bakersfield is 16.0°C (~61°F) to 18.5°C (~65°F) (O'Dell and Ryan, in prep). Average annual precipitation from the northern limit to the southern limit is 267 mm (~10.5 in.) to 137 mm (~5.5 in.). The most concise delineation of the San Joaquin Desert is a polygon encompassing areas of the San Joaquin Valley and South Coast Range with annual average precipitation ≤ 267 mm (O'Dell and Ryan, in prep). The San Joaquin Desert harbors a high diversity of endemic plant and animal species. Most of the land comprising the San Joaquin Desert has been converted to agriculture and much of the endemic flora and fauna is now rare and endangered (USFWS 1998; O'Dell and Ryan, in prep).

There is little fossil record, flora or fauna, of the Quaternary paleoclimate of the San Joaquin Desert. A fossil pollen study from Tulare Lake bed suggests the presence of Great Basin Desert-like flora in the San Joaquin Desert through the very late Pleistocene (Davis 1999). The McKittrick and Maricopa tar seeps provide information about the southernmost part of this area, with radiocarbon dates that range from approximately 15,000 to 5,000 years before present (YPB) depending on locality (Fox-Dobbs et al. 2014). Plant macrofossils of *Arctostaphylos glauca* (Ericaceae) and *Juniperus californica* (Cupressaceae) from one of the McKittrick asphalt seeps (Mason 1944) suggest the presence of cooler and wetter climate conditions in the San Joaquin Desert during the late Pleistocene, but floral data from these sites are limited. Discovery of the fossiliferous nature of the oil-sands deposit at Oil Canyon (OC) near Coalinga in the San Joaquin Valley is the northernmost locality yet found in the San Joaquin Desert and provides an important new source of data for understanding the paleoecosystems and paleoclimate of the San Joaquin Desert during an apparent period of rapid climate change during the early Holocene (Fig. 1A, B).

Figure 2. A. View of the stratified Oil Canyon deposit looking northeast, UCMP PA1340. **B.** Image of deposit showing the well-consolidated upper strata of the unit and the unconsolidated loose sand in the lower portion representing a decomposition sequence of the hydrocarbons from youngest at the top (10,150 YBP) to oldest at the bottom (>11,320 YBP). **C, D.** Closer views of the finely-stratified nature of the deposit. Note the fragments of white marine shale (Temblor) imbedded in the deposit (D).

Locality, age, and depositional setting

The fossiliferous nature of the OC site (UCMP PA1340) was discovered by the lead author (REO) in 2015 and brought to the attention of the co-authors. The site is located in a small, seasonal, tributary drainage to OC at an elevation of 396 m (1,299 ft.) and 12.4 km (7.7 mi.) north of the city of Coalinga (Fig. 1). It consists of an approximately 1.4 m thick and 465 m^2 exposed deposit of finely stratified sandy alluvium bound by oil and tar (bitumen matrix) (Fig. 2A–D). Excavations of approximately 10 m^3 of the matrix in 2015 yielded a diversity of plant, invertebrate, and vertebrate specimens (Figs. 3–5). The specimens consist of both three-dimensional and compressed carbonized plant and insect remains, while the vertebrate material includes partially articulated skeletons, isolated bones, and feathers. The age of the deposit has been radiocarbon dated from carbonized wood fragments to ≥11,320 YBP at the bottom of the unit and ~10,150 YBP at the top

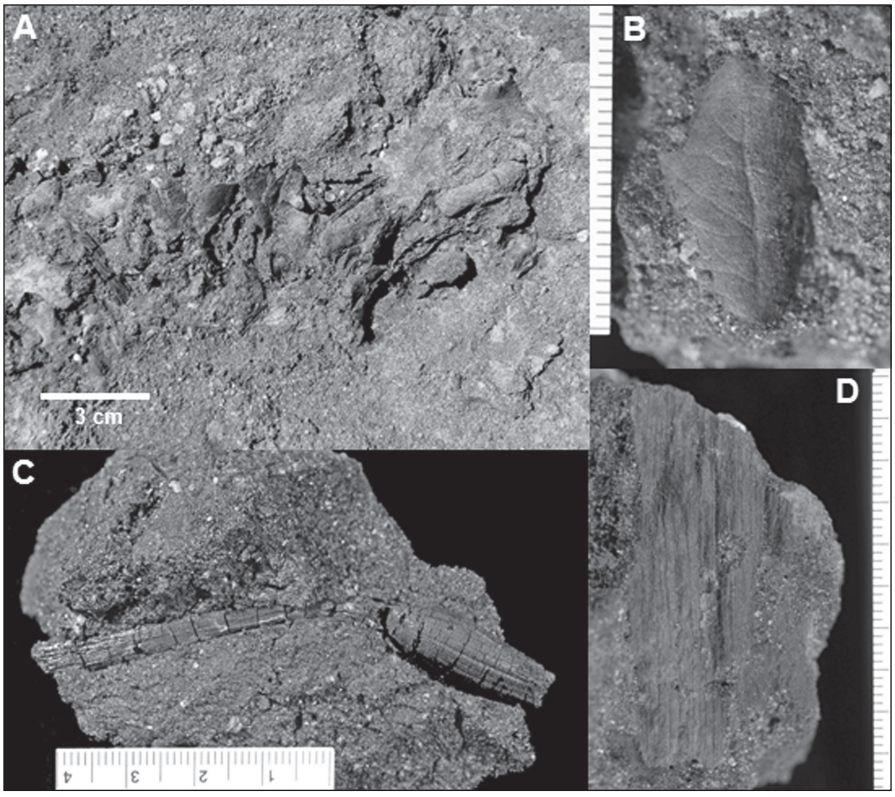

Figure 3. Oil Canyon plant megafossils. **A.** Rock surface with cluster of *Quercus john-tuckeri* leaves oriented at varying angles to the bedding plane indicative of transport prior to deposition, UCMP 401227. **B.** Detail of *Q. john-tuckeri* leaf showing venation and large tooth on upper left margin, UCMP 401210. **C.** Carbonized cast of an inflated inflorescence stem reminiscent of the buckwheat *Eriogonum nudum* var. *indictum*, UCMP 401232. **D.** Leaf fragment of *Typha* UCMP 401231. B–D: scale in mm.

(early Holocene; Beta Analytic, Miami, Florida, USA). The density and friability of the strata transitions from a hard asphalt pavement near the top (least breakdown of hydrocarbons) through moderately soft, friable oil-infused sandstone in the middle to very soft, verging on loose sand at the base due to nearly complete hydrocarbon decomposition (Fig. 2A–D). Much of the material fractures coarsely along bedding planes (Fig. 2C, D), but is fragile and highly susceptible to crumbling due to friability of the matrix. Butvar, a polyvinyl butyral resin dissolved in ethanol, was applied to most fossil specimens to stabilize them.

Oil Canyon flora and fauna

Plants – Plant specimens include fragments of woody stems that are not readily identifiable to taxon, fine leaf impressions of *Quercus john-tuckeri* (Fig. 3A, B), inflated inflorescence internal stem casts of *Eriogonum nudum* var. *indictum* (Fig. 3C), and fine leaf impressions of *Typha* sp. (Fig. 3D). Leaf impressions of *Q. john-tuckeri* are very abundant throughout the strata (>10,500 YBP) except near the very top of the deposit (<10,500 YBP) where they abruptly disappear. As seen in Figure 3A, some horizons show concentrations of leaves oriented in various planes suggesting transport prior to deposition, e.g., those in Figure 3A are at relatively steep angles to the bedding plane. *Eriogonum nudum* var. *indictum* inflated inflorescence stem casts (Fig. 3C) and leaf impressions reminiscent of *Typha* (Fig. 3D) are distributed throughout the unit from the lowermost through the uppermost layers, but do not occur in large numbers. The fragmentary nature of these specimens also suggests water and wind transport prior to burial.

Insects – Invertebrate specimens include a diversity of insects preserved as fine, detailed compressions-impressions, but preservation in some cases is a combination of compression and three-dimensional carbonized cast, e.g., the wings of the dragonfly specimen in Figure 4A are compressed, whereas the body is three-dimensionally preserved. The surfaces of many rock specimens show mass accumulations of grasshoppers (Orthoptera) (Fig. 4B) and dragonflies (Odonata). Other insect orders identified include Coleoptera (beetles) (Fig. 4C), Lepidoptera (butterflies and or moths) (Fig. 4D) and Hymenoptera (ants and bees). The large beetle (length >3.0 cm; >1.2 in.) in Figure 4C is most similar to the giant water scavenger beetles in the genus *Hydrophilus* (Hydrophilidae). They are typically found in shallow ponds with abundant vegetation, and in streams. The OC insects are distributed throughout the seep with the most finely preserved occurring near the top of the deposit, where the hydrocarbons are less decomposed. The OC seep is exceptional in California's oil-sands sites in the abundance, diversity, and fine-detailed preservation of the insects.

Vertebrates – Twelve fossil vertebrate specimens representing a minimum of four taxa were found. All specimens are still largely embedded in sediments; identifications should be regarded as tentative pending preparation of the most diagnostic elements. The largest animal represented is *Lynx rufus*, the bobcat. The fragmentary jaw (UCMP 235585) (Fig. 5A) can be assigned to this taxon based on the size and number of preserved alveoli. Rodents are represented by five partial skeletons (UCMP 235586, 276791–276794). The most complete of these (UCMP 276792) have bisected skulls with small grooved incisors (Fig. 5B), indicating these were heteromyid rodents. Comparison of the relative proportions of the cranial bones and overall size indicates these are likely *Perognathus inornatus*, the San Joaquin pocket mouse, a species that occurs in the area today.

The most notable specimens are those of birds, which include both feather impressions (Fig. 5D, F) and articulated limb material (Fig. 5C, E). At least two taxa are present. The smaller of the two (UCMP 276788) is a passeriform and includes a complete, unbroken carpometacarpus, which was compared with a range of extant taxa. In size and morphology it is most similar to *Bombycilla cedrorum* (cedar waxwing) and *Sialia currucoides* (mountain bluebird; UCMP 119166). The element is distinctly larger than that found in any sparrows, wrens, or swallows in our comparative sample and smaller than an American robin or Brewer's blackbird. This size bracketing suggests that UCMP 276788 was a 16–20 cm bird.

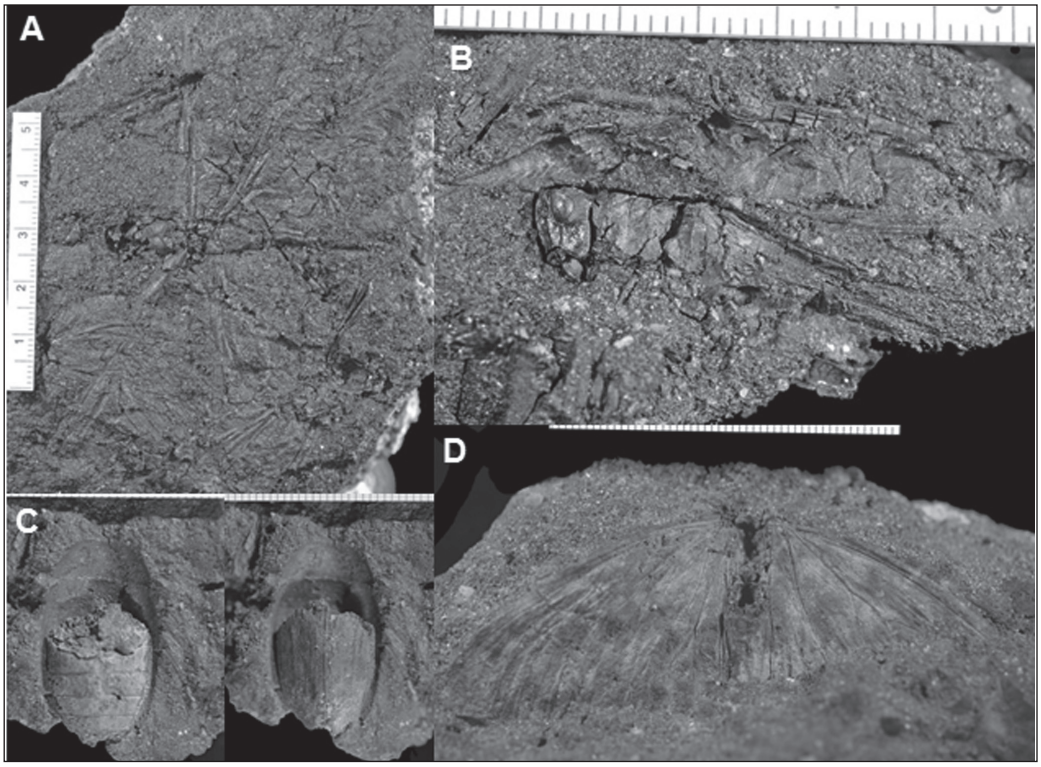

Figure 4. Oil Canyon fossil insects. **A.** Carbonized compression-cast of a large dragonfly. UCMP 401228. **B.** Carbonized cast of a grasshopper, UCMP 401233. **C.** Ventral (left) and dorsal (right) views of the impression and partial cast of the abdomen of a large beetle, cf. *Hydrophilus* sp., 401230. **D.** Compression of a relatively large lepidopteran, UCMP 401229. All scales in mm.

A second specimen, UCMP 276790, is a part and counterpart preserving bones of the hindlimb and articulated feather impressions of a bird with a tarsometatarsus approximately 50 mm in length (Fig. 5C–E). The best comparison in size is with *Corvus brachyrynychos* (American crow); it is distinctly larger than that of the American robin or scrub jays and smaller than that of the common raven.

All of these appear to represent taxa occurring in the area today. They are most notable for the varied modes of preservation and the potential for other tissues to be preserved. The preservation of the OC feathers is unusual and merits further investigation to determine if it represents one of the known modes of microbially-mediated preservation or permineralization (e.g., Davis and Briggs 1995, Briggs 2003).

Oil Canyon paleoenvironmental interpretation

The Oligocene-Miocene Temblor Formation underlies the OC seep and the small drainage (Fig. 1A, B). Adjacent and upstream of the site the Temblor strata form well-exposed slopes comprised of shale (white, diatomaceous, acidic soil) and sandstone (Fig. 6A). The OC seep consists of finely stratified alluvium in a matrix of oil and asphalt. The exposed area of the seep is ~465 m^2 and lies at the southwestern edge of the watershed area (~100 km^2) at an elevation of 396 m (1299 ft.) (Fig. 6B). The watershed's western boundary extends up to ~442 m (1450 ft.), the eastern and southern boundaries near ~475 m (1560 ft.), with the present drainage channel extending to an elevation of ~415 m (1360 ft.) (Fig. 6B). The alluvial sediments consist of sand and gravel eroded from sandstone in the eastern portion of the drainage and white Temblor marine shale fragments eroded from the northern and southern portions of the drainage. Since the deposit contains representative rock types from the entire drainage, it may be assumed that the deposit also contains plant material from species representative from throughout the small drainage during that time (Fig. 6B). Invertebrate and vertebrate fossil species are likely representative of the local fauna. Current average annual temperature at the site is about 17.6°C (63.7°F) and average annual precipitation is about 178 mm (7 in.). The dominant vegetation type of the drainage is typical of upland areas of the San Joaquin Desert and includes *Atriplex polycarpa* (Chenopodiaceae), *Eriogonum fasciculatum* var. *polifolium* (Polygonaceae), *Gutierrezia californica* (Asteraceae), and *Eastwoodia elegans* (Asteraceae). Herbaceous perennial species include *Eriogonum nudum* var. *indictum* (Polygonaceae; restricted to the marine shale), *Marah fabacea* (Cucurbitaceae), and

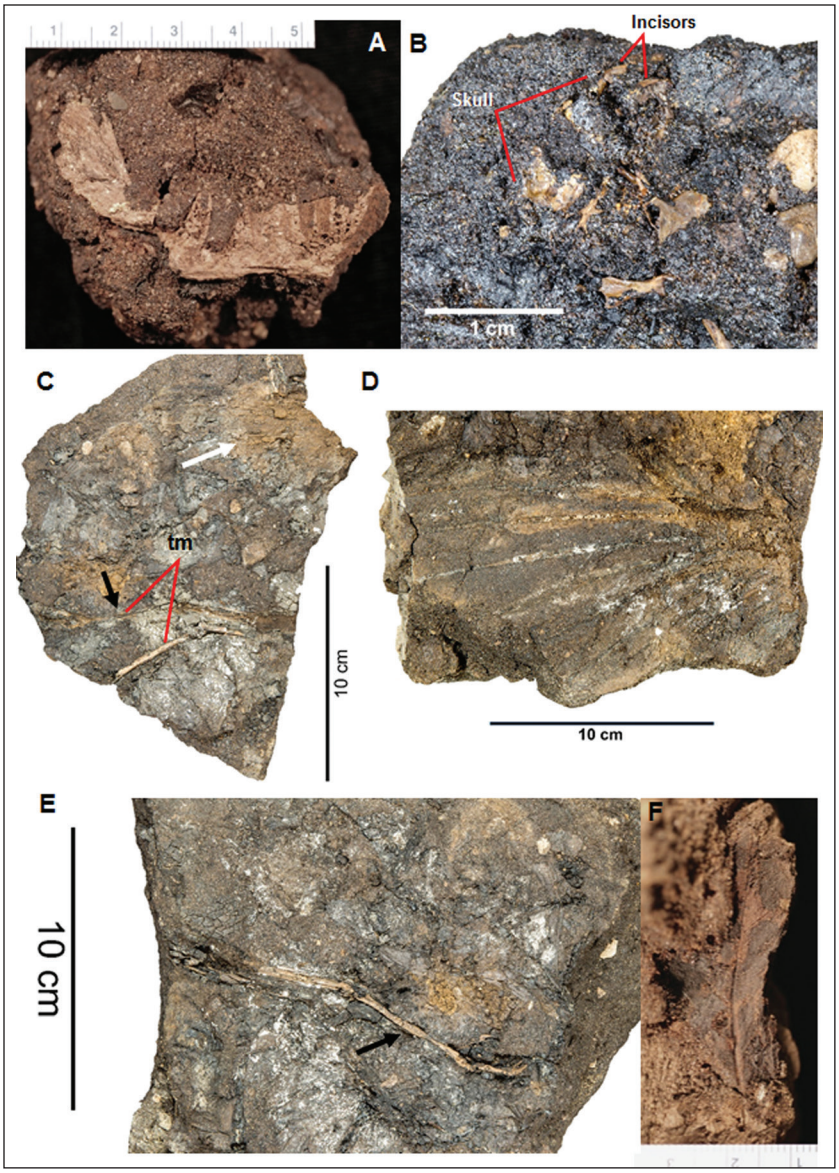

Figure 5. Oil Canyon fossil vertebrates. **A.** Lower jaw of a bobcat, *Lynx rufus,* UCMP 235585. **B.** Partial skull and associated skeletal elements preliminarily identified as a pocket mouse, *Perognathus inornatus*, UCMP 276792. **C–D.** Remains of partial legs and feathered wing or tail (white arrow in C) of medium-sized bird, UCMP 276790. Tarsometatarsals (**tm**) labeled and black arrow in C points to the counterpart of the more complete leg in D (arrow). **E.** Isolated compressed feather, UCMP 276795. A, F: scale in mm.

Poa secunda (Poaceae). The nearest *Quercus john-tuckeri* to the site occurs on Temblor shale approximately 12 km (~7.5 mi.) north-northwest and 91 m (~300 ft.) higher in elevation than the OC seep. There is no perennial water present in the drainage upstream of the deposit and no *Typha* sp. grow in the area today.

The OC seep contains fossils of two upland plant taxa, *Quercus john-tuckeri* and *Eriogonum nudum* var. *indictum*, and one obligate perennial wetland taxon, *Typha*, indicating the presence of dry upland habitat on the slopes and localized perennial wetland within the drainage bottom. We hypothesize that oil, asphalt, and water seeped to the surface in the drainage bottom not far upslope from the seep, forming a small pond where oil and asphalt were suspended on the water's surface. *Typha* would have grown on the edges of the pond providing habitat for water beetles and other aquatic insects. Terrestrial insects and small vertebrates including reptiles, birds, and rodents attracted to the water may have fallen into the pond, and become trapped in oil and asphalt on the surface. Potentially, larger vertebrates may also have become trapped, but their bodies remained within the deeper pond basin.

During flash flood events in spring and summer, sediment and upland plant material may have been washed into and through the pond, mixing with *Typha* leaves and the entrapped insects and small vertebrates, and then overflowing and accumulating as layered strata downstream of the pond. The flash flood events occurred with a frequency of once every three to four years based on the total number of distinct strata counted in the deposit. The pond overflowing to an alluvial fan-type depositional environment would explain the presence of *Typha* leaves; the presence of mass accumulations of insects (water surface accumulation); the presence of only small vertebrates (surface float); and the finely stratified nature of the deposit. The hypothesized pond basin, which may contain large vertebrate fossils, is suspected to be buried by sediment immediately upslope of the stratified OC seep. This hypothesis will be tested using augers to sample the deeper, covered portion of the basin.

Quercus john-tuckeri leaf impressions are abundant throughout the deposit, but the remains of other woody plant species that dominate at slightly cooler (15.5°C; 60°F) and wetter (279 mm; 11 in.) climates in the region are entirely absent. Those species include *Q. douglasii*, *Pinus sabiniana*, *Q. berberidifolia*, and *Arctostaphylos glauca*. Curiously, although *Juniperus californica* commonly co-occurs with *Q. john-tuckeri*, even at its warmest, driest locations, no macrofossils that may be attributed to *Juniperus* have been found in the deposit.

The abundance and distribution of *Q. john-tuckeri* throughout the stratified deposit provides clear evidence for climate change in the early Holocene at the western margin of the San Joaquin Valley, eastern edge of the central Southern Coast Ranges. Leaf impressions of the species are abundant throughout the seep, but abruptly disappear near the top of the unit. The species is currently absent from the OC watershed, with the nearest extant

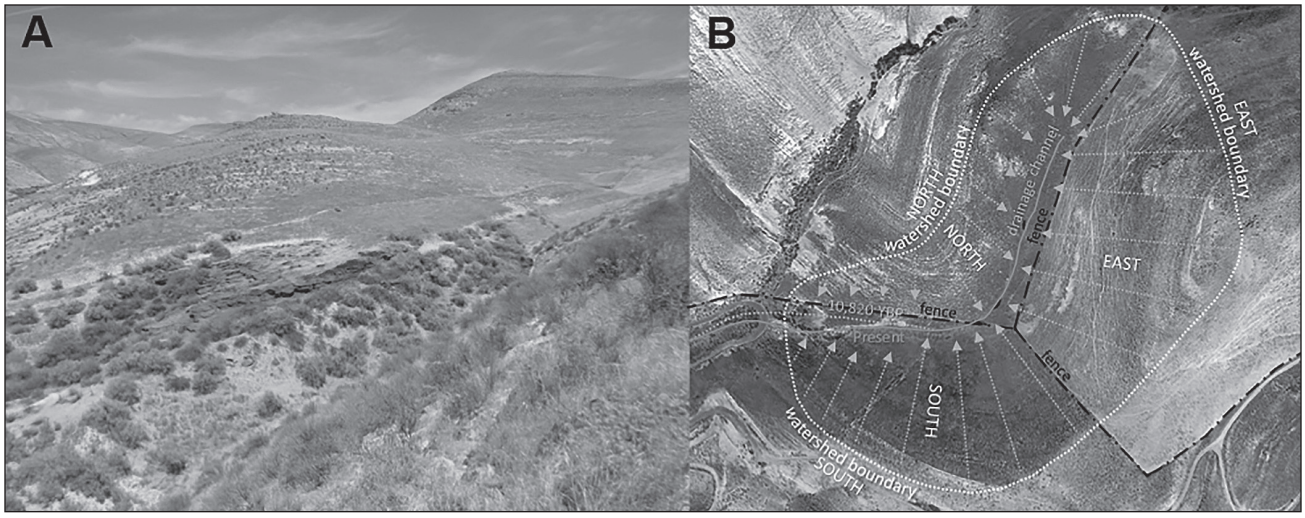

Figure 6. A. View of the Oil Canyon locality looking northeast (dark brown, center of photo) showing the small drainage upslope and current vegetation. The deposit is surrounded by *Atriplex polycarpa*. *Eriogonum nudum* var. *indictum* occurs immediately uphill from the deposit. *Eriogonum fasciculatum* var. *polifolium*, *Gutterezia californica*, and *Eastwoodia elegans* occur on the hillslope in the foreground and on the ridge in the background. **B.** Google Earth satellite view of the Oil Canyon deposit (far left edge of the dotted white polygon) and the extent of the drainage. Sandstone is located in the eastern part of the drainage and marine shale in its northern and southern portions. Dot-lined arrows indicate dominant direction of water flow and movement of sediment. Solid line indicates the position of the current drainage channel.

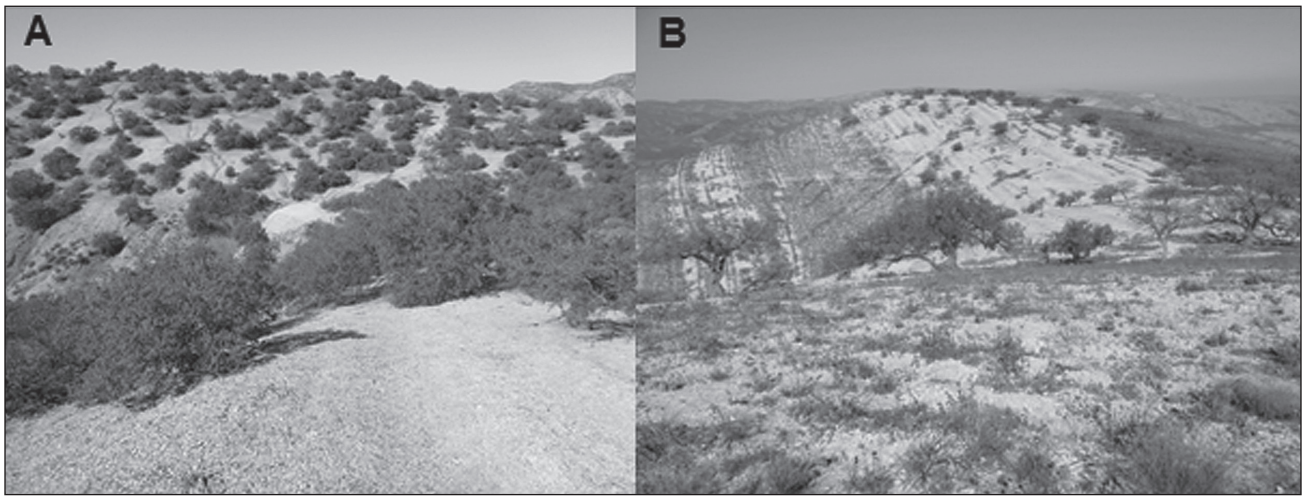

Figure 7. A. ~11,310 YBP Oil Canyon analog plant community. *Quercus john-tuckeri* is abundant. Lat. 36.388536°, Lon. -120.489775°. **B.** ~10,800 YBP Oil Canyon analog plant community. *Quercus john-tuckeri* greatly declines in abundance and disappears by 10,500 YBP as the climate becomes warmer and drier and transitions to the San Joaquin Desert. Lat. 36.358679°, Lon. -120.407082°

population located 12 km (~7.5 mi.) north-northwest and 91 m (300 ft.) higher in elevation (Figs. 7, 8). The climate at the nearest extant *Q. john-tuckeri* population and others in the region is cooler (~16.1°C; 61°F) and wetter (267 mm; ~10.5 in.) than the OC seep (~17.6°C, 64°F; ~178 mm,7 in.). Simply using the present-day OC area geographic distribution of *Q. john-tuckeri*, its temperature and precipitation requirements, and apparent population decline in the OC watershed by ~10,150 YPB, suggests the OC area climate since this time has warmed by at least 1.5°C and average annual precipitation has declined by about 50%.

Currently, the distribution of *Q. john-tuckeri* occurs just outside of the San Joaquin Desert, at its margins. The apparent rapid disappearance of *Q. john-tuckeri* post 10,500 YBP from the OC site suggests expansion of the current San Joaquin Desert climate and ecosystems into the Coalinga area by the early Holocene (Fig. 8). The early Holocene timeline for establishment of the San Joaquin Desert is also supported by the work of Raven and Axelrod (1978), with Davis' paleoclimate estimates from Tulare Lake fossil pollen data showing temperature and precipitation values approaching those of today's SJD by 7,000 YPB (see Fig. 4 in Davis, 1999).

Acknowledgements

We thank the AERA Energy Corporation for access and facilitating our request to excavate the site by providing backhoe assistance, the Museum of Vertebrate Zoology for access to modern comparative mammals, David Strauss for the specimen images in Figures 6B–E, and comments

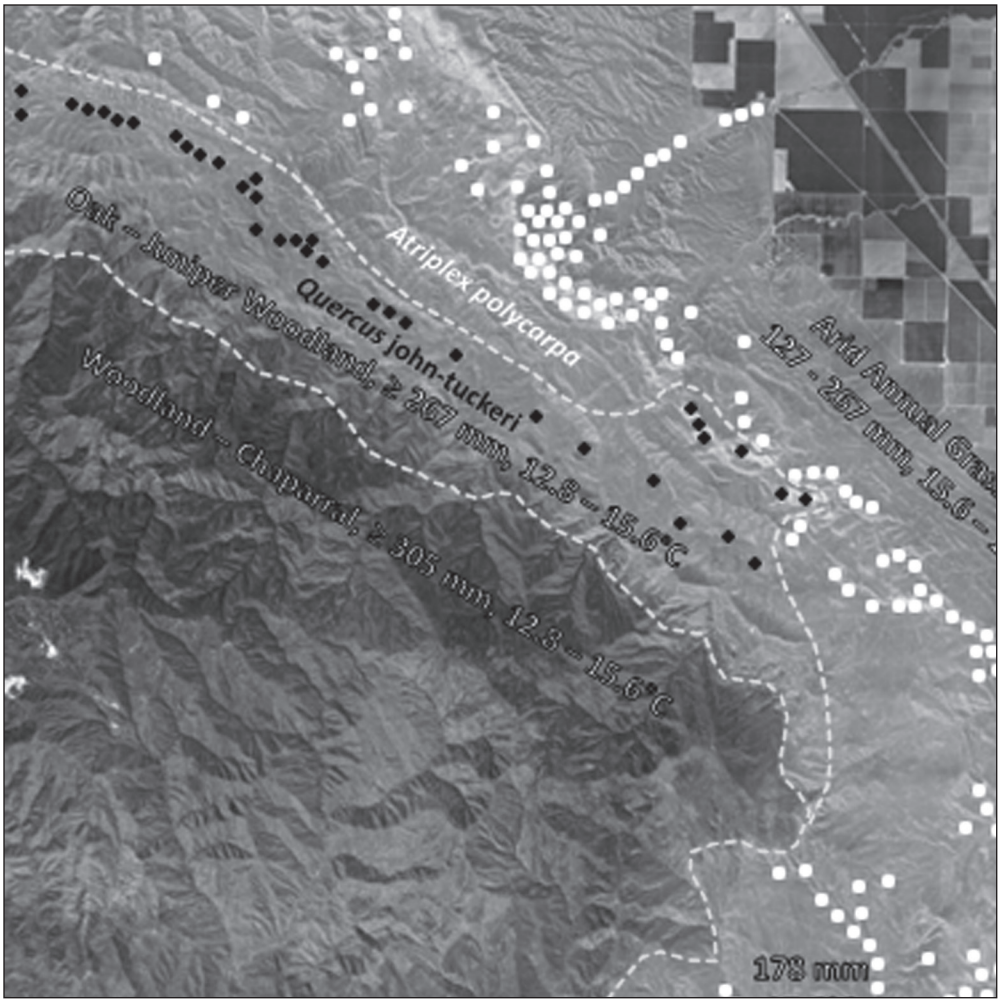

Figure 8. Google map satellite view of Oil Canyon oil seep fossil deposit ( ), and climate relative to the current distribution of *Atriplex polycarpa* (○) and *Quercus john-tuckeri* (●). The climate and vegetation of the Oak-Juniper Woodland zone is interpreted to have extended to the area of the Oil Canyon site to at least 10,500 YBP and gradually increased in elevation as the climate became warmer and drier through the early Holocene, giving way to the current San Joaquin Desert flora, represented here by *A. polycarpa*.

from an anonymous reviewer that improved the paper. Support for this project was provided to DME, PAH, BDR and MIE by the University of California Museum of Paleontology Annie Alexander Endowment. We also wish to thank the Bureau of Land Management for providing support to REO making this study possible. It was also facilitated by a National Science Foundation grant for Advancing the Digitization of Biological Collections (NSF grant #PEN-1503671) to DME. This is UCMP Contribution No. 2081.

Literature cited

Briggs, DE, 2003. The role of decay and mineralization in the preservation of soft-bodied fossils. Annual Review of Earth and Planetary Sciences, 31(1), pp.275-301.

Chaney RW and HL Mason. 1933. A Pleistocene flora from the asphalt deposits at Carpenteria, California. In: Studies of the Pleistocene paleobotany of California. Pp. 45–79, Carnegie Institution of Washington, DC.

Davis OK. 1999. Pollen analysis of Tulare Lake, California: Great Basin-like vegetation in Central California during the full-glacial and early Holocene. Review of Palaeobotany and Palynology 107:249–257.

Davis, PG, and Briggs, DE, 1995. Fossilization of feathers. Geology, 23(9), pp.783-786.

Fox-Dobbs, K, RG Dundas, RB Trayler, and PA Holroyd. 2014. Paleoecological implications of new megafaunal ^{14}C ages from the McKittrick tar seeps, California. Journal of Vertebrate Paleontology 34:220-223, DOI:10.1080/02724634.2013.791694

Germano DJ, LR Saslaw, Cypher BL, EA Cypher, and LM Vredenburgh. 2011. The San Joaquin Desert of California: Ecologically misunderstood and overlooked. Natural Areas Journal 31:138–147.

Mason HL. 1944. A Pleistocene flora from the McKittrick asphalt deposits of California. Proceedings of the California Academy of Sciences 25:221–234.

O'Dell RE and AB Ryan. In prep for Madroño. Mojave Desert microrefugia on south aspect hillslopes of the San Joaquin Desert: An ecological model for projected future climate change.

Raven PH and DI Axelrod. 1978. Origin and relationships of the California flora. University of California Press, Berkeley, CA.

Northern flying squirrel (*Glaucomys sabrinus*) from Kuffel Canyon, San Bernardino Mountains, California

Tom Howe and Peg Eby Howe
P.O. Box 1231, Lake Arrowhead, CA, peby2thowe@cs.com

Flying squirrels were first noted in the San Jacinto Mountains in 1897, with populations subsequently described in the San Bernardino and San Gabriel Mountains, making the Transverse Ranges in California the southernmost populations of the northern flying squirrel, *Glaucomys sabrinus*. In recent history, they have not been observed in the San Jacinto or the San Gabriel Mountains, but are still regularly sighted in the San Bernardino Mountains, giving wildlife biologists concern that *G. sabrinus* southern populations are becoming threatened or endangered.

In July of 2016, Peggy Howe and I began assisting in observations of Northern flying squirrels after answering an inquiry in the local newspaper placed by the San Diego Natural History Museum (SDMH) and the California Department of Fish and Wildlife (CDFW). After meeting with SDNHM and CDFW researchers, we were given an observer's kit that included a "critter camera", a suet holder and suet, an instructional DVD, and directions to download and post photos on iNaturalist.org. We were hoping to gain more information about the nocturnal *G. sabrinus*, which we had previously encountered at our home in Kuffel Canyon in the San Bernardino Mountains. We were interested in examining events that resulted in the flying squirrels "stranding" away from populations in the southern Sierra Nevada and Tehachapi Mountains.

Flying squirrels are represented by two species: the northern flying squirrel *Glaucomys sabrinus* ranging from Alaska to southern California, and southern flying squirrels, *G. volans*, in the eastern part of the United States. Flying squirrels represent a widespread and successful mammalian species over time in North America that is indicative of specific habitat constraints. Its presence in southern California is most recently related to climatic changes at the end of the Pleistocene that also precipitated the emergence of the Mojave Desert, finalizing their isolation.

During the first fifteen days of observation, we collected more than 400 different photos of the squirrels eating and cavorting on our deck and the adjacent trees, thirty-five feet above the canyon floor. This spurred us to invest in our own cameras to gain more angles and views, including videos, of the squirrel activity.

We began further research to expand our background knowledge of Glaucomys. Our interest in our local flying squirrels converged with our ongoing fossil preparation and study activities, when we recalled ancestral Petauristodon flying squirrel fossils collected from early Miocene rocks, 16ma, in nearby Cajon Pass. Since our modern local squirrel populations are considered the southernmost occurrence of northern flying squirrel we became interested in gaining a better understanding of their original distribution in the mountains of southern California. Three isolated populations initially described by Rhoads in 1897 occurred in the San Jacinto, San Bernardino, and San Gabriel Mountains in Southern California's Transverse Ranges. However, they have become conspicuously absent in the San Jacinto and San Gabriel Mountains. In 1944 Willet mentioned that flying squirrels probably were present in the San Gabriels, and Vaughan noted in 1954 that Sabrinus californicus (Glaucomys sabrinus?) occurred in the San Gabriel Mountains, though there are no recorded museum observations, and no recorded sightings (Brylski, 1998).

In contrast, in the San Bernardino Mountains, *Glaucomys* have been visibly active. However, the Center for Biological Diversity voiced concerns that the San Bernardino Mountains' populations are also in danger and may be going the way of the San Jacinto and San Gabriel Mountain population. There is specific concern for habitat being compromised and destroyed.

Glaucomys prefer pine/deciduous forest ranging in elevation from 4000 to 8000 feet, living in tree hollows and stick/branch nests. There is a definitive correlation between specific slope delineation; flying squirrels prefer gentler, less steep slopes and are absent in steeper forests. Populations in old growth tree stands are denser, particularly in trees with abundant snags and tree hollows (also found in Kuffel Canyon). Squirrels can adapt to young trees, but populations are adversely affected by fragmentation of habitat. Open spaces hinder *Glaucomys* movement to, and habitation of, unoccupied areas. Fragmentation and loss of habitat are the probable causes for the isolation of *Glaucomys*' populations. Conifer and hardwood seed, acorns and other nuts, native fruits, insects, lichen, fungi, and tree resin are common food. The Kuffel Canyon population also eats truffles, lichen, dogwood berries in season, and—wherever available—bird seed mixes from residents' bird feeders. In our observations, the canyon flying squirrel population was actually "less than threatened" because of the prolific consumption of bird seed from our feeders. In Kuffel

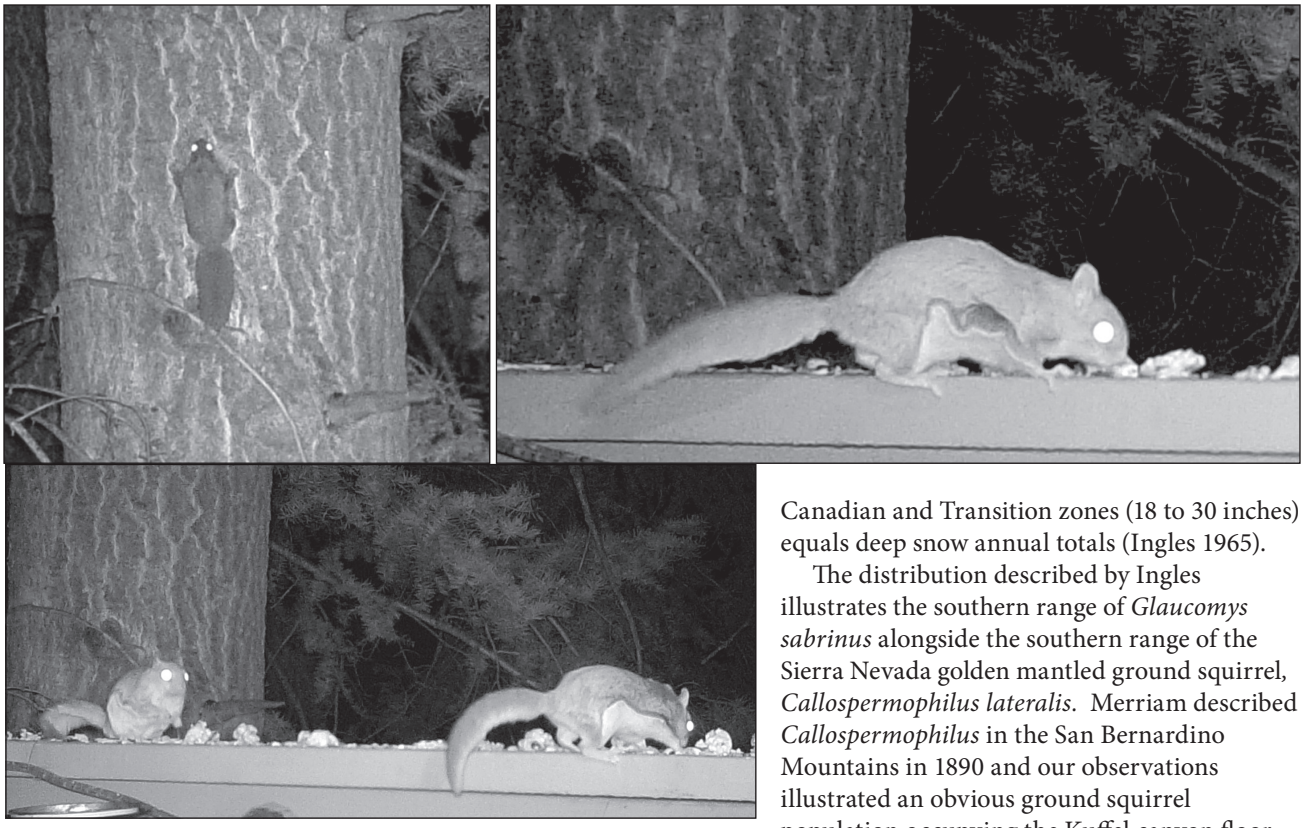

Flying squirrels at Kuffel Canyon, San Bernardino Mountains. Upper left image shows squirrel in landing position.

Canyon, flying squirrels exist quite comfortably with humans. Healthy squirrels appear in snow, rain, and fog, not out of necessity but out of convenience when seasonal food items aren't available. Conversely, when dogwood berries were available our bird feeders and suet were remarkably untouched.

Glaucomys southernmost occurrence was likely a result of significant climate change at the start of the interglacial approximately 11,500 years ago, which completely altered potential squirrel habitat and range. "Quaternary climatic fluctuation and associated changes in location and extent of forest habitats…" which precipitated "geographically isolated peripheral populations in high-elevation habitats at the, southern extremes of each species, (*G. sabrinus* and *G. volans*) range." (Arbogast 2007). The initial Sierra Nevada uplift 7 Ma (million years ago) and the onset of the uplift of the San Bernardino Mountains 3 Ma began the initial isolation of *Glaucomys* southern range. The habitat of *Glaucomys* described by Ingles (1965) included: "forested areas of yellow pine, red fir, spruce, hemlock, and redwood forest in Transition and Canadian life zones…". The Sierra Nevada squirrel population is part of the Canadian life zone (25 to 30 inches of precipitation annually, fir/aspen forest). The San Bernardino Mountain squirrels live in the Transition life zone (open deciduous, Ponderosa pine forest, 18 -26 inches of precipitation annually). The yearly precipitation average between the Canadian and Transition zones (18 to 30 inches) equals deep snow annual totals (Ingles 1965).

The distribution described by Ingles illustrates the southern range of *Glaucomys sabrinus* alongside the southern range of the Sierra Nevada golden mantled ground squirrel, *Callospermophilus lateralis*. Merriam described *Callospermophilus* in the San Bernardino Mountains in 1890 and our observations illustrated an obvious ground squirrel population occupying the Kuffel canyon floor below the Dogwood trees, among the fungi, the lichen, and below the bird feeders on our deck. It is likely, *Glaucomys* and *Callospermophilus* are utilizing extremely similar food sources within the Transition zone biota detailed by Ingles (1965).

References

Arbogast, B. S. (2007, Aug). A Brief History of the New World Flying Squirrels: Phylogeny, Biogeography, and Conservation Genetics. *Journal of Mammalogy*, Vol.88, Issue 4, pg(s) 840-849. Retrieved August 14, 2016 from http://www.bioone.org/doi/full/10.1644/06-MAMM-S-322R1.1

Basgall, M. (2003, February). Squirrels' Evolutionary Family Tree Reveals Influence of Climate, Geology. *Duke Today*, Retrieved August 14, 2016, from https://today.duke.edu/2003/02/squirreltree0302.html.

Brylski, P. V. (1998). San Bernardino flying squirrel, *Glaucomys sabrinus californicus*, in Bolster, B.C., editor. 1998. Terrestrial Mammal Species of Special Concern in California. Draft Final Report prepared by P.V. Brylski, P.W. Collins, E.D. Pierson, W.E. Rainey and T.E. Kucera. Report submitted to California Department of Fish and Game Wildlife Management Division, Nongame Bird and Mammal Conservation Program for Contract No.FG3146WM.

Ingles, L. G. (1965). *Mammals of the Pacific States, California, Oregon and Washington*. Stanford University Press, Stanford, California.

Reynolds, R. E. (1991) "Biostratigraphic Relationships of Tertiary Small Vertebrates from Cajon Valley, San Bernardino County, California", San Bernardino County Museum Association Quarterly, Vol. 38, Fall 1991.

Fecundity and reproductive phenology of female Agassiz's desert tortoises (*Gopherus agassizii*) in the Sonoran Desert region of Joshua Tree National Park

Jeffrey E. Lovich[1,*], Shellie R. Puffer[1], Mickey Agha[2], Joshua R. Ennen[3], Kathie Meyer-Wilkins[4], Laura A. Tennant[1], Amanda L. Smith[5], and Michael S. Vamstad[6]

[1]*U.S. Geological Survey, Southwest Biological Science Center, 2255 North Gemini Drive, Flagstaff, AZ 86001, USA*

[2]*Department of Wildlife, Fish, and Conservation Biology, University of California, Davis, One Shields Avenue, Davis, CA 95616, USA*

[3]*Tennessee Aquarium Conservation Institute, Tennessee Aquarium, 175 Baylor School Rd, Chattanooga, TN 37405, USA*

[4]*19233 Stratford Way, Apple Valley, CA 92308, USA*

[5]*University of Arizona, College of Architecture, Planning and Landscape Architecture, 1040 Olive Road, Tucson, AZ 85719, USA*

[6]*National Park Service, Joshua Tree National Park, 74485 National Park Drive, Twentynine Palms, CA 92277-3597, USA*

**Corresponding author: e-mail: jeffrey_lovich@usgs.gov*

Effective conservation of any species requires detailed knowledge of population vital rates (births and deaths). Sensitivity of populations to human-induced and natural stresses can result in population declines or extinction in extreme cases. Agassiz's desert tortoise (*Gopherus agassizii*) is federally protected as a threatened species. Many monitored populations throughout the range in portions of Arizona, California, Nevada and Utah have experienced declines (Averill-Murray et al. 2012; Esque et al. 2010; Lovich et al. 2014a) since final listing occurred in 1990. These declines occurred despite the fact that *G. agassizii* is well-studied (Lovich and Ennen 2013) and more than $100 million dollars were expended on recovery actions (U.S. General Accounting Office 2002) in the first 12 years after listing, rising to $200 million dollars more recently (Averill-Murray et al. 2012).

Most research on *G. agassizii* has focused on populations living the in the Mojave Desert of California (Ernst and Lovich 2009), especially research on their reproductive ecology (e.g., Averill-Murray et al. 2014; Henen 2002; Rostal et al. 1994; Turner et al. 1986; Turner et al. 1984; Wallis et al. 1999). Comparatively little is known of this aspect of their life history near the southern distributional limit of their range in the California portion of the Sonoran Desert other than research conducted near Palm Springs, California (Agha et al. 2013; Ennen et al. 2012; Lovich et al. 2012; Lovich et al. 2014b; Lovich et al. 2015) and limited information from Joshua Tree National Park (Lovich et al. 1999). Given the ecoclimatological differences between the Mojave and Sonoran deserts, it is possible that reproductive attributes such as clutch size, clutch frequency and clutch phenology differ between the two ecoregions.

We studied the reproductive ecology of *G. agassizii* at two locations in the Sonoran Desert portion of Joshua Tree National Park during two time periods. From 1997–1999 we studied a population in the Pinto Basin, an area characterized largely by relatively flat, gently sloping terrain with a creosote bush/bursage scrub plant community. During 2015 and 2016, we radiotracked a separate population of tortoises about 20 km south along the Cottonwood Road entrance to the Park. This area

Figure 1. Radiograph of a female Agassiz's desert tortoise from Joshua Tree National Park taken 3 June 2015. Note the presence of two clutches of eggs: one with four eggs in the middle that is thickly-shelled, and another, more thinly-shelled, consisting of five eggs. A penny is visible for scale in the upper left, and the radio transmitter and antenna are visible on the right shoulder of the tortoise.

was at the base of the steep, boulder-strewn Cottonwood Mountains grading south onto tilted bajadas interspersed with ironwood, blue palo verde, smoke tree, and ocotillo "woodlands". Four to seven females were monitored each year and X-rayed about once every 10 days from April-July to determine their reproductive condition (Figure 1). Droughts occurred during several years, and 1998 and 2015 were characterized by wet El Niño conditions.

Across all years, mean clutch size was 4.3 ± 0.27 eggs/clutch, clutch frequency was 1.78 clutches/female/year, and mean X-ray egg width was 36.51 ± 0.13 mm, all of which are comparable to other published studies both in the Sonoran and Mojave deserts of California. Our results support earlier published findings that *G. agassizii* utilize a bet-hedging strategy of consistently producing small clutches almost every year, even during times of low annual primary productivity. However, during one year (1997) following a short drought, all radioed females in our study forwent reproduction, failing to produce shelled eggs. Regionally warmer climate in the Sonoran Desert of California appears to have an effect on the timing of egg production, as the earliest dates of egg visibility in our study (April 6) were approximately two weeks earlier than the earliest dates reported for *G. agassizii* in the Mojave Desert. In all years but one following exceptional rainfall, the tortoises in our study concluded reproductive efforts by mid-June, about two weeks earlier than in Palm Springs during approximately the same time period (Lovich et al. 2012). The exception was 1998 when shelled eggs in second clutches were visible in X-radiographs into July.

Literature cited

Agha, M., J. E. Lovich, J. R. Ennen, and E. Wilcox. 2013. Nest-guarding by female Agassiz's desert tortoise (*Gopherus agassizii*) at a wind-energy facility near Palm Springs, California. Southwestern Naturalist 58:254-257.

Averill-Murray, R. C., C. R. Darst, K. J. Field, and L. J. Allison. 2012. A new approach to conservation of the Mojave Desert tortoise. BioScience 62:893-899.

Averill-Murray, R.C., L.J. Allison, and L.L. Smith. 2014. Nesting and reproductive output among North American tortoises. Biology and Conservation of North American Tortoises, (eds. D. Rostal, E.D. McCoy, & H.R. Mushinsky), pp. 110–117. Johns Hopkins University Press, USA.

Ennen, J. R., J. E. Lovich, K. P. Meyer, C. Bjurlin, and T. R. Arundel. 2012. Nesting ecology of a population of *Gopherus agassizii* at a utility-scale wind energy facility in southern California. Copeia 2012:222-228.

Ernst, C. H., and J. E. Lovich. 2009. Turtles of the United States and Canada, Second Edition. Baltimore, Johns Hopkins University Press.

Esque, T. C., K. E. Nussear, K. K. Drake, A. D. Walde, K. H. Berry, R. C. Averill-Murray, A. P. Woodman et al. 2010. Effects of subsidized predators, resource variability, and human population density on desert tortoise populations in the Mojave Desert, USA. Endangered Species Research 12:167-177.

Henen, B. T. 2002. Energy and water balance, diet, and reproduction of female desert tortoises (*Gopherus agassizii*). Chelonian Conservation and Biology 4:319-329.

Lovich, J. E., P. Medica, H. Avery, K. Meyer, G. Bowser, and A. Brown. 1999. Studies of reproductive output of the desert tortoise at Joshua Tree National Park, the Mojave National Preserve, and comparative sites. Park Science 19:22-24.

Lovich, J., M. Agha, M. Meulblok, K. Meyer, J. Ennen, C. Loughran, S. Madrak, and C. Bjurlin. 2012. Climatic variation affects clutch phenology in Agassiz's desert tortoise *Gopherus agassizii*. Endangered Species Research 19:63-74.

Lovich, J. E., and J. R. Ennen. 2013. A quantitative analysis of the state of knowledge of turtles of the United States and Canada. Amphibia-Reptilia 34:11-23.

Lovich, J. E., C. B. Yackulic, J. Freilich, M. Agha, M. Austin, K. P. Meyer, T. R. Arundel, J. Hansen, M.S. Vamstad, and S.A. Root. 2014a. Climatic variation and tortoise survival: has a desert species met its match? Biological Conservation 169:214-224.

Lovich, J. E., M. Agha, C. B. Yackulic, K. Meyer, C. Bjurlin, J. R. Ennen, T. R. Arundel, and M. Austin. 2014b. Nest site characteristics, nesting movements, and lack of long-term nest site fidelity in Agassiz's desert tortoises (*Gopherus agassizii*) at a wind energy facility in southern California. California Fish and Game 100:404-416.

Lovich, J. E., J. R. Ennen, C. B. Yackulic, K. Meyer-Wilkins, M. Agha, C. Loughran, C. Bjurlin, M. Austin and S. Madrak. 2015. Not putting all their eggs in one basket: bet-hedging despite extraordinary annual reproductive output of desert tortoises. Biological Journal of the Linnean Society 115:399-410.

Rostal, D.C., V.A. Lance, J.S. Grumbles, and A.C. Alberts. 1994. Seasonal reproductive cycle of the desert tortoise (*Gopherus agassizii*) in the eastern Mojave Desert. Herpetological Monographs 8:72-82.

Turner, F. B., P. A. Medica, and C. L. Lyons. 1984. Reproduction and survival of the desert tortoise *(Scaptochelys agassizii*) in Ivanpah Valley, California. Copeia 1984:811-820.

Turner, F. B., P. Hayden, B. L. Burge, and J. B. Roberson. 1986. Egg production by the desert tortoise (*Gopherus agassizii*) in California. Herpetologica 42:93-104.

U.S. General Accounting Office. 2002. Research Strategy and long-term monitoring needed for the Mojave desert tortoise recovery program, Pages ii + 53 pp, Report to Congressional Requesters. GAO-03-23.

Wallis, I. R., B. T. Henen, and K. A. Nagy. 1999. Egg size and annual egg production by female desert tortoises (*Gopherus agassizii*): the importance of food abundance, body size, and date of shelling. Journal of Herpetology 33:394-408.

Mesocarnivore visitation and interactions with Agassiz's desert tortoises (*Gopherus agassizii*) and their burrows

Shellie R. Puffer[1*], Mickey Agha[2], Amanda L. Smith[3], Jeffrey E. Lovich[1*], David Delaney[4], Joshua R. Ennen[5], Jessica Briggs[6], Leo J. Fleckenstein[7], Laura A. Tennant[1], Andrew Walde[8], Terence R. Arundel[1], Steven J. Price[7], and Brian D. Todd[2]

[1]*U.S. Geological Survey, Southwest Biological Science Center, 2255 North Gemini Drive, MS-9394, Flagstaff, AZ 86001, USA*
[2]*Department of Wildlife, Fish, and Conservation Biology, University of California, One Shields Avenue, Davis, CA 95616, USA*
[3]*University of Arizona, College of Architecture, Planning, and Landscape Architecture, 1040 Olive Road, Tucson, AZ 85719, USA*
[4]*U.S. Army Construction Engineering Research Laboratory, P.O. Box 9005, Champaign, IL 61826-9005, USA*
[5]*Tennessee Aquarium Conservation Institute, Tennessee Aquarium, 175 Baylor School Road, Chattanooga, TN 37405, USA*
[6]*Colorado State University, Fort Collins, CO 80523, USA*
[7]*Department of Forestry, University of Kentucky, Lexington, KY 40546, USA*
[8]*Walde Research and Environmental Consulting, Atascadero, CA 93422, USA*
**Corresponding authors: e-mails: mpuffer@usgs.gov; jeffrey_lovich@usgs.gov*

Agassiz's desert tortoise (*Gopherus agassizii*) has been federally listed as threatened since 1990, but thus far recovery efforts have been largely unsuccessful (U.S. Fish and Wildlife Service [USFWS] 2015). Populations of *G. agassizii* suffer from declines which have been attributed to a number of factors, including increased predation pressures potentially related to climate change (Peterson 1994; Lovich et al. 2014a) and subsidized predators (Esque et al. 2010). Because of the life history characteristics of desert tortoises, increasing predation pressure can have significant effects on desert tortoise population size or structure. Therefore it is an important part of the conservation of this species to study, understand, and manage for predator-prey dynamics (USFWS 2011). Mesocarnivores, such as coyotes (*Canis latrans)*, bobcats (*Lynx rufus)*, gray foxes (*Urocyon cinereoargenteus*), skunks (family: Mephitidae*)*, and American badgers (*Taxidea taxus*), are all documented or suspected predators of various life stages of Agassiz's desert tortoises (Luckenbach 1982; Ernst and Lovich 2009). This diverse group of small- to medium-sized mammals has a diet consisting of predominantly animal protein. They can influence community structure by playing a top-down role in regulating populations of prey species at lower trophic levels (Prugh et al. 2009; Roemer et al. 2009). Mesocarnivore predation and interactions with desert tortoises are frequently reported but poorly documented with real time observations, especially due to the fact that many mesocarnivores are secretive, nocturnal animals (Peterson 1994).

Agassiz's desert tortoises are important as ecosystem engineers. They construct and maintain shelter sites that act as thermal refugia (Mack et al. 2015). Many other vertebrates are known to use tortoise burrows for various reasons as commensals, including a variety of lizards, birds, and small mammals (Woodbury and Hardy 1948; Walde et al. 2009; Walde et al. 2015). These small vertebrates are often used as prey by various mesocarnivores, and therefore the presence of these types of commensals at desert tortoise burrows may attract predators (Coombs 1979; Winegarner 1985; Toland 1991). The objective of our study was to document mesocarnivore visitation of desert tortoise burrows, and specifically determine what mesocarnivore species interact with desert tortoises or their burrows, how frequently these interactions occur, and what factors resulting from human activities influence mesocarnivore presence at burrows, such as proximity to the nearest wind turbine or road.

The study site is located at a utility-scale wind energy facility (Mesa) near Palm Springs, California. It is situated at the intersection of several ecosystems, including Sonoran Desert, Mojave Desert, montane, and coastal sage scrub (Lovich and Daniels 2000). It also has many anthropogenic features such as wind turbines, electrical transformers, and an extensive network of unpaved roads. Beginning 1 June 2013, 48 infrared motion sensor cameras were placed near the entrances of active *G. agassizii* burrows, and wildlife visitation was recorded as a series of five to ten photographs taken at 0.2 s trigger speed. One photographic set, or even multiple photographic sets triggered by the same animal within a five minute period, were considered to be one 'event' to reduce autocorrelation in our analyses. Data were downloaded every 15–30 days until the cameras were removed on 14 November 2013.

We recorded approximately 5,000 wildlife camera trap events inside or near tortoise burrows. Of these, we documented 22 mesocarnivore events; hundreds of reptile and small mammal events; thousands of bird events; and one event of an adult black bear (a macro-omnivore) and her cub (Lovich et al. 2014b). A total of 35 species were observed utilizing desert tortoise burrows, including 3 species of lizards, 4 species of snakes, 7 species of small mammals, and 14 species of birds. On two occasions, a

Figure 1. A bobcat triggers a photograph while investigating a tortoise burrow at 2122 h on 11 October 2013.

direct interaction of a mesocarnivore and a desert tortoise was recorded when a bobcat approached a sleeping desert tortoise on a burrow apron. Additionally, we recorded coyotes, gray foxes, bobcats (Fig. 1), and a western spotted skunk investigating burrow entrances. Although mesocarnivores are documented predators of various life stages of desert tortoises, no evidence of predation was observed in our study. Statistical analyses performed using generalized linear modeling also show the number of times mesocarnivores were observed at desert tortoise burrows increased closer to dirt roads and decreased closer to wind turbines.

It is possible that mesocarnivore visits to desert tortoise burrows were motivated by searching for alternative prey items or shelter. Scent marking by mesocarnivores was observed, demonstrating that some animals identified the burrow as a resource within their home range. It is also possible that the anthropogenic infrastructure of the utility-scale wind energy facility may have altered the behavior of mesocarnivores, potentially due to mechanisms such as ground vibrations and sound emissions. Our results suggest that mesocarnivore visits to burrows arise from complex interactions between burrows, the local food web, and the anthropogenic landscape, and these visits do not necessarily result in predation on tortoises. The multitude of species associated with desert tortoise burrows emphasizes the desert tortoises' intricate role in their ecosystem. Declining populations of *G. agassizii* may alter the availability of desert tortoise burrows that act as a resource for shelter, food, or thermal refugia for other species associated with the burrows, including mesocarnivores.

Any use of trade, product, or firm names is for descriptive purposes only and does not imply endorsement by the U.S. Government.

Literature Cited

Coombs, E. M. 1979. Food habitats and livestock competition with the desert tortoises on the Beaver Dam Slope, Utah. Pp. 132–147 in E. St. Amant (ed.), Desert Tortoise Council Proceedings of 1979 Symposium. Desert Tortoise Council, Long Beach, California.

Ernst, C. H., and J. E. Lovich. 2009. Turtles of the United States and Canada, 2nd Edition. Johns Hopkins University Press, Baltimore, 827 pp.

Esque, T. C., K. E. Nussear, K. K. Drake, A. D. Walde, K. H. Berry, R. C. Averill-Murray, A. P. Woodman, W. I. Boarman, P. A. Medica, J. Mack, and J. S. Heaton. 2010. Effects of subsidized predators, resource variability, and human population density on desert tortoise populations in the Mojave Desert, USA. Endangered Species Research 12:167–177.

Lovich, J. E., and R. Daniels. 2000. Environmental characteristics of desert tortoise (*Gopherus agassizii*) burrow locations in an altered industrial landscape. Chelonian Conservation Biology 3:714–721.

Lovich, J. E., D. Delaney, J. Briggs, M. Agha, M. Austin, and J. Reese. 2014b. Black bears (*Ursus americanus*) as a novel potential predator of Agassiz's desert tortoises (*Gopherus agassizii*) at a California wind energy facility. Bulletin of the Southern California Academy of Sciences 113:34–41.

Lovich, J. E., C. B. Yackulic, J. Freilich, M. Agha, M. Austin, K. P. Meyer, T. R. Arundel, J. Hansen, M. S. Vamstad, and S. A. Root. 2014a. Climatic variation and tortoise survival: Has a desert species met its match? Biological Conservation 169:214-224.

Luckenbach, R. A. 1982. Ecology and management of the desert tortoise (*Gopherus agassizii*) in California. Pp. 1–39 in R. B. Bury (ed.), North American Tortoises: Conservation and Ecology. U.S. Department of the Interior, U.S. Fish and Wildlife Service, Wildlife Research Report 12.

Mack, J. S., K. H. Berry, D. M. Miller, and A. S. Carlson. 2015. Factors affecting the thermal environment of Agassiz's desert tortoise (*Gopherus agassizii*) cover sites in the central Mojave Desert during periods of temperature extremes. Journal of Herpetology 49:405–414.

Peterson, C. C. 1994. Different rates and causes of high mortality in two populations of the threatened desert tortoise *Gopherus agassizii*. Biological Conservation 70:101–108.

Prugh, L. R., C. J. Stoner, C. W. Epps, W. T. Bean, W. J. Ripple, A. S. Laiberte, and J. S. Brashares. 2009. The rise of the mesopredator. BioScience 59:779–791

Roemer, G. W., M. E. Gompper, and B. Van Valkenburgh. 2009. The ecological role of the mammalian mesocarnivore. BioScience 59:165–173.

Toland, B. 1991. Spotted skunk use of a gopher tortoise burrow for breeding. Florida Scientist 54:10–12.

U.S. Fish and Wildlife Service. 2011. Revised recovery plan for the Mojave population of the desert tortoise (*Gopherus agassizii*). U.S. Fish and Wildlife Service, Pacific Southwest Region, Sacramento, California, USA.

U.S. Fish and Wildlife Service. 2015. Range-wide monitoring of the Mojave Desert tortoise (*Gopherus agassizii*): 2013 and 2014 annual reporting. Report by the Desert Tortoise Recovery Office, U.S. Fish and Wildlife Service, Reno, Nevada, USA.

Walde, A. D., A. Currylow, and A. M. Walde. 2015. Discovery of a new burrow associate of the Desert Tortoise (*Gopherus agassizii*), the Long-nosed Leopard Lizard (*Gambelia wislizenii*). Herpetology Notes 8:107–109.

Walde, A. D., A. M. Walde, D. K. Delaney, and L. L. Pater. 2009. Burrows of desert tortoises (*Gopherus agassizii*) as thermal refugia for horned larks (*Eremophila alpestris*) in the Mojave Desert. The Southwestern Naturalist 54:375–381.

Winegarner, M. S. 1985. Bobcat family utilize tortoise burrow. Florida Field Naturalist 13:32–33.

Woodbury, A. M., and R. Hardy. 1948. Studies of the desert tortoise, *Gopherus agassizii*. Ecological Monographs 18:145–200.

From butterflies to bighorns: Multi-dimensional species-species and species-process interactions may inform sustainable solar energy development in desert ecosystems

Steven M. Grodsky[1,2], Kara A. Moore-O'Leary[3], and Rebecca R. Hernandez[1,2]
[1]*Department of Land, Air and Water Resources, University of California – Davis, Davis, CA 95616*
[2]*Energy Ecology Center, Davis, CA 95616*
[3]*Pacific Southwest Region, U. S. Fish and Wildlife Service, Sacramento, CA 95819*

ABSTRACT — Solar energy development is a contemporary, anthropogenic driver of disturbance in desert ecosystems. Although solar energy may contribute to global deep decarbonization and mitigation of climate change through emissions reductions, net effects of solar energy development on desert ecosystems are largely unknown. Siting, construction, and operation of solar energy infrastructure in natural desert environments may affect interactions between soils, plants, and animals, inducing "bottom-up" and/or "top-down" trophic responses to disturbance and modified environmental conditions. Understanding species-species and species-process interactions may elucidate systematic effects of solar energy development on desert ecosystem function and integrity more comprehensively than addressing effects of solar energy on individual desert biosphere constituents exclusively. Further, ecological effects of disturbance-mediated biological invasions specific to solar energy development in deserts are intrinsically better demonstrated when interactions among native and invasive species and ecological processes are considered. If "umbrella" species are used in studies at the desert ecology-solar energy nexus, we recommend adoption of species representative of species-process interactions at a variety of spatial scales. Consideration of these novel and integrative approaches to solar ecology may help guide future research objectives, thereby leading to better understanding of the complex interface between solar energy and desert conservation.

Introduction

Concerns regarding finite fossil fuel resources, increased energy demand, and climate change, coupled with current socioeconomic drivers, have bolstered global renewable energy development (Shafiee and Topal 2009, IPCC 2011). Solar energy in the form of ground-mounted, utility-scale [i.e., ≥1 megawatt$_{DC}$ (MW)] photovoltaic and concentrating solar power technologies is a burgeoning renewable energy option that has exhibited significant industrial growth over the last decade (Bazilian et al. 2013, Hernandez et al. 2014**a**). Favorable environmental conditions and abundant public lands (e.g., Bureau of Land Management) may make deserts of the southwest United States the ideal recipient environment for solar energy development (BLM 2012, Hernandez et al. 2015). Although solar energy may help advance decarbonization, sensitive desert ecosystems may be imperiled by solar energy development (Lovich and Ennen 2011). For example, construction of solar facilities creates a series of biophysical disturbances, including grading of soils and vegetation removal, which in turn may affect biota via "bottom-up" trophic interactions (e.g., degraded soils → decreased plant growth → reduced food and cover for wildlife; Hernandez et al. 2014**b**). Meanwhile, aridland Southwest ecosystems support exceptional biodiversity and many endemic, threatened and endangered species already stressed by climate change (Lovich and Bainbridge 1999, Mittermeier et al. 2001).

Studies explicitly quantifying potential effects of solar energy development on desert ecosystems are limited (Lovich and Ennen 2011); however, these data and the body of desert-disturbance literature provide a conceptual framework for guiding sustainable solar energy development (Moore-O'Leary et al., *in review*). Few past studies measured effects of solar energy facilities on biodiversity (e.g., birds – McCrary et al. 1986). However, effects of other forms of anthropogenic disturbance on desert ecosystems have been documented, which may

Figure 1. Some potential indirect effects of solar energy development on soils, plants, and animals in desert ecosystems. Photo credit: Steve Grodsky.

inform future ecosystem response to disturbance caused by solar energy development (Hernandez et al. 2014**b**).

Solar energy development may negatively or positively affect desert ecosystems via direct (i.e., proximate) or indirect effects. Proximate effects of solar energy on biodiversity may involve direct mortality of organisms, theoretically ranging from soil microbes to birds of prey. Disturbance from construction of solar facilities and associated infrastructure may lead to mortality of exposed soil biota and burrowing and/or fossorial wildlife, including reptiles and invertebrates (Lovich and Bainbridge 1999). Increased densities of transmission lines stemming from solar facilities may result in increased avian fatalities caused by direct collision with power lines (Smith and Dwyer 2016). Extreme heat radiating from beams of light reflected by heliostats towards central heating towers in concentrating solar plants may incinerate flying wildlife, including birds (McCrary et al.1986, Walston et al. 2016) and butterflies (S. M. Grodsky, *unpublished data*). Anecdotal evidence suggests that some bats, birds, and insects may mistake the surface of photovoltaic solar panels for water (i.e., lake effect), leading to direct mortality via collision with panels (Greif and Siemers 2010). Similarly, light pollution from photovoltaic panels and heliostats may attract insects (Horváth et al. 2009), which in turn may increase the likelihood of collision for insectivorous birds.

Given the extensive web of possible ecological interactions driven by anthropogenic disturbance, indirect effects of solar facilities on desert ecosystems are inherently more numerous than proximate effects. We describe some of the primary, potential indirect effects of solar energy development on desert ecosystems in Fig. 1. Lovich and Ennen (2011) and Hernandez et al. (2014**b**) comprehensively reviewed potential indirect effects of solar energy facilities on desert ecosystems.

Potential effects of solar energy development on desert ecosystems have been covered in several reviews and a conceptual framework for solar energy and the land-energy-ecology nexus is forthcoming (i.e., Moore-O'Leary et al., *in review*). While existing reviews mostly present potential effects of solar energy development on individual species or groups of species, we recognize the opportunity to enhance this framework by exploring integrative approaches to desert ecology based on species-species and species-process interactions. As such, our objectives are to: 1) exemplify how the study of trophic interactions may holistically inform systematic, desert biosphere response to solar energy; 2) demonstrate the inherent connection between disturbance-mediated invasion ecology and native-invasive species interactions and resultant ecosystem effects; and 3) examine how species-process interactions may help inform selection of study species representative of spatially explicit ecosystem processes. Consideration of these novel and integrative approaches to solar ecology may guide future research objectives, thereby leading to better understanding of the complex interface between solar energy and desert conservation.

Trophic interactions: the Milkweed–Monarch Nexus example

When considering effects of solar energy development on entire desert ecosystems, a "bottom-up" approach can be useful for elucidating interconnected rather than isolated impacts on representative desert systems (Hunter and Price 1992). For example, studying how solar energy facilities affect soils, which in turn affect milkweed, which in turn affect monarchs (and vice versa) may reveal mechanisms behind ecological responses to associated disturbance and environmental change (Fig. 2**a**). In contrast, measuring response of one individual element of the milkweed-monarch nexus (i.e., the series of interactions between soil, milkweed, and monarchs and indirectly associated flora and fauna) to solar energy-mediated disturbance may uncover patterns, but is less

likely to reveal causation. Pre-construction site preparation at solar facilities may vary in intensity (e.g. blading vs. mowing), which dictates levels of soil disturbance and consequently plant community response (Hernandez et al. 2014**b**). Heliostat presence and configuration may alter microclimate conditions of soils via shading and altered water dynamics, including availability, runoff, and erosion (Tanner et al. 2014). Soil variables may in turn affect milkweed physiology, photosynthetic rate, and overall plant health, potentially leading to variable rates of herbivory and granivory (Moore-O'Leary et al., *in review*). Positive and/or negative feedback loops between individual milkweed plants and monarch caterpillars may result in further "bottom-up" implications, including individual caterpillar survival. We summarize trophic interactions of the milkweed-monarch nexus in Fig. 2**b** (*see also* Fig. 2**a**).

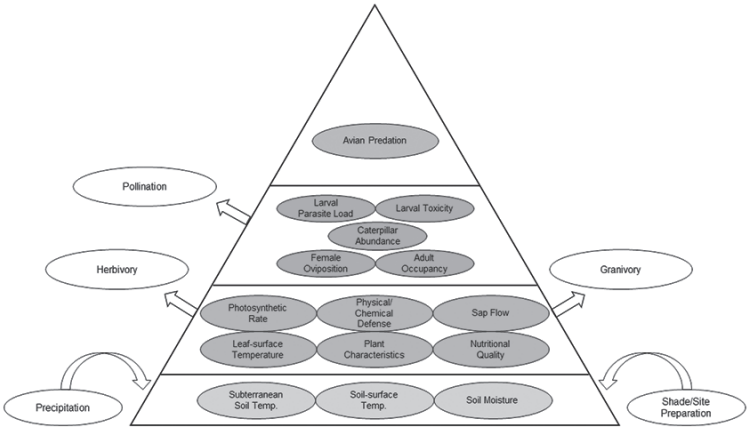

Figure 2**a**. Measurements informing "bottom-up" effects of solar facility site preparation, configuration, and operations on desert monarchs at the Ivanpah Solar Facility. From bottom to top of pyramid: soil (beige), Mojave milkweed (green), monarch butterfly (orange), and monarch predators (blue).

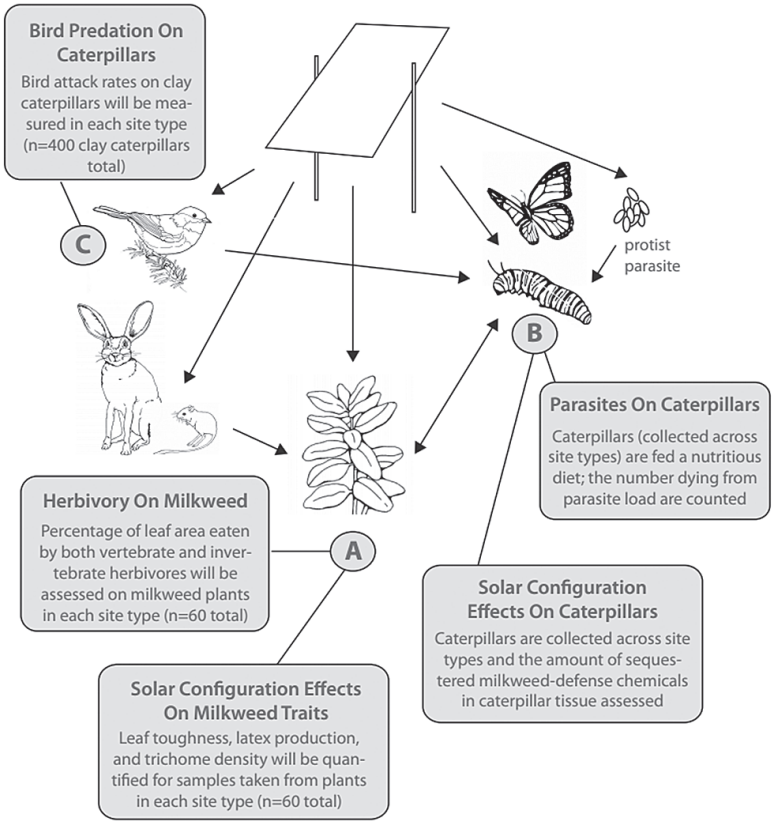

Figure 2**b**. Interconnectedness between Mojave milkweed, monarch, and their associates potentially affected by solar energy infrastructure.

Disturbance-mediated biological invasions interactively affect desert ecosystems

Conceptually, ecological disturbance events often lead to "winners and losers" (Grodsky et al. 2016**a**). For example, clearcutting a forest will benefit wildlife species that thrive in early-successional vegetation communities, but will inherently displace wildlife reliant on mature forest canopy. In desert ecosystems, the "winners" responding to disturbance may mostly consist of invasive species [e.g., Saharan mustard (*Brassica tournefortii*)] because native desert species are often not adapted to frequent or large-scale disturbances. Colonization of invasive species may be further facilitated by the fact that native desert communities often take centuries to naturally restore following disturbance (Lovich and Bainbridge 1999).

Anthropogenic disturbance in the form of solar energy development may alter desert disturbance regimes and facilitate spread of invasive species (e.g. invertebrates, plants), which in turn may reshape species-species and species-process interactions (D'Antonio and Vitousek 1992, Lovich and Ennen 2011, Tanner et al. 2014). In general, disturbance in deserts often facilitates colonization of invasive species (Gelbard and Belnap 2003, Zink et al. 2015). While endemic, desert flora and fauna are adapted to a relatively narrow range of environmental conditions and historically infrequent disturbance, invasive species can occur within a wide range of environmental and habitat conditions (Sakai et al. 2001). Roads associated with solar facilities also may perpetuate spread of invasive plants (Gelbard and Belmap 2003). Once populations of invasive species become established in and around solar facilities, propagules may disperse to adjacent undisturbed desert and potentially outcompete native species for resources (Zink et al. 1995). For example, invasive ants may outcompete native, seed-dispersing ants for nesting substrate and food; ecosystem-wide effects may consequently occur, since many invasive ants are far less efficient seed dispersers than the native ants they displace

(Warren et al. 2015). Disturbance from solar energy development may facilitate the spread of flammable, invasive annual plants [e.g., cheatgrass (*Bromus tectorum*)] in the desert Southwest (Brown and Minnich 1986, Abatzoglou and Kolden 2011). Southwestern deserts and the species that live there are not fire-adapted (Brooks and Esque 2002). As such, increased fire frequency resulting from a combination of abundant, invasive plant fuels and higher likelihood of anthropogenic ignitions could have potentially severe ecosystem effects in deserts, adversely affecting sensitive plant communities and wildlife (Esque et al. 2003, Lovich et al. 2011).

Species representative of systematic interactions in the desert ecosphere

At first glance, the concept of "umbrella" species appears to contradict our proposed conceptual framework aimed at addressing effects of solar energy on system-wide, ecological interactions. However, "umbrella" species have disproportionate conservation value relative to some other species in that their protection often cascades to multiple species. Further, "umbrella" species also promote and help fund desert ecology research. For example, conservation concerns regarding solar energy development in deserts of the southwest United States have largely centered on the Agassiz's desert tortoise (*Gopherus agassizii*), a federally threatened species and important ecosystem engineer (Lovich and Ennen 2011). Indeed, the desert tortoise serves as a useful "umbrella" species in areas currently supporting utility-scale solar energy development, potentially extending protection from some anthropogenic disturbance to entire desert communities (Tracy and Brussard 1994). If "umbrella" species must be used, we suggest including study species that encapsulate species-process interactions at multiple spatial scales to enhance desert conservation in the face of solar energy development. We exemplify use of two such species for desert ecosystems threatened by solar energy development: 1) desert bighorn sheep (*Ovis canadensis nelson*) to address integrated, landscape-level effects on animal movement; and 2) monarch butterfly (*Danaus plexippus*) to explore local-scale, trophic interactions.

Desert bighorn sheep (Fig. 3) are charismatic megafauna emblematic of the ruggedness of the desert Southwest with large home ranges and expansive movements, and thus may serve as a sentinel species indicative of landscape-level effects of solar energy development on animal movement and dispersal. The desert bighorn sheep, a subspecies of bighorn sheep, has been particularly susceptible to anthropogenic changes, including habitat loss, overgrazing by livestock, diseases contracted from domestic livestock, and loss of water resources, throughout its range (Papouchis et al. 2001). Independent desert bighorn populations are generally demographically separated by intervening desert, making connectivity among populations essential for maintaining genetic diversity in the regional metapopulation (Bleich et al. 1990, Bleich et al. 1996). Fragmentation caused by highways has blocked gene flow and significantly reduced genetic diversity in bighorn sheep (Epps et al. 2005). Solar energy development and associated roads and corridors also may increase fragmentation in desert landscapes at large-spatial scales (Lovich and Ennen 2011), which in turn may similarly restrict desert bighorn movement and gene flow. Further, desert bighorns may demonstrate long-term avoidance of solar energy facilities, although they do occupy areas developed long ago for wind energy (Agha et al. 2015). Analogous avoidance behavior exhibited by mule deer (*Odocoileus hemionus*) was observed in areas supporting oil and gas development in the Intermountain West, which lead to disconnection between breeding populations of the species (Sawyer et al. 2009). Recent upgrades in GPS collar-technology enable collection of high fidelity, spatiotemporal data of individual animals; desert bighorn sheep equipped with these collars would provide sufficient data to quantify landscape-level effects of solar energy development on bighorn movement. Concurrent collection of DNA samples from these sheep populations would help researchers better understand how genetic connectivity relates to recorded movement of individuals.

Figure 3. Desert bighorn sheep (*Ovis canadensis nelson*) in the Mojave Desert. Photo credit: Rebecca Hernandez.

Monarch butterflies may be especially useful as an indicator of "bottom-up" effects of solar energy development in novel desert ecospheres. Given their holometabolous live cycle, inextricable ties to milkweed, and

contribution to ecosystem services, monarchs are model organisms for addressing trophic interactions. Further, invertebrates are excellent ecological indicators of land use change, including renewable energy development, at micro-sites with highly integrated ecological processes (Grodsky et al. 2015). Variable environmental and microclimate conditions created by solar energy infrastructure may affect soils and thereby milkweed species serving as host plants for monarchs (Moore-O'Leary et al. *in review*). In turn, overall milkweed health and fitness may affect factors contributing to monarch caterpillar survival, including cardenolide sequestration, susceptibility to predation and parasitism, and forage quality.

The western population of the monarch butterfly has precipitously declined in response to severely reduced populations of milkweed host plants, loss and reduced quality of overwintering sites along the California coast, and climate change (Monroe et al. 2017). In fact, nationwide population declines of the monarch butterfly have been so precipitous that the species currently is under consideration for listing under the Endangered Species Act, with a final protection decision scheduled for 2019. A western monarch migration route begins in southern California and passes through much of the desert Southwest, which is inhabited by several species of desert milkweed and thus serves as a spring and summer breeding-ground for the butterflies (Moore and André 2014, Xerces Society 2015).

Conclusions

Research at the nexus of solar energy development and desert ecology will be essential for informing sustainable development of solar energy in the desert Southwest. Among major renewable energy technologies, solar energy has a high propensity for large-scale development in undisturbed, sensitive ecosystems with high biodiversity (Hernandez et al. 2015). In contrast, wind energy facilities may be sited in agricultural areas with typically low biodiversity (McDonald et al. 2009), and woody biomass harvests for forest bioenergy often occur after timber harvest in industrial forests (Fritts et al. 2014, Grodsky et al. 2016**b**). We suggest that desert ecology studies on solar energy development will be enhanced by prioritizing research efforts that address species-species and species-process interactions. Specifically, we recommend that future studies focus on "bottom-up" ecological interactions, ecosystem-wide effects, and landscape-level impacts. We encourage desert researchers to consider connections and intersections of their own work with solar energy development in the desert Southwest.

Literature cited

Abatzoglou, J. T. and C. A. Kolden. 2011. Climate change in western US deserts: Potential for increased wildfire and invasive annual grasses. Rangeland Ecology and Management 64: 471–478.

Agha, M., D. Delaney, J. E. Lovich, J. Briggs, M. Austin and S. J. Price. 2015. Nelson's big horn sheep (Ovis canadensis nelsoni) trample Agassiz's desert tortoise (Gopherus agassizii) burrow at a California wind energy facility. Bulletin of the Southern California Academy of Sciences 114:58–62.

Bazilian M., *et al*. 2013. Reconsidering the economics of photovoltaic power. Renewable Energy 53:329–338.

Bleich, V. C., J. D. Wehausen, and S. A. Holl. 1990. Desert-dwelling mountain sheep: conservation implications of a naturally fragmented distribution. Conservation Biology 4: 383–390.

Bleich, V. C., J. D. Wehausen, R. R. Ramey II, and J. L. Rechel. 1996. Metapopulation theory and mountain sheep: implications for conservation. In: Metapopulations and Wildlife Conservation (ed. McCullough, D.R.). Island Press, Covelo, pp. 353–373.

BLM (Bureau of Land Management). 2012. Approved resource management plan amendments/record of decision (ROD) for solar energy development in six southwestern states.

Brooks, M. L. and T. C. Esque. 2002. Alien plants and fire in desert tortoise (*Gopherus agassizii*) habitat of the Mojave and Colorado Deserts. Chelonian Conservation and Biology 4:330–340.

Brown, D.E. and R. A. Minnich. 1986. Fire and changes in creosote bush scrub of the western Sonoran Desert, California. American Midland Naturalist 116:411–422.

D'Antonio, C. M., and P. M. Vitousek. 1992. Biological invasions by exotic grasses, the grass/fire cycle, and global change. Annual Review of Ecology and Systematics 23:63–87.

Epps, C. W., P. J. Palsbøll, J. D. Wehausen, G. K. Roderick, R. R. Ramey II, and D. R. McCullough. 2005. Highways block gene flow and cause a rapid decline in genetic diversity of desert bighorn sheep. Ecology Letters 8:1029–1038.

Esque, T. C., C. R. Schwalbe, L. A. DeFalco, R. B. Duncan, and T. J. Hughe. 2003. Effects of desert wildfires on desert tortoise (*Gopherus agassizii*) and other small vertebrates. Southwestern Naturalist 48:103–111.

Fritts, S. R., C. E. Moorman, D. W. Hazel, and B. D. Jackson. 2014. Biomass harvesting guidelines affect downed wood debris retention. Biomass and Bioenergy 70:382–391.

Gelbard J. L. and J. Belnap. 2003. Roads as conduits for exotic plant invasions in a semiarid landscape. Conservation Biology 17:420–432.

Greif, S. and B. M. Siemers. 2010. Innate recognition of water bodies in echolocating bats. Nature Communications 1.

Grodsky, S. M., R. B. Iglay, C. E. Sorenson, and C. E. Moorman. 2015. Should invertebrates receive greater inclusion in wildlife research journals? Journal of Wildlife Management 79:529–536.

Grodsky, S. M., C. E. Moorman, and K. R. Russell. 2016**a**. Forest Wildlife Management. Pp. 47-85 in G. Larocque (ed.) Ecological Forest Management Handbook. Taylor and Francis Group, LLC/CRC Press. Boca Raton, FL, USA.

Grodsky, S. M., C. E. Moorman, S. R. Fritts, D. W. Hazel, J. A. Homyack, S. B. Castleberry, and T. B. Wigley. 2016**b**. Winter bird use of harvest residues in clearcuts and the implications

of forest bioenergy harvest in the southeastern United States. Forest Ecology and Management 379:91–101.

Hernandez, R. R., M. K. Hoffacker, and C. B. Field. 2014**a**. Land-use efficiency of big solar. Environmental Science and Technology 48:1315–1323.

Hernandez, R. R., *et al*. 2014**b**. Environmental impacts of utility-scale solar energy. Renewable and Sustainable Energy Reviews 29:766–779.

Hernandez, R. R., M. K. Hoffacker, M. L. Murphy-Mariscal, G. C. Wu, and M. F. Allen. 2015. Solar energy development impacts on land cover change and protected areas. Proceedings of the National Academy of Sciences 112: 13579–13584.

Horváth G., G. Krisk, P. Malik P, and B. Robertson. 2009. Polarized light pollution: a new kind of ecological photopollution. Frontiers in Ecology and the Environment 7:317–25.

Hunter, M. D. and P. W. Price. 1992. Playing chutes and ladders: Heterogeneity and the relative roles of bottom-up and top-down forces in natural communities. Ecology 73: 724–732.

IPCC. 2011. IPCC Special Report on Renewable Energy Sources and Climate Change Mitigation. Prepared by Working Group III of the Intergovernmental Panel on Climate Change [O. Edenhofer, R. Pichs-Madruga, Y. Sokona, K. Seyboth, P. Matschoss, S. Kadner, T. Zwickel, P. Eickemeier, G. Hansen, S. Schlömer, C. von Stechow (eds)]. Cambridge University Press, Cambridge, United Kingdom and New York, NY, USA, 1075 pp.

Lovich, J.E. and D. Bainbridge. 1999. Anthropogenic degradation of the southern California desert ecosystem and prospects for natural recovery and restoration. Environmental Management 24:309–326.

Lovich, J. E. and R. Daniels. 2000. Environmental characteristics of desert tortoise (*Gopherus agassizii*) burrow locations in an altered industrial landscape. Chelonian Conservation and Biology 3:714–721.

Lovich, J. E. and J. R. Ennen. 2011. Wildlife conservation and solar energy development in the Desert Southwest, United States. BioScience 61:982–992.

Lovich, J.E., J.R. Ennen, S. Madrak, C. Loughran, K. Meyer, T.V. Arundel, and C. Bjurlin. 2011. Long-term post fire effects on spatial ecology and reproductive output of female desert tortoises at a wind energy facility near Palm Springs, California. Fire Ecology 7:75-87.

McCrary M. D., R. L. McKernan, R. W. Schreiber, W. D. Wagner, and T. C. Sciarrotta.1986. Avian mortality at a solar energy power plant. Journal of Field Ornithology 57:135–141.

McDonald R. I., J. Fargione, J. Kiesecker, W. M. Miller, and J. Powell. 2009. Energy sprawl or energy efficiency: Climate policy impacts on natural habitat for the United States of America. PLoS ONE 4:e6802. doi:10.1371/journal.pone.0006802.

Mittermeier R. A., C. G. Mittermeier, P. R. Gil, G. Fonseca, T. Brooks, J. Pilgrim, and W. R. Konstant (eds). 2002. Wilderness: Earth's Last Wild Places. Conservation International.

Moore, K. A. and J. M. André. 2014. Rare plant diversity in the California deserts: Priorities for research and conservation. Fremontia 42: 9–14.

Moore, K. A., R. R. Hernandez, D. Johnston, S. R. Abella, K. E. Tanner, A. C. Swanson, J. Kreitler, and J. E. Lovich. *In review*. Critical ecological concepts for sustainable solar energy and the land-energy-ecology nexus. In review. Frontiers in Ecology and the Environment.

Monroe, M., E. Pelton, S. McKnight, C. Fallon, D. Frey, and S. Stevens. 2017. Western Monarch Thanksgiving Count Data from 1997–2016. Available at: http://www.westernmonarchcount.org.

Papouchis, C. M., F. J. Singer, and W. B. Sloan. 2001. Responses of desert bighorn sheep to increased human recreation. The Journal of Wildlife Management 65:573–582.

Sakai, A. K., et al. 2001. The population biology of invasive species. Annual Review of Ecology and Systematics. 32 305–332.

Sawyer, H., M. J. Kauffman, and R. M. Nelson. 2009. Influence of well pad activity on winter habitat selection patterns on mule deer. Journal of Wildlife Management 73:1052–1061.

Shafiee, S. and E. Topal. 2009. When will fossil fuel reserves be diminished? Energy Policy 37:181–189.

Smith, J. A. and J. F. Dwyer. 2016. Avian interactions with renewable energy infrastructure: An update. The Condor: Ornithological Applications 118:411–423.

Tanner K. K. Moore, and B. Pavlik. 2014. Measuring impacts of solar development on desert plants. Fremontia 42.

Tracy C. R. and P. F. Brussard. 1994. Preserving biodiversity: Species in landscapes. Ecological Applications 4:205–207.

Walston L. J., K. E. Rollins, K. E. LaGory, K. P. Smith, and S. A. Meyers. 2016. A preliminary assessment of avian mortality at utility-scale solar energy facilities in the United States. Renewable Energy 92:405–14.

Warren, R. J., A. McMillan, J. R. King, L. Chick, and M. A. Bardford. 2015. Forest invader replaces predation but not dispersal services by a keystone species. Biological Invasions 17:3153–3162.

Xerces Society for Invertebrate Conservation. 2015. Monarch Migration: Spring and Fall. Available at: http://www.xerces.org/wp-content/uploads/2015/10/MonarchMap-NatureServe-10.20.png.

Zink T. A., M. F. Allen, B. Heindl-Tenhunen, and E. B. Allen. 1995. The effect of a disturbance corridor on an ecological reserve. Restoration Ecology 3:304–310.

Icebows

David K. Lynch[1] and David S. P. Dearborn[2]
[1]*Thule Scientific;* [2]*Lawrence Livermore National Laboratory*

ABSTRACT—When sunlight falls on spherical water drops (refractive index n=1.33), two bright rainbows (primary and secondary) are produced that are separated by Alexander's Dark Band. In studying rainbows that could form in other planetary atmospheres, we noticed that when n ≈1.31, the primary and secondary bows overlap. Water ice has an index near 1.31 so we investigated the possibility that transparent ice balls could produce the predicted bow. Laboratory studies show that the composite bow—*icebow*—does indeed exist. To our knowledge, no natural icebow has ever been reported.

1. Introduction

The geometrical optics of rainbows are well understood, and have been since Descartes first ray-traced them.[1] The wave theory of rainbows has also been solved.[2-3] Yet much less attention has been paid to rainbows produced in substances other than water. Seawater is known to produce rainbows at scattering angles that are slightly different than that of pure water.[4-5] Some work has also gone into possible rainbows on other planets, for example those produced by H_2O, CH_4, and H_2SO_4, each of which is known to exist in liquid form in the solar system[6-7].

While investigating rainbows from spheres with different indices of refraction, we noticed that when the refractive index n is near 1.31, the primary and secondary rainbows nearly overlap (Figure 1). Since water ice's index is about 1.31, it seemed that transparent ice spheres could produce an unusual rainbow, an "icebow". In this paper we explore this possibility.

2. Requirement for precise overlap

For the primary and secondary bows to precisely overlap, the index of refraction must be such that each bow's ray emerges from the drop traveling parallel to one another. Using geometrical optics[3,8] and the conditions for minimum deviation in a sphere, the require index is n = 1.3120125. For water ice, this index corresponds to a wavelength ~530 nm, squarely in the green part of the spectrum[9], and therefore easily seen by the eye.

Dispersion aside, this index assures that the primary and secondary bows will leave the drop travelling in the same direction, i.e., parallel to each other, though emerging from opposite sides of the drop. From the observer's view point, the scattering angle would be 134.8°, essentially 135°, and seen at 45° from the antisolar point.

To a distant observer, both bows would appear as a single bow because the light from them would be coming from the same direction. The colors would be dominated by the much brighter primary bow, and colors would be further muted by the oppositely directed dispersions.

3. Laboratory experiments.

Ice spheres and cylinders were made in a freezer and illuminated with collimated white light from an LED flashlight in a goniometer system on an optical bench. The distance between the observer and the ice ball, and between the light source and ice ball were both approximately six meters. The ice ball subtended an angle of 0.5°, an amount smaller than the width of either bow. Being close enough to the sphere to resolve it allowed us to move around the sphere and watch each bow ray come and go. Observing from a large but not infinite distance meant that the bow rays coming from the ball were not precisely parallel, but dispersion allowed us to identify each unambiguously.

Both rainbow rays were found at the expected scattering angle, 135° (Figure 3). Because of the additional internal reflection experienced by secondary rays, the two rays emerged from opposite sides of the sphere, and therefore could be seen as separate bright spots on the sphere. Surface irregularities caused by the melting ice distorted the rainbows but the bows were nonetheless unquestionably present. This was verified as the bows appeared and disappeared when the observer's line-of-sight (i.e., scattering angle) changed.

To check if both spots on the ice ball were the two sought-after rainbow rays, other spheres were examined under the same circumstances (water, acrylic and glass, n = 1.33, 1.48 and 1.52 respectively). In no case were both bow rays visible from a single location. Specifically, when viewed from a direction showing the primary bow, the secondary bow was not seen (Figure 4). This is to be expected because the spheres had refractive indices that were very different than 1.31, and thus the primary and secondary rays would not be parallel.

4. Discussion

It is not surprising that ice spheres can produce rainbows. But it is interesting that ice has exactly the right refractive index to cause the primary and secondary bows to overlap. This happens because both bows emerge from the drop at the same scattering angle.

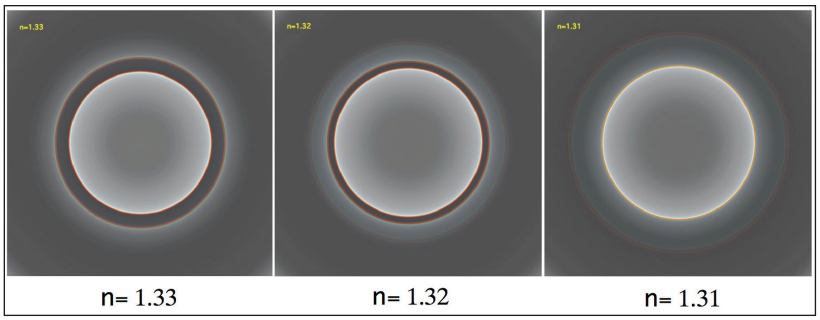

Figure 1. Rainbow simulations centered on the antisolar point. For water (n = 1.33), the familiar primary and secondary bows are evident with Alexander's Dark Band between them. As the index is reduced, the two bows come closer together until when n = 1.31, they overlap. When n < 1.3, the secondary bow is inside the primary bow.

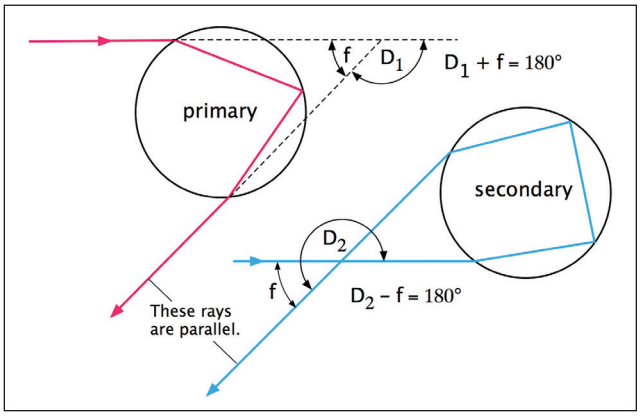

Figure 2. The conditions for perfect overlap is that D1 + D2 = 360°, where D1 and D2 are the minimum deviation angles of the primary and secondary bows, respectively.

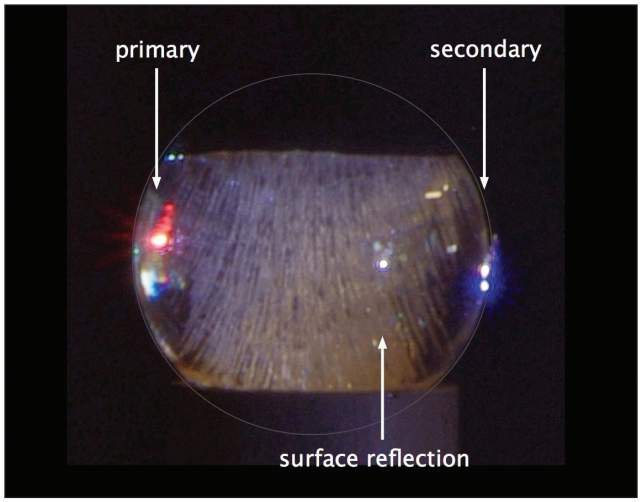

Figure 3. Ice sphere observed at a scattering angle of 135°. The primary and secondary bows are evident on opposite sides of the sphere. Irregularities in the surface distort the bows. Ice sphere was 5.3 cm in diameter and viewed from a distance of about six meters. Illumination was from a collimated white light LED flashlight.

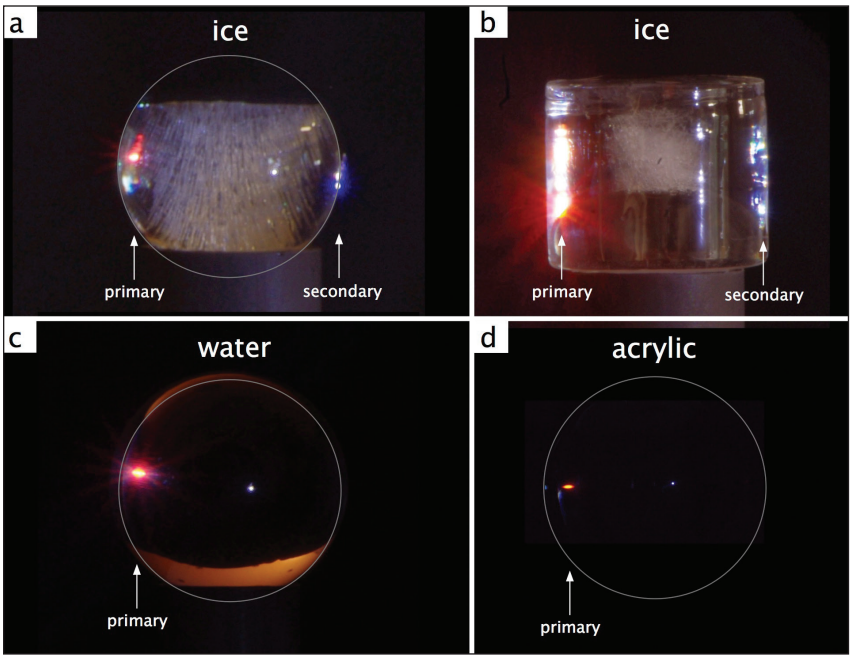

Figure 4. (4a) Ice sphere viewed at a scattering angle135°. The primary and secondary bows are evident, as they are in an ice cylinder (4b). Figures 4c and 4d (water and acrylic, respectively) viewed from the angle necessary to see the primary bow. As expected, the secondary bows are absent because they emerge from the spheres at angles that are significantly different than the scattering angles of their primary bows. The water sphere (Figure 4c) was a thin-walled hollow glass sphere filled with water, and the orange glows are due to ambient room lights. In Figure 4a, 4c and 4d, the outlines of the spheres have been drawn in.

To form natural icebows, one needs spherical or cylindrical ice particles larger than a few tens of microns in size. Such particles would need to be well separated from one another and illuminated by the sun. Possible places to look are in mixed phase clouds, sleet, hail, old snow, frozen waterfalls, and icicles.

There is abundant evidence in the cloud community that "quasi-spherical" or spherical ice particles exist in some cold clouds.[10-13] The claim that the particles are made of ice is based on *in situ* collection methods and lidar measurements showing no polarization in backscatter. Visual observations of clouds that "look like cirrus" have shown cloud coronae, though coronae can also be formed by small nonspherical particles. No rainbows have been reported in these clouds and it is not known if the particles were transparent.

Icicles offer a more accessible chance to see icebows. They are numerous

and transparent. Observing the bow is simply a matter of finding icicles with circular cross sections that are illuminated by the sun in such a way that the observer can view them 45° from the antisolar point. To our knowledge, no such natural icebow has ever been reported. It seems likely, however, that casual observers have seen icebow glints in icicles but have not recognized them as being significant or interesting.

As a final note, observers should take care to measure the image scale on their photographs, and then measure the radii or other defining feature of rainbows and ice crystal haloes. Odd radius halos are often only a degree or two different that the common halos, and such small angular distance would pass unnoticed by eye. This is especially true for an icebow, which is only three degrees larger than the primary rainbow.

5. Summary and conclusions

Theory and experiments reported here show that overlapping primary and secondary rainbows occur in ice spheres and ice cylinders. So far, no naturally-occur icebows have been reported but they should be relatively easy to observe in icicles.

References

1. Descarte, René, *Discours de la Méthode Pour Bien Conduire Sa Raison et Chercher la Vérité dans les Sciences (second appendix) La Dioptrique* (1637)

2. Mie, Gustav, "Beiträge zur Optik trüber Medien, speziell kolloidaler Metallösungen". *Annalen der Physik* **330** (3): 377–445 (1908)

3. Adam, John A., The mathematical physics of rainbows and glories, Physics Reports, Volume 356, Issue 4-5, p. 229-365 (2002)

4. See photograph by J. Dijkema. http://www.atoptics.co.uk/rainbows/seabow.htm

5. Dijkema's photograph has been reproduced many places, e.g., Lynch, D.K. and Livingston, W.C., *Color and Light in Nature*, 2nd Edition reprint, Thule Scientific, Topanga USA (2010)

6. Rainbows on Titan, http://science.nasa.gov/science-news/science-at-nasa/2005/25feb_titan2/

7. Markiewicz, W.J., E. Petrova, O. Shalygina, M. Almeida, D.V. Titov, a, S.S. Limaye, N. Ignatiev, T. Roatsch, K.D. Matz, Glory on Venus cloud tops and the unknown UV absorber, Icarus 234, 15 May, 200–203 (2014)

8. Tricker, R. A. R., *Introduction to Meteorological Optics*, London: Mills and Boon (1970)

9. Warren, S. G., and R. E. Brandt, Optical constants of ice from the ultraviolet to the microwave: A revised compilation, J. Geophys. Res., 113, (2008).

10. Baumgardner D., H. Chepfer, G. B. Raga, and G. L. Kok, The shapes of very small cirrus particles derived from in situ measurements, Geophys Res. Letters, 32, L01806 (2005)

11. Korolev, A. V., M.P. Bailey, J. Hallett, G.A. Isaac, Laboratory and In Situ Observation of Deposition Growth of Frozen Drops. J of Applied Meteorology, 43, No. 4, pp. 612–622. (2004)

12. Sassen, K., Optical Backscatter from near-spherical water, ice and mixed phase drops, Applied optics, 16(5), 1332-1341 (1977)

13. Del Guasta, M., Massimo, Marco Morandia, Leopoldo Stefanutti, Stefano Balestri, Esko Kyro, Markku Rummukainen, Rigel Kivi, Vincenzo Rizi, Bernhard Stein, Carsten Wedekind, Bernd Mielke, Renaud Matthey, Valentin Mitev, Mathilde Douard, Lidar observations of spherical particles in a- 65°C cold cirrus observed above Sodankyla (Finland) during S.E.S.A.M.E., J. Aerosol Sci., 29, 357-374 (1998)

Abstracts from proceedings: the 2017 Desert Symposium

Robert E. Reynolds, compiler
Research Associate, Desert Studies Center, bob.reynolds220@gmail.com

Barbequed burro baffles bureaucrats!

Brian Brown
China Ranch, Tecopa, CA, dates@chinaranch.com

In 1978 an incident at the Warm Springs mining camp in Death Valley resulted in the destruction of a patch of critical riparian habitat in the driest, hottest place on earth. The incident pitted the National Park Service against a private mining company, and was a test exercise in how the agency might enforce the new environmental laws that would change mining in Death Valley forever. The author was an employee at the mine at the time and a peripheral participant and observer as the story unfolded. These are personal reflections and recollections based on the incident, a forgotten but entertaining bit of Death Valley history.

Hydrogeologic framework modeling of two groundwater basins at Fort Irwin National Training Center in the Mojave Desert, California

G. Cromwell[1] and Lindsay B. Ball[2]
[1]USGS, California Water Science Center, 4165 Spruance Rd Suite 200, San Diego, CA 92101 (gcromwell@usgs.gov); [2]USGS, Crustal Geophysics and Geochemistry, DFC Box 25046, MS 964, Denver, CO 80225

As part of a broader investigation of water availability at the Fort Irwin National Training Center (NTC), a three-dimensional (3D) hydrogeologic framework model is being constructed for two groundwater basins that have potential to supply water to Fort Irwin NTC: Superior and Goldstone.

Previous studies conducted by the United States Geological Survey in Fort Irwin NTC have mapped the surficial geology of Superior and Goldstone basins, identified major faults, and defined general stratigraphic relationships. This initial characterization of the geology in the two basins was aided by the examination of cuttings from newly drilled wells, inclusion of depth-to-crystalline basement estimates derived from gravity measurements, and interpretation of airborne electromagnetic (AEM) survey lines collected throughout Fort Irwin NTC.

The new 3D hydrogeologic model incorporates the geologic maps, sections, and fault information from this initial work, and combines it with updates to the depth-to-crystalline basement, and AEM survey datasets for the two groundwater basins. From this suite of information, a 3D hydrogeologic framework model was developed by using EarthVision[1] software. The datasets are loaded into EarthVision, and used to extrapolate the subsurface extent of four lithostratigraphic units: 1) Mesozoic metamorphic and plutonic crystalline basement (Bmt); 2) Tuffaceous and volcaniclastic Miocene deposits (Tv); 3) Miocene mafic-felsic lava flows and domes (Tf); and 4) Quaternary sediments (Q). AEM resistivity zones are calibrated to the regional geology by using surficial maps and known geologic structures. In general, Bmt and Tf are highly resistive, Q is moderately resistive/conductive, and Tv is highly to moderately conductive. The thickness and extent of the Tv is particularly important as it is the primary groundwater-producing unit.

The 3D hydrogeologic model shows elevated outcrops of Bmt and Tf serve as the boundary for both Superior and Goldstone. The two basins range in thickness from ~40 to 1400 meters, and are filled primarily by interlayered sequences of Tv and Tf. Deposits of the Q unit are generally present in the uppermost 50 m of each basin and, in Superior, are divided by a thin and extensive young basalt flow. These interpretations are consistent with known geologic interpretations in Fort Irwin NTC and correspond well with AEM resistivity interpretations from neighboring groundwater basins. Quantification of the subsurface extent and structure of the four lithostratigraphic units, especially Tv and Tf, will allow for improved evaluations of groundwater availability in Superior and Goldstone basins.

[*] For descriptive purposes only and does not imply endorsement by the U.S. Government.

Timing and style of deformation of the Soda–Avawatz fault system, easternmost Eastern California Shear Zone

Andrew J. Cyr and David M. Miller
US Geological Survey, 345 Middlefield Road, MS973 Menlo Park, CA 94025, acyr@usgs.gov

The Soda and Avawatz Mountains, eastern Mojave Desert, are somewhat contiguous ranges considered the easternmost expression of the Eastern California Shear Zone (ECSZ), a NW-striking zone of distributed dextral shear that accommodates ~10% of motion along the Pacific–North American plate boundary. The eastern Soda Mountains, ~6 km west of Baker, CA, expose Precambrian and younger rocks uplifted by Mesozoic and Cenozoic faulting. Cenozoic faults include a set of roughly parallel, NW-striking sub-vertical faults that offset Tertiary and Quaternary alluvial deposits, which we refer to as the Soda–Avawatz fault zone. Recent geologic mapping of

latest Miocene and younger alluvium and Quaternary alluvial fan surfaces in the eastern Soda Mountains reveals that deformation along the S–AFZ is kinematically different than the regional ECSZ dextral deformation. Rather, evidence indicates that the S–AFZ alternated between i) folding and uplift, likely with a dextral-oblique component, in Tertiary time, followed by ii) discrete right-lateral displacement of alluvial fan surfaces developed post late Pleistocene time (~40 ka via IRSL chronology), and iii) younger uplift and incision of early Holocene (~9-14 ka) alluvial fan surfaces. This temporal pattern of deformation in the S–AFZ indicates an overall transpressional deformation regime since at least late Miocene time, punctuated by a short episode of discrete dextral strike-slip during the late Pleistocene. This observation implies that the NW-striking fault zones of the ECSZ, that are colinear with the S–AFZ to the northwest (the Avawatz fault zone) and southeast (the Bristol-Granite Mountains fault zone), should exhibit similar temporal patterns of transpression and discrete slip.

We also conducted preliminary mapping along the southeastern front of the Avawatz Mountains in order to determine the timing and nature of fault related deformation along what we refer to here as the East Avawatz fault zone (EAFZ), and how fault-related deformation might relate to the S–AFZ in the eastern Soda Mountains to the southeast. Our mapping demonstrates that i) late Pleistocene alluvial fan surfaces have been uplifted and incised along a N-NW-striking range front fault and, ii) late Pleistocene, and perhaps younger, alluvial fan deposits ~3 km from the mountain front, have been folded, possibly above a blind reverse fault. However, we found no evidence of right-lateral displacement of alluvial fan surfaces. These observations indicate that deformation along the northern part of the eastern boundary of the ECSZ has been primarily transpressional since at least late Miocene time, punctuated by a short interval of discrete fault slip. Although the S–AFZ is considered part of the ECSZ, discrete slip related to Pacific–North American plate boundary motion may be focused on to parallel strike slip faults either to the west (e.g., Red Pass fault) or to the east (e.g., to unidentified faults in Silurian valley). This conclusion suggests that the amount of compression and uplift must be better accounted for in order to better define the amount of Pacific–North American plate boundary slip accommodated by the eastern margin of the ECSZ.

The Mojave Trails National Monument presidential proclamation–Identifying the objects and values whose protection and preservation take precedence over the Bureau of Land Management's multiple use mission.

Christopher S. Dalu
Bureau of Land Management, Needles, CA

On February 12, 2016, President Barak Obama designated 1,601,441 acres of public land as the Mojave Trails National Monument. National Monuments can be designated by Congress through legislation or by the president through proclamation under the authority of the Antiquities Act of 1906. The Antiquities Act of 1906 gives the president the authority to ". . . declare by public proclamation historic landmarks, historic and prehistoric structures and other objects of historic or scientific interest that are situated on [public] land to be national monuments." Proclamations designating national monuments list the various objects of scientific or cultural interest that are to be protected. Such protection takes precedence over the BLM's multiple use mission, which is consistent with the second half of FLPMA § 302(a) "The Secretary shall manage the public lands according to the principles of multiple use and sustained yield . . . except where a tract of such public land has been dedicated to specific uses according to any other provisions of law it shall be managed in accordance with such law. The BLM follows the procedures within BLM Manual 622 – National Monuments, National Conservations Areas, and Similar Designations to implement the intent of the proclamation. The primary focus of this poster will be to provide those parts of Mojave Trails National Monument Proclamation that describe the objects that are to be protected. Visual elements will include a map of the monument, photos of some of the objects, and general references to the Antiquities Act and statistics on National Monuments.

Icons in peril: ecology and conservation of the *Encelia* alliance in México and the U.S.

Christopher T. DiVittorio
Scholar in Residence, University of California, Institute for México and the U.S. (UC-MEXUS), chrisdivittorio@gmail.com

The *Encelia* alliance comprises 25 described taxa from *Encelia*, *Enceliopsis* and *Geraea*, and together make up one of the most striking adaptive radiations found among the angiosperms. These species inhabit some of the most extreme environments on Earth including Death Valley, the San Felipe Desert, and even the Atacama Desert of Chile and Peru. They are also charismatic, with the Panamint daisy *Enceliopsis covillei* appearing on the historic logo of the California Native Plant Society. Other species such as *Encelia farinosa* are model ecophysiology study organisms and ubiquitous features of Mojave and Sonoran Desert landscapes. However, there are also a number of species—among them some

of the most unique in the alliance—that are at serious risk of being lost. For example, *Encelia ravenii*, one of the only white-flowered species in the entire tribe, is known from a single population of only 15 individuals with recent declines of up to 75%. Another species known from a single population of less than 100 individuals is *Encelia densifolia*, which possesses a large number of unique ancestral traits, but is actively hybridizing with the widespread *Encelia farinosa*. Motivated by recent rains and the potential for a good seed production year, we are beginning a campaign (www.EnceliaAlliance.org) to promote, study, and conserve some of these taxa, leveraging partnerships with academics, non-governmental organizations (NGOs), and federal agencies forged over the past decade. Our first steps will involve seed banking, genomic analysis, and propagation of five of the rarest taxa, by partnering with academics from UNAM and officials from the federal Vizcaíno Biosphere Reserve, to set up community-based Jardines Botanicos/Viveros de Plantas Raras Nativas. These Viveros will allow us to "close the loop" by providing genetically healthy seed and plantings for restoration efforts, and would eventually become independent, promoting sustainable tourism and generating alternative income streams for fishing-dependent communities in the San Felipe and Vizcaino Deserts. We are also trying to "close the loop" in the US by partnering with NGOs and private donors to identify and propagate additional species that are at-risk of imminent extinction or loss of genetic diversity. Together, our program seeks to provide a safety net against extinction for species from overlooked ecosystems in the Mojave, Sonoran, and Great Basin deserts.

Analysis of vegetation diversity, density and cover on maturing substrates of an alluvial fan at Zzyzx, CA

Adrian Escobar[1], Andrew Roxas[2], Maureen Kelley[2]
Advisers—Drs. Darren Sandquist and Jennifer Garrison
Departments of 1Geological Sciences and 2Biological Science, California State University, Fullerton<aescobar24@csu.fullerton.edu

A comparative analysis of vegetation on maturing alluvial fan substrates was performed using cover, density and diversity characteristics of perennial shrubs. Development of desert varnish and pavement on lobes of the Springer and Zzyzx alluvial fans near the Desert Studies Center (Zzyzx, California) were used as indicators of relative substrate age. Based on previous studies we hypothesized that intermediate-aged lobes would possess higher plant cover and density than older and younger lobes because intermediate substrates are less active than younger channels and more permeable than significantly varnished older lobes. We also hypothesized that there would be greater plant diversity at the distal end of the fan, regardless of substrate age, due to higher water input and retention, and greater nutrient availability. Our results showed that plant density was highest on the intermediate-aged lobes (0.21 plants/m2), plant cover was highest on youngest lobe (6.5%), and plant diversity was higher at distal portions of the fan (0.12 plants/m2). While the results show a trend in support of our initial hypotheses, larger sample sizes are needed for greater confidence in these finding and to better understand alluvial fan vegetation development within the Mojave.

Along the troubled trail: travels with Nicholas Porter Earp past every bloody massacre site on the Mormon Wagon Road through the Mojave (The 1864 Diary of Sarah Jane Rousseau)

Walter Feller
PO Box 401780, Hesperia, Ca. 92340-1780 walter@aeve.com

Travel on the Mormon wagon road/Salt Lake Road between Salt Lake City, Utah, and San Bernardino, California, was laborious as it crossed through southwestern Utah, southern Nevada and the arid Mojave Desert in the mid-nineteenth century. The jagged trail was known to be fraught with topographical challenges, danger, mystery and massacres at many places along the way.

The captain of one wagon train in 1864 was Nicholas Porter Earp, patriarch of the Earp clan (Virgil, 16 year old Wyatt, Morgan, James, and Warren). Nick had a temper and could definitely make things interesting. The wagon train was made up of four families, with diarist Sarah Jane Rousseau observing and recording his moments of raucous leadership.

Rousseau kept a daily record of locations, mileage traveled, weather, and events. Through her diary we can follow the trip from Mountain Meadows to the Cajon Pass in California and examine not only her hardships and trials, but the history of wildness and violence that had recently preceded the company along the way.

Geology and timing of megabreccias at Black Butte, Mesquite Valley, NV and relation to the Stateline fault system

[1]R.J. Fleck, [1]J.P. Calzia, and [2]O.T. Rämö
[1]U.S. Geological Survey, 345 Middlefield Rd, Menlo Park, CA 94025; [2]Dept of Geosciences and Geography, University of Helsinki Finland FI-00014

Carbonate megabreccias of Paleozoic limestone and dolomite, emplaced in the Resting Springs Formation at Black Butte in Mesquite Valley, Nevada, have been used to constrain the offset on part of the dextral Stateline Fault System (SFS) (Guest et al., 2007). Seismic reflection studies by Scheirer et al. (2010) indicate that Black Butte is located immediately southwest of and near the northern end of the Mesquite Valley segment of the SFS. In Pahrump Valley, the next basin to the north, the SFS steps to the west, resulting in a left-stepping, en-echelon fault system between Mesquite and Pahrump Basins.

The resulting contractional domain between right-lateral en-echelon faults is documented by the dramatic 90° counterclockwise rotation of structural trends in Black Butte from about N50°W at its southeast end to about S40°W at the northwest, a distance less than 5 km.

The megabreccias are composed of variably brecciated slide blocks or sheets, ranging from several meters to two kilometers, tectonically overriding and locally deforming Tertiary lacustrine deposits and volcanic rocks of the Resting Springs Formation. The megabreccias are depositionally overlain by fanglomerate deposits that are now tilted 20° to 40° to the northeast. West of the northern part of Black Butte a thin-bedded limestone with a clearly non-marine present-day 87Sr/86Sr of 0.71869±1 represents the oldest part of the Resting Springs Formation. The fresh-water limestone is overlain by biotite latite flow(s), thin-bedded porcellanite, tuffaceous siltstone, and volcanic ash that were subsequently overridden by the megabreccia at the northern end of Black Butte. Biotite from the latite yielded a K-Ar age of 13.8±0.3 Ma (Dixie Hambrick, written commun., 1988). Although these Resting Springs strata are faulted and tightly folded in places, they are not brecciated.

The timing of megabreccia emplacement at Black Butte is constrained by the ages of the overridden volcanic ash of the Resting Springs Formation and by the deposition of the overlying fanglomerates. $^{40}Ar/^{39}Ar$ ages on sanidine from three samples of tuff overridden by megabreccia sheets in the main mass of Black Butte yield a weighted mean of 12.81±0.03 Ma, placing a maximum age on emplacement of those megabreccia sheets. These results confirm U-Pb zircon ages reported by Guest et al (2007) and a biotite K-Ar age (Dixie Hambrick, written commun., 1988) from nearly identical locations that yield average ages of 12.84±0.23 Ma and 12.8±0.3 Ma, respectively. Biotite and plagioclase from an obsidian-bearing block of volcanic breccia overlying the same tuff yield a mean $^{40}Ar/^{39}Ar$ age of 13.18±0.06 Ma, statistically older than the sanidines. These data are consistent with emplacement of allocthonous obsidian and carbonate blocks on the 12.8-Ma Resting Springs rocks at Black Butte from similar units exposed at the 13.2- to 13.6-Ma Devil Peak (Guest et al, 2007). These deposits are now located some 30 km to the southeast, translated dextrally along the SFS. With at least some of the Black Butte megabreccias emplaced after 12.8 Ma, their origin as a culminating volcanic avalanche following 13.2-13.6 Ma eruption and collapse at Devil Peak seems insufficient.

References cited

Guest, Bernard, Niemi, Nathan, and Wernicke, Brian, 2007, Stateline fault system: A new component of the Miocene-Quaternary Eastern California shear zone: Geological Society America Bulletin, v. 119, p. 1337-1346.

Scheirer, D.S., Sweetkind, D.S., and Miller, J.J., 2010, Multiple phases of basin formation along the Stateline fault system in Pahrump and Mesquite Valleys, Nevada and California: Geosphere, v. 6, p. 23-129.

Inventory and analysis of landslides in the Mojave Desert, California

C. Gentile,[1], N.C. Barth,[1], and H. Steinmuller[2]
[1]University of California, Riverside. 900 University Ave, Riverside, CA 92521 (cgent001@ucr.edu); [2]Riverside City College. 4800 Magnolia Ave, Riverside, CA 92506

We present the first "complete" GIS database of landslides for the Mojave Desert region of California between the San Andreas and Garlock fault systems. We start by compiling all pre-existing literature and geological maps (both Quaternary surficial deposits and bedrock) at various scales and extract previously mapped landslides. We then use a variety of available imagery (aerial photos, terrain models, slope maps, hillshades, airborne lidar data) to systematically search the landscape for landslides, including deep-seated bedrock slumps and debris flows. Targeted fieldwork then follows to confirm key findings. With this database in hand, we can then build rich metadata for all the landslide deposits identified (type, volume, rock type, failure direction, age if known, etc.). This allows us to use the GIS to spatially interpolate landslide parameters across about 70000 km2 of the Mojave Desert and test correlations to causative factors (rock strength, slope steepness, geology, precipitation, earthquake shaking potential, etc.). The motivation for this work is to test the feasibility of a southern California-wide landslide database to better understand spatiotemporal trends and hazards.

Faults, mountains, lakes, and caves, the geologic story of San Bernardino County

Ian Gilbert[1], Robert Reynolds[2]
[1]Division of Earth Sciences, San Bernardino County Museum, 2024 Orange Tree Lane, Redlands, CA 92374, [2]Redlands, CA 92373, igilbert@sbcm.sbcounty.gov

The San Bernardino County Museum (SBCM) in Redlands, California, is in the final stages of developing a new permanent installation for the second floor of the Earth Sciences Gallery. Planned exhibits will tell the interconnected story of our region's geologic and paleontological history through the means of interactive displays, sculpted landforms, tactile objects, visual cues, interpretive text, and thought-provoking questions. Much of our region's spectacular topography is the result of active diastrophism, therefore, visitors will first be oriented by observing the nearby San Andreas fault zone and Transverse Ranges from an elevated viewing tower. As visitors progress through the exhibition they will encounter elasmosaurs, echolocating dolphins, bear dogs, and saber-tooth cats from the Mojave within exhibits that will focus on our region's tectonism, erosion and sedimentation, Pleistocene fluvial and pluvial systems, caves, and life through deep geologic time. All exhibits will incorporate and emphasize SBCM's vast collections,

encouraging visitors to make connections between the incredible geologic and paleontological history of our region, while simultaneously learning the important role museums serve to local and scientific communities. In addition, the content and design of this exhibition was developed for the "Next Generation Science Standard for California Public Schools, grades K-12" , supporting an interdisciplinary approach so visitors have the opportunity to build connections that link science to technology and societal impacts, ensuring pertinent, focused, and rewarding educational experiences.

Colonization of the zone-tailed hawk (*Buteo albonotatus*) in Mojave National Preserve

Lori Hargrove[1], Philip Unitt[1], Lea Squires[1], and Troy Maikis[2]
[1]Department of Birds and Mammals, San Diego Natural History Museum, San Diego, CA; [2]Department of Science and Resource Stewardship, Mojave National Preserve, Barstow, CA, troy_maikis@nps.gov

Large-scale monitoring programs tend to be insufficient for tracking changes in the distribution of rare or localized species, and it can be difficult to distinguish between a truly biological expansion and range extensions discovered through increased coverage by biologists. The zone-tailed hawk (*Buteo albonotatus*) nests from South America north into Texas, New Mexico, and Arizona and is considered rare throughout its range. Between 1862 and 1944, only five observations of zone-tailed hawks were known for the state of California, mostly near the Mexican border, and consequently it was considered only a rare vagrant in fall and winter. A literature review revealed that California's first record during the late spring / early summer breeding season was at Morongo Valley in 1970. Since then, fall and winter records have increased, and since 2003 there has been at least one bird recorded during the nesting season in Southern California annually.

In the 1980s a pair of zone-tailed hawks nested unsuccessfully in the Santa Rosa Mountains, Riverside County, and a pair at Hot Springs Mountain, San Diego County, fledged one young. However, neither of these nestings was followed by colonization. In Mojave National Preserve, a pair was first observed in 2004 and occurrences in spring / summer have been regular since 2009, including a nest in the Granite Mountains in 2011, a fledged juvenile at Mid Hills Campground in 2012, a nest in Cedar Canyon in 2014, and now at these sites two successful nests that we documented in 2016. Thus, a colonization in this region is apparent. A northward expansion has also been documented in the neighboring state of Arizona. Previous intensive scientific surveys in Mojave National Preserve over the past 100 years provide greater confidence that the colonization of zone-tailed hawk is a real change, and not an artifact of increased coverage

Desert Renewable Energy Conservation Plan

Tanya Henderson
Executive Director, Amargosa Conservancy, tanya@amargosaconservancy.org

Something about the vast spaces, technical color sunsets and cleverly adapted organisms of the California deserts have inspired curiosity, love, and loyalty amongst the desert rats. That affection for the open vistas and harsh conditions has inspired many to devote their time and energies to protect these desert lands through the ages.

The Desert Renewable Energy Conservation Plan (DRECP) was officially adopted when the Record of Decision was published in September of 2016. This legislation considers the deserts of California at landscape scale. It is one of the most comprehensive management plans ever launched. But what is it?

This talk will introduce the DRECP in the context of history and the scope of the plan—how does it relate to Death Valley National Park? To the Desert Protection Act of 1994? What other management plans exist at this landscape scale? What makes the DRECP unique? It will discuss why this groundbreaking planning effort took place—is it just about renewable energy? And it will discuss what the plan means to those of us on the ground in the desert, what we should pay attention to and how we can take part in the management process, even though the bulk of the plan is approved.

A two-stage fluid history for the Orocopia Schist and associated rocks related to flat subduction and exhumation, southeastern California

Gregory J. Holka[1], Marty Grove[2], Carl E. Jacobson[3,], Gordon B. Haxel[4]
[1]Department of Geological Sciences and the Institute for Integrated Research in Materials, Environments, and Societies, California State University, Long Beach, Long Beach, California 90840-3902, USA gregory.holk@csulb.edu; [2]Department of Geological Sciences, Green Earth Sciences, Stanford University, Stanford, California 46202-2115, USA; [3]Department of Geological and Atmospheric Sciences, Iowa State University, Ames, Iowa 50011-3212, USA and Department of Earth and Space Sciences, West Chester University of Pennsylvania, West Chester, Pennsylvania 19355, USA; [4]Geology Program, School of Earth Sciences and Environmental Sustainability, Northern Arizona University, Flagstaff, Arizona 86011, USA

Stable isotopes combined with preexisting 40Ar/39Ar thermochronology at the Gavilan Hills and Orocopia Mountains in southeastern California record two stages of fluid-rock interaction: (1) Stage 1 is related to prograde metamorphism as Orocopia Schist was accreted to the base of the crust during late Cretaceous–early Cenozoic Laramide flat subduction. (2) Stage 2 affected the Orocopia Schist and is related to middle Cenozoic exhumation along detachment faults. There is no local evidence that schist-derived fluids infiltrated structurally overlying continental rocks. Mineral δ18O values from

Orocopia Schist in the lower plate of the Chocolate Mountains fault and Gatuna normal fault in the Gavilan Hills are in equilibrium at 490–580°C with metamorphic water (δ18O = 7–11‰). Phengite and biotite δD values from the Orocopia Schist and upper plate suggest metamorphic fluids (δD ~ –40‰). In contrast, final exhumation of the schist along the Orocopia Mountains detachment fault (OMDF) in the Orocopia Mountains was associated with alteration of prograde biotite and amphibole to chlorite (T ~ 350–400°C) and the influx of meteoric-hydrothermal fluids at 24–20 Ma. Phengites from a thin mylonite zone at the top of the Orocopia Schist and alteration chlorites have the lowest fluid δD values, suggesting that these faults were an enhanced zone of meteoric fluid (δD < –70‰) circulation. Variable δD values in Orocopia Schist from structurally lower chlorite and biotite zones indicate a lesser degree of interaction with meteoric-hydrothermal fluids. High fluid δ18O values (6–12‰) indicate low water-rock ratios for the OMDF. A steep thermal gradient developed across the OMDF at the onset of middle Cenozoic slip likely drove a more vigorous hydrothermal system within the Orocopia Mountains relative to the equivalent age Gatuna fault in the Gavilan Hills.

KEY WORDS: stable isotopes, flat subduction, exhumation, meteoric-hydrothermal fluids

Selected trace elements in alluvium and rocks, western Mojave Desert, southern California

Krishangi D. Groover and John A. Izbicki
USGS, 4165 Spruance Rd Ste 200, San Diego, CA 92101, kgroover@usgs.gov

The chemistry and age of groundwater in the western Mojave Desert combine to create conditions that may allow naturally occurring trace elements (such as arsenic, chromium, or uranium) in alluvium and rock to enter groundwater at concentrations that may be a public health concern. A study of trace element concentrations in alluvium and rock is necessary to understand potentially harmful trace element concentrations in groundwater. More than 650 analyses were done on 189 samples of alluvium and rocks within the western Mojave Desert, southern California, to evaluate geologic sources of selected elements that could potentially enter groundwater. Portable (pXRF) and laboratory (LXRF) X-ray fluorescence was used to determine the concentrations of 27 elements, including naturally occurring water-quality contaminants such as arsenic, chromium, and uranium. The pXRF data were within 10 percent of traceable reference standards for most trace elements. Correlation of pXRF and LXRF data was good for many trace elements such as chromium, manganese, and uranium, with least-squares regression slopes near one and intercepts near zero. The pXRF overestimated iron compared to LXRF. Arsenic concentrations were greater than the average for continental crust in all analyses, with a maximum concentration of 125 mg/kg in alluvium from hydrothermally altered volcanic terrain. Chromium concentrations were less than the average for continental crust in 93 percent of measurements, although maximum concentrations of 300 mg/kg in alluvium and 8,600 mg/kg in rocks were measured in mafic terrains. Uranium (reporting limit 2.8 mg/kg) was detected in 13 percent of measurements, with most uranium detections in alluvium eroded from felsic terrain. Rubidium and potassium were associated with alluvium eroded from felsic terrain; but iron, copper, chromium, and, to a lesser extent, titanium, manganese, and nickel were associated with alluvium eroded from mafic terrain. Zinc, vanadium, and arsenic were associated with alluvium eroded from hydrothermally altered terrain. Comparison of pXRF with sequential extraction data from 40 samples showed arsenic and uranium were more abundant on the surfaces of mineral grains, while chromium and vanadium remained mostly within primary mineral grains. These data suggest that dissolution into groundwater as a result of changes in pH or redox state is more likely for arsenic and uranium than for chromium or vanadium.

Cave Mountain faulting and landsliding

V Frank F. Jordan, Jr.
San Bernardino County, Land Use Services Department, Frank.Jordan@lus.sbcounty.gov

Cave Mountain is a small, northeast-trending mountain ridge located immediately southeast of Interstate 15, about 10 miles southwest of Zzyzx and about 16 miles southwest of Baker. Jennings et al. (1962) mapped the southwest half of the ridge as granitic rock of Cretaceous age and the northeast half of the ridge as mixed pre-Cenozoic granitic and metamorphic rocks. The highpoint of the range is measured at 3624 feet/1104 meters above mean sea level. The relatively steep flanks of the ridge lie up to 2350 feet/700 meters above the surrounding alluvial valleys. Google Earth Pro was used to analyze the geologic aspects of Cave Mountain. These steep slopes are angled at 60% to 65% grade. These steep flanks are the result of relatively youthful normal faulting. A prominent, unmapped, northwest-striking normal fault separates the toes of rock slopes on the southeast from coalescing alluvial fans to the northwest. The USGS mapped a northeast-striking fault of Pleistocene age located approximately 3,000 feet/900 meters northwest of this fault. A parallel, unmapped northeast-striking normal(?) fault is situated along the southeast side of the ridge, and separates the steeply inclined rock of the spine of the ridge from the lower flanks of the mountain. Additional north-northeast-striking and east-northeast-striking faulting shows evidence of lateral as well as lesser vertical offset of these lower flanks. A prominent, but unmapped north-northeast-striking fault is coincident with the contact between the mapped granitic and metamorphic rock bodies. However, tonal reflectance of the imagery suggests that the rock underlying the ridge is genetically similar. Geomorphology of the steep slopes suggests that

northwest-failing landsliding affects the near surface rock mantling the northwest flank of the ridge. An argument can be made that the low flanks on the southeast side of the ridge may also be the result of deep-seated landsliding. This geologic analysis of Cave Mountain is presented with the aid of Google Earth Pro.

Mohave ground squirrel 2016 trapping results for the "Bowling Alley," San Bernardino County, California.

Ed LaRue
Circle Mountain Biological Consultants, Inc.

Between March 8 and June 22, 2016, 22 biologists trapped 11 grids in the region north of Edwards Air Force Base, which has been colloquially referred to as the "Bowling Alley." Thirteen Mohave ground squirrels (MGS), including 4 adults and 9 juveniles, were captured on 6 of the 11 grids. Eleven of these MGS were captured in creosote bush scrub and 2 were captured in saltbush scrub communities.

Pending collection of new scientific data such as provided in this report, both the Bureau of Land Management and San Bernardino County Board of Supervisors have tentatively identified the larger region encompassing the Bowling Alley as the "North of Edwards Development Focus Area." In the California Department of Fish and Wildlife's latest draft of its MGS Conservation Strategy, the Bowling Alley is located within the "North of Edwards Key Population Center."

That 13 Mohave ground squirrels were captured from the north end to the south end of the study area during the 2016 trapping effort is considered reliable evidence that the MGS occurs throughout the Bowling Alley, persists within this area even though regional populations are in decline and may have been extirpated from the southern and western portions of the historic range, and in spite of recent years of drought.

Based on information provided in this report, we found:

- MGS have persisted in the Bowling Alley from 2011 to 2016 with 100% trapping success of the only two MGS studies ever performed in the region;
- MGS were detected in 2016 when long-term known MGS populations have been in decline over the past five years and were detected at reduced levels region-wide in 2016; and
- The Bowling Alley is comprised of suitable substrates; moderate-to-high diversity of perennial plants; a prevalence of ecologically-important spiny hopsage and winterfat plants; habitat for at least 10 other special status plant and animal species and resources detected during the study; and is minimally affected by low levels of human impacts (with the exception of sheep grazing).

Based on the positive MGS trapping results given herein, the presence of requisite suitable habitat components as identified by the MGS TAG, two decades of programmatic failure to trap MGS populations in the southern and western portions of its range, and confirmation of MGS persistence over the past five years in spite of drought, we recommend that:

- The BLM withdraw the Bowling Alley area from further consideration as a Development Focus Area under the Desert Renewable Energy Conservation Plan; and
- The San Bernardino County Board of Supervisors no longer consider this as one of the five Development Focus Areas identified for energy development in their 17 February 2016 Resolution.

Geometric, kinematic, and temporal patterns of Quaternary surface rupture on the eastern Pinto Mountain fault zone relative to fault intersections near Twentynine Palms, southern California

Christopher M. Menges, Jonathan C. Matti, and Stephanie L. Dudash
U.S.Geological Survey, 520 N. Park Ave, STE 355, Tucson AZ 8571, (cmmenges@usgs.gov)

Detailed geologic mapping along the eastern Pinto Mountain fault zone (PMfz) in the Twentynine Palms area reveals previously unrecognized temporal and spatial variations in internal geometry, kinematics, and Quaternary surface-rupture timing; these variations appear to reflect fault-zone position relative to intersections with several NW-oriented transverse faults at both ends of the section of fault zone mapped in this study. The PMfz is an approximately E-W-trending, 80-km-long sinistral fault that forms the structural boundary between domains of transverse NW-trending dextral faults in the central Mojave Desert to the north and subparallel E-W-trending left-lateral faults in the eastern Transverse Ranges to the south. The PMfz displays evidence for an estimated 16-20 km of cumulative displacement of basement rocks. Existing data suggest that most mid- to late Quaternary activity is concentrated on the 40-km long western and middle sections of the PMfz in and westward of the Twentynine Palms area. We have produced a detailed geological map, focusing the relations of surface rupture to surficial deposits along a 10-km section of the PMfz where it traverses the southern and southwestern part of Twentynine Palms and continues another 4 km beyond the town to the southeast. This mapping indicates that the overall zone of faulting increases in complexity and width to the east concomitant with abrupt changes or deflections in the average fault zone orientation from an E- to a more SE-direction. The zone of surface ruptures increases in width eastward across this mapped section from < 150 m at the W-end to a >1.5-km near the intersection with the NW-trending Mesquite Lake dextral fault zone (MLfz) on the eastern edge. This width increase is not uniformly distributed but occurs abruptly via a series of E-directed branches and (or) right steps within the composite fault zone. That is, the most significant component strands of the fault zone

commonly either abruptly deflect and (or) branch onto new primary faults strands reoriented to ESE, with very little or much reduced levels of faulting observed on any continuation of the original strands eastward past these branch-deflections points. Geometrically, the composite fault zone consists of multiple internal zones of clustered faulting, <5 m- to >200 m in width and increasing from one to 4-5 in number eastward across the map area. These commonly subparallel zones of clustered faulting are separated by relatively undeformed intervening blocks. Each fault-rich domain comprises a complex array of subparallel to branching discrete multiple component zones of shears and fractures, 2- 8+ in number and centimeters to meters in width, that collectively suggest wide zones of distributed surface rupture.

The ages of most recent ruptures — constrained by fault-zone stratigraphy and scarps — vary among individual components of the composite fault zone. Our age estimates for the youngest set of surface ruptures include: (1) late Pleistocene rupture ages on the two main northern zones; and (2) multiple (minimum 2-3) Holocene-age ruptures, commonly as young as late Holocene, on the two southern zones.

Many internal fault strands in the PMfz display geomorphic and structural features (vertical scarps, fault-bounded escarpments and popup structures, oblique slickenlines, net displacement estimates, and folded or tilted strata) indicative of secondary transpression, commonly localized at SE-trending right-shifted constraining bends, branches, or step-overs on internal fault zones; this secondary deformational component increases eastward in intensity and coverage on both the overall zone and individual strands as the PMfz approaches dextral-fault intersections such as the MLfz. In many areas the northernmost and southernmost strands of the overall fault zone are associated with inward directed south-facing ridges and N-facing escarpments, respectively, that topographically bound an intervening lowland area containing low-relief mostly translational internal fault strands commonly associated with the most complex and recently active surface displacement patterns. Collectively this fault-generated topography defines a variable-width trough, tens of meters deep, that widens to the east in concert with the increasing width and complexity of the overall PMfz as it approaches intersection with the eastern dextral fault zone (MLfz).

The PMfz and associated fault trough themselves occupy the crest of a large broad arch-like elongate elongated topographic high increasing in elevation from 30 to 100^{+} m from west to east on a N-facing slope above lower terrain to the north. This feature suggest an additional component of regional uplift, oriented transversely (N-S) across the PMfz , which is likely contractional in nature, based on the persistent transpressional component observed along the associated PMfz. Bedrock dissection and erosion patterns along the adjacent north escarpment of the Eastern Transverse Ranges suggest this uplift is transmitted southward across the PMfz into this adjoining range block.

The cumulative spatial-temporal patterns of fault geometry and kinematics define a complicated stepwise increase in the width, complexity, transpressive component, and ages of surface displacements to the E and SE along the mapped section of the PMfz that appears strongly influenced by eastward approach to the NW-trending dextral MLfz.

Recent detailed mapping of the southern and western Coyote Mountains, Imperial County, southern California.

George J Morgan and JR Morgan
georgemorgan@cox.net

Since 2001, our ongoing detailed mapping of the Coyote Mountains (CM) we have found:

1) Active left and right lateral faulting in some instances reactivating older faults;
2) Cenozoic thrusting and three episodes of extensional tectonics associated with Basin and Range extension, opening of the Gulf of California and the West Salton Detachment Fault;
3) Mullion structures;
4) Landslides, several terraces and stream piracy associated with the recent, rapid, episodic, differential uplift of the CM;
5) Named a new formation Viejo, lower Imperial Group consisting of +9 interfingering transgressional-regressional marine sequences and +5 terrestrial fanglomerates;
6) At least one Viejo Formation of marine sediments that interfingers with a Viejo terrestrial fanglomerate;
7) Two Viejo Formation fresh-water limestones associated with two Viejo terrestrial fanglomerates;
8) Two Viejo Formation sedimentary sequences that interfinger with Miocene Alverson Canyon Formation volcanics;
9) Alverson Canyon (17 Ma) plugs, cinder cones, lahars flows, etc.;
10) Jurassic (~162 Ma) age igneous rocks;
11) Folded and faulted metamorphic rocks consisting of marbles, schists, gneisses, banded chert, quartzite, and amphibolite with pillow structures.

Evidence of synextensional deposition of the Early Miocene Jackhammer and Pickhandle formations in the Amphitheatre Canyon area of the northeastern Calico Mountains, CA

Bryan P. Murray
Department of Geological Sciences, California State Polytechnic University, Pomona, CA 91768

This study in the Amphitheatre Canyon area of the northeastern Calico Mountains (~2 km NNW of Calico

Peak) presents new evidence of synextensional deposition of the Early Miocene Jackhammer and Pickhandle formations in a normal fault-bounded basin within the upper plate of the Waterman Hills detachment fault of the central Mojave metamorphic core complex (CMMCC). The Jackhammer Formation at this locality consists primarily of a ~130 m-thick welded ignimbrite, herein named the "Mammut ignimbrite." This ignimbrite is crystal-rich (30–40% quartz, biotite, sanidine, and hornblende phenocrysts, to 2 mm-diameter) with 15–20% lithic fragments (most 0.5-5 cm-diameter, max ~50 cm). In addition to the Mammut ignimbrite, the Jackhammer Formation consists of locally interbedded alluvial conglomeratic sandstone, tuffaceous sandstone, lacustrine limestone, avalanche megabreccia, and mafic lava. The Pickhandle Formation conformably overlies the Jackhammer Formation and consists of two members: 1) a lower member of a dacitic block and ash flow and monomict (dacitic) debris flow breccia (max clast size ~1.25 m-diameter), and 2) an upper member of alluvial polymict (basement-derived and dacitic) conglomeratic sandstone and conglomerate, primary and reworked lapilli tuff, and localized rhyodacitic lava and block and ash flows. During and following deposition of the Pickhandle Formation in the study area, reddish porphyritic dacitic plugs and lavas were emplaced.

In the study area, stratigraphic evidence suggests syndepositional displacement of the "Amphitheatre Fault," a high-angle NW-striking, SW-dipping normal fault that bounds the northeastern margin of an extensional basin. The deposits of the Jackhammer and Pickhandle formations thicken and coarsen eastward toward the Amphitheatre Fault in the hanging wall block, with the Jackhammer Formation generally absent or thin on the footwall block of the fault where deposits of the lower Pickhandle Formation deposited directly on nonmylonitic basement Mesozoic granitoids. Paleocurrent indicators suggest primarily WSW-directed flow away from the footwall block, with clasts mainly derived from the basement and intrabasinal dacitic rocks. Growth strata (fanning bedding dips and intraformational angular unconformities) within the hanging wall deposits and the interbedded alluvial debris flow, megabreccia, and lacustrine deposits located adjacent to the Amphitheatre Fault suggest deposition in a half-graben basin formed during CMMCC extension. Future geochronological analyses of coeval volcanic rocks will provide additional age constraints on CMMCC extensional basin development.

Distributed deformation associated with the eastern termination of the Cady Fault, Eastern California Shear Zone

K. M. Schmidt[1] and P. Nuriel[2]
[1]U.S. Geological Survey; [2]Geological Survey of Israel, kschmidt@usgs.gov, nuriel@gsi.gov.il

Previous research by others, our new field mapping, and analysis of aeromagnetic data indicate that the Cady Fault (CF) is a significant structural boundary acting as the southern boundary to the Mojave block within the Eastern California Shear Zone (ECSZ) that separates northwest-striking dextral faults to the south, from east-northeast-striking sinistral faults to the north. To constrain the timing and interpret strain distribution in the tectonic accommodation zone east of the termination of the CF, an east-striking, steeply dipping, sinistral fault, we mapped bedrock and surficial geology and acquired U/Pb dates of syn-tectonic opaline precipitates within faults displacing alluvial sediment. Here we provide evidence for distributed oblique dextral shear east of the CF towards the topographic low of Broadwell Lake.

At its eastern terminus, the CF intersects or merges with an east-vergent, west-dipping, N-NE striking thrust, hereafter referred to as the Elephant Seal fault (ESF). This abrupt, eastward change in displacement kinematics generated rock uplift that has exhumed crystalline basement with high relief, the Cady Mountains, which decreases southward from the CF and the local high of Cady Peak. This may indicate decreased total reverse fault slip on the ESF to the south toward the Lavic Lake Fault.

Immediately east of the ESF lies an extensive, deeply incised, alluvial sequence composed of sediments with a clast composition consistent with a local source from Cady Mountains exhumed along the ESF. This alluvial sequence is displaced by numerous, newly recognized, discontinuous, steeply west dipping (65-85°), low-strain faults ranging in structural orientation from N-NW to N-NE, situated a distance of ~ 1 to > 2 km east of the ESF. Abundant, conspicuous opaline precipitates that display evidence of multiple-generations of syn-tectonic precipitation core these faults. We used U/Pb techniques to determine the ages of these opaline-cored faults to constrain the timing of displacement outboard of the CF/ESF system. These ages range from ~0.46-5.2 Ma; with a mean and standard deviation of 2+/-1.4 Ma calculated from 24 analyses representing 7 separate outcrops of faulted alluvium. This chronologic control on age of faulting indicates the sediments in the tectonic accommodation zone east of the CF/ESF to be of at least Pleistocene to Pliocene in age. Additional evidence of Quaternary activity for these opaline-cored faults includes gouge zones up to 0.35 m thick, which displace Stage III Bk horizons near the present ground surface. These same faults produced back-facing scarps evident on local topographic highs of fan surfaces and likely

represent horst-like structures associated with east-vergent shortening of this alluvial fill.

Although deformation features in this accommodation zone are consistent with shortening associated with a right step in a broader left-lateral fault system with reverse faulting oriented roughly orthogonal to primary sinistral faults, evidence for a through-going surface trace of an east-striking sinistral fault east of the CF is presently lacking. The Broadwell Mesa fault is such a candidate, but it lies 20 km to the east and the intervening area is separated by numerous north-striking, likely oblique dextral, faults. Such complexity of accommodation zone fault structure may indicate that i) deformation associated with the CF is a spatially and temporally evolving feature that may be lengthening eastward or, more probable that, ii) reverse deformation associated solely with the ESF is stepping eastward. Additionally, the orientation of many of the structures are generally orthogonal, or at a high angle, relative to the expected NNE regional stress field within the ECSZ, and hence represent local complexity of Quaternary tectonic deformation.

Hydrologic and geologic controls on groundwater recharge along the Mojave River floodplain aquifer

Whitney A. Seymour[1] and Trent W. Biggs[2]
[1]USGS California Water Science Center, 4165 Spruance Road, Suite 200, San Diego, CA 92101, wseymour@usgs.gov; [2]Storm Hall 308C, Department of Geography, San Diego State University, 5500 Campanile Dr., San Diego, CA 92182-4493

The Mojave River and its underlying ground-water basin are important water sources for the Mojave Desert. More than 80% of natural recharge to the basin comes from transmission losses of Mojave River stormflow. The majority of this recharge remains in the Mojave River floodplain aquifer, the most productive aquifer in the basin. Therefore, it is necessary to understand the quantity and spatial distribution of natural recharge in the Mojave River floodplain aquifer. The objectives of this study were to determine: 1) how stormflow duration (days), peak flow rate (m^3/second), and magnitude (volume, in million cubic meters) control the quantity of groundwater recharge at a given distance downstream from where the Mojave River enters the floodplain aquifer; and 2) how geologically-mediated features (including aquifer and channel morphology) and depth to the water table prior to a stormflow event control the quantity and spatial distribution of recharge.

Univariate and multivariate regressions used hydrologic and geologic variables to estimate groundwater-level rise for 10 floodplain aquifer segments along the Mojave River during 6 stormflow events. Regressions using the inverse distance weighting (IDW) interpolation method to determine average observed water-level rise best represent the system, because IDW captures the spatial variability within each segment. Results indicate that stormflow magnitude is the dominant predictor of groundwater-level rise for the entire floodplain aquifer. The quantity of recharge for individual segments downstream from the Mojave River headwaters is controlled by both hydrologic and geologic variables. Pre-event groundwater level controls recharge from stormflow in the segment directly below the headwaters, flow duration and magnitude control recharge in the middle segments of the river, and peak flow rate controls recharge in the downstream segments of the river. Morphological variables such as aquifer width, channel width, pre-event groundwater level, and aquifer storage (aquifer width × pre-event groundwater level), were statistically significant predictors of groundwater-level rise for five out of six stormflow events ($p < 0.05$).

A water budget was constructed for three gauged stream reaches along the Mojave River. Results indicate that transmission loss is the largest contributor to groundwater recharge for all 3 stream reaches, supporting the existing research finding that the Mojave River is the primary source of recharge to the floodplain aquifer. Contrary to expectation, the largest amount of recharge did not occur in the coarsest-grained upstream reach. Segment regression analysis indicated that recharge in the upstream reach is limited by a combination of narrow channel and aquifer widths, and by high pre-event groundwater levels. The largest amount of recharge occurred in the middle reach where these factors are not limiting.

Influence of resource availability on the growth and reproduction of the invasive annual *Brassica tournefortii* (Sahara mustard)

Laura Song and Joel K. Abraham
California State University, Fullerton (ljsong@csu.fullerton.edu)

The spread of invasive non-native plant species threatens native plants in most California ecosystems. *Brassica tournefortii* (Sahara mustard) is a highly invasive non-native annual herb that is spreading rapidly in arid ecosystems of southern California. *B. tournefortii* displaces native annual species by forming dense, persistent populations. Resource variability in California, particularly in soil nitrogen and water, may be linked with the expansion of *B. tournefortii* in California's arid ecosystems, which historically are relatively resistant to invasions. We conducted a greenhouse experiment to explore the possible interactive effects of water and nitrogen availability on growth, allocation, and reproduction of *B. tournefortii*. We applied two fully crossed factors to *B. tournefortii*: two levels of watering and three levels of nitrogen addition. Higher water and nitrogen availability resulted in increased total dry biomass and higher average fruit and seed count. *B. tournefortii* stem mass ratio was greater with higher available nitrogen, while specific leaf area increased with lower available nitrogen; allocation did not differ across watering treatments. Although both water and nitrogen impacted growth and reproduction, we found no evidence

of interactions between water and nitrogen availability. Previous studies have shown that higher water availability can lead to greater expansion of *B. tournefortii* in favorable conditions, but this study demonstrates that nitrogen may have a stronger influence on productivity and reproduction. Future studies on how nitrogen availability influences the competitive impacts of *B. tournefortii* on native species will add to our understanding of this invasion, and may aid in the management of existing populations in the arid regions of California.

Keywords: Invasion, arid ecosystems, resource availability, *Brassica tournefortii*

Fossil wood from Scoop Wash, Mohave County, Arizona

Thomas Spinks
Anza Borrego Desert State Park, tlspinks217@gmail.com

The petrified wood found in the Colorado River delta area of the Salton Trough has been studied extensively. As a result, seven genera of fossil trees have been identified that comprise the Carrizo Local Flora. Petrified wood from the Colorado River outside of the delta area has not yet been examined systematically. This poster represents the preliminary results of identifying samples of petrified wood collected from the Scoop Wash area in Mohave County, Arizona, one of the northernmost areas of the lower Colorado River.

Scoop Wash is the first of 10 wood localities in the Pliocene Bullhead Formation that crop out along the lower Colorado River where samples of Pliocene age petrified wood occur. Samples are being collected for taxonomic comparison with the petrified woods found in the delta area of the river in the Salton Trough.

First record of vertebrate fossils in the Searles Basin: in another desert paleosol

J. D. Stewart and Marjorie Hakel.
Natural History Museum of Los Angeles County, 900 Exposition Blvd., Los Angeles, CA 90007; fossil50@pacbell.net

Searles Lake lies in northwestern San Bernardino County, California. Many paleontologists have assumed, based on the abundance of vertebrate fossils at nearby China Lake, that vertebrate fossils should be found at Searles Lake. However, evaporite minerals are mined at Searles Lake and are rare at China Lake, indicating that the two lakes, although linked, have quite different histories.

George Smith, a USGS geologist, spent years studying the geology of the Searles Basin, and published two USGS Professional Papers on this topic in 1979 and 2009. He never witnessed a single vertebrate fossil from the lake sediments in all the years of his research, but he identified three paleosols within the lacustrine sequence that mark low stands of the lake. Because of his many radiocarbon dates on tufa and mollusks within the lakebed sequence, the ages of these paleosols are well constrained.

On the western slopes of the basin among many tufa-coated rocks, a paleosol can be found in places with very little digging. It is a reddish-tan color and is marked by white nodules of pedogenic carbonate formed within relatively fine-grained alluvium or against and between cobble-size clasts in coarser sediments. Paleosols, like modern soils, conform to topography. In the relatively small area where we studied this soil, its elevation varies by 20 feet, as does the existing surface. Smith's published mapping of the geology indicates that the areas where we have observed this paleosol correlate with his middle paleosol, bracketed by radiocarbon dates of 15 ka to 13.5 ka. The fauna observed thus far includes a lizard, a bird, *Ammospermophilus leucurus*, *Dipodomys* sp., and cf. *Thomomys* sp. Some of the specimens show substantial development of manganese oxide coating. All show some degree of calcium carbonate coating. In most cases, the coating is pedogenic carbonate. In the case of the avian fossil, it could be lacustrine carbonate.

This area joins the growing list of California desert areas where Pleistocene paleosols have produced vertebrate fossils. Scientists and others concerned with the conservation and management of paleontological resources in the Searles Basin should shift their focus from the lacustrine sediments to the paleosols.

— Notes —